Australian Academy of Science

International Association of Geodesy

Proceedings of Symposium on Earth's Gravitational Field and Secular Variations in Position

Editors

R. S. MATHER

P. V. ANGUS-LEPPAN

The School of Surveying
The University of New South Wales
Sydney, Australia

Published by
The School of Surveying
The University of New South Wales
Sydney, Australia
June 1974

National Library of Australia card number and ISBN
0 85839 016 7

Australian
Academy
of
Science

International
Association
of
Geodesy

PROCEEDINGS OF SYMPOSIUM ON THE EARTH'S GRAVITATIONAL FIELD AND SECULAR VARIATIONS IN POSITION

ORGANIZING COMMITTEE

P.V. Angus-Leppan
(Chairman) School of Surveying
The University of New South Wales

A.G. Bomford
Division of National Mapping
Department of Minerals and Energy

J.C. Dooley
Bureau of Mineral Resources
Department of Minerals and Energy

R.S. Mather
School of Surveying
The University of New South Wales
Secretary, Section V, International
Association of Geodesy

The members of the organizing committee are members of the Sub-Committee on Geodesy of the Australian National Committee on Geodesy and Geophysics

---

VENUE: Theatre B
Sciences Building
The University of New South Wales
Sydney
Australia
26 - 30 November 1973

PROCEEDINGS: SYMPOSIUM ON

EARTH'S GRAVITATIONAL FIELD & SECULAR VARIATIONS IN POSITION

PREFACE

The International Symposium on the Earth's Gravitational Field and Secular Variations in Position was held in Sydney, Australia from 26 to 30 November 1973. The venue of this Symposium which was organized by the Australian Academy of Science for the International Association of Geodesy, was the Sciences Theatre B, University of New South Wales, in the Sydney suburb of Kensington.

On behalf of the Australian Academy of Science and the International Association of Geodesy, the Organizing Committee takes pleasure in making the following acknowledgments.

. Financial and/or material assistance was received from the following organizations. The listing is in chronological order of receipt of commitment.

Department of Science, Government of Australia
International Union of Geodesy and Geophysics
School of Surveying, University of New South Wales
IBM Australia Pty Ltd
Wild Australia Pty Ltd
Ansett Airlines of Australia
Hewlett Packard Australia Pty Ltd
D.R. Johnston & Co.
Carl Zeiss Pty Ltd
AGA Products (Aust) Pty. Ltd.

. The co-operation and intellectual stimulus of the various session chairmen, listed on pages ix to xv.

. Mr. Edward G. Anderson for making sound recordings and notes of all discussions.

. Mrs Margeri Mather who as a gesture of goodwill to the geodetic community, prepared the bulk of the typescript for the Proceedings.

. Messrs L. Jeffrey & M. Legge, Mrs. W.S. Lennon, Dr. S.U. Nasca, Miss M. O'Hara and Mr. G. Umadhay of the School of Surveying assisted in the organization of the Symposium.

R.S. Mather accepts responsibility for the accuracy of the transcripts of the discussions, and with P.V. Angus-Leppan, who did the final proof-reading, prepared the material for typing. Author co-operation in proof-reading typescripts is also acknowledged

ORGANIZING COMMITTEE

LIST OF PARTICIPANTS

AUSTRALIA

Australian Capital Territory

1. Mr Henry J. M. Abraham
   Mt Stromlo & Siding Spring Observatory
   Australian National University
   Private Bag, Woden
   Canberra 2606

2. Mr W. Anfiloff
   Bureau of Mineral Resources
   PO Box 378 Canberra 2601

3. Mr Brian C. Barlow
   Bureau of Mineral Resources
   PO Box 378 Canberra 2601

4. Mr Anthony G. Bomford
   Division of National Mapping
   PO Box 667 Canberra 2601

5. Mr James C. Dooley
   Bureau of Mineral Resources
   PO Box 378 Canberra 2601

6. Dr John G. Fryer
   Division of National Mapping
   PO Box 667 Canberra 2601

7. Mr Bruce P. Lambert
   Division of National Mapping
   PO Box 667 Canberra 2601

8. Mr Klaus Leppert
   Division of National Mapping
   PO Box 667 Canberra 2601

9. Mr John McK. Luck *
   Division of National Mapping
   PO Box 667 Canberra 2601

10. Dr Peter Morgan
    Division of National Mapping
    PO Box 667 Canberra 2601

11. Mr Adrian Roelse
    Division of National Mapping
    PO Box 667 Canberra 2601

12. Mr W. Wassermann
    School of Liberal Studies
    Canberra College of Advanced Education
    PO Box 381 Canberra 2601

New South Wales

13. Mr Maurice Aliprandi
    School of Civil Engineering
    Sydney Technical College
    Broadway 2007

14. Dr John S. Allman
    School of Surveying
    University of New South Wales
    PO Box 1 Kensington 2033

15. Mr Edward G. Anderson
    School of Surveying
    University of New South Wales
    PO Box 1 Kensington 2033

16. Professor Peter V. Angus-Leppan
    School of Surveying, Univ. of New South Wales
    PO Box 1 Kensington 2033

17. Mr Gordon E. Baker
    1/64 Mullens Street
    Balmain 2041

18. Mr George A. Bell
    CSIRO/National Standards Laboratory
    Chippendale 2008

19. Mr Leonard Berlin
    School of Surveying
    University of New South Wales
    PO Box 1 Kensington 2033

20. Professor George G. Bennett
    School of Surveying
    University of New South Wales
    PO Box 1 Kensington 2033

21. Mr Alan Brady
    School of Civil Engineering
    New South Wales Institute of Technology
    Broadway 2007

22. Mr Karl Bretreger
    35 Gough Street
    Granville West 2142

23. Professor V. T. Buchwald
    School of Mathematics
    University of New South Wales
    PO Box 1 Kensington 2033

24. Mr Glenn Bush
    12 Birdwood Ave
    Pagewood 2035

25. Mr Frank L. Clarke
    Department of Civil Engineering
    University of Newcastle 2308

26. Mr Richard Coleman
    78 Tryon Road
    East Lindfield 2070

AUSTRALIA (contd)

New South Wales (contd)

27. Mr R. Nigel Davies
43 Sunshine Street
Manly Vale 2093

28. Mr T. L. Duyet
School of Surveying
University of New South Wales
PO Box 1 Kensington 2033

29. Mr R. Fleeton
Aero Service Australia
514 Miller Street
Cammeray 2062

30. Mr John G. Freislich
School of Surveying
University of New South Wales
PO Box 1 Kensington 2033

31. Mr P. G. Friedmann
90 Woronora Crescent
West Como 2226

32. Mr D. M. Geyer
Aero Service Australia
514 Miller Street
Cammeray 2062

33. Dr J. Stuart Godfrey
CSIRO/Division of Fisheries
& Oceanography
PO Box 21 Cronulla 2230

34. Mr Graham J. Hall
6 Cressfield Avenue
Carlingford 2118

35. Dr Leonard U. Hibbard
CSIRO/National Standards Laboraaory
Chippendale 2008

36. Dr B. David Johnson
School of Earth Sciences
Macquarie University
North Ryde 2113

37. Mr John T. Judge
Central Mapping Authority
67-69 Regent Street
Chippendale 2008

38. Mr A. H. William Kearsley
School of Surveying
University of New South Wales
PO Box 1 Kensington 2033

39. Mr P. C. Kelly
11 Wangi Avenue
Cronulla 2230

40. Mr Aksheya Kumar
School of Applied Geology
University of New South Wales
PO Box 1 Kensington 2033

41. Mr Ronald D. Lister
School of Surveying
University of New South Wales
PO Box 1 Kensington 2033

42. Mr Ian D. Lloyd
School of Surveying
University of New South Wales
PO Box 1 Kensington 2033

43. Mr Jeffrey Lovell
School of Civil Engineering
Sydney Technical College
Broadway 2007

44. Mr John R. Masters
1 Aden Street
Seaforth 2092

45. Dr Ronald S. Mather
School of Surveying
University of New South Wales
PO Box 1 Kensington 2033

46. Dr Salvatore U. Nasca
School of Surveying
University of New South Wales
PO Box 1 Kensington 2033

47. Mr Bruno Purins
Central Mapping Authority
PO Box 39 Sydney 2001

48. Dr. I. Qureshi
School of Applied Geology
University of New South Wales
PO Box 1 Kensington 2033

49. Dr J. A. Roberts
CSIRO/Division of Radiophysics
PO Box 76 Epping 2121

50. Dr Artur Stolz
School of Surveying
University of New South Wales
PO Box 1 Kensington 2033

51. Dr Peter H. Sydenham
Department of Geophysics
University of New England
Armidale 2351

52. Mr Grigorio Umadhay
School of Surveying
University of New South Wales
PO Box 1 Kensington 2033

53. Mr Ross S. Walker
39 Glenwall Street
Kingsgrove 2208

54. Mr A. P. Henry Werner
School of Surveying
University of New South Wales
PO Box 1 Kensington 2033

Queensland

55. Dr Ian A. Harley
Department of Surveying
University of Queensland
St Lucia 4067

56. Mr Paul C. Miller
Department of Surveying
University of Queensland
St Lucia 4067

57. Professor Frank D. Stacey
Department of Physics
University of Queensland
St Lucia 4067

South Australia

58. Mr Lyall E. Bishop
School of Surveying
South Australian Institute of Technology
Box 1 Ingle Farm 5098

59. Dr John S. Gubbay
WRE/Space Research Group
PO Box 2151 Adelaide 5001

60. Dr Kenneth J. W. Lynn
WRE/Space Research Group
PO Box 2151 Adelaide 5001

Tasmania

61. Mr Anthony Sprent
Department of Surveying
Tasmanian College of Advanced Education
Mount Nelson 7007

Victoria

62. Mr Henry D. Couchman
Department of Surveying
Royal Melbourne Institute of Technology
124 Latrobe Street
Melbourne 3000

63. Mr N. F. Edwards
Department of Surveying
Royal Melbourne Institute of Technology
124 Latrobe Street
Melbourne 3000

64. Mr Brian T. Murphy
Department of Surveying
University of Melbourne
Parkville 3052

65. Mr G. H. V. Thomson
Department of Surveying
Royal Melbourne Institute of Technology
124 Latrobe Street
Melbourne 3000

Western Australia

66. Mr Kenneth J. Lyons
Department of Surveying
West Australian Institute of Technology
Hayman Road
South Bentley 6102

67. Mr Harvey L. Mitchell
Department of Civil Engineering
University of Western Australia
Nedlands 6109

A U S T R I A

68. Professor Helmut Moritz
Institute of Geodesy IV
Technical University
Steyrergasse 17
A 8010 Graz

B E L G I U M

69. Professor Paul Melchior
Observatoire Royale de Belgique
3 Ave Circulaire
Uccle, Bruxelles 18

70. Dr Paul Paquet *
Observatoire Royal de Belgique
3 Ave Circulaire
Uccle, Bruxelles 18

C A N A D A

71. Dr Dezso Nagy *
Gravity Division
Department of Energy, Mines & Resources
Ottawa, Ontario K1A 0E4

72. Dr Richard I. Walcott
Earth Physics Branch
Department of Energy, Mines & Resources
Ottawa, Ontario K1A 0E4

C Z E C H O S L O V A K I A

73. Dr G. Nedoma *
Ceskoslovenska Akad. Ved
Geofysikalni Ustav
Bocni 11 CP1401
Praha 4 Sporilov

F R A N C E

74. Miss Martine Feissel
Bureau International de l'Heure
61 Ave de l'Observatoire
75014 Paris

75. Professor Kurt Lambeck
Section d'Astrophysique
Observatoire de Paris
92190 Meudon

76. Dr A. Sakuma
Bureau International des Poids et Mesures
Pavillon de Breteuil
92 Sevres

GERMANY (FEDERAL REPUBLIC OF)

77. Professor Erik Grafarend
Institut für Theoretische Geodäsie
Universität Bonn
D 53 Bonn, Nussallee 17

78. Professor Erwin Groten
Astronomische Geodäsie und
Satellitengeodäsie
Technische Hochschule Darmstadt
61 Darmstadt, Petersenstrasse 13

79. Dr Guenter Seeber
Geodetic Institute
University of Bonn
D 53 Bonn, Nussallee 17

GREAT BRITAIN

80. Mr John R. Hollwey
Department of Land Surveying
North East London Polytechnic
Forest Road, London E17 4JB

GREECE

81. Professor Constantinos Cladas
University of Saloniki
Boucouzestiou 35
Athens

INDIA

82. Dr J. C. Bhattacharji *
Geodetic Survey Research Branch
Survey of India
Dehra Dun, UP

INDONESIA

83. Professor Jacub Rais
Badan Koordinasi Survey
Dan Pemetaan Nasional
Jalan Wahidin I/II
Jakarta

ITALY

84. Professor Armando Norinelli
Instituto de Fisica Terrestre
Geodesia e Geografia Fisica
Universita di Padova
Via VIII Febbraio 9
35100 Padova

JAPAN

85. Dr Naomi Fujita
Crustal Research Office
Geographical Survey Institute
24-13, 3-Chome Higashiyama
Meguro-ku, Tokyo

86. Dr Yukio Hagiwara *
Earthquake Research Laboratory
University of Tokyo
Bunkyo-ku, Tokyo 113

KOREA

87. Mr Moo Woong Choi
(present address)
Department of Geography
Tokyo University of Education
Misuzuso 604, 1-Chome Ikebukuro
Toshimaku, Tokyo 170

NEW ZEALAND

88. Professor John B. Mackie
University of Otago
Box 56, Dunedin

89. Mr W. Ian Reilly
DSIR/Division of Geophysics
Box 8005, Wellington

NIGERIA

90. Dr Gabriel F. T. Obenson *
Faculty of Engineering
University of Lagos
Lagos

PAPUA & NEW GUINEA

91. Mr Alan J. McCarthy
Department of Surveying
TPNG University of Technology
Box 793, Lae

SWEDEN

92. Professor Arne Bjerhammar *
Kungl. Tekniska Högskolan
Instituionen för Geodesi
S-100 44 Stockholm 70

UNITED STATES

93. Mr. Peter J. Dunn
Wolf Research & Development Corporation
Riverdale, Md.

94. Dr Donald Eckhardt
AFCRL/L.G. Hanscom Field
Terrestrial Sciences Laboratory
Bedford, Mass. 01730

95. Mrs Irene Fischer
Defence Mapping Agency
Topographic Center
7500 Brooks Lane
Washington DC 20315

96. Mr Stanford Holdahl
US National Geodetic Survey
N O A A
Rockville Md 20852

97. Mr John Hopkins
Defence Mapping Agency
Aerospace Center
St Louis, Missouri 63118

98. Professor William M. Kaula
Institute for Planetary & Space Sciences
University of California
Los Angeles, California 90024

99. Mr Peter F. MacDoran *
Jet Propulsion Laboratory
California Institute of Technology
Pasadena, California 91103

100 Professor William Markowitz
Physical Oceanography Laboratory
Nova University
8000 N Ocean Drive
Dania, Florida 33004

101 Professor Ivan I. Mueller
Department of Geodetic Science
Ohio State University
1958 Neil Avenue
Columbus Ohio 43210

102 Dr Robert D. Nason *
Earthquake Research Laboratory
US Geological Survey
390 Main Street
San Francisco, California 94105

103 Dr Kwok M. Ong
Jet Propulsion Laboratory
California Institute of Technology
Pasadena, California 91103

104 Dr Henry H. Plotkin
Advanced Data Systems Division
NASA/Goddard Space Flight Center
Greenbelt Md 20771

105 Professor Richard H. Rapp
Department of Geodetic Science
Ohio State University
1958 Neil Avenue
Columbus Ohio 43210

106 Dr Joseph W. Siry
NASA/HQ
Washington DC 20546

107 Professor Wilton Sturges
Department of Oceanography
Florida State University
Tallahassee, Florida 32306

108 Professor Byron D. Tapley
Department of Aerospace Engineering
& Engineering Mechanics
University of Texas at Austin
Austin, Texas 78712

109 Mr Samir Vincent
Computer Sciences Corporation
8728 Colesville Road
Silver Spring, Md 20910

110 Mr Charles A. Whitten
9606 Sutherland Road
Silver Spring, Md 20901

111 Mr James D. Williams
Haleakala Observatory
University of Hawaii
Box 157, Kula, Maui
Hawaii 96790

U S S R (SOVIET UNION)

112 Professor Yuri D. Boulanger
President, IAG
Soviet Academy of Sciences
117296 Molodezhnaya 3
Moscow

113 Dr J. A. Maslov
Soviet Academy of Sciences
117296 Molodezhnaya 3
Moscow

* Paper to be presented in absentia

ASSOCIATES

Australia

114 Mrs Betty Allman
115 Mrs G. A. Bell
116 Mrs Barbara Berlin
117 Mrs Molly Bennett
118 Mrs Barbara Bishop
119 Mrs Nanette Dooley
120 Mrs Eulie Freislich
121 Mrs Rosalind Kearsley
122 Mrs Gwen Lambert
123 Mrs Margeri Mather
124 Mrs H.L.Mitchell
125 Mrs Heidi Stolz

Italy

126 Mrs A. Norinelli

United States

127 Dr Erik Fischer
128 Mrs Brena Whitten

RESOLUTIONS ADOPTED AT THE CLOSING SESSION

NOVEMBER 30 1973

1. This Symposium wishes to draw attention to the valuable contribution being made to geodesy by the work of the Federation of Astronomical and Geophysical Services (FAGS). The form of presentation of the results of these services is in need of re-examination, and with this in mind, this Symposium suggests that a study group be set up for this purpose. In the meantime this Symposium recommends that the work of FAGS should be maintained and extended.

   Carried unanimously

2. This Symposium,
   noting the discrepancies in the definition of a height datum,
   recommends detailed studies of the relation between geodetic and oceanographic height datums.

   Carried

3. This Symposium,
   noting that, in Australia, although geodetic and geophysical survey activities appear to be proceeding on effective operational lines, fundamental research in geodesy has, for the most part, tended to be incidental to these activities and to specific space projects;
   further noting the advantageous location of Australia for participation in geodetic and geophysical research projects, and indeed, that such participation is often essential to the successful completion of some international research projects;
   recommends that the Australian Academy of Science do all it can, to bring about the development of adequate facilities in Australia for continuing fundamental research in geodesy.

   Carried unanimously

4. The International Association of Geodesy, on behalf of the participants at the Symposium on the Earth's Gravitational Field and Secular Variations in Position, expresses its appreciation to the Australian Academy of Science, the University of New South Wales, and the Organizing Committee for the excellent arrangements and facilities provided and for the hospitality extended during the Symposium.

   Carried by acclamation

SYMPOSIUM PROGRAM AND TABLE OF CONTENTS

Session C — Tuesday 27 November 1973 — 0900 hrs

Geoid Determinations

Chairman: H. MORITZ (Austria)

Session D — Tuesday 27 November 1973 — 1100 hrs

Secular Variations in Gravity

Boundary Value Problem in Physical Geodesy

Chairman: E. GROTEN (Federal Republic of Germany)

Page

Session I — Thursday 29 November 1973 — 0900 hrs

Statistical Techniques

Chairman: E.W. GRAFAREND (Federal Republic of Germany)

Session J — Thursday 29 November 1973 — 1100 hrs

Mathematical Models and Earth Parameters

Chairman: I.I. MUELLER (United States)

Page

Session M — Friday 30 November 1973 — 1100 hrs

Metrology

Chairman: G.A. BELL (Australia)

Session N — Friday 30 November 1973 — 1330 hrs

Future Trends

Chairman: J.D. BOULANGER (Soviet Union)

† Invited Review Papers

* Presented by

§ Presented in absentia

OPENING ADDRESS

by Professor Rupert Myers
Vice-Chancellor of the University of New South Wales

It is a great pleasure to welcome you here today at the start of this important international symposium - to welcome in particular our overseas visitors, in order of precedence, to Australia, to Sydney and to the campus of the University of New South Wales.

We are honoured to act as hosts for an international symposium of significance, sponsored as it is by the Australian Academy of Science and under the auspices of the International Association of Geodesy.

I understand that, of the 114 distinguished delegates to the symposium, 37 of you have come from 16 countries overseas and most of you have travelled half way around the world. In itself, this is a reflection of the importance of this gathering, and we in Australia and in the University can, I think, justifiably take some pride in your selection of this venue for the symposium.

Valuable research activity in geodesy is spread widely throughout our nation. On thumbing through your splendidly presented program booklet, I counted a total of 10 different institutions in Australia represented among the speakers, coming from 6 universities and 4 Australian Government instrumentalities.

In the University of New South Wales, we have what I have been told is the largest school of surveying in the English speaking world. Under Professor Angus-Leppan, who is Chairman of the Organising Committee of this symposium, our School of Surveying has a staff of 19 academics and this year had 330 students in the course leading to the degree of Bachelor of Surveying. The School of Surveying also provides service courses for another 300-odd students of engineering.

We find there's a big demand for our graduates; after all, there's an awful lot of surveying to do in the development of Australia's 7½ million square kilometres of land, not to mention the rapidly increasing need for surveying work in our oceans as we develop our vast continental shelf.

The professional work of surveyors is, of course, an increasingly vital pre-requisite for all kinds of development and control of our habitat - urban, suburban, rural and industrial. But I'm sure you'll agree with the proposition that the practice of surveying would fall stagnant - indeed it could not keep up with new demands on it for greater precision and reliability - without the backing of a major and dynamic effort of scientific research in geodesy. And that, of course, is what this symposium is all about.

Geodesy has a noble tradition in the development of classical physical science. Great names like GAUSS, LAPLACE, BESSEL, NEWTON and EULER have all left their mark on science through their studies of geodesy. The exact nature of the Earth's shape and rotation has fascinated not only these great scientists but, like the study of the universe, it seems to have captured the imagination of the layman for generations.

Only the other day I read in our popular press of the recent hypothesis that the Earth is shaped like

a pear. I don't know whether this symposium will confirm or refute this suggestion, but what I have observed with great interest is that there is much latent excitement among geodesists about the new instrumentation which will surely bring about a revolution in our understanding of our own planet. The program of this symposium eloquently reflects this mood.

The very notion that we shall shortly be able to measure the actual rate of movement of continents across the face of the earth is, to many outside observers, quite a staggering achievement - every bit as remarkable as the discoveries of the astronomers about our universe in the past decade.

As you all know better than I, we have only been able to *infer* the existence of continental drift from geological and geophysical evidence collected from the records preserved in rocks millions of years old. But now, I note from the abstracts of your proceedings, it is quite realistic to expect that, within a few years, it will be possible to measure continuously the precise position and gravity of any point on the earth with accuracies approaching one part in 100 million.

The use of specialised satellites will not only make this possible but will also allow extremely precise measurement of sea level, which is of vital importance in the study of, among other things, ocean currents - a highly practical application which will benefit ocean navigation.

While the applications of satellites might appear the most dramatic developments in the near future, we must note the great strides made in the complementary and equally essential research work on the earth's gravitational field, on very long baseline interferometry and on oceanography - to mention but a few of the interlocking fields of study which go to make up the matrix of your subject.

But satellites do hold the solution for some long-standing problems in surveying. At a professional gathering earlier this year, Professor Angus-Leppan concluded that, if you want to measure a distance on earth longer than 40 kilometres, the most accurate way is to do so via a satellite or via the moon. And we here know of the potential for satellite geodesy as a result of the year spent recently with NASA, the American space agency, by our Associate Professor Mather, who is also a member of the organising committee of this symposium.

It is a matter of some concern, though, to Australian geodesists that they may not be able to participate fully in these developments. The equipment needed for a satellite tracker which uses laser ranging techniques to obtain maximum accuracy costs of the order of $1 million. Whether Australia and other nations can become actively involved in the international programs of NASA called the GEOS-C satellite, and Earth and Ocean Physics Applications Project will be dependent on the availability of such instruments. These programs are being organised, like this symposium, on an international basis. Perhaps it is not too much to expect that the work of the international fellowship of geodesists, which will be strengthened by this symposium, will be strengthened even further by a widespread availability of the new, sophisticated but expensive instruments needed for development of research.

I wish you every success in your deliberations this week. I hope you will enjoy your stay in Sydney and at the University. And, I have much pleasure in formally declaring open this International Symposium on the Earth's Gravitational Field and Secular Variations in Position.

FISCHER, I.
Defense Mapping Agency Topographic Center
Washington, DC 20315

Proc.Symposium on Earth's Gravitational Field & Secular Variations in Position (1973),3-10.

INTERIM REPORT OF SPECIAL STUDY GROUP V-29, IAG

ABSTRACT

The title of Special Study Group V-29 is "Astrogravimetric and Astrogeodetic Methods for Determining the Shape of the Geoid". The statements in this Report on the current activities of the Group have been taken from communications received from the members.

This Symposium, taking place approximately halfway between the IAG General Assemblies in Moscow 1971 and in Paris 1975, provided the impetus to get in touch with the members of the Special Study Group V-29, to find out who was still interested in this Group and what the members were doing pertinent to its topic. Whether the reportable news at this time is much or little, seems less important than the opportunity to communicate and mutually stimulate a renewed interest in contributing to the Group's Report for the next General Assembly in Paris in 1975. Several people joined the SSG V-29 at this time. A listing of the current membership is given below. We have lost PROFESSOR EDUARDO E. BAGLIETTO of the University of Buenos Aires, Argentina, who had been a contributing member since 1968; he passed away on 6 June 1972.

The last report of SSG V-29 at Moscow in 1971 (FISCHER 1972) gave a geographical overview of activities. Recent communications from members tell of further developments.

To being with our host country, Australia: The completion of the astrogeodetic geoid chart of Australia, constructed from a wealth of astrogeodetic deflections of the vertical with some gravimetric interpolations, has been reported at Moscow (FRYER 1971, FRYER 1972), but - according to A. G. BOMFORD - the definition of its reference datum has since run into a minor, yet intriguing snag. It involves the geoidal height of the datum point at Johnston, which originally, in 1965, had been adopted as the customary zero meters. In 1971, this choice was changed to -6m in order to produce a closer geoid-to-ellipsoid fit. A third value, +4.9 m, resulted from the fact that the official definition of the datum included the height above the reference ellipsoid with the numerical value 571.2 m of the elevation above mean sea-level, while the 1972 national levelling adjustment gave 566.3 m, that is, 4.9 m less. This levelling adjustment (GRANGER 1972) was based on mean sea-level, as established at 30 tide gauges around the continent from 3-year simultaneous observations. These mean values were held fixed at zero elevation to represent the geoid.

As the requirements for numerical precision increase, we will be faced more and more with the practical implications of such interrelationships between the concepts of geoidal height at a datum point, ellipsoidal height, elevation above mean sea-level, and mean sea-level versus geoid. This topic falls outside the scope of this Study Group, but it concerns the basic geodetic definitions and the adoption of numerical values which might be subject to change in the future.

In Europe, G. BOMFORD's astrogeodetic geoid chart of 1971 (BOMFORD 1972) had provided corrections of previous errors in the southern parts, so that the loop around the Mediterranean Sea does seem to close now. D. BALODIMOS (1972) contributes a strengthening of the geoid chart in Greece by

including a newly observed geoidal section in a recomputation for Greece and surrounding areas. This section starts near Athens, goes north to Salonica and then east to Drama, and thus provides geoidal information for the central part of Greece and a better geoidal connection to other Balkan countries. The inclusion of some deflections beyond the border permits the formation of geoidal loops. Starting the recomputation with BOMFORD's value for Corfu, the main profile in BOMFORD's chart connecting Italy with Turkey via Corfu and Athens is upheld, since the data are the same. TENGSTRÖM's gravimetric profile from Athens to El Alamein is confirmed. But there are some changes in Yugoslavia and Bulgaria. The chart was constructed on European Datum and then converted to the Greek datum on the BESSEL Ellipsoid, and also to a geocentric datum using the Reference Ellipsoid of 1967. In an attempt to explain the rapid variation of deflections in some areas and possibly provide a method of interpolation, isostatically compensated topographic deflections were computed along the new section. The expected smooth residuals were not smooth, however, and further investigations were made into possible correlations with recorded high seismic activities. Indeed, such correlation seems to exist not only for these irregular deflection stations, but also for other areas of irregular geoidal features. A fascinating connection is pointed out with a recent theory of a separate small tectonic plate, the Aegean Sea plate (McKENZIE 1970), whose boundaries pass through the regions of the large irregularities, as shown on Map 8.03 in BALODIMOS (1972). The geoid contours have the same shape as the SW-S-SE boundary of that plate, and the slope of the geoid is very steep near the junction with the African plate. It seems that the Aegean Sea plate, which is moving to the S-W relative to the European plate, is dipping under the African plate. The special features of the geoid and the deflection values appear to support McKENZIE's theory.

In Austria, Hungary, and Yugoslavia we may expect another geoidal strengthening. J. J. LEVALLOIS is currently engaged in working out a solution to some long-standing geoidal mysteries there, by combining gravimetric and astrogeodetic data. He further intends to use the strengthened European geoid chart in a synthesis with all other available data of various types towards a world geoid chart.

S. BAKKELID reports that new astrogeodetic deflection values in Norway have become available. In preparation for the computation of gravimetric deflections with topographic corrections, the mean elevations are being determined for 5' x 10' area squares covering Norway and extending 20 km into neighbouring countries. RUDZKI anomalies will be used first.

In Czechoslovakia, M. BURŠA computed the differences between astrogeodetic and gravimetric deflections of the vertical, which form the basis for astrogravimetric levelling, in 29 interpolation areas of the territory of Czechoslovakia of an average of 9500 sq. km, using the MOLODENSKY method. In introducing the PELLINEN corrections for condensation, the accuracy of these differences can be characterised by the mean square error on the average of about ±0.3" including high mountain areas. The differences were represented graphically and expressed analytically by the interpolation functions (BURŠA 1972). They serve on the given territory as a firm basis for an accurate interpolation of astrogeodetic, or gravimetric deflections of the vertical, as well as accurate determinations of the relative quasi-geoid heights. On the basis of deflections, corrected for the effect of topographic masses, also partial undulations of the geoid due to deeply deposited masses were computed (BURŠA 1973).

PICK & JAKUBCOVA (1972) used the astrogeodetic deflections from the IAG listing for a tentative determination of the shape of the Moho-discontinuity in Central Europe. Referring to earlier work by M. BURŠA (1970) and H. WOLF (1971) and to the ambiguity of the problem, they combine the evidence of deep seismic sounding with all types of geodetic data characterising the gravity field, and com-

pute the effects of various mathematical models of the discontinuity, in order to single out the most probable one consistent with the evidence. Pick pursues related topics in an effort to generalise the definition of the normal height system to make it applicable for points in the upper part of the earth (PICK 1970); he investigates the effect on geoid heights and deflections when neglecting higher order terms in the boundary condition and computes an example in the Czechoslovakian test area in the High Tatras (PICK 1973a); and he also considers time dependent changes in deflections of the vertical when describing movements in the upper parts of the earth, since geodetic measurements are made in a local coordinate system related to the local plumb line direction which changes with the pole motion and with local changes (PICK 1973b).

U. SHOSHANI has a report on the progress of astrogeodetic work done in Israel. The mail, however, has not arrived at the time of this writing.

B. M. JONES & E. FITSCHEN observed a geoidal section in the center of South Africa. Also this report did not arrive in time.

G. A. CORCORAN reports that the Geodetic Survey of Canada has been working towards an astrogeodetic profile of the geoid from the east coast to the west coast across Canada. The past field season (1972), one of the larger gaps across northern Ontario has been closed with a traverse of deflection points. A small gap still exists in the profile in southern British Columbia. It is hoped that this may be closed sometime in the near future. Some preliminary computations for geoid separation have already been carried out.

G. LACHAPELLE (1973) copes with the scarcity of deflections in central Canada by computing the Canadian geoid in separate adjustments for the eastern and the western parts. The connection is provided by five satellite tracking stations whose positions and geoidal heights from a NASA solution were adopted as fixed values. Geoid charts for eastern Canada and for western Canada were computed on two systems, a geocentric datum and the North American Datum of 1927, after choosing transformation formulas between them from several published values. The results are compared with I.FISCHER's astrogeodetic chart for North America on North American Datum (1967) and also with NASA's gravimetric chart (1972) on a geocentric datum. Both comparisons show agreements within five meters.

C. L. MERRY & P. VANICEK (1973a) point to the omission of geoid-to-ellipsoid corrections in the Canadian horizontal control adjustment on NAD 27 and to the possibility that neglecting to correct directions for the deflections of the vertical may have caused an apparent rotation of the control net. In view of the need to relate satellite geodesy to terrestrial networks, the authors review the basic concepts of a geodetic datum (MERRY & VANICEK 1973b) and of datum transformation formulas derived from geoid height comparisons, considering translation and rotation of the coordinate axes. In a practical application to various regions in North America, the influence of expected regional bias is shown. The authors also experiment with a least-squares-surface-fitting technique (VANICEK & MERRY 1973), computing a geoid chart from a two-dimensional algebraic polynomial of the n-th order, where the derivatives of the coefficients are set equal to the given deflection values. Various parts of Canada and also North America without Alaska and Mexico were so treated, each with different assumptions about the order of the polynomial.

In all of these Canadian geoid studies, the 1967 astrogeodetic geoid chart of North America by I. FISCHER et al (1967) was used for comparison and the discrepancies were shown to be within a few

meters. D. A. RICE has applied new deflection values available for the USA to a computation of very dense geoid profiles along the new precise traverses which form large loops from coast to coast. A comparison of these geoidal loops with Fischer's map shows discrepancies of a few meters in a systematic pattern, possibly indicating a slight east-west tilt. The planned readjustment of the US control network should yield a refinement of the geoidal information.

GEMAEL ET AL (1973) sends another set of his series of topographic-isostatic gravity reduction charts, this time for the State of Minas Gerais, Brazil. There are charts for the Pratt-Hayford System, T=113.7 km, and for the Airy-Heiskanen System, T=20 km, 30 km, and 40 km.

A. A. CERRATO established a tie between the triangulation net in the Province of Mendoza, referred to Uspallata Datum, with the Argentinian national triangulation net, referred to Campo Inchauspe Datum. This independent Uspallata triangulation net had been established in the mountainous regions of Mendoza by the Geodetic Institute of the University of Buenos Aires (Professor E. E. BAGLIETTO). In 1971, measurements of lengths and azimuths were made to establish four points of the Uspallata net in the Campo Inchauspe system. From the calculated coordinates a datum transformation between the two systems was derived, and applied to the 17 astrogeodetic deflection stations of the Uspallata net. The transformed deflection values were larger, particularly the prime vertical components. It appears that towards the north and towards the west, the ellipsoid of the Uspallata datum is above that of the Campo Inchauspe datum. Gravimetric observations in the area were continued with a view towards computation of gravimetric deflections there.

The new continental South American Datum of 1969, designed by I. FISCHER (1973a) has been officially accepted by the Pan American Institute of Geography and History (PAIGH). Its datum point is Chua, Brazil, in the center of the low and densely settled regions of the continent. The geoid has been computed from the astrogeodetic deflections of the vertical, and checked by several satellite-derived three-dimensional transcontinental distances. The geoid separation was utilised to reduce the base lines to the ellipscid. An estimate of the geoidal features in the interior was obtained by datum transformation from the 1968 modification of the Mercury Datum (1968).

A pacific atoll in the Marshall Islands has been used to study the possibility of interpolating astrogeodetic deflections of the vertical in an ocean setting (I. FISCHER, 1973c). As an alternative to an expensive dense gravimetric survey, from which gravimetric deflections can be computed by the Vening-Meinesz formula, bathymetric maps were used to compute topographic deflections directly. The topography of the ocean bottom provides information on the volume of the ocean masses to a depth of 5 km with the known density of the ocean water. Together with reasonable assumptions about the rock density down to 5 km depth, the major part of the deflection value can be computed. Assumptions about density distributions below 5 km depth are guided by geophysical data about the thickness and density of the earth's crust beneath the oceans, but the essential ambiguity is approached by several density models, with and without isostatic compensation. The deflections produced by these density models are compared with the observed astrogeodetic deflections on the atoll, whereby a feedback for further modifications of the model is obtained.

This excursion into marine geodesy reflects the current interest in detailed ocean geoids and deflections, and the question whether the astrogeodetic approach can be adapted for this purpose (I.FISCHER 1973b). The already proven feasibility of placing geodetic markers on the ocean floor, the plans of establishing calibration ranges, and the attempts of observing astros on stabilised platforms provide the basic ingredients for extending the astrogeodetic approach into the sea, if combined with satel-

lite geodesy as a surveying tool. Deflections established on islands, above geodetic ocean markers, or derived from satellite altimetry can be used as control values to derive detailed deflections from gravimetric and bathymetric interpolation. This will assist, for instance, inertial navigation in the recovery of positions at sea. The prospect of exploiting economic resources in ocean areas will make it important to establish identifiable boundaries for exploration and development areas in the High Seas - an ancient obligation of geodesy on land.

2. References

BALODIMOS, D. 1972. *Geoidal Studies in Greece.* Oxford.

BOMFORD, G. 1972. The Astrogeodetic Geoid in Europe & Connected Areas 1971. *Travaux IAG.* Paris.

BURŠA, M. 1970. On the Correlation between Deflections and Axes of Zones of Increased Macroseismic Mobility. *Studia geophys. et geod.* 14, 2, 183.

BURŠA, M. 1972. Accuracy Differences of Astrogeodetic and Gravimetric Deflections of the Vertical on the Territory of Czechoslovakia. *Travaux Inst.Géophys.Acad.Tchéchosl.Sc.* No.319. Geofysikální sbornik 1970, Academia, Praha.

BURŠA, M. 1973. Undulations of the Geoid Due to Deep Anomalous Masses on the Territory of Czechoslovakia. *Travaux Inst. Géophys.Acad.Tchéchosl.Sci.* No.345, Geofysikální sbornik 1971, Academia, Praha.

FISCHER, I., SLUTSKY, M., SHIRLEY, R. & WYATT, P.III. 1967. Geoid Charts of North and Central America. *US Army Map Service.* Techn.Rept.No.62. Washington, DC.

FISCHER, I., SLUTSKY, M., SHIRLEY, F.R., WYATT, P.Y. III. 1968. New Pieces in the Picture Puzzle of an Astrogeodetic Geoid Map of the World. *Bull.Géod.* 88.

FISCHER, I. 1972. Report of the Special Study Group V-29, Moscow 1971. *Travaux IAG.* Paris.

FISCHER, I. 1973a. The Basic Framework of the South American Datum of 1969. *Revista Cartográfica.*

FISCHER, I. 1973b. *Is the Astrogeodetic Approach in Geodesy Obsolete?* GEOP Research Conf.IV. Boulder, Colorado.

FISCHER, I. 1973c. Deflections at Sea. *Proc.Symposium "The Earth's Gravitational Field and Secular Variations in Position".* Sydney, Australia.

FRYER, J.G. 1971. The Geoid in Australia - 1971. *Div.Nat.Map.Tech.Rep.* 13, Canberra, Australia.

FRYER, J.G. 1972. The Australian Geoid. *Aust.Surv.* 24, 4.

GEMAEL, C. & HATSCHBACH, F. 1973. Cartas de Redução Topo-Isostática para o Estado de Minas Gerais. *Bol.Univ.Fed.do Paraná, Geodésia.* 14, Brasil.

GRANGER, H.W. 1972. The Australian Height Datum. *Aust.Surv.*24, 4.

LACHAPELLE, G. 1973. *A Study of the Geoid in Canada.* Dept. of Surveying & Geodesy, Univ. of Oxford.

McKENZIE, D.P. 1970. Plate Tectonics of the Mediterranean Region. *Nature.* 226.

MERRY, C.L. & VANIČEK, P. 1973a. Horizontal Control and the Geoid in Canada. *Canadian Surv.* 27, 1.

MERRY, C.L. & VANIČEK, P. 1973b. *The Geoid & the Positioning of Geodetic Datums.* Univ. of New Brunswick, Fredericton (unpublished).

PICK, M. 1970. Generalization of the System of Normal Heights. *Bull.Géod.* 97.

PICK, M. 1973a. On the Boundary Condition of the Gravity Disturbing Potential. *Studia geophys. et geod.* 17.

PICK, M. 1973b. *Recent Movements and the Variation of the Earth's Gravity Field.* Symposium "Geodesy & Physics of the Earth". Potsdam.

PICK, M. & JAKUBCOVA, J. 1972. Determination of Mohorovicic Discontinuity from Deep Seismic Soundings & the Characteristics of the outer Earth's Gravity Field. *Bull.Géod.* 106.

VANIČEK, P. & MERRY, C.L. 1973. Determination of the Geoid from Deflections of the Vertical Using a Least-Squares Surface Fitting Technique. *Bull.Géod.* 109.

VINCENT, S.F., STRANGE, W.E. & MARSH, J.G. 1972. A Detailed Gravimetric Geoid of North America, the North Atlantic, Eurasia, and Australia. *Goddard Space Flight Center Rep.* X-553-72-331, Greenbelt, Md.

WOLF, H. 1971. Geoid und Mohorovicić Diskontinuität. *Zeitschr.f.Vermesswes.* 96, 9, 373.
Communications from the members of SSG-V-29, IAG, 1973.

3. Special Study Group V-29,IAG - Membership List as of September 1973

Irene Fischer (Chairman)	Defense Mapping Agency Topographic Center, Washington DC USA
Ing.S.Bakkelid	Geographical Survey of Norway, Oslo, Norway
Dr D. Balodimos	Surveying Laboratory, National Technical University, Athens, Greece
Brig. G. Bomford	Hainton Lodge, Sutton Courtenay, Berkshire, England
Mr A. G. Bomford	Ass.Dir., Div. of National Mapping, Canberra, Australia
Dr M. Burša	Research Inst. of Geodesy, Dept. of Theoretical Geodesy, Praha, Czechoslovakia
Ing. A.A.Cerrato	Dir., Inst. of Geodesy, Univ. of Buenos Aires, Buenos Aires, Argentina
Mr G.A.Corcoran	Geodetic Survey of Canada, Ottawa, Canada
Agrim.Ing.P.Dragan	Inst. Geogr.Militar, Buenos Aires, Argentina
Dr H.M.Dufour	Inst. Geogr.National, Paris, France
Mr E. Fitschen	Trigonometrical Survey, Mowbray C.P., South Africa
Prof. C. Gemael	Centro de Estudos e Pesquisas de Géodésia, Univ. of Paraná, Curitiba, Paraná, Brazil
Akad.Prof.V.K.Hristov	Bulgarische Akad.der Wissenschaften, Sofia, Bulgaria
Dr B.M.Jones	Dept. of Land Surveying, Univ. of Natal, Durban, South Africa
Dr G. Lachapelle	Geodetic Institute, Helsinki, Finland
Mr B. P. Lambert	Dir., Div. of National Mapping, Canberra, Australia
Dr J.J.Levallois	Secretary General, IAG, Inst.Geogr.National, Paris, France
Mr C. L. Merry	Dept. of Surveying Engineering, Univ. of New Brunswick, Fredericton, Canada
Dipl.Ing.A.Muminagić	President of Yugoslav.Comm. of Geodesy & Geophysics, Beograd, Yugoslavia
Mr S. Perlman	Dept. of Surveys, Tel-Aviv, Israel
Dr Ing.M.Pick	Geophysical Inst., Czech.Acad.of Science, Praha, Czechoslovakia
Mr W. I. Reilly	Geophysics Div., Dept. of Scientific & Industrial Research, Wellington, New Zealand
Mr D. A. Rice	National Oceanic & Atmospheric Administration, Rockville, USA
Dr A. R. Robbins	Dept. of Surveying & Geodesy, Oxford, England
Mr U. Shoshani	Deputy Dir., Dept. of Surveys, Tel-Aviv, Israel
Eng.N.de Sousa Afonso	Inst.Geogr.e Cadastral, Lisbon, Portugal
Dr E. Tengström	Inst. of Geodesy, Univ. of Uppsala, Hällby, Sweden
Dr P. Vaníček	Dept. of Surveying Engineering, Univ. of New Brunswick, Fredericton, Canada
Dr H. Wolf	Inst. für Theoretische Geodäsie, Univ. of Bonn, Bonn, Germany
Dr A. Živhović	Univ. of Beograd, Beograd. Yugoslavia

4. Discussion

ANGUS-LEPPAN (Chairman): Would Lambert (Director of National Mapping, Australia) like to comment on the intriguing relationship in Australia between the geoid, ellipsoid and mean sea level?

LAMBERT: I would like someone to advise me on it. We "cleverly" got the elements of the Australian Geodetic Datum written into the legislation dealing with the off-shore petroleum. This will forever establish the Australian Geodetic Datum for Australia. Later (1971) we completed our geoid contour map for Australia. When we compared this with the original height that was used, we found that there was a difference and have quite a problem to resolve there. We cannot get the legislation altered, and our contour map will just have to fit the legislation.

KEARSLEY: I am impressed by the stated accuracy of the deflections of the vertical given by Bursa in Czechoslavokia of 0".3. Could you tell me exactly what methods he used to compute this? He mentions the Pellinen corrections. Could you go into a little more detail about that?

FISCHER: I do not have too many details. The statement is the information Bursa sent me for this report. However there are more details about his earlier work on the same topic in my report presented at Moscow in 1971 (*AIG Travaux* 24,351) and in his publication quoted there. He has a very detailed gravimetric chart of Czechoslavokia with extra detail around the many astrogeodetic deflection stations, between which he wants to interpolate. The distance between these stations is small, which keeps the interpolation error down. He also uses Bouguer reductions and terrain corrections. The overlapping set of 29 interpolation areas gives a way to compute interpolations by Molodensky's method from two or more, slightly different groups of astrogeodetic stations and evaluate accuracies from the comparisons. Also, tests are made with astrogeodetic deflections not used in the interpolation procedure.

BARLOW: I have a question which is really a request for advice from this meeting. We have a gravity map of Australia with a good degree of accurate coverage. There are many reasons which can be put forward when seeking funds to do gravity work over a continent like Australia. One of these is gravimetric deflections of the vertical and undulations of the geoid. The literature is not very helpful in advising on what station spacing should be used. In Australia we have stations on a grid of not more than 11 km, station to station; the data available at present has a standard deviation of about 1, perhaps 2 mgal in bad areas. Do we require better accuracy than this? Do we require a station spacing closer than this? We are computerizing all gravity information which we would like to have on a common datum. It will cost about half a million dollars to do this as accurately as we can, but we are proceeding with it. As a lot of money is required to recompute the gravity data to a higher accuracy, I would like arguments in case someone were to ask "Is this worthwhile?". Is 1 mgal accuracy enough for your purpose?

FISCHER: Well I think you ought to ask Mather.

MATHER: I think so provided there is no systematic error in the gravity data. The systematic errors will come primarily from either the gravity datum or the elevations. If you do not have systematic error, I think you could tolerate a much larger noise in the 11 km grid than the figure you quoted. But of course, this means that if you really wanted to do detailed calculations over an area for deflections of the vertical, the station spacing would have to be considerably lessened. But it is impractical to establish a field on that basis for all of Australia; this densification is done in local areas where deflections are to be computed.

BARLOW: When you talk about systematic error do you mean over a $15' \times 15'$ area or a $1^\circ \times 1^\circ$ area?

MATHER: I mean an error that will have a long wavelength in global terms.

DOOLEY: There are several papers written on this by Hirvonen and Kaula in the late fifties in which the requirements for accuracy were given. Accuracies for both geoid heights and deflections of the vertical were well and truly worked out and published.

RAPP : I think the question is a very difficult one. The papers referenced, by Hirvonen and Kaula, do not direct themselves to detailed analysis of what we would get in a specific situation, dealing primarily with idealized situations. Also studies were done by Moritz who investigated the gravity requirements for very precise determinations such as computations of deflections of the vertical and geoid undulations, again primarily on a global basis. They are continuing studies in the west Alps for the computation of gravimetric deflections of the vertical in a highly disturbed area. One of their problems was that they could not get dense enough gravity material to a degree considered adequately accurate for the definition of deflections to 0".2. They need a much denser field than 4-5 km. So it is not an easy issue and I appreciate the problems in trying to get appropriate specifications.

MARKOWITZ, Wm.
Physical Oceanographic Laboratory
Nova University
Dania, Fla 33004
United States of America

Proc. Symposium on Earth's Gravitational Field & Secular Variations in Position (1973), 11-19.

ASTRONOMICAL PROGRAMS FOR THE STUDY OF SECULAR VARIATIONS IN POSITION †

ABSTRACT

Secular changes in relative position might be detected by stations which observe common stars. Five chains of stations on nearly the same latitude are in operation: the International Latitude Service (ILS), three PZT chains, and one astrolabe chain.

The latitude and longitude of a station change secularly in consequence of the secular motion of the mean pole of rotation. Corrections for such changes can be obtained from the secular motion determined from ILS observations.

At initial determination is made of the secular motion from BIH observations.

1. Introduction

Early theories of continental drift envisioned large drift rates. In a few cases large differences in position were obtained for two epochs of observation, e.g. 3" in latitude and 5 s in longitude for a field station in Greenland, for epochs 1870 and 1932. These large changes, however, could be accounted for by errors in the methods of observation. Continued observations at permanent observatories indicated that secular changes in position are very small, if not null.

Modern theories of continental drift, based on plate motions, lead to much smaller estimates of relative continental drift rates, of the order of 3 cm/yr. This corresponds to 0".001/yr in arc and, for middle latitudes, about 0.1 ms/yr in longitude. The detection of such small drift rates through optical astronomy is possible but difficult. Not only is the rate extremely small, but new, precise definitions of reference axes and co-ordinates are required. The basic problem in formulating precise definitions is that no set of axes "fixed in the Earth", with respect to which positions may be referred, exists.

The detection of secular changes in position is simplified if the participating stations observe stars in common and use the same reduction constants. This eliminates errors in star positions, proper motions, and the observational ephemeris. The stations must therefore be on nearly the same latitudde. Five such stations, listed in table 1, are now in operation.

The International Latitude Service (ILS), which began observing in September 1899, was the first astronomical program formed in which all stations observe the same stars. Observations made during the past 74 years provide information on the periodic motions of the instantaneous axis of rotation about the axis of figure and the secular motion of the latter. The secular motion of the axis of figure, whose pole is identified with the mean pole of rotation, causes a drift in latitude and longitude which is not related to crustal displacements. Hence, this secular motion must be taken into account in determining relative drift in position.

† *Revised February 1974*

TABLE 1. Astronomical Chains

	Longitude	Latitude
1. ILS		
Mizusawa (Japan)	141° E	+39° 8' 31".602
Kitab (USSR)	67° E	1.850
Carloforte (Italy)	8° E	8.941
Gaithersburg (USA)	77° W	13.202
Ukiah (USA)	123° W	12.096
2. PZT		
Washington (USA)	77° W	+38° 55'
Mizusawa (Japan)	141° E	+39° 8'
Mt. Stromlo (Australia)	149° E	-35° 19'
Punta Indio (Argentina)	57° W	-35° 21'
Herstmonceux (UK)	0°	+50° 52'
Calgary (Canada)	114° W	+50° 52'
3. Astrolabe		
Paris (France)	2° E	+48° 50'
Dolbeau (Canada)	72° W	+48° 50'

2. The Gravity Vector; Astronomical Observations

Astronomical determinations of latitude and longitude are based on two axes, the *vertical* and the *instantaneous axis of rotation*.

At any point, P, on the Earth there exists a gravity vector $\underset{\sim}{G}$, whose direction is that of the vertical (plumb line) and whose magnitude is g, the acceleration of gravity at P. $\underset{\sim}{G}$ is the resultant of the attractions of the Earth, Moon, and Sun and the centrifugal force of rotation. The magnitude undergoes variations, periodic certainly and secular probably.

When we say that $\underset{\sim}{G}$ is variable we must state with respect to what the variation occurs. The answer is simple as regards the magnitude, g, which is measured in units of length and time. These units are defined by two electromagnetic radiations produced by quantum transitions: 1 metre = 1 650 763.73 wavelengths of a specific Kr-86 transition, and 1 second = 9 192 631 770 periods of a specific Cs-133 transition. Consideration is being given to using one transition to define both the units of length and time, and to using the speed of light as a base SI unit. However, no matter what changes are made two adopted constants will be involved in the measurement of g.

Specifying the direction of $\underset{\sim}{G}$, rigorously, presents difficulties. At any instant $\underset{\sim}{G}$ has a definite orientation with respect to a set of axes fixed with respect to external galaxies. The orientation changes rapidly, however, and we wish to refer $\underset{\sim}{G}$ to axes fixed in the Earth. The Earth, however, is not a rigid body, and such axes cannot be defined rigorously.

Let E_r denote a fictitious rigid body which approximates the Earth. Associated with E_r is an axis of

figure, A_F, an instantaneous axis of rotation, A_I, and a momentum axis, A_M. These are co-planar with A_M in between and close to A_I (about 3 cm at the Earth's surface, at maximum, for the motion observed). The 3 axes describe motions about each other in accordance with the representation of L. Poinsot, which involves rolling cones. A_M undergoes precession and nutation with respect to extra-galactic axes. A_F is fixed with respect to E_r, and A_I undergoes periodic motion about A_F (Euler nutation).

The actual Earth is not rigid and A_F does not necessarily retain a fixed position relative to the crust. However, there is an instantaneous axis for all practical observational purposes, A_I, which is used as a primary reference. It is the angles between the vertical at each station and their relation to A_I, which define the astronomical longitude and latitude of each station.

The newer techniques such as Doppler, laser ranging of the Moon and artificial satellites, and VLBI, do not employ the vertical. Hence, they cannot be used to determine astronomical longitude and latitude; they are used to determine other co-ordinates.

The co-latitude is the angle between the vertical and A_I. Latitude and time are determined in practice with specialised instruments which determine the angle between the zenith and stars whose *relative positions* are known with very high accuracy. The zenith is determined with a mercury reflecting basin or with a level.

The ILS chain includes 5 stations. A solution is made each month for 3 unknowns, x and y, the coordinates of the pole, and z, a constant term. All errors which affect the 5 stations alike, such as errors in star positions, proper motions, and constants of reduction, are absorbed by z. The observational data are the differences in the 5 mean monthly latitudes from the 5 initial latitudes adopted for each station.

3. Recently Started Programs

Beginning about 1957, and partly in connection with the International Geophysical year (IGY), a number of photographic zenith tubes (PZT) and astrolabes came into use. These instruments determine both time and latitude, and with high precision.

In consequence of the interest in verifying the hypothesis of continental drift, steps were taken to utilise these newer instruments in programs for the detection of secular variations in position. Definite secular changes in latitude had not been detected by the ILS observations. However, modern theories indicate that relative drifts are occurring chiefly in longitude; hence, the importance of time determinations with common stars.

A symposium on Continental Drift, Secular Motion of the Pole, and Rotation of the Earth, organised by the International Astronomical Union (IAU) in cooperation with the International Union of Geodesy and Geophysics (IUGG), was held in Stresa, Italy, in March 1967 (MARKOWITZ & GUINOT 1968). The symposium recommended that chains of two or more PZT's or astrolabes be established on nearly the same parallel of latitude, to observe the same stars. Also, the symposium adopted initial latitudes for the ILS stations, given in Table 1. These define an origin for the position of the pole,

now called the *Conventional International Origin*, or CIO. These recommendations were adopted by both the IAU and the IUGG in 1967.

Chains in operation are listed in table 1. The Washington and Mizusawa PZT's have only about one-half of their lists in common. This, however, is sufficient to link the star lists. S. Takagi, at Mizusawa, has begun analyzing the observations.

Steps are being taken to install a PZT at each ILS station in addition to the visual latitude instrument. Only Mizusawa has a PZT now. The completion of a 5-station ILS-PZT chain would be of very high value in studying the secular motion of the pole and secular changes in position of stations.

4. The CIO

The reson for adopting the CIO was to end the confusion which had arisen because a multitude of origins had come into use, often not specifically defined. The CIO is specifically defined by the adopted initial latitudes of the 5 ILS stations, which may be regarded as five arbitrary constants. It does not matter what constants were selected since we are interested chiefly in the motion of the pole, and not in its absolute position. Nor does it matter that the 5 ILS stations may be in motion. The important thing is that the CIO provides a standard origin for specifying the latitude and longitude of a station and the co-ordinates of the pole.

5. Secular Motion of the Pole

A displacement of the pole of rotation from the origin to a point at x, y (with the conventional notation) causes changes in latitude, ϕ , and longitude, λ , as follows:

$$\phi = \phi_o + x \cos \lambda + y \sin \lambda \quad , \tag{1}$$

$$\lambda = \lambda_o + (x \sin \lambda - y \cos \lambda)(\tan \phi)/15 \quad , \tag{2}$$

where ϕ_o and λ_o are the latitude and longitude when the pole is at the origin. (Note: West longitude is reckoned positive in astronomy; λ is in time in equation (2))

Secular changes in x and y would cause secular changes in latitudes and longitudes not caused by crustal displacements.

Figure 1 shows the recent motion of the pole of rotation and the motion of the mean pole since 1903.0, as derived from ILS observations.

6. Characteristics of the Secular Motion

The nature of the secular motion and indeed, its reality, have long been the subject of discussion.

The ILS secular motion was first determined, in 1916, by B. Wanach from a short interval, 1900-1915.

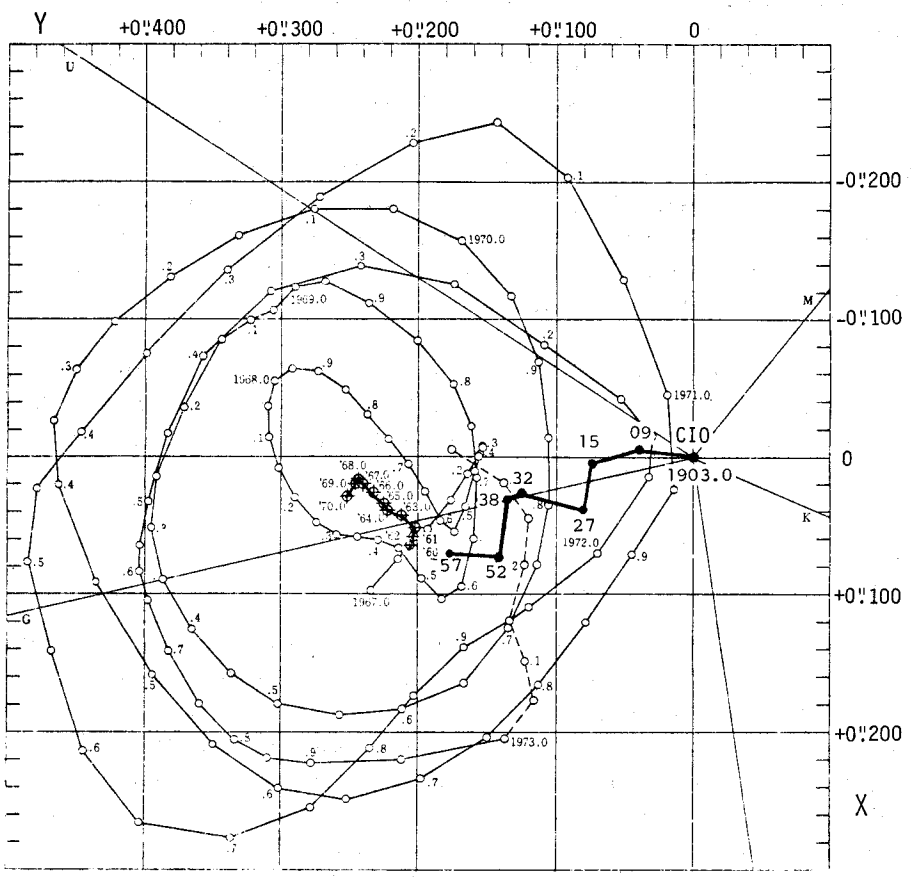

Figure 1. Secular Motion of the Pole

The ILS polar motion for 1968.00 to 1973.35; from YUMI (1973b). Crosses mark the position of the mean pole from 1960.0 to 1968.0, obtained by Yumi, based on 6-year running means of **x** and **y**. Solid circles are 6-year means for epochs from 1903.0 to 1957.0; from (MARKOWITZ 1960).

He obtained 0".003/yr along 55°W. N. Sekiguchi found in 1954 that a random motion was superimposed on a progressive motion. MARKOWITZ (1960) found that the secular motion was well represented by a progressive component of 0".0032/yr along 60°W plus a librational component of period 24 years. He noted that the motion is empirical and it was not known whether it would continue. Figure 1 shows that the progressive and librational motions have continued, although the librational motion is not strictly of period 24 yr.

The ILS observations thus indicate a secular motion of the mean pole relative to the stations. However, suggestions have been made that this motion is not a real motion of the pole. Alternate explanations which have been given are that the apparent motion is due to

(a) errors in proper motions, or

(b) non-polar changes in latitude of some stations, due either to crustal drift or to observational effects.

A study of the way in which the *definitive* ILS polar motion co-ordinates, x and y, are derived shows that they are independent of any external catalogues, e.g., GC or FK4, and therefore, of their errors in position or proper motion. The computation of control latitudes (MARKOWITZ 1961) confirms this independence. Hence explanation (a) is excluded, although (b) remains.

Plots of the variations in latitude of the 5 ILS stations showed progressive and oscillatory changes which agree in magnitude, phase, and sign with those expected from the derived progressive and librational motions of the mean pole (MARKOWITZ 1968; MARKOWITZ 1970). It is difficult to see how the phases of the variations at the five stations could maintain the proper relation if the variations were due to independent effects at the stations.

Nevertheless, an independent determination of the secular motion was greatly desired, and it was therefore decided to begin a study of the secular motion provided by the observations of the Bureau International de l'Heure (BIH). The importance of the BIH secular motion lies in the large number of stations which form the basic BIH system.

7. 1968 BIH System

In 1967 the BIH introduced a new method of deriving the polar motion, from both latitude and time observations, on a rigorously homogeneous basis (GUINOT & FEISSEL 1968). Details are given by FEISSEL (1972). The BIH reference system, called the *1968 BIH System*, is defined by a weighted set of instruments which were in operation in 1966. This includes 34 for latitude and 17 for time, with appreciable weight, at 29 observatories. The 5 ILS instruments are included, but their weight is only 0.09 of the total. Corrections are applied each year so that the reference system remains that of the 1968 BIH System. The system is unaffected by the addition of new participating stations, changes in catalogues used, or changes in the adopted co-ordinates of any station.

Corrections were applied back to 1962.0. However, as FEISSEL (1972) noted, the accuracy of the early years, particularly 1962 and 1963 is reduced; fewer stations were in operation than in 1966, and some corrections were uncertain. The annual differences in both x and y between the BIH and ILS show discontinuities at 1964/65, which indicates that the results from 1965 on are on the 1968 BIH System, but those for 1962, 1963, and 1964 may not be.

7.1. Proper Motions

The equations of condition contain x and y with coefficients sin λ, and cos λ, where λ is the station's longitude. In consequence, a fictitious, *constant* drift of the mean pole could occur if the average error in proper motion (in either co-ordinate) is correlated with longitude. There is no drift if the same error affects all stations.

The BIH stations, with few exceptions, are independent. Proper motions are tied nominally to the same system, FK4, but residual differences between stations may exist. GUINOT & FEISSEL (1968) estimated that the probable error of the fictitious drift is 0".000 2/yr. My estimate is of the same order. The fictitious drift due to proper motion errors is negligible for present purposes.

7.2 Systematic Errors

Because of the large number of instruments which form the 1968 BIH System, the BIH secular motion is

much less affected than the ILS by systematic errors which may affect one or two stations, sometimes for years.

7.3 BIH Secular Motion

It follows that the BIH secular motion is determined with high accuracy, is negligibly affected by errors in proper motion, and is little affected by systematic errors at individual stations. We may use the results from 1965 with high confidence to check the ILS secular motion.

8. Comparison of Secular Motions

The co-ordinates of the barycentre are the 6-yr running means, which include nearly 5 Chandler periods, of **x** and **y**. The ILS values for the mean epochs 1965.0 to 1970.0 were given by YUMI (1973a; 1973b), and the BIH values were kindly furnished by Dr. B. GUINOT. The results are shown in figure 2. The BIH 6-yr means for epochs 1965.0 to 1967.0 include observations made through 1964, and the corresponding motion is shown dotted.

The ILS and BIH secular motions show certain similarities. A marked change in direction is indicated for the ILS about 1968 and for the BIH about 1967. More significant, however, is the similarity of motions during the last 8 years, which is given by mean epochs 1968.0 to 1970.0. The ILS motion is 0".007/yr along 37° W longitude and the BIH is 0".005/yr along 24° W, which is fairly good agreement. This 8-yr interval is too small, however, to permit drawing conclusions regarding the secular motion. We may be able to do so by 1980.

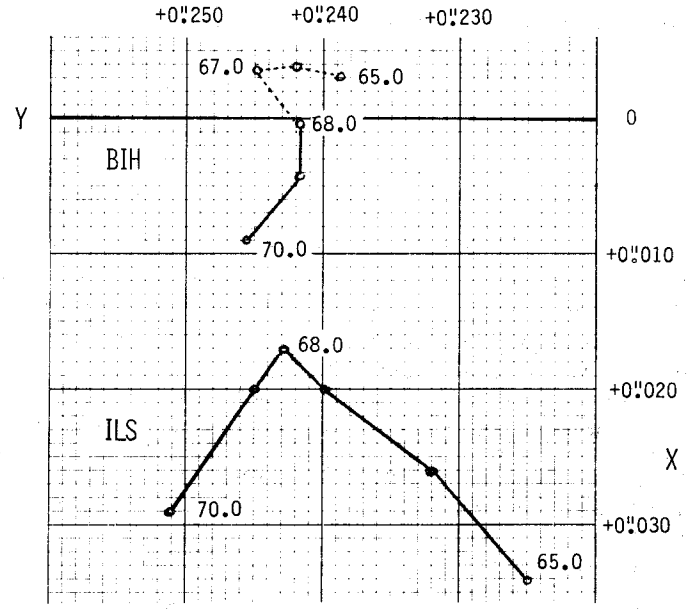

Figure 2. Mean Pole

ILS and BIH positions from 6-yr running means of **x** and **y**.

9. Discussion and Summary

The Earth is not a rigid body, and no axes fixed in the Earth can be defined to serve as a reference system for measuring secular changes in position. Use is made of the instantaneous axis of rotation and the vertical at a station to define astronomical latitude and longitude. These are determined with classical optical instruments, e.g., zenith telescope, PZT, and astrolabe.

The CIO, based on ILS observations, serves as a standard origin for latitude and longitude and for the polar motion.

The newer techniques, such as Doppler, laser ranging, and VLBI, do not employ the vertical; these would detect continental drift by techniques other than changes in astronomical latitude and longitude.

The axis of figure of the Earth, identified with the mean pole of rotation, has a secular motion, as indicated by the ILS observations. The BIH observations during the last 8 years indicate a similar secular motion, but the interval is too short to permit drawing conclusions. In a few more years the combination of ILS and BIH results should provide a reliable determination of the secular motion.

Several chains of stations on nearly the same parallel of latitude have been established to observe stars in common. These might detect secular changes in astronomical latitude and longitude.

The probable error of a yearly mean difference in longitude between two PZT's or astrolabes, as indicated by the BIH results, is about 3 ms. The probable error in drift rate would be about 0.1 ms/yr for 20 years of continuous observation and about 0.03 ms/yr for 40 years. If relative secular drifts in longitude of 0.1 ms/yr (about 3 cm/yr at latitude 45°) are occurring then we may obtain some evidence through classical optical astronomy towards the end of this century.

10. References

FEISSEL, M. 1972. In *BIH Rapport Annuel Pour 1971*, Section E, Paris.

GUINOT, B. & FEISSEL, M. 1968. In MARKOWITZ, W & GUINOT, B. (ed.) *Continental Drift, Secular Motion of the Pole, and Rotation of the Earth.* Reidel, Dordrecht, p.63.

MARKOWITZ, W. 1960. Latitude and Longitude, and the Secular Motion of the Pole. In RUNCORN, S.K. (ed.) *Methods and Techniques in Geophysics.* Interscience, New York, p.325.

MARKOWITZ, W. 1961. Internation Determination of the Total Motion of the Pole. *Bull. géodés.* 59,29.

MARKOWITZ, W. 1968. In MARKOWITZ, W & GUINOT, B. (ed.) *Continental Drift, Secular Motion of the Pole, and Rotation of the Earth.* Reidel, Dordrecht, p.28.

MARKOWITZ, W. 1970. Sudden Changes in Rotational Acceleration of the Earth and Secular Motion of the Pole. In MANSINHA, L., SMYLIE, D.E. & BECK, A.E. (ed.) *Earthquake Displacement Fields and Rotation of the Earth.* Reidel, Dordrecht, p.78.

MARKOWITZ, W. & GUINOT, B. (ed.) 1968. *Continental Drift, Secular Motion of the Pole, and Rotation of the Earth.* Reidel, Dordrecht.

YUMI, S. 1973a. *Annual Report of the IPMS for 1971.* Mizusawa, p.4.

YUMI, S. 1973b. *Report of the IPMS (1972.0 - 1973.4).* Mizusawa, p.7.

11. Discussion

FREISLICH: Can you comment on the relative accuracy of the astrolabe as compared with the PZT?

MARKOWITZ: I cannot give a (simple) answer to this question.

BOMFORD: These days we do not think of our latitude observatories as fixed points. They are on tectonic plates. There may be no real secular motion of the pole at all. It may just be that the five International Latitude Stations and the thirty BIH stations are moving about with their tectonic plates, and what appears at the moment to be secular motion of the pole may just be random noise as the stations move around. Has this argument been put to you before and is there any good compelling argument in the other direction?

MARKOWITZ: What is obtained is the relative motion between the mean pole and the observing stations. Since the Earth is not rigid, one cannot say whether the stations are moving or the pole is moving. The suggestion that there is plate motion has been made before. However the problem which has not yet definitely been solved is whether the apparent motion observed is real or arises from local observational effects. If it turns out that the motion is real then we can attack the problem of trying to determine what is moving.

FEISSEL, M.
Bureau International de l'Heure
Observatoire de Paris
75014 Paris
France

Proc.Symposium on Earth's Gravitational Field & Secular Variations in Position (1973),20-28.

AN ASTRONOMICAL MEASUREMENT OF THE PRESENT DAY DRIFT OF THE EURASIAN AND AMERICAN PLATES

ABSTRACT

A measurement of the displacement of the Eurasian and American plates on the Earth's spherical surface is made by using the 1962-1972 local drifts in latitude and longitude of 45 astronomical observatories with respect to the coordinates reference system of the Bureau International de l'Heure (BIH).

These displacements are described by three parameters: geographical coordinates of the rotation pole and angular velocity. Opposite to the geophysical computation of these parameters, which give the relative motions of the plates over several million years, the astronomical data used make it possible to measure the relative as well as the absolute (relative to an external reference system) motions over a short time period.

However, the noise level of one annual mean position derived from the observations is larger than the drift, the method used by the BIH in order to preserve a fixed reference system in the computation of the pole motion and the rotation of the earth gives local drifts which are homogeneous between 1962 and 1972 and independent of the Earth's rotation pole drift. Among the 80 observatories which measured time and/or latitude during this period, it was possible to compute one or both components of the local drifts of 35 stations belonging to the Eurasian plate and 10 belonging to the American plate.

For each of those two plates, the rotation parameters are obtained by a least-square fitting of the individual drifts of the stations it bears. The coordinates found for the Eulerian pole of their relative motion is in accordance with the geophysical results, while the angular velocity is found larger than the one admitted for the past 100 million years. The parameters of the absolute motion of the two plates are also computed, the BIH coordinates system being taken as an external reference system.

1. Introduction

The parameters of the relative motion of Eurasia and America have been determined on the basis of geophysical data. They are deduced from the relative displacement along the common boundary of the two plates and they describe the movement in a geological time scale. The geographical coordinates (Φ ,Λ) of the eulerian pole of the rotation and the amplitude(ω) of the rotation vector according to different authors are given in Table 1.

Table 1

Rotation parameters of the motion of America relative to Eurasia

Reference	Φ	Λ	ω (10^{-7}deg/yr)	Name in Figure 1
BULLARD et al (1965)	73°N	97°E	--	BU 65
LE PICHON (1968)	78°N	102°E	- 2.8	LP 68
LE PICHON (1971)	79°N	16°W	--	LP 71
CHASE (1972)	48°N	155°E	- 2.36	CH 72

2. The Astronomical Measurements

A completely different kind of measurement of the motions can be made by using astronomical data : time and latitude observations give the position of a station referred to a system linked to a given star catalogue. In order to study the Earth's rotation, such observations are regularly made in a large number of stations. Once the effect of the variations in the Earth's rotation is removed from the universal time and latitude measurements made in a station, the residual values show secular variations due to errors in the star catalogue, possible local drifts or drift of the mean pole, but also to the motion of the plate to which the station belongs.

Precise latitude observations have been made since 1899. The time observations are actually a comparison of the universal time with a laboratory time-scale; the time scale used nowadays is the atomic time scale, TAI, given by atomic clocks and time signals, so that one can be sure that the local time scales actually used in the observatories are consistent within about 1 microsecond; but this accuracy was achieved only recently, and it can be concluded that the series of time observations made prior to 1955 may contain large systematic errors. Furthermore, the two modern instruments measuring both time and latitude, i.e. the PZT and the Danjon astrolabe which increase the accuracy of the observations themselves, were not in use before 1954-55.

The possibility of measuring the present day continental drift (which amplitude is of the order of 0".001 per year) by use of the residuals of some well chosen astronomical observatories has been examined. The difficulties encountered can be described as being due to the lack of homogeneous reference available during a period long enough to get rid of the observation errors.

A way to ensure the homogeneity of the reference is to consider concurrent observations of two or more instruments located on different plates and observing common stars. A pair of such stations makes it possible to measure the drift after about 30 years (MARKOWITZ 1968). A study of the latitude observations made since 70 years at the International Latitude Stations yields an evaluation of the position of the pole of the motion Eurasia-America : $\Phi = 82^{\circ}$ N, $\Lambda = 57^{\circ}$ W (PROVERBIO & QUESADA 1972).

The above method is a strict one, but its use needs a coordination in the measurement process (location of the instruments, common program, equivalent reduction procedures) which is not easily

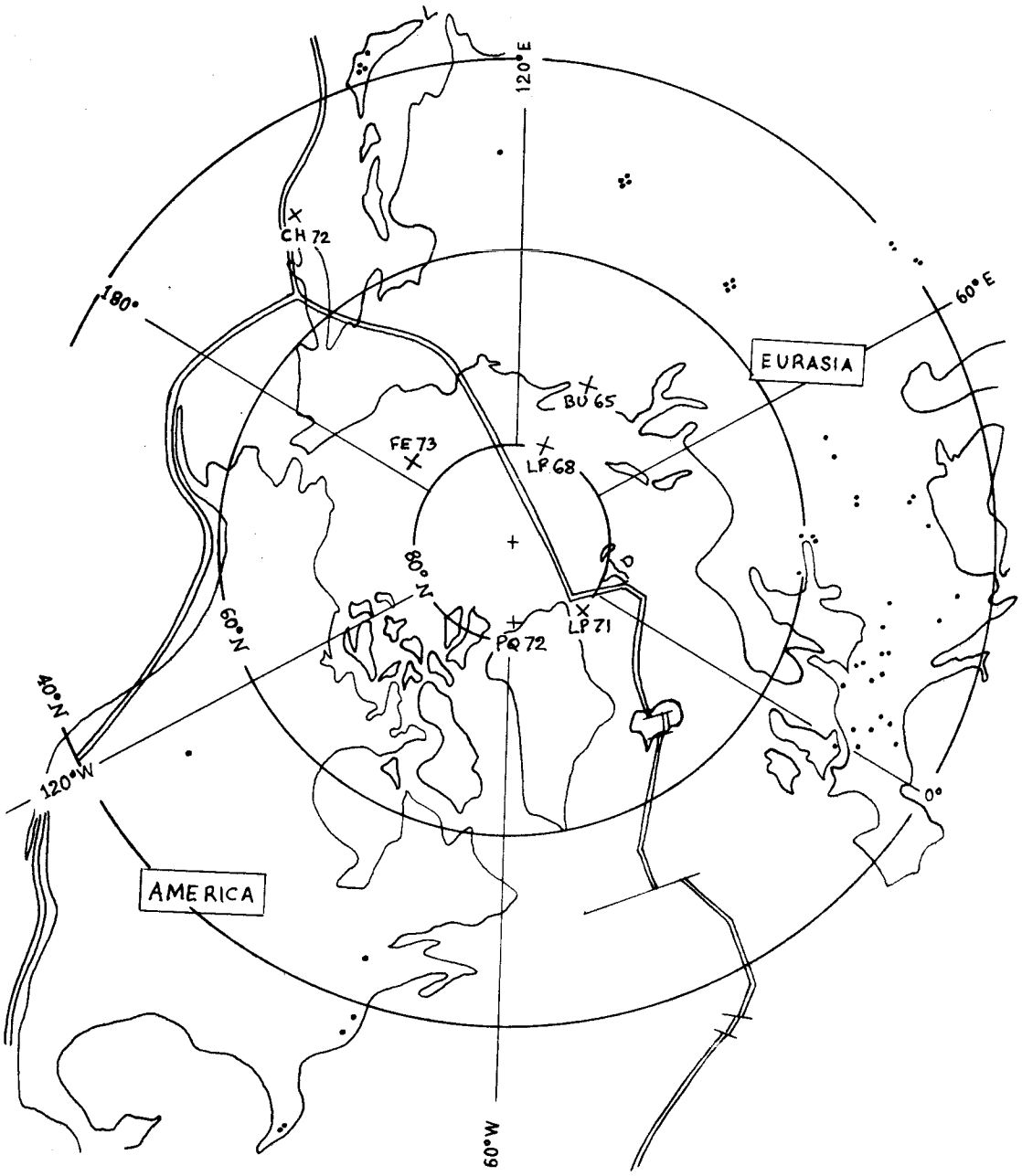

Figure 1 - America and Eurasia

- Time and latitude instruments (those of South America have the latitudes -0^{o}, -23^{o}, -23^{o}, -33^{o}, -34^{o}.)

+ proposed eulerian poles of the relative motion

realised. Moreover, it does not allow the use of the numerous instruments which do not fulfil these conditions. The Bureau International de l'Heure computes time series of UT1-UTC and of the pole coordinates deduced from all the existing series of measured quantities directly related to the Earth Earth's rotation vector, i.e. the present 80 astronomical time and/or latitude series as well as the series obtained, sometimes as byproducts, by the modern methods (satellite observations, VLBI, etc). These series may show individual deviations related not only to continental drift. However, some plates bear a number of observations large enough to reduce the accidental errors and to make it possible to compute their motion relative to the BIH reference system. This provides the new way of measuring plate motions from astronomical observations which is used in this work. The parameters of the motion of a plate relative to the BIH system are obtained by a least square fitting in the individual drifts of the stations it bears, referred to this system; the errors caused by accidental deviations in the stars proper motions are averaged due to the number of stations.

The motion of a plate relative to another one is then computed by combining the two rotation vectors and thus eliminating the intermediate reference system; as the different star catalogues used are not independent, the effect of common systematic deviations in the proper motions is well eliminated if the stations of both plates are located in the same latitude zone.

3. The Local Drifts in the BIH Reference System and the Motion of the Plates

a) The data

In the computation method used by the BIH (GUINOT & FEISSEL 1968) predicted corrections are applied to the different series which contribute to the global computation (FEISSEL 1972). The correction used is the sum of a constant term a, and two periodical terms (annual and semi annual), its prediction being renewed every year according to its actual value for the preceding years. This method is applied in the current computation since 1968. It has been applied to older data, so that homogeneous time series of the pole coordinates and UT1-UTC are available starting from 1962.0. It gives also the individual annual residuals, a, of all the participating observatories, which allow the computation of the drifts 1962-1972 of the stations relative to the system BIH 1968. We thus obtained the individual drifts of $\frac{da}{dt}$ for about 40 instruments in latitude and 50 in longitude. These drifts are referred to the BIH system and they are not affected by the real drift of the mean Earth rotation pole relative to the plates.

The spacing of the stations on the different plates is very unequal. Only two of the six main plates bear enough observatories to make possible the computation of their motion. The American plate has 10 stations which give 8 values in latitude and 9 in time; the Eurasian plate has 35 observatories, 25 in latitude and 27 in time. Five of the ten American stations are in the same latitude zone as the Eurasian observatories (25^{o} N to 60^{o} N).

b) The equations of the Motion

Figure 2 shows P the Earth's pole, Π the Eulerian pole of a plate, A a point of this plate. The movement of A is a rotation with the angular velocity ω around Π. The velocity of the movement along a parallel of the pole Π is $V = \omega \sin \alpha$. The positive rotation is anticlockwise. For this study, we can assume that the Earth is a sphere centred on the centre of mass. If we call ϕ_A the annual residual in latitude and θ_A the annual residual in time observations, the drift in latitude

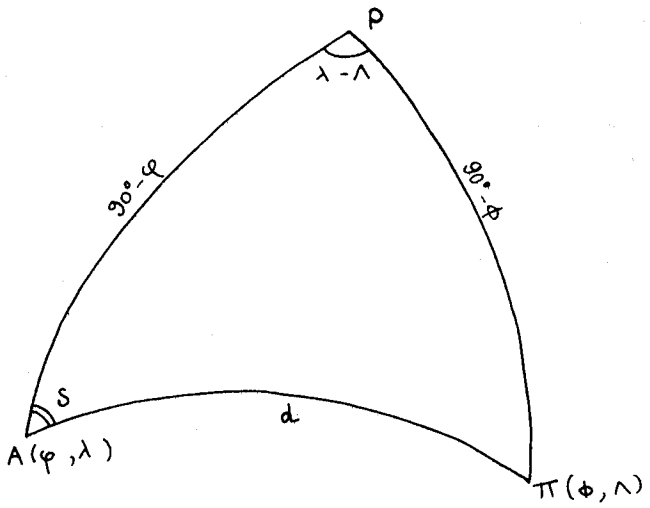

Figure 2

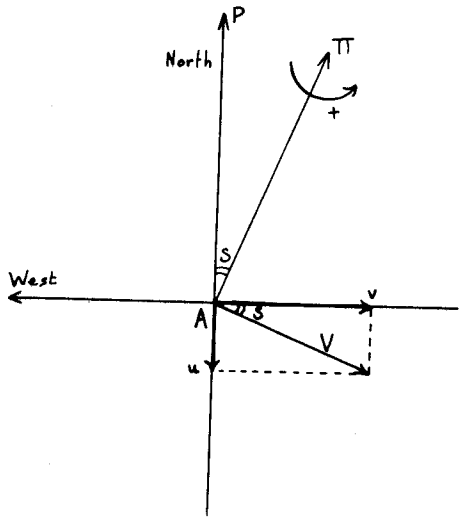

Figure 3

$u = \frac{d\phi_A}{dt}$ is the projection of V on the meridian of A ; the positive motion is northward. The drift along the great circle perpendicular to the meridian of A is

$$v = - \frac{d\theta_A}{dt} \cos \phi$$

the positive motion is westward, as for longitudes; if the local observed UT-UTC decreases, it means that the observatory has a westward drift. Taking into account the different positive directions of V, u, v, the velocity of A is related to the astronomical data by (Figure 3) :

$$\begin{cases} u = -\omega \sin \alpha \sin S & \text{(latitude)} \\ v = -\omega \sin \alpha \cos S & \text{(time)} \end{cases}$$

The trigonometric relations in the spherical triangle PAΠ yield:

$$u = -\omega \cos \Phi \sin (\lambda - \Lambda)$$
$$u = \omega \cos \Phi [\sin \Lambda \cos \lambda - \cos \Lambda \sin \lambda]$$

One has too:

$$v = -\omega(\sin \Phi \cos \phi - \cos \Phi \sin \phi \cos (\lambda - \Lambda))$$

$$v = -\omega \sin \Phi \cos \phi + \omega \sin \phi \cos \Phi \cos \Lambda \cos \lambda + \omega \sin \phi \cos \Phi \sin \Lambda \sin \lambda$$

The change of coordinates:

$$\begin{cases} x = \omega \cos \Phi \cos \Lambda \\ y = \omega \cos \Phi \sin \Lambda \\ z = \omega \sin \Phi \end{cases} \quad \text{, i.e.} \quad \begin{cases} \omega = (x^2 + y^2 + z^2)^{\frac{1}{2}} \\ \Phi = \arccos \left(\frac{x^2 + y^2}{\omega^2} \right)^{\frac{1}{2}} \\ \Lambda = \arctan \frac{y}{x} \end{cases}$$

yields

$$u = - x \sin \lambda + y \cos \lambda$$

$$v = + x \sin \phi \cos \lambda + y \sin \phi \sin \lambda - z \cos \phi$$

Or, when replacing u and v by their values,

$$\frac{d\phi_A}{dt} = - x \sin \lambda + y \cos \lambda \qquad (1)$$

$$- \frac{d\theta_A}{dt} \cos \phi = x \sin \phi \cos \lambda + y \sin \phi \sin \lambda - z \cos \phi \qquad (2)$$

The order of magnitude of the errors are 25^{o} in Φ, 30^{o} in Λ and 6×10^{-7}deg/yr on ω.

5. References

ARUR, M.G. & MUELLER, I.I. 1971. Latitude Observations in the Detection of Continental Drift. *J. Geophys.Res.* 76,2071-2076.

BULLARD, E.C., EVERETT, J.E. & SMITH, A.G. 1965. The fit of the Continents around the Atlantic, in *A Symposium on Continental Drift.* BLACKET, P.M.S., BULLARD, E. & RUNCORN, S.K. (eds) *Phil.Trans.Soc.London,A.* 1088, 41.

CHASE, C.G. 1972. The N Plate Problem of Plate Tectonics. *Geophys.J.R.astr.Soc.*29, 117-122.

FEISSEL, M. 1972. La conservation du système de référence des résultats du Bureau International de l'Heure, in *Rapport Annuel pour 1971 du BIH*, Paris.

FRANCHETEAU, J. & SCLATER, J.C. 1970. Comments on paper by E. IRVING & W.A.ROBERTSON, Test for Polar Wandering and some possible implications. *J.Geophys.Res.* 75, 1023-1027.

GUINOT, B. & FEISSEL, M. 1968. Nouvelles méthodes de calcul du Bureau International de l'Heure, in *IAU Symposium n° 32, Continental drift, polar motion and rotation of the Earth.* MARKOWITZ, W. & GUINOT, B. (eds). Reidel, Dordrecht.

LE PICHON X. 1968. Sea floor spreading and continental drift. *J.Geophys.Res.*73, 3661-3697.

LE PICHON X. 1970. Correction to "Sea floor spreading and continental drift". *J.Geophys.Res.* 75, 2793.

LE PICHON X. & FOX, P.J. 1971. Marginal offsets, Fracture Zones, and the Early Opening of the North Atlantic. *J.Geophys.Res.* 76, 6295-6308.

LE PICHON X, 1972. Cinématique de la tectonique des plaques, in *Structure et dynamique de la lithosphère.* Hermann, Paris.

MARKOWITZ, W. 1968. Concurrent astronomical observations for studying continental drift, polar motion, and rotation of the Earth, in *IAU Symposium 32, Continental drift, polar motion, and rotation of the Earth.* MARKOWITZ, W. & GUINOT, B (eds). Reidel, Dordrecht.

MORGAN, W.J. 1968. Rises, Trenches, Great Faults and Crustal Blocks. *J.Geophys.Res.*73, 1959-1982.

PROVERBIO, E. & QUESADA, V. 1972. Velocity and direction of plate displacements by latitude observations, Presented at the *Journées Luxembourgeoises de Géodynamique.*

STOYKO, N. 1968. Variation séculaire des longitudes in *IAU Symposium 32, Continental drift, polar motion, and rotation of the Earth.* Reidel, Dordrecht.

TANNER, R.W. 1972. The estimation of Plate Motions by Astronomical Methods. *Canad.J.Earth Sc.*9, 8, 1052.

WILSON, J.T. 1965. A new class of faults and their bearing on continental drift. *Nature.* 207, 343-347.

6. Discussion

WHITTEN: Rather than ask a question, I would like to make a comment. Your paper is extremely interesting. Let us compare it with data presented by Markowitz. Looking at figure 2 of his paper, we see an illustration representing the change in latitude of the five ILS stations. About five years ago, after Markowitz had prepared his paper for the meeting in Stresa, I was interested in the effect of possible rotation of continents. I used the data Markowitz had shown, that over the seventy year period Gaithersburg had moved north with respect to Ukiah in California. Taking these points as the ends of a baseline, I made a rough calculation that there would be about 5° minus rotation (anticlockwise) in ten million years. This was in agreement with what geophysicists had said was happening in North America - twenty five degrees in the past fifty million years. I took the three Eurasian stations and found about a four degree clockwise rotation over the ten million year period. These numbers are in general agreement with the results you have found. The observations for the ILS stations do not include longitude, as Markowitz points out, so I could not get a true rotation, but I can get an element of rotation. I can't get the translation, but by using the latitude data, I think it is interesting to see that there is agreement with your work.

FEISSEL: For my computation I considered that Ukiah did not belong to the main American plate and I did not use Carloforte, which is too close to the Africa-Eurasia boundary. As the pole of the motion of America relative to Eurasia lies near the Earth's rotation pole, latitude variations give little information on the displacement.

WHITTEN: That is right; using the latitude only, you cannot determine the pole of rotation, but I could determine an element of plate rotation.

ABRAHAM, H. J. M.
Mt Stromlo & Siding Spring Observatory
Australian National University
Canberra ACT 2600
Australia

Proc. Symposium on Earth's Gravitational Field & Secular Variations in Position (1973), 29-35.

THE EARTH'S SECULAR LIBRATIONS

ABSTRACT

Three components of the secular polar motion are described:

a) a minor libration which varies in frequency with the amplitude of the Chandler wobble;

b) the major libration which appears to be increasing in period and amplitude;

c) the progressive motion which is fairly steady in rate and direction.

Librations appear to affect the phase of the Chandler wobble. It is suggested that libration characteristics are due to time-dependent responses.

1. The Data

Figure 1 shows the positions of the barycentre according to YUMI & WAKO (1966) and YUMI (1966-1973a; 1973b). Those based on the data from Mizusawa (M), Carloforte (C) and Ukiah (U) extended from 1903 to 1963. Those that also include Kitab (K) and Gaithersburg (G) extend from 1936 to 1970. It is clear that different stations report very different progressive motions.

Figure 2 shows the result of simply applying -0".004/yr to the y values as a rough correction for the progressive motion. The main feature is then the librations. Its departures from a smooth oscillation appear to vary in amplitude and frequency with R, the amplitude of the Chandler wobble. (R was greatest around 1910 and 1953). Arrows indicate the approximate direction of displacements by the minor libration.

Figure 3 indicates that the frequency response has not remained constant. The period of the strongest spectral line has increased, and the relative response at the shorter periods has changed. It was found that each of these corresponds to a particular value of R. Consequently, the strength of the line depends upon the number of times that a particular value of R occurs in the sample, e.g. small values of R were frequent before 1936, but not afterwards; this caused the 16-year period to be strong in the data for 1904-66, but not in the data for 1936-1967.

THE MODEL

In the words of JEFFREYS (1952):

> The behaviour can be represented better if we regard the solid as composed of pieces, all perfectly elastic when the stress is not too great, but flowing when it is great enough, the transitions being at different stresses for different portions. ... Thus the rate of deformation will increase more rapidly than in proportion to the

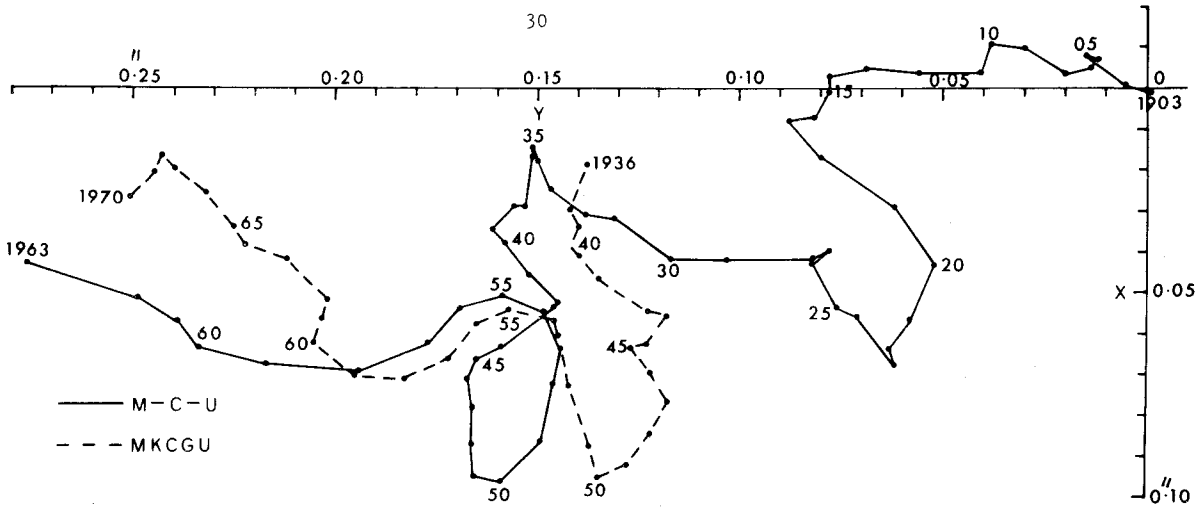

Figure 1. Positions of the barycentre

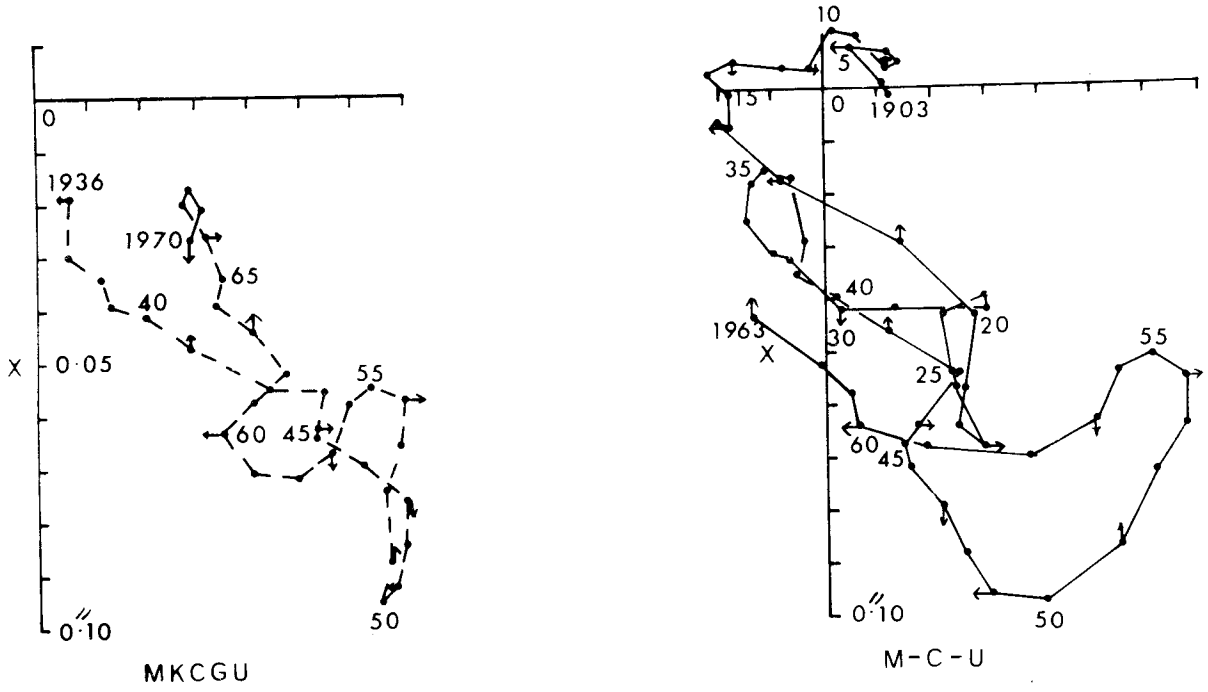

Figure 2. Positions of the barycentre partly corrected for progressive motion

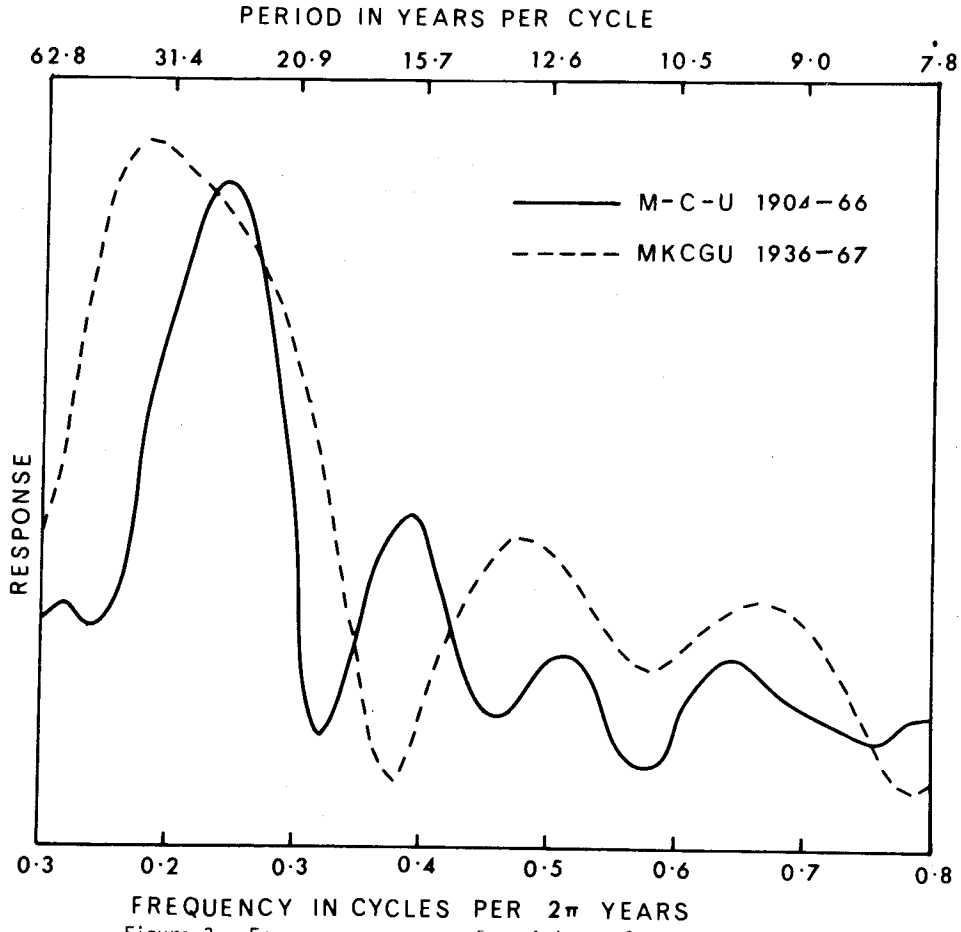

Figure 3. Frequency response of positions of the barycentre

> stress. ... If the stress is in an intermediate range the weaker parts may adjust themselves to a hydrostatic state, leaving the whole deforming stress to be borne by the stronger parts. If this happens the displacement will tend to a finite limit, the rate of approach being limited by the viscosity of the weak parts. If the stress is removed the strong parts will tend to spring back and, in doing so, apply deforming stresses to the weak ones, which will again flow, but in reverse direction.

This is the model which has been used here to interpret the strains that are associated with the polar motions. The presence of periodic strains is indicated by the deformations that accompany the wobbles. In the notation of MUNK & MACDONALD (1960), when the rotation pole P is displaced from its current position of rest O to some point $\underline{\underline{m}}$ then $\underline{\underline{m}}$ can serve as a measure of the stress $\underline{\underline{S}}$. Let the rate of relaxation of an excitation ψ be

$$\dot{\psi} = -\psi/\tau \qquad (1).$$

The strain in an actual body is indicated by the deformation excitation

$$\underline{\underline{\psi}}_D = (\underline{\underline{k}}/k_f)\underline{\underline{m}} \equiv (k/k_f)\underline{\underline{m}} - i(k/k_f)\,(\tfrac{1}{2}\mu/Q)\underline{\underline{m}} \qquad (2)$$

where k is the Love number; k_f is the value that k would have if the Earth had the shape of a rotating fluid and its density distribution were equal to that of the actual Earth; μ is the dimensionless rigidity; and $1/Q$ is the 'specific dissipation function' which indicates sharpness of resonance.

The existence of systematic stress is shown by the progressive motion. Along the meridian of this motion weak material is assumed to yield or fracture until the stress is borne by stronger material. Then the stress can rise until the yield strain is reached, and so the mean rigidity of the material that still resists will also rise. In the meridian normal to the progressive motion the rigidity would not become so great. Whenever the stress is reduced the material would tend to recover.

The strain ε depends not only on the stress S and the rigidity; as shown in Jeffreys' approximation (GUTENBERG 1959) there is also the time-dependent increase which depends on $\int S dt$ and the viscosity; and there is the time-dependent decrease (due to relief of stress) which depends on $\dot{\varepsilon}$ and the time of retardation. It is evident that terms in $\int S dt$ may be unimportant if the period is short but they can become important or even dominant if the period is long. The retarded elastic response is important in the period of the Chandler wobble, and the rate of response is important in the periods of librations.

2. The Minor Libration

An empirical formula is used provisionally for the frequency of this small libration. It was derived as follows:

Let R be the radius of the Chandler wobble
b be the semi-minor axis of the annual wobble
σ and σ_0 be the angular speed of the annual and Chandler wobble respectively

and let $$\psi = R - (k/k_f)R. \qquad (3)$$

When the annual excitations with a steady excitation give rise to the annual and Chandler wobbles then the departure of the rotation pole P from its initial position O can be given in the form

$$\underline{\underline{m}} = \underline{\underline{R}}(1 - e^{i\sigma_0 t}) + \underline{\underline{m}}^{+}(1 - e^{i\sigma t}) - \underline{\underline{m}}^{-}(1 - e^{-i\sigma t}) \qquad (4).$$

During every period $2\pi(\sigma - \sigma_0)^{-1}$ the mean position of P is

$$\underline{\underline{R}} + \underline{\underline{m}}^{+} - \underline{\underline{m}}^{-} = \underline{\underline{R}} + \underline{\underline{b}} \qquad (5).$$

Thus in each period $2\pi(\sigma - \sigma_o)^{-1}$ the rotation pole moves with apparent annual speed $R(\sigma_o - \sigma)$ about a mean position $\underline{\underline{R}} + \underline{\underline{b}}$. Consequently the apparent angular speed of the annual mean positions of the pole is

$$\frac{-R(\sigma - \sigma_0)}{R + b} \equiv -\upsilon_1 \qquad (6).$$

3. The Major Libration

It is suggested that this libration arises from the Earth's response to stress in the presence of anelastic material.

Let $\underline{\overline{R}}$ be the mean position of the modified excitation pole of the free wobble with respect to O during each period $2\pi(\sigma - \sigma_0)^{-1}$. The corresponding anelastic deformation excitation due to strong material is $\underline{\overline{R}}\,\underline{k}/k_f$ so the unrelieved mean excitation is $\underline{\overline{R}}(1 - \underline{k}/k_f) \equiv \underline{\overline{\psi}}$. This excitation urges the weak material to yield or fracture and thus relieve the remaining stress. The consequent motion of $\underline{\overline{\psi}}$ with respect to O would be

$$\frac{d\underline{\overline{\psi}}}{dt} = -\left(1 - \frac{k}{k_f} + \frac{i}{2}\frac{k}{k_f}\frac{\mu}{Q}\right)\frac{\underline{\overline{R}}}{\tau} \qquad (7).$$

The real term shows the rate at which $\underline{\overline{\psi}}$ would attempt to move to O. However, it is well known that R has a continuing mean value of about 0".15. Therefore there is evidently an energy source as well, and this compensates for the damping and maintains the value of $\underline{\overline{\psi}}$, so the real term can be disregarded. Then

$$\frac{d\underline{\overline{\psi}}}{dt} = \frac{k_f - \underline{k}}{k_f}\frac{d\underline{\overline{R}}}{dt} = -\frac{i}{2}\frac{k}{k_f}\frac{\mu}{Q}\frac{\underline{\overline{R}}}{\tau}.$$

Therefore $\underline{\overline{R}}$ revolves with radius $\overline{R}$ and frequency

$$-\upsilon_2 = -\frac{k\mu}{2Q(k_f - \underline{k})\tau} \qquad (8).$$

A simple example is that in which the strong material on its own would respond to the Chandler wobble as a Kelvin-Voigt body, i.e. like a spring with rigidity $\tilde{\mu}_s$ in parallel with a dashpot with viscosity $\tilde{\eta}_s$. There would be no permanent strain; and the relaxation time $\tau_s = \eta_s/\tilde{\mu}_s$. It can be shown (MUNK & MACDONALD 1960) that $1/(2Q) = \sigma_0\tau_s/(1 + \mu)$. The relaxation time for the actual Earth is τ. $(\tau > \tau_s)$. Then equation 8 becomes

$$-\upsilon_2 = -\frac{k}{k_f - \underline{k}}\frac{\mu}{1 + \mu}\frac{\tau_s}{\tau}\sigma_0 \simeq -\frac{k}{k_f}\frac{\tau_s}{\tau}\sigma_0 \qquad (9).$$

Let us now consider some of the effects of a stress $S \sin \upsilon_2 t$ in a material that gives a retarded elastic response. The stress equation is of the type $\ddot{y} + 2p\dot{y} + q^2 y = q^2 s \sin \upsilon_2 t$ in which $\upsilon^2 < q^2$. Then the steady state solution is $y \simeq SA \sin(\upsilon_2 t - \tan^{-1}\upsilon_2\tau)$ where $A = (1 + \upsilon_2^2\tau^2)^{-\frac{1}{2}}$ (SOKOLNIKOFF 1941). Similarly in the case of $\overline{R}\exp(-i\upsilon_2 t)$; let $t = 0$ be an instant when this excitation is acting in the meridian of reference, and let $\tau = \tilde{\eta}/\tilde{\mu}$ be the relaxation time along that meridian. Let τ_i be the relaxation time along the meridian which is normal to this. Then the deformation excitation is

$$\overline{R}\,A\cos(\upsilon_2 t - \tan^{-1}\upsilon_2\tau) - i\overline{R}\,A_i\sin(\upsilon_2 t - \tan^{-1}\upsilon_2\tau_i)$$

$$\simeq \overline{R}\,A\{\sin\upsilon_2 t + i(A_i/A)\cos(\upsilon_2 t + \lambda)\} \qquad (10),$$

where $$\lambda = \tan^{-1}\upsilon_2\tau - \tan^{-1}\upsilon_2\tau_i \simeq (\upsilon_2\tau_i)^{-1} \qquad (11).$$

According to these expressions the oblique axis should be A_i/A times greater than that in the meridian of reference, and it should lie $\pi/2 - \lambda$ radians to the west of that meridian, approximately. It seems likely that τ would be greatest in the meridian of the progressive motion.

4. Variations

The model helps to explain several phenomena. The observed period of the libration has been increasing, as can be seen in Figure 1 and in the line shift in Figure 3. The rate of increase is about 0.4 year/year. This can be expected if the stress is continuing to make the strong material give way. Then the mean value of $\tilde{\mu}_s$ would rise, τ_s would fall, and υ_2 would decrease according to equation (9). υ_2 would also decrease if the more viscous conditions increase or last longer and thus cause τ to rise.

The observed amplitude of the librations varies with the Chandler amplitude (e.g. R was relatively large about 1910 and 1953 and small from about 1922 to 1942), and it appears to have been increasing as well. According to equation (10) there should be an increase in amplitude on account of the decrease in υ_2 in A.

A small eastwards rotation of this libration axis would also occur, according to equation (11) but further treatment will be needed to verify this.

The progressive motion appears to be far more stable, as shown by the compact libration pattern when a constant rate correction is applied.

Finally, the model is relevant to the problem of why the Chandlerian wobble *was not* disturbed in phase when it *was* disturbed in amplitude (around 1910 and 1953), and *was* disturbed in phase when it *was not* disturbed in amplitude (1925.5 to 1928.5) (GUINOT 1972). The explanation appears to be that the period of the wobble is strongly related to the librations as well as to the amplitude of the wobble (ABRAHAM & BOOTS 1972). This is because the period of the wobble increases with the integrated deformation, and this is affected by librations.

Least squares solutions are now being fitted to obtain greater precision.

5. References

ABRAHAM, H. J. M. & BOOTS, J. N. 1972. On Variations in the Chandler Frequency, in *IAU Colloquium No. 1*. O. CACERES (ed). National University of La Plata.

GUINOT, B. 1972. *Astron. and Astrophys.* 19. 207.

GUTENBERG, B. 1959. *Physics of the Earth's Interior.* Academic Press, London.

JEFFREYS, H. 1952. *The Earth.* University Press, Cambridge.

MUNK, W.H. & MACDONALD, G.J.F. 1960. *The Rotation of the Earth.* Cambridge University Press, Cambridge.

SOKOLNIKOFF, I.S. & E. S. 1941. *Higher Mathematics for Engineers and Physicists.* McGraw-Hill Book Co, London.

YUMI, S. & WAKŌ, Y. 1966. *Publ.Int.Lat.Obs.Mizusawa.* 5, 61.

YUMI, S. 1966-1973a. *Annual Reports IPMS.*

YUMI, S. 1973b. *Report of the IPMS* (1972.0 - 1973.4).

FISCHER, I.
Defence Mapping Agency
Topographic Center
Washington DC 20315
United States of America

Proc. Symposium on Earth's Gravitational Field & Secular Variations in Position (1973),36-50.

DEFLECTIONS AT SEA

ABSTRACT

As the frontiers of geodesy are pushed forward into the ocean areas, the determination of ocean geoids is being discussed in anticipation of the forthcoming GEOS-C satellite altimeter experiment. Independent methods will be needed for checks and verification, but also for interpolating the finer details of the geoid and/or deflections of the vertical in areas of interest. This paper explores the possibility of utilising bathymetric data to determine deflections of the vertical at sea, if gravimetric anomalies are not or not sufficiently available. A Pacific atoll where a number of astrogeodetic deflections of the vertical have been observed, is studied as a test case to determine the accuracy with which the given deflection values can be reproduced.

1. Introduction

The current extension of geodesy from detailed and highly accurate land data into the vast ocean regions takes several different forms. Foremost is satellite geodesy which establishes positions of islands and ships with increasing accuracy. The feasibility of placing geodetic markers on the ocean floor provides the prospect of a geodetic control network with calibration ranges in the oceans, to aid all other endeavours with recoverable checkpoints. Satellite altimetry is expected to yield geoidal profiles and slopes of the ocean surface. Methods of determining deflections of the vertical directly by a ship's inertial navigation system are tried and the possibility of observing astros from stabilised platforms is explored. The standard procedure of deriving geoid undulations and deflections of the vertical from gravity anomalies by STOKES' and VENING MEINESZ' formulas requires an extensive collection of gravimetric measurements at sea, with great density around the points of interest. The ocean bottom topography is being mapped with increasing completeness as well as detail, but so far this data has not been used for direct computation of deflections. Suppose good bathymetric maps of an area are available, then it should be possible to compute from them deflections directly as the horizontal components of mass attractions. This paper explores the feasibility of this approach from a practical viewpoint; that is, real data from existing maps will be used and the results will be tested against observed deflection values. The exasperating difficulties and pitfalls of numerical data will thus show up, while they do not appear in theoretical treatises or smooth textbook examples. A realistic feel for achievable accuracies can be gained from the comparison of computed with observed deflection values. As a significance gauge for deflections at sea, we quote from the literature (MOURAD 1971), that VON ARX achieved an accuracy of ± 12 seconds of arc for astrogeodetic deflections across the Puerto Rican Trench; and that BUTERA et al determined deflections across the same Trench from the difference between the positions from a ship's inertial navigation system (SINS) and from LORAC or LORAN, which differed by up to 70" from those by VON ARX.

2. The Test Area

An atoll in the Marshall Islands in the Pacific Ocean was selected as a test case to see whether and how accurately deflection values could be produced from bathymetric maps, as an alternative procedure to computing deflections from an extensive collection of gravity anomalies. An evaluation of the accuracy achieved was provided by the comparison with a set of sixteen astrogeodetic deflections, observed on the islands surrounding the lagoon, and referred to a local geodetic datum. The deflection values range from -24.49" to +28.89" in the meridian, and from -19.12" to +21.83" in the prime vertical, rather large variations across an area of less than $3/4^{\circ}$ in diameter.

Considering the dependence of astrogeodetic deflection values on the arbitrary choice of the geodetic datum, one might wonder whether or not a change to a world datum or a best fitting regional datum might be appropriate before a comparison is made with values computed from ocean bottom topography. As it turns out, a change to any other datum for such a small area amounts practically to a blanket correction in either component, and would thus be easily recognisable, if needed in the comparison.

The bathymetric maps available for this study were Hydrographic Office charts at about 1:1 000 000, at 1:100 000, 12 000, 10 000 and Army Map Service maps at 1:25 000. Here we ran into our first exasperating difficulties with real numbers: plotting the sixteen stations on these maps according to the given coordinates made them fall into the water. Then a reference statement for an overall blanket correction was discovered which should align the geodetic coordinates with the map grid. This correction brought the stations nearer to the islands but not yet onto them. A search of the field books and station descriptions helped to locate the stations on the large scale maps in proper relation to buildings or roads. The correct relationship was thus established, station by station, between the geodetic coordinates on the local datum and the map coordinates.

Next came the reading of the bathymetric information, requiring a decision about the degree of detail and the extent of coverage to be used, versus the effort to be expended. It was decided to use the "rectangular" method throughout (FISCHER 1966), with area units of $\frac{1}{2}' \times \frac{1}{2}'$, 2.5' x 2.5', and 5' x 5', and the delineation between them to be assigned by trial and error, and by the detail, or rather the lack of detail shown on the maps. The trial was compounded by the poor quality of the maps, with little or different information given on different- scale sheets in some regions. Eventually, the overall extent of coverage adopted for this pilot study was an area of 5° in latitude and 4° in longitude, so that each station was at least 1.5° from the boundary. A refinement in the vicinity of each station was added, however: the 0.5' x 0.5' square containing the station had been subdivided into four parts by the meridian and prime vertical through the station; this arrangement was now replaced by 5" x 5" readings, and by 10" x 10" readings in the eight 0.5' x 0.5' squares around it. A further refinement of 2" x 2" instead of the 5" x 5" was tried for one island. The gain seemed too insignificant to justify the expense for the others. It is assumed that the adopted coverage provides 80-90% of even the large deflection values.

A verification of this assumption may be seen in Figure 1, where the accrual with distance is plotted for each deflection component at a specific station, showing a gradual levelling off. The vertical line marks the end of the centrally symmetric coverage for this station. The additional accrual stems from the lopsidedness of a fixed data area for all stations of the region. This brings up the old question of a necessarily limited data extent: should one use the same fixed area for all

sixteen stations of the region, or should one use centrally symmetric areas for the individual stations, which then would differ from station to station. For purposes of computing interpolation values between given deflections, the first approach works on the assumption that distant neglected masses will affect all stations in the same or slowly varying amount, which can be taken care of within the interpolation process; this approach is less expensive, since the area can be kept relatively small. To reproduce one individual deflection value independently, one would have to go out far enough so that the accrual from the next distance-belt would be insignificantly small. Figure 1 suggests a distance of about 350 km.

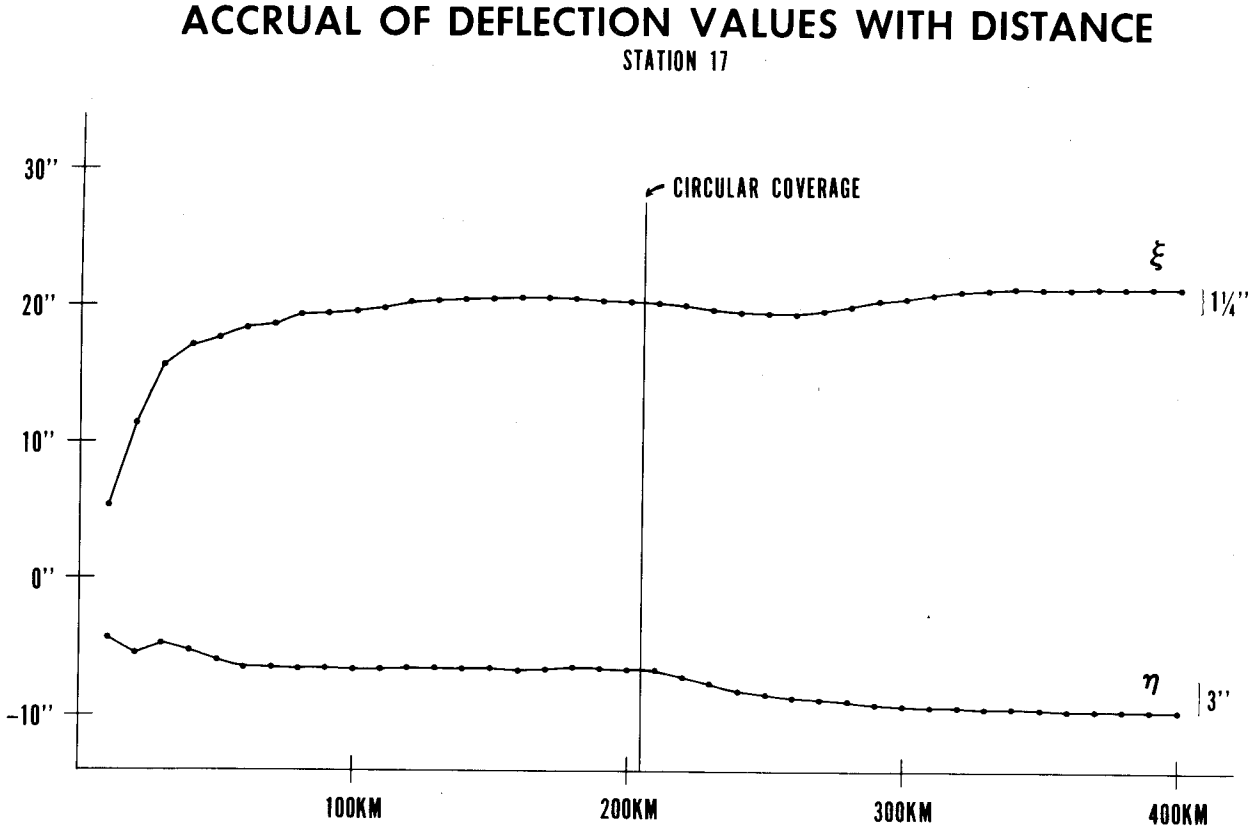

Figure 1

3. Isostatic Models

The basic expression for the horizontal attraction of a mass m on a station A, formulated as meridional and prime vertical deflection components in a rectangular coordinate system, is given by

$$\left.\begin{matrix}\xi \\ \eta\end{matrix}\right\} = - \frac{k\,m}{g\,s^3} \left\{\begin{matrix}x_m - x_A \\ y_m - x_A\end{matrix}\right. ,$$

where k = gravitational constant
g = mean value of gravity
s = distance Am

For a numerical integration of the effect of all given masses around A, the data area is subdivided into a system of rectangular area units with pre-assigned dimensions $(a \times b)_i$. The mass m_i of a rectangular column with the given cross section $(a \times b)_i$ is described by the height H_i and the density σ_i. For the small region of this study the assumption of a flat earth is adequate. As a further simplification, the mass m_i is treated as a point mass at the center of the column.

The primary input of the ocean depths read from the maps and associated with the adopted density value $\sigma = 1.027$ for sea water must be supplemented by reasonable assumptions about the rock density in the area, variations from an average density value, the existence of isostatic compensation, depth of compensation, different types of isostatic theories, or other density models. One may hope that, in turn, a distinction between some of these assumptions can be made from comparing the computation results with the observed deflection values.

As a first model, we tried the textbook approach of PRATT-HAYFORD's isostatic theory with density $\sigma = 2.67$ and depth of compensation at 113.7 km. A land column with zero elevation above mean sea level is taken as the standard, and a water column as deficient in mass by comparison. Traditionally, the water column is thought to be compressed to rock density, leaving an "empty" space as a clear deficiency, which is compensated by an excess mass distributed from the ocean bottom down to 113.7 km below mean sea level. For computational simplification, the deficiency and the excess are thought to be concentrated at the midpoints of their respective columns.

The sixteen deflections computed from this model were compared with the sixteen given astrogeodetic deflection values. The residuals (observed minus computed values) are listed in Table 1. Variations of this model with rock density values from 2.3 to 2.8 were computed to see the sensitivity of this parameter. With a criterion of the average error in absolute value and of the number of "hits" within 1.5" the density value 2.5 seemed best, with 2.4 a close second. To pinpoint a bias which could be interpreted as a datum shift, seemed to be premature and insignificant at this stage. Figure 2 is a graphic representation of these residuals which permits a visual interpolation for other density values and the following conclusions:

a. The "best" σ would be indicated by the shortest vector, that is the perpendicular to a line connecting the other solutions. Apparently, no "best" value would lead to zero residuals.
b. The "best" σ would be different for different stations or different regions. The east and west regions seem to behave differently, with 2.4 better in the east, and 2.5 - 2.6 better in the west.
c. An overall "good" value would be between 2.4 and 2.5, but it would not be 2.67.

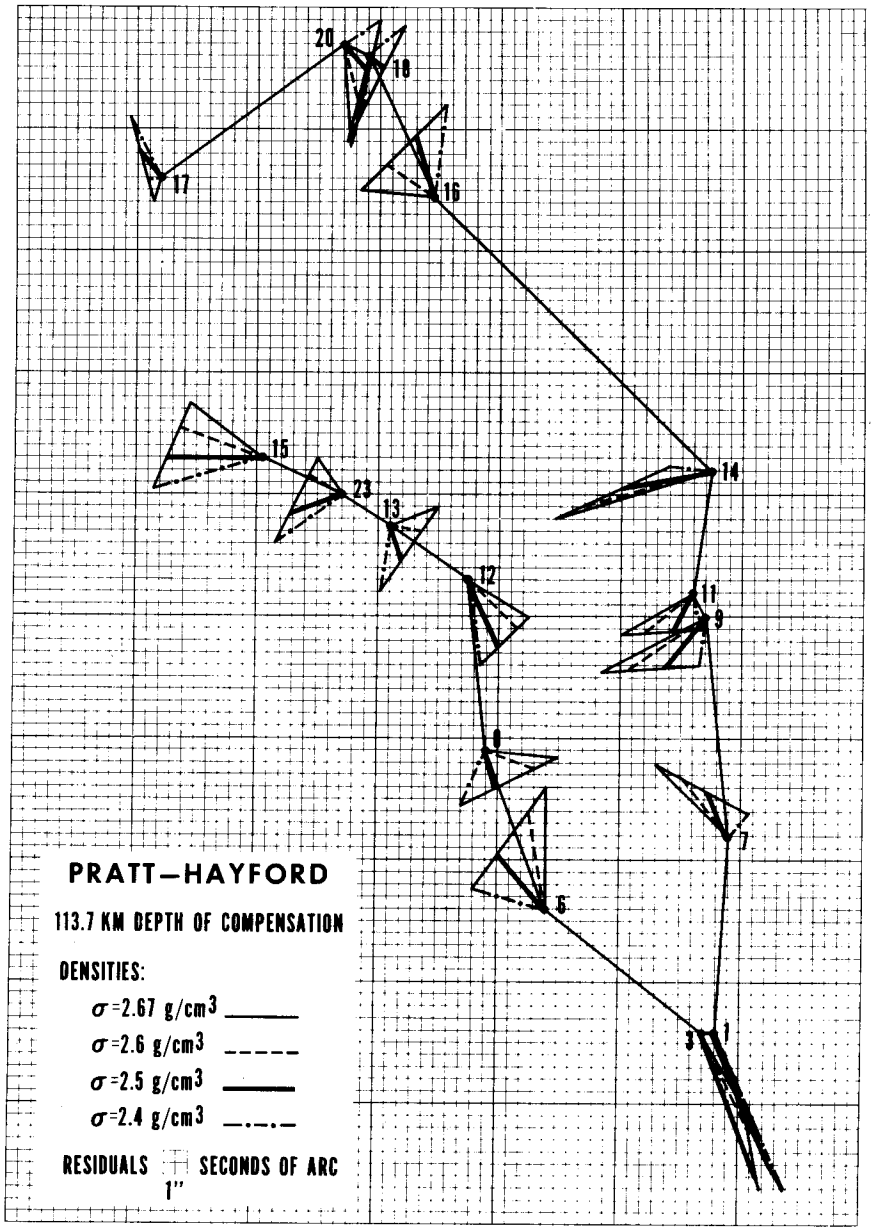

Figure 2. Pratt-Hayford Residuals for Various Rock Densities

TABLE 1. Pratt-Hayford Isostatic Models
Residuals for Various Densities and Depths of Compensation

Sta	Depth of Compensation 113.7 km σ =2.67 v_ξ''	v_η''	σ =2.5 v_ξ''	v_η''	σ =2.4 v_ξ''	v_η''	57 km σ =2.4 v_ξ''	v_η''	227 km σ =2.4 v_ξ''	v_η''	σ =2.5 v_ξ''	v_η''
1	-3.26	+1.39	-5.26	+2.36	-6.44	+2.94	-8.70	+3.61	-5.51	+3.43	-4.26	+2.90
3	-2.95	+1.75	-5.16	+2.04	-6.46	+2.21	-8.79	+2.69	-5.48	+2.75	-4.11	+2.62
6	+5.05	+0.01	+2.35	-1.95	+0.76	-3.10	-2.09	-4.01	+2.00	-2.42	+3.69	-1.22
7	+2.92	-3.12	+1.74	-0.72	+1.05	+0.69	-0.64	+2.52	+1.71	+0.66	+2.45	-0.76
8	-0.29	+3.00	-1.47	+0.54	-2.17	-0.90	-4.68	-1.84	-1.10	-0.42	-0.33	+1.06
9	-2.24	-4.21	-2.07	-1.67	-1.97	-0.17	-2.23	+2.41	-1.81	-0.63	-1.90	-2.15
11	-1.74	-2.97	-1.59	-0.89	-1.50	+0.34	-1.60	+2.87	-1.40	-0.12	-1.48	-1.39
12	-1.47	+2.49	-2.70	+1.28	-3.42	+0.57	-4.69	+0.58	-2.92	+0.69	-2.16	+1.41
13	+0.72	+1.92	-1.40	+0.53	-2.66	-0.29	-3.99	-0.77	-2.19	-0.04	-0.90	+0.79
14	-2.07	-6.51	-0.66	-3.60	+0.17	-1.88	+1.27	+1.26	-0.19	-2.59	-1.05	-4.36
15	+2.30	-3.09	0.00	-4.01	-1.35	-4.55	-2.58	-5.63	-0.95	-4.10	+0.43	-3.53
16	+0.29	-2.92	+2.46	-0.73	+3.73	+0.57	+6.64	+2.19	+2.63	+0.16	+1.28	-1.16
17	-1.03	-0.27	+1.26	-0.96	+2.61	-1.36	+5.13	-2.06	+1.78	-1.13	+0.37	-0.71
18	-3.45	-0.82	-0.48	+0.62	+1.28	+1.46	+5.22	+2.47	-0.24	+1.12	-2.11	+0.25
20	-4.19	+0.27	-0.96	+1.03	+0.94	+1.47	+4.97	+2.32	-0.61	+1.16	-2.63	+0.69
23	+1.46	-0.91	-0.72	-2.04	-2.00	-2.71	-3.27	-3.39	-1.59	-2.40	-0.28	-1.71
a	2.2	2.2	1.9	1.6	2.4	1.6	4.2	2.5	2.0	1.5	1.8	1.7
b	6/16	6/16	8/16	9/16	7/16	10/16	2/16	3/16	6/16	10/16	8/16	10/16

a = $\Sigma |v| / 16$
b = number of $|v| \leq 1.5''$ out of 16 cases

A variation of the traditional depth of compensation at 113.7 km to half and twice its value, holding the density value of 2.4, leads to other sets of residuals which are listed also in Table 1, and graphed in Figure 3. It appears that 57 km is no improvement, while 227 km is a strong competitor, although the gain is small and not evident at all stations. It suggests, however, that isostatic compensation takes place further down rather than nearer to the ocean bottom.

Although the PRATT-HAYFORD theory may be too simple for geophysical insight, it is a very convenient tool as an intermediary step for interpolating deflections. In fact, the thirty-two deflection components were modelled with an average error of 1.8" and 1.7" respectively and 18 "hits" within 1.5", without even applying any further possible sophistication in the model or the procedure. That is not too bad for a first try, considering the 12" accuracy quoted in MOURAD's Report.

The AIRY-HEISKANEN theory of isostasy takes more cognisance of geophysical factors and some of its findings have been corroborated by seismic evidence. We know now that the crust under the oceans is thinner than in the continental blocks, and we know some density magnitudes involved. Figure 4 is a simplified density model for our area adapted from the literature (HEISKANEN & VENING MEINESZ 1958; STRAHLER 1971). It takes the 5 km ocean depth shown on the maps, as the standard, and assumes underneath a 1 km sediment layer, a 6 km basaltic crust, and heavier ultrabasic rock beyond the Mohorovičič discontinuity at 12 km depth. The thin crust under the oceans can be interpreted as the result of a compensating antiroot, coming up from a theoretical depth of compensation at around

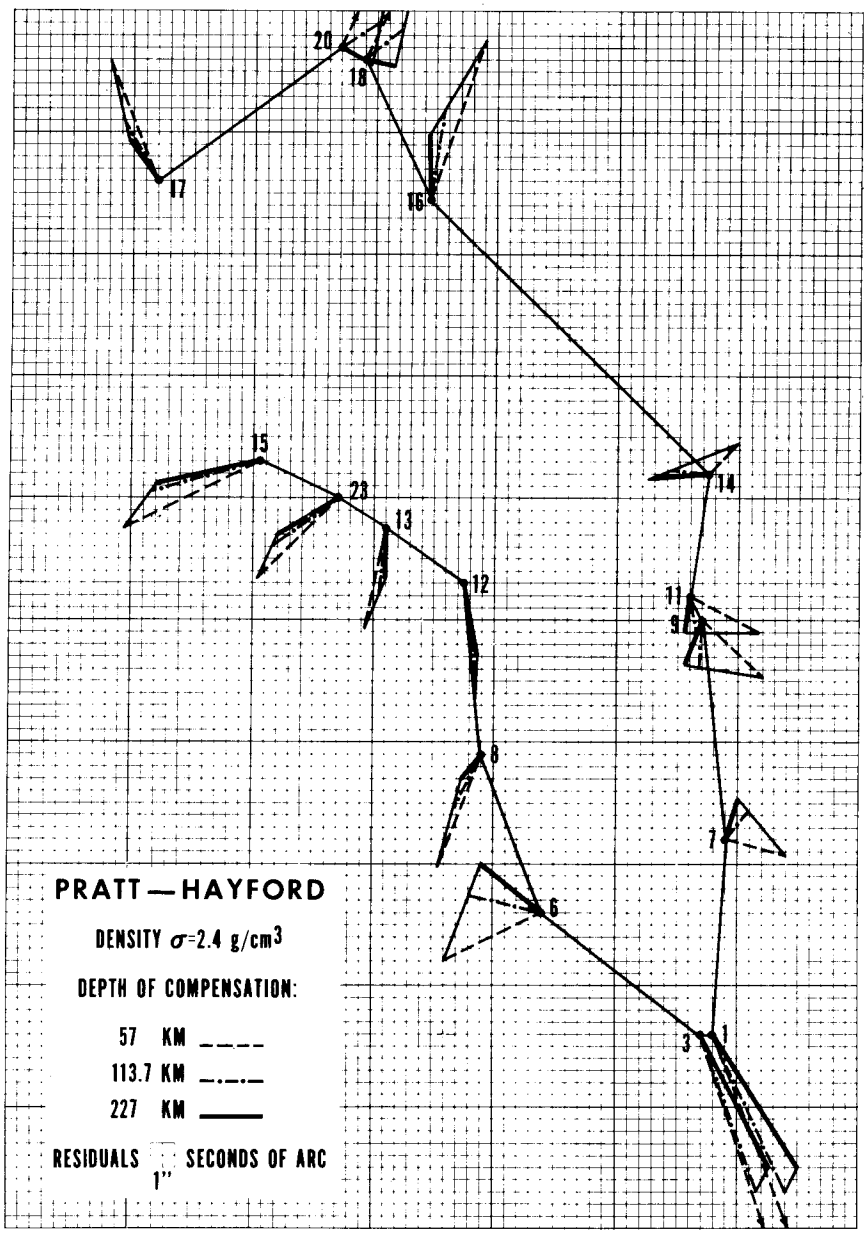

Figure 3. Pratt-Hayford Residuals for Various Depth of Compensation

30 km, which balances the mass deficiency of the ocean waters. So the overall fact of isostasy is already included in our standard model, which will now be modified by the specific depth readings D, in order to compute the deflections at each station.

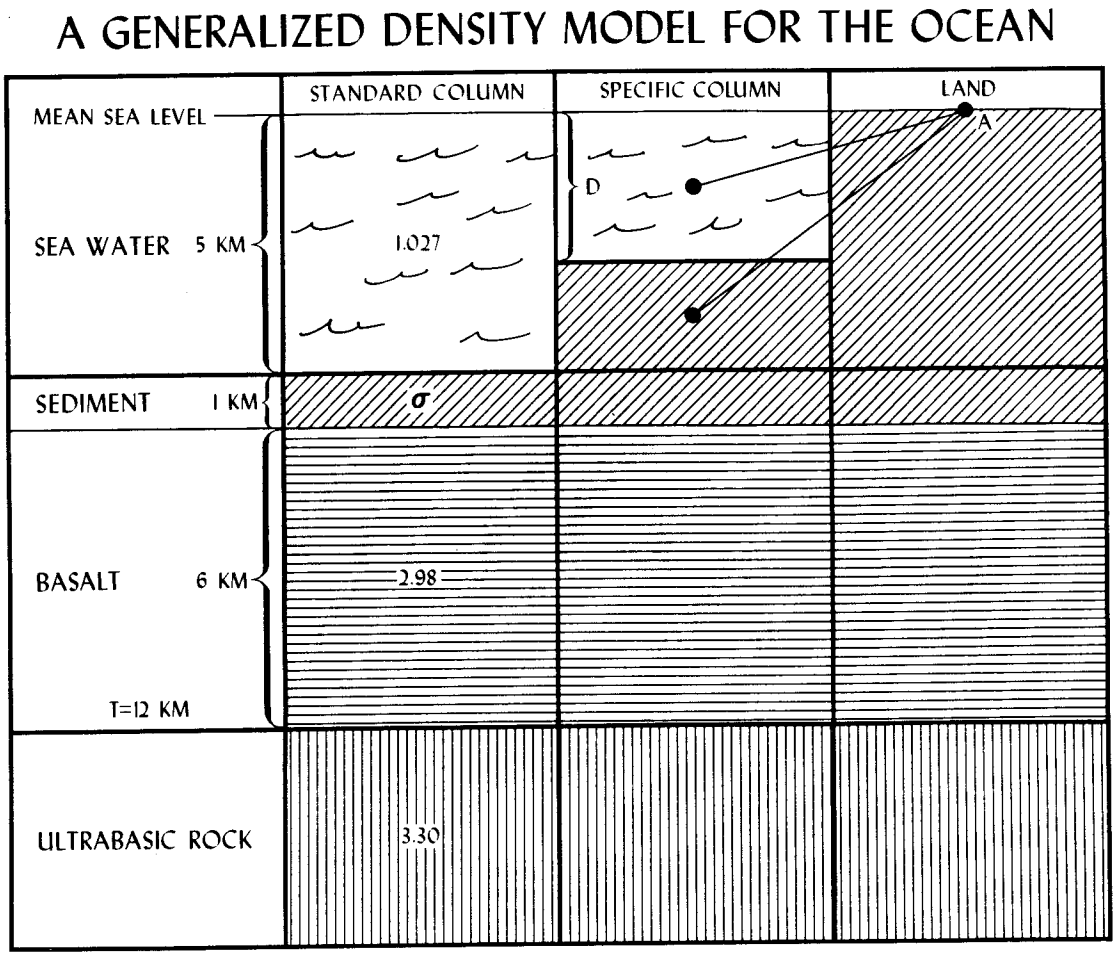

Figure 4

To allow for a similar variation of parameters (density and depth of compensation) as for the PRATT-HAYFORD theory above, the computations were carried out in two steps: first, the effect of the "visible" topography was computed, that is the land and water distribution down to 5 km depth as read from the maps. The effect of assumed compensating masses, modifying the standard model of Figure 4, is computed separately and added.

The effect of the "visible" topography was computed for various rock densities and 2.4 was found to give the smallest residuals. The depth of compensation was varied from T = 12 km to T = 30 km and T = 55 km, at an assumed boundary of rigidity within the ultrabasic layer. The residuals are listed in Table 2 and graphed in Figure 5. Interpolating by sight for the "best" T, one can see again that east and west behave differently, but that an overall "best" depth of compensation is further down

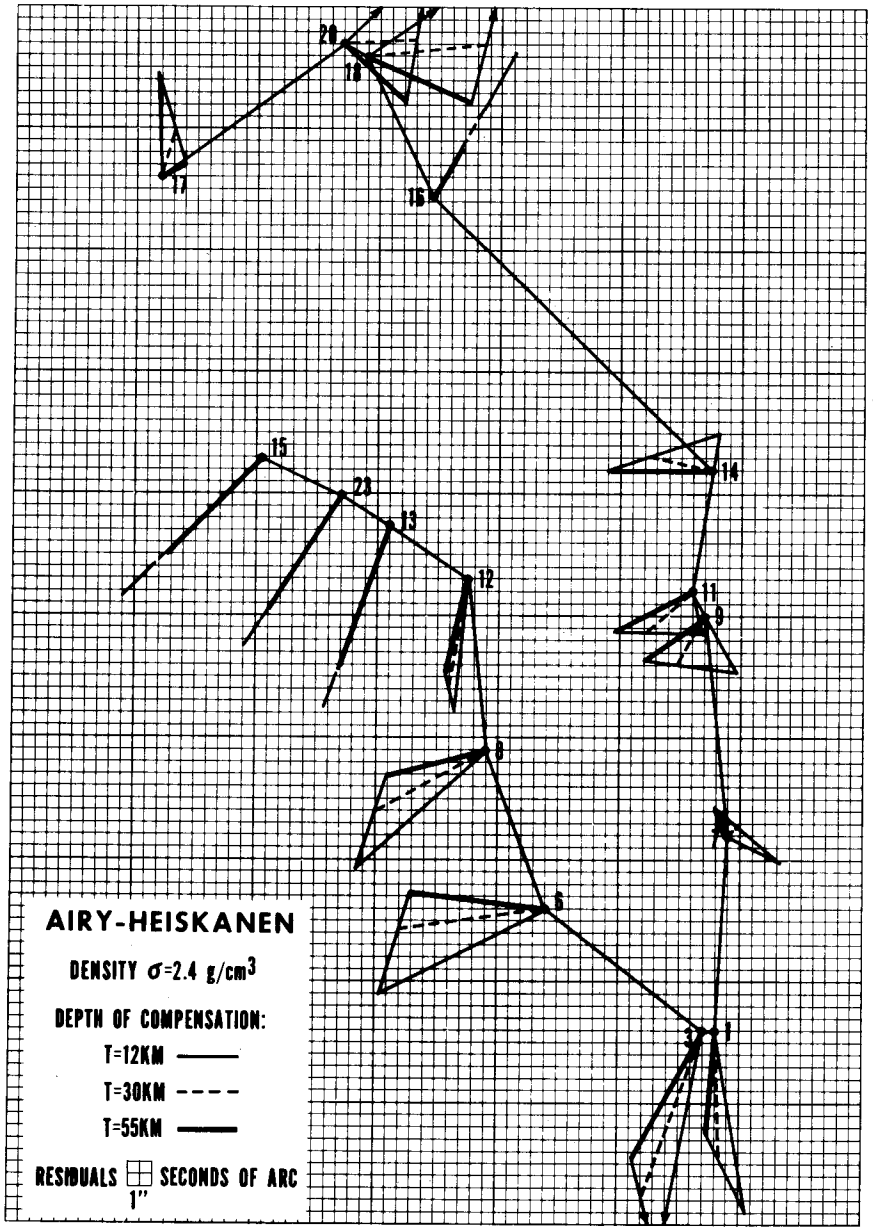

Figure 5. Airy-Heiskanen Residuals for Various Depths of Compensation

rather than up. Residuals in Table 2 are less attractive than those in Table 1.

It appears that further improvement would come from considering the different behaviour of the different regions.

TABLE 2. Airy-Heiskanen Isostatic Models
Residuals for Various Depths of Compensation

σ =2.4	T=12 km		T=30 km		T=55 km	
Sta	v_ξ"	v_η"	v_ξ"	v_η"	v_ξ"	v_η"
1	-7.51	+1.13	-5.50	+0.13	-4.29	-0.26
3	-9.15	-1.66	-7.09	-2.43	-5.83	-2.71
6	-3.49	-6.78	-0.89	-5.91	+0.69	-5.52
7	-1.31	+2.29	+0.29	+0.39	+1.22	-0.62
8	-4.81	-5.32	-2.41	-4.52	-1.03	-4.19
9	-2.30	+1.29	-2.06	-1.15	-1.87	-2.55
11	-1.81	+0.37	-1.73	-2.01	-1.62	-3.39
12	-5.40	-0.59	-4.30	-0.72	-3.68	-0.85
13	-7.50	-2.67	-6.39	-2.29	-5.81	-2.10
14	+1.51	+0.37	+0.47	-2.62	-0.09	-4.33
15	-5.70	-5.74	-4.54	-4.69	-4.06	-4.04
16	+6.06	+3.35	+3.55	+1.90	+2.00	+1.15
17	+4.24	-0.13	+1.96	+0.50	+0.54	+1.07
18	+3.93	+5.52	+0.44	+4.73	-1.86	+4.29
20	+3.74	+3.47	+0.13	+2.83	-2.21	+2.48
23	-6.24	-4.00	-5.18	-3.39	-4.69	-3.04
a	4.6	2.8	2.9	2.5	2.6	2.7
b	1/16	6/16	5/16	5/16	5/16	5/16

a = Σ |v| / 16
b = number of |v| $\leq$ 1.5" out of 16 cases

4. Other Density Models

Since the practical goal of this study and the degree of its success lies in small residuals (what is small?), the residuals themselves may help to define a density model that will decrease them further. This approach permits to accommodate the apparent differences of specific regions.

Figure 6 shows the residuals due to the "visible" topography down to a depth of 5 km, assuming 2.4 as the "best" overall rock density. The direction and magnitude of the residual vectors point to or from additional mass deficiencies or excesses that would counteract these vectors. A deepening of the sediment layer into the basalt below 6 km depth (see Fig.4) would constitute a mass deficit against the model, with a density difference $\Delta\sigma$ = 2.4 - 2.98 = -.58. Similarly, a deepening of the basalt beyond the 12 km depth would act as a deficiency of $\Delta\sigma$ = 2.98 - 3.3 = -.32. A mass excess

could be produced by letting the ultrabasic rock come up above the 12 km line with a density difference of +.32 or by letting the basalt come up above the 6 km line with a density difference of +.58. In the latter case one must take care not to contradict the map readings of the water depths. A little inspection with some simplified computational experimentation placed some hypothetical yet reasonable "holes" H and "loads" L where the residual vectors seemed to indicate (Fig.6).

Obviously, the choices are not unique; while some are clearly better than others, some are also equivalent. A large mass at the 12 km density discontinuity may have the same deflection effect as a smaller mass at the 6 km level, and so on. Table 3 gives the details of one choice of a fairly obvious and simple combination of such holes and loads, all on the 6 km level. For simplicity, they were treated as point masses at the center of the layer.

TABLE 3. A Tentative Density Model

Feature	Position of Center horizontal	vertical	Thickness	Horizontal Extent	Density Difference
Hole 1	see Fig.6	- 8 km	4 km	12' x 12'	-.58
Hole 2	"	- 8	4	8' x 8'	-.58
Load 1	"	- 5	2	8' x 8'	+.58
Load 2	"	- 5	2	10' x 10'	+.58
Load 3	"	- 5	2	6' x 6'	+.58

The cumulative effect on the residuals of adding one such point mass after another is given in Table 4 and in Figure 6, showing a dramatic improvement. In 23 of the 32 cases the error is within 1.5", with none larger than 2.9". No optimization was applied, although it is clear that further refinements could be made.

Seven additional observed deflection stations were used as test points for this preliminary model. Table 5 shows an r.m.s. error of 1.17" in each component at these test points.

5. Conclusions

This study showed that bathymetric data can be utilised to compute deflections of the vertical with an r.m.s. accuracy of about 1½" or better in each component, as tested against observed deflection values. This result compares favourably with the current attempts to observe deflections at sea, with an accuracy of ± 12" so far.

Considering modern techniques of ocean bottom mapping, one can expect even better results from these than from the maps which were available for this pilot study. Although the numerical results must be considered preliminary, the feasibility of the bathymetric method has been demonstrated. Geophysical interpresentation and a distinction between several possible density models will have to

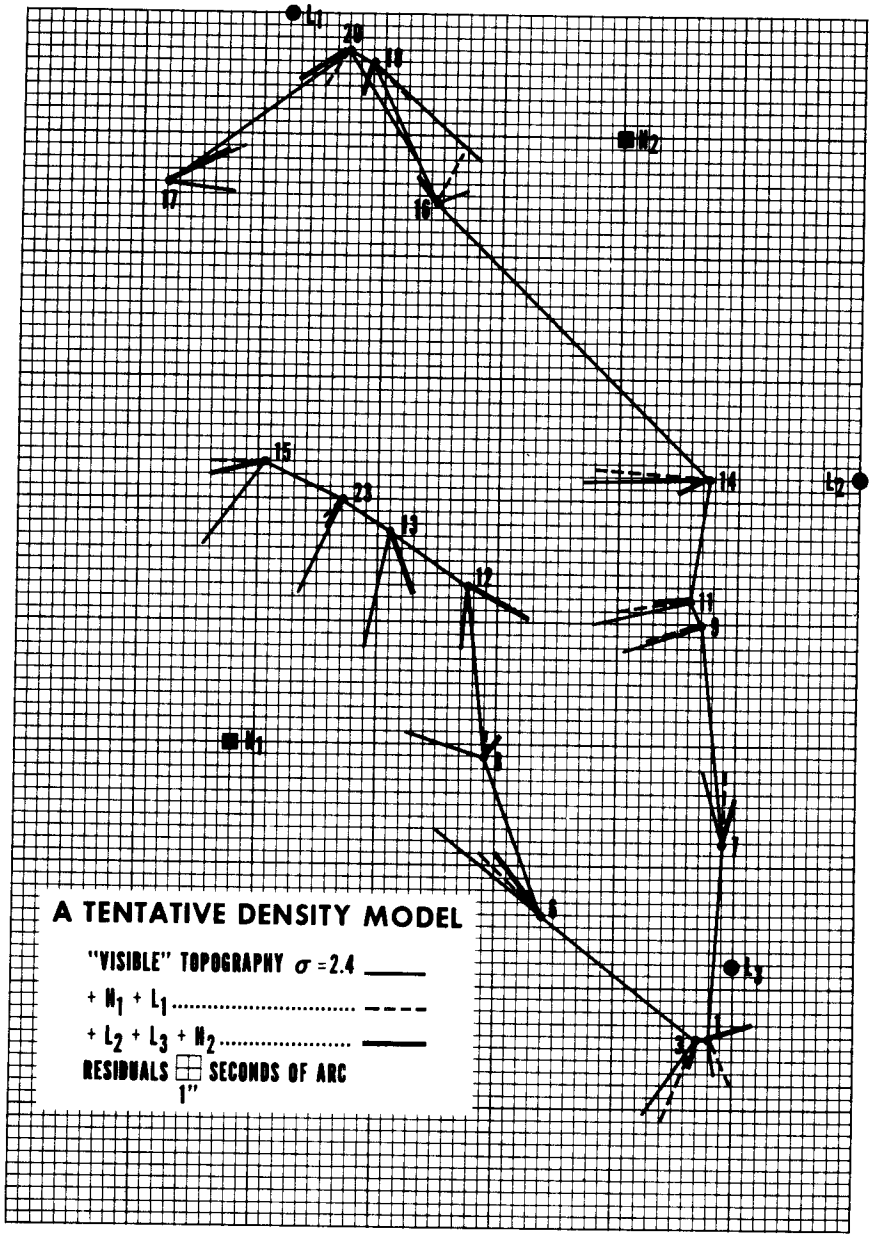

Figure 6. Residuals from a Combination of Point Masses

TABLE 4. Effect of a Tentative Density Model

Residuals from a Combination of Point Masses

Sta	"Visible" Topography σ =2.5 v_ξ''	"Visible" Topography σ =2.5 v_η''	"Visible" Topography σ =2.4 v_ξ''	"Visible" Topography σ =2.4 v_η''	+ H_1 v_ξ''	+ H_1 v_η''	+ L_1 v_ξ''	+ L_1 v_η''	+ L_2 v_ξ''	+ L_2 v_η''	+ L_3 v_ξ''	+ L_3 v_η''	+ H_2 v_ξ''	+ H_2 v_η''
1	-0.23	-0.40	-1.62	+0.18	-2.04	+0.88	-1.99	+0.86	-1.72	+0.93	+0.54	+1.72	+0.49	+1.73
3	-1.65	-2.40	-3.10	-2.16	-3.54	-1.44	-3.49	-1.46	-3.22	-1.38	-1.09	-0.32	-1.24	-0.31
6	+5.19	-3.21	+3.44	-4.39	+2.54	-2.73	+2.61	-2.75	+2.87	-2.56	+2.69	-1.85	+2.49	-1.87
7	+3.86	-2.28	+3.06	-0.89	+2.87	+0.10	+2.93	+0.07	+3.50	+0.28	+1.95	+0.43	+1.72	+0.47
8	+1.99	-1.74	+1.11	-3.15	+0.95	+0.17	+1.05	+0.14	+1.30	+0.48	+1.11	+0.71	+0.82	+0.65
9	-1.12	-4.82	-1.08	-3.25	-0.81	-2.21	-0.72	-2.27	+0.51	-0.94	+0.23	-0.91	-0.24	-0.83
11	-0.98	-5.41	-0.94	-4.06	-0.61	-3.01	-0.51	-3.08	+0.59	-1.54	+0.35	-1.51	-0.16	-1.43
12	-1.73	+0.52	-2.54	-0.21	-0.99	+2.12	-0.83	+2.07	-0.68	+2.60	-0.81	+2.69	-1.29	+2.53
13	-3.57	-0.29	-4.79	-1.11	-2.27	+0.76	-2.06	+0.72	-2.01	+1.13	-2.09	+1.20	-2.56	+0.92
14	-0.99	-7.19	-0.17	-5.38	+0.25	-4.62	+0.36	-4.72	+0.36	-1.54	+0.22	-1.53	-0.62	-1.31
15	-1.87	-1.83	-3.21	-2.47	-0.37	-2.16	-0.08	-2.15	-0.09	-1.89	-0.14	-1.84	-0.47	-2.20
16	-0.78	-0.06	+0.60	+1.20	+1.34	+1.48	+2.07	+0.89	+1.88	+1.19	+1.83	+1.21	+1.13	-0.77
17	-1.82	+3.19	-0.39	+2.64	+0.43	+2.53	+1.42	+3.24	+1.36	+3.39	+1.33	+3.41	+1.27	+2.89
18	-5.86	+3.83	-3.92	+4.55	-3.37	+4.66	-1.59	+1.55	-1.73	+1.72	-1.76	+1.73	-1.38	+0.39
20	-6.45	+2.41	-4.36	+2.80	-3.82	+2.88	-1.42	-1.11	-1.55	-0.95	-1.58	-0.94	-1.23	-2.08
23	-2.52	-1.13	-3.78	-1.85	-0.95	-0.57	-0.70	-0.60	-0.68	-0.26	-0.75	-0.20	-1.18	-0.53
a	2.5	2.5	2.4	2.5	1.7	2.0	1.5	1.7	1.5	1.4	1.2	1.4	1.1	1.3
b	5/16	5/16	6/16	5/16	9/16	7/16	9/16	8/16	8/16	9/16	10/16	8/16	13/16	10/16

a = $\Sigma |v| / 16$

b = number of $|v| \leq 1.5''$ out of 16 cases

TABLE 5. Seven Test Points

Model: Density 2.4, Two "Holes" and Three "Loads"

Station	Observed Deflection ξ''	Observed Deflection η''	Residuals v_ξ''	Residuals v_η''
2	- 23.59	+ 11.69	- 0.80	+ 1.86
4	- 23.79	+ 6.95	- 0.45	+ 0.72
5	- 21.82	+ 11.73	+ 1.41	+ 1.91
10	+ 0.05	+ 21.11	+ 1.81	- 0.37
19	+ 28.89	+ 10.49	+ 0.21	+ 0.09
21	+ 26.27	+ 10.14	- 1.87	- 1.28
22	+ 28.75	+ 11.16	+ 0.03	+ 0.50
$\Sigma \|v\|/7$			0.94	0.96
r.m.s.			1.17	1.17

wait, however, until the truncation error due to the limits of the data area has been sufficiently reduced.

6. Acknowledgment

Mr Philip Y. WYATT III, Defense Mapping Agency Topographic Center, assembled the data tapes from 14 000 readings and carried out the computations on the UNIVAC 1108.

7. References

FISCHER, I. 1966. Slopes and curvatures of the geoid from gravity anomalies by electronic computer. *J.Geophys.Res.* 71, 4909.

HEISKANEN, W.A. & VENING MEINESZ, F.A. 1958. *The earth and its gravity field.* McGraw-Hill, New York.

MOURAD, A.G. 1972. Marine geodesy 1967 - 1971, IAG Special Study Group I-25. *Travaux de l'Ass. Int.de Géod.* Tome 24, Paris.

STRAHLER, A.N. 1971. *The Earth Sciences.* 2nd ed. Harper & Row, New York.

8. Discussion

KAULA: On the question of determining gravity anomalies from the topography at sea with a wavelength of a couple of hundred kilometres. I was wondering if you had considered using a regional type of isostatic compensation?

FISCHER: Yes, I did. I had started with the usual approach given in the textbooks: local compensation and regional. The Vening Meinesz regional compensation was considered at length but was put aside for the moment because the differences in results as compared to the other hypotheses were too small to explain the large residuals. I had bigger problems at that stage as the effect of various density models on the residuals is larger than the fine distinction between local compensation and regional, with the data used so far. When I started, it was thought that computing the deflections from mass attractions should tell us what type of compensation applied here. Maybe it will later on, after we have studied further the effect of truncating the data area, and of various density distributions.

BOMFORD: I do not quite understand how you locate your masses.

FISCHER: This is obtained from the residual vectors (Observed minus Computed): if that vector is large, and since the observed values cannot be changed, you have to make another assumption about the computed value. A mass excess or mass deficiency is added to the model to make the residual smaller. The vector points towards the area where a deficiency is needed to make that vector smaller. A point mass is placed there, which could be spread out later to make it more realistic, if one wants to. The point mass is assumed to be of a certain size, say a 10' × 10' square and a specified density difference, located at the centre of the mass column; and the resulting effect studied. It is a little trial and error, but using simple computation which does not require a big computer.

BOMFORD: You did a number of computations, iterating to make your residuals as small as possible?

FISCHER: Theoretically you could do so by making a lot of such assumptions. That is why I didn't pursue it any further beyond using just big ones - five of them - that have major effects. Hundreds could be used if desired, but of very local effect which would not help you predict effects elsewhere. Some conclusions can be drawn from the major effects: there is either some deficiency here or excess there; and there is some isostatic compensation. One could combine such findings, for example with the Vening Meinesz regional model or some other hypothesis so that the residuals would be small. Then one could try some geophysical interpretation. While that is premature, I was careful not to put any deficiency or excess arbitrarily which might contradict other evidence such as the depth readings from the maps.

GRAFAREND: How did you define your datum?

FISCHER: The datum of the astrogeodetic deflections is a given local datum. This is not the same datum as the one corresponding to the computations of mass attractions. I considered changing to a world datum or a regionally well-fitting datum. Since the Earth is practically flat for such a small region, such a datum transformation amounts to a constant correction of, say, about 3" in latitude and longitude to the given deflection values. One can apply a tentative correction on this account to begin with, or one can leave it for the inspection of the residuals. If the residuals were constant (rather than near zero), they could be interpreted as a datum shift. If the purpose is the interpolation of astrogeodetic deflections, such constant correction is taken care of within the interpolation process.

DOOLEY: Is there any gravity information in the area in which you are working?

FISCHER: Yes, but not enough for a computation of gravimetric deflections.

KEARSLEY: I would be interested to know how the station geodetic position was found.

FISCHER: There is a first order survey on a local datum. That survey connects all these islands and the positions are internally consistent. There are also some geoceiver stations. We checked the distances between these with the survey and they agreed. So we believe the claim that the survey is first-order.

RAPP, R.H.
Department of Geodetic Science
The Ohio State University
Columbus Ohio 43210
United States of America

Proc.Symposium on Earth's Gravitational Field & Secular Variations in Position (1973),51-75.

THE EARTH'S GRAVITATIONAL FIELD FROM THE COMBINATION OF SATELLITE AND TERRESTRIAL DATA *

ABSTRACT

This paper reviews techniques and results in the combination of gravimetric and satellite data. The first section of the report deals with theoretical procedures, while the second section deals with current solutions. In the first section, the estimation of mean anomalies for use in combination studies is discussed with the location of current gravity material being described. Specific techniques for combination solutions are discussed for various models. These models include those where the gravitational field is represented by a set of potential coefficients, or by a set of discrete blocks distributed on the Earth. The potential coefficient solutions compared are those of the SAO Standard Earth II and III, the Goddard Earth Model 6 (GEM 6) and a solution by the author. These solutions are compared in terms of root mean square coefficients,undulations and anomaly differences, and implied anomaly degree variances. In addition, comparisons were made through terrestrial anomaly comparisons, astro-geodetic undulation comparisons and orbit fitting tests. Some solutions compared reveal certain solutions to be better for some purposes than others.

1. Introduction

The purpose of this paper is to discuss some of the procedures used for the combination of gravimetric and satellite data and to compare some of the current solutions that attempt to describe the Earth's gravitational field.

We should first define what we mean by the Earth's gravitational field. We note first that in some cases it is convenient to talk about the gravity field of the Earth instead of the gravitational field. Gravity and gravitation are related in that gravity, for a point rotating with the Earth, is the vector sum of the gravitational attraction and the centrifugal force. For points located on the surface of the Earth we are primarily concerned with gravity while for points located at satellite altitude we are interested in the gravitational field.

On the surface of the Earth we can determine gravity by making measurements of its normal component (using gravimeters) and its other components through the determination of the deflection of the vertical. Primarily, however, we can consider that we can determine the normal component of gravity at various discrete points on the surface of the Earth. These points may be located on the land, on the oceans, on ocean bottoms, or (in a few cases) at points of aircraft altitude. (Here we should note that measured gravity is a function not only of the Earth's attracting masses and centrifugal force, but also is effected by lunar and solar tides, by Earth tides, and to a very minor extent, the atmosphere. Formally, these latter effects are removed from measured gravity to yield a result independent of these quantities.) If we could obtain a dense global coverage of point gravity measurements we could say that the gravity field on the Earth has been determined and through the application of suitable equations, the gravitational vector at points in space could be determined (HEISKANEN & MORITZ 1967,chapter 5). Unfortunately the area gravity coverage for the Earth is not complete with

* Revised January 1974

wide areas (especially in some oceanic areas) having little gravity data, or data not generally available to the scientific community. A discussion of gravity measuring techniques may be found in HEISKANEN & VENING MEINESZ (1958) while a discussion on the utilization of gravity data for various geodetic purposes may be found in HEISKANEN & MORITZ (1967).

This lack of data had prevented an accurate analysis of the broad variations of the Earth's gravity field until artificial satellites were launched. A satellite moves within the gravitational field of the Earth (plus other forces, of course). Observing the precise motion of the satellite allows us to infer information with respect to the Earth's gravitational field. Since a satellite's position will be perturbed only in a minor way, due to local gravity irregularities, we generally think of the analysis of satellite information being used to determine the broader variations of the Earth's gravitational field. (These statements do not consider new satellite observation techniques such as satellite-to-satellite tracking, or satellite gradiometry that provide a measurement at satellite altitudes, of quantities that depend on the gravity field of the Earth.) A discussion on how a satellite's motion depends on the Earth's gravitational field may be found in (KAULA 1966a), or (MUELLER 1964).

If we say that the local variations of the Earth's gravity field are best determined by direct gravity measurements, and that the broad variations are determined through the analysis of satellite motion, the most complete description of the Earth's gravitational field must come from some combination of the two techniques.

This paper specifically concerns itself with some of the techniques used for this combination. I will not attempt to analyze all techniques used for combination solutions. Rather, I will discuss certain techniques that are currently being used, with appropriate references to other pertinent papers when necessary.

2. Gravity Material

Discrete measurements of gravity (g) are generally converted to gravity anomalies, Δg, by subtracting from the observed gravity some reference gravity due (generally) to an equipotential rotational ellipsoid. We have

$$\Delta g = g' - \gamma \qquad (1),$$

where g' is the observed gravity reduced to some reference surface. In most applications carried out to date, this reference surface has been taken to be the geoid with no masses external to it. The specific way in which the reduction is done in obtaining g' from g will yield different types of anomalies. The starting anomaly for use in combination studies is the free-air anomaly. For this and other types of anomalies, see (HEISKANEN & MORITZ 1967, chapter 3). (We will discuss later modifications to the free-air anomaly for more precise statements of the combination procedures.)

The discrete anomalies available on the surface of the Earth are not directly usable for most combination solutions. (However, BJERHAMMAR (1963) has, for example, proposed to use discrete values for some purposes.) Because of this, the anomalies are formed into values representative of various size areas on the Earth's surface. We write:

$$\overline{\Delta g} = \frac{1}{A}\iint_A \Delta g \, dA \qquad (2),$$

where $\overline{\Delta g}$ is the mean anomaly in a block whose area is A. Usually A is defined to be an area bordered by meridians and parallels. These areas (or blocks) may be equiangular (such as 1° × 1°) or equal area (RAPP 1971a) in size. For a given basic block area there will be fewer equal area blocks than equiangular blocks on the surface of the Earth. Thus, for computational efficiency and statistical effectiveness, it is most efficient to use equal area blocks in combination studies. However, the gravity data used in recent combination studies has been supplied in 1° × 1° blocks (ACIC 1971). Such blocks need to be used in the estimation and prediction of mean anomalies in five degree equal area blocks, The larger size blocks are currently used in some types of combination studies. Other types of combination work use mean anomalies in ten degree and fifteen degree blocks (HAJELA 1973). The estimation of the five degree equal area blocks from the 1° × 1° data requires several decisions on the appropriate procedure. KAULA (1966b) used a linear regression technique to determine five degree equal area anomalies based on 1° × 1° data. RAPP (1972a) used a modification of Kaula's work that carried out anomaly prediction, and the prediction accuracy considering the location of the 1° × 1° anomalies within the 5° equal area blocks, as well as the accuracy of the 1° × 1° data. The specific procedure used is as follows. The 1° × 1° means were first formed into mean anomalies for areas 60 nautical miles (nm) (in latitude) and 60±30 nm (in longitude). These anomalies were then used to estimate the mean anomalies in 300 nm (in latitude) and 300±30 nm (in longitude) blocks by predicting, in the 300 nm block any missing 60 nm blocks by linear regression. The 300 nm mean anomaly was then formed as a straight average of the 25, 60 nm blocks in the 300 nm blocks. No estimations were made for a 300 nm block unless it contained one or more observed 60 nm blocks.

The specific equation used for predicting a 60 nm anomaly (g*) was given by MORITZ (1969):

$$g^* = \underline{C}_p (\underline{C} + \underline{D})^{-1} \underline{g} \qquad (3),$$

where $\underline{C}_p$ is a column vector whose elements are the covariance between the block (p) to be predicted and the observed anomalies; $\underline{C}$ is a matrix whose elements are the covariances between the observed anomalies; $\underline{D}$ is an error covariance matrix for the observed anomalies; and $\underline{g}$ is a column vector of the observed anomalies within the 300 nm block in which g* was situated. For these computations $\underline{D}$ is taken as a diagonal matrix with each diagonal element being equal to m_j^2, where m_j is the standard deviation of the observed anomaly g_j. The standard deviation (m) of the 300 nm anomaly was computed from (IBID,p.11)

$$m^2 = \overline{\overline{C}} - \underline{\overline{C}}_i (\underline{C} + \underline{D})^{-1} \underline{\overline{C}}_i \qquad (4),$$

where $\overline{\overline{C}}$ is the mean square value (or variance) of the 300 nm mean anomalies, and $\underline{\overline{C}}_i$ is a column vector representing the covariance between the i-th observed anomaly and the 300 nm block in which it lies.

The above equations were applied to a set of 23,355 1° × 1° anomalies which were based on a set of 1° × 1° anomalies of ACIC (1971) supplemented by additional material not present in the ACIC set. For example, using data not made available by ACIC, 323 ACIC anomalies in the Canadian area were replaced by updated values, and 1989 new, 1° × 1° values in the Canadian area were added. This data enables the prediction of 1283, 5° equal area anomalies and their accuracy. The location of these blocks is shown in figure 1. Since these predictions have taken place, new gravity material has

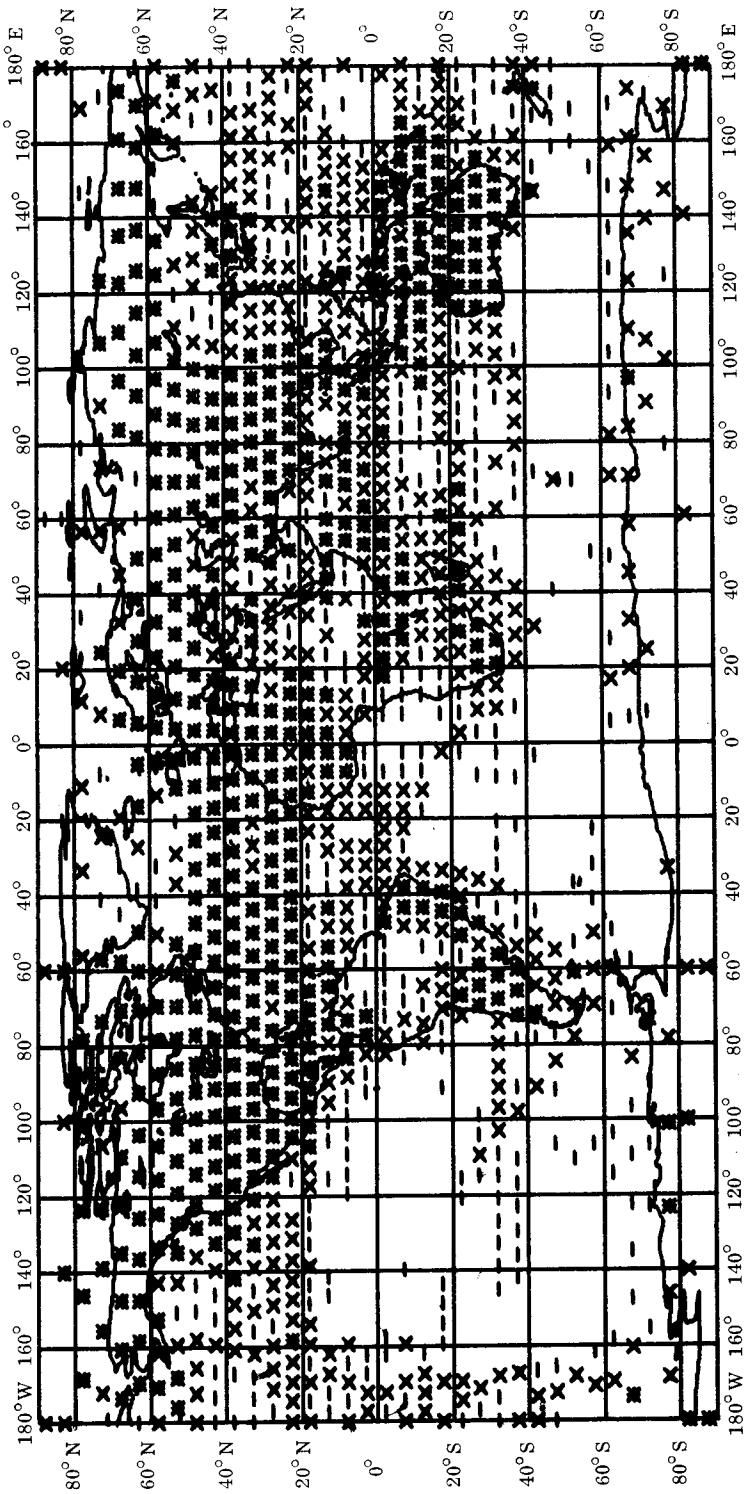

Figure 1. Quality and Distribution of Terrestrial Gravity Data Used by RAPP (1972a)
(Symbols are Located at the Centre of the 5° Equal Area Blocks)

become available in several areas. One large block of data are the results from Project SEAMAP of the National Geodetic Survey.

The procedures described above are only one of several that have been used by various investigators. More sophisticated techniques are possible. For example, the use of a localized covariance as opposed to global functions in developing the C matrices of equations 3 and 4 may lead to more precise estimates of some quantities. However, RAPP (1964) found that localized covariances did not yield significantly different anomaly predictions but did yield different anomaly standard deviation predictions. The inclusion of more 60 nm anomalies in the prediction of a 300 nm mean may be warranted but the resultant error correlation between the 300 nm blocks may cause more problems than is worth. The studies of GROTEN (1966) indicate the addition of known anomalies somewhat distant from anomalies to be predicted have little influence on the predicted anomaly.

Since we do not have global gravity coverage, a decision must be made for combination solutions as to what anomalies should be assigned (if any) for these empty areas. (Some combination methods do not require global estimates for the terrestrial gravity field. However, to assure that distortion - in terms of geoid heights or anomalies - is not given to the empty areas, it is usual practice to utilize global anomaly estimates in any combination solution.) The estimation of anomalies in unsurveyed areas is a field of study in itself (ORLIN 1966) which will not be gone into here. For recent combination solutions the following procedures may be found:

1) estimation of empty areas by linear regression from known 5° equal area anomalies (KAULA 1966a);
2) incorporation of model anomalies computed on the basis of topography and an isostatic hypothesis (RAPP 1968);
3) computing anomalies from a set of potential coefficients derived from satellite orbital analysis (KÖHLNEIN 1967); and
4) setting the anomalies in the unsurveyed areas to zero with large standard deviations (GAPOSCHKIN & LAMBECK 1971).

The linear regression is valuable because of its well defined applicability. However, its accuracy is subject to how well is the linear regression model formed (e.g., is the correlation of free air anomalies with topography considered) and how strong are the correlations between the known anomalies and the anomalies to be predicted. The model anomalies are useful as they incorporate independently estimated data (such as topographic heights). They may not reflect actual mass anomalies. The use of satellite anomalies in the empty areas is fine when we can ignore the havoc that such a procedure raises in trying to carry out a rigorous least squares solution. The use of a zero anomaly admits our ignorance and keeps the combination solution from "blowing up" in the empty areas if no other information were used.

3. Satellite Data

The fundamental satellite observations are the direct observation of satellites. These observations include those of right ascension and declination, range, and range-rate (or some function of range-rate). This data is generally processed to extract gravitational field information (as well as station co-ordinates, tidal parameters, orbital parameters, etc.). This gravitational field information is then combined with terrestrial gravity information in a variety of ways which are discussed

in the following section.

4. Combination Methods

There are many methods to combine satellite and terrestrial gravity data. A summary of some of these may be found in (HOPKINS 1972). Space does not permit a discussion of all methods nor complete details of methods to be described. Basically, there are two types of combination methods that differ in the manner in which the gravitational field is represented. The first method represents the Earth's gravitational field using potential coefficients while the second method uses discrete blocks on the surface of the Earth.

4.1 Combination Methods Using Potential Coefficients

We represent the Earth's gravitational potential (V) by a set of fully normalized potential coefficients $(\overline{C}_{\ell m}, \overline{S}_{\ell m})$ as follows:

$$V = \frac{kM}{r}\left(1 + \sum_{\ell=2}^{\infty}\left(\frac{a}{r}\right)^{\ell}\sum_{m=0}^{\ell}\left(\overline{C}_{\ell m}\cos m\lambda + \overline{S}_{\ell m}\sin m\lambda\right)\overline{P}_{\ell m}(\sin\overline{\Phi})\right) \qquad (5),$$

where: kM is the geocentric gravitation constant;

r is the geocentric latitude
$\overline{\Phi}$ is the geocentric latitude
λ is the longitude
} of the point at which V is being computed;

a is a nominal equatorial radius; and

$\overline{P}_{\ell m}$ are the fully normalized associate Legendre functions.

Potential coefficients can be related to gravity anomalies in two ways. The first is through the following equation:

$$\begin{pmatrix}\overline{C}_{\ell m}\\ \overline{S}_{\ell m}\end{pmatrix} = \begin{pmatrix}\overline{C}_{\ell m}\\ \overline{S}_{\ell m}\end{pmatrix}_{ref} + \frac{1}{4\pi\gamma(\ell-1)}\iint_{\sigma}\overline{\Delta g}\begin{pmatrix}\cos m\lambda\\ \sin m\lambda\end{pmatrix}\overline{P}_{\ell m}(\sin\overline{\Phi})\,d\sigma \qquad (6)$$

where: $(\overline{C}_{\ell m}, \overline{S}_{\ell m})_{ref}$ are potential coefficients implied by the reference figure (or gravity formula) to which the mean anomalies $\overline{\Delta g}$ (given as blocks $d\sigma$) are referred to. When the anomalies are referred to a rotational equipotential ellipsoid gravity formula, all $(\overline{C}_{\ell m}, \overline{S}_{\ell m})_{ref}$ are zero except for $\overline{C}_{\ell 0}$ when ℓ is even. In that case the reference values of $\overline{C}_{\ell 0}$ with $\ell > 4$ are generally considered negligible. The integration in equation 6 is taken over the Earth which is here approximated by a spherical surface. Equation 6 follows from the discussion in (HEISKANEN & MORITZ 1967, section 2-20).

The combination adjustment is carried out by estimating $\overline{\Delta g}$ values and their standard deviations from terrestrial gravity material, and by taking values of the potential coefficients and their standard deviations from satellite analysis. Then equation 6 is used as a mathematical model to formulate a weighted least squares adjustment where the following quantity is minimized:

$$V_g' D_g^{-1} V_g + V_c' D_c^{-1} V_c \qquad (7),$$

where V_g and V_c are the residual vectors for the gravity anomalies and potential coefficients, and

D_g and D_c are the variance-covariance matrices of the observed anomalies and the a priori known potential coefficients.

The details of the adjustment procedure using this method are found in (RAPP 1969a). The first computation using this approach was done by KAULA (1966b) where an adjusted set of potential coefficients complete to $\ell = 6$ plus some additional terms were sought. The results of this method will be a set of adjusted potential coefficients and a set of mean gravity anomalies consistent with the adjusted potential coefficient set, yet retaining the greater detail that would exist in anomaly blocks smaller than that defined by a set of potential coefficients solved for up to a degree less than $180°/\theta°$, where θ is the block size in which the $\overline{\Delta g}$ values are given.

Anomalies and potential coefficients may also be related by the following equation (RAPP 1967)

$$\Delta g = \frac{kM}{r^2} \sum_{\ell=2}^{\ell_{max}} \left(\frac{a}{r} \right)^{\ell} (\ell - 1) \sum_{m=0}^{\ell} \left(\overline{C}^{*}_{\ell m} \cos m\lambda + \overline{S}_{\ell m} \sin m\lambda \right) \overline{P}_{\ell m}(\sin \overline{\phi}) \qquad (8),$$

where ℓ_{max} is the maximum degree for which potential coefficients are to be found or are given. $\overline{C}^{*}_{\ell m}$, $\overline{S}_{\ell m}$ are the potential coefficients referred to an ellipsoid whose flattening is specified. Actually, equation 8 does not give the standard anomaly, but rather the anomaly component in the radial direction. The difference is insignificant (RAPP 1972b). In some combination studies spherical approximations to equation 8 have been used by letting r be a mean radius (R) of the Earth. Considering the accuracy of current gravity material such approximations do not appear critical.

Knowing terrestrial estimates of $\overline{\Delta g}$ and **a** priori values (from satellite analysis) of the potential coefficients, equation 8 may be used as a mathematical model to obtain weighted least squares estimates of the potential coefficients under the same condition as specific in equation 7. The details of the adjustment procedure are given in (RAPP 1969a). This method was used by RAPP (1968) to obtain adjusted potential coefficients to $\ell = 14$ plus some additional terms.

It should be noted that both equations 6 and 8 can be used to determine potential coefficients given only terrestrial gravity material. Whether these equations are used in this manner, or as the foundation for a combination solution, the results for the two methods (assuming equivalent spherical approximations) will be different unless all anomalies (given in equal area blocks) have the same standard deviations (RAPP 1969a).

PELLINEN (1965; 1969) also discusses combination solutions using equations similar to 6 or 8.

The exclusive use of equations 6 or 8 ignores the fact that satellite estimated potential coefficients are not estimates independent of other unknowns such as station co-ordinates and parameters dependent on the satellite orbit (such as initial condition, drag effects, etc). To consider this information we consider two sets of normal equations, one arising from the satellite adjustment and the other arising from the potential coefficient solution from terrestrial data using equation 8. We have:

$$q N_{S,X} X + (q N_{S,P} + N_G) P = q U_S + U_G \qquad (9),$$

where X are station co-ordinate parameters, P are the potential coefficient parameters, $N_{S,X}$ are the normal equations for the station co-ordinates from the satellite data; $N_{S,P}$ and N_G are the normal

equations for the potential coefficients from the satellite and terrestrial gravity data respectively. U_S and U_G are the constant vectors of the normal equation, q is a scaling parameter used to provide the most effective weighting between the satellite and terrestrial information. Equation 9 is solved to obtain the X and P vectors. The arc (or orbit) dependent parameters do not appear in equation 9 as they are usually eliminated by the technique described by KAULA (1966a,p.105). The combination technique represented by equation 9 with some version of 8, has been used by GAPOSCHKIN & LAMBECK (1971), LERCH ET AL (1972a;1972b) and GAPOSCHKIN (1973). BJERHAMMAR (1969) gives a more general view of combining data from different satellite solutions where he shows how observation and/or normal equations may be combined to determine station co-ordinates and potential coefficients on a basis of normal equations supplied by different investigators.

The preceding method has only used gravity information to infer information with respect to potential coefficients. However, gravity data may also be used to determine deflections of the vertical and geoid undulations which may be used to determine geocentric station positions. This additional information can be incorporated into a combined solution with satellite data to determine not only station positions and potential coefficients but datum shifts and an equatorial radius. This general method is described by RAPP (1971b) with computer programs for the implementation of the method given by GOPALAPILLAI ET AL (1971). To date no results from this procedure have been published.

FISCHER (1968a;1968b) and GROTEN (1970) have described techniques where astro-geodetic undulation solutions can be incorporated in combination solutions. Although no numerical results were given by Groten, Fischer computes a set of potential coefficients to degree 13. Because of the non-global extent of astro-geodetic undulation, the development of global information from them is more a theoretical procedure than a practical one.

MORITZ (1970) derived a procedure that can be used for a combination solution using the concept of least squares collocation. In this type of solution, the quantity minimized is

$$s' C^{-1} s + V_g' D_g^{-1} V_g + V_c' D_c^{-1} V_c \qquad (10),$$

where s is the signal array and C is the covariance matrix of the signal. When a combination solution using equation 6 is considered, the signal array corresponds to the gravity anomalies. When equation 8 is used, the signal is considered to be the potential coefficients. In this latter case the relationship between a set of potential coefficients, p_o, estimated under the usual least squares principle (equation 7) can be related to a set, p, determined from the least squares collocation principle through :

$$p = (I + N^{-1} C^{-1})^{-1} p_o \qquad (11),$$

where N are the coefficients of the unknowns (NX = U) in the usual least squares solution (where N contains a priori information on the estimated potential coefficients) and C is the covariance matrix between the potential coefficients that are being estimated.

4.2 Combination Methods Using Discrete Representation of the Earth's Gravitational Field

The use of a spherical harmonic expansion to represent the Earth's gravitational field has played the major role in combination solutions because of the advantageous manner in which the potential coefficients can be used for satellite orbital analysis (KAULA 1970). However, for future data acquisition schemes and as an independent alternative to potential coefficients, it is reasonable to consider the

surface of the Earth (or some approximation to it) divided into discrete areas for which a function related to the Earth's gravitational field is to be determined.

In 1965, Arnold proposed a method where gravity anomalies in discrete blocks could be determined throught the analysis of the orbital variations of various satellites. In this procedure the perturbations on the orbital elements were related to the gravity anomalies through the generalized Stokes' equation and its derivatives. In the Arnold procedure, known anomalies were held fixed in solving for a limited number of anomalies considered as unknowns. Additional details may be found in (ARNOLD 1966; ARNOLD 1972).

OBENSON (1970; 1972) extended the idea of Arnold to the extent that a global anomaly field could simultaneously be found from a generalized least squares solution with satellite data alone, or in combination with terrestrial gravity material. Obenson's procedure considered the influence of the gravity anomalies on the satellite position expressed through orbital element variations.

KOCH (1968) proposed that the Earth's gravitational field be represented by a low degree set of potential coefficients plus a disturbing potential represented by the potential of a single layer distributed in discrete blocks on the surface of the Earth. The density of the surface layer for each of the blocks can be determined from orbital analysis and in combination with surface gravity material if necessary.

RAPP (1971c) outlined a procedure where the Earth's gravitational field could be represented simply by a set of discrete gravity anomalies. Such anomalies can be determined from orbital analysis or can be solved in a combination solution with observed terrestrial gravity material. As with the Koch solution, a global set of discrete parameters is determined in a generalized least squares adjustment where the terrestrial material is incorporated as a priori information.

For either the Koch or Rapp procedure we may represent a set of satellite observations as follows:

$$O(r_o, \dot{r}_o, t_o, t, R, A, G, P) = 0 \qquad (12),$$

where r_o and $\dot{r}_o$ are the initial position and velocity vectors at time t_o. t is the time from t_o, R represents a reference set of potential coefficients, A are parameters depending on the satellite arc; G are the parameters of the gravitational field, and P are the co-ordinates of the observed station. The unknowns of greatest interest are G and P.

To further consider G, we represent the gravitational potential, W, as a sum of a normal potential due to a low degree reference field and a disturbing potential T.

$$W = U + T \qquad (13).$$

In Koch's case, T is:

$$T = \iint_E \frac{\chi'(\phi,\lambda)}{\ell} dE \qquad (14),$$

where χ' is an auxiliary density of the surface layer (referred to the U field) in a surface element dE and ℓ is the distance between the block and the point at which the evaluation of T is done. In

Rapp's case, T is given by the generalized Stokes' equation (HEISKANEN & MORITZ 1967,p.93):

$$T = \frac{R}{4\pi} \iint_E S(r,\psi^*)\ \Delta g'\ dE \qquad (15),$$

where $S(r,\psi^*)$ is the generalized Stokes' function dependent on the distance from the centre of the Earth to the point at which T is being computed, and ψ^* is the spehrical arc between the element dE on the spherical approximation to the Earth, and the sub-computation point. The anomalies $\Delta g'$ are referenced to the U field.

In order to develop the observation equations for this type of procedure is is necessary to differentiate equations 14 or 15 in three directions to determine the accelerations acting on the satellite due to the density layer or the anomalies. These derivatives can then be used in the variational equations which are numerically integrated (along with the equations of motion of the satellite) to obtain the derivatives of the satellite observation with respect to the gravitational parameters.

For a combination solution with the surface gravity material and the surface density solution, a global terrestrial field must be transformed into surface density values using the following equation (KOCH & MORRISON 1970):

$$\chi = \frac{\Delta g - G}{2\pi} + \frac{3}{(4\pi)^2} \iint (\Delta g - G)\ S(\psi)\ dE \qquad (16),$$

where G is the mean global anomaly. The standard deviations of the χ values can then be determined from an error propagation with equation 16 using the standard deviation of the terrestrial anomalies. This terrestrial derived information may be used as a priori information in a generalized least squares adjustment.

A combination solution with surface gravity material, and the analysis with anomalies incorportaed as unknowns is made simply by adding the a priori anomaly data into the adjustment scheme. No transformation is required. Details of this adjustment are in (RAPP 1971c). For comparisons with the usual potential coefficient determinations, the density values or the anomalies resulting from these discrete block solutions can be converted into potential coefficient sets. In the case of anomalies, equation 6 can be used. In the case of surface density values, the following equation can be used (KOCH & WITTE 1971):

$$\begin{Bmatrix} \overline{C}_{\ell m} \\ \\ \overline{S}_{\ell m} \end{Bmatrix} = \begin{Bmatrix} \overline{C}_{\ell m} \\ \\ \overline{S}_{\ell m} \end{Bmatrix}_{ref} + \frac{1}{(2\ell+1)k\,M\,a^{\ell}} \iint_E \chi'\, r \begin{Bmatrix} \cos m\lambda \\ \\ \sin m\lambda \end{Bmatrix} dE \qquad (17)$$

where the integration is carried out numerically over the blocks used in the solution.

The use of surface density values as unknowns has the advantage of computational simplicity over the use of anomalies in the evaluation of the derivatives needed in the observation equations. In addition, the use of surface density values may have a strong theoretical basis when considered with respect to the assumptions on the use of the generalized Stokes' equation. On the other hand, the use of anomalies as unknowns permits a very simple combination solution to be carried out without the

need for any transformation of data. In addition, any theoretical problems can apparently be resolved by proper interpretation of what anomaly is being found, or what precisely is the anomaly to be used in a combination solution.

4.3 Theoretical Concerns

Further discussion is warranted with respect to some problems connected with the combination procedures discussed in the preceding sections.

Equation 7 has two approximations connected with it. First, the reference surface on which the anomalies are given is assumed spherical. LELGEMANN (1972) gives equations that show how corrections for this assumption can be made and that in fact such corrections are negligible at least up to degree 30. An analogous discussion may be found in OSTACH & PELLINEN (1966) who do not give numerical results. We also have assumed in equation 7 and also in equation 15 that our terrestrial anomalies (or the anomalies being solved for), refer to a spherical surface. In fact, the terrestrial anomalies we use refer to the surface of the Earth. Formally these anomalies may be reduced to a common spherical surface (e.g., the Bjerhammar sphere) using procedures discussed by BJERHAMMAR (1969). PELLINEN (1969) and OSTACH & PELLINEN (1970) indicate that the anomalies, used in formulas such as equation 7, should be $\Delta g + G_1$, where G_1 is the Molodensky correction term, which is near the mean terrain correction for the $d\sigma$ area. Thus, the anomaly to use in the combination studies is not the free air anomaly but rather the Faye anomaly which contains the terrain effect. The large size of the anomaly blocks used to date and the inaccuracy of the terrestrial data, has not warranted such corrections to data (RAPP 1970).

A related concern is often expressed with respect to the convergence at the surface of the Earth, of the spherical harmonic series expressed by equation 8. If the series diverges (which formally it does) some concern is then stated with respect to combination solutions made with terrestrial gravity data given at the Earth's surface. The concern is bypassed by the knowledge that we are not solving for an infinite set of potential coefficients, but rather for a finite set which are being determined from a finite data set.

PELLINEN (1965) also suggests that the G_1 correction be made to the anomalies used in equation 8.

At the current data accuracy level, and in the size of the anomaly blocks being used, and the highest degree to which potential coefficients are being determined, the theoretical refinements considered above are probably not important at this time. On the other hand, PELLINEN (1962) showed that the effect of neglecting the G_1 terms in the coefficient determinations from anomalies may lead to errors on the order of 15-20% for low degree coefficients. Since we purport to know these low degree coefficients to better than this relative accuracy, we need to look in more detail at the case of the G_1 terms in our terrestrial anomaly data. As smaller block sizes are used, with different types of satellite observation data, the precise definition of the boundary value problem as related to satellite and gravimetric data will be needed both in the theoretical and practical sense.One start in this area is the work of BAUSSUS VON LUETZOW (1972).

OSTACH & PELLINEN (1970) continue the discussion on the proper anomalies to be used in determining, in essence, potential coefficients. In this paper, a spherical harmonic expansion of the G_1 correction term is given. Such an expression could be used to determine a global, but smoothed representation of G_1, which in turn could be used to find the corresponding effect on the potential coefficients.

5. Results

In this section we will discuss some of the current (Nov 1973) solutions that are postulated to describe the Earth's gravitational field. Although results exist for both potential coefficient determinations and discrete block determinations, more discussion will be devoted to the former as this is the area in which extensive computational effort has been expended.

5.1 Potential Coefficient Results

We will consider four potential coefficient determinations computed from the combination of gravimetric and satellite data. These are:

A: 1969 Smithsonian Standard Earth II (GAPOSCHKIN & LAMBECK 1970; GAPOSCHKIN & LAMBECK 1971) (called SE II). This solution consisted of 316 (20 of which were fixed zonal coefficients) potential coefficients which are complete to degree 16 with additional zonal and resonance terms to degree 22. The combination procedure was carried out basically using equation 9 with equation 8, solving simultaneously for the geocentric co-ordinates of 46 stations. The terrestrial gravity data used consisted of 935, 5° equal area anomalies used by KAULA (1966b), with the empty areas estimated from a linear regression procedure applied to the 935 anomalies.

B: Smithsonian Institution Standard Earth III (GAPOSCHKIN 1973). This solution consisted of 386 potential coefficients which are complete to degree 18 with additional zonal coefficients to degree 36 and resonance terms to degree 23. The combination procedure was carried out as with SE II but with an updated anomaly set, setting anomalies in the empty areas to zero. In addition, no partial derivatives of the anomalies with respect to the zonal harmonics or tesseral harmonics less than the 9th degree were computed. The justification for this was that such derivatives are negligibly small. The results of RAPP (1969b) whereby potential coefficients were found solely from terrestrial data do not support this justification.

C: GEM6. The GEM6 solution is the combination solution made with the pure satellite solution GEM5. These new models are updated models of the GEM1 and GEM2 solutions (LERCH ET AL 1972b), and the GEM3 and GEM4 solutions (LERCH ET AL 1972a). The GEM6 solution consists of 337 potential coefficients and the geocentric co-ordinates of 134 tracking stations. The coefficients are complete to degree 16 with additional terms to degree 22. The combination procedure was carried out using essentially equations 8 and 9. The anomalies used for the combination solution were those used by RAPP (1972; 1973a).

D: RAPP (1973a). This solution is a combination solution made with equation 11 using the least squares collocation principle. This model, which started from the GEM3 potential coefficient set, contains 449 coefficients being complete to degree 20, with additional terms to degree 22. The gravity data used in this solution was based on 23,355 $1° \times 1°$ anomalies processed using equations 3 and 4 to determine 1283, 5° equal area anomalies and their standard deviations (RAPP 1972). The remaining blocks were filled up using model anomalies based on topographic isostatic information (UOTILA 1964). In addition to the potential coefficients, this solution provided a set of 1654, 5° equal area anomalies adjusted, through equation 6 to be consistent with the adjusted potential coefficient set.

5.2 Potential Coefficient Comparisons

5.21 Potential Coefficient Differences

In this section we will compare the four potential coefficient sets in several ways. In table 1, we give the root mean square difference (Δ), the average percentage difference ($\overline{\%}$), the root mean square undulation (ΔN) and the anomaly difference (δg), when the coefficient sets are compared in terms of common coefficients. In table 2, we give the root mean square undulation and anomaly difference between the solutions when all the coefficients of a solution are considered. To estimate the maximum undulation or anomaly difference between a solution, multiply the RMS difference by four.

Table 1

Root Mean Square Potential Coefficient, Undulation and Anomaly Differences, for Various Potential Coefficient Sets

	SEII				SEIII				GEM6			
	$\Delta\times10^6$	$\overline{\%}$	RMS ΔN (m)	RMS δg (mgal)	$\Delta\times10^6$	$\overline{\%}$	RMS ΔN (m)	RMS δg (mgal)	$\Delta\times10^6$	$\overline{\%}$	RMS ΔN (m)	RMS δg (mgal)
SEII	--	--	--	--	0.066	81	7.5	10.6	0.049	90	5.5	9.3
SEIII	0.066	81	7.5	10.6	--	--	--	--	0.056	80	6.4	8.6
GEM6	0.049	90	5.5	9.3	0.056	80	6.4	8.6	--	--	--	--
Rapp	0.049	62	5.5	9.2	0.058	72	7.2	10.0	0.026	49	3.0	5.3

Table 2

Root Mean Square Undulation and Anomaly Differences Between Complete Potential Coefficient Sets

	SEII		SEIII		GEM6	
	RMS ΔN (m)	RMS δg (mgal)	RMS ΔN (m)	RMS δg (mgal)	RMS ΔN (m)	RMS δg (mgal)
SEII	--	--	7.7	11.4	5.5	9.4
SEIII*	7.7	11.4	--	--	6.6	9.6
GEM6	5.5	9.4	6.6	9.6	--	--
Rapp	5.9	10.8	7.4	11.1	3.7	7.7

* SEIII to $\ell = 23$ only

5.22 Anomaly Degree Variance Comparisons

The potential coefficients may be converted to anomaly degree variances using the following:

$$\sigma_\ell^2(\Delta g) = \gamma^2(\ell - 1)^2 \sum\left(\overline{C}_{\ell m}^2 + \overline{S}_{\ell m}^2\right) \qquad (18),$$

where the $\overline{C}_{20}$ and $\overline{C}_{40}$ are referred to an ellipsoid of a specified flattening. Values of the anomaly degree variances as computed from the potential coefficient sets described in section 5.1 are given

in table 3 along with the anomaly degree variances computed from gravity data alone (RAPP 1972) using the procedures described by KAULA (1966b).

Table 3

Anomaly Degree Variances†

$(mgal)^2$

ℓ	SEII	SEIII	GEM6	Rapp	Gravity*
2	7.4	7.2	7.5	7.5	12.7
3	33.0	33.5	33.7	33.9	31.3
4	20.0	20.4	19.3	19.2	13.6
5	17.8	25.9	21.7	21.6	15.1
6	15.7	18.2	20.1	18.9	19.9
7	15.5	19.3	17.5	18.8	15.5
8	6.7	19.6	8.4	10.4	7.5
9	12.7	11.7	8.8	11.1	16.1
10	12.9	11.0	11.4	11.4	9.6
11	12.2	10.0	7.7	8.4	10.8
12	5.1	9.1	4.2	4.8	3.9
13	11.1	9.3	10.7	11.7	8.2
14	8.4	8.1	5.9	5.5	8.3
15	13.2	8.3	8.6	7.3	8.6
16	13.8	10.1	6.8	6.5	8.7
17		9.9		5.7	8.6
18		8.7		10.7	9.6
19				11.0	7.4
20				8.9	6.8

* RAPP (1972) † Reference Flattening 1/298.256

The biggest difference between the SEII and the SEIII occur at ℓ = 5 and 8 where the SEIII values are 8.1 and 12.9 $mgal^2$ higher than the SEII values. For these two cases the SEII values agree better with the gravimetrically derived anomaly degree variances than the values obtained from the SEIII. The lower value at ℓ = 8 also occurs in the GEM6 and Rapp solutions.

5.23 Astro-Geodetic Undulation Comparisons

A set of potential coefficients can be used to derive a set of geoid undulations which may be compared to astro-geodetic undulations after an appropriate transformation. The agreement of the transformed undulations with the astro-geodetic undulations (as judged by the root mean square undulations differ difference after the transformation) can be used to infer the value of the potential coefficients in describing geoid undulations.

Results for such comparisons have been described by RAPP (1973a) for all solutions given here except for the SEIII which is reported here along with the other values. These comparisons have been made on the North American Datum with 3112 points and on the Australian Datum with 1084 points. The root mean square differences are given in table 4. Considering the information from both datums, the best agreement is found with the GEM6 coefficients with the poorest agreement found from the SEIII set.

Table 4

RMS Difference (After Adjustment) Between Astro-geodetic Undulations and Undulations Computed from Potential Coefficients (metres)

	North American Datum	Australian Datum
SEII	± 5.2	± 2.9
SEIII	± 6.1	± 2.6
GEM6	± 3.9	± 2.2
Rapp	± 4.4	± 2.0

5.24 Anomaly Comparisons

Anomalies may be computed from potential coefficients as seen from equation 8. These anomalies may then be compared to the actual terrestrial anomalies to consider their agreement. KAULA (1966a) gave procedures for such comparisons when the potential coefficients were determined solely from satellite data. These comparisons have also been made with potential coefficients derived from combination solutions. The analysis of these comparisons must be balanced against the fact that the anomalies against which comparisons are being made have usually been used in the combination solution being judged. Thus, the comparisons may not reveal absolute truth, but rather relative truth. In this section we carry out these comparisons with the four potential coefficient sets of section 5.1, recognizing that 2 out of 4 sets used different gravimetric data in the combination solution. The terrestrial anomalies used for the comparisons are the 927 values given by RAPP (1972) (with the anomalies in the Canadian area corrected by -2 mgal), having standard deviations less than or equal to ±10 mgal. Other subsets of the terrestrial field were tested, but the results to be reported here are representative.

The comparison terms are as follows:

$E\left((g_T - g_S)^2\right)$: the mean square difference between terrestrial anomalies (g_T) and those derived from potential coefficients (g_S);

$E\left(\varepsilon_S^2\right)$: mean square value of the error associated with the potential coefficients;

$E\left(\delta g^2\right)$: mean square value of neglected higher order terms in the computation of g_S; and

$E\left(\delta g_H^2\right)$: mean square effect of the true contribution to g_S from the potential coefficients

The above values have been computed for two subsets (to ℓ = 12, and 16) of each potential coefficient set as well as the complete set. The results are given in table 5. The results of the comparison made to ℓ = 12 indicate that the SEIII coefficients are less accurate than the other three sets. The agreement with the terrestrial anomalies is about the same in the SEII and SEIII, and the GEM6 and Rapp solutions.

The results of the comparisons made to ℓ = 16 indicate that the SEII coefficient set is less accurate than the other three sets all of which are about the same accuracy. The comparison of the complete coefficient sets indicates the SEII is again poorer than the other sets. The Rapp set shows a slightly better agreement with the terrestrial field but this is due to the inclusion of more potential coefficients in its solution than are found in the other solutions. In all cases, the

Table 5

Comparison of Anomalies Derived from Potential Coefficients with Terrestrial Anomalies

$(\text{mgal})^2$

	To ℓ = 12				To ℓ = 16				Complete			
	$E\{(g_T-g_S)^2\}$	$E\{\varepsilon_S^2\}$	$E\{\delta g^2\}$	$E\{g_H^2\}$	$E\{(g_T-g_S)^2\}$	$E\{\varepsilon_S^2\}$	$E\{\delta g^2\}$	$E\{g_H^2\}$	$E\{(g_T-g_S)^2\}$	$E\{\varepsilon_S^2\}$	$E\{\delta g^2\}$	$E\{g_H^2\}$
SEII	174	28	110	160	177	57	84	186	182	66	80	187
SEIII*	175	45	94	176	148	42	70	200	141	48	56	213
GEM6	154	25	93	177	138	31	71	199	143	38	69	201
Rapp	164	34	95	175	146	39	71	199	133	47	50	220

* Complete to ℓ = 23

GEM6 coefficients appear to be the most accurate as judged by $E\{\varepsilon_S^2\}$.

5.25 Orbit Fitting

A set of potential coefficients can be used in the representation of the Earth's gravitational field for satellite orbit computations. In the fitting of an orbit to the observations, the fit (as judged by the root mean square residual after adjustment) is a measure of how well the gravitational field is represented by the set of coefficients being tested. For complete testing of a set of coefficients, orbits not used in the original estimation of the potential coefficient sets should be used. In addition, the testing should be over as wide of range (in terms of inclinations, heights, etc) of orbits as possible. For this paper, however, I have the results (table 6) of orbit fitting for a single Geos 1 arc using laser data in a seven day arc.

Table 6

Root Mean Square Orbit Fit

(metres)

Solution	Fit
SEII	± 4.8
SEIII	7.9
GEM6	7.2
Rapp	5.0

The poorest fit is found with the SEIII coefficients with little difference between the SEII and the Rapp sets. More extensive testing in this area needs to be carried out similar to what was done by MARSH & DOUGLAS (1970) and WAGNER (1972).

5.26 Undulation and Anomaly Maps

Potential coefficients can be converted to geoid undulations through the following equations which are spherical approximations:

$$N = R \sum_{\ell=2}^{\ell_{max}} \sum_{m=0}^{\ell} \left(\overline{C}^{*}_{\ell m} \cos m\lambda + \overline{S}_{\ell m} \sin m\lambda \right) \overline{P}_{\ell m}(\sin \overline{\Phi}) \qquad (19),$$

and

$$\Delta g = \gamma \sum_{\ell=2}^{\ell_{max}} (\ell - 1) \sum_{m=0}^{\ell} \left(\overline{C}^{*}_{\ell m} \cos m\lambda + \overline{S}_{\ell m} \sin m\lambda\right) \overline{P}_{\ell m}(\sin \overline{\Phi}) \qquad (20),$$

where $\overline{C}^{*}_{\ell m}$ are the differences between the observed values and those values implied by an equipotential ellipsoid of a defined flattening. As mentioned in section 4.1, the differences involving $\overline{C}_{2,0}$ and $\overline{C}_{4,0}$ are the only ones usually considered. The ellipsoid to which the N and Δg values refer is a mean Earth ellipsoid (see HEISKANEN & MORITZ 1967, section 2-20 & 2-21). R is a mean Earth radius, and γ is an average value of gravity over the Earth. Values of N and Δg computed through equations 19 and 20 with the coefficients of RAPP (1973b) referred to a flattening of 1/298.256 are given in figures 2 and 3. To demonstrate some of the differences between the various solutions, figure 4 gives the anomaly differences between the RAPP (1973a) solution and the SEII solution. The maximum anomaly difference is 40 mgal occurring in the south Pacific area. This area is represented in more detail in figure 5 where anomalies in the block -10° to -40° latitude, and 190° to 235° east longitude are given. The anomalies have been computed for the SEII, SEIII, GEM5, GEM6 and the Rapp potential coefficient solutions from an integration over 5° equal area blocks strating from equation 8. In addition, we give the terrestrial anomalies (and their standard deviations) where they existed in the area. The GEM5 solution, which is based on satellite data alone, shows a smooth anomaly field in this area where the maximum anomaly range was 16 mgal. The SEII solution and the SEIII solution have a high and a low in this area with the maximum anomaly variation reduced by 19 mgal in the SEIII solution relative to the SEII. No observed gravity data was used in this area in the SEII. What gravity material was used in this area for the SEIII is not known. The Rapp solution also shows several maxima and minima, but not to the extent found in the other solutions. Additional gravity material is needed to verify the actual existence of the highs and lows in this area, or to see if, in fact, they are simply the result of a distortion introduced into the area by the adjustment procedure.

5.26 Summary

Current potential coefficients found from a combination of gravimetric and satellite data differ because of the satellite data used, the gravity data used, the combination procedure, and the degree at which the coefficients have been truncated. It is difficult to define what is the best coefficient set, although some of the comparisons made in the preceding sections indicate that one or more of the sets tested may be better suited for a specific purpose than one of the others.

5.3 Discrete Block Solutions

Gravitational field solutions using discrete blocks have been reported by ARNOLD (1972), KOCH & MORRISON (1970), KOCH (1970), KOCH & WITTE (1971), and RAPP (1973b). Arnold estimated 52, 20° × 20° mean anomalies out of 101 values on the Earth, assuming 49 anomalies as perfectly known, using 1182 observation equations based on the observation of six satellites. Koch & Morrison solved for 48, 30° × 30° surface density values based on 8692 optical observations of five satellites and a set of surface density values determined from terrestrial gravity material. They give potential coefficients to degree 8, based on a satellite solution and on the combined solution. KOCH (1970) used the 48 block satellite solution in conjunction with more detailed gravity material to estimate a 192 block solution which must be dominated by the gravity material since only the 30° × 30° blocks from the satellite solution were used.

KOCH & WITTE (1971) reported a satellite alone solution for 104, 20° surface elements computed using Doppler data from five satellites. The potential coefficients derived from their solution implied

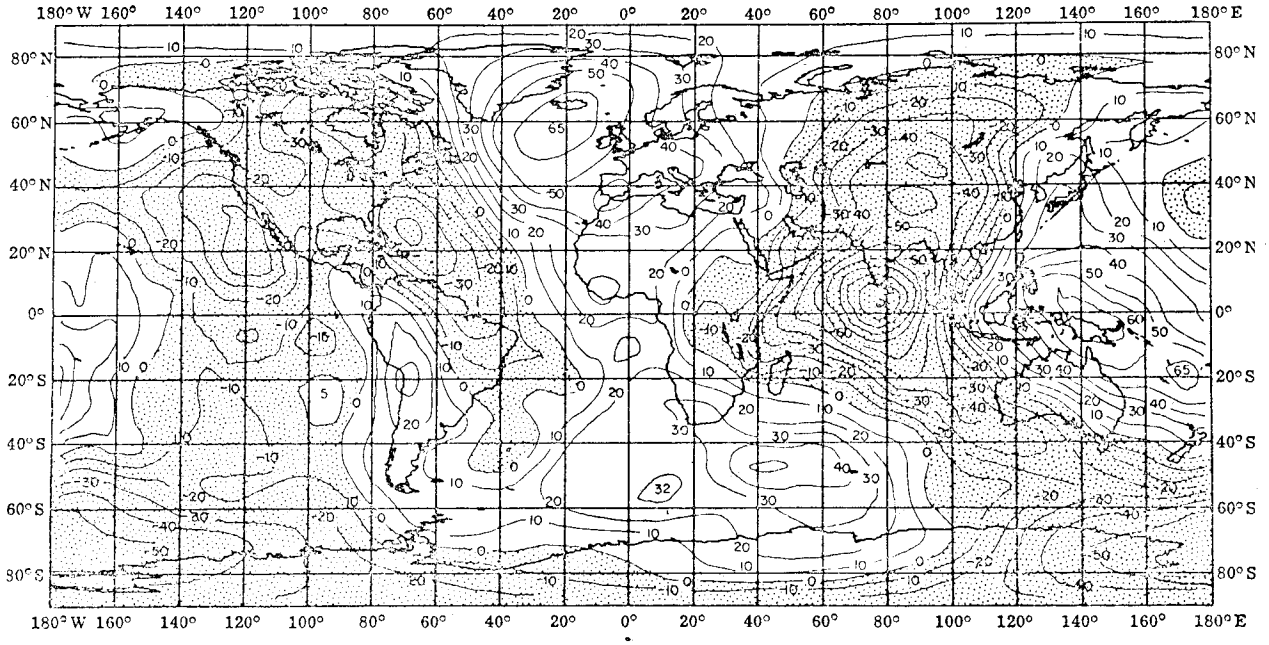

Figure 2. Geoid Undulations from Rapp Coefficients
Contour Interval: 10 m ; Reference Flattening = 1/298.256

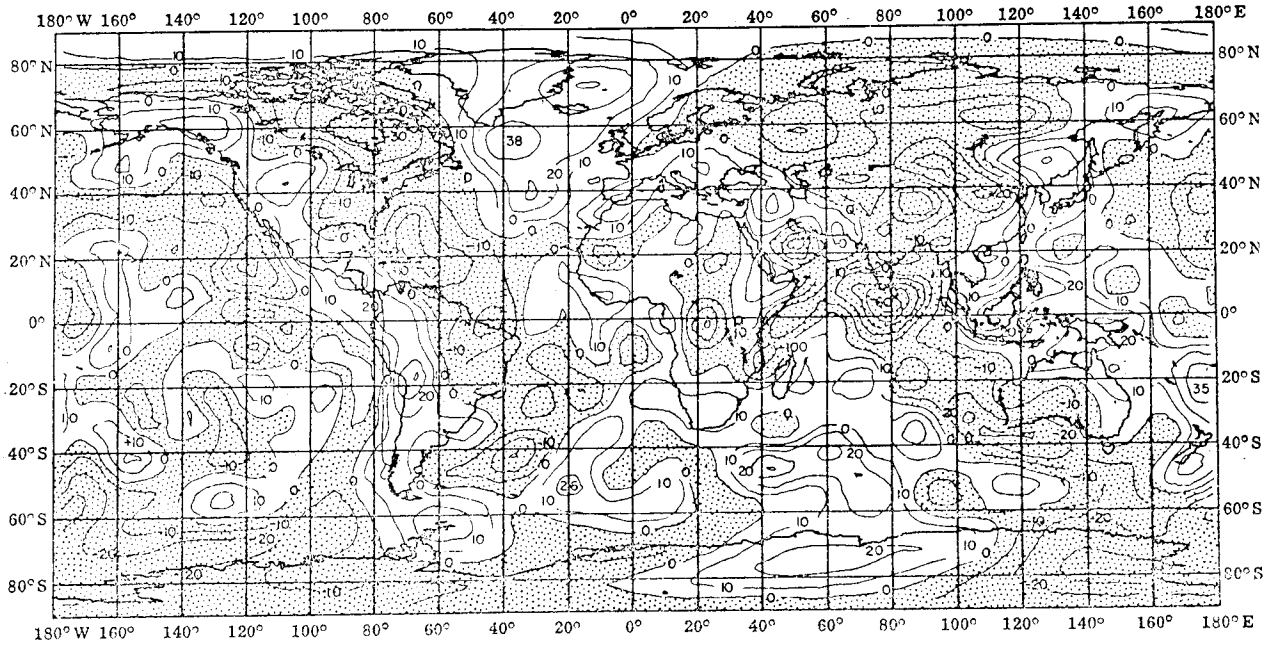

Figure 3. Anomalies from Rapp Coefficients
Contour Interval: 10 mgal; Reference Flattening = 1/298.256

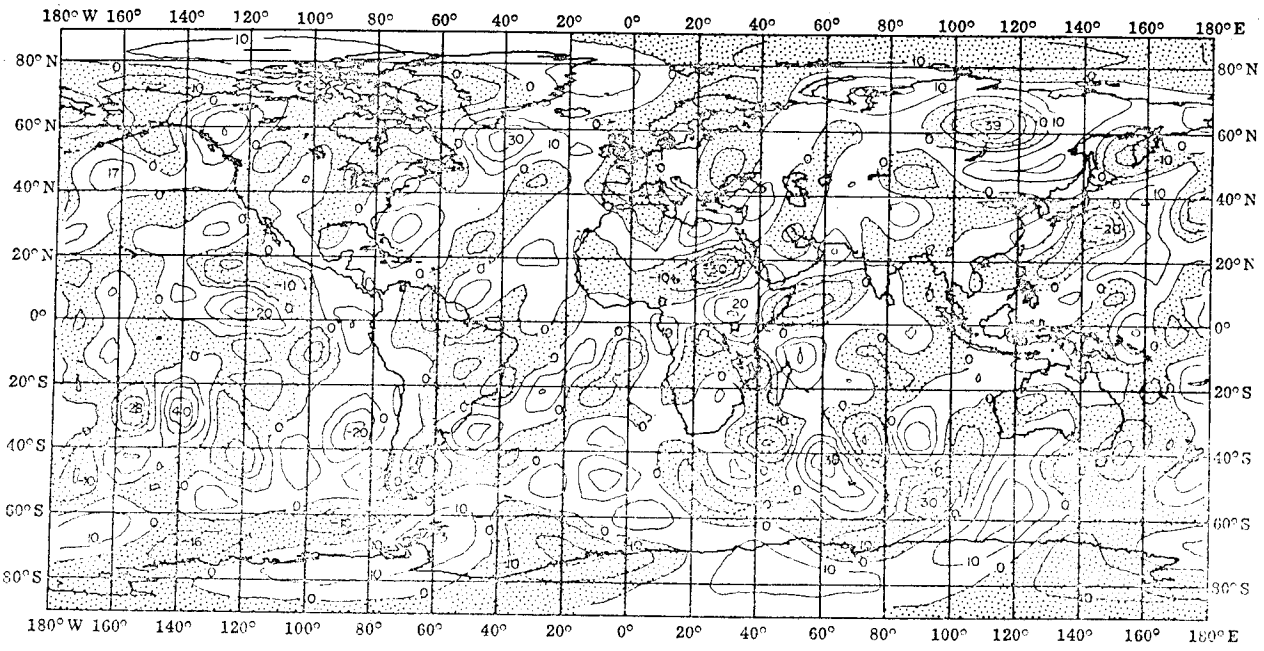

Figure 4. Anomaly Differences: Rapp Solution minus SEII solution
Contour Interval: 10 mgal; Maximum Difference = 40 mgal;
RMS Difference = 10.8 mgal

anomaly degree variances much larger than found by other investigations (at least up to degree 11) indicating that their solution has distorted potential coefficients.

RAPP (1973b) using the generalized Stokes equation (e.g., see equation 15), solved for 184, 15° equal area anomalies, and selected station co-ordinates. A satellite alone, and a combination solution were made. The satellite solution processed 17,651 optical observations from ten satellites in 29, 5 to 7 day arcs. The anomalies and their standard deviations for the 29 arc combination solution are shown in figure 6.

As with the potential coefficient combination solution, the combination solutions of a least squares nature, require some decision on a relative weighting between the two data types. This is needed as the satellite alone solution yields standard deviations for the unknown anomalies of unrealistically small value. For example, the standard deviation of the anomalies found from the 29 arc satellite solution average ±2 mgal where comparisons of the solution anomalies to well known terrestrial anomalies indicated a realistic standard deviation to be on the order of ±6 mgal. Thus, a scaling factor was applied to the satellite normal equations, before the combination solution was made, to yield a more realistic weighting scheme between the satellite and terrestrial information.

The potential coefficients implied by the anomalies found in the RAPP (1973b) solution agreed fairly well with potential coefficients derived from the more standard type of analysis. In addition, the anomaly degree variances computed from the potential coefficients agreed well with those computed from other sources.

The results obtained from current discrete block solutions represent sets of methods rather than

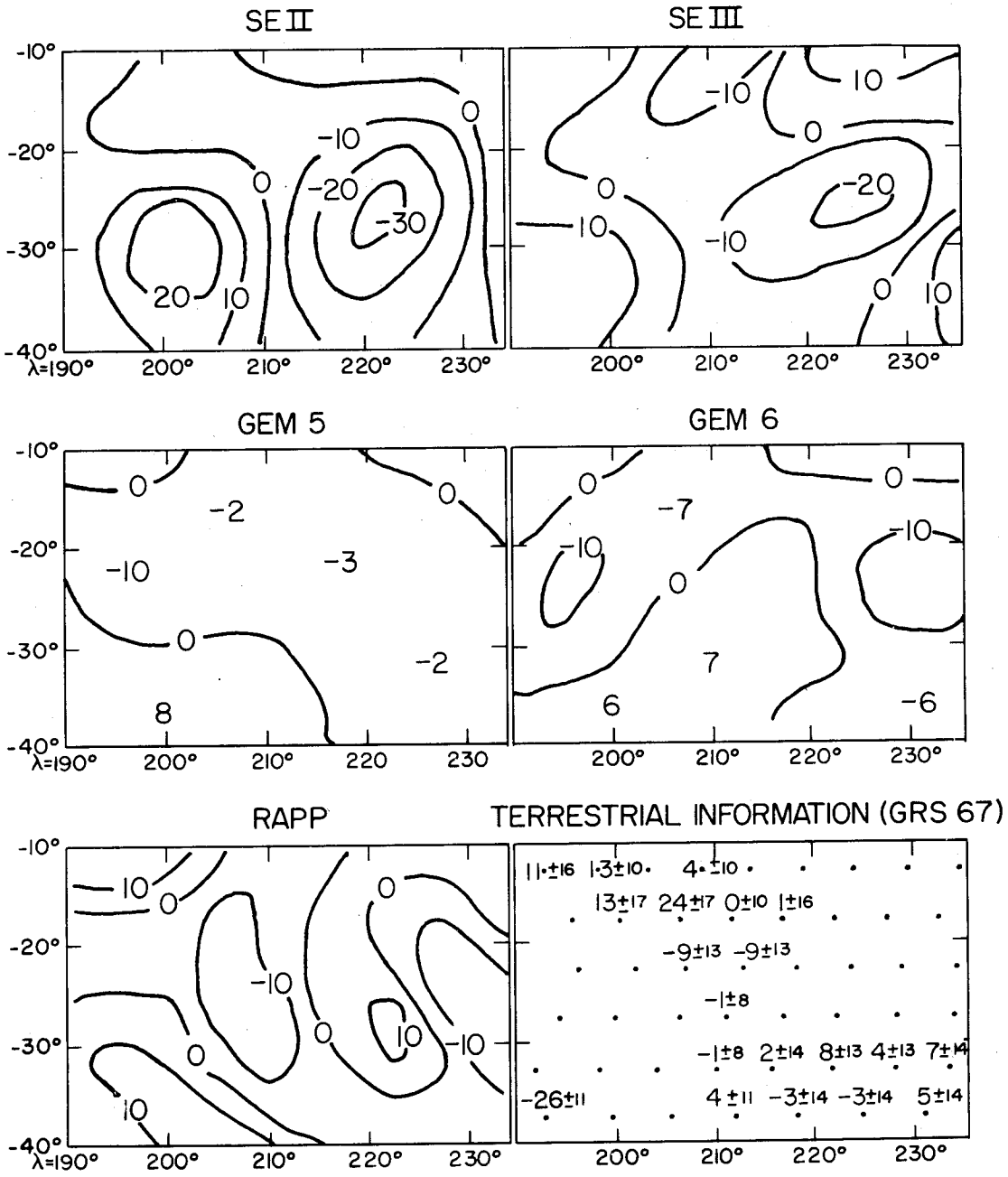

Figure 5. Anomalies in a South Pacific Area

results that are to be regarded as most current representations of the gravitational field. This is because the amount of satellite data analysed in the discrete block solutions is considerably less than that used in such solutions as the SEII, SEIII, or GEM6.

6. The Representation of the Earth's Gravitational Field

The combination of satellite and gravimetric data in the future will face the use of new observation

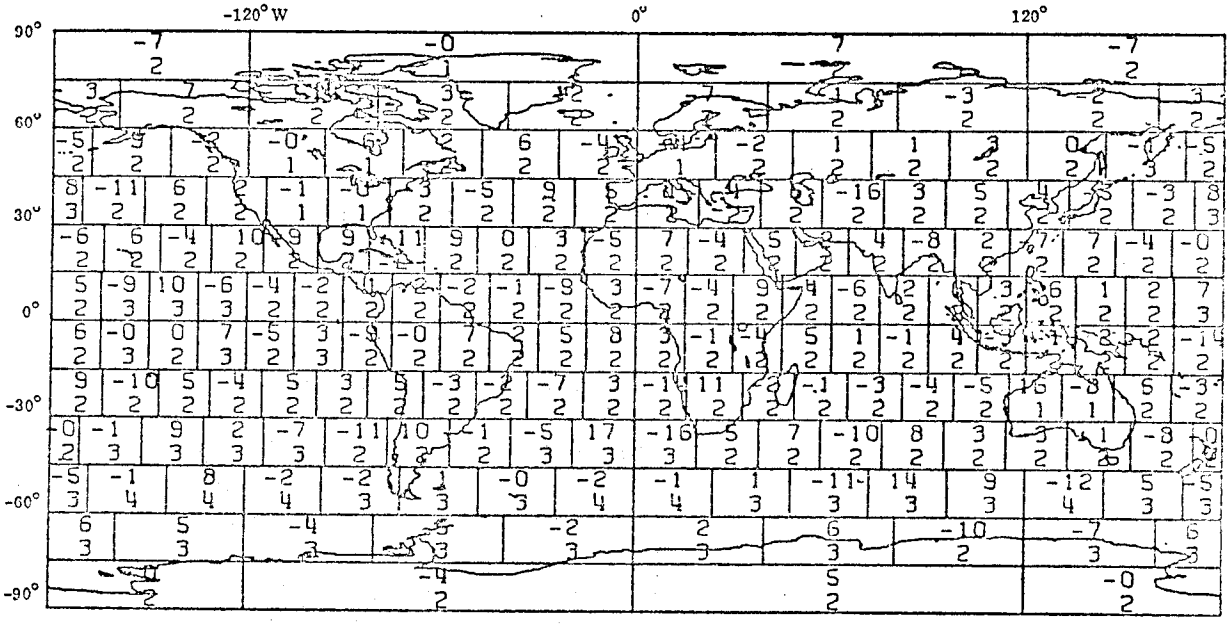

Figure 6. Anomalies (Upper Figure) and their Standard Deviations From 29 Arc Combination Solution (RAPP 1973b) - (mgal)

data obtained from satellites. The two new data types that will be available are satellite altimetry and satellite-to-satellite tracking. In using this data, and of course, existing satellite data, the proper way in which to represent the Earth's gravitational field must be considered. In addition, it may be that a global gravity field will not be sought in one given solution. Rather, solutions for the gravity field in local or regional areas could be found with the global field constructed from regional sets.

The representation problem is a rather important one at this time with a good deal of effort being placed on trying to define a system that can define the gravity field in an appropriate manner. In addition, to the potential coefficient and discrete block (surface densities or gravity anomalies) representative investigations have been carried out with point masses (BALMINO 1972; NEEDHAM 1970); sampling functions (LUNDQUIST & GIACAGLIA 1972; LUNDQUIST, GIACAGLIA & GAY 1973); or some analytic description of the anomaly field through some power series (STRANGE 1972), or through "regional functions" (DUFOUR & KOVALESKY 1970), or through the disturbing potential being represented in an analytic way, by a surface density layer distributed over a sphere bounding the Earth (VINTI 1971).

For future work several of the above systems will undoubtedly be used to describe the local part of the Earth's gravitational field. What procedure is best is not clear at this time. If we wish to easily incorporate existing terrestrial gravity material into a combination solution with a new type of representation; if we wish a function or quantity that can theoretically be related to the gravimetric boundary value problem, so that the external gravitational field as well as the field on the Earth's surface can be defined, and if we wish to be able to geophysically interpret the parameters of the local representation, it would appear that discrete blocks of gravity anomalies referred to

some high degree (e.g., ℓ = 12 or 20) potential coefficient field may be the appropriate form of representation desired.

7. Summary

This paper has attempted to outline some of the procedures, problems and results that are found in the combination of satellite and terrestrial gravity material. Details have been relegated to the references where possible. We have now just about passed the era of the broad wavelength determination of the Earth's gravitational field. Although current solutions do not agree in detail, the broad character is well defined.

If detailed gravity material were available on a global basis, we could consider the gravity field determined. Such is not the case because of unsurveyed ocean areas and land areas for which data is not available. Gravity material in the ocean areas is increasing but complete coverage cannot be expected for many years, and in some areas perhaps not in the foreseeable future. Consequently, the need for satellite systems that can refine our knowledge of the Earth's gravity field. The use of this new data could, in the limit, provide a global gravity coverage in 2° × 2° blocks on the surface of the Earth. The future accuracy of this field is not clear although the studies of SCHWARZ (1972) and REED (1973) indicate the possibility of obtaining anomalies to a standard deviation on the order of 1 to 3 mgal. Such results on a global basis can be used to satisfy almost all but the most local requirements for our knowledge of the Earth's gravitational field.

8. Acknowledgment

The work presented here was sponsored, in part, by the Air Force Cambridge Research Laboratories under Contract No. F 19628-72-C-0120, and by the National Aeronautics and Space Administration (Goddard Space Flight Center) under research grant no. NGR 36-008-161. Jim Marsh of GSFC provided the information for table 6. Some computer support was received through the Instruction and Research Computer Center of the Ohio State University.

9. References

ACIC 1971. 1° × 1° Mean Free-Air Gravity Anomalies. *ACIC Reference Publication* 29, St. Louis Missouri.

ARNOLD, K. 1965. The Orbits of Artificial Satellites as a Function of Gravity Anomalies. *Veroffenttichungen des Geodatischen Instituts in Potsdam* 27, Deutsche Akademie des Wissenschaften zu Berlin.

ARNOLD, K. 1966. On the Influence of Gravity Anomalies on Satellite Orbits. In "Gravity Anomalies: Unsurveyed Areas". *Am.geophys.U.Monograph* 9, Washington DC.

ARNOLD, K. 1972. Determination of Gravity Anomalies by Satellite Geodesy. In "The Use of Artificial Satellites for Geodesy". *Am.geophys.U.Monograph* 15, Washington DC.

BALMINO, G. 1972. Representation of the Earth Potential by Buried Masses. *Op.cit.*

BAUSSUS VON LUETZOW, H. 1972. The Determination of the Anomalous Gravity Potential from Satellite and Terrestrial Data Under Utilization of Modern Gravimetric Theory. (Abstr.) *EOS Trans. Am.geophys.U.* 53,892.

BJERHAMMAR, A. 1963. *Gravimetric Geodesy Free of Density Estimates Through Analysis of Discrete Gravity Data.* US Army GIMRADA, Alexandria Virginia.

BJERHAMMAR, A. 1969. Studies of a Coalescent World Geodetic System. *Tellus* 21,517-548.

DUFOUR, H. & KOVALEVSKY, J. 1970. *Formulation Practique Due Champ de Gravite Terrestre Par Des Fonctions Regionalisees.* Institut Geographique National,IGN-2,Paris.

FISCHER, I. 1968a. *A 1968 Modification of the Mercury Datum.* 49th Annual Meeting,American Geophysical Union,Washington DC.

FISCHER, I. 1968b. A Modification of the Mercury Datum. *Tech.Rep.* 67, US Army Map Service, Washington DC.

GAPOSCHKIN, E.M. 1973. *Smithsonian Institution Standard Earth III.* 54th Annual Meeting,American Geophysical Union,Washington DC.

GAPOSCHKIN, E.M. & LAMBECK, K. 1970. 1969 Smithsonian Standard Earth (II). *Spec.Rep.* 315, Smithsonian Astrophysical Observatory,Cambridge Mass.

GAPOSCHKIN, E.M. & LAMBECK, K. 1971. Earth's Gravity Field to the Sixteenth Degree and Station Coordinates from Satellite and Terrestrial Data. *J.geophys.Res.* 76,4855-4883.

GOPALAPILLAI, S., KARKI, P. & RAPP, R.H. 1971. Two Fortran IV Computer Programs for the General Combination of Satellite and Gravity Field Determinations. *Rep.* 168,Department of Geodetic Science,The Ohio State University,Columbus Ohio.

GROTEN, E. 1966. On Linear Regression Prediction of Mean Gravity Anomalies. In "Gravity Anomalies: Unsurveyed Areas". *Am.geophys.U.Monograph* 9,Washington DC.

GROTEN, E. 1970. Outline of Alternative Combination Solutions in Satellite Orbit Analysis. *Boll. Di Geofisica Teorica Ed Applicata* XIII,250-255.

HAJELA, D.P. 1973. The Computation of 15 and 10 Equal Area Block Terrestrial Free Air Gravity Anomalies. *Rep.* 194,Department of Geodetic Science,The Ohio State University,Columbus Ohio.

HEISKANEN, W.A. & MORITZ, H. 1967. *Physical Geodesy.* Freeman,San Fransisco.

HEISKANEN, W.A. & VENING MEINESZ, F.A. 1958. *The Earth and its Gravity Field.* McGraw-Hill,New York.

HOPKINS, J. 1972. Analysis of Methods for Computing an Earth Gravitational Model from a Combination of Terrestrial and Satellite Data. In "The Use of Artificial Satellites for Geodesy". *Am.geophys.U.Monograph* 15,Washington DC.

KAULA, W.M. 1966a. *Theory of Satellite Geodesy.* Blaisdell,Waltham Mass.

KAULA, W.M. 1966b. Tests and Combination of Satellite Determinations of the Gravity Field with Gravimetry. *J.geophys.Res.* 71,5303-5314.

KAULA, W.M. 1970. The Appropriate Representation of the Gravity Field for Satellite Geodesy. *Proc. Fourth Symposium on Mathematical Geodesy*,Comm.Geod.Stal.,Bologna,57-65.

KOCH, K.R. 1968. Alternate Representation of the Earth's Gravitational Field for Satellite Geodesy. *Boll.Di Geofisica Teorica Ed Applicata* X,318-325.

KOCH, K.R. 1970. Surface Density Values for the Earth from Satellite and Gravity Observations. *Geophys.J.R.astr.Soc.* 21,1-12.

KOCH, K.R. & MORRISON, F. 1970. A Simple Layer Model of the Geopotential from a Combination of Satellite and Gravity Data. *J.geophys.Res.* 75,1483-1492.

KOCH, K.R. & WITTE, B. 1971. Earth's Gravity Field Represented by a Simple Layer Potential from Doppler Tracking of Satellites. *J.geophys.Res.* 76,8471-8479.

KÖHLNEIN, W. 1967. The Earth's Gravitational Field as Derived from a Combination of Satellite Data with Gravity Anomalies. In *Spec.Rep.* 264,Smithsonian Astrophysical Observatory, Cambridge Mass.

LELGEMANN, D. 1972. *Spherical Approximation and the Combination of Gravimetric and Satellite Data.* Fifth Symposium on Mathematical Geodesy,Florence.

LERCH, F.J. ET AL 1972a. Gravitational Field Models for the Earth (GEM 1 & 2). *Doc.X*-553-72-146, Goddard Space Flight Center,Greenbelt Md.

LERCH, F.J. ET AL 1972b. Gravitational Field Models GEM3 and GEM4. *Doc.X*-592-72-476,Goddard Space Flight Center,Greenbelt Md.

LUNDQUIST, C.A. & GIACAGLIA, G.E.O. 1972. Geopotential Representation with Sampling Functions. In "The Use of Artificial Satellites for Geodesy". *Am.geophys.U.Monograph* 15,Washington DC.

LUNDQUIST, C.A., GIACAGLIA, G.E.O & GAY, R. 1973. *Experiments with Combining Satellite and Surface Gravity Data.* First International Symposium,The Use of Artificial Satellites for Geodesy & Geodynamics,Athens.

MARSH, J.G. & DOUGLAS, B.C. 1971. Tests and Comparisons of Gravity Models. *Celestial Mechanics* 4, 309-325.

MORITZ, H. 1969. A General Theory of Gravity Processing. *Rep.* 122,Department of Geodetic Science, The Ohio State University,Columbus Ohio.

MORITZ, H. 1970. Combination of Satellite Harmonics and Gravimetry. *Rep.* 146,Dept. of Geodetic Science,The Ohio State University,Columbus Ohio.

MUELLER, I.I. 1964. *Introduction to Satellite Geodesy.* Ungar,New York.

NEEDHAM, P. 1970. The Formation and Evaluation of Detailed Geopotential Models Based on Point Masses. *Rep.* 149,Department of Geodetic Science,The Ohio State University,Columbus Ohio.

OBENSON, G.F.T. 1970. Direct Evaluation of the Earth's Gravity Anomaly Field from Orbital Analysis of Artificial Earth Satellites. *Rep.* 129,Department of Geodetic Science,The Ohio State University,Columbus Ohio.

OBSENSON, G.F.T. 1972. Evaluation of Gravity Anomalies Directly from Satellite Observations. *Geophys. J.R.astr.Soc.* 30,69-83.

ORLIN, H. (ed.) 1966. Gravity Anomalies: Unsurveyed Areas. *Am.geophys.U.Monograph* 9,Washington DC.

OSTACH, O.M. & PELLINEN, L.P. 1966. The Effect of the earth's Ellipticity on its Stokes' Constants. *Transactions of the Central Scientific Research Institute of Geodesy, Aerial Survey & Cartography* 171 (ACIC Technical Translation TC1282,AD 661810),92 pp.

OSTACH, O.M. & PELLINEN, L.P. 1970. Determination of Stokes' Constants of the Earth from Gravity Anomalies. *Studia geophysica et geodetica* 14,121-126.

PELLINEN, L.P. 1962. Accounting for Topography in the Calculation of Quasigeoidal Heights and Plumb-line Deflections from Gravity Anomalies. *Bull.géodés.* 63,57-65.

PELLINEN, L.P. 1965. Determination of the Coefficients of Expansion of the Earth's Gravitational Potential into Spherical Functions from Joint Processing of Gravimetric and Satellite Data. *Geodesy and Aerophotography* 5 (transl. American Geophysical Union).

PELLINEN, L.P. 1969. Joint Adjustment of Gravimetric and Satellite Data in the Determination of the Earth's Gravitational Field. *Byulletin Stantsiy Opticheskogo Nablyudenuja Iskusstvennykh Sputnikov Zemli* 55 (transl. DMA Aerospace Center,1970,AD715152),55-68.

RAPP, R.H. 1964. The Prediction of Point and Mean Gravity Anomalies Through the Use of a Digital Computer. *Rep.* 43,Department of Geodetic Science,The Ohio State University,Columbus Ohio.

RAPP, R.H. 1967. Comparison of Satellite Geoids and Anomaly Fields. *Rep.* 80,Department of Geodetic Science,The Ohio State University,Columbus Ohio.

RAPP, R.H. 1968. Gravitational Potential of the Earth Determined from a Combination of Satellite, Observed and Model Anomalies. *J.geophys.Res.* 73,6555-6562.

RAPP, R.H. 1969a. Analytical and Numerical Differences Between Two Methods for the Combination of Gravimetric and Satellite Data. *Boll.Di Geofisica Teorica Ed Applicata* XI,108-118.

RAPP, R.H. 1969b. *Gravitational Potential Coefficients from Gravity Data Alone (II).* 50th Annual General Meeting,American Geophysical Union,Washington DC.

RAPP, R.H. 1970. Corrections to a Mean Free-Air Surface Anomaly to be Used in the Combination of Gravimetric and Satellite Data. *Proc.Fourth Symposium on Mathematical Geodesy.* Comm. Geod.Stal.,Bologna,107-116.

RAPP, R.H. 1971a. Equal Area Blocks. *Bull.géodés.* 99,113-125.

RAPP, R.H. 1971b. A Procedure for Combining Satellite and Gravimetric Data for Position and Gravity Field Determinations. *J.geophys.Res.* 76,4986-4990.

RAPP, R.H. 1971c. The Direct Combination of Satellite and Gravimetric Data for Mean Anomaly Determinations. *Rep.* 131,Department of Geodetic Science,The Ohio State University, Columbus Ohio.

RAPP, R.H. 1972a. The Formation and Analysis of a 5 Equal Area Block Terrestrial Gravity Field. *Rep.* 178,Department of Geodetic Science,The Ohio State University,Columbus Ohio.

RAPP, R.H. 1972b. Improved Models for Anomaly Computations from Potential Coefficients. *Rep.* 181, Department of Geodetic Science,The Ohio State University,Columbus Ohio.

RAPP, R.H. 1973a. Numerical Results from the Combination of Gravimetric and Satellite Data Using the Principle of Least Squares Collocation. *Rep.* 200,Dept. of Geodetic Science,The Ohio State University,Columbus Ohio

RAPP, R.H. 1973b. *Results from the Direct Combination of Satellite and Gravimetric Data.* First International Symposium,The Use of Artificial Satellites for Geodesy and Geodynamics, Athens.

REED, G.B. 1973. Application of Kinematical Geodesy for Determining the Short Wave Length Components of the Gravity Field by Satellite Gradiometry. *Rep.* 201,Dept. of Geodetic Science,The Ohio State University,Columbus Ohio.

SCHWARZ, C.R. 1972. Refinement of the Gravity Field by Satellite-to Satellite Doppler Tracking. In "The Use of Artificial Satellites for Geodesy". *Am.geophys.U.Monograph* 15,Washington DC.

STRANGE, W.M. 1972. Numerical Testing of an Altimeter Reduction Method. (Abstr.) *EOS Trans.Am.geophys. U.* 53,968.

UOTILA, U.A. 1964. Gravity Anomalies for a Mathematical Model of the Earth. *Publ.* 43,Isostatic Institute,International Association of Geodesy,Helsinki.

VINTI, J.P. 1971. Representation of the Earth's Gravitational Potential. *Celestial Mechanics* 4,348.

WAGNER, C.A. 1972. The Accuracy of Geopotential Solutions from Resonant Satellite Data. *Doc. X*-553-72-472,Goddard Space Flight Center,Greenbelt Md.

10. Discussion

TAPLEY: What technique of weighting did you use to combine your satellite data with surface data?

RAPP: Are you referring to the block data or the geopotential data?

TAPLEY: The original geopotential data.

RAPP: There was not a unique weighting factor applied to the whole system. A systematic analysis of every single potential coefficient was gone through to estimate uniquely for each potential coefficient, a standard deviation. When those standard deviations were used, we found that it was not possible to get good orbit fits. So we tightened up the standard deviations on the a priori potential coefficients from satellites. On doing so, we got good orbit fits. A whole series of solutions were obtained. We finally picked the one which would give good orbit fits but did not distort terrestrial gravity data significantly.

TAPLEY: The second question is on your single orbit fits for laser tracking data. Which tracking station locations were used?

RAPP: The tracking station locations used were those obtained by Marsh, Douglas & Klosko using the GEODYN program.

DUNN: For a forty degree inclination satellite, what gravity model would you go for?

RAPP: I don't know. If I were to say "My own solution", I would be said to be biased. GEM 6 looks quite good.

GROTEN, E.
Dept. of Geodesy & Satellite Geodesy
Technical University
61 Darmstadt
Federal Republic of Germany

Proc.Symposium on Earth's Gravitational Field & Secular Variations in Position (1973),76-92.

EFFICIENCY OF METHODS FOR IMPROVING THE PRESENTLY AVAILABLE INFORMATION ON THE EARTH'S GRAVITY FIELD

ABSTRACT

Test computations and statistical considerations are used in estimating the possible improvement of geoid and gravity field computation based on satellite orbit analysis. Satellite altimetry and gradient measurements are mainly dealt with.

New methods and techniques for improving the present knowledge of the Earth's figure and gravity field have been discussed more or less in detail, e.g.WILLIAMSTOWN REPORT (1969). Altimetry from artificial satellites (GREENE 1972; STANLEY ET AL 1972) and, to some extent, gravity gradient observations (FORWARD 1972) might be of primary importance in this connection besides satellite-to-satellite techniques which will not be dealt with in the present paper. The full exploitation of such new methods will, of course, lead to improved computational methods and theoretical procedures. Until now, satellite altimetry was mainly considered in connection with other methods, leading to new types of "combination solutions"; see, for instance RAPP (1971). A somewhat different approach in altimetry has been proposed by ARNOLD (1972). The latter paper leads to the question to what extent can geoid undulations be directly predicted.

A similar question could be raised in considering the present knowledge of the gravity field. Ten years ago, the prediction of gravity in un-surveyed areas was a major topic in physical geodesy; meanwhile large scale information is obtained, e.g., from satellite orbit analysis. In many areas where detailed geoid heights are to be computed, detailed knowledge in the neighbourhood zones is available. Because of

$$-\Delta g = \frac{\partial T}{\partial n} - \frac{1}{\gamma}\frac{\partial \gamma}{\partial n} T \qquad (1),$$

where T = disturbing potential;
γ = normal gravity;
n = normal direction; and
Δg = gravity anomaly,
the prediction of T and the geoid undulation

$$N = T/\gamma \qquad (2)$$

is, in general, simpler than the Δg-prediction. For the prediction of any quantity is in most cases easier than the prediction of its derivatives. The discrepancy, in general,is not so big at sea where altimetry is relevant as on land, but even when dealing with mean values or smoothed data, T-prediction is remarkably advantageous.

In order to get information on the statistical parameters of N, we have analyzed the global gravimetric geoid by VINCENT & MARSH (1973); as this geoid has been basically evaluated from $1^\circ \times 1^\circ$ mean free

air anomalies, it might be used, within its reliability, to study the spectrum of the gravity field up to degree $n \doteq 180$. However, as the corresponding gravity material is certainly affected by bias, spectral methods might lead to perturbed results, with severe perturbations in areas where biased gravity material has been used. On the other hand, the direct evaluation of statistical parameters of T and N from those of Δg by simple integral transform is not basically superior.

Accuracy investigations for the zone of geographic longitudes λ and latitudes ϕ

$$20^\circ \leq \phi \leq 80^\circ \quad \text{(north)} \qquad ; \qquad 200^\circ \geq \lambda \geq 50^\circ \quad \text{(east)},$$

and specifically for continental areas within this zone, indicate sufficient reliability for determining statistical parameters. A comparison has, for instance, been done with a very local geoid section (GROTEN & RUMMEL 1973) in central Europe. Figures 1 to 3 show the latter geoid section where regional gravity data have been combined with the latest coefficients model by RAPP (1973a), the SAO Standard Earth III and the Goddard Earth Model (GEM) 5. When $N_o = -17.0$ m is added to the numbers given in these figures, they are then related to the 1967-reference ellipsoid adopted at Lucerne where, however, Rapp's latest set of constants (GM, a, ω,...) was used in evaluating N_o. For details, see (GROTEN & RUMMEL 1973).

Under the assumption of isotropy and stationarity, the autocovariance functions within the above given area were evaluated for the global geoid, and for the local geoid within the zone shown in figures 1 to 3. In eliminating the trend, simply the effect of the outer zones corresponding to the above mentioned (global) coefficient sets has been omitted. Even though the local shape of the geoid section changes remarkably with changes in the outer zones, corresponding variations in the statistical parameters are small.

In addition, assuming stationarity, autocorrelation functions along meridians (λ = const) and latitude circles (ϕ = const) have been studied. Even when the samples are relatively small, they indicate systematic changes in cov(N) for profiles of constant latitude which are not fully explained by the heterogeneity of Δg-material. Figure 5 shows a few examples for ϕ = const; more details will be given in a forthcoming paper (GROTEN 1974). Figures 6 to 9 show a few examples for the autocorrelation along meridians λ = const. As these data are basically obtained from $1^\circ \times 1^\circ$ mean gravity values, the corresponding N-values are, of course, smoothed data. But on comparing the results for the local geoid with those for the global section it is seen that the tendency in very high harmonics seems to corroborate earlier assumptions by Kaula and specifically those by RAPP (1972).

On applying the well known linear autoregression prediction formulas to the local geoid section, it was found that within $d \doteq 20$ km or so, N can be predicted along profiles with a relative error of about 5 to 10 %. For the global geoid, the same accuracy is obtained within $d \doteq 50$ km. These accuracy estimates were evaluated by directly comparing "observed" with predicted values.

Unless collocation procedures are applied from the very beginning in satellite altimetry, it might be useful to extend the geoid obtained along altimeter profiles to "unsurveyed" areas.

In order to get a few hints on the very high harmonics we compared the local geoid section with a small geoid part obtained from astro-geodetic* and torsion balance measurements within the same area. It came out that even though the gravimetric geoid section was basically obtained from mean Δg-values for $6' \times 10'$ blocks, the corresponding loss of information is quite small. Such a comparison is, of course, always affected by local bias. Part of it is removed by topographic and terrain correction;

---

* Heitz-geoid as transformed by GROTEN (1970)

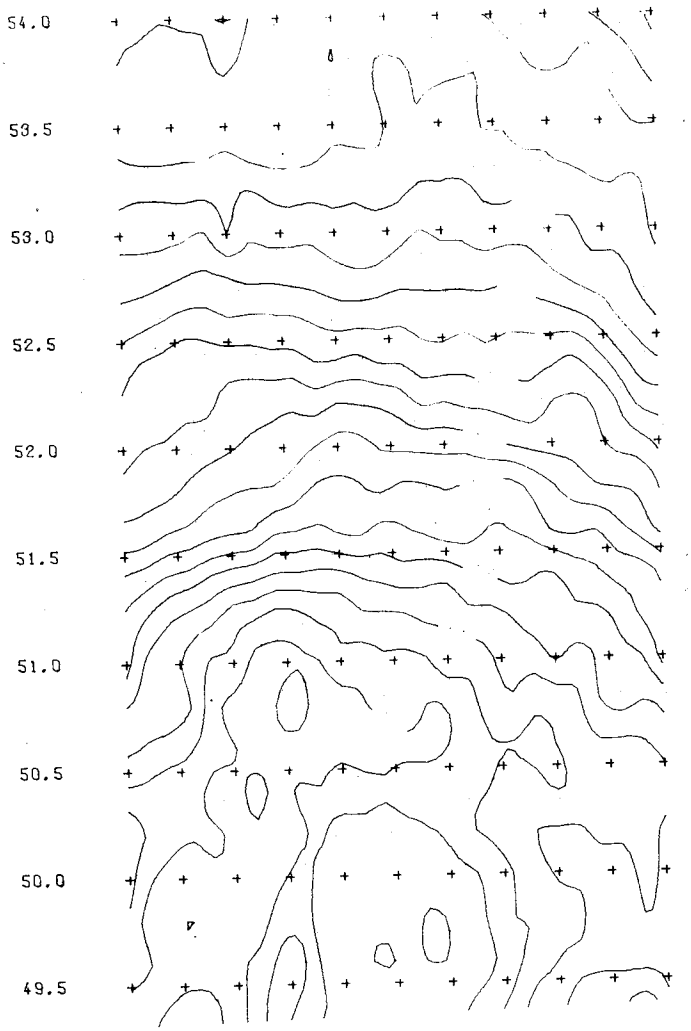

Figure 1.
Geoid Section at
Central Europe
from
Regional Gravity
and
Rapp's Coefficients

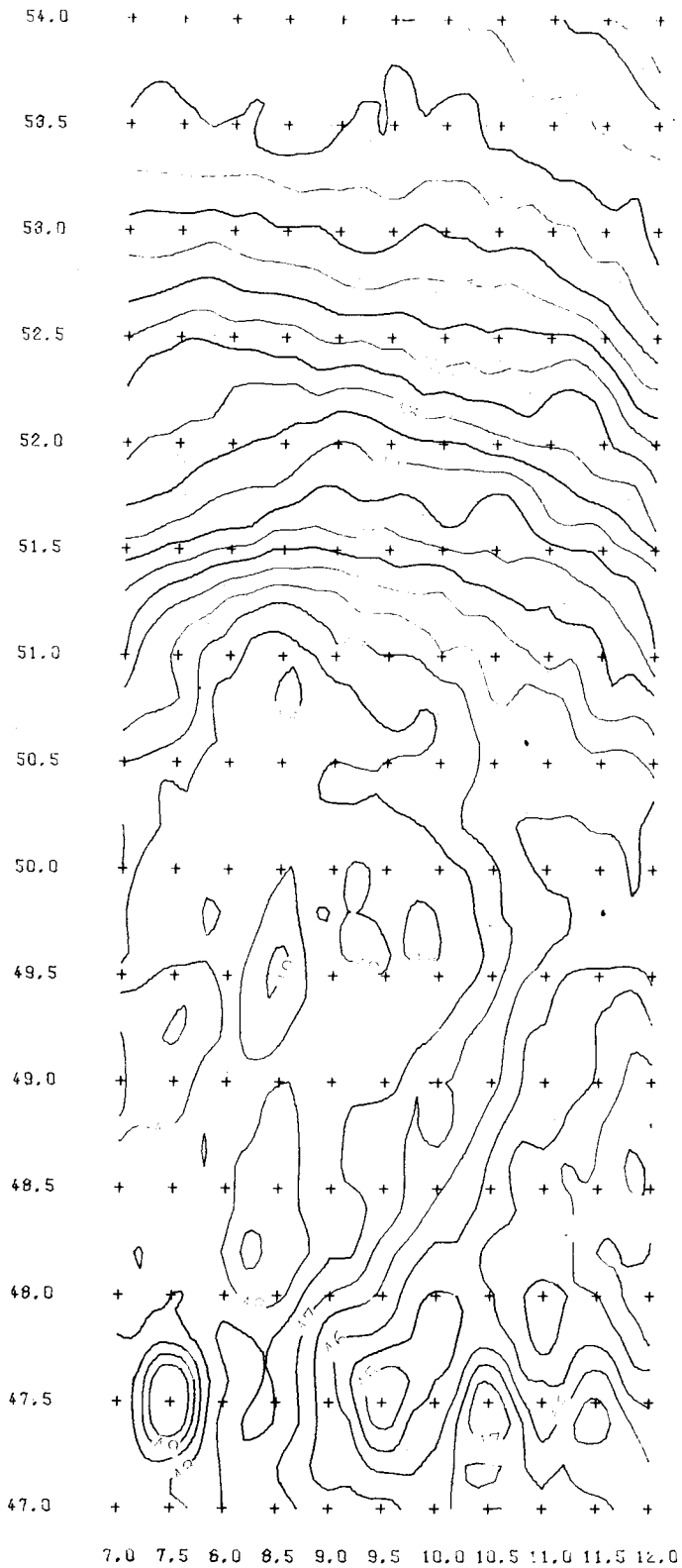

Figure 2.
Geoid Section at
Central Europe
from
Regional Gravity
and
SAO SE!!!

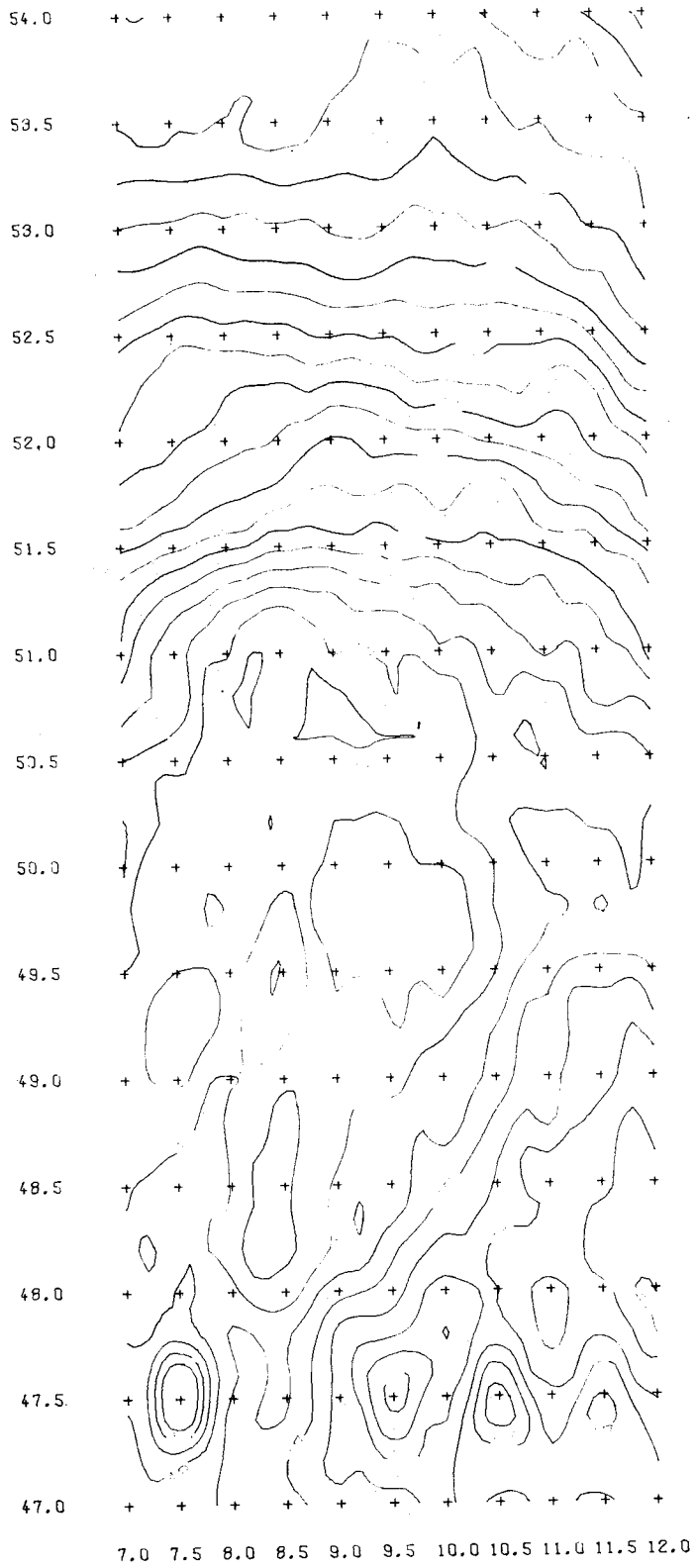

Figure 3.
Geoid Section at
Central Europe
from
Regional Gravity
and
GEM 5

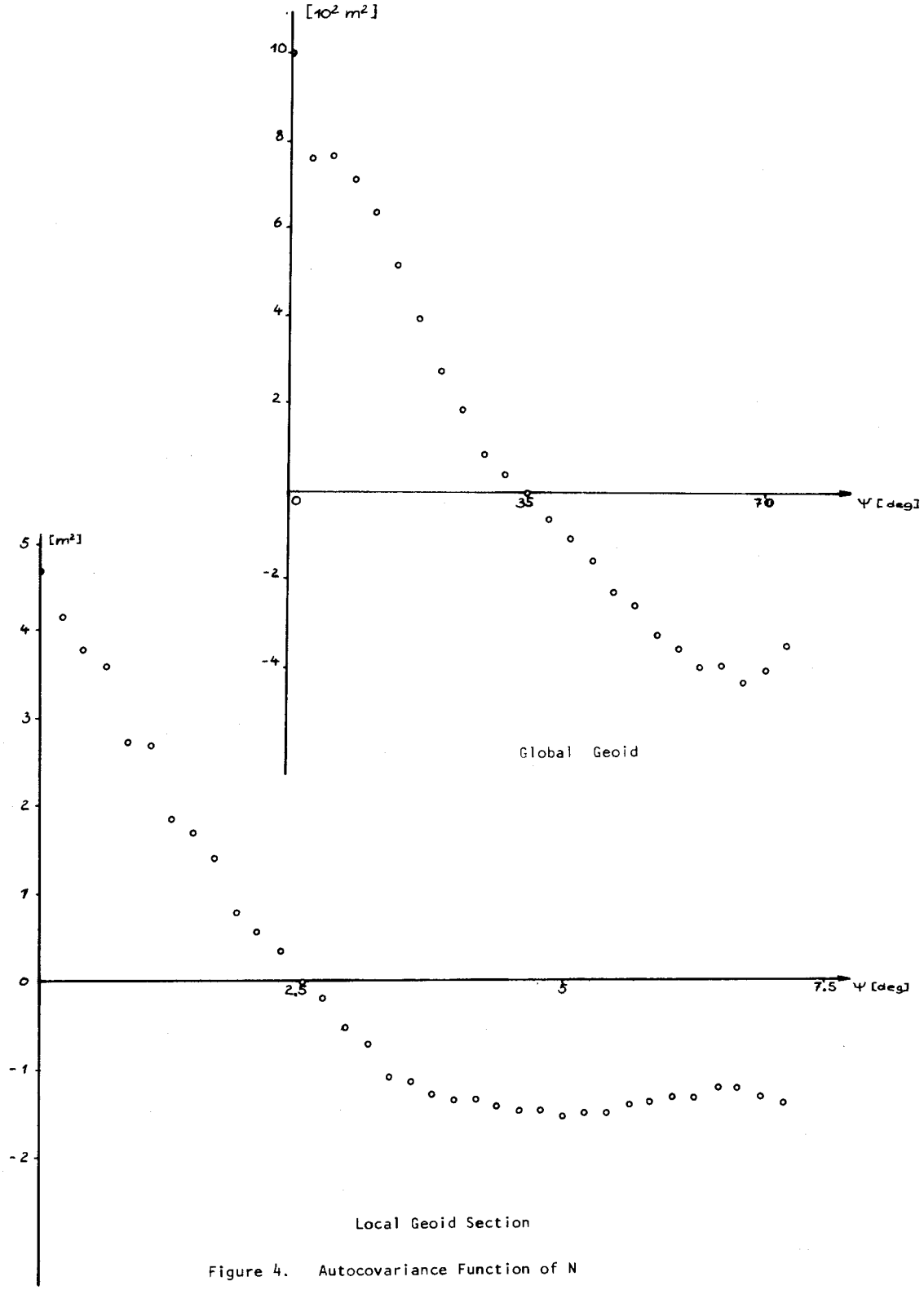

Figure 4. Autocovariance Function of N

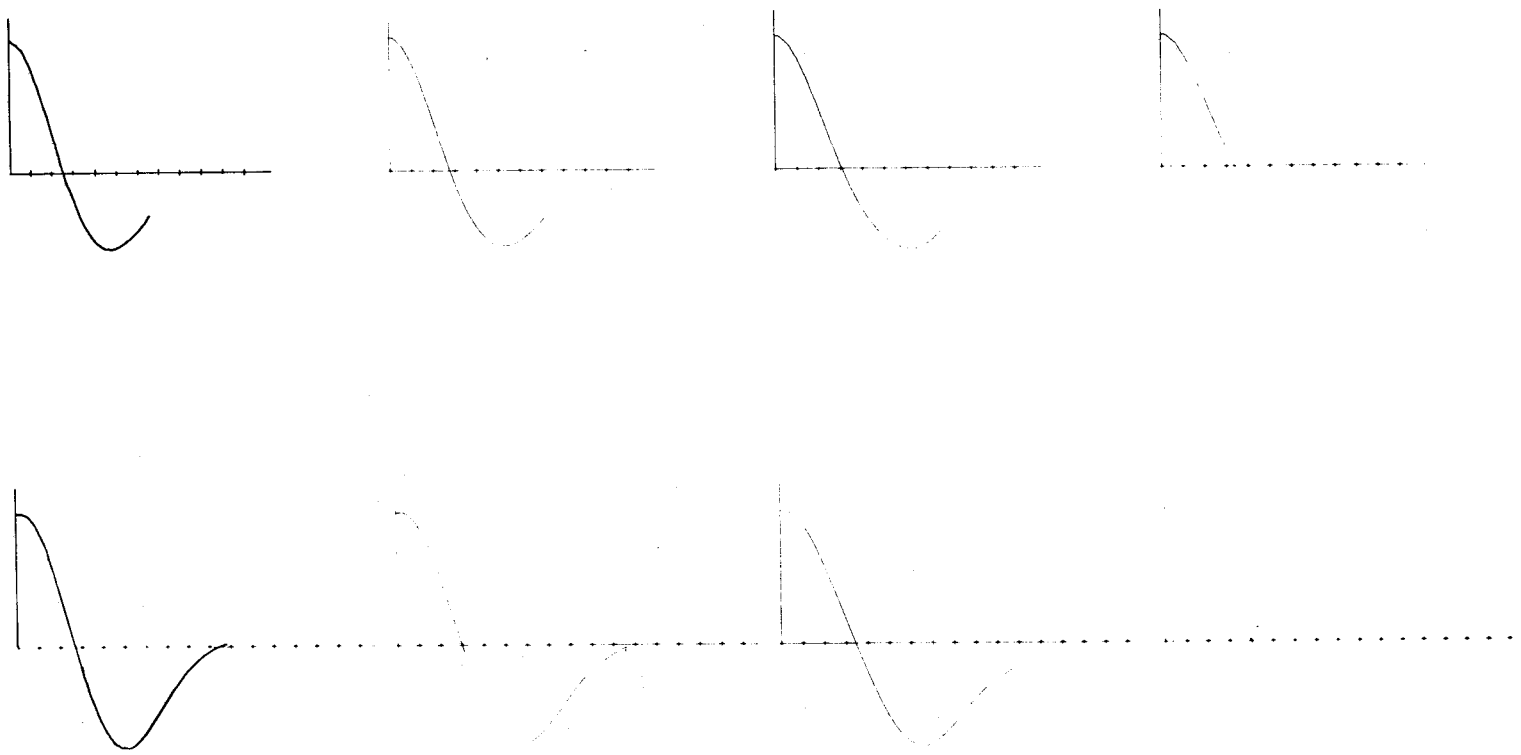

Figure 5. Autocorrelation* of **N** along ϕ = Constant around $\phi = 50°$**

* where in the upper part $cov(t) = \frac{1}{T-t} \sum_i N_i N_{i+t}$,

and in the lower row $cov(t) = \frac{1}{T} \sum_i N_i N_{i+t}$

was used with T = length of profile, t = separation and N_k = centred geoid heights

** one part on abscissa corresponds to 4000 km

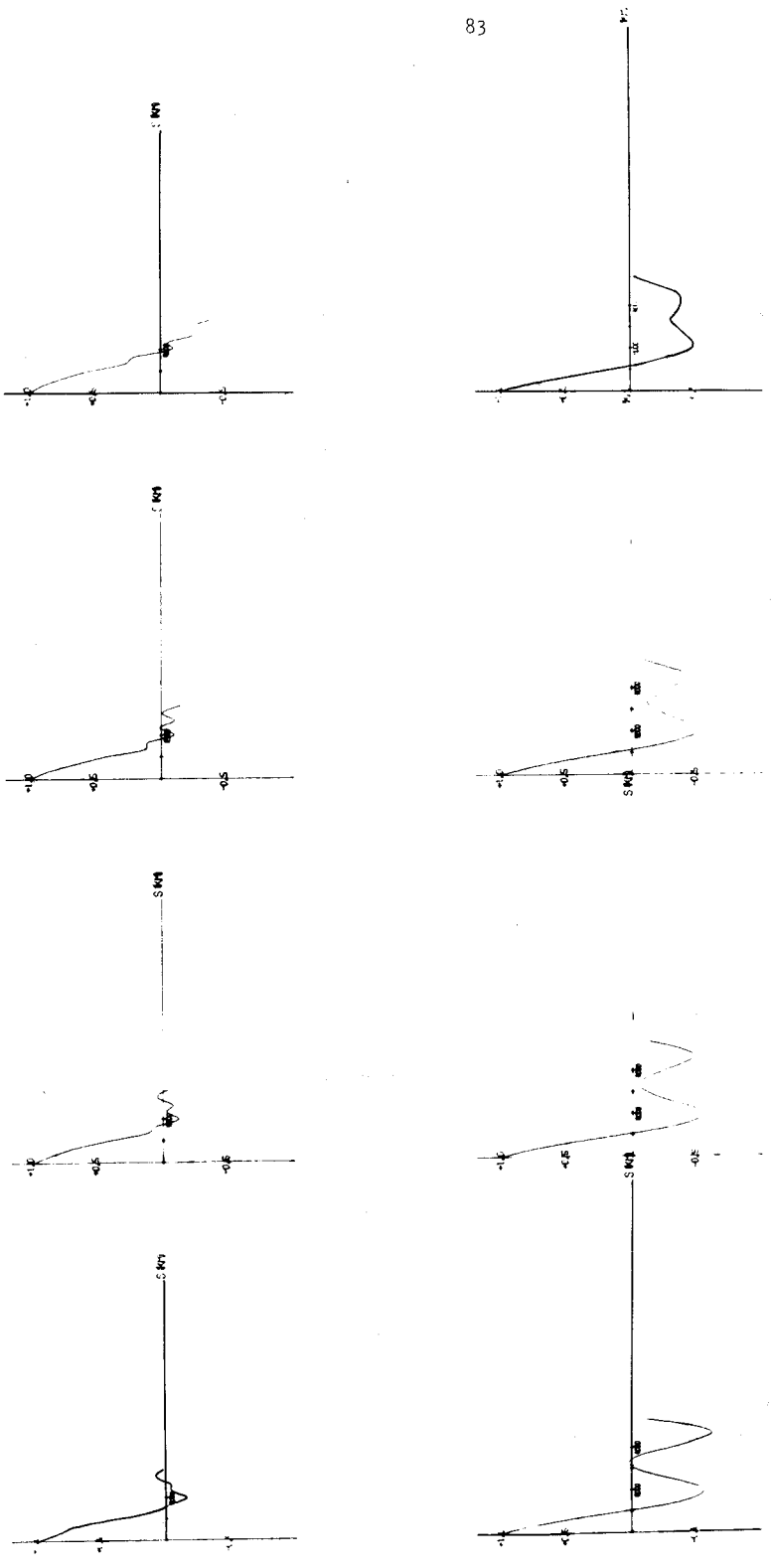

Figure 6. Autocorrelation* of N along λ = Constant for the Pacific Area ($\lambda \doteq 200°$)

*Refer note to figure 5

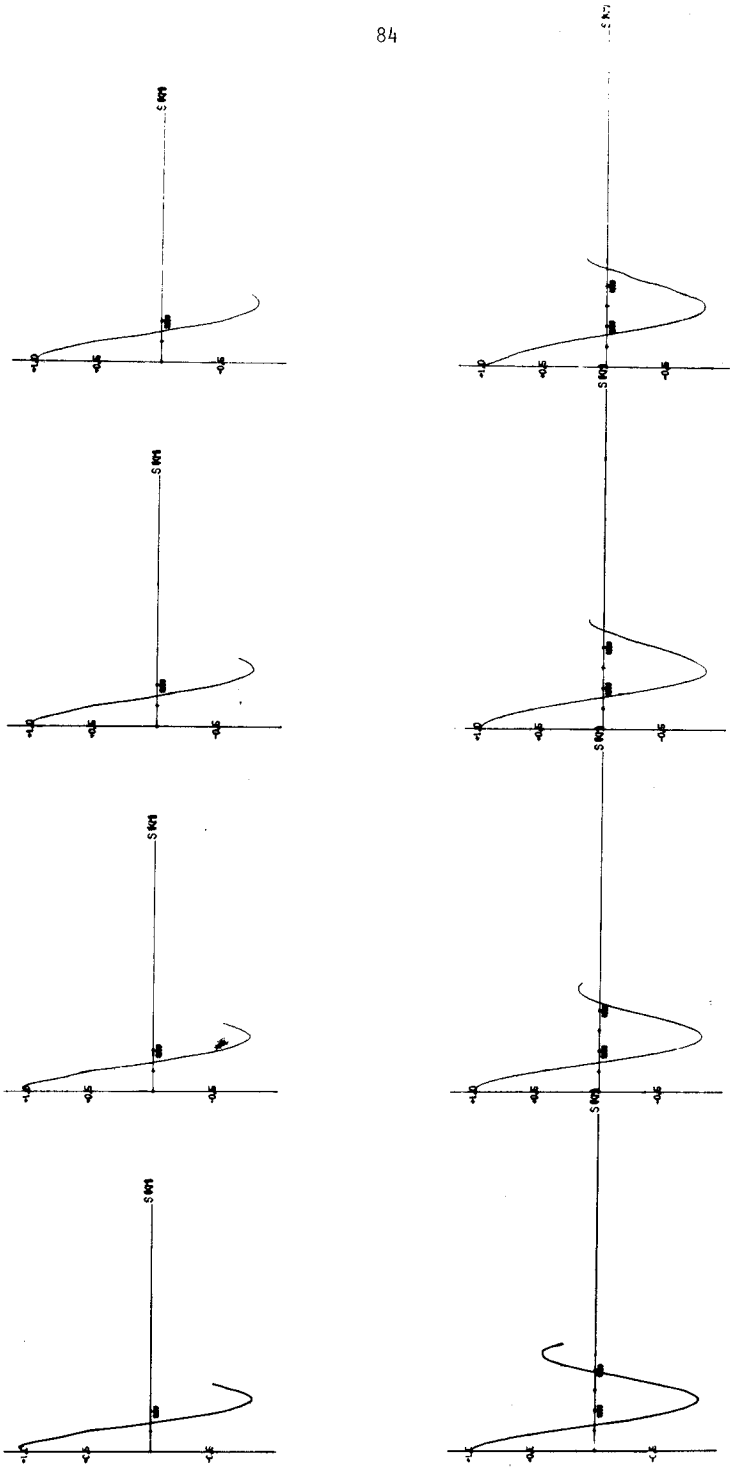

Figure 7. Autocorrelation* of **N** along λ = Constant for the North American Continent

* Refer note to figure 5

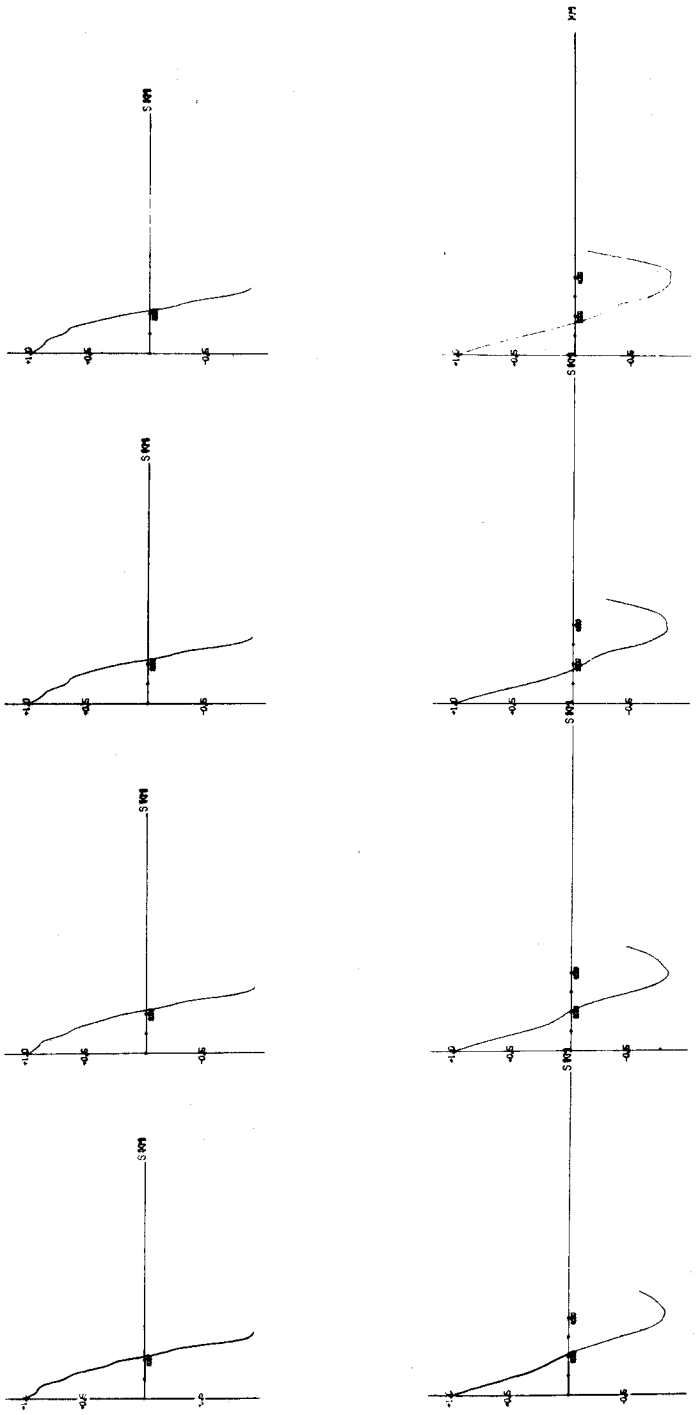

Figure 8. Autocorrelation* of **N** along λ = Constant for the Atlantic Ocean

*Refer note to figure 5

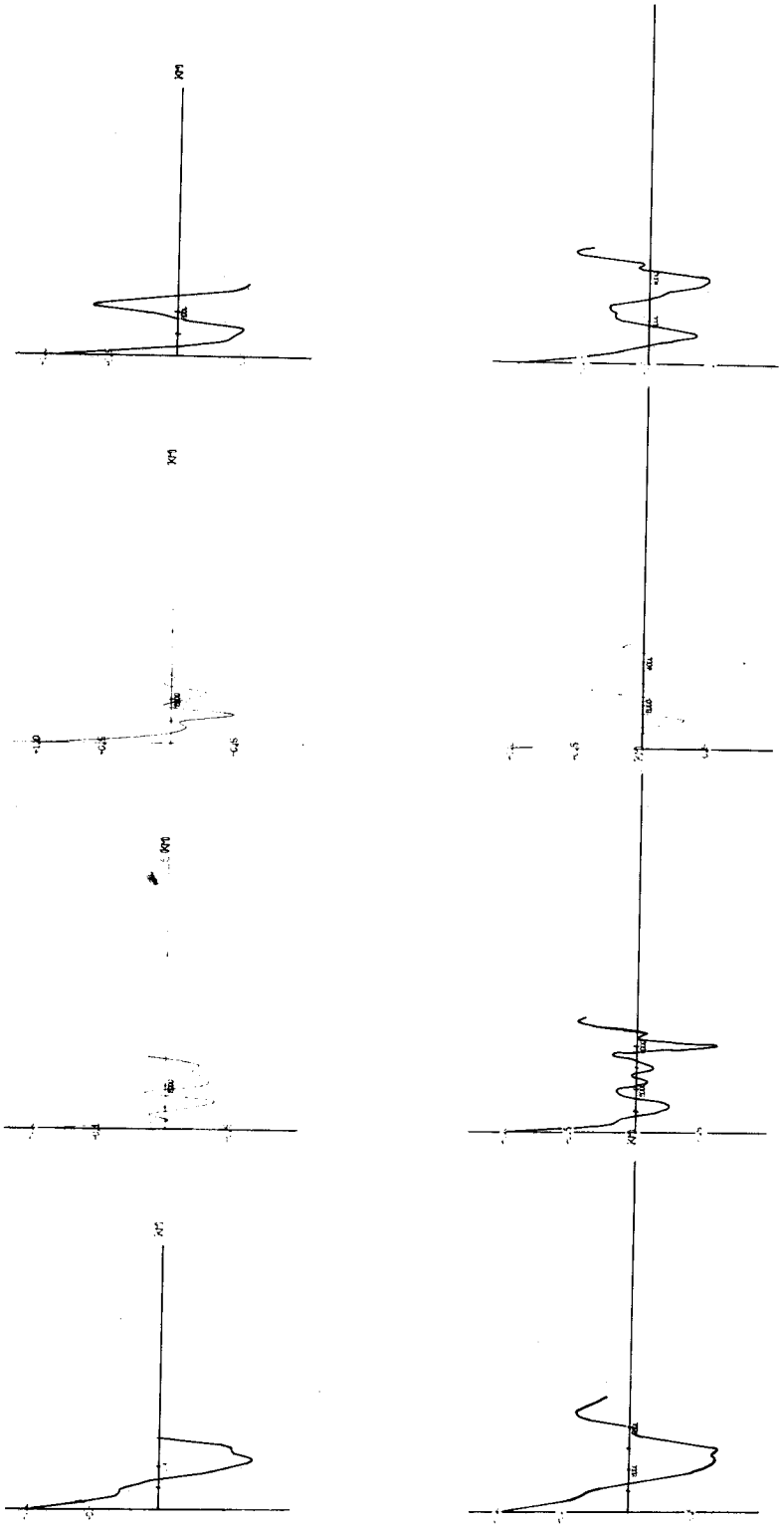

Figure 9. Autocorrelation* of **N** along λ = Constant for the European-African Area

*Refer note to figure 5

but local geology cannot be fully taken into account in most cases.

By comparing the autocorrelation functions given by KAULA (1963) with those few examples given here, the potentialities in predicting N or T directly become evident. In contrast to the above discussion of N-values alone, the detailed results of combination solutions with altimetry, etc. as given in (GROTEN 1970a) will be dealt with in (GROTEN 1974).

The application of recent gradiometry techniques in space and in the air as presented for example during the Symposium on Dynamical Gravimetry at Fort Worth in 1970, give rise to methods which are not so affected by very local topographic influence which bother gradiometer observers on the Earth's surface for several decades. One of the basic advantages of such methods lies in the fact that the influence of Δg at P (at the Earth's surface) on $\partial\Delta g/\partial h$ at a point P' (at elevation h) decreases as ℓ^{-5}, where $\ell = \overline{PP'}$. This rule holds for the lower altitudes above the Earth's surface. The basic *principles* are in these cases best represented by using Fourier series where for Δg_h at elevation h we get the well known relation

$$\Delta g_h = \sum F_{nm} \exp\left[i(u_n x + v_m y) - h(u_n^2 + v_n^2)^{\frac{1}{2}}\right] \qquad (3).$$

By transforming to a series of trigonometrical functions using Euler's formula we usually get for $\partial\Delta g/\partial h$ the coefficients

$$- a A_{nm} e^{-ah} \qquad (4)$$

and so on, whenever the coefficients of the corresponding Δg-series are A_{nm}, B_{nm} ....., where

$$a = \sqrt{(n^2 + m^2)}.$$

Analogously, the coefficients for the horizontal gradients are found to be

$$nm\, A_{nm} e^{-ah} \qquad (5)$$

and so on. For "two dimensional models" as often used in exploration geophysics, we have

$$n \gg m \qquad \text{or} \qquad n \ll m,$$

one of them being small. In these cases both types of gradients do not differ significantly; otherwise the latter formula behaves approximately like

$$a^2 A_{nm} e^{-ah} \qquad (6).$$

For $A_{nm} = 1$, the above expressions are discussed in figures 10 and 11. From gradients observed at elevations h, we arrive of course, at Δg at the Earth's surface by factor multiplications using

$$a\, e^{+ah} \qquad (7)$$

for vertical gradients, and by using

$$(nm)^{-1} e^{ah} \qquad (8).$$

The advantage, at least in theory, becomes evident by comparing the corresponding factor in downward

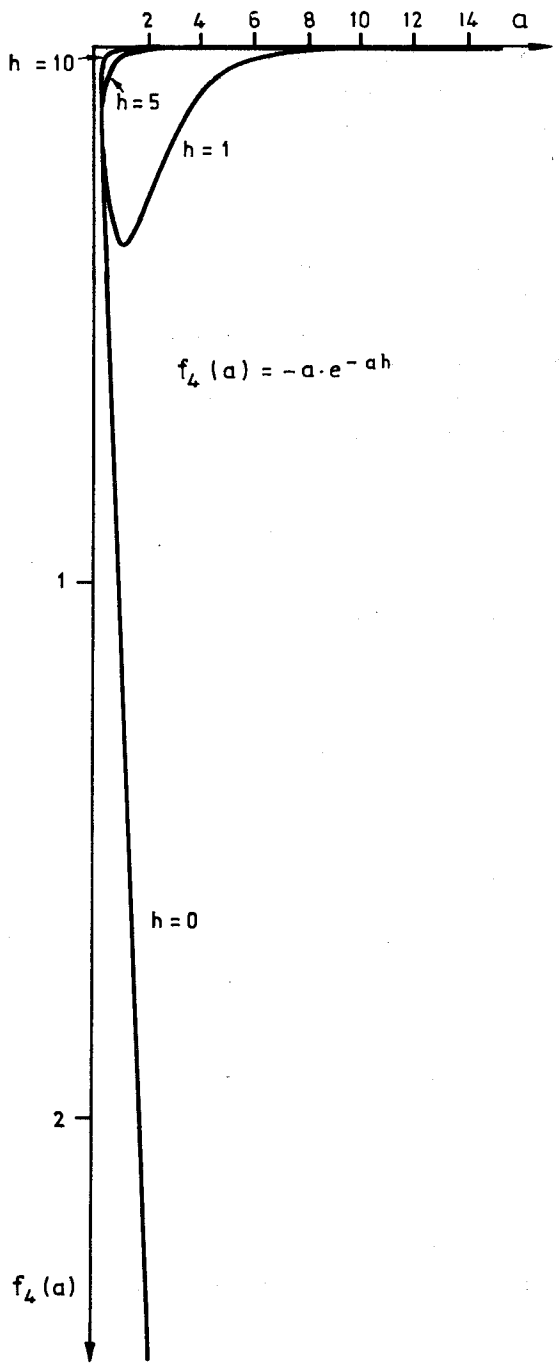

FIGURE 10: BEHAVIOUR OF TRIGONOMETRIC COEFFICIENTS DEPENDING ON a

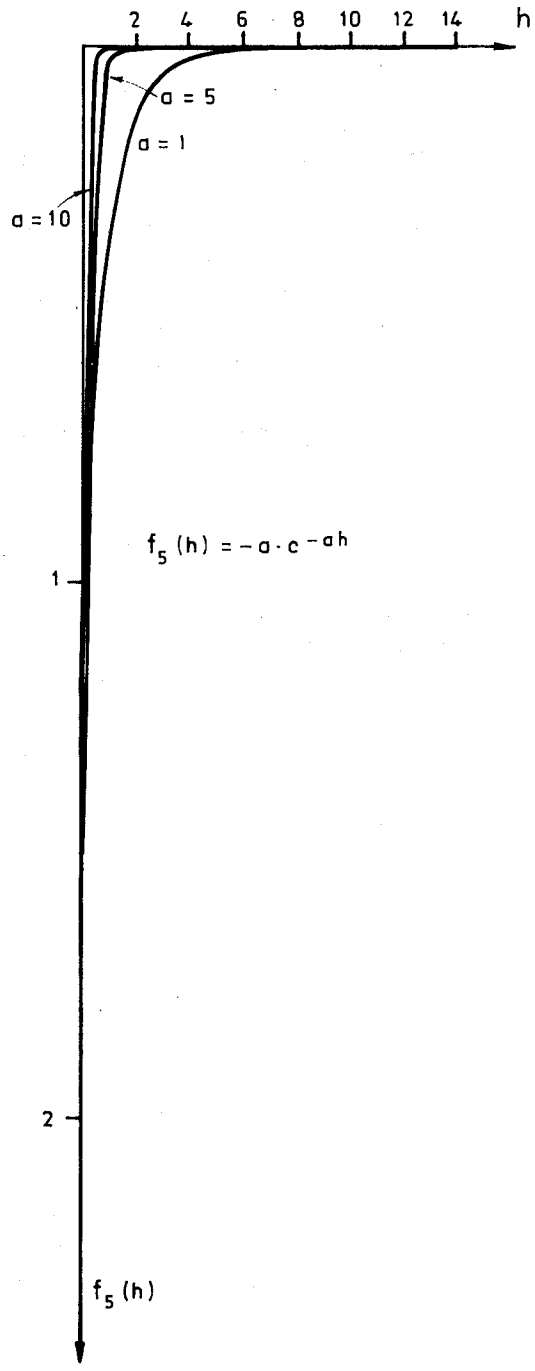

FIGURE 11: BEHAVIOUR OF TRIGONOMETRIC COEFFICIENTS DEPENDING ON h

continuation of Δg.

At higher elevations, the decrease of the effect of local phenomena is advatageous. FORWARD (1972) has given results of detailed studies using Kaula's rule $10^{-5}/n^2$. The difference in information obtained at high altitudes h > 250 km, at one side, and at altitudes h ≒ 10 km is best explained by figures 12 in the case of the "vertical gradient". It is realized that the superiority of gradient observations at satellite altitudes is relevant for harmonics of degree n > 40.

Figures 12 are self explaining as far as the general features are concerned. In dealing with spherical harmonic series, the slow decrease of the high harmonics of $\partial g/\partial h$ with increasing degree can be a remarkable disadvantage whenever real orbits are considered instead of the simple model orbits. For in this case averaging out of harmonics beyond a certain degree is no longer feasible so truncation errors arise which are higher than in the case of conventional orbital analysis. Even if the harmonic series is replaced by alternative representations of the gravity field, as done for example by Koch and others, any improvement cannot be anticipated. A term-by-term attribution of $\partial g/\partial h$ to the potential does not seem to be feasible in space, in any case. But in the case of "low" altitudes as for example in the case of aircraft profiles (as earlier mentioned), the application of linear integral equations is superior to spherical harmonic expansions as flat approximations are sufficient. Then, of course, truncation errors are avoided by simply smoothing the data.

2. References

ARNOLD, K. 1972. Das Geoid aus Beobachtungen der Satellitenaltimetrie. *Veroff. Deutsche Akad.Wiss. Zentralinst.Phys.der Erde* 7,Potsdam.

FORWARD, F.L. 1972. Geodesy with Orbiting Gradiometers. In "The use of Artificial Satellites for Geodesy" (Henriksen, S.W., Mancini, A. and Chovitz, B.H. (ed.)). *Am.geophys.U.Monograph* 15,239-244.

GREENE, A.H. 1972. Accuracy of Satellite Radar Altimeter Measurements. *Op.cit.supra.*,227-237.

GROTEN, E. 1970. Absolute Orientation of an Astrogeodetic Geoid Section and its Correlation with Geophysical Data. *Stud.geophys.et Geodet.* 2,212-221, Prague.

GROTEN, E. 1970a. Outline of Alternative Combination Solutions in Satellite Orbit Analysis. *Boll.geof. Teor. ed Appl.* XIII,250-255.

GROTEN, E. & RUMMEL, R. 1973. Improved Gravimetric Geoid for $7 \leq \lambda \leq 12^{\circ}$(E) and $47^{\circ} \leq \phi \leq 54$(N). *Allg.Vermessungsnachr.* (in press)

GROTEN, E. 1974. Geoid Computations using Heterogeneous Data Sets. Paper to be presented at *International Marine Geodesy Symposium,* Columbus Ohio.

KAULA, W.M. 1963. Determinations of the Earth's Gravitational Field. *Rev.geophys.* 1,507-551.

RAPP, R.H. 1971. Accuracy of Potential Coefficient Determinations from Satellite Altimetry and Terrestrial Gravity. *Rep.* 166,Dept. of Geodetic Science,The Ohio State University, Columbus Ohio.

RAPP, R.H. 1972. Geopotential Coefficient Behavior to High Degree and Geoid Information by Wavelength. *Rep.* 180,Dept. of Geodetic Science,The Ohio State University,Columbus Ohio.

RAPP, R.H. 1973. *Comparison of Least Squares and Collocation Estimated Potential Coefficients.* Presentation at International Summer School on Mathematical Methods in Physical Geodesy at Ramsau, Austria.

STANLEY, H.R., ROY, N.A., & MARTIN, C.F. 1972. Rapid Global Geoid Mapping with Satellite Altimetry. In "The Use of Artificial Satellites for Geodesy" (Henriksen, S.W., Mancini, A. & Chovitz, B.H. (ed.)). *Am. geophys.U.Monograph* 15,209-216.

VINCENT, S. & MARSH, J.G. 1973. Global Detailed Gravimetric Geoid. *International Symposium on the Use of Artificial Satellites for Geodesy & Geodynamics*,Athens.

WILLIAMSTOWN REPORT 1969. *The Terrestrial Environment: Solid Earth and Ocean Physics.* M.I.T. Measuring Systems Lab.,Cambridge Mass.

3. Acknowledgments

E. Tengstrom kindly made available recent data material of SSG 5:16, International Association of Geodesy; J. Brennecke and R. Rummel did most of the computer work.

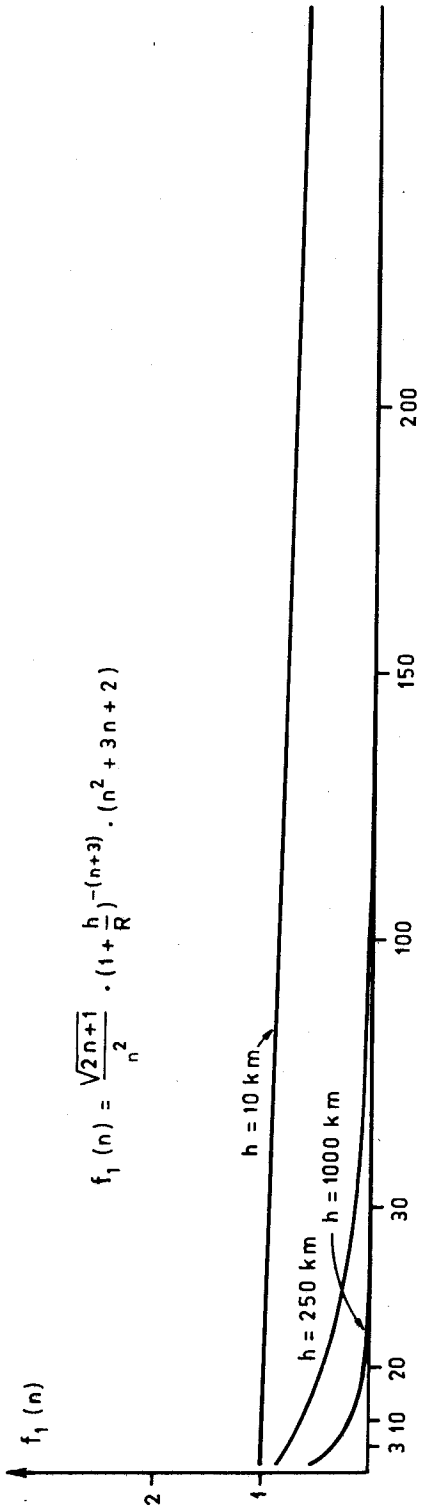

FIGURE 12 a: VERTICAL GRAVITY GRADIENT AT DIFFERENT ELEVATIONS.

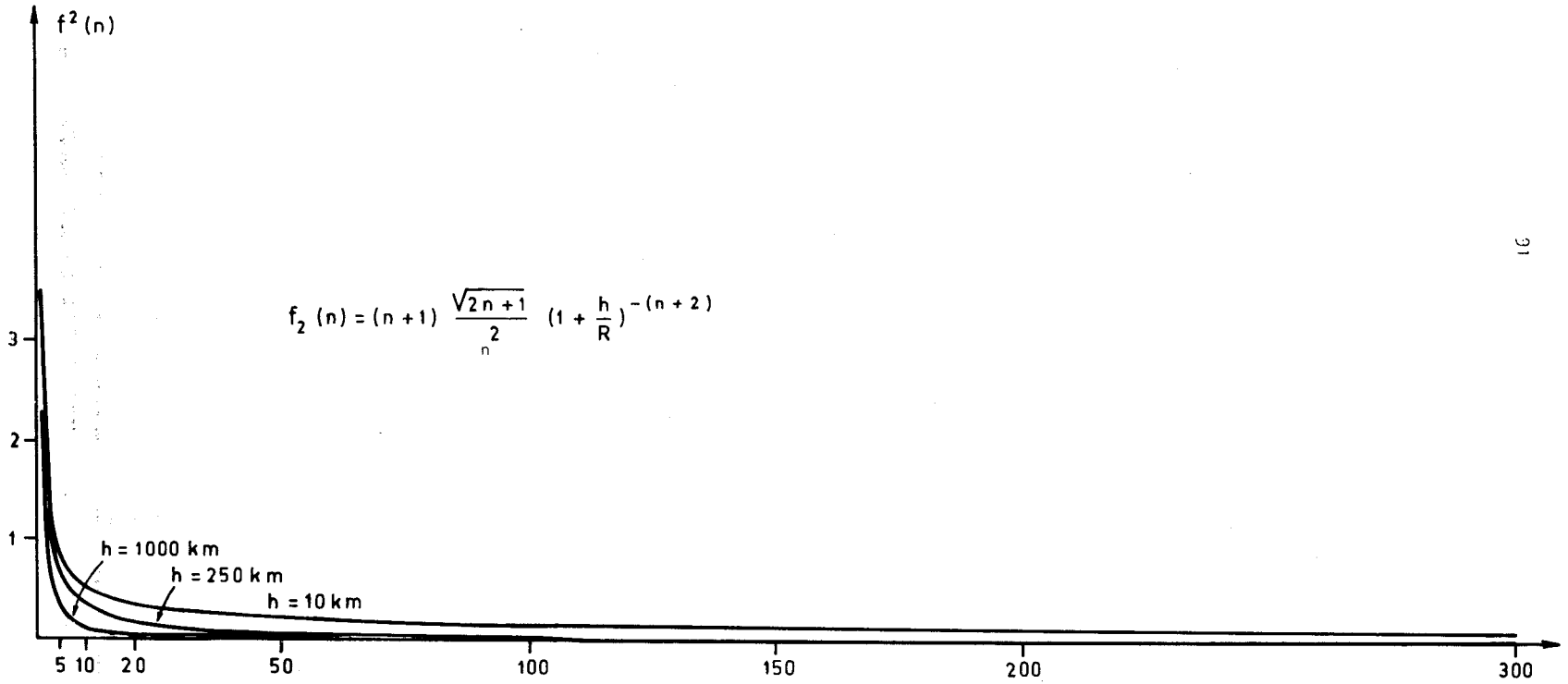

FIGURE 12 b: VERTICAL GRAVITY GRADIENT AT DIFFERENT ELEVATIONS

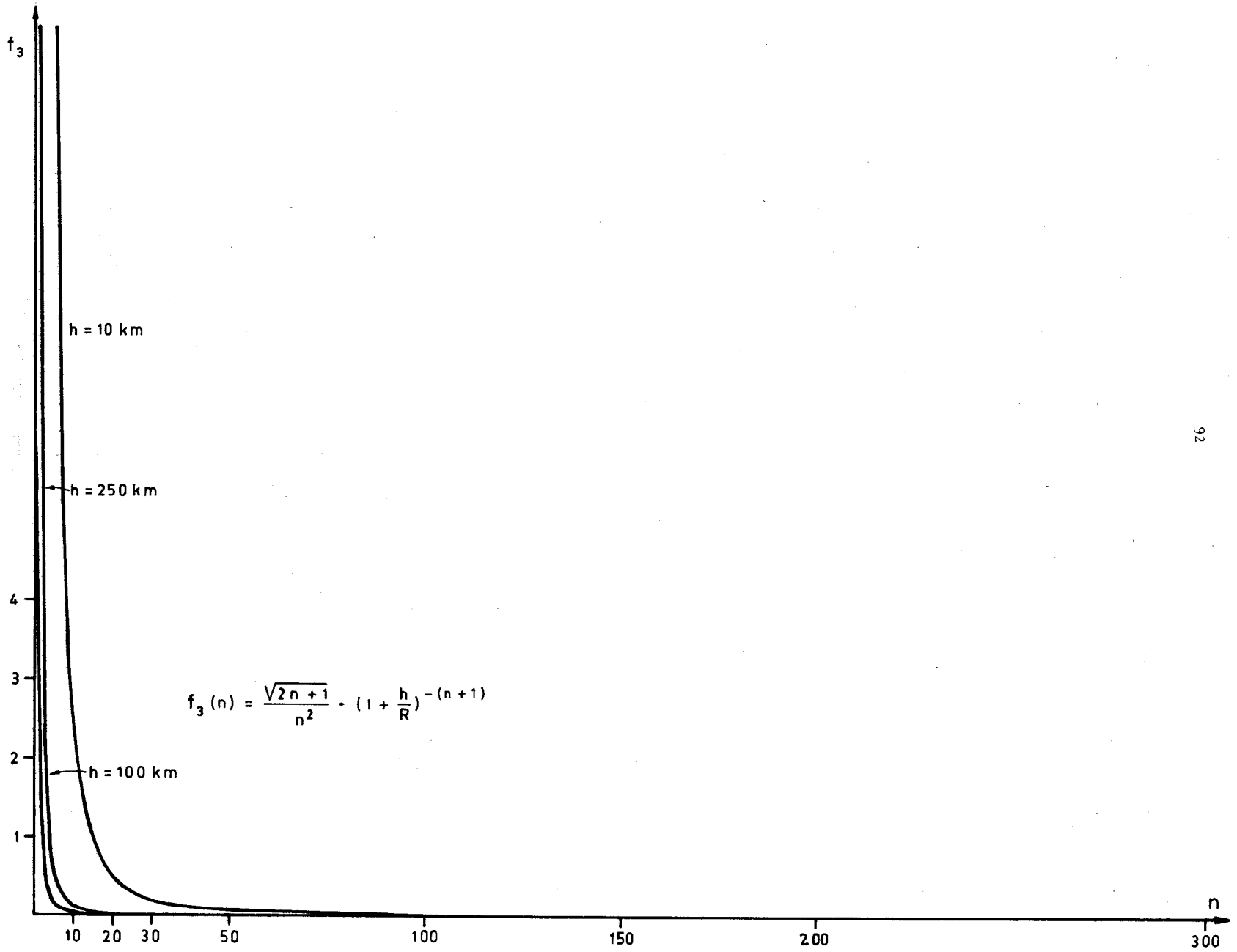

FIGURE 12 c: VERTICAL GRAVITY GRADIENT AT DIFFERENT ELEVATIONS.

HOPKINS, J.
Defence Mapping Agency
Aerospace Center
St. Louis AFS, Missouri 63118
United States of America

Proc. Symposium on Earth's Gravitational Field & Secular Variations in Position (1973), 93-105.

MATHEMATICAL MODELS OF GEOPOTENTIAL GRADIENTS

ABSTRACT

The gravitational potential of the Earth and its gradients are most frequently expressed in terms of spherical harmonics. This representation can be wasteful of computer time and/or core storage and can present numerical difficulties when higher degree coefficients are involved. A few viable alternatives to spherical harmonics such as point mass sets and surface density layers are examined. This evaluation is conducted in terms of goodness of fit and second order gradients of the geopotential and in terms of facility of computation.

1. Introduction

The most frequently used expression for the gravitational potential of the Earth at an exterior point is a summation of spherical harmonics. This expression can be easily differentiated with respect to the spherical co-ordinates of the external point to derive expressions for the first, second and higher order gradients (spatial derivatives) of the geopotential. The number of coefficients required for the spherical harmonic representation increases as the square of the highest degree used. In the electronic computer, then, this representation might utilize an undesirable amount of processing time and core storage. Further, numerical difficulties are encountered in many computers due to exponent limits on floating point numbers.

What we seek, then, is an alternate model which meets three criteria

(1) readily differentiable to any desired order;

(2) minimal number of coefficients; and

(3) avoidance of very large or very small exponents in the computations.

Representations considered in this paper are

(a) point masses (EALUM 1971);

(b) density layers (KOCH & WITTE 1971); and

(c) Taylor's series (JUNCOSA & JOHNS 1965).

Although the partial derivatives required for these representations are not as succint as those in the spherical harmonic representation, a little care is all that is required.

We might select a "best" model from these alternatives by considering the goodness of fit to test data in various applications. Possibly, we may select as "best" that model which is most conservative of computer time and/or core storage. Again, we may wish to consider the trade-offs between goodness of fit and computer resource conservation. The purpose of this paper is to present the derivation of the models rather than propose a definitive selection of a "best" model.

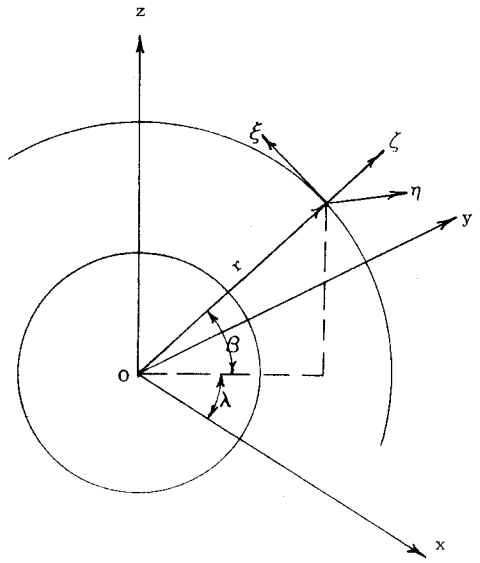

Figure 1. Global and Local Co-ordinate Systems

2. Fundamentals

The geopotential and its gradients are herein represented in terms of global spherical co-ordinates, global Cartesian co-ordinates, and local Cartesian co-ordinates (see figure 1). We define the global spherical co-ordinates (β,λ,r) in the usual sense, i.e., β is the geocentric latitude for the exterior point, λ is its geocentric longitude (from Greenwich), and r its geocentric radius. We define the global Cartesian co-ordinates (x,y,z) as being Earth centred - Earth fixed with the z axis coincident with the Earth's rotational axis and the xy plane coincident with the Earth's equatorial plane. The x axis is directed through the Greenwich meridian and the y axis completes the right-handed orthogonal triad. The local Cartesian co-ordinates (ξ,η,ζ) are defined as being centred at the exterior point and oriented so that the ζ axis coincides with the outward directed radius vector. The $\xi\eta$ plane is normal to this axis with the ξ and η axes directed north and east, respectively.

The first order derivatives of the geopotential express the components of the gravity vector at the exterior point. In terms of partial derivatives with respect to spherical co-ordinates, they are (MORITZ 1971)

$$V_\zeta = V_r \quad ; \quad V_\xi = -\frac{1}{r} V_\beta \quad ; \quad V_\eta = \frac{1}{r \cos\beta} V_\lambda \qquad (1),$$

where $V_r = \partial V/\partial r$, etc. The second order derivatives express the components of the gravity gradient tensor at the exterior point. Again, in terms of partial derivatives with respect to the spherical co-ordinates (IBID)

$$V_{\xi\xi} = \frac{1}{r^2} V_{\beta\beta} + \frac{1}{r} V_r \qquad (2a),$$

$$V_{\xi\eta} = -\frac{1}{r^2 \cos\beta} V_{\beta\lambda} + \frac{1}{r^2 \sec\beta \tan\beta} V_\lambda = V_{\eta\xi} \qquad (2b),$$

$$V_{\xi\zeta} = -\frac{1}{r} V_{r\beta} + \frac{1}{r^2} V_{\beta} = V_{\zeta\xi} \quad (2c),$$

$$V_{\eta\eta} = \frac{1}{r^2\cos^2\beta} V_{\lambda\lambda} + \frac{1}{r} V_r + \frac{1}{r^2}\tan\beta\, V_{\beta} \quad (2d),$$

$$V_{\eta\zeta} = \frac{1}{r\cos\beta} V_{r\lambda} - \frac{1}{r^2\cos\beta} V_{\lambda} = V_{\zeta\eta} \quad (2e),$$

and

$$V_{\zeta\zeta} = V_{rr} \quad (2f).$$

Gradients can be transformed between local and global Cartesian co-ordinates by a rotation matrix (IBID)

$$\begin{pmatrix} V_x \\ V_y \\ V_z \end{pmatrix} = A \begin{pmatrix} V_\xi \\ V_\eta \\ V_\zeta \end{pmatrix} \quad (3),$$

and

$$\begin{pmatrix} V_{xx} & V_{xy} & V_{xz} \\ V_{yx} & V_{yy} & V_{yz} \\ V_{zx} & V_{zy} & V_{zz} \end{pmatrix} = A \begin{pmatrix} V_{\xi\xi} & V_{\xi\eta} & V_{\xi\zeta} \\ V_{\eta\xi} & V_{\eta\eta} & V_{\eta\zeta} \\ V_{\zeta\xi} & V_{\zeta\eta} & V_{\zeta\zeta} \end{pmatrix} A^T \quad (4)$$

where

$$A = \begin{pmatrix} -\sin\beta\cos\lambda & -\sin\lambda & \cos\beta\cos\lambda \\ -\cos\beta\sin\lambda & \cos\lambda & \cos\beta\sin\lambda \\ \cos\beta & 0 & \sin\beta \end{pmatrix} \quad (5),$$

or by its inverse, which equals its transpose due to orthogonality

$$\begin{pmatrix} V_\xi \\ V_\eta \\ V_\zeta \end{pmatrix} = A^T \begin{pmatrix} V_x \\ V_y \\ V_z \end{pmatrix} \quad (6)$$

and

$$\begin{pmatrix} V_{\xi\xi} & V_{\xi\eta} & V_{\xi\zeta} \\ V_{\eta\xi} & V_{\eta\eta} & V_{\eta\zeta} \\ V_{\zeta\xi} & V_{\zeta\eta} & V_{\zeta\zeta} \end{pmatrix} = A^T \begin{pmatrix} V_{xx} & V_{xy} & V_{xz} \\ V_{yx} & V_{yy} & V_{yz} \\ V_{zx} & V_{zy} & V_{zz} \end{pmatrix} A \quad (7).$$

We note here, also, that the gradient tensors, both local and global are symmetric. Also, per Laplace's equation

$$V_{xx} + V_{yy} + V_{zz} = V_{\xi\xi} + V_{\eta\eta} + V_{\zeta\zeta} = 0.$$

3. Mathematical Models

3.1 Spherical Harmonics

The usual expression for the gravitational potential of the Earth on an external point in terms of spherical harmonics is (e.g., HOTINE 1969)

$$V(\beta,\lambda,r) = \frac{GM}{r}\left[1 + \sum_{n=2}^{\infty}\left(\frac{a}{r}\right)^n \sum_{m=0}^{n} P_{nm}(\sin\beta)\left(C_{nm}\cos m\lambda + S_{nm}\sin m\lambda\right)\right] \quad (8),$$

where (β,λ,r) = global spherical co-ordinates of exterior point,
GM = Earth's gravitational constant,
a = Earth's equatorial radius,
$P_{nm}(\sin\beta)$ = associated Legendre functions, and
C_{nm}, S_{nm} = conventional geopotential coefficients.

This expression can be easily differentiated to yield the required partial derivatives.

We see that frequent references to sine and cosine routines are required in the computation process. as the coefficient set grows larger, the number of associated Legendre functions required increases rapidly. Recursive relations (HOPKINS 1973; BURINGTON 1949) are available to relieve the situation somewhat. Still, the process is quite formidable. If in the above equation, we choose to eliminate the effects of the constant term and of the coefficients C_{20} and C_{40}, we operate upon the anomalous potential T, i.e.,

$$T = V - U \quad (9)$$

where

$$U = \frac{GM}{r}\left[1 + \left(\frac{a}{r}\right)^2 P_{20}(\sin\beta)\, C_{20} + \left(\frac{a}{r}\right)^4 P_4\right.$$

a readily differentiable form. The anomalous potential le
(e.g., HEISKANEN & MORITZ 1967,p.86)

$$\Delta g = -\frac{\partial T}{\partial r} - \frac{2}{a}T$$

In terms of spherical harmonics (e.g., RAPP 1972)

$$\Delta g = \frac{GM}{r^2}\left[\sum_{n=2}^{\infty}\left(\frac{a}{r}\right)^n (n-1)\sum_{m=0}^{n} P\right.$$

where the C_{20} and C_{40} are omitted.

3.2 Point Masses

The basic formulation for the gravitational potential at a p
terms of point masses is (EALUM 1971)

$$V_i(\beta,\lambda,r) = GM \sum_{j=1}^{N}\left(\frac{m_j}{M}\right)\frac{1}{\rho_{ij}}$$

where

(m_j/M) = ratio of the j-th point mass to the Earth's mass;

ρ_{ij} = distance from the point mass j to the exterior point i; and

N = number of point masses in the set.

In the global Cartesian co-ordinate system (x,y,z),

$$\rho_{ij}^2 = (x_i - x_j)^2 + (y_i - y_j)^2 + (z_i - z_j)^2 \qquad (14),$$

while in the global spherical co-ordinate system (β,λ,r)

$$\rho_{ij}^2 = r_i^2 + r_j^2 - 2r_i r_j \cos\psi \qquad (15).$$

The subscript $_i$ refers to the exterior point and the subscript $_j$ refers to the j-th point mass. The spherical distance ψ is given by

$$\cos\psi = \sin\beta_i \sin\beta_j + \cos\beta_i \cos\beta_j \cos(\lambda_i - \lambda_j) \qquad (16).$$

The partial derivatives which are form-invariant within and between the global co-ordinate systems, by the chain rule, are

$$V_s = GM \sum_{j=1}^{N} \left(\frac{m_j}{M}\right) \frac{1}{\rho_{ij}^2} \frac{\partial \rho_{ij}}{\partial s} \qquad (17a)$$

and

$$V_{st} = GM \sum_{j=1}^{N} \left(\frac{m_j}{M}\right) \left(\frac{2}{\rho_{ij}^3} \frac{\partial \rho_{ij}}{\partial s} \frac{\partial \rho_{ij}}{\partial t} - \frac{1}{\rho_{ij}} \frac{\partial^2 \rho_{ij}}{\partial s \partial t}\right) \qquad (17b),$$

where $s,t = x_i, y_i$ or z_i or $s,t = \beta_i, \lambda_i$ or r_i.

Computations of gradients in the global Cartesian co-ordinates (x,y,z) is accomplished directly by taking the partial derivatives in the above equation with respect to x, y and z. Should gradients be required in the local Cartesian co-ordinate system (ξ,η,ζ), transformations reflected by equations 6 and 7 are applied.

On the other hand, if the partial derivatives are taken with respect to β, λ and r, the computation of gradients in the local Cartesian co-ordinates (ξ,η,ζ) proceeds through equations 1 and 2. Should gradients be required in global Cartesian co-ordinates (x,y,z), transformations reflected by equations 3 and 4 are applied.

The gravity anomaly, a function of the anomalous potential, can readily be expressed in global Cartesian co-ordinates (NEEDHAM 1970) as

$$\Delta g_i = GM \sum_{j=1}^{N} \left(\frac{m_j}{M}\right) \left(\frac{r_i^2 - F_{ij}}{\rho_{ij}^3 r_i} - \frac{2}{\rho_{ij} r_i}\right) \qquad (18),$$

where

$$F_{ij} = x_i x_j + y_i y_j + z_i z_j .$$

3.3 Density Layers

The basic formulation for the gravitational potential at a point exterior to the Earth expressed in terms of density layers is (KOCH & WITTE 1971)

$$V_i(\beta,\lambda,r) = \frac{GM}{r_i}\left\{1 + \sum_{n=2}^{n_{max}} \left(\frac{a}{r_i}\right)^n \sum_{m=0}^{n} P_{nm}(\sin\beta_i)\left(C_{nm}\cos m\lambda_i + S_{nm}\sin m\lambda_i\right)\right\} + \sum_{j=1}^{N} \chi_j \iint_{\Delta E_j} \frac{dE_j}{\rho_{ij}} \quad (19),$$

where χ_i = density function of layer;

E_j = area of layer;

n_{max} = maximum degree of spherical harmonic portion; and

N = number of density layers.

If the potential be represented as the sum of the spherical harmonic portion and the density layer portion, i.e.,

$$V = U + T,$$

the density layers can be used to represent the residual potential above a certain harmonic degree n_{max}. Now let

$$T_i = \sum_{j=1}^{N} \chi_j \iint_{\Delta E_j} \frac{dE_j}{\rho_{ij}} \quad (20).$$

This equation expresses a critical point in the density layer model. Since the integral over the surface element E_j is solved numerically, it is subject to errors of quadrature. KOCH (1971) develops analytical expressions for the surface elements on ellipsoidal and spherical surfaces which can be used in lieu of the integral. Fineness of the grid about the computation point is analogous to the well known scheme for computation of geoid heights from surface mean gravity anomaly elements.

The integral in equation 20 is replaced by the area of the layer, i.e.,

$$E_j/\rho_{ij} = \iint_{\Delta E_j} dE_j/\rho_{ij} \quad (21)$$

and the anomalous potential can be expressed as

$$T_i = \sum_{j=1}^{N} \chi_j \frac{E_j}{\rho_{ij}} \quad (22).$$

The development of expressions for the gradients in the local Cartesian co-ordinate system (ξ,η,ζ) closely parallels the development in terms of point masses, i.e., equation 17. Quite simply,

$$T_p = \sum_{j=1}^{N} -\chi_j E_j \frac{1}{\rho_{ij}^2} \frac{\partial\rho_{ij}}{\partial p} \quad (21a)$$

and

$$T_{pq} = \sum_{j=1}^{N} \chi_j E_j \left(\frac{2}{\rho_{ij}^3} \frac{\partial\rho_{ij}}{\partial p} \frac{\partial\rho_{ij}}{\partial q} - \frac{1}{\rho_{ij}^2} \frac{\partial^2\rho_{ij}}{\partial p\partial q}\right) \quad (21b)$$

where

$$p,q = (\beta_i,\lambda_i,r_i).$$

The computation of the gradients then proceeds through equations 1 and 2.

3.4 Taylor Series

While the coefficients in the point mass and density layer approaches have some physical meaning, the Taylor series approach (JUNCOSA & JOHNS 1965) is unique in that the coefficients do not. For the basis of this method we return to fundamental potential theory. Let (β,λ,r) and (β',λ',r') be the spherical co-ordinates of the exterior point and some mass element dm of the attracting mass, as illustrated in figure 2. For the potential the the exterior point, we have

$$F(\beta,\lambda,r) = \frac{G}{r}\iiint \frac{dm(\beta',\lambda',r')\, d\beta'\, d\lambda'\, dr'}{\left(1 + (r'/r)^2 - 2(r'/r)\cos\theta\right)^{\frac{1}{2}}} \qquad (22).$$

The integration is taken over the Earth's total volume. Denoting the direction cosines of the two vectors by

$$(u,v,w) = (\cos\lambda\cos\beta, \sin\lambda\cos\beta, \sin\beta) \quad ; \quad \text{and}$$
$$(\xi,\eta,\zeta) = (\cos\lambda'\cos\beta', \sin\lambda'\cos\beta', \sin\beta'),$$

we have

$$\cos\theta = u\xi + v\eta + w\zeta .$$

Then equation 22 can be expressed in the form of a Taylor series

$$F(\beta,\lambda,r) = \frac{G}{r}\iiint \sum_i \sum_j \sum_k C_{ijk} u^i \xi^i v^j \eta^j w^k \zeta^k \left(\frac{r'}{r}\right)^{i+j+k} dm\, d\beta'\, d\lambda'\, dr' \qquad (23),$$

where C_{ijk} are coefficients that depend upon the various derivatives of the integrand with respect to $u\xi$, $v\eta$ and $w\zeta$ up to the (i+j+k)-th order.

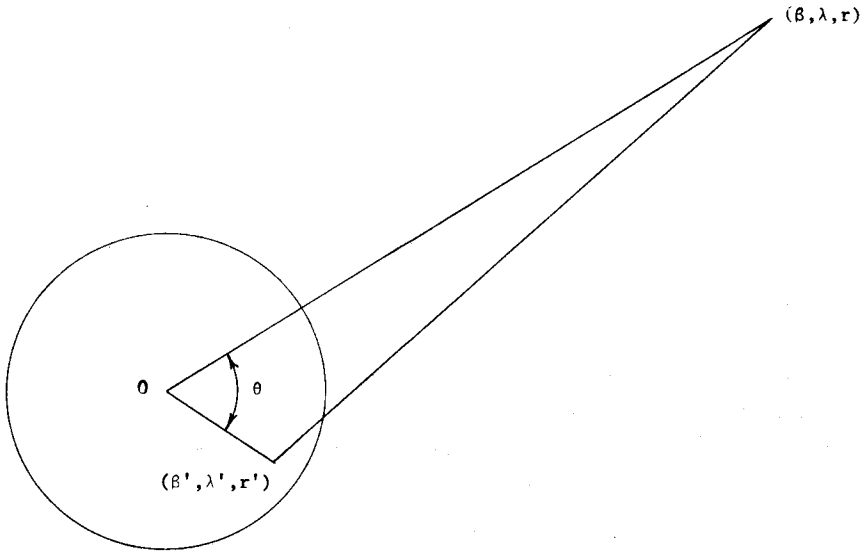

Figure 2. Geometry of Potential Theory

We now invert the order of integration and summation and perform the summations in the order

$$i + j + k = 0 \; ; \quad i + j + k = 1 \; ; \quad i + j + k = 2 \; ; \quad \text{etc.}$$

Recognizing here that the possible derivatives are linearly dependent since $u^2 + v^2 + w^2 = 1$, we may finally write for the potential

$$\begin{aligned} F(\beta,\lambda,r) = {} & \frac{A}{r} + \frac{1}{r^2}\left(B_1 u + B_2 v + B_3 w\right) + \frac{1}{r^3}\left(C_1(3u^2 - 1) + C_2(3v^2 - 1) + C_3 uv + C_4 uw + C_5 vw\right) + \\ & \frac{1}{r^4}\left(D_1(5u^2 - 3)u + D_2(5v^2 - 3)v + D_3(5u^2 - 1)v + D_4(5v^2 - 1)u + D_5(5u^2 - 1)w + \right. \\ & \left. D_6(5v^2 - 1)w + D_7 uvw\right) + \frac{1}{r^5}\left(E_1(35u^4 - 30u^2 + 3) + E_2(35v^4 - 30v^2 + 3) + \right. \\ & E_3(7u^2 - 3)uv + E_4(7v^2 - 3)uv + E_5(7u^2 - 3)uw + E_6(7v^2 - 3)vw + E_7(35u^2v^2 + 5w^2 - 4) + \\ & \left. E_8(7u^2 - 1)vw + E_9(7v^2 - 1)uw\right) \end{aligned} \qquad (24),$$

where A, B_1, B_2, ... E_9 are coefficients to be determined. While this expansion is given to the fifth power of r^{-1}, the pattern is readily seen, should it be desirable to extend the representation to higher powers of r^{-1}.

Obtaining the required partial derivatives of equation 24 with respect to the spherical co-ordinates of the exterior point is quite tedious, but the derivatives themselves are rather simple. The partial derivatives with respect to r, i.e., F_r and F_{rr} are direct, while the remaining partial derivatives involve the chain rule, i.e.,

$$F_x = \frac{\partial F}{\partial u}\frac{\partial u}{\partial x} + \frac{\partial F}{\partial v}\frac{\partial v}{\partial x} + \frac{\partial F}{\partial w}\frac{\partial w}{\partial x} \qquad (25),$$

and

$$F_{xy} = \frac{\partial^2 F}{\partial u^2}\frac{\partial u}{\partial x}\frac{\partial u}{\partial y} + \frac{\partial^2 F}{\partial v^2}\frac{\partial v}{\partial x}\frac{\partial v}{\partial y} + \frac{\partial^2 F}{\partial w^2}\frac{\partial w}{\partial x}\frac{\partial w}{\partial y} + \frac{\partial F}{\partial u}\frac{\partial^2 u}{\partial x \partial y} + \frac{\partial F}{\partial v}\frac{\partial^2 v}{\partial x \partial y} + \frac{\partial F}{\partial w}\frac{\partial^2 w}{\partial x \partial y} \qquad (26),$$

where

$$x,y = \beta, \lambda \text{ or } r.$$

We then proceed through equations 1 and 2 to obtain gradients in the local Cartesian co-ordinate system (ξ,η,ζ).

4. Characteristics of Observations

While the gravitational potential is not usually measured directly, satellite-to-satellite tracking provides a means of doing so (COMFORT 1971). Equations 8, 13, 19 and 24 express the potential in the various mathematical models under discussion. The first order gradient is the gravity vector at the exterior point. In practice, it might be measured as range and/or angular rates, but for the sake of this paper, it will be used directly.

The second order gradients or gravity gradients can be measured directly by gradiometers at or near the surface of the Earth or at satellite altitudes (HOPKINS 1972). In the surface case, we expect that a three sensor system will yield all nine components of the gradient tensor (of which five are independent). In the orbit case, the principal contribution to the signal is (GLASER & SHERRY 1971)

$$V_{\zeta\zeta} - V_{\xi\xi} = V_{rr} - \frac{1}{r^2} V_{\beta\beta} - \frac{1}{r} V_r \qquad (27).$$

Currently, the best data we have available for determining the geopotential is the set of mean gravity anomalies. Using potentials, first order gradients, second order gradients, or mean gravity data as observations, equations can readily be written for computation of spherical harmonic coefficients, point mass ratios, density values, or Taylor series coefficients by a least squares process. Generation of pseudo-observations for numerical tests is described in the following section.

5. Numerical Tests

Pseudo-observation data generated using the spherical harmonic model was used as a norm against which to compare the alternative models. Using a set of spherical harmonic coefficients complete to degree and order 36, potentials, gravity vector components and gravity gradients were computed for 1440 points defined in global spherical Earth fixed co-ordinates selected from polar, circular orbit at an altitude of about 300 km. A set of surface gravity gradient pseudo-observations was computed in a latitude band extending 45 degrees each side of the equator. The harmonic coefficients were themselves derived from recent unclassified mean free air gravity anomaly data.

Initially, a set of 186 point mass ratios, spaced over the Earth at a 900 nautical mile interval, was computed from the anomalous potential data, i.e., the input observations were adjusted to remove the contribution of the reference ellipsoid. The masses were placed at a distance of 5400 km from the Earth's centre. From these mass ratios, the first and second order gradients and mean gravity anomalies were computed and compared with the test data. The required gradients were computed both in local co-ordinates directly and in global co-ordinates rotated to local. To assess the effect of increasing the mass set size, a set of 410 point mass ratios, spaced over the Earth at 600 nautical mile intervals were computed from the V_ζ component of the orbit data. From this data the potential and the remaining gradients and gravity anomaly data were computed and compared with the test data. The density layer concept was applied by computing a set of density layer values located on the surface of the Earth coincident with the location of the point masses. The anomalous potential data was used to derive these values, without application of the quadrature techniques to represent the surface element. As in the point mass tests, the first and second order gradients were computed and compared with test values.

The Taylor series coefficients were computed from the full potential values. A total of 25 coefficients were computed, incorporating the fifth power of r^{-1}. From the coefficients, the first and second order gradients were computed and compared with the test data. Test results are given in Table 1.

We expect a good comparison between potentials as this is the data used to derive the coefficients for the representation. All comparisons are within an order of magnitude of the desired accuracy. The computation of the gravity vector components directly in local co-ordinates, more complex mathematically, yields no better results than the simpler global to local computation. The gravity gradients, especially those in orbit, are reasonably well predicted by either route. Generally the mean anomaly results are somewhat poor. However, a spherical harmonic representation for gravity anomalies can be just as poor for certain coefficient sets derived solely from orbit data (DECKER 1972). Another

important consideration is that of computer time. One may wish to consider trade-offs in computer time versus accuracy. Typical computer times are given in table 2.

A substantial savings of computer time in the application of the point mass model can be achieved by the computation of the gradients in global co-ordinates and applying the appropriate rotation matrices. Each alternative model represents a savings over the spherical harmonic model in terms of computer time, the price being a loss of accuracy to some degree.

6. Conclusions

It is reasonable to conclude that all three alternatives to the spherical model are viable. The limited size of the point mass, density layer or Taylor series coefficient sets introduces a limit to the precision of representation. Each representation can be made more accurate by increasing the number of defining coefficients.

The Taylor series representation provides the most compact representation and is highly conservative of computer time. The point mass and density layer models are competetive with it and with each other. The trade off is an order of magnitude difference in computer time requirements versus a factor of two improvement in accuracy.

In such applications as orbit computations using a numerical integration scheme such as Runge-Kutta or Cowell's method, the necessity to re-compute the gravity vector component several times in one integration step makes the Taylor series model quite attractive. It is for this reason that heretofore ignored Taylor series model ought to be given further study. It is my intention to do so.

7. Acknowledgments

The assistance rendered to me by my son, John L. Hopkins, student at Florissant Valley Community College, St. Louis, Missouri, in checking my mathematics is sincerely appreciated. His satisfaction in detecting errors committed by his father has enhanced my confidence in the algebra involved.

8. References

BURINGTON, J.S. 1951. *Handbook of Mathematical Tables and Formulas.* (3rd ed.) Handbook Publishers, Sandusky, Ohio.

COMFORT, G.C. 1971. The Determination of Gravitational Potential from the Measurement of Relative Velocity between Satellites. *Rep.* T-545, Charles Stark Draper Lab., Massachusetts Institute of Technology, Cambridge, Mass.

DECKER, B.L. 1972. Present Day Accuracy of the Earth's Gravitational Field. *Proceedings (microfilm) International Symposium on Earth Gravity Models and Related Problems*, St. Louis, Mo.; (Abstr.) *EOS Trans. Am. geophys. U.* 53,891.

EALUM, R.L. 1971. *Gravity Field Representation by Point Mass Sets.* Doctoral Dissertation, Cornell University, Ithaca, NY.

GLASER, R.J. & SHERRY, E. 1971. *Relationship of Gravity Gradients to Spherical Harmonics.* Jet Propulsion Laboratory, Pasadena Calif.

HEISKANEN, W.A. & MORITZ, H. 1967. *Physical Geodesy.* Freeman, San Fransisco.

HOPKINS, J. 1973. Computation of Normalized Associated Legendre Functions Using Recursive Relations. *J. geophys. Res.* 78,476-477.

Table 1

Data Comparisons (RMS - Computed vs Test Data)

Model	Potential cm^2/sec^2	V_ζ	V_η cm/sec^2	V_ξ	$V_{\zeta\zeta}$ (Surface) EU**	$V_{\zeta\zeta} - V_{\xi\xi}$ EU**	Δg cm/sec^2
Point Masses(186)	8.9×10^4						
Local		3.0×10^{-3}	2.1×10^{-3}	2.2×10^{-3}	4.2×10^{-1}	1.6×10^{-1}	1.1×10^{-2}
Global to Local		1.1×10^{-2}	7.2×10^{-3}	6.9×10^{-3}	*	1.6×10^{-1}	1.1×10^{-2}
Point Masses(410)	1.5×10^6						
Local		1.6×10^{-3}	1.7×10^{-2}	3.4×10^{-3}	1.3	8.5×10^{-1}	4.6×10^{-2}
Global to Local		1.6×10^{-3}	1.7×10^{-2}	3.2×10^{-3}	*	3.3×10^{-1}	4.6×10^{-2}
Density Layers	2.7×10^5	4.1×10^{-2}	9.0×10^{-3}	7.6×10^{-3}	*	7.7×10^{-1}	*
Taylor Series	6.4×10^5	7.6×10^{-3}	5.4×10^{-3}	4.7×10^{-3}	4.2×10^{-1}	2.1×10^{-1}	1.3×10^{-2}
Representative Values	6.0×10^{11}	8.8×10^2	7.6×10^{-3}	1.2	3.1×10^3	4.5×10^3	1.4×10^{-2}
Desired Accuracy	1.0×10^5	3.0×10^{-3}	3.0×10^{-3}	3.0×10^{-3}	1.0	1.0×10^{-1}	2.0×10^{-3}

* Computation not made

** 1 EU = 10^{-9} cm $sec^{-2} cm^{-1}$ (Eötvos unit)

Table 2

Computation Times (UNIVAC 1108)

Model	Derive Coefficients (Total)	V_ζ, V_η, V_ξ sec/pt	$V_{\zeta\zeta}$ sec/pt	$V_{\zeta\zeta} - V_{\xi\xi}$ sec/pt	Δg sec/pt
Point Masses (186)	$8^m\ 15^s$				
Local		0.253	0.103	0.231	0.138
Global to Local		0.064	*	0.121	0.058
Point Masses (410)	$1^h\ 23^m\ 45^s$				
Local		0.491	0.206	0.815	0.292
Global to Local		0.114	*	0.212	0.094
Density Layers	$9^m\ 08^s$	0.220	*	0.226	*
Taylor Series	$0^m\ 28^s$	0.026	0.009	0.035	0.015
Spherical Harmonics	*	0.377	0.145	0.378	0.150

* Not computed

HOPKINS, J. 1972. The Combination of Gradiometer and Satellite Data for an Earth Gravitational Model. Defence Mapping Agency Aerospace Center, St. Louis, Mo.; (Abstr.)*EOS Trans.Am. geophys.U.* 53,967.

HOTINE, M. 1969. Mathematical Geodesy. *ESSA Monograph* 2, Washington, DC.

JUNCOSA, M.L. & JOHNS, R.K.C. 1965. A Chebyshev Approximation to the Earth's External Gravipotential with Internally Unrestricted Mass Distribution. *Memorandum* RM-4677-PR, The Rand Corporation, Santa Monica, California.

KOCH, K.-R. 1971. Errors of Quadrature Connected with the Simple Layer Model of the Geopotential. *NOAA Tech.Memo. NOS* 11, Rockville, Md.

KOCH, K.-R. & WITTE, B.U. 1971. Earth's Gravity Field Represented by a Simple Layer Potential from Doppler Tracking of Satellites. *J.geophys.Res.* 76,8477-8479.

MORITZ, H. 1971. Kinematical Geodesy II. *Rep.* 165,Dept. of Geodetic Science,The Ohio State University, Columbus,Ohio.

NEEDHAM, P.E. 1970. The Formulation and Evaluation of Detailed Geopotential Models Based on Point Masses. *Rep.* 149,Dept. of Geodetic Science, The Ohio State University, Columbus,Ohio.

RAPP, R.H. 1972. Improved Models for Anomaly Computations from Potential Coefficients. *Rep.* 181, Dept. of Geodetic Science, The Ohio State University, Columbus,Ohio.

WITTE, B.U. 1971. Computational Procedures for the Determination of a Simple Layer Model of the Geopotential from Doppler Observations. *NOAA Tech. Rep. NOS* 42,Rockville,Md.

9. Discussion

RAPP: Let me add a comment about gravity gradiometers because I think it is something that may be coming along. Many people think that gravity gradiometry is primarily going to help us determine the details of the gravity field; if you observe a gradiometer over an area it reacts very locally.

HOPKINS: I should like to add that gravity gradiometry can assist in getting global information of long wavelength.

RAPP: The question is whether the gravity gradiometer will be accurate enough to obtain the resolution obtained presently from potential coefficients using the orbital technique.

HOPKINS: The accuracy of the gradiometer is one part in a billion plus or minus another twenty (bias).

RAPP: Second; the representations you tested. There is another one that would have been nice to test - the gravity anomaly, which is something you can measure. You don't measure point masses or terms in a Taylor series. So if you are looking for a representation which can easily be combined, you use the anomaly. A report was completed nine months ago by a graduate student (G. REED of the US Army) at the Ohio State University on satellite gradiometry and its implications in determining the gravity field of the Earth. He studied the problem of recovering gravity anomalies or point masses from rotating gradiometer data or a hard mounted system. He concluded that the most reasonable representation was obtained using anomalies. The use of an anomaly representation allows straightforward combination solutions to be made. So I add that as a comment; there are additional views to those expressed by you.

ECKHARDT: I have a question on Taylor series. You have a spherical solid harmonic converted to a Cartesian type solid harmonic. Is it the identical thing whether you do it in spherical or rectangular harmonics. The Taylor series should give the same answer as the spherical harmonics. You are comparing your models with much higher degree models. In a way it is not fair.

HOPKINS: That's what I am doing with the point masses. I am comparing smaller models with the rather larger spherical harmonic models.

ECKHARDT: You should compare Taylor series models with the same degree spherical harmonic models - with the same amount of information - and see what you get in the shortest time. That will give the answer.

GRAFAREND: You mention the transformation between the local system and the geocentric system done by Moritz. This only holds for a spherical Earth. It does not hold for an ellipsoidal Earth or the real Earth. Your formulae are therefore restricted. The exact transformation is given in (HOTINE, M. *Mathematical Geodesy*. ESSA Monograph 2,Washington DC 1969).

ANDERSON, E.G.
School of Surveying
University of New South Wales
Kensington N.S.W. 2033
Australia

Proc.Symposium on Earth's Gravitational Field & Secular Variations in Position (1973),106-116.

EVALUATION OF THE GRAVITATIONAL POTENTIAL AND ATTRACTION OF A MODEL OF THE EARTH'S TOPOGRAPHY AND COMPENSATION

ABSTRACT

Development of a method of directly computing the gravitational potential and attraction of the earth's topography and isostatic compensation, at geoidal, surface, and orbital elevations, is reported. Some preliminary results, from a programme of world-wide numeric evaluation, illustrate the basic features of these fields and demonstrate some practical limitations to the attainable accuracy.

1. Introduction

In a recent study by FRYER (1970) estimates of the global indirect effect for the free-air geoid were computed. It has been shown (e.g. HEISKANEN & MORITZ 1967, p. 145; MATHER 1968 A, p. 45) that the free-air "co-geoid" closely approximates the geoid, and the associated indirect effect is, therefore, expected to be comparatively small. Fryer's estimates (summarized in figure 1) displayed appreciably greater magnitude than anticipated and remarkably slow attenuation of the effect with increasing distance from the major topographic masses.

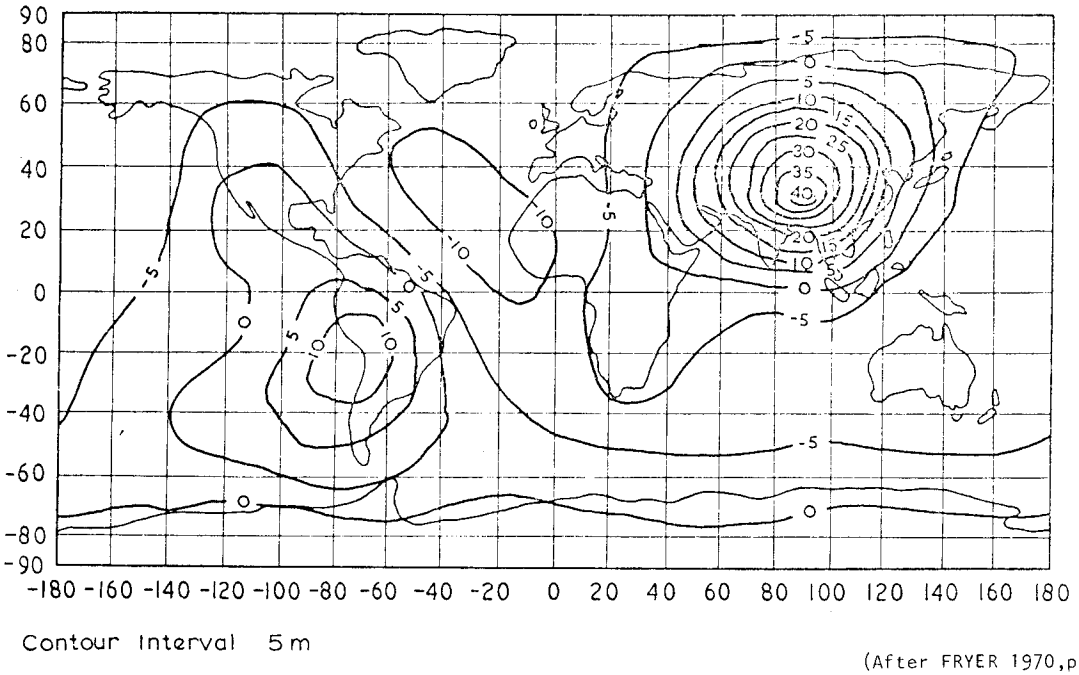

(After FRYER 1970,p.155)

Figure 1. Total Indirect Effect for Global Solution

Consequently, the study reported here has been directed towards a general assessment of the effects of the earth's topography and isostatic compensation on its gravitational field and thus ultimately, the evaluation of the geoid. The approach has been to evaluate directly the Newtonian gravitational potential and attraction of a digital model of the topography and compensation. This procedure has assumed the compensated topography to be in complete isolation from the remainder of the earth, and all other energetic influences. The direct nature of this approach and its investigative bent, may be contrasted with the solution oriented, and thus more involved, derivations of Fryer, wherein the properties of the effect were not of primary concern.

As the major computational work for this study is continuing, only results of preliminary investigations are presented, and any conclusions must be tentative.

2. The Indirect Effect

Stokes' formula for the determination of the geoid requires gravity anomalies representing boundary values at the geoid. Consequently, matter exterior to the bounding surface (that is, topography above the geoid) is mathematically removed or displaced inside the boundary. The resulting disturbance of the gravitational potential, and hence the geoid, is referred to as the indirect effect. A formulation of the indirect effect for the free air geoid has been derived by MATHER (1968 A, 1968 B) and shown to comprise, like the geoid solution itself, a zero-order term, a potential dependent term, and a term with Stokesian characteristics. The free air geoid closely approximates a non-regularized geoid, in that the "direct" effect, due to the attraction of the topography and compensation, is dismissed from the reduction procedure.

Fryer's detailed derivations of the potential and Stokesian terms for the indirect effect (FRYER 1970, p. 45 et seq) show the former to be predominantly a function of a residual potential, representing the difference between the potential due to the topography exterior to the geoid and that of its mathematical condensation as a surface layer on the geoid. The major contributing component of the Stokesian term arises from a Stokes integration of the differential terrain correction, being the difference in attraction of the topography between the surface and the geoid. Fryer's global estimates of these terms are illustrated by figures 2 and 3, respectively.

3. Computational Methods

Evaluation of the potential and attraction of the topography and compensation at a point, requires the solution of the following fundamental integrals, in 3 dimensions, derived from Newton's law of gravitation, (see figure 4).

$$\text{POTENTIAL:} \quad V = k \iiint \frac{\rho \, dv}{r}$$

$$\text{ATTRACTION COMPONENTS:} \quad x_i = -k \iiint \frac{(x_i - \xi_i)\rho \, dv}{r^3} \qquad (i = 1, 3)$$

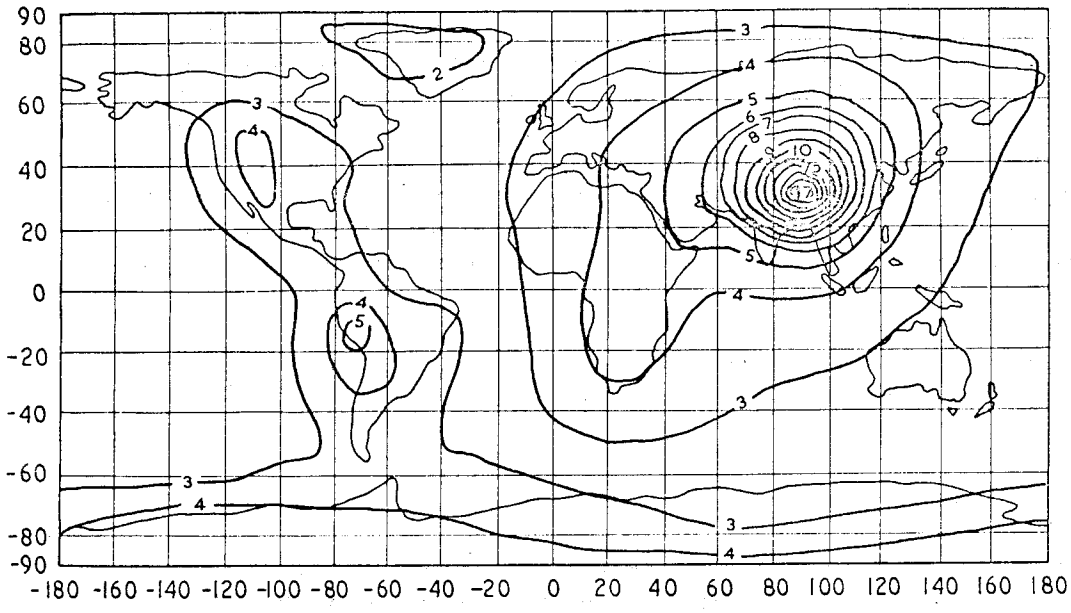

(After FRYER 1970,p.153)

Figure 2. Non-Stokesian Term in Global Indirect Effect Solution Derived from Numerical Integration Method. Contour Interval 1 m

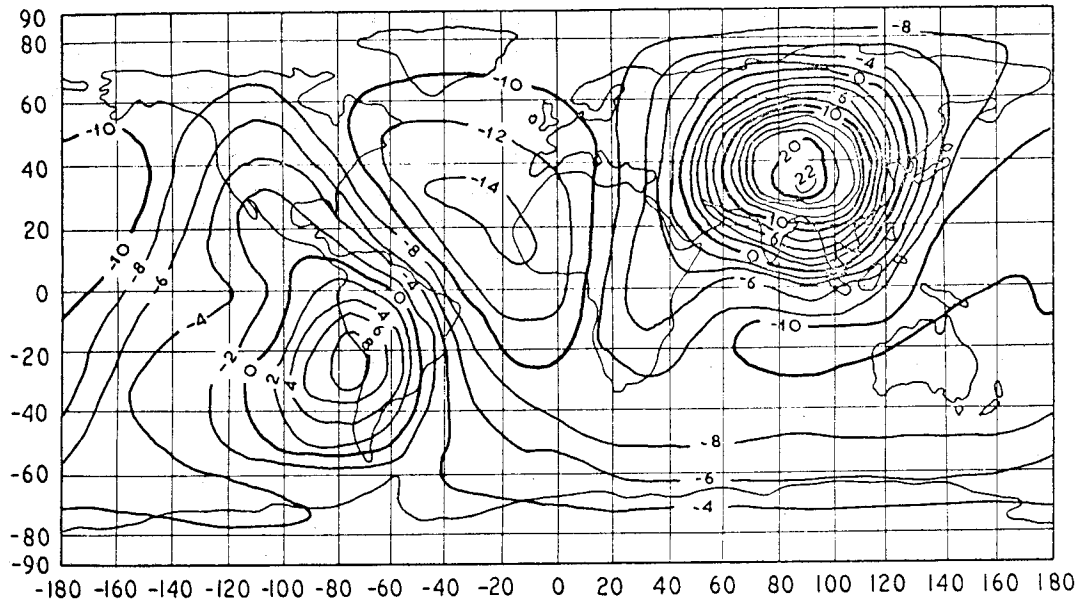

(After FRYER 1970 ,p.154)

Figure 3. Stokesian Term to Order (6,6) in Global Indirect Effect Solution Contour Interval 2 m

where: k is the gravitational constant (6.67×10^{-11} $m^3kg^{-1}s^{-2}$)

dv is an elemental volume of matter,

ρ is the density of matter

r is the distance of the elemental volume from the point of computation,

x_i are the rectangular coordinates of the point of computation, and

ξ_i are the rectangular coordinates of the elemental volume.

A total solution for a particular point requires the limits of integration to be such as to include the whole of the topography and compensation. Then, to determine the spacial qualities of the gravitational field, evaluation may be repeated for a number of points distributed globally. Bearing in mind the contributing terms of the indirect effect, these points may be chosen at the geoid and at the surface of the earth. Points at an elevation representative of satellite orbits (500 km) may be similarly considered.

Whatever method of evaluating the integrals is employed, the limits of integration must be defined by adopting mathematical models to represent the extent of both the topography and compensation. The most commonly available digital data representing the topography is in the form of mean elevations, based on various "square" subdivisions of the geographical coordinate graticule. Isostatic compensation limits are defined in terms of the topographic elevations, after adopting a particular compensation model. Topographic elevations are usually referred to the geoid, however it is necessary to assume that this coincides everywhere with some basic figure of the earth, so as to enable definition of the spatial distribution of the topographic masses with respect to a local coordinate system at each computation point. Polar coordinates in the local system are easily derived by a transformation from the general, geocentric reference frame.

A number of methods are available for solution of the integrals, including rigorous evaluation, numerical integration (cubature), and series expansion. If each topographic block, defined by a geographical coordinate system, is approximated by a homogeneous, rectangular parallelopiped, a rigorous solution of the potential and attraction integrals is available in general form (MACMILLAN 1930, p. 72). Alternatively, without need of the rectangular approximation, conventional numerical integration techniques can be applied, by dividing the block into smaller elements. A further solution is provided by series expansion of the reciprocal distance (1/r) in terms of Legendre polynomials (Ibid, p. 81), however the convergence of this series as r approaches zero requires careful consideration. The applicability of each of these methods is dependent upon the accuracy sought, and is therefore governed mainly by the distance of the topographic block from the computation point. This leads naturally to the introduction of a set of zones, surrounding the computation point, within each of which, a particular method is applied, consistent with the required accuracy. Accuracy is also affected by the degree of subdivision in each zone, because of the redistribution of matter which results from adopting a mean elevation over the extent of each block.

4. Assumptions and Their Effects

In view of the nature of the indirect effect as essentially a small correction term in the overall determination of the geoid, it has been assumed that accuracy corresponding to the order of the flattening should be sought throughout the derivations and calculations. This criterion may not always be fulfilled in practice, largely because of external limitations imposed by the available data. The major assumptions and models involved in the evaluations are summarized in table 1.

TABLE 1

ASSUMED MATHEMATICAL MODELS

1. Figure of the Earth:
   International Ellipsoid, 1967
   Semi-Major Axis $a = 6\ 378\ 160$ m
   Flattening $f = 1/298.25$

2. Isostatic Compensation:
   Airy-Heiskanen Model
   Crustal Thickness $T = 30\ 000$ m
   Sub-crustal Density $\rho = 3270$ kg m^{-3}

3. Density of Topography:
   de Graaff-Hunter Model
   Density of Column (kg m^{-3}) $= 2770 - h/21$ $(h \leq 2100$ m$)$
   $= 2670$ $(h > 2100$ m$)$
   where h is the mean elevation in metres.

4. Topographic Data:
   A Set of Digital Models, Comprising Mean Elevations
   Based on Geographical "Square" Subdivisions of 5' and 1°.

A figure of the earth is required to determine the distribution of the topography with respect to the computation point, but the influence of its departures from reality on the results is negligible. Indeed a plane model would be adequate in the inner zone and the difference between a spherical and a spheroidal model in the outer zones is quite insignificant. A spheroidal model was adopted, since only a slight saving in computation time would accrue from the use of any less realistic model.

The Airy-Heiskanen model for compensation was adopted as one which reasonably fits the available evidence, without introducing the unmanageable complexity of a regional model into the process of storing and accessing the digital data. It has the further advantage of facilitating comparisons with results of other studies.

Rather more concern must arise from the choice of a density model. Any departure from reality of the densities used is propagated directly into the solution, since they act much like a common scaling factor in the calculations. It is most unlikely that any available model is correct to the order of the flattening and the effect of mass stratification on the gravity field is ignored. Certainly, a better model could be compiled, from the available geological mapping at least, though the task would be a major undertaking.

Topographic mean elevations introduce two important sources of error. The first depends on the primary accuracy of the data, which is determined by its source and method of compilation. Clearly, the user of such data has little or no control over these factors. Mean elevation data used in the present study has been gathered from four sources:

(1) One degree mean values were compiled from the available five minute data, as listed in (2) and (3) below and, where this coverage is incomplete, from one degree values prepared by W. H. K. Lee of the University of California.

(2) Five minute data for North America and Europe was supplied by the U.S.A. Defense Mapping Agency (CZARNECKI 1970).

(3) Five minute values for Australia were derived by linear interpolation from the tenth degree data compiled by MATHER (1968 A).

(4) Five minute values for the remainder of the world are being simulated. A linear correlation of regional geomorphology, based on the one degree data, is used to provide a linear model for conversion of known five minute values to areas where such data is lacking.

There are approximately 3.2 million positive five minute mean values in the global model.

The second prominent source of error relates to the use of a digital model composed of mean values. Representation of the topographic elevations within some finite and relatively large area, imposes an apparent shifting of mass and an overall smoothing of gradients. Both factors contribute to a distortion of the gravity field being evaluated, to the extent that the digital model misrepresents reality. It should be noted that the five minute data, including the simulated values, enter into the calculations pertaining to the inner zones only. Outer zone calculations are therefore based entirely on "realistic" data.

5. Preliminary Investigations

A number of preliminary comparisons of formulae and methods and numerical checks have been completed. In particular, the behaviour of formulae, and the effect of approximations in the contact zone (within 5' of the computation point), where the value of r approaches zero, have been closely investigated. A comparison of evaluations of the potential of the topography in this zone, using a cylindrical assumption (Ibid, pp. 92 - 104), by numerical integration based on Simpson's formula, and by a rigorous formula for a rectangular prism, is summarized in table 2.

TABLE 2

COMPARISON OF METHODS OF EVALUATION OF THE POTENTIAL OF THE CONTACT ZONE

Dimensions of Block: 11 120 m ($0^{\circ}.1$) sq. x 5000 m high
Density: 2670 kg m^{-3}

METHOD	POTENTIAL (Jkg^{-1})
Cylindrical Assumption	58.42
Rad. = 12 547 m	
Numerical Integration	
No. of Intervals = 2 x 2 x 2	79.20
4 x 4 x 4	55.63
6 x 6 x 6	61.20
8 x 8 x 8	57.40
10 x 10 x 10	59.21
12 x 12 x 12	57.78
Rigorous Formula	57.68

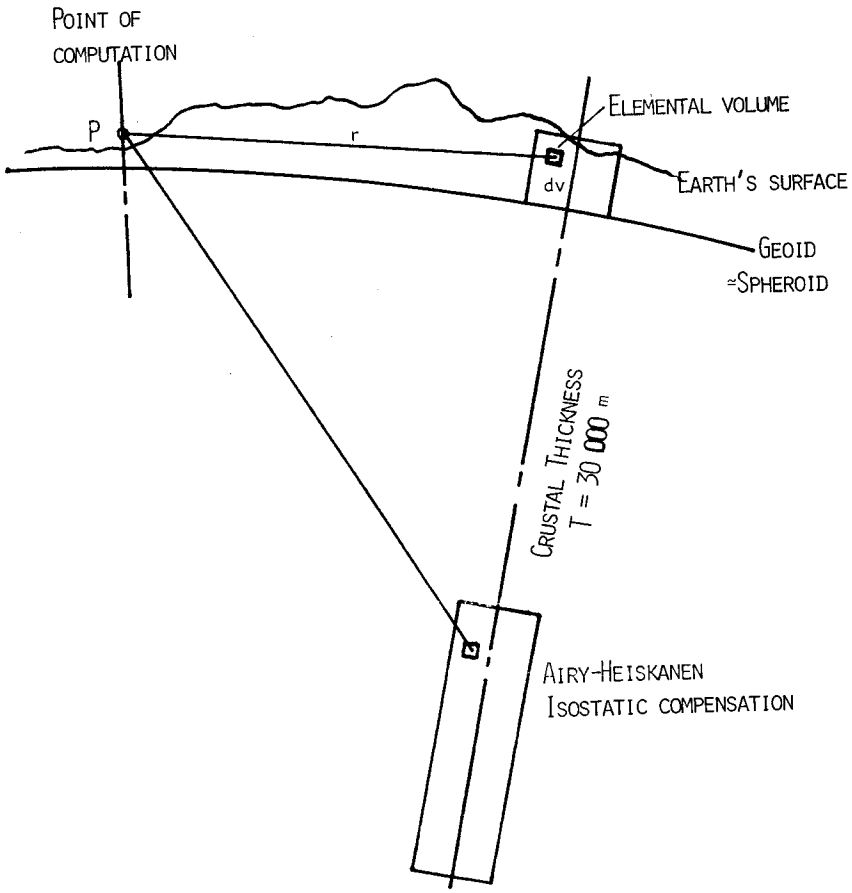

Figure 4. Integration of Topography and Compensation

As might be anticipated, the cylindrical assumption tends to slightly over-estimate the solution, though it provides a valid result in this unstable region, near the discontinuity in the reciprocal distance. Although numerical integration does not entirely fail under these circumstances, it is seen to present an oscillating solution as the number of intervals is increased. Further investigation has revealed that this effect is not present beyond the contact zone. However, any saving in computation time for this method, relative to a rigorous solution, is marginal.

Another method, relevant to all but the contact and inner zones, is provided by expansion of the reciprocal distance in a series, dependent on Legendre polynomials. The first term of such a series is no more than the commonly employed sphere, or point mass, approximation. Experimental calculations, with up to five terms, have shown that the first term alone provides a satisfactory result, when the distance r is greater than about ten times the maximum dimension of the topographic block. Consequently, this approximation may be safely applied beyond about 30' from the computation point.

Table 3 contains the definition of zones used, the size of data subdivisions within each zone, and the method of evaluation employed. A degree of flexibility of zone boundaries and data subdivisions has been programmed into the computer routines.

TABLE 3

METHODS OF EVALUATION AND DEFINITION OF ZONES

ZONE	LIMITS	SIZE OF DATA SUBDIVISIONS	METHOD
CONTACT	0 to 5'	5' x 5'	RIGOROUS
INNER	5' to <2°*	5' x 5'	RIGOROUS
NEAR	30' to 2°*	5' x 5'	SERIES EXPANSION
OUTER	>2°	30' x 30' † 1° x 1° 5° x 5°	SERIES EXPANSION

* Boundary of inner and near zones varied, depending on mean elevations

† Data subdivisions in outer zone varied, depending on "ruggedness" of topography

Hence the change from rigorous formula to series evaluation is varied depending on the mean elevations. A similar refinement is included in the outer zone evaluation, where the presence of steep topographic gradients within a data subdivision can introduce a significant error, if they are not depicted more realistically by smaller data subdivisions. For instance, if a 1° block of topography, 5° from the computation point, contains elevation differences of about 3000 metres (such as may occur in the Himalayas), an error approaching 3% is introduced by adopting a mean elevation for the whole area. Under these circumstances, the computer routines are designed to resort to a smaller data subdivision.

Results of some early evaluations for the contact zone are illustrated in figure 5. Gravitational potential at the surface, due to the topography and compensation within five minutes of the computation point is plotted for a profile along the 19° north parallel of latitude, where it crosses the Eastern Sierra Madre in Mexico. This area depicts well the effects of steep topographic gradients, relatively large elevations, and the sea coast. A high degree of correlation clearly exists between the potential and the elevations, and there is no evidence of slow attenuation of the field. The vertical component of the gravitational force behaves similarly. Simplified test evaluations have also provided a provisional indication of the general trends to be expected for the outer zones. Apparently, the influence of the topography and compensation on the gravitational field extends further than anticipated, resulting in a noticeable smoothing out of the high correlation with local topographic variations, seen in the contact zone. This is substantially in agreement with Fryer's results, where the outer zone contribution to the potential term was found to be fairly constant at 6.3 metres, or about 37% of the total (FRYER 1970, p. 127).

6. Summary

1. Fryer's global estimates of the indirect effect for the free air geoid are larger than expected and display slow attenuation away from the sources of topographic influence.

2. This study attempts to investigate these results, using a different approach, based on a direct global evaluation of the gravitational potential and attraction components due to the topography and isostatic compensation.

3. Mathematical models have been adopted to define the figure of the earth, the isostatic compensation, and the density. A digital model, including some simulated data, is used to represent the topography.

4. Preliminary investigations indicate that the influence of nearby topography (the contact zone) does not contribute to the effect described by Fryer. These investigations further suggest that the topography in the outer zones (at distances of the order of the separation of the continents) may exert a significant influence on the magnitude and gradient of the gravitational field.

7. References

CZARNECKI, W. 1970. *The Geodetic Importance of Mean Elevation Data.* Paper presented at the 1970 ACSM/ASP Convention, Control Surveys Division, Washington, D.C.

FRYER, J. G. 1970. The Effect of the Geoid on the Australian Geodetic Network. UNISURV Rep. 20, University of New South Wales, Kensington N.S.W.

HEISKANEN, W. A. & MORITZ, H. 1967. *Physical Geodesy*, Freeman, San Francisco.

MACMILLAN, W. D. 1930. *The Theory of the Potential*, Dover, New York.

MATHER, R. S. 1968A. The Free Air Geoid in South Australia and its Relation to the Equipotential Surfaces of the Earth's Gravitational Field UNISURV Rep. 6, University of New South Wales, Kensington, N.S.W.

MATHER, R. S. 1968B. The Free Air Geoid as a Solution of the Boundary Value Problem. *Geophs. J. R. astr. Soc.* 16, 515-530.

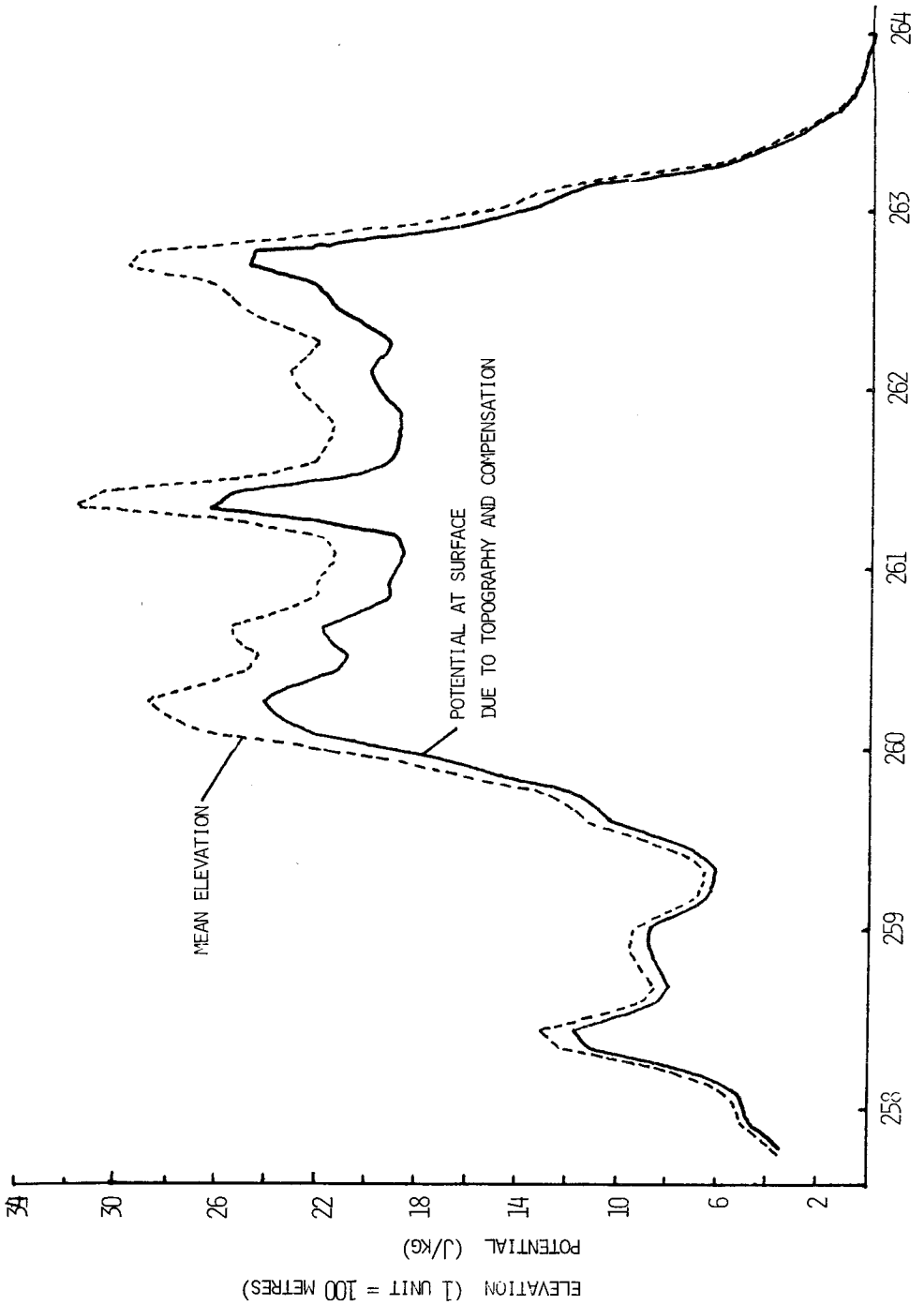

Figure 5. Gravitational Potential Due to Contact Zone (4 × 5' Squares) and Mean Elevations at Latitude 19° north

8. Discussion

FRYER: About the matter of slow attenuation; my calculations agreed with ANDERSON's that the attenuation from a topographic block in isolation is quite rapid and can be modelled against topographic shape - however, when considered from a global calculation, the actual distribution of data has a cumulative effect, making the attenuation around a large mass appear slow.

ANDERSON: I can't comment at this stage as I don't have global solutions but only preliminary calculations over selected areas.

QURESHI: Is the calculation being carried to an angular distance of 5 degrees from the computation point?

ANDERSON: At each point I evaluate; so all topography is taken into account at each computation point.

REILLY: In the topographic-isostatic model you are adopting, are the masses of the topography and compensation of a given column equal and opposite? I note that you use a variable density for the topography.

ANDERSON: The variable density is constant for a given block. It varies from block to block. As the density of compensation is based on the value assumed for the density of the topography, the net effect is equal and opposite.

MATHER, R.S.
School of Surveying *
The University of New South Wales
Kensington NSW 2033
Australia

Proc.Symposium on Earth's Gravitational Field & Secular Variations in Position (1973),117-153.

POSITION FROM GRAVITY

ABSTRACT

Procedures for obtaining position from surface gravity observations and reviewed and their relevance assessed in the context of the application of modern geodetic techniques to programs of Earth and ocean physics. Solutions based on the use of surface layer techniques, the discrete value approach, and the development from Green's third identity are stated in summary, the latter being extended to order e^3 in the height anomaly.

The representation of the surface gravity field which is required in order that this accuracy may be achieved is discussed. Interim techniques which could be used in the absence of such a representation are also outlined.

The role which can be played by the determination of changes in observed gravity to a few microgal, in the definition of geodetic reference systems for long period studies in Earth physics, is discussed and the consequences of changes of zero degree summarized. The possible use of these techniques in future geodetic practice is also assessed.

1. Introduction

1.1 Preamble

At first glance, it would appear that geodesists of today should be grateful for the activities of exploration geophysicists which have made significant contributions to all the well known data banks available at present. After all, it is only in the past two decades that the course of events has looked favourably on the collection of gravity information with solely geodetic objectives in view. All the available surface gravity information has still not been able to provide meaningful definitions of position on its own at the time of writing. The techniques of satellite geodesy revolutionized practical determinations related to position from a consideration of the Earth's gravity field, and there is little argument that these methods give relevant position-related parameters with a precision of about 2 - 4 %, the higher precision estimate being obtained on the use of combination techniques incorporating surface gravity information with satellite data.

Many factors have changed since the advent of the satellite era less than two decades ago. A technical advance of importance is the development of the surface ship gravimeter which provides a means of defining the surface gravity field in ocean areas with a resolution which if used advantageously, can be shown to be adequate for all present day requirements in Earth and ocean physics. A second development of great significance is the sensational improvement achieved in the precision with which absolute determinations of gravity based on interferometric techniques can be made (e.g., COOK 1965; FALLER 1965). The permanent installation maintained by the Bureau International des Poids et Mesures (BIPM) at Sevres, France, has been achieving a measuring precision of ±3 μgal for some years now (SAKUMA 1971), improving the resolution of g from 2 parts in 10^6 to about 3 parts in 10^9 in less than a decade. To this should be added the capability which has been available for some time, and enables the measurement of *differences* in gravity with an accuracy better than 1 part in 10^5 on land

* Prepared while at NASA/Goddard Space Flight Center, Greenbelt, Md, USA - *X Doc.*-592-73-164(June 1973)

without any appreciable measurement time.

These significant improvements in metrology pose a series of interesting problems which must be dealt with before the maximum geodetic information can be obtained from surface gravity measurements. In the first instance, it becomes necessary to review the implications of adopting a rigid body model for the Earth as the basis for computations of position from surface gravity data. Further effect to be considered is the change in the Earth space location of the rotation vector and their influence on the determination of position from gravity. Short period mass changes smaller in magnitude than Earth tide effects, and possibly more difficult to model, may also have to be considered. Into this category fall changes in atmospheric circulation patterns from some model, variations in the water table and similar phenomena. Over a long time scale, it is necessary to consider the implications of a possible secular variation in the gravitational constant G.

As most of these effects are 7 - 8 orders of magnitude smaller than that of g, it has been accepted practice to convert observed gravity g to the gravity anomaly Δg by differencing g from the value γ of normal gravity for a model of the Earth, afforded by the value of GM, the rate ω of rotation of the Earth, assumed to be constant, together with the equatorial radius a and flattening f of an ellispoid of revolution which "best fits" the geoid. No allowance is made for the possibility of variations with time, in any of the parameters defining this system of reference. This is not inconsistent with the concept of determinations relevant to a certain epoch, provided

(a) the observations used are all made during the epoch considered; and

(b) the accuracy sought is less than 1 part in 10^7 in g.

The magnitude of gravitational deviations from a solid Earth model are smaller than $o\{10^{-6}g\}$. The largest effect is the diurnal Earth tide variation with magnitude $o\{10^{-7}g\}$. It has not been considered necessary at the present time, to recommend the adoption of a systematic procedure for modelling and removing the effect of the Earth tides from observed gravity except when establishing gravity standardization networks, in view of the limited accuracy of elevation data used in computing the gravity anomaly. This would call for the adoption of a universally acceptable model for Earth tides, which would then be used as a matter of routine to correct observed gravity prior to use in geodetic computations. Such corrections are only necessary at fundamental gravity stations where determinations are made with the highest possible resolution for either the definition of global gravity standardization networks (MATHER 1973,p.68) or when attempting to locate changes in the position of the Earth's centre of mass (geocentre) with time (MATHER 1972,p.13). The need for applying such corrections at other stations will depend on the extent of gravity coverage available locally and whether elevation datums have been unified at the 50 cm level.

Current practice accepts the validity of each individual nation's elevation datum as well as its gravity datum. The continuance of such a practice is unwise if systematic errors at the 50 cm level are not to occur in the final results. The most taxing goal is the definition of the geoid in ocean areas to the highest possible accuracy, in order that such results could be used with satellite altimeter data to study ocean circulation by defining the sea surface topography. On present trends, it would appear that 5-10 cm accuracy is desirable in geoid determinations for this purpose.

It is in this context that the use of gravimetric techniques in the determination of geodetic position should be reviewed. The present development covers

(a) the basic developments underlying the determination of position from gravity;

(b) a review of some of the methods suggested to the present time, for solving the boundary value problem in physical geodesy;

(c) techniques for the preparation of data sets for this task; and

(d) the geodetic interpretation of such solutions in Earth space.

In all sections, an assessment is made of the requirements which will have to be met in order that the independent evaluation of selected geodetic characteristics available from surface gravity determinations, can be used in the resolution of some possible ambiguities from other methods when applied to studies of high precision for Earth and ocean physics.

1.2 A guide to notation

1.2.1 Recurring Symbols

a = equatorial radius of the ellipsoid of reference

$\vec{d}$ = separation vector between equivalent points P on the Earth's surface and Q on telluroid

dz = increment in orthometric elevation

$d\sigma$ = element of surface area on unit sphere

e = eccentricity of the meridian ellipse; $e^2 = 2f - f^2$

$F(\psi) = f(\psi) \sin \psi$

f = flattening of meridian ellipse

$f(\psi)$ = Stokes' function = $\operatorname{cosec} \frac{1}{2}\psi + 1 - 5 \cos \psi - 6 \sin \frac{1}{2}\psi - 3 \cos \psi \left(\log\{\sin \frac{1}{2}\psi(1 + \sin \frac{1}{2}\psi)\}\right)$

g = gravity as observed at the surface of the Earth

h = ellipsoidal elevation

h_d = height anomaly

h_n = normal elevation

M = mass of the Earth, including the atmosphere

$M\{X\}$ = global mean value of X

$m = a\omega^2/\gamma_e$

$m' = a^3\omega^2/GM = m + o\{f^2\}$

N = elevation of geoid above ellipsoid

$\vec{N}$ = unit vector normal to the surface of the Earth

N_f = free air geoid; the Stokesian contribution to h_d

N_c = indirect effect to free air geoid; non-Stokesian contribution to h_d

R = geocentric distance

$\overline{R}$ = radius of sphere containing all topography - the Brillouin sphere

R_b = radius of sphere which is internal to the Earth's surface - the Bjerhammar sphere

R_m = mean radius of the Earth

r = distance between the point of computation P and the element of surface area dS

$\overline{r} = 2\overline{R} \sin \frac{1}{2}\psi$

$r_o = 2R_m \sin \frac{1}{2}\psi$

S = surface of the Earth

U = spheropotential due to the system of reference

U_o = spheropotential on the surface of the reference ellipsoid

V_d = disturbing potential

W = geopotential

W_o = potential of the geoid

X_i = geocentric rectangular Cartesian co-ordinate system $X_1X_2X_3$

x_i = local rectangular Cartesian co-ordinate system $x_1x_2x_3$ with the x_3 axis along the local normal, the x_1x_2 plane defining the local horizon, with axes oriented north, east.

α = azimuth

β = ground slope; subscripts $_1$ and $_2$ refer to components north and east

γ = normal gravity due to reference system; subscripts $_o$ and $_e$ refer to values on reference ellipsoid and equatorial gravity respectively.

Δg = gravity anomaly at the surface of the Earth, defined by equation 10

ΔW = geopotential difference with respect to the geoid

δg = gravity disturbance

λ = longitude, positive east

ξ = components of deflection of the vertical; subscripts $_1$ and $_2$ refer to valuesin the north and east directions respectively

ζ = deflection of the vertical, positive if outward vertical lies north, east of normal

Φ = density of surface layer, except in section 3.4

ϕ = latitude, positive north; subscripts $_c$, $_a$, $_g$, refer to geocentric, astronomically determined and geodetic latitudes respectively.

ψ = angular distance at geocentre between the point of computation P and the element of surface area dS

ω = angular velocity of rotation of the Earth

$$\vec{\nabla} = \sum_{i=1}^{3} \frac{\partial}{\partial x_i} \vec{i}$$

1.2.2 Conventions

$a = b + o\{b^2\}$ ≡ terms whose order of magnitude is equal to or less than b^2 are neglected $(b < 1)$

$$x_\alpha y_\alpha = x_1 y_1 + x_2 y_2$$

$x_i = a_{ij} b_j$ ≡ $x_i = a_{i1} b_1 + a_{i2} b_2 + \ldots$, there being as many equations as possible values of i

$a \doteq c$ ≡ a is approximately equal to c

2. Basic principles

2.1 The system of reference

The principle behind the determination of Earth space position from gravity observations made at the surface of the Earth is implied from deviations of observed gravity from values at an "equivalent" point on some Earth model, whose parameters are completely defined. Current geodetic practice (IAG 1970,p.12) specifies a rigid body model by the following parameters.

(a) The value $\mu (= GM)$ where G is the gravitational constant & M the mass of the Earth.

(b) The constant rate ω of rotation of the rigid Earth model.

(c) The equatorial radius a of an ellipsoid of revolution which presumably is one of best fit to the geoid.

(d) The dynamic form factor J_2 which is equivalent to a value for the flattening f for the reference ellipsoid.

It is conventional to choose the value for a such that the ellipsoid has the same volume as the geoid. This is not a necessary condition if zero degree effects are taken into account when formulating a solution for the boundary value problem. What is more important in solutions which aspire to accuracies greater than the order of the flattening (i.e., ±30 cm in the height anomaly), is that the ellipsoid lies everywhere within the physical surface of the Earth. This permits the use of Laplace's equation in the representation of the appropriate disturbing potential without approximation. The adoption of such a procedure without an equivalent adjustment in μ could cause larger numerical values of the gravity anomaly, which would in turn, call for greater caution in developing computer algorithms for evaluation purposes.

It can be stated without being contentious that the value adopted for a has to be based on some determination of the scale of Earth space. This would be provided by either the measurement of long arcs at the surface of the Earth by classical techniques (e.g., the PAGEOS baselines) or else by laser ranges to either satellites or the moon. All determinations of scale are therefore based on the velocity of light and the definition adopted for the basic interval of time. The value of the flattening f of the reference ellipsoid is best deduced from the second degree zonal harmonic obtained from the secular variations in the right ascension Ω of the node and the argument ω of perigee of near Earth satellites. The precision claimed at the present time (e.g.,LERCH ET AL 1972,

p.27) for this harmonic is 1 part in 10^5, the required relation being (e.g., MATHER 1971a,p.85)

$$C_{20} = \frac{1}{3} m' - \frac{2}{3} f - \frac{3}{7} m'f + \frac{1}{3} f^2 + o\{f^3\} \quad (1),$$

where

$$m' = \frac{a^3\omega^2}{GM},$$

ω being the angular velocity of rotation of the Earth. The exact relation between the observed secular variations $\dot{\Omega}_{20}$ and C_{20} is (e.g., IBID,p.151)

$$\dot{\Omega}_{20} = \frac{3(GM)^{\frac{1}{2}}}{2(1 - e_s^2)^2} \frac{a^2}{a_s^{7/2}} \cos i \, C_{20} \quad (2),$$

a_s being the equatorial radius of the satellite orbit, e_s its eccentricity and i the inclination.

The change df in f due to changes da, $d\omega$ and d(GM) in a, ω and GM are given by

$$df = \frac{3}{2} m' \left(3 \frac{da}{a} + 2 \frac{d\omega}{\omega}\right) - \frac{1}{2} \frac{d(GM)}{GM} (3m' + C_{20}) + o\{f^2 df\} \quad (3).$$

The ratio df/f is therefore of the same order of magnitude as d(GM)/GM for a specified value of a as the ratio $d\omega/\omega$ is at least an order of magnitude smaller, if these ratios reflect the precision with which each of these quantities are determined.

It is all-important that the rotational characteristics assigned to the reference model are exactly equivalent to those influencing gravity as measured at the Earth's surface. This is implicit in deriving equation 60 from equations 58 and 59. The rotation vector in Earth space is not fixed and hence deviations from the rigid body model occur in practice. The rate ω of rotation is subject to secular variations due to tidal friction. Certain shorter period effects have to be accounted for, at least in theory, when reducing gravity to a rigid body equivalent of the Earth; the practical consequences are negligible as their magnitude is less than 1 part in 10^9 in g. A second factor is the change in position of the instantaneous axis of rotation with respect to the Earth's crust. The total contribution of the rotation to observed gravity is the appropriate resolute of

$$g_r = p\omega^2 \quad (4)$$

directed away from the axis of rotation and perpendicular to it. The changes dg_r in g_r due to changes dp in p, which is the distance of the point at which gravity is measured, from the axis of rotation, and $d\omega$ in ω is given by

$$dg_r = g_r \left(2 \frac{d\omega}{\omega} + \frac{dp}{p} + o\{10^{-12}\} \right) \quad (5).$$

The effect of the ratio $d\omega/\omega$ will be less than 1 μgal on observed gravity for a 10 msec variation in the length of day, and hence this term is not of significance in the reduction of observed gravity if the latter were restricted to some epoch of observation. The effect of polar motion is reflected in the second term in equation 5 and is o{1 μgal} (BURSA 1972).

Short period changes in observed gravity with larger magnitudes have been reported by SAKUMA (1971) after modeling the effects of Earth tides. It should be noted that a 1% change in the local atmospheric density is of order 10 microgal, while quasi-stationary changes in the local geological formations, e.g., in the local water table, could cause gravitational effects of this same magnitude.

It is therefore important that both the atmosphere and the local geology be modeled in the vicinity of those gravity stations at which g is to be re-measured at regular intervals with the highest possible precision.

The dominant gravitational variation with time is that due to Earth tides, with magnitude o{10^2 μgal} and Earth models for this effect are well known in the literature (e.g., MELCHIOR 1966). It is important that an unambiguous Earth tide model at the 10 μgal level be uniformly adopted when specifying gravity values at stations comprising the global gravity standardization network described in section 4.

The final parameter defining the reference system is $\mu(=GM)$. The commonly accepted values of GM are presently based on the analysis of interplanetary space probes. The technique used can be briefly summarized as follows (ESPOSITO & WONG 1972). Doppler data from inter-planetary space probes is analysed using numerical integration procedures for the determination of the motion of the probe with reference to a geocentric inertial co-ordinate system. Perturbations due to the Earth's departure from a sphere, solar radiation pressure, planetary and lunar gravitational effects and spacecraft attitude control forces are modeled when effecting this solution, which also provides revised estimates of tracking station co-ordinates as a by-product of the solution. The main conclusions of relevance to the present review are the following. Firstly the value of GM is based on the velocity of light. Secondly, the potential U_o on the surface of the reference ellipsoid, assumed to be an equipotential, is related to the values adopted for ω, a, f and μ by the relation (e.g., MATHER 1971a,p.83)

$$U_o = \frac{GM}{a} \frac{\sin^{-1} e}{e} + \frac{1}{3} a^2 \omega^3 ,$$

where

$$e^2 = 2f - f^2.$$

As GM has an uncertainty of 1 part in 10^6 at the present time, it follows that U_o will differ from the true potential of the geoid consistent with Newtonian gravitation, as scaled by the velocity of light by at least 1 part in 10^6. If U_o were assumed to be equal to the potential W_o of the geoid, it would be tantamount to imposing a second scale constraint when using gravitational techniques in geodesy. The only way out of this impasse is to use external geometrical information which when combined with the gravitational solution, will give an improved estimate of W_o as discussed in section 5. Such an estimate would be consistent with the scale provided by the velocity of light. In the interim, it should be borne in mind that all position determinations based on gravity alone may have a constant scale error of upto 1 part per million on this account.

In summary it may be stated that

(a) Only Earth tide effects need be allowed for in all work except those determinations required for the monitoring of co-ordinate systems;

(b) Position determinations based on gravity alone are liable to have a constant scale error of upto 1 part per million due to the uncertainty in the assumption $U_o = W_o$.

The following conclusions may therefore be drawn about the adoption of a rigid body model of the Earth as an intermediary in the definition of position from gravity, with the highest possible precision as the ultimate goal.

(i) The only departures from rigidity which need be considered for solutions of the boundary value problem are the effect of Earth tides on gravity observations especially when establishing gravity standardization networks.

(ii) An error in GM will give rise to ambiguities in scale if W_o is forced to be equal to U_o. For further discussion, see section 5.1

2.2 Data requirements

Observed gravity will be the result of two kinds of determinations. The first type will be absolute determinations with the highest precision possible, while the second will be point values established by differential techniques based on the former, and with a precision which is about one order of magnitude inferior. The practice adopted in gravimetric determinations is the use of gravity observations and a knowledge of the surface topography of the Earth to determine the separation vector $\vec{d}$ between equivalent points on the reference model, whose Earth space position is known, and the physical surface of the Earth, as illustrated in figure 1. The separation vector can be completely defined by the height anomaly h_d and the angles ξ_α which are more completely defined in the next sub-section.

The most exacting requirements are called for in the definition of position from gravity when determining the geoid for ocean physics applications, where present estimates of requirements call for resolution at the ±10 cm level. The equivalent order of magnitude is e^3 (i.e., 5 parts in 10^4) which can be assessed as ±50 μgal in the gravity anomaly Δg. On the basis of the discussion in the previous sub-section, it would be adequate to maintain a rotating rigid body model as the system of reference and apply the appropriate reductions to observed gravity to make the measurements compatible with the model. The position so defined will be unaffected by short period time variations in the Earth's gravitational field.

The nature of the reductions necessary will depend on the purpose for which the gravity data is required, the accuracy with which it has been established and the nature of the elevation data available for its reduction. Earth tide corrections necessary at stations monitoring changes in g for global reference system definition (MATHER 1972,section 3.3) should be capable of resolution to 1 gal. Some difficulty may be experienced in removing ocean lodaing effects, especially in coastal areas, as these could influence the tidal correction in the second significant figure (HENDERSHOTT 1972). Corrections for short period variations of the atmosphere and the stratigraphy in the vicinity of gravity stations monitoring the reference system, are also necessary. This presupposes the existence of "accepted" models for both the atmosphere and the local stratigraphy, and the effect meteorological changes may have on them. While Earth tide effects should be allowed for when making any gravity determination, the summary in section 4 indicates that the effect of omitting the correction on determinations of position from gravity is likely to be negligible as the tidal effect has the characteristics of a random measurement error. All further discussion will therefore assume observed gravity g as having been observed on a rigid Earth, rotating with uniform angular velocity, the gravitational effects of polar motion being corrected for when using gravity data for the definition of geodetic reference systems.

The formulation of relations at the surface of the Earth is based on the following principles.

(a) An estimate is available of the geocentric co-ordinates of the point P at the surface of the Earth. In classical terms, these surface co-ordinates (ϕ_a,λ_a) are related to the vertical at P by astronomical determinations, and can be evaluated at best to a factor of one or two better than 1 part in 10^6 (i.e., ±6 m in each co-ordinate). This estimate differs from the true geocentric co-ordinate by amounts upto 10^{-4} radians depending on the magnitude of the local deflection of the vertical.

(b) The displacement of P above the equivalent point P_o on the ellipsoid is defined by the normal elevation h_n, which is related to the difference in geopotential ΔW between the equipotential datum for elevations (the geoid) and P as obtained from levelling, by the relation

$$\Delta W = - \int_{\text{geoid}}^{P} g \, dz,$$

g being the observed gravity for the section of the line of levelling where the orthometric height difference is dz. The equation defining h_n in terms of ΔW is the relation (e.g., MATHER 1971a,p.100)

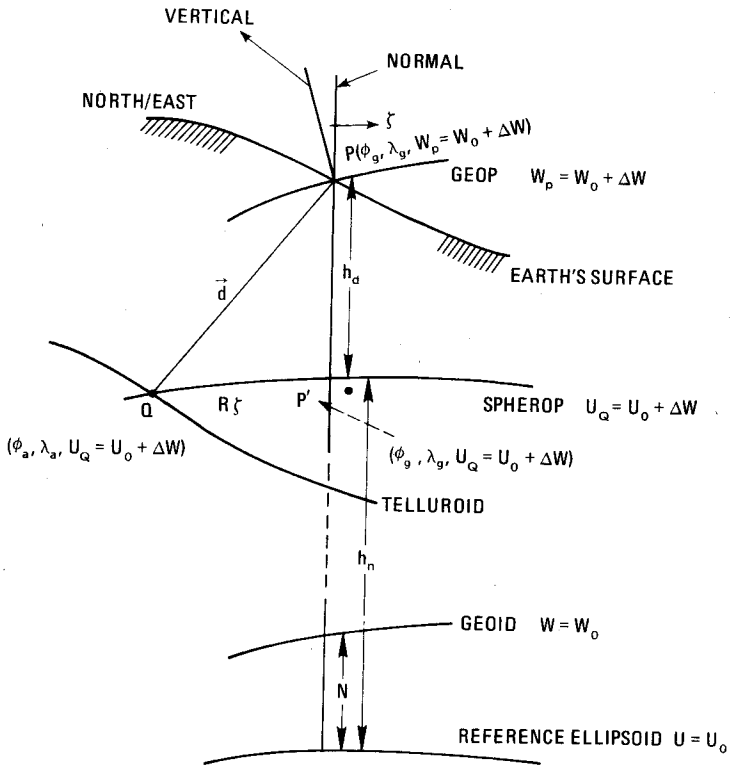

FIGURE 1 : The Separation Vector $\vec{d}$ and the Reference System

$$h_n = \frac{\Delta W}{\gamma_o}\left\{1 + \frac{\Delta W}{a\gamma_o}\left(1 + m + f - 2f\sin^2\phi\right) + \left(\frac{\Delta W}{a\gamma_o}\right)^2 + o\{f^3\}\right\},$$

where γ_o is the value of normal gravity on the reference ellipsoid, and

$$m = \frac{a\omega^2}{\gamma_e} \qquad (6),$$

γ_e being the value of normal gravity at the equator, and ΔW is treated without regard to sign for points exterior to the geoid.

It has been shown (MATHER 1973, section 4.3) that the data requirements for the determination of the height anomaly h_d with a precision equivalent to that possible in establishing h_n are well within the capabilities of measuring and data sampling techniques available at the present time. Thus position determination from gravity in any absolute sense

(i) requires a knowledge of astronomical co-ordinates; and

(ii) calls for a global representation of the gravity anomaly field.

The resolution of the information from positional astronomy at the present time will have to improve by a factor of 50 before the horizontal determinations are of adequate accuracy for the complete determination of position by this method alone. Such a determination will also require the determinations of the deflections of the vertical ξ_α to $o\{10^{-4}\xi_\alpha\}$.

It can therefore be concluded that the determination of geocentric position from positional astronomy and surface gravity to accuracies much in excess of 1 part in 10^6 may not be a practical possibility in the foreseeable future. The determination of the height anomaly on the other hand, will remain a problem of fundamental interest as it forms an integral part in the definition of sea surface topography from space. The ensuing development will continue to deal with the complete development necessary

for the determination of position from gravity, but only in outline. More detailed review will be confined to the techniques for determining the height anomaly.

2.3 Basic Relations

The formulation of the Molodenskii problem (HEISKANEN & MORITZ 1967,p.291) can be treated as one which seeks the determination of the separation vector $\vec{d}$ between "equivalent" points $P(\phi_g,\lambda_g,W_p=W_o+\Delta W)$ on the Earth's surface and $Q(\phi_a,\lambda_a,U_Q=U_o+\Delta W)$ on the associated spherop $U=U_Q$ of the reference system, as illustrated in figure 1. If the subscripts $_a$ refer to values determined astronomically at P, the separation vector is given by

$$\vec{d} = R_\alpha \xi_\alpha \vec{\alpha} + h_d \vec{3} \qquad (7),$$

where R_α are the meridian and prime vertical radii of curvature of the associated spherop, $\vec{\alpha}$ are unit vectors oriented along the tangent plane to the spherop at Q in the meridian and prime vertical respectively, while $\vec{3}$ is the unit vector along the outward normal at Q. The subscripts $_g$ refer to the surface co-ordinates of the point P' in figure 1 on the associated spherop $U = U_Q$ whose normal passes through P.

The locus of the point Q is called the telluroid and mirrors the physical surface of the solid Earth and oceans to order f^2. The system of reference is based on the family of spherops $(U=U_o+\Delta W)$ exterior to the reference ellipsoid defined by the geometrical parameters a and f, and the gravitational characteristic $\mu(=GM)$, with the constraint that the surface of the reference ellipsoid is the equipotential surface $U = U_o$. As pointed out in section 2.1, there is no necessity for the ellipsoid to be forced to have the same volume as the geoid $(W=W_o)$ provided terms of zero degree were retained in the solution. In such circumstances it is no difficult to show that (e.g., MATHER 1973, p.14) the height anomaly (h_d in figure 1) is given by

$$h_d = \frac{1}{\gamma}\{V_d - (W_o - U_o)\} + o\{10^{-3}m\} \qquad (8),$$

where the disturbing potential at P is given by

$$V_{dp} = W_p - U_p \qquad (9).$$

The quantity W_p is defined by the value W_o of the geopotential on the equipotential surface used as the datum for geodetic levelling, and the observed difference of geopotential ΔW between this surface at P, by the relation

$$W_p = W_o + \Delta W.$$

The datum in use at the present time is that afforded by mean sea level derived from tide gauge readings over periods in excess of one year. As solutions of the geodetic boundary value problem require definitions which are applicable globally, it is essential that all regional definitions of mean sea level are correlated on a world wide basis to a common epoch in the first instance before the differences in geopotential ΔW can be considered to be referred to an equipotential surface of the Earth's gravitational field. It has been estimated that systematic errors of $o\{\pm 10$ cm$\}$ could result in solutions of the boundary value problem if errors on this account were of $o\{\pm 30$ cm$\}$ and each datum covered $o\{10^6$ km$^2\}$ (IBID,p.68).

A second problem of consequence and of which little is known at the present time, is the possibility of quasi-stationary departures of the sea surface from the equipotential surface defined by the

results of geodetic levelling. The phenomenon, known as stationary sea surface topography, has been reported along coastlines in many parts of the world. A summary of some results is given by HAMON & GREIG (1972), indicating magnitudes of 30-50 cm being commonplace, with one reported as large as 1.7m over 3000 km. This effect is discussed further in section 4.

The gravity anomaly Δg at the surface of the Earth is defined by

$$\Delta g = g_p - \gamma_{p'} \qquad (10),$$

where g_p is the value of gravity observed at P, corrected for departures of the Earth from a rigid body model, as described in section 2.1, and $\gamma_{p'}$ is obtained from the equivalent value γ_o of normal gravity on the reference ellipsoid, given by the commonly used relations of the type (e.g., HEISKANEN & MORITZ 1967,p.79)

$$\gamma_o = \gamma_e\{1 + \beta \sin^2\phi_g + \beta_2 \sin^2 2\phi_g + o\{f^3\}\} \qquad (11),$$

where γ_e is equatorial gravity defined by the values adopted for a, f, GM and ω(e.g., IAG 1970,p. 48;MATHER 1971a,p.87), $\beta = o\{f\}$ and $\beta_2 = o\{f^2\}$, using the relationship (e.g., IBID,p.101)

$$\gamma_{p'} = \gamma_o - 2\frac{\Delta W}{a}\{1 + f + m - 2f \sin^2\phi - \frac{1}{2}\frac{\Delta W}{a\gamma} + o\{f^2\}\} \qquad (12),$$

ΔW having the same significance as in equation 6.

Possible sources of systematic error in the computed value of $\gamma_{p'}$ and hence Δg arise in the definition of ϕ_g and ΔW. While the effect of errors in the latter have already been described, ϕ_g should be defined to ±0.4 arcsec if $\gamma_{p'}$ is not to have an error of approximately ± 10 μgal. It is therefore important to use any of the global solutions available at the present time for the definition of geocentric position, to evaluate geocentric orientation parameters for each of the regional geodetic datums (MATHER 1973,p.16) before computing gravity anomalies for high precision determinations, rather than use values referred to regional geodetic datums.

The equation described as the fundamental equation in physical geodesy (HEISKANEN & MORITZ 1967,p.86) defines the relationship between the disturbing potential V_d and the gravity anomaly Δg as (MATHER 1973,p.18)

$$\frac{\partial V_d}{\partial h} = -\Delta g + \frac{\partial \gamma}{\partial h} h_d \left(+ \frac{1}{2} g \zeta^2 + o\{1 \text{ μgal}\}\right) \qquad (13),$$

where the terms within the bracket take into account effects smaller than $o\{f\,\Delta g\}$, ζ being the deflection of the vertical at the point considered.

The philosophy underlying equation 13 is the contention that the geocentric position of P is not known, though estimates adequate for the linearization of the quantities involved are available. Circumstances may well arise in the future where accurate horizontal and vertical surveys may be available and the principal practical role of techniques in physical geodesy is the determination of the geoid in ocean areas for study of ocean circulation. In such a situation, it is envisaged that all the land masses are linked to a geocentric system of reference using laser ranging methods and/or VLBI, giving at least one fundamental station on each geodetic datum. Horizontal survey methods together with geodetic and astro-geodetic levelling, will provide data for completely defining geocentric position of points on any regional network which includes at least one fundamental station, with an accuracy of 1 part in 10^6. As surface ship locations can be routinely

determined to within one order of magnitude greater, it is of relevance to examine the gravity disturbance δg(e.g., HOTINE 1969,p.312), given by

$$\delta g = g_p - \gamma_p = -\frac{\partial V_d}{\partial h} + \frac{1}{2} g\zeta^2 + o\{1\ \mu gal\} \qquad (14),$$

where the uncertainties in defining the position of P can be estimated as ±0.2 arcsec in horizontal position and ±2 m in normal displacement, if the astro-geodetic levelling is based on an adequate distribution of stations. The effect of errors due to the first source on δg are $o\{1\ \mu gal\}$ while that of those due to the second are $o\{5\times10^2\ \mu gal\}$. Thus the gravity disturbance, whose order of magnitude is not significantly different to that of the gravity anomaly, is likely to have errors of $o\{5\times10^2\ \mu gal\}$ which are probably correlated with wavelengths in excess of 1000 km (e.g., MATHER, BARLOW & FRYER 1971,figure 4.2) unless radically new techniques are available for determining

either geocentric position at each gravity station such that the radial component is resolved with systematic biases of wavelengths longer than 1000 km held to below the 20-30 cm level;

or the contribution of astro-geodetic levelling with the same resolution as geodetic levelling.

The projection of present day techniques does not lead to the conclusion that there would be significant advantages in using the gravity disturbance δg in preference to the gravity anomaly Δg in formulating solutions of the boundary value problem.

The separation vector $\vec{d}$, illustrated in figure 1, can be represented by components along the axes of a local Cartesian co-ordinate system x_i at Q, with the x_3 axis oriented along the spherop normal at Q, as illustrated in figure 2, in accordance with equation 7. $\vec{d}$ is of importance in defining the geocentric orientation vector $\vec{0}$ for regional geodetic datums using surface gravity data (MATHER 1971b, p.62). A description of how such information could be used to assemble a world geodetic system linking the major land masses by comparing the separation vectors as obtained from gravimetry and astro-geodesy is given by MATHER (1971c).

The mainstream of practical endeavours at the present time is in the determination of the height anomaly h_d. Over 90% of the power in such determinations comes from the "free air geoid" N_f, obtained by the use of free air anomalies (i.e., surface gravity anomalies to the order of the flattening) in Stokes' integral which is set out out in equation 15. The latter is a solution of the boundary value problem for a spherical Earth which is exterior to all matter and whose bounding surface is an equipotential (STOKES 1849).

The deflections of the vertical ξ_α are usually obtained using the principles generally attributed to VENING MEINESZ (1928). Working on a spherical reference system, he showed that if the separation N_f between the physical and reference surfaces were given by Stokes' integral

$$N_{fp} = \frac{R}{4\pi\gamma} \iint f(\psi)\ \Delta g\ d\sigma \qquad (15),$$

where Δg is the value of the gravity anomaly at the element of surface area $d\sigma$ on unit sphere which is at an angular distance ψ from the point of computation P, $f(\psi)$ being Stokes' function (e.g., HEISKANEN & MORITZ 1967,p.94), then

$$\xi_\alpha = -\frac{\partial N}{\partial x_\alpha} \qquad (16),$$

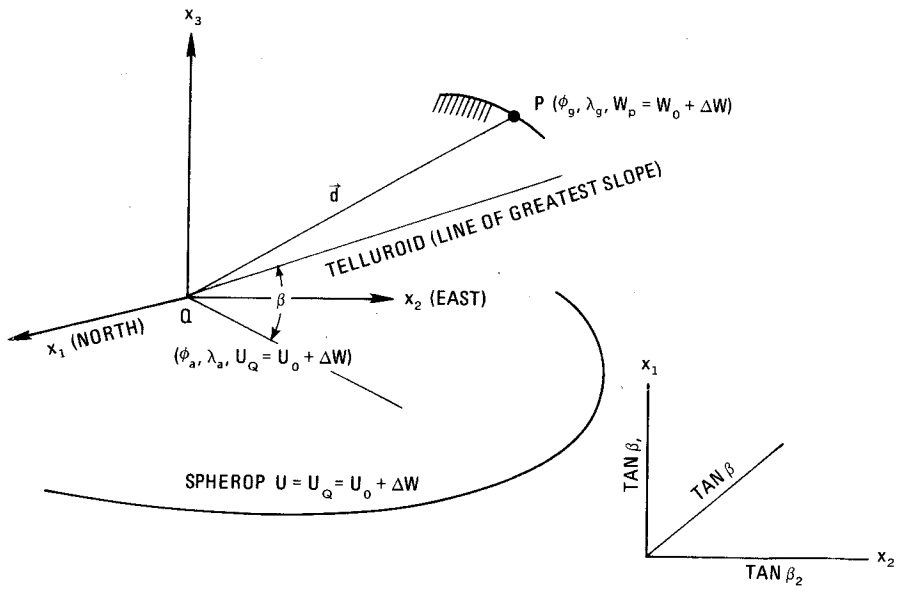

Figure 2. The Separation Vector and the Local Cartesian Co-ordinate System

as illustrated in figure 3, where x_α is a two dimensional Cartesian system in the horizontal plane at the point of computation P, with the x_1 axis oriented north and x_2 axis east. It is not difficult to show in the case of Stokes' problem that

$$\xi_\alpha = \frac{1}{4\pi\gamma} \iint \frac{\partial\{f(\psi)\}}{\partial\psi} \cos A_\alpha \; \Delta g \; d\sigma \qquad (17),$$

as

$$\frac{\partial}{\partial x_\alpha} = -\frac{1}{R} \frac{\partial}{\partial\psi} \cos A_\alpha \qquad (18),$$

where

$$A_1 = \alpha \qquad \text{and} \qquad A_2 = \tfrac{1}{2}\pi - \alpha \qquad (19),$$

α being the azimuth of $d\sigma$ from P. This follows as only ψ in the kernel of the integral at 15 varies as the point of computation changes from P to some adjacent point Q in the case of the Stokes problem.

The required expression for the Molodenskii problem is not the same as the elevation h_p of P appears in the kernel of the integral. As the deflection of the vertical at the surface of the Earth is obtained from the height anomaly h_d (IBID, p.312), which is given by

$$h_d = h_d(\phi,\lambda,h_p) = h_d(\psi,\alpha_\sigma,h_p) \qquad (20),$$

where α_σ is the azimuth of P from the element of surface area $d\sigma$, it can be shown that (MATHER 1971c, p.88)

$$\xi_\alpha = \frac{1}{h_\alpha} \left(\frac{\partial h_d}{\partial\psi} \frac{\partial\psi}{\partial u_\alpha} + \frac{\partial h_d}{\partial\alpha_\sigma} \frac{\partial\alpha_\sigma}{\partial u_\alpha} \right) \qquad (21),$$

u_α being the set of curvilinear surface co-ordinates on the reference surface, and h_α the associated

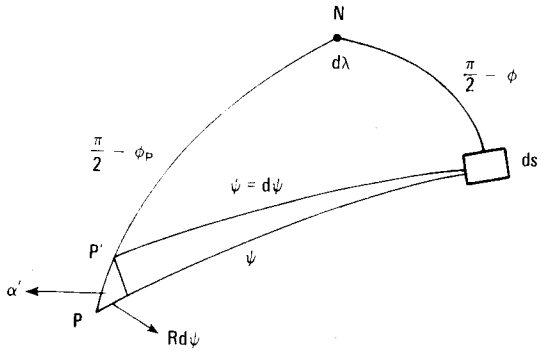

Figure 3. The Vening Meinesz Problem

linearization parameters. For the latitude-longitude system

$$u_1 = \phi \quad ; \quad u_2 = \lambda \tag{22},$$

while

$$h_1 = R \quad ; \quad h_2 = R \cos \phi \tag{23}$$

for a spherical approximation of the Earth. In the case of solutions to order e^3,

$$h_1 = \rho + h; \quad h_2 = (\nu + h) \cos \phi \tag{24},$$

ρ and ν being equivalent to the R_α defined in equation 7. The detailed development of solutions of the boundary value problem in this case use the geocentric latitude ϕ_c instead of the geodetic latitude ϕ, all parameters referring to quantities relating angular displacements between the geocentric radii to the pole P and dψ.

As explained above, the principal task in determining position from gravity is the definition of the height anomaly h_d, which is equal to the geoid height N in ocean areas, where $\Delta W = 0$. The next section deals in summary with some of the methods which have been proposed for defining the height anomaly.

3. Techniques for the Solution of the Boundary Value Problem

3.1 Introduction

Attention will be confined to three techniques whose use to obtain solutions to the boundary value problem have been extensively reported in the literature. The methods considered deal with formulations of solutions to what is known as Molodenskii's problem, at the physical surface of the Earth. It is not intended to formulate solutions for surfaces other than that of the Earth, e.g., the geoid, obtained by defining N instead of h_d. Neither is any attempt made to discuss the merits of regularization (e.g. MOLODENSKII ET AL 1962,p.45), where the conditions applicable to Stokes' problem are artificially created by the transfer of mass to within the geoid. The main advantage claimed for such techniques is a utility which is desirable when the surface gravity coverage is poor, as the adoption of certain types of mass transfers enables a more reliable prediction of gravity anomalies *for the chosen model*. The validity of such claims is open to question if the end-product

of the calculations is to be a meaningful determination of positional parameters, *which can only be as good as the available data.*

The three techniques which will be covered, ostensibly do not require a knowledge of the stratification of matter within the Earth, defining solutions in terms of an "adeqate sampling" of the gravity field at the surface of the Earth, in conjunction with a complete definition of the associated topography. They can be classified as

(1) Surface layer solutions;

(2) Solutions from data sampled at discrete points on the Earth's surface; and

(3) Solutions from Green's third identity.

It is of interest to summarize the basis of each of these methods.

3.2 The Surface Layer Technique

This method, initially developed by Molodenskii (MOLODENSKII ET AL 1962,p.118 et seq.) was first published in 1949. Considerable material is available on the problems associated with the practical use of this technique by MORITZ (1966; 1970; 1972) and members of the Soviet school (e.g., BROVAR 1964; MARYCH 1969; YEREMEEV 1969; PELLINEN 1972). The derivation calls for the representation of the disturbing potential V_d at the surface of the Earth by a surface layer of density Φ such that the former can be represented at any point P either on the surface of the Earth or exterior to it by the relation

$$V_{dp} = \iint_S \frac{\Phi}{r}\, dS \qquad (25),$$

where there is no restriction on the shape of the surface S. It can be shown that

$$\left(\frac{\partial V_d}{\partial h}\right)_p = -2\pi\Phi_p \cos\beta_p + \frac{\partial}{\partial h_p}\left(\iint_S \frac{\Phi}{r}\, dS\right) \qquad (26),$$

where the subscript $_p$ refers to evaluation at P, β_p being the ground slope at P. The first term on the right appears because of the indeterminance at P itself. The inner zone in this region is treated as a disk (e.g., HEISKANEN & MORITZ 1967,p.129), the negative sign being introduced as the outward derivative is required, while the attraction of the disk is toward the geocentre. The cos β term allows for the slope of the surface of the disk with respect to the vertical. No approximations are involved in the derivation of equation 26.

The ensuing development which is well documented (IBID,p.300) can be summarized as follows, on retaining those terms whose contributions are greater than $o\{fh_d\}$. On using equations 8,13,25 and 26,

$$\Delta g = 2\pi\Phi_p \cos\beta_p - \frac{W_o - U_o}{\gamma_p}\left(\frac{\partial\gamma}{\partial h}\right)_p - \iint\left[\frac{\partial}{\partial h_p}\left(\frac{1}{r}\right) - \frac{1}{\gamma_p}\left(\frac{\partial\gamma}{\partial h}\right)_p \frac{1}{r}\right]\Phi\, dS + o\{f\,\Delta g\} \qquad (27).$$

As

$$\frac{1}{\gamma_p}\left(\frac{\partial\gamma}{\partial h}\right)_p = -\frac{2}{R_p} + o\left\{f\,\frac{1}{\gamma}\frac{\partial\gamma}{\partial h}\right\} \qquad (28),$$

and

$$r = (R_p^2 + R^2 - 2R\,R_p \cos\psi)^{\frac{1}{2}} \qquad (29),$$

it follows from figure 4 that

$$\frac{\partial}{\partial h_p}\left(\frac{1}{r}\right) = \frac{\partial}{\partial R_p}\left(\frac{1}{r}\right) + o\{f^2 \frac{\partial}{\partial h_p}\left(\frac{1}{r}\right)\} = -\frac{1}{r^3}(R_p - R\cos\psi) = -\frac{R_p}{2r^3} + \frac{R^2}{2R_p r^3} - \frac{1}{2R_p r}.$$

Thus

$$\frac{\partial}{\partial h_p}\left(\frac{1}{r}\right) - \frac{1}{\gamma_p}\left(\frac{\partial \gamma}{\partial h}\right)_p \frac{1}{r} = \frac{3}{2R_p r} + \frac{R^2 - R_p^2}{2R_p r^3} + o\{f\,\frac{1}{R_p r}\} \qquad (30).$$

Equation 27 can therefore be written as

$$\Delta g = 2\pi\Phi_p \cos\beta_p - \frac{W_o - U_o}{\gamma_p}\left(\frac{\partial \gamma}{\partial h}\right)_p - \iint \left\{\frac{3}{2R_p r} + \frac{R^2 - R_p^2}{2R_p r^3}\right\}\Phi\, dS + o\{f\,\Delta g\} \qquad (31).$$

The solution suggested by Molodenskii for equation 31 is based on the method of successive approximations where the surface of the Earth (S) is transformed into the surface $\bar{S}$ using a parameter k which specifies the relationship between the geocentric radii R and $\bar{R}$ to equivalent points on S and $\bar{S}$ by the relation (MOLODENSKII ET AL 1962,p.120)

$$\bar{R} = R_m + k(R - R_m) \qquad (32),$$

where R_m is the mean radius of the Earth and $0 \leq k \leq 1$. Thus S and $\bar{S}$ coincide when $k = 1$, while the classical Stokesian case in which no topography exists exterior to the geoid, is obtained when $k = 0$. This is equivalent to scaling all elevations and grades by k from h and $\tan\beta$ to $\bar{h}$ and $k \tan\beta$ where

$$\bar{h} = kh,$$

and the related angle $\bar{\beta}$ is given by

$$\bar{\beta} = \cos^{-1}\{(1 + k^2\tan^2\beta)^{-\frac{1}{2}}\} \qquad (33).$$

Other relevant conversions are

$$\bar{r} = \{r_o^2 + k^2(h - h_p)^2\}^{\frac{1}{2}} + o\{f\bar{r}\} \qquad (34),$$

where r_o is the expression for the spherical case, given by

$$r_o = 2R_m \sin\tfrac{1}{2}\psi \qquad (35).$$

Molodenskii simplifies the solution by introducing the parameter χ defined by the equation

$$\chi = \frac{R^2}{R_m^2}\,\Phi\,\sec\beta \qquad (36),$$

which, when taken in conjunction with the relation

$$dS = R^2 d\sigma \sec \beta \qquad (37),$$

where $d\sigma$ is the element of surface area on unit sphere, enables equation 31 to be written as

$$\Delta g = \frac{R_m^2}{R_p^2} 2\pi\chi_p \cos^2\beta_p - \frac{W_o - U_o}{\gamma_p}\left(\frac{\partial\gamma}{\partial h}\right)_p - \frac{3R_m^2}{2R_p}\iint \frac{\chi}{r}\, d\sigma - \frac{R_m^2}{2R_p}\iint \frac{R^2 - R_p^2}{r^3}\chi\, d\sigma + o\{f\ \Delta g\} \qquad (38).$$

It can be shown that (IBID,p.121) that if χ were expanded in a power series of the form

$$\chi = \sum_{i=0}^{\infty} \chi_i k^i \qquad (39),$$

and on introducing a set of functions G_i, the use of equations 33, 34 and 39 in equation 38 gives the system of integral equations

$$G_i = 2\pi\chi_i + 2\frac{W_o - U_o}{R_m} - \frac{3}{2} R_m \iint \frac{\chi_i}{r_o}\, d\sigma, \qquad i=1,\infty \qquad (40),$$

on equating the coefficients of k^i, and as $R^2 - R_p^2 = 2R\,(h - h_p) + o\{fR^2\}$. The quantities G_i are obtained in this manipulation as

$$G_o = \Delta g \qquad (41),$$

$$G_1 = R_m^2 \iint \frac{h - h_p}{r_o^3}\, \chi_o d\sigma \qquad (42),$$

with more complex expressions for higher values of i (IBID,p.122), being of the form

$$G_i = G_i(h, h_p, \chi_0, \chi_1, \ldots\ldots \chi_{(i-1)}) \qquad (43).$$

Equation 38 reduces to equation 40 when $h = h_p = 0$ and $\beta = 0$. The Molodenskii problem is equivalent to Stokes' problem in such a case, the solution of which is equation 15; which, on taking zero degree effects into account (MATHER 1971c,p.85), can be written as

$$N_f = \frac{1}{\gamma}(V_d + W_o - U_o) = \frac{W_o - U_o}{\gamma} - R_m \frac{M\{\Delta g\}}{\gamma} + \frac{R_m}{4\pi\gamma}\iint f(\psi)\ \Delta g\, d\sigma \qquad (44),$$

where $M\{\Delta g\}$ is the global mean value of Δg. The substitution of equation 25 in equation 40, in an appropriately modified form gives

$$\chi_i = \frac{1}{2\pi}\left(G_i + \frac{3V_{di}}{2R_m}\right) \qquad (45)$$

on adoption of the representation

$$V_d = \sum_{i=0}^{\infty} k^i V_{di} = \sum_{i=0}^{\infty} \iint k^i \frac{\chi_i}{r_o} d\sigma + o\{fV_d\} \qquad (46).$$

The second equality in equation 46 would be consistent with equation 25 only if there were no topography. If this inconsistency were removed (MOLODENSKII ET AL 1962,p.123), the final expression for the height anomaly would be aseries in G_i embedded in the form set out at 44 with some topographic correction terms whose effects are purely local in character and need only be considered in areas of rugged topography, being functions of r_o^{-3}, the series being obtained when $k = 1$. In this case,

$$h_d = \frac{W_o - U_o}{\gamma} - R_m \frac{M\{G\}}{\gamma} + \frac{R_m}{4\pi\gamma} \iint f(\psi)\, G\, d\sigma + T \qquad (47),$$

where

$$G = \sum_{i=0}^{\infty} G_i \qquad (48)$$

and T are the series of topographic correction terms whose form is given by MOLODENSKII (IBID). MORITZ (1966,p.91) has given alternate forms for G_1, and shows that if the gravity anomalies are linearly correlated with elevation, G_1 reduces to the terrain correction. Thus the combination of equations 42 and 45 gives

$$G_1 = \frac{R_m}{2\pi} \iint \frac{h - h_p}{r_o^3} \Delta g\, d\sigma = \frac{1}{2}\pi \rho R_m^2 \iint \frac{(h - h_p)^2}{r_o^3} d\sigma \qquad (49),$$

the second equality being based on the assumption of linear height correlation of gravity anomalies (IBID,p.88).

Notes

(1) This technique will be practically effective only if the contributions of the higher G_i are significantly smaller than those obtained for $i = 0$ and 1. The evaluation of any particular G_i presupposes a knowledge of all $\chi_j (j < i)$, which in turn are defined through equation 45. The solution is therefore iterative, and as the series in χ_i is theoretically infinite, it is desirable that

$$\chi_i = o\{10^{-1}\ \chi_{i-1}\} \qquad (50)$$

for efficient practical evaluation. As G_o is the gravity anomaly, the first iteration gives the free air geoid, which contains over 90% of the power in the solution. It should therefore require only three iterations to obtain a solution to order e^3 in h_d if equation 50 were satisfied.

(2) There would be little difficulty in meeting this criterion if the ratio $(h - h_p)/r_o = o\{10^{-1}\}$. As the oceans comprising 70% of the Earth's surface and non-mountainous regions make little or no significant contribution to topographical effects, the magnitude of the corrections to the free air geoid would be small if the above criterion were satisfied. All topography with grades in excess of 5° pose problems in this respect when they occur within a few km of the point of computation, distant zone effects being rapidly submerged by the r_o^{-3} term. Also see section 3.5

(3) Serious embarrassment is caused when slopes exceed $\frac{1}{4}\pi$. Divergent series are obtained, making an iterative approach unstable. Discussions on the problem of convergence are available in the literature (MORITZ 1970; MORITZ 1972; KRARUP 1972). For a further discussion see section 3.5

(4) The quantity G can have no first degree harmonic, as the solution of Stokes' problem forbids the existence of such harmonics. Consequently the reference ellipsoid used for computing normal gravity is situated at the centre of mass of the mass distribution needed to produce values of gravity at the surface of the Earth which would give rise to a gravity anomaly distribution equivalent to that of G. The writer is not aware of any detailed investigation of this problem but it is unlikely that the nett effect would exceed o{5×10 cm}.

(5) The extension of this theory to orders of accuracy greater than that of the flattening is possible in theory. Such a solution could be obtained on including all effects of relevant magnitude in equations 27 and 28, and on allowing for the existence of the atmosphere, noting that Stokes' integral is strictly valid only if there is no mass exterior to the phsyical surface. In addition, it is necessary to take into account the Earth's ellipticity, when utilizing the orthogonal properties of surface harmonics.

3.3 Solution from Discrete Values

This technique was originally proposed by Bjerhammar who summarizes the problem as follows (BJERHAMMAR 1964,p.14).

> "A finite number of gravity data (gravity anomalies) is given for a non-spherical surface, at it is required to find such a solution that the boundary values for the gravity data (gravity anomalies) are satisfied in all given points."

The Bjerhammar problem is differently posed to that of Molodenskii and a different approach is used for the representation of the gravity anomalies at the surface of the Earth. Working on the basis that the representation of the surface gravity field can only be in terms of samples taken at discrete points at the Earth's surface, Bjerhammar proposes the interpretation of such data in terms of a set of model anomalies Δg^* on the surface of a sphere of radius R_b which is less than or equal to the polar radius of the best fitting ellipsoid. The appropriate requirement in Earth space is that any point on the Earth's surface lies exterior to the sphere of radius R_b (the Bjerhammar sphere), whose centre is collocated with the geocentre.

The technique of solution can be summarized as follows. The surface of the Bjerhammar sphere is partitioned into a grid, each element of which has a surface area $R_b^2 d\sigma$, and is represented by the model gravity anomaly Δg^*, assumed constant over the area. The disturbing potential V_{dp} at any exterior point P whose geocentric distance, as illustrated in figure 4, is R_p, is given by

$$V_{dp} = \frac{R_b^2}{4\pi R_p} \iint \Delta g^* \sum_{n=2}^{\infty} \frac{2n+1}{n-1} \left(\frac{R_b}{R_p}\right)^n P_{no}(\cos\psi)\, d\sigma \qquad (51)$$

under conditions applicable to Stokes' problem. Δg^* obviously cannot have a first degree harmonic and the possibility of satisfying this condition in conjunction with the geocentric collocation of the Bjerhammar sphere is subject to the same arguments as outlined in note 4 to section 3.2.

The observational data is in the form of gravity anomalies Δg as determined at discrete points at the surface of the Earth. Using the fact that Poisson's integral

$$H_p = \frac{R_b(R_p^2 - R_b^2)}{4\pi} \iint \frac{H}{r^3}\, d\sigma \qquad (52)$$

applies without approximation to any function H which is harmonic exterior to the Bjerhammar sphere, is is possible to define gravity anomalies Δg at all exterior points, if a surface distribution of the data set Δg^* were available on the sphere. Alternately, if Δg_i are the gravity anomalies measured at the surface of the Earth, the equation defining Δg_i in terms of the Δg^* is obtained from equation 52 as

$$\Delta g_i = \frac{R_b(R_{pi}^2 - R_b^2)}{4\pi R_p} \sum_j \frac{\Delta g_j^*}{r_{ij}^3} d\sigma_j \qquad (53),$$

where r_{ij} is the distance between P_i on the Earth's surface, with geocentric distance R_{pi}, and the surface element $d\sigma_j$ on the Bjerhammar sphere.

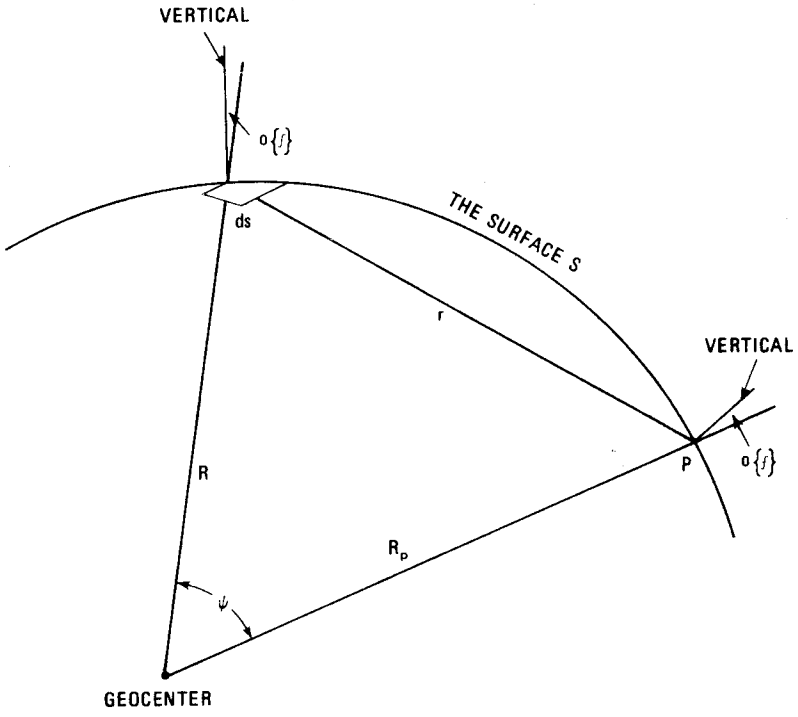

Figure 4. Relations for r

Equation 53, called the *discrete integral equation* by BJERHAMMAR (1968,p.6), can be treated as a set of observation equations which can be solved by standard techniques for the elements Δg^*. The technique is subject to certain practical difficulties when tested on models with heavy point masses between the sphere and the Earth's surface (IBID,p.67). In such cases, Bjerhammar advocates the use of the disturbing potential rather than the gravity anomaly in equation 53, presumably by recourse to an iterative procedure. The validity of the technique hinges on whether the disturbing potential computed at all points P_i at the Earth's surface due to the Bjerhammar system is identical with that due to the Earth. For a summary of the proof of this condition, see (BJERHAMMAR 1969, pp.452-6).

The instability of the inversion procedure due to the nature of gravitational attraction and its susceptibility to large masses locally (e.g., mountainous regions) led Bjerhammar to suggest that the more stable disturbing potential V_d^* on the Bjerhammar sphere be used as an intermediary in the solution on the following lines (IBID,p.498 et seq). The disturbing potential V_{di} at P_i on the Earth's surface is given by equation 52 as

$$V_{di} = \frac{R_b(R_{pi}^2 - R_b^2)}{4\pi} \iint \frac{V_d^*}{r_i^3} d\sigma \qquad (54).$$

As

$$\left\{\frac{\partial V_d}{\partial h}\right\} = \frac{R_b}{8\pi R_{pi}} \iint \frac{4R_{pi}^2 r_i^3 - 3r_i(R^2 - R_b^2 + r^2)(R_p^2 - R_b^2)}{r_i^6} V_d^* \, d\sigma + o\{f^2 \frac{\partial V_d}{\partial h}\} \qquad (55),$$

Δg is obtained from equation 13 on considering terms larger than $o\{f\,\Delta g\}$, as

$$\Delta g_i = -\frac{R_b}{8R_{pi}} \iint \left\{ \frac{4R_{pi}^2}{r_i^3} - \frac{3(R_{pi}^2 - R_b^2)^2}{r_i^5} + \frac{R_{pi}^2 - R_b^2}{r_i^3} \right\} V_d^* \, d\sigma + o\{f\,\Delta g\} \qquad (56).$$

Equation 58 is simplified by differencing V_d^* from the value V_{do}^* which is the value of V_d^* at the point on the Bjerhammar sphere corresponding to P. It can be shown (IBID,p.499) that equation 56 can be transformed to

$$\Delta g_i = -\frac{R_b V_{do}^*}{R_p^2} - \frac{R_b}{8\pi R_{pi}} \iint \left\{ \frac{5R_{pi}^2 - R_b^2}{r_i^3} - \frac{3(R_{pi}^2 - R_b^2)^2}{r_i^5} \right\} (V_d^* - V_{do}^*) d\sigma + o\{f\,\Delta g\} \qquad (57),$$

which is a generalized version of the Molodenskii inverse of Stokes' integral (MOLODENSKII ET AL 1962, p.50).

Notes

(1) The use of this system would, at first glance appear to be a prohibitive task. This is not the case as the terms being integrated are scaled by r^{-3} and hence only limited regions need be considered around each primary point at which evaluations are made. Details of tests in the West Alps using a 5^ox 5^o area with a 15^ox 15^o buffer zone, with basic sub-divisions of 5'x 5', are given by Bjerhammar (IBID,p.508), an iterative procedure being used to recover Δg^*.

(2) The intellectual elegance of the method is enhanced by its ability to combine all manifestations of the Earth's gravitational field into a single solution entity. It must be added that this same end can be achieved by using the methods proposed by KRARUP (1969), though the problems associated with practical implementation have yet to be tackled in the case of high precision determinations.

(3) The factors which have to be taken into account to extend the solution to orders smaller than that of the flattening are similar to those outlined in section 3.2(5).

(4) The solution, like that from Krarup's method, is unique for a given distribution of data. This of course, doen not mean that the answer obtained is correct to the order of accuracy with which the problem is formulated. Data needed for solutions of the boundary value problem are dealt with in section 4.

(5) For completeness, the solution should incorporate terms of zero degree as in section 3.2.

3.4 Solutions from Green's Third Identity

Considerable work has been done in this field (e.g., ARNOLD 1959; KOCH 1965; MORITZ 1965; MATHER 1971c). The basic integral used is Green's third identity which is obtained by the application of Green's theorem to two scalars r^{-1} and W which is harmonic in the volume V_e exterior to a surface S. On combining the gravitational and rotational effects (e.g., HEISKANEN & MORITZ 1967,p.15), the final expression obtained for the gravitational potential (W_p) at a point P on the surface S, on the assumption that all matter is contained within S and rotates with constant angular velocity ω, is

$$W_p = \frac{1}{2\pi} \iint \left(\frac{1}{r} \vec{\nabla} \cdot \vec{N} \, W - W \, \vec{\nabla} \cdot \vec{N} \, \frac{1}{r} \right) dS - 2\omega^2 \iiint \frac{1}{r} \, dV_i \qquad (58),$$

where $\vec{\nabla} = \frac{\partial}{\partial x_i} \vec{i}$, $\vec{i}$ being unit vectors along the axes x_i of a Cartesian co-ordinate system and r the distance of the elements of surface area dS and volume dV_i interior to S, from P.

A similar expression is obtained for the potential U_p at P due to a gravitating ellipsoid of reference which has the same gravitational characteristics as the Earth, including rotation. On considering the same surface S which is that of the Earth,

$$U_p = \frac{1}{2\pi} \iint \left(\frac{1}{r} \vec{\nabla} \cdot \vec{N} \, U - U \, \vec{\nabla} \cdot \vec{N} \, \frac{1}{r} \right) dS - 2\omega^2 \iiint \frac{1}{r} \, dV_i \qquad (59),$$

$\vec{N}$ in both equations 58 and 59 being the unit vector normal to S at dS. Both equations hold exactly if U and W are harmonic exterior to S. This condition requires that no matter exists on either system exterior to the Earth's surface. The practical consequences, which are of significance when resolution approaching the order of the flattening is sought as the end result of computations, are the following.

1. The reference ellipsoid must always lie within S. As S councides with the ocean surface over 70% of the Earth, the reference ellipsoid must be smaller than the ellipsoid which best fits the geoid by an amount greater than the largest negative geoid undulation if no condition is to be be imposed on the mass distribution within the equipotential ellipsoid.

2. There should be no atmosphere exterior to S if equation 60 is to hold to accuracies in excess of order $10^{-2}V_d$.

3. Both the reference ellipsoid and the Earth are assumed to rotate with the same constant angular velocity ω. Irregularities in the Earth's rotation have to be allowed for as corrections to observations in instances where such magnitudes are of significance. For details, see section 2.2 and 4.

The practice to date has been to treat the atmospheric effects as those which should be modeled and allowed for as corrections to observations prior to use in computations (e.g., IAG 1970,p.18). In a recent solution MATHER (1973,p.28 et seq.) formulated a solution of the boundary value problem to $o\{e^3 h_d\}$ by separating the gravitational effects of the atmosphere from those of the solid Earth and oceans.

In conventional solutions, the disturbing potential V_d is obtained on differencing equations 58 and 59, when

$$V_{dp} = W_p - U_p = \frac{1}{2\pi} \iint \left(V_d \, \vec{\nabla} \cdot \vec{N} \, \frac{1}{r} - \frac{1}{r} \vec{\nabla} \cdot \vec{N} \, V_d \right) dS \qquad (60).$$

This equation is not valid to orders smaller than $o\{10^{-2}V_d\}$ as it assumes the geopotential to be harmonic outside S. A function which does satisfy Laplace's equation exterior to S is the potential W' due to the solid Earth and oceans, which is related to W by the relation

$$W' = W - V_a \qquad (61),$$

where V_a is the potential of the atmosphere, which is of order $10^{-6}W$, and more significantly, $V_a = o\{10^{-2}V_d\}$. As such, it is desirable to construct a theory which allows for its existence in the course of the derivation.

The final solution using this technique can only be obtained by iteration, the number of iterations required, as in the surface layer method, being a function of the accuracy sought. Favourable conditions for the adoption of an iterativeprocedure are the following.

a. A significant amount (> 90%) of the power should be generated in the first iteration.

b. The iterative procedure should have the ability to converge to the correct result.

c. The number of iterations necessary for achieving the desiring degree of resolution should be as small as possible.

When surface gravity is the sole source of information, the only procedure available for obtaining an adequate first approximation to the height anomaly h_d is the use of Stokes' approach. Fundamental to this technique is the assumption that the disturbing potential is harmonic exterior to and on the surface S, and therefore can be expressed in the form

$$V_d = \sum_{n=0}^{\infty} \frac{A_n}{R^{n+1}} \quad , n \neq 1 \qquad (62),$$

where

$$A_n = \sum_{m=0}^{n} A_{nm} \qquad (63),$$

and

$$A_{nm} = P_{nm}(\sin \phi_c)\{C_{nm}\cos m\lambda + S_{nm}\sin m\lambda\} \qquad (64),$$

the last equation being the standard expression for a surface harmonic.

The adoption of this model enables the combination of the effects of the disturbing potential V_d and its vertical gradient $\partial V_d/\partial h$ on using equation 13, thereby transforming the formulation to a representation of the observed quantity, the gravity anomaly Δg. Details of the problems involved in obtaining a solution of the boundary value problem to order $e^3 h_d$ are dealt with by MATHER (1973,p.31 et seq.). To preserve flexibility in the formulation of results to any required order of accuracy, it is desirable to retain physical relevance in the derivation by constructing the integral at 60 such that the disturbing potential V_d is replaced by the quantity

$$V_d' = V_d - V_a \qquad (65),$$

where V_a is the potential of the atmosphere.

A generalized solution which did not consider either the existence of the atmosphere or the fact that the potential of the geoid was not known, the latter being disregarded after due consideration as a quantity which correctly cannot be determined from gravimetric methods alone (MOLODENSKII ET AL

1962,p.104), was formulated by Molodenskii in 1945 (IBID,p.93). A specific solution was given by ARNOLD (1959), which could be written as

$$h_{dp} = \frac{R_m}{4\pi\gamma}\iint (\Delta g - \gamma\,\xi_\alpha \tan\beta_\alpha) f(\psi)\, d\sigma + \frac{R_m^2}{2\pi\gamma}\iint \frac{1}{r_o^3}\left\{(h_p - h) + R \sin\psi \frac{dh}{dr}\right\} V_d\, d\sigma \qquad (66),$$

where ξ_α are the components of the deflections of the vertical, $f(\psi)$ is Stokes' function, $\tan\beta_\alpha$ being the components of the gradient of the ground slope in the north and east directions,

$$\frac{dh}{dr} = \cos A'_\alpha \tan\beta_\alpha \qquad (67),$$

where

$$A'_1 = \alpha_\sigma \quad ; \quad A'_2 = \tfrac{1}{2}\pi - \alpha_\sigma \qquad (68),$$

and r_o is given by equation 35. A revision of the derivation to the order of the flattening showed that (MATHER 1971c,p.85)

$$h_{dp} = \frac{W_o - U_o}{\gamma} - R_m \frac{M\{\Delta g\}}{\gamma} + \frac{R_m}{4\pi\gamma}\iint f(\psi)\ \Delta g\, d\sigma + \frac{R_m^2}{2\pi\gamma}\iint \frac{1}{r_o}\left\{\left\{(h_p - h) + R_m \sin\psi \frac{dh}{dr}\right\}\frac{V_d}{r_o^2} - \gamma\,\xi_\alpha \tan\beta_\alpha\right\} d\sigma$$

$$+ o\{f\, h_d\} \qquad \text{if} \qquad \left(\frac{(h_p - h)}{r_o}\right)^2 = o\{f\} \qquad (69),$$

and Laplace's equation were satisfied to $o\{f\,\vec{\nabla}^2 V_d\}$ at all points exterior to and on S. Equations 66 and 69 would then be equivalent if

$$\frac{1}{2}\iint \gamma\,\xi_\alpha \tan\beta_\alpha\, f(\psi)\, d\sigma = R_m \iint \frac{1}{r_o}\gamma\,\xi_\alpha \tan\beta_\alpha\, d\sigma \qquad (70).$$

The effect of the terms common to the kernels of the integrals on either side of the equality in equation 70 can be expected to arise from only 30% of the surface area of the globe. Significant contributions to h_d will be restricted to only about 5% of the surface area, being about one order of magnitude smaller than Δg if $\xi_\alpha = o\{10^{-4}\}$ and $\tan\beta = o\{10^{-1}\}$. The high probability of correlation between the signs of ξ_α and β_α in regions where the latter is significant magnitude, indicates that this effect is likely to be always positive. As $h_d = o\{10^2 m\}$, it is realistic to estimate the effect of the above term as $o\{5\times10\ cm\}$, the effect being consequential if regions of mountainous topography occur near the point of computation.

The first term in the second integral at 69 converges much more quickly with increase of r_o and can be treated as a purely local effect. The advantage of the solution at 69 over that at 66 is the fact that all terms due to the interaction between the ground slope and the slope of the equipotential can be treated as purely local effects, giving solutions where the neglected effects do not have magnitudes much in excess of the order of the flattening. Another advantage of the solution at 69 is its unambiguous definition in Earth space as the Stokesian term defined a contribution with reference to an ellipsoid whose centre is at the geocentre of the Earth with no atmosphere.

The generalization to order e^3 in h_d (i.e., ±5 cm) deals not only with the effect of the topography, the interactions between the slopes of the topography and the equipotential surfaces of the Earth's gravitational field, as well as the atmosphere, but is also in keeping with the physical

characteristics of the scalar potential (MATHER 1973). It also establishes the nature of the relationship between the Stokesian term and the indirect effect without limitations imposed by the simplistic approximations permitted by the adoption of a lower order of accuracy and identifies the anomaly to be used in Stokes' integral. The geometry of the solution is also specified in Earth space, as the centre of the reference ellipsoid is located at the centre of mass G' of the solid Earth and oceans, whose co-ordinates $\overline{X}_{ei}$ with respect to a geocentric Cartesian co-ordinate system are given by (IBID,p.26)

$$\overline{X}_{ei} = - \frac{M_a}{M_e} \overline{X}_{ai} \qquad (71),$$

where $\overline{X}_{ai}$ are the co-ordinates of the centre of mass of the model adopted for the Earth's atmosphere, M_a and M_e being the mass of the atmosphere and the solid Earth and oceans respectively. The final formulae obtained in the solution referred to are summarized below.

$$h_{dp} = N_{fp} + N_{cp} \qquad (72),$$

where the Stokesian term N_{fp} is given by

$$N_{fp} = \frac{W_o - U_o}{\gamma_p} - \overline{R} \frac{M\{\Delta g_c\}}{\gamma_p} + \frac{\overline{R}}{4\pi\gamma_p} \iint f(\psi) \quad \Delta g_c \, d\sigma \qquad (73),$$

γ_p being the value of normal gravity at P' in figure 1, $\overline{R}$ being the radius of the Brillouin sphere whose centre is collocated with the centre of mass of the solid Earth and oceans G', and contains the solid Earth and oceans. The gravity anomaly Δg_c is defined by

$$\Delta g_c = \Delta g_1 + \Delta g_2 \qquad (74),$$

where

$$\Delta g_1 = \Delta g + \frac{\partial V_a}{\partial h} + 2 \frac{V_a}{R_m} \qquad (75),$$

V_a being the potential of the atmosphere, and

$$\Delta g_2 = \frac{2V'_d}{R_m} c_\phi - \frac{1}{2} g \zeta^2 + dR \frac{\partial \Delta g}{\partial h} + o\{e^3 \Delta g\} \qquad (76),$$

if

$$\frac{1}{2}(dR)^2 \frac{\partial \Delta g}{\partial h} = o\{e^3 \Delta g\},$$

where

$$dR = \overline{R} - a(1 - f \sin^2\phi_c) - h + o\{f \, dR\} \qquad (77),$$

$$\frac{\partial \Delta g}{\partial h} = - \gamma \left(\sum_{\alpha=1}^{2} \frac{\partial \xi_\alpha}{\partial x_\alpha} - \frac{\xi_1 \tan \phi_c}{R_m} - 2 \frac{N_f}{R_m^2} + o\{f \frac{\partial \Delta g}{\partial h}\} \right) \qquad (78),$$

and

$$c_\phi = f + m - 3f \sin^2\phi_c + o\{f^2\} \qquad (79).$$

The angle ψ is computed in calculations to $o\{e^3 h_d\}$ from the geocentric latitude ϕ_c and longitude λ as

$$\psi = \cos^{-1}(\sin\phi_c \sin\phi_{cp} + \cos\phi_c \cos\phi_{cp} \cos d\lambda) \tag{80},$$

where

$$d\lambda = \lambda - \lambda_p \tag{81},$$

the value without subscript referring to $d\sigma$, and those with subscript $_p$ to the point of computation P. The indirect effect N_{cp} is given by

$$N_{cp} = \frac{V_{ap}}{\gamma_p} + \frac{1}{2\pi\gamma_p}\iint \frac{R^2}{r}\left\{\frac{\partial V'_d}{\partial x_\alpha}\tan\beta_\alpha + V'_d\frac{x_\alpha \tan\beta_\alpha}{r^2} + \frac{1}{2R}\left\{3\left(c_\Delta + 3\frac{dR}{R}\right) - \Phi\right\} - dR\frac{\partial\Delta g}{\partial h} + \Delta g'\left(c_\Delta + \frac{3}{2}\frac{dR}{R}\right) + o\{e^3\Delta g\}\right\} d\sigma \quad \text{if } \frac{1}{2}(dR)^2\frac{\partial^2\Delta g}{\partial h^2} = o\{e^3\Delta g\} \tag{82},$$

r being the distance between $d\sigma$ and P, R being the geocentric distance, given by

$$R = a(1 - f\sin^2\phi_c) + h + o\{f^2 R\} \tag{83},$$

and h the ellipsoidal elevation. The other expressions which need definition are

$$\frac{\partial V'_d}{\partial x_\alpha}\tan\beta_\alpha = -\gamma\,\xi_\alpha\tan\beta_\alpha + N_f\frac{\partial\gamma}{\partial x_1}\tan\beta_1 + o\{f^2\Delta g\} \tag{84},$$

the two dimensional co-ordinate systems x_α having the same significance as in figure 2,

$$\frac{x_\alpha}{r^2}\tan\beta_\alpha = \frac{R}{r^2}(1 + c_x)\sin\psi\frac{dh}{dr} \tag{85},$$

where dh/dr is defined by equation 67,

$$c_x = \frac{\cos(\frac{1}{2}\psi - \theta)}{\cos(\frac{1}{2}\psi + \theta + \delta)} - 1 \tag{86},$$

$$= -\tan^{-1}\left\{\frac{2\sin\delta\sin\frac{1}{2}\psi - \frac{\Delta R}{R_m}\cos(\frac{1}{2}\psi + \delta)}{2\cos\delta\sin\frac{1}{2}\psi + \frac{\Delta R}{R_m}\sin(\frac{1}{2}\psi + \delta)}\right\} + o\{f^2\tan\theta\}$$

$$= \frac{1}{2}\frac{\Delta R}{R_m}\cot\tfrac{1}{2}\psi - \delta + o\{f^2\} \quad \text{if } \psi > 5^o \tag{87},$$

$$\Delta R = R_p - R \tag{88},$$

and

$$\delta = f\sin 2\phi_c\cos\alpha_\sigma + o\{f^2\} \tag{89}.$$

The term Φ is given by

$$\Phi = \frac{2R}{r}\left\{R - R_p\cos(\psi + \delta)\right\} - 1 \qquad (90),$$

and

$$c_\Delta = \frac{1 + 2\frac{dR}{R}}{(1 + c_{\frac{-}{r}})^{\frac{1}{2}}} - 1 \qquad (91),$$

where

$$c_{\frac{-}{r}} = \left(\frac{\Delta R}{\bar{r}}\right)^2 - \frac{dR + dR_p}{R_m} + o\{f^2\} \qquad (92),$$

and

$$\bar{r} = 2\bar{R}\sin\tfrac{1}{2}\psi \qquad (93).$$

Notes

(1) The adoption of an iterative procedure to solve equations 72 to 93 cannot be avoided. See note 1 to section 3.2 for background. Mather (IBID,p.49 et seq.) has suggested an iterative procedure which should require three stages in the computation for determining N_c to 5 parts in 10^4 (i.e., $o\{e^3h_d\}$), while the Stokesian contribution need be evaluated only once, but in two stages.

(2) The first two terms in equation 73 are of zero degree and are meaningful only when the *surface gravity field* is sufficiently well defined to give an adequate value for the global mean surface gravity anomaly. Present day solutions which are heavily dependent on satellite determined low degree harmonics of the Earth's gravitational field, are insensitive to the effects of these terms. For a further discussion of zero degree effects which would be of conseqeunce in solutions based on adequate distributions of surface gravity data alone, see section 5.

(3) It could be construed that the conditions attached to equations 76 and 82 are a limitation on the development outlined above. The relevant terms which are omitted have a nett differential effect of

$$\frac{1}{4\pi\gamma}\iint\left\{\frac{1}{2}\bar{R}\,f(\psi) - \frac{R^2}{r}\right\}(dR)^2\,\frac{\partial^2\Delta g}{\partial h^2}\,d\sigma$$

on h_d which would be negligible if the quantity $\partial^2\Delta g/\partial h^2$ had random error characteristics over areas larger than 10^4 km^2 with magnitudes of order 10^{-8} mgal m^{-2}, which is only one order of magnitude smaller than that of $\partial^2\gamma/\partial h^2$.

(4) The components of the deflections of the vertical ξ_α are computed on the principles outlined in equations 16 to 24. A series of expressions which include effects with magnitudes of the order of the flattening are given by MATHER (1971c,p.86 et seq.). Such expressions should be adequate for the evaluation of h_d to $o\{e^3h_d\}$, but fail if accuracies of this type are required from the deflections themselves. Extension would principally require the use of an ellipsoidal co-ordinate system and a more careful evaluation of some of the higher derivatives of characteristics of the gravitational field which have been assessed as having insignificant effects on the height anomaly.

3.5 Conclusion

The formulation of a solution of the boundary value problem at the physical surface of the Earth, in contrast to Stokes' problem where there is no topography exterior to the geoid, calls for the evaluation of "topographical" terms which arise as a consequence of

(a) departures of the Earth's surface from a level surface; and

(b) elevation of the point of computation above or below the surrounding topography.

The first effect has contributions with long wavelength which, on present assessment of geoid

determinations, should not have effects in excess of o{50 cm} unless rugged topography occurs in the vicinity of the point of computation. The second effect is a purely local one as it is scaled by the factor r^{-3}, as seen in equations 42, 57 and 69.

The limitation in theory of the surface layer method is the heavy reliance it places on the convergence of the series in G_i, defined at 43, in the mathematical sense. It may appear to be paradoxical in practical terms, that the *slope* of the topography of distant areas, which at least to a first order of approximation, are in isostatic compensation, can affect computations of the height anomaly. These terms occur because the gravity anomaly used in computations and defined by equations 10 and 11, reflect the mass distribution of the Earth as it exists. If, on the other hand, a suggestion similar to that made by DE GRAAFF HUNTER (1958) calling for the smoothing of the topography such that slopes in excess of 5^o did not exist, were adopted, there would be little to choose between the methods outlined in this section for the solution of the boundary value problem. In such a case, each of the iterative methods mentioned would not require more than three iterations to achieve a 5 cm resolution in h_d.

The conclusion that a model had to be adopted for the topography was also reached by MORITZ (1972, p.49) after a detailed study of the convergence of Molodenskii series. This approach has in the latter half of this century, become anathema to physical geodesists (e.g., MOLODENSKII ET AL. 1962, p.118) as it involves making assumptions about the density of material comprising the upper layers of the Earth's crust. In contrast, the quantities Δg, h, tan β and $\partial^i \Delta g/\partial h^i$ must be considered those which can be observed. In this sense, the solution described in section 3.4 exhibits favourable convergence characteristics, as the solutions involved are not open ended, but controlled in magnitude as terms in a rapidly convergent power series in the parameter f (= $o\{10^{-3}\}$). In practical terms however, the higher differential coefficients $\partial^i \Delta g/\partial h^i$ are unlikely to be determined with sufficient density to be of practical use, and the adequacy of equation 69 will depend largely on the magnitude and wavelength of the series $(i!)^{-1} h^i (\partial^i \Delta g/\partial h^i)$. Cumulative magnitudes of o{±0.5 mgal} with wavelengths of 100 km or less can be considered to be acceptable for solutions to order $e^3 h_d$, as discussed in section 4.

Reverting to the question of smoothening the topography in order that grades do not exceed 10^{-1}, the following problems will have to be attended to if such a procedure were adopted as everyday practice in physical geodesy

(a) The principles underlying the transfer of mass and their associated consequences should be clearly defined.

(b) The question of assigning a density for each element transferred will have to be dealt with, as the resulting corrections to observed gravity will depend on the model adopted for these masses.

If such procedures were deemed to be necessary, it would be madatory to adopt a model for the Earth with surface slopes less than 5^o. The transfer of matter to achieve this goal will change both observed gravity as well as the location of the center of mass of the physical system. The exact numerical values of the corrections made will depend on the principles adopted for the mass transfer. Physical geodesists advocating this type of approach will have to face up to the philosophical problem of which elements of topography to flatten out or fill. It is most important that a single model be adopted in order that the geodetic community is not subject to a confusing variety of results which are not in agreement, not because of significant factors, but merely as a consequence of the adopted smoothing procedure. The limited surface gravity data available at the present time continues to keep the above problem in the area of academic interest alone. It is one in which continued discussion is to be encouraged.

The solution of Molodenskii's problem by means of analytical continuation (MORITZ 1969; MARYCH 1969) has not been dealt with as it has been shown to be equivalent to the solution obtained using the surface layer approach (MORITZ 1970). Another method which may prove to have some benefits is the use of numerical integration techniques, on which published material is hard to come by.

4. Practical Considerations

4.1 Introduction

Practical considerations fall into two distinct categories. The first concerns the optimum sampling of data in order that the necessary precision can be achieved in numerical computations. The second is the extraction of the most probable results from whatever (inadequate) data is available. The second falls beyond the scope of this review and is covered elsewhere in this Symposium. One exception is the use of Molodenskii and Cook truncation functions to obtain the maximum information from satellite determined gravity anomalies and local gravity fields.

The problem can be summarized as follows. Over 90% of the power in h_d comes from Stokes' integral. Many regions exist where dense local gravity fields are available, but where beyond some limiting angular distance ψ_o, the available gravity data from the analysis of the orbital perturbations of near Earth satellites on combination with whatever surface gravity data exists, can be represented as a set of surface harmonics of the type given in equations 63 and 64. The free air geoid at equation 73 can be written as (MOLODENSKII ET AL 1962,p.147)

$$N_{fp} = \frac{W_o - U_o}{\gamma} - R\,\frac{M\{\Delta g\}}{\gamma} + \frac{R}{4\pi\gamma}\int_0^{\psi}\int_0^{2\pi} f(\psi)\,\Delta g\,\sin\psi\,d\psi\,d\alpha + \frac{R}{2\gamma}\sum_{n=2}^{\infty} Q_n\,\Delta g_n \qquad (94),$$

where the gravity anomaly Δg to be used in Stokes' integral is expressed by the set of surface harmonics

$$\Delta g = \sum_{n=0}^{\infty} \Delta g_n, \quad n \neq 1 \qquad (95).$$

Q_n is Molodenskii's truncation function, given by

$$Q_n = \int_{\psi_o}^{\pi} f(\psi)\,P_{no}(\cos\psi)\,\sin\psi\,d\psi \qquad (96),$$

$P_{no}(\cos\psi)$ being the Legendre zonal harmonic. Values of Q_n for various ψ_o are given by Molodenskii and his co-workers (IBID,p.150) to n=8, DE WITTE (1967) to n=25, and HAGIWARA (1972) to n=18. The computational efficiency of this method over the use of surface quadrature techniques for distant zone effects, in the present era where distant zone fields are heavily dependent for quality on satellite data, is a factor of 70 (OJENGBEDE 1973,p.32). In practice, only a limited number (at present, upto degree and order 20) of such harmonics are available and a rounding off error will occur in computations, due to the existence of a residual in the power spectrum of gravity anomalies on adopting the surface harmonic representation. Molodenskii uses an elegant technique to show that the use of harmonics to n=8 with surface gravity representations up to $\psi_o=23^o$, results in errors less than ±2 m, while extension of surface gravity coverage to $\psi_o=35^o$ reduces the truncation error to less than ±50 cm (MOLODENSKII ET AL 1962,p.164).

Similar considerations apply to the computation of the Vening Meinesz contribution to the deflections of the vertical using Cook's truncation function (COOK 1950,p.377), the equation equivalent to 94 in this case being (DE WITTE 1967,p.455)

$$\xi_\alpha = \frac{1}{4\pi\gamma}\int_0^{\psi_o}\int_0^{2\pi} \frac{\partial\{f(\psi)\}}{\partial\psi}\,\Delta g \cos A_\alpha \sin\psi\, d\psi\, d\alpha + \frac{1}{2}\sum_{n=2}^{\infty}(n-1)C_{n1}q_n \qquad (97),$$

where

$$C_{\alpha n1} = \frac{1}{4\pi(n-1)\gamma}\iint \Delta g_n\, p_{n1}(\cos\psi)\cos A_\alpha\, d\sigma \qquad (98),$$

A_α being defined by equation 19 while Cook's truncation function q_n is given by

$$q_n = \int_{-1}^{\cos\frac{1}{2}\psi_o}\frac{\partial}{\partial\psi}\{f(\psi)\}\, p_{n1}(\cos\psi)\, d(\cos\psi) \qquad (99).$$

The relationship between the functions Q_n and q_n has been established by HAGIWARA (1972,p.461) who gives a proof of the equivalence of the developments of Molodenskii and Cook. On using the same values of n and ψ_o described in the previous paragraph, Molodenskii shows that the truncation errors in ξ_α are less than 1.1 arcsec and 0.2 arcsec respectively in the two cases given. It can be concluded with confidence that the use of truncation functions is capable of giving a resolution equivalent to the best astro-geodetic results as is borne out by determinations in Australia (MATHER, BARLOW & FRYER 1971,p.19) and the tests carried out by OJENGBEDE (1973,p.41).

4.2 The Sampling of the Gravity Field at the Surface of the Earth

The overwhelming majority of surface gravity data available at the present time have been established for geophysical purposes motivated by regional considerations. Such information has to be carefully screened before being put to geodetic use. There are problems that arise in the establishment of the value of observed gravity itself. Until recently, most gravity determinations of quality were made by differential means using gravimeters. It is now possible to carry out an absolute determination of g with a resolution of ±50 μgal using a transportable apparatus (MORELLI ET AL 1971,p.17) while resolution at the ±3 μgal level has been reported by the apparatus at Sevres, France (SAKUMA 1971).

It is all-important in the first instance that all values of observed gravity are correctly referred to the unified gravity standardization network defined by the *International Gravity Standardization Network 1971* (IGSN71) or an equivalent global control network, in order that datum discrepancies may be minimized, if not eliminated. The solution of the geodetic boundary value problem requires an evaluation of the gravity anomaly. This calls for a knowledge of

(a) the geodetic latitude ϕ_g of the gravity station to 0.04 arcsec (± 1 m) for an accuracy of ±1 μgal; and

(b) the geopotential difference ΔW with respect to the geoid to ±0.003 kgal m for a resolution of ±1 μgal in the gravity anomaly Δg,

in addition to the requirements stated earlier for values of observed gravity. This also calls for the definition of a datum for the geopotential differences on a global basis, and to some desirable degree of resolution.

The status at the present time is as follows. While IGSN71 is available, it is most unlikely that any of the large gravity data banks are reliably connected to this network in toto at the present time. Most values of normal gravity are computed from regional geodetic co-ordinates of gravity

stations which are unlikely to differ from geocentric values by more than ±10 arcsec. Thus all values of normal gravity computed in a given continental area covered by one of the regional datums (usually up to 5% of the Earth's total surface area), are subject to systematic errors not exceeding ±¼ mgal. The lack of a global datum for geopotential cannot cause errors much in excess of ±½ mgal if the datum for elevations were based on at least one year's tide gauge readings, and there is no evidence available at present which indicates that the magnitude of stationary sea surface topography is much in excess of ±2 m. While these magnitudes appear to be small, their effect on the evaluation of Stokes' integral is significant, being systematic in character.

Present day geoid computations from surface gravity data are therefore limited in effectiveness as a consequence of irregularly distributed data which could be subject to systematic errors due to the effect of inadequately defined datums on the data set used in the computations. The existence of such effects cannot be tolerated when the data is required for the determination of the geoid with the highest possible precision in the study of sea surface topography, whose magnitude is unlikely to exceed 2-3 m. The term sea surface topography refers to departures of the ocean surface from an equipotential surface of the Earth's gravitational field and is partially due to salinity, meteorological and tidal effects. The magnitude of the residual departures on allowing for these factors, and termed stationary effects, can only be estimated from manifestations along coastlines which have been obtained by comparing the results of geodetic levelling with tide gauge readings. Departures which cannot as yet be explained, have been reported in Australia (e.g., HAMON & GREIG 1972), the United States (e.g., STURGES 1972) and elsewhere with slopes approaching or in excess of 0.1 arcsec. On balancing satellite altimeter technology presently available against oceanographic requirements, it would appear that a 10 cm resolution in the determination of the geoid is a desirable goal for this purpose (WILLIAMSTOWN REPORT 1969,3-2).

The criteria governing the factors which constitute a "desirable" representation of the gravity field for the solution of the geodetic boundary value problem is dependent on the requirements for the solution of Stokes' integral which, as discussed earlier, provides over 90% of the power. This would apply to any of the techniques of solution described in section 3. The following is a summary of a recent look at this problem (MATHER 1973,p.53 et seq.). A suitable form of Stokes' integral for quadratures evaluation is

$$N_f^{(cm)} = K \sum_i n_i \sum_j \mu_{ij} f(\psi_{ij}) \Delta g_{ij}^{(mgal)} \qquad (100),$$

where Δg_{ij} is the value of the gravity anomaly representing a $n_i^o \times n_i^o$ square,

$$K \doteqdot 1.58 \times 10^{-2} \qquad (101),$$

and $\mu_{ij} = \cos \phi_{cij}$ or $\sin \psi_{ij}$ depending on whether a latitude-longitude or azimuth-angular distance system of co-ordinates is used. Equation 100 would be adequate if the subdivision of the basic $n_i^o \times n_i^o$ into $N(= n_i^2/m^2)$ $m^o \times m^o$ squares $(m < n_i)$, where the k-th such square will be represented by the gravity anomaly Δg_k at an angular distance ψ_k from the point of computation P such that

$$\Delta g_k = \overline{\Delta g} + c_{gk} \quad ; \quad F(\psi_k) = \overline{F(\psi)} + c_{\psi k} \qquad (102),$$

$\overline{\Delta g}$ and $\overline{F(\psi)}$ being given by

$$\overline{\Delta g} = \frac{1}{N}\sum_{k=1}^{N} \Delta g_k \quad ; \qquad \overline{F(\psi)} = \frac{1}{N}\sum_{k=1}^{N} f(\psi_k) \tag{103},$$

and the use of these smaller sub-divisions in the quadratures evaluation in lieu of the $n_i^o \times n_i^o$ squares together with the appropriate area mean, did not reduce the quadratures error to below the desired order of accuracy ($o\{\varepsilon\}$). This would happen if

$$\sum_{k=1}^{N} c_{gk}\, c_{\psi k} = o\{\varepsilon\} \tag{104},$$

implying no correlation whatever between variations in $f(\psi)$ and Δg over the $n_i^o \times n_i^o$ area. While the function $F(\psi)$, given by

$$F(\psi) = f(\psi) \sin \psi \tag{105},$$

has predictable variations, Δg defies accurate prediction free from systematic bias except over very short distances and under carefully controlled conditions. As gravity has to be sampled at discrete points, the quadratures approach makes a representation procedure mandatory. Consequently, some finite element of surface area has to be represented by a single observation. It is useful to bear in mind that

(a) the global gravity standardization network available at present has a station accuracy of ±0.2 mgal (MORELLI ET AL 1971 ,p.6);

(b) errors in gravimeter ties seldom exceed ±0.2 mgal if performed with adequate instruments and any sort of minimal care; and

(c) geopotential errors of $o\{\pm 3$ kgal m$\}$ give rise to an error of $o\{\pm 1$ mgal$\}$ in the gravity anomaly.

A precision of ±1 mgal in the gravity anomaly is relatively easy to obtain in areas where the regional geodetic level network is reasonably dense. The gravity anomaly also undergoes changes with position within the basic square it is expected to represent. This penchant was characterized by a quantity introduced by de Graaff Hunter, called the error of representation $E\{\Delta g\}_{nm}$ for an $n^o \times m^o$ square, which in the case of a fully represented square, is given by (DE GRAAFF HUNTER 1935)

$$\left(E\{\Delta g\}_{nm}\right)^2 = \sum_{i=1}^{N} \frac{(\Delta g_i - \overline{\Delta g})^2}{N} \tag{106}.$$

A reliable value for $E\{\Delta g\}_{nm}$ is obtained from N evenly spaced values of Δg_i covering the $n^o \times m^o$ square, $\overline{\Delta g}$ being the mean value of the gravity anomaly, given by

$$\overline{\Delta g} = \frac{1}{N}\sum_{i=1}^{N} \Delta g_i \tag{107}.$$

Several estimates of this statistical characteristic of the gravity anomaly field at the surface of the Earth are available in the literature (e.g., IBID; HIRVONEN 1956; MOLODENSKII ET AL 1962,p.172; MATHER 1967,p.131). Samples which are available at the present time from different parts of the globe reflect the flatter continental areas. $E\{\Delta g\}_n$ in such areas is a function of square size and in general terms, can be expressed by the relations

$$E\{\Delta g\}_n = \begin{cases} \pm C_1 \sqrt{n} & \frac{1}{4}^o < n < 5^o \\ \pm C_2\, n & n < \frac{1}{4}^o \end{cases} \tag{108}$$

for an $n^o \times n^o$ square, where n is in degrees and $E\{\Delta g\}_n$ in mgal, when $C_1 \doteq 12$ and $C_2 \doteq 3 \times 10$. It can also be shown that $E\{\Delta g\}_n$ is a function of unsigned ground slope $|\beta|$, with magnitudes which can be as much a five times as great in very rugged areas, especially when n is small. As such variations are functions of ground slope and not elevation, it is estimated that about 2-5 % of the Earth's surface will require values of C_1 and C_2 which are significantly greater than those given above, for an adequate representation of variations in the gravity anomaly.

The number of terms involved in the quadratures evaluation is a function of the accuracy desired in the computation. If the requirments of sea surface topography determinations (1 part in 10^4) were to be met, it would be necessary, for estimation purposes, to restrict square sizes to those over which the contribution of the terms containing the second differential coefficient of $F(\psi)$ were held to $o\{e^3 h_d\}$. The required number of summations is $o\{10^6\}$. The study of the propagation of systematic and random error characteristics through equation 100 under these circumstances shows that an adequate representation of the surface gravity field which would enable the achievement of an accuracy of ±10 cm in the final result would be one which had an $E\{\Delta g\}$ value of ±3 mgal, if the data were not subject to systematic error in excess of ± 50 μgal. Such a representation is afforded by a 10 km grid in non-mountainous areas. While the estimation characteristics of gravitationally disturbed regions are covered by the above figures, which assume that oceanic fields will have a similar tendency to vary as continental data, regions characterized by larger ground slopes have significantly greater values of $E\{\Delta g\}$. It would be necessary to reduce the size of the grid in such cases to retain $E\{\Delta g\}$ at ±3 mgal. The use of the smoothening techniques described in section 3.5 would of course reduce these values. It follows that present day techniques for establishing surface gravity anomalies are adequate for the determination of sea surface topography. It is interesting to note that the station spacing required on the above basis, is already available over large continental areas like the United States, Canada and Australia, at the present time.

The consequences of systematic errors in Δg which hold the same sign over considerable extents, on the values of h_d computed, are significant. A systematic error $e_{\Delta g}$ which holds its magnitude and sign over a $n^o \times n^o$ area, but has random characteristics over larger extents, is shown to have an effect e_{Ns} on the computed value of h_d given by (IBID,p.65)

$$e_{Ns} = \pm o\{K'' n\, e_{\Delta g}\} \qquad (109),$$

where $K'' \doteq 10$, for e_{Ns} in cm, n in degrees and $e_{\Delta g}$ in mgal. If e_{Ns} were held at ±5 cm, the estimate of the magnitude of the tolerable systematic error e_g, which is inversely proportional to its wavelength, varies from $o\{\pm 5$ mgal$\}$ when $n = 0.1^o$ to $o\{\pm 0.1$ mgal$\}$ when $n = 5^o$.

Likely sources of systematic error have been listed at the commencement of this sub-section. The following conclusions can be drawn.

(1) IGSN71 would be an adequate gravity standardization network for sea surface topography studies only if the station density were 1 per 5×10^4 km^2 and the errors of adjacent stations were not correlated at the 200 μgal level. Neither of these conditions is likely to be satisfied. An adequate net would be afforded by stations at which absolute determinations had been carried out with ±50 μgal resolution, and a representation of 1 station per 10^6 km^2. In the interim, it would be advisable that all gravity data should be subject to randomization procedures at the level of the precision of the gravity standardization network, prior to use in solutions of the boundary value problem.

(2) Gravity anomaly information on each geodetic datum should be corrected for changes in normal gravity due to the datum not being geocentric (IBID,p.16).

(3) The term "geoid" which is synonymous with both the global datum for elevations

as well as the "undisturbed" free level of the sea, should be defined on the basis of models which afford resolution with an accuracy of ±10 cm.

A possible problem of some significance in the determination of sea surface topography and other high precision determinations of h_d, is the existence of the sea surface topography itself with not insignificant amplitudes (e.g., 3-4 m) and substantial wavelengths. The evidence for the existence of such phenomena is widespread but based on purely coastal phenomena, as obtained from levelling- tide gauge comparisons. Extended studies of the sea surface using short pulse high resolution altimeters should go a long way toward clarifying whether stationary sea surface topography is merely a coastal phenomenon, and if not, the dominant wavelengths with which it is prone to occur. The existence of stationary sea surface topography with 4000 km wavelengths and 2 m amplitudes would cause errors of $o\{\pm 1\ m\}$ in h_d. While this estimate is based on the maximum magnitude of the phenomenon reported to date, the existence of such an effect will require an iteration in the determination of h_d. (For a later perspective on this problem, see the other paper by Mather in these Proceedings. The rapidity with which these iterations converge is more a function of the wavelength of the stationary sea surface topography than of its amplitude.

5. Gravity and Earth Space

5.1 Gravity and Scale

A problem which requires careful scrutiny is the possibility or otherwise of defining a scale for Earth space from gravity determinations at the surface of the Earth. It must be clearly emphasized that the ensuing development excludes the consideration of satellite data which constitutes the basis of low degree representations of the Earth's gravity field at the present time. The problem could be stated as follows. Given an adequate distribution of determinations of surface gravity, how are the effects of zero degree h_{do} in the global distribution of height anomalies to be interpreted. This effect can be written as

$$h_{do} = \frac{W_o - U_o}{\gamma} - R\frac{M\{\Delta g_c\}}{\gamma} + N_{co} + o\{fh_{do}\} \qquad (110),$$

on considering equations 73 and 74, N_{co} being the contribution of zero degree by the indirect effect N_c. *W_o is not known* and it is common practice to assume the first term to be zero. The second and third terms will have finite magnitudes. A change in the value of GM will provide nearly equal and opposite changes in the terms containing U_o and $M\{\Delta g_c\}$. Hence equation 110 cannot be evaluated unless the value of W_o were known, which is certainly not the case to order ±1 m at the present time.

Equation 110 could however be used to find out the potential of the geoid W_o if h_{do} were known from some independent determination (e.g, geometrical satellite geodesy). The numerical value of h_{do} can be established by analyzing the differences

$$v_i = h_{di} + h_{ni} - h_i \qquad (111),$$

where the subscript $_i$ refers to evaluation at the i-th station in a global satellite station network, h_d being determined gravimetrically with the first term in equation 110 supressed. The value so obtained for h_{do} on use in equation 110 will give a value for W_o which is consistent with the set of units defined.

Any "improvement" in the value of GM obtained from gravimetric determinations in the strictest sense

will have to be based on the assumption that the potential of the geoid W_o is equal to that of the equipotential ellipsoid of revolution U_o. The geoid is a physical reality, being a manifestation of the mass distribution which gives the observed gravitational phenomena at the surface of the Earth, while U_o is defined by the chosen values for the parameters a, GM, ω and f which define the system of reference. It has been deduced that the term $(W_o - U_o)/\gamma$ is approximately 3 m if the ellipsoid were one of best fit to the geoid and the value adopted for GM was the best estimate available for the Earth (MATHER 1971c,p.98), provided the free air anomaly had no zero degree harmonic.

Thus any deductions which can be drawn about scale from gravimetric determinations alone are subject to ambiguity, if restricted to a single epoch. The effect of zero degree deduced from comparisons between geometrical satellite solutions and surface gravity determinations of h_d described by equation 111, should be used only for the purpose of determining the value of W_o. A second effect of importance is the term of zero degree obtained on studying changes in observed gravity determined by the use of absolute techniques with a resolution approaching ±1 μgal, as determined on specially designed observing platforms, well distributed about the Earth, between successive epochs in time. Such changes can be interpreted as either reflecting an expansion of the Earth, as measured within the framework of the velocity of light and the adopted standard for the measurement of time intervals, or else as a change in the value of GM. For a discussion see (MATHER 1972,p.15).

5.2 Gravity and Geodetic Reference Systems

The preceding development has assumed that the Earth has a fixed mass distribution subject to some periodic changes due to effects like Earth tides. Such a description would be adequate only if the observations were taken over a limited period of time, such as one or two decades. There is considerable evidence which seems to point to the large scale re-distribution of at least the masses constituting the Earth's crust, over very long periods of time, with the attendant possibility of mass variations at greater depth depending on the nature of the mechanism which could produce such crustal motions.

A possible consequence of such mass re-distributions could be the motion of the Earth's centre of mass (geocentre) with respect to the Earth's crust. The analysis of high precision determinations of absolute gravity at a well distributed net of observing platforms as described in the previous subsection, could provide a means of recovering the motion of the geocentre between epochs, on analyzing the first degree harmonic of changes in absolute g (IBID). It should be pointed out that a problem in filtering out short period effects due to meteorological causes has to be overcome before results of reliability are likely to be obtained. Fortunately an estimate of the same effect can be obtained on studying changes in geocentric position of a global network of laser tracking stations using dynamic techniques, to provide a verification of the effectiveness of the determination.

5.3 The Role of Gravimetric Methods in Earth and Ocean Physics

Until recently, it was generally held that gravimetric methods if used with adequate data, provided the only non-controversial technique for computing ellipsoidal elevations with the same resolution as that available from geodetic levelling, thus completing the definition of geocentric position of points on the Earth's surface in three dimensions. Position determination at the present time has not provided resolutions which can confidently claimed to be better than 1 part in 10^6.

It is now clear that the most precise determination of geocentric position is required primarily for studies in Earth and ocean physics, rather than for any direct engineering or technological purpose. It would not be exaggeration to state that resolution to 1 part in 10^8 would be the aim of geodetic techniques being currently developed for such schemes. While there is no clear indication that surface methods, subject to restrictions imposed by atmospheric uncertainties, can be improved to

meet these goals, extra-terrestrial techniques like laser ranging to near Earth satellites and VLBI, promise that such goals may well be achieved in the near future. There is also no reason to doubt at this stage, that transportable versions of these systems could not achieve this same degree of resolution.

It would therefore appear that, with the passage of time, there would be less use of geodetic levelling and the systems of reference implicit in its concept, for use in Earth physics. The exception is of course the study of the instantaneous geocentric position of the ocean surface, and the interpretation of these results for the study of ocean circulation. The determination of the geoid with the highest possible precision is a necessary prerequisite for such studies. Gravity information will still have to be assembled and anomalies computed on the basis of elevations referred to an equipotential surface, the most convenient being the geoid.

Three matters of significance which should be closely studied before undertaking the task of assembling an adequate gravity anomaly field for computation of geoid heights to ±10 cm, are the following.

(a) The definition of the physical model to serve as a datum for elevations with an accuracy which is not more than a factor of three less than the highest precision sought in the geoid solution.

(b) Techniques to be used for minimizing the effect of gravity base station errors on geoid computations.

(c) The question of whether it is necessary to adopt a model for the "surface of measurement" and, if so, the nature of an acceptable model and the procedure to be adopted in converting measurements on the Earth's surface to equivalent quantities on the model.

6. Acknowledgments

This paper was written while the author was the holder of a National Academy of Sciences Resident Research Associateship at National Aeronautics and Space Administration's Goddard Space Flight Center, Greenbelt, Maryland, while on leave of absence from the University of New South Wales.

7. References

ARNOLD, K. 1959. Zur Bestimmung der Geoidundulationen aus Freiluftanomalien. *Rep.*12, Geodatischen Instituts in Potsdam.

BJERHAMMAR, A. 1964. A New Theory of Geodetic Gravity. *Trans. R. Inst.Techn.*243,75 pp,Stockholm.

BJERHAMMAR, A. 1968. *On Gravity*. Royal Inst. of Techn.,Division of Geodesy,Stockholm,129 pp.

BJERHAMMAR, A. 1969. On the Boundary Value Problem of Physical Geodesy. *Tellus* 21,451-516.

BROVAR, V.V. 1964. On the Solution of Molodensky's Boundary Value Problem. *Bull.geodes.* 72,167-173.

BURSA, M. 1972. Variations of the Earth's Gravity Field due to the Free Nutation. *Studia geophys. et geod.* 16,122-125.

COOK, A.H. 1950. The Calculation of Deflexions of the Vertical from Gravity Anomalies. *Proc.R.Soc. A* 204,374-395.

COOK, A.H. 1965. A New Absolute Determination of g. *Nature* 208,5007,279.

DE GRAAFF-HUNTER, J. 1935. On the Figure of the Earth from Gravity Observations etc. *Phil.Trans.R. Soc.* 234,377-431.

DE GRAAFF-HUNTER, J. 1958. Reduction of Observed Gravity, Report of Study Group 8. *Bull.geodes.* 50, 1-16.

DE WITTE, L. 1967. Truncation Errors in the Stokes and Vening Meinesz Formulas for Different Order Spherical Harmonic Gravity Terms. *Geophys.J.R. astr.Soc.* 12,449-464.

ESPOSITO, P.B. & WONG, S.K. 1972. Geocentric Gravitational Constant Determined from Mariner 9 Radio Tracking Data. *Proceedings(microfilm) International Symposium on Earth Gravity Models & Related Problems*,St. Louis;(Abstr.)*EOS Trans.Am geophys.U.* 53,891.

FALLER, J.E. 1965. An Absolute Interferometric Determination of the Acceleration of Gravity. *Bull. geodes.* 77,203-204.

HAGIWARA, Y. 1972. Truncation Error Formulas for the Geoidal Height and the Deflection of the Vertical. *Bull. geodes.* 106,453-466.

HAMON, B.V. & GREIG, M.A. 1972. Mean Sea Level in Relation to Geodetic Land Leveling Around Australia. *J.geophys.Res.* 77,7157-7162.

HEISKANEN, W.A. & MORITZ, H. 1967. *Physical Geodesy*. Freeman, San Fransisco.

HENDERSHOTT, M.C. 1972. The Effect of Solid Earth Deformation on Global Ocean Tides.*Geophys.J.R.astr. Soc.* 29, 389-402.

HIRVONEN, R.A. 1956. On the Precision of the Gravimetric Determination of the Geoid. *Trans. Am. geophys.U.*37,1-8.

HOTINE, M. 1969. Mathematical Geodesy. *ESSA Monograph* 2,416 pp.

IAG 1970. *Geodetic Reference System 1967*. Spec.Publ.,International Association of Geodesy,Paris.

KOCH, K.-R. 1965. Der Einfluss der Topographie auf die Forme von Stokes. *Z.f.VermessWes.* 90,356-361.

KRARUP, T. 1969. A Contribution to the Mathematical Foundation of Physical Geodesy. *Rep.* 44,Danish Geodetic Institute, Copenhagen.

KRARUP, T. 1972. *Letters on Molodenskiy's Problem*. Unpublished circulation to Members of Study Group 4:31, International Association of Geodesy.

LERCH, F.J., WAGNER, C.A., SMITH, D.E., SANDSON, M.L., BROWND, J.E. & RICHARDSON, J.A. 1972. Gravitational Field Models for the Earth (GEM 1 & 2)(GEM 3 & 4). *X Doc.* 553-72-146, Goddard Space Flight Center, Greenbelt, Md.

MARYCH, M.J. 1969. On the Second Approximation of Molodenskii for the Perturbing Potential (in Russian). *Geodezija, Kartografija i Aerofotos'jemka* 10,17-27, L'vov.

MATHER, R.S. 1967. The Extension of the Gravity Field in South Australia. *Oster.Z.f.VermessWes.*25, 126-138.

MATHER, R.S. 1971a. The Analysis of the Earth's Gravity Field. *Monograph* 2,School of Surveying, University of New South Wales, Kensington NSW, 172 pp.

MATHER, R.S. 1971b. The Geocentric Orientation Vector for the Australian Geodetic Datum. *Geophys.J. R.astr.Soc.* 22,55-81.

MATHER, R.S. 1971c. A World Geodetic System from Gravimetry. *Geophys.J.R.astr.Soc.* 23,75-100.

MATHER, R.S. 1972. Four Dimensional Studies in Earth Space. *X Doc.*553-72-230, Goddard Space Flight Center, Greenbelt Md, 25 pp; also *Bull.geodes.*108,187-209.

MATHER, R.S. 1973. A Solution of the Geodetic Boundary Value Problem to Order e^3. *X Doc.* 592-73-11, Goddard Space Flight Center, Greenbelt Md, 126 pp;(Abstr.)*EOS Trans.Am.geophys.U.* 54,229.

MATHER, R.S., BARLOW, B.C. & FRYER, J.G. 1971. A Study of the Earth's Gravitational Field in the Australian Region, XV General Assembly, IAG, Moscow. (in *UNISURV Rep.*22,1-41, University of New South Wales, Kensington NSW.

MELCHIOR, P. 1966. *The Earth Tides*. Pergamon, New York.

MOLODENSKII, M.S., EREMEEV, V.F. & YURKINA, M.I. 1962. *Methods for Study of the External Gravitational Field and Figure of the Earth*. Israel Program for Scientific Translations, Jerusalem.

MORELLI, C., GANTAR, C., HONKASALO, T., MCCONNELL, R.K., SZABO, B., TANNER, J.G., UOTILA, U.A. & WHALEN, C.T. 1971. *The International Gravity Standardization Net 1971*. XV General Assembly, IAG, Moscow.

MORITZ, H. 1965. The Boundary Value Problem of Physical Geodesy. *Suomal.Tiedeakat.Toim A III* 83.

MORITZ, H. 1966. Linear Solutions of the Geodetic Boundary Value Problem. *Rep.*79, Dept. of Geodetic Science, Ohio State University, Columbus Ohio, 135 pp.

MORITZ, H. 1969. Nonlinear Solutions of the Geodetic Boundary Value Problem. *Rep.* 126,Dept. of Geodetic Science, Ohio State University, Columbus Ohio, 56 pp.

MORITZ, H. 1970. Molodensky's Series and Analytical Continuation, *Rep.* 145,Dept. of Geodetic Science, Ohio State University, Columbus Ohio, 35 pp.

MORITZ, H. 1972. Convergence of Molodensky's Series, *Rep.* 183,Dept. of Geodetic Science, Ohio State University, Columbus Ohio, 50 pp.

OJENGBEDE, O.A. 1973. *The Use of Truncation Functions in the Gravimetric Solution of the Geoid.* Dissertation,School of Surveying,University of New South Wales, Kensington NSW,109 pp.

PELLINEN, L.P. 1972. On the Identity of Various Solutions of the Molodensky's Problem with Help of a small parameter κ. *Proceedings (microfilm) International Symposium on Earth Gravity Models and Related Problems*, St. Louis Mo; (Abstr.) *EOS Trans.Am.geophys.U.* 53,894.

SAKUMA, A. 1971. Une Tendence de la Variation de la Pesanteur Observee au BIPM, Sevres, France. *XV General Assembly, IAG*, Moscow.

STOKES, G.G. 1849. On the Variation of Gravity at the Surface of the Earth. *Trans.Camb.Phil.Soc., Math.Phys.* 2,131-171.

STURGES, W. 1972. Comments on Ocean Circulation with Regard to Satellite Altimetry. (in Sea Surface Topography from Space (Apel, J.R. (ed)),Vol 2,24(1-17) *NOAA Tech. Rep.* ERL 228-AOML 7-2).

VENING MEINESZ, F.A. 1928. A Formula for Expressing the Deflection of the Plumb Line in the Gravity Anomalies and some Formulae for the Gravity Field and the Gravity-Potential outside the Geoid. *Koninkl.Akad.van Wetenschap. (Science Sec.)* 31,315-331, Amsterdam.

WILLIAMSTOWN REPORT 1969. *Solid Earth and Ocean Physics.* MIT Measuring Systems Lab., Cambridge Mass.

YEREMEEV, V.F. 1969. On the Numerical Solution of the Molodensky's Integral Equation for Layer Density. *TsNIIGAiK* 176,16-23.

8. Discussion

QURESHI: What role do geological anomalies play in this type of work?

MATHER: In trying to determine geodetic information, it is preferable to treat the gravity effect in terms of the free air anomaly and to keep the other contributions as a set of topography dependent terms which are treated separately in terms of elevations or their geopotential equivalents.

QURESHI: But geological anomalies are not always related to the topography.

MATHER: Yes. For example if you take an isostatic type anomaly and use it in Stokes' integral, you obtain a co-geoid. Provided you compute the correct indirect effect by taking all factors into consideration, you will get the correct answer. But this is not the same problem. In this case you are trying to make a *geoid* determination; you are trying to create Stokes' conditions by manipulating the topography. But most geodesists want to avoid making assumptions about (the density distribution of) the topography.

MORITZ: This old question of density and its effects is more or less obsolete. We know that density does not have such a large effect on the problem. A much larger effect is introduced, as you mention, through the interpolation problem.

VINCENT, S.
Computer Sciences Corp.
Colesville Rd
Silver Spring Md 20910
United States of America

MARSH, J.G.
Geodynamics Br.
Goddard Space Flight Center
Greenbelt Md 20771
United States of America

Proc.Symposium on Earth's Gravitational Field & Secular Variations in Position (1973), 154-171.

GLOBAL DETAILED GEOID COMPUTATION AND MODEL ANALYSIS

ABSTRACT

A global detailed gravimetric geoid has been computed by combining the Goddard Space Flight Center (GSFC) GEM-6 gravity model derived from satellite and surface gravity data and surface 1°- by - 1° mean free air gravity anomaly data. The accuracy of the geoid has been assessed at ±2 m on the continents, and 5 to 7 m in areas where surface gravity data are sparse.

The GSFC GEM-4, -6 models, the SAO 2, 3 models and the Rapp '73 model were considered in order to arrive at the best base gravity model for use in detailed geoid computations. RMS differences between GEM-6 and the other models ranged from 3 m to 7 m. The maximum differences in all cases occurred in the southern hemisphere where surface data and satellite observations are sparse. These differences exhibited wavelengths of approximately 30° to 50° longitude. To study the source of these differences, detailed geoid heights were computed with models truncated to twelfth degree and order, as well as eighth degree and order. This truncation resulted in a reduction of the rms differences to a maximum of 5 m. Comparisons have been made with the astro-geodetic data of Rice (United States), Bomford (Europe) and Mather (Australia). Comparisons have also been carried out with geoid heights from satellite solutions for geocentric station co-ordinates in North America and the Caribbean.

1. Introduction

A global detailed gravimetric geoid has been computed by combining the Goddard Space Flight Center (GSFC) GEM-6 gravity model (LERCH ET AL 1973) derived from satellite perturbations and surface gravity data, with 1°- by - 1° mean surface free air gravity anomaly data. Previously, a local detailed geoid combining the above model and 1°- by - 1° surface gravity data was computed for the north east Pacific and the north Atlantic area to provide an independent base of comparison for the GEOS-C altimeter experiment (MARSH ET AL 1973).

In the process of computing the geoids presented in this reference, several satellite gravity models published in the past four years were tested in order to determine the best base gravity model for detailed geoid computations. The models used in the geoid computations, in addition to the GEM-6 model were GSFC GEM-4 (LERCH ET AL 1972), the SAO-2 (GAPOSCHKIN ET AL 1970), SAO-3 (GAPOSCHKIN 1973) models and the Rapp '73 model. The rms differences between geoid heights computed using the GEM-6 gravity model and those computed using other gravity models, ranged from 3 m for the Rapp 1973 model to 7 m for the SAO-3 gravity model when the computations utilized the complete set of spherical harmonic coefficients.

The largest geoid height differences occurring in the above comparisons were located in the southern hemisphere. These differences exhibited a wavelength of approximately 30° in longitude, indicating errors in the middle degree and order coefficients of the various models. This finding prompted recomputations of the geoid with the satellite models truncated to lower degree and order, starting with (12,12). As a result, the rms difference was reduced to 1 m for GEM-4, and to 5 m for SAO-3. Geoid profiles at 10° intervals in latitude were drawn for all models (complete and truncated).

Differences between the geoids along these profiles were generally 5 m in areas of relatively dense surface gravity data and as large as 25 m in areas of sparse or absent gravity data. However, when truncated models were used, the differences were reduced to a maximum of about 15 m.

The accuracy of the GEM-6 detailed geoid is assessed at ±2 m in areas of dense surface gravity coverage and 5 to 7 m in areas of less dense coverage based on comparisons with astro-geodetic geoids and dynamically derived station heights.

2. Method of Computations and Data Source

The method of computation is presented in detail in (VINCENT ET AL 1973). The detailed geoid heights were computed by combining the GEM-6 satellite gravity field and surface 1°- by - 1° gravity data. The component of the detailed geoid obtained using the GEM-6 gravity field is derived as a function of the spherical harmonic coefficients of the gravity model and the surface geoidal heights are derived by incorporating surface 1° - by - 1° gravity data into Stokes' equation for areas 20°- by - 20° centred at the computational points.

The surface gravity data used in the computations consisted of 23,947 records of 1°- by - 1° mean free air gravity anomalies obtained from the Defence Mapping Agency/Aerospace Center. This data set was complemented with collections from the National Ocean and Atmospheric Agency, and the Hawaii Institute of Geophysics. However, whenever possible, local data collected by local agencies were considered first in data preparation. When these data were not sufficient, the above mentioned sources were used to fill in the voids. The data file is discussed in detail in (IBID).

3. Analysis

The base gravity model used in detailed geoid computations provides information on the long wavelength (approximately $\geq$ 1000 km) undulations of the geoid. The short wavelength information is provided by the 1°- by - 1° surface gravity data. All models tested were complete to degree and order 16 with selected higher degree terms, and were therefore capable of providing the 1000 km information on the geoidal undulations. Since all models were combined with the same set of 1°- by - 1° surface gravity data, the resultant differences in the detailed geoid heights are due to variations in the gravity models. The analyses of the models and the final choice of the base model for use in detailed geoid computations were carried out by

1. inter-comparing the respective geoids of these models; and
2. comparison with external standards such as astro-geodetic geoids and dynamically derived tracking station co-ordinates.

3.1 Inter-Model Comparisons

Detailed geoids were computed using the full set of coefficients of the five gravity models and profiles were drawn along parallels of latitude around the entire globe at 10° intervals in latitude. Figures 1 through 5 present representative examples of these profiles. In the northern hemisphere, representative profiles were chosen at 20° and 40° north latitude (figures 1 and 2). These profiles show an average variability of about ±5 m; however, individual differences as large as 10 m do appear. For example, in figure 2, at longitude 180°E, the geoid computed using the SAO-2 model differs from the geoid computed using the GEM-6 solution by 10 m. The models show the largest scatter at 180°E mainly because of a lack of surface gravity data available. The dominant

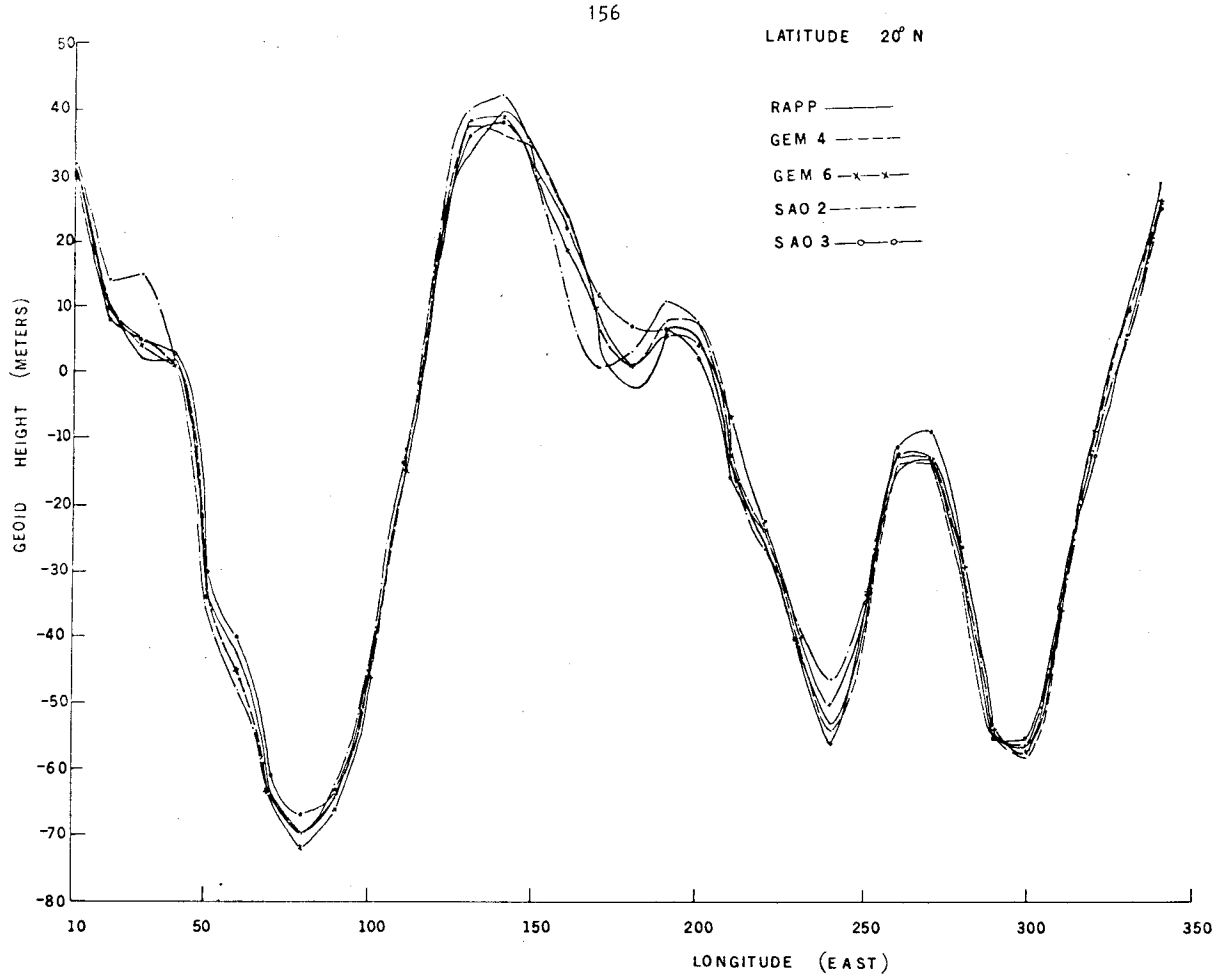

Figure 1. Detailed Geoid Profiles at Latitude 20°N

differences in these profiles are the amplitudes of the main features, rather than the slopes of the geoids. It is noted that there are many places along these profiles where the respective geoid profiles vary only by a few percent.

In figures 3 through 5 (southern hemisphere), a completely different picture emerges. The scatter is much more prevelant. This is largely attributed to the sparsity of surface gravity data, as well as a lack of satellite observational data. The scatter in the profiles increases gradually towards the Antarctic. For example, in figure 3, the scatter is evident only along longitudes 200°E to 350°E, but in figures 4 and 5, the divergence is noted along the entire length of the profile. In figure 5, the maximum difference reaches approximately 25 m at longitude 180°E. In contrast to the northern hemisphere, the geoid slopes in the southern hemisphere exhibit large variations.

MARSH ET AL (1973) showed differences between GEM-6 and other models to exhibit a wavelength of approximately 30° to 50° in longitude. This variation, when translated into spherical harmonic terms, corresponds to middle degree and order. The orbital perturbations arising from spherical harmonic coefficients of degree and order larger than (8,8) are generally on the order of a few metres, a fact which makes accurate recovery of the individual coefficient values difficult except in the case of resonance. This fact, plus the findings of BROWND & RICHARDSON (1973)

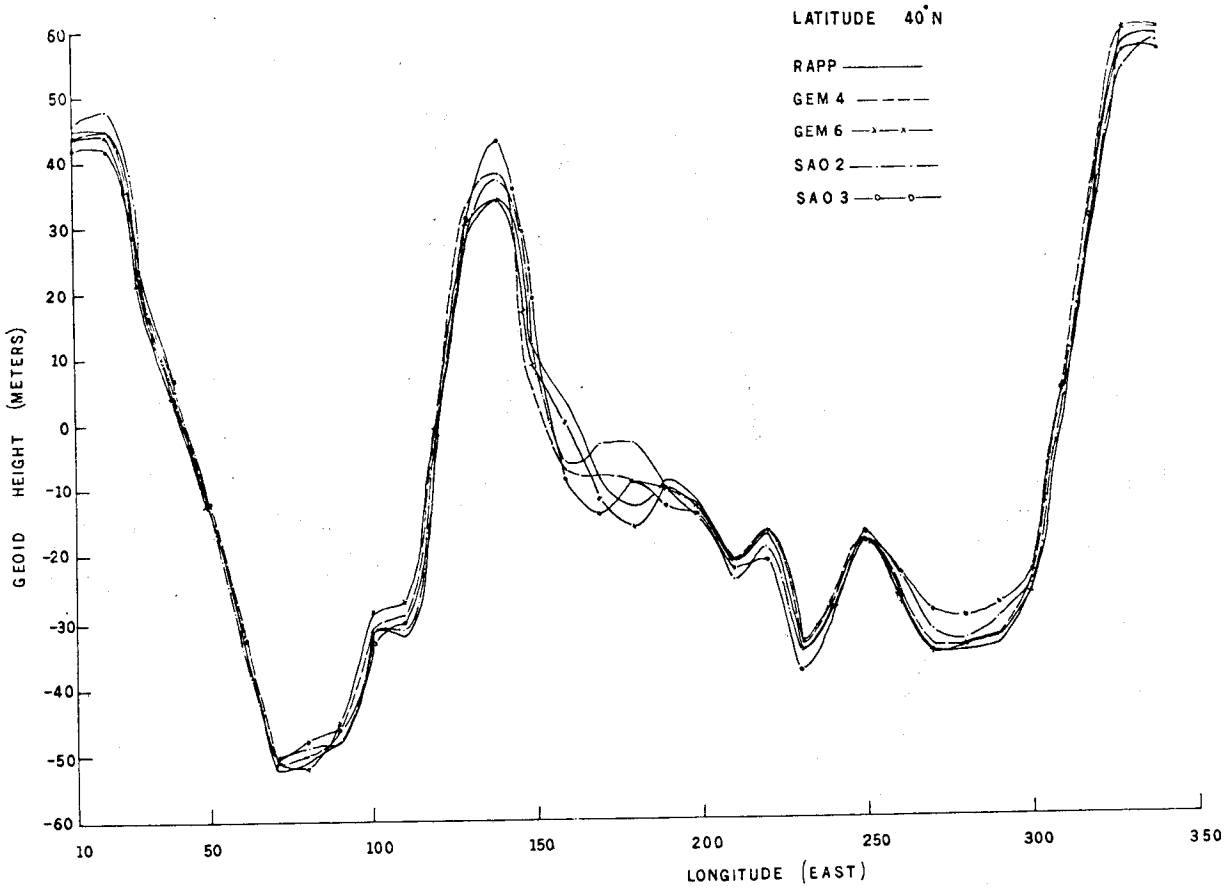

Figure 2. Detailed Geoid Profiles at Latitude 40°N

when conducting tests on the gravity anomalies derived from various gravity fields, coupled with the scarcity of surface gravity data in the southern hemisphere, led to the re-computation of the detailed geoids using truncated gravity models (12,12) and (8,8). Brownd & Richardson found that when satellite derived gravity anomalies were compared with surface gravity data using truncated models, the (12,12) field agreed best with the surface gravity data while the lower and higher degree models were divergent from the surface data.

Figures 6 through 10 present profiles of detailed geoids computed using models truncated to (12,12), plus SAO-2, and SAO-3 truncated to (8,8). One point noted throughout these profiles is that truncation to (12,12) for the GEM-4, GEM-6 and Rapp '73 models reduces the differences between then to an envelope of about 2 m. The SAO-2, SAO-3 (12,12) models on the other hand, show variations as large as 5 m with respect to each other. They are also in disagreement with the general trend of the other truncated models, as well as indicating features not portrayed by the general trend. However, further truncation of the SAO-2 and SAO-3 models to (8,8) generally reduces the differences along the main features and eliminates some of the extraneous features. As one truncates back to lower degrees, the results of the geoid computations tend to become identical because the satellite coefficients are nearly equal. But since the surface data within 10° of the computation point cannot completely represent the effect of the truncated wavelengths, this does not necessarily mean

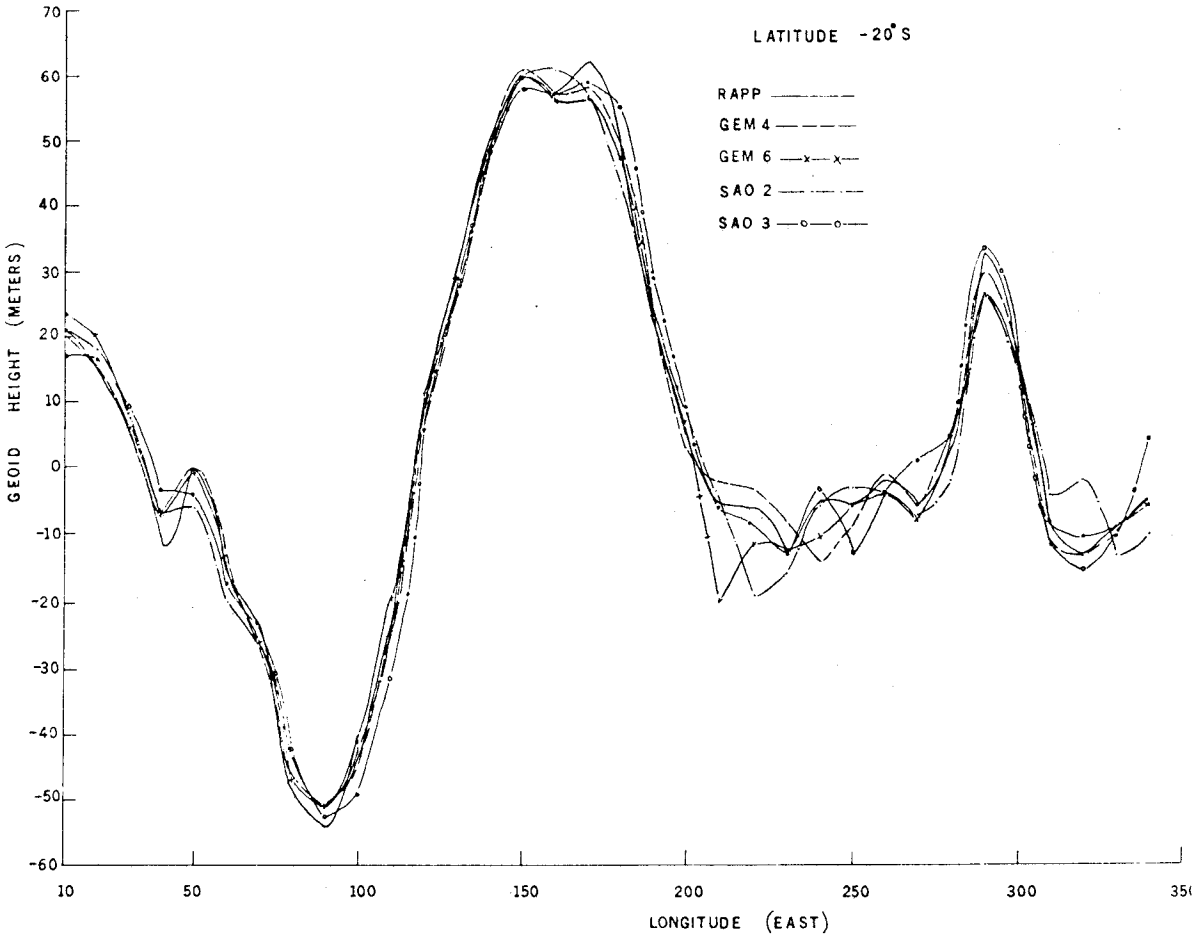

Figure 3. Detailed Geoid Profiles at Latitude 20°S

that the answers are getting better, but rather that the truncated models are identical. The GEM models and the Rapp '73 model represent the geoid better because of the higher accuracy of their higher harmonics as further upcoming tests show.

RMS differences have also been computed for the complete and truncated models versus GEM-6.

GEM-6 versus	Complete Model	(12,12)
Rapp	± 2.7 m	± 1.6 m
GEM-4	± 3.7 m	± 1.3 m
SAO-2	± 4.5 m	± 3.3 m
SAO-3	± 6.5 m	± 5.2 m

It is felt that global rms differences are probably not too meaningful, since the differences in the southern hemisphere are much larger than in the northern hemisphere. Furthermore, these relative differences could be interpreted as a lower bound for the absolute accuracy of the geoid. Figures 11 through 14 present geoid height differences in histogram form. As is noted in these histograms,

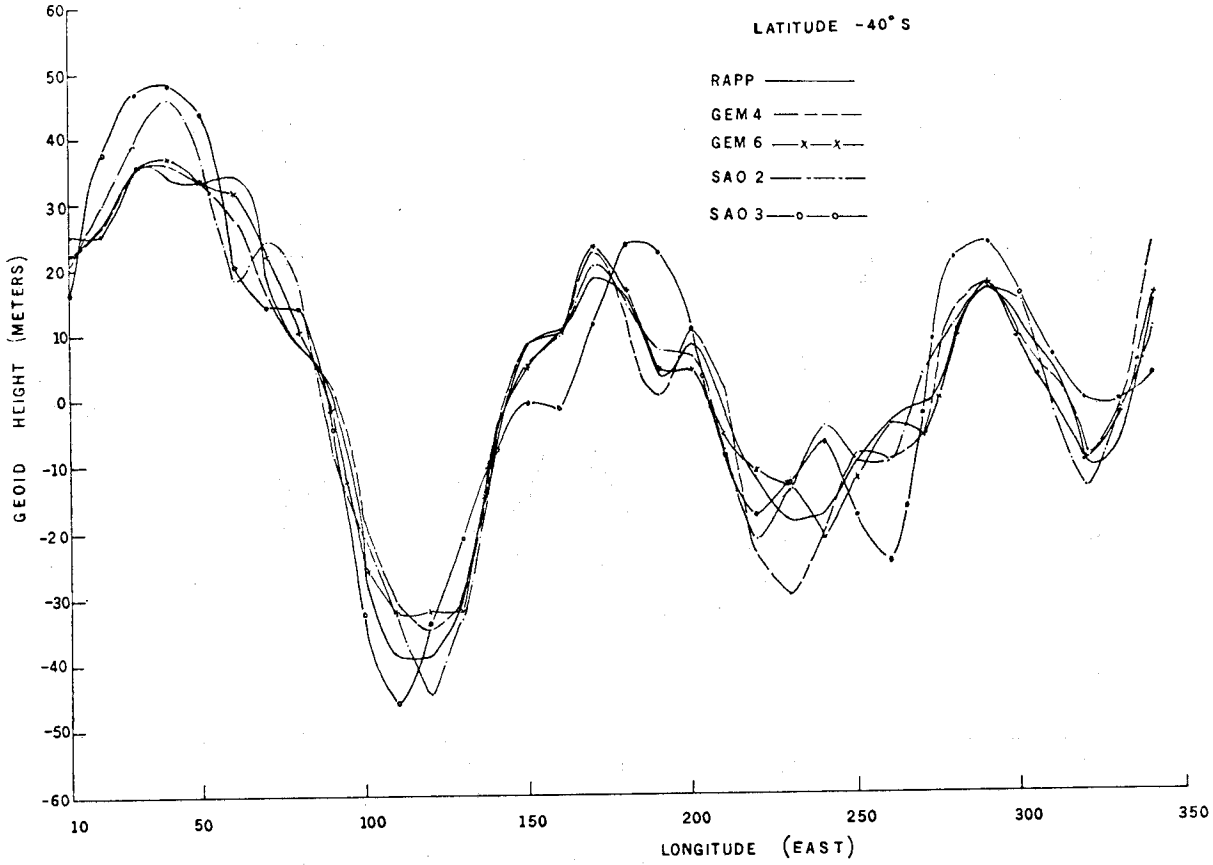

Figure 4. Detailed Geoid Profiles at Latitude 40°S

the most frequent differences are in the range of -5 to +5 m.

3.2 Comparison with External Standards

3.2.1 Comparisons with Astro-geodetic Geoids

Detailed gravimetric geoids computed with the above mentioned models were compared with the astro-geodetic geoids of BOMFORD (1971) in Europe, RICE (1973) in the United States, and MATHER ET AL (1971) in Australia. In all cases, the astro-geodetic geoids were transformed to a centre of mass system using transformation sets of MARSH ET AL (1973) before comparisons were made.

In Europe, detailed gravimetric geoids were computed with the Stokes' functions integrated 10° and 20° around the point of computation. This was done

1. because of the availability of 1°- by - 1° data; and
2. to assess the long wavelength contribution of the gravity models.

A profile at latitude 48°N recommended by Bomford as being the most representative, was used for the comparison. The SAO-2 and SAO-3 profiles were similar, but they were different from those for GEM-4, GEM-6 and the Rapp '73 models. In the case of 10° integration, the detailed geoid using the SAO-3 model showed a tilt of 1.6 arcsec with respect to the astro-geodetic geoid.

However, when the GEM-6 model was considered, the differences became much less systematic and were

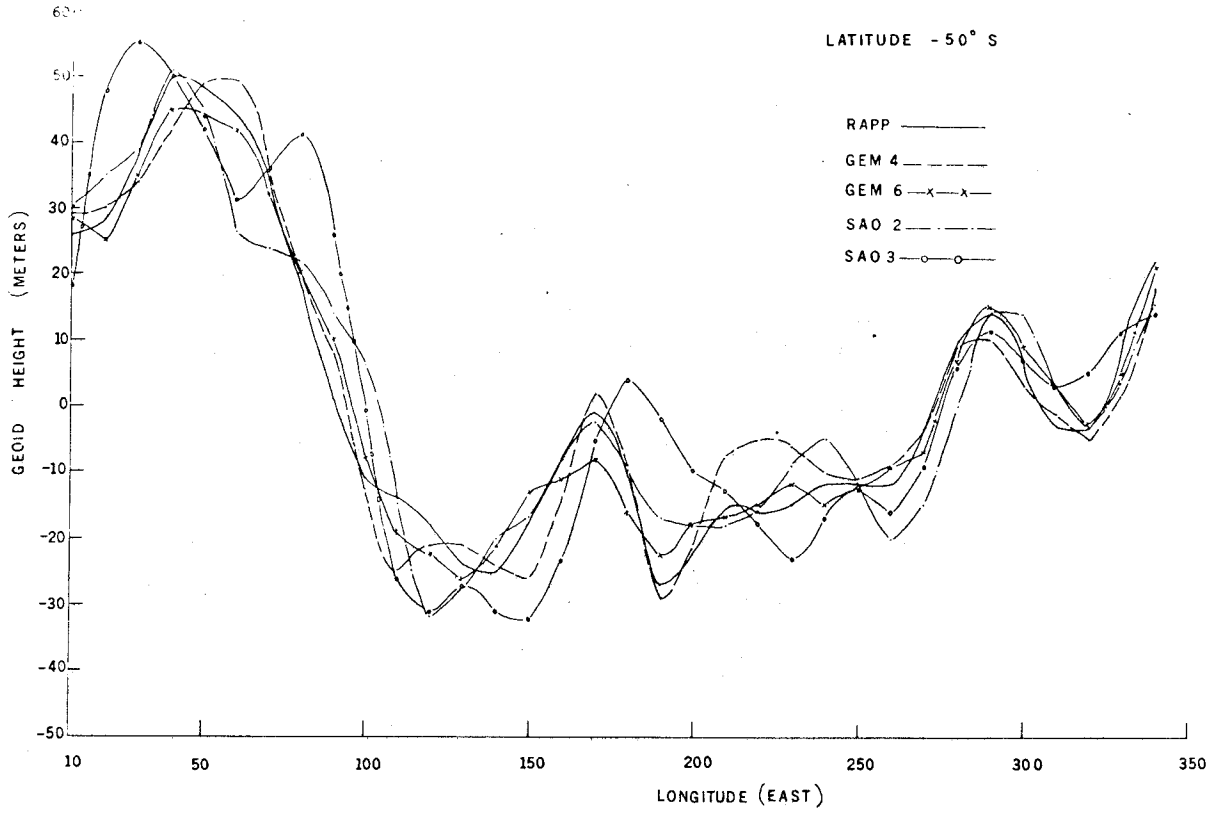

Figure 5. Detailed Geoid Profiles at Latitude 50°S

of the order of ±2 m (figure 15). When the 20° integration was performed, the SAO-3 model and the GEM-6 model both agreed well with the astro-geodetic geoid (figure 16). The GEM-6 detailed geoid did not change when the integration interval was increased from 10° to 20°, indicating a more accurate representation of the long wavelength features by the GEM and Rapp '73 models. In Australia, the comparisons with Mather's astro-geodetic geoid were conducted along a profile 26°S (figure 17). The detailed geoid, when based upon the SAO-3 model, exhibited a tilt of 1 arcsec with respect to Mather's geoid. However, the detailed geoid based upon the GEM-6 model showed only 0.5 arcsec tilt. GEM-6 matched the results Mather found in his studies on the Australian datum.

Another comparison was made with Rice's astro-geodetic geoid for a profile in the United States at latitude 35°N. Table 1 presents the differences between Rice's geoid and the detailed geoids computed using the various models. The differences in the geoid heights for all models were random except for SAO-3 and GEM-6 where an additional constant value of 2 m for SAO-3 and 1 m for GEM-6 had to be added. The agreement between Rice's geoid and all the models was on the order of ±2 m.

3.2.2 Comparison with Dynamic Station Heights

Goddard Space Flight Center Long-Arc Orbital Analyses have provided geocentric co-ordinates for tracking stations (MARSH ET AL 1973). Geoid heights of the tracking stations derived from this

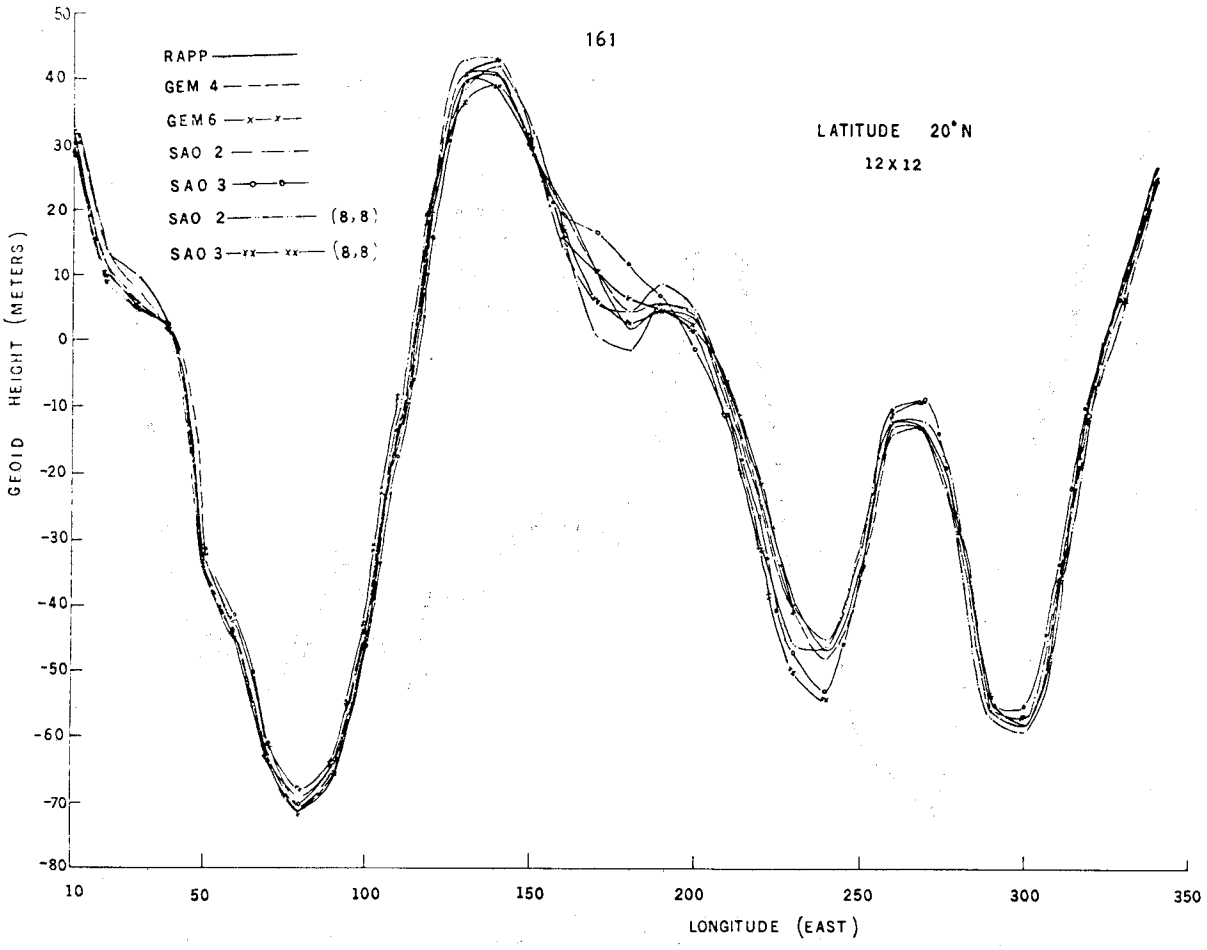

Figure 6. Detailed Geoid Profiles at Latitude 20°N (Truncated Models (12,12) and (8,8))

Table 1

Profile at Latitude 35°N

Difference Between Rice's Converted Astro-geoid and Detailed Geoid Computed using Various Models (units metres)

Longitude (deg)	Rice	GEM-4 *	GEM-6 *†	SAO-II *	SAO-III * ††	RAPP *
81	-34	-1	-2	-2	-2	-1
83	-30	1	0	0	-2	1
85	-32	-1	-1	-2	-2	-1
87	-29	0	0	-1	-2	0
91	-29	0	1	0	-2	0
92	-29	0	2	0	-1	0
93	-31	-1	1	-1	-1	-1
96	-29	2	3	1	-1	2
99	-28	1	1	0	0	1
101	-28	0	1	0	1	1
105	-20	1	2	2	3	3
107	-21	0	0	0	2	1
110	-23	0	-1	0	2	1
113	-27	0	-1	-1	2	0
115	-30	1	-1	0	1	0
117	-31	2	1	2	2	2

KEY:-

* Rice minus GEM-4 detailed geoid height, GEM-6, ...

† Systematic difference of 1 m has been added

†† Systematic difference of 2 m has been added

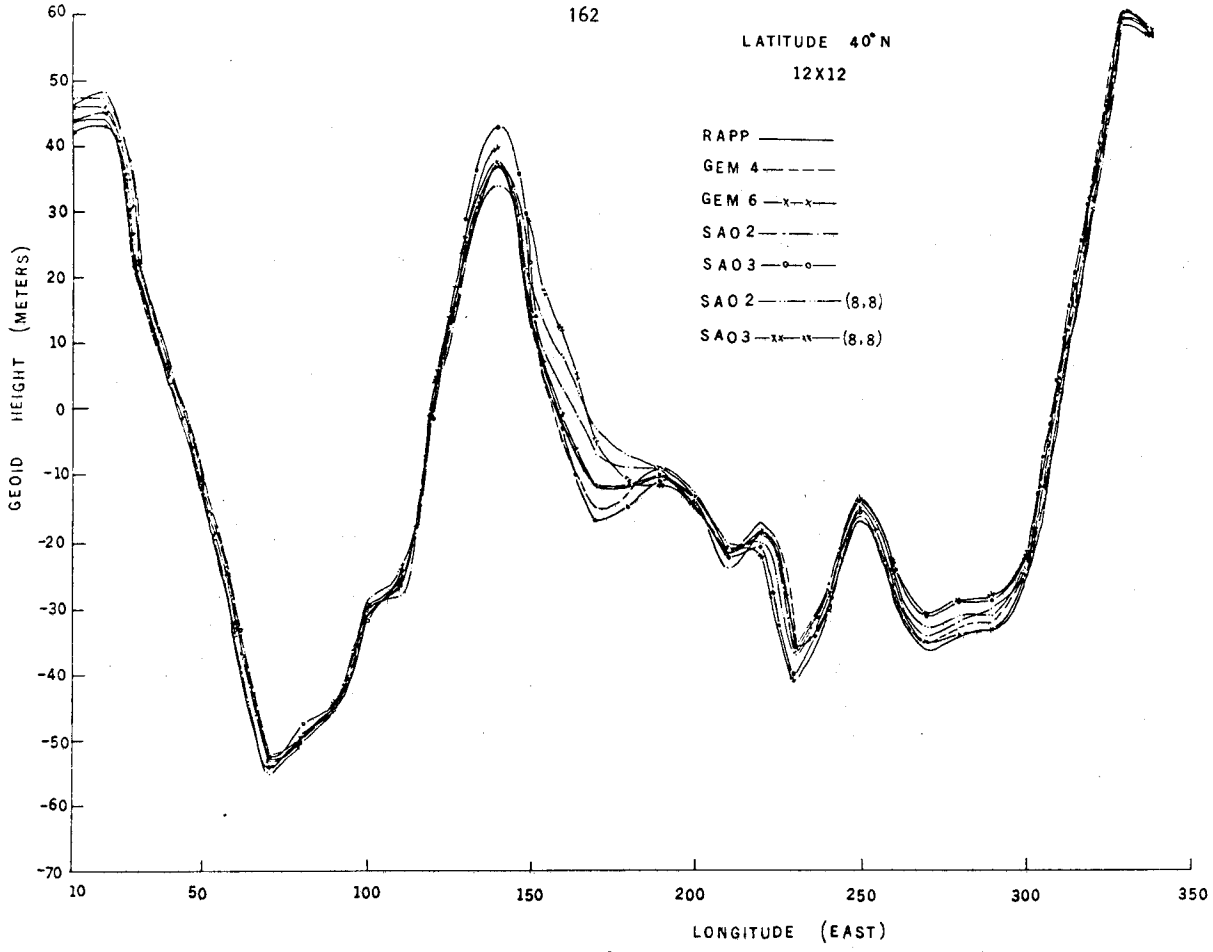

Figure 7. Detailed Geoid Profiles at Latitude 40°N (Truncated Models (12,12) and (8,8))

solution were compared with detailed geoid heights. Table 2 presents the results of these comparisons for stations in the United States and the Caribbean. The results obtained using all the satellite models are similar, except for those computed using the SAO-3 model where differences as large as 5 m versus the average are apparent. The rms agreement for all models is about ± 3 m. This agreement is considered excellent considering the various error sources inherent in this type of comparison. For example, errors can be attributed to

a. dynamically derived station heights;
b. mean sea level values; and
c. gravimetric geoid heights.

4. The Goddard Earth Model (GEM-6) Detailed Geoid

The GEM-6 gravity model was chosen to be the base model for detailed geoid computations. The GEM-6 model consists of a geopotential field in spherical harmonics and a centre of mass system of tracking stations. The GEM-6 solution was computed from a combination of the GEM-5 solution with surface gravimetric data and simultaneous satellite tracking data (LERCH ET AL 1973). The GEM-5 solution is based on satellite data only. The satellite data consisted of 350 weekly orbital arcs of optical, electronic and laser tracking data on 27 close Earth satellites. In addition, approximately 100 one- and two-day arcs of GEOS tracking data were employed for refinement of tracker co-ordinates. The surface gravimetric data consisted of a global collection of 300-by-300

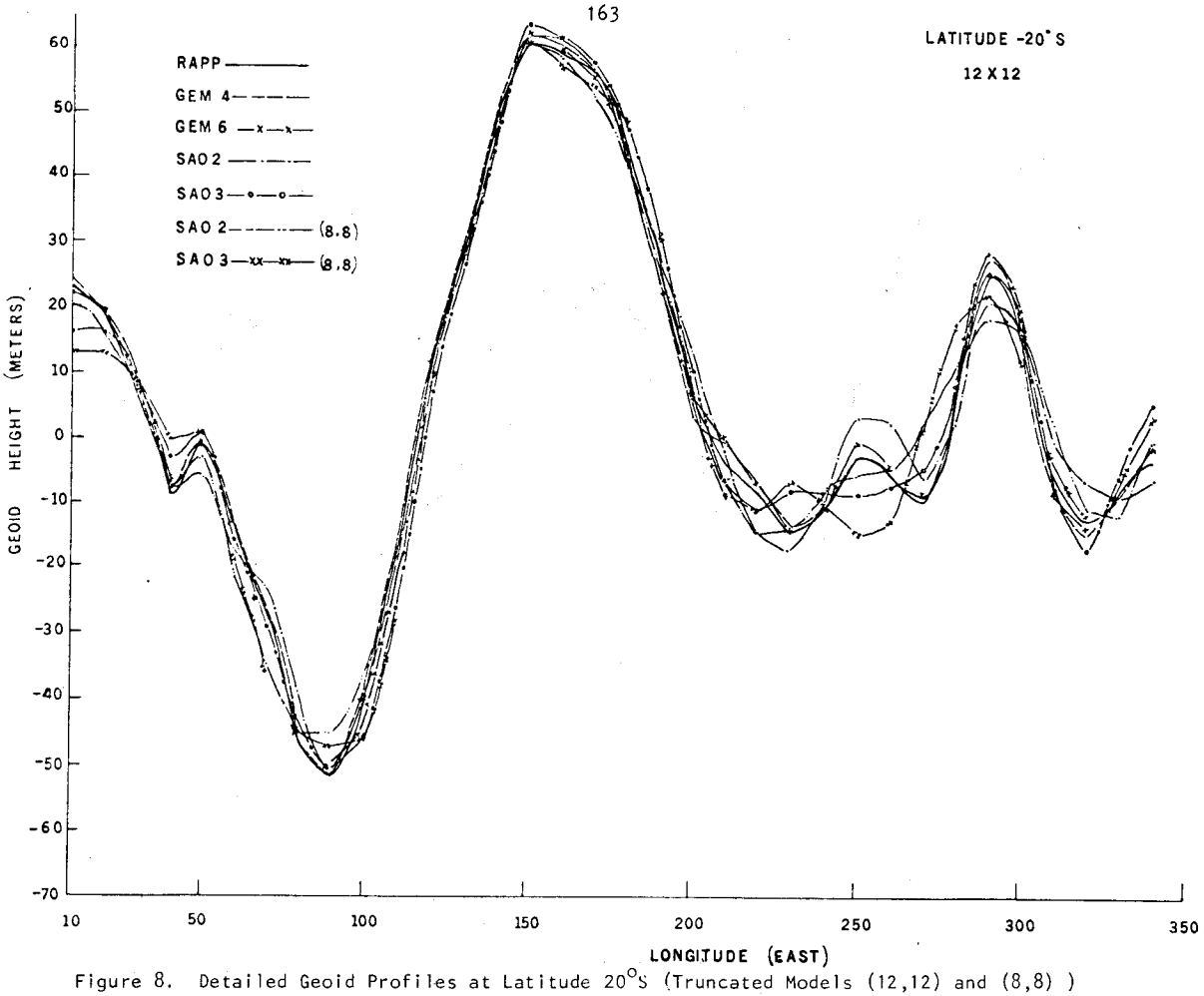

Figure 8. Detailed Geoid Profiles at Latitude 20°S (Truncated Models (12,12) and (8,8))

Table 2

Comparison Between Dynamic Station Heights and Gravimetric Geoid Using Various Models (Metres)

Station Number	Latitude (deg)	Longitude (deg)	GSFC 73* Long Arc	GEM-4†	GEM-6†	SAO-II†	SAO-III†	RAPP*	KEY
1032	48	307	12	-1	0	5	1	1	* Geoid Height =
1021	38	283	-43	-9	-10	-9	-14	-9	(Dynamic height
1022	27	278	-29	2	1	-1	-3	1	above ellipsoid)
1030	35	243	-30	5	3	2	3	3	minus
1034	48	263	-27	1	-1	-3	-3	2	(Mean Sea Level height)
1042	35	277	-34	-2	-3	-4	-7	-3	
7036	26	262	-27	-2	-3	-3	-5	-2	† GSFC '73 (MARSH, DOUGLAS & KLOSKO 1973)
7037	39	268	-35	-1	-1	-2	-6	-1	minus
7050	39	283	-40	-6	-8	-6	-12	-6	GEM-4 detailed
7045	40	255	-18	0	0	1	-2	-1	geoid, GEM-6,....
9001	32	253	-22	1	1	6	1	2	
9021	32	249	-30	-1	-2	-8	-2	-1	
7072	27	280	-32	4	0	-1	-2	1	
7075	46	279	-32	5	5	5	1	6	
7039	32	295	-35	4	4	6	2	6	
7040	18	294	-46	4	4	2	3	3	

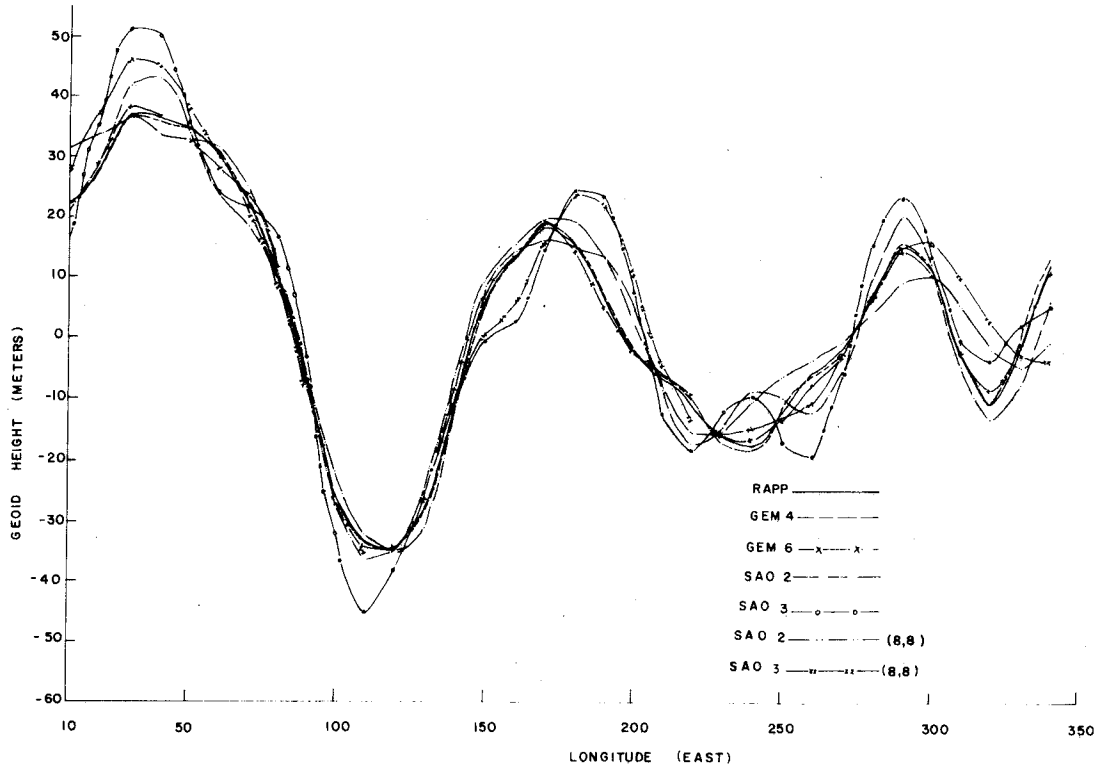

Figure 9. Detailed Geoid Profiles at Latitude 40^{o}S (Truncated Models (12,12) and (8,8))

nautical mile equal area anomalies developed by RAPP (1972). The simultaneous observational data from the North American MOTS-Laser network and from the global BC-4 network were processed geometrically before inclusion in the the GEM-6 solution. The GEM-6 model is complete to degree and order 16, with higher degree zonal harmonics and selected satellite resonant terms extending to degree 22.

The global detailed geoid (GEM-6) is presented in figure 18. The parameters used in the computation of the detailed geoid are :

W_o = 6263687.5 kgal m,
γ_e = 978032.2 mgal,
a_e = 6378.142 km,
1/f = 298.255,
GM = 3.986009×10^5 $km^3 sec^{-2}$, and
ω = $0.72921151467 \times 10^{-4}$ rad sec^{-1}.

The general difference between the satellite geoid (GEM-6) and the detailed geoid are on the order of 10 m or less. However, large variations in geoid heights do exist in certain areas. For example, in Australia, prominent differences of 10-12 m occur in the eastern part of the country due to the dominance of mountain ranges that adjoin relatively flat plains and shallow continental slopes. A difference of 15 m over the Puerto Rico trench occurs, which is a function of a large gravity gradient over a small region. These differences, coupled with numerous others, are the representation of the surface gravity short wavelength contributions to the geoid that are

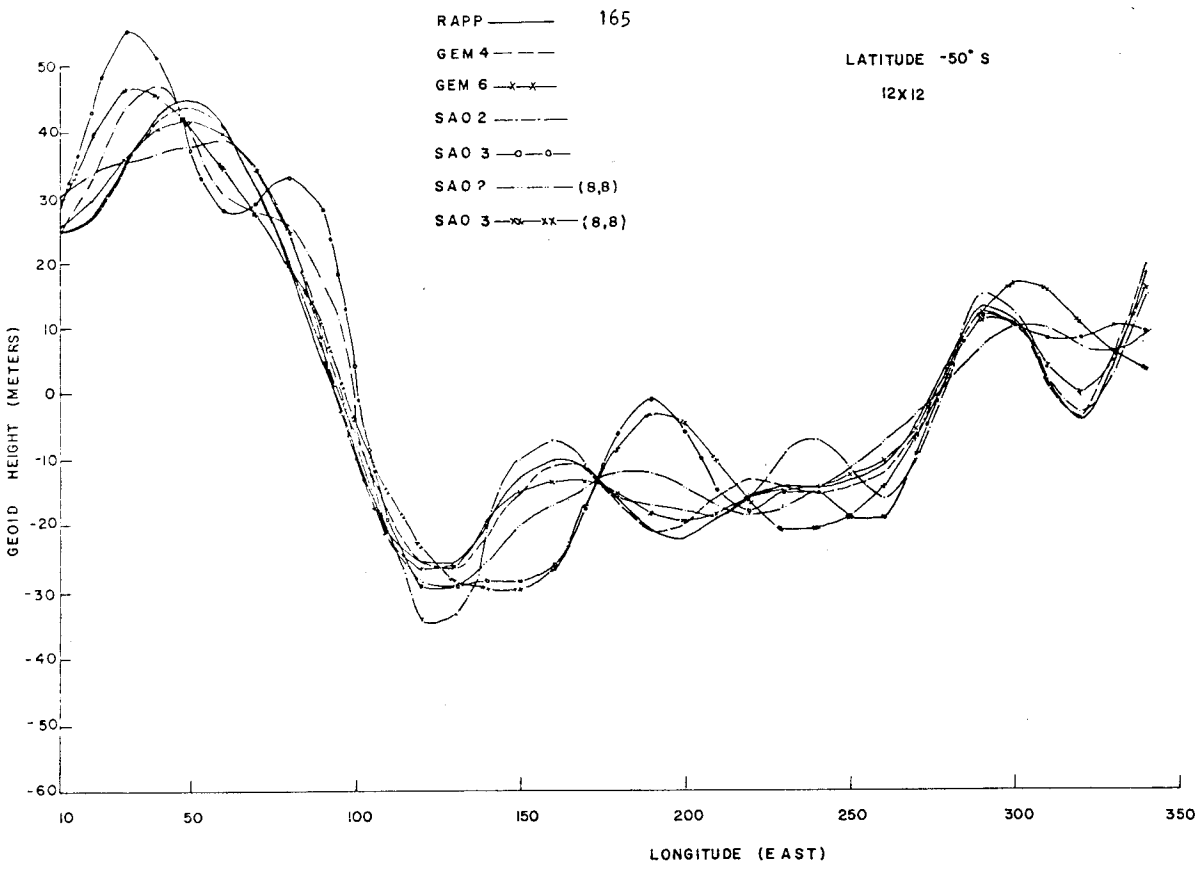

Figure 10. Detailed Geoid Profiles at Latitude 50°S (Truncated Models (12,12) and (8,8))

not provided by the above satellite model.

5. Conclusions

The accuracy of the GEM-6 detailed geoid is assessed as ±2 m in areas of dense surface gravity coverage.

The greatest divergence in these models appears in areas of sparse surface data coverage, notably in the southern hemisphere. The magnitude of these differences was as large as 25 m with a wavelength of approximately 30° to 50°,

Analysis in the southern hemisphere with models truncated to (12,12) indicated that caution should be exercised in interpreting geoid details provided by higher degree and order harmonic coefficients when surface data is lacking.

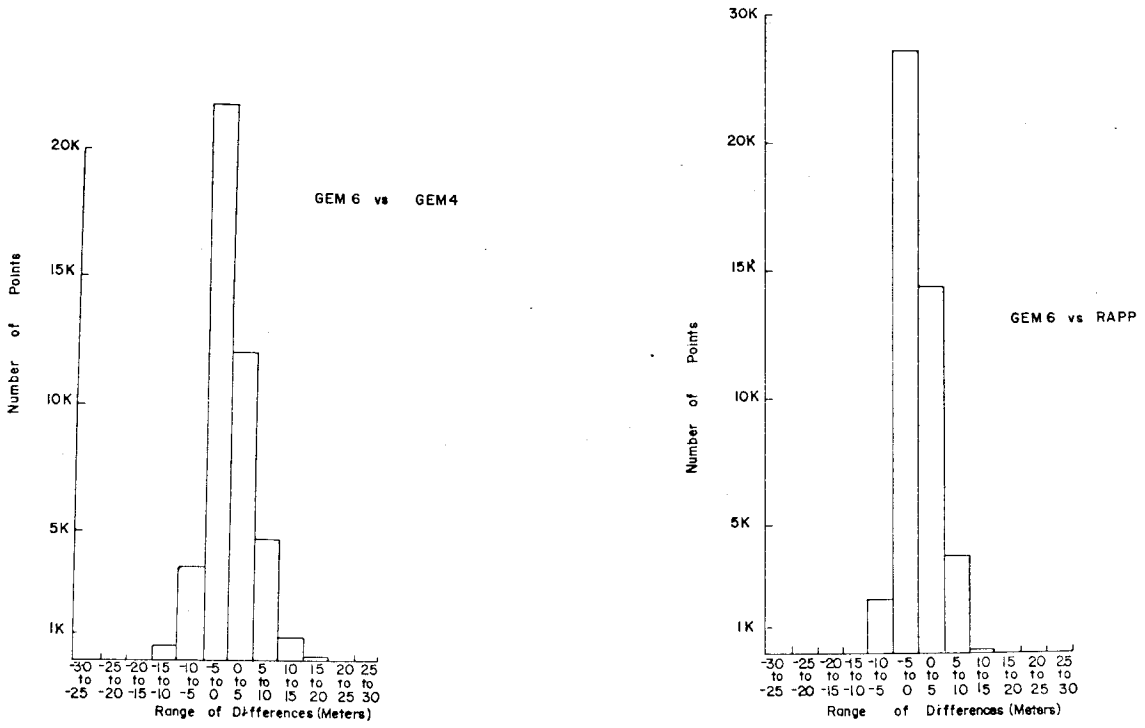

Figure 11. Histogram Showing Differences Between GEM-6 Detailed Geoid versus Detailed Geoids of GEM-4 and Rapp '73 (Complete Model)

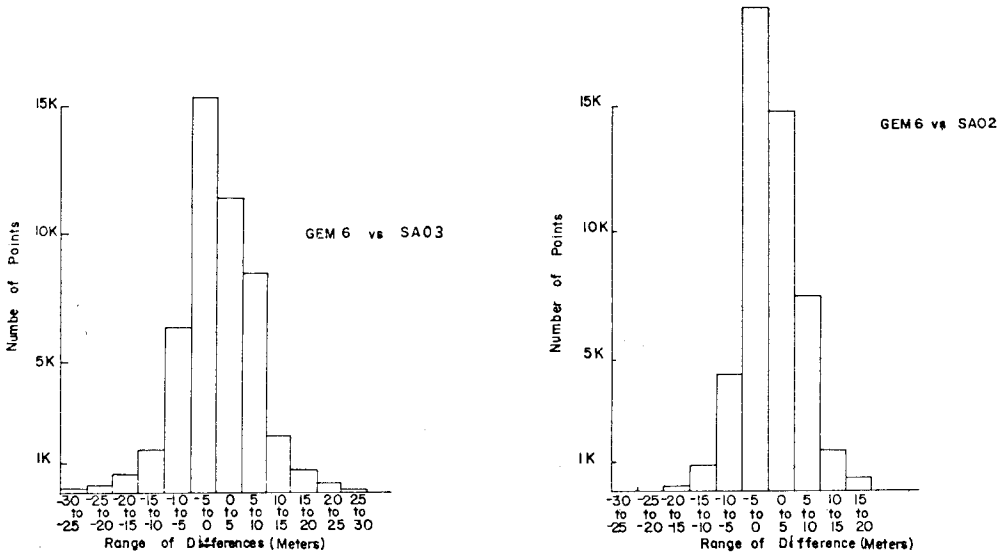

Figure 12. Histograms Showing Differences Between GEM-6 Detailed Geoid versus Detailed Geoids of SAO-2 and SAO-3 (Complete Models)

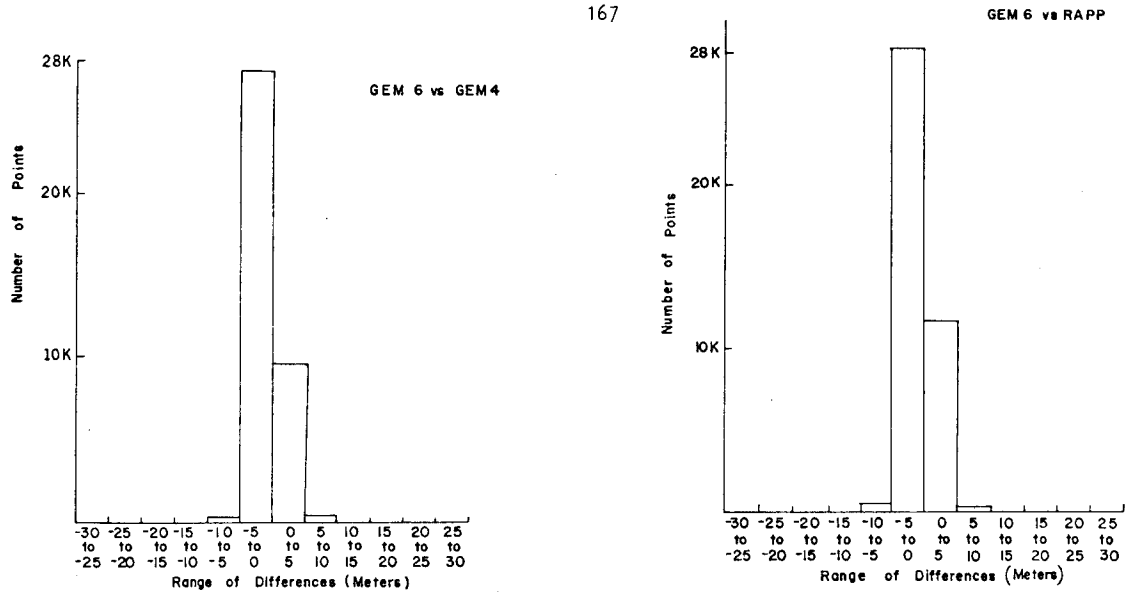

Figure 13. Histograms Showing Differences Between GEM-6 Detailed Geoid Versus Detailed Geoids of GEM-4 and Rapp [Truncated Models (12,12)]

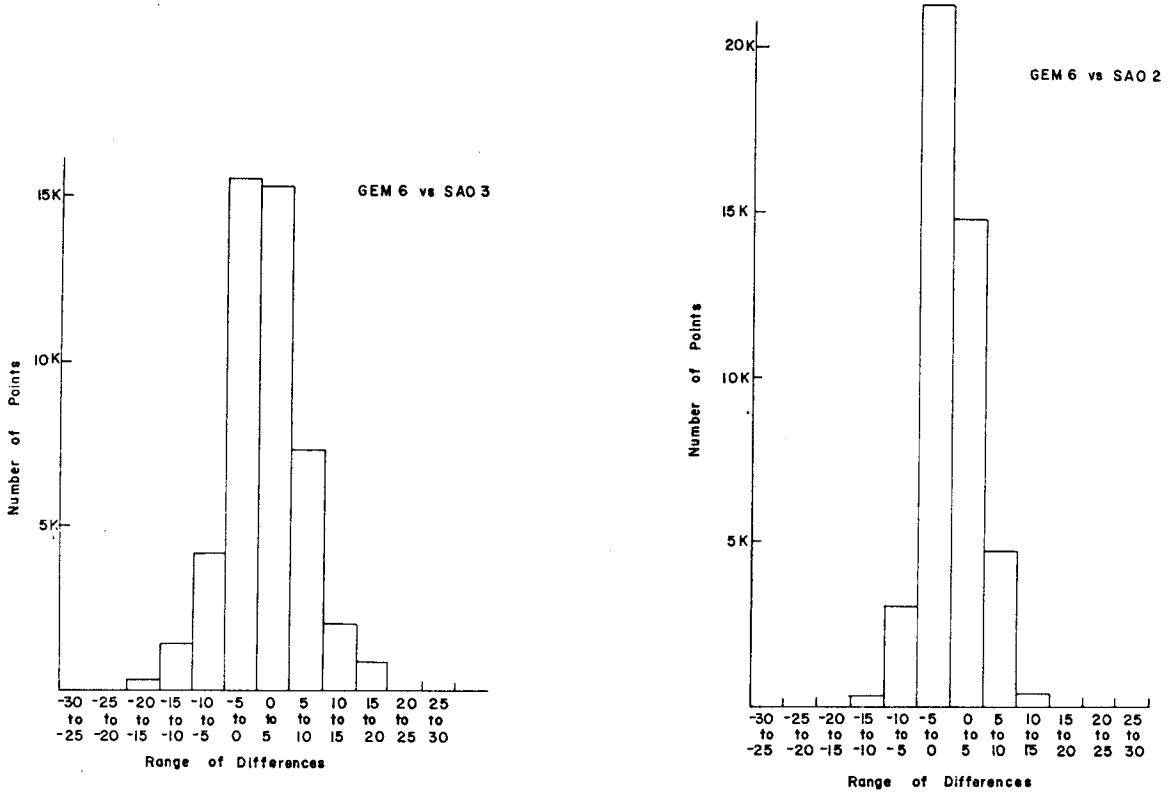

Figure 14. Histograms Showing Differences Between GEM-6 Detailed Geoid versus Detailed Geoids of SAO-2 and SAO-3 [Truncated Models (12,12)]

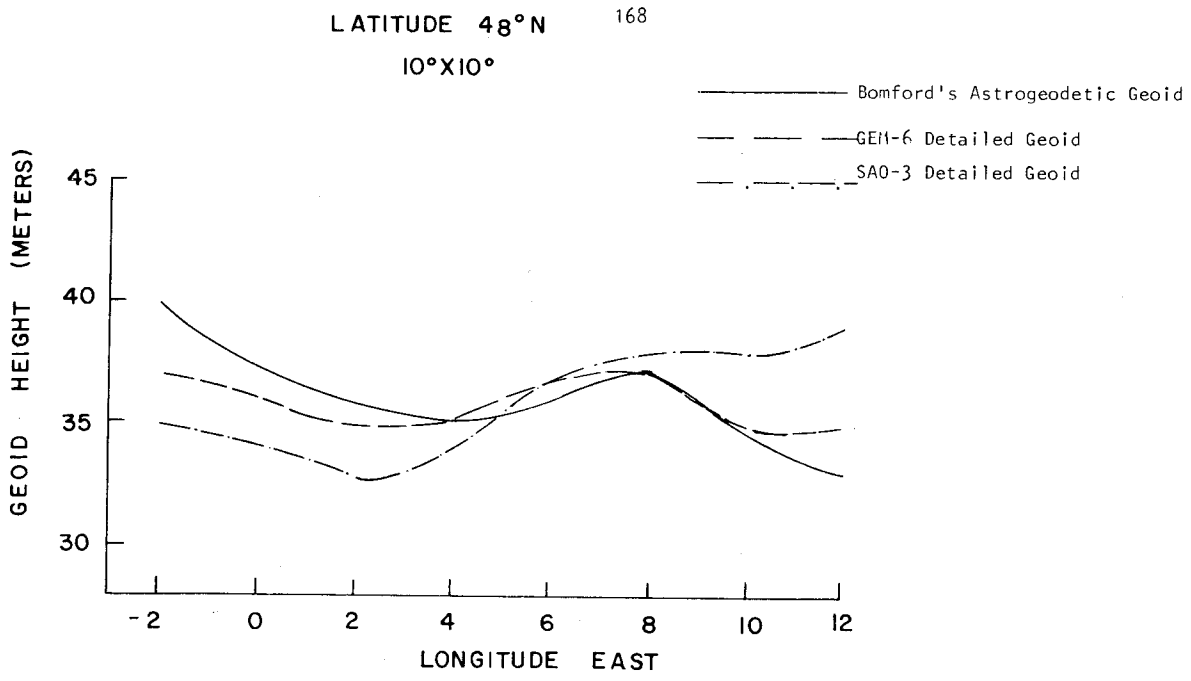

Figure 15. Comparison Between Bomford's Transformed Astrogeodetic Geoid and Detailed Gravimetric Geoid (GEM-6 and SAO-3) Integrated 10^{o} Around Computation Point in Europe

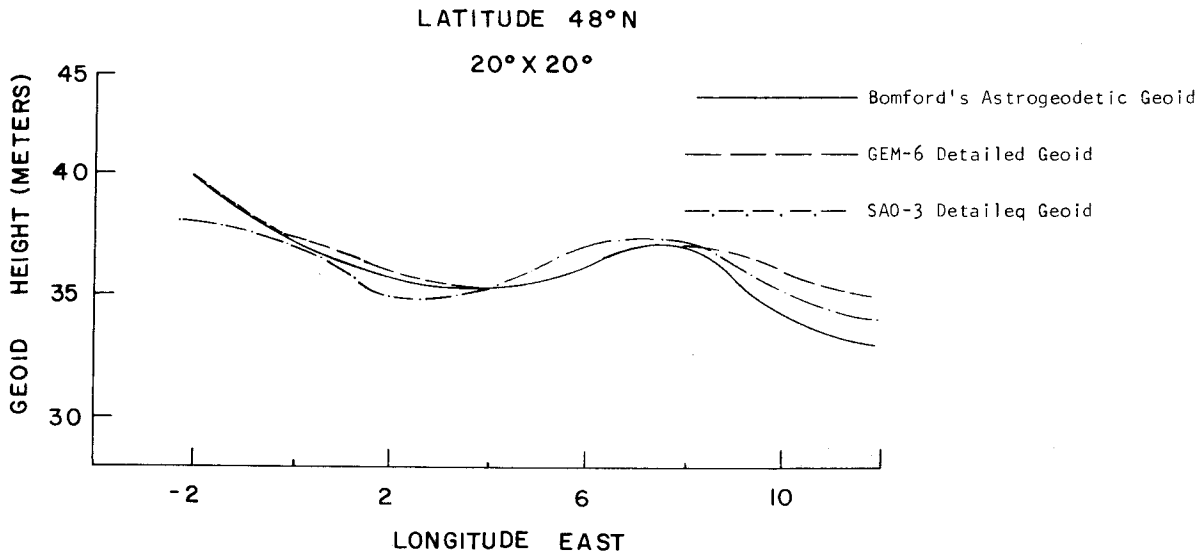

Figure 16. Comparison Between Bomford's Transformed Astrogeodetic Geoid and Detailed Gravimetric Geoid (GEM-6 and SAO-3) Integrated 20^{o} Around Computation Point for Europe

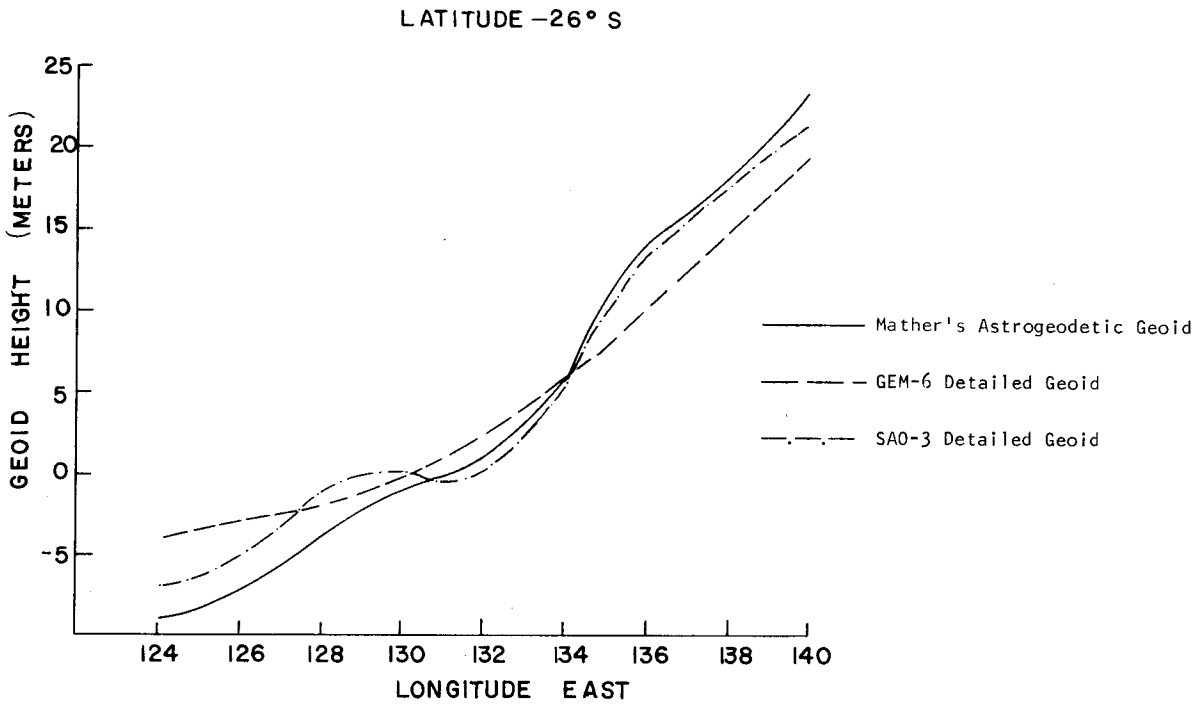

Figure 17. Comparison Between Mather's Transformed Astrogeodetic Geoid and Detailed Gravimetric Geoid (GEM-6 and SAO-3) in Australia

6. References

BOMFORD, G. 1971. The Astro-geodetic Geoid in Europe and Connected Areas. Appendix to "Report of Special Study Group V-29"(Author-I. FISCHER). *Travaux L'Assoc. Intern. Géodés.* 24,357-371.

BROWND, G. & RICHARDSON, J.A. 1973. Personal Communication. Computer Sciences Corporation,Silver Spring Md.

GAPOSCHKIN, E.M. 1973. *Smithsonian Standard Earth III.* Fifty Fourth Annual Meeting, American Geophysical Union,Washington DC.

GAPOSCHKIN, E.M. & LAMBECK, K. 1970. Smithsonian Standard Earth II. *Smithsonian astrophys.Obs. Spec.Rep.* 315,Cambridge Mass.

LERCH, F. ET AL 1972. Gravitational Field Models GEM-3 and GEM-4. *Doc X*-592-72-476,Goddard Space Flight Center,Greenbelt Md.

LERCH ET AL 1973. Gravitational Field Models GEM-5 and GEM-6. Contribution to *National Geodetic Satellite Program Final Report*,Goddard Space Flight Center,Greenbelt Md.

MARSH, J.G., DOUGLAS, B.C. & KLOSKO, S.M. 1973. Global Station Co-ordinate Solution Based Upon Camera and Laser Data -GSFC 1973. *Doc. X*-592-73-171,Goddard Space Flight Center, Greenbelt Md.

MARSH, J.G. & VINCENT, S. 1973. *Detailed Geoid Computations for GEOS-C Altimeter Experiment Area.* Fourth GEOP (Geodesy/Solid Earth and Ocean Physics) Conference, Boulder Colorado.

MATHER, R.S.,BARLOW, B.C. & FRYER,J.G. 1971. A Study of the Earth's Gravitational Field in the Australian Region. *UNISURV Rep.* 22,University of New South Wales,Kensington NSW,1-41.

RAPP, R.H. 1973. *The Earth's Gravitational Field from the Combination of Satellite and Terrestrial Data.* Fifty Fourth Annual Meeting,American Geophysical Union,Washington DC.

RICE, D.A. 1973. Personal Communication. National Ocean Survey,Rockville Md.

VINCENT, S. & MARSH, J.G. 1973. Global Detailed Gravimetric Geoid. *First International Symposium on the Use of Artificial Satellites for Geodesy & Geodynamics.* Athens.

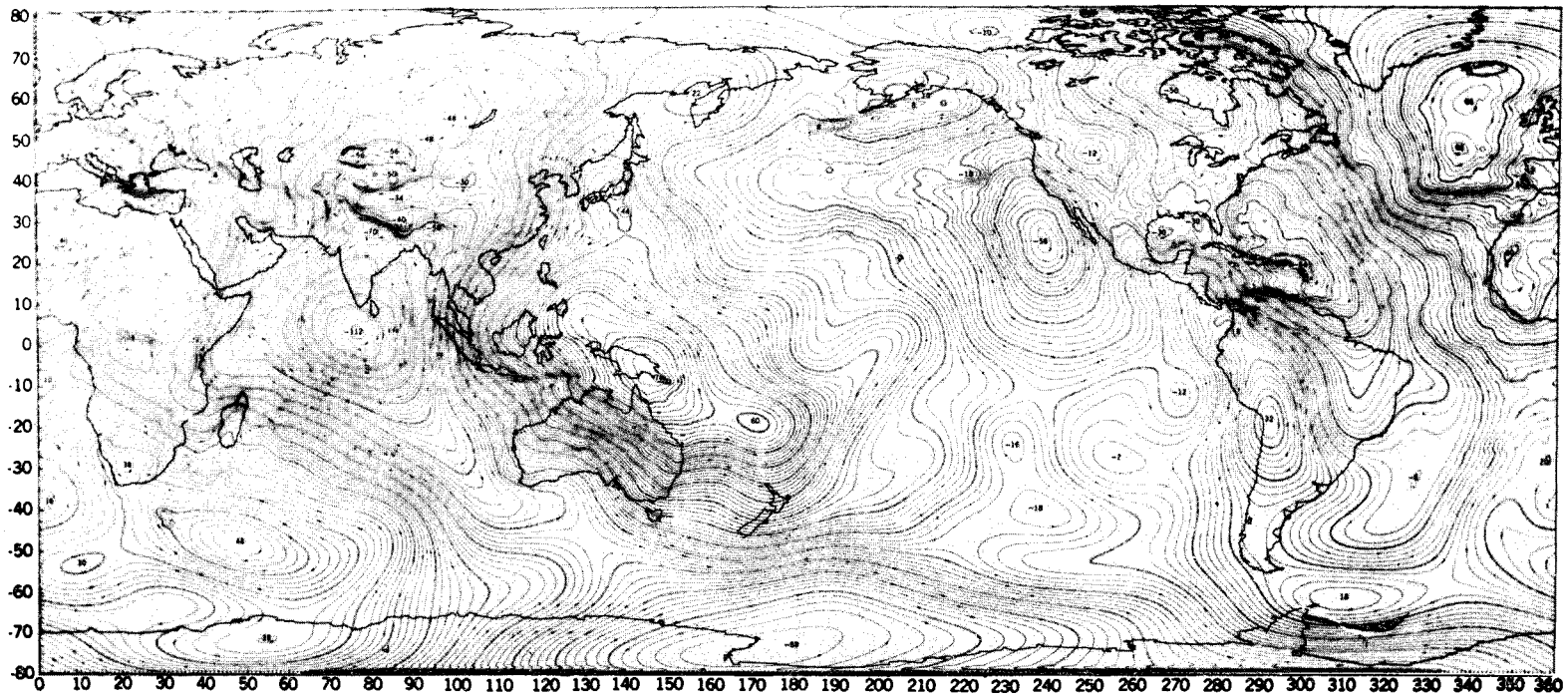

NASA/GODDARD SPACE FLIGHT CENTER

GLOBAL DETAILED GRAVIMETRIC GEOID BASED UPON A COMBINATION OF THE GSFC GEM-6 EARTH MODEL AND 1°×1° SURFACE GRAVITY DATA

CONTOUR INTERVAL 2 METERS, EARTH RADIUS: 6378.142 KM,
1/F=298.255, GM=398600.9 KM^3/SEC^2

562-2188
DEC. 73

7. Discussion

STOLZ: Why did you choose these particular sections for illustrating the comparisons?

VINCENT: The selection was arbitrary.

WALCOTT: What is the basis for the ±2 m figure quoted for accuracy?

VINCENT: It is based on values of dynamic station parameters and astro-geodetic geoid comparisons.

MATHER: Did you always go out to twenty degrees (from the point of computation)?

VINCENT: No; only when data was available. If there was no information, the value of the difference was put to zero.

OBENSON, G.
Faculty of Engineering
University of Lagos
Lagos
Nigeria

Proc.Symposium on Earth's Gravitational Field & Secular Variations in Position (1973),172-187.

A 1973 GRAVIMETRIC GEOID OF AFRICA

ABSTRACT

Results of a preliminary gravimetric geoid computed on the Geodetic Reference System 1967 (GRS67) are given in the form of undulation and deflection maps.

For the computations, $1^{o} \times 1^{o}$ mean free air gravity anomalies formed the inner zone and five degree equal area values the outer zone around each computation point. Some of the required $1^{o} \times 1^{o}$ means, together with their accuracies, were obtained by statistical prediction methods using an autocovariance function derived from the known $1^{o} \times 1^{o}$ values.

The results confirm the general south-easterly down slope of the geoid undulations. The average computed standard errors are about 3.6 m in the undulations and 0".6 in the deflections.

1. Introduction

Research in geodesy on Africa within Africa is generally very frustrating, mainly because of lack of data (and funds). One usually starts off by writing to related departments in the various countries in the continent. Most of these departments never reply and the few that do, refer one to either Britain, France or the United States of America. With some luck, one may receive some data from Britain or (in most cases), from the USA several letters and months later!

Computation of the geoid (undulations and deflections) and the related accuracies from gravity anomalies is a straightforward application of well-known formulae. However, as far as we know, this has never been done for the whole African continent. This paper is thus a primary attempt at computing what is, in fact, a "free air co-geoid" which, it is hoped, would be improved upon as more gravity data becomes available.

2. Gravity Data Used

The free air gravity anomaly data used consisted basically of: United States Aeronautical Chart and Information Center $1^{o} \times 1^{o}$ mean values (ACIC 1971), Rapp's five degree equal area values (RAPP 1972) and Bureau Gravimetrique International Bouguer anomaly map and $5^{o} \times 5^{o}$ means (BGI 1971). A total of 5450 $1^{\circ} \times 1^{\circ}$ sub-blocks, enclosed within 197 5° equal area blocks, were required. 2500 of the $1^{o} \times 1^{o}$ values were given in the ACIC report and 210 of these were replaced by what were considered to be better values. Of the remaining 2950 $1^{o} \times 1^{o}$ values, 350 were obtained from Bouguer anomalies either given as point values or read off from several maps that were available to us. The rest, 2600 of them, were predicted using the minimum variance or contouring methods. Figure 1 shows the area covered by the $1^{o} \times 1^{o}$ mean values.

For the minimum variance method, an autocovariance function was developed from the 2850 known $1^{o} \times 1^{o}$ means. This function was then used to predict the unknown $1^{o} \times 1^{o}$ values in any area within the limits of the maximum range of the function. The prediction equations given by MORITZ (1969) were used.

Thus, using matrix notation,

$$\Delta g = \overline{C} \, (C + D)^{-1} \, \Delta g \qquad (1),$$

and

$$m^2_{\Delta g} = \overline{\overline{C}} - \overline{C} \, (C + D)^{-1} \, \overline{C}^{T} \qquad (2),$$

where $\hat{\Delta g}$ is the predicted $1^{o} \times 1^{o}$ value;

Δg is the column vector of known $1^{o} \times 1^{o}$ means;

m^2 is the variance of the predicted anomaly;

C is the matrix whose elements are the covariance between the known blocks;

$\overline{C}$ is a row vector whose elements are the covariances between the block p being predicted and the known blocks i used in the prediction; thus

Thus

$$\overline{C}_i = C_{pi} \qquad (3);$$

D represents the given variances of the known $1^{o} \times 1^{o}$ anomalies used in the predict prediction; and

$\overline{\overline{C}}$ is the variance of the $1^{o} \times 1^{o}$ anomalies.

Thus

$$\overline{\overline{C}} = C_{ii} \qquad (4).$$

However, there were some areas, particularly south of the West African coast, where contouring was used owing to the short range nature of the covariance function.

As a result of the new and predicted $1^{o} \times 1^{o}$ values, 168 five degree equal area means were replaced, 116 of them differing by 5 mgal or less from the Rapp values. The variance of each new value was obtained from equation 2 with appropriate definitions of the matrices.

Finally, the one degree and five degree anomalies were transformed into the GRS67 system to which the computed deflections and undulations were referred. The transformation equations were

$$\Delta g_{67} = \Delta g_R + 1.71 + 0.11 \sin^2\phi \ \text{mgal} \qquad (5),$$

where Δg_R are the Rapp five degree anomalies referred to a differently defined reference system, and

$$\Delta g_{67} = \Delta g_I + 2.33 - 13.6 \sin^2\phi \ \text{mgal} \qquad (6),$$

where Δg_I are the $1^{o} \times 1^{o}$ values referred to the International Gravity Formula.

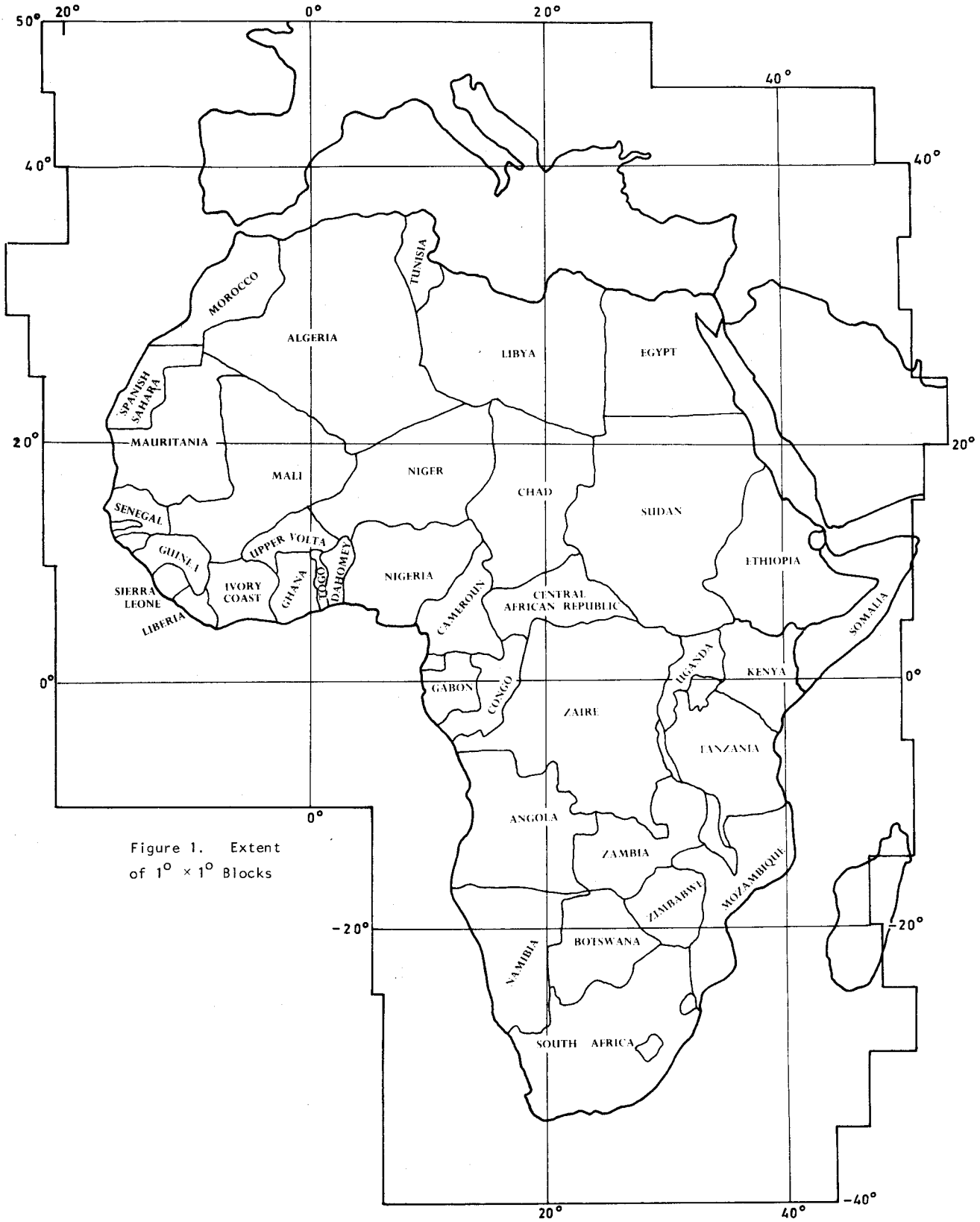

Figure 1. Extent of $1^{\circ} \times 1^{\circ}$ Blocks

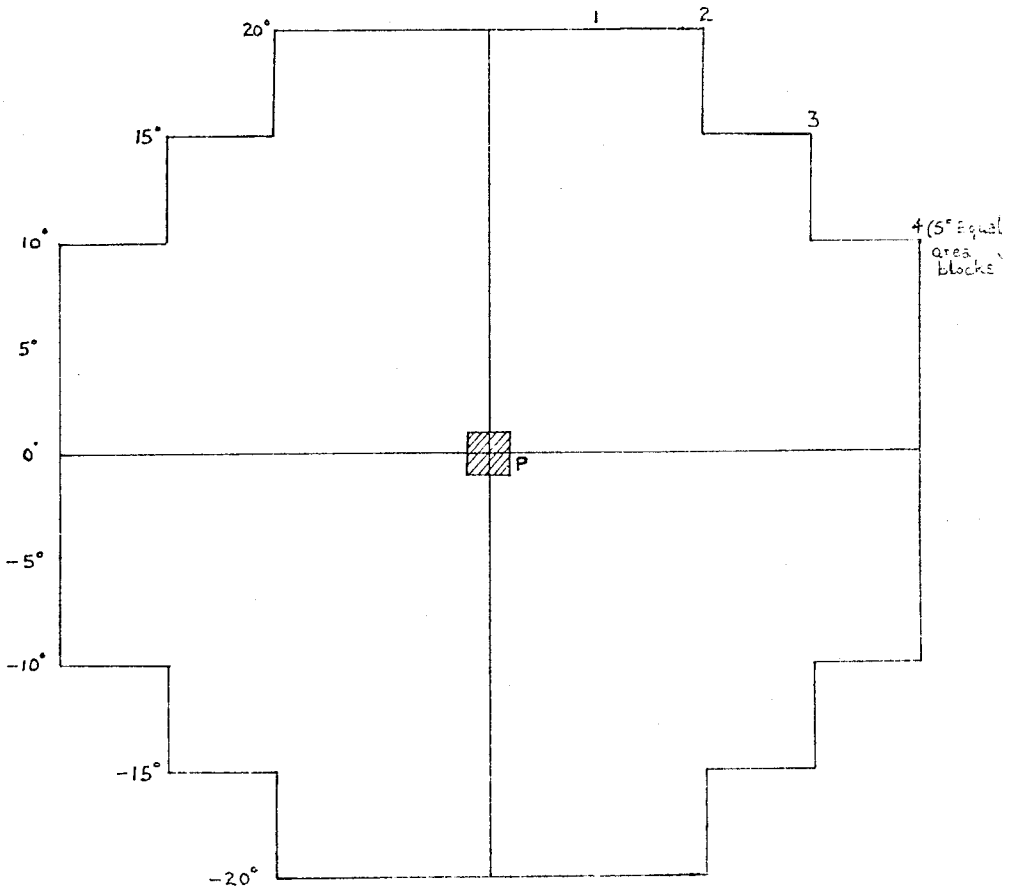

Figure 2. Limits of Inner Zone Around Each Computation Point P. The Four Shaded $1^{o} \times 1^{o}$ blocks were not included in the Computations

Both equations 5 and 6 imply a Potsdam correction of -14 mgal (IAG 1971) and an atmospheric gravity correction of -0.87 mgal (ECKER & MITTERMAYER 1969)

3. Computational Techniques

Stokes' and Vening Meinesz equations are the relevant equations for the computation of the undulations and deflections of the vertical respectively. Thus

$$\begin{Bmatrix} N \\ \xi \\ \eta \end{Bmatrix} = \frac{1}{4\pi G} \begin{Bmatrix} R \iint \Delta g \; S(\psi) \; d\sigma \\ \\ \rho \iint \Delta g \; \frac{dS(\psi)}{d\psi} \begin{Bmatrix} \cos \alpha \\ \sin \alpha \end{Bmatrix} d\sigma \end{Bmatrix} \qquad (7),$$

where $S(\psi)$ is Stokes' function;

G is the mean Earth gravity ;

R is the mean Earth radius;

Δg are free air anomalies;

$d\sigma$ is the element of area of the surface σ whose anomaly is Δg and at an azimuth α from the computation point; and

ρ = cosec 1''.

In practice the required values are computed from any of several numerical forms of equation 7. For example,

$$\begin{Bmatrix} N \\ \xi \\ \eta \end{Bmatrix} = \frac{1}{4\pi G} \begin{Bmatrix} R \sum_m \Delta g \; S(\psi) \; \Delta\sigma \\ \\ \rho \sum_m \Delta g \; dS(\psi) \begin{Bmatrix} \cos\alpha \\ \sin\alpha \end{Bmatrix} \Delta\sigma \end{Bmatrix} \tag{8}$$

or

$$\begin{Bmatrix} N \\ \xi \\ \eta \end{Bmatrix} = \frac{1}{4\pi G} \begin{Bmatrix} R \sum_m \Delta g \; \frac{1}{n} \sum_n S(\psi) \; \Delta\sigma \\ \\ \rho \sum_m \Delta g \; \frac{1}{n} \sum_n dS(\psi) \begin{Bmatrix} \cos\alpha \\ \sin\alpha \end{Bmatrix} \Delta\sigma \end{Bmatrix} \tag{9},$$

where m is the number of large blocks covering the Earth's surface; and

n is the number of sub-blocks in each large block m.

Equation 8 was used for the computations done in this paper. Because of the behaviour of Stokes' function and its derivative as the computation point is approached, the computations are usually done for an inner zone using smaller blocks, and for an outer zone using larger blocks, $1° \times 1°$ and $5°$ equalarea mean values respectively for this paper. Thus, symbolically,

$$\begin{Bmatrix} N \\ \xi \\ \eta \end{Bmatrix} = \begin{Bmatrix} N \\ \xi \\ \eta \end{Bmatrix}_{\text{Inner}} + \begin{Bmatrix} N \\ \xi \\ \eta \end{Bmatrix}_{\text{Outer}} \tag{10}.$$

Equations 8 and 10 can be written in matrix form as

$$E = K_I A_I + K_0 A_0 \tag{11},$$

where E represents the computed undulations and deflections;

A represents the gravity anomalies for the inner zone I and the outer zone 0; and

K represents the coefficients of the anomalies, whose elements are given by

$$\begin{Bmatrix} k_{N_i} \\ k_{\xi_i} \\ k_{\eta i} \end{Bmatrix} = \begin{Bmatrix} \frac{R}{4\pi G} \; S(\psi_i) \; \Delta\sigma_i \\ \\ \frac{\rho}{4\pi G} \; dS(\psi_i) \begin{Bmatrix} \cos\alpha_i \\ \sin\alpha_i \end{Bmatrix} \Delta\sigma_i \end{Bmatrix} \tag{12}.$$

The covariance matrix of the computed undulations and deflections Σ_E follows from equation 11 OBENSON (1973). Thus

$$\Sigma_E = K_I \Sigma_{A_I} K_I + K_0 \Sigma_{A_0} K_0 + K_I \Sigma_{A_I A_0} K_0 + K_0 \Sigma_{A_I A_0} K_I \qquad (13),$$

where

Σ_A is the covariance matrix of the given anomalies. Only the first two terms on the right of equation 13 were used in the evaluations done here since $\Sigma_{A_I A_0}$ is generally not known in practice.

3.1 Determining the Limits of the Inner Zone

The spherical cap defining the inner zone has been variously given as extending up to between 10^o to 40^o away from the computation point (UOTILA 1959; MATHER 1969; NEEDHAM 1970). It was however determined here by comparing the deflections and the undulations, computed separately, from a five degree equal area anomaly block and from $1^o \times 1^o$ values within the five degree block at various points. The location of this block was varied in distance and azimuth from the computation point. Though the spherical distance differed with the position of the computation point, it was found that the lengths, in terms of $\Delta\phi$ and $\Delta\lambda$ for any spherical range of differences between the one degree and five degree contributions to the deflections and undulations, were the same for all points. Table 1 illustrates this for a maximum difference of not more than 0.08 m for the undulation and 0".02 for the deflection components.

From these tests, the inner zone was then defined as a circle of radius $S = \sqrt{[\Delta\phi^2 + \Delta\lambda^2]} = 20^\circ$ around the computation point. This limit produces a total maximum average error of about 1.5 m in the undulation and 0".3 in the deflections. However, owing to the shape of the given anomaly blocks, the inner zone for each computation point was taken as shown in figure 2.

Since five degree equal area blocks were used, the east-west lengths were chosen in terms of whole blocks - hence a maximum of four blocks on either side of the point. For most points within the

T a b l e 1

Sample Results Used to Determine the Limits of the Inner Zone

Computation Point ϕ (deg)	Computation Point λ (deg)	ψ (deg)	$S = \sqrt{(\Delta\phi^2+\Delta\lambda^2)}$ (deg)	Differences ($5^\circ - 1^\circ$) Contributions ξ (sec)	η (sec)	N (m)
70	0	6.1	17.3	0.003	0.004	0.01
45	5	12.3	17.3	0.010	0.018	0.08
20	0	16.5	17.3	0.001	0.001	0.01
0	15	17.7	17.3	0.001	0.001	0.01
-10	20	17.5	17.3	0.001	0.005	0.03
-35	25	14.7	17.3	0.000	0.003	0.01
-60	0	9.4	17.3	0.018	0.010	0.04

continent, the arrangement in figure 2 applied, but there were other points, especially near the coast where $\Delta\phi$ and $\Delta\lambda$ were as low as 10° or two 5° equal area blocks away. However, the average number of 1° × 1° blocks inside the inner zone was about 1200. For lack of more detailed data, the four 1° × 1° blocks immdeiately surrounding the computation points were not used in the computations.

4. Results

The undulations and deflections of the vertical were computed at 91 points at the intersection of the five degree equal area blocks within the continent. Figures 3, 5 and 7 show the contour maps of N, ξ and η respectively. Figures 4, 6 and 8 are their accompanying standard errors.

To obtain the total value of either the undulation of deflections at any point, the contribution of the four 1° × 1° blocks surrounding the point should first be computed from a more detailed anomaly field and simplified forms of equation 7, and then added to the value read off maps. For the undulations and their accuracies, these values are generally negligibly small. However figure 3 confirms the general south-easterly down slope of the undulations, decreasing from a maximum of 56 m in northern Morocco to -8 m in Somalia and Kenya. Figures 4, 6 & 8 indicate average standard errors of about 3.6 m in the undulations and 0".6 in each deflection component throughout the continent.

5. Discussion

It is usual to compare free air undulations with equivalent astro-geodetic values in order to determine absolute accuracies; hence some information on the effect of the "indirect effect" and the reliability of the estimated anomalies and their accuracies. It was not possible to do this here because of the lack of numerical data on any astro-geodetic geoids computed in any part of the continent. A suitable comparison would have been the recently-completed 12° latitude astro-geodetic geoid profile connecting western Sudan, just north of the Chad/Central African Republic boundary with Dakar in Senegal (WALKER 1971; MCCALL 1970; YATER 1971). However this was not possible as none of the papers mentioned above contained any discrete values either of the profile or of the Adindan datum on which the profile was based. But a visual comparison between a profile taken approximately along latitude 12°N in figure 3 and that given by Walker shows that both "rise steeply from Sudan to central Nigeria and then drop smoothly from central Mali to Dakar" (WALKER 1971).

The results given here should be useful in the determination of various Earth parameters and transformations between the various geodetic datums on the continent.

6. Acknowledgments

The research for this paper was supported in part by a research grant for computer time from the Faculty of Engineering through the Dean, Professor I.O. Oladapo. The author is grateful and also wishes to thank all those who contributed advice and/or gravity data, in particular Professor R.H. Rapp, Elmer Hauer and Enilo Ajakaiye.

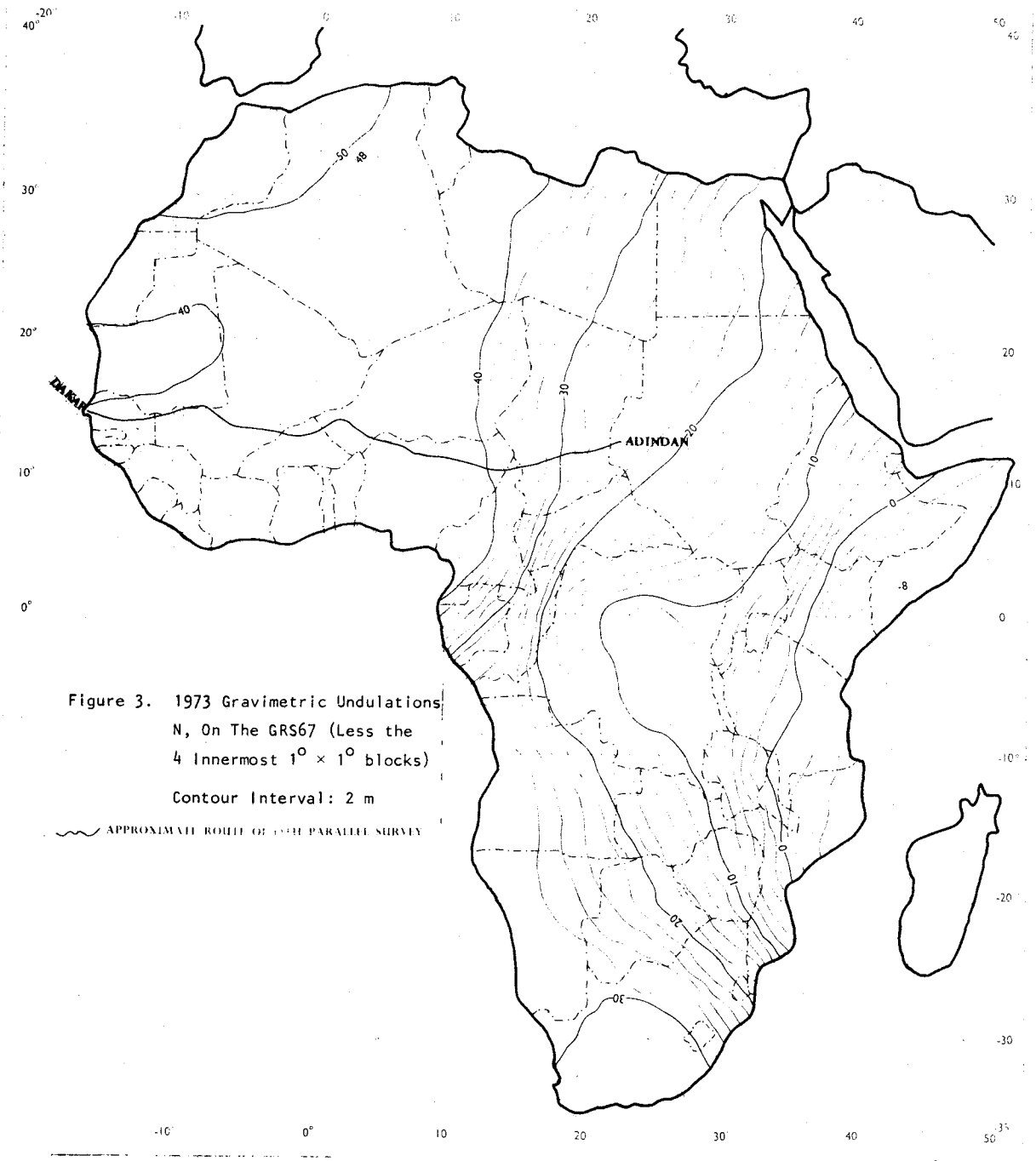

Figure 3. 1973 Gravimetric Undulations N, On The GRS67 (Less the 4 Innermost $1^{o} \times 1^{o}$ blocks)

Contour Interval: 2 m

APPROXIMATE ROUTE OF [illegible] PARALLEL SURVEY

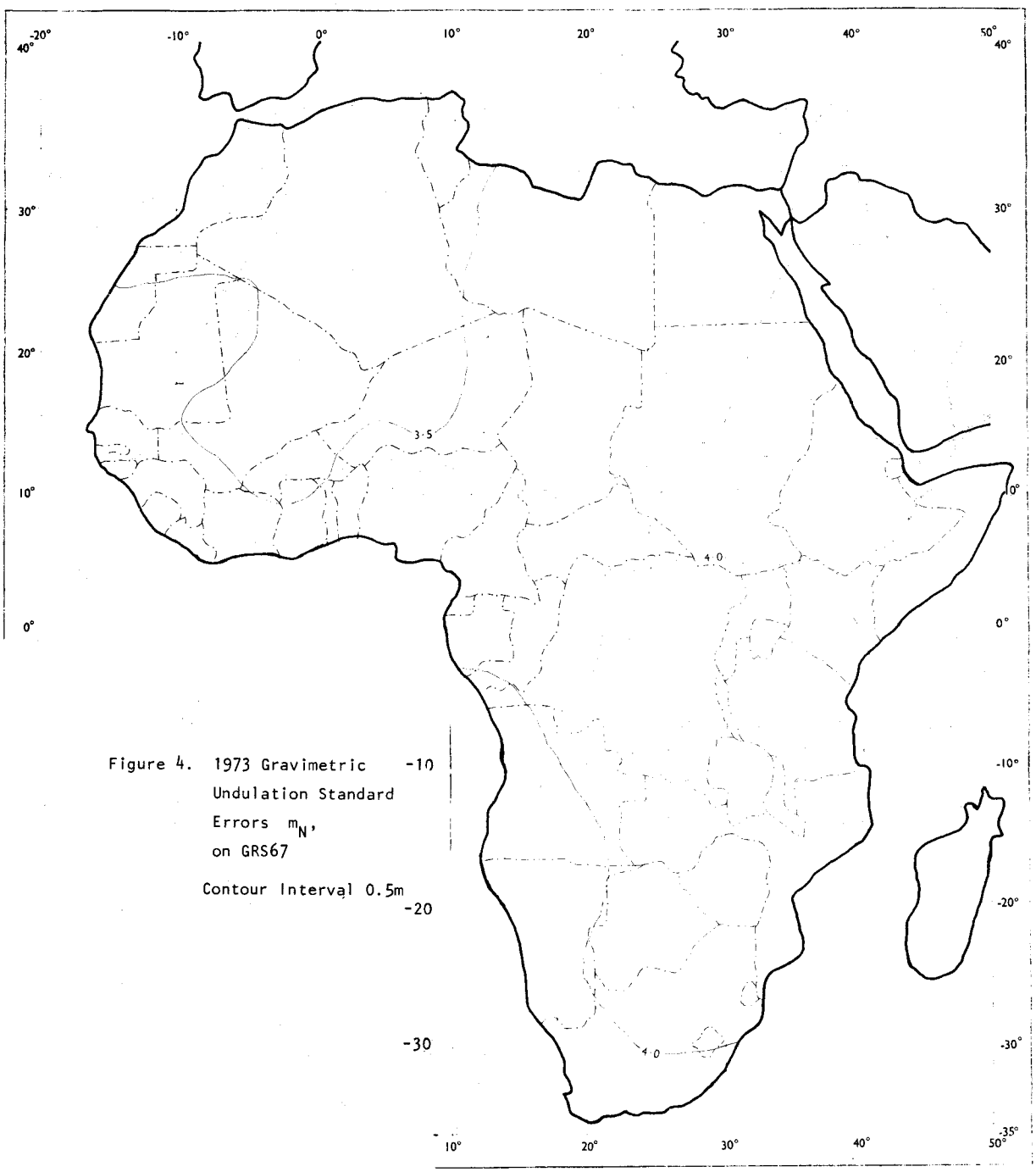

Figure 4. 1973 Gravimetric Undulation Standard Errors m_N, on GRS67

Contour Interval 0.5m

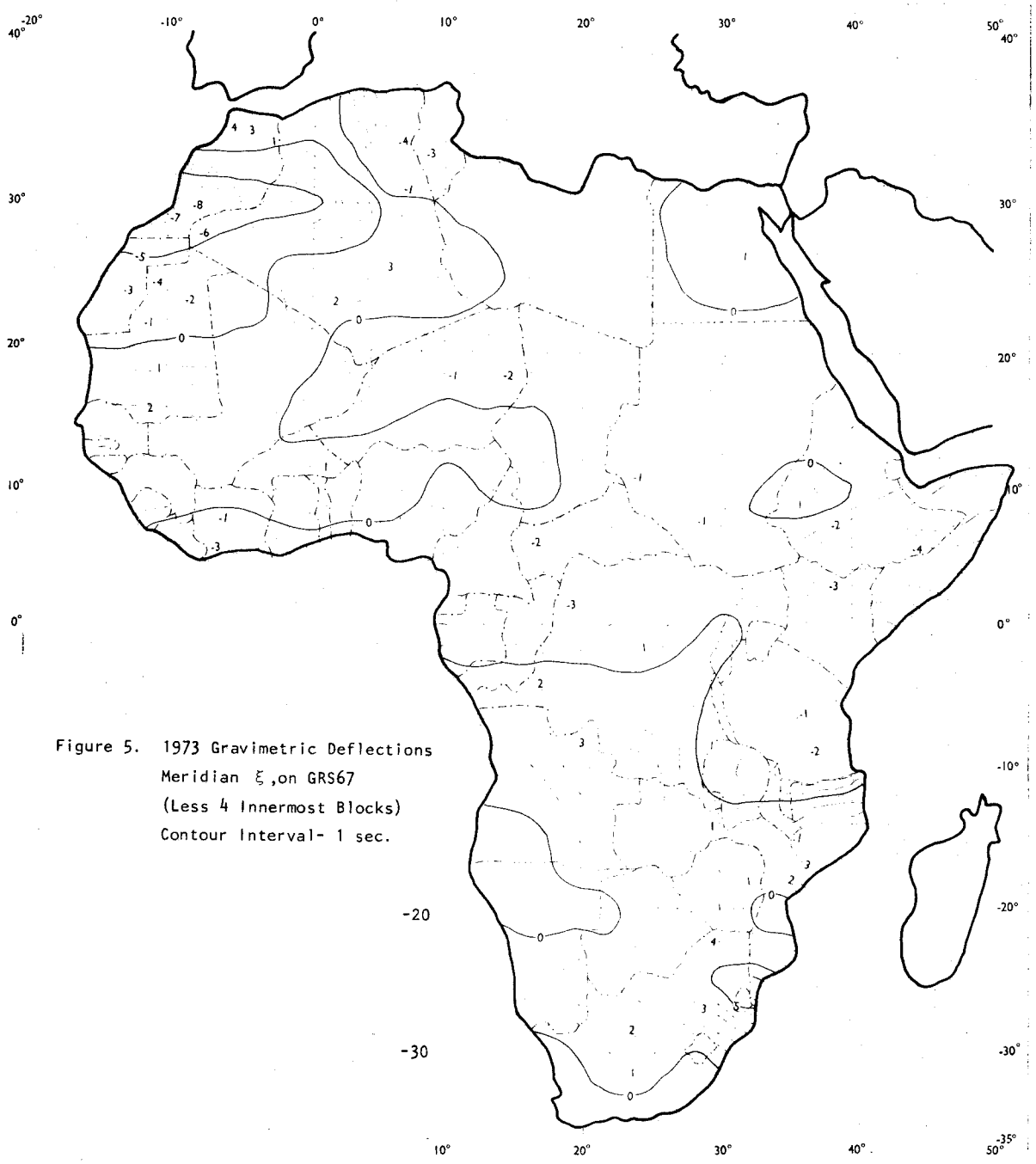

Figure 5. 1973 Gravimetric Deflections
Meridian ξ, on GRS67
(Less 4 Innermost Blocks)
Contour Interval- 1 sec.

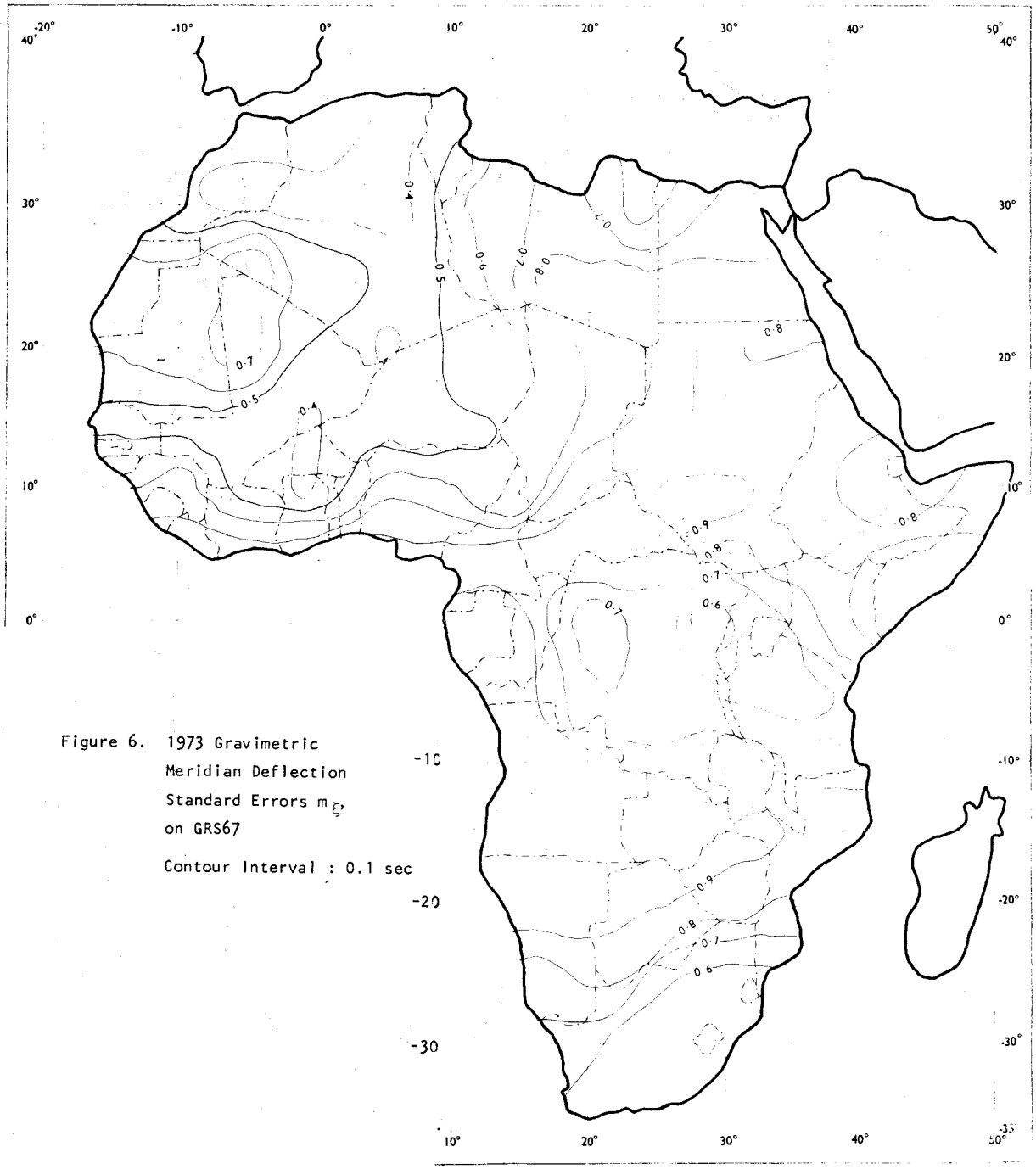

Figure 6. 1973 Gravimetric Meridian Deflection Standard Errors m_ξ, on GRS67

Contour Interval : 0.1 sec

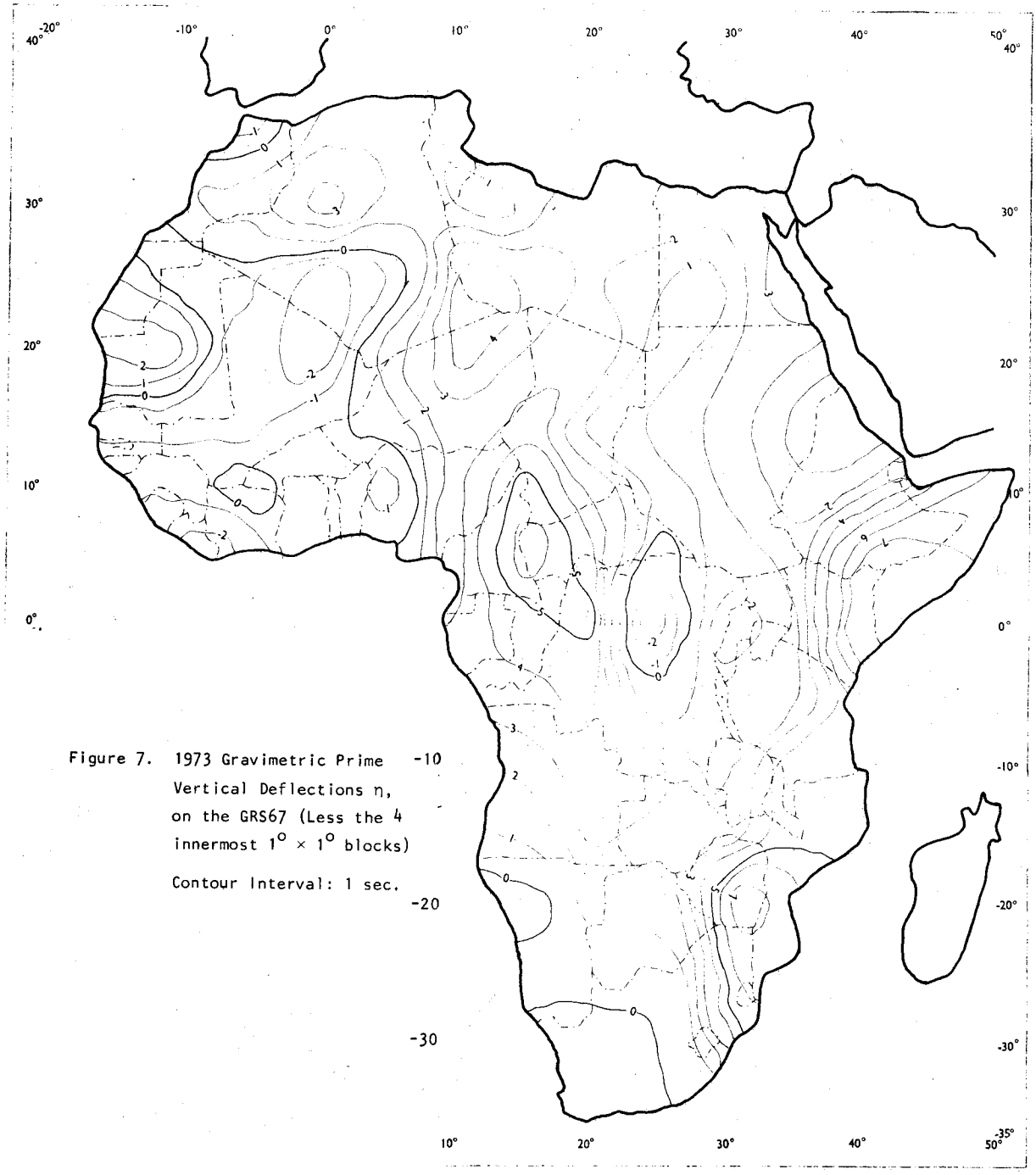

Figure 7. 1973 Gravimetric Prime Vertical Deflections η, on the GRS67 (Less the 4 innermost $1^{\circ} \times 1^{\circ}$ blocks)

Contour Interval: 1 sec.

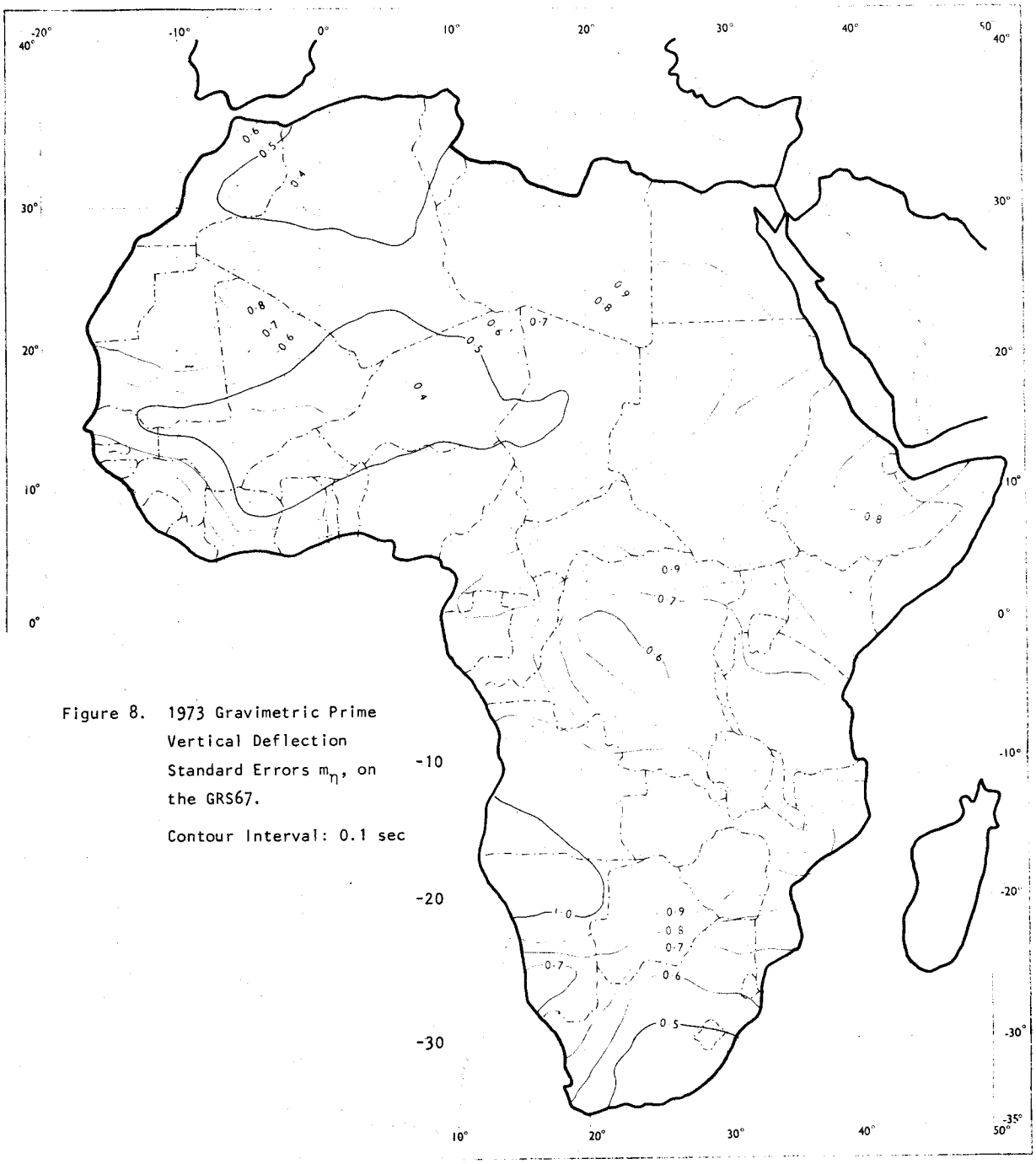

Figure 8. 1973 Gravimetric Prime Vertical Deflection Standard Errors m_η, on the GRS67.

Contour Interval: 0.1 sec

Dave Gordon of the University Computer Centre helped with programming problems and Rowland Asoegwu and Jimoh Ogunsanya (both post-graduate students in the department), carried out some of the prediction and map contouring.

7. References

ACIC 1971. 1° × 1° Mean Free Air Anomalies. *Ref.Publ.* 29, Aeronautical Chart & Information Center.

AJAKAIYE, D.E. & BURKE, K. 1973. A Bouguer Gravity Map of Nigeria. *Tectonophysics* 16

BGI 1971. *Anomalies de Bouguer, Europe-Afrique.* 3e edition, Bureau Gravimetrique International, Paris.

ECKER, E. & MITTERMAYER, E. 1969. Gravity Correction for the Influence of the Atmosphere. *Boll.di geofis.Teorica ed Appl.* XI,41-42.

HEISKANEN, W.A. & MORITZ, H. 1967. *Physical Geodesy.* Freeman,San Fransisco.

IAG 1971. *Geodetic Reference System 1967.* Spec.Publ.,International Association of Geodesy,Paris.

MATHER, R.S. 1969. The Free Air Geoid for Australia. *Geophys.J.R.astr.Soc.* 18,499-516.

MCCALL, J.S. 1970. Report on Completion 12th Parallel Survey - Africa. *United Nations Regional Cartographic Conference for Asia and the Far East*,Teheran.

MORITZ, H. 1969. A General Theory of Gravity Processing. *Rep.*122,Dept. of Geodetic Science,The Ohio State University, Columbus Ohio.

NEEDHAM, P.H. 1970. The Formation and Evaluation of Detailed Geopotential Models Based on Point Masses. *Rep.* 149,Dept. of Geodetic Science,The Ohio State University,Columbus Ohio.

OBENSON, G.F.T 1973. Error Analysis of Deflections of the Vertical and Undulations from the Accuracies of Gravity Anomalies. *Bull.geodes.* 108,141-155.

OLAJIGA, O.B. 1972. *Collection and Processing of Gravity Data in Nigeria.* M.Sc. Thesis, University of Lagos, Lagos.

QURESHI, I.R. 1971. Gravity Measurements in the North-Eastern Sudan and Crustal Structure of the Red Sea. *Geophys.J.R.astr.Soc.* 24.

RAPP, R.H. 1972. The Formation and Analysis of a Five Degree Equal Area Block Terrestrial Gravity Field. *Rep.* 178,Dept. of Geodetic Science,The Ohio State University,Columbus Ohio.

UOTILA, U.A. 1959. Investigations on the Gravity Field of the Earth. *Rep.* 6,Institute of Geodesy, Photogrammetry & Cartography,The Ohio State University, Columbus Ohio.

WALKER, J.W. 1971. Adjustment of the 12th Parallel Geodimeter Traverse. *Annual Convention,American Congress of Surveying & Mapping*,Washington DC.

YATER, R.R. 1971. 12th Parallel Survey. *Commonwealth Survey Officers' Conference*,Paper B2, Cambridge,England.

8. Discussion*

WALCOTT: As an outsider, I have a question. Gravity is measured with respect to the geoid .. ?

RAPP: Gravity is measured with respect to the Earth's surface. The question is what you should do with this gravity. In all solutions of the boundary value problem you work with some residual. The main question relates to how you formulate the boundary value problem. In the days of Stokes, you formulated it on the geoid by eliminating the masses exterior to it. This was incorrect and from developments between 1932 and 1945, it was accepted that we would try to compute the surface of the Earth (i.e., deflections of the vertical and height anomalies). The next question is deciding on the best way to do that. As Mather said (earlier) this morning, all sorts of complications arise.

WALCOTT: Is there a difference in datum between Δg_T and Δg_S?

RAPP: You have to be careful to make sure there is not a difference in the datum. To do that we have to define the reference ellipsoid (or the reference surface to which the undulations are to be referred) very carefully. If this is not done, for example, if the gravity anomalies were computed using a certain gravity formula which is not compatible with that used for satellite potential coefficient determinations, there will be a systematic error in the undulations which are computed. Some recent work (RAPP, R.H. 1973 . Accuracy of Geoid Undulation Computations. *J.geophys.Res.*78,7589) showed that an error of 1 mgal in defining the proper gravity formula can give a 1 - 3 m error in this type of formulation. It is really a critical issue.

KEARSLEY: Can you comment on the stated accuracy of the deflections of the vertical?

RAPP: They sound reasonable when you consider that the effect of the four inner blocks is excluded. A big inaccuracy comes from the inner area.

MATHER: I would like to comment on that. Once we were doing some work for (the Division of) National Mapping, gravimetrically checking astro-geodetic deflections of the vertical. Computation out to 150 km using a tenth degree grid enabled us to recover all but about 1½ arcsec in the long wavelength component and the effect of the innermost zone (within 5 km of the point of computation).

MORITZ: If the inner zones are not known, instead of excluding them altogether, it would be advisable to rather fit a polynomial to the four inner zone mean values.

ECKHARDT: We are discussing the separation of N_1, N_2 & N_3 and presumably hoping that N_3 is small. Another way of doing this for a limited area like Africa or North America is to modify Stokes' function. If we can say that what we measure on ground is error free, except that it doesn't cover the whole Earth. If we take the difference between (this field and) say, a (12,12) satellite model, the contribution of the difference will only be in the higher degree harmonics. Stokes' function can therefore be modified by subtracting the lower degree harmonics arbitrarily such that the outer zone effects become zero, on subtracting a set of Legendre polynomials $P_n(\psi)$ from Stokes' function $S(\psi)$ such that

$$S(\psi) - \sum h_n P_n(\psi)$$

becomes small. I have done this for example, for a (12,12) solution and say 15°(radius of surface gravity). This is one way of modifying Stokes' kernel and ignoring the (outer zone) term. (For illustration see figure on p.187).

RAPP: This type of approach can be found in (MOLODENSKII, M.S. ET AL 1962. *Methods for Study of the External Gravitational Field & Figure of the Earth.* Israel Program for Scientific Translations,Jerusalem) where it is shown how you can modify Stokes' kernel to any particular degree and the idea of truncation theory was developed for many functions by DE WITTE (1967. *Geophys.J.R.astr.Soc.*12,449-464). The objection I have to this that there is no reason to believe that the anomalies computed from potential coefficients to say degree 12, are sufficiently accurate that we can justify forcing contributions from degree two upwards to be zero. We force the low degree terms to be zero by summing Stokes equation not from n = 2, but from $n = n_{max}$ which will force any information in the lower degree terms to be essentially zero. It will be necessary to guarantee that there is no error in these particular anomalies. I can show that N is generally small. A recent publication (RAPP

1973. *Op.cit.supra*) shows that the magnitudes from this region are quite small in relation to the errors in the gravity field.

MATHER: I would like to comment that Molodensky truncation functions were used to prepare a geoid map of Australia by GRUSHINSKY AND SAZHINA (1971. *J.geol.Soc.Aust.* 18,183-199) of the Soviet Union and we find that this technique gives good agreement with the Stokesian approach.

* This paper was presented on G. OBENSON'S Behalf by R.H. RAPP.

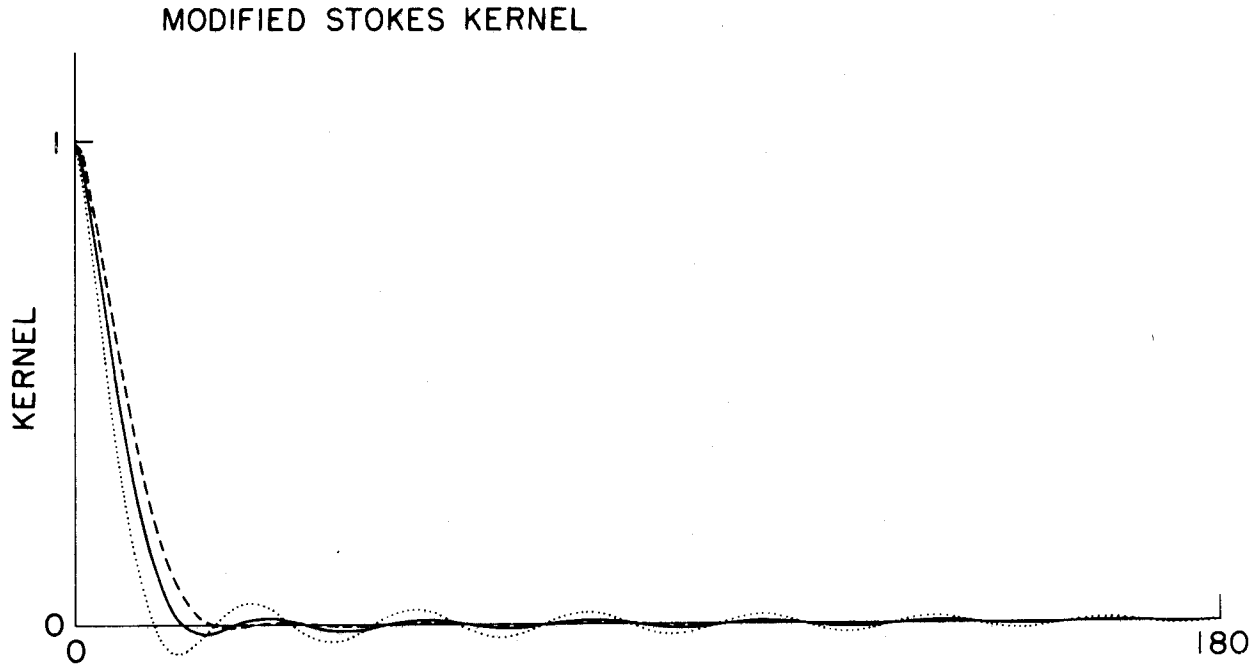

See comment by D. Eckhardt on p.186

NAGY, D.*
PAUL, M.K.
Gravity Division, Earth Physics Br,
Dept. of Energy, Mines & Resources
Ottawa K1A 0E4
Canada

Proc. Symposium on Earth's Gravitational Field & Secular Variations in Position (1973), 188.

GRAVIMETRIC GEOID OF CANADA *

ABSTRACT

A gravimetric geoid over Canada has been calculated from Stokes' formula. The gravity data used in this computation are in the form of $\frac{1}{2}^\circ$ block averages over Canada and a three degree belt beyond her southern boundary, $1^\circ \times 1^\circ$ mean values over a large part of U.S.A. and $5^\circ \times 5^\circ$ block averages over elsewhere.

The computed geoid refers to Reference System 1967 and indicates a marked depression of geoidal height at the western edge of Hudson Bay. While the position of the depression is in good agreement with similar studies made earlier, its magnitude of 60 m is significantly higher. Another local depression of the geoid is at the southern part of British Columbia-Alberta border.

The "local variations" of geoidal height due to $\frac{1}{2}^\circ$ and $1^\circ \times 1^\circ$ data set have been separately computed and their accuracy has been estimated to better than 1.0 m. The standard error of the regional contribution to the geoid height may, however, be as large as 5.0 m, when 20 mgal is assumed for the standard error of $5^\circ \times 5^\circ$ block averages.

1. Publication Details

The text and diagrams of this paper have been published. The relevant details are:

Contribution 499, Earth Physics Branch, Department of Energy, Mines & Resources, Ottawa, Canada.

2. Discussion *

LAMBERT: I understood you wanted a solution of the geoid to reduce satellite observations. Won't satellite observations themselves give all the accuracy required for geoid determinations?

WALCOTT: The contribution from the local geoid is the part not included in the coefficients and is as large as 20 m in some areas. The geoid obtained is very smooth. The main point I want to make is that if I took out the difference between observed gravity and that computed from satellite geoids, it would give a contribution of N_2 which is about 20 m. We want an accuracy of about 1 m.

LAMBERT: I was under the impression you could get 1-2 m from X, Y and Z.

WALCOTT: The X, Y and Z have been obtained to 1-2 m, but to obtain elevation at the point, you need the geoid to better than 1-2 m.

---

* This paper was presented on behalf of D. NAGY & M.K. PAUL by R.I. WALCOTT.

KEARSLEY, A. H. W.
School of Surveying
University of New South Wales
Kensington N.S.W. 2033
Australia

Proc.Symposium on Earth's Gravitational Field & Secular Variations in Position (1973),189-201.

DEFLECTIONS OF THE VERTICAL FROM GRAVIMETRY IN THE NARRABRI REGION OF NEW SOUTH WALES

ABSTRACT

The Narrabri-Manilla region of New South Wales has been chosen as a suitable area for testing the theories used for the computation of the deflection of the vertical by gravimetric means. This is because:

i) the national astro-geodetic networks through the area reveal it as a disturbed region; and

ii) the region contains a cross-section of terrains which enables testing under greatly varying conditions.

The expressions used in the computation are examined to test their relevance, both as to basic concepts used in their derivation and also to see the limitations inherent in terms related to correction for topography.

1. Introduction

1.1 Aim of the Paper

The computation of the deflection of the vertical by gravimetric means has received a lot of attention. Most of this has sprung from the solution offered by Molodensky, and has aimed at modifying his original formulae to obtain a more convenient computation and easier interpretation. To date the formulae have been successfully applied to theoretical models (e.g. MOLODENSKII ET AL 1962, p. 217) but, to the author's knowledge, these formulae or their modifications have yet to have had unqualified success in application to a real-life situation. There are two aspects which are the main cause of such failures, and it is naturally, difficult to tell how much either aspect is contributing to this failure. One is the lack in the coverage of gravity data and the other is the uncertainty of the behaviour of the terrain correction terms in areas of steep terrain.

The aim of this paper is to look at two of the approaches which have been developed for the computation of the deflection at the surface, to discuss the assumptions made at the various stages of the derivation, to try and predict the points of weakness in the resulting expressions when these are applied in the test region and to consider their adaptability for computational purposes.

1.2 Symbols

$d\sigma$	=	element of surface area on unit sphere.
dS	=	element of surface area on earth's surface.
dz	=	increment in orthometric elevation
$\frac{d}{d\psi}\{f(\psi)\}$	=	Vening-Meinesz function

$f(\psi)$	=	Stokes function
g	=	observed gravity at the Earth's surface
h	=	normal height above ellipsoid
h_d	=	height anomaly
$M\{\Delta g\}$	=	global mean value of Δg
N	=	elevation of geoid above spheroid
N_f	=	free air geoid
r	=	distance between point at which computation is taking place (P) and element of surface area dS
r_o	=	r on the surface of the sphere
r_1	=	r on the earth's surface
R_m	=	mean radius of the earth
R_p	=	radius vector at P
S_ϕ	=	distance along the meridian

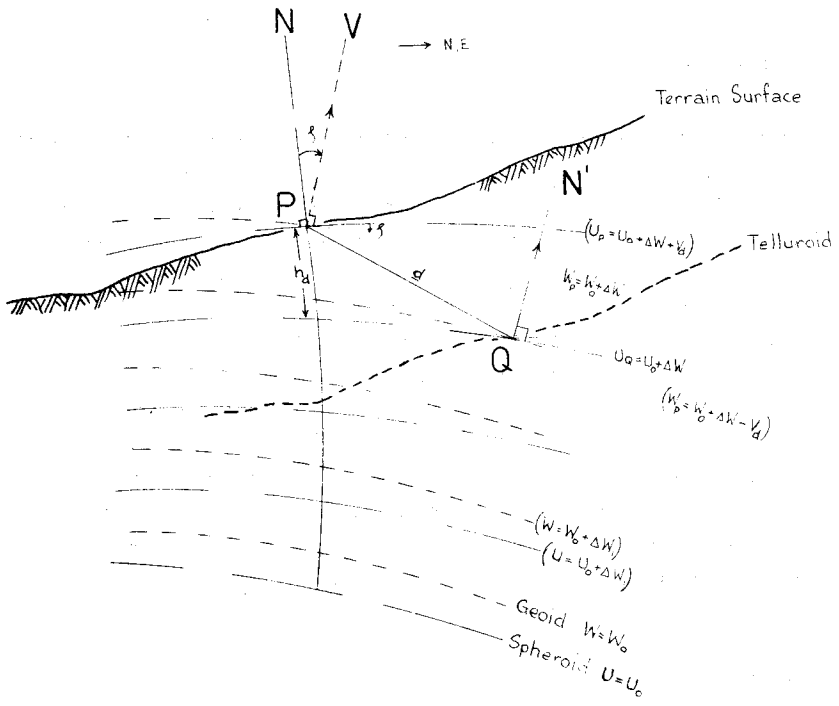

Figure 1. Deflections at the Surface

S_λ = distance along the prime vertical

U = potential due to the reference system (normal potential or spheropotential)

U_o = normal potential at the surface of the ellipsoid

V_d = disturbing potential

W = geopotential

W_o = potential of the geoid

x_i = local rectangular Cartesian coordinate system, where x_3 lies along the normal, and the x_1x_2 plane defines the local horizon (x_1 is North, x_2 is East)

α = azimuth

β = ground slope; subscripts 1, 2 refer to components in N, E directions respectively.

γ = normal gravity due to reference system.

Δg = free-air gravity anomaly at Earth's surface

ΔW = difference in potential between geoid and a generalised geop

λ = longitude, positive East

ξ = components of the deflection of the vertical; subscripts 1, 2 refer to component in N, E directions respectively; subscript p refers to deflection at P.

ε = deflection of the vertical; positive of outward normal lies North and East of the normal

Φ = a function of the density of the surface layer

ϕ = latitude, positive North

ψ = angle subtended at the geocentre between computation point P and element of the surface area, dS

2. The Test Area

2.1 Location and Nature

The area chosen for the test area is the Narrabri-Manilla region in the state of New South Wales, and lies 600 km north-west of Sydney and 300 km inland. It is bounded roughly by $-30^\circ07'$ to $-30^\circ52'$ in latitude and $+149^\circ45'$ in longitude. This region contains the junction of four sections of the astro-geodetic levelling network of Australia, and distributed through it are 12 astro-geodetic stations spaced about 30 km apart along the loops. These stations are reckoned to be fixed to an accuracy of about 0.4 arcsec in latitude and 0.8 arcsec in longitude (see MATHER ET AL 1971, p. 11).

There were a number of reasons for choosing this area. One was the abundance and distribution of control stations mentioned above. More importantly, computations already carried out showed large differences between the astro-geodetic values and those determined gravimetrically, indicating the shortcomings of the method used for computation in this disturbed region. The area encompasses a great variety of topographical types, ranging from the completely flat plains of the Wee-Waa district to the West to the very rugged and broken terrain of the Kaputar National Park. The control stations themselves are situated in terrain of varying types, grading from the flat, through the small symmetrical ad isolated hills, to foothills and finally rugged mountain ranges. It must be realised that the terrain itself is largely the reason for the anomalous deflections, nevertheless it is an advantage to have such a gradation as this should indicate at what stage the theory, especially that for inner and middle zones, will break down, and how much 'reinforcement' is needed to satisfy the limits of accuracy.

2.2 Gravity Data

Gravity in the area has been surveyed by the Bureau of Mineral Resources, Geology and Geophysics as part of their programme to provide a complete gravity coverage of the continent (see IBID, p. 7). This has resulted in a density of gravity readings of about 1 station per 16 km^2 in flat areas to 1 station per 8 km^2 in the mountains in the area of this test region. The density required for accurate computations is still somewhat a matter of conjecture, but has been variously thought to be (for mountainous areas) 1 point every 0.5 to 1 km within several kilometres of the control station (PELLINEN 1968) and "a .05 degree (5 km) grid within 0.5^o (5 km) of the control point, in addition to the 0.01^o grid within 0.1^o when evaluating using a computer" (MATHER ET AL 1971, p. 27).

Several field trips have been made to intensify the existing gravity field. As a general rule the aim has been to encircle the station with 6 to 10 gravity readings at a radius of about 2-3 km, with the existing density doubled to a distance of 8 km (all of these being chosen with an overriding consideration that the points be chosen in critical positions, such as at the foot of the hill or mountain).

Gravity was measured by a Worden gravimeter (kindly loaned by the Bureau of Mineral Resources) with traverses terminating at the Isogal Stations at either Narrabri or Tamworth. Height was determined in a number of ways. In some cases it was possible to use the third-order control stations or level runs placed for the mapping programme in the area, but usually (especially for inner zone stations) height was determined by trigonometric heighting with distances observed direct by EDM or found by subtense methods. In some cases height was fixed by single base altimetry over short distances. Position was found either by radiation from a known station or by scaling from the excellent 1:31 680 (2 inches to a mile) maps which cover most of the area.

The final accuracy of gravity values, especially those determined from the later trips, is expected to be of the order of 0.3 mgal.

3. The Gravimetric Approach to Plumb-Line Deflections

3.1 The Classical Approach

In the gravimetric approach to this problem, one is trying to determine the tilt of the normal equipotential surface, the spherop, to the actual equipotential surface, the geop. The classical approach to this is to consider these two surfaces at the level of the reference surface. It then becomes a matter of finding the rate of change of the separation of the geoid from the spheroid, N, in the direction of the two axes defining the local coordinate system.

Hence, (e.g. MEISKANEN & MORITZ 1967, p. 112)

$$\xi = -\frac{dN}{dS_\varphi} = \xi_1$$

$$\eta = -\frac{dN}{dS_\lambda} = \xi_2 \qquad \ldots (1)$$

which, when applied to Stokes Integral, result in the Vening-Meinesz expressions

$$\xi_j = \frac{1}{4\pi\gamma}\iint \Delta g \frac{d}{d\psi}\{f(\psi)\}\cos \alpha_j . d\sigma \quad \ldots j = 1, 2 \qquad \ldots (2)$$

where $\alpha_1 = \alpha$; and $\alpha_2 = 90 - \alpha$

It is worth emphasising that the problems associated with the solution of (2) are a direct consequence of the difficulties associated with Stokes solution and the evaluation of the separation of the geoid-ellipsoid system. This problem is well expressed by Brovar when he states " Geodesy can and must solve this problem (i.e.,of relating the geodetic survey at the surface to the ellipsoid - Author's comment) without involing any hypotheses concerning the internal structure of the earth" (BROVAR ET AL 1964, p. 91).

3.2 The Contemporary Approach

In 1945 Molodensky devised an approach which by-passed the need to reduce information to the elusive geoid. This approach has had a great impact on physical geodesy and methods are still being developed to provide efficient and practical means of solving the rather cumbersome expressions which derive directly from his formulation. Some of these methods will be treated later, but firstly it is necessary to show in simple terms the new geometrical concepts which evolved as a result of this new approach.

The surfaces of the earth (S) is thought to be represented by a second surface known as the telluroid. This was defined originally by HIRVONEN (1960, p. 39) as the locus of points whose positions were defined by the geodetic ϕ and λ of the surface point P and whose spheropotential was equal to the geopotential at the P. This (see figure 1) was the intersection of the normal through P with the spherop $U = W_p$. Definition in this way was inconclusive and a modified definition was suggested by DE GRAAFF-HUNTER (1960, p. 193). In this system the "Terroid" became the locus of associated points defined by the astronomically observed values of ϕ and λ for P on the spherop $U = W_p$ (see point Q, figure 1),

$$\text{i.e. } \phi_Q = \phi_{P_A} \quad , \quad \lambda_Q = \lambda_{P_A} \quad , \quad U_Q = U_o + \Delta W_P \qquad \ldots (3)$$

In terms of location and derivation this modification made little difference, but it did provide a more absolute definition for the position of the reference surface (hereafter called the telluroid) as its planimetric location was no longer relative to the local ellipsoid chosen for the geodetic computations. It can be seen that the telluroid is still a reflection of the terrain but is now slightly displaced (the displacement being a function of the deflection of the vertical) and that the normal to the spherop through Q has the same spatial orientation as the vertical through P. (For a more formal explanation, see MATHER 1968, pp. 34 and 42).

It is the height anomaly (h_d) between the geop W_p and the spherop $U = U_o + \Delta W$ which is the subject of the solution and, incidentally, which substitutes for N to produce a surface known as the "quasi-geoid" when referred to the reference surface, the ellipsoid. (See HEISKANEN & MORITZ 1967, p. 293; MOLODENSKII ET AL 1962, p. 76).

3.3 The Deflection at the Surface

The deflection of the vertical at P can now be defined as the small change in the separation between U_p and W_p for an increment in the distance along the surface W_p. This change in separation manifests itself as a change in the height anomaly (h_d) and hence the two components at the surface in the meridian and the prime vertical can be seen to be

$$\xi_{1_p} = \frac{dh_d}{dS_\phi}$$

$$\xi_{2_p} = \frac{dh_d}{dS_\lambda} \qquad \ldots (4)$$

The variable h_d is calculated at the telluroid, hence it is necessary to relate the separation of the two surfaces W_Q, U_Q at Q to the equivalent separation between W_p and U_p at P. This has been expressed as (MATHER 1971, p. 86; HEISKANEN & MORITZ 1967, p. 313)

$$\xi_{j_p} = -\frac{dh_d}{dx_j}_{W=W_p} = -\left(\frac{dh_d}{dx_j}\right)_{Tell} + \frac{dh_d}{dx_3} \cdot \frac{dx_3}{dx_j} \quad \ldots j = 1, 2 \qquad \ldots (5)$$

Where the second term is the correction to the differential at the telluroid and is seen to be the change in the height anomaly with height compounded with the change in the height of the telluroid in the direction being considered.

For completeness it should be recognised that the 3-dimensional axis system at Q does not have the same spatial orientation as the axis system at P, having suffered the small displacement ζ. The axis system at Q must therefore be resolved into the axis system at P.

$$\text{viz.} \quad \xi_j = \left\{-\left(\frac{dh_d}{dx_j}\right)_{Tell} + \frac{dh_d}{dx_3}\,\frac{dx_3}{dx_j}\right\} \cos \xi_j \quad \ldots j = 1, 2$$

which, on expanding cos ξ_j and accounting for the magnitude of ξ in Australia, will degenerate to (5).

The second term on the right hand side of (5) evaluates as $-\frac{\Delta g}{\gamma} \cdot \tan \beta_j$ where β_j is the slope of the ground (this being equivalent to the telluroid slope at the associated point). This term, as has been shown in HEISKANEN & MORITZ (1967, p. 314) and MATHER (1971, p. 88) compensates with part of the first term in the expression being considered when this term is expanded.

The evaluation of this first term will obviously depend upon the approach adopted to find the height anomaly. Two approaches will be referred to (i) Molodensky's approach, using surface layer techniques and (ii) the approach which uses as a starting point Green's third identity. A summary of these approaches can be found in (MATHER 1973, pp. 21-28 and pp. 32-43), but for a more detailed development the reader is referred to MOLODENSKII ET AL (1962, pp. 118-124) and HEISKANEN & MORITZ (1967, pp. 300-312) for the former approach, and for the latter approach MATHER 1970, pp. 10-21 and MATHER 1971, pp. 78-86.

4. The Height Anomaly and its Differential

4.1 By Surface Layer Techniques

4.1.1 Derivation

This approach is based on the premise that the potential relating to a body can be expressed in terms of an attracting layer on the surface of that body. This is extended to express the disturbing potential (and not the potential) in terms of the layer

$$\text{i.e.} \qquad V_{d_p} = \iint_\sigma \frac{\Phi}{r} \, dS \qquad \ldots (6)$$

where Φ is related to the density of the surface layer on S which is held to be producing the disturbing potential V_{dp} at P.

The development of the theory is well known (see MOLODENSKII ET AL 1962, pp. 118-124) and will not be repeated here. The end product is an expression which gives both the height anomaly and (subsequently) the deflection in terms on a series of successive approximations of the density of the anomalous surface layer, in turn expressed as a function of the surface gravity anomalies and corrections to these at each point for the irregularities of the earth's surface.

Hence, to the second order, it is found that

$$h_d = \frac{R}{4\pi\gamma} \iint_\sigma (\Delta g + G_1 + G_2) \, f(\psi) \, d\sigma - \frac{R^2}{4\pi\gamma} \iint \frac{(h-h_p)^2}{r_o^3} \, \Delta g \, d\sigma \qquad \ldots (7)$$

and

$$\xi_j = \frac{1}{4\pi\gamma} \iint_\sigma (\Delta g + G_1 + G_2) \frac{d}{d\psi} (f\psi) \cos \alpha_j \, d\sigma$$

$$+ \frac{3R^2}{4\pi\gamma} \iint_\sigma \frac{\cos \frac{1}{2}\psi}{r_o^4} (h-h_p)^2 \, \Delta g \cos \alpha_j \, d\sigma - \frac{\Delta g + G_1}{\gamma} \tan \beta_j \qquad \ldots j = 1, 2 \qquad \ldots (8)$$

where

$$G_1 = \frac{R^2}{2\pi} \iint_\sigma \frac{h-h_p}{r_o^3} \, \Delta g \, d\sigma$$

and

$$G_2 = \frac{R^2}{2\pi} \iint_\sigma \frac{h-h_p}{r_o^3} \, G_1 \, d\sigma + \Delta g . \tan^2 \beta$$

α_j is defined in (1).

Some of the methods devised to modify the above are considered below.

4.1.2 Practical Evaluation

A summary of some of the approaches developed to evaluate equation (8) can be found in (PELLINEN 1968). Some use mathematical devices to simplify the expressions. Others, by modifying the original concept have used a different physical model as the starting point and have thus made modifications.

(a) In 1962, Pellinen suggested an approach which aims at removing the effect of the topography from the general solution and independently evaluating the effect the 'removed' topography will have on the deflection. This method as originally developed is given by PELLINEN (1962) and is also outlined by MORITZ (1969, pp. 27-30).

The free-air anomaly at the surface is adjusted to account for the contribution made to this anomaly by the topography above a stated reference surface.

i.e. $\Delta g_c = \Delta g - \Delta g_T$

where Δg_c is the anomaly corrected for topography
Δg is the free-air anomaly at the surface
and Δg_T is the contribution to g of the topography

Δg_c is substituted for Δg in the Equations (7) and (8) to find the parameters defining the anomalous field at the reference surface. Thus, to a first order approximation, we find

$$\xi_j = \frac{1}{4\pi\gamma} \iint_\sigma (\Delta g_c + G_{1_c}) \cdot \frac{d}{d\psi} \cdot \{f(\psi)\} \cdot \cos\alpha_j \cdot d\sigma + \Delta\xi_{j_T} \qquad \ldots (9)$$

where

$$\xi_{j_T} = -\frac{k\rho R^3}{\gamma} \iint \frac{h-h_p}{r_o^2 r_1} \cdot \sin\psi \cdot \cos\alpha_j \cdot d\sigma$$

G_{1_c} = G_1 with Δg_c substituted for Δg.

As mentioned by Moritz, an advantage in this approach is that the G_{1_c} values will be similar and smoother than the G_1 values in the original expression (8). However, Δg_c may attain large values being in essence the Bouguer anomaly, as might the corrections $\Delta\xi_{j_T}$. A device to alleviate this problem has also been suggested by PELLINEN (1968) (see also MORITZ 1969, pp. 30-33).

A spherical surface, concentric to the original reference surface at sea level and passing through the computation point P, is held to have a surface layer of density ρh which produces an anomalous potential field. The gravity anomaly resulting from this surface layer will have a compensating influence on the mass of the topography removed in the aforementioned approach. If the anomaly accumulating in this way (which is shown to be the Faye anomaly, the free-air anomaly plus the terrain correction only) is now used in place of Δg_c in the earlier expression (9), and due consideration given to the correction term which results, it is found that (MORITZ 1969, p. 31)

$$\xi_j = \frac{1}{4\pi\gamma}\iint_\sigma (\Delta g + C)\,\frac{d}{d\psi}\{f(\psi)\}\,\cos\alpha_j\,d\sigma$$

$$+ \sum_{n=1}^{\infty}\frac{1}{4\pi\gamma}\iint_\sigma \bar{g}_n\,\frac{d}{d\psi}\,f(\psi)\,\cos\alpha_j\,d\sigma + \delta\xi_j \qquad \ldots\ j = 1, 2$$

where $\Delta g + C$ is the Faye anomaly.

$\bar{g}_n$ are the correction terms computed using the Bouguer anomalies

$$\text{and } \delta\xi_j = \frac{k\rho R^3}{\gamma}\iint \frac{h-h_p}{r_o}\left(\frac{1}{r_o} - \frac{1}{r_1}\right)\sin\psi\,\cos\alpha_j\,d\sigma \qquad \ldots\ j = 1, 2$$

$$C = k\rho R^2 \iint_\sigma \left(\frac{1}{r_o} - \frac{1}{r_1}\right) d\sigma \qquad \ldots\ (10)$$

By using this device the gravity anomalies and the correction term $\delta\xi$ are both reduced in size. Also, as with the first approach, the uncertainty of the density of the sub-surface is overcome because it is compensated when the correciion term is added. The adoption of the reference surface passing through the computation point (as in the second approach) should also improve the convergence of the higher order terms, and improve the accuracy of the first order approximation.

(b) The other type of approach used in solving Molodensky's expression use mathematical devices in order to simplify them. In this respect it is worth mentioning a method developed by MORITZ (1969) who uses analytical continuation of the gravity anomaly from surface to sea level and thus gains a solution by means of successive approximations. While some doubts about the validity of this approach (i.e. continuation below the surface of the attracting body) are expressed, it is felt to be justified by the equivalence gained with matched terms of the modified Molodensky approach. In this way, MORITZ (1969, pp. 35-37) derives to second-order accuracy

$$\xi_j = \frac{1}{4\pi\gamma}\iint_\sigma (\Delta g + g_1 + g_2)\,\frac{d}{d\psi}\,\{f(\psi)\}\,\cos\alpha_j\,d\sigma \qquad \ldots\ j = 1, 2$$

where

$$g_1 = -(h-h_p)\,L_1(\Delta g)$$

$$g_2 = -\tfrac{1}{2}(h-h_p)^2\,L_1\{L_1(\Delta g)\} - (h-h_p)\,L_1(g_1)$$

$$\text{with } L_1(f) = \frac{R^2}{2\pi}\iint \frac{f-f_p}{r_o^3}\,d\sigma \qquad \ldots\ (11)$$

Moritz claims that, though for all practical purposes this is identical with Molodensky's original expressions, it is an easier statement to evaluate. A big advantage from the computing viewpoint is that successive terms of the series are evaluated recursively, although it is probable that the 2nd order is as high an order as is needed for most cases.

Nevertheless, their expressions do appear simpler to evaluate than those in (6), although care must be taken to ensure the terms converge significantly. To assist in this, as Moritz states, it is possible to substitute the Faye anomaly for the free-air anomaly in (11) and apply the corrections as per (10). Now the g_1 and g_2 terms being computed from the Bouguer anomalies will be smaller and this should aid convergence.

Obviously for inner zone computations a device such as is used in 4.2(b), or as suggested in ARONOV ET AL (1971), using an intermediate step, will have to be adopted.

4.2 By Green's Third Identity

4.2.1 Derivation

The disturbing potential when expressed in terms of Green's Third Identity is used to obtain the height anomaly

$$h_d = \frac{W_o - U_o}{\gamma} - R_m \{\Delta g\} + \frac{R_m}{4\pi\gamma} \iint_\sigma \Delta g . f(\psi) . d\sigma$$

$$+ \frac{R_m^2}{2\pi\gamma} \iint_\sigma \frac{1}{r_o} \left[\{(h_p - h) + R_m \sin\psi \frac{dh}{dr}\} \frac{V_d}{r_o^2} - \gamma \xi_j \tan\beta_j \right] d\sigma$$

(See MATHER 1971, pp. 78-86 for derivation)

Differentiating this with respect to the two axes defining the horizontal plane at P, the tilts of the two equipotential surfaces in these directions result as the sum of two components, that directly contributed by the Vening-Meinesz expressions, and a correction to this for the departure of the topography from the (ideal) reference surface, viz.:

$$\xi_{p_j} = \frac{1}{4\pi\gamma} \iint_\sigma \Delta g \frac{d}{d\psi} \{f(\psi)\} \cos\alpha_j \, d\sigma$$

$$+ \frac{R}{2\pi\gamma} \iint_\sigma \left[\left(\{ (R.\sin\frac{dh}{dr_o} + h_p - h) \frac{-3\cos\frac{1}{2}\psi}{2\sin\frac{1}{2}\psi} + R\cos\psi \frac{dh}{dr_o} \right\} \frac{V_d}{8R^3 \sin^3\frac{\psi}{2}} \right.$$

$$\left. + \frac{\gamma\cos\frac{1}{2}\psi}{4R\sin^2\frac{1}{2}\psi} \xi_j \tan\beta_j \right) \cos\alpha_j + (-1)^j \frac{R\sin\psi}{8R\sin^3\frac{1}{2}\psi} \frac{d}{dx_o} \left(\frac{dh}{dr_o}\right) V_d \frac{\sin\alpha_j}{\sin\psi} \Bigg] d\sigma$$

$$\ldots j = 1, 2 \qquad \ldots (12)$$

(see IBID, pp. 86-89 for full development)

4.2.2 Practical Evaluation

For computation purposes (12) can be greatly simplified by dividing the area involved into 3 zones, (see outer, central and inner zones) and assuming a planar approximation for the inner and central zones, with outer zone computations ($>3^o$) made on a spherical model. This reduces the expression (15) to

(a) *The Stokesian Term*

$$\xi_{f_{p_j}} = \frac{1}{4\pi\gamma}\int_{\psi_o}^{\pi}\int_{0}^{2\pi} \Delta g \frac{\partial}{\partial\psi}\{f(\psi)\}\cos\alpha \, d\sigma \qquad \ldots j = 1, 2$$

$$- \frac{1}{2\gamma} r_i \left(\frac{d\Delta g}{dx_j}\right)\left(1 + \frac{3x_i}{4R}\right)$$

The first term being the familiar Vening-Meinesz formula applied to central and outer zones, and the second term the inner zone contribution to this quantity.

(b) *The Terrain Correction Term*

$$\xi_{c_{p_j}} = \frac{1}{2\pi}\int_{\psi_o}^{\psi}\int_{o}^{2\pi} \left\{\frac{1}{\psi^2}\sum_{k=1}^{2} \xi_{f_k} \tan\beta_k - \left[\left(2\frac{dh}{dr_o} + 3\frac{h_p - h}{R}\right)\cos\alpha_j + \right.\right.$$

$$\left.\left.(-1)^j \frac{\partial}{\partial A_c}\left(\frac{dh}{dr_o}\right)\sin\alpha_j\right]\frac{N_f - N_{f_p}}{\psi^3}\right\} d\sigma \qquad \ldots j = 1, 2 \qquad \ldots (13)$$

where $\psi' = 3^o$, $\psi_o = 0.01^o$ i.e. 1 km

and $\frac{dh}{dr_o} = \cos\alpha_c \tan\beta_1 + \sin\alpha_c \tan\beta_2$

$$\frac{d}{dx_c}\frac{dh}{dr_o} = -\sin\alpha_c \tan\beta_1 + \cos\alpha_c \tan\beta_2$$

$$\alpha_c = 180^o - \alpha$$

Here the introduction of the term $N_f - N_{f_p}$ is an equivalent to a zero-degree datum shift and is analogous to the introduction of a reference surface through P mentioned in 4.1 (a) of the surface layer solution. It entails a knowledge of the geoid-spheroid separation at all points involved in the middle zone computation and this can be obtained (if not already known) from the data which is to be used in the computations.

Similarly the term $\xi_\alpha \tan\beta_\alpha$ will generally be small, so zero-approximation values for these can be computed as a first step and stored ready for use as part of the programme.

5. Conclusions

Although the above expressions have not yet been tested for the region under investigation, it is worthwhile trying to predict how they will behave under the conditions which prevail there. It is, in this respect, useful to note the results of an investigation by DIMITRIJEVICH (1972) who calculated the affect of the terrain correction (equivalent to G_1 in expression (8)) on the deflection at a number of control stations in the United States.

The greatest topographic effect is down the west coast of the continent where mountains reach about 4 000 metres above sea level, and it was mainly in this region that the gravity anomalies received the correction. The results of the computation showed that for a station lying 4^{o} east of the mountain range the terrain corrections introduced about .4 arcsecs into the prime vertical component (with, understandably little effect being felt in the meridional component). This effect attenuated as the computation point moved eastward. It also lessened when the computation point was taken in the mountains themselves, suggesting a compensatory effect due to the rough symmetry of the terrain about the control station.

In the test region under investigation a similar situation exists. On the western edge plains stretch north west and south with the Nandewar Ranges to the east. The inner zone will easily satisfy the planar assumption, but the central zone, being unsymmetrical in the east-west direction is expected to introduce large corrections into the value for ξ_2. This will be further complicated by the irregularity and steepness of the terrain to the east manifesting as an uncertainty in the β or $h-h_p$ and N_f-N_f terms. There may also be problems in obtaining convergence in the G_1 and G_2 terms in this area, and the use of the Faye anomaly should help to alleviate this. There will be a further uncertainty in ξ_2 introduced by the fact that for the outer zone, the region to the East becomes ocean. This means that, although the spherical approximation will hold good, Δg values will be poorer. The use of the Stokesian approximation for the expansions of the outer zone in the other three directions will also be valid particularly to the west. The north/south extensions will probably not hold so well, as to the south at $\psi = 6^{o}$ one meets the Snowy Mountains region with mountains reaching 2 500 m and to the north at $\psi = 22^{o}$ lies New Guinea with its rugged mountain systems. Also, the use of the free-air anomaly in such large mountain passes as the Himalayas is a source of systematic error, and here the technique which applies terrain corrections should prove stronger.

Moving eastward into the mountains themselves one is confronted with more problems relating mainly to the assumptions of planarity in the derivation. It will be necessary to reduce the inner-zone radius, perhaps even to as little as 200 m, and it may well be that the intensified gravity field may still prove insufficient. It is fortunate that the area is well mapped andinterpolations may prove to be sufficient to strengthen the field. There will be some 'balancing' of the terrain effects due to a closer approximation to symmetry in the central zone. Even so it may well be that the assumptions prove inadequate and a more rigorous approach will have to be applied.

6. Acknowledgements

Thanks is due to the Bureau of Mineral Resources, Geology and Geophysics (Canberra) for the loan of the Worden Gravimeter used in the surveys to date.

7. References

ARONOV, V. E. & GORDON, V. M. ET AL 1971. "A Program for computing Deflections of the Vertical in a Central Zone". *Geodesy and Aerophotography* (Trans.) 4, 190-192.

BROVAR, V.V., MAGNITSKIY, V.A. & SHIMBIREV, B.P. 1964. *The Theory of the Figure of the Earth.* (Transl.) Clearinghouse for Federal Scientific & Technical Information, Washington DC, AD 608975.

DIMITRIJEVICH, I.J. 1972. The Use of Terrain Corrections in Computing Gravimetric Deflections of the Vertical Components and Geoid Heights. *53rd Annual Meeting of American Geophysical Union*,Washington DC.

GRAAFF-HUNTER, J.DE 1960. The Shape of the Earth's Surface in Terms of Gravity at Ground Level. *Bull.géodés.* 56,191-200.

HEISKANEN, W.A. & MORITZ, H. 1967. *Physical Geodesy.* Freeman,San Fransisco.

HIRVONEN, R.A. 1960. New Theory of the Gravimetric Geodesy. *Suomal.Tiedeakat.Toim A III* 56.

MATHER, R.S. 1968. The Free Air Geoid in South Australia ..... Gravitational Field. *UNISURV Rep.* 6,University of New South Wales,Kensington NSW,491 pp.

MATHER, R.S. 1970. The Australian Geodetic Datum in Earth Space. *UNISURV. Rep.* 19,University of New South Wales,Kensington NSW,130 pp.

MATHER, R.S. 1971. A World Geodetic System from Gravimetry. *Geophys.J.R.astr.Soc.* 23,75-100.

MATHER, R.S. 1973. Position from Gravity.* *Doc.X*-592-73-164,Goddard Space Flight Center,Greenbelt Md.

MATHER, R.S., BARLOW, B.C. & FRYER, J.G. 1971. A Study of the Earth's Gravitational Field in the Australian Region. XV General Assembly IUGG,Moscow. In *UNISURV Rep.* 22,1-41.

MOLODENSKII, M.S., EREMEEV, V.F. & YURKINA, M.I. 1962. *Methods for Study of the External Gravitational Field and the Figure of the Earth.* Israel Program for Scientific Translations,Jerusalem.

MORITZ, H. 1968. On the Use of the Terrain Correction in Solving Molodensky's Problem. *Rep.* 108, Department of Geodetic Science,The Ohio State University,Columbus Ohio.

MORITZ, H. 1969. Non-Linear Solutions of the Geodetic Boundary Value Problem. *Rep.* 126,Department of Geodetic Science,The Ohio State University,Columbus Ohio.

PELLINEN, L.P. 1962. Accounting for Topography in the Calculation of Quasi-Geoidal Heights and Plumb Line Deflections from Gravity Anomalies. *Bull.géodés.* 63,57-65.

PELLINEN, L.P. 1968. Comparison of Different Methods for Computing the Plumb Line Deflections in Mountainous Areas. *Bull.géodés.* 89,345-354.

8. Discussion

RAPP: About eight months ago a dissertation was submitted by a graduate student (EMRICK, H.) at Ohio State University that discussed, among other things, techniques for computing deflections of the vertical at Pike's Peak in the Colorado Rockies. The idea was to use the G_1 term of Molodenskii, the modification $\overline{G}_1$, the terrain correction and the two corrections you mention g_1 and g_2. He used blocks down to 200 m squares and carried out computations to about 150 km from the computation point at several points. He computed deflections of the vertical using four different techniques including the Bjerhammar iteration down to the reference sphere and compared the differences. The maximum difference was probably less than one second between the uncorrected deflections and the various correction terms. The differences between the various correction term models was a maximum of 0.5 sec.

---

* See pp. 117-153 of these Proceedings

GENERAL DISCUSSION ON SESSION C - (H.MORITZ AS CHAIRMAN)

MUELLER: (To MATHER) How can you get a value of W_o from a global geoid solution like that produced by VINCENT ?

MATHER : Stokes' integral as commonly known is insensitive to terms of zero degree. The formulation of the boundary value problem in terms of gravity anomalies at the surface of the Earth can be made without making any assumptions on this account. It is not possible to draw any conclusions about the term of zero degree without external constraints as there is one term W_o which is unknown at *some* level of precision. We do not know the potential of the geoid to 1 part in 10^7 at the present time.

MUELLER: You therefore state that in addition to a solution of the boundary value problem, it is necessary to have an external constraint before a value can be obtained for W_o?

MATHER: Yes.

MORITZ: How does the geoid in Canada compare with the VINCENT-MARSH global geoid?

WALCOTT: I couldn't say at this time as I haven't seen the detail of their geoid.

MUELLER: You said that the N_3 term is in the order of 0 - 20 m. You also stated that it is negligibly small. Which statement is true?

WALCOTT: My statement is true. What may not be true is the data in the Bulletin Geodesique reference. RAPP might like to comment on that?

RAPP: I am trying to recall the Bulletin Geodesique article and I dont recall the global five degree anomaly field.

WALCOTT: The techniques are right but the data may be questionable.

MATHER : I would like to comment on the methods of solution used, assuming we are using the level of data dealt with in the preparation of the three geoid maps presented today. VINCENT mentioned that only an (8,8) solution was needed to adequately represent distant zone effects in such solutions. The use of Molodenskii truncation functions should adequately cover the contribution of outer zone effects, provided the inner zone were well represented by surface gravity. This technique has been used by some Russian groups to prepare geoid maps. There is a certain uncertainty in the present techniques as it is not clear where the surface gravity representation ends. A presentation later in this symposium by Y. HAGIWARA will illustrate the use of this technique.

WALCOTT: Surely the technical problem is that there is insufficient data?

MATHER: The practical consequences are marginal, but the technique is neater.

MUELLER: I would like to refer to VINCENT's map. From strictly geometrical satellite solutions, we compared his undulations at 158 stations around the globe and the average difference was 0.2 m. This is a pretty good geoid solution.

WALCOTT: A stepwise function was used to fit data across the US border. There are differences between ACIC data as compared with our (Canadian) data in contiguous positions.

MATHER: Has the discrepancy between the Ottawa datum and the Washington Datum been taken into account (when preparing the Canadian geoid map)?

WALCOTT: Yes they have. The differences between ACIC data and our data are not systematic.

MUELLER: As MATHER pointed out, the question is the extent of the wavelength of the systematic error. Hopefully they are not of long wavelength.

GRAFAREND: A comment to MATHER. You mentioned the approximation of your solution up to the order of e^3. I have some doubts because the basic formulation of the problem is only correct to the order of e^2. We have studied the linearity and non-linearity problems in some detail and have found that especially vertical deflection calculations are very sensitive to higher order terms in the formulation. A recent reference to the problem of a non-linear formulation of the geodetic boundary value problem is the contribution of M. PICK (1973. *Studia geod. et geophys.* 17,173) where the influence of the higher order terms on regional effects is shown for the region of CSSR and cannot be ignored, even for geoidal undulations. Thus, the accuracy of some solution is also dependent on the accuracy of the formulation of the problem. The central question is how accurate the linear formulation is. *

MORITZ: As far as the accuracy of the data goes, the present formulation should be sufficient and there are many other factors that come in, for example, problems of computing those second and third order terms in the linear formulation. There is also the question of numerical errors due to lack of data which may be much larger.

MATHER: Another important question is deciding on whether or not a uniform method should be adopted for processing gravity information so that the "best" solution can be obtained from irregularly distributed information. Take the three geoid maps presented today. VINCENT ignored higher degree effects in those areas where no one degree information was available (equivalent to representation by the spherical harmonic model); I presume NAGY & PAUL adopted a similar procedure, while it would appear that OBENSON did a covariance analysis for prediction purposes. These are different approaches. There is a case to be put forward for a uniform approach. I do not know whether there is a clear cut answer to this problem.

MORITZ: I don't quite know what you mean by uniform processing. There is a related topic which can be more fully discussed at the appropriate session (Session I) - the optimum treatment of existing data since this problem involves statistical considerations.

MATHER: Maybe something could be said in general terms as it is felt that the differences in the solutions is due in part, to the different methods used to process the data.

MORITZ: Yes. Since the data is largely the same, differences in answers will always be due to the different procedures used. The various procedures should be encouraged so long as they are proceeding on valid lines.

QURESHI: How do you define random and systematic error? We talk about different persons processing data differently. A systematic error in one set of data (processed by one person) may be random in the global context.

MATHER: Significant sources of systematic error in surface gravity anomalies are firstly those in the datum for observed gravity, and secondly those in the height datum. We assume that

all datums are located on the same equipotential surface. The boundary value problem, as commonly formulated is dependent on the term ΔW with respect to the geoid. Irrespective of whether errors on this account are due to levelling errors (as maintained by oceanographers) or so-called sea surface topography, we still have the effect on the data. These are sources of systematic error of long wavelength. A numerical manipulation could be performed to get rid of these effects. An example of random effects are elevation errors at individual gravity stations.

QURESHI: How about marine gravity observations where we have large errors with an accuracy of ± 5 mgal?

MORITZ: There are two different sorts of errors. Firstly there are measuring errors and secondly there are interpolation errors in gravity observations which are taken along profiles. The latter errors may be larger.

---

*Post-Symposium Reply from MATHER: Having since read PICK's paper, it can be stated that the basis for his development had already been taken into consideration in the solution to order e^3 referred to.

BOULANGER, J.D.
Institute of Physics of the Earth
Academy of Sciences of the USSR
Moscow
U S S R

Proc. Symposium on Earth's Gravitational Field & Secular Variations in Position (1973), 205-212.

SECULAR VARIATIONS IN GRAVITY

1. Text

The problem of secular variations of gravity is one of the acute problems of gravimetry and has fundamental interest for such sciences as metrology, physics, astronomy, geodesy, geophysics and geology. This is explained by the fact that the complex set of data on recent crustal movements, gravity variations, irregularity of the Earth's rotation and oscillations of the world ocean level allows the evaluation of the displacement of masses within the Earth, thus providing new data about the dynamics and, consequently, the history of development of our planet.

This is a complex task which shall demand long-standing efforts of an extensive group of specialists. Its integral part is the study of gravity changes in time in a wide spectrum of frequencies caused both by endogenous and exogenous processes. In this study, the determination of the fact of gravity changes in time is decisive.

The initial stage of researches in this field started as far back as the twenties when such great discrepancies in the g values were obtained at repeated gravity determinations, that it was difficult to explain them only in terms of the errors of measurement. This gave grounds for some of the authors (ABAKELIA 1936a; ABEKELIA 1936b) to draw a conclusion about the possibility of considerable gravity variations in time, which reach several microgal per year, associating them with tectonic processes occurring in the Earth's interior.

Further works proved these conceptions to be erroneous. Thus PARIISKY (1937), analysing the processes which can cause the irregularity of the Earth's rotation, has shown for the first time that such processes can be either the vertical movements of large sections of the Earth's crust or the transformation of the matter within the Earth with a noticeable change of density. Both these reasons can cause the change of gravity on the Earth's surface, but they must be small and not exceed tenths of microgal.

Much later BARTA (1957; 1962; 1963; 1965; 1967) and then VOGEL (1968) have suggested a hypothesis about the possible gravity changes in time, caused by the displacement of the Earth's core in respect of its mantle. According to their calculations, the gravity variations can reach tenths of microgal per year and can have quasi-periodic character with the period of about 500 - 1000 years.

As a result of researches of vertical crustal movements carried out by KALASHNIKOVA (1970), it was established that a large part of depressions and uplifts develops independently of the basic gravitational fields. This provides grounds for supposing that vertical movements are caused by compression or extension of deep material without change of the general mass, i.e., in this case, transportation of the matter within the Earth does not cause gravity changes on its surface.

Comparison of these two concepts indicates our extremely limited knowledge of processes that cause the dynamics of the globe. At the same time, success in experimental gravimetry, in measurements of variations in the rotation rate of the Earth, in geodetic measurements provide opportunities to approach the solution of this problem not only from the point of view of theoretical studies, but also by special experiments. We already have the capability to accumulate experimental data, without which the solution of this most important problem is impossible.

What are the data available to us at the present moment?

Of outstanding importance in the field of experimental gravimetry for the last decade are the works of Sakuma who elaborated the instrument for absolute gravity determinations with the accuracy of ±1 to ±2 parts in 10^9. By means of this instrument he has established the gravity acceleration in Sèvres, France, with the rate of about 20 microgal per year. This result is of extreme importance and opens new ways to further studies in this field.

At the same time, since it is as yet the only result, it is rather difficult to have a clear conception even whether the phenomenon is of global, regional or local character. Only the establishment of similar stations in other regions of the globe or the undertaking of special additional measurements with highly sensitive gravimeters can provide grounds to obtain the answer to this problem in the future.

I am not aware of any attempts to find explanations of causes of this change. A certain exception is the paper by BURSA (1972). He showed the influence of the movement of the pole which can reach 5 microgal per year, and is in agreement with the results obtained by Sakuma.

During the last 15 - 20 years, several attempts were made to discover the secular or spontaneous changes of gravity of both regional and local character. Of greatest interest as regards the results obtained are the works of Torge (SCHLEUSENEER & TORGE 1971) and of the Japanese colleagues Satomura and Nakagawa (SATOMURA & NAKAGAWA 1972; NAKAGAWA 1972).

The changes of gravity obtained in Iceland by Torge are not large and on the verge of measurement accuracy. Though their analysis and processing are carefully done, actual comparisons can be carried out only between two epochs of measurements conducted in 1965 and 1970. Thus, for this region, only one result was obtained with relative reliability. And in the case where the measured values are on the accuracy limit, it is difficult to consider such conclusions as reliable. It is widely acknowledged that in similar cases it is sufficient to have an insignificant systematic effect on measurements in one of the epochs and the result, based even on very well statistically processed data, can be erroneous.

At the same time, the works of Torge deserve serious attention, since for the first time they experimentally establish the fact of gravity change caused, perhaps, by tectonic processes.

Of no lesser interest are the works on the study of gravity changes in the region of Lake Biwo-Ko. As a result of these measurements, a decrease of gravity was established in the southern part of the lake for three years on the average 50 - 100 microgal, i.e., with a rate of the order of 15-30 microgal per year. These results were compared with the variations of the level of the lake and changes of heights caused by recent crustal movements. However, agreement is obtained only in tendency. The changes in heights of water level can explain only a small part of the variations. The authors therefore tend to ascribe these changes to the variations in the crustal density caused by tectonic

processes.

In the Soviet Union, the works on the study of secular gravity variations were started in 1935. But only in 1954-55 were the first measurements accomplished for that purpose along the line Potsdam - Petropavlovsk-on-Kamchatka, and on several points in the Caucasus and in middle Asia. The points were chosen in such a way as to cover with measurements, regions tectonically quiet and seismically active (BOULANGER & SCHEGLOV 1971). Repeated observations were carried out ten years later in 1964. Notable changes of gravity were not detected. All the measurements were much less than the errors of their determination. As the result of their careful processing, a conclusion was made that if gravity changes occurred at the indicated points, they did not exceed 10 microgal per year.

Similar observations were conducted at a number of points in eastern Europe in 1958 and 1968. The same result was obtained here. The changes of gravity were less than the errors in their determination and the annual rates could not be more than 10 microgal.

Commencing in 1970, systematic repeated observations of gravity were carried out at points along a closed polygon Moscow - Sverdlovsk - Perm - Petrozavodsk - Moscow. These measurements have also not detected changes in gravity. All deviations were less than their errors.

In recent years in the scientific publications of the Soviet Union, a number of works (SOBOKAR 1968; FAITELSON 1969a; FAITELSON 1969b; FAITELSON & AZARKINA 1970; FAITELSON & AZARKINA 1972; SHRAIBMAN 1971; SIROTOV & PARFENOV 1970) were published, which present data on gravity variations with time, obtained as the result of comparison of gravimetric maps compiled in different years. Comparisons were made of the maps of the Baikal region, the Ukraine, the Volga region and the northern Caucasus. According to the opinion of the authors of these works, they have discovered gravity variations which have a good correlation with the tectonics of these regions. Moreover, the variations reached several tenths of microgal per year.

The experience of highly accurate repeated relative determinations of gravity testifies to considerable difficulties of comparison of data of different epochs. It is done with reliability only for separate points with their precise identification and the presence of complete information on the metrology of measurements. At the slightest inaccuracy in this information, as a rule, the measurements show systematic errors which considerably distort the conclusions. It is therefore rather difficult to agree with the reality of the data obtained on the basis of comparison of repeated area surveys.

Thus, careful analysis of the world literature shows that at the present moment, extremely scanty data are available for characterising gravity changes in time. The problem arises, what is to be done to accumulate them at a greater rate, so that we can have as soon as possible, the data characterising the dynamics of the globe by gravimetric data.

In this connection, I would like to make a few comments on the possible organization of international works for the study of gravity changes in time.

In the first place, it would be necessary to find out the representativeness of secular variations of gravity obtained in Sèvres. This can be done by comparatively simple means using relative methods of measurements. In order to reveal the local component, it is necessary to establish a reliable control of the stability of the altitude of the station and organize a network of gravimetrical points located at distances ranging from 1-2 km to 25-30 km from Sèvres, and to tie them directly to the

point at Sèvres. At the rate of changes around 20 microgal per year, using modern gravimeters, in 2-3 years we can obtain a reliable answer to the problem whether the observed phenomenon is local or regional.

In the case when the local character of the phenomenon is not evident, then gravimetrical measurements should be conducted along the line of latitudinal direction several hundreds of km long, and passing through Sèvres. Repeated observations on that line already in three years should be able to considerably elucidate this problem, and in five years produce an unequivocal answer about the character of the observed phenomena in Sèvres.

Considering the importance of measurement of secular variations of gravity in the equatorial zone, since actually in this zone the displacement of mass has its greatest influence on the Earth's rotation, it seems apparent to ask the countries having portable equipment for the absolute determination of gravity, to undertake absolute determinations annually at a number of points. In the first place, according the calculations of Barta, these observations should be organized in the region of Rangoon (Burma), Teheran (Iran), Tripoli (Libya), Accra (Ghana) and in the central part of Brazil. With an accuracy of measurements even of the order of ±1-2 parts in 10^8, we can expect in 3 - 5 years to obtain a positive answer about the possibility of displacement of the centre of the Earth's mass.

Since the measurements with instruments for absolute gravity determinations shall be conducted on a limited scale in the next few years, it would be useful to establish a network of international gravimetric points of high precision on the basis of the stations indicated above. These points of high precision should be located in regions with supposed maximum and minimum gravity changes. The connections of these points with points of absolute determinations by modern means can be carried out with an accuracy of the order ± 15 microgal. During repeated determinations once every 2 - 3 years, we can expect to obtain already in 5 - 6 years the first conception of the regional gravity changes. Using the network of points, the interested countries could conduct the study of local gravity changes.

Naturally, the suggested program can be realised only on the basis of international co-operation and in close collaboration of scientists, whose efforts provide the possibility of obtaining the necessary financial support and sufficient number of gravimeters well qualified for highly precise measurements.

In the Soviet Union, within the framework of this project, a program has been elaborated on for the study of secular variations of gravity for 10 years. This program envisages the establishment of a network of stations on the territory of eastern Europe and in the west of the Asiatic part of the USSR. This network will be based on Sèvres. The stations shall be located both in aseismic regions and in regions seismically and tectonically active. Simultaneously, studies of local gravity measurements shall be continued in middle Asia, the Baikal region, in Crimea, on the Caucasus, in the Ukraine amd Karelia.

The Soviet Geophysical Committee is prepared to participate in the establishment of the international network of gravimetrical points with the purpose of the study of secular variations of gravity.

2. References

ABAKELIA, M.S. 1936a. On the Changes of Gravity in Time and in Association with Geotectonic Movements on the Caucasus. *Problems of Soviet Geology* VI,117-122.

ABAKELIA, M.S. 1936b. On the Organization of Gravity Observations in the Trans-Caucasus. *Problems of Soviet Geology* VI,452-454.

BARTA, G. 1957. On the Variations of Gravity. *Ann.Univ.Scient.Budapest,Sec.geol.* I,13-19.

BARTA, G. 1962. Recommendation for Detecting and Surveying the Secular Variation of the Earth's Gravity Field. *Abhandl.Deutsch.Akad.Wiss.,Berlin,Rl. Bergbau Hütten* 2,433-436.

BARTA, G. 1963. The Secular Variation in the Geomagnetic Field and Other Geophysical Phenomena. *Ann.Univ.Scient.Budapest,Sec.geol.* 7,71-81.

BARTA, G. 1965. The Evolution of the Idea of the Secular Variations in Gravity. *Bull.geofis.Teor. e Appl.* 7,3-5.

BARTA, G. 1967. The Asymmetric Structure of the Earth and its Secular Process. *Öster.Z.f.VermessWes* 25,77-79.

BOULANGER, J.D. & SCHEGLOV, S.N. 1971. On Secular Changes of Gravity. *Bull.geodes.* 100.175-177.

BURSA, M. 1972. Variations of the Earth's Gravity Field due to Free Nutation. *Stud.geophys.et geod.* 16,122-125.

FAITELSON, A.SH. 1969a. Secular Variations of Gravity in the Aral-Caspian Region. *Doklady AN SSSR* 189,1240-1241.

FAITELSON, A.SH. 1969b. Secular Variations of Gravity on the Russian Platform. *Doklady AN SSSR* 188,577-582.

FAITELSON, A.SH & AZARKINA, E.A. 1970. Secular Variations of Gravity in the Ukraine. *Doklady AN SSSR* 195,89-90.

FAITELSON, A. SH. & AZARKINA, E.A. 1972. Secular Variations of Gravity on the Caucasus. *Izvestia AN SSSR,Fizika Zemli* 9,93-94.

KALASHNIKOVA, I.V. 1970. On the Connection of Recent Vertical Crustal Movements with the Gravity Field. *Geomorphologia* 3,62-68.

NAKAGAWA, I. 1972. Secular Change of Gravity near Lake Biwo-Ko. *J.geodet.Soc.Japan* 18,23-29.

PARIISKY, N.N. 1937. Studies of Time Gravity Changes on the Caucasus. *Intern.geol.Congress,* XVIII Session,Abstract of Reports N.-L.,pp.189-190.

SATOMURA, M. & NAKAGAWA, I. 1972. Secular Change of Gravity near Lake Biwo-Ko. *Contributions, geophys. Inst., Kyoto Univ.* 12,101-115.

SCHLEUSENEER, A. & TORGE, W. 1971. Investigations of Secular Gravity Variations in Iceland. *Z.f. geophys.* 37,679-701.

SHRAIBMAN, V.I. & FAITELSON, A.SH. 1971. Quantitative Estimations of Connections between Variations of Gravity Field and Geostructural Elements. *Bull.Moscow Soc.Naturalists,Sec.geol.* 46,152-153.

SIROTOV, YU.N. & PARFENOV, A.I. 1970. Studies of Gravity Field Variations with Time in the Region of the Baikal Rift Zone. In the collection of papers *Problems of Regional Geology & Petrography of Diberia and methods of Geochemical and Geophysical Researches* 2,123-125, Novosibirsk.

SOBOKAR, G.T.1968. Quasi-periodic Variations of Gravity in the Ukraine.*Dopovidi ANU SSR B* 9,781-783.

VOGEL, A. 1968. The Question of Secular Variations in the Earth's Gravity Field from Mass Displacements in the Earth's Deep Interior. *Bull.geodes.* 88,223-226.

3. Bibliography

BENRENDT, J.C. 1967. Gravity Increase at the South Pole. *Science* 155,1015-1017.

BENTLEY, C. 1971. Secular Increase of Gravity at the South Pole Station. *Antarctic Snow & Ice Stud.* 2,191-198,Washington,DC.

BIRO, P. 1971. Die Vertikale Erdkrustenbewegungen und Sekular Variationen des Erdschwerfeldes. *XV General Assembly, IUGG, Moscow.*

FUJITA, N. 1971. *J.geodet.Soc.Japan* 17,8-13.

HONKASALO, T. 1966. Gravity and Land Upheaval in Fennoscandia. *Suomal.tiedeakat.Toim A III* 90,139-141.

HONKASALO, T. 1967. Variation of Gravity Caused by Land Uplift in Fennoscandia. *XIV General Assembly IUGG, Lucerne.*

KUKKAMÄKKI, T.J. 1969. On Observation of Secular Variation of Gravity in Fennoscandia. In *Problems of Recent Crustal Movements*, 494-495.

LEVALLOIS, J.-J. 1971. Quelques Consequences Géophysiques des Nouvelles Méthodes de Haute Précision de Mesures Absolues de g. *Bull.géodes.* 99,111-112.

NOWORU, I. 1968. A Study on the Time Change of Gravity in Ooshima Island. *J.geodet.Soc.Japan* ,146-150.

RIZAWA, T. 1970. Recordings with Askania Gravimeters Before and After Important Earthqakes. In *Rep. Symposium on Coastal Geodesy* (SIGL, R.(ed)),613-614,Munich.

SZABO, Z. 1967. Néhány magjegyzés a gravitácios tér évszázados válto zásával kapcsolatban. *Geofiz. Közl.* 16,109-111.

TADZIMA MINORU 1970. Possibility of Gravity Change Accompanying Crustal Movement. *J.geod.Soc. Japan* 16,60-67.

T a b l e 1

Secular Change in Gravity (units milligal)

	m_g(1955)	m_g(1967)	$\delta = g_{1967} - g_{1955}$		$\delta' = \delta - \Delta$	$m_{\delta'}$	$\delta'/m_{\delta'}$
Potsdam	±0.00	±0.00	0.00	±0.00	-0.07	±0.04	-
Moscow	0.16	0.05	-0.10	0.17	-0.17	0.17	1.0
Riga	0.26	0.09	+0.31	0.28	+0.24	0.28	0.9
Kazan	0.25	0.07	-0.01	0.26	-0.08	0.26	0.3
Sverdlovsk	0.30	0.07	+0.02	0.31	-0.05	0.31	0.2
Tschita	0.51	0.12	+0.20	0.52	+0.13	0.52	0.2
Tahtamigda	0.58	0.11	+0.12	0.59	+0.05	0.59	0.1
Petropavlovsk	0.72	0.14	+0.16	0.73	+0.09	0.73	0.1
		Mean: Δ'	= +0.10	± 0.05			
Tbilisi	±0.32	±0.10	-0.03	±0.34	-0.10	±0.34	0.3
Ashkhabad	0.46	0.10	+0.03	0.47	-0.04	0.47	0.1
Dushanbe	0.51	0.12	-0.13	0.52	-0.20	0.52	0.4
Alma-Ata	0.49	0.11	+0.18	0.50	+0.11	0.50	0.2
Balhash	0.50	0.12	+0.18	0.51	+0.11	0.51	0.2
		Mean: Δ''	= +0.05	± 0.06			
		Mean: Δ	= +0.07	± 0.04			

T a b l e 2

The Tie "Potsdam" - "Moscow (Ledovo)"

Year	Δg	M(Δg)
1958	290.63	± 0.16 mgal
1968	.55	0.05
1970	.31	0.04
1971	.31	0.03

Table 3

Changes of Gravity on the European Part of the Soviet Union

Name of Point	Changes (mgal)	Error (mgal)
	1968 - 1973	
Moscow (Ledovo)	0.00	± 0.000
Kazan	-0.01	0.045
Sverdlovsk	+0.02	0.059
	1970/1971 - 1972/1973	
Moscow (Ledovo)	0.000	± 0.000
Kazan	-0.005	0.022
Sverdlovsk	+0.030	0.030
Perm	-0.005	0.038
Kirovsk	-0.005	0.038
Petrozavodsk	+0.005	0.030

Table 4

Results of Repeated Measurements in Countries of Eastern Europe
Units - mgal

Names of Points	1958 M(g)	1968 M(g)	Differences δg	Differences $M(\delta g)$
Potsdam	±0.00	±0.00	0.00	± 0.00
Berlin	0.01	0.01	-0.04	0.01
Warsaw	0.09	0.02	-0.13	0.09
Prague	0.09	0.02	+0.10	0.09
Budapest	0.13	0.04	-0.04	0.14
Bucarest	0.16	0.04	0.00	0.16
Sofia	0.16	0.07	+0.07	0.17

4. Discussion

HOPKINS: Talking about 2/100 th mgal; are these instrumental errors?

BOULANGER: Yes. ±0.02 mgal is the error of the measurements. But each apparatus gives us more error than this. That is the error of the mean. We work with a minimum of 7-8 instruments and we measure each Δg 3 to 4 times. That is the error of the mean of all measurements.

HOLDAHL: You compared changes in gravity with changes in elevation. How did you measure the changes in elevation?

BOULANGER: In the fundamental sense we cannot control elevations, but it could be done in the following manner. We combine measurements of gravity with very comprehensive measurements of elevation in eastern Europe where we have many loops along which measurements are taken. These results give us vertical crustal movement. The movement is of the order of 1-3 mm per year.

HOLDAHL: Specifically what measuring method was used? Was it precise levelling?

BOULANGER: Yes. The points in the net were tied to check points at each station in the system of points. Having measured a change in gravity, you take the vertical component and relate it to the nearby points. The effects of microseisms, man made vibrations, temperature, etc. can be eliminated from the observations.

HOLDAHL: What is the distance between the two standard points?

BOULANGER: Quite different. Between satellite points situated around the principal points from 2 to 12 km.

HOLDAHL: Overall?

BOULANGER: Between principal points and standard points the mean is 300 - 400 km.

SAKUMA: Within two years, a portable gravity meter (for measuring absolute gravity) of 10 μgal accuracy will become available commerically.

MUELLER: When we get down to these sort of numbers, what do you do when the ground water level changes? How can you separate these changes and changes in climate?

BOULANGER: Yes; there is probably a change in level that can be attributed to water level changes to 0.02 mgal.

ECKHARDT: A base gradiometer at M I T (Mass. Inst. Technology) was sensitive to changes in water on the roof, sewage level, etc.

BARTA, G.
Eötvös Loránd Tudományegyetem
Geofizikai Tanszék
Budapest VIII
Hungary

Proc. Symposium on Earth's Gravitational Field & Secular Variations in Position (1973), 213-217.

DISTORTION OF THE GRAVITY FIELD AND ITS CONSEQUENCES

1. Text

It is known that the geoid can be represented as a sum of two rotation-symmetrical forms, the axes of which are found in the plane of the equator. One of these axes originating from the centre of the Earth is directed towards India, while the other is directed towards Australia. The former has no ellipticity in contrast to the latter which has it (BARTA 1973a). (These two figures must not be confused with polar oblateness which also possesses a rotational symmetry.)

The combined form represents the true observed geoid with such an accuracy that it is worthwhile to publish the well known diagram again and to subject it to further discussion (figure 1). The proving force of similarity is a strong one because the computed figure is based only on the equatorial data of the geoid; thus the similarity is not a result of a simple approximation, but it is an evidence of principle of the suppositions used in the computations. Thus the equatorial data system of the geoid implicitly contains the four anomalies of the temperate zones too, together with sign, form and dimension.

Deviations between the two diagrams present themselves only in the orientation of the positive and negative anomalies of the temperate zones. On the observed figure (A), these directions show a certain oblique angle with the equator, while on the computed one (B) they are perpendicular to it. As it is easy to see, this is only as a consequence of our computations having been based only on equatorial data. Removing this constraint enables us to obtain also the oblique anomaly-directions seen on the measured diagram (A) and we can assure a similarity even better than seen in the figure.

This interpretation of the figure of the geoid has far reaching consequences within the domains of many branches of science. For example, the polar oblateness belonging to hydrostatic equilibrium increases owing to the reported ellipticity of the Australian form and if the axes of the two rotation-symmetrical forms do not fall exactly into the equatorial plane, then there must exist a deviation between the northern and southern hemispheres (the pear shape of the globe, etc.).

But let us disregard the geodetic aspects of the phenomenon and let us consider first of all, the consequences in connection with the internal structure of the Earth. In that respect, the most important consequence of the statement is that the geoid figure is determined only by a small number of relevant factors, i.e., the six big anomalies of the geoid are not formed by near-surface gravitational phenomena, but by two large scale effects only, against which the globe behaves as a fluid, and the influence of which makes itself felt on the whole surface of the Earth, even at opposite sides. These effects, owing just to their small number, do not intermingle with one another on the other side within the framework of measurement-noise, as it could be supposed in the case of a great number of acting sources. Thus they can be separated and discussed individually, so that we can draw exact

A

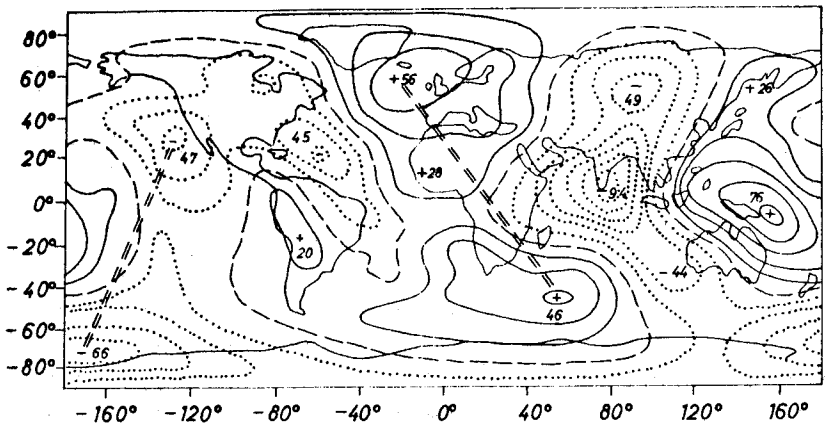

Figure 1 (A): The "Smithsonian 1966" geoid

B

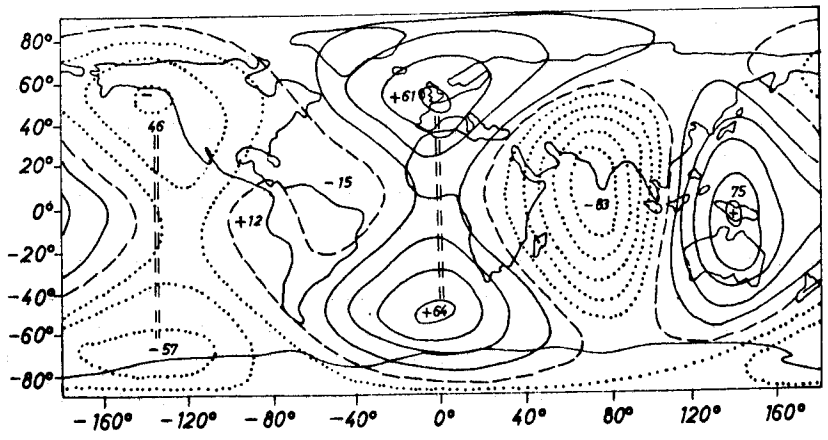

Figure 1(B): Geoid Figure Computed from Two Rotation-Symmetrical Anomaly Systems

consequences as regard their cause and different characteristics.

A mass anomaly of such a great dimension cannot exist in the material of the crust and mantle owing to the tendency towards isostasy. Under the influence of the gravity field, the anomalous mass would

have been shifted up or down depending on its density during geologic ages. Thus, an anomaly of such a character can exist only either on the surface or at great depth. On the surface of the Earth, no sign of such a density anomaly can be found in the areas involved. Thus we have to direct our attention to the domains at great depth.

The mobile, plasmatic material of the outer core, however, is even less suitable for maintaining a significant inhomogeneity. It is strange enough that there is only one domain of the globe capable of holding the source of such a large-scale anomaly system, i.e., the inner core of the Earth. The inner core or its centre, respectively, represents namely a singular point of the gravity potential field. For this material domain the notion of "up" and "down" ceases to exist, because it does not exert any influence on itself as a unit, by its gravity field. The masses of the crust-mantle and the outer core (taken in first approximation as spherical shells) , do not exert an attracting force on it, their gravitational interaction manifests itself in a pressure only. That is the reason why we need not - or even must not - suppose a central position of the inner core.

The eccentricity of our magnetic dipole - long known - indicates that the inner core does not show in fact a central symmetrical position. This is supported also by the fact that the component anomaly of the geoidal figure, which has a rotational symmetry from the direction of Australia, is showing an ellipticity in the direction of the eccentricity of the magnetic dipole. Thus both force fields indicate a general asymmetry of the internal structure of our globe. According to the indications of the two fields, the inner core of the Earth possesses an eccentric position in the direction towards Australia.

If the material of the crust and mantle shows a central symmetry in the form of spherical shells, then on the Gutenberg-Wiechert surface we have a constant pressure; the shells do not exert any internal effect. Thus they need not be taken into account in what follows. If however the material of the outer core can be compressed, then for the inner core of an arbitrary position, there exists a density distribution producing a constant pressure on the Lehman surface, this being the condition for a hydrostatic equilibrium of the inner core at the given location.

Thus assuming a suitable density distribution, one can arrive naturally at any desired value of the eccentricity. Therefore some force or effect must exist maintaining the eccentricity on the one hand and the inhomogeneity of the material of the external core on the other. One of such effects is the centrifugal force acting on the inner core, directed outwards and increasing linearly with the distance from the axis of rotation.

To define another such force we have to take recourse to the following considerations. When computing pressure we have taken into account the gravity interaction of the materials of the inner and outer core, but we did not consider the gravity effect of the material parts of the outer core on one another, though these are counteracting the inhomogeneity of the outer core in the direction of promoting the development of homogeneous conditions. This force is directed towards the centre and increases - as an approximation - quadratically with the distance from the centre. A rough estimation shows that the two forces equal one another at an approximate distance of 100 km from the centre. Thus the present eccentricity of the magnetic dipole amounting to 430 km can be related to the eccentricity of the inner core of the Earth, and what is more, it is an inevitable consequence of the hydrostatic equilibrium of the inner core when interpreted correctly (BARTA 1973b).

Thus the mechanism producing the eccentricity of the inner core of the globe is similar to the

working method of speed regulators found on the old steam machines. The eccentricity does exist as long as the Earth rotates. In case of a stopping of rotation, central symmetry will be restored if the physical characteristics of the materials of the outer core remained unchanged.

The direction of the eccentricity however, would not be determined by the physical causes mentioned above. According to the reasoning, the rotation axis of the Earth is surrounded by a potential-trench where the inner core is lying, taking some direction. Owing to its eccentric position, it is not in an equilibrium state in the system Sun-Moon-Earth, so that it is shifting within this trench towards west, which may be the cause of the westward drift of the magnetic field.

Because of the westward drift of the the inner core, the material of the outer core must flow off the direction of movement and flow behind the inner core. The plasmatic material around the spot of divergence (under India) begins whirling, producing by its flow the magnetic secular variation; while by its dynamic effect, it produces the other rotation-symmetrical anomaly-configuration in agreement with the determination of the geoid (this has no ellipticity; the zonal spherical harmonics used for its representation have significant members only of odd orders (BARTA 1973a)).

The eccentricity and movement of the inner core furnishes - of course - much information about the material characteristics (compressibility, viscosity, etc.) of the outer core. Setting aside these opportunities for now, let us consider the possibilities for studying the variation phenomena represented by this movement.

The factual shifting of the core may cause a significant change in time of the internal mass distribution of our globe and of its gravity field as well. The interconnections are however very complex ones. The crust - and mantle - domain, not having the form of a spherical shell and in reality not being homogeneous, exerts an influence inside, while the asymmetrically located inner core is also influencing these masses above, and what is more, it keeps them moving too. Thus we cannot know what amplifying or compensating effects will result on the surface as a result of these complex interactions. It is clear that the anomalies determining the shape of the Earth must shift towards the west with the speed of the westward drift. We do not know any details as yet and many contradicting observations may support the development of deviating views. With the interpretation of measurements lacking sufficient accuracy, observational errors may be taken as signs of a secular change, while - owing to a great scattering of measurements - even the existence of such change can be contested.

Thus from the point of view of internal structure and processes of the Earth, it is of decisive importance to subject to an investigation - besides measurements regarding the eccentricity of the magnetic dipole and the magnetic secular variation - similar parameters of the gravity field too, and by increasing - as far as possible - the observational accuracy to the order of magnitude of the variations. Measurements should be arranged - of course - first of all on spots where variations of a maximum intensity may be expected. In case of an eccentricity and shifting of the inner core, it seems probable that the greatest changes will present themselves along the equator, and even here, at points where the sources of the two anomalies are near one another, i.e., between India and Australia.

But irrespective of any theory, a simple logical reasoning supports the inference that the greatest change in time is to be expected there, where the spatial gradient of the fields is the biggest one. The biggest positive anomaly of the geoidal figure can be found near New Guinea - northern Australia, while the greatest negative anomaly is near Ceylon.

It is not possible to establish a continuous measuring profile between these points owing to the presence of the ocean. Besides the theoretical considerations (the magnetic dipole being eccentric at present north of Australia towards the Marshall Islands, while the magnetic secular variation, also having a significant symmetry-point in the northern hemisphere near Pakistan) practical possibilities also indicate that the measuring profile should be laid along the line: north Australia - Indonesia - south east India - east India - Iran.

The surveying of this line as well as its repeated re-surveying would be needed for the accurate recognition of the inner structure of the Earth and if its internal processes. In the event of successful observations, we would obtain a way to understand the causes of tectonic movements, too. That is why Working Group 6 of the Inter-Union Commission on Geodynamics has included among its resolutions, the setting up of the above mentioned measuring line and has addressed the conference of the International Association of Geodesy at Sydney, as well as the teritorially competent national commissions to support the plan and to make arrangements for its implementation.

When investigating the asymmetry of the globe, we inevitably risk the loss of the elegant and well applicable symmetry characteristics of the mathematical techniques applied as yet for the description of the fields of forces. Nevertheless, the accuracy of measurements has been increased recently to such an extent that the study could be extended to the details too. But clinging to the results of these more accurate measurements we have to re-examine these symmetry-characteristics and to apply an approximation procedure of higher order which adapts itself better to reality for the interpretation of the fields of forces.

In exchange for the loss of symmetry we get a compensation however, through the appearance of the possibility and idea of a variation itself and through the greater flexibility obtained by the abandonment of the rigorously symmetrical systems. It is possible that just on the basis of these advantages, some basic geophysical-geodetical problems will near their solution.

2. References

BARTA, G. 1973a. Physical Background of the Geoidal Figure. *Nature* 243,156-158.

BARTA, G. 1973b. Zu den Physikalischen Zusammenhängen des asymmetrischen Baus des Erdkörpers. *Gerlands Beiträge Geophysik* 82,257-266.

FUJITA, N.
FUJII, Y.
Geographical Survey Institute
Meguro-ku, Tokyo
Japan

Proc. Symposium on Earth's Gravitational Field & Secular Variations in Position (1973), 218-221.

GRAVITY CHANGE IN JAPAN

ABSTRACT

Gravity changes accompanying the Niigata earthquake, the Matsushiro swarm earthquakes, Mihara volcanic activity in Ooshima island, and crustal activities in Hokkaido, South Kanto and Shikoku districts have been found in Japan.

The correlation between gravity change and height change in Matsushiro is discussed under consideration of the mechanism of the Matsushiro swarm earthquakes. There are examples in which the gravity changes are often larger than expected. Some of them might be related with dilatancy of the crust. It is considered that the gravity survey is useful for earthquake prediction.

1. Text

Recent developments in gravimeter instrumentation and measuring techniques enable us to detect significant gravity change that may accompany various kinds of geophysical phenomena such as earthquakes, volcanic activity, tectonic movements and so on. Recently, many examples of gravity changes have been reported in Japan, as shown in table 1. These studies were recently reviewed by HAGIWARA & TAJIMA (1973a).

Table 1
Examples of Gravity Change in Japan

Phenomena	Location	Reference
Earthquake	Niigata	FUJII 1966
	Matsushiro	HARADA 1968
	Gifu	TANAKA & TSUKAHARA 1969
	Nemuro	OKAWA, YAMASHITA & YOKOYAMA 1973
Volcanic eruption	Oshima island	INOUCHI, KANO & FUJII 1972
Ground subsidence	Niigata	FUJITA 1971
	Tokyo	FUJITA 1971
	Mobara	HAGIWARA & TAJIMA 1973b
Tectonic movement	Kii & Muroto	FUJII & NAKANE 1972
Others	South Kanto	TAJIMA 1970
	Lake Biwa	SATOMURA & NAKAGAWA 1972

A typical example of gravity changes accompanying earthquake activity is the case experienced during the Matsushiro swarm earthquakes. This example seems to show that the observed gravity change cannot be interpreted by the deformation of continuous medium (TAZIMA 1970), but by the dilatancy model of earthquake occurrences (KASAHARA 1970; SCHOLZ, SYKES & AGGARWAL 1973).

Observed gravity changes associated with the Matsushiro swarm earhquakes are shown in figure 1. In stage I, the land around Mt. Minakami began to upheave by Δh and the gravity decreased by Δg. The observed $\Delta g/\Delta h$ is approximately equal to the free air gradient (-0.3086 mgal m^{-1}). In stage II, the most active period of earthquakes, the large amount of underground water started to flow out. The land upheaval and gravity decrease still continued. The observed gradient is quite different from the free air gradient and the Bouguer gradient (-0.1967 mgal m^{-1}). In stage III, with decrease of seismic activity, the land began to subside, the ground water flowed out of the crust and the gravity began to increase. The observed gradient returned to the free air gradient again. The results of seismological observation (pull and push) and geomagnetic survey showed the existence of east-west compression around Matsushiro.

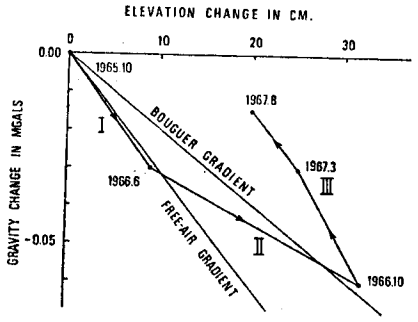

Figure 1. Relation between Changes in Gravity and Elevation Observed at the Matsushiro First-order Gravity Station

When the thickness of the Bouguer plate varies from h to $h+\Delta h$, and the density from ρ to $\rho+\Delta\rho$, the gravity on the plate varies from g to $g+\Delta g$. Then the observed gradient is expressed as

$$\Delta g/\Delta h = -0.3086 + 2\pi k\rho + 2\pi k\, \Delta\rho\, h/\Delta h.$$

In stage I, the development of the open cracks in the porous medium might have caused the land upheaval. The gravity decreases along the free air gradient because of $\rho = -\Delta\rho\, h/\Delta h$. In stage II, the observed gradient of -0.12 mgal m^{-1} results in $\Delta\rho \doteqdot +1 \times 10^{-4}$ g cm^{-3}. The porosity of the crust might have decreased together with the mass intrusion. The ground water might have also penetrated from neighbouring regions into the porous medium. A part of the ground water flowed out of the crust. In stage III, the closing of these cracks might have occurred. The ground water remaining in the crust might have been forced to come out of the crust when the cracks closed. Then the observed gradient is nearly equal to the free air gradient. The free air gradient in stage III may be explained mainly by the closing of the cracks. The explanation mentioned above is schematically shown in figure 2.

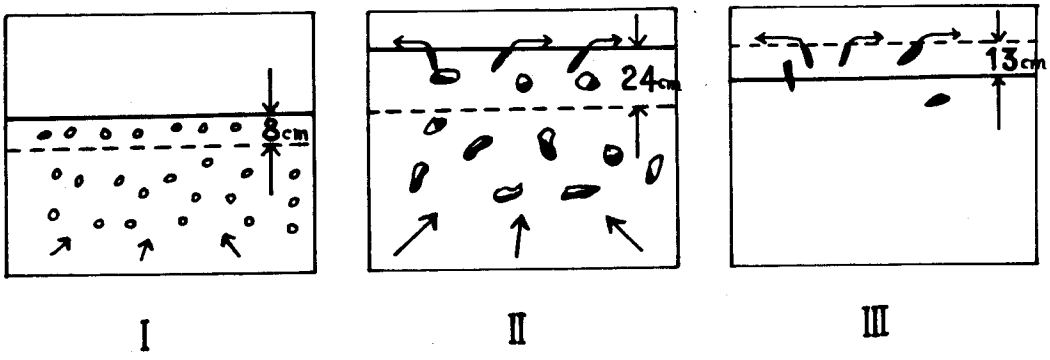

Figure 2. A Dilatancy Model for Gravity Change at Matsushiro
I : Stage 1. Dilatancy II : Stage 2. Mass Intrusion & Density Increase III : Stage 3. Shrinkage

The writers proposed the pattern of the seismic crustal deformation (FUJITA & FUJII 1973). In figure 3, the β_1 phase corresponds to the dilatancy process and the γ_3 phase to the shrinkage process. It is expected that the free air gradient may appear in the β_1 and γ_3 phases. And the gravity change can be one of the precursory phenomena to earthquakes.

The gravity changes have been discussed around the accuracy of the gravity survey. At first, the accuracy of the gravity survey should be improved. In 1968, the Gravity Meters Comparison Group was organized. In 1969-1971, three symposia were held on Gravity and High Accuracy Levelling under the auspices of the Geodetic Society of Japan. In accordance with the resolution adopted at the symposia, the gravity survey of the south Kanto district has been carried out several times by using several La-Coste gravity meters since 1969 (NAKAGAWA 1971). It has been clarified that the gravity increase prevails in the south Kanto district. It is considered that the gravity value at the datum in the University of Tokyo may be decreasing by 0.01 mgal yr^{-1} (HAGIWARA & TAJIMA 1973a). It seems that the ground water level around the datum is dropping faster than the mean level of ground water in the other areas being surveyed.

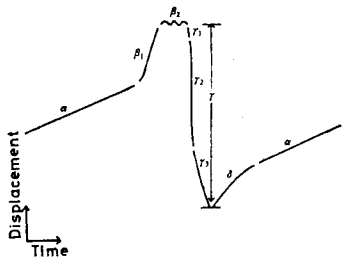

Figure 3. A Typical Pattern of Seismic Crustal Movement

α : Steady State
γ_1 : Pre-Seismic Slip
γ_2 : Co-Seismic Slip
γ_3 : Post-Seismic Slip
γ : Geodetic Slip
β_1 : Dilatant State
β_2 : Unstable State
δ : Transient State

When discussing the gravity change, the local conditions, such as open cracks and ground water level in the upper crust, cannot be neglected.

2. References

FUJII, Y. 1966. Gravity Change in the Shock Area of the Niigata Earthquake, 16 June 1964 (in Japanese). *Zisin II* 19,200-216.

FUJII, Y. & NAKANE, K. 1972. Crustal Deformation and Secular Change of Gravity Accompanied by Interaction of Plates (in Japanese). *J.geodet.Soc.Japan* 18,180-190.

FUJITA, N. 1971. Notes on Gravity Change (in Japanese). *J.geod.Soc.Japan* 17,8-13.

FUJITA, N. & FUJII, Y. 1973. Detailed Phases of Seismic Crustal Movement. *J.geodet.Soc.Japan* 19, 55-56.

HAGIWARA, Y. & TAJIMA, H. 1973a. Secular Changes in Gravity (in Japanese). *Publications for the 50th Anniversary of the Great Kanto Earthquake, 1923*, 311-327.

HAGIWARA, Y. & TAJIMA, H. 1973b. Secular Gravity Changes in Chigasaki and Mobara Ground Subsidence Areas (in Japanese). *J.geodet.Soc.Japan* 19,70-75.

HARADA, Y. 1968. Geodetic Work in Japan with Special Reference to the Matsushiro Earthquakes. *Trans. Am.geophys.U.* 50,390-391.

INOUCHI, N., KANO, K. & FUJII, Y. 1972. A Study on the Time Change of Gravity in Ooshima Island (II) (in Japanese). *J.geodet.Soc.Japan* 18,104-111.

KASAHARA, K. 1970. The Source Region of the Matsushiro Swarm Earthquakes. *Bull.Earthq.Res.Inst.* 48, 581-602.

NAKAGAWA, I. 1971. Some Remarks on Gravity Survey (in Japanese). *J.geodet.Soc.Japan* 17,67-75.

OKAWA, S., YAMASHITA, I. & YOKOYAMA, I. 1973. Resurvey of Gravity and Geomagnetism after the Off Nemuro Peninsula Earthquake (in Japanese). *Abstract, Autumn Meeting, Seismological Society of Japan* 2,120.

SATOMURA, M. & NAKAGAWA, I. 1972. Secular Change of Gravity near Lake Biwako. *Contr.geophys.Inst. Kyoto University* 12,101-115.

SCHOLZ, C.H., SYKES, L.R. & AGGARWAL, Y.P. 1973. Earthquake Prediction:A Physical Basis. *Science* 181,803-810.

TAJIMA, H. 1970. On Precise Gravity Survey in Miura and Boso Peninsulas (on the Results of Re-survey) (in Japanese). *J.geodet.Soc.Japan* 16,54-59.

TANAKA, M. & TSUKAHARA, K. 1969. Crustal Movements in the Epicentral Area of Gifu Earthquake of September 9,1969 (in Japanese). *J.geodet.Soc.Japan* (in press).

TAZIMA, M. 1970. Possibility of Gravity Change Accompanying Crustal Movement (in Japanese). *J.geodet. Soc.Japan* 16,60-67.

3. Discussion

WALCOTT: The gravity change at Matsushiro is of great interest and, if correct, of considerable importance. You have small changes of 50 microgal but show your data as points. I presume there are error bounds on your gravity data. What are they?

FUJITA: ±0.02 - ±0.03 mgal.

NEDOMA, J.
Geophysical Institute
Czech. Academy of Sciences
Prague 4-Spořilov, Boční II
Czechoslavokia

Proc. Symposium on Earth's Gravitational Field & Secular Variations in Position (1973), 222-226.

CONTRIBUTION TO THE VARIATIONAL FORMULATION OF THE BOUNDARY VALUE PROBLEM OF THE GRAVITY FIELD AND THE DISCRETE GRAVITY FIELD

ABSTRACT

The possibility of the variational formulation of the boundary value problem of the gravity potential is discussed. The method under consideration will be derived quite generally without any hypothesis about the mass distribution between the Earth's surface and the geoid. We shall start from the gravity data given on the Earth's surface. The relation between the variational formulation and the discrete gravity field is shown.

1. Introduction

In this contribution, a possibility of the solution of the variational formulation of the boundary value problem of the gravity field will be discussed. We start from the gravity data given on the Earth's surface and we do not make any hypothesis about the mass distribution between the Earth's surface and the geoid. The Earth's surface is assumed to be sufficiently smooth with a finite number of singular points and with the demand that the fundamental boundary value condition of gravity is fulfilled with the predetermined accuracy. Let us assume also that the total mass of the normal body is equal to the mass of the Earth and, further, both bodies turn around the same axis going through the identical centre of gravity with the same angular velocity ω.

2. Theory

We shall consider two cases of the formulation of studying the outer gravity field:

Case 1

1. The disturbing potential T fulfils the Laplace equation

$$\Delta T = 0$$

outside the Earth (i.e., in Ω).

2. It fulfils the condition

$$\frac{\partial T}{\partial n} + \frac{2T}{R} = -\Delta g$$

on the Earth's surface S, where n is the direction of the normal to the Earth, R is the distance from the point P on the Earth's surface to the centre of the Earth, Δg is the free air anomaly at the same point P.

3. It fulfils the condition of regularity

$$\lim_{r\to\infty} rT = 0$$

at infinity.

This problem is equivalent to another boundary value problem with a homogeneous boundary condition. By putting

$$t = T - w,$$

where T is the disturbing potential of the original problem and w is a suitable sufficiently smooth function fulfilling the boundary value conditions given in (2) and (3). We then obtain

$$\Delta t = 0 \qquad \text{outside the Earth,}$$

where

$$\theta = -\Delta w \qquad (1),$$

$$\frac{\partial t}{\partial n} + \frac{2t}{R} = 0 \qquad \text{on the Earth's surface S} \qquad (2),$$

and

$$\lim_{r\to\infty} rt = 0 \qquad \text{at infinity} \qquad (3),$$

or, in the operator's form

$$L\,t = -\theta.$$

Let us define the domain $D/\Omega/$ of the operator L as a set of all finite functions* twice continuously differentiable on the closure $\overline{\Omega}$ $(C^2/\Omega/)$, which satisfy the boundary conditions 2 and 3. We shall consider the completion of the $D/\Omega/$ with respect to the energetic norm. We call this space *energetical space* and denote it by $V/\Omega/$. In fact, we have

$$/Lt, t/ = /-\Delta t, t/ = \int_\Omega /\mathrm{grad}\ t/^2\, d\Omega + \int_S \frac{2}{R} t^2\, dS \geq 0.$$

If $/Lt, t/ = 0$, then $t = C = \text{const.}$ As t is a finite function, we have $C = 0$ and hence $t = 0$. Thus $/Lt, t/ > 0$, $t \neq 0$ and the operator L is positive.

As the operator L is a positive operator, the problem leads to the minimization of the following functional

$$F/t/ = \int_\Omega /\mathrm{grad}\ t/^2\, d\Omega + \int_S \frac{2}{R} t^2\, dS + \int_\Omega 2\theta\, t\, d\Omega \qquad (4).$$

This means that in order to find the disturbing potential T outside the Earth, we have to minimize the functional $F/t/$ from equation 4 over a special Hilbert space - the so-called energetical space $V/\Omega/$ (see NEDOMA 1973b) and using the expression

$$T = t + w.$$

As the author shows in the reference quoted, there exists exactly one disturbing potential T. This

---

* A real function f belongs to the class of finite functions if there is a $r > 0$ and a sphere

$$K_r = \{/x,y,z/ \in R^3, x^2+y^2+z^2 \leq r^2,\ r > 0\}$$

such that $f/x/ = 0$ for $x \notin K_r$

is a consequence of the following facts:

a. That

$$\theta = -\Delta w = -\operatorname{div}\operatorname{grad} w = \operatorname{div} F/x/,$$

where

$$|F/x/| = |-\operatorname{grad} w| \in L_2/\Omega/,$$

and

$$\int_\Omega t_n\,\theta\,d\Omega = -\int_\Omega \operatorname{grad} t_n \operatorname{grad} w\,d\Omega + \int_S t_n \frac{\partial w}{\partial n}\,dS,$$

where

$t_n \in V/\Omega/$ is the finite function, $\frac{\partial w}{\partial n} \in L_2/S/$ (see IBID);

and then the assumption of theorem 42.2 of MIKHLIN (1966) are satisfied.

b. That the disturbing potential T does not depend on the choice of the function w.

Case II

The same problem may be studied from the point of view of the other formulation in which any satellite's measurement can be used. We shall construct a certain surface of known form, which will be assumed to lie at a height H above the Earth's surface and that the angle between the direction of the normal n to it at the point Q and the direction of the normal n_1 to the level surface, passing through the same point Q, is small. We assume that it turns around the same axis passing through the same centre of gravity with the same angular velocity ω. We may then consider the fundamental boundary condition of gravity on the discussed surface in the form

$$\frac{\partial T}{\partial n} + \frac{2T}{R_1} = -\Delta g_1,$$

where n_1 is the normal to the mentioned surface Σ, R_1 is the distance of the point Q from the centre of the Earth and Δg_1 is the free-air anomaly obtained from the satellite measurement or from measurements at the Earth which were recalculated on the measured surface Σ. As in the case of the formulation discussed earlier, the disturbing potential T fulfils Laplace's equation outside the Earth and the fundamental boundary value condition of gravity on the Earth's surface. Using ideas analogous to the above, we obtain the equivalent problem for the disturbing potential t:

$\Delta t = \hat{\theta}$ in the space outside the Earth's surface, which we denote as $\hat{\Omega}$, and where

$$\hat{\theta} = -\Delta w_1 \qquad (1'),$$

$$\frac{\partial t}{\partial n} + \frac{2t}{R} = 0 \quad \text{on the Earth's surface S} \qquad (2'),$$

$$\frac{\partial t}{\partial n_1} + \frac{2t}{R_1} = 0 \quad \text{on the surface } \Sigma \qquad (3'),$$

i.e.,

$$At = -\hat{\theta},$$

where A is a positive definite operator (see NEDOMA 1973b), as

$$(At, t) \geq \gamma^2 ||t||^2_{W_2^1},$$

$$\gamma = \min/\frac{2}{R}, \frac{2}{R_1}, 1/ \Big/ \min\ \pi^{-2}/\,/a-a_1/^{-2} + /b-b_1/^{-2} + /c-c_1/^{-2}\,/^{-1},\ c_1\,\pi^{-2}//a-a_1/^{-2} + /b-b_1/^{-2} + /c-c_1/^{-2}/^{-1},$$

$$+ c_2\pi^{-2}//a-a_1/^{-2} + /b-b_1/^{-2} + /c-c_1/^{-2}/^{-1}/,$$

$$c_1 \geq \frac{1}{f}\left|\frac{\partial f}{\partial n}\right| \Big|_S \quad , \qquad c_2 \geq \frac{1}{f}\left|\frac{\partial f}{\partial n_1}\right| \Big|_\Sigma \quad ,$$

where

$$f = \sin \frac{\pi x}{a-a_1} \sin \frac{\pi y}{b-b_1} \sin \frac{\pi z}{c-c_1} \quad , \qquad f \neq 0 \quad \text{in } \hat{\Omega},$$

and where $a, a_1, \ldots, c_1$ are the parameters of the cube K (see figure 1) which contain the region $\hat{\Omega}$. The study of this problem leads to the minimization of the following functional

$$F/t/ = \int_{\hat{\Omega}} /\text{grad } t/^2 \, d\hat{\Omega} + \int_S \frac{2}{R} t^2 \, dS + \int_\Sigma \frac{2}{R_1} t^2 \, d\Sigma + \int_{\hat{\Omega}} 2\theta t \, d\hat{\Omega} \qquad (5).$$

Minimization of this functional takes in the special concrete Hilbert space $V/\hat{\Omega}/$, where $V/\hat{\Omega}/$ is the closure of $D/\hat{\Omega}/$ in the sense of the metric of the Sobolev space $W_2^1/\hat{\Omega}/$ (see IOSIDA 1965), and where $D/\hat{\Omega}/$ is the set of all functions $v \in C_2/\hat{\Omega}/$ which satisfy boundary conditions (2') and (3'). As shown in (NEDOMA 1973b), there exists exactly one disturbing potential T. This follows from the fact that the corresponding bilinear form $B/t,v/$, where

$$B/t,v/ = \int_{\hat{\Omega}} \text{grad } t \;\; \text{grad } v \, d\hat{\Omega} + \int_S \frac{2}{R} t\, v \, dS + \int_\Sigma \frac{2}{R_1} t\, v \, d\Sigma,$$

for all $v \in V/\hat{\Omega}/$ is V-elliptic *, and from the fact that T does not depend on the choise of the function w_1.

The space outside the Earth Ω and $\hat{\Omega}$ in the case where the gravity data from satellite observations are used, respectively, will be covered by a finite complex M_h of simple bodies, e.g., simple prisms, etc., in such a way that each surface has the following property:

Two elements of M_h have in common either a face or an edge or a vertex or are disjoint. The index h characterizes the maximum diameter of the elements of M_h. Let V_h be a finite dimensional subspace of V consisting of all functions whose restrictions to each element of M_h are polynomials of a prescribed degree. It is known that the disturbing potential t is the unique function in V which minimizes over V the functional at 4 and 5 respectively. The discrete disturbing potential t_h is a function from V_h which minimizes equation 4 (or equation 5) over V_h, i.e.,

$$F/t_h/ = \min_{v \in V_h} F/v/.$$

Let $\{\phi_k\}_{k=1}^n$ be a basis for V_h. Then $t_h/P/$ can be uniquely expressed in the form

$$t_h/P/ = \sum_k a_k \, \phi_k/P/ \qquad (6)$$

with some coefficients $a_1, \ldots, a_n$. Substituting successively $t_h/P/$ and ϕ_k $k = 1, \ldots, n$ into bilinear form corresponding to equations 4 and 5 respectively, we obtain the following system of linear algebraic equations for determining the unknown coefficients $a_1, \ldots, a_n$, i.e.,

$$\sum_{k=1}^{n} a_k (L\phi_k, \phi_m) = (-\theta, \phi_m), \qquad m=1, \ldots, n.$$

---

* The bilinear form $B/u,v/$ is V-elliptic if

$$B/u,v/ \geq c \, \|v\|^2_{W_2^1/\hat{\Omega}/} \quad , \qquad v \in V, \quad c = \text{const} > 0.$$

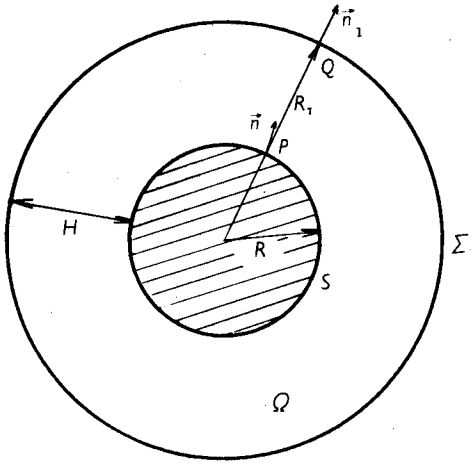

Figure 1.

Then the problem for studying the outer gravity field is transformed to the problem of studying the discrete outer gravity field. For a suitable choice of the basic functions, it may be shown that the discrete outer gravity field has similar properties to the outer gravity field (NEDOMA 1973a) concerning the maximum principle.

3. Conclusion

In the contribution presented, the possibility of studying the outer gravity field from the point of view of its discretization is discussed. This discretization of the outer gravity field was established from the variational formulation. An idea of a possible utilization of the satellite measurements performed on the Earth's surface was also given. However, there remains the question of transferring the gravity data received from the satellites to the above discussed surface Σ, as it turns with a different velocity around its axis than that of the satellite moving in its orbit. It appears that the discretization of the outer gravity field gives possibilities for using both types of measurements but the final answer cannot be given immediately.

4. Acknowledgments

I would like to thank Professor E. Grafarend who kindly delivered my lecture.

5. References

IOSIDA, K. 1965. *Functional Analysis.* Springer Verlag,Berlin.

MIKHLIN, S.G. 1966. *Čislennaja realizacija variacionnych metodov.* Nauka,Moscow.

NEDOMA, J. 1973a. On the Discrete Outer Gravity Field. *Pure & Applied geoph.* 110,1899.

NEDOMA, J. 1973b. The Variational Formulation of the Boundary Value Problem .. *Studia geoph.et geodet.* (in press).

BHATTACHARJI, J.C.
Geodetic & Research Branch
Survey of India
Dehra Dun UP
India

Proc. Symposium on Earth's Gravitational Field & Secular Variations in Position (1973),227-239.

GEOID, ISOSTATIC GEOID, ISOSTATIC CO-GEOID AND INDIRECT EFFECT OF GRAVITY IN INDIA

ABSTRACT

The terms relating to the geoid, isostatic geoid, isostatic co-geoid and indirect effect on gravity, are briefly explained in this paper with their implications in physical geodesy. After defining the geoid, the indirect effects of gravity are computed first with the help of Heiskanen's tables and then the isostatic geoidal heights derived for as many as 456 points uniformly distributed throughout the entire country after taking into account in the case of the latter, the shifting of the Earth's centre of gravity as is essentially needed in problems connected with the figure of the Earth in order to make the discussion complete. Finally the isostatic co-geoid (i.e., the actual geoid *minus* the computed isostatic geoid) is computed by making use of the actual geoidal data available in India till 1972. It has also been made clear that the procedure of deriving isostatic co-geoid direct from the geoid - isostatic differences is much more precise, economical and less time-consuming than what is normally obtained by first computing the isostatic deflections and then integrating the corresponding isostatic deflection anomalies circuit by circuit.

Relevant charts have been prepared and included to depict the geoid, isostatic geoid, isostatic co-geoid and indirect effect on gravity in contoured forms for extensive use in physical geodesy and various geophysical investigations in India.

1. Geoid

The figure of the Earth is a level surface whose potential is principally due to the gravitational attraction of the Earth's mass and the centrifugal force of the axial rotation. By convention, this level surface coincides with mean sea level which gives very nearly a physical representation of an equipotential surface, and is defined as the geoid (LAMBERT 1930,p.112). The elevations and depressions of this geoid with respect to the spheroidal surface of reference in use, i.e., the International spheroidal surface (see figure 1), and known as geoidal undulations, are depicted in maps in the form of geoidal contours. These undulations are normally determined either gravimetrically by the reputed Stokes' formula on utilizing the free air gravity anomalies all around the Earth or astro-geodetically as is usually done, by direct integration of plumb-line deflections observed at appropriate intervals or by satellite geodesy.

The Indian geoid fixed with respect to the adopted International spheroid of reference having the initial values at Kalianpur H.S. as

$$\xi_o = +2''.42 \quad ; \quad \eta_o = +3''.17 \quad ; \quad N_o = 9.5 \text{ m},$$

is obtained by the astro-geodetic method on utilizing about 1600 plumb-line deflections observed along geoidal circuits covering the entire country (GULATEE 1955,p.5).

Chart 1 depicts the positions of the geoidal circuits in India with the individual closure errors given

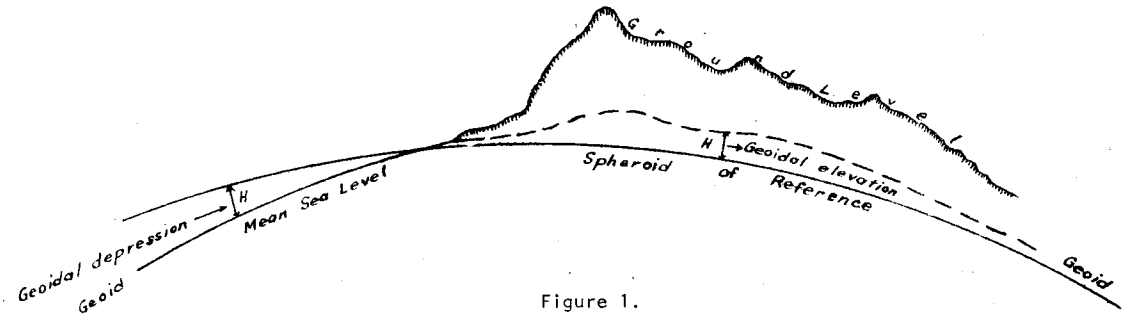
Ground Level
Geoidal elevation
H
Spheroid of Reference
Geoid
Geoidal depression
H
Mean Sea Level
Geoid

Figure 1.

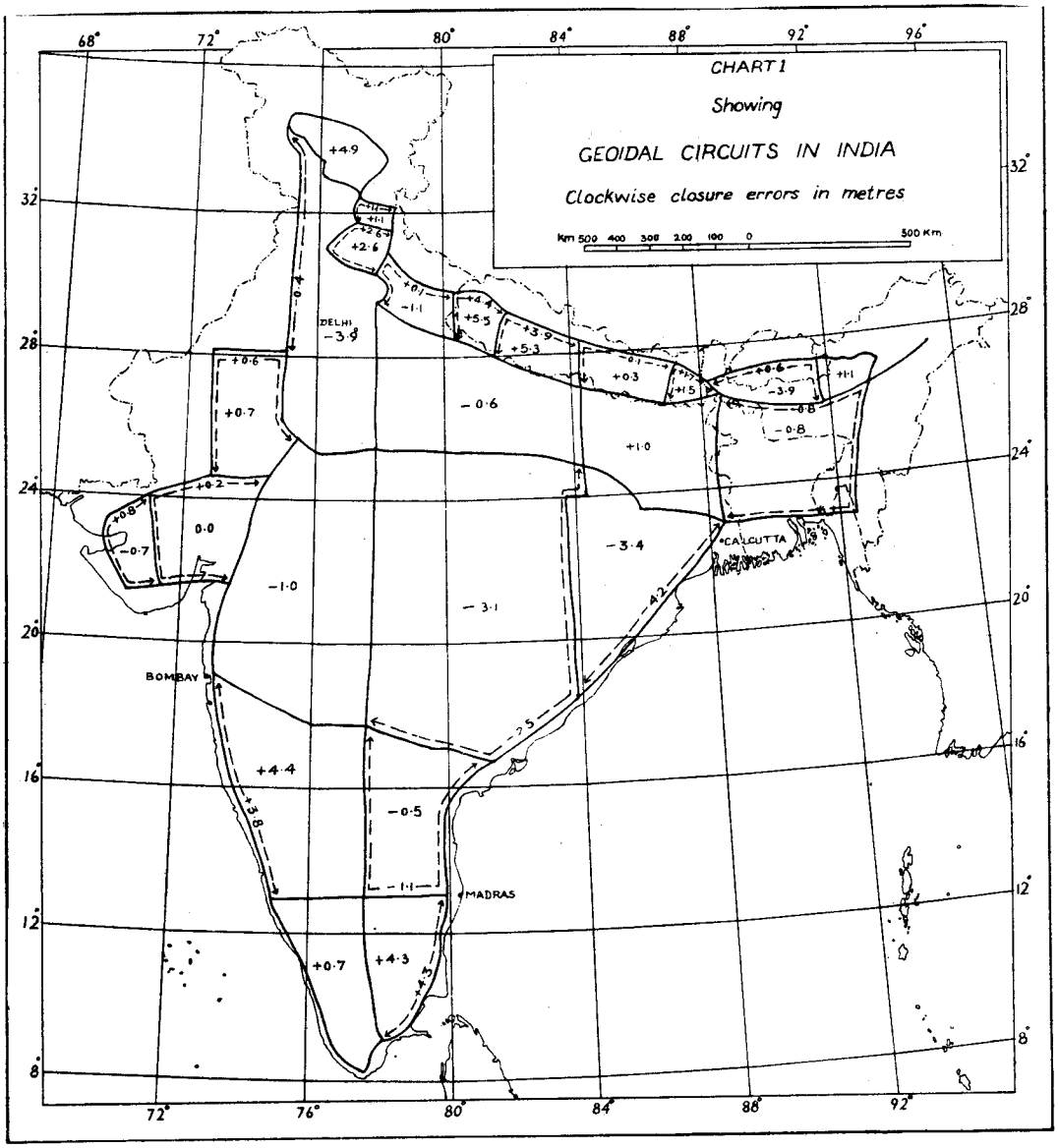
CHART 1
Showing
GEOIDAL CIRCUITS IN INDIA
Clockwise closure errors in metres
Km 500 400 300 200 100 0 500 Km
DELHI
BOMBAY
CALCUTTA
MADRAS
+4·9
+2·6
+0·7
+0·2
0·0
−0·7
−1·0
−0·6
+1·0
−3·4
−3·1
+4·4
−0·5
+0·7
+4·3
68°
72°
76°
80°
84°
88°
92°
96°
8°
12°
16°
20°
24°
28°
32°

within brackets, along which plumb-line deflection stations were established at 20 - 30 km intervals covering the entire country. The general procedure followed in carrying out the circuit to circuit figural adjustment of the closure errors is also indicated in the same chart.

Chart 2 depicts the geoid in India, based on the arbitrarily assigned value of +9.5 m for the geoid-spheroid separation at the initial point at Kalianpur H.S., showing the geoidal contours at intervals of 3 m in the high hills of the Himalayas and 1 m in the rest of the country. The chart comprises the synthesized results of about 1600 plumb-line deflections observed throughout the country, providing thereby a more realistic picture regarding not only the relative shape of the Indian part of the geoid, but also the underground crustal variations inside the Earth, than that provided by the isolated plumb-line deflections alone. But on referring to chart 1, it will appear necessary to have a much closer network of geoidal circuits in India in order to ensure a more precise and dependable geoidal map for the country. However, while delineating the geoidal lines inside the wider gaps between the existing deflection lines, attempts have been made to utilize the general trends of the theoretical geoid contours based on the isostatic considerations also (see chart 6) in order to make them more representative and precise. In fact, the geoidal undulations as given in chart 2, constitute a complete geoidal cover for India, and display a number of interesting features in the form of geoidal abnormalities. The chief among these is indicated by a broad band of average breadth 500 km with an average elevation of over 10 m running across the whole breadth of peninsular India, which has been given the appellation of the Hidden Range of Burrard, lying practically parallel to the Himalayan Range. This if followed by a region of marked depression of over 8 m along the Himalayan foot-hills, characterized by the alluvial plains of the Ganges, and then again by a region of elevated geoid of the order of 15 to 20 m or more towards the high Himalayas. On the whole, India in fact is a region of excessive geoid which again appears to rise as as we go east, west and north of the Indian frontiers. But unfortunately, the Indian part of the geoidal framework being yet based on a more or less arbitrary orientation, no definite conclusions can be drawn on them without further considerations.

2. Indirect Effect on Gravity

According to Clairaut's theorem, if the value of gravity is given at a single point on or outside a level surface whose form is known and coincides with the physical surface of a uniformly rotating body, then gravity due to the body at all points outside the level surface is uniquely determined. But the converse is not necessarily always true. In case, however, the level surface is not very different from an ellipsoid of revolution, the values of gravity on the level surface pre-determine the form of the surface itself. But in applying this theorem to the Earth, we face an obvious difficulty because of the implied condition for the level surface to coincide with the physical surface of the body, being not fulfilled by the Earth's geoidal surface (LAMBERT 1930,p.113). "The expedient adopted in the circumstances, is to substitute in imagination for the actual Earth, an idealized Earth in which the masses lying outside the geoid are replaced by masses within it. This process of substituting internal masses for external ones, changes, in general, both the values of gravity and the form of the geoid" (IBID).

When the masses involved and their old and new positions are known, those changes become calculable. Similarly, the transfer of matter implied in the usual isostatic reduction of observed values of gravity to the sea level, also means a warping of the geoid giving rise to a new surface which may be called an isostatically reduced warped geoid, with its centre of gravity having been shifted from that of the Earth during the process of computation. Hence, in applying the isostatic method to the

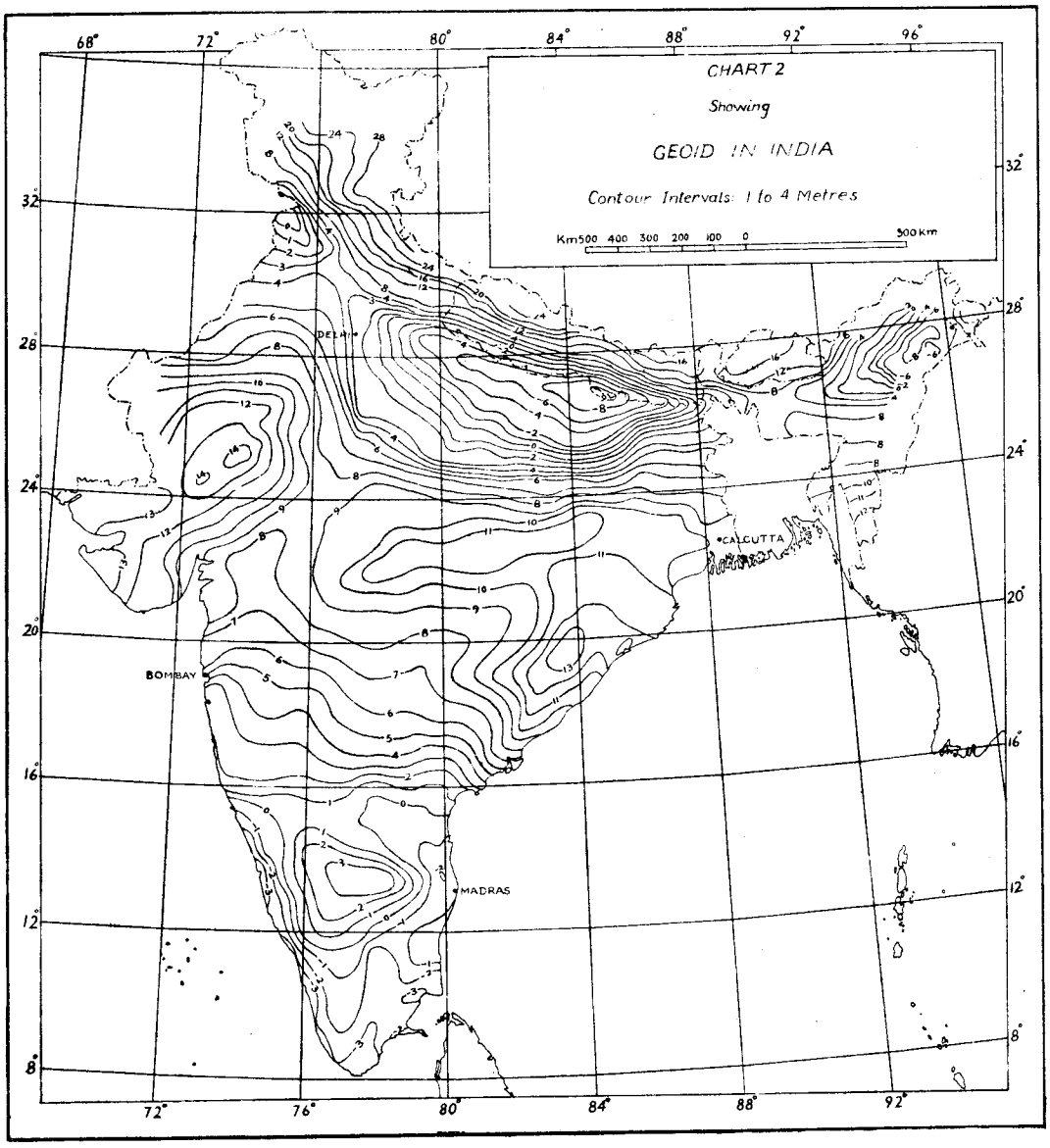

problem of the figure of the Earth, it must be remembered that the geoid differs from the warped geoid and an allowance has to be made accordingly by reducing observations to the latter instead of the former, in the form of an additional correction which is termed the *indirect effect* $\Delta_2 g$. Why the warped geoid referred to, is not required to be corrected at this stage, for the shifting of its centre of gravity will be explained later.

Now, the deviation of the warped geoid varying quite slowly, the topography and the compensation corresponding to the matter between the geoid and the warped geoid are practically equal, so that the resultant isostatic correction becomes very negligible reducing the indirect effect $\Delta_2 g$ ultimately to a simple free air correction only. In the free air method of reduction also, the intervening topography being condensed immediately below the level of the warped geoid, the indirect effect $\Delta_2 g$ is reduced to the same simple free air correction as before (IBID,p.143). The necessary tables have been provided by HEISKANEN & NISKANEN (1941) for direct evaluation of the indirect effect $\Delta_2 g$, i.e.,

the correction required to reduce the gravity values from the geoid to the warped geoid, obtained on account of the isostatically reduced visible topography considered on the entire surface of the Earth, so that the reduced isostatic anomalies can be rightly utilized in Stokes' formula. But the question of displacement of the Earth's centre of gravity due to the mass transfer implied in the isostatic reduction, is necessarily irrelevant at this stage as far as the reduced isostatic gravity anomalies are concerned; for, if the shifting occurs, the direct and indirect effects, $\Delta_1 g$ and $\Delta_2 g$ are both affected, and we do not ordinarily treat $\Delta_1 g$ and $\Delta_2 g$ separately, but only their sum which is never affected (IBID,p.162).

Chart 3 depicts the indirect effect on gravity $\Delta_2 g$ for India on Hayford's hypothesis of d = 113.7 km,

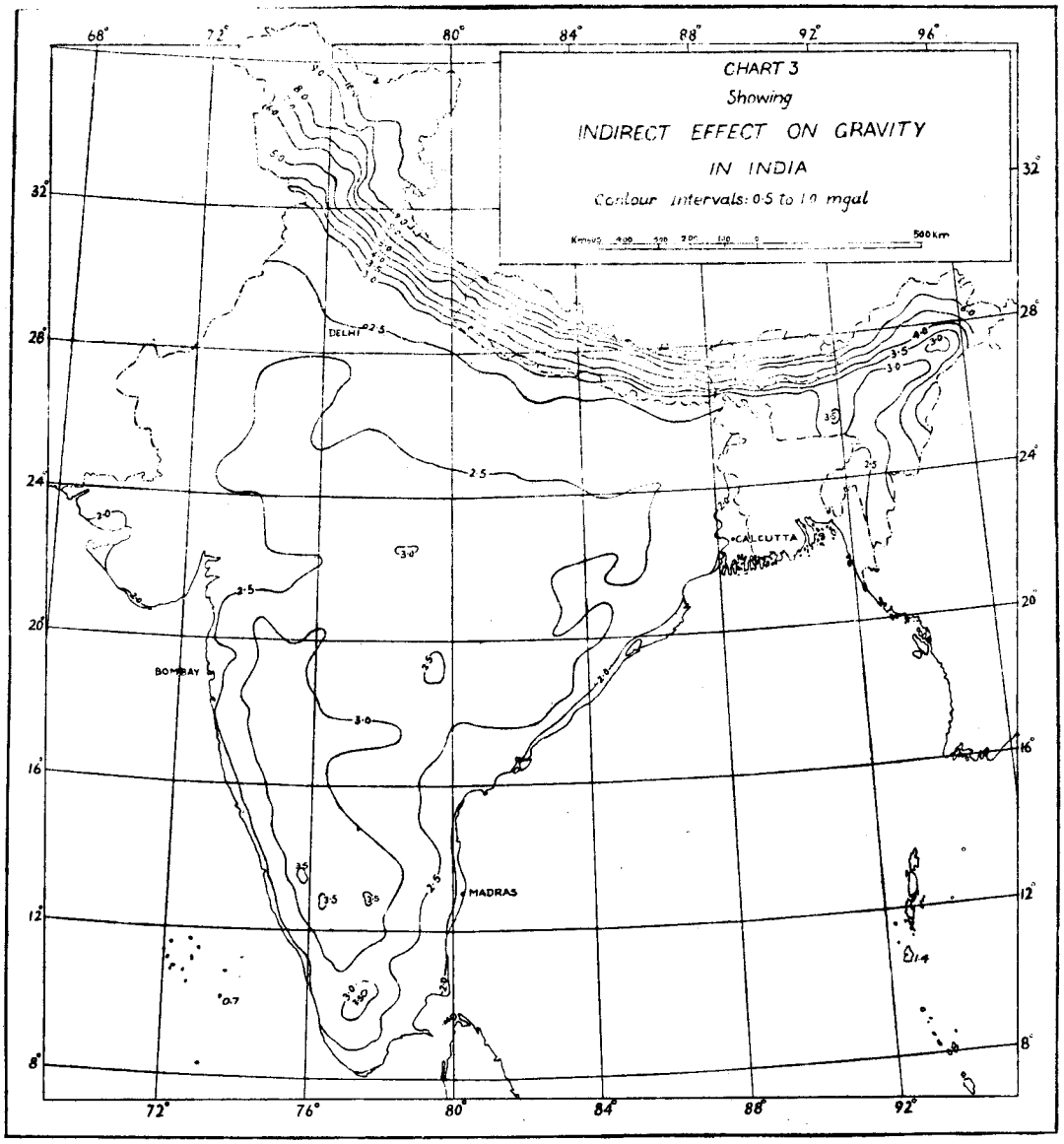

showing the $\Delta_2 g$ contours at intervals of 1 mgal in the high hills of the Himalayan region, and at 0.5 mgal in the rest of the country. The chart has been prepared for the first time for the Indian peninsula to the present high degree of precision, by making use of as many as 456 computed points throughout the country, in accordance with the recommendations of the International Union of Geodesy & Geophysics. The computations are based on the tables of HEISKANEN & NISKANEN (1941) for the effects up to Hayford zone 12, and a specially designed chart 4 for the effects of zones 11 to 1 is included in this paper.

The indirect effect has practically no use in geophysics by way of delineations of local structures, but plays an important role in physical geodesy in correcting relevant isostatic gravity anomalies for

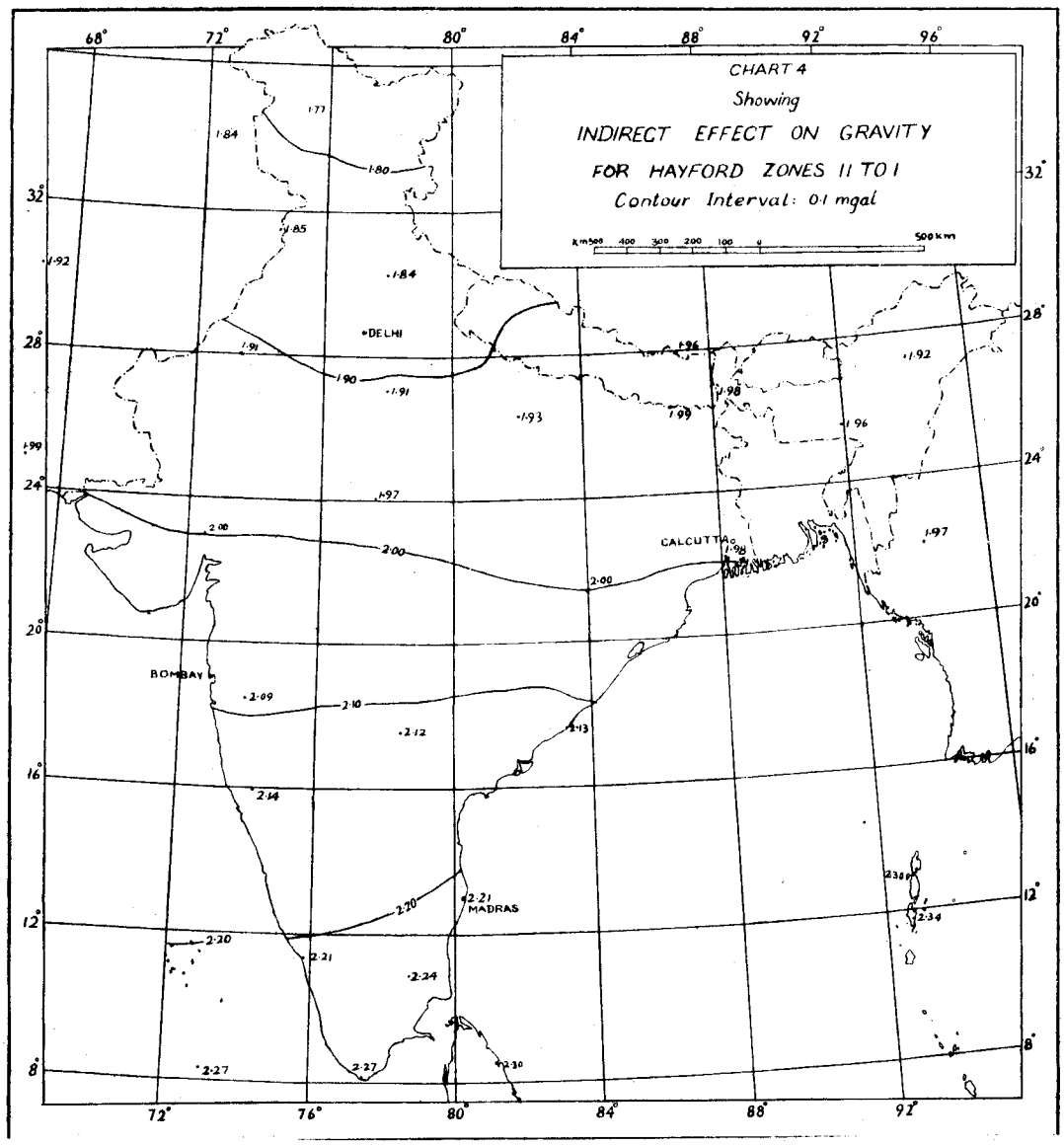

use in the Stokes and Vening Meinesz formulae for the determination of absolute undulations of the geoid and plumb-line deflections.

3. Isostatic Geoid and Isostatic co-geoid

As already mentioned, the overall transfer of the Earth's external topography above the geoid implied in the isostatic method of reduction, means not only the warping of the geoid but would also obviously displace the centre of gravity of the Earth. Moreover, since Stokes' formula furnishes the undulations of the same warped geoid having its centre of gravity coincident with that of the Earth and in no other position, the warped geoid has to be corrected for its deformation due to the displacement of its centre of gravity, while deducing the undulations of the geoid from the corresponding undulations derived from the Stokes formula. The warped geoid in its true position, duly corrected for the displacement of its centre of gravity, is termed as the *co-geoid* or more appropriately the *isostatic co-geoid* and is known in the Survey of India as the *compensated geoid*, as shown in figure 2. In fact there are many co-geoids of which the considered isostatic co-geoid on Hayford's hypothesis for $d = 113.7$ km, is one, as there are systems of substituting internal masses for external ones lying outside the geoid.

The necessary formulae are in existence for computing the required corrections for the displacement of the centre of gravity of the Earth in both magnitude and direction implied by the isostatic method of reduction on Hayford's hypothesis. The resultant displacement $\overline{X}_R$ of the centre of gravity of the Earth in passing from the geoid to the isostatic co-geoid, due to the addition of the isostatically compensated topography in the form of a cap of angular radius θ, height h, density ρ, Earth's mean density ρ_m and mean radius a, and depth of compensation d, is denoted by (LAMBERT 1930,p.162)

$$\overline{X}_R = \frac{3}{4} \frac{\rho}{\rho_m} \sin^2\theta \frac{h\ d}{a} \ ,$$

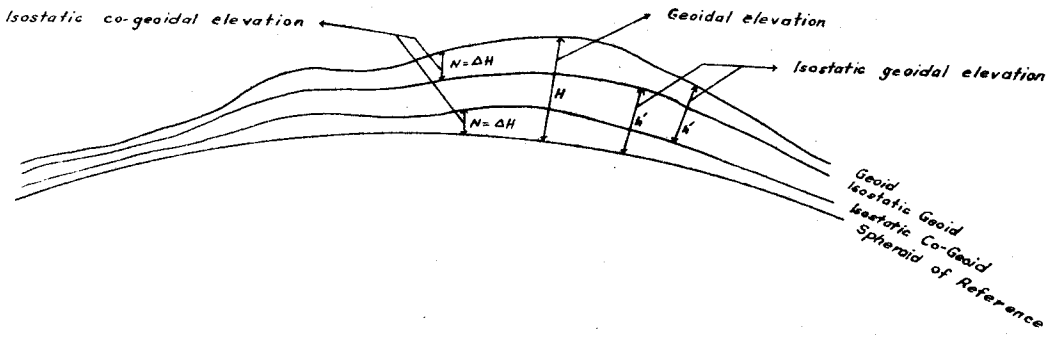

Figure 2.

and the summation for the separate zones furnishes the total resultant displacement. In practical applications, if the continents are considered as extra loads and the oceans as deficits of matter on the Earth's surface, the addition of these surpluses and deficits is to displace the centre of gravity. Let the latitude $\overline{\phi}$ and longitude $\overline{\lambda}$ denote the direction and $\overline{r}$ denote the amount of the displacement when the excesses and deficits are isostatically compensated on Hayford's hypothesis to a depth d (IBID, p.168). The results as obtained by Lambert and Prey for the case (d = 100 km) are as follows

$$\overline{r} = 4.9 \text{ m} \quad ; \quad \overline{\phi} = 43^{\circ}\ 57'\ \text{N} \quad ; \quad \overline{\lambda} = 31^{\circ}\ 01'\ \text{E}.$$

For any other depth d', the values of $\overline{\phi}$ and $\overline{\lambda}$ remain unchanged while the value of $\overline{r}$ gets changed approximately in the ratio d'/d (IBID,pp.168-169), the corresponding values in the case of Hayford's compensation for the depth of 113.7 km reduce to

$$\overline{r} = 5.6 \text{ m} \quad ; \quad \overline{\phi} = 43^{\circ}\ 57'\ \text{N} \quad ; \quad \overline{\lambda} = 31^{\circ}\ 01'\ \text{E}.$$

Now, since the displacement for any other point on the Earth's surface varies as the cosine of its angular distance from $(\overline{\phi},\overline{\lambda})$, the corrections can be worked out as above for only a limited number of uniformly distributed points and the values of the isostatic geoidal undulations as deduced from the corresponding values of the indirect effect on gravity ($\Delta_2 g$), with the help of the usual free air corrections only, can be adequately corrected for the displacement of the Earth's centre of gravity without any difficulty.

The vertical separation between the geoid and the isostatic co-geoid in its proper position, when reckoned positively downwards and superimposed on the surface of the spheroid of reference in the opposite sense, is termed the *isostatic geoid* on Hayford's hypothesis for d = 113.7 km (see figure 2). Indeed, if the particular hypothesis of isostasy used in the computation were exactly fulfilled in nature, and if the computations were rigorously made, the *isostatic geoid* and the *geoid* would have been exactly identical. But since the Earth is not constituted in that way, this can never be the case in actual practice. The undulations of the isostatic co-geoid or the Survey of India compensated geoid are thus equivalent to the *differences* (actual geoid *minus* isostatic geoid), i.e.,

$$N = H - h' = \Delta H \quad \text{(see figure 2)},$$

which can also rightly be designated as *isostatic geoidal anomalies* on the relevant Hayford's hypothesis for d = 113.7 km, providing an indirect measure of the regional departures of isostatic equilibrium inside the Earth. Similarly the undulations of the geoid are obtainable from the *sums* (isostatic co-geoid - derived gravimetrically from Stokes' formula - *plus* isostatic geoid), i.e.,

$$H = N + h' = \Delta H + h' \quad \text{(see figure 2)}.$$

The undulations of the isostatic co-geoid or the compensated geoid are determined either gravimetrically from Stokes' formula on utilizing the isostatic gravity anomalies all around the Earth or astro-geodetically, as is usually done, by direct integration of Hayford anomalies or more precisely isostatic deflection anomalies, i.e., the observed deflection *minus* the isostatic deflection computed on the Hayford hypothesis on considering compensated topography right up to the antipodes. The Indian isostatic co-geoid or compensated geoid has been obtained by the astro-geodetic method on utilizing about 1031 isostatic deflection anomalies computed till 1956 and adopting the initial value of the elevation of the isostatic co-geoid above the International spheroid of reference, at Kalianpur H.S. as +6.7 m which was originally derived by subtracting the approximate value of the

isostatic geoidal elevation computed on considering compensated topography upto a distance of 600 km only instead of the whole Earth, from that of the natural geoid more or less arbitrarily fixed with respect to the International spheroid of reference. As mentioned earlier, since the necessary tables are available (HEISKANEN & NISKANEN 1941) for the precise computations of the indirect effect $\Delta_2 g$ on considering the compensated topography all around the Earth, which can be straight away converted into the corresponding values of the undulations of the isostatic co-geoid by making use of the usual free air reduction factor and the corrections for the displacement of the Earth's centre of gravity from the relevant chart, it has been easily possible to derive for the first time the isostatic geoidal values with all the needed corrections applied, for as many as 456 uniformly distributed points in India, including the one at the initial point, which will provide not only a reliable isostatic geoidal picture for the whole country, but also a firm value for the isostatic co-geoidal elevation of +4.8 m instead of the old approximate figure of +6.7 m at Kalianpur H.S., relative to the more or less arbitrarily defined geoidal undulations in India. Since the undulations of the isostatic co-geoid as determined gravimetrically are considered absolute, these would, however, obviously differ from those obtained astro-geodetically, because of the arbitrariness in the orientation of the Indian geoid with respect to the International spheroid of reference. In fact, the astro-geodetic method of computing the undulations of the isostatic co-geoid by making use of the isostatic geoid as described above, is obviously much simpler and less time-consuming and therefore much more economical than that of direct integration of the Hayford or isostatic deflection anomalies on Hayford's hypothesis for d = 113.7 km, adopted later by the Survey of India as a routine procedure considering the latter presumably more precise (GULATEE 1955,p.7). But it can be seen from the comparative statement given below that if the considered corrections are duly applied, the procedure now adopted in this articale, apart from its remarkable simplicity in application, is much more accurate also than the existing one, because of not only the possible accumulation of errors in the individual isostatic co-geoidal circuits deduced from the large number of point to point isostatic deflection anomaly values, but also partly due to the computed isostatic deflection in use being not duly corrected for the displacement of the Earth's centre of gravity in the isostatic method of reduction.

Chart 5 depicts the corrections for the displacement of the Earth's centre of gravity on Hayford's hypothesis for (d = 113.7 km) in contoured forms at an interval of 0.1 m, for the entire country, to be applied to the undulations of the isostatic co-geoid in passing from the geoid to the isostatic co-geoid or straight away to those of the isostatic geoid with respect to the International spheroid of reference. The correction contours are based on only seven uniformly distributed points (see chart 5) computed by making use of the figures derived by Lambert and Prey.

Chart 6 depicts the isostatic geoid in India on Hayford's hypothesis for (d = 113.7 km) , prepared for the first time in its proper form, considering the compensated topography all round the Earth and also duly corrected for the shifting in the Earth's centre of gravity by making use of chart 5, and shows the isostatic geoidal contours at intervals of 3 m in the high hills of the Himalayas and 1 m in the rest of the country. The chart has been drawn by utilizing a dense network of computed isostatic geoidal elevations comprising the same 456 uniformly distributed points as for the indirect effects $\Delta_2 g$, thus making both charts 3 and 6 extremely precise and dependable. But critical examination of charts 2 and 6 will obviously indicate a lack of resemblance between the two, which will only show that Bowie's generalized statement

"The proof of isostasy has made it possible to compute an approximate geoid without all these observational data"

(BOWIE 1927,p.227) is not correct at least so far as India is concerned. In fact, the above

COMPARATIVE STATEMENT OF ISOSTATIC CO-GEOIDAL UNDULATIONS IN A CIRCUIT IN SOUTH INDIA DERIVED BY BOTH GEOID-ISOSTATIC GEOID AND ISOSTATIC DEFLECTION ANOMALY METHODS

Sl. No.	Sheet No.	Name of Station	Geoid	Isostatic geoid (corrected for shifting of earth's C.G.)	Isostatic co-geoid by Geoid-Isostatic Geoid Method No. 1 (4)−(5)	Isostatic co-geoid by Isostatic deflection anomaly Method No. 2 after having corrected for initial error of 1·9 m (including shifting of earth's C.G.) in isostatic geoid at Kalianpur H.S.	Discrepancy Method No. 1 *minus* Method No. 2 (6)−(7)	Correction to Method No. 2 for variation of error due to shifting of earth's C.G.	Isostatic co-geoid by Method No. 2 after correction* (7) + (9)	Discrepancy Method No. 2 *minus* Method No. 2 after correction* (6)−(10)
(1)	(2)	(3)	(4)	(5)	(6)	(7)	(8)	(9)	(10)	(11)
			metres	*metres*	*metres*	*metres*	*metres*	*metres*	*metres*	*metres*
1	56 G	Alipur ..	+4·0	+6·1	−2·1	+0·2	−2·3	−0·4	−0·2	−1·9
2	56 G	Sodaseopet ..	+4·2	+6·1	−1·9	+0·5	−2·4	−0·4	+0·1	−2·0
3	56 K	Muttanji ..	+4·2	+6·1	−1·9	+0·7	−2·6	−0·4	+0·3	−2·2
4	,,	Bolarum ..	+4·3	+6·0	−1·7	+0·9	−2·6	−0·5	+0·4	−2·1
5	56 K	Tuprampet ..	+3·6	+5·8	−2·2	+0·5	−2·7	−0·5	0·0	−2·2
6	56 O	Yalmanaid ..	+3·1	+5·4	−2·3	+0·5	−2·8	−0·5	0·0	−2·3
7	,,	Katangur ..	+2·6	+5·1	−2·5	+0·5	−3·0	−0·5	0·0	−2·5
8	,,	Suriapet ..	+2·5	+4·8	−2·3	+0·8	−3·1	−0·6	+0·2	−2·5
9	56 O	Munagala ..	+2·6	+4·5	−1·9	+0·9	−2·8	−0·6	+0·3	−2·2
10	65 D	Anumanchipalli ..	+2·8	+4·3	−1·5	+1·5	−3·0	−0·6	+0·9	−2·4
11	,,	Nandigama ..	+3·0	+4·0	−1·0	+1·9	−2·9	−0·6	+1·3	−2·3
12	,,	Ibrahimpatnam ..	+3·2	+3·6	−0·4	+2·5	−2·9	−0·6	+1·9	−2·3
13	,,	Anantavaram ..	+2·6	+3·6	−1·0	+1·9	−2·9	−0·6	+1·3	−2·3
14	,,	Dhulipalla S. ..	+1·0	+3·8	−2·8	+0·2	−3·0	−0·6	−0·4	−2·4
15	65 D	Kitapa S. ..	+0·6	+3·7	−3·1	−0·3	−2·8	−0·6	−0·9	−2·2
16	57 M	Danapa H.S. ..	0·0	+3·5	−3·5	−0·8	−2·7	−0·6	−1·4	−2·1
17	66 A	Medaimata ..	+0·1	+3·5	−3·4	−0·3	−3·1	−0·6	−0·9	−2·5
18	66 A	Ongole H.S. ..	−0·1	+3·3	−3·4	−0·4	−3·0	−0·7	−1·1	−2·3
19	57 M	Puripad ..	−0·5	+3·3	−3·8	−0·9	−2·9	−0·7	−1·6	−2·2
20	57 M	Darutippa S. ..	−1·1	+3·3	−4·4	−1·4	−3·0	−0·7	−2·1	−2·3
21	57 N	Nishanbadu ..	−1·9	+3·0	−4·9	−2·0	−2·9	−0·7	−2·7	−2·2
22	,,	Kistama H.S. ..	−2·2	+3·4	−5·6	−2·9	−2·7	−0·7	−3·6	−2·0
23	57 N	Bandaldura ..	−3·0	+3·0	−6·0	−3·0	−3·0	−0·7	−3·7	−2·3
24	66 B	Gudali H.S. ..	−2·9	+3·0	−5·9	−2·9	−3·0	−0·7	−3·6	−2·3
25	57 O	Ammapudi ..	−3·1	+3·0	−6·1	−3·2	−2·9	−0·7	−3·9	−2·2
26	,,	Satyanedu ..	−3·3	+3·4	−6·7	−3·6	−3·1	−0·8	−4·4	−2·3
27	57 O	Chambedu ..	−3·1	+3·1	−6·2	−3·1	−3·1	−0·8	−3·9	−2·3
28	57 P	Bimantangal ..	−2·6	+3·1	−5·7	−2·5	−3·2	−0·8	−3·3	−2·4
29	,,	Sembarambakkam ..	−2·6	+3·6	−6·2	−3·2	−3·0	−0·8	−4·0	−2·2
30	57 P	Chinnasamudram ..	−2·3	+4·1	−6·4	−3·5	−2·9	−0·8	−4·3	−2·1
31	57 O	Timmayyapalli ..	−1·2	+4·9	−6·1	−3·4	−2·7	−0·8	−4·2	−1·9
32	57 K	Venkatagiri ..	+0·1	+5·9	−5·8	−2·9	−2·9	−0·7	−3·6	−2·2
33	,,	Pattikonda ..	+1·2	+6·4	−5·2	−2·6	−2·6	−0·7	−3·3	−1·9
34	,,	Anantapura ..	+2·0	+5·9	−4·9	−2·4	−2·5	−0·7	−3·1	−1·8
35	57 K	Chunchadenahalli ..	+2·2	+7·2	−5·0	−2·4	−2·6	−0·7	−3·1	−1·9
36	57 G	Hoskote ..	+2·2	+7·6	−5·4	−2·7	−2·7	−0·7	−3·4	−2·0
37	,,	Bangalore ..	+1·9	+7·7	−5·8	−2·7	−3·1	−0·7	−3·4	−2·4
38	,,	Halasurbetta ..	+2·2	+7·6	−5·4	−2·5	−2·9	−0·7	−3·2	−2·2
39	,,	Kalkote h.s. ..	+2·2	+7·5	−5·3	−2·3	−3·0	−0·7	−3·0	−2·3
40	,,	Gudem hill staff ..	+1·7	+7·2	−5·5	−2·5	−3·0	−0·6	−3·1	−2·4
41	,,	Konduru white ridge ..	+1·1	+6·9	−5·8	−3·0	−2·8	−0·6	−3·6	−2·2
42	57 G	Bommasandra s. ..	+0·6	−6·8	−6·2	−3·3	−2·9	−0·6	−3·9	−2·3
43	57 F	Penukonda h.s. ..	+0·4	+6·7	−6·3	−3·4	−2·9	−0·6	−4·0	−2·3
44	,,	Urakonda H.S. ..	−0·2	+6·5	−6·7	−3·8	−2·9	−0·6	−4·4	−2·3
45	,,	Gollapalle h.s. ..	−0·9	+6·3	−7·2	−4·2	−3·0	−0·6	−4·8	−2·4
46	,,	Devarakonda H.S. ..	−1·2	+6·2	−7·4	−4·5	−2·9	−0·6	−5·1	−2·3
47	57 F	Kanampalli Rock peak	−1·7	+6·0	−7·7	−4·7	−3·0	−0·6	−5·3	−2·4
48	57 E	Namthabad S. ..	−1·8	+5·9	−7·7	−4·9	−2·8	−0·6	−5·5	−2·2
49	,,	Koitkonda h.s. ..	−1·6	+5·8	−7·4	−4·7	−2·7	−0·5	−5·2	−2·2
50	,,	Pullikonda H.S. ..	−1·5	+5·6	−7·1	−4·6	−2·5	−0·5	−5·1	−2·0
51	,,	Palakurti rock ..	−1·5	+5·4	−6·9	−4·5	−2·4	−0·5	−5·0	−1·9
52	57 E	Kere Belagal H.S. ..	−1·3	+5·4	−6·7	−4·2	−2·5	−0·5	−4·7	−2·0
53	56 H	Induvasi h.s. ..	−0·7	+5·4	−6·1	−3·6	−2·5	−0·5	−4·1	−2·0
54	,,	Tuagat h.s. ..	−0·4	+5·4	−5·8	−3·4	−2·4	−0·5	−3·9	−1·9
55	,,	Tonsalgutta s. ..	0·0	+5·4	−5·4	−3·0	−2·4	−0·5	−3·5	−1·9
56	,,	Jaganpalli rock ..	+0·5	+5·6	−5·1	−2·5	−2·6	−0·5	−3·0	−2·1
57	,,	Impagat H.S. ..	+1·5	+5·9	−4·4	−1·8	−2·6	−0·5	−2·3	−2·1
58	56 H	Dorapalli h.s. ..	+2·2	+6·3	−4·1	−1·4	−2·7	−0·5	−1·9	−2·2
59	56 G	Linganapalle h.s. ..	+2·7	+6·3	−3·6	−0·9	−2·7	−0·4	−1·3	−2·3
60	,,	Devanur s. ..	+2·9	+6·2	−3·3	−0·7	−2·6	−0·4	−1·1	−2·2
61	,,	Marepalli s. ..	+3·2	+6·2	−3·0	−0·4	−2·6	−0·4	−0·8	−2·2
62	,,	Kandenmarai T.S. ..	+3·7	+6·2	−2·5	−0·1	−2·4	−0·4	−0·5	−2·0
63	56 G	Alipur ..	+4·0	+6·1	−2·1	+0·2	−2·3	−0·4	−0·2	−1·9

* This still includes the error of + 9 m in co-geoid accumulated from Kalianpur H.S. to Alipur.

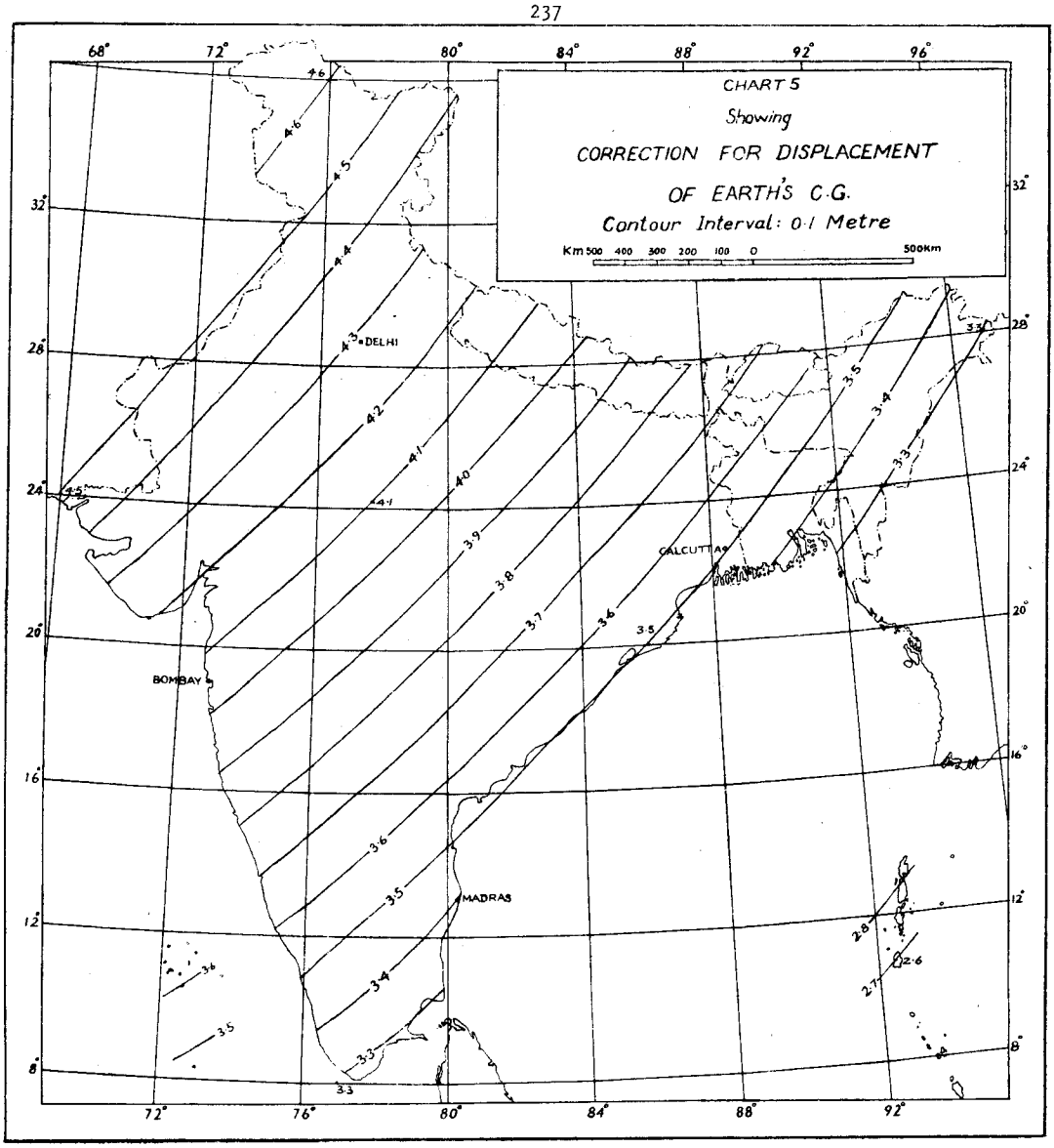

discrepancies are in a way, indirect measures of the deviation of isostatic equilibrium prevalent in the respective regions inside the Earth, and more vividly and completely represented in chart 7 (see next paragraph). But the isostatic geoidal undulations as given in chart 6, being duly corrected for the shifting of the Earth's centre of gravity, have ample applications in physical geodesy in obtaining the actual geoidal undulations directly from the corresponding isostatic co-geoidal values computed gravimetrically by the Stokes formula.

Chart 7 depicts the isostatic co-geoid in India on Hayford's hypothesis for (d = 113.7 km), prepared with the help of the same charts 2 and 6 by making use of their differences only at a sufficiently large number of, or simply the same 456 common points (as for $\Delta_2 g$) and as such, is expected to be as accurate as chart 2, the precision of chart 6 being unquestionable as indicated before. The chart

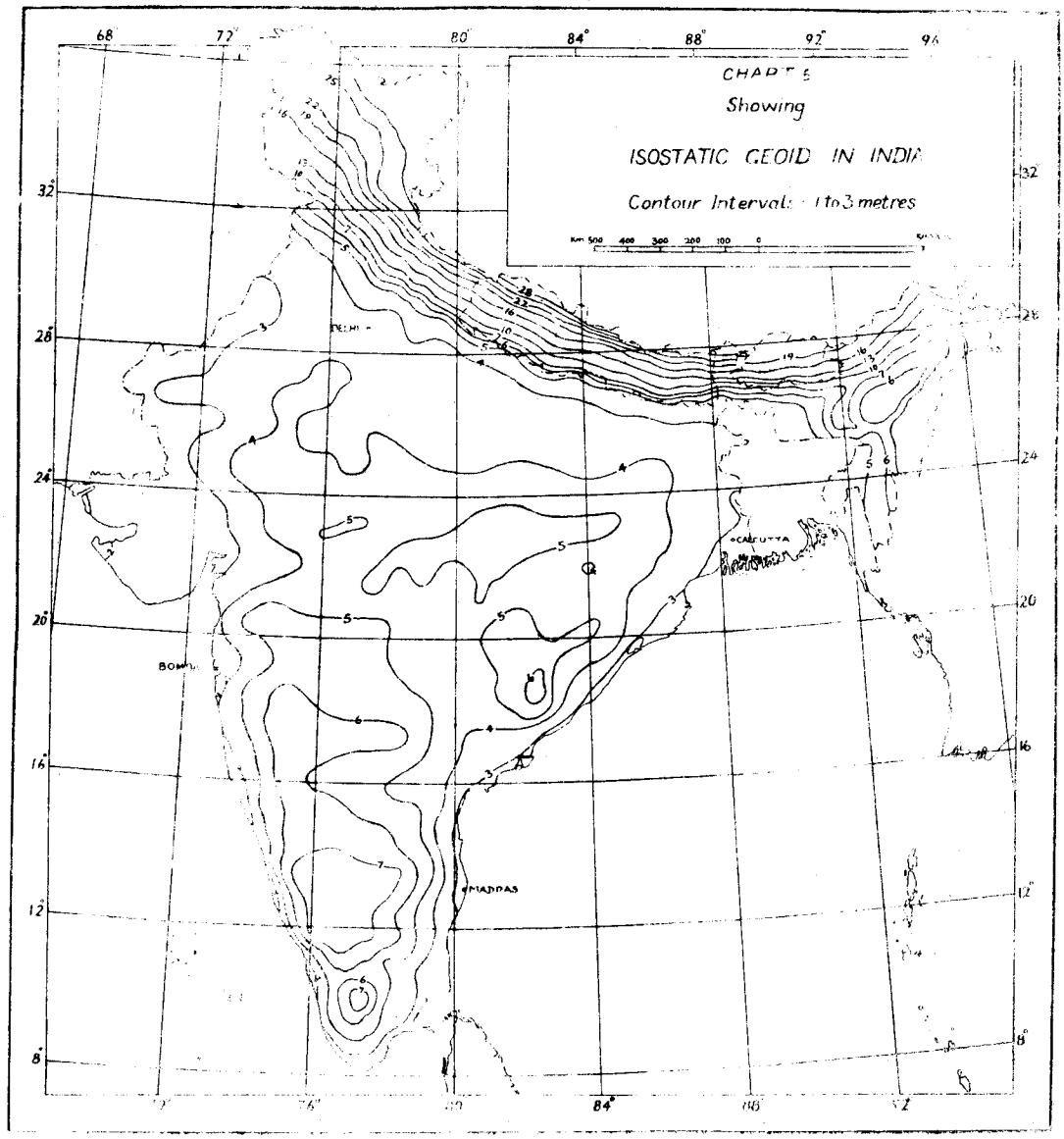

gives the isostatic co-geoidal contours relative to the assigned geoidal elevation of +9.5 m at Kalianpur H.S., at intervals of 3 m in the high hills of the Himalayan region and 1 m in the rest of the country.

The isostatic co-geoidal undulations as given in chart 7, indicate more or less, the same pattern of feature, slightly reduced, as the actual geoidal undulations in chart 2, showing thereby that the isostatic co-geoid has no significant correlation with the isostatic geoid derived according to isostatic theory from a purely theoretical consideration of the Earth's topographical features.

4. Acknowledgments

I am thankful to the Director, Geodetic and Research Branch, Survey of India, for his guidance, encouragement and offering of necessary facilities and data for writing this paper. My grateful

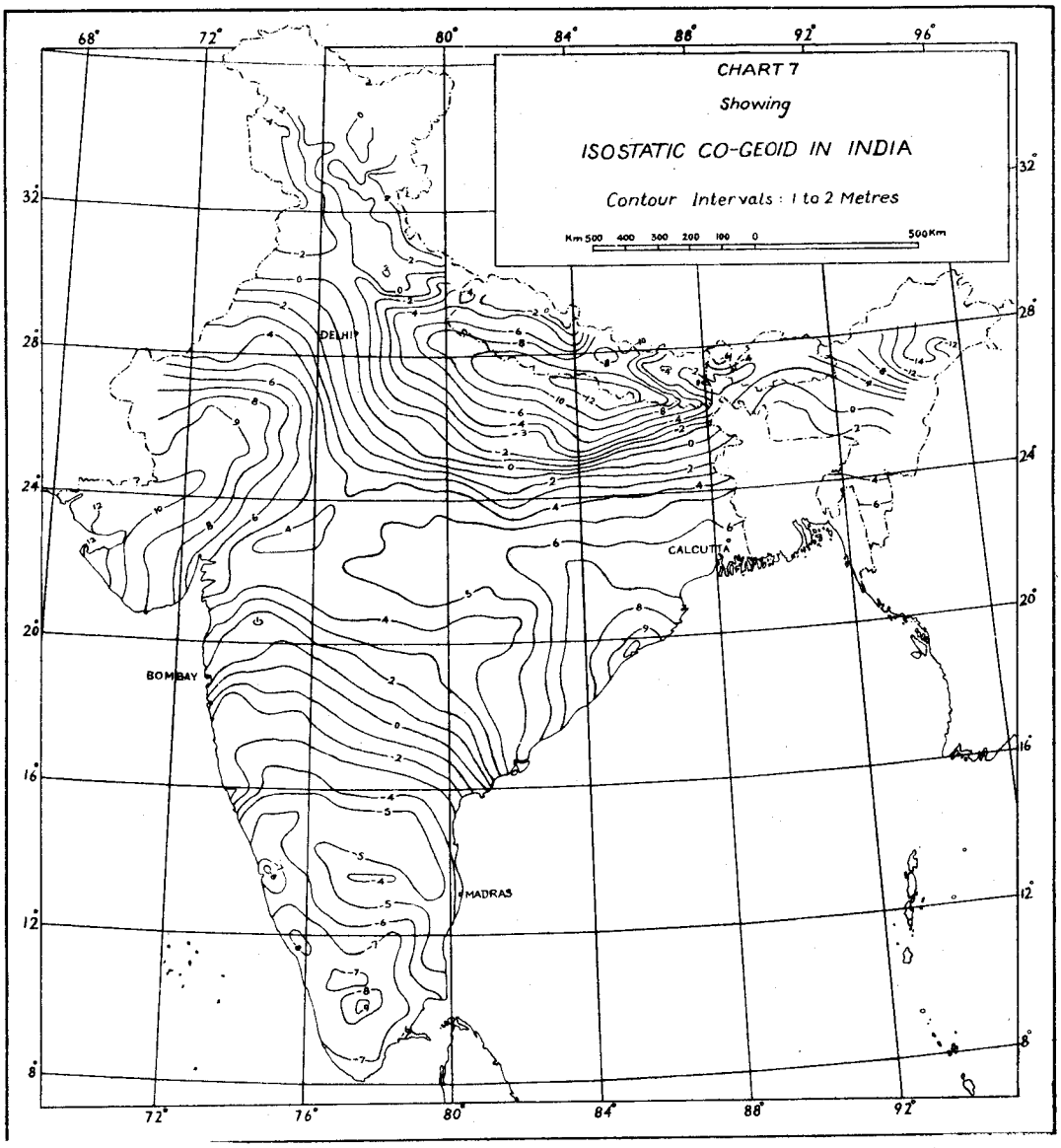

thanks are also due to the Surveyor General of India for his kindly granting me necessary permission to present the paper at the symposium.

5. References

BOWIE, W. 1927. *Am. J. Sci.* 81,227.

GULATEE, B.L. 1955. Deviations of the Vertical in India. *Tech.paper* 9,Survey of India, Dehra Dun.

HEISKANEN, W.A. & NISKANEN, E. 1941. World Map for the Indirect Effect of the Undulations of the Geoid on Gravity Anomalies. *Publ.Isostatic Inst.,International Association of Geodesy* 7.

LAMBERT, W.D. 1930. The Reduction of Observed Values of Gravity to Sea Level. *Bull.geodes.* 26, 107-181.

KAULA, W.M.
Institute of Planetary & Space Sciences
University of California
Los Angeles California 90024
United States of America

Proc.Symposium on Earth's Gravitational Field & Secular Variations in Position (1973),240-247.

MANTLE CONVECTIVE MODELS RELATED TO THE GRAVITY FIELD AND TECTONIC MOTION

ABSTRACT

A comprehensive mantle convective flow model will not be forthcoming for a long time. Difficulties include the highly non-linear character of the problem, the strong temperature and stress dependence of mantle rheology, and the complexity of the lithospheric boundary condition. Considerable improvement is being made in understanding simplified models. The principal regions in which more geodetic data would be of value are

1. major fault zones,
2. interiors of seismically active continents, and
3. post-glacial rebound areas.

1. Introduction

It is a truism of science that the aim of science is to find the fundamental causes of phenomena. However, this truism is an insufficient guide to action; to say, for example, that the Earth's gravity field is one of many consequences of a "big bang" origin of the universe does not yield any insight. In practice, the causes we seek are those which are proximate enough that the processes connecting them to observable phenomena are reasonably comprehensible and incontrovertible.

For much geodetic data the dominant cause is well known: isostasy. However, at this late date, the prevalence of isostasy is not very interesting: mainly the manifestation of the fact that, over 4.6×10^9 years of Earth history, density irregularities which are isostatically compensated tend to persist, while those which are not tend to die away by rock creep.

Of more interest are the indicators of current activity within the Earth. Most significant are:

1. the 10^3 year time scale of post glacial adjustment;
2. the approximately 45 ergs/cm^2/sec of heat coming from below the crust;
3. the 10^7 year time scale of the current plate tectonic pattern indicated by sea floor remanent magnetism; and
4. the marked compositional differentiations associated with igneous activity.

The creep rate inferred from the post glacial data, together with the density of heat sources indicated by the heat flow, imply that the Earth's interior is a highly non-linear flow system. The much longer time scale of plate tectonics indicates that this flow system is close to steady state. The compositional differentiations suggests that compositional inhomogeneities may be as important in driving the flow as thermal effects. A further complication is that the distribution of radiogenic heat sources is strongly correlated with variations in the bulk chemical composition, the U, Th, K being normally associated with CaO and Al_2O_3 (DICKINSON & LUTH 1971; GAST 1972; WYLLIE 1973).

2. Fundamental Considerations

If we assume a constant linear viscous rheology (i.e., strain rate proportionate to stress); assume all the heat sources are associated with the minor component δn_A; assume incompressibility; let potential $V = V_o + \delta V$, density $\rho = \rho_o + \delta\rho$, pressure $p = p_o + \delta p$; and take $\delta\rho$ to be composed of a thermal part $-\rho_o \alpha\, \delta T$ and a compositional part $\Delta\rho\, \delta n_A$, then the momentum and energy equations become:

$$\rho\left(\dot{\underset{\sim}{v}} + \underset{\sim}{v}\cdot\nabla\underset{\sim}{v}\right) = \rho_o \nabla\delta V - \nabla\delta p + \underset{\sim}{\lambda}\, g\left(\rho_o\alpha\, \delta T - \Delta\rho\, \delta n_A\right) + \eta\, \nabla^2\underset{\sim}{v} \tag{1}$$

and

$$\dot{T} + \underset{\sim}{v}\cdot\nabla T = \kappa\, \nabla^2 T + \frac{q n_A}{\rho C_V} + \frac{\eta}{2\rho C_V} E^2 \tag{2},$$

where $\underset{\sim}{v}$ is velocity, $\underset{\sim}{\lambda}$ is the radial unit vector, g is gravity, η is viscosity, T is temperature, κ is thermal diffusivity, q is energy release per unit volume of heat sources n_A, C_V is heat capacity and E is the strain rate tensor.

If we further use as a unit of length the distance d between upper and lower boundaries; of time, d^2/κ; of mass, $d^2\eta/\kappa$; and of temperature, $q n_A d^2/(3\kappa\rho C_V)$, then the equations become

$$\frac{1}{Pr}\left(\dot{\underset{\sim}{v}} + \underset{\sim}{v}\cdot\nabla\underset{\sim}{v}\right) = \frac{1}{Pr}\delta V - \nabla\delta p + \underset{\sim}{\lambda}\left(Ra\, \delta T - Co\, \delta n_A\right) + \nabla^2\underset{\sim}{v} \tag{3},$$

and

$$\dot{T} + \underset{\sim}{v}\cdot\nabla T = \nabla^2 T + Di\, E^2 + 3\left(1 + \delta n_A/n_A\right) \tag{4},$$

where, using typical values for the Earth's mantle with $d \simeq 2900$ km,

$$\left.\begin{aligned} Pr &= \eta/(\rho_o\kappa) && \simeq 3\times 10^{24} \\ Ra &= \alpha q\, n_A d^5 g/(3\kappa^2\eta C_V) && \simeq 4\times 10^{7} \\ Co &= \Delta\rho\, g\, d^3/(\kappa\eta) && \simeq 10^{8} \\ Di &= 3\kappa^2\eta/(2q\, n_A d^4) = \alpha dg/(C_V Ra) && \simeq 10^{-8} \end{aligned}\right\} \tag{5},$$

The large Prandtl number Pr means that the flow is non-turbulent; evolution of the system from within takes place only through the energy equation. The large Rayleigh Ra, about 10^4 times critical, indicates the flow is highly non-linear, and the large Co indicates that compositional variations could be of comparable significance to thermal variations. The small Di suggests dissipation is negligible; however (unlike Pr), this parameter has a strong dependence on the length scale d. Furthermore, the strain rate tensor E depends strongly on the aspect ratio of the flow. Hence if the flow cells are confined to a relatively shallow zone of less than about 500 km, dissipation can be significant. This also corresponds roughly to the length d which will make the Rayleigh number Ra close to the value found as critical for the onset of convective flow, 1100.

Laboratory experiments indicate that the assumptions on which the aforegoing discussion is based may be a gross over-simplification (WEERTMAN 1970; STOCKER & ASHBY 1973). Assuming variations in

the gravity field Δg are due to density variations $\delta\rho$ spread over some zone h, the resulting stress differences of order $g\,\delta\rho\,h$ are large enough that the rock strain rate has a strongly non-linear dependence on stress, to a third or higher power of the stress. Furthermore, there are strongly non-linear dependences of viscosity η and density ρ on temperature, the latter arising from phase transitions. The most evident consequence of the temperature dependence of the viscosity is the lithosphere, a layer 30 - 100 km thick for which an elastic rheology is appropriate. The lithosphere is a strong stress guide horizontally, as evidenced by the wide extent of some of the tectonic plates. It also must have a strong thermal effect where it is thrust down into the asthenosphere. On the other hand, the lithosphere is rather thin on a global scale, so that it is not at all resistant to broad scale vertical stresses, and acts essentially as a free boundary.

Laboratory experiments and theoretical studies both indicate that contained heat sources and temperature dependence of properties have complicating effects, making stable patterns three-dimensional rather than two-dimensional (BUSSE 1967). As might be expected, the non-linear dependence of strain rate on stress has the effect of concentrating the flow considerably.

3. Model Studies

At present, a true mantle convection model does not exist. The combination of macroscale problems (essentially, the high degree of non-linearity) and microscale problems (the great number of plausibly significant effects) makes all modeling to date piecemeal. The problem which has been most thoroughly studied is simple Bernard convection; i.e., equations 3 - 4 simplified to

$$\left.\begin{aligned} 0 &= -\nabla\delta p + \underset{\sim}{\lambda}\,Ra\,\delta T + \nabla^2\underset{\sim}{v} \\ \dot{T} + \underset{\sim}{v}\cdot\nabla T &= \nabla^2 T \\ T(1) &= 0 \\ T(0) &= 1 \end{aligned}\right\} \quad (6),$$

This has been solved analytically up to about $Ra \simeq 10^5$ (IBID) and numerically up to $Ra \simeq 10^7$ (MCKENZIE ET AL 1973). The conclusions are that as Ra increases, rolls remain stable but cells are smaller and plumes and boundary layers become narrower.

Partial models related to understanding mantle convection can be grouped into about five classes, in accordance with their limitations.

(1) Analytic expansions at moderate Ra (MALKUS & VERONIS 1958; BUSSE 1967; RICHTER 1973). These expansions are in terms of one to three small parameters, such as $(Ra - Ra_{cr})/Ra$. Linear dependencies of properties on temperature, contained heat sources, phase transitions, and two component effects have been analysed in plane layers, and some in spherical geometry. Some results suggestive for application at still higher Ra are :
   (a) the persistence of flow planforms as Ra is increased;
   (b) the breakdown of the flow into three-dimensional patterns with internal heat sources or temperature dependent properties; and
   (c) the correspondence of steady state flow to maximization of heat transport.

(2) Two dimensional numerical integration (IBID; TORRANCE & TURCOTTE 1971; ANDREWS 1972; MCKENZIE ET AL 1973). The computer is the obvious device for higher Ra. However, the capacity and speed of present-day computers makes a full three-dimensional integration too expensive. A variety of effects -- contained heat sources, exponential temperature dependence on viscosity, dissipation, etc. -- have been examined. Phase transitions enhance the rate of flow. Contained heat sources result in broad up-plumes and narrow down-plumes, while the higher order temperature of viscosity results in narrow up-plumes and broad down-plumes. Integrations combining these effects have not yet been made. Also there have been virtually no attempts to extrapolate inferences to three dimensional flow.

(3) Long wavelength analyses (MCKENZIE 1968; KAULA 1974). The spectra of the topography, gravitational potential, and plate tectonic velocities suggest that a dominant part of the flow is broad scale, appropriate for expressions in terms of spherical harmonic coefficients $C_{\ell m}(x)$, $S_{\ell m}(x)$. If we define for scalar quantities x:

$$S_\ell(x) = \sum_{n=1}^{\ell} \sum_{m=0}^{n} \{ \overline{C}^2_{nm}(x) + \overline{S}^2_{nm}(x) \} \qquad (7),$$

and for vector quantities v:

$$S_\ell(v) = \sum_{n=1}^{\ell} n(n+1) \sum_{m=0}^{n} \{ \overline{C}^2_{nm}(v_s) + \overline{S}^2_{nm}(v_s) + \overline{C}^2_{nm}(v_T) + \overline{S}^2_{nm}(v_T) \} \qquad (8),$$

where the subscript $_s$ denotes poloidal and the subscript $_T$ denotes toroidal, then the values of $S_\ell(x)/S_{36}(x)$ are:

ℓ	Topography	Potential	Velocity
2	0.48	0.65	0.64
4	0.68	0.90	0.76
6	0.81	0.95	0.85
8	0.86	0.97	0.89

However, the continental part of the topography is largely accounted for by static isostasy, while the potential spectrum ($10^{-5}\ n^{-2}$ "rule of thumb") corresponds to a white spectrum in density. Only the velocity spectrum is found to have implications for deep flow in solutions optimizing heat transfer. The observational fact of plate tectonics is the main rationale for pursuing this approach.

(4) Boundary layer or plume studies (SCHUBERT & TURCOTTE 1971; RICHTER 1973; ANDREWS 1972; References in section 6.7) . Models confined to the lithosphere and its interaction with the asthenosphere have been rather successful in explaining characteristics of certain types of features, particularly oceanic rises (ANDREWS 1972; SCLATER & FRANCHETEAU 1970; LACHENBRUCH 1973; PARKER 1973) and underthrust lithospheric zones (SCHUBERT & TURCOTTE 1971; MCKENZIE 1969; TOKSÖZ ET AL 1971; GRIGGS 1972). These models necessarily assume a level of isostasy or zero work a few hundred kilometres deep. Recent developments in understanding the phase transition dependences on water (GREEN 1973) may allow the extension of oceanic rise models to explain the topographic and gravity lows of ocean basins as a consequence of accelerations arising from a thickening lithosphere.

More speculative work in this category are models of continental break up due to contained heat

sources, and of narrow up-plumes leading to "hot spots" (MORGAN 1972; DEFFEYES 1972).

(5) Purely mechanical studies. This category comprises the response of viscous or elastic-viscous layered media to known changes in load. Post-glacial uplift studies, which yield the principal evidence that the mantle indeed flows, are the best known examples (see references in section 6.8). Because of inadequate data on the peripheral bulge zone, there are still differences by a factor of ten as to the lower mantle viscosity. Other doubts arise from the transient nature of the uplift, and from the possible importance of non-linear dependence of strain rate on stress.

Another area of study which should develop considerably in the near future is anelastic deformation in fault zones. The inability to account for Chandler wobble with elastic dislocation models suggests that anelastic flow may be the significant excitation. In this instance, the layered elastic and viscous layered medium is broken by a fault, which is loaded by motions prescribed from the kinematic plate tectonic model. The problem is to reconcile deformation patterns from models with those observed near a fault.

4. Conclusions

Current efforts applicable to mantle convection are still rather far from directly explaining the observed gravity field and plate motions. The inferences are still quite qualitative, but progress is considerable. A list in rough order of decreasing firmness and increasing speculativeness might be :

- Compositional variations are of comparable importance to thermal variations.
- Phase transitions reinforce and amplify thermal expansion and contraction
- The smallness of variations in the gravity field indicates that the driving density differences are too small to force all the return flow through a thin asthenosphere; there must be a deeper flow.
- The temperature dependence of viscosity probably leads to a fairly constant mean viscosity as a function of depth below the asthenosphere.
- Gravity anomalies tend to reflect rather shallow conditions, while plate velocities reflect deeper conditions.
- The observed plate velocities of some centimetres per year indicate a depth of flow several hundred kilometres at least, so that the dissipation (i.e., friction) is not too great.
- If thermal plumes are narrow and do not move with time, then the mantle is significantly differentiated in heat sources and composition.

Relevant to the purposes of this conference to prescribe observations of the gravity field and secular motions, the more fundamental studies of mantle convection seem to be of little help, since they are still far from explaining existing data. A lot more modeling is needed to develop the necessary insight. It can be said, however, that for the broad scale of more than a thousand km, it is virtually certain that refinement of geodetic data would not help, particularly over oceanic areas. The system is so sluggish that on this scale there can be no doubt that the relative velocities obtained from remanent magnetism prevail in an essentially steady state manner.

The areas in which more geodetic data would help are of three types.

1. Fault zones: the margins between tectonic plates, be they tensile, compressive or strike slip. Although the plates themselves must move very steadily, at the edges there is a lot of irregular jerky motion which it is desirable to understand better for scientific as well as practical reasons, such earthquake alleviation.

2. Active continental areas: regions in which a minor (less than 1%) but perceptible portion of seismic energy is released, such as the United States from the Rockies eastward, or the Tien-Shan - Baikal belt in the USSR. In such regions there may be smaller tectonic plates or incipient rifts, but the remanent magnetism is too mixed up, and the rates too slow, to get any indication of relative motion between parts of continent to the accuracy attained for oceanic areas.

3. Post glacial uplift. As mentioned earlier some ambiguity as to interpretation still exists, which could be solved by more detailed data.

5. Acknowledgments

This work is supported by NSF grant GA-10963. This paper is Institute of Geophysics & Planetary Physics Publication No. 1233.

6. References

For each of several subject areas some references are suggested. The list is not intended to be complete or representative.

6.1 Rheology of Mantle Materials

STOCKER, R.L. & ASHBY, M.F. 1973. On the Rheology of the Upper Mantle. *Revs.geophys.space phys.* 11,391-426.

WEERTMAN, J. 1970. The Creep Strength of the Earth's Mantle. *Revs.geophys.space phys.* 8,145-168.

6.2 Compositional Considerations

CLARK, S.P.,Jr. & RINGWOOD, A.E. 1964. Density Distribution and Constitution of the Mantle. *Revs.geophys.* 2,35-88.

DICKINSON, W.R. & LUTH, W.C. 1971. A Model for Plate Tectonic Evolution of Mantle Layers. *Science* 174,400-404.

GAST, P.W. 1972. The Chemical Composition of the Earth, the Moon, and Chondritic Meteorites. In (ROBERTSON, E.C. ed.) *The Nature of the Solid Earth.* McGraw-Hill, New York,19-40.

GREEN, D.H. 1973. Contrasted Melting Relations in a Pyrolite Upper Mantle Under Mid-Oceanic Ridge, Stable Crust, and Island Arc Environments. *Tectonophysics* 17,285-297.

WYLLIE, P.J. 1973. Experimental Petrology and Global Tectonics - a Preview. *Tectonophysics* 17, 189-209.

6.3 Fundamental Stability Analyses

BACKUS, G.E. 1955. On the Application of Eigenfunction Expansions to the Problem of the Thermal Instability of a Fluid Sphere Heated Within. *Phil.Mag.Ser.7* 46,1310-1327.

CHANDRASEKHAR, S. 1961. *Hydrodynamic and Hydromagnetic Stability.* Clarendon Press,Oxford,652 pp.

JEFFREYS, H. & BLAND, M.E.M. 1951. The Instability of a Fluid Sphere Heated Within. *Mon.Not.R. astr.Soc.,geophys.Suppl.*6,148-158.

SCHUBERT, G. & TURCOTTE, D.L. 1971. Phase Changes and Mantle Convection. *J.geophys.Res.* 76, 1424-1432.

6.4 Analytical Developments at Small Rayleigh Number

BUSSE, F.H. 1967. The Stability of Finite Amplitude Cellular Convection and its Relation to an Extremum Principle. *J. fluid mech.* 30,625-649.

MALKUS, W.V.R. & VERONIS, G. 1958. Finite Amplitude Cellular Convection. *J.fluid mech.* 4,225-260.

RICHTER, F.M. 1973. Dynamical Models for Sea Floor Spreading. *Revs.geophys.space phys.*11,223-287.

6.5 Numerical Integrations in Two Dimensions

The last reference in section 6.4 plus

ANDREWS, D.J. 1972. Numerical Simulation of Sea-Floor Spreading. *J.geophys.Res.* 77,6470-6481.

MCKENZIE, D.P., ROBERTS, J. & WEISS, N. 1973. Numerical Models of Convection in the Earth's Mantle. *Tectonophysics* 19,89-103.

TORRANCE, K.E. & TURCOTTE, D.L. 1971. Structure of Convection Cells in the Mantle. *J.geophys.Res.* 76,1154-1161.

6.6 Long Wavelength Analyses

KAULA, W.M. 1974. Thermal Convection in a Sphere as an Inverse Problem, with Applications to the Earth and Moon. *J.geophys.Res.* 79 (in press).

MCKENZIE, D.P. 1968. The Influence of the Boundary Conditions and the Rotation on Convection in the Earth's Mantle. *Geophys.J.R.astr.Soc.* 15,457-500.

6.7 Boundary Layer and Plume Computations and Speculations

The last reference in sections 6.3 and 6.4, the first reference in section 6.5, plus

DEFFEYES, K.S. 1972. Plume Convection with an Upper Mantle Temperature Inversion. *Nature* 240, 539-544.

GRIGGS, D.T. 1972. The Sinking Lithosphere and the Focal Mechanism of Deep Earthquakes . In (ROBERTSON, E.C. ed.) *The Nature of the Solid Earth.* New York,361-384.

JACOBY, W.R. 1970. Instability in the Upper Mantle and Global Plate Movements. *J.geophys.Res.* 75, 5671-5680.

KAULA, W.M. 1972. Global Gravity and Mantle Convection. *Tectonophysics* 13,341-359.

LACHENBRUCH, A.H. 1973. Differentiation and the Gravitational Driving Force for Material Rising at an Ocean Ridge. *J.geophys.Res.* 78,825-831.

MCKENZIE, D.P. 1969. Speculations on the Consequences and Causes of Plate Motions. *Geophys.J.R. astr.Soc.* 18,1-32.

MORGAN, J.W. 1972. Plate Motion and Deep Mantle Convection. *Mem.geol.Soc.Am.* 132,7-22.

PARKER, R.L. 1973. Thermal Model of Ocean Ridges. *Nature phys.science* 242,137-139.

SCLATER, J.G. & FRANCHETEAU, J. 1970. The Implications of Terrestrial Heat Flow Observations on Current Tectonic and Geochemical Models of Crust and Upper Mantle on the Earth. *Geophys.J.R.astr.Soc.* 20,493-509.

TOKSÖZ, M.N., MINEAR, J.W. & JULIAN, B.R. 1971. Temperature Field and Geophysical Effects of a Downgoing Slab. *J.geophys.Res.* 76,1113-1138.

TURCOTTE, D.L. & OXBURGH, E.R. 1967. Finite Amplitude Convection Cells and Continental Drift. *J.fluid.mech.* 28,29-42.

6.8 Post-Glacial Rebound Analyses

CATHLES, L.M. 1971. Lower Mantle Viscosity Inferred from Post Glacial Adjustment of the Ocean Basins and Canada. *EOS Trans.Am.geophys.U.* 52,353.

MCCONNELL, R.K.,Jr. 1968. Viscosity of the Mantle from Relaxation Time Spectra of Isostatic Adjustment. *J.geophys.Res.* 73,7089-7105.

O'CONNELL, R.M. 1971. Pleistocene Glaciation and the Viscosity of the Lower Mantle. *Geophys.J.R. astr.Soc.* 23,299-327.

WALCOTT, R.I. 1973. Structure of the Earth from Glacio-Isostatic Rebound. *Ann.Rev.Earth plan. Sci.* 1,15-37.

7. Discussion

HOLDAHL: Do you think that VLBI and lunar laser ranging measurements will help improve the value for the drift rates?

KAULA: The remanent magnetism has a resolution of roughly 10^5 years. That is the time in which the distance the plate moves is about the same as the depth of the ocean. It is about a third of the average time between reversals. Because the driving forces are shifted only by the convection underlying the plate motion, it is plausible that the spatial average plate motion this year or any other year, will be close to the temporal average over 10^5 years. You will not find geophysicists asking for the measurement of continental drift. You will find geophysicists asking for measurement of relative motion in confused areas like the San Andreas fault region in California. This is the sort of situation to which geodetic measurements can contribute. Somewhere between the 5000 km scale of major plates and the few km scale on which marked relative motion on faults occur, *variations* in relative motion of say a centimetre per year occur. 1000 km seems to be a conservative upper limit.

MUELLER: Are you saying that the separation of VLBI stations over several thousand km is not useful anymore from the geophysicists' point of view to determine plate motion?

KAULA: Suppose you detected differences from the remanent magnetism motion between, say, stations in Hawaii and Japan. It would be a moot point whether this result reflected local or regional effects in Hawaii or Japan or both, and not motions of the entire plates.

GUBBAY: The VLBI measurement should be across a minimum distance, say a fault. This is because the maintenance of the accuracy may be bedevilled by Earth tides of much larger amplitudes. If the stations are in the same local region, this effect will be minimized.

KAULA: Of course, the experiment is better if the error sources are isolated. But you also want to measure something significant. Several hundred km baselines are desirable. If you have portable VLBI, you have a series of stations which you move along.

DUNN: You mention that the relative motion of the plates across the San Andreas fault is about 5 cm per year. Can you give a sigma on that?

KAULA: The figure of 5.5 cm per year has a sigma of 0.4 cm per year. It refers to the average motion of the entire Pacific plate with respect to the North American. I think you are referring to geodetic measurement in the region of the fault zone. This is 3.2 cm per year north at Hollister on the San Andreas, but varies elsewhere.

WHITTEN: That sounds a reasonable number. In some places it is 6 cm per year and in others it is 3 cm per year. There are places where it is locked. Back from the fault there is strain accumulation.

WALCOTT: The lithosphere is a low pass filter and we have considerable information of short wavelength (less than 5000 km) on lower mantle behaviour. What we are really lacking is long wavelength information (> 6000 km) and the only way we can get this is by studying loading on scales such as the Pacific ocean. My own personal feeling is that the data is available; you can go out and get it.

KAULA: You mean shore line features ... ?

WALCOTT: Yes; I mean sea level changes with time.

DOOLEY, J.C.
Bureau of Mineral Resources
Canberra ACT 2600
AUSTRALIA

Proc.Symposium on Earth's Gravitational Field & Secular Variations in Position (1973),248-260.

THE GRAVITY ANOMALIES OF CENTRAL AUSTRALIA AND THEIR SIGNIFICANCE FOR LONG-TERM TECTONIC MOVEMENTS*

ABSTRACT

The Bouguer gravity map of Australia shows five prominent elongated negative anomalies striking approximately east-west with peak-to-peak distances of about 80 km and amplitudes up to 160 mGal. These anomalies correlate approximately with the Officer Basin, the southern and northern parts of the Amadeus Basin, the Ngalia Basin, and the Lander Trough in the Wiso Basin. The anomalies are too large to be explained by the sediments in these basins alone, and imply substantial density variations at a depth near the crust/mantle boundary. The absence of any evidence of major tectonic activity since the Carboniferous suggests that these anomalies have existed more or less in their present form for some hundreds of millions of years. This implies that the lithosphere in this region has a long-term strength of about 100 to 200 bar.

Over this area, whose dimensions are about 10° to 15°, the average free-air anomaly is negative, with a minimum of about -30 mGal. This could arise from erosion of about 0.3 km of sediments without corresponding isostatic compensation; a time lag of intracratonic isostatic readjustment of the order of 5×10^7 years, and a lithospheric strength of one or two kbar over this time, would be implied. This anomaly may be partly associated with the deeper mantle structure as revealed by studies of satellite orbits.

On the basis of seismicity evidence some authors have proposed that the Australian continent is rifting apart. There is a well defined seismic zone running northwards from Spencer Gulf in South Australia to about latitude 30°S, but north of this the available data are far from conclusive. One hypothesis suggests that a 'Fitzroy-Spencer lineament' has been a major zone of shearing displacement since the Precambrian; this must be ruled out as the lineament intersects the gravity anomalies discussed above, and any substantial movement along it would have caused offsets of these anomalies; no such offsets are evident.

It is suggested that the central block containing the gravity anomalies has been a stable feature at least since the late Palaeozoic, and that stresses are adjusted along zones of weakness shown by minor seismicity around the boundaries. These zones approximately coincide with lineaments truncating the gravity anomalies and the major geological features, and it is probable that movements along them may have persisted for a long time, particularly on the western boundary.

1. Text

This paper is an attempt to see what can be deduced about secular variations in position from the Earth's gravity field in the Australian region, together with some evidence from seismicity.

The preliminary Bouguer gravity map of Australia (BMR, 1973) (see also ANFILOFF & SHAW 1974 , Figure 2) shows five prominent negative gravity anomalies in Central Australia between latitudes

---

* *Record 1973/205, Bureau of Mineral Resources*

20° and 30° S approximately.

These gravity anomalies correlate with five ancient basins - from south to north, the Officer Basin, southern and northern Amadeus Basins, Ngalia Basin, and the Lander Trough in the Wiso Basin. PLUMB (1972), and also the Tectonic Map of Australia (GSA, 1971) (see also Ibid, figure 1), describe the history of this area in terms of orogenies, transitional periods, cratonisation, and platform cover deposition, from the Archaean through to the early Palaeozoic.

The depth of these basins is fairly well known from seismic and aeromagnetic work, but only about half of the gravity anomalies can be accounted for by sediments unless we assume unreasonable density values. Models by ANFILOFF & SHAW (1974), MATHUR (1973); FORMAN & SHAW (1973), have all resorted to density changes deep in the crust. The negative gravity anomalies generally overlap the outcropping basement rocks, suggesting major overthrusting. Basement outcrops generally appear as low mountain ranges between comparatively low-lying and flat sediments; thus the correspondence between Bouguer anomalies and elevation is the reverse of that expected for isostasy.

The free-air anomaly profiles along longitudes 129°E and 132°E (figure 1, after WELLMAN, in prep.) show this lack of isostasy. The surface altitudes between basins are not shown to full advantage because they are plotted from gravity station heights, which are generally sited so as to avoid peaks.

No major tectonic activity has occurred in the area since the Carboniferous (PLUMB 1972), nor is there, as far as is known, any present-day seismic activity in the area (figure 2, after DENHAM et al, in prep.). Presumably the anomalies must have originated during a period of intense tectonic activity, with compressive stress and overthrusting, and then have been frozen into the crust or lithosphere and are now supported by its strength.

An estimate of the strength needed to support these anomalies can be obtained from a simple model of McKENZIE (1967). In figure 3, the upper layer is taken as a solid resting on an asthenosphere which is effectively a liquid over the geological periods concerned. An applied load centred at C causes an elastic deformation of the crust (greatly exaggerated in the diagram). Depending on the parameters involved the maximum shear stress σ_{max} will occur either at AA' and CC', or at BB'. The free-air gravity anomaly Δg at C relative to A can also be readily calculated, and thus can be related to the maximum stress by means of the equation:

$$\sigma_{max} = \Delta g \quad f(\lambda/T),$$

where λ is the width of the deflected part of the lithosphere and T is the thickness. $f(\lambda/t)$ follows different laws according to whether σ_{max} occurs at BB' or CC'; the resulting function is plotted in figure 3.

Estimates of amplitude and wavelength of the anomalies over the five basins are listed in table 1. The Amadeus Basin was treated firstly as two separate basins, and secondly as one basin with the central gravity high smoothed out. Estimates of the shear strength scaled from figure 3 are listed for a lithosphere 40, 60, and 100 km thick.

Thus this leads to a minimum strength of the lithosphere of say 100 or 200 bars. Laboratory measurements give somewhere about 4000 bars (GRIGGS et al 1960). Naturally it is expected that strength over geological periods is much less, as stress applied for long periods causes deformation without

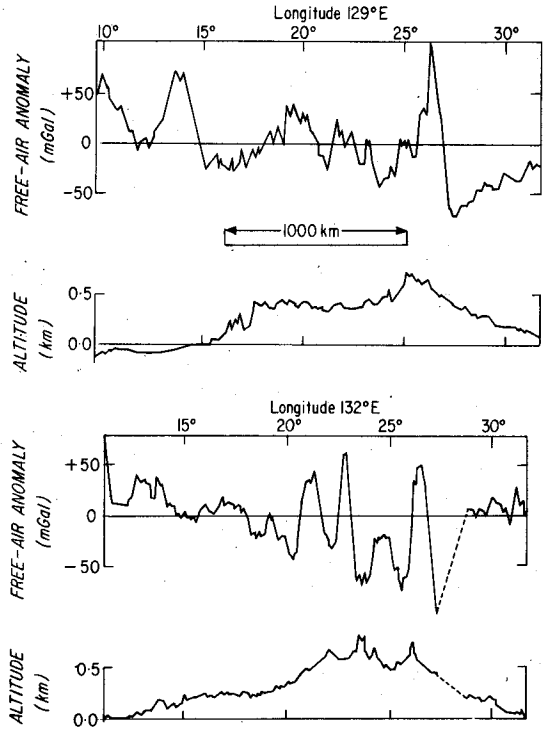

Figure 1. Gravity and Altitude Profile Across Australia

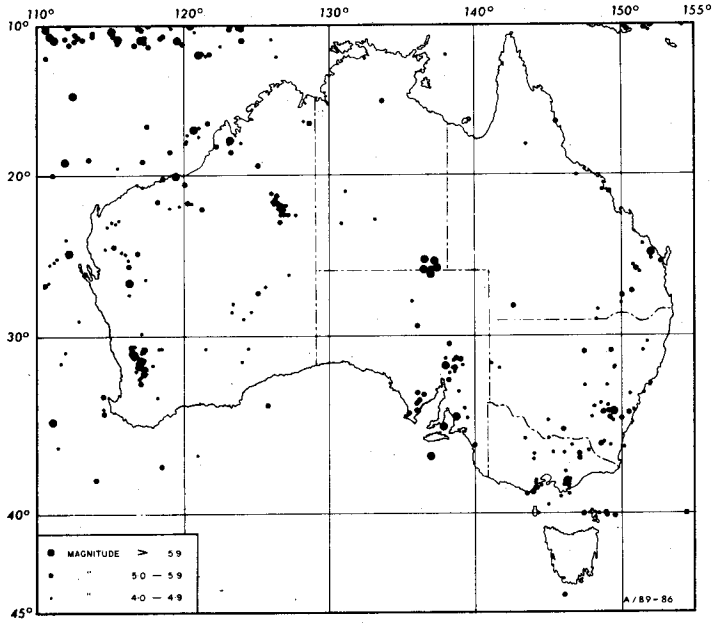

Figure 2. Australian Seismicity 1900-1972

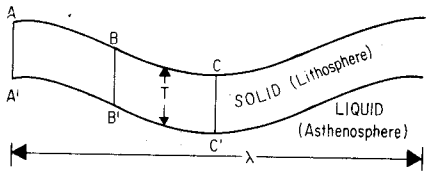

Maximum stress in bars at AA', BB', or CC'

$\sigma_{max} = \Delta g \, f(\lambda/T)$

$f(\lambda/T)$ as below

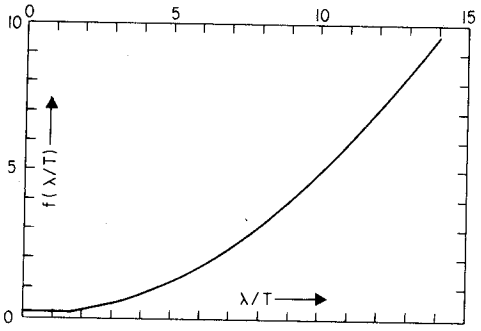

Figure 3

Table 1

Basin	Anomaly (mGal)	Width (km)	Maximum Stress T = 40 km	60 km	100 km
Officer	140	225	210	98	42
Amadeus South	105	175	95	42	21
Amadeus North	115	225	173	80	35
Amadeus (whole)	100	400	480	240	80
Ngalia	110	200	132	55	28
Lander Trough	60	250	114	54	21
Regional Anomaly (a)	30	2000	3600	1590	570
(b)	20	2000	2400	1060	380

breaking. CAREY (1954) has proposed the concept of 'rheidity', or relaxation time beyond which stresses cannot persist without viscous flow becoming important. For igneous rocks he estimates about 10^9 years. Also he defines 'practical strength', which is a function of time and is the stress which can be supported for a given period. Thus we say that the practical strength of the lithosphere in central Australia is at least 100 or 200 bars for a period of about 2×10^8 years This is consistent with CAREY's estimate of rheidity for igneous rocks.

If we examine the free-air anomaly profiles (figure 1), particularly along 132°E, we note that, if local effects of these major anomalies are smoothed out, there is a general negative value in the

central portion compared with the southern and northern ends, with a width of 1000 km or more. To study this in more detail a compilation of free-air anomalies of 1^{o} x 1^{o} lat/long 'squares' has been made for the Australian area. This is based largely on MATHER's (1969a, 1969b) figures, but includes more data recently available, some from anomalies on tape in BMR national gravity repository, some calculated by WELLMAN (in preparation) and others estimated from Bouguer anomaly maps and then corrected to the mean elevation of the square for land squares. For more recent BMR marine surveys south and west of the continent the average was estimated directly from preliminary free-air anomaly maps. With coastal squares (i.e. part marine and part land) a combination of these two methods was used.

Some of these data are in a preliminary form and should not be regarded as the best that could be derived from available data for 1^{o} x 1^{o} squares; however, if averaged over larger squares errors become much smaller. The series of maps presented here (figures 4, 5, 6 and 7) show contours for means of 3^{o}, 5^{o}, 7^{o}, and 10^{o} squares based on running averages of the 1^{o} square means.

These all show a persistent gravity low in central Australia.

Consider an infinite slab of density anomaly $\Delta\rho$ and thickness T; the gravitational attraction is $\overline{g} = 2\pi\ k\ \Delta\rho\ T$. If the slab has finite width, then by calculating the integrated anomaly of a simple step fault we find that by averaging over a slab of width about 10T we get about $0.9\overline{g}$, the remaining $0.1\overline{g}$ being in the 'tails' of the anomaly.

Similarly, if we consider that the Earth is homogeneous below a depth T, the average excess pressure on a level surface at depth L below this slab is $g_o \Delta\rho T$, where g_o is the surface gravity (actual variation with depth being very small near the surface). The gravity anomaly of such a slab is approximately proportional to the anomalous stress on a level surface beneath it.

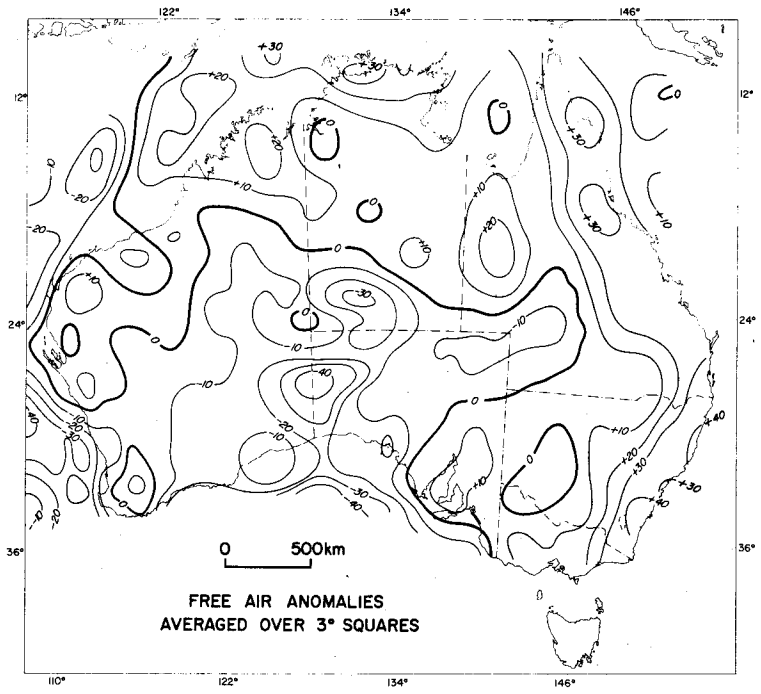

Figure 4.

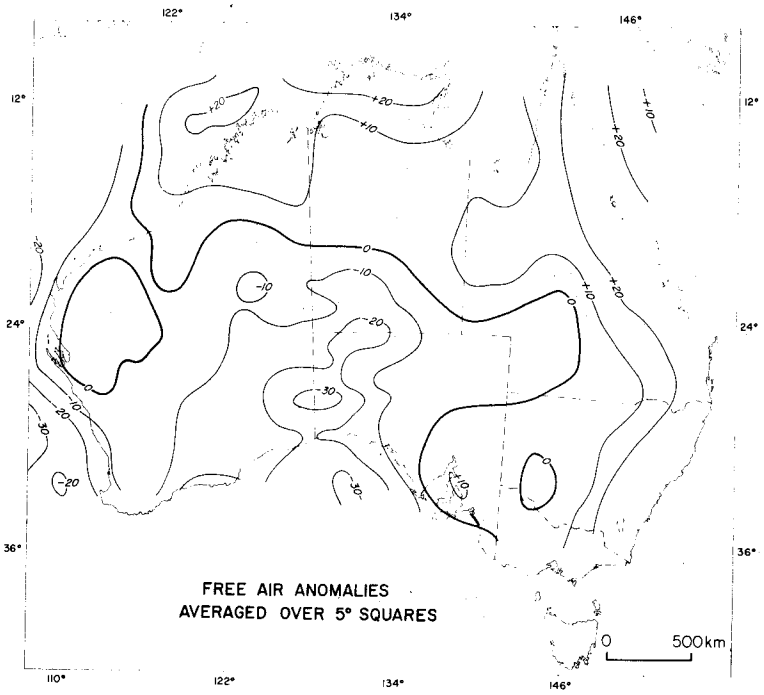

Figure 5.

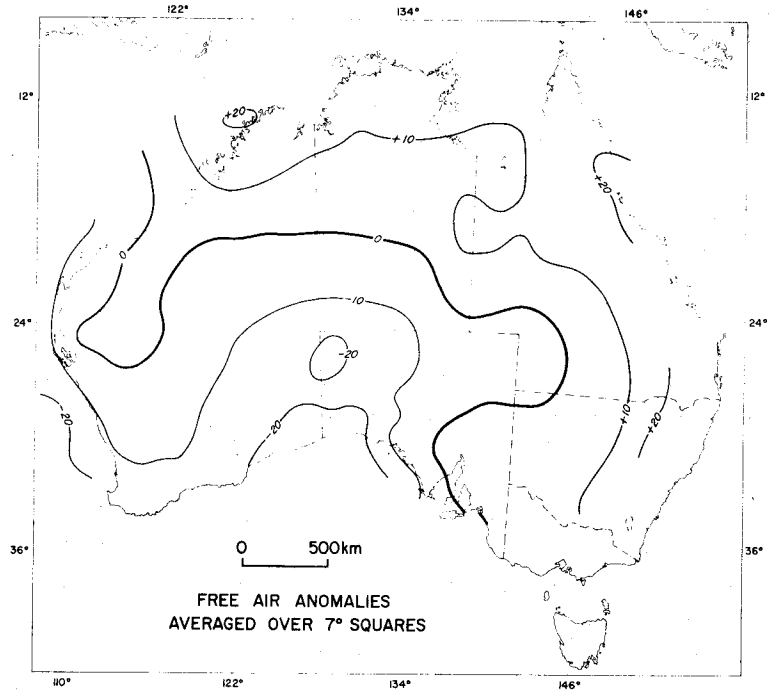

Figure 6.

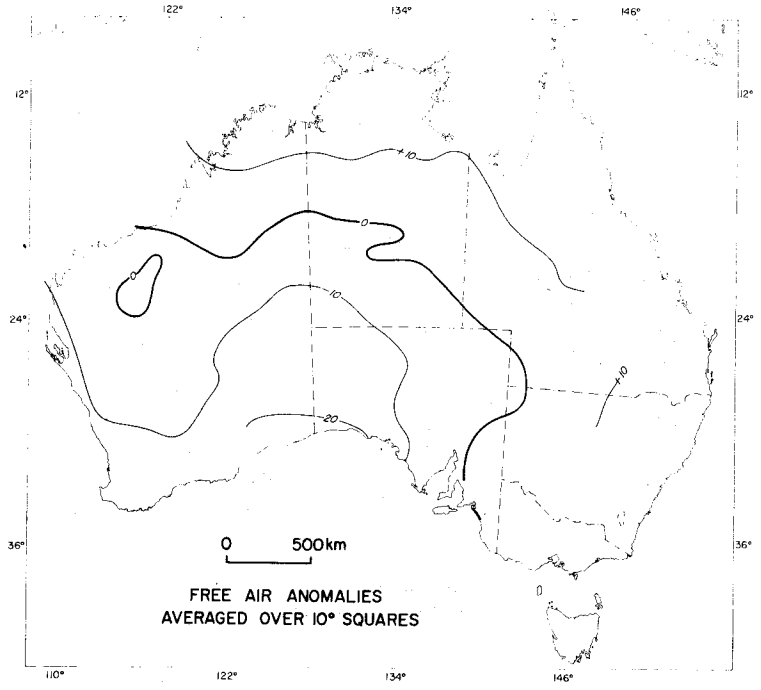

Figure 7

WELLMAN (in preparation) has concluded from Fourier analysis that there is very little lateral density variation beneath about 60 km depth, except for the sources of the very broad anomalies in the low-order spherical harmonics of the Earth's field, as shown for example by satellite orbits. If we neglect these and assume that the whole anomaly is associated with sources in the upper 60 km, then horizontal averages over 600 km, or about 5°, would represent the stress at or just below this depth, and give an indication of strength. This gives a figure of say 1600 bars.

If part of the anomaly is due to much deeper sources, then the strength at great depth needs to be of this order. Assume all of the anomaly is caused by density variations below the surface at depth L; then for the slab, ρ and T are constant, and $\frac{\Delta(g\rho T)}{g\rho T}$ is the order of $\frac{\Delta g}{g}$, or about 1 in 10^4 and can be neglected.

Thus we need to separate anomaly sources about 60 km from deeper, presumably much deeper, sources. This is the old problem of separating residual and regional, and of course there is no unique way of doing this.

As one possible approach to this problem, the satellite harmonic field of 2-16th order was used as a regional (figure 8, from figure 1 of ANDERSON et al 1973) based on data of GAPOSCHKIN & LAMBECK (1971). This is based purely on satellites - published fields based on combination of satellite and terrestrial data use part of the Australian data but not all, and hence are likely to introduce bias in different areas. The 16th-order harmonics have a wavelength of about $22\frac{1}{2}^{\circ}$; thus this probably represents effects from about 300 km depth or more. The residual derived from 5° means minus 2-16th order satellite field is shown in figure 9. We can still see an anomaly of say -20 mGal and about 2000 km wavelength; this gives a strength of, for T = 100 km, 380 bars; for T = 60, 1060 bars.

Elsewhere, (DOOLEY 1973) I have suggested that this anomaly could be due to slow erosion of the higher parts of the shield, with a long time constant in the process of isostatic compensation. The rate of

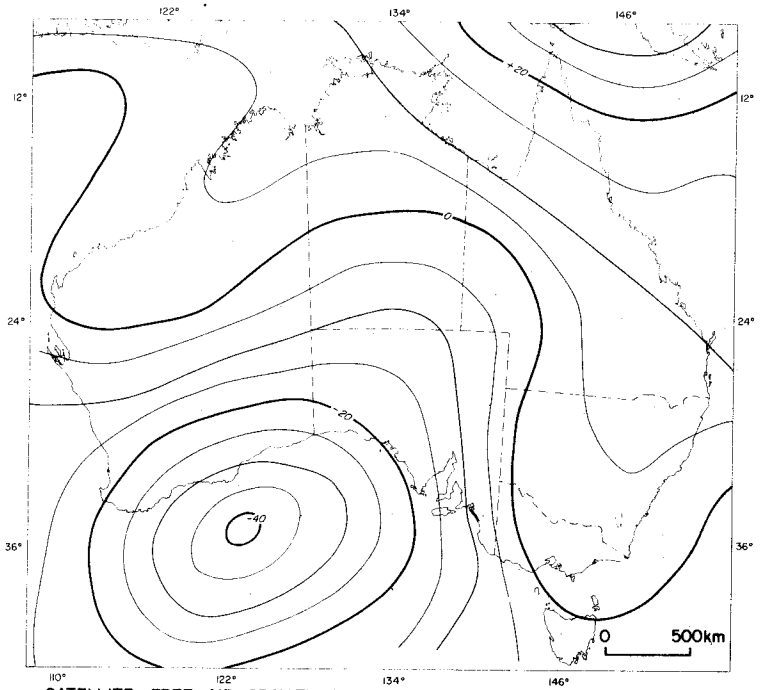

Figure 8

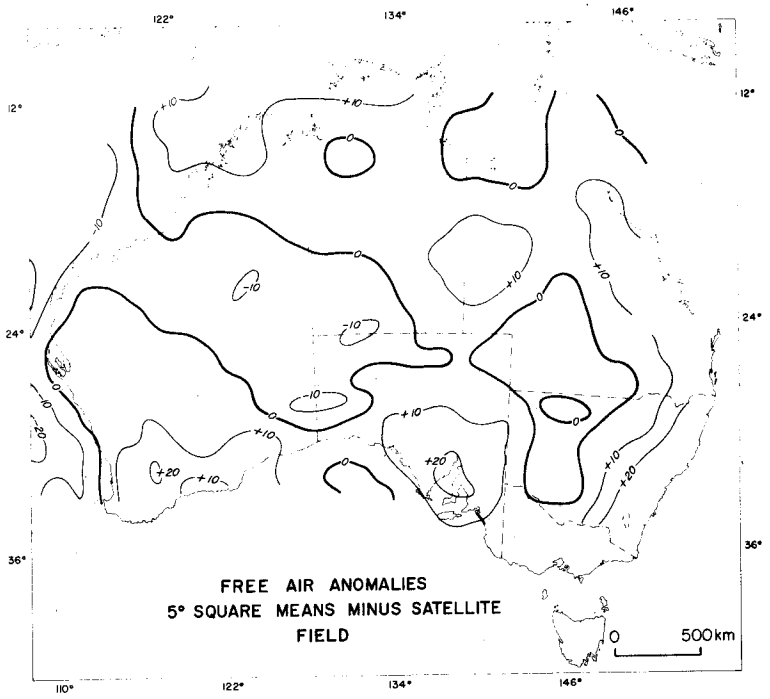

Figure 9

erosion was estimated at something of the order of 10^{-5} m/yr. Erosion without compensation of 1 km of sediments would produce a negative anomaly of about 100 mGal ($41.85\rho_s$, where ρ_s is the density of the material removed), so the anomaly estimated above of 20-30 mGal would imply a time-lag of isostatic compensation of about 20-30 M.y., and the lithospheric strength of the order of 1 kbar estimated above would be the effective strength for this period. Note the great difference in time of isostatic adjustment from that estimated from the Fennoscandian shield post-alluvial rebound of about 15 000 yr. The latter is usually regarded as referring to upper mantle rheidity. If my conclusions are correct and give representative strengths and time constants for shield lithospheres, it may be that the shields move fairly rapidly into a position of isostatic equilibrium as a whole, while maintaining intra-shield stress differences in the lithosphere for much longer periods of time.

We note in passing that LAMBECK (1972) has estimated that the harmonics of order as low as 8 or 9 could be supported in the lithosphere with a strength of 1500 bars.

The relation between earthquake magnitude and stress is anything but precise, but the available data suggest that earthquakes of magnitude M_s = 7 or 8 would be associated with stresses of the order of 1000 bar.

The seismicity map of Australia (DENHAM et al, in preparation) is shown in Figure 4. It must be borne in mind that the distribution of earthquakes shown is affected by density of population and instrumentation; the distribution can probably be regarded as fairly unbiased by these factors for magnitudes greater than 5. As Australian seismicity is low, this does not leave much data for statistical generalisation. In fact, in several cases, one earthquake and its aftershocks have changed the picture entirely.

As regards central Australia, there is a well defined seismic zone running northwards from Adelaide to about 30°S, fairly large recent earthquakes in the Simpson Desert (STEWART & DENHAM 1974) and Canning Basin (DENHAM et al, in preparation), and a few minor events.

Several authors have proposed that the Australian continent is rifting or shearing along a plate boundary through the centre. Figure 10 shows three proposed lineaments - that of COOK (1966; 1971), which initially was based partly on gravity evidence; that of CLEARY & SIMPSON (1971) based on seismicity and a proposed relation to a displacement of the Southern Ocean mid-ocean ridge south of Adelaide; and that of STEWART & MOUNT (1972) who describe the 'Fitzroy-Spencer lineament' on the basis mainly of seismicity.

Cook's proposed lineament was based on correlation of widely separated gravity anomalies across areas where few or no observations were available at the time. Subsequent surveys have made these correlations improbable.

STEWART & MOUNT postulate that the Fitzroy-Spencer lineament has been a zone of shearing relative movement between two blocks of the continent since Precambrian times. However, we note that their lineament intersects at an angle the major gravity anomalies in central Australia. If indeed shearing movement had continued for a prolonged geological period, then we would expect it to show in a large offset displacement of these gravity anomalies, since we have shown that they are some hundreds of millions of years old. Examination of the gravity map shows no indication of such displacement. The same could be said for the major geological boundaries of the associated basins and blocks.

CLEARY & SIMPSON's proposed zone cannot be dismissed on these grounds, as it skirts along the eastern edge of the supposed stable block and then trends westwards along the length of the Ngalia Basin.

However, in view of the low seismicity it seems premature to draw any firm conclusions about trans-continental zones of activity. The central block which we have studied above appears to have shown little or no seismicity for the period for which data are available, but there is a suggestion that earthquakes tend to occur around its edges. In view of the figures for the lithospheric strength inferred above for the central block, it seems that this may be a comparatively strong and stable slab surrounded by weaker material, or zones of weakness, in which stress adjustments are occurring.

Moreover, recent studies of earthquake first motions by DENHAM (pers.comm.) suggest different stress regimes - north-south compression in south-eastern Australia, and NE-SW compression in the north-western part of the continent.

ANFILOFF & SHAW (1974, figure 2) have drawn attention to a NNE trending lineament which truncates the major gravity anomalies on the western side, and which also truncates the major geological features - the Arunta and Musgrave blocks, and the Officer, Amadeus, and Ngalia Basins. The zone of seismicity forming the western boundary of the stable block proposed above is approximately linear and coincides approximately with ANFILOFF & SHAW's lineament. Thus it appears that movement may still be taking place along or close to this lineament, which is apparently of ancient origin; the time of commencement of these movements is difficult to estimate.

Further, ANFILOFF & SHAW postulate a south-east trending lineament truncating the northern gravity anomalies and geological features of the block (IBID, figure 10). The Simpson Desert earthquakes occurred somewhat to the east of this lineament. Examination of the gravity (BMR 1973) and tectonic (GSA 1971) maps show that it would be reasonable to move the line of truncation eastwards so as to pass through these earthquakes. The seismicity zone southwards from here shows some agreement with the trend of the eastern boundary of the gravity anomalies and geological features; however, both the boundaries and the seismicity zone are irregular in shape, and this boundary cannot be defined clearly.

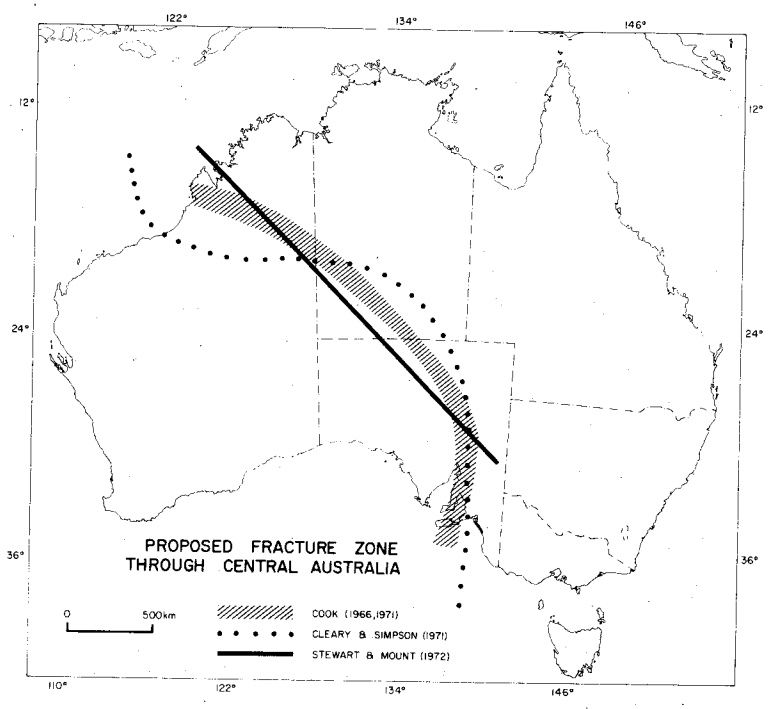

Figure 10

2. Conclusions

1) The largest gravity anomalies in the shield area are not associated with evidence of seismicity. This is distinct from the situation in island arcs.

2) These anomalies are very old and imply a significant long-term strength of the shield lithosphere.

3) The lack of noticeable displacement of the anomalies along the proposed Fitzroy-Spencer lineament precludes any significant long-term strike-slip motion along this lineament.

4) Much more seismicity data are required to enable reliable confirmation or rejection of proposed trans-continental rupture zones.

5) Four lines of evidence, i.e. truncation of gravity anomalies, truncation of geological features, the estimated strength of the central block, and the seismicity zones, suggest that the central block has been a stable feature since late Palaeozoic (or possibly earlier) and that

stresses in the continental plate have been relieved by movements along the boundaries of this block throughout a considerable period of geological time.

3. Acknowledgment

The permission of the Director, Bureau of Mineral Resources, Australia, to publish this paper is acknowledged.

4. References

ANDERSON, R.N., McKENZIE, D.P. & SCLATER, G.P. 1973. Gravity, bathymetry and convection in the Earth. *Earth plan. Sci.Letters.* 18, 391.

ANFILOFF, W. & SHAW, R.D. 1974. The gravity effects of two large uplifted granulite blocks in separate Australian shield areas. (This volume,273-289).

BMR 1973. Preliminary Bouguer Anomalies, Australia, scale 1:5 000 000. Government Printer, Canberra.

CAREY, S.W. 1954. The rheid concept in geotectonics. *J. geol.Soc.Aust.* 1, 67.

CLEARY, J.R. & SIMPSON, D.W. 1971. Seismotectonics of the Australian continent. *Nature.* 230, 239.

COOK, P.J. 1966. The Illamurta structure, central Australia: its development and relationship to a major fracture zone. *Bur.Miner.Resour.Aust.Rec.* 1966/46 (unpublished).

COOK, P.J. 1971. Illamurta diapiric complex and its position on an important central Australian structural zone. *Bull.Amer.Ass.petrol.Geol.* 55, 64.

DENHAM, D., EVERINGHAM, I.B. & GREGSON, P.J. East Canning Basin Earthquake, March 1970. (In preparation).

DENHAM, D., SIMPSON, D.W., GREGSON, P.J. & SUTTON, D.J. 1972. Travel times and amplitudes from explosions in Northern Australia. *Geophys.J.* 28, 225.

DOOLEY, J.C. 1973. Is the Earth Expanding? *Search.* 4, 9.

FORMAN, D.J. & SHAW, R.D. 1973. Deformation of the crust and mantle in central Australia. *Bur.Miner.Resour.Aust.Bull.* 144.

GAPOSCHKIN, E.M. & LAMBECK, K. 1971. Earth's gravity fields to 16th degree and station co-ordinates from satellites and terrestrial data. *J.geophys.Res.* 76. 4855.

GRIGGS, D.T., TURNER, F.J. & HEARD, H.C. 1960. Deformation of rocks at 500 to 800°C. *Geol.Soc.Amer.Mem.* 79, Chap.4.

GSA. 1971. Tectonic Map of Australia, 1971. *Geol.Soc.Aust.* Sydney.

LAMBECK, K. 1972. Gravity anomalies over ocean ridges. *Geophys.J.R.astron.Soc.*30, 37.

McKENZIE, D.P. 1967. Some remarks on heat flow and gravity anomalies. *J.geophys.Res.* 72, 6261.

MATHER, R.S. 1969a. The free air geoid for Australia. *Geophys.J.R.astron.Soc.* 18, 499.

MATHER, R.S. 1969b. The free air geoid for Australia from gravity data available in 1968. *Unisurv.Rep.* University of New South Wales, Sydney.

MATHUR, S.P. A proposal for a deep seismic sounding survey in central Australia. *Bur.Miner. Resour.Aust.Rec.* (in preparation).

PLUMB, K.A. 1972. Tectonic evolution of Australia, summary. *Bur.Miner.Resour.Aust.Rec.* 1972/37 (unpublished).

STEWART, I.C.F. & DENHAM, D. 1974. Simpson Desert earthquake, central Australia, August 1972. *Geophys.J.R.astron.Soc.* (in press).

STEWART, I.C.F. & MOUNT, T.J. 1972. Earthquake mechanisms in South Australia in relation to plate tectonics. *J.geol.Soc.Aust.* 19, 41.

WELLMAN, P. Australian gravity and altitude spectra. (In preparation).

5. Discussion

KAULA: Is there any evidence of a low-velocity layer under Australia? If so, what is the depth to the top of this layer?

DOOLEY: DENHAM ET AL (1972), as a result of refraction recordings from large explosions in the Ord River area, have found indications of a low-velocity layer with a lower boundary of about 160 km depth. The thickness of the zone could not be determined.

PURINS*: To what extent has a study of the Earth's density distribution been carried out in Australia and what are the future plans?

DOOLEY: WELLMAN (in.prep.) has modelled the free air gravity field in Australia in terms of average density and thickness of $2^\circ \times 2^\circ$ crustal blocks on the assumption that each such block is isostatically compensated.

A computer-based file is being established in the Bureau of Mineral Resources (Canberra) for density measurements of bore cores and rock specimens; however no comprehensive analysis has yet been made of these data.

* Written Question.

JOHNSON, B. D.
LEE, T. J.
School of Earth Sciences
Macquarie University
North Ryde NSW 2113
AUSTRALIA

Proc. Symposium on Earth's Gravitational Field & Secular Variations in Position (1973), 261-272.

A RAPID METHOD FOR THE COMPUTATION OF THE GRAVITATIONAL ANOMALY DUE TO COMPLEX THREE DIMENSIONAL STRUCTURES

ABSTRACT

A rapid method for the evaluation of the gravity field over complex structures can be developed by representing the structure as a sum of cubic elements of side a and density ρ.

The vertical component of the gravitational attraction for each cubic element is calculated from

$$g_z = G\rho \left[\frac{a^3 z}{R^3} + \frac{7}{96} \frac{a^7}{R^7} \left(3z - \frac{9z(x^4 + y^4 + z^4)}{R^4} + \frac{4z^3}{R^2}\right)\right]$$

where x, y and z are the coordinates of the observation point with respect to the centre of the cube, G is the gravitational constant and $R^2 = x^2 + y^2 + z^2$. The above formula is obtained by a multipole expansion of the integral expression for the potential of a cube, neglecting terms above order 4, and is valid when the required accuracy A_4 is less than

$$\frac{Ga^3}{R^2} \left(\frac{a\sqrt{3}}{2R}\right)^8 / \left(1 - \frac{a\sqrt{3}}{2R}\right) .$$

A further simplification may be obtained by only using the first term of the expansion when the specified accuracy, A_o, is less than

$$\frac{Ga^3}{R^2} \left(\frac{a\sqrt{3}}{2R}\right)^4 / \left(1 - \frac{a\sqrt{3}}{2R}\right)$$

The exact expression for the cube is only used in the restricted region close to the cube.

An array of attraction values for the cube is calculated once for each level in the model and then convoluted with an observation array. The convolution is limited by the lateral extent of the model at that level. Density variations within the model require the attraction array to be multiplied by a constant value when changing from one density region to another.

The ability to specify the required accuracy enables extremely rapid preliminary calculations to be performed. A final calculation can be carried out using a greater accuracy when the model is deemed to be correct.

1. Introduction

Several methods exist in the literature for the computation of the gravitational attraction of three-dimensional models. The methods vary greatly in the complexity of the models, the speed of calculation and in the resulting accuracy.

The most widely used method is that of TALWANI & EWING (1960) in which the model is divided into horizontal polygonal laminae the attractions of which are summed at each observation point. The amount of work involved is the product of the number of stations, the number of laminae, and the

number of faces on each lamina. The resulting calculations are relatively rapid and accurate, however, it is difficult to change the model easily unless the polygonal laminae form parts of vertical prisms.

A more rapid method which is based on vertical prisms is that of BOTT (1959) who replaces prisms by a line mass approximation. This is shown to be accurate at a great enough distance from the prisms, figure 2, but leaves us with the problem of calculating the points nearest to the model. The amount of work involved is the product of the number of prisms and the number of stations.

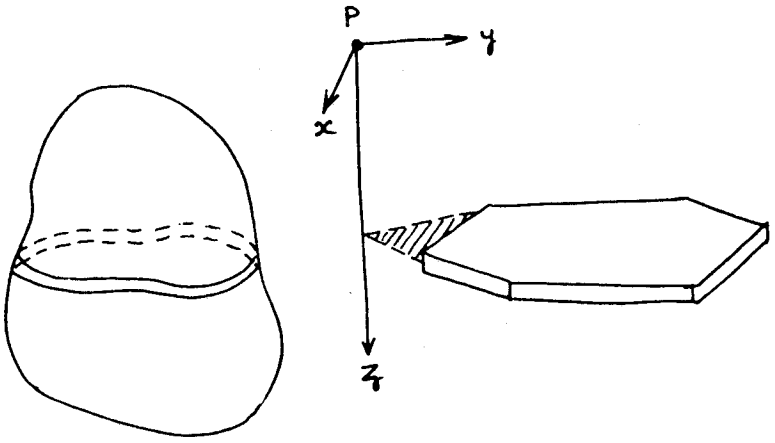

Figure 1. Principle of Lamina Method
Attraction at P due to shaded area

$$g_z = G\rho \left| \tan^{-1} \left\{ \frac{z(by - az^2)}{x\left[(1 + a^2)z^2 + b^2\right] - (a^2z^2 + b^2)\sqrt{x^2 + y^2 + z^2}} \right\} \right|_{x_{k+1},\, y_{k+1}}^{x_k,\, y_k}$$

where $a = \dfrac{x_{k+1} - x_k}{y_{k+1} - y_k}$ $\qquad$ $b = \dfrac{x_k y_{k+1} - x_{k+1} y_k}{y_{k+1} - y_k}$

after TALWANI & EWING (1960)

In order to overcome the accuracy problem an exact expression for the attraction of a prism was formulated by NAGY (1966), figure 3.

The expression is a result of performing a volume integration of a point mass over the prism volume

$$\Delta g_z = G\rho \int_V \frac{z\,dv}{r^3}$$

The complete expression contains 24 terms, each of which contains a logarithmic or inverse trigonometric function together with square roots.

A much neater form of the expression has been given by GOODACRE (1973) and this may be further

simplified to give

$$g_z = G\rho \left|\left|\left| \; x \ln \left\{\frac{y+r}{(x^2+z^2)^{\frac{1}{2}}}\right\} + y \ln \left\{\frac{x+r}{(y^2+z^2)^{\frac{1}{2}}}\right\} \right.\right.\right.$$

$$- z \arctan \left\{\frac{xy}{zr}\right\} \Bigg|_{x_1}^{x_2} \Bigg|_{y_1}^{y_2} \Bigg|_{z_1}^{z_2}$$

which may be written as a subroutine.

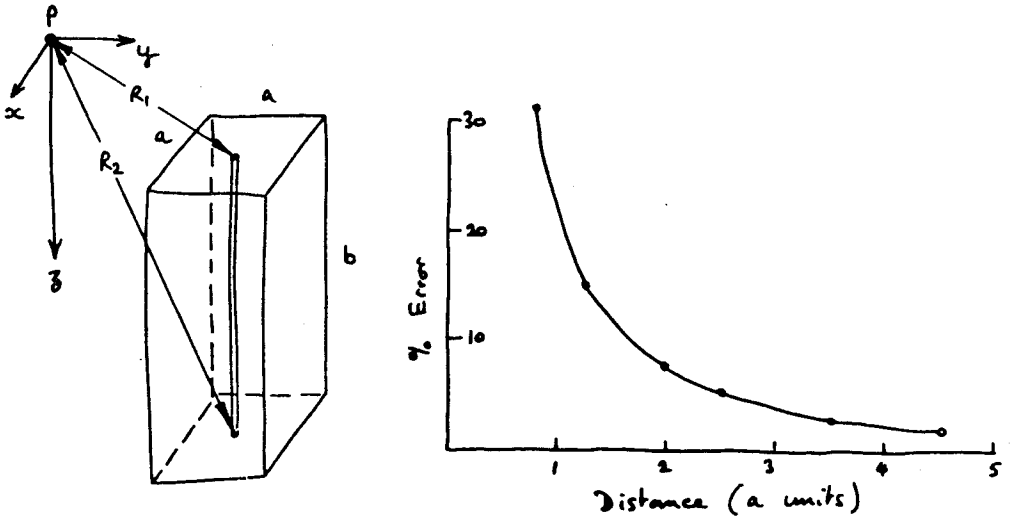

Figure 2. Principle of Line Mass Method

Attraction at P due to line mass

$$= G\rho\, a^2 \left\{\frac{1}{R_1} - \frac{1}{R_2}\right\}$$

after BOTT (1959)

The method although producing an exact solution, is very lengthy, particularly when it is noted that the evaluation is carried out for every prism and for every station.

There is therefore a considerable difference in the accuracy and speed of the various presently used methods. ST.JOHN & GREEN (1967) attempted to overcome these difficulties by using the exact formula close to the station and the line mass formula at distances removed from the station. There is, however, no provision in their method for ascertaining the accuracy of the calculations in ord to either change the formula used or to truncate the calculations.

There is therefore a choice in existing techniques between exact and slow methods and more rapid in which the calculations may be inaccurate in certain points. The aim in this paper was to devise a method in which the required accuracy determines the complexity of the calculation required at any point.

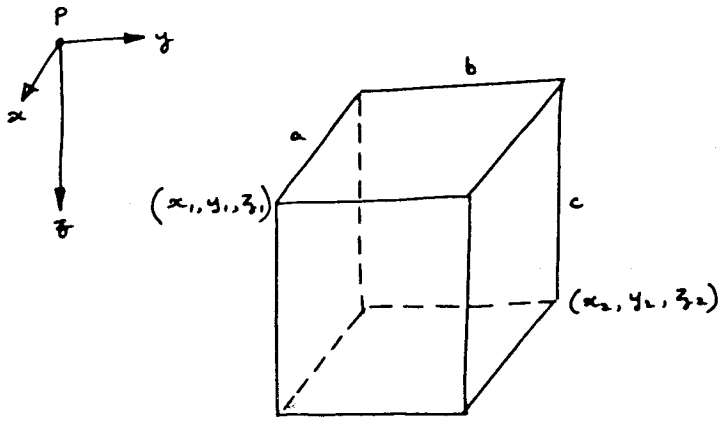

Figure 3. Principle of Prism Method.

2. Development of Approximation Formula for the Cube

The gravitational potential, U, due to an arbitrary volume v, and density ρ, may be written as

$$U = G\rho \int_v \frac{dv}{|\vec{R} - \vec{r}|} \qquad (1),$$

where G is the gravitational constant.

Expanding the reciprocal distance term as a series of Legendre functions (MACROBERT 1967, p.79) of argument cos γ, γ being defined in Figure 4,

$$U = \frac{G}{R}\rho \int_v \sum_{n=0}^{\infty} \left(\frac{r}{R}\right)^n P_n (\cos \gamma)\, dv \qquad (2).$$

We shall now restrict ourselves to the special case where the volume is a cube of dimension a and R is the distance of the observation point from the centre of the cube.

The integration can be performed by interchanging the order of integration and summation and expanding the Legendre functions by their addition formula (MACROBERT 1967, p.128).

$$\text{Thus } U = G\rho \left(\frac{a^3}{R} + \frac{7}{60} \frac{a^7}{R^9} \frac{1}{2^4} \{3R^4 - 5 (x^4 + y^4 + z^4)\} \right) \qquad (3)$$

where harmonic terms of greater than order 4 have been neglected (see Appendix).

The vertical component of the gravitational attraction due to a cube is then obtained by differentiating with respect to z, the above expression for the potential.

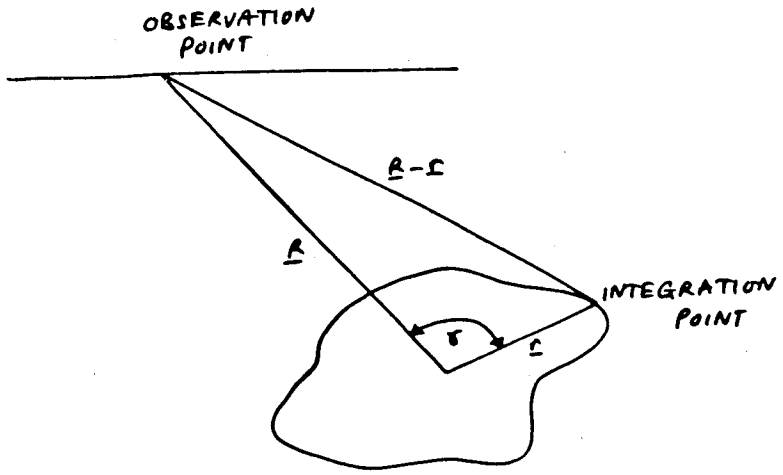

Figure 4.

$$\text{Thus } \Delta g_z = G\rho \left\{ \frac{a^3 z}{R^3} + \frac{7}{96} \frac{a^7}{R^7} \left(3z - \frac{9z(x^4+y^4+z^4)}{R^4} + \frac{4z^3}{R^2}\right)\right\} \qquad (4)$$

GRANT (1952) has shown that the remainder, A_n, satisfies the inequality

$$A_n < \frac{Ga^3\rho}{R^2} \left(\frac{a\sqrt{3}}{2R}\right)^{n+1} / \left(1 - \frac{a\sqrt{3}}{2R}\right) \qquad (5)$$

where n is the highest order of the terms included. Because of the symmetry of the cube, the terms included in equation 4 are for $n = 0$ and 4 and the first term neglected is for $n = 8$.

In equation 4, the first term in the expansion represents a sphere centred at the centre of the cube and having the same mass as the cube. The remaining terms approximate the deviation of the cube from a sphere.

In a similar problem, GRANT (ibid) used expansions of up to and including order 2 to determine the position and shape of a gravitational source.

In practice, it has been found necessary to scale the coordinates with respect to the distance R in order that computer accuracy be maintained. The working formulation for equation 4 is thus

$$\Delta g_z = G\rho z \left\{ \left(\frac{a}{R}\right)^3 + \frac{7}{96} \left(\frac{a}{R}\right)^7 \left[3 - 9\left\{\left(\frac{x}{R}\right)^4 + \left(\frac{y}{R}\right)^4 + \left(\frac{z}{R}\right)^4\right\} + 4\left(\frac{z}{R}\right)^2\right] \right\}$$

In a similar manner the exact expression has been rearranged and normalised with respect to z.

$$\Delta g_z = G\rho z \left|\left|\left| \frac{x}{z} \ln \left\{ \left(\frac{y}{z} + \frac{R}{z} \right) \Big/ \left(\frac{x^2}{z^2} + 1 \right)^{\frac{1}{2}} \right\} + \frac{y}{z} \ln \left\{ \left(\frac{x}{z} + \frac{R}{z} \right) \Big/ \left(\frac{y^2}{z^2} + 1 \right)^{\frac{1}{2}} \right\} \right.\right.\right.$$

$$\left. - \arctan \left\{ \left(\frac{x}{z} \frac{y}{z} \right) \Big/ \frac{R^2}{z^2} \right\} \right|_{x_1}^{x_2} \Big|_{y_1}^{y_2} \Big|_{z_1}^{z_2}$$

3. Application

In practice, the simple sphere calculation is sufficient for all but the closest parts of the body where the more accurate multipole expansion or the exact formulations may be required.

The required formulation is predetermined by the examination of the remainder term as calculated by equation 5 and comparing this with the required accuracy. The same remainder term may be used to truncate the calculation so that observation points beyond a certain distance are omitted.

The procedure is then to divide the model into levels of the dimension of the cube heights. An attraction array is calculated for a cube in the highest level. The calculations are performed in order with increasing distance from the centre of the cube, so that each calculation is tested against the remainder term to determine the use of the next simplest form of the calculation. This attraction array is calculated for a 45° segment since the symmetry properties of the cube allow the remaining area to be copied from the calculated segment (Figure 5).

The attraction array is then convolved with the observational array, the convolution being performed with the origin of the attraction array over the centre of each cube in the level of the model (Figure 6). Since the density may vary from one prism to another, a multiplying factor is applied to the attraction array when changing from one density to another.

The calculation proceeds by moving to the next level down in the model and computing a new attraction array and continuing as before. The calculation proceeds level-by-level until either the model is complete or the attraction array at any particular level has its maximum value below the required accuracy.

Figure 7 is a plot of the terms used in the calculation of the attraction array as a function of x, y and z being the coordinates of the observation point with respect to the centre of the cube. It can be seen that the exact expression is required only for the closest calculations and even the multipole expansion gives way to the simple sphere calculation. The distance at which the calculations are terminated is seen to decrease the size of the attraction array very rapidly and levels deeper than this distance need not be considered in the calculation. A plot of the relative times for each level is shown down the right side of the diagram.

The resulting effects of the approximation method are that the very lengthy calculations for the large numbers of blocks required for complex bodies are replaced by a relatively small number of more rapid calculations.

The present program is currently being used to calculate the topographic correction of the region around Macquarie Island, an area of over 600 km square. Initial tests on this model show that reasonably accurate results are being obtained in a time much less than for the exact methods.

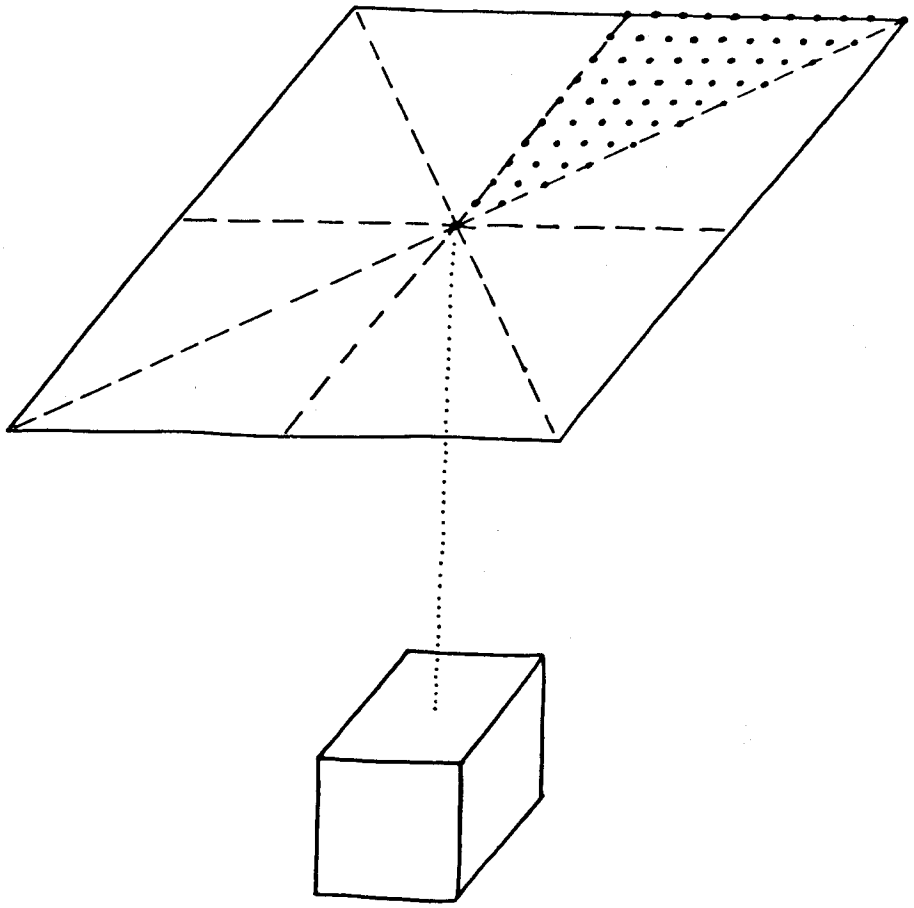

Figure 5. Calculation of Attraction Array

4. Developments

The efficiency of the program may be improved by writing the crucial part of the calculation in assembler language as there is a considerable amount of array address calculation involved. This however, makes the program machine dependent.

A correction could be easily incorporated to allow for a spherical earth distortion after the manner of TAKIN & TALWANI (1966). The restriction, that the model, the attraction array and the observation array lie on a rectilinear grid, however, restricts the model to lie within a relatively small segment of the sphere.

In some applications the computation of the magnetic field together with the gravity field is required. Similar expressions for the exact, multipole and spherical dipole magnetic attractions have been derived and will be presented elsewhere. Extra storage is required since the summation must be carried out for each of the three vector components. The resulting total field anomaly can only be calculated on completion of the model.

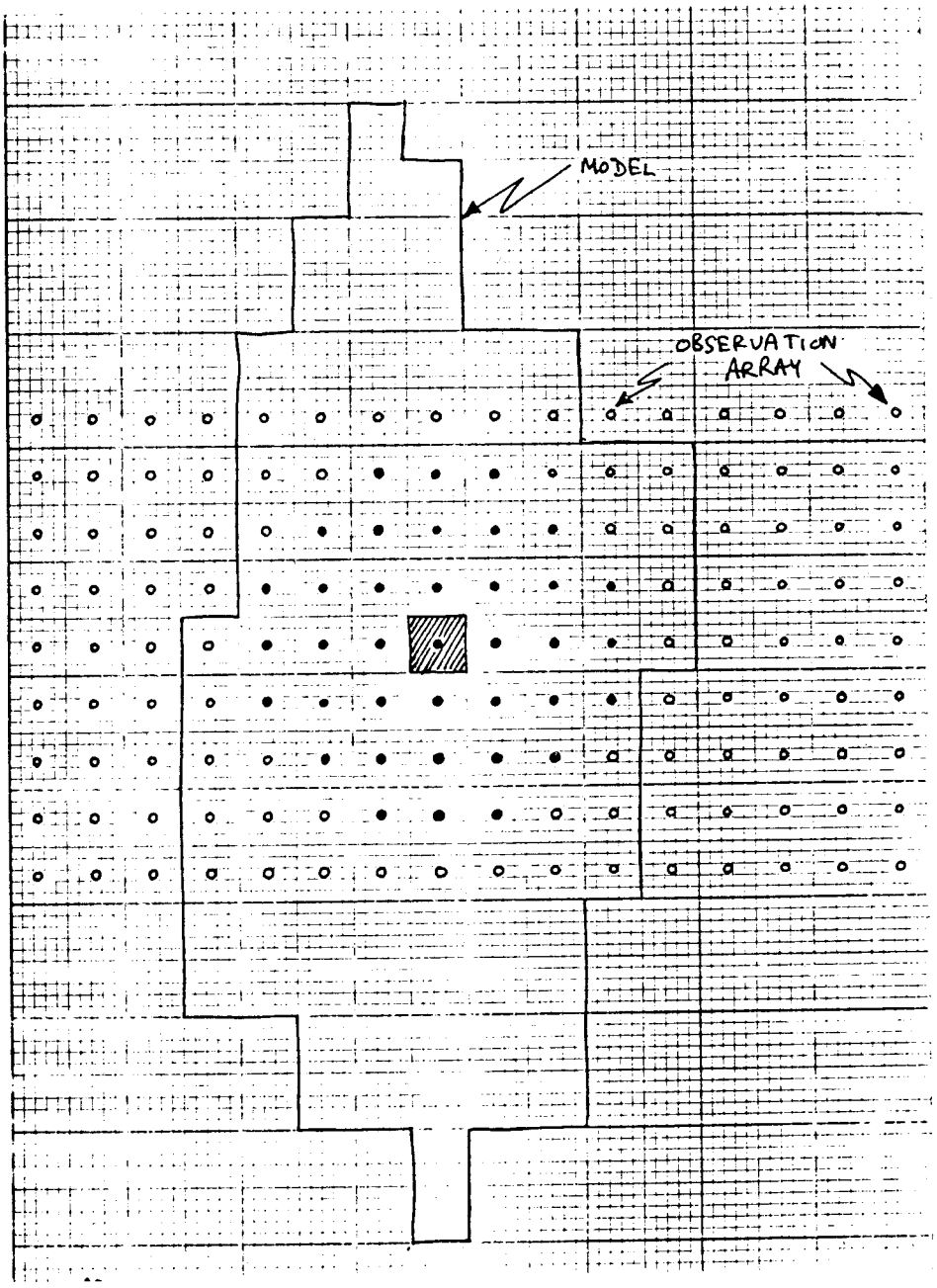

Figure 6. Addition of Attraction Due to One Cube to the Observation Array.

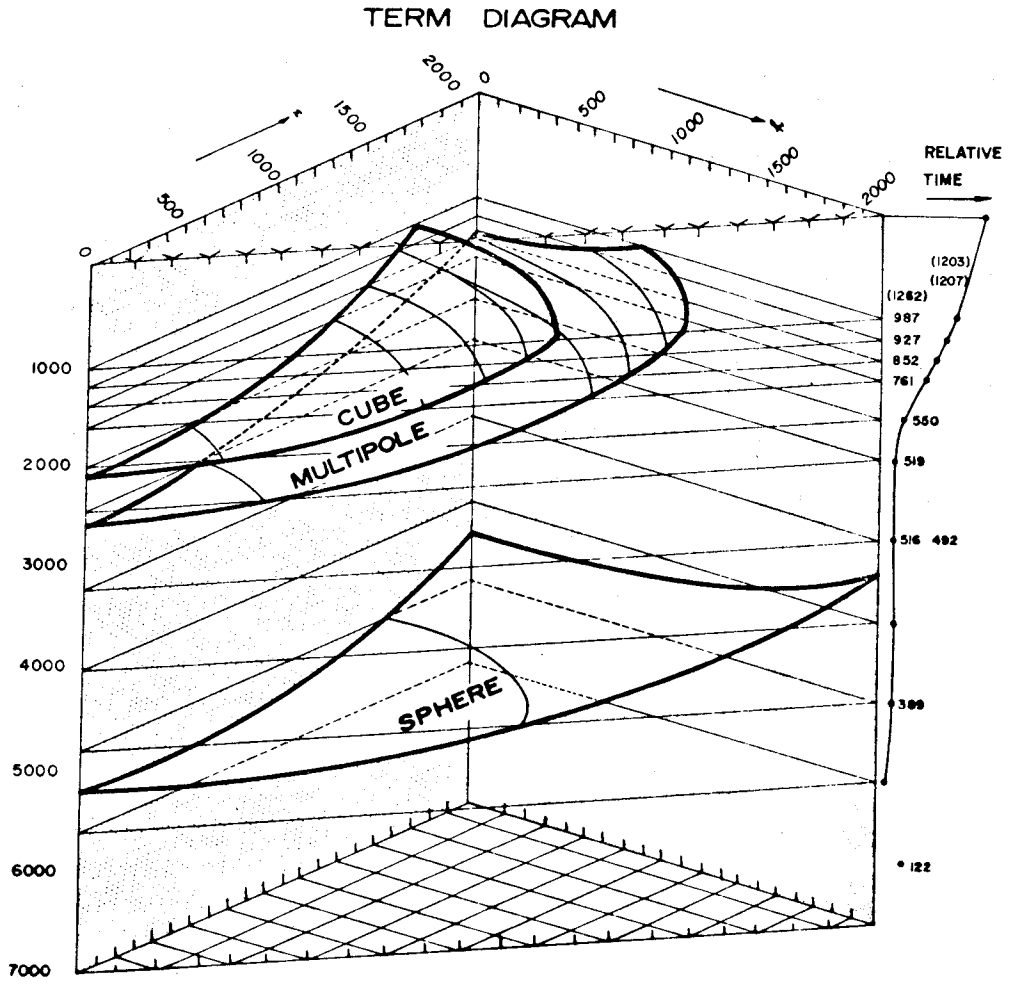

Figure 7.

5. Conclusions

While the expansion of the gravitational field in terms of multipoles has been used successfully for a number of years, it has up to now been neglected in the forward problem. It has here been shown to be an efficient method of calculating the gravity anomaly due to complex three-dimensional structures.

6. Acknowledgments

The authors wish to acknowledge the provision of a Macquarie University Research Grant to cover the computing costs involved.

7. References

BOTT, M.H.P. 1959 . The use of electronic digital computers for the evaluation of gravimetric terrain corrections. *Geophys.Prosp.* 7. 46-54

GOODACRE, A.K. 1973. Some comments on the calculation of the gravitational and magnetic attraction of a homogenous rectangular prism. *Geophys.Prosp.* 21. 66-69

GRANT, F.S. 1952. Three-dimensional calculation of gravitational anomalies. *Geophysics.* 17. 344-364

MACROBERT, T.M. 1967. *Spherical Harmonics.* Pergamon,New York.

NAGY, D. 1966. The gravitational attraction of a right rectangular prism. *Geophysics.* 31, 362-371

ST JOHN, V.P. & GREEN, R. 1967. Topographic and isostatic corrections to gravity surveys in mountainous areas. *Geophys.Prosp.* 15, 151-162

TAKIN, M. & TALWANI, M. 1966. Rapid computation of the gravitational attraction of topography on a spherical earth. *Geophys.Prosp.* 14. 119-142

TALWANI, M. & EWING, M. 1960. Rapid computation of gravitational attraction of three-dimensional bodies of arbitrary shape. *Geophysics.* 25. 203-225

8. Appendix

The expansion for the potential, due to an arbitrary volume v of density ρ

$$U = G\rho \int_v \frac{\rho dv}{|\vec{R}-\vec{r}|}$$

can be derived as follows.

Expanding the reciprocal distance, $|\vec{R}-\vec{r}|$, in terms of the Legendre functions (MACROBERT, 1967, p79) yields

$$U = \frac{G\rho}{R} \int_v \sum_{n=0}^{\infty} \left(\frac{r}{R}\right)^n P_n(\cos\gamma)\, dx'dy'dz'$$

where $R = (x^2 + y^2 + z^2)^{\frac{1}{2}}$, $r = (x'^2 + y'^2 + z'^2)^{\frac{1}{2}}$ and $\cos\gamma$ is as previously (Figure A1).

Let (R, θ, ϕ) be the spherical polar coordinates of the observation point (x, y, z) and (r, θ', ϕ') those of the point of integration (x', y', z').

Since (MACROBERT 1967,p.128)

$$P_n(\cos\gamma) = P_n(\cos\theta)\, P_n(\cos\theta') + 2 \sum_{m=1}^{n} \frac{(n-m)!}{(n+m)!} \cos m(\phi-\phi') \times$$

$$P_n^m(\cos\theta)\, P_n^m(\cos\theta').\cos m(\phi-\phi'),$$

$$U = \frac{G\rho}{R} \int_V \sum_{n=0}^{\infty} \left(\frac{r}{R}\right)^n P_n(\cos\theta)\, P_n(\cos\theta') + 2 \sum_{m=1}^{n} P_n^m(\cos\theta)$$

$$P_n^m(\cos\theta')\ \cos m(\phi-\phi')\ dx'\, dy'\, dz'$$

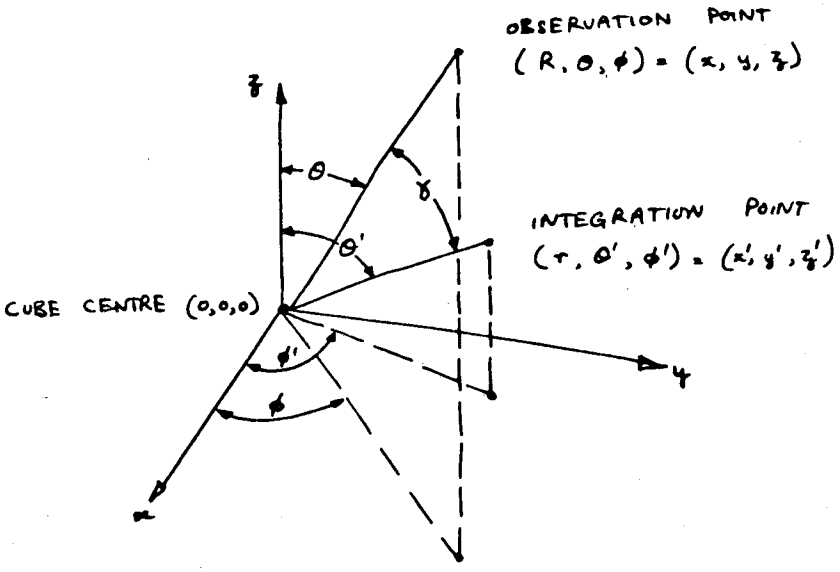

Figure A1. Coordinate Transformation

The origins of the coordinate systems are at the centre of the cube whose sides are parallel to the rectangular coordinates and of length a. By noting that

$$P_n^m(x) = (1 - x^2)^{m/2} \frac{d^m}{dx^m} P_n(x) \qquad \text{and}$$

$$P_n(x) = \frac{1}{2^n n!} \frac{d^n}{dx^n} (x^2 - 1)^n ,$$

the integration can be performed by interchanging the order of summation and integration and transforming back to the rectangular coordinate system (Figure A1)

$$\therefore \quad U = G\rho \left[\frac{a^3}{R} + \frac{7}{60} \frac{a^7}{R^9} \frac{1}{2^4} \left[3R^4 - 5\,(x^4 + y^4 + z^4) \right] \right]$$

9. Discussion

QURESHI: Do you specify an error for one calculation or for the whole series of calculations, as you will calculate the effect of a number of block elements for your model at a point? That means in any of your calculations you will have a total error. How would you describe this ?

STACEY: If I understand your question correctly, I think you are only concerned with fractional errors which cant be large.

QURESHI: You can specify that the error of your calculation at a point be less than 0.1 mgal. You are going to calculate at this point the effect of 100 elements which constitute your model. You can have a hundred errors. How would you specify the individual errors?

JOHNSON: If you have relative errors, you can work out the effect of each error. An error of a tenth mgal can be added, say, every ten times. You work out the maximum possible error in each calculation. The final error is the sum.

UNIDENTIFIED: Have you run an analysis program?

JOHNSON: No; we have been running against an exact calculation by the Nagy method.

KAULA: The same formulae can be found in *Theory of the Potential* by MacMillan.

JOHNSON: The one I used is at least a factor of ten more accurate than the computer software.

ANDERSON: I have been using similar formualae, and with regard to the references given by JOHNSON, all formulae are given in detail by MACMILLAN (*The Theory of the Potential*. Dover,New York)

JOHNSON: The development here is in the design of the type of convolution involved.

ANFILOFF, W.
SHAW, R.D.
Bureau of Mineral Resources
Department of Minerals & Energy
Canberra, ACT 2600
Australia

Proc.Symposium on Earth's Gravitational Field & Secular Variations in Position (1973),273-289.

THE GRAVITY EFFECTS OF THREE LARGE UPLIFTED GRANULITE BLOCKS IN SEPARATE AUSTRALIAN SHIELD AREAS

ABSTRACT

The three biggest linear gravity features on the Australian continent have a common form, and are an order of magnitude larger than any anomalies of comparable origin in Australia with the possible exception of the Perth Basin. They correspond with three belts of Proterozoic deformation involving narrow zones of crustal uplift, coupled with downwarping and the interpreted formation of large granulite batholiths on both sides. The development of all three belts appears to have been controlled by two major north-trending crustal dislocations.

Model studies of the gravity anomaly at the Fraser Range, south-western Australia, suggest that the Fraser Range mafic granulite has been thrust upward at least 4 km through granitic cover, with no corresponding displacement in the Conrad and Mohorovicic Discontinuities below the granulite. Two major granites on either side of the granulite are both interpreted as terminating at about 12 km.

Model studies of the anomalies in central Australia aid in delineating the southern Arunta and Musgrave upthrust granulite blocks and suggest the possible presence of four large bodies of granite and metasediment which terminate at a common depth horizon, possibly the Conrad Discontinuity. The horizon is interpreted as relatively flat. Because no gravity interpretation is unique, other models of the central Australian region which explain the gravity anomalies in terms of crustal warping or thrusting are also plausible. The models presented here are acceptable alternatives because they are consistent with the observation by Cleary of a Conrad Discontinuity at an average depth of about 20 km in many parts of Australia, and a crustal thickness which does not vary more than 5 km from an average value of about 40 km.

The termination of the gravity features associated with the southern Arunta granulite abruptly eastwards against a pronounced gravity lineament is taken to imply that a north-south compression was the cause of deformation, and that stress was released across a major crustal dislocation.

There is geological evidence of compressive events in the central Australian region at approximately 1700, 1000, 600 and 300 m.y., all consistent with stresses resulting from a primary north-south compression vector acting through central Australia. The permanence of a principal compression direction would be a limiting factor for theories of continental drift involving the rotation of the Precambrian Australian plate relative to its surroundings.

1. Introduction

This paper deals with the gravity anomalies associated with the Fraser Range, Musgrave, and southern Arunta mafic granulitic belts located in southwest and central Australia (figure 1). In terms of amplitude and length, these are three of the biggest linear gravity features in Australia, and are prominent on the gravity map of Australia (figure 2).

The systematic reconnaissance gravity coverage of most of Australia has enabled the anomalies to be compared with other gravity features, and their common characteristics to be assessed. Three belts of gravity anomalies are recognized. Each consists of a gravity ridge flanked by gravity troughs and each corresponds to a deformed belt consisting of an upthrust mafic granulite block flanked by combinations of granite and sediment. These are referred to as the Fraser Range, Musgrave, and southern Arunta Gravity Belts and Deformed Belts respectively. A model is suggested for the three structural belts

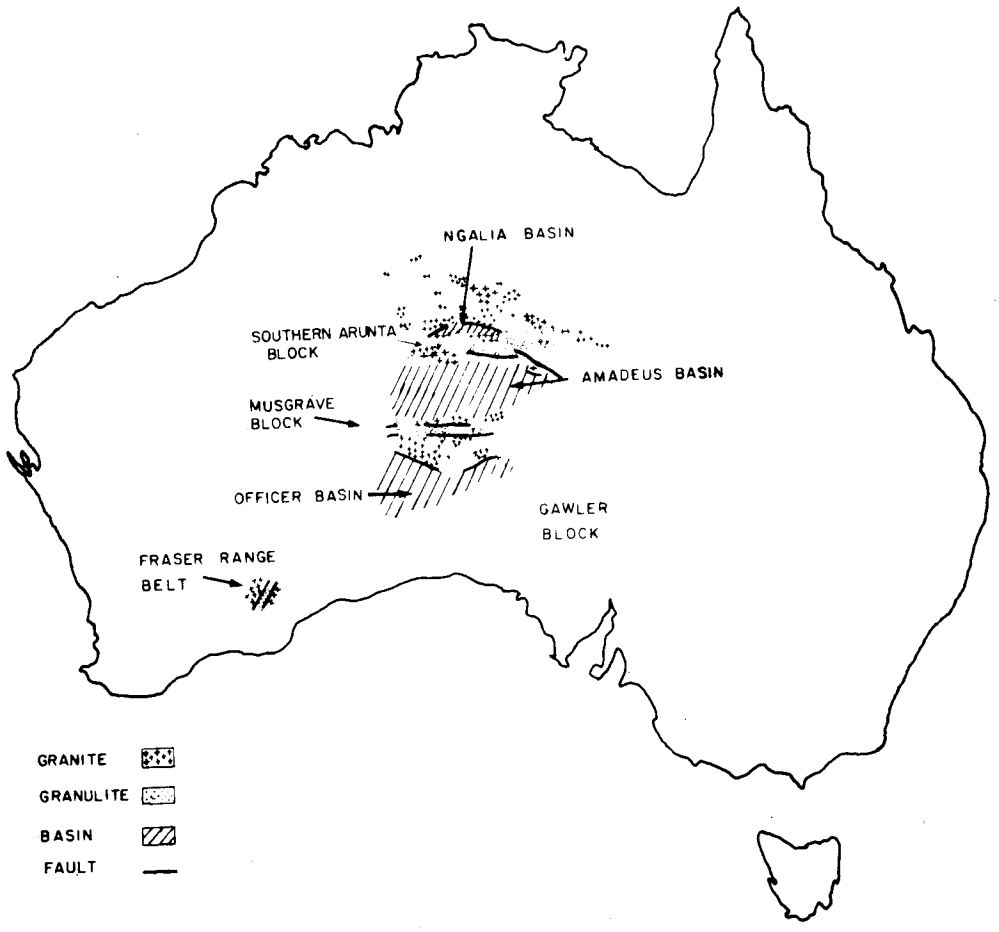

Figure 1. Granites, Granulites and Sedimentary Basins in Central and Southwestern Australia

which explains their present structure, and has some far-reaching, though speculative, implications.

Gravity profiles across the Fraser Range Gravity Belt along sections F1-F5 are shown in figure 3, and profiles across the Musgrave and southern Arunta Gravity Belts along sections C0-C5 in figure 4. The profiles of all three belts have a similar form, maintained over large distances. The maximum peak-to-trough amplitude is 170 mgal and gradients reach 4 mgal/km. In relation to the gravity levels in surrounding areas, the anomalies reach 60 mgal above and 110 mgal below surrounding levels.

Whereas the gravity ridges can be directly attributed to narrow zones of crustal uplift resulting in the exposure at the surface, of belts containing a major component of mafic granulite at the surface (MARSHALL & NARAIN 1954), the adjacent gravity lows have been interpreted in various ways. EVERINGHAM (1966) attributes the low east of Fraser Range to a granite 10 km thick; FLAVELLE (1965) explains the major low associated with the Ngalia Basin, N.T., mainly in terms of granite; MILTON & PARKER (1973) attribute the major low in the eastern part of the Officer Basin, S.A., mainly to a sediment in a basement trough with a 0.45 g cm^{-3} density contrast; and MATHUR (in prep.) attributes all four major lows in the central Australia region mainly to downwarping of the lower crust, based on the original concept

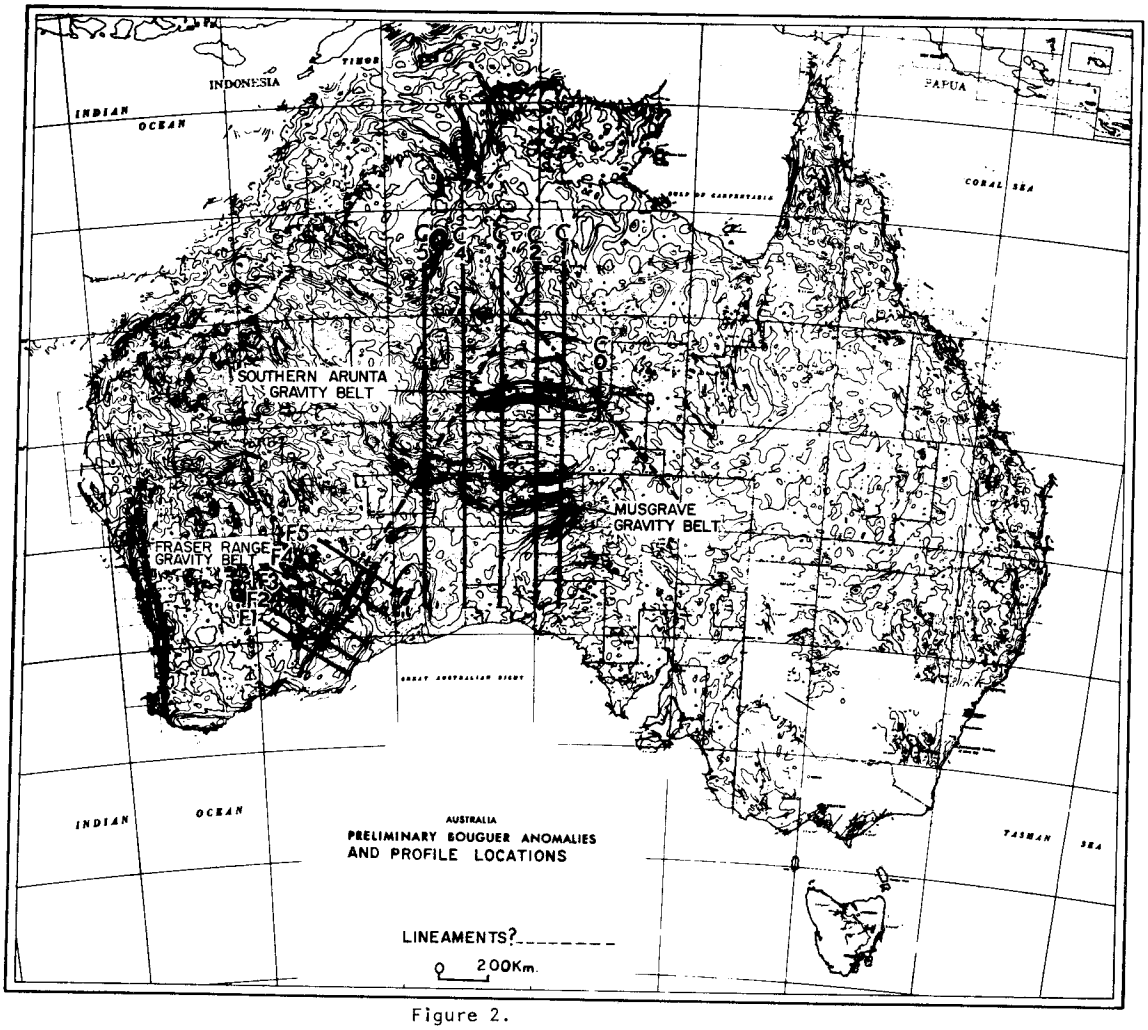

Figure 2.

of MARSHALL & NARAIN (1954) and Forman (in WELLS ET AL 1970; FORMAN & SHAW 1973). The crustal models shown in figures 5 and 9 explain the Bouguer anomalies in terms of density contrasts between rock units within the upper 20 km of the crust. However, because interpretations of gravity data are seldom unequivocal, a model such as that of MATHUR (in prep.) involving crustal warping is equally plausible in terms of available data. In the gravity models shown in figures 5 and 9, the local interpretations of granite made by EVERINGHAM (1966) and FLAVELLE (1965) have been extended with some modifications to all six major lows. The lows are postulated to have been caused by large blocks of low-density material consisting of granitic rock and variable amounts of metasediments overlain in the central Australian region by sedimentary basins. The distribution of exposed granitic rocks is sketched in figure 2. Granites and low density metasediments account for the bulk of exposed rock in the area corresponding to the greater part of the gravity low north of the Ngalia Basin. Similar rocks occur along the northern margin of the Amadeus Bsin and include large batholiths in the Mount Liebig and Mount Rennie 1:250,000 Geological Sheet areas. Large granitic bodies also crop out at the southern margin of the Amadeus Basin near Kulgera and at the northern margin of the Officer Basin in the Birksgate and Lindsay 1:250,000 Geological Sheet areas.

Two interpreted sections are presented, one across the Fraser Range Deformed Belt, and one across

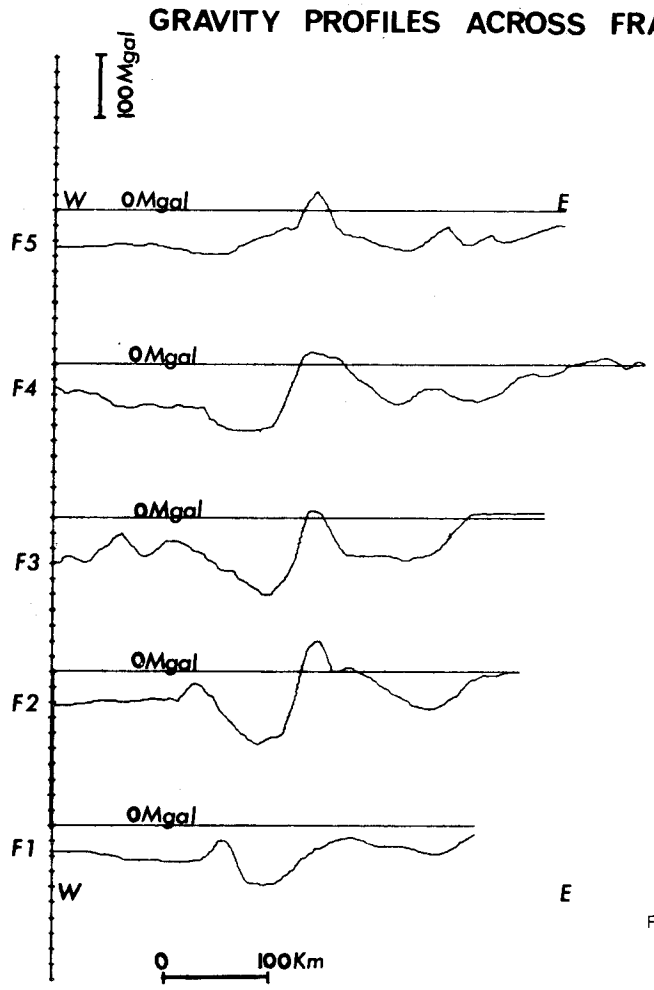

Figure 3

central Australia (the Central Australian Deformed Province) including the Musgrave and south Arunta Deformed Belts. Undeformed areas beyond the deformed belts are included in each section, so that the deformed belt structures can be interpreted in terms of mass variations relative to undeformed crustal layering.

The gravity ridges are interpreted in terms of varying amounts of mass excess caused by the uplift of granulites, and the lows are assumed to be substantially caused by large granitic bodies and variable amounts of metasediments extending down to specific depths. Large-scale compressive forces are postulated to cause the uplift of the granulite belts, subsidence and the preservation of low-density metasediments and older granites, and the formation of new granites.

2. Interpretation of the Fraser Range Gravity Belt in Southwestern Australia

The interpretation of the anomalies associated with the Fraser Range Deformed Belt is made along section F2, taken across the belt (figure 2). This particular section was chosen because detailed gravity information is available along it and the geology is better known than elsewhere in the Fraser Range. The section length is 300 km and includes Archaean gneisses and greenstones of the Yilgarn

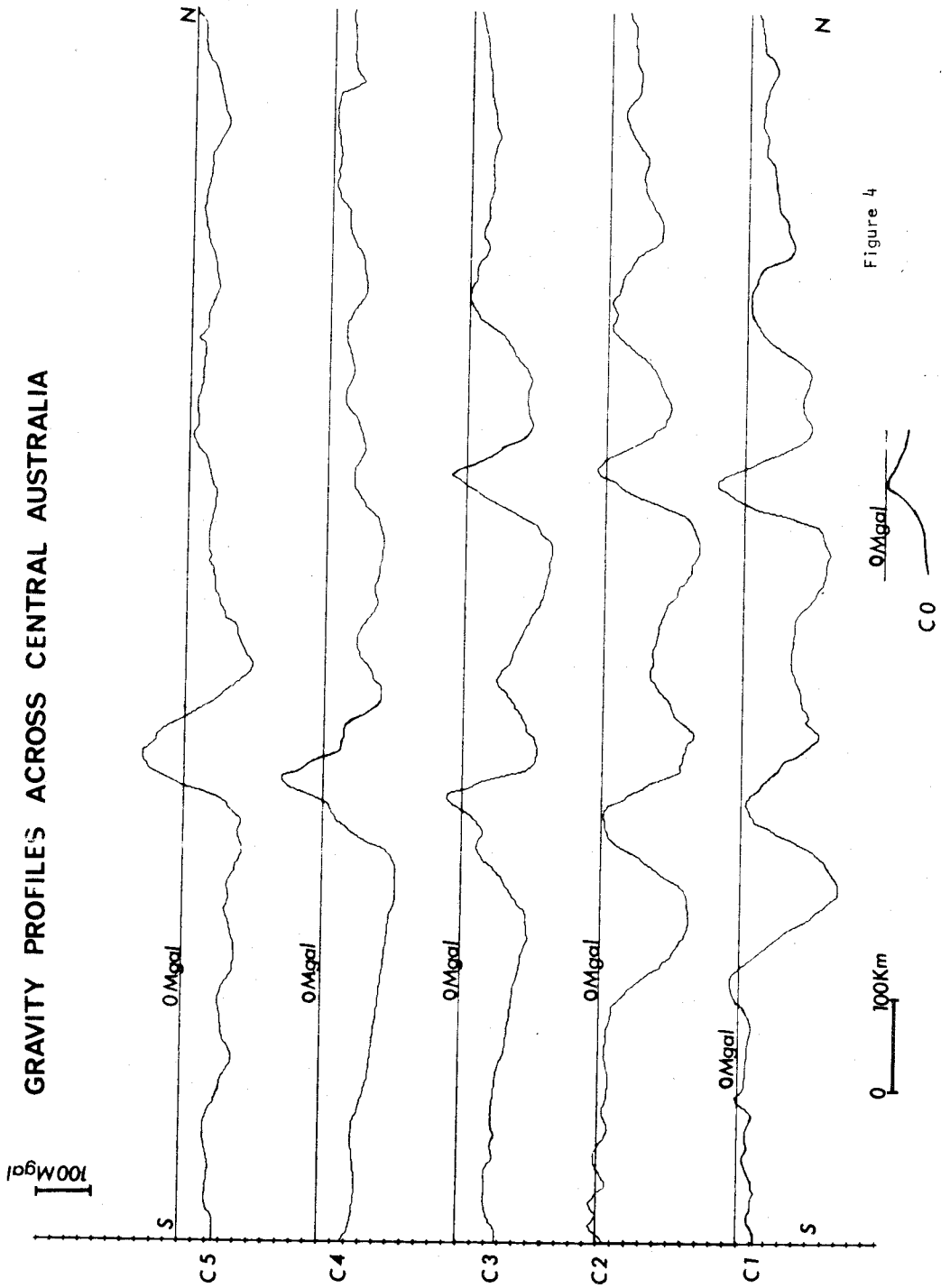
GRAVITY PROFILES ACROSS CENTRAL AUSTRALIA
100Mgal
N
S
0Mgal
C5
C4
C3
C2
C1
C0
0
100Km

Figure 4

FRASER RANGE GEOLOGY
AND INTERPRETED SECTION
- LINE F2

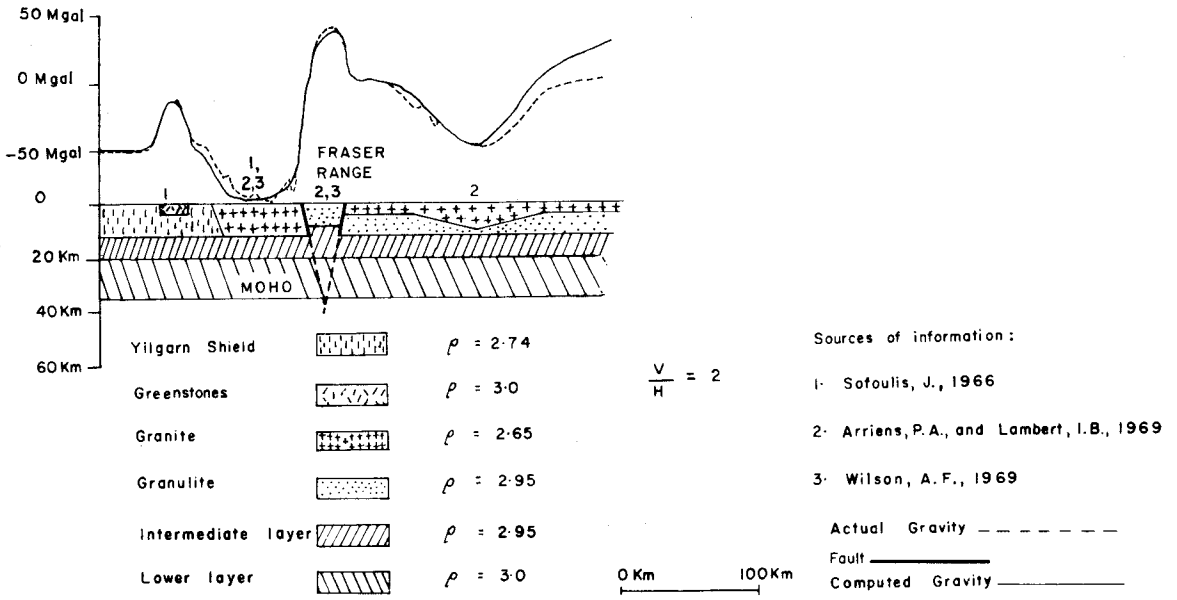

Figure 5

Shield in the west, Proterozoic granite, the Proterozoic Fraser Range mafic granulite, and the Balladonia granite and associated low-density rocks in the east.

The two granites and the mafic granulite may be interpreted as constituting a structural belt deformed against the Archaean shield by compression in the Proterozoic. Compression may have caused crustal buckling, resulting in the formation of two zones of subsidence flanking a zone of uplift. The subsidence is envisaged as causing the formation and preservation of large granite batholiths, and the uplift as causing the thrusting of mafic granulites into the upper levels of the crust. The upper part of the interpreted section (figure 5) is based on the geology of SOFOULIS (1966), WILSON (1969), and ARRIENS & LAMBERT (1969), and is modelled to consist of three main rock types:

- Archaean gneiss with a mean density of 2.74 g cm^{-3} to 12 km depth;
- two granitic bodies of density 2.65 g cm^{-3} both bottoming at about 12 km depth; and
- a mafic granulite of density 2.95 g cm^{-3}.

The lower part of the interpreted section depicts horizons at 20 and 35 km, based on the seismic results in the eastern part of the Yilgarn Shield (MATHUR in prep.), and also a subsurface granulite layer east of the Fraser Range.

The main features of the interpretation are:

1. The particular shape of the gravity anomaly over the Fraser Range granulite suggests that the granulite may have been thrust at least 4 km upwards through granitic cover.
2. The granites on either side of the Fraser Range granulite are present to a similar depth.
3. The very close agreement between the interpreted width of the Fraser Range granulite (33 km) and the mapped width (about 35 km) implies that the Conrad and Mohorovicic Discontinuities are both flat under the Fraser Range, as any upward displacement of these horizons would

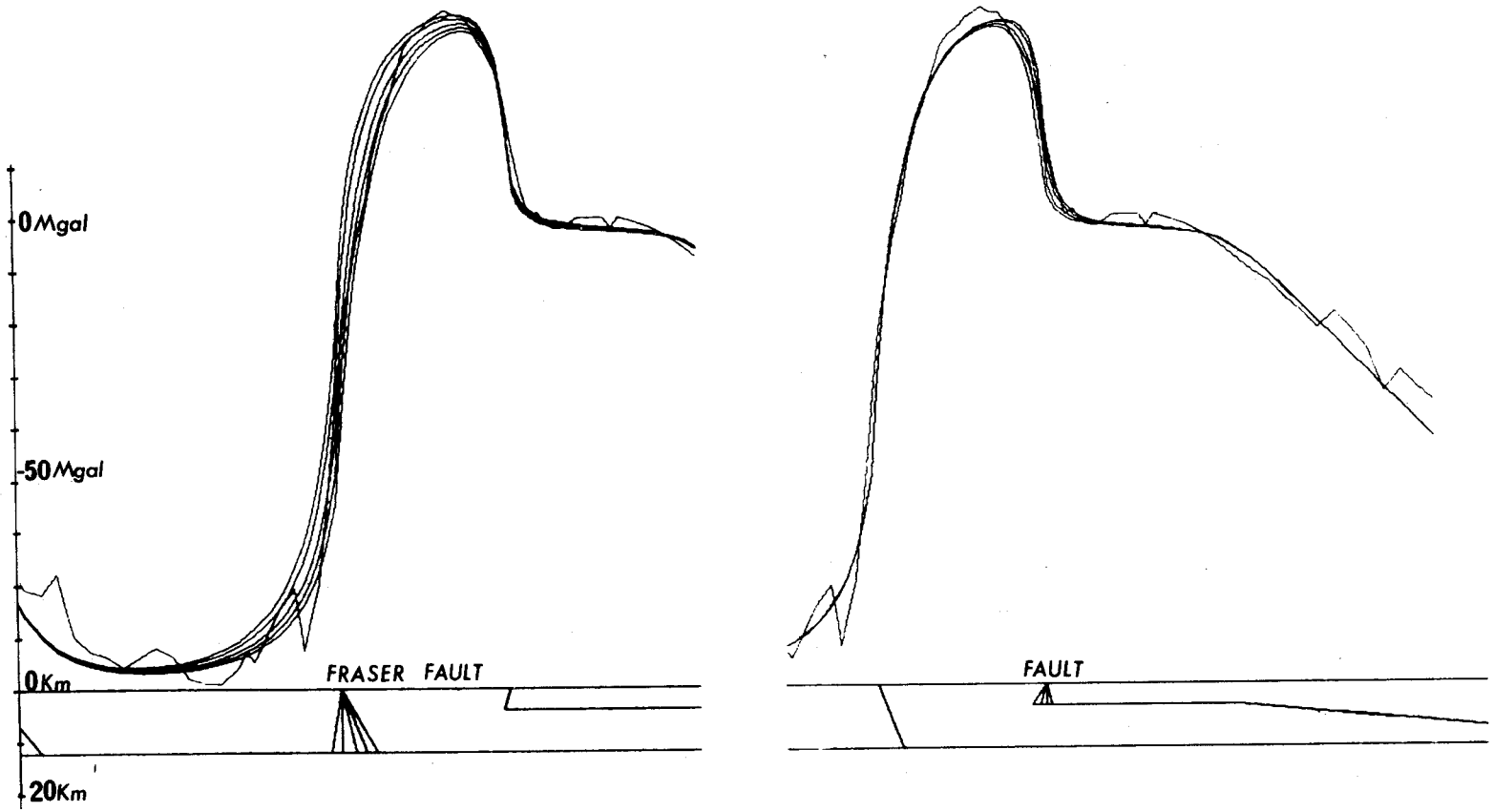

Figure 6. Sensitivity of the Computed Anomaly Over Fraser Range to Changes in the Fault Angles - Line F2

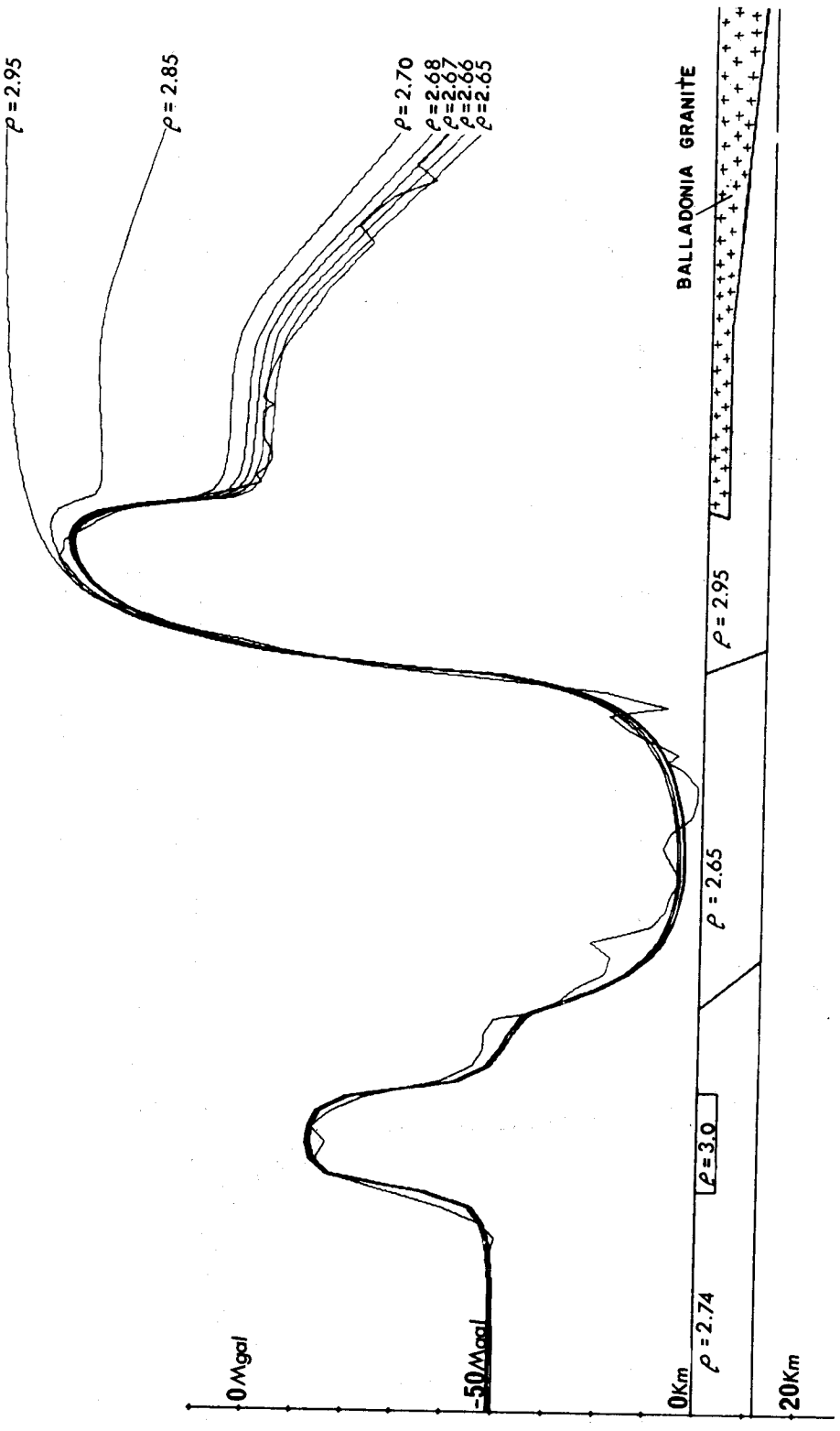

Figure 7. Sensitivity of the Computed Anomaly Over Fraser Range to Changes in the Density of the Balladonia Granite - Line F2

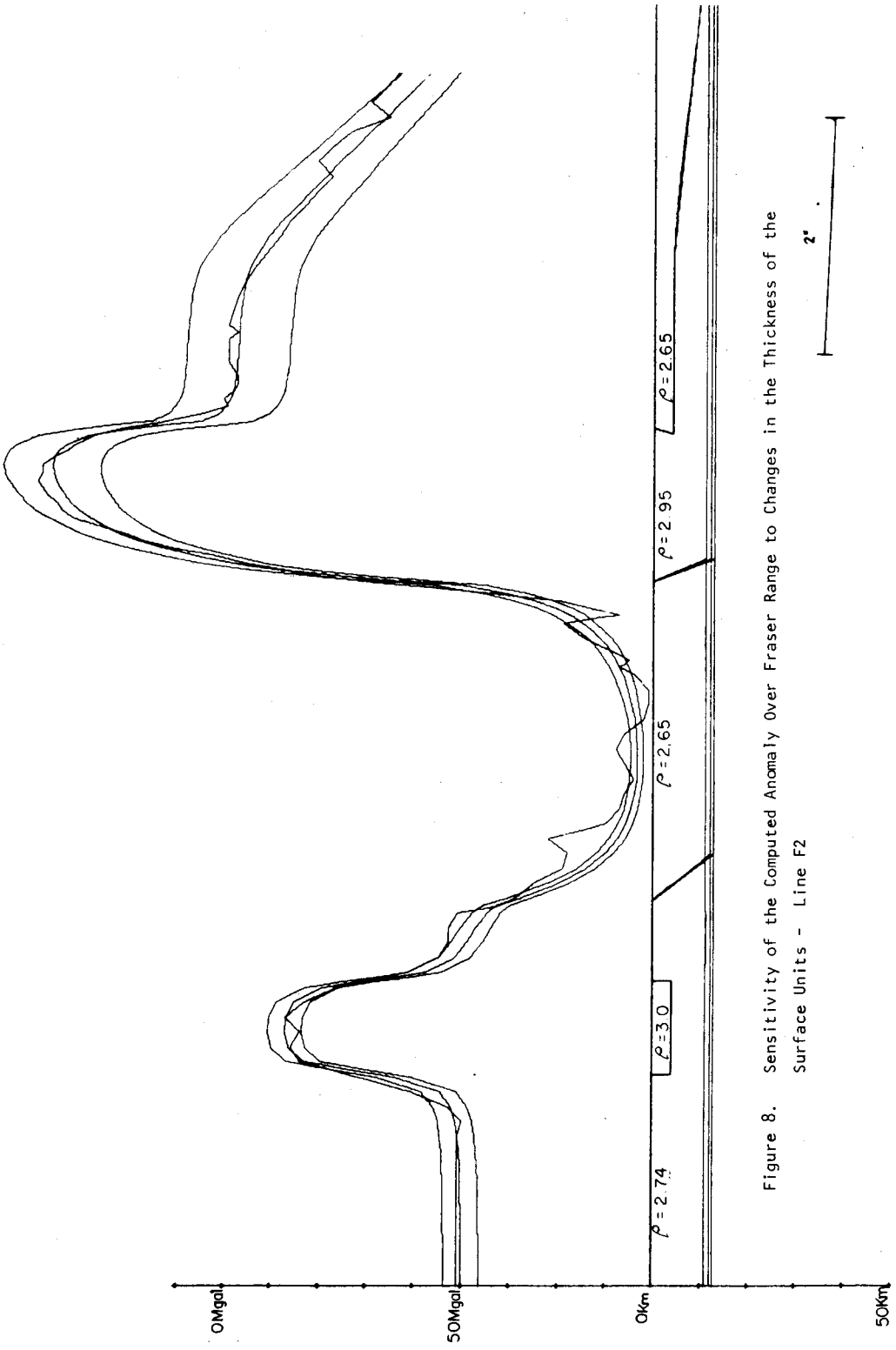

Figure 8. Sensitivity of the Computed Anomaly Over Fraser Range to Changes in the Thickness of the Surface Units - Line F2

constitute a mass excess at depth, and would have produced a much broader gravity anomaly over the granulite than is observed.

Figures 6, 7 & 8 are included to demonstrate the sensitivity of the computed anomaly to changes in various aspects of the interpreted model, and show the degree of resolution of the gravity modelling.

3. Interpretation of the Musgrave and Southern Arunta Gravity Belts in Central Australia

The Musgrave and Arunta Gravity Belts are interpreted along C1 (figure 1). This line is along 133° longitude and crosses the Gawler Block, the East Officer Basin, the Musgrave Block, the Amadeus Basin, the southern Arunta Block, the Ngalia Basin, and the northern Arunta Block. On the basis of the gravity effects, the area crossed is subdivided into two zones of undeformed crust, in the south and north, and two structural belts of deformation, the Musgrave and Arunta Deformed Belts (figure 9). The Officer Basin and its associated granites, the Musgrave Block upthrust granulites, and the southern Amadeus Basin and its associated granites are included in the Musgrave Deformed Belt. The northern Amadeus Basin and its associated granites, the upthrust granulites of the Arunta Block, and the Ngalia Basin and its associated granites are included in the southern Arunta Deformed Belt. Both belts may be considered to consist of two zones of subsidence flanking a zone of uplift, the subsidence being inferred from the accumulation of sediments, and the uplift from the presence of narrow zones of basic granulites in association with thrust faults.

Our interpretation of the gravity anomalies in central Australia assumesthat most of the gravity effects can be accounted for by density variation in the top 20 km of the crust (figure 9). The anomalies are interpreted in terms of lateral variation in density relative to two areas of undeformed crust at each end of the section. Assuming a mean crustal density of 2.81 g cm^{-3} to 20 km for the undeformed crust, the zones of subsidence can be considered to contain 20 km of granitic material of density 2.65 g cm^{-3}, and the zones of upthrust to contain crust of density 2.85 upthrust 5 km above its level in undeformed crust; and in the southern Arunta Block, 12 km of dense lower crustal material of density 3.0 g cm^{-3} all cratonized above the Conrad Discontinuity. The postulated Conrad Discontinuity at about 20 km in central Australia is consistent with its widespread distribution throughout many parts of the Australian continent (CLEARY 1973).

Three factors emerge from the interpreted model:

1. The similarity of gravity levels over undeformed crust at each end of the section is consistent with the crust there having a similar composition, and with the postulate that deformation in central Australia is intracratonic.
2. The gravity levels of all four gravity lows are consistent with equal thicknesses of low-density rock, interpreted as granite and lesser amounts of low-density metasediment in each case, over a distance of 600 km. This suggests that an essentially flat discontinuity, possibly the Conrad at 20 km depth, exists in the central Australian region.
3. The gravity levels over the upthrust zones suggest that up to 12 km of crustal uplift occurred along narrow zones relative to the undeformed crust, and that, if this caused displacements deeper in the crust, they have since been annulled by a process of density equilibration.

It is postulated that at about 1600-1700 m.y. (SHAW & STEWART 1973; MARJORIBANKS & BLACK 1973) in the

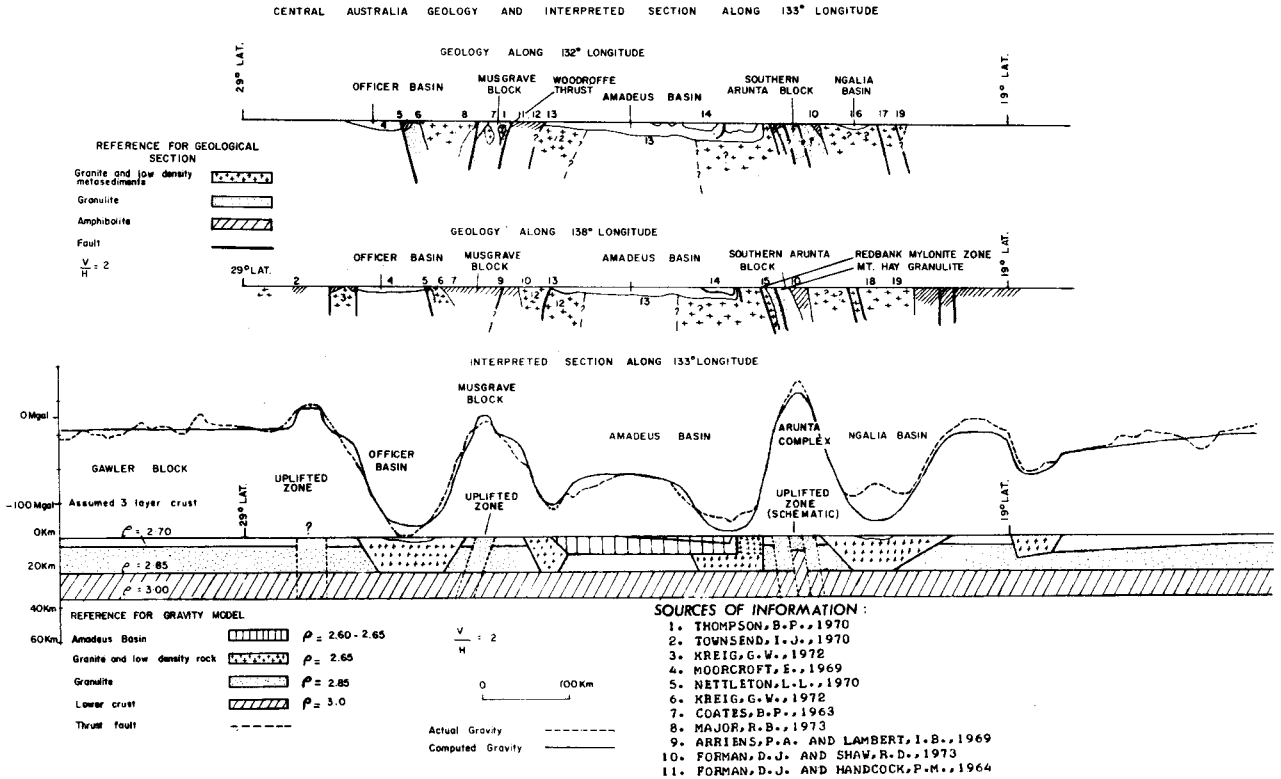

Figure 9

SOURCES OF INFORMATION :

1. THOMPSON, B.P., 1970
2. TOWNSEND, I.J., 1970
3. KREIG, G.W., 1972
4. MOORCROFT, E., 1969
5. NETTLETON, L.L., 1970
6. KREIG, G.W., 1972
7. COATES, B.P., 1963
8. MAJOR, R.B., 1973
9. ARRIENS, P.A. AND LAMBERT, I.B., 1969
10. FORMAN, D.J. AND SHAW, R.D., 1973
11. FORMAN, D.J. AND HANDCOCK, P.M., 1964
12. STEWART, A.J., 1967
13. YOUNG, G.A. AND SHELLEY, E.P., 1966
14. WELLS, A.T., FORMAN, D.J., RANFORD, L.C. AND COOK, P.J., 1970
15. MARJORIBANKS, R.W. AND BLACK, L.P., IN PREP.
16. WELLS, A.T., MOSS, F.J. AND SABITAY, A., 1972
17. WELLS, A.T., 1972
18. EVANS, T.G. AND GLIKSON, A.Y., 1969
19. SHAW, R.D. AND STEWART, A.J., IN PREP.

southern Arunta Deformed Belt and at 1000 m.y. or earlier (THOMSON 1970) in the Musgrave Deformed Belt, a strong north-south compressive stress caused the crust to buckle and consequently subside in two zones flanking a zone of uplift in a manner similar to that suggested by FORMAN & SHAW (1973). Anatectic granites are envisaged to have formed as sediments and perhaps older granites became deeply buried in the sinking troughs. Magmatic granites may also have formed at greater depths in the deformed zones. By the time crustal movements ceased, vast quantities of low-density material had accumulated to considerable depths. Conversely, in the zone of uplift, dense lower crustal material became cratonized in the upper levels of the crust. The southern Arunta Deformed Belt was reactivated, about 300-400 m.y. (IBID; SHAW & STEWART 1973) resulting in similar uplift and subsidence along roughly the same zones and the Musgrave Deformed Belt was similarly reactivated at about 600 m.y. (FORMAN *in* WELLS ET AL 1970; FORMAN & SHAW 1973).

It is postulated that after each main deformation the thickness of the structural units was reduced both by surface peneplanation and by their obliteration at depth due to large scale diffusion and largely vertical separation of elements particularly at about the level of migmatization. Additional equilibration of densities at depth might also be expected due to post-uplift phase changes in minerals as a result of adjustment to new PT conditions. Partial disruption of lateral density differences might be a result of granite intrusion late in the tectonic cycle. There is geological evidence that an event involving granite intrusion in the Musgrave Block between 1100-1200 m.y. (THOMSON 1970) extended to the southern Arunta Block as a migmatite event (MARJORIBANKS & BLACK 1973). No igneous activity is known to be associated with the later deformations considered to involve crustal warping and thrusting at 600 m.y. and 400-300 m.y. (FORMAN & SHAW 1973). Possibly the effective crustal strength was greater because the level of partial melting had, by that time, dropped to greater depths or because compression was maintained throughout the tectonic cycle. The continuous obliteration below a certain depth of the original density irregularities caused by the deformations may have produced a horizon that is conceivably the Conrad Discontinuity.

The gravity model shown in figure 9 is a much simplified representation of a complex history, but demonstrates how the gravity effects could be accounted for by density variations in the top 20 km of crust and how low-density rocks may terminate downwards at a common level.

4. Evidence for the Existence of a Primary North-South Compressive Force in Central Australia Over a 1400 m.y. Time Span

The causes of the uplift of the southern Arunta and Musgrave granulites are not known unequivocally, but circumstantial evidence suggests that the granulites of the southern Arunta Block were elevated by thrusting resulting from a strong north-south compressive force. Crustal buckling and fracturing in response to horizontal compressive forces has been proposed by MARSHALL & NARAIN (1954) to account for the main Bouguer anomaly features in the Central Australian Deformed Province. The marked similarilty in form, symmetry, and spatial periodicity of the main Bouguer anomaly features could be explained by such compressive deformation, especially if the initial buckles were formed during part of a continuous compressive episode. FORMAN & SHAW (1973) imply horizontal compression as a cause, but place more emphasis on overthrusting. Continuous or recurring compression would also help to explain the preservation of the original upthrust and downwarped crust, especially during any period of relative plasticity before the crust cooled and cratonized.

The eastern edge of the south Arunta Gravity Belt is truncated by a transverse lineament against which

both the gravity ridge and adjacent troughs are terminated abruptly. The change in gravity level of the ridge across the lineament is 50 mgal (figure 10). This aspect of the gravity anomalies suggests that the ridge and the two troughs were formed together as the result of an overall process of deformation, and that the overall deformation was terminated laterally by a crustal dislocation. This implies that the deformation is likely to have been caused by compressive stress acting on a relatively rigid plate, since only stress release across a dislocation would have sharply limited deformation along a lineament.

A similar dislocation would be expected to have occurred at the same time on the western side of the deformations, and there is evidence of a gravity lineament which extends from the Fraser Range Deformed Belt, past the western edge of the Musgrave and south Arunta Deformed Belts, and intersects the eastern lineament at a point centrally north of the Central Australian Deformed Province (figure 2). It is suggested that an exceptionally large primary north-south compressive force may have acted through the intersections of the two lineaments, causing the uplift of granulites and the subsidence of the flanking troughs.

Geological evidence indicates that the pattern of dominantly east-west structures in central Australia has been produced by a series of events involving overthrusting and overfolding which extended from the mid-Proterozoic to the mid-Carboniferous. In each event the geological structures can be interpreted to be the result of a major north-south compressive stress of constant orientation. There is evidence for the following events:

1700-1600 m.y. A major deformed zone (Redbank mylonite zone) separates the south Arunta granulites (Mt. Hay granulites) from an adjacent zone to the south containing migmatized granitic gneisses and low density metasediments. The mylonite foliation of the deformed zone is overprinted by a migmatite event at 1070 m.y. (concordant Rb/Sr total rock and mineral age - MARJORIBANKS & BLACK 1973). The gneisses have been dated at 1620 ± 70 m.y. (Rb/Sr total rock - OP.CIT.) and the uplift is possibl of this age or younger. Overthrusting consistent with compressive stress is suggested by the steep northerly dip of the mylonite foliation.

1000 m.y. or earlier Woodroofe Thrust is thought to be related to the intrusion of mafic and ultramafic igneous rocks (MAJOR 1973; THOMSON 1970) and related to structures in the granulites (COLLERSON, OLIVER & RUTLAND 1972), which have been dated at 1380 ± 120 m. y. by ARRIENS & LAMBERT (1969) (Rb-Sr total rock). Northerly directed overthrust and flattening suggests a primary north-south compressive stress.

600 m.y. The Petermann Range Nappe developed as a large recumbent anticline and complementary syncline involving both crystalline basement and sedimentary cover. Formation of the nappe at 600 m.y. is based on its stratigraphic relationships (FORMAN 1972) and Rb/sr mineral ages for metamorphosed granite intruding gneiss in the core of the nappe (LEGGO *in* FORMAN 1972). The extreme overfolding in a northerly sense is consistent with a major component of north-south compressive stress. The Woodroffe Thrust may have been reactivated during the 600 m.y. event (FORMAN & SHAW 1973).

300-400 m.y. Alice Springs Orogeny has been dated by K-Ar methods by STEWART (1971) and by Rb-Sr methods by ARMSTRONG & STEWART 1973). Deformation involved movement along a zone up to 10 km wide and the southward translation of a number of overthrusts in the northern margin of the Amadeus and Ngalia Basins (MARJORIBANKS & BLACK 1973; SHAW ET AL 1971). This implies a major component of north-south compressive stress.

In each event, the deformations produced are very elongate and regular. These large-scale yet narrow zones of uplift which developed with parallel orientation repeatedly over a time span of 1400 m.y. can be simply interpreted as the product of recurring compressive stress consistently oriented relative to the Central Australian Deformed Province.

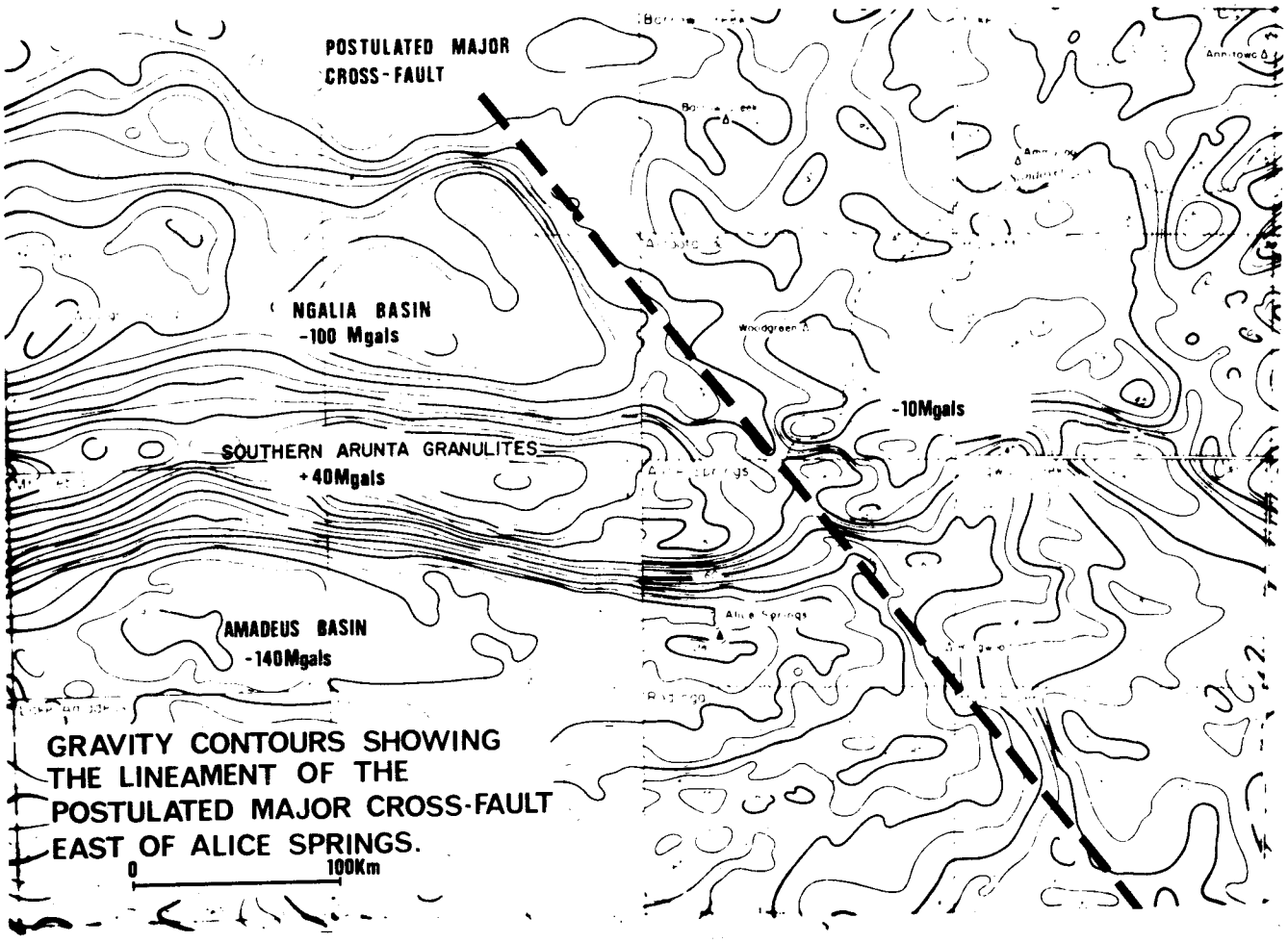

Figure 10

5. Conclusions

Three very similar structural belts, the Fraser Range, Musgrave, and southern Arunta Deformed Belts, and three corresponding belts of anomalies, the Fraser Range, Musgrave, and southern Arunta Gravity Belts are recognized. Each structural belt is interpreted as a narrow zone of uplift characterized by granulites and thrust faults and flanked by zones of subsidence characterized by sediments and large anatectic and magmatic granites. The three gravity belts have the same form and are an order of magnitude larger in amplitude than any other anomalies of comparable origin in Australia.

The Fraser Range interpretation indicates that two large granites flank the granulite. The large

gravity gradients across the faults bounding the granulite indicate that a sharp contact exists between it and the granites, suggesting that the granulite was thrust into a granitic cover. Both granites are interpreted as bottoming at about 12 km on each side of the granulite, and this may reflect the presence of a crustal horizon at that depth.

In particular, the Fraser Range anomaly negates the possibility of local uplift or warping at depth under the Fraser Range because the width of the anomaly closely matches the known width of the granulite. This strongly suggests that the Conrad and Mohorovicic Discontinuities are flat. The interpretation across central Australia suggests that the discontinuities are flat there also. Mass deficiencies caused by four postulated bodies consisting of granites and variable amounts of metasediment appear to terminate downwards at a common depth, and mass excesses caused by the uplift of the Musgrave granulites can also be placed above the common granite depth. This suggests that the granites and associated metasediments may terminate downwards at a flat discontinuity, possibly the Conrad Discontinuity at about 20 km depth, below which density irregularities do not occur.

Geological evidence suggests that the major east-west structures in central Australia were caused by a recurring primary north-south compressive stress over the interval 1700 - 300 m.y. We believe that compression can also be deduced from the gravity information. The prominent truncation of the gravity features at the eastern edge of the Central Australian Deformed Province suggests that a major NNW crustal dislocation terminated stress and resulting deformation farther eastwards. A similar dislocation is interpreted to extend north-north east from the Fraser Fault along the western edge of the Central Australian Deformed Province, and, if extrapolated, the two would intersect at a point centrally north of the deformed zone.

The deformation of the Fraser, Musgrave, and south Arunta belts can therefore be considered to have occurred between two intersecting major crustal dislocations. The interpreted relationship between the crustal dislocations and the Central Australian Deformed Province implies that the deformed province was an intracontinental feature from at least the time of formation of the 1700 m.y. old southern Arunta Deformed Belt.

There is evidence of deformations involving north-south compressive stress in the Central Australian Deformed Province at 1700, 1000, 600, and 300 m.y. Immediately after the main 1700 m.y. and 1000 m.y. deformations, anisotropy may have affected the direction of stress, but considering the length of time and the magnitude and consistency of the later strains involved, it is unlikely that anisotropy markedly affected the stress direction in the more recent events. The overall history of stress in the Central Australian Deformed Province therefore appears to be one of compressive stresses resulting from a more or less consistent north-south primary compression vector. This suggests that the main Australian Precambrian plate did not rotate relative to its surroundings if it underwent continental drift between 1700 and 300 m.y., since this would probably have produced new principal stress directions.

6. Acknowledgments

The authors wish to thank A.Y. Glikson, A.J. Stewart and R.W. Marjoribanks for their helpful comments on the initial manuscript.

This paper is published with the permission of the Director, Bureau of Mineral Resources, Geology & Geophysics, Canberra, ACT.

7. References

ARMSTRONG, R.L. & STEWART, A.J. 1973. Rubidium-Strontium Dates and Excess Argon in the Arltunga Nappe Complex, Northern Territory. *Bur.Min.Resour.Aust.Rec.* (in preparation),Canberra ACT.

ARRIENS, P.A. & LAMBERT, I.B. 1969. On the Age and Strontium Isotopic Geochemistry of Granulite-Facies Rocks from the Frazer Range, Western Australia, and the Musgrave Ranges, Central Australia. *Geol.Soc.Aust.Spec.Publ.* 2,377-388.

CLEARY, J. 1973. Australian Crustal Structure. *Tectonophysics* (in press).

COATES, R.P. 1963. The Geology of the Alberga 4-Mile Military Sheet. *Geol.Surv.S.Aust.Rep.Invest.* 22.

COLLERSON, K.D., OLIVER, P.L. & RUTLAND, R.W.R. 1972. An Example of Structural and Metamorphic Relationships in the Musgrave Orogenic Belt, in Central Australia. *J.geol.Soc.Aust.* 18, 379-393.

EVANS, T.G. & GLIKSON, A.Y. 1969. The Geology of the Napperby Sheet Area, Northern Territory. *Bur. Miner.Resour.Aust.Rec.* 1969/85, Canberra ACT.

EVERINGHAM, I.B. 1966. *Gravity Anomalies on the Precambrian Shield of Southwestern Australia.* M.Sc. Thesis, University of Western Australia, Perth WA.

FLAVELLE, A.J. 1965. Helicopter Gravity Survey by Contract, Northern Territory and Queensland. *Bur.Miner.Resour.Aust.Rec.* 1965/212,Canberra ACT.

FORMAN, D.J. 1972. Petermann Ranges, N.T. - 1:250,000 Geological Sheet. *Bur.Miner.Resour.Aust.explan. Notes* SG/52-1,Canberra ACT.

FORMAN, D.J. & HANCOCK, P.M. 1964. Regional Geology of the Southern Margin, Amadeus Basin, Rawlinson Range to Mulga Park Station. *Bur.Miner.Resour.Aust.Rec.* 1964/41,Canberra ACT.

FORMAN, D.J. & SHAW, R.D. 1973. Deformation of the Crust and Mantle in Central Australia. *Bur.Miner.Resour.Aust.Bull.* 144,Canberra ACT.

KRIEG, G.W. 1972a. Everard, S.A. - 1:250,000 Geological Map. *Geol.Surv.S.Aust.explan.Notes* SG/53-13, Adelaide SA.

KREIG, G.W. 1972b. The Ammaroodina Inlier. *Geol.Surv.S.Aust.Quart.geol.Notes* 41,Adelaide SA.

MAJOR, R.B. 1973. Woodroffe, S.A. - 1:250,000 Geological Map. *Geol.Surv.S.Aust.explan.Notes* SG/52-12,Adelaide SA.

MARJORIBANKS, R.W. & BLACK, L.P. 1973. The Geology and Geochronology of the Arunta Complex North of Ormiston Gorge,Central Australia. *Bur.Miner.Resour.Aust.Rec.* 1973/181, Canberra ACT.

MARSHALL, C.E. & NARAIN, N. 1954. Regional Gravity Investigations in the Eastern and Central Commonwealth. *Mem.* 1954/2,Department of Geology & Geophysics,University of Sydney,Sydney NSW.

MATHUR, S.P., BRANSON, J.C. & MOSS, F.J. 1973. Geotraverse Seismic Survey, W.A. *Bur.Miner.Resour. Aust.Rec.* (in preparation),Canberra ACT.

MATHUR, S.P. 1973. A Proposal for Deep Crustal Seismic Sounding Survey in Central Australia. *Bur. Miner.Resour.Aust.Rec.* (in preparation),Canberra ACT.

MILTON, B.E. & PARKER, A.J. 1973. An Interpretation of Geophysical Observations on the Northern Margin of the Eastern Officer Basin. *Geol.Surv.S.Aust.Quart.geol.Notes* 46,Adelaide SA.

MILTON, B.E. & THORNTON, R.C.N. 1970. Discovery of a Dense Lower to Middle Palaeozoic Dolomite in the Northwest Arckaringa Basin. *Geol.Surv.S.Aust.Quart.geol.Notes* 36,Adelaide SA.

MOSSFROFT, E. 1969. Sesmic Reflection, Refraction and Gravity Survey,Eastern Officer Basin, 1966. *Min.Rkv.Adelaide* 126,58-70.

NETTLETON, L.L. 1970. *Eastern Officer Basin Gravity Survey PEL 10 & 11, South Australia.* Geophysical Associates Pty Ltd, Report for Murumba Oil N.L. (S.Aust.Dept. Mines open file Env.1196),Adelaide SA.

SOFOULIS, J. 1966. Widgemooltha, W.A. - 1:250,000 Geological Map. *Geol.Surv.W.Aust.explan.Notes* SH/51-14,Perth WA.

SHAW, R.D. & STEWART, A.J. 1973. Regional Geology of the Precambrian Arunta Block. In *Economic Geology of Australia and Papua and New Guinea.* Australian Institute of Mining and Metallurgy,Melbourne Vic.

SHAW, R.D., STEWART, A.J., YAR KHAN, M. & FUNK, J. 1971. Progress Reports on Detailed Studies in the Arltunga Nappe Complex, N.T., 1971. *Bur.Miner.Resour.Aust.Rec.* 1971/66,Canberra ACT.

STEWART, A.J. 1967. Kulgera, N.T. - 1:250,000 Geological Series. *Bur.Miner.Resour.Aust.explan.Notes* SG/53-5,Canberra ACT.

STEWART, A.J. 1971. K-Ar dates from the Arltunga Nappe Complex,Northern Territory. *J.geol.Soc.Aust.* 17,205-211.

THOMSON, B.P. 1970. A Review of the Precambrian and Lower Palaeozoic Tectonics of South Australia. *Trans.R.Soc.S.Aust.* 94,193-221.

TOWNSEND, I.J. 1970. Stratigraphic Drilling Programme 1969. Western Archaringa Basin. *S.Aust.Dep. Mines Rep.* BK70/40,Adelaide SA.

WELLS, A.T., FORMAN, D.J, RANFORD, L.C. & COOK, P.J. 1970. Geology of the Amadeus Basin, Central Australia. *Bur.Miner.Resour.Aust.Bull.* 100,Canberra ACT.

WELLS, A.T., MOSS, F.J. & SABITAY, A. 1972. The Ngalia Basin, Northern Territory - Recent Geological and Geophysical Information Upgrades Petroleum Prospects. *APEA J* 12,144-151.

WELLS, A.T. 1972. Mount Doreen, N.T. - 1:250,000 Geological Series. *Bur.Miner.Resour.Aust.explan. Notes* SF/52-12,Canberra ACT.

WHITWORTH, R. 1970. Reconnaissance Gravity Survey of Parts of Northern Territory and Western Australia, 1967. *Bur.Miner.Resour.Aust.Rec.* 1970/15,Canberra ACT.

WILSON, A.F. 1969. Granulite Terrains and Their Tectonic Setting and Relationship to Associated Metamorphic Rocks in Australia. *Geol.Soc.Aust.Spec.Publ.* 2,243-258.

YOUNG, G.A. & SHELLEY, E.P. 1966. The Amadeus Basin Airborne Magnetic and Radiometric Survey, N.T. *Bur.Miner.Resour.Aust.Rec.* 1966/64,Canberra ACT.

Proc.Symposium on Earth's Gravitational Field & Secular Variations in Position (1973),290.

TAPLEY, B.D.
Department of Aerospace Engineering & Engineering Mechanics
University of Texas at Austin
Austin, Texas 78710
United States of America

Chairman's Introduction to Session F - "Laser Ranging to Satellites"

The application of laser ranging to Earth satellites has opened up a number of new and interesting areas of study and has given rise to a potential for contributing to a number of problems in geodesy and geodynamics.

Position range measurements are routinely made to the order of 50 cm with the expectation that this accuracy can be improved to the order of 10 cm.

Such precision holds promise for contributing to the solution to such problems as the study of solid Earth tides, short term polar motion, gravitational field definition, geoid determinations, etc.

The session this morning has four papers dealing with problems in these areas.

The first paper deals with the problem of dynamic determination of position and has the advantage that the information obtained is referenced to the Earth's centre of gravity (SMITH ET AL).

The second paper (by ONG) considers the role of geometrical determinations and has the advantage of being free from gravitation and other model errors, but has the associated disadvantage of requiring a large number of stations simultaneously tracking the vehicle if a solution is to be obtained.

The third paper (by PLOTKIN) will give some insight into the potential for achieving a range measuring accuracy in the 10 cm range, while the fourth paper (by PAQUET & DEJAIFFE) will discuss the Doppler measuring systems.

SMITH, D.E.
KOLENKIEWICZ, R.
AGREEN, R.W.
NASA Goddard Space Flight Center
Greenbelt Md 20771
United States of America

DUNN, P.J.
Wolf Research & Development Corporation
Riverdale Md
United States of America

Proc.Symposium on Earth's Gravitational Field & Secular Variations in Position (1973),291-314.

DYNAMIC TECHNIQUES FOR STUDIES OF SECULAR VARIATIONS IN POSITION FROM RANGING TO SATELLITES

ABSTRACT

During the last few years NASA Goddard Space Flight Center has been applying satellite laser range measurements to problems in Earth and ocean physics. Primary attention has been directed towards the measurement of the variation of latitude arising from polar motion and to the determination of the solid-Earth and ocean tidal distortion of the Earth's gravity field. These investigations have been successfully conducted using data obtained by a single laser station tracking a single satellite. It has further been demonstrated that these data can also be used to monitor the height or radial distance of the station and can contribute substantially to our knowledge of the gravity field.

Experiments involving two stations have also been conducted. Simultaneous range measurements to a satellite from two stations several hundred km apart have been used to determine the relative location of one station with respect to the other. This technique is now being used in an experiment (SAFE) to measure the motion between points 900 km apart on opposite sides of the San Andreas fault system in California. A simulation of this experiment for a seven year observing period has indicated that it should be possible to determine the average relative motion of the two sides of the fault to an accuracy of about 5 mm per year.

At the present time, all spacecraft equipped with laser retroreflectors are in relatively low orbits of 500 to 2000 km but in the next few years it is anticipated that geodynamic satellites at much greater altitude will be launched. At these greater altitudes of several thousand km, the perturbing effects of the Earth's gravity field will be much smaller and should permit an improvement of at least an order of magnitude in the determination of the product of the Earth's mass and gravitational constant.

In a few years it is anticipated that laser ranging measurements to high altitude satellites from a single site will permit the station to monitor its own latitude and height variations at the 5 to 10 cm level on a daily basis and determine the length of day to about 0.2 milliseconds. Multiple station experiments should enable crustal and tectonic motions to be measured to an accuracy of a few mm per year over a few years from which large scale strain fields could be derived. Observations of lower altitude satellites will yield information on the gravity field, the elastic response of the solid-Earth to tidal forces and the amplitudes and phases of certain components of the ocean tides.

1. Introduction

The successful development of high precision laser tracking systems over the last decade is now beginning to to permit the investigation of geophysical parameters of considerable interest and importance. At Goddard Space Flight Center the accuracy of laser ranging has improved nearly two orders of magnitude since 1964, and toward the end of 1973, reached a level of about 10 cm. With this quality, it can reasonably be expected that laser ranging to satellites will be able to contribute significantly to the measurement of the motions of the Earth, such as tectonic, polar, tidal and crustal, and to the determination of the Earth's gravitational field in both space and time. However, until very recently, the quality of the range measurements was of the order of 50 cm, a capability

achieved in 1970, and it is upon data of this quality that all our experience so far has been based. In this paper we attempt to review the major aspects of the analysis of satellite laser range measurements conducted at Goddard Space Flight Center since 1970 for ultimate application to geodesy and geodynamics.

The investigations at Goddard Space Flight Center (GSFC) have been restricted so far to those that can be achieved with one or two tracking systems. Until late 1973, GSFC possessed one fixed laser system sited at its optical facility in Greenbelt, Maryland and one mobile tracking system that could be driven, or shipped, almost anywhere. Both these systems were one joule ruby lasers with a pulse rate of one-per-second.

A major factor that influenced the analyses was the limited knowledge of the perturbing forces affecting the motion of the satellite. In 1970, our long wavelength knowledge of the gravitational field was almost entirely derived from optical satellite tracking data accurate to about two seconds of arc (10 m at about 1000 km range) (GAPOSCHKIN & LAMBECK 1970). Thus, the laser observations were about an order of magnitude better than the data used to derive the field and thus any analysis might ultimately be limited by errors in force field rather than the data. The position is hardly any different in 1973 than in 1970, and in none of the investigations conducted at GSFC in the last few years has any real evidence been uncovered which suggests that we have been limited by the quality of the data; even at the 50 cm level. Consequently, any modest achievements that can be established in the present environment should be well exceeded (even with the same data) when improved force models are available. It is therefore essential that research continue in the area of improving the Earth's gravity field and in the modeling of other perturbing influences of satellite orbits for the full potential of the orbit dynamic technique to be fully realized.

Because of the difficulty of assessing the full value of the range data already available, predictions of future capabilities, such as detecting plate motion, are almost entirely dependent on simulations or error analyses; which are themselves based on assumed error models. In the absence of any other technique this approach has been used at GSFC for projecting future capabilities with future satellites. It is from these simulations and error analyses, as well as from our own work over the last few years, that much of our optimism for the future is drawn.

In the following sections the major results obtained at GSFC over the last three years from the analysis of laser range data are described and discussed; followed by a brief description of some of our own ideas and plans for the future.

2. Laser Data

There are seven satellites presently in orbit carrying laser retroreflectors, Beacon Explorers B and C, and GEOS 1 and 2 launched by the United States, and three satellites launched by France, D1-C, D1-D and PEOLE. At GSFC most of our tracking operations have been on the U.S. satellites, particularly Beacon Explorer C (BE-C), and it is the analyses of tracking data on this spacecraft that is described here.

The orbit of BE-C is nearly circular at an altitude of about 1000 km with an orbital inclination of 41°. A typical pass of BE-C near a ground station lasts about 8 to 10 minutes and can be tracked by the laser station down to elevations of 20° or less fairly routinely (weather permitting) and some-

times below 10°; thus, with a pulse rate of one-per-second, 500 or more range measurements are obtained on a "good" pass of the satellite. Less than 100 measurements are considered "poor" passes but this does not necessarily imply that the data or the pass is any less valuable than a "good" pass. The average number of measurements per pass over nearly 18 months of tracking of BE-C by the fixed laser at GSFC was about 150.

The basic measurement of the laser system is the round-trip travel time of the laser pulse from the transmitter to the satellite and back down to the receiver (JOHNSON ET AL 1967). This time interval is corrected for system delays (calibration constants), for variation in the pulse shape and height, converted to a range, and corrected for atmospheric effects and for spacecraft size and attitude. The whole system is calibrated by ranging to a calibration target at a known distance from the tracking system before and after every satellite pass. The tropospheric correction amounts to about 2.5 m at zenith and is applied to each individual range measurement according to the elevation (E), pressure (P), temperature (T), and the station height above mean sea level (H), as shown below:

$$\delta\rho = \frac{2.238 + 0.0414\, P\, T^{-1} - 0.238\, H}{\sin E + 10^{-3} \cot E} \qquad (1).$$

The above formula is believed to provide the correction accurate to about 5 cm at 20° elevation.

A correction for spacecraft attitude and size is also made before the data are analyzed. The laser pulse is reflected from the surface of the spacecraft and yet the orbital dynamics are concerned with the motion of the spacecraft centre of mass. Thus, a range correction from the spacecraft surface to the centre of mass is made to each measurement. For BE-C, which is magnetically stabilized, this correction is on the average about 20 cm and varies slowly during a pass observed at GSFC between 15 cm and 27 cm.

After all corrections are applied, the final range measurements are checked for internal consistency by fitting an orbit or a polynomial through each pass of data for each station. This procedure provides the rms noise level of the data and identifies and measurements that are obvious errors. Further, the noise level can be used as an initial check that the system appears to be working correctly. For example, a sudden increase in the noise level from 50 cm to 100 cm between two consecutive passes probably indicates a change in performance of the system that needs to be investigated.

Figure 1 shows the range residuals to an orbit fitted to each of four passes of data obtained by the fixed Goddard laser (GODLAS). These four passes were obtained by the fixed Goddard laser (GODLAS) on September 2, 1970. The rms fits of the data about these orbits varies between 48 cm and 53 cm. The noise levels associated with each pass only indicate the internal consistency of the data and say nothing about possible biases that could exist. It will be seen in later sections, that if these pass-to-pass biases exist, they are extremely constant or probably no larger than the noise level. The quality of the data shown in figure 1 is typical of that collected during the Summer and Fall of 1970. During the latter part of 1971 the noise level of the data was generally higher at about 80 cm and is believed to have been the result of an unintentional increase in the length of the ruby pulse from about 20 to nearly 40 nanoseconds.

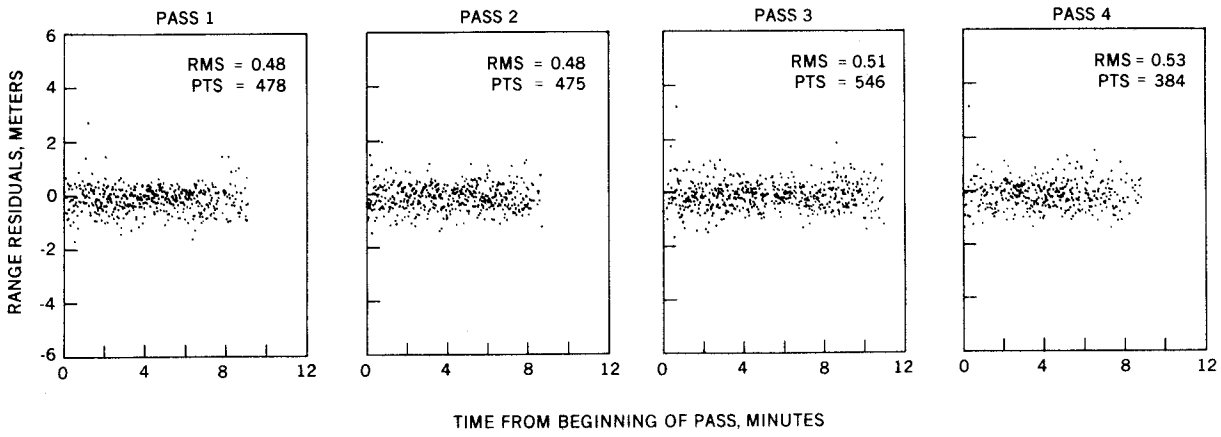

Figure 1. Laser Range Residuals to Four Beacon Explorer C Passes on September 2, 1970

The laser systems also output the direction of the receiving telescope at the time of each return pulse but we have never used these data in any of our investigations because of their relatively low accuracy and high probability of biases. The angular field of the receiving telescope is about one minute of arc and the return pulse could come from anywhere in the field of view. Further, the telescope is computer driven to follow a predicted path across the sky and if the satellite is acquired in one segment of the field of the receiving telescope, it may well remain in that "off-centre" position throughout the pass. The angle measurements would then be biased by anything up to about 30 arcseconds. On a number of occasions the quality of the angle data has been estimated by comparing the position of the satellite computed from a large number of range measurements, with the angle data. This comparison suggested the rms noise of the angle data was about 30 arcseconds with biases of the order of 15 arcseconds.

3. Orbit Determination

The latitude of the GSFC Optical Site is approximately 39°N and because this is comparable to the orbital inclination of BE-C (41°), the apparent motion of the satellite from the site is predominantly west to east. In addition, the site sees four consecutive passes of BE-C spanning about 6 hours each day (when the weather permits). In the analysis, an orbit has been determined for BE-C from laser

data on every occasion that four consecutive passes were observed at the GSFC site (GODLAS). Thirty-six sets of orbital elements have been determined in a five-hundred day period between July 1970 and November 1971. In order to assess the quality of these BE-C orbits, a simple analysis of the variations in the orbit parameters was conducted. For this test, 28 sets of orbital elements obtained for the Summer and Fall of 1970 were used in a short arc minus long arc analysis.

The short minus long arc approach involves comparing orbit parameters obtained from short arcs (for example, four passes) with the same parameters obtained from a long arc (several weeks or months) and is basically equivalent to comparing observations (short arcs) with theory (long arcs). In situations, such as at GSFC, where numerical integration is used in the orbit determination programs, no "theory" exists and must be replaced with a numerical computation. This computation must provide the best orbit available and be equally representative of the true orbit at each of the observation points (short-arc orbits). The way this "theoretical" orbit can be produced is by fitting one single orbit to all the data covered by the short arcs. If this long-arc is sufficiently long, it will average through perturbations that are not accounted for in the integration of the orbit and it then becomes equivalent to the theoretical orbit. The short arcs, on the other hand, are unable to average through any unmodeled perturbation that has a periodicity longer than the time span of the short arc. The short arc therefore (in contrast to the long arc) absorbs the perturbations into the orbit parameters. Subtracting the orbit parameters of the long arc from the parameters of the short arcs therefore reveals perturbations that are not computed in the long arc as well as errors, or deficiencies, in the modeling of forces that are included. Figure 2 shows residuals in semi-major axis, argument of perigee, right ascension of the node, eccentricity and mean anomaly obtained from a short minus long arc analysis of the BE-C data. The residuals in inclination are not shown in figure 2 bacause they are described and discussed in considerable detail in later sections of this paper. It will be seen in these sections that the orbital inclination is the best determined parameter.

Figure 2 shows the variation in semi-major axis is bounded by about plus and minus 3 m with the suggestion of a 70 to 80 day oscillation. This oscillation is probably more evident in the orgument of perigee and mean anomaly, and to a lesser extent in the eccentricity. There is no evidence, however, of an oscillation in the nodal residuals which are dominated by a linear acceleration of about 1.5×10^{-5} degrees/day, equivalent to an error of about 3 parts in 10^6 in the precession of the node. In terms of satellite position, the residuals in mean anomaly and semi-major axis indicate a maximum difference between the short arc and long arc positions of less than 1 km. A fact to be noticed in figure 2 is that the eccentricity and argument of perigee are negatively biased. The cause of these, and other trends and patterns in figure 2 are at present unknown. The connection between these residuals and a possible error in **GM**, the product of the gravitational constant and the Earth's mass, is being investigated. It should also be noted from figure 2 that each of the elements appears to have high internal consistency suggesting that the patterns and trends clearly visible are caused by errors in the Earth parameters (gravity, station position, etc.) rather than the data.

In general, the fit of the orbit to the laser data in a four-pass orbit never equals the quality of the data. Typically, the rms of fit of the laser data in a four-pass orbit is between 1 and 3 m (in contrast to 40 to 60 cm on a single pass) and we have found that the fit is very dependent on the gravitational field being used in the orbit analysis. For the Goddard Earth Model 1 (GEM 1), the average rms of fit over 36 four-pass orbits containing nearly 36,000 laser range measurements is

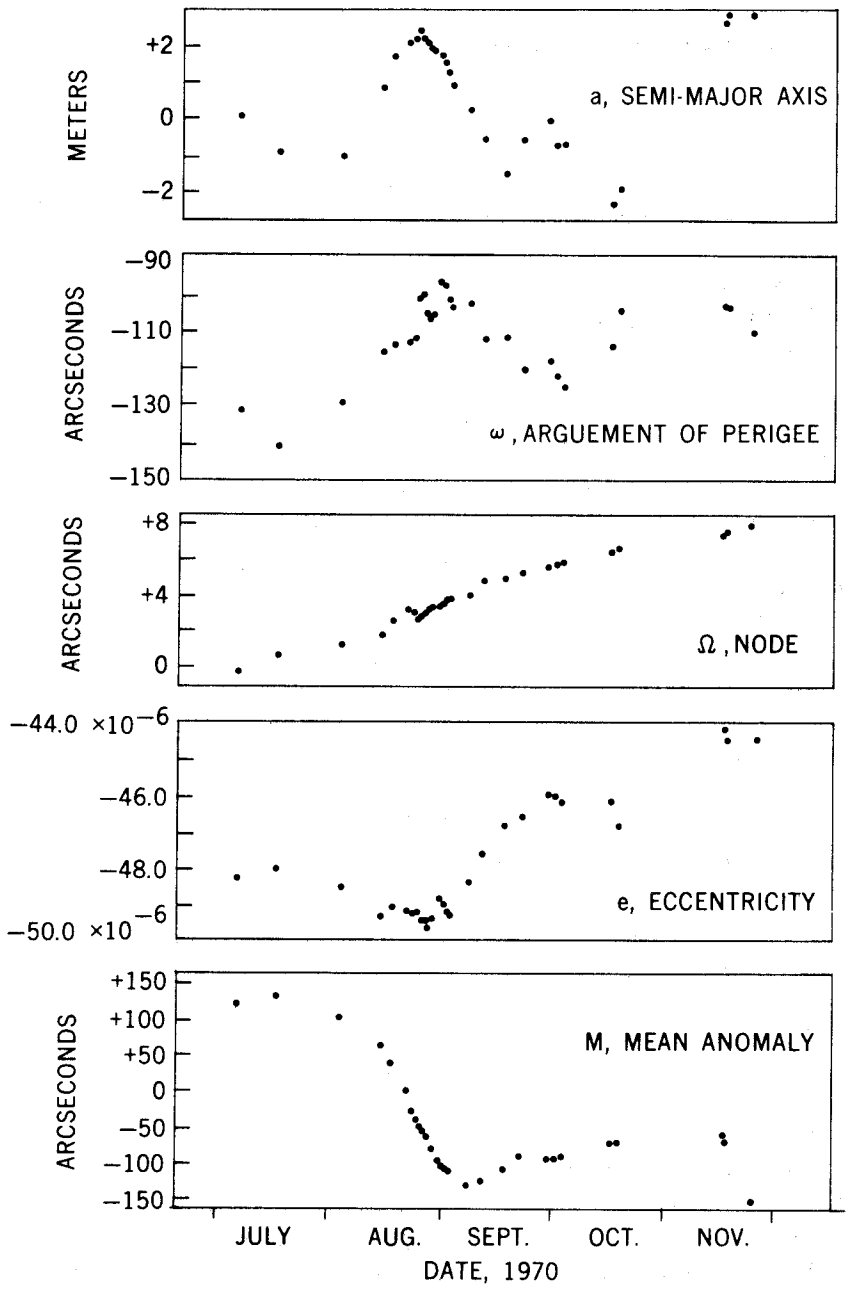

Figure 2. Beacon Explorer C Orbital Element Residuals

1.32 m. There appears to be no correlation between the number of measurements and the rms of the fit. Further, we have found no evidence of poor data in the orbital arcs with the larger rms deviations.

Table 1

Results of the Determination of the Position of the Seneca Laser and the Baseline Between Goddard and Seneca

TIME OF FIRST PASS Y – M – D	RANGE MEAS. GODDARD	RANGE MEAS. SENECA	R.M.S. FIT TO ORBIT GODDARD (cm.)	R.M.S. FIT TO ORBIT SENECA (cm.)	ADJUSTED SENECA POSITION LAT. 42° 42'	ADJUSTED SENECA POSITION LONG. 283° 10'	ADJUSTED SENECA POSITION HEIGHT	BASELINE DEVIATION FROM MEAN
70–08–22	1792	580	153	135	4.900"	17.278"	191.48 m.	+96 cm. (max.)
70–09–01	2002	817	105	106	4.845	17.334	189.16	–80 cm. (min.)
70–09–02	1883	1522	128	134	4.874	17.282	190.95	+14 cm.
70–09–07	1351	1399	147	145	4.848	17.253	189.81	–69 cm.
70–09–11	778	917	82	202	4.879	17.218	193.48	+38 cm.

MEAN BASELINE	408,701.92 m.	INDIVIDUAL BASELINE SIGMA	74 cm.
BASELINE SPREAD	176 cm.	MEAN BASELINE SIGMA	33 cm.

An inspection of the residuals on a 4-pass arc shows that they are far from random. Periodic trends are clearly evident in the residuals, of which a good example is shown in figure 3a. This pattern reflects the errors or deficiencies in the gravitational field model (in this case GEM 1) and changes with the field. Thus the residual pattern for the Standard Earth II field is quite different from that for GEM 1 although the pattern is still quasi-sinusoidal. The possibility that these patterns are a result of other errors, such as the position of the tracking station, has been explored but this has been rejected because another tracking station only a few hundred km away has the same pattern when the same gravitational field is used. It is not difficult to show that modifying the solar radiation pressure perturbation model has no effect on the residual patterns of the short four-pass orbits. It should be further mentioned that all four-pass orbits derived from data collected at the same station exhibit almost identical patterns.

It is interesting to note that if orbits are fitted to only two or three consecutive passes (instead

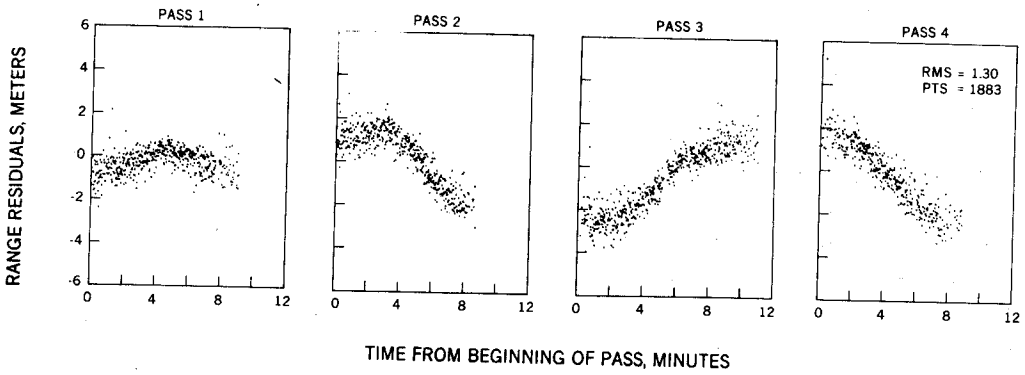

Figure 3a. Laser Range Residuals to Beacon Explorer C - Four Pass Orbit

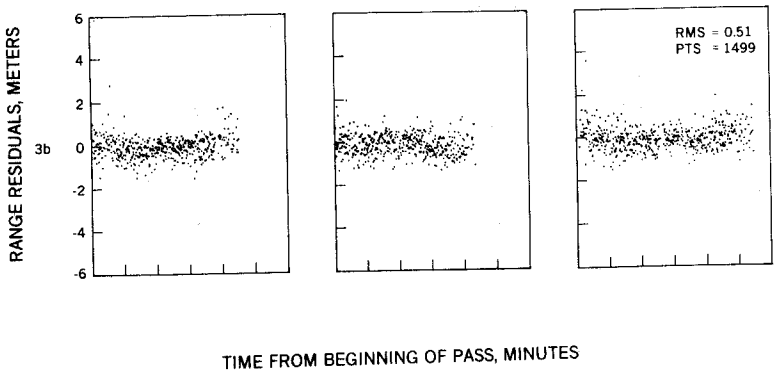

Figure 3b. Laser Range Residuals to Beacon Explorer C - A Three-Pass Orbit

of four), the rms fits of the observations about the orbits are significantly improved and the patterns less pronounced. Indeed, on two pass orbits, the patterns are no longer evident. Figures 3b and 3c show a three-pass and a two-pass orbit. The data in figures 3b and 3c are subsets of that shown in figure 3a.

The average range residual on a four pass orbit is usually a few cm but in our initial investigations we usually found this average to be a few decimetres and we postulated that it was caused by an error in the height of the station. Consequently, we made a determination of the station height from each four pass orbit in a simultaneous solution with the six orbit parameters. In all 36 cases, the average residual was less than 10 cm in in most cases only a few cm. The values of the height recovered from each four-pass orbital arc are shown in figure 4. They range over nearly 20 m about a weighted mean of 9.29 m with a rms deviation of 3.85 m. The mean height is only a few metres larger than the *a priori* value and was adopted as the "true" height of the station. The results shown in figure 4 were obtained with the GEM 1 gravity field and from earlier experiments employing different gravity models we know that the distribution of the points is almost completely dependent on the gravity field used in the analysis. For example, one might reasonably suspect some of the outlying points in figure 4 to be a result of poor data but this is not the case. The analysis of these data with other gravity fields has shown other points to be outliers and convinced the authors that figure 4 is unable to shed any light on the general quality of the data but rather on the

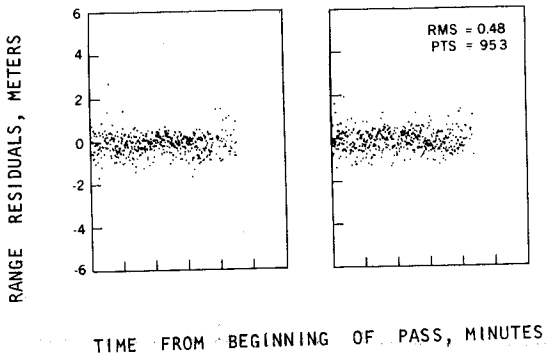

Figure 3c. Laser Range Residuals to Beacon Explorer C - A Two-Pass Orbit

quality of the gravity field.

In order to aid in the interpretation of figure 4, a kind of spectral analysis of the 36 heights has been performed by fitting a large number of sine curves through the data and by determining the least squares amplitude and phase for different frequencies. The results of this analysis are shown in figure 5 in which the square of the amplitude is plotted against frequency. A proper spectral analysis of the data could not be performed because of its sparcity and the irregular intervals between the measurements. If data had been obtained on all possible occasions, the interval between the measurements would (on average) have been about 23 hours 39 minutes (determined by the precession of the orbit with respect to the sun). Thus the highest frequency that was removed was one cycle/day; the lowest was 0.01 cycles/day.

Figure 5 is essentially noisy throughout the whole frequency range. One peak around 0.032 cycles/day (31.2 days) might be significant but those near 0.31 (3.2 days) are almost certainly noise. The 31 day period is difficult to explain. It is close to a month and therefore one is tempted to ask if it is indirectly caused by the moon. This is unlikely, however, because most lunar effects have periods determined primarily by the motion of the moon with respect to the orbit, which for BE-C are around 11 and 85 days.

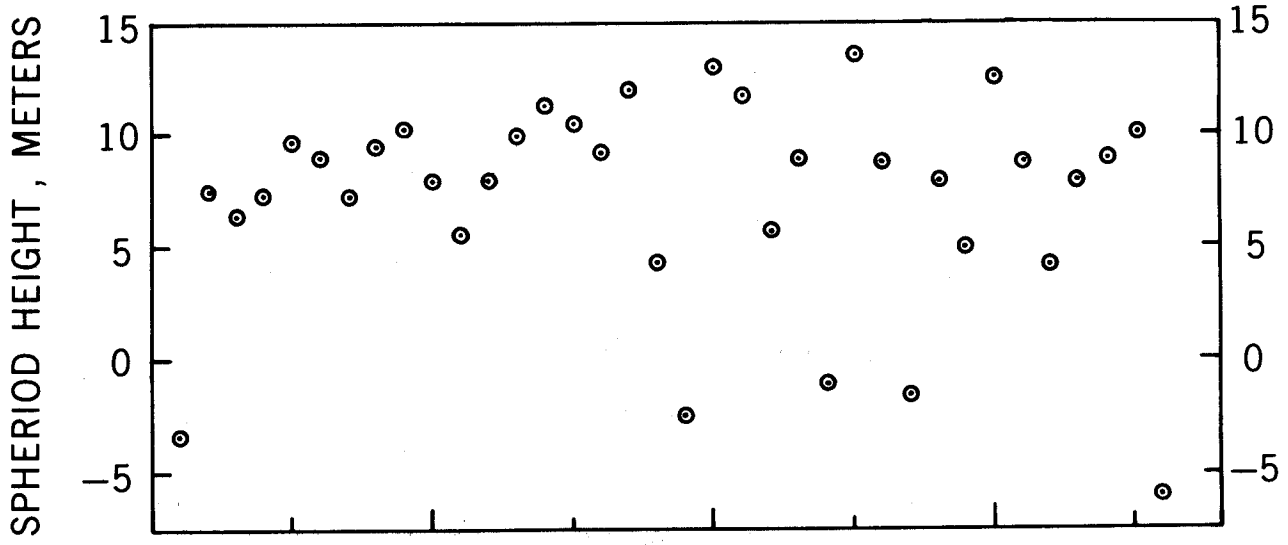

Figure 4. Height of Goddard Laser Obtained from Thirty-Six Four-Pass Orbital Arcs of Beacon Explorer C. The rms Deviation of a Single Height Measurement is 3.85 m

4. Solid Earth and Ocean Tides

One of the major aims of this analysis was the detection of the perturbations of the orbit by the solid-Earth and ocean tides. Since the latitude of the Goddard tracking station (GODLAS) was within a few degrees of the apex of the Beacon Explorer C orbit, most of the observations were obtained when the satellite had a predominant motion from west to east. Thus, during a four-pass observing period, the observations were clustered around the position of maximum latitude attained by the satellite and hence the orbital inclination was a well determined parameter. The variations in orbital inclination obtained from the 36 four-pass orbits have been analyzed using the "short-arc minus long-arc" technique in order to isolate the tidal perturbations.

The largest perturbations of the orbital inclination result from the non-sphericity of the Earth, which causes both short and long period effects. The largest short period term is caused by the Earth's oblateness, given by (MERSON 1961)

$$\delta i = -\frac{3}{2} J_2 \left(\frac{R}{p}\right)^2 \sin 2i \left[\left\{\frac{1}{2}\sin^2 u + \frac{1}{3} e \cos\omega\right\} + \left\{\frac{1}{3} e \sin^2 u \cos\nu - \frac{1}{3} e \cos u \cos\omega\right\}\right] +$$

$$\text{terms of order } J_2 \text{ squared} \qquad (2),$$

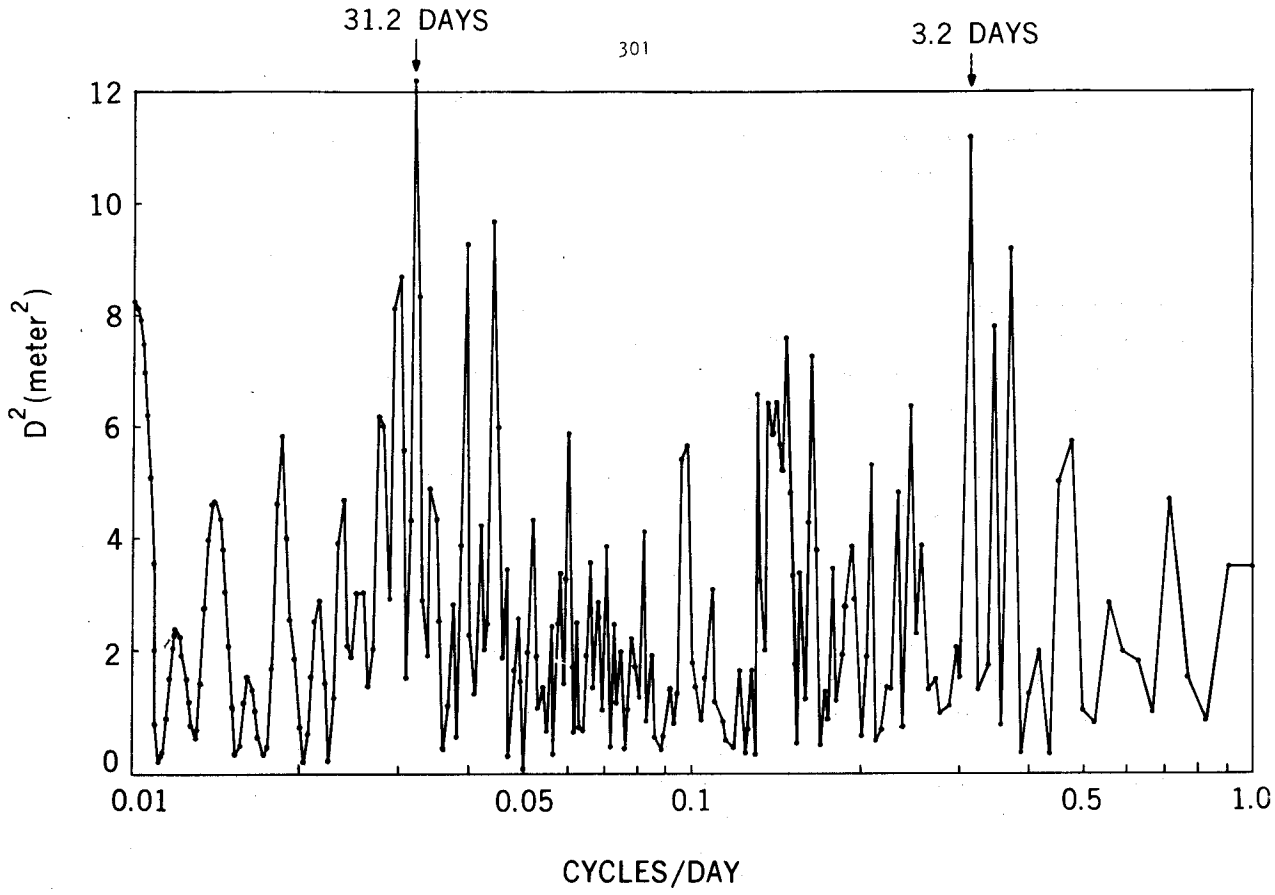

Figure 5. Frequency Analysis of the Height Determinations of the Goddard Laser

where δi is the perturbation in inclination, J_2 is the second degree zonal harmonic coefficient, R is the Earth's equatorial radius, p is the semi-latus rectum, i is the orbital inclination, u is the argument of latitude, e is the eccentricity and ω is the argument of perigee. Since $J_2 \sim 1.1 \times 10^{-3}$, the amplitude of δi is about 60 arcseconds, or about 2 km projected onto the Earth's surface. An important aspect of the perturbation given by equation 2 is that the major term ($\frac{1}{2} \sin^2 u$) is only a function of the projected motion of the satellite on the Earth's surface and consequently can be ignored if the orbital inclination is determined for the same argument of latitude (u). For example, suppose the orbit of the satellite is determined at the position of maximum northerly latitude ($u=\frac{1}{2}\pi$) then the terms inside the brackets in equation 2 reduce to

$$\frac{1}{2} + \frac{2}{3} e \sin \{\tfrac{1}{2}(\omega - \nu)\}$$

which has an amplitude of about 120 m for BE-C. Thus, the short period perturbations of the inclination by the gravity field can be kept to a minimum by determining the orbit at the maximum latitude position.

The J_2^2 terms and other geopotential coefficients cause short period perturbations (in the inclination) of about 10 m. Slightly longer period terms, the so-called M-daily terms of low order (M), can cause perturbations equivalent to a few tens of metres in the orbital inclination with periods of 24 hours,

12 hours, 8 hours, etc. The next largest period is that of the primary resonance which is about 5.5 days for Beacon Explorer C and associated with terms of order 13. The argument of the primary thirteenth-order resonance is

$$\omega + M + 13(\Omega - \theta),$$

where M is the mean anomaly, Ω is the right ascension of the node, and θ is the sidereal time. After approximately $5\frac{1}{2}$ days the ground track of the satellite repeats itself, that is, when the argument of the primary resonance has moved through 2π. The amplitude of this resonance (for BE-C) is about 0.35 arcseconds in the inclination (11 m).

There are also long-period perturbations in the inclination that are associated with the odd zonal harmonics in the gravity field. The principal terms take the form (MERSON 1961)

$$\delta i = (A J_3 + B J_5 + C J_7 + \ldots) \sin \omega \qquad (3),$$

where A, B, C .. are functions of the orbit parameters, and J_3, J_5, J_7, .. are the odd zonal harmonics. The perigee rotation period, and therefore the period of the perturbation, for BE-C is 70 days, and the amplitude of the perturbation is about 2 arcseconds and is equivalent to about 60 m projected onto the Earth's surface. Other long period perturbations are caused by the gravitational attraction of the sun and moon, and contain several periods ranging from 10 days to 85 days. In addition, there are very long period terms with periods up to about 19 years, but all these luni-solar perturbations can be computed with adequate accuracy from a knowledge of the positions of the sun and moon.

The major unknown perturbations of long period are those associated with the solid-Earth and ocean tides and are effectively indirect luni-solar perturbations. The sun and moon raise ocean and body tides that involve sufficient mass that they perturb the motion of the satellite. These tidal disturbances of the gravity field can be largely represented by a second degree spherical harmonic with axial symmetry in the approximate direction of the tide rising body. With this representation, the major terms in the tidal perturbation of inclination can be written (KOZAI 1965; FISHER & FELSENTREGER 1966; MUSEN & FELSENTREGER 1973)

$$\delta i = \frac{3}{4} m_D \frac{n_D^2}{n} \left(\frac{R}{a} \right)^5 \frac{k_2}{(1-e^2)^2} \cos^2(\tfrac{1}{2} i_D) \left\{ \frac{\sin i \cos^2(\frac{1}{2} i_D)}{2(\dot{L} - \dot{\Omega})} \cos 2(L-\Omega) - \frac{2 \cos i \tan(\frac{1}{2} i_D) \cos i_D}{(\dot{\Omega} - \dot{\Omega}_D)} \cos(\Omega - \Omega_D) - \right.$$

$$\left. \frac{\cos i \sin i_D}{(2\dot{L} - \dot{\Omega})} \cos(2L - \Omega) \right\} \qquad (4),$$

where m_D is the ratio of the mass of the tide raising body to the mass of the Earth, n_D is the mean motion of the disturbing body, n the mean motion of the satellite and a the semi-major axis. k_2 is Love's number of second degree, i_D is the orbit of the disturbing body to the Earth's equator, L is the longitude of the disturbing body and Ω and Ω_D are the right ascensions of the ascending nodes of the orbits of the satellite and disturbing body. The dot quantities refer to time derivatives. The Love number is defined as the ratio of the tidal potential to the tide raising potential.

The amplitudes of these perturbations (of BE-C) amount to a few tenths of an arcsecond for each of the terms in equation 4 for both the sun and moon. Their periods are about 10, 12 and 85 days for the moon and 35 days, 58 days and 85 days for the sun. For Beacon Explorer C the expected total perturbations has a peak-to-peak variation of about 2.1 arcseconds, or about 70 m projected onto the Earth's surface.

The initial step in isolating the tidal perturbations was to determine the maximum latitude reached by the satellite on each pass of the 36 four-pass orbits. This was accomplished with the aid of an ephemeris which was generated for each orbital arc from a least squares fit to the data. The second step was to derive the maximum latitude on each pass from the long-arc orbit described in section 3. Finally, the long-arc maximum latitudes were subtracted from the short-arc maximum latitudes and the "max-lat" residuals showed very clearly the effects of the tide on the orbit. From these residuals we made an estimation of the Love number k_2 (amplitude) and the phase of the tides. Initially this estimate was only made from the first five months of data (SMITH ET AL 1973) and subsequently extended through the following year (KOLENKIEWICZ ET AL 1973). The observed max-lat residuals are shown in figure 6, together with the best fit theoretical curve for $k_2 = 0.245$ and ϕ (phase) $= 3.2°$. The precision with which the data fit the curve indicates a standard deviation of 0.005 for k_2 and $0.5°$ for ϕ.

The actual procedure for deriving the values of k_2 and ϕ extended over several months (DUNN ET AL 1973). In the initial analysis of the tides, the differences between the laser data and the theory shown in figure 6, contained an oscillation of amplitude about 2 m and period 5.5 days. This pattern is characteristic of an error in the resonance terms (order 13 for BE-C) in the gravity field and consequently an adjustment was made to two coefficients. An approximately 19% decrease in $C_{19}{}^{13}$ and approximately 18% increase in $S_{19}{}^{13}$, with respect to the GEM 1 values, removed the sinusoidal residual pattern (KOLENKIEWICZ ET AL 1973). At this stage the analysis was restarted from the beginning with this new gravity field which we referred to as GEM 1*. Having re-analyzed the orbits and redetermined the station heights (with GEM 1*) we found almost no change from out original analysis with GEM 1 with the exception of removing the patterns in the residuals in inclination (maximum latitude) in the tide analysis. It is with the GEM 1* field that the laser points in figure 6 have been computed and from which the Love number and phase already given were derived.

Because the determination of k_2 and ϕ was obtained from a separate analysis of the residuals in inclination rather than from a large least squares adjustment from the raw laser data, it was neccesary to undertake a second re-analysis of all the observational data with the tides modeled (using the recovered values of k_2 and ϕ) in order to check that the tidal solution had converged. Only insignificantly small changes in the recovered heights for the Goddard laser were obtained and there was no change from the original best fit values for k_2 and ϕ.

The most important single result evident from figure 6 is that the amplitude of the perturbation is significantly smaller than expected. From seismic data we know that k_2 should be around 0.30 and therefore that there must be some additional perturbations of the BE-C orbit that are tending to compensate for the solid-Earth tides. Since the agreement between the theoretical curve and the data is so good in figure 6, it must be concluded that the functional form of the perturbation must be very similar to that of the solid-Earth tide, that is, a second degree spherical harmonic. Thus, it has been suggested that the additional perturbation is caused from the global ocean tides (LAMBECK

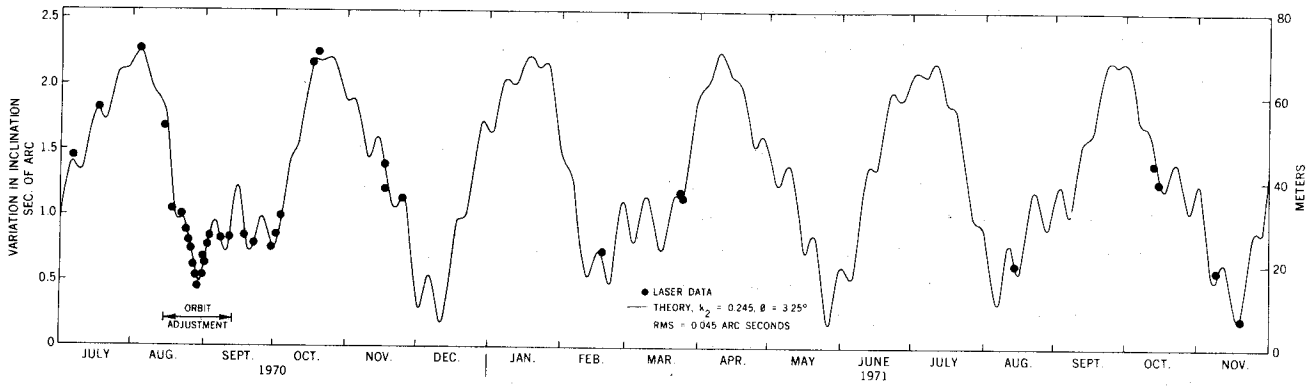

Figure 6. Tidal Perturbations of the Orbital Inclination of Beacon Explorer C

& CAZENAVE 1973). The ocean tides, however, contain many components which can be represented in spherical harmonic form but it is only those of second order, and principally second and fourth degree, that actually perturb the spacecraft to any significant extent (MUSEN 1973). We may therefore argue that this tidal analysis has identified a perturbation equivalent

$$(k_2)_{ocean} = 0.30 - 0.245 = 0.055$$

from the ocean tides.

The solution for the phase of the tidal perturbations (ϕ=3.2°) is more difficult to interpret. The phase of the solid-Earth tide is believed to be small, of the order of a degree or less, and the difference with the result here suggests a larger phase lag for the ocean tides. This is not inconsistent with observations of the tides except that each tidal component is believed to have a different phase and thus a single observation of the phase lag of the tidal gravitational field (of even degree and order two) must be a composite value and hence difficult to interpret. We must await further observations of the ocean tidal perturbations of other satellites before the contributions and phase lags from each tidal component can be identified.

5. Variation of Latitude

In the analysis previously described it was necessary to include polar motion which has the effect of

changing the latitude, and to a small extent longitude, of the laser tracking station. The magnitude of the variation in latitude (MUNK & MACDONALD 1960) amounts to about 0.3 arcseconds in a year (10 m on the Earth's surface) and is monitored routinely by the Bureau International de l'Heure (BIH). In our computations the 5-day smoothed mean position of the pole published by the BIH has been used. The accuracy of the BIH data is probably about 0.02 arcseconds but because these values are averaged over 5 days it is possible for real departures of several hundredths of an arcsecond to exist with respect to a continuous smooth curve.

During the 17 months of laser data, the latitude of the Goddard station varied by approximately 15 m due to the combined effects of the annual and Chandlerian motions of the pole. In order to determine our sensitivity to these motions we suppressed the modeling of polar motion in the 36 short orbital arcs so that the variation of latitude of the tracking station would be forced into the orbital inclination and hence into the values of maximum latitude. Subtracting the long arc maximum latitudes from the short-arc maximum latitudes revealed, as expected, the variations in latitudes of the tracking site (SMITH ET AL 1972b;KOLENKIEWICZ ET AL 1973) shown in figure 7. In analyzing this variation it was essential to include the tidal effects and use the improved resonant gravity terms described in the previous section. The BIH smoothed variation of latitude is also shown in figure 7 and the rms fit of the laser data about the BIH curve is 1.38 m (0.045 arcseconds). At the present time it is probably correct to assume that the differences between the laser and BIH results of figure 7 are primarily due to errors in the laser values rather than in the BIH and that the scatter reflects errors in the gravitational field model used in the orbit computations. As our knowledge of the gravity field improves over the next few years, the scatter in the latitude variation (from the laser data) of figure 7 should decrease correspondingly.

In order to better understand the causes of the scatter of residuals in figure 7, an attempt was made to determine any major periodicities within the residuals to the BIH curve. The same method as used in analyzing the station heights of section 3 (figure 5) was employed. A set of sinusoidal oscillations was fitted through the residuals with frequencies between 1 cycle/day and 0.01 cycles/day. The square of the amplitudes (D) of the recovered oscillations are shown against frequency in figure 8. As might be expected, the variation of D^2 with frequency is largely noise but there may be one or two peaks that are significant. There is a peak near 0.165 cycles/day (6.0 day period) which is one of the resonant periods for the odd degree thirteenth order geopotential terms, and another unidentified peak at about 0.035 cycles/day (28.2 day period). A comparison of figures 5 and 8 is important in their interpretation since the laser data are the source of both the height and latitude measurements. The only difference in technique used to generate these figures is that figure 8 is an analysis of residuals obtained from differencing short and long orbit arcs, while figure 5 is based purely on short arc analysis. Hence errors in the short-arc orbit computation will appear in both figures while errors in the long arc only affect figure 8. There is probably only one significant peak in the height analysis of figure 5, at about 0.032 cycles/day (31.2 day period). This frequency is reasonably close to the peak at 0.035 cycles/day seen in figure 8, but a frequency this low in the orbit perturbations is difficult to explain. Further, the amplitudes of these oscillations (if they exist) are so large, 3.5 m in height and 0.034 arcseconds (1 m) in latitude, that their origin cannot be geophysical. However, it is possible that the orbit is resonant with terms of very high degree and order, say 27, and this possibility is being investigated.

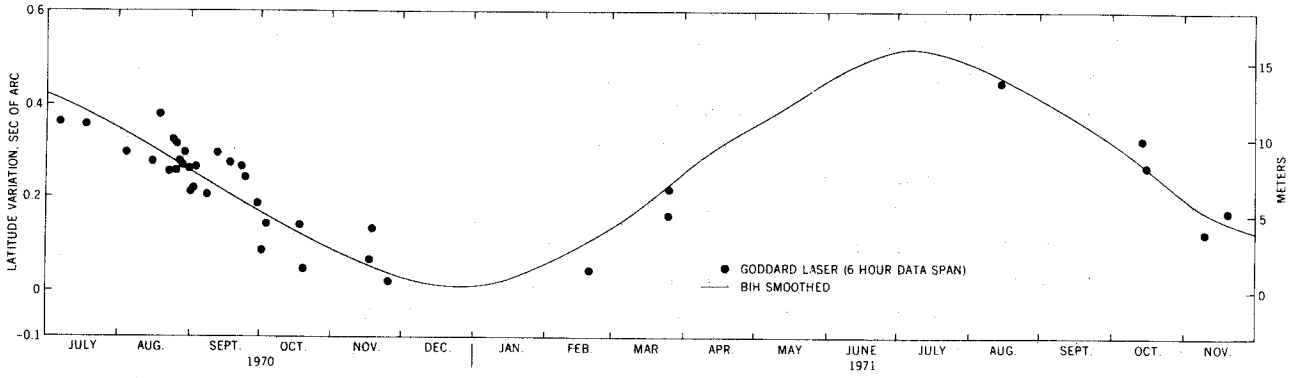

Figure 7. Variation of Latitude of the Goddard Laser

6. Two Station Experiments

The results described in the previous sections were obtained with a single laser tracking system and the fundamental objective of that work was to try and develop techniques that will permit a laser tracking system to monitor its own latitude and height variation at a geophysically useful level. In this section we describe some of our experiments using two laser systems in which the fundamental objective is the measurement of phenomena, such as tectonic and fault motion by the precise determination of the position of one of the tracking systems with respect to the other.

During August and September 1970 a second GSFC laser tracking system was operating from a site near Seneca Lake, New York (SMITH ET AL 1972a). This station was 408 km due north of the laser system at the GSFC Optical Site with which the polar motion and tidal data were obtained. The original purpose of establishing the Seneca station was to determine polar motion in a joint experiment with the Goddard laser. However, it was subsequently found that the second station was not essential for polar motion studies but that with two stations tracking the same satellite on the same passes, it was possible to determine the distance between the lasers very precisely.

There were 5 occasions when the Seneca station observed four consecutive passes of BE-C simultaneously with the Goddard station. From these data, during August and September 1970, the position of the

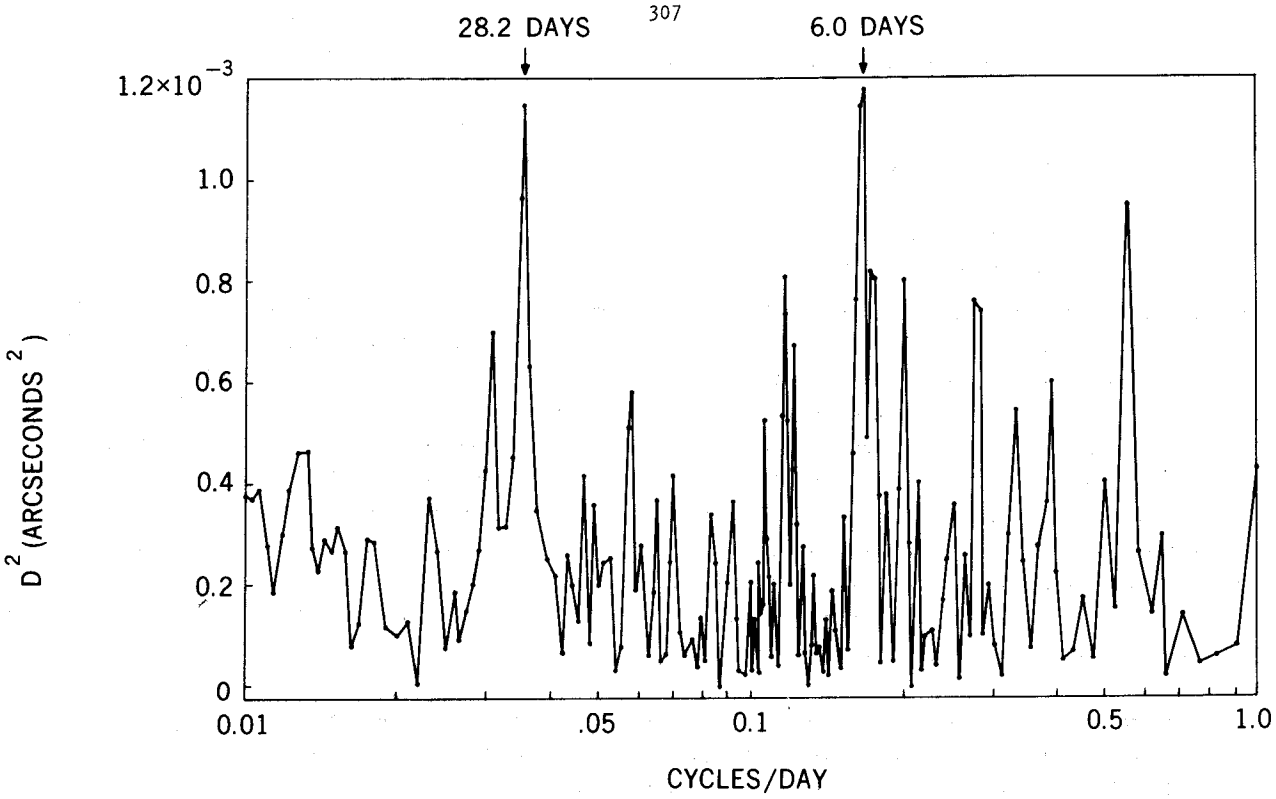

Figure 8. Frequency Analysis of the Variation in Latitude of the Goddard Laser

Seneca station has been determined. In these calculations the position of the Goddard station has been assumed known with the following co-ordinates:

Goddard: Latitude 39° 01' 13.88" N; Longitude 283° 10' 18.50" E; Height 9.29 m.

The values of the latitude and longitude were adopted from early work at GSFC on tracking station positions and are not crucial in the analysis. The height value is a dynamic average of the values in figure 4, derived by simultaneously adjusting the orbital parameters on each of the 36 orbital arcs together with the station height (a single least squares value for all 36 arcs). The numerical value of the height is dependent on the latitude adopted for the station (as above), the product of the gravitational constant (G) and the mass of the Earth (M), the gravitational field (GEM 1*, see section 4) and the mean equatorial radius (R_E) of the Earth. Throughout these analyses we have used the following values:

$$GM = 3.986\,013 \times 10^{20}\ cm^3/sec^2 \quad ; \quad R_E = 6\,378\,155\ m.$$

The results of our determination of the Seneca position are shown in table 1.† The position of Seneca has been determined from each four-pass orbital arc and table 1 shows the range of values of latitude is 0.055 arcseconds (1.7 m), of longitude is 0.116 arcseconds (2.7 m at the latitude of Seneca) and 4.32 m in height. Because Seneca is due north of Goddard, the baseline values have the same range as the latitude values. The baseline length according to survey is 408,698.77 m which is about 3 m less than the value obtained from the co-ordinates given in table 1; the accuracy of the survey is about ± 2 m.

†p.297

The major sources of error in the satellite solution for the Goddard-Seneca baseline are estimated to be:

gravity	2.5 m;
GM (1 part in 10^6)	0.2 m;
range biases (1 m)	0.3 m;
refraction (5%)	0.1 m; and
Goddard height (10 m)	1.6 m,

where the gravity error model (MARTIN & ROY 1972) is taken as one quarter the difference between the Smithsonian Astrophysical Observatory's Standard Earth I field (LUNDQUIST & VEIS 1966) and the Applied Physics Laboratory's 3.5 Model (GUIER & NEWTON 1965). There is of course considerable uncertainty in the above estimates for the accuracy of the parameters used in the analysis but a total accuracy of 2 to 3 m appears reasonable. Gravity errors dominate the solution but because of the technique that has been employed, all the orbital arcs (4 passes) have very similar geometric distribution with respect to the tracking stations. Hence, the errors on one 4-pass orbit are very similar to the errors on any other 4-pass orbit so that the repeatability of the baseline measurement can be expected to be considerably better than the accuracy. This situation is supported by table 1 in which the standard deviation of an individual baseline measurement is probably better than 1 m even though our best estimate of the accuracy is, perhaps, 3 m.

The internal accuracies (noise standard deviation) of the Goddard-Seneca experiment are of particular interest because they represent the ultimate capability of the technique if our knowledge of everything affecting the motion of the spacecraft were known perfectly. Based on laser range measurements of 1 m noise (no biases), the standard deviation of latitude would be about 15 cm, longitude about 8 cm, and height 9 cm. Thus, the technique has the capability of reaching the 1 cm level in all co-ordinates with laser systems of the 5-10 cm noise level, which are projected to be available in 1974.

With the introduction of radar altimeters, satellite-to-satellite tracking techniques and more accurate laser data in greater quantities, significant improvements in the gravity field, GM and station co-ordinates can be projected such that 10 cm precision relative positioning should be a realizable objective from a single four-pass orbital arc. In 1972, a plan was formulated for applying this technique to the measurement of motion along the San Andreas fault in California, which is the boundary between the tectonic plates of the Pacific and North America. In its simplest concept, one laser tracking station would be established on the western side of the fault, that is, on the Pacific plate, near San Diego and a second station on the eastern side of the fault, the North American plate, near Quincy in northern California (see figure 9). The distance between the two stations is nearly 900 km and the angle between the baseline and the fault is about 15° so that the change in baseline length over several years will be very similar to the gross fault motion across the plate boundary. Present estimates of the fault motion are between 3 and 5 cm/yr.

A simulation of this experiment (AGREEN & SMITH 1973), the San Andreas Fault Experiment (SAFE), has been completed and is summarized in table 2. The experiment has been simulated to last for 8 years, using the BE-C satellite and stations at San Diego and Quincy. Table 2 shows the effects of various errors on the baseline between the two stations when each year of measurements is composed of 16 simultaneous short-arcs of three consecutive passes. (Three passes were used because the

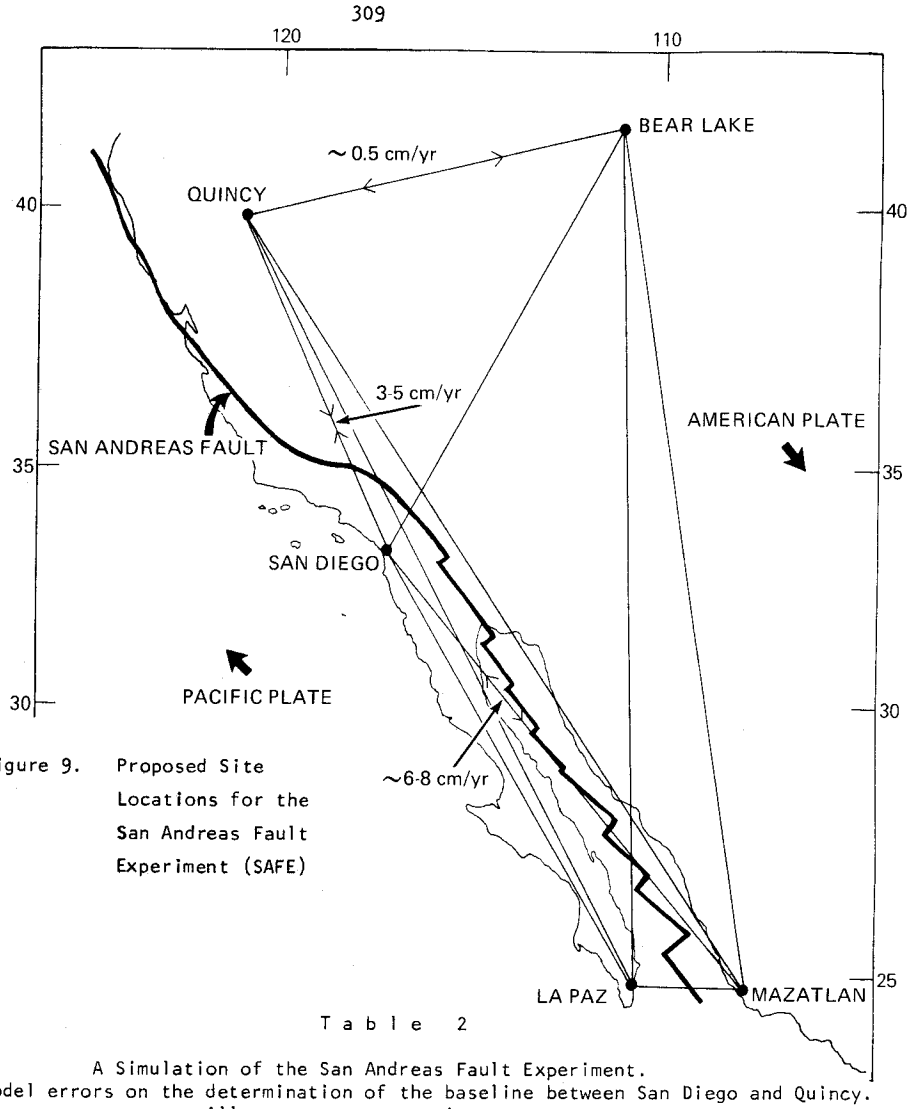

Figure 9. Proposed Site Locations for the San Andreas Fault Experiment (SAFE)

Table 2

A Simulation of the San Andreas Fault Experiment.
Effects of model errors on the determination of the baseline between San Diego and Quincy.
All measurements are in cm.

Year	GM	Gravity Model	Quincy Bias	San Diego Bias	Solar Radiation	Atmospheric Drag	C 19,13	S 19,13	San Diego Longitude	San Diego Latitude	San Diego Height
1970	102	-62	-2	7	-1	-1	1	1	0	-14	-110
1971	95	-68	-2	8	-2	-1	0	0	0	0	-99
1972	109	-53	-3	7	0	-1	1	0	0	-2	-113
1973	102	-66	-2	7	0	-1	0	0	0	-9	-107
1974	102	-57	-2	7	0	-1	1	0	0	-8	-108
1975	98	-61	-2	7	1	-1	0	0	0	-4	-103
1976	102	-75	-3	7	1	-1	1	0	0	-9	-107
1977	99	-64	-3	7	0	-1	0	0	0	-5	-104
Average	101	-63	-2.4	7.1	-0.1	-0.5	0.5	0	0	-6.4	-106
RMS	3.8	6.3	0.3	0.3	0.9	0	0.5	0	0	4.2	4.1

simulation suggested that three passes gave a greater precision than four passes). The error sources in the simulation were 1 part in 10^6 for GM, ½(SAO Standard Earth 1 - APL 3.5) for gravity, 10 cm range biases, 10% error in solar radiation and air drag models, ½ nominal values of the 19th degree, 13th order resonant terms in the geopotential, and 5 m in each co-ordinate at San Diego.

From table 2 we obtain the root-sum-squares as ±9.5 cm for the baseline precision based on the *a priori* magnitudes of the error sources already given. These *a priori* estimates are believed to reflect our knowledge in 1972-73 and can be expected to improve considerably during the present decade. If we postulate that there will be the following improvements in our knowledge by 1980 (over 1972-73 values)

GM	by a factor	20	(to 5 parts in 10^8);
Gravity	by a factor	7;	
San Diego Position	by a factor	20	(to 25 cm); and
Laser Systems	by a factor	5	(to 2 cm),

the precision of the baseline measurement will be 1 to 2 cm with an accuracy of about 10 to 15 cm. This will permit the determination of the change in baseline (plate motion) to better than 0.5 cm/yr over a 7 year period.

The full plans for SAFE include the establishment of a third laser site near Bear Lake, Utah and proposals for two sites in Mexico, on either side of the Gulf of California. These additional sites will enable the gross plate motion and crustal deformation to be measured along a 2000 km stretch of the western United States and Mexico. Motions along the fault in the Gulf of California are estimated to be much larger than those in southern California, with estimates generally in the 6 to 8 cm/year range. The site in Utah will enable the spreading rate across northern California and Nevada to be estimated, although this motion is probably only of the order of 0.5 cm/year and consequently very difficult to measure.

The SAFE experiment is planned to begin in the Spring of 1974 but a preliminary tracking experiment was conducted in September 1972 between the San Diego and Quincy sites (SMITH & VONBUN 1973). In this test experiment, both sites successfully tracked four consecutive passes of BE-C on four simultaneous occasions from which estimates of the position of Quincy with respect to San Diego have been obtained. During this period the laser systems were performing at about the 60 to 80 cm noise level, implying biases of this order could be in the data. Essentially the same techniques were used in this analysis as had been used in the Goddard-Seneca experiment. From all the four-pass orbital arcs obtained at San Diego, the height of the station was derived. The latitude, longitude and recovered height of the station used in the subsequent analysis were

San Diego: Latitude 32° 36' 02.53" N; Longitude 243° 09' 32.87" E; Height 989.5 m.

Based on the above co-ordinates, the results shown in table 3 were obtained with the GEM 1* gravity field. Unfortunately, there are only four determinations and any statistics concerning the solutions must, therefore, be treated with caution. However, the four solutions do agree at least as well as might be expected from our knowledge of the data and the models. Further, there is a very obvious correlation among the recovered latitudes and longitudes in table 3. In addition, this linear variation is approximately perpendicular to the direction of the San Diego-Quincy baseline, showing that there is a tendency for the Quincy solutions to lie on an arc centered on the primary station

Table 3

Results of the Determination of the Position of the Quincy Laser and the Baseline Between San Diego and Quincy

TIME OF FIRST PASS Y – M – D	RANGE MEAS. QUINCY	SANDIE	R.M.S. FIT TO ORBIT QUINCY (cm.)	SANDIE (cm.)	ADJUSTED QUINCY POSITION LAT.	LONG.	HEIGHT	BASELINE DEVIATION FROM MEAN
					39° 58'	239° 03'		
72–09–17	623	1047	299	357	24.447"	37.787"	1062.76 m.	+35 cm. (max.)
72–09–18	327	920	205	250	24.411	37.732	1061.42	–19 cm.
72–09–30	649	926	190	153	24.402	37.686	1062.24	+15 cm.
72–10–03	439	578	127	98	24.373	37.659	1064.24	–30 cm. (min.)

MEAN BASELINE	896,275.17 m.	INDIVIDUAL BASELINE SIGMA	30 cm.
BASELINE SPREAD	65 cm.	MEAN BASELINE SIGMA	15 cm.

(San Diego) thereby giving a better determination of the baseline length than of the individual co-ordinates of the second station (Quincy).

7. Future Satellites and Investigations

In the course of the investigations described in the previous sections it became increasingly obvious that the full potential of the techniques could not be achieved without significant improvements in many geophysical parameters, including GM and the gravity field. The major problem area has probably been the gravity field so far, partly because our experience has been with relatively low altitude spacecraft like BE-C . However, this may change if the planned high altitude satellites such as TIMATION III and LAGEOS are launched. TIMATION, expected to be at an altitude of about 14,000 km, will be much less affected by a lack of knowledge of the higher harmonic coefficients of the gravity field and therefore, in principle, a much better spacecraft to use for satellite geodynamic research.

In order to assess the impact of TIMATION III on an experiment, such as SAFE, a series of simulations of the determination of the San Diego-Quincy baseline have been completed. In summary, the major error sources are now only GM and the position of San Diego. Further, results of the same accuracy and precision can be obtained from a few days of TIMATION tracking compared to about 2 months of BE-C tracking and because the gravity perturbations are very small, high altitude spacecraft offer the possibility of determining GM. Simulations of a small world-wide network of laser stations indicate that an improvement in GM by about two orders of magnitude (to 1 part in 10^8) should be realizable in the next five years (CARPENTER ET AL 1972). Thus, the TIMATION and LAGEOS type spacecraft are expected to have a major impact on this type of investigation.

Projecting the type of techniques used on Beacon Explorer C into the future with more advanced spacecraft and better orbits, and further realizing that there will be substantial improvements in our knowledge of the gravity field through the application of newer tracking techniques, such as satellite-to-satellite tracking and altimetry, we anticipate that geophysically useful measurements of fault motion, tectonic plate motions and polar motions will be obtained within the next five years.

The accuracies which will be achievable from about one week of data will probably be of the order of 5 to 10 cm in distance measuring for distances up to about 10,000 km, and about 5 to 10 cm in the variation of latitude and 10 to 20 cm in the variation in height of a station from 6 to 12 hours of tracking. In addition, it should also be possible to determine the variations in the length of day (LOD) to a few tenths of a millisecond on a daily basis, although other techniques, such as very long baseline interferometry, may be better suited to this measurement. In the laser technique for LOD studies, the essential requirement is a suitable satellite in a highly inclined orbit to the equator so that a station, or stations, can measure the time and longitude of the satellite crossing a given latitude. Daily measurements of this type permit the rotation of the Earth with respect to the plane of the orbit of the satellite to be derived.

8. References

AGREEN, R.W. & SMITH, D.E. 1973. A Simulation of the San Andreas Fault Experiment. *Rep. X*-592-73-216,Goddard Space Flight Center,Greenbelt Md.

CARPENTER, L. (ed.) 1972. Preliminary Study of the Application of the TIMATION III Satellite to Earth Physics. *Rep. X*-553-72-50,Goddard Space Flight Center,Greenbelt Md.

DUNN, P.J., SMITH, D.E. & KOLENKIEWICZ, R. 1973. Techniques for the Analyses of Geodynamic Effects Using Laser Data. *First International Symposium, Use of Artificial Satellites for Geodesy & Geodynamics*,Athens.

FISHER, D. & FELSENTREGER, T. 1966. Effects of the Solar and Lunar Tides on the Motion of an Artificial Earth Satellite. *Rep. X*-547-66-560,Goddard Space Flight Center,Greenbelt Md.

GAPOSCHKIN, E.M. & LAMBECK, K. 1970. 1969 Smithsonian Standard Earth II. *Spec.Rep.* 315, Smithsonian Astrophysical Observatory,Cambridge Mass.

GUIER, W.H. & NEWTON, R.R. 1965. The Earth's Gravitational Field Deduced from the Doppler Tracking of Five Satellites. *J.geophys.Res.* 70(18),4613-4626.

JOHNSON, T.S., PLOTKIN, H.H. & SPADIN, P.L. 1967. A Laser Satellite Ranging System, 1, Experiment Description. *IEEE J.Quantum Electron.* QE-3(11),435-439.

KOLENKIEWICZ, R., SMITH, D.E. & DUNN, P.J. 1973. Polar Motion and Earth Tides from Beacon Explorer C. *First International Symposium,Artificial Satellites for Geodesy & Geodynamics*,Athens.

KOZAI, Y. 1965. Effects of the Tidal Deformation of the Earth on the Motion of Close Earth Satellites. *Publ.astron.Soc.Japan* 17,395-402.

LAMBECK, K. & CAZENAVE, A. 1973. Fluid Tidal Effects on Satellite Orbits and Other Temporal Variations in the Geopotential. *Bull.* 7,Groupe Recherches de Geodesie Spatiale,Paris.

LUNDQUIST, C.A. & VEIS, G. (Ed.) 1966. Geodetic Parameters for a 1966 Smithsonian Institution Standard Earth, Vol. 1. *Spec.Rep.* 200,Smithsonian Astrophysical Observatory, Cambridge Mass.

MARTIN, C.F. & ROY, N.A. 1972. An Error Model for the SAO 1969 Standard Earth. In HENRIKSEN, S.W., MANCINI, A & CHOVITZ, B.H. (ed.). "The Use of Artificial Satellites for Geodesy". *Geophys.Monograph* 15,American Geophysical Union,Washington DC,161-167.

MERSON, R.H. 1961. The Motion of a Satellite in an Axi-Symmetric Gravitational Field. *Geophys.J. R.astr.Soc.* 4,17-52.

MUNK, W.H. & MACDONALD, G.J.F. 1960. *The Rotation of the Earth.* Cambridge University Press,London.

MUSEN, P. 1973. A Semi-Analytical Method of Computation of Oceanic Tidal Perturbations in the Motion of Artificial Satellites. *Rep. X*-590-73-190,Goddard Space Flight Center,Greenbelt Md.

MUSEN, P. & FELSENTREGER, T. 1973. On the Determination of the Long Period Tidal Perturbations in the Elements of Artificial Earth Satellites. *Celestial Mechanics* 7,256-279.

SMITH, D.E., KOLENKIEWICZ, R. & DUNN, P.J. 1972a. Geodetic Studies by Laser Ranging to Satellites. In HENRIKSEN, S.W., MANCINI, A. & CHOVITZ, B.H. (ed.). "The Use of Artificial Satellites for Geodesy". *Geophys.Monograph* 15,American Geophysical Union,Washington DC,187-196.

SMITH, D.E., KOLENKIEWICZ, R., DUNN, P.J., PLOTKIN, H.H. & JOHNSON, T.S. 1972b. Polar Motion from Laser Tracking of Artificial Satellites. *Science* 178,405-6.

SMITH, D.E., KOLENKIEWICZ, R. & DUNN, P.J. 1973. A Determination of the Earth Tidal Amplitude and Phase from the Orbital Perturbations of the Beacon Explorer C Spacecraft. *Nature* 244, 498.

SMITH, D.E. & VONBUN, F.O. 1973. The San Andreas Fault Experiment. *24th Congress,International Astronautical Federation*,Baku.

9. Discussion *

GUBBAY: You have listed the longitude of the adjusted stations to a thousandth of an arcsecond. I wonder how well you know systematic errors and how well you can hold down the measurement errors to astronomical position?

DUNN: The expression of the results to 0.001 arcseconds may be optimistic. Your question regarding this is interesting. We claim that the absolute time co-ordinate is irrelevant to baseline consistency monitoring and we are happy to have incestuous time reference systems common to both lasers, in order to monitor baselines on a regular basis. There are other ways of getting absolute values of errors in the rotation rate of the Earth. I haven't addressed these problems in this particular presentation because our attempts to do so would have been frustrated by lack of data. The paper itself addresses the problem of monitoring the Earth's rotation rate.

WALCOTT: What is the future of satellite laser ranging in view of the sensitivity to weather, the very high cost of installation as compared with electronic distancing?

DUNN: Among the electronic systems, the most competetive is VLBI. One advantage of the laser system is that the results are obtained very quickly. To obtain a range from a laser return is a relatively simple technique, and we can obtain a 6 hour orbit just a few minutes after the last results have come in, which makes the technique very useful for quasi-real time observations for polar motion and earthquake prediction. So one practical advantage of laser ranging is very quick measurement capability compared with the more complex technique of VLBI which requires complicated software for searching for fringes and producing the time delay and fringe rate measurements.

WALCOTT: It seems to me to be very unreliable. How many days was the Seneca-Goddard experiment washed out by the weather?

DUNN: Too many. The returns in the California experiment are much better. During the SAFE experiment, we plan to return to the same location every year to monitor the change in the baseline length. We will try to get started earlier in the fall to use the better weather.

MUELLER: Referring to the slide on the Earth tide effect; does the solid line represent the values for some model and the dots the observations?

DUNN: Yes; the solid curve represents the simple second degree model of the disturbing potential of the sun and the moon through its effect on the inclination of BE-C as an Earth tide. The values fitted were the amplitude of the curve and indirectly, the phase of the curve, as we concentrated the effect into two parameters.

MUELLER: The distribution of the dots is poor.

DUNN: Yes; although there are two peaks and three well defined valleys, and though areas are sparse, in the critical areas of the peaks and the valleys, good agreement was obtained.

RAPP: Did you run the baseline experiment with different gravity models and if so what was the difference of baseline lengths with different models?

DUNN: I do not have exact figures; but up to week before last, there was no model that gave better results than GEM 1. We find that different GEM models give different fits up to ±3 m.

RAPP: I don't understand your statement that you are not concerned about length.

DUNN: Absolute length is tied to GM; we are concerned with relative length measurements.

RAPP: I'd like to know how the gravity model affects the length.

DUNN: We'd like to know ourselves. The gravity model adopted influences the consistency of the results in the precision to which one can monitor changes in baselines. We usually obtain worse consistency in the baselines with gravity models generated outside Goddard (Space Flight Center).

STOLZ: Why do you calculate only changes in latitude? Can you be sure that you have removed the effects of the other parameters?

DUNN: We claim to have solved for the tidal parameters and geopotential resonance terms which can affect our latitude measurements.

STOLZ: You assume the values obtained are error free?

DUNN: We assume the form of the tidal model is error free. The value of the Love number k_2 is an adjusted parameter and is quite controversial. We have claimed for k a precision which is related to the value of the sigma in amplitude of the Earth tide perturbation to inclination. As the noise level of our data about the BIH polar motion curve is 138 cm over 18 months, it does suggest that our modeling is adequate.

---

* Paper presented by P.J. DUNN

ONG, K. M.
Tracking and Orbit Determination Section
Jet Propulsion Laboratory
California Institute of Technology
Pasadena, California
UNITED STATES OF AMERICA

Proc.Symposium on Earth's Gravitational Field & Secular Variations in Position (1973),315-327.

3-D MULTILATERATION FOR MEASUREMENT OF EARTH CRUSTAL DEFORMATION AND NETWORK DENSIFICATION*

ABSTRACT

This paper presents a discussion of how range and range-difference data types can enable precise three dimensional measurement of ground station positions and the position of an artificial signal source, without explicit dependence upon the signal source trajectory.

Previous analysis of range only multilateration has shown a capability of determining relative station locations with 1 cm accuracy given ranging accuracy of a few centimeters. Such ranging accuracy could be obtained by either laser or possibly by radio methods. Because all-weather operation is so desirable, a radio implementation is the preferred mode.

Another possible radio approach is range-difference multilateration. Very Long Baseline Interferometry (VLBI) has demonstrated few cm range-difference measurements using cross correlation techniques. The analysis of VLBI multilateration is not yet as well developed as the range only multilateration; however, preliminary results indicate comparable few cm performance potential.

Although a multilateration system is capable of stand-alone operation, the need for intercontinental geodetic measurements would require a high flying earth orbiting satellite with its associated disadvantage of substantial costs, particularly when data are needed over many years.

A more effective strategy is to combine the multilateration approach with a VLBI system using natural radio sources. The VLBI methods would provide a coarse grid of three dimensional benchmark locations on a regional and global scale. Multilateration stations would then occupy these coarse grid locations and provide a means for highly portable, relatively low cost units to then densify networks on a regional and local scale.

Because a multilateration approach can make use of strong artificial radio sources, it makes possible the use of relatively low cost, highly mobile stations. Such mobile stations are virtually essential for three dimensional surveying in heavily urbanized areas or in rugged terrain. Accurate three dimensional station location determinations on a fine scale are likely to play an important role in the search for earthquake premonitory phenomena. For example, Southern California (like many other regions of the world) is tectonically very complex with faulting and possible earthquake premonitory crustal uplift occurring over regions of a few km. Therefore, there is an obvious need for dense three dimensional network establishment for which multilateration techniques offer great promise.

This paper presents the results of one phase of research carried out at the Jet Propulsion Laboratory, California Institute of Technology, under Contract No.NAS 7-100, sponsored by the National Aeronautics and Space Administration.

1. Introduction

It is of great worldwide geophysical interest to develop a global tectonic monitoring system which can accurately measure secular variations in three-dimensional position on the earth's crust. Such a monitoring system, if accurate to the centimetre level, will no doubt revolutionalise the field of geodesy, with no less dramatic impact on geodynamic and seismological research such as the search for earthquake premonitory phenomena, the test of continental drift and plate tectonic theories etc.

Through the advent of new aerospace and electronic technology, together with the new concepts of systems approach to large-scale problems, it is now believed that setting up such a global tectonic monitoring system is a distinct possibility. Specifically, in this paper, geometric techniques (multilateration) will be outlined which will enable the relative three-dimensional coordinates of a group of ground stations to be determined using electronic techniques for slant range or range-difference measurements to an artificial satellite or signal bearing vehicle in space. Another technique (Very Long Baseline Interferometry or VLBI) which employs natural radio sources is described by MacDORAN (1973). Both of these techniques have the potential of determining station coordinates to a few centimeters.

Even though historically the techniques of multilateration and of VLBI have been pursued separately, it has recently been realised that the two techniques can be combined into a network densification system in a cost-effective manner. Such a system, which may be called VLBI Multilateration, will operate with a high flying aircraft emitting artificial radio sources, simultaneously received at several ground stations. The processing of these signals will then determine the relative station coordinates in a combined solution. These coordinates may then be tied to the inertial coordinates determined from VLBI measurements established on a global scale. It is the merging of these two techniques which will make the establishment of a global tectonic monitoring system a practical possibility.

In the following sections, range-only and range-difference multilateration concepts will be discussed. Justification of the required accuracy will be provided for a range-only system using laser ranging stations. The same system can of course be operated in a radio ranging mode implementation, at the sacrifice of some precision, but with the advantage of all-weather operation.

The other radio mode implementation, namely, range-difference multilateration, makes use of differential time of arrival measurements or interferometrically derived values for the range-difference. Such a system to date is not as well developed as the range-only system, but preliminary analysis shows that it also has promise for centimeter level position determination if properly designed.

2. Range-Only Multilateration

A laser ranging multilateration system based on range-only multilateration has been designed at the Jet Propulsion Laboratory and reported in ESCOBAL et al (1973a). This section reviews the systems analysis and section 3 the hardware implementation aspects of that work.

Suppose we are given a number of ground stations simultaneously ranging to an earth orbiting satellite. It proves to be convenient to work in a relative coordinate system as indicated in figure 1, where station coordinates are denoted by $(0, 0, 0)$, $(X_2, 0, 0)$, $(X_3, Y_3, 0)$ and (X_j, Y_j, Z_j), $j = 4, 5, \ldots 1$, and the vehicle trajectory coordinates are denoted by (x_n, y_n, z_n),

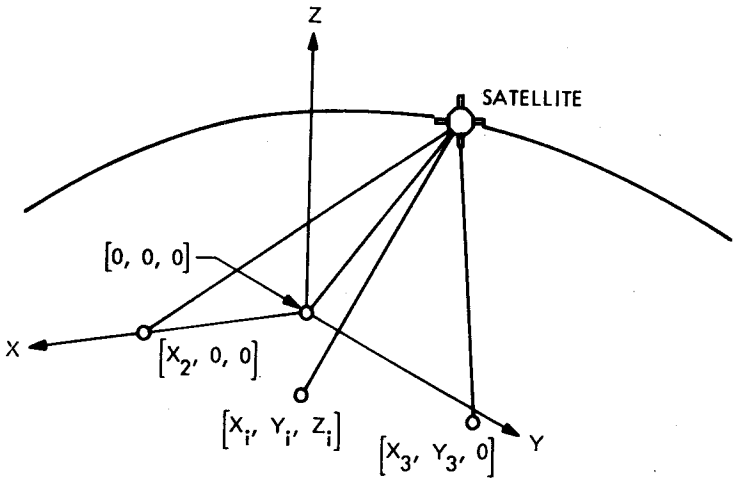

Figure 1. Adopted geometric coordinate system.

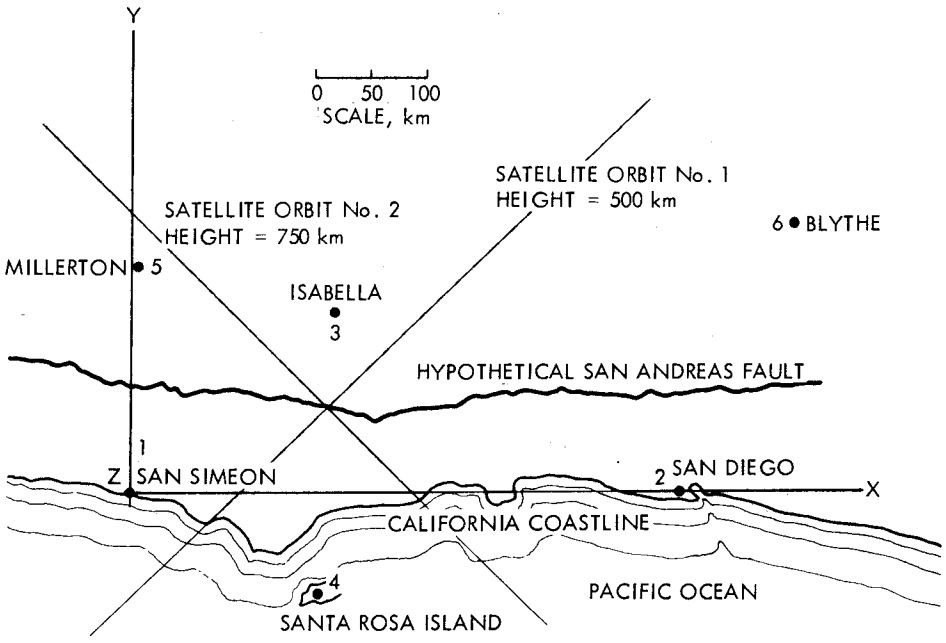

Figure 2. A six station multilateration network along the San Andreas Fault in Southern California.

$n = 1, 2, \ldots N$. Let ρ_{in} be the slant range from the i-th station to the n-th trajectory point. Furthermore, let all the non-vanishing station coordinates be collectively denoted by the vector $\vec{S}$:

$$\vec{S} \equiv (X_2, X_3, Y_3, X_4, Y_4, Z_4, \ldots Z_1)$$

and all the measurement date ρ_{in} be denoted by the data vector $\vec{\rho}$

$$\vec{\rho} \equiv \left\{ \rho_{in} \mid i = 1, 2, \ldots 1; \quad n = 1, 2, \ldots N \right\}$$

It is shown in ESCOBAL et al (1973) that the following "multilateration equations" can be formulated for the determination of $\vec{S}$ from the observed ranges:

$$F_{jn}(\vec{S}, \vec{\rho}) = X_j^2 + Y_j^2 + Z_j^2 - 2x_n X_j - 2y_n Y_j - 2z_n Z_j - \delta_{jn} = 0 \qquad (1)$$

$$j = 4, 5, 6, \ldots 1, \qquad n = 1, 2, 3, \ldots N$$

where the satellite coordinates (x_n, y_n, z_n) can be expressed in terms of station locations and the data by the following equations:

$$x_n = (X_2^2 - \delta_{2n})/(2X_2)$$

$$Y_n = \left(X_3^2 + Y_3^2 - \delta_{3n} - \frac{X_3}{X_2}(X_2^2 - \delta_{2n})\right)/(2Y_3) \qquad (2)$$

$$z_n = \left(\rho_{1n}^2 - x_n^2 - y_n^2\right)^{\frac{1}{2}}$$

and

$$\delta_{in} \equiv \rho_{in}^2 - \rho_{1n}^2$$

Solution of equation system 1 in the appropriate least squares sense will then yield the required station coordinates which will in turn determine the satellite positions through equations 2.

The minimum number of stations required in a range only multilateration system is four for which at least six range points must be taken. If the four stations lie on the same plane, it turns out that the solution to the multilateration equations is degenerate; i.e. a unique set of station coordinates cannot be obtained no matter how many range points are taken. Although in a real-world situation, stations will not exactly lie on a plane, however, a nearly coplanar configuration will lead to high sensitivity of station coordinate errors with respect to ranging errors. Such difficulties associated with station coplanarity can be overcome only if 6 or more stations are used. In addition to degeneracies due to the placement of stations, there is also the class of degeneracies due to orbit selections. The general mathematical problems of singularities encountered in ranging systems has been discussed by ESCOBAL et al (1973b), BLAHA (1971) and ONG & ESCOBAL, (1972).

To ascertain the accuracy of the range only multilateration system under measurement uncertanties, a number of hypothetical configurations involving baselines of local to intercontinental magnitudes have been simulated. Figure 2 shows the location of six hypothetical stations placed along a region of great tectonic interest, i.e. the Southern California portion of the San Andreas fault. Two

circular-orbit satellite passes, whose projections on the XY plane of the adopted coordinate system are as indicated, were used in the simulation. The altitudes of the two satellites are approximately 500 km and 750 km respectively. Fifty points from each orbital arc were generated with X-coordinates varying from San Simeon to San Diego. Assuming ranging errors to be Gaussian distributed with zero mean and 1 cm (1σ), the standard deviations of the computed station coordinates from solving the multilateration equations are displayed in table 1.

TABLE 1

Errors in Station Coordinates for
Southern California Stations Assuming
1 cm Normal Random Errors in Ranging

Station	σ_x (cm)	σ_y (cm)	σ_z (cm)
1. San Simeon	/	/	/
2. San Diego	2.06	/	/
3. Isabella	1.11	3.56	/
4. Santa Rosa I	1.31	1.76	0.99
5. Millerton	1.14	4.16	0.71
6. Blythe	2.64	4.74	1.18

Another hypothetical configuration suitable for the study of continental drift and global plate tectonics is depicted in figure 2. Again a total of 100 points from two satellites at altitudes of 6000 and 10000 km were employed. With ranging errors again assumed to be Gaussian distributed with zero mean and 1 cm (1σ), the errors in calculated station coordinates are given in Table 2.

TABLE 2

Errors in Station Coordinates for the
Intercontinental Configuration Assuming
1 cm Normal Random Error in Ranging

Station	σ_x (cm)	σ_y (cm)	σ_z (cm)
1. Mexico City	/	/	/
2. London	1.87	/	/
3. New York	1.43	1.20	/
4. Freetown	2.08	2.81	1.45
5. Reykjavik	2.01	1.00	1.33
6. Caracas	0.09	1.64	0.51

3. Laser Implementation of 3-D Multilateration

The 3-D Multilateration technique can be implemented through use of a number of ground stations which simultaneously transmit laser pulses to compact reflectors on a moving vehicle, e.g. an airplane or a satellite. Each station evaluates station-to-vehicle range by measuring the time interval between transmission of the original pulse and reception of the reflected pulse. Simultaneous range measurements are then processed so as to yield relative station locations in three dimensions.

The hardware subsystem for measuring station-vehicle ranges is identical for all station configurations. In order to attain high accuracy range measurements, the subsystem utilises a new type of pulsed laser. This laser is a mode-locked, Q-spoiled ruby laser, and has the capability of emitting light pulses of very short duration (0.1 ns or less). The subsystem employs a tracking mount to aim transmitting and receiving telescopes at the vehicle. A measurement is made of the time required for a laser pulse to make a round-trip flight from the station to the vehicle-borne retroreflector. This time, measured with a resolution of 0.1 ns, is used in conjunction with an atmospheric model to calculate the range to the vehicle.

Each ground station also contains an X-Y tracking mount for steering the two telescopes, a small computer to direct the tracking mount toward the satellite, timing ciruitry, recording equipment, and power supplies. In order to satisfy the requirement for "simultaneous" ranging, the clocks at each station must be synchronised to 3 μs; such synchronisation is easily achievable using low-cost components. Synchronisation of laser firing to 1 ms is adequate and well within the state of the art; variations of laser firing within this range are compensated for by time-tagging range measurements, and interpolating between successive measurements so as to obtain effective simultaneity among stations.

It is emphasised that the system errors caused by the satellite, Earth constants, and orbital perturbations do *not* enter into the process. In fact, since the proposed techniques are independent of the location of the retroreflector, the only error sources which enter into the range measurement are:

1) Bias error due to atmospheric delay
2) Random error due to atmospheric turbulence
3) Random equipment measurement error
4) Equipment bias error

A demonstration ranging system was assembled using commercially available components in order to evaluate the measurement errors produced by current hardware. This system simulated a long distance ranging system over short path lengths by using attenuated return signals. The results obtained with this system show that hardware-related errors in range measurement can be made acceptably small, typically less than 3 cm. Future systems can be expected to operate at satellite distances with 1-cm ranging accuracy.

Figure 4 indicates the schematic of hardware components in the system. These can be assembled from commercially available components, packaged compactly, and placed in a transportable van as indicated in figure 5.

4. Range Difference Multilateration

The laser ranging multilateration system discussed in section 3 suffers from one great drawback in

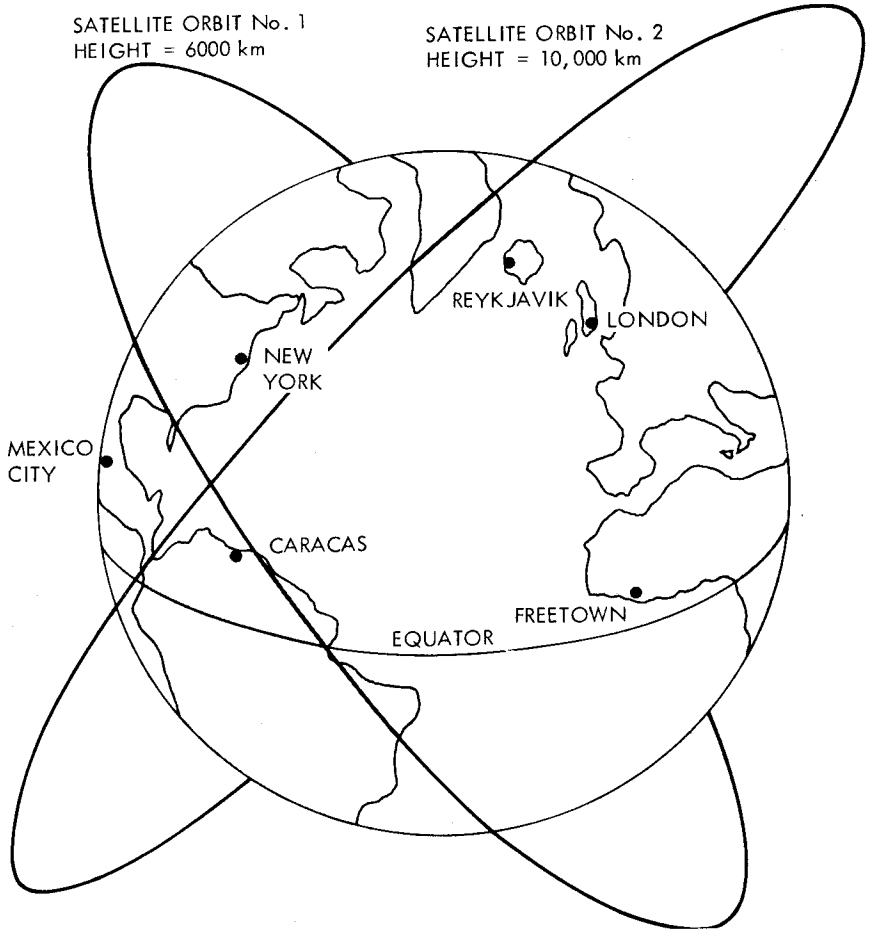

Figure 3. A global multilateration system

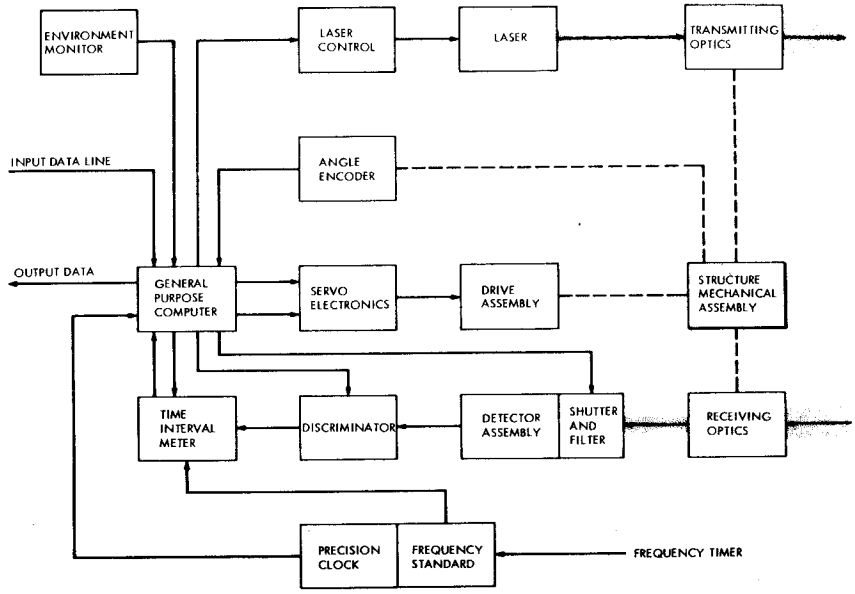

Figure 4. Schematic of laser ranging station hardware

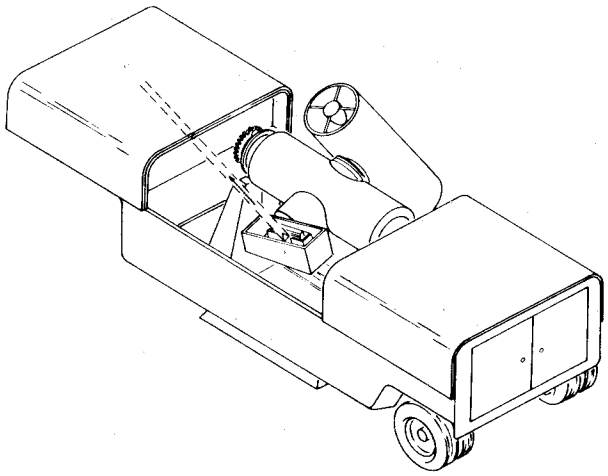

Figure 5. Artist's conception of laser tracking station

that simultaneous observation from 4 to 6 stations to an orbiting vehicle may be easily weathered out. On the other hand, a radio (radar) implementation of range only multilateration, while it has the distinct advantage of all-weather operation capability, can not be expected to yield the same degree of accuracy as laser ranging insofar as present-day technology is concerned. There is, however, another kind of data type, i.e. range differences, which can be measured via radio interferometric techniques and yet has the potential of centimeter-level accuracy comparable to the laser range data type. For a discussion of the instrumentation and methodology for measuring range differences via radio interferometry, the reader is referred to THOMAS (1973). In the present section, only the theoretical foundation relative to such a "range-difference multilateration" technique is discussed. A complete systems study of this problem comparable to the laser ranging technique is presently under way.

The standard relative, station-based coordinate system of figure 1 is again adopted for this analysis. The observables of the system are the differences in slant ranges between station 1 (the origin) and another (say the i-th) station to the vehicle:

$$\varepsilon_{in} \equiv \rho_{in} - \rho_{1n}$$

The problem is to determine the (3I - 6) - component station coordinate vector:

$$\vec{S} = (X_2, X_3, Y_3, X_4, Y_4, Z_4, \ldots X_I, Y_I, Z_I)$$

in terms of the data vector $\vec{\varepsilon}$:

$$\vec{\varepsilon} = \left\{ \varepsilon_{in} \mid i = 2, 3, 4, \ldots I; \quad n = 1, 2, \ldots N \right\}$$

This mathematical problem has been solved in ESCOBAL et al (1973), where it was shown that at least 5 stations are needed for unique determination of $\vec{S}$, and that at least 6 stations will be required in the case of coplanar configurations. The components of $\vec{S}$ are determined by solving the following

systems of equations:

$$F_{jn}(\vec{S}, \vec{\varepsilon}) = X_j^2 + Y_j^2 + Z_j^2 - 2x_n X_j - 2y_n Y_j - 2z_n Z_j - \varepsilon_{jn}^2 - 2\varepsilon_{jn} u_n = 0$$

$$j = 5, 6, \ldots J \qquad (3)$$

$$n = 1, 2, \ldots N$$

where x_n, y_n, z_n can be expressed as functions of the station coordinates and the data vector $\vec{\varepsilon}$ by means of the following equations:

$$x_n = A_{1n} + B_{1n} u_n,$$

$$y_n = A_{2n} + B_{2n} u_n,$$

$$z_n = \left(u_n^2 - x_n^2 - y_n^2\right)^{\frac{1}{2}}, \text{ always positive by definition,}$$

$$A_{1n} = \left(X_2^2 - \varepsilon_{2n}^2\right) / \left(2X_2\right)$$

$$B_{1n} = -\varepsilon_{2n}/X_2$$

$$A_2 = \left(X_3^2 + Y_3^2 - \varepsilon_{3n}^2 - 2X_3 A_{1n}\right) / \left(2Y_3\right)$$

$$B_{2n} = -\left(X_3 B_{1n} + \varepsilon_{3n}\right) / Y_3$$

The quantities u_n are the ranges from station 1 to each of the vehicle trajectory points. They are determined from the coordinates of the first 4 stations by the following equations:

$$\Gamma_{1n} u_n^2 + \Gamma_{2n} u_n + \Gamma_{3n} = 0 \qquad (4)$$

where

$$\Gamma_{1n} = B_{3n}^2 - 4Z_4^2\left(1 - B_{1n}^2 - B_{2n}^2\right)$$

$$\Gamma_{2n} = 2\left[A_{3n} B_{3n} + 4Z_4^2\left(A_{1n} B_{1n} + A_{2n} B_{2n}\right)\right]$$

$$\Gamma_{3n} = A_{3n}^2 + 4Z_4^2\left(A_{1n}^2 + A_{2n}^2\right)$$

$$A_{3n} = X_4^2 + Y_4^2 + Z_4^2 - 2\left(A_{1n} X_4 + A_{2n} Y_4\right) - \varepsilon_{4n}^2$$

$$B_{3n} = -2\left(B_{1n} X_4 + B_{2n} Y_4 + \varepsilon_{4n}\right)$$

Note that u_n is determined from a quadratic equation. In the coplanar case ($Z_4 = 0$), the left-hand side of equation 4 turns out to be a perfect square and hence u_n is uniquely determined. In general when $Z_4 \neq 0$, there may exist two physically acceptable solutions to u_n. The choice between the 2 solutions can be made by using approximate, a-priori knowledge of the ranges u_n, or by bringing in

additional stations.

The above system of equations can be solved by means of Newton-Raphson iteration in the appropriate least-squares sense. Preliminary analysis indicates that error magnification factors, i.e., the ratio of the errors (standard deviations) occasioned in station coordinates to the error assumed for the data, for suitably chosen configurations are quite small. Since this study has not been completed at the time of writing, such results will be left for a future paper.

5. Network Densification by Means of VLBI Multilateration

The range only and range difference multilateration systems considered in the previous sections are capable of stand-alone operations, i.e., it is not necessary to provide additional information other than the fundamental data types (range or range difference). However, for intercontinental geodetic measurements, high flying earth-orbiting satellites with varying altitudes will be required in order to yield respectable accuracy in the solution. Such high flying satellites and their associated equipments will incur substantial costs since data will be required over many years for the tectonic monitoring program. It is thus not cost-effective to use multilateration for intercontinental measurements.

Another difficulty which may be encountered in the use of multilateration techniques for large scale tectonic monitoring may be traced to the relative nature of the coordinate system adopted for such analysis. It can be readily seen that the station coordinate vector $\vec{S}$ will remain invariant if the whole ensemble of multilateration stations undergoes *rigid* displacement or rotation. Geophysically this means that if all the stations lie on the same rigid tectonic plate, then motion of the plate itself with respect to the rest of the earth cannot be detected through multilateration. It is therefore advantageous to be able to tie these relative coordinates determined by multilateration to a more inertial frame of reference, perhaps independently established by other techniques. The technique of Very Long Baseline Interferometry (VLBI), which has the potential of determining accurately three-dimensional coordinates of baselines of arbitrary magnitudes in a coordinate reference frame defined by extragalactic radio sources, appears to satisfy these needs (MacDORAN 1973). However, because the radio flux density of natural sources (quasars) are of the order of magnitude of 10^{-26} watts/m^2/Hz when received at the surface of the earth, it takes highly sophisticated electronic equipments to receive and record such signals, making even a portable VLBI station difficult to be moved from place to place. (Conventional VLBI stations are usually permanent tracking stations such as the Goldstone and the Canberra Radio Tracking Stations.) It is, nevertheless, important to be able to determine 3-dimensional station locations on a fine scale in a tectonically complex region such as Southern California. It would therefore seem extremely desirable to have available a system making use of highly portable equipment for the purpose of regional and local tectonic monitoring augmenting the coarse-grid VLBI network. Range difference multilateration with low-flying vehicle-borne artificial signal sources appears to meet these requirements.

A simple calculation shows that a one-watt transmitter broadcasting random noise over a 100 MHz bandwidth received at a distance of 100 km will exhibit a radio flux density of approximately 10^{-19} watts/m^2/Hz. This improvement of 7 orders of magnitude relative to a natural radio source can be exploited in the form of a vast reduction in the sophistication of the radio interferometer stations and a corresponding increase in mobility. The range difference multilateration technique as discussed in the previous section can be used in conjunction with these small portable interferometers for densifying the regional or local geodetic networks.

Thus, conceptually, a global tectonic monitoring system works as following. First, intercontinental bechmarks are established via conventional (natural source) VLBI techniques such as Project ARIES presently carried out at the Jet Propulsion Laboratory. This will enable the establishment of a coarse grid network in a quasi-inertial reference frame defined by the extragalactic objects. Range difference multilateration stations (or laser ranging stations if applicable) will then occupy these sites. Each of these sites will then serve as the origin of a denser network of multi-lateration stations covering the local region. Low flying vehicles bearing laser retroflectors or radio noise transmitters are then used in conjunction with the multi-lateration stations. Simultaneous determination of the relative station and vehicle coordinates is then possible through the use of the developed analytic techniques. Such a network densification scheme is illustrated in figures 6a and 6b.

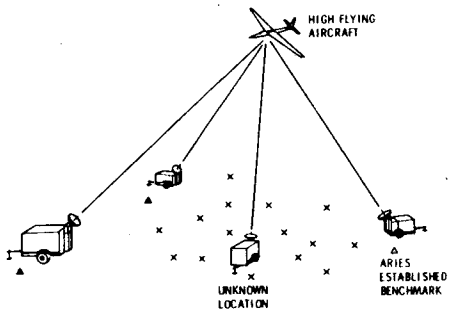

Figure 6(a). Network densification by 3-D Multilateration

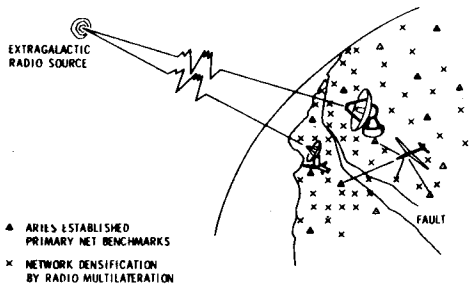

Figure 6(b). VLBI Multilateration Earthquake Monitoring System

6. Summary

In this paper, analytical methods of range only and range difference multilateration for relative 3-dimensional station location determination have been discussed. Implementation of range only multilateration through the use of laser ranging stations has also been outlined. Because of the desirability of all-weather operation capability, a radio mode implementation is preferred.

This can be accomplished through radio ranging, or through interferometric range difference multilateration. The latter technique makes use of low-flying artificial signal bearing vehicles and small diameter dish antennae for ground reception. This makes such a system highly mobile and thus suitable for network densification purposes in tectonically complex regions such as Southern California. Dense local networks, combined with a global, coarse-grid network established by natural source VLBI in a global reference frame will enable the worldwide monitoring of tectonic events and the detection of secular variations in position on earth.

7. Acknowledgment

The author wishes to thank P. R. Escobal, H. F. Fliegel, R. M. Jaffe, P. M. Muller, M. S. Shumate and O. H. von Roos for their contributions to the 3-D Multilateration project, and P. F. MacDoran and J. B. Thomas for their advice on the concepts of VLBI systems and network densigifcation.

8. References

BLAHA, G. 1971. "Investigation of Critical Configurations for Fundamental Range Networks", Ohio State University Dissertation, and references cited therein.

ESCOBAL, P.R., ONG, K.M., VON ROOS, O.H., SHUMATE, M.S., JAFFE, R.M., FLIEGEL, H.F. & MULLER, P.M. 1973a. "3-D Multilateration: A Precision Geodetic Measurement System". *NASA Technical Memorandum* 33-605, Jet Propulsion Laboratory, Pasadena California.

ESCOBAL, P.R., ONG, K.M. & VON ROOS, O.H. 1973b. "Range Difference Multilateration for Obtaining Precision Geodetic and Trajectory Measurements", submitted to *Astronautica Acta*.

MacDORAN, P.F. November 1973. "Very Long Baseline Interferometry (VLBI) Applications to Secular Geodynamics and Earth Strain Measurement", presented at the International Symposium on Earth's Gravitational Field and Secular Variations in Position, Sydney, Australia (This volume,380-395).

ONG, K.M. & ESCOBAL, P.R. 1972. "Multilateration: A Nondegenerate Method of Obtaining Station Coordinates and Satellite Ephemerides", submitted to *Journal of Astronautical Sciences*.

THOMAS, J.B. August 1973. "An Analysis of Long Baseline Radio Interferometry, Part III". *Jet Propulsion Laboratory Technical Report* 32-1526, Vol.XXVI.

9. Discussion

STOLZ: Do you see any application of your technique to lunar laser ranging?

ONG: We have not analyzed the multilateration geometry for lunar laser ranging. I think it is possible that the orbit of the moon could serve as the positions in space for multilateration. It might cause certain problems in that we have only one pass of a satellite (i.e., the moon). There might be an accuracy problem involved which could degrade the accuracy of the station locations. You should have sufficient separation in space co-ordinates to achieve an adequate accuracy.

MUELLER: The obvious problem is that of the weather; to obtain six station simultaneity is almost impossible. We have statistics now about this. For example the (US) National Geodetic Survey global satellite triangulation observed 2,200 events, and they always tried to co-ordinate observations between three, four and five stations if possible. From memory there were less than 25% of the three station events and less than 2% of the four station events.

ONG: Yes, this is a problem, but it should be possible to use the method over small areas with aeroplane type experiments.

MUELLER: In the case of the second method, the problem is one of range differences. I'd like to draw your attention to the work done with geoceivers, using them in an integrated mode and getting range differences. The whole geometry of the adjustment technique and the receiver configuration was thoroughly analyzed by several groups working with geoceivers, most of the work coming from Duane Brown Associates.

DUNN: With the Goddard lasers, very stringent precautions are taken to prevent aircraft flying into laser beams.

ONG: I think the safety precautions taken about laser beams have been over-emphasized. In a study reported in (*Laser Focus* 8,22-27,May 1972), and in our report (*NASA/JPL Technical Memorandum* TM 33-605) which studied the safety problem, it was shown that correct safety measures as to the use of lasers are not difficult to achieve.

ECKHARDT: I would like to answer the question as to whether the multilateration approach can be used with lunar ranging from different sites but not exactly simultaneously. You have the direction of the moon in space from which you can pick up the orbit of the moon.

GUBBAY: I've heard we are measuring position, and keep wondering what we are measuring with respect to; what the prevailing system of reference is. I know we are thinking in terms of complementary techniques but the reference systems are different. How do we fuse all these measurements together? They are liable to small errors. Can these errors be recovered?

ONG: No. The assumption is that VLBI uses an inertial co-ordinate system while multilateration could use a local system on a relative basis. By fine filtering or referencing multilateration networks together with VLBI, it will be possible to provide the global co-ordinates of all stations relative to an inertial reference system. The problem we are looking at now is a very difficult one and might include transformations which would introduce additional error sources. It does not appear likely that these errors can be recovered to the degree of accuracy we are talking about.

GUBBAY: Even with VLBI, you need one position to start with. Where can you start from?

ONG: In defining a co-ordinate system for geodetic applications we are not too interested where the dynamical centre of the Earth is. We are more interested in relative positions and relative motion and relative motion of stations with respect to one another. The search for an "absolute" reference frame is important, but for applications in monitoring changes in position, this is not important. We can therefore start from any convenient station.

PLOTKIN, H.H.
NASA Goddard Space Flight Center
Greenbelt Md 20771
United States of America

Proc.Symposium on Earth's Gravitational Field & Secular Variations in Position (1973),328-346.

LASER TECHNOLOGY FOR HIGH PRECISION SATELLITE TRACKING

ABSTRACT

Fixed and mobile laser ranging stations have been developed to track satellites equipped with retro-reflector arrays. These have operated consistently at data rates of once per second with range precision better than 50 cm, using Q-switched ruby lasers with pulse durations of 20 to 40 nanoseconds. Improvements are being incorporated to improve the precision to 10 cm, and to permit ranging to more distant satellites. These include improved reflector array designs, processing and analysis of the received reflection pulses, and use of sub-nanosecond pulse duration lasers.

1. Text

There are now 7 satellites in near Earth orbit fitted with retroreflectors, commencing with the first in the BE series (figure 1). There are two more such satellites scheduled for launch by the

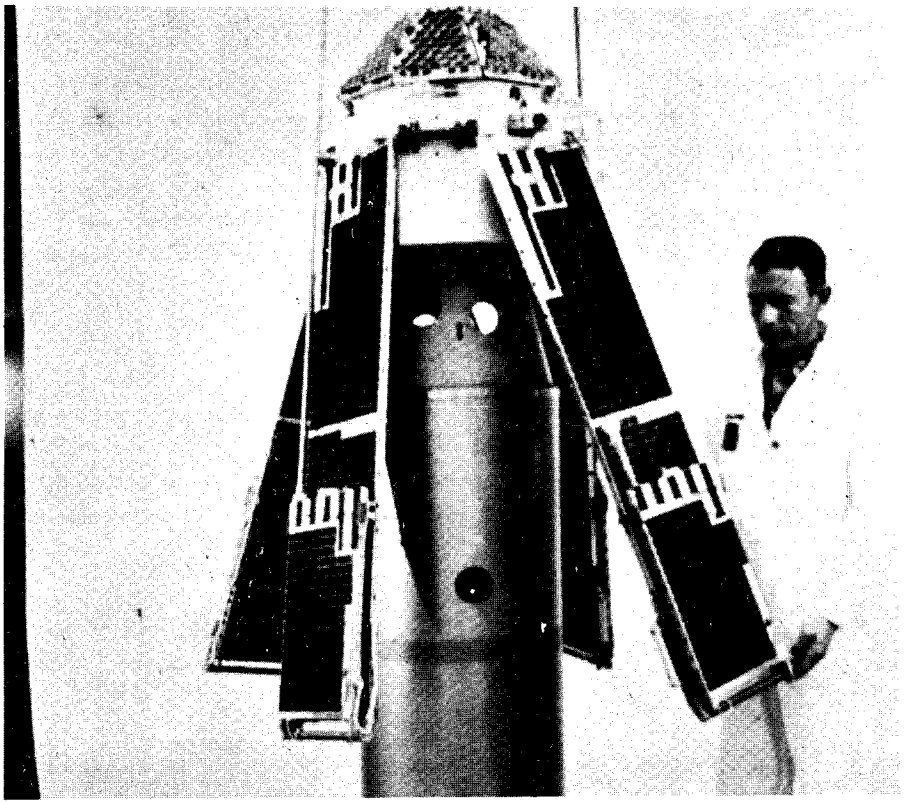

Figure 1. **Beacon-Explorer B. The First Satellite Orbited (October 1964) with Retroreflectors for Laser Tracking** *(Goddard Space Flight Center)*

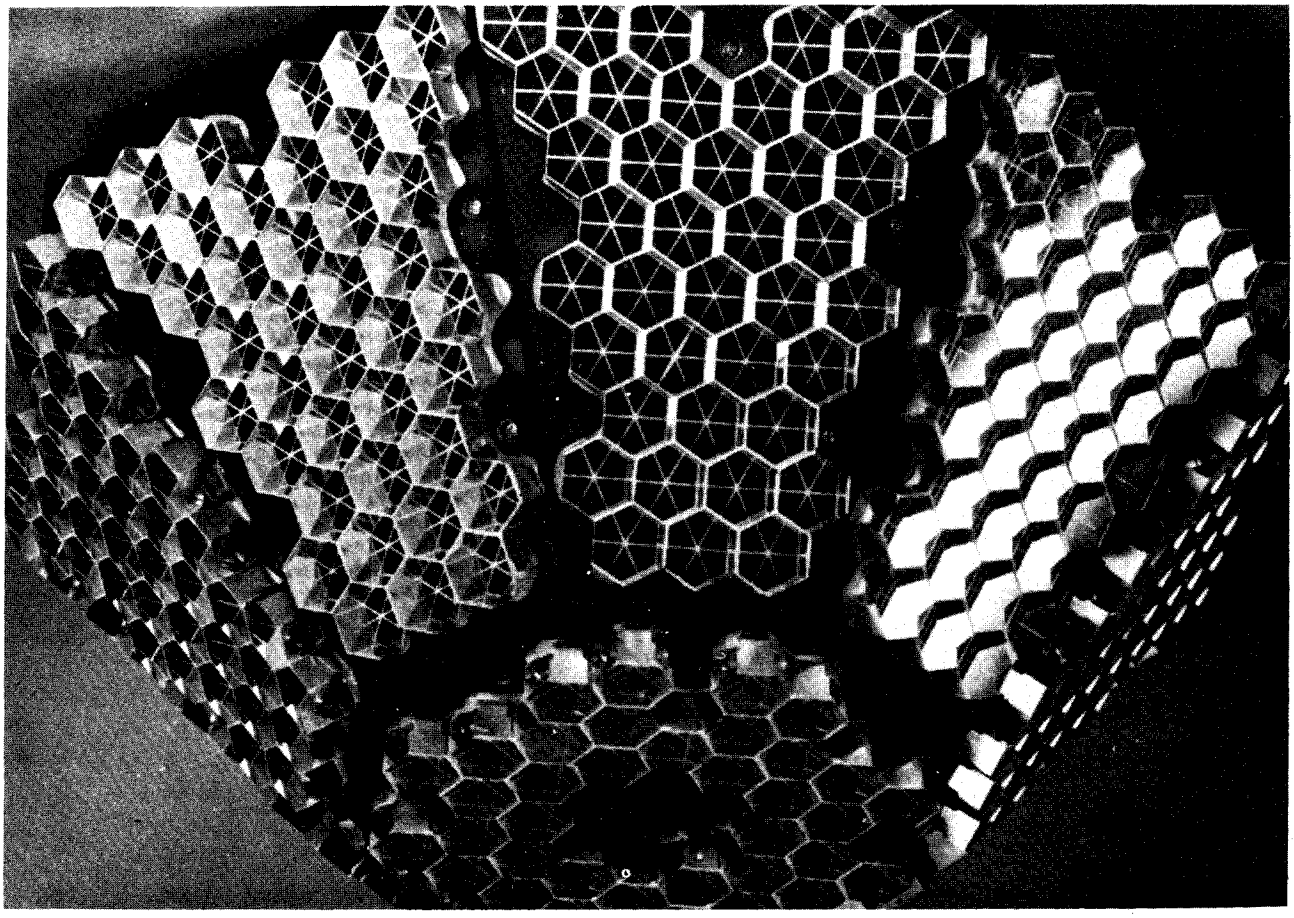

Figure 2. Retroreflector Array on Beacon-Explorer

United States in 1974, and another in 1976. There are large quantities of data that have been taken , with rms scatter in range measurement (and, presumably, accuracy) of ±50 cm.

We are now preparing a new generation of satellite laser trackers which have a precision of ±10 cm. Our plans are to further improve the precision to ±2 cm over several years. We think this can be done , but as users of this data you must understand the source of our confidence in the accuracy, and ultimately draw your own conclusions. The only way I can impart this degree of confidence is to describe the design features of our technique, in more detail than some would like and too rapidly for others.

The retro-reflector array (figure 2) is composed of a number of fused silica corner cubes; these

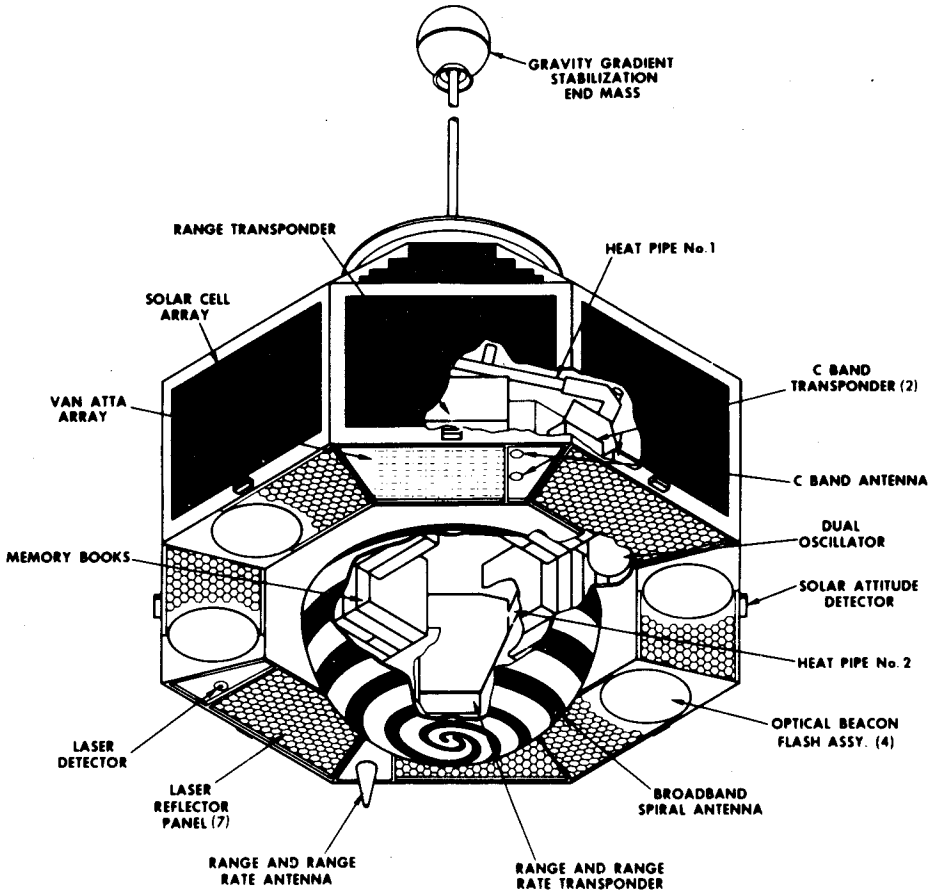

Figure 3. GEOS-B Spacecraft

corner cubes have the property that a beam of light incident on them is reflected directly back towards the transmitter. The Beacon-Explorer (BE) satellites are magnetically stabilized and a pyramid reflecting cap was placed on the north-seeking end of the spacecraft. I am embarrassed to say that this made it particularly useless for observations from Australia. But we have learned from our errors. The GEOS-A and GEOS-B spacecraft (figure 3) which are stabilized by the gravity field gradient, and all our future satellites, will *not* be useless for observations from Australia. In these cases, the retro-reflectors will be mounted on the Earth-viewing surface of the spacecraft, pointing down so that they can be seen from all hemispheres of the Earth.

The signal depends on three terms (figure 4). The *first* term is the incident energy on the reflectors and that depends on the energy which is transmitted, the number of reflectors, the area of the individual reflectors and the divergence of the transmitted beam. The *second* term depends on

CLASSICAL BISTATIC RADAR EQUATION

$$S = \underbrace{\frac{P_T G_T}{4\pi R^2}}_{\text{POWER DENSITY AT TARGET}} \times \underbrace{\frac{\sigma(\alpha)}{4\pi R^2}}_{\text{POWER DENSITY AT RECEIVER PER UNIT POWER AT TARGET}} \times \underbrace{\frac{G_R \lambda^2}{4\pi}}_{\text{EFFECTIVE ANTENNA RECEIVING AREA}}$$

$$G = \left(\frac{\pi D}{\lambda}\right)^2 \quad \text{ANTENNA GAIN}$$

$$\sigma(\alpha) = \frac{4\pi A^2}{\lambda^2} \quad \text{RADAR CROSS SECTION}$$

Figure 4. Classical Bistatic Radar Equation

the area or gain of the individual reflectors because they will determine the spot size of the downward reflected beam. The *third* term is the area of the receiving telescope.

In addition to these terms we also have to remember that when you look at the cube corner at an oblique angle (figure 5), the effective area will be less since there will be a tilt effect. There are also losses in the optics and losses in the atmosphere. Finally, there is also an effect due to the fact that the satellite is moving - a velocity aberration effect. All these effects will affect the design of a satellite.

For instance, we want to look at the satellite at a very low elevation angle so that we get maximum coverage. In order to do that, we have to mount the cube corners at an angle on the surface of a cone and tilt them outward so that we can see them even when the satellite is at a very low elevation angle. We must also mount the cube corner in such a way that the return pulse is spread

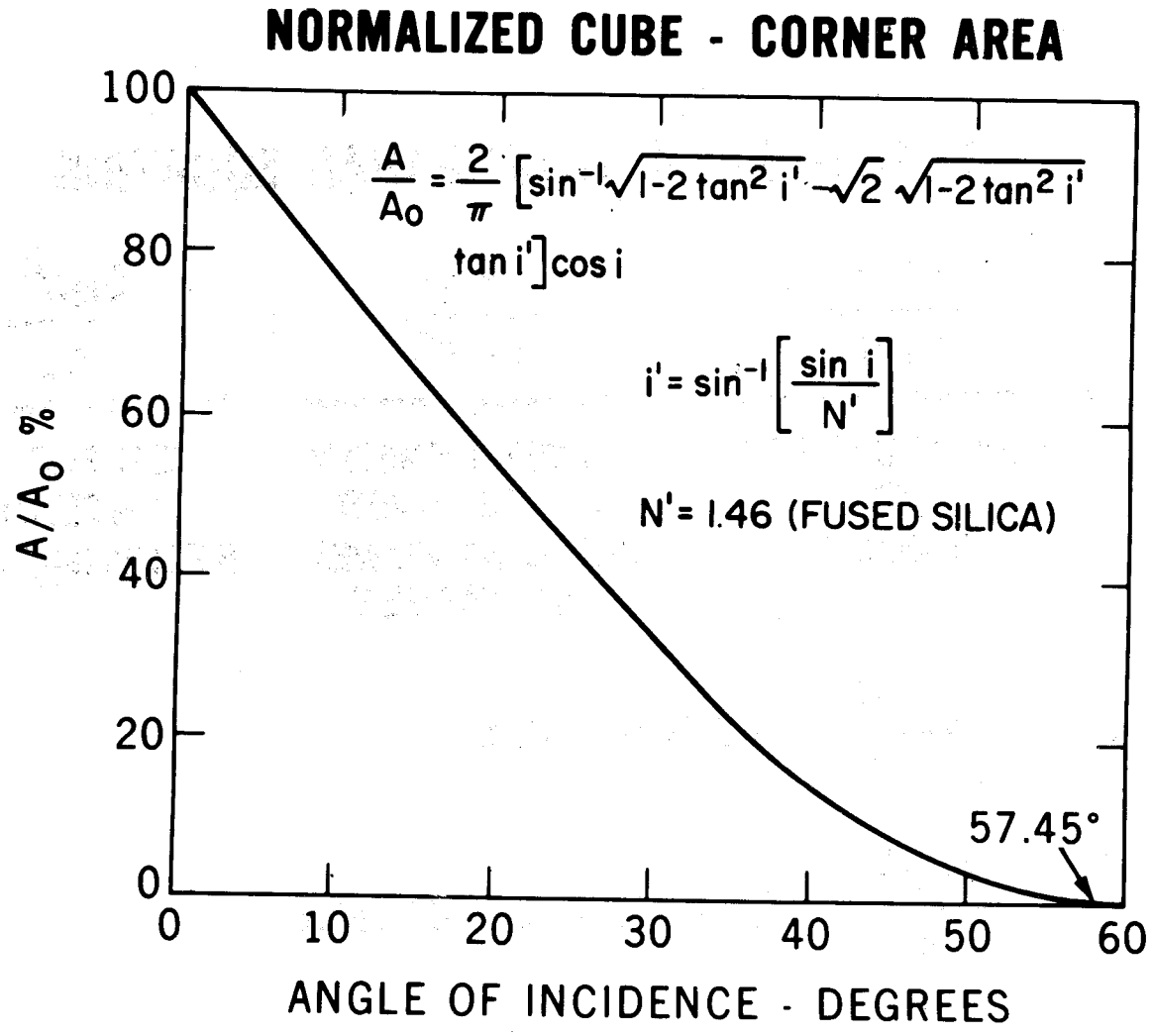

Figure 5. Normalized Cube-Corner Effective Area

in a very well defined manner so that we can measure the range with respect to the centre of mass of the spacecraft. Unless we can measure that range accurately with respect to the centre of gravity, the precision we are going to talk about will be senseless. For these reasons, the reflector arrays on GEOS-C (figure 6) has a well defined geometry and is tilted outward at an angle of 45°.

Now, how large shall the individual cube corners be? That will be decided upon by the velocity aberration. In figure 7, a ray of laser light hits the satellite and gets reflected. But because the satellite is moving with a velocity v, the reflected spot doesn't come back to the source but is displaced. The size of the spot will depend on the diffraction effect at the individual cube corners. The larger the cube corner is, the smaller the spot will be. If the spot is very small, it will miss the transmitter and you will get no signal. If the spot is very large, the energy is spread over a large area and you are making inefficient use of the return signal.

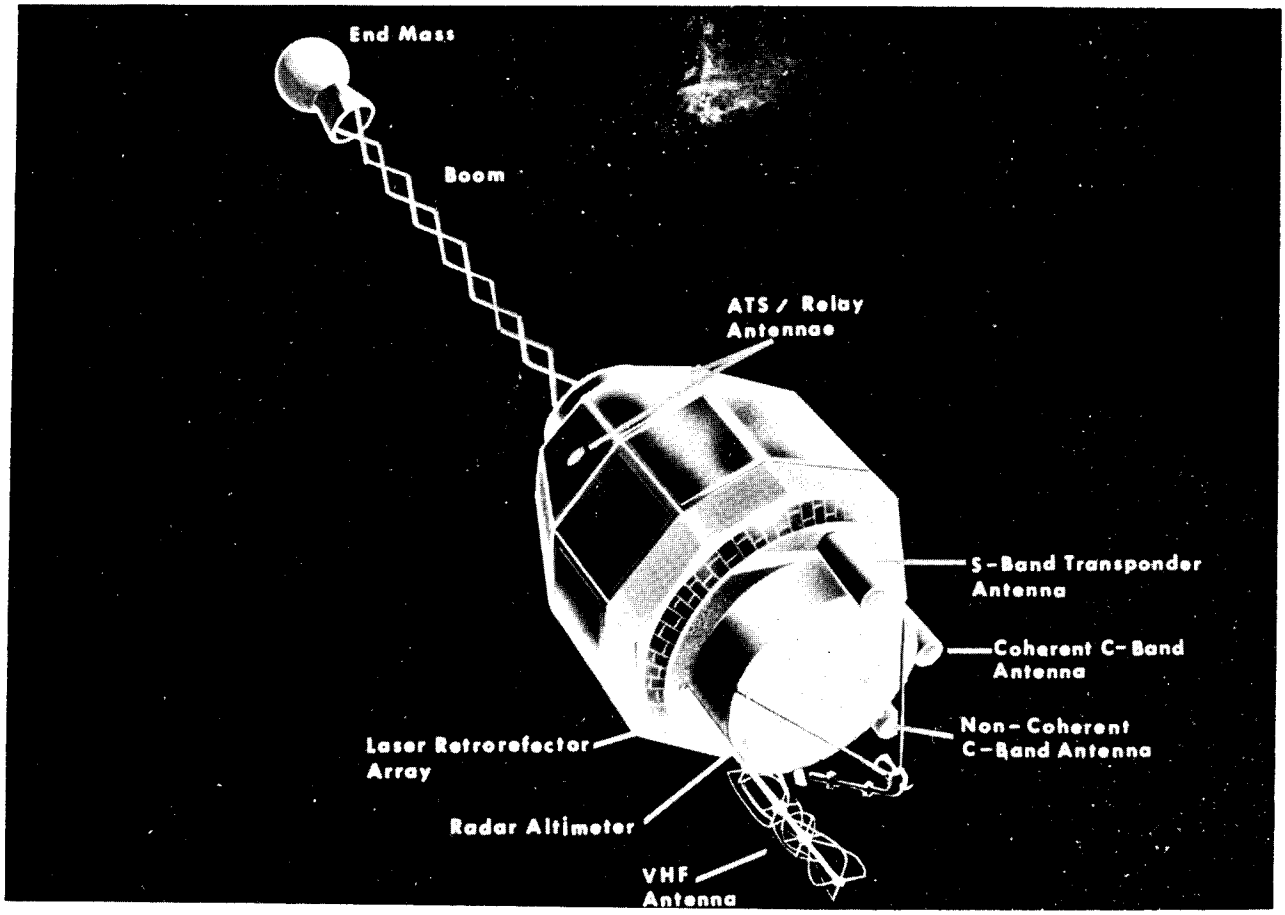

Figure 6. GEOS-C - To be Launched by NASA in 1974

If you look at the spot in detail, the intensity profile of the diffraction pattern is given by a Bessel function and the optimum value is a function of the velocity itself. But the velocity is a function of the satellite altitude (figure 8). For GEOS-C, the optimum cube corner size is about 4 mm in radius. On the other hand, TIMATION III is a satellite we also plan to launch in 1974 at an altitude of 14,000 km. Its reflectors should have an optimum diameter of about 7 mm. For the TIMATION satellite, we will indeed use the optimum diameter as given in figure 8. However, for GEOS-C, 4 mm is too small for convenience. In order to get the required total area, you would have to mount a great many such 4 mm reflectors, and it would be too expensive. Therefore, we essentially ignored figure 8 to design GEOS-C.

Instead we use 3½ cm diameter reflectors. This would ordinarily produce a very small spot which would miss the transmitter. What we did was to introduce errors into the angles of the cube corners and because of these errors, the returned ray split into 6 spots forming a toroidal distribution and the amount of the splitting was designed so that it compensated for the velocity

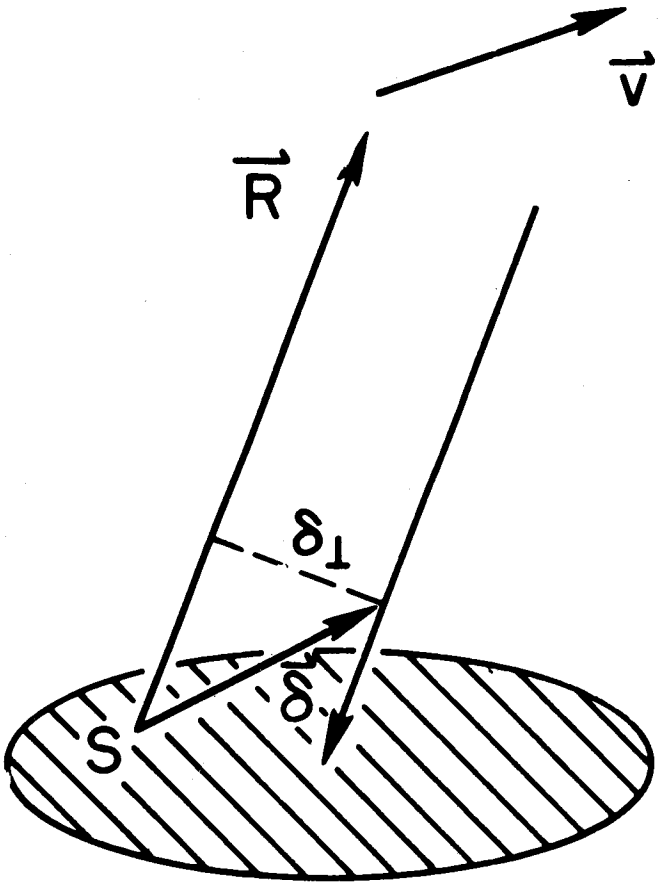

$$|\delta| = 2\frac{v}{c}R$$

$$\delta_\perp = \frac{(\vec{R}\cdot\vec{\delta})^2 - \delta^2 R^2}{R\,|\vec{R}\times\vec{\delta}|}$$

Figure 7. Displacement of Reflected Spot Due to Velocity Aberration

aberration. The receiving telescope will find itself out on the toroid ring, where the intensity has been optimized. This turns out to be a better design than the optimum small reflector.

Figure 9 is a quick summary of the returned signal we would expect if we were to assume we use a pulsed ruby laser with 1 J of energy per pulse, a transmitter divergence of 1 mrad, a 50 cm diameter receiver, and satellite reflectors which are 3½ cm in diameter. There will be 270 of these on GEOS-C. Here we can't use the diffraction formula for 3½ cm cube corners. We lose a factor of 36 which comes about because we have split the reflected beam into 6 spots. The range of GEOS-C will be approximately 1000 km.

The received signal, if all reflectors were facing downward, would be 2×10^5 photoelectrons. This is further reduced by a factor of 20 because we tilted them away from the zenith. The signal received is therefore 10^4 photoelectrons - a goodly number - one with which we should be very comfortable.

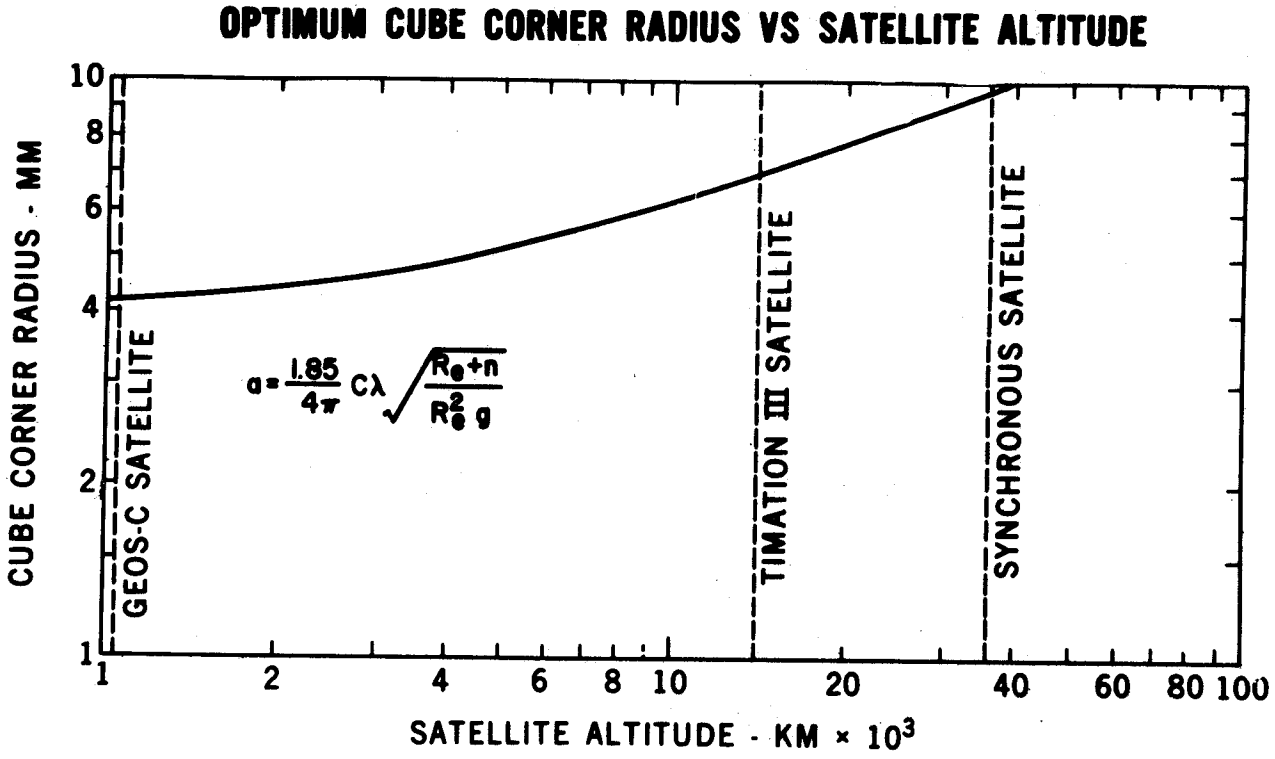

Figure 8. Optimum Cube-Corner Radius as a Function of Satellite Altitude. This optimization assumes perfect cube-corners with metallized reflecting surface.

Figure 10 is a picture of the mobile laser ranging station which is now reaching completion at the Goddard Space Flight Center. It is self-contained in its own van. The back closes up for road travel. The laser is mounted underneath the van and is accessible through a door. The laser light comes up through a smaller collimating telescope at the right. The reflected light is received by the larger telescope and is detected in the photo-multiplier mounted at the Cassegrain focus. The system is directed toward the satellite by a computer program which derives the expected satellite orbit, and all preliminary data processing and recording is done within the van.

I now want to come to the real reason for my talk. The question is :

How will we know what the accuracy of the measurement is?

The accuracy will depend on the degree to which we can calibrate the system and out ability to measure pulse position (figure 11). Up to now, the laser pulses we have used for satellite tracking have had a duration of about 20 nanoseconds. The laser at McDonald Observatory used for ranging

$$S_0 = \frac{P_T G_T G_R \lambda^2 \sigma L_S}{(4\pi)^3 R^4}$$

		dB	Value
P_T	Power Transmitted	0	1 J
G_T	Transmitter Gain	81.1	$\theta_T = 5 \times 10^{-4}$
G_R	Receiver Gain	127.1	$D_R = .5$ M
λ^2		-123.2	$\lambda = .6943$ um
σ	Radar Cross Section		
	$\sigma = N \frac{4}{36} \frac{A^2}{2}$	82.5	$D_C = 3.5$ cm $N = 270$
$(1/4\pi)^3$		-33.0	
$1/R^4$	Range	-238.7	$R = 9.27 \times 10^5$ M
L_S	System Losses	-11.1	$\rho = 7.8\%$
S_0	Received Signal	-115.3	2.95×10^{-12} J
	$N_S = \eta \frac{S_0}{H\nu}$		
η	Quantum Efficiency	-17.0	0.02
$(H\nu)^{-1}$	Photon Energy	185.4	
N_S	Received Photoelectrons (Flat Array)	53.1	2×10^5
N'_S	GEOS-C Array = .05 N_S		10^4 P.E.

Figure 9. GEOS-C Signal Calculation

to the moon has a pulse duration of 3 nanoseconds. We are now designing lasers which will have pulse durations of 0.2 nanoseconds. However, for the next few years, we are stuck with pulse durections of 20 nanoseconds. A 20 nanosecond pulse is 600 cm long, whereas we are trying to range to a few cm. The question is:

Can we get 10 cm accuracy with pulses 600 cm long?

Once we have developed the necessary position measuring technique , we must ask whether the system is stable. What is the effect of clock synchronization; what is the effect of atmospheric propagation; what is the spreading effect on reflector geometry? Remember that a short pulse is going to come back spread by the reflector and we have to know what the effect of the spacecraft array will be on that pulse.

Under these circumstances, how can we claim something like 10 cm in precision? There are a number of ways we can sense the position of a returned pulse (figure 12). When we started, we used a fixed threshold. We used a very simple circuit and our range precision was ±1½ m. The next improvement was to use a constant fraction trigger threshold. This was something which did

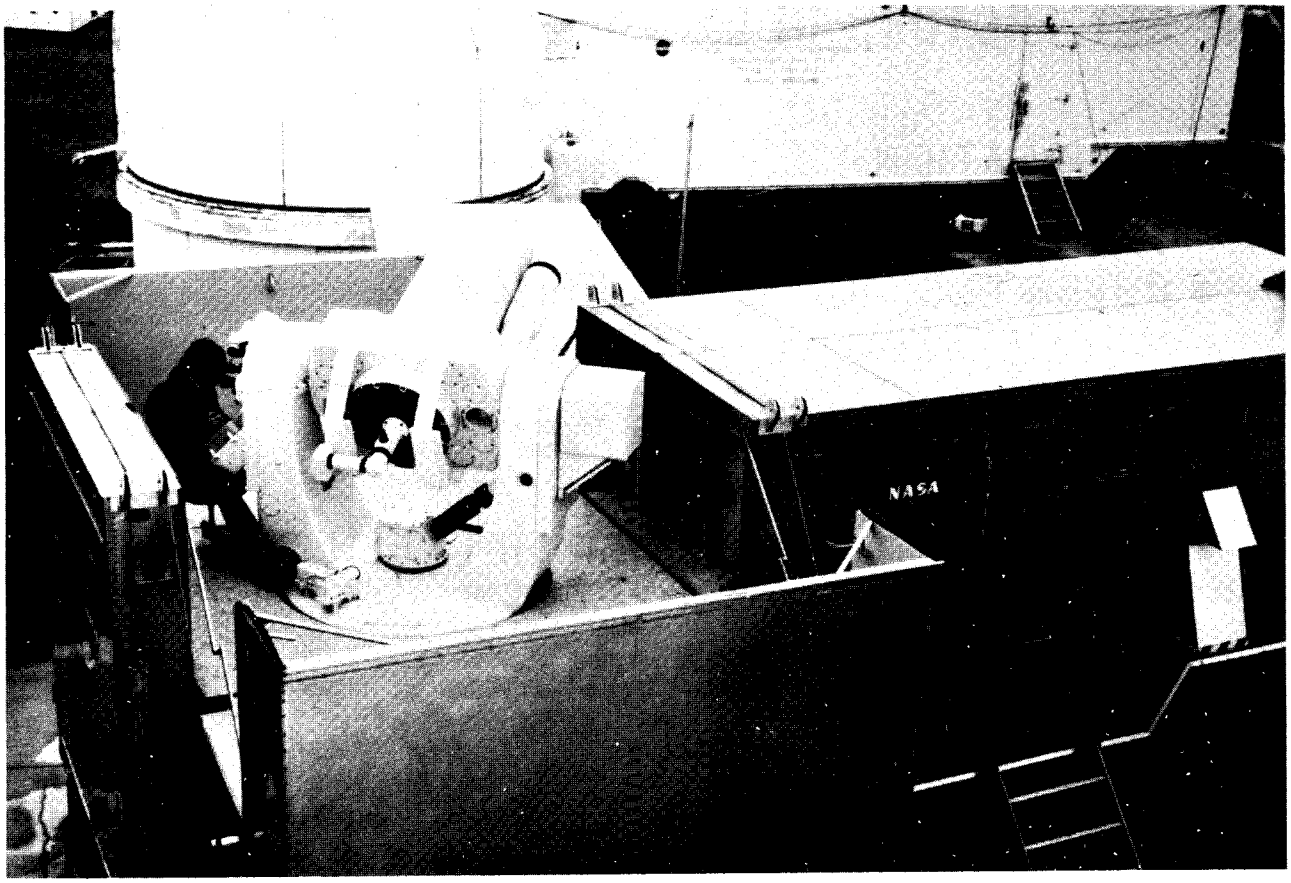

Figure 10. Photograph of MOBLAS 2, NASA Goddard Space Flight Center's Mobile Laser Ranging System

not change much as a function of pulse height but it did depend on pulse shape. The result of using this technique was a precision of ±50 cm.

The next generation will have to do better than the constant fraction trigger. We will measure the centroid of the 600 cm pulse (figure 13). We fire the laser once per second. We pick up a little of the outgoing pulse with a photo diode and use that to start a range interval timing system. At the same time, we also detect the centroid of the transmitted pulse, and record in the computer the position of that centroid with respect to the time at which we actually start timing the range interval. When the received pulse arrives, we use that to stop the range interval timing system. But at the same time, we make a careful analysis of the wave form because now the pulse has changed in both amplitude and shape. It will scintillate a great deal, with wide fluctuations in intensity. It will also be affected by the spreading of the reflector.

In the transmitted pulse, the centroid measuring technique is very simple. We just measure the width of the pulse and add half the width to the time at which the trigger was activated. That represents very well the centroid of the pulse because the pulse is fairly symmetrical and

KEY FACTORS IN LASER RANGING ACCURACY

- CALIBRATION
- PULSE POSITION MEASUREMENT
- SYSTEM STABILITY
- CLOCK SYNCHRONIZATION BETWEEN STATIONS
- ATMOSPHERIC PROPAGATION
- SPACECRAFT RETROREFLECTOR ARRAY GEOMETRY

Figure 11. Key Factors in Laser Ranging Accuracy

reproducible. On the other hand, the pulse which comes back in the returned signal fluctuates over a wide range in amplitude (figure 14) (as much as 1000 or 2000 to 1) and has unpredictable shapes. On the reflected pulse we, therefore, have to use a different technique - we measure the wave form in a digitizer, actually recording the value of the signal amplitudes in a number of channels. As can be seen in figure 15, even though the trigger point would have been the same in the two pulses, the position of the centroid will vary considerably, and must be taken into account.

We now have three such systems in operation:

- A stationary laser at Goddard, and
- Mobile Laser (MOBLAS) systems one and two.

In figure 16 are the results we have been getting in range precision. The rms scatter is about 15 cm on the average. If we assume there are no systematic errors, and that the fluctuations are random, then we can smooth over several measurements. If we do smooth over 10 points, the precision of ranging is about 4.7 cm.

TYPES OF PULSE POSITION SENSING

- FIXED THRESHOLD TRIGGER ON LEADING EDGE OF PULSE.
  - ADVANTAGE: VERY SIMPLE CIRCUIT.
  - DISADVANTAGE: MEASURED POSITION IS A FUNCTION OF PULSE HEIGHT AND PULSE SHAPE.
- CONSTANT FRACTION TRIGGER ON LEADING EDGE OF PULSE.
  - ADVANTAGE: MODERATELY SIMPLE CIRCUIT AND MEASURED POSITION ONLY WEAKLY DEPENDENT ON PULSE HEIGHT.
  - DISADVANTAGE: MEASURED POSITION IS A FUNCTION OF PULSE SHAPE.
- PULSE CENTROID MEASUREMENT.
  - ADVANTAGE: MEASURED POSITION INDEPENDENT OF PULSE HEIGHT AND ONLY WEAKLY DEPENDENT ON PULSE SHAPE.
  - DISADVANTAGE: COMPLICATED CIRCUITRY.

Figure 12. Types of Pulse Position Sensing

What shall we expect for the calibration error ? (See figure 17.) We calibrate by ranging to a tower 3 km away. The surveyors tell us that they trust the survey to 1½ cm. We have propagation errors in measuring the distance to the target and we have the precision with which we can measure the range to that target. Usually, during calibration we fire a hundred shots, with an rms range scatter of ±15 cm for the ensemble.

Having calibrated such a system, how well does the system maintain its calibration with high stability?

Figure 18 shows typical five hour runs on two independent systems. The calibration constant remains stable within an rms of ±4 cm. To accomplish clock synchronization, we have caesium standards at all our stations and we synchronize using LORAN-C.

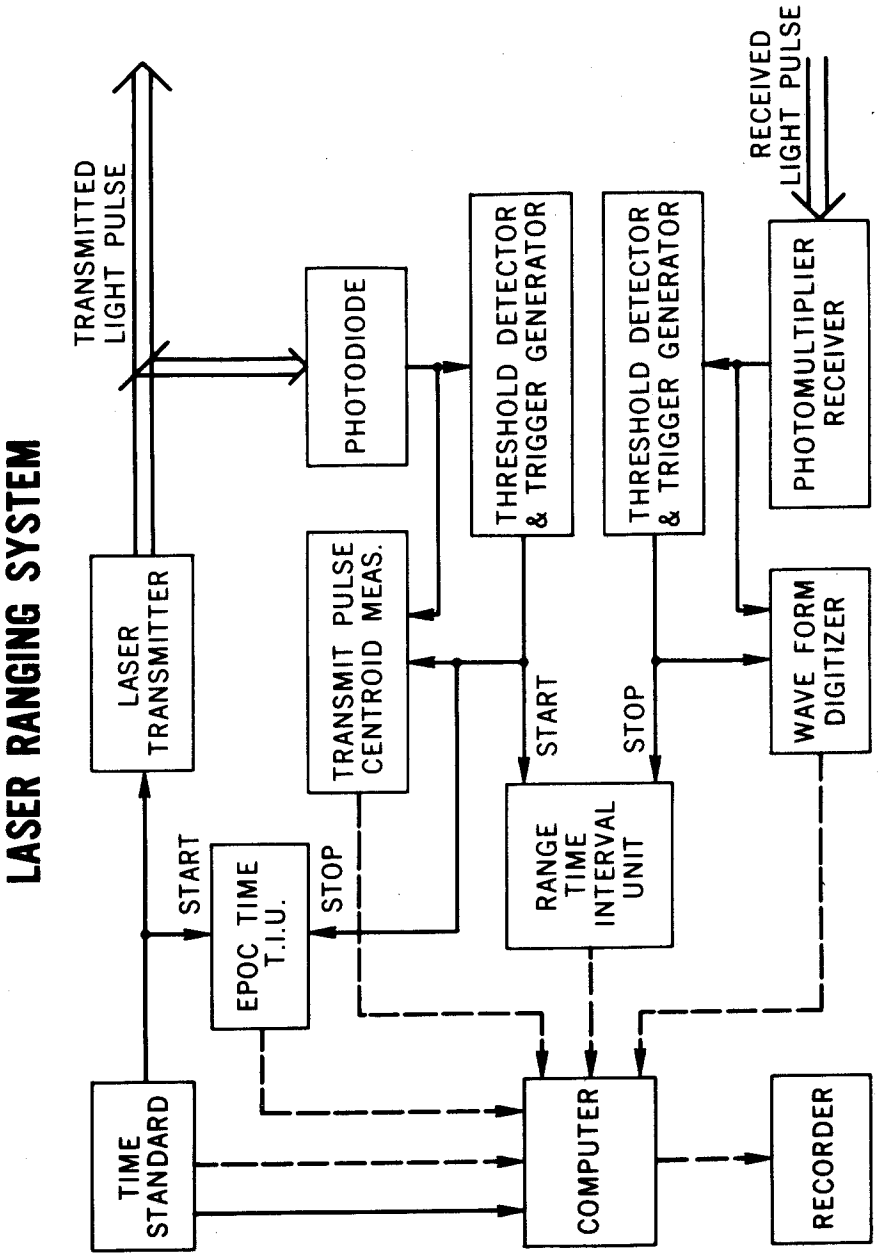

Figure 13. Block Diagram of Laser Ranging System

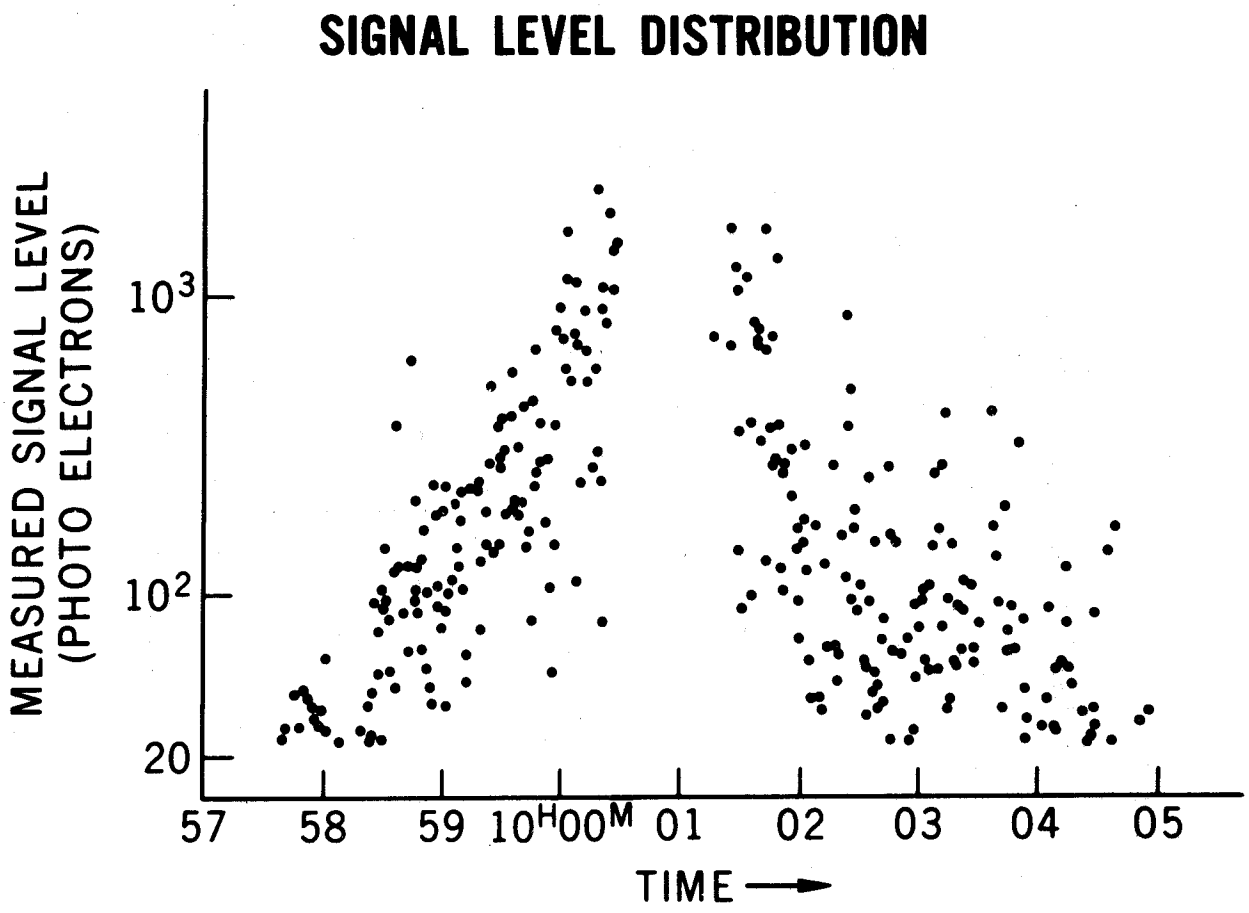

Figure 14. Signal Level Fluctuations from GEOS-B

The kind of performance we get is epoch precision of five microseconds, which is equivalent to space tracking errors of ±3½ cm. The range correction of two metres for the atmospheric refraction delay is known to ±3 cm. The spacecraft array geometry for GEOS-C for a 20 nanosecond pulse, results in an uncertainty in the centroid of the spacecraft's position of about 3 cm. This is because the GEOS-C reflector array is one metre in diameter, the pulse gets spread on its way back, and within that pulse, there is scintillation due to interference between the cube corners of the GEOS-C array. This scintillation gives an uncertainty of ±3 cm. Finally, as summarized in figure 19, the total rms error is about 10 cm, using laser pulses 20 nanoseconds

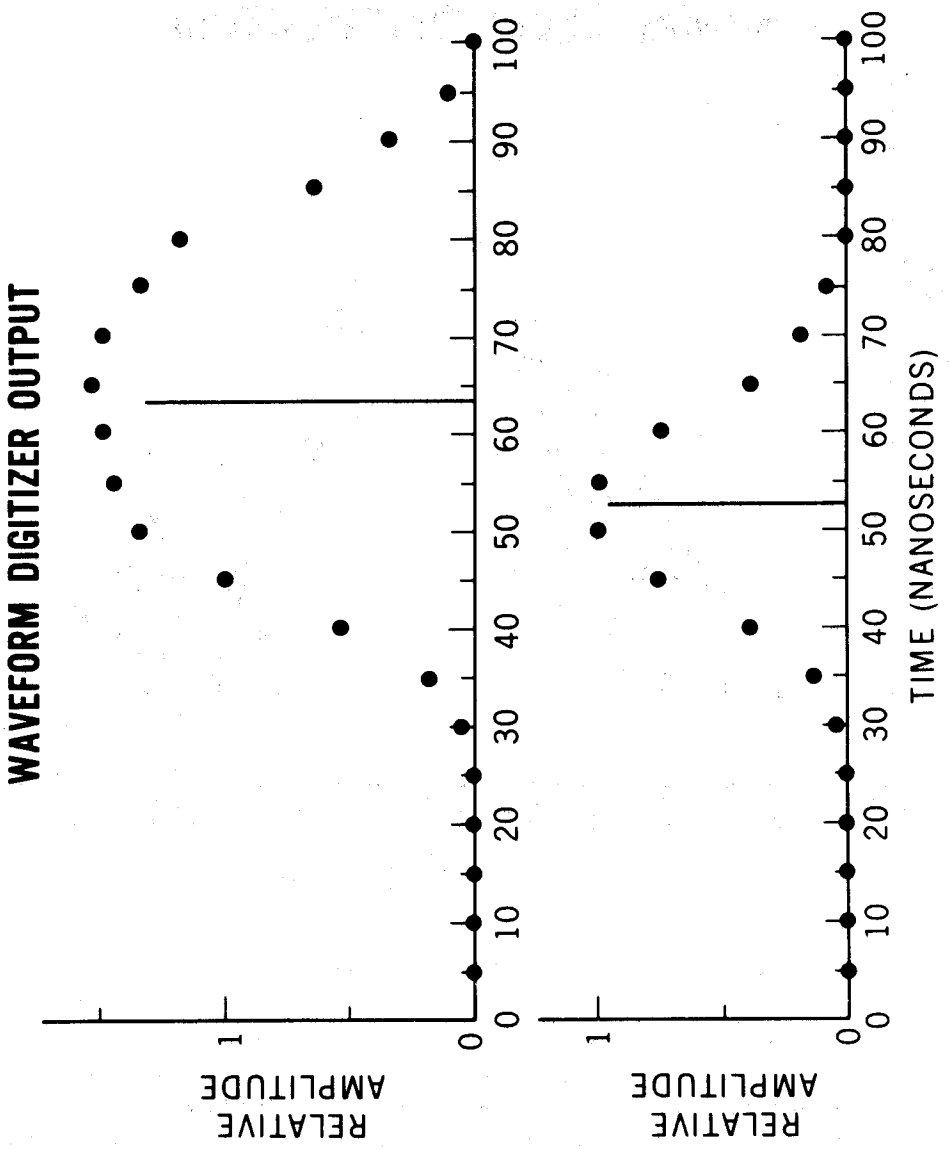

Figure 15. Results from Use of Waveform Digitizer

RANGING DATA RMS

STALAS	9 TO 16 cm	(11 cm AVE.)
MOBLAS 1	11 TO 25 cm	(16 cm AVE.)
MOBLAS 2	10 TO 16 cm	(13 cm AVE.)

PULSE POSITION MEASUREMENT ACCURACY

$$\frac{\text{DATA RMS}}{\sqrt{10}} = \frac{15}{\sqrt{10}} = 4.7 \text{ cm}$$

Figure 16. RMS Ranging Scatter Obtained During Calibration Tests of Goddard Space Flight Center Systems

CALIBRATION ERROR SOURCES

DISTANCE FROM TRACKER AXIS TO CALIBRATION TARGET	± 1.5cm
ATMOSPHERIC PROPAGATION	± 0.6
TIME INTERVAL MEASUREMENT PRECISION	$\frac{\text{RMS MEASUREMENTS}}{\sqrt{\text{NO. OF MEASUREMENTS}}}$

Figure 17. Calibration Error Sources

long.

That is the basis of my confidence. We are now developing a 0.2 nanosecond system. The first of these is being sent to the Haleakala lunar ranging station. As shown in the right hand column of figure 19, if we did very little more than replace a 20 nanosecond system with a 0.2 nanosecond system, we would end up with a 5 cm uncertainty.

This should happen with the NASA mobile stations within the next few years. After the short pulse lasers are introduced, we can further improve the detection systems for measuring the pulse position and we can improve the clock synchronization and get down to about 2 cm. I am confident this can be done.

The above is a slightly edited transcript of a presentation to Session F on Wednesday 28 November 1973.

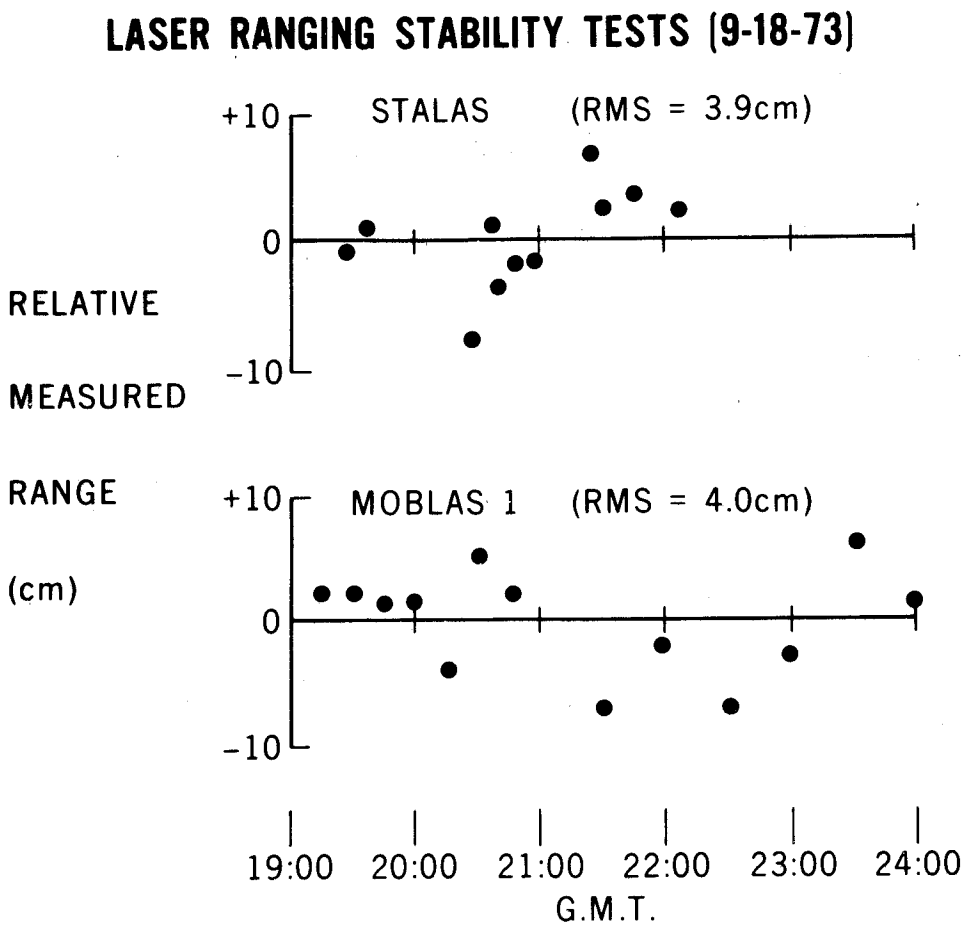

Figure 18. Tests to Monitor the Stability of Calibration on Two of the Goddard Ranging Systems

2. Discussion

ANGUS-LEPPAN: Any special reason why few technical details have been published on the Goddard laser ranging systems?

PLOTKIN: There is no reason for this other than sloth.

WALCOTT: Is there going to be a synchronous satellite with retro-reflectors?

PLOTKIN: There are none now planned. The highest is TIMATION III at 14,000 km. LAGEOS planned for launch in 1976 will be at 6,000 km. Incidentally, these two satellites will satisfy ONG's geometry very well.

ONG: You mentioned an array size of 1 m diameter and a 3 cm accuracy over the range. I am puzzled as to how that can be done.

PLOTKIN: These are figures for GEOS-C. If you have a very short pulse incident on GEOS-C, it would only illuminate a few reflectors facing the incident ray and the returned pulse

LASER RANGING ACCURACY

	20 NS LASER		0.2 NS LASER
• CALIBRATION	2.2cm		1.6cm
• PULSE POSITION MEASUREMENT $(15/\sqrt{10})$	4.7	$(1.5/\sqrt{10})$	0.5
• SYSTEM STABILITY	4.0		0.4
• CLOCK SYNCHRONIZATION (5 μs)	3.5		3.5
• ATMOSPHERIC PROPAGATION	3.0		3.0
• S/C ARRAY GEOMETRY $(9/\sqrt{10})$	2.9	$(2/\sqrt{10})$	0.6
TOTAL RSS	8.5cm		4.9m

Figure 19

would be about 20 cm long. If the signal is very good, as it is for GEOS-C, you should be able to trace the shape of the pulse in a waveform synthesizer and locate the centroid. If the signal strength were infinitely good, this can be done with extreme precision. However, what happens here is that within the pulse there will be scintillations bacause the different reflectors will interfere with one another. Because of those random scintillations we cannot determine the centroid of the 20 cm long pulse with infinite precision; for that geometry and a 20 cm pulse, the uncertainty will be about 20 cm.

PÂQUET, P.
DEJAIFFE, R.
Observatoire Royal de Belgique
Avenue Circulaire 3
B-1180 Bruxelles,
B E L G I U M

Proc. Symposium on Earth's Gravitational Field & Secular Variations in Position (1973), 347-359.

ANALYSIS OF THE FIRST DOPPLER OBERVATIONS PERFORMED AT THE ROYAL OBSERVATORY OF BELGIUM

ABSTRACT

This paper contents a comparative analysis of the results obtained in Brussels by both astronomical and doppler measurements. This study is limited at the internal and external errors distributions. However, the existence of a drift between the NWL and the BIH system is clearly shown. The geodetic coordinates of the station deduced from doppler observations are:

$\lambda = 4^{o}21'31''.113 \pm 0.007, \quad \phi = 50^{o}47'54''.893 \pm 0.003$

1. Introduction

In May 1972 one of the TRANET Doppler Stations was loaned by the US Navy to the Royal Observatory of Belgium, in Brussels. Operational on 23 June, 1972, this station - referred to as TRANET station 021 - is uninterruptedly observing since this date.

Radioelectric observations performed by these Tranet stations permit determinations of the polar motion besides other geodetic goals. Since 1969 the Naval Weapons Laboratory (NWL, Dahlgren, Va.) determines the polar motion generally from the observations of the 1967-92A satellite which is one of the five still in operation Transit satellites.

The deflection of the vertical prevents any direct comparison between astronomical coordinates and results obtained by the Doppler method. However, these two techniques can be compared according to the following points of view:

- global results such as for example, polar motion curves deduced by each of these two techniques;
- evolution of the longitude differences;
- residuals associated with observed elements.

A comparison of the instantaneous astronomical latitude of the Uccle-Brussels station deduced from the BIH (Bureau International de l'Heure, Paris) and the NWL polar motion is presented in figure 1. This figure clearly shows apparently a reduction of the amplitude and a phase of a few days in the NWL observations. These characteristics indicate the existence of a drift in one of these two systems with respect to the other. An homogeneous series extended over some years will probably permit the unification of these two coordinate systems.

In this paper the analysis of the results is limited to the study of the internal and external errors distribution of the doppler method. Also included is a comparison of the same kind of errors tied with the astronomical observations performed at Uccle with a Danjon astrolabe.

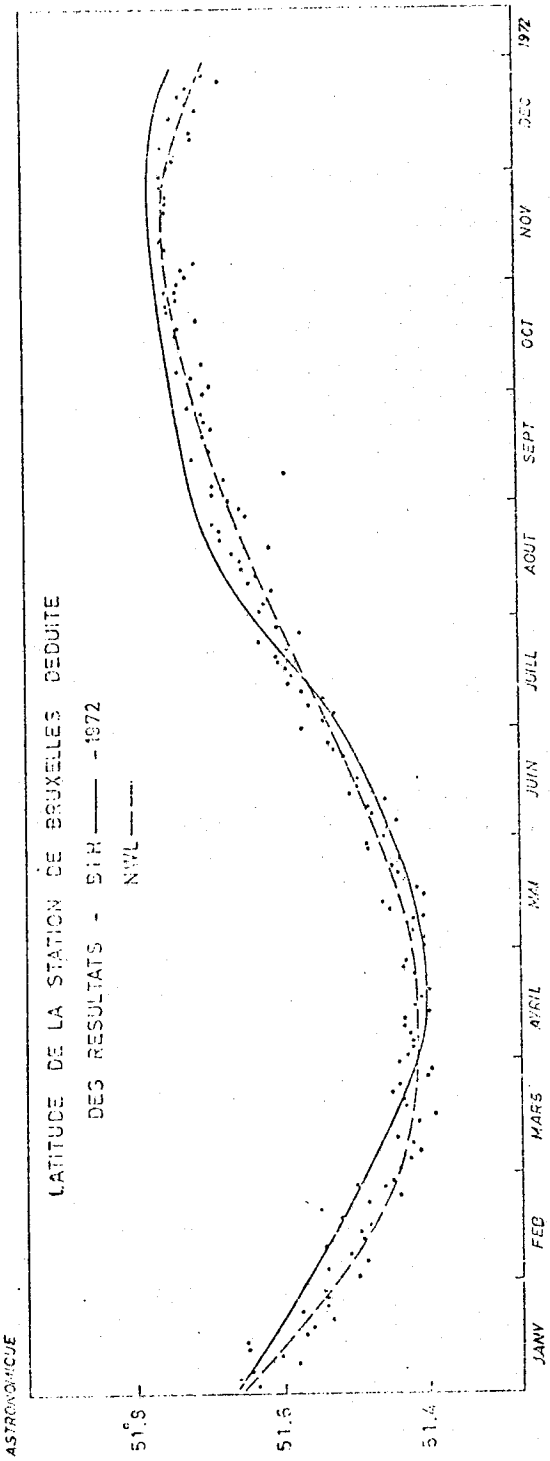

Figure 1. Comparison of the Instantaneous Astronomical Latitude of the Uccle - Bruxelles Station Deduced from the BIH and the NWL Polar Motions

2. Data Reduction

The observed data reduction procedure for the whole Doppler stations has been described by R. J. ANDERLE (1970; 1971). For a better understanding of the elements at our disposal, we indicate that the procedure in use is divided in two steps:

i) On each period of two days and from the complete observational material provided by the whole stations, NWL computes one improved orbit of which the orbital parameters are known in the instantaneous frame of reference;

ii) then this improved orbit and the mean coordinates (λ_M, ϕ_M) of the stations are used for an individual analysis of all the passes considered in the first reduction phase.

The differences between theoretical and experimental values of the frequencies drifts, due to the Doppler effect, lead to the observational equations of which the station coordinates and the frequency of the embarked oscillator in the satellite are the unknowns.

Practically these coordinates of the considered station are indirectly determined by the intermediate of two particular coordinates tied to the orbit.

The origin is located at the point which corresponds to the theoretical minimal distance between the station and the satellite. This origin is then fixed from the station mean coordinates and from the improved orbit. At this particular point there is no Doppler effect. The $\underline{r}$ vector along the origin-station direction and the $\dot{\underline{r}}$ vector directed perpendicular to the $\underline{r}$ vector are two of the coordinate axis system. These two components are respectively defined as slant range and along track components.

For polar orbits, as it is the case for the satellites observed by the Tranet stations, figure 2 shows that the observed along track displacement is nothing else than the Δu difference between the instantaneous and the reference equators. Indeed if the Earth rotation axis did not change the station S would follow the nonperturbed path AA_1; due to the displacement of the pole from CIO (Conventional International Origin) to P the station S really moves along BB_1. During the successive passes above the horizon of station S the along track component (ATC) successively measures the Δu_i displacements.

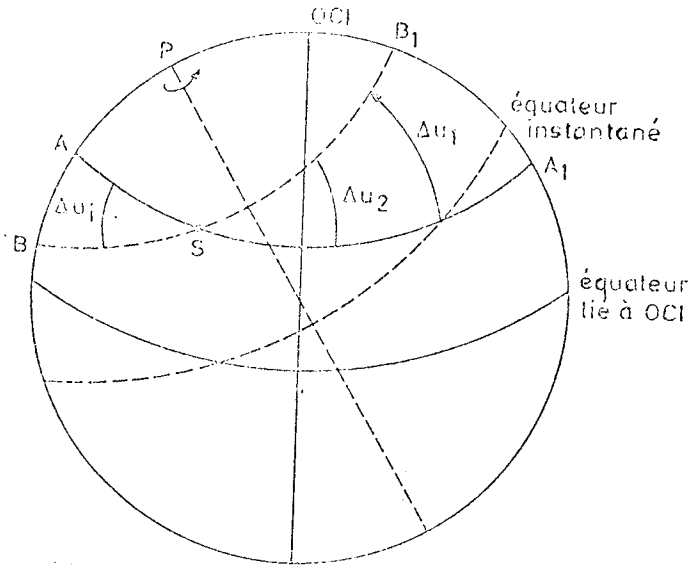

Figure 2. Geometrical Configuration

In each 48 hours time interval the ATC presents two diurnal periods tied with the polar motion. In analysing this component NWL deduces the amplitude and the phase or yet the (x,y) coordinates of the instantaneous pole (ANDERLE 1970).

3. Internal Coherence

From each individually analysed pass one can deduce:

i) the along track and slant range displacements;

ii) the observed ellipsoidal coordinates at which the polar motion corrections have already been applied;

iii) the mean square errors (mse) associated with each of these elements.

As they result from the individual analysis of passes these mse are tied with the *internal errors*.

Table 1 contains the arithmetic mean of these mse computed for the 503 first observed passes in Uccle and the standard deviation σ of their distribution. In (a) all the passes have been considered while the results in (b) have been obtained after elimination of the values greater than 2.57σ. In this same table one can also find the internal errors computed from the results of 343 astronomical observations performed in Uccle with a Danjon astrolabe. These errors are the errors associated with each latitude and longitude determination from the observations of only one group of stars.

T A B L E 1

Internal Coherence

Doppler Measurements				
	Longitude	Latitude	Along Track	Slant Range
N	503	503	503	503
(a) Mean	0''109	0''038	1.27 m	0.93 m
σ	0''248	0''043	1.77 m	1.51 m
N	491	486	491	495
(b) Mean	0''079	0''033	1.07 m	0.78 m
σ	0''081	0''022	0.82 m	0.55 m

Astrolabe Observations		
	Longitude	Latitude
N	343	343
(a) Mean	0''113	0''111
σ	0''101	0''101
N	336	334
(b) Mean	0''104	0''101
σ	0''043	0''043

The distribution in percentage of the internal errors in the four components has been plotted in figures 3 through 6 for the totality of the considered passes. On figures 4 and 5 the same distribution has also been represented for the astrolabe observations. It must be noticed that if the internal coherence may be compared for the longitude, the Doppler measurements are really better than the astrolabe results for latitude determinations. This is due to the fact that the analysis is performed only with polar satellites.

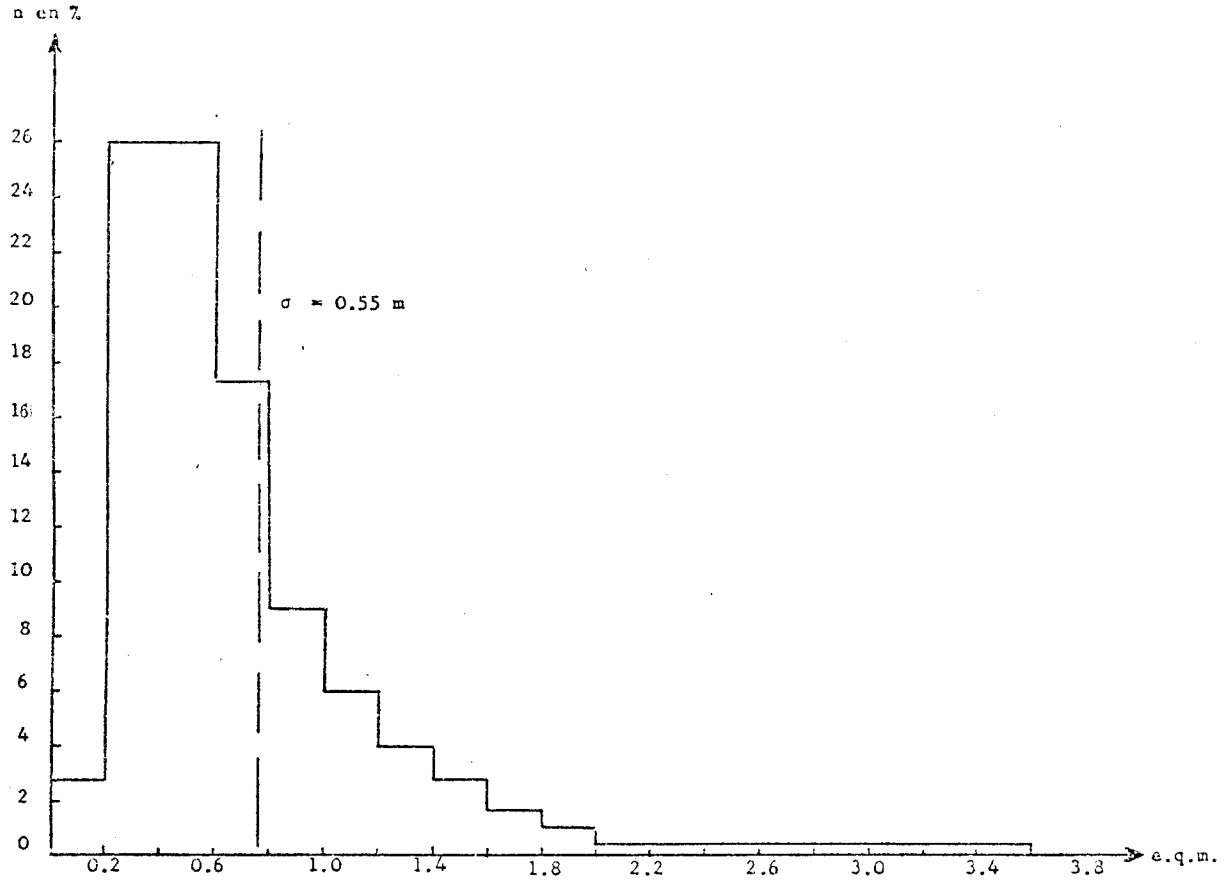

Figure 3. Internal Errors : mse Range Distribution
Mean Value : 0.78 m

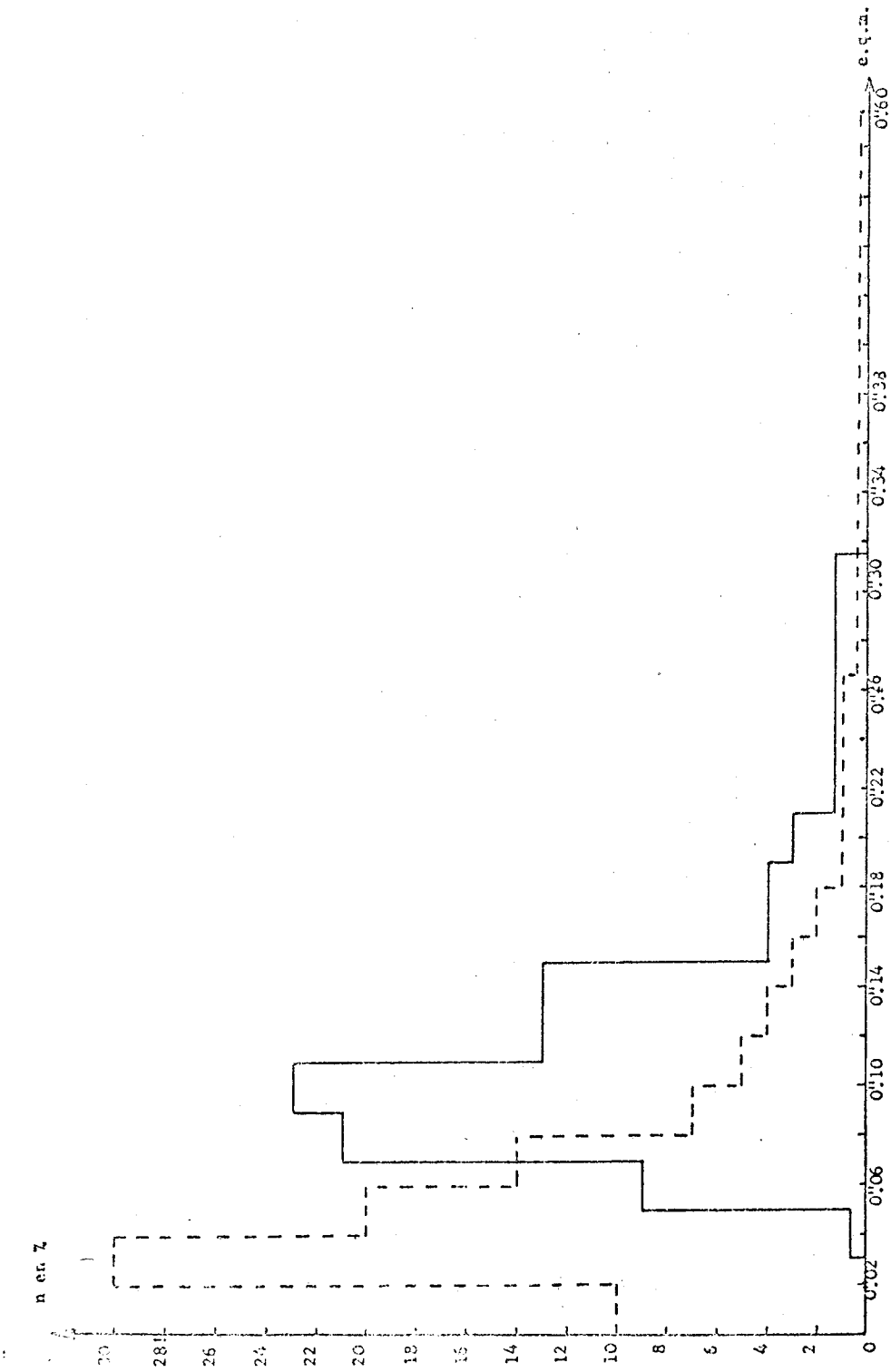

Figure 4. Internal Errors : mse Longitude Distribution -
Mean Values: (D) 0"079; (A) 0"104

——— Astrolabe ---------- Doppler

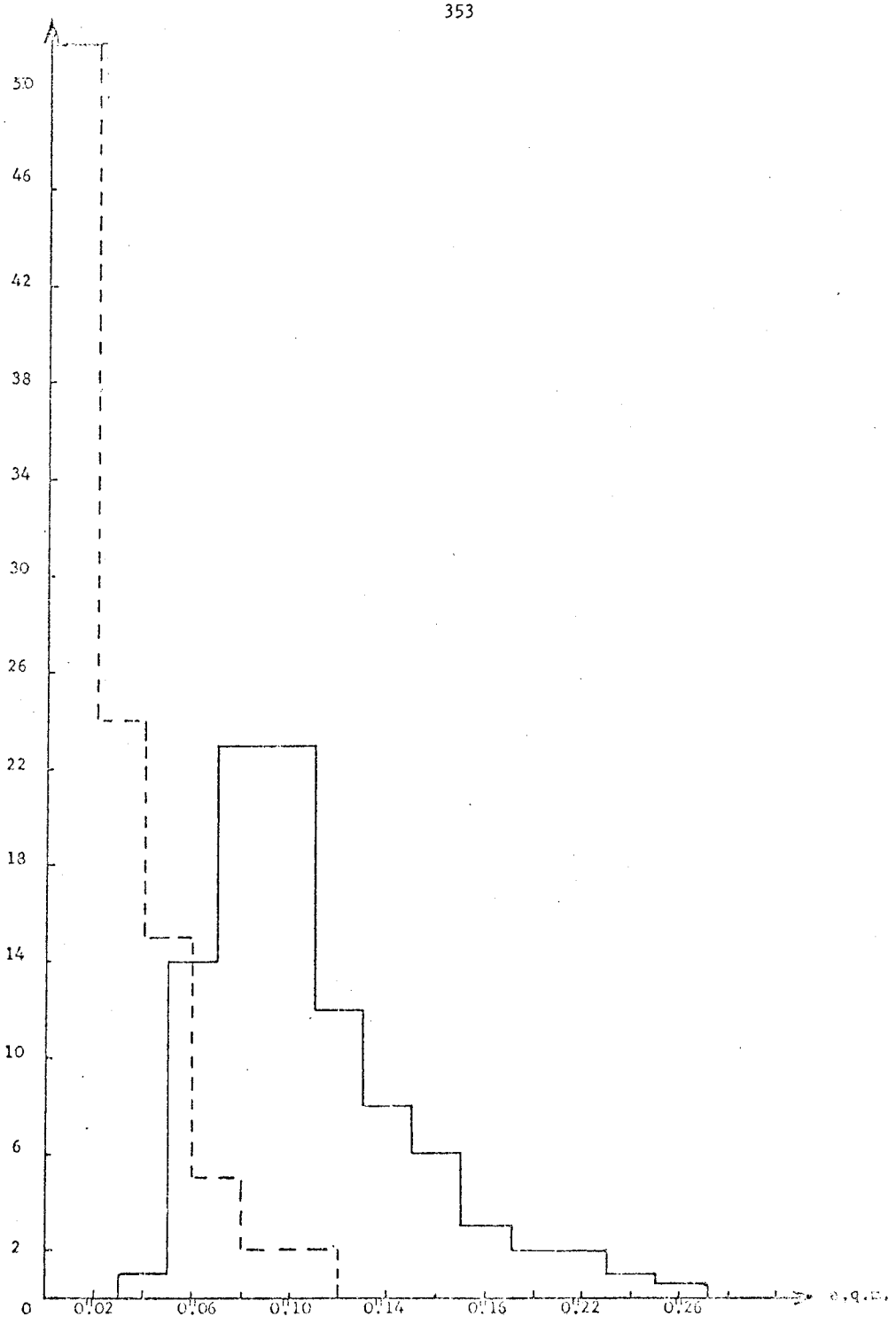

Figure 5. Internal Errors : mse Latitude Distribution -
Mean Values: (D) 0".033; (A) 0".101
——— Astrolabe ---------- Doppler

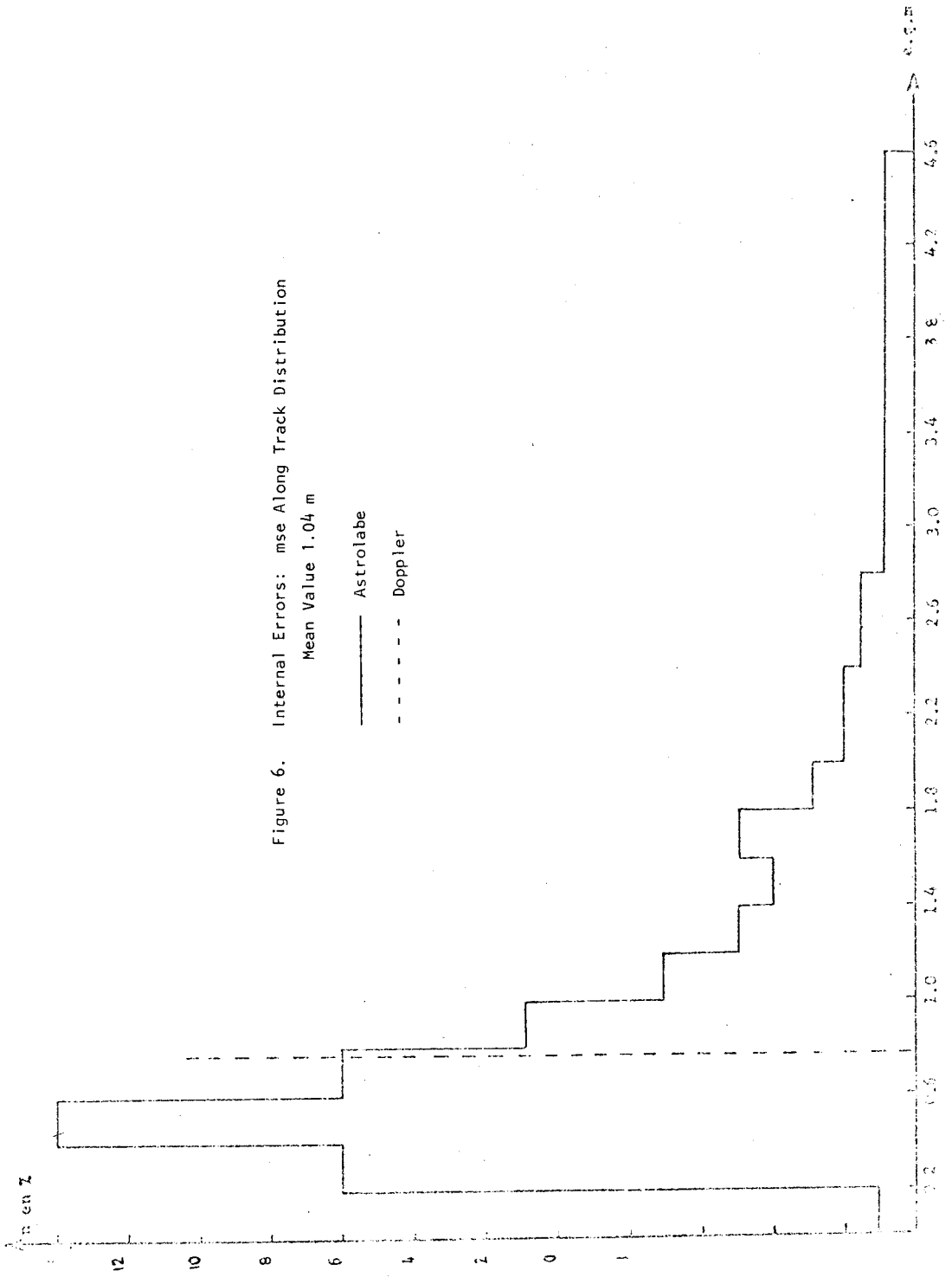

Figure 6. Internal Errors: mse Along Track Distribution
Mean Value 1.04 m

4. External Coherence

If (λ_N, ϕ_N) denote the mean coordinates of a station in the fixed NWL frame of reference, the instantaneous coordinates $(\lambda_{inst}, \phi_{inst})$ deduced from the individual analysis of each pass are brought back in this NWL frame of reference by the relations :

$$\lambda_{obs,N} = \lambda_{inst} + x \tan \phi_N \sin \lambda_N - y \tan \phi_N \cos \lambda_N$$

$$\phi_{obs,N} = \phi_{inst} - x \cos \lambda_N - y \sin \lambda_N.$$

The residuals

$$r_\lambda = \lambda_N - \lambda_{obs,\,N}$$

$$r_\phi = \phi_N - \phi_{obs,\,N}$$

are defined as the *external errors*.

Table 2 gives the standard deviation σ_D of these errors distribution. This table also contains the standard deviations of the distributions of the external longitude and latitude errors obtained with an astrolabe:

$$r'_\lambda = (UT_o - UTC)_{Ucc} - (UT_o - UTC)_{BIH}$$

$$r'_\phi = \phi_{obs} - \phi_{Ucc,BIH}$$

where $\phi_{Ucc,BIH}$ denotes the instantaneous Uccle latitude deduced from the BIH polar motion curve. $(UT_o\text{-}UTC)$ and ϕ_{obs} are deduced from each group of stars. Each line of Table 2 represents the standard deviation of a new distribution obtained in eliminating residuals which are greater than 2.57 the σ value of the precedent line.

The distribution of the random errors of the measurements made by the Doppler and by the astronomical method are shown in figures 7 and 8.

5. Conclusions

In order to obtain a standard deviation value for the longitude which may be compared with the astrolabe one (0".20) about five passes in one hundred have to be abandoned. If one tries to obtain a significant improvement, this percentage rises up to 7.5 . In any case this elimination does not seem excessive in practice.

In the calculation of the astrolabe external errors the annual corrections published by the BIH have not been applied. The latitude internal and external coherences are of the same order of magnitude; that corresponds to the well-known quality of the astrolabe. But in longitude a variation by a factor two occurs. This last remark is a peculiar characteristic of the Uccle astrolabe which has always given less good results in longitude than in latitude (GUINOT et al 1972).

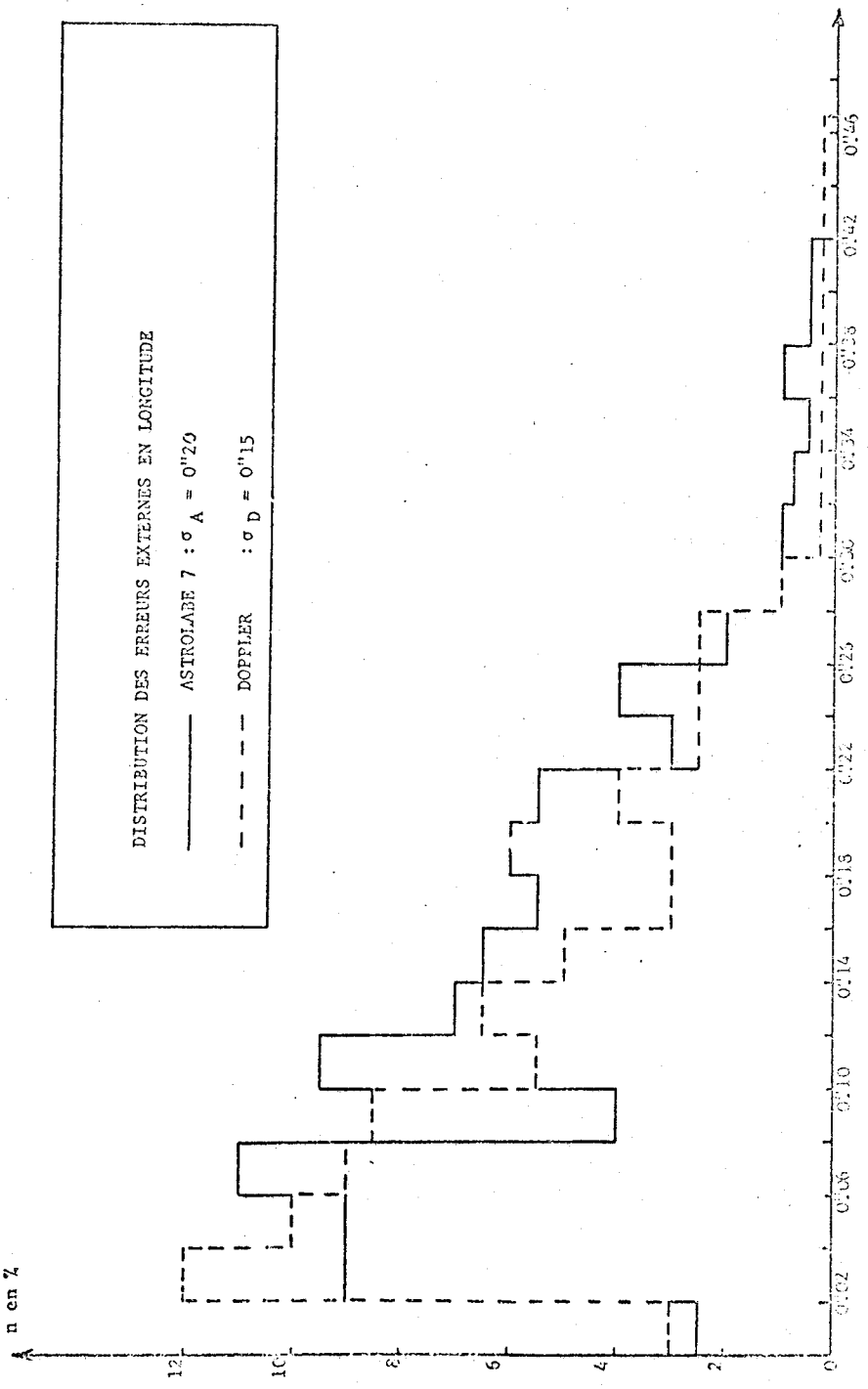

Figure 7. Longitude External Errors Distribution

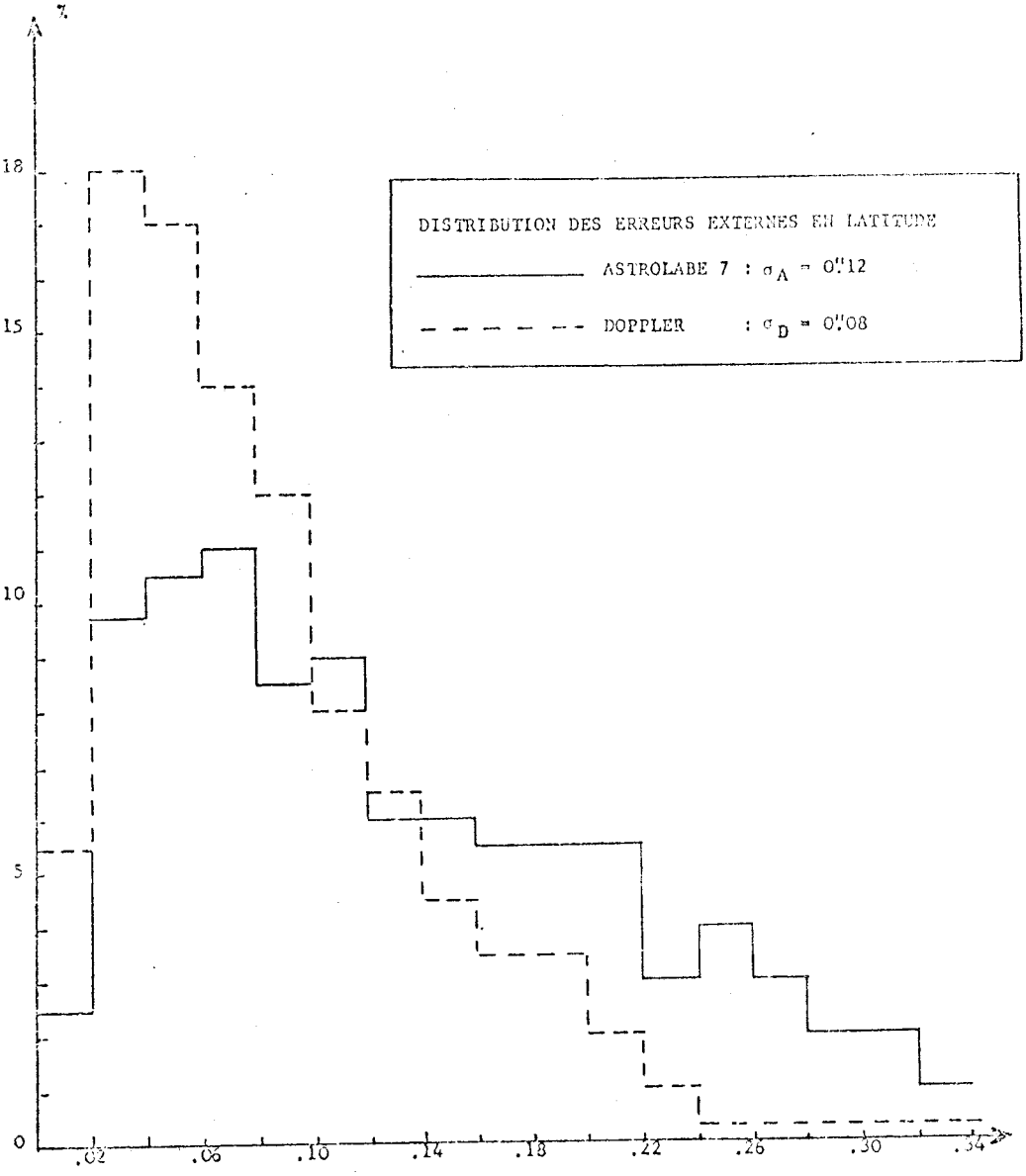

Figure 8. Latitude External Errors Distribution

Finally, in making use of the doppler observations mentioned in the last line of table 2, the coordinates and the corresponding accuracy of the Uccle-Brussels station have been deduced and this important result is given hereafter:

$\lambda = 4^{o}21'31''.113 \pm .007 \qquad \phi = 50^{o}47'54''.893 \pm .003$

TABLE 2

External Coherence

Doppler Measurements			
Longitude		Latitude	
N	σ	N	σ
503	0''667	503	0''116
493	0''279	496	0''091
476	0''189	486	0''084
465	0''154	484	0''083
Astrolabe Observations			
Longitude		Latitude	
N	σ	N	σ
274	0''222	274	0''141
270	0''207	268	0''131
268	0''202	266	0''128

6. References

ANDERLE, R.J. 1971. Refined geodetic results based on Doppler satellite observations. *NWL Technical Report TR-2889.*

ANDERLE, R.J. 1970. Polar motion determinations by US Navy Doppler satellites observations. *NWL Technical Report TR-2432.*

GUINOT, B., FEISSEL, M. & GRANVEAUD, M. 1972. Rapport annuel pour 1971. *Bureau International de l'Heure.* Paris.

7. Discussion *

LLOYD: What method is used to correct for refraction, especially for ionospheric effects and secondly for lower atmosphere effects?

MELCHIOR: Corrections for atmospheric effects are made by NWL. There are two frequencies 400 MHz and 150 MHz. By using that you can eliminate the ionospheric effect because the Doppler effect is proportional to the frequency, while the ionospheric effect is inversely proportional to the frequency. A better precision could be obtained if we had a third frequency in GHz. I don't believe the lower atmosphere has any effect on Doppler. As regards the tropospheric effect, ten years ago when they developed the Doppler system, they made meteorological

measurements to try and correct the Doppler. But it was not successful and finally they just adopted a model and this seems to be the best way.

WALCOTT: In addition to your operation, there will also be satellite Doppler alongside the two PZT's in Canada. It will be interesting to compare the results.

MUELLER: As the computations were done by NWL (US Naval Weapons Laboratory, Dahlgren Virginia), I presume the NWL ephemeris was used in these calculations.

MELCHIOR: Yes.

* The paper was presented on behalf of the authors by P. MELCHIOR.

SIRY, J.W.
National Aeronautics & Space Adminsitration
Washington, DC 20546
United States of America

Proc.Symposium on Earth's Gravitational Field & Secular Variations in Position (1973),360-379.

SATELLITE TECHNIQUES FOR THE STUDY OF SECULAR VARIATIONS IN POSITION

ABSTRACT

Secular variations in position are associated with seismic activity on a number of occasions. Crustal motions of the order of several centimetres, for example, have been observed to precede earthquakes. SCHOLZ, SYKES & AGGARWAL (1973) propose a model which relates these and other precursory phenomena to dilatancy. They present evidence linking the precursor time interval with the earthquake magnitude and the length of the aftershock zone. Dilatant regions of the order of a few tens of kilometres in scale and precursor time intervals ranging from roughly half a year to a year and a half are expected to be of interest in connection with earthquakes of magnitude six, for example. The dilatancy mechanism seems to be operative in the case of thrust faults and probably also in the case of some strike-slip events. A system for sensing precursory crustal motions should thus have the capability for determining site positions with an accuracy of the order of a couple of centimetres in a time interval of approximately a quarter of a year at spacings of roughly ten kilometres in a region of interest such as a fault zone. Several hundred such locations are needed to cover the fault systems in the California area.

A system for monitoring such precursory crustal motions is presented. It involves a set of automated corner reflector stations tracked by means of a laser operating in the Geopause satellite. It should be possible to range some three times during every Geopause pass to each of the sites in such an ensemble, weather permitting. One centimentre range data gathered during a quarter of a year should yield position component accuracies of the order of a couple of centimetres. A laser beam of a tenth of a milliradian in diameter would, in general, illuminate a single station in such an array. A broader beam would generate reflections from several sites, yielding overlapping data. A chain or pattern of such overlapping regions can strengthen the solution for site positions. Pressure, temperature and humidity gauges can provide refraction correction data. Turnaround transponders interrogated by the Geopause radio tracking system can furnish corresponding data in excessively cloudy regions.

This concept based on satellite techniques offers the prospect of a practical approach to the problem of monitoring secular variations in position such as precursory crustal motions.

1. Introduction

Secular variations in position of more than one kind are associated with seismic activity on a number of occasions. Some are viewed in terms of strain in regions near earthquake fault zones. Others associated with dilatancy are thought to have a more specific precursory nature.

2. Crustal Motions which are Precursory to Earthquakes

Precursory phenomena of several types have been observed to precede earthquakes. Among these are crustal motions, variations in the ratio of the seismic compressional velocity, V_p, to the seismic shear velocity, V_s, and changes in the electric resistivity, magnetic fields, radon emission, and

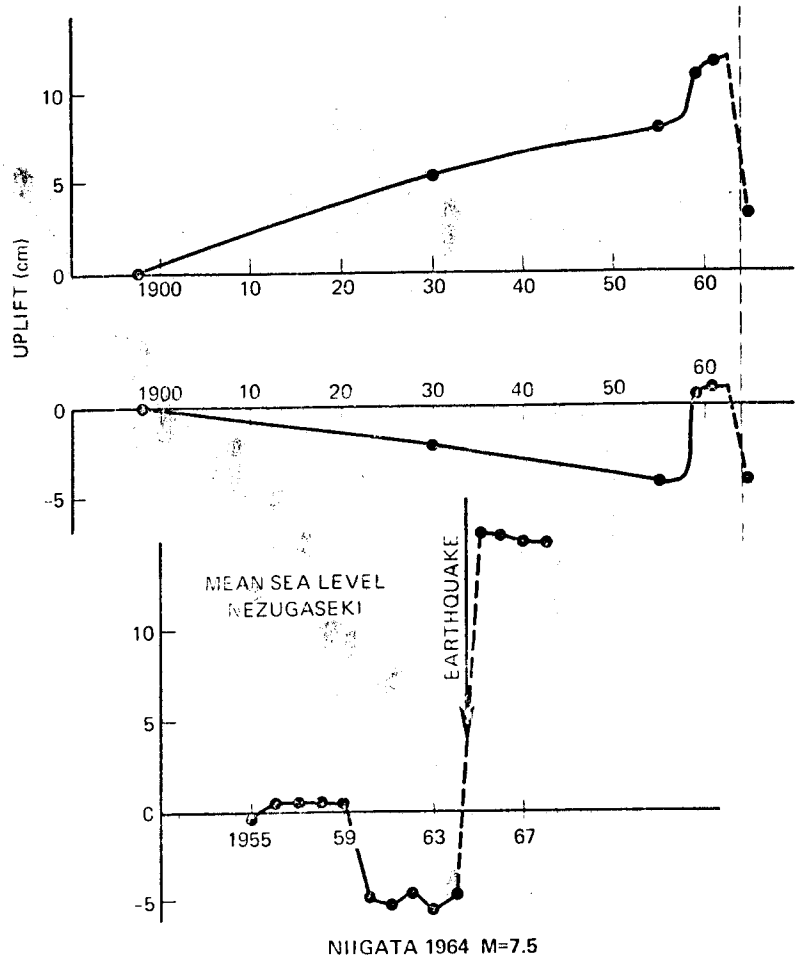

Figure 1. Earthquake Related Secular Variations in Position in Japan (SCHOLZ ET AL 1973). Sea Level Data corrected for oceanographic and meteorological conditions (YAMAGUTI 1968); Levelling data from (TSUBOKAWA ET AL 1968)

the relative numbers of large and small seismic shocks (SCHOLZ ET AL 1973; WHITCOMB ET AL 1972; KELLEHER ET AL 1973). An example of vertical crustal motion occurring before a large earthquake is seen in figure 1.

A model which relates these various premonitory effects to dilatancy has been proposed by SCHOLZ, SYKES & AGGARWAL (1973). They present evidence linking the precursor time interval with the magnitude of the subsequent earthquake. This is seen in figure 2. The long term precursory effects occur months and even years prior to large earthquakes. They also find a connection between the precursory time interval and the length of the aftershock zone, which is taken as a characteristic dimension. This is exhibited in figure 3. These data relating a variety of different phenomena are in good agreement with the diffusion relation. This circumstance lends further support to the dilatancy theory as an explanation of the array of effects.

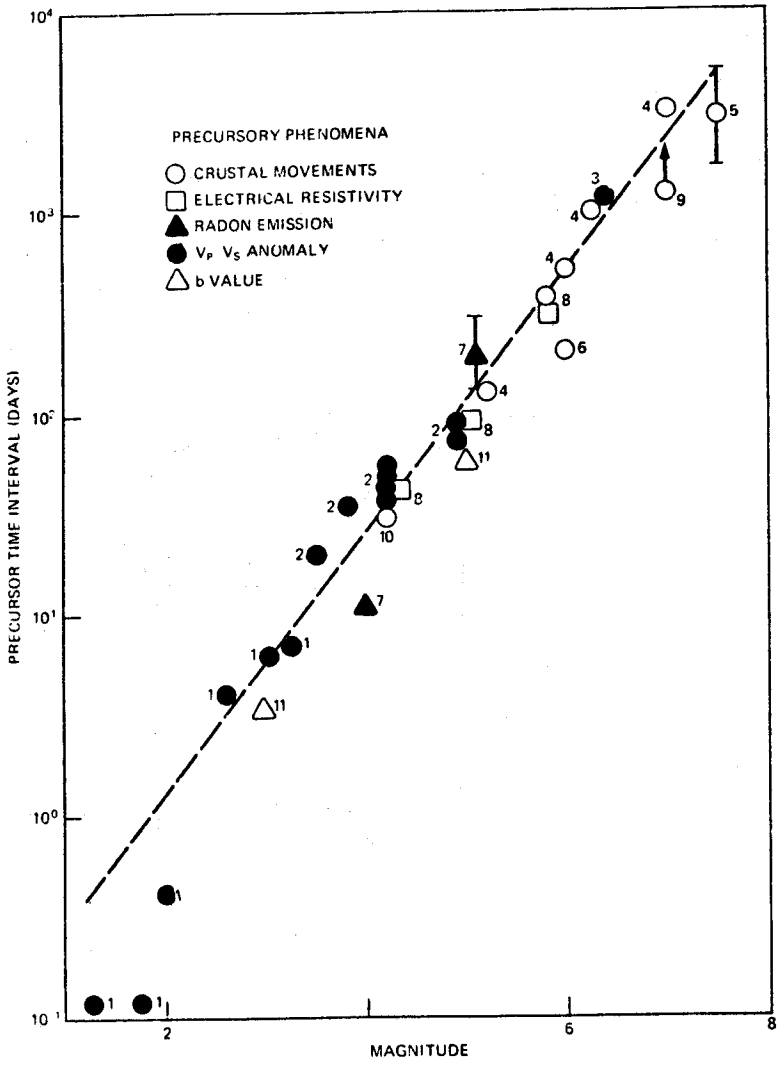

Figure 2. Precursor Time Interval as a Function of Earthquake Magnitude (SCHOLZ ET AL 1973)

The scale of the dilatant region is thus an indicator both of the magnitude of the subsequent earthquake and of the time interval between the earthquake and the precursory phenomena such as crustal motion. The dilatant region itself is about twice the length of the fault or the aftershock zone.

At thrusting faults the vertical precursory crustal motions are of the order of several centimetres. There is also some evidence in connection with the Danville, California earthquake which indicates that it is appropriate to view at least some strike-slip events in terms of the dilatancy mechanism. The vertical components of the motion will be approximately a third of the horizontal strain for shallow earthquakes, i.e., ones for which the depth is small relative to the dimension of the source. This is true for the moderate and large California earthquakes. Scholz, Sykes & Aggarwal point out

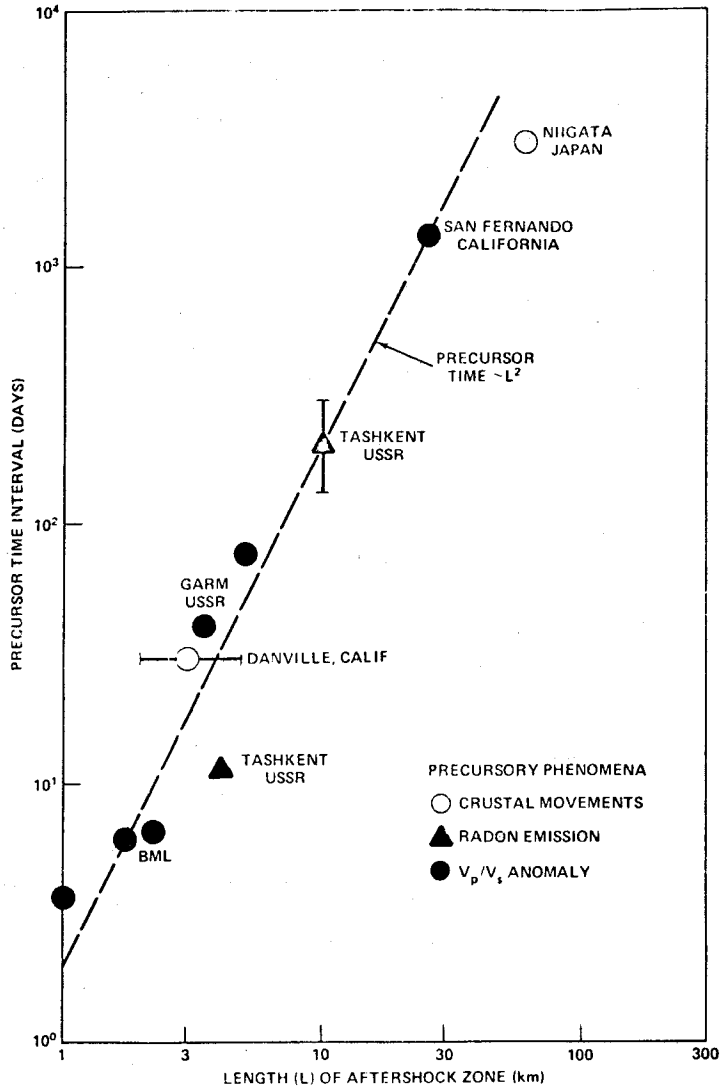

Figure 3. Precursor Time Interval as a Function of the Length of the Aftershock Zone (SCHOLZ ET AL 1973)

that, although they cannot demonstrate that premonitory effects occur before shocks deeper than about 10 to 15 km, the depth range where the effect is observed includes virtually all earthquakes on or near the San Andreas fault system in California and most of the world's damaging earthquakes (SCHOLZ ET AL 1973).

Earthquakes of magnitude six or larger can cause significant damage as is pointed out, for example in figure 4 which is presented in the NASA Earth and Ocean Physics Applications Program (EOPAP) Plan (NASA 1972).

Earthquake	Magnitude	Estimated Property Damage ($ × 10^6) Contemporary $	1966 $*	Estimated Loss of Life
San Fransisco, Calif. April 18, 1906	8.3	400	2600	700
Alaska March 27, 1964	8.5	311		114
Long Beach, Calif. March 10, 1933	6.3	50	170	120
Kern County, Calif. July 21, 1952	7.7	50		12
Aleutian Islands April 1, 1946	7.4	25**		173**
Puget Sound, Wash. April 13, 1949	7.0	25		8
Puget Sound, Wash. April 29, 1965	6.5	12		6
Hegben Lake, Mont. August 17, 1959	7.1	11		28
Santa Barbara, Calif. June 29, 1925	6.3	8	26	13
Imperial Valley, Calif. May 18, 1940	7.1	5		9
Montana Series October & November 1935	up to 6.2	4		4
San Fernando, Calif.† February 9, 1971	6.6	553		64

Figure 4. Property Damage and Loss of Life from Major Earthquakes in the United States in the Present Century

* Based on *Engineering News Record* Building Cost Index

** Most of the damage and loss of life resulted from the tsunami that hit the Hawaiian Islands

† The San Fernando, California Earthquake of February 9, 1971. *Professional Paper* 733, U.S. Geological Survey, U.S. Government Printing Office, Washington DC.

3. Preliminary Design Parameters for a Precursory Crustal Motion and Regional Strain Field Monitoring Network

3.1 Crustal Motion Characteristics of the Dilatancy Model with Particular Reference to Major Earthquakes

A magnitude six earthquake can be characterized in an order of magnitude way in terms of the preceding discussion as one associated with a dilatancy which precedes the earthquake by a time interval of the order of half a year to a year and a half, and a dilatant region some 20 to 30 km long, which is marked by crustal motions having a scale of several cm in the case of thrusting faults and at least some strike-slip faults (figure 5).

A system for monitoring such precursory crustal motions can be an important element of an earthquake prediction capability. Such a system would involve an array of stations about 5 to 10 km apart along the fault deployed in two lines symmetrically placed on each side of it and separated by a distance

A Magnitude 6 Earthquake can be Characterized in an Order of Magnitude Way as Follows:

Precursor Time Interval:	0.5 - 1.5 yr
Fault Length:	10 - 15 km
Dilatant Region Length:	20 - 30 km

Crustal Motion in Dilatant Region:
At Thrusting Fault - Several cm Vertical Motion
At Strike-Slip Fault -
Vertical Motion ∿ 1/3 Horizontal Motion

Scale of Dilatant Region is an Indicator of Time and Magnitude of Subsequent Earthquake

Figure 5

comparable to the interval between the sites in each line. This arrangement is indicated in figure 6. This means an average of one site for roughly every four km of fault line. Position components should be measured to the order of a centimetre or two in times of approximately a quarter of a year or less.

3.2 The California Region Viewed from the Standpoint of Possible Criteria for Predicting Earthquake Locations

An extensive study of possible criteria for predicting earthquake locations has been conducted by KELLEHER, SYKES & OLIVER (1973). They have categorized segments of the circum-Pacific belt in terms of the following initial set of criteria:

1. The segment is a part of a major shallow seismic belt characterized predominantly by strike-slip or thrust faulting (plate boundaries other than spreading ridges according to plate tectonic theory).

2. The segment has not ruptured for at least 30 years .

The shallow seismic belts which they studied here, i.e., those which satisfy the first of these criteria, are indicated in figure 7a. The segments which meet both of the initial criteria and hence

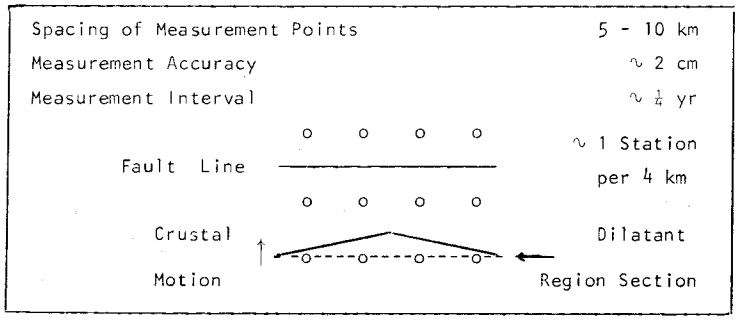

Figure 6. Precursor Crustal Motion Monitoring Network for Major Earthquakes, i.e., M ≥ 6. Preliminary Design Parameters

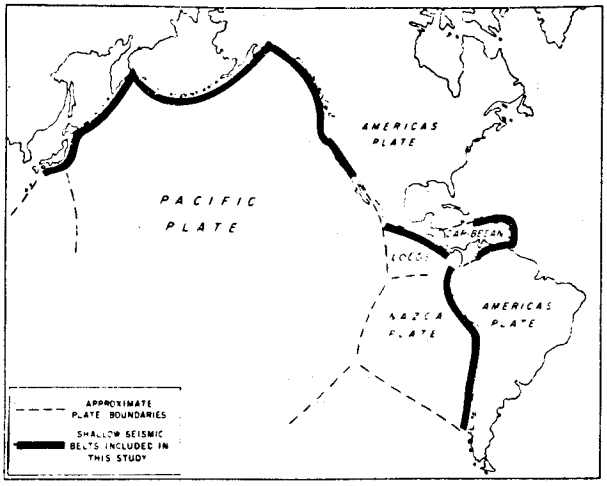

Figure 7a. Major Shallow Seismic Belts Examined by KELLEHER, SYKES & OLIVER (1973)

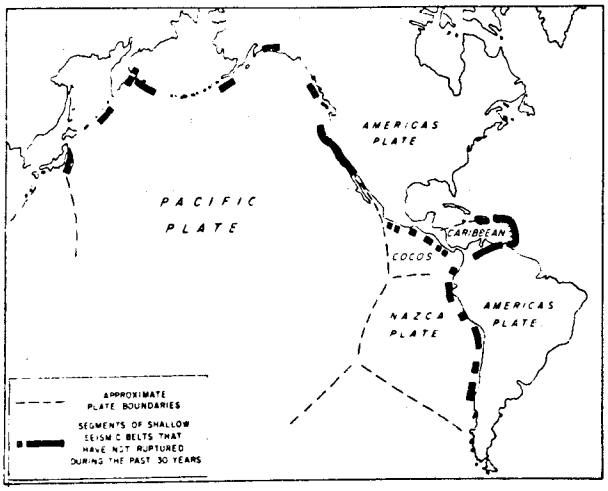

Figure 7b. Shallow Seismic Zones of Figure 7a with Rupture Zones of the past 30 years removed. Zones of Sea Floor Spreading also removed (IBID)

are designated by them as areas of "special seismic potential" are indicated in figure 7b.

Interest in certain of these latter segments of special seismic potential is further heightened if at least one of the following three criteria is fulfilled.

1. A historic record of one or more large earthquakes along a segment is taken as evidence that large earthquakes can again occur along that segment. This criterion is not trivial since several segments along the major plate boundaries examined in this study are not known to have experienced large earthquakes during historic times

2. Evidence based on historical data and relative plate motions suggests that the recurrence interval for large earthquakes is near the duration of the time interval since the most recent large earthquake of that segment.

3. The segment appears to be the site for the next event of a series of earthquakes progressing regularly in space and time.

(IBID)

Areas of special seismic potential which meet at least one of three criteria are shaded doubly in figure 8. Looking more closely at a small part of this region, they find a picture of the San Andreas fault system which is seen in figure 9, where the shading conventions are the same as in the previous figure. Added in figure 9 are indications of the zones of the great earthquakes of 1857 and 1906 (IBID).

Allen views the San Andreas fault system as being composed of five segments for the purpose of estimating the potential for future great earthquakes (ALLEN 1968). He proposed that the 1857 and 1906 earthquake zones are probable locations for infrequent great earthquakes and that the three other segments of the San Andreas system release strain energy by means of creep and small - and moderate- magnitude earthquakes more or less continuously and hence are not likely locales for great earthquakes (KELLEHER ET AL 1973; ALLEN 1968). Significantly, however, SCHOLZ, MOLNAR & JOHNSON (1972) found in the laboratory that a small amount of stable slip always precedes stick slip. It is of interest to note in this connection that the Imperial Valley neighbourhood south east of the 1857 break is an area where strain may be accumulating even though the region is active, as is indicated in figure 10. Similarly, fault creep slippage along the San Andreas is widespread between the 1857 and 1906 earthquake zones, yet the question as to whether strain is accumulating or is already high there is a controversial one (SAVAGE & BURFORD 1970; 1971; SCHOLZ & FITCH 1969; 1970; 1971; NASON 1971; KELLEHER ET AL 1973). KELLEHER, SYKES & OLIVER (1973) point out that special interest must be attached to creeping segments of the San Andreas if creep at active faults indicates high stress. They point, too, to the region southeast of the 1857 earthquake zone as also being of special interest since it has not broken during historic time. Conspicuously high apparent stresses

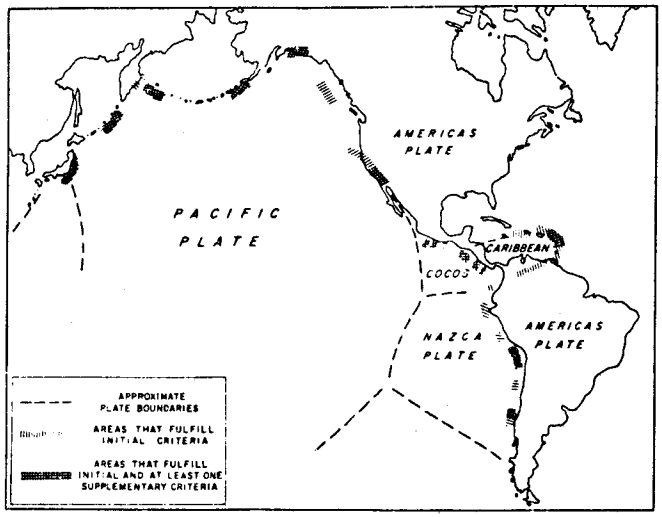

Figure 8. A Summary of Segments and Plate Boundaries that Fulfill the criteria of KELLEHER ET AL (1973) for Identifying Likely Locations for Large Earthquakes of the near future. *All areas that meet these criteria are designated regions of special seismic potential. Because of the scale, the areas indicated are approximate. See reference for detailed description and qualifications.*

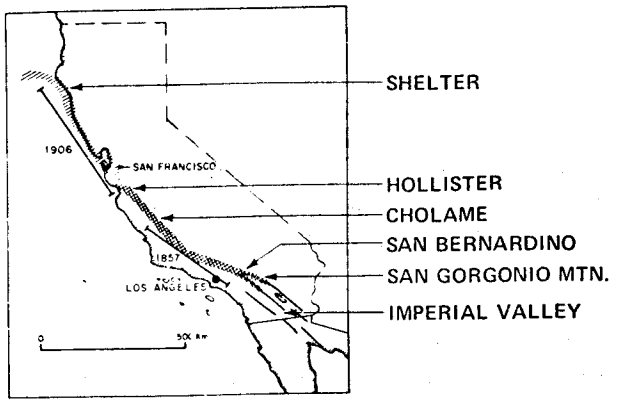

Figure 9. Segments of the San Andreas System that Fulfill Initial or Supplementary Criteria of KELLEHER ET AL (1973)

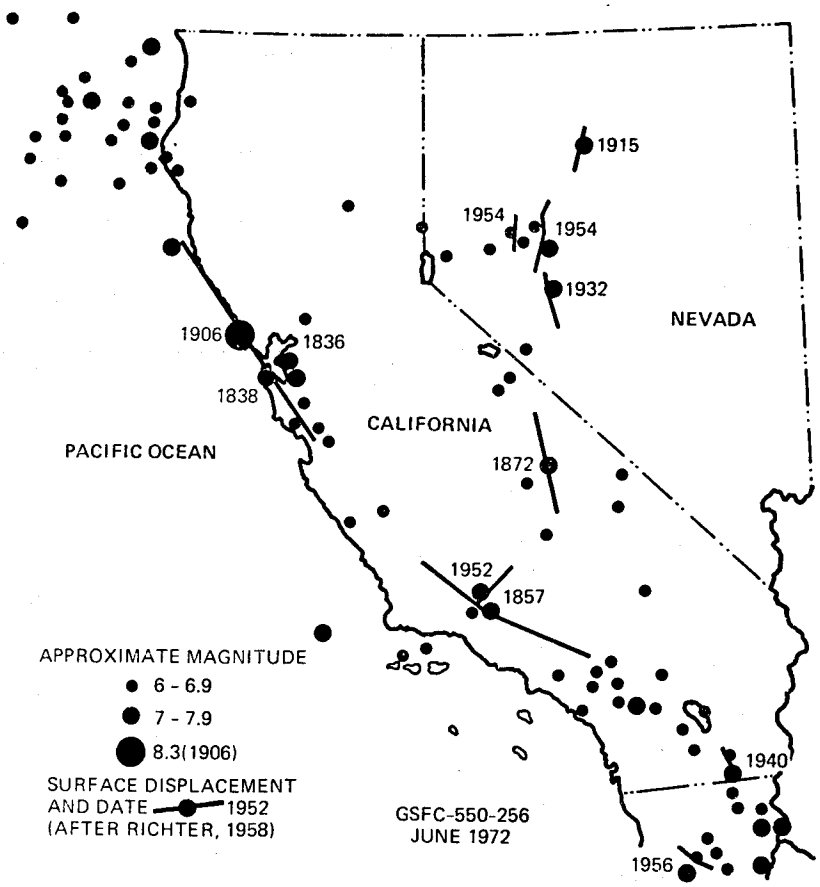

Figure 10. Major Earthquakes Along the San Andreas Fault and in Neighbouring Regions of California and Nevada.

from earthquakes in the area between San Bernardino and the San Gorgonio mountain were observed by WYSS & BRUNE (1971). The location of major earthquakes occurring in eastern California and western Nevada including, for example, the Owens Valley earthquake of 1872 are also seen in figure 10. The segment of the San Andreas fault system having special seismic potential is some 1100 km long, as can be seen in figure 9. The zones of the 1857 and 1906 earthquakes, which are probable locations for future great earthquakes, and hence are of particular interest from the standpoint of the present discussion, are together nearly 800 km long. The San Andreas fault system as a whole is some 1400 km long.

3.3 A Regional Strain Field Monitoring Network

KELLEHER, SYKES & OLIVER (1973) call attention to the clear need for surveys across faults which are paralliel to the Cholame-Hollister fault zone but many tens of km from it. The measurement of regional strain fields is contenplated in the NASA EOPAP Plan (NASA 1972). In California, some of the arrays for this purpose would be roughly normal to the San Andreas fault at spacings of, e.g., 10, 30, 100, 300, and perhaps 1000 km, say. There would be at least several such lines on each side of the fault, to the extent that land and island geography permits. Techniques for determining positions of ocean floor points such as those described by MOURAD ET AL (1972) may be applicable here. Selection of sites to the eastward would take due account of the complex structure and patterns of activity extending at least as far as the Wasatch region.

As the preceding discussion indicated, it will probably be of interest to locate such lines near the ends and centres of the 1857 and 1906 earthquake zones, and also north of Shelter Cove, between Cholame and Hollister, and one or more south east of San Bernardino, e.g., in the Imperial Valley region, and perhaps south of it. Such locations are indicated schematically in figure 11.

The San Andreas Fault Experiment (SAFE) constitutes the first step in the NASA EOPAP regional strain field measurement program (NASA 1972; VONBUN 1972; SMITH ET AL 1972; PLOTKIN ET AL 1973). The SAFE project is aimed at determining the changing distance between mobile laser stations near Quincy and San Diego in California. The locations of these two sites are also indicated in figure 11.

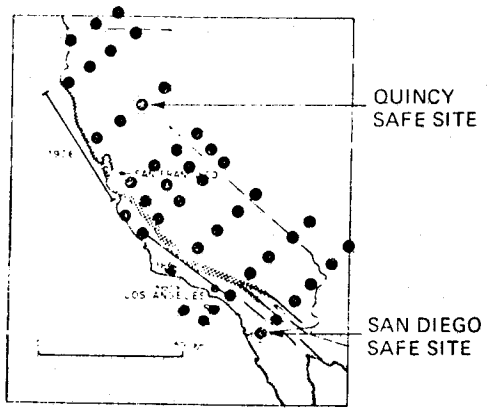

Figure 11. The San Andreas Fault System as depicted by KELLEHER ET AL ET AL (1973)
Added are schematic possible locations for regional strain field measurement sites. The locations of the present SAFE sites near Quincy and San Diego are also shown.

Data obtained through laser tracking of existing satellites such as Beacon Explorer-C will be used for the initial intersite distance determinations.

3.4 The Precursory Crustal Motion and Regional Strain Field Monitoring Network

The regions of interest in figures 9 and 10, in all, have a linear extent of the order of a quarter to a half on Earth's radius. This corresponds to some 400 to 800 stations.

The preliminary design parameters for a premonitory crustal motion and regional strain field measurement network system presented in this section do indeed pose formidable problems which arise chiefly due to the stringent accuracy requirements associated with station location determination and the extremely large number of sites involved.

4. A Precursory Crustal Motion and Regional Strain Field Monitoring System

4.1 General Characteristics

An alternative approach to the problem of monitoring precursory crustal motions and regional strain fields can be based on the use of corner reflectors at the sites indicated in the preceding discussion which are tracked by means of a laser system operating in the Geopause satellite (SIRY 1971). Each of the automated ground stations would also be equipped with simple apparatus for measuring atmospheric pressures, temperatures and humidities, and telemetering them via Geopause. Sites troubled by excessive cloudiness would also be equipped with turnaround transponders operating in conjunction with the Geopause radio tracking system. Such a Precursory Crustal Motion and Regional Strain Field Monitoring System is indicated schematically in figure 12.

In this approach, the problems associated with the site location accuracies are attacked by means of the Geopause spacecraft equipped with accurate laser and radio range tracking systems, and the challenge posed by the very large number of sites is met by means of the relatively simple and inexpensive ground stations.

4.2 The Geopause spacecraft

The state of the art orbit analysis and station position determination is roughly an order of magnitude away from the accuracy levels required for this precursory crustal motion application. The realization of the required accuracies awaits the solution of four kinds of problems, namely, those involving orbit determination and the lack of sufficient knowledge of tracking station biases, the gravity field and tracking station locations.

The Geopasue satellite system concept offers promising approaches in connection with all of these areas (IBID). A typical Geopause satellite orbit has a fourteen hour period, a mean height of about 4.6 Earth radii, and is nearly circular, polar, and normal to the ecliptic. At this height only a relatively few gravity terms have uncertainties corresponding to orbital perturbations above the decimetre level. Refer to figure 13. The orbit is, in this sense, at the geopotential boundary, i.e., the "geopause". The few remaining environmental quantities which may be significant can be handled by means of orbit analyses and surface force compensation systems or accelerometers.

The Geopause satellite system also provides the tracking geometry and coverage needed for determining the orbit, the tracking system biases and the station locations. This is indicated in figures

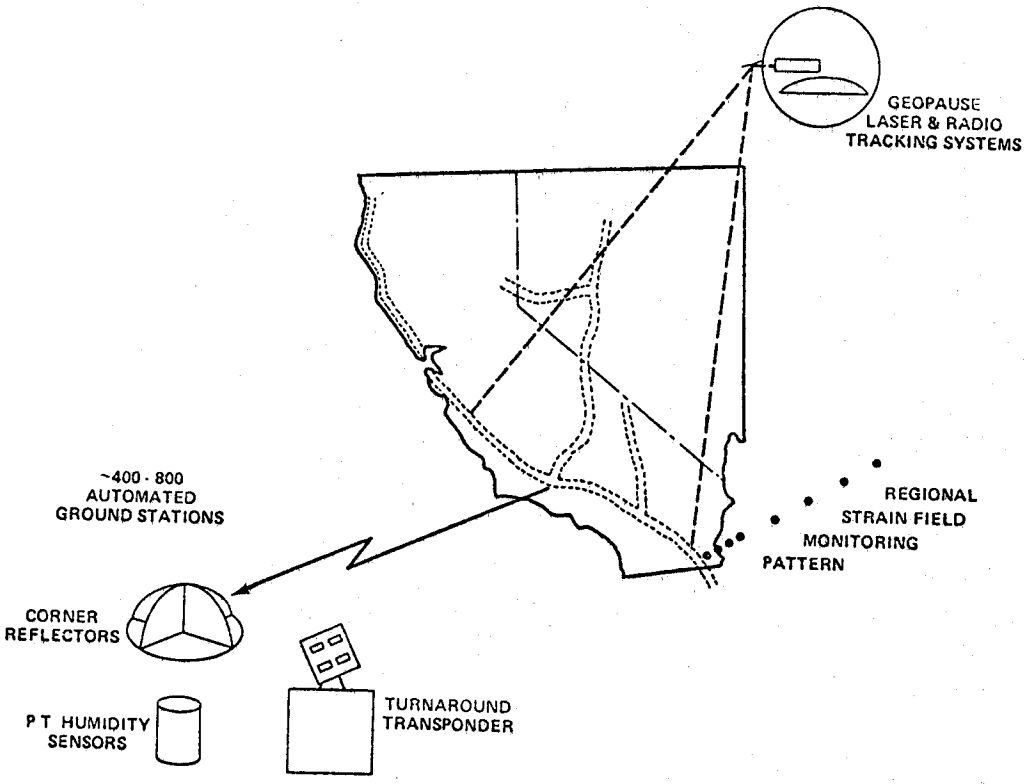

Figure 12. Precursory Crustal Motion and Regional Strain Field Monitoring System Based on the Geopause Satellite

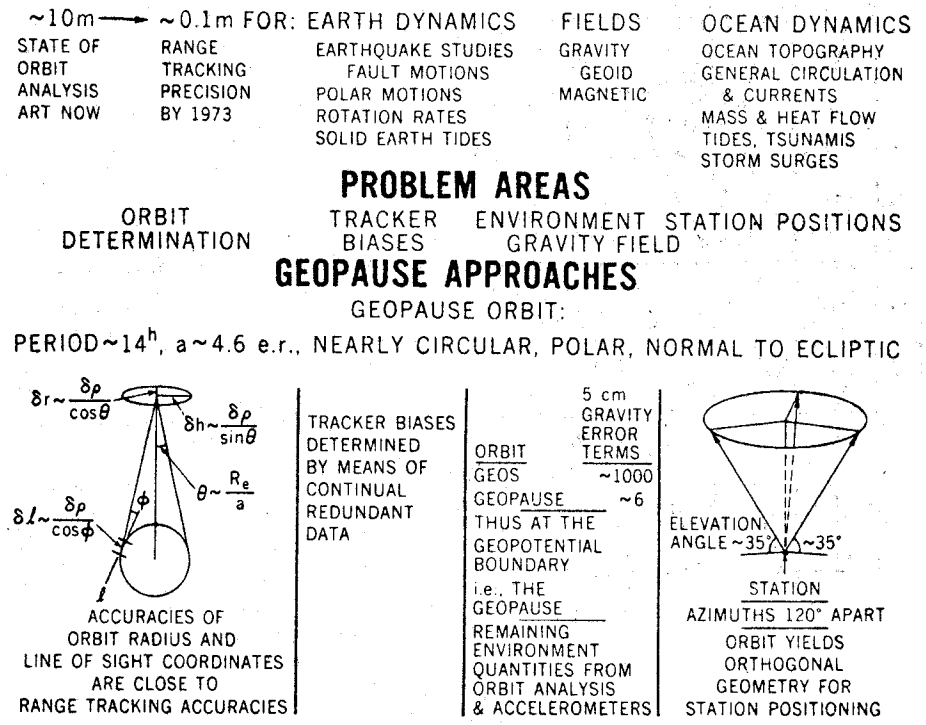

Figure 13. Geopause Approaches to the Meeting of Earth and Ocean Physics Applications Program Goals

13 and 14.

Results of an analysis based on a week of simulated observations from ten NASA affiliated sites are shown in figure 15. It was assumed that range data having a two cm bias were taken at intervals of a quarter of a minute. The uncertainties in the geopotential coefficients were taken to be a quarter of the difference between the SAO 1969 Standard Earth Model and the APL 3.5 Model (LUNDQUIST & VEIS 1966; GUIER & NEWTON 1965; MARTIN & ROY 1971). This assumption has been found to be consistent with some observational experience (IBID). The quantities solved for were the station position co-ordinates, GM and the sets of geopotential coefficients listed in figure 15. The resulting uncertainties in these quantities are also shown there. The designation "Rosman L" denotes a site whose longitude was effectively fixed and taken to be 90°W for reasons of convenience associated with the program. The study was carried out using the program system employed in connection with the analyses of SIRY (1971) and MARTIN & ROY (1971). The uncertainties in the station co-ordinates obtained in this case are listed in figure 15. The largest is 4.8 cm. The root mean square value and the mean value of the magnitudes are 3.1 cm and 2.7 cm respectively.

Since the Geopause spacecraft will be simultaneously visible from four or more sites in several parts of its orbit, it will become practical to determine tracking instrument biases on a continuing basis.

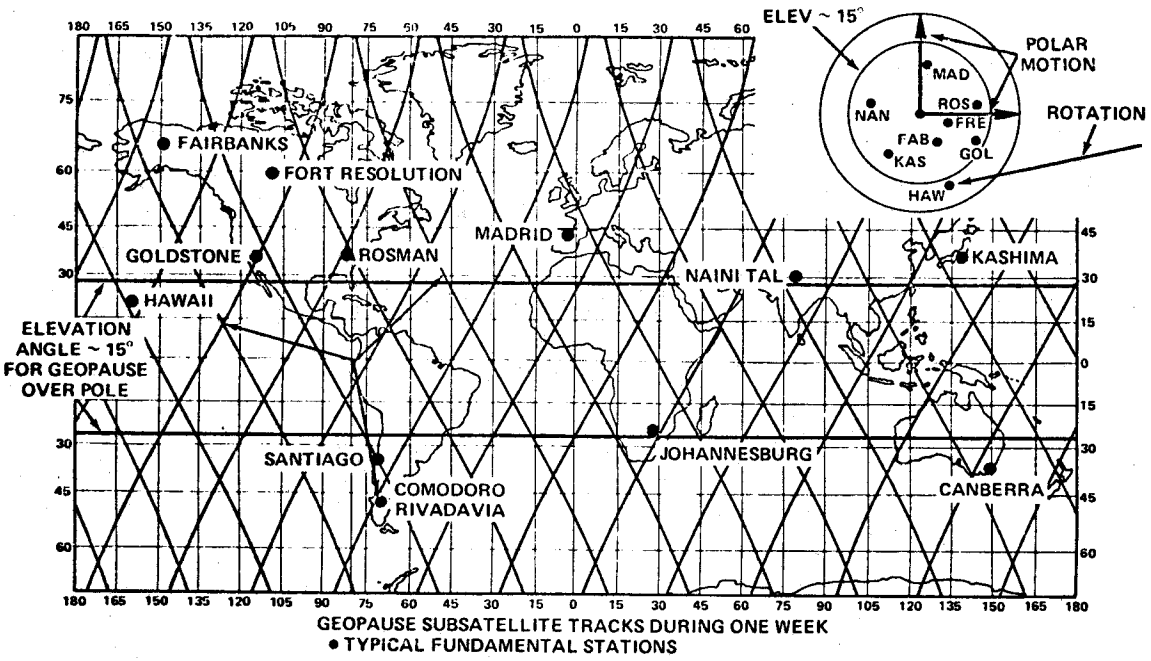

Figure 14. Geopause Orbit Yields the Geometry for Determination of Orbit, Tracker Biases, GM, Station Locations, Fault Motions, Polar Motions, Rotation Rates, Tides

For example, when Geopause is over the North Pole, it is visible at elevation angles above about 10° not only from the Arctic zone but also from the entire temperate zone, i.e., from all stations north of the Tropic of Cancer. This includes most of the Northern Hemisphere stations affiliated with NASA. Similar remarks apply to the visibility of Geopause when it is over the South Pole or near the equatorial plane. This visibility of Geopause over very wide zones of the Earth not only means that tracking system biases can be determined on a regular continuing basis, but also that the effects of the Earth's polar motions and rotational rate variations can also be observed frequently. Accordingly, it will be possible to decrease correspondingly the adverse effects of these factors on the accuracy of site position determinations.

It is anticipated that it will also be helpful to include as fundamental stations some locations in regions of relative crustal stability such as a Canadian shield site at Fort Resolution, for example.

The analysis summarized in figure 15 was based on tracking data obtained during a single week, which is the basic time interval during which a geometrically strong set of data can be obtained with Geopause for all stations over the globe. Much of the geometrical strength of the result is obtained from the three normal place observations during each pass which occur on the rising and setting branches and near culmination.

The Geopause satellite will be visible from a point or a region such as California for about 5 hours during a nearly overhead pass. If, say, 5 seconds are allowed for both the ranging to a ground site and the pointing motion to the next site, there would be enough time during a nearly overhead pass to

Adjusted Parameter	Standard Deviation ($\times 10^{10}$)	Adjusted Parameter	Standard Deviation (mm)	Adjusted Parameter	Standard Deviation (mm)
GM	9	ROSMAN X	5	JOHANNESBURG X	31
C(2, 2)	2	ROSMAN Y	34	JOHANNESBURG Y	40
S(2, 2)	35	ROSMAN Z	39	JOHANNESBURG Z	35
C(3, 1)	270	SANTIAGO X	3	KASHIMA X	26
S(3, 1)	140	SANTIAGO Y	37	KASHIMA Y	33
C(3, 2)	5	SANTIAGO Z	40	KASHIMA Z	41
S(3, 2)	5	ROSMAN-L Y	33	CANBERRA X	7
C(3, 3)	7	ROSMAN-L Z	39	CANBERRA Y	45
S(3, 3)	1	GOLDSTONE X	20	CANBERRA Z	38
C(4, 2)	21	GOLDSTONE Y	33	FAIRBANKS X	4
S(4, 2)	160	GOLDSTONE Z	39	FAIRBANKS Y	20
C(4, 3)	1	COMODORO RIVADAVIA X	5	FAIRBANKS Z	48
S(4, 3)	3	COMODORO RIVADAVIA Y	30	HAWAII X	9
C(4, 4)	0.1	COMODORO RIVADAVIA Z	45	HAWAII Y	37
S(4, 4)	2	MADRID X	19	HAWAII Z	38
		MADRID Y	32		
		MADRID Z	41		

Assumptions: Range bias, 2 cm. Range rate bias, 0.05 mm/s. Geopotential Harmonic Coefficient Uncertainties, 0.25 (SAO M1-APL 3.5). Tracking Interval, 1 week. Rms and mean of magnitudes of station coordinate standard deviations are 3.1 and 2.7 cm, respectively.

Figure 15. Geopause Satellite Orbit Properties
Determination of Gravitational Parameters and Co-ordinates for Stations of a Typical Fundamental Network

make a total of some 3000 site observations, or 3 or more observations per site.

Laser beams having a diameter of some 20 arc seconds corresponding to a spot size at the ground of 3 to 6 km are practical. Such a beam would, in general, illuminate a single site. Somewhat broader beams of 15 or 20 km spot size would generate reflections from several sites, yielding overlapping data. A chain or pattern of such overlapping data sets would strengthen the solution for the site positions in general, and the relative site positions in particular.

The different returns could, in general, be easily distinguished on the basis of prior knowledge of the ranges. The latter would usually differ by km, while knowledge of the positions of the sites and of the Geopause satellite would be orders of magnitude smaller than this, i.e., of the order of less than 1 m. The information which could be generated on the basis of the range predictions could be used, say, to program range gates.

It also appears that it will be feasible to maintain knowledge of the Geopause attitude with adequate adequacy, i.e., of the order of 5 to 10 arc seconds, and hence to control or point the laser mirror beam correspondingly (see, for example TRW 1972).

Programs for pointing the laser to the numerous targets could be generated in a ground-based computer and transmitted to the Geopause control system computer. The laser system might alternately range to a site and then move to the next one. On the other hand, it might simply move continuously at a slowly varying or infrequently changing rate, ranging to the sites in a linear array at the appropriate

times as it passes them (KANT 1973). In either case, the pointing motions and rates involved are reasonable. Thus it appears that during nearly overhead Geopause passes, it will be technically feasible from the standpoint of controls and pointing to obtain three normal places, each based on several individual measures, for each of the hundreds of sites in a regional network such as the California-Nevada one contemplated in figure 12. Power resources of a specific Geopause design will govern the rate at which data would be gathered. It appears that this point will probably not be a critical one, however, since it is estimated that the time available for determining the site positions is an order of magnitude or more longer than the basic one week interval during which Geopause affords the opportunity for complete geometrical coverage.

Experience indicates that the data set actually required to achieve a given result may be larger than that implied by an analysis such as the one described above in connection with figure 15. This may be due, in part at least, to the fact that weather and other practical factors tend to increase the amount of time which is needed to achieve a geometrically strong data set. Even so, it seems that a reasonable margin is available here.

The Geopause radio tracking system will, in general, interrogate more than one transponder if several neighbouring sites are equipped with them. The remarks made above in connection with laser ranging concerning the ability to distinguish between the various returns apply here too. Control and pointing capabilities needed for the laser system are more than adequate for the radio system.

4.3 The Automated Ground Stations

The automated ground stations would include laser retro-reflector arrays, meteorological sensors and, as appropriate, radio turnaround transponders. Four corner reflectors in a Cartesian array would provide the hemispherical coverage. These would be suitably mounted on rock formations or occasionally on concrete piers. A transparent cover could be hemispherical, or consist simply of four face planes perhaps at a fairly steep angle forming a spire. It could be kept sufficiently clear by wipers and/or a blower. Power could be furnished by batteries which might be powered by solar cells if experience indicates such an approach to be cost effective. Servicing of non-responding sites and periodic maintenance, battery replacement, etc. could be accomplished by truck and helicopter patrols. Fencing may be useful in some cases to discourage souvenir hunters. Additional meteorological ground stations forming a larger linear array with roughly 20 km separations straddling the basic sites would provide a two-dimensional data base for refraction corrections. Laser corner reflectors and turnaround transponders at such outlying sites could provide additional data concerning fault motions having a corresponding scale. The dilatant regions may not extend out to these distances very often (SCHOLZ 1973). Accordingly, if reflectors and transponders were placed at such sites, they would serve primarily to provide some additional information about regional strain fields.

The turnaround transponders would be, in general, of the type which are already being readied in connection with the ATS-Nimbus satellite-to-satellite tracking (SST) experiment and the SMS tracking system. The antenna, for example, could be of moderate size and gain, comparable to the Nimbus SST transponder antenna, for example. This would provide the necessary link margins, and yet not place excessively stringent requirements on the pointing control system. Antennas with a beam width of the order of 0.1 radian or so would need to be re-pointed only every minute or even only once every several minutes in order to follow the relatively slow motion of Geopause as it is seen from a ground

Geopause Range Tracking Systems	*Automated Ground Stations*
Laser System	*Laser Corner Reflector Stations*
0.1 - 0.2 mrad beam; 2 - 8 km spot size	4 large open corner reflectors in Cartesian array
6 arc seconds attitude control	Rock mounting or concrete pier
Range to: ~ 720 sites/hr	Hemispherical or spire transparent cover-wipers/blowers
~ 3000 sites/overhead pass ~ 3 ranges/site/overhead pass ~ 2 cm position component accuracy in $\frac{1}{4}$ yr	Pressure, temperature & humidity gauges at corner reflector sites and at peripheral sites for 2-dimensional data measures relayed through Geopause
	Truck & Helicopter maintenance patrols servicing non-responding sites and for periodic maintenance, battery replacement, etc.
Radio System	*Radio Turnaround Transponder Stations*
Multiple return discrimination via programmed range gates	Added at low visibility sites, e.g., under persistent dog or clouds, etc.
~ 2 cm position component accuracy in $\frac{1}{4}$ yr	Commands from Geopause for antenna pointing, etc.
Laser & radio systems also track low-altitude spacecraft yeilding oceanographic and gravity data	Radiometer for water vapour refraction correction

Figure 16. Precursory Crustal Motion Monitoring System

station. Commands to point the turnaround transponder antennas would come from Geopause. The turnaround transponder sites would also be equipped with radiometers for gauging the water vapour contribution to the refraction correction where this is necessary. The Geopause laser and radio tracking systems should be able to provide ranging data with an accuracy of the order of 1 cm once the refraction correction data are applied (see, for example HOPFIELD 1972).

Characteristics of the Precursory Crustal Motion and Regional Strain Field Monitoring System are summarized in figure 16.

Once the warning is given and the dilatant region has been located with this system, other equipment can be brought to bear on the problem. For example, seismic velocity measurements can be used to trace out the history of the V_p/V_s curve. Resistivity measurements might also be made. Data gathered by means of various additional techniques would generate further confidence in the earthquake predictions.

The cost of an automated ground station may turn out to be of a lower order than the cost of preparing a site for a mobile ground station.

The Geopause laser and radio tracking systems would also be used to track the low-altitude Earth and Ocean Physics Applications Program spacecraft yielding oceanographic and gravity data (e.g., NASA 1972;

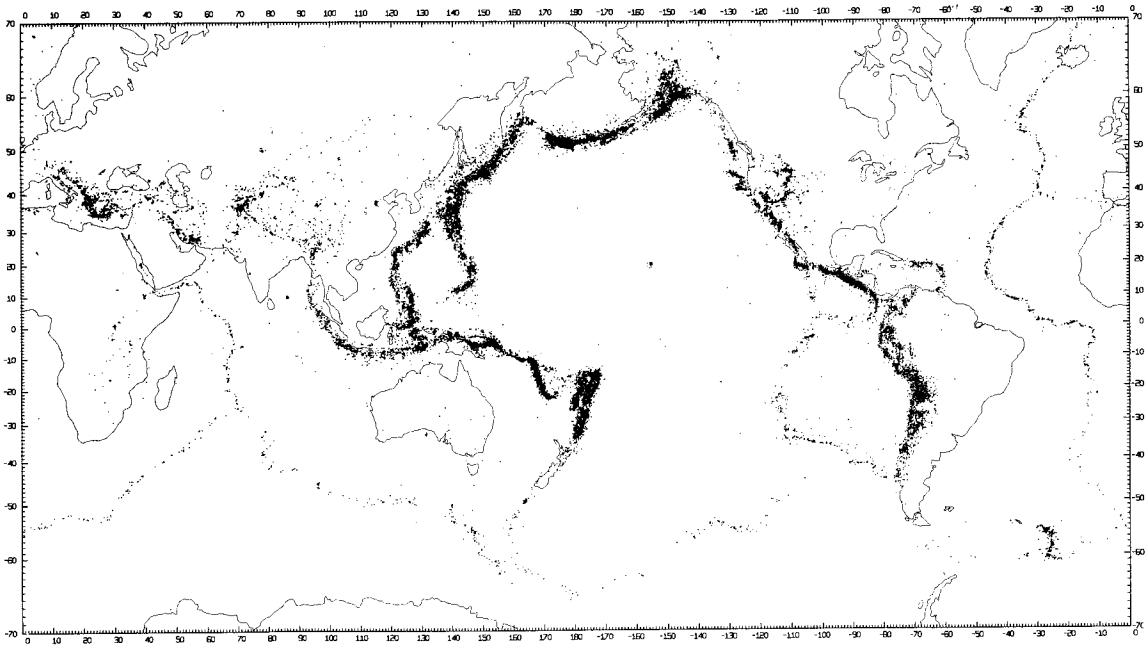

Figure 17. Seismicity of the Earth, 1961-1967. Depths to 700 km (KELLEHER ET AL 1973; BARAZANGI & DORMAN 1969)

SIRY 1971; VONBUN 1972). Some conventional laser. VLBI, and radio ground stations of the type already planned will still be needed as part of the overall Geopause system in connection, for example, with the determination of its orbit and the validation and calibration of the Geopause tracking systems (see figure 14, for example).

The concept outlined here based on Geopause satellite techniques offers the prospect of a practical approach to the problem of monitoring secular variations in position such as precursory crustal motions and regional strains, and providing data potentially useful for earthquake predictions.

The above discussion is in terms of the California region. Similar approaches might be applied in some of the other areas shown in figures 7 and 8, and in other parts of the world indicated in figure 17 which are troubled by seismicity, such as the Middle East, to the extent that geography and other factors allow.

Areas of high seismic risk in central and eastern North America indicated in figure 18 may also be of interest from the standpoint of crustal motion measurement. Crustal motions which may occur in the region between the Rocky Mountains and the eastern United States could also be monitored by this approach (DRAKE 1973).

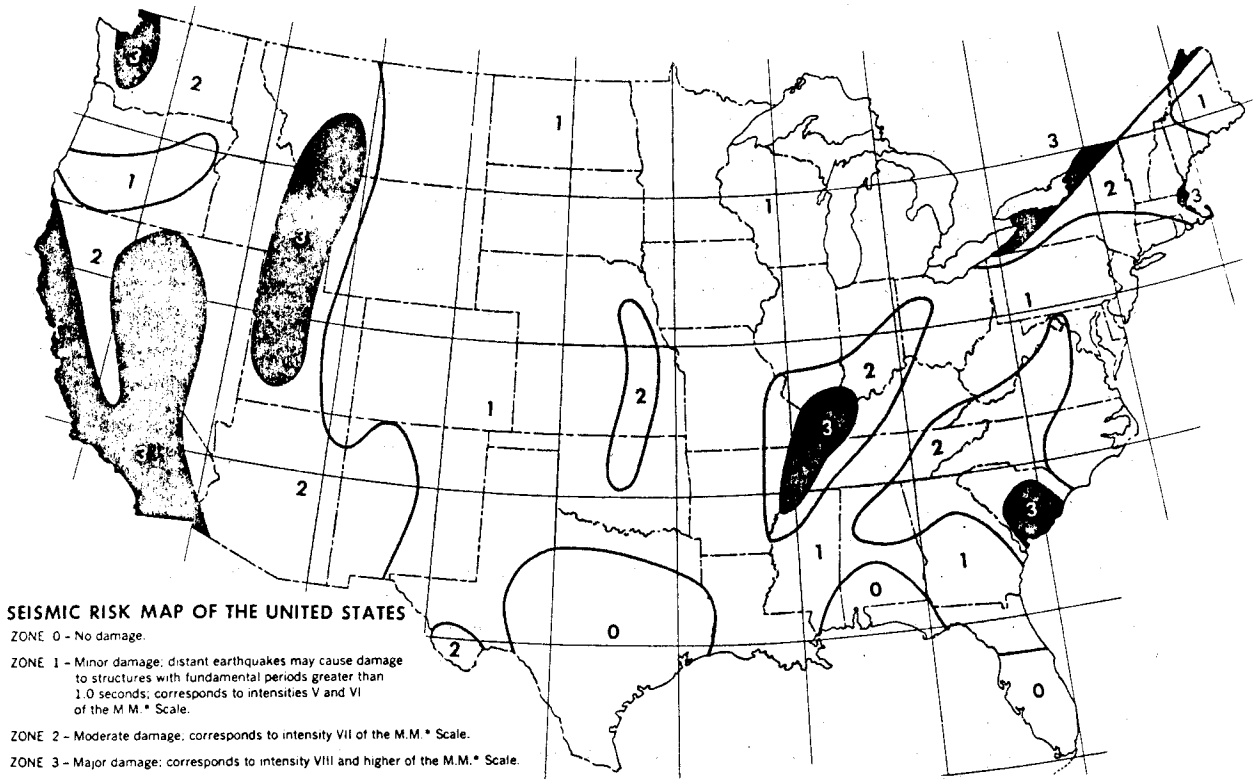

Figure 18. Seismic Risk Map of the United States. (From ALGERMISSEN 1969) (NASA 1972)

5. Acknowledgments

It is a pleasure to achnowledge helpful discussions with Drs. C. Scholz, C. Drake, C. Allen, F. Vonbun, H. Plotkin and D. Smith, and Messrs H. Hoffman, S. Kant, P. Minott, P. Schmid and S. Stevens.

6. References

ALGERMISSEN, S.T. 1969. Seismic Risk Studies in the United States. *Fourth World Conference on Earthquake Engineering*, Vol 1,26.

ALLEN, C. 1968. The Tectonic Environments of Seismically Active and Inactive Areas along the San Andreas Fault System. *Publ.Geol.Sci.* 11,Stanford University, Stanford Calif.,70.

BARAZANGI, M. & DORMAN, J. 1969. World Seismicity Maps of ESSA, Coast and Geodetic Survey Epicenter Data for 1961-1967. *Bull.seismol.Soc.Amer.* 59,369.

DRAKE, C. 1973. Private communication.

GUIER, W.H. & NEWTON, R.R. 1965. The Earth's Gravitational Field as Deduced from the Doppler Tracking of Five Satellites. *J.geophys.Res.* 70,4613-4626.

HOPFIELD, H.S. 1972. Tropospheric Range Error Parameters: Further Studies. *Rep.* CP 015,Applied Physics Laboratory,Johns Hopkins University,Silver Spring Md.

KANT, S. 1973. Private Communication.

KELLEHER, J., SYKES, L.R. & OLIVER, J. 1973. Possible Criteria for Predicting Earthquake Locations and Their Applications to Major Plate Boundaries of the Pacific and the Carribean. *J.geophys.Res.* 78(14).

LUNDQUIST, C.A. & VEIS, G. 1966. Geodetic Parameters for a 1966 Smithsonian Institution Standard Earth. *Spec.Rep.* 200,Smithsonian Astrophysical Observatory,Cambridge Mass.

MARTIN, C.F. & ROY, N.A. 1971. An Error Model for the SAO 1969 Standard Earth. *Third International Symposium, Use of Artificial Satellites for Geodesy.* American Geophysical Union,Washington DC.

MOURAD, A.G., FUBARA, D.M., HOPPER, A.T. & RUCK, G.T. 1972. Geodetic Location of Acoustic Ocean-Bottom Transponders from Surface Positions. *EOS Trans.Amer.geophys.U.* 53,644-649.

NASA 1972. *NASA Earth and Ocean Physics Applications Program.* National Aeronautics & Space Administration,Washington DC.

NASON, R. 1971. *Investigation of Fault Creep Slippage in Northern and Central California.* Ph.D. Thesis,University of California, San Diego Calif.,250 pp.

PLOTKIN, H., JOHNSON, T. & MINOTT, P. 1973. Progress in Laser Ranging to Satellites: Achievements and Plans. *COSPAR,IAG Symposium*, Technical University,Athens.

SAVAGE, J. & BURFORD, R. 1970. Strain Accumulation in California. *Bull.seismol.Soc.Amer.* 60,1877.

SAVAGE, J. & BURFORD, R. 1971. Discussion of paper by C.H. Scholz & T.J. Fitch "Strain Accumulation along the San Andreas Fault". *J.geophys.Res.* 76,6469.

SCHOLZ, C. 1973. Private Communication.

SCHOLZ, C. & FITCH, T.J. 1969. Strain Accumulation Along the San Andreas Fault. *J.geophys.Res.* 74,6649.

SCHOLZ, C.H. & FITCH, T.J. 1970. Strain and Creep in Central California. *J.geophys.Res.* 75,4447.

SCHOLZ, C.H. & FITCH, T.J. 1971. Reply to "Discussion of Paper by C.H. Scholz & T.J. Fitch, 'Strain Accumulation along the San Andreas Fault' by J.C. Savage & R.O. Burford". *J.geophys.Res.* 76,6480.

SCHOLZ, C., MOLNAR, P. & JOHNSON, T. 1972. Detailed Studies of Frictional Sliding of Granite and Implications for the Earthquake Mechanism. *J.geophys.Res.* 77,6392.

SCHOLZ, C.H., SYKES, L.R. & AGGARWAL, Y.P. 1973. The Physical Basis for Earthquake Prediction. *54th Annual Meeting,American Geophysical Union*,Washington DC; and Earthquake Prediction: A Physical Basis. *Science* 181,803-810.

SIRY, J.W. 1971. A Geopause Satellite System Concept. *Space Science Reviews* 14(2),314-341; and *Third Internationa Symposium, Use of Artificial Satellites for Geodesy*,Washington DC.

SMITH, D., SAVAGE, J., TOCHER, D. & SCHOLZ, C. 1972. The San Andreas Fault Experiment. *EOS Trans. Amer.geophys.U.* 53(4).

TRW 1973. Precision Pointing Control System Design and Analysis. *Rep.* 13900-6012-R0-01,TRW Systems Group,Redondo Beach Calif.

TSUBOKAWA, V., DAMBARA, T & OKADA, A. 1968. In KAWASUMI, H. (ed.) *General Report on the Niigata Earthquake.* Tokyo Electical Engineering College Press,p.129.

VONBUN, F.O. 1972. Earth and Ocean Physics Applications Program (EOPAP). *XXIII International Astronautical Congress*,Vienna.

WHITCOMB, J.H., GARMANY, J.D. & ANDERSON, D.L. 1972. Earthquake Prediction: Variation of Seismic Velocities Before the San Fransisco Earthquake. *Science* 180,632-635.

WYSS, M. & BRUNE, J. 1971. Regional Variations of Source Properties in Southern California Estimated from the Ratio of Short-to-Long-Period Amplitudes. *Bull.seismol.Soc.Amer.* **61**,1153.

YAMAGUTI, S. 1968. *Bull.Earthquake Res.Inst.* **46**,1269.

7. Discussion

ANGUS-LEPPAN: Can you give us some idea of the cost of such a system?

SIRY: I refer the question to Plotkin.

PLOTKIN: This is a difficult question to answer. We are developing laser systems to go into spacecraft for communications and, more recently, for tracking spacecraft-to-spacecraft. These developments are at a very early stage. We certainly can think in terms of space-borne laser systems. To say what such a system would cost is not possible at the present time.

MUELLER: What is a reasonable estimate of the weight of a satellite which could carry a system like that described?

PLOTKIN: The collecting area need not have to be so large because the reflectors on ground are not limited in size as the spacecraft reflectors are. The difference is going to be in carrying a laser and power supply on board, as well as (systems for) pointing. 1/10th mrad is quite feasible from ground because we have reference directions. Your are talking about doing this from space with very high accuracy but with essentially no beacons, and pointing to a passive reflector. This could be difficult. It is a concept we will have to study.

MACDORAN, P.F.
Tracking & Orbit Determination Section
Jet Propulsion Laboratory
California Institute of Technology
Pasadena California 91103
United States of America

Proc. Symposium on Earth's Gravitational Field & Secular Variations in Position (1973), 380-395.

VERY LONG BASELINE INTERFEROMETRY (VLBI) APPLICATIONS TO SECULAR GEODYNAMICS AND EARTH STRAIN MEASUREMENT *

ABSTRACT

An instrumental technique from radio astronomy, known as Very Long Baseline Interferometry (VLBI) offers significant promise for the problem of accurate long distance, three dimensional surveying and determination of whole Earth geodynamical phenomena. The methods of VLBI make it possible for receiving stations to be independently operated at arbitrary separations using extragalactic radio sources at its frame of time invariant angular reference. Feasibility demonstrations at S-band (13 cm) wavelengths have been performed, and accuracies of a few centimetres for three-dimensional surveying over a short distance (16 km) have been demonstrated. VLBI operation on longer baselines (8400 km) have been performed between Goldstone, California, and Madrid, Spain in order to develop the capability for determination of Universal Time variations, in addition to the measurements of this intercontinental baseline. Systems analysis indicates that necessary calibrations can be developed so as to make possible the implementation of a transportable radio interferometer station concept. Using a transportable 9-m diameter dish antenna, operated in combination with a 64-m dish, receiving at X-band wavelengths (4 cm), it will be possible to measure the three-dimensional separation between antennas with a few cm accuracy for separations up to several hundred km. With simultaneous S- and X-band reception at each antenna, the transportable antenna could be operated at even intercontinental distances with 10 cm baseline accuracy. Earth platform parameters of Universal Time and polar motion could be calibrated to 0.25 msec and 10 cm, respectively, and radio source positions determined to 0.005 arcsec accuracies by S/X-band reception, using large antennas of the Deep Space Network in an extended synoptic observational mode.

The importance of accurate Earth parameter calibrations and the determination of secular appearing phenomena is extremely important, particularly in the light of recent geophysical theories. Continental plate tectonics and its resultant Earth crustal deformations (typically a few cm per year) in the zones of plate contact, appears to be intimately related with Earthquake occurrence on a local and global scale. In addition, recent research by Russian and American seismologists has led to a theory for earthquake prediction based on rock dilatancy. A consequence of the dilatancy models is that large areas (100's of km^2) of the Earth's crust must undergo many cm of vertical uplift which is also precursory to earthquakes. Because the VLBI technique is capable of full three-dimensional baseline determinations, it offers great promise for both vertical crustal uplift detection as well as measurement of horizontal strain accumulation, and perhaps significantly contribute to the search for reliable earthquake prediction methods.

1. Historical Origins of VLBI

Historically, applications of interferometry have been primarily for astronomical purposes beginning with the work of A.A. Michelson and F.G. Pease in 1920. These early experiments used optical wavelengths to measure the angular diameters of stars. The method operated by combining star light received via two separate optical paths which had to be established and maintained at equal optical

* This paper presents the results of one phase of research carried out at the Jet Propulsion Laboratory, California Institute of Technology, under Contract No NAS 7-100, sponsored by the National Aeronautics & Space Administration.

lengths (figure 1). This task proved to be extremely difficult and prevented the primary mirrors from being separable by more than 20 ft, mainly because of atmospheric dissimilarities in the two interferometer arms. A dissimilarity in optical path of only 0.2 μ($\frac{1}{2}$ an optical wavelength) is sufficient to destroy the interference pattern (or fringes) which is the output of any interferometer system.

With the emergence of radio astronomy as a discipline in the 1930's came the desire to create the analog of the Michelson/Pease stellar interferometer using radio waves instead of optical wavelengths. These early radio interferometers were the so-called "hard-wired" systems, because cables or some other phase stable communications link were needed to derive the first oscillator signals (figure 2). As with its optical forerunner, the radio paths must be stable to better than one-half an RF wavelength to maintain the fringe output of the interferometer. The practicality of laying cables has limited short baseline interferometers to about 1 km, whereas microwave relay links have allowed antenna separations up to about 100 km. Because the resolving power of an interferometer is dependent on the ratio of the wavelength to the antenna separation, there was the inevitable desire to move the antenna spacing to intercontinental distance, if possible. The breakthrough in achieving these very long baselines occurred in 1967 (BROTEN ET AL 1967; BARE ET AL 1967) because of improvements in quantum electronic frequency systems which afforded essentially identical performance of two or more separate devices for generating local oscillator signals. The improved frequency systems eliminated the need for a phase-stable link between the two receiving stations, making it possible for the stations to be separated by arbitrarily large distances limited only by the Earth's diameter. This, then was the origin of the radio astronomy technique of Very Long Baseline Interferometry (VLBI). Perhaps it would have been more apt to term the method independent station radio interferometry, so as not to imply that only very long baselines were allowed.

When the baselines are comparatively short, and phase stable communication links are available, the outputs of the heterodyne receivers are conveniently combined at a common site to produce fringes. However, on a very long baseline the output of the receivers must be handled differently. The only

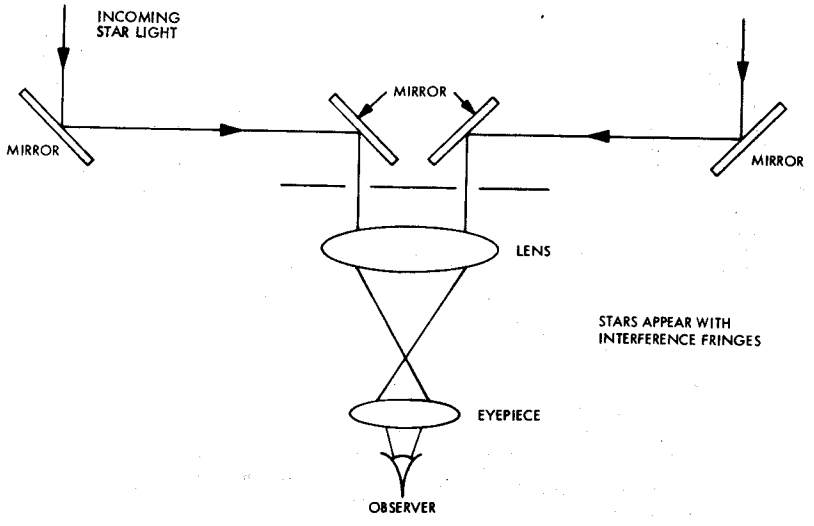

Figure 1. Michelson/Pease Stellar Interferometer

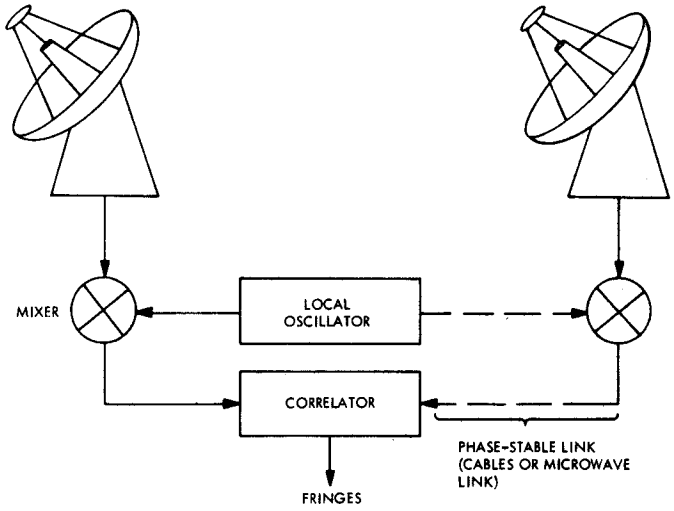

Figure 2. Conventional "Hard-Wired" Radio Interferometer

method so far demonstrated consists of recording receiver output on magnetic tapes along with time codes from each station. Two implementations exist in this type of recording:

an analogue approach favoured by the Canadians; and

a digital method used by virtually all US teams.

These magnetic tapes are brought together for cross-correlation processing usually several days to weeks after the time they were recorded. It is the cross-correlation process which yields the fringe response of the interferometer. A schematic diagram of the VLBI technique is given in figure 3.

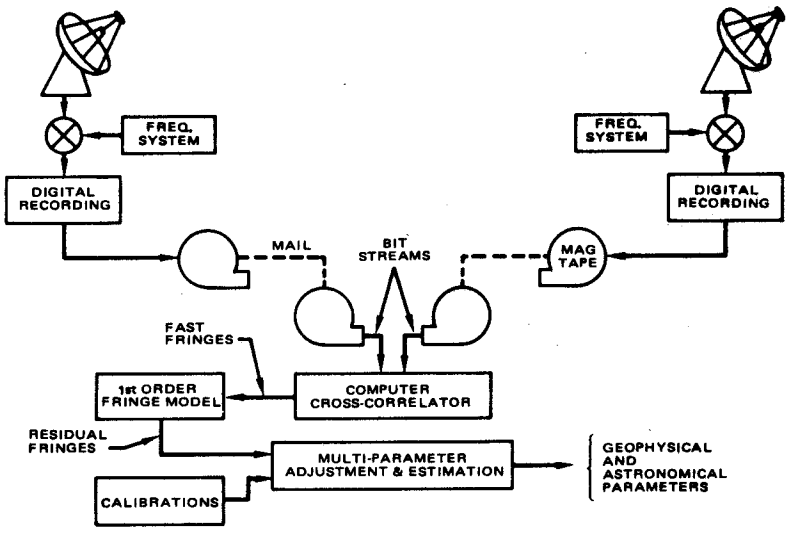

Figure 3. The VLBI Technique

Since the original experiment in 1920, interferometry has been used for astronomical applications and particularly for measuring the angular diameters of the source of the light, or radio waves. The early publications on VLBI however, correctly identified applications to geophysics (GOLD 1967; MACDONALD 1967) although the prediction of centimetre level measurements are yet to be realized over very long baselines.

For those interested in the general VLBI literature and its use in the study of spatial structure of celestial radio sources, general survey articles (KLEMPERER 1972; KELLERMAN 1971) will be found useful.

2. The VLBI Technique

In VLBI measurements, the radio signal produced by a distant source is recorded simultaneously at the two radio antennas. Because of a difference of ray paths, reception of the signal will be delayed in time at one antenna relative to the other. By cross-correlating the two signals, the time delay and/or its time derivative may be determined (THOMAS 1972a; THOMAS 1972b). When narrow-band recording equipment is used, only the time derivative of the time delay may be measured with adequate precision to be useful. If the radio signal is generated by an extra-galactic object, the radio source may be regarded as a fixed object because of its great distance.

The time variation of the time delay is due entirely to the Earth's motion, but depends, of course, on the source location and the baseline vector between the two antennas. In general, measurement of the derivative of the time delay for many natural sources can lead, by means of a least-squares analysis, to the determination of source locations, the baseline vector, and Earth-motion parameters, such as UT1 (Universal Time), and polar motion.

Figure 4 shows a schematic diagram of a radio interferometer station pair, while figure 5 gives the geometry of the situation. As these two antennas are separated by a distance $|\vec{D}|$, there will be a difference in the time of reception of the signal at the two antennas. This delay τ_g is given by

$$\tau_g = \frac{\vec{D}}{c} \cdot \vec{s} \qquad (1),$$

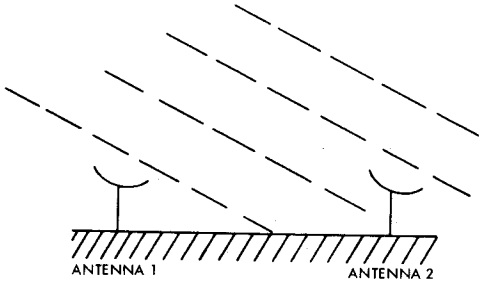

Figure 4. Interferometer Pair

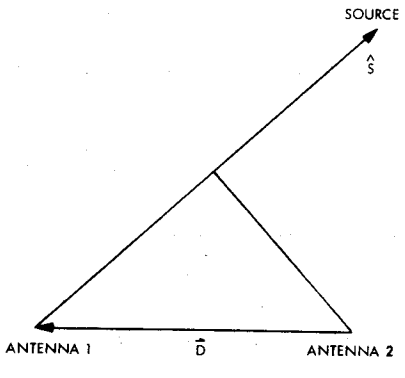

Figure 5. Interferometer Geometry

where c is the speed of light and $\vec{s}$ is a unit vector opposite the direction of propagation of the wave front (assumed to be a plane for simplicity only). This time delay has a maximum possible value of (Earth's radius)/c, or 0.021 sec. The quantity

$$\nu_F = \omega_o \frac{\partial \tau_g}{\partial t} \tag{2}$$

is known as the fringe rate, where ω_o is the received frequency and is just the negative of the Doppler shift between the two stations. In general, cross-correlation of the two data streams allows the time delay τ_g and the fringe rate ν_F to be measured.

The dot product in equation 1 is most usefully expanded in terms of the equatorial co-ordinate system of date. In this system, the right ascension and declination of the source are given by α_s, δ_s while the equivalent quantities for the baseline vector D are α_b, δ_b.

Explicitly writing out the dot product in equation 1,

$$\tau_g = \frac{|D|}{c}\left(\cos\delta_b\cos\alpha_b\cos\delta_s\cos\alpha_s + \cos\delta_b\sin\alpha_b\cos\delta_s\sin\alpha_s + \sin\delta_b\sin\delta_s\right)$$

$$= \frac{|D|}{c}\left(\sin\delta_b\sin\delta_s + \cos\delta_b\cos\delta_s\cos(\alpha_b - \alpha_s)\right) \tag{3},$$

the fringe rate - equation 2 - is then

$$\nu_F = -\frac{|D|\omega_o}{c}\left(\cos\delta_b\cos\delta_s\sin(\alpha_b - \alpha_s)\right)\frac{\partial}{\partial t}(\alpha_b - \alpha_s) \tag{4}.$$

If the equatorial projection of $|D|$ is called r_b,

$$r_b = |D|\cos\delta_b \tag{5},$$

since

$$\frac{\partial}{\partial t}(\alpha_b - \alpha_s) = \omega_e \tag{6},$$

where ω_e is the angular velocity of rotation of the Earth (0.73×10^{-4} rad sec^{-1}),

$$\nu_F = \frac{\omega_o r_b}{c}\,\omega_e\cos\delta_s\sin(\alpha_b - \alpha_s) \tag{7}.$$

Equation 3 emphasizes the cylindrical co-ordinates are the natural units for this problem. The problem however, is also conveniently expressed in terms of a right handed Cartesian co-ordinate system fastened to the Earth with the x axis through Greenwich and the z axis along the instantaneous rotation axis. If $\alpha_G(t)$ is the right ascension of Greenwich, and λ_b is the longitude of the baseline in the Earth-fixed system, then

$$\lambda_b = \tan^{-1}\left(\frac{y_2 - y_1}{x_2 - x_1}\right) \tag{8},$$

where x_i, y_i, z_i refer to the Earth-fixed, geocentric co-ordinates of the i-th station, and the right ascension of the baseline vector becomes

$$\alpha_b(t) = \lambda_b + \alpha_G(t) \tag{9}.$$

In a system fixed to the Earth,

$$X = |D| \cos \delta_b \cos \lambda_b \quad ; \quad Y = |D| \cos \delta_b \sin \lambda_b \tag{10},$$

and

$$Z = |D| \sin \delta_b \tag{11},$$

where X, Y and Z are the projections of the baseline on the x, y, and z axes. The geometry of a typical baseline is illustrated in figure 6.

Substituting equation 9 in equation 3, one can obtain

$$\tau_g = \frac{1}{c}\left(Z \sin \delta_s + \cos \delta_s \{X \cos[\alpha_G(t) - \alpha_s] - Y \sin[\alpha_G(t) - \alpha_s]\}\right) \tag{12},$$

and

$$\nu_F = -\frac{\omega_e \omega_o}{c}\left(\cos \delta_s \{X \sin[\alpha_G(t) - \alpha_s] + Y \cos[\alpha_G(t) - \alpha_s]\}\right) \tag{13}.$$

3. Recent History of VLBI Geodetic Experiments

Various research teams have been active in the development of the VLBI technique for applications to geophysics. There has been considerable variety in instrumentation methods and lengths of baselines

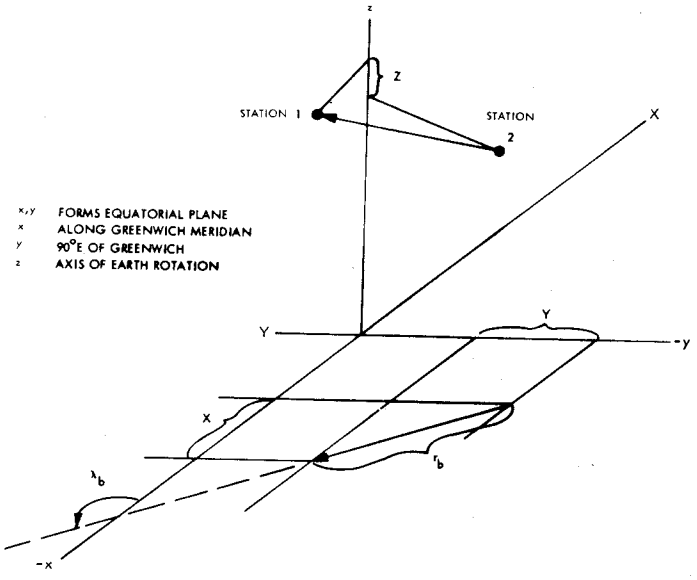

Figure 6. Intrinsic Co-ordinates of an Interferometer Baseline Vector

Table 1

VLBI Geodetic Experiments Summary

Reporting Date	Group	Baseline	Length (km)	Reference
April 1970	MIT	Haystack / Greenbank	845	HINTEREGGER ET AL 1970
September 1971	GSFC	Rosman / Mojave	3000	RAMASASTRY ET AL 1973
October 1971	JPL	Goldstone only	16	FANSELOW ET AL 1972a
April 1972	GSFC/SAO	Agassiz / OVRO	2900	RAMASASTRY ET AL 1973
October 1972	MIT/GSFC	Haystack / Greenbank	845	HINTEREGGER ET AL 1972
December 1972	JPL	Goldstone / Madrid	8400	FANSELOW ET AL 1972b
December 1972	JPL	Goldstone only	16	THOMAS ET AL 1972

which are illustrated in table 1.

In order to give some insight into the progression of such research, the following is a brief historical account of the experience at JPL.

VLBI Earth physics experiments began by using two stations of the Goldstone Deep Space Communications Complex (DSCC), the 64 m Mars and 26 m Echo antennas, separated by 16 km. In January 1971, a 30 cm two dimensional (equatorial components only) baseline measurement accuracy relative to a ground survey, was obtained by fringe frequency observations. Those fringe frequency measurements were disturbed by instabilities at the first local oscillator which were corrected for subsequent experiments by construction of a fixed frequency multiplier.

In the summer of 1971, a series of intercontinental baseline experiments were conducted between the 64 m Goldstone and 26 m Madrid stations of the Deep Space Network (DSN). The goals for the experiment were to measure variations in the Earth's rotational rate (UT1), the equatorial components of this inter-continental baseline (approximately 8400 km), and to begin the establishment of a catalogue of extragalactic radio sources. As reported by FANSELOW ET AL (1972b), each of these goals was achieved. The variations in UT1 were measured with a precision of the state of the art (2 msec) and found to be in agreement with those derived optically by the Bureau International de l'Heure (BIH), Paris, France. The equatorial baseline components were derived with an accuracy of 1.5 m and found to be within 2 m of the baseline derived by the DSN from doppler tracking of interplanetary spacecraft. A catalogue of ten extragalactic radio sources has been determined with a relative accuracy of 0.1 to 0.02 arcsec.

The experience gained from these Goldstone/Madrid measurements enabled a quantitative systems analysis to be made. The results indicate that a small antenna could be fielded for surveying over short, moderate or even intercontinental baselines. With the assistance of the geophysical community, particularly the Caltech Seismological Laboratory, sites of geophysical significance were suggested, and perhaps more importantly, the requirement for extremely high measurement accuracy was clearly established. It became recognized that the major geophysical contribution which a VLBI type measurement can make is the rate of Earth crustal strain taking place over hundreds of kilometres on either side of earthquake fault zones. However, in order to be of worth in the near term (within 5 years), measurements need to be made with 5 cm or better accuracy in three dimensions. Because the strain

rate can be at most about 6 cm yr^{-1}, and resolution of at least 2 cm yr^{-1} is required to adequately distinguish between various competing geophysical theories, a measurement accuracy of 5 cm would require 5 years to achieve a rate determination uncertainty of 2 cm yr^{-1}.

Since a radio interferometer has never achieved such high accuracies, it became necessary to conduct a series of feasibility demonstrations, and beginning in 1972, experiment emphasis returned to the Mars and Echo stations of the Goldstone DSCC. In April 1972, the first JPL test of two channel bandwidth synthesis was made with a channel spacing of 10 MHz. Bandwidth synthesis schemes were pioneered by MIT (ROGERS 1970) and allowed the measurement of the time delay interferometer function. The April experiment determined the third component of the baseline vector with an accuracy of 50 cm. Based on the April 1972 experiment, the radio system and computer software were redesigned to perform a synthesis over a 40 MHz channel separation. As reported by THOMAS ET AL (1972), the results of three experiments (16 August, 14 and 18 October 1972) are 5 cm, 4 cm and 4 cm in three dimensions, respectively. The comparison of the interferometer determinations with an existing ground survey indicates good agreement in the length of the baseline, within the 20 cm uncertainty of the horizontal geodetic control.

In August 1972, a surplus US Army transportable 9 m diameter satellite communications station was transferred to NASA/JPL to become a portable radio interferometer station.

4. Error Sources

4.1 Transmission Media

The most important of the VLBI error sources for geodynamic applications arises from the transmission media. Any interferometer is inherently a differential device, and thus the differential phase-delays in paths between the receiving antennas and the source are the important factors.

The transmission media consists mainly of the wet and dry components of the Earth's troposphere (the lower 11 km of our atmosphere) and the charged particles. Charged particles are mainly contributed by the Earth's ionosphere and space plasma. The general magnitude of the errors is given in table 2.

Table 2

Transmission Media Corrections for Typical Very Long Baseline Observations at S-Band (Elevation Angles Greater Than 10°)

	Troposphere	Ionosphere (S-band)	Space Plasma (S-band)
Delay	0 - 10 m	0 - 6 m	0 - 1 m
Fringe Frequency (f.f.) (S-band)	0 - 20 mHz	0 - 3 mHz	0 - 0.5 mHz
10 cm Fractional Correction	1% - delay 0.3% - f.f.	2% - delay 2% - f.f.	10% - delay 10% - f.f.

The transmission media are important error sources to VLBI because of their potential for introducing correlated or systematic errors in the observations. As the Earth rotates, the length traversed by the radio waves varies. At rise, when the radio source is first visible for a given station, the path through the ionosphere and the troposphere is longest. As the source apparently moves to higher elevation angles, the length through these media decreases, becoming a minimum at zenith and increasing as the source approaches set. Thus, the path length through the ionosphere and the troposphere has a diurnal variation. As was previously discussed, both the VLBI time-delay and fringe-frequency functions have diurnal signatures and thus diurnal phase-delay from the atmosphere will appear correlated with the VLBI data types (time delay and fringe frequency).

The fact that only the differential atmospheric delay enters as an error source is generally no help in eliminating the correlated effects. When the stations are far apart, the atmosphere above one station is essentially independent of that above another.

4.2 Frequency and Timing System

It is highly desirable, and perhaps mandatory, from a geophysical point of view, that VLBI baselines be ultimately measurable with 3 cm accuracy. Some data averaging will probably be done to achieve 3 cm, but averaging more than ten days of data is likely to be self-defeating because of correlated errors and the likelihood of washing out geophysically significant signatures. This implies that the accuracy of VLBI data from a single day should not be worse than 10 cm (0.3 nsec).

There is a necessity for observing extragalactic radio sources at widely separated declinations, in order to accomplish parameter separations in simultaneous solutions for geophysical, astronomical and instrumental effects. The requirement for the length-of-data arc is determined by the inherent information content of the interferometric observables for particular source declinations and baseline orientations. A VLBI "pass" on a particular source may be as short as 3 hours to as much as 12 hours.

A 0.3 nsec VLBI accuracy over a pass can be translated to a fractional frequency deviation ($\Delta f/f$) of between 3×10^{-14} (over 3 hours) to 7×10^{-15} (over 12 hours).

Performance at, and occasionally better than 7×10^{-15} has been demonstrated* in laboratory environments. However, extreme care must be taken when using the hydrogen maser outputs of 1, 5 or 100 MHz in mutiplying these frequencies up to the local oscillator frequencies of S- and/or X-band. Apparently small phase shifts or rapid phase variations have destroyed many VLBI experiments in the past.

There are circumstances when a frequency system other than a hydrogen maser will suffice. One such case occurs when using the VLBI technique on short to moderate length baselines (< 1000 km). For baselines of such lengths, five or more radio sources can be rapidly (3 hours or less) observed over a wide range of declinations and hour angles, and a self-contained data set obtained from which it is possible to simultaneously solve for baseline and instrumental parameters. In this way it is possible to make use of $\Delta f/f = 1 \times 10^{-13}$ performance which can be obtained from rubidium frequency systems of modern design and still achieve baseline measurement accuracies of 5 cm or better.

---

* by hydrogen masers

5. Calibration of Transmission Media Errors

Interestingly, the largest single transmission media error, the dry component of the toposphere, is also the least difficult to correct. The dry component amounts to about 2 m at zenith and about 80 m at the horizon, but it is *a priori* predictable with centimetre accuracy for elevation angles larger than 15° using local meteorological data and empirical principles.

The next largest error source is the Earth's ionosphere. This error source varies between 0.5 m and 2 m of group delay at zenith for S-band (2 GHz). At X-band (8 GHz), the delay effects are lower by a factor of 16. The variability is due to solar illumination on the Earth's upper atmosphere, being smallest at night and largest at a little past local noon. Empirical models for the ionosphere are essentially useless for VLBI applications because of the considerable variability of the ionosphere on a day to day basis. Another approach is to use the indirect calibration procedure of VHF Faraday rotation (MULHALL ET AL 1970) to measure the columnar electron content along some particular fixed direction, and then to map that electron content to an arbitrary line of sight depending on the radio source being observed. Such indirect methods are now being employed for a UT1 experiment using DSN stations, and it appears that baseline accuracies better than 1 m are unlikely.

What is needed is a direct calibration approach. Such an approach is to make VLBI measurements of radio sources (e.g., quasars and radio galaxies) simultaneously at two frequencies, S-band and X-band for example. Such an observing mode would afford the opportunity of exploiting the physical phenomenon of electromagnetic dispersion. Charged particle dispersion causes group delay effects which are inversely proportional to the square of the radio frequency being observed. Thus, X-band is less affected by charged particles than S-band. By differencing VLBI time-delay measurements at S- and X-band, a direct measurement of the differential columnar charged-particle content between the two Earth-based stations and the extragalactic radio source being observed, is obtained. This technique measures the aggregate differential charged particles contributed by the ionosphere, solar wind, interstellar and intergalactic media. Given a direct calibration capability of this S-/X-band type, it should be possible to calibrate the total charged particle problem with an accuracy of 10 cm or better.

Having calibrated the dry troposphere and charged particles, the only remaining significant transmission media error is the wet component of the troposphere. This error varies between 5 and 30 cm depending upon the time of the year. Published analytic studies on this topic (SCHAPER ET AL 1970) have shown that even in relatively humid areas, the zenith phase delay of tropospheric water vapour is predictable to 4 cm, given extensive past radiosonde balloon weather data; with water vapour radiometry and local surface weather data, the zenith water vapour delay can be ascertained to within 1 cm. The question of what accuracies will exist when no large body of historic radiosonde data is available for an arbitrary station location is receiving further study. However, the achievement of a 5 cm or better calibration using historical precipitable water data and surface weather from each station, appears reasonable (ONG ET AL 1973).

6. Phenomena to Which VLBI is Sensitive

6.1 Universal Time

Universal Time can be thought of as the time integration of the Earth rotation rate. The term UT1

is used to denote the instantaneous angular position of the Greenwich meridian with respect to the mean sun. Variations in UT1 exhibit a pronounced seasonal dependence and are thought to be at least in part the result of atmospheric transport, altering the Earth's moment of inertia (MUNK & MACDONALD 1960). There is also considerable randomness in UT1, which is unexplained.

Data on UT1 are obtained principally from the US Naval Observatory (USNO) and the Bureau International de l'Heure (BIH), Paris, France. Both of these UT1 services employ optical methods, either photographic zenith tubes (PZT) or transit circles. Both instruments possess msec (of time) resolution limits. It is the reliance on optical stars, however, which imposes the fundamental limit on accuracy.

Problems arise from two sources:

- refractive effects of the atmosphere above the observatory; and
- proper motion effects of the stars in the catalogue.

Ideally, the observatory would view the stars through a layered atmosphere at normal incidence. However, the atmosphere is not sufficiently layered in parallel planes nor free from random effects to allow uncorrupted observations; observations on a given night are likely to have individual standard deviations of 30 msec. It is only by taking 20 or more stars that the formal standard deviation can be reduced to about 7 msec.

The standard deviations of five day measurements of UT1 are approximately 3 msec, and the two time services (USNO and BIH) in the past have been in substantial disagreement regarding UT1.

A more subtle problem results from the stars themselves. There is a need for the stars in the catalogue to be sufficiently bright (brighter than eighth magnitude) to be measured with precision. However, bright stars are also likely to be local stars (0.1 to 1 kpc *) having larger proper motions. Random errors in proper motions are large. Furthermore, these stars are a part of our own galaxy and are undergoing a rotation which imparts a systematic catalogue drift, the uncertainty of which is about an arcsec per century (0.01" per year). Thus proper motion and rotation corrections for the individual catalogue stars must be derived from the observations so that UT1 will not drift at a rate of 30 cm per year. The method of solving for the proper motions of the catalogue from the UT1 observations themselves is difficult at best.

The VLBI resolution potential can be extremely high: a fraction of the wavelength/baseline ratio. For a 10,000 km baseline at X-band (λ = 3 cm), the resolution could be smaller than 6×10^{-4} arcsec or 0.04 msec of UT1, however, the accuracy of the UT1 will probably be 0.5 msec or about one order of magnitude improvement in the state of the art.

6.2 Polar Motion

The phenomenon of polar motion (PM) is the movement of the Earth's crust with respect to the axis of rotation. These motions are conventionally decomposed into rotations about three Cartesian axes. The x and y components are in the equatorial plane, while z is the spin axis; x points to the Greenwich meridian. Strictly speaking, only the rotational motions about the x and y axes are categorized as polar motion; rotations about the z axis become part of the phenomenon of UT1. Polar motion data are conventionally obtained from the Bureau International de l'Heure (BIH), Paris, France, or the International Polar Motion Service (IPMS), Mizusawa, Japan. Both IPMS and BIH

---

* 1 kpc = 1000 parsec ; 1 parsec = 2×10^5 astronomical units

utilize observatories at various latitudes and observe stars at several declinations. As was discussed in the context of UT1 measurements, optical astrometric methods of this type suffer from limited instrument resolution, atmospheric refraction which is uncorrectable, and star catalogue drifts. Because of these common error sources, the PM measurement precisions are quite similar to those of UT1, approximately 1 m. Also, as in the case of UT1, the two sources of PM data occasionally disagree by as much as 5 m.

Polar motion is observable by VLBI because it changes the x and y projections of the baseline onto the equatorial plane. Maximum sensitivity to PM is obtained from a north-south oriented baseline (WILLIAMS 1970). Baseline measurement with 1 m accuracy should be achievable using a single frequency (S-band for example) and introducing external transmission media calibrations. A two-frequency (S- and X-band) wideband VLBI system with water-vapour radiometric tropospheric calibrations should allow PM to be measured with an accuracy of 20 cm or better from a single day of data. These observations are, of course, with respect to an extragalactic radio source (ERS) frame.

6.3 Earth Tides

In much the same way that the moon and sun deform the ocean surface to generate ocean tides, the solid land masses undergo tidal oscillations. Amplitudes of the Earth tides are typically less than 0.5 m with diurnal and longer period variations. *In situ* gravimeters possess more than sufficient sensitivity for measuring this effect; however, it is not possible to separate tidal deformations from changes in the gravity field of the Earth itself. Once VLBI accuracies are in the domain of 10 cm or better, Earth tides should be measurable interferometrically, allowing separation of the geometrical deformations from mass transport phenomena. It would therefore be desirable for gravimeters to be co-located with VLBI stations.

6.4 Continental Plate Tectonics and Regional Fault Monitoring

The theory of continental drift has had remarkable success in blending apparently diverse geophysical disciplines into a single model of the Earth's crust. The model consists of several large continental plates which are in relative motion, at least in the geological past. Some of these plates are undergoing collisions with one another and these collisions frequently result in seismically violent events. Any global understanding of earthquakes must certainly concern itself with the probable fact of continental drift.

The drifts of continental plates are generally small, less than 20 cm per year. These rates have been indirectly deduced from phenomena such as sea floor spreading data. However, no direct measurement of the relative motions of the major continental plates has been possible to date because operational global geodetic technology is currently at the 10 m accuracy level.

The potential of VLBI for measuring intercontinental separations with 10 cm accuracies clearly will have great impact on determining contemporary drift rates and developing more advanced models of global earthquake mechanisms.

The issue of regional fault monitoring is another area where VLBI can make a valuable contribution. Fault systems are frequently complex as discontinuities do not simply occur at some defineable interface. For example, locked portions of the San Andreas fault system of California are probably storing strain energy, and elastic deformations may be going on hundreds of kilometres from the fault. Thus, conventional high accuracy geodimeter point-to-point measurements across the "fault" will measure little or no change over a 20 km baseline, while over a several hundred km baseline, substantial strains may be occurring.

A point which is not widely appreciated is that state-of-the-art geodimeter measurements have high accuracy (1 part in 10^6) only in a horizon control sense (in only two dimensions). Vertical control is most accurately obtained by a method known as differential levelling. Levelling is explicitly dependent on local gravity as a reference and is therefore directionally sensitive to deflections of the vertical. These deflections make it difficult to distinguish geometric relationships from those of a geodetic nature which have been gravitationally affected. In addition, differential levelling is accomplished in 100 m increments, making frequent long distance surveys through rough terrain logistically difficult. Accurate vertical crustal uplift measurements are assuming a very important role in studying the earthquake mechanism (WHITCOMB ET AL 1973; ANDERSON & WHITCOMB 1973) and coupling that with the horizontal crustal deformations predicted by continental plate tectonics, there is a great need for highly accurate three dimensional Earth measuring methods.

Because VLBI is capable of determining three-dimensional station locations with 10 cm or better accuracies on baselines of arbitrary length (10 km to 10,000 km), operates virtually under all weather conditions, and makes its observations relative to an essentially time-invariant co-ordinate frame of extragalactic radio sources, its potential for defining earthquake strain fields is indeed great.

6.5 The Extragalactic Radio Source (ERS) Frame

The co-ordinate system to which VLBI is sensitive is the frame of compact (emissions from regions less than 0.001 arcsec in diameter) extragalactic radio sources. These sources are primarily quasars, and are probably more than 10 to 100 Mpc away. Even if these sources have proper motions, they are not likely to accumulate the magnitude of errors encountered with local stars. For example, suppose a radio source 100 Mpc away was moving at one-tenth the speed of light perpendicular to the line of sight. Such a movement would be equivalent to 10^{-4} arcsec per year or about 3 mm per year drift in longitude. The issue of whether such motions actually exist, and whether they would be systematic, is far beyond the scope of this discussion. The current ERS catalogue for the 24 kHz recorded bandwidth system for VLBI Earth physics has about 50 objects suitable for use at S-band. With a future 2 MHz VLBI system, the catalogue of objects usable at both S- and X-band will remain at about 50. A catalogue of ten sources would serve well for a global geodynamics program.

7. Development Potential

7.1 Primary Network

The need for direct charged particle calibrations clearly indicates the desirability of simultaneous S/X-band VLBI as previously discussed. Given this type of calibration, the highly correlated errors due to the Earth's ionosphere can be effectively corrected to the 10 cm level or better. The wet component of the troposphere appears correctable given regional meteorological data and some type of direct calibrations such as water vapour radiometry at each antenna site.

Given these capabilities, impressive geodynamical measurements with the following accuracies should result:

$$\sigma_{UT1} = 0.5 \text{ msec (of time)} \; ; \quad \sigma_{\text{polar motion}} = 10 \text{ cm} \; ; \; \sigma_{\text{Earth tides}} = 10 \text{ cm};$$

three dimensional station locations to 10 cm; extragalactic radio source catalogue to 0.005 arcsec.

The foregoing results should be attainable with a few days of data. Thus, in continental drift

regions of 10 cm per year, VLBI could provide definitive information on drift rates in 2 years or perhaps less.

7.2 Portable Applications *

The need for VLBI data from remote locations obviously suggests some type of portable VLBI station. Fortunately the physics of the situation lends itself readily to this type of portable station. The observation of extragalactic radio sources is possible because the interferometer performance is governed by the geometric mean of the antenna areas (SHAPIRO & KNIGHT 1970). Thus, if only a small diameter antenna (< 10 m) can be put into the field, the lack of its sensitivity can be mitigated by having a larger antenna serve as the other receiving element of the interferometer.

It is also possible to further reduce the data acquisition requirements on the portable station by having it operate as an adjunct to a primary VLBI network. The primary net would be responsible for measuring UT1, polar motion, and determining radio source positions. Thus, only five parameters directly connected with the portable station must be solved for;

- the three co-ordinates for the station location;
- the clock offset; and
- the frequency offset.

Each radio source observed would provide three elements of information. Observing two sources, one at high declination and another at moderate low declination, would be sufficient to uniquely provide the portable station's location in three dimensions.

The particular implementation of received wavelengths would depend on the particular mission. For example, if data were desired on possible motions of some island in Japan, the portable station could be equipped for S/X-band simultaneous VLBI reception and a water vapour radiometer for tropospheric calibration. If this portable station had a 10 m diameter antenna and operated with a 26 m fixed station, five or more radio sources would be available, enabling the portable station to be located with a 10 cm accuracy, given only a few days data and operated in conjunction with a primary network.

For applications of regional tectonic monitoring, the situation is somewhat less complex. If a large fixed antenna is located in the approximate vicinity of a fault system, as is the case of the Goldstone antennas relative to the southern California portion of the San Andreas fault system, the baseline lengths can be limited to 1000 km or less. Having baselines of 1000 km or less enables a significant self-cancellation of the Earth's ionosphere, particularly the ionosphere's diurnal characteristic. If furthermore, the VLBI observations are made at X-band wavelengths, then the charged particle effects are esentially random at each station. This leaves only the tropospheric water vapour to be explicitly calibrated. Local meteorological data from the portable and fixed antennas, together with water-vapour radiometer measurements for each station should allow overall data accuracy of 7 cm from a single day of data. Four days of data from the portable station should allow a 3 to 5 cm accuracy in determining the station's location in three dimensions.

Such short to moderate length baselines tend to be insensitive to UT1, polar motion and source location; uncertainties of 3 msec in UT1 and 1 m in polar motion would amount to about 10 cm in the portable station location.

To operate portable stations at 1000 km separations from fixed stations would require primary

---

* Portable VLBI applications to earthquake research are being pursued under a concept name of ARIES (Astronomical Radio Interferometric Earth Surveying)

network performance equivalent to 0.005 arcsec. so that station locations would not have systematic errors above 3 cm from UT1, polar motion, and source location uncertainties.

Given a situation of no high-accuracy UT1, polar motion, and source locations, the portable stations could be designed to stand alone. That is, with moderately more sensitive receivers on the portable antennas, 10 m diameter stations could make up their own network, with station-to-station separation always less than about 200 km or with an observing program that makes sufficient observations to solve for the required UT1, polar motion, and source locations in a similar manner to that which would have been employed by the large antenna primary network.

8. Acknowledgments

The author wishes to thank P.S. Callahan, H.F. Fliegel, J.L. Fanselow, J.B. Thomas and J.G. Williams of the Jet Propulsion Laboratory, and J.H. Whitcomb of the Caltech Seismological Laboratory for advice on the many diverse elements concerned in the preparation of this paper.

9. References

ANDERSON, D.L. & WHITCOMB, J.H. 1973. *Time Dependent Seismology.* (in press) Seismological Laboratory,California Institute of Technology,Pasadena California.

BARE, C., CLARK, B.G., KELLERMANN, K.I., COHEN, M.H. & JAUNCEY, D.L. 1967. Interferometer Experiment with Independent Local Oscillators. *Science* 157,189-191.

BROTEN, N.W., LEGG, T.H., LOCKE, J.L., MCLEISH, C.W., RICHARDS, R.S., CHISOLM, R.M., GUSH, H.P., YEN, J.L. & GALT, J.A. 1967. Long Baseline Interferometry: a New Technique. *Science* 156,1592-1593.

FANSELOW, J.L., MACDORAN, P.F., THOMAS, J.B., WILLIAMS, J.G., FINNIE, C.J., SATO, T., SKJERVE, L. & SPITZMESSER, D.J. 1972a. The Goldstone Interferometer for Earth Physics. *Tech.Rep.* 32-1526,Jet Propulsion Laboratory,California Institute of Technology,Pasadena California, 45-57.

FANSELOW, J.L., MACDORAN, P.F., THOMAS, J.B., WILLIAMS, J.G., SPITZMESSER, D.J., SKJERVE, L. & URECH, J. 1972b. The Equatorial Projection of a California/Spain Baseline and Irregularities in the Earth's Rotation Rate as Obtained by a Radio Interferometer. *EOS Trans. Am.geophys.U.* 53,968.

GOLD, T. 1967. Radio Method for the Precise Measurement of the Rotation Period of the Earth. *Science* 157,302-304.

HINTEREGGER, H.F. ET AL 1970. *EOS Trans.Am.geophys.U.* 51,267.

HINTEREGGER, H.F. ET AL. 1972. Precision Geodesy via Radio Interferometry: First Results. *Science* 178,396.

KELLERMANN, K.I. 1971. Intercontinental Radio Astronomy. *Scientific American.* November Issue.

KLEMPERER, W.K. 1972. Long Baseline Radio Interferometry with Independent Frequency Standards. *Proc.IEEE* 60, May Issue (No 5).

MULHALL, B.D., CHAO, C.C., MOTTINGER, N.A., MULLER, P.M., ONDRASIK, V.J., SJOGREN, W.L., THULEEN, K.L. & TRASK, D.W. 1970. Tracking System Analytic Calibration Activities for the Mariner Mars 1969 Mission. *Tech. Rep.* 32-1499,Jet Propulsion Laboratory,California Institute of Technology,Pasadena California.

MUNK, W.H. & MACDONALD, G.J.F. 1960. *The Rotation of the Earth:A Geophysical Discussion.* Cambridge University Press.

ONG, K.M., CHAO, C.C. & MACDORAN, P.F. 1973. Unpublished Material. Jet Propulsion Laboratory, California Institute of Technology,Pasadena California.

ROGERS, A.E.E. 1970. Very Long Baseline Interferormetry with Large Effective Bandwidth and Phase Delay Measurements. *Radio Science* 5,1239.

MACDONALD, G.J.F. 1967. Implications for Geophysics of the Precise Measurement of the Earth's Rotation. *Science* 157,305-306.

RAMASASTRY, J. ET AL 1973. Presentation to *XVI-th Meeting of COSPAR*,Konstanz, Federal Republic of Germany.

SCHAPER, L.W., Jr., STAELIN, D.H. & WATERS, J.W. 1970. The Estimation of Tropospheric Electrical Path Length by Microwave Radiometry. *Proc. IEEE* February Issue.

SHAPIRO, I.I. & KNIGHT, C.A. 1970. Geophysical Applications of Long-Baseline Radio Interferometry. In (MANSINHA, L., SMYLIE, D.E. & BECK, A.E. ed.) *Earthquake Displacement Fields and the Rotation of the Earth*. Reidel Dordrecht,285-301.

THOMAS, J.B. 1972a. An Analysis of Long Baseline Interferometry. *Tech.Rep.* 32-1526,Vol.VII,Jet Propulsion Laboratory,California Institute of Technology,Pasadena California,37-50.

THOMAS, J.B. 1972b. An Analysis of Long Baseline Interferometry,Part II. *Tech.Rep.*32-1526,Vol.VIII, Jet Propulsion Laboratory,California Institute of Technology,Pasadena California,29-38.

THOMAS, J.B., FANSELOW, J.L., MACDORAN, P.F., SPITZMESSER, D.J. & SKJERVE, L. 1972. Radio Interferometry: Feasibility Demonstration for Monitoring Tectonic Motion. *EOS Trans.Am. geophys.U.* 53,968.

WHITCOMB, J.H., GARMANY, J.D. & ANDERSON, D.L. 1973. Earthquake Prediction: Variation of Seismic Velocities Before the San Fernando Earthquake. *Science* 180,632.

WILLIAMS, J.G. 1970. Very Long Baseline Interferometry and Its Sensitivity to Geophysical and Astronomical Effects. *Space Programs Summary* 37-62,Vol.II,Jet Propulsion Laboratory California Institute of Technology,Pasadena California,49-55.

10. Discussion*

MELCHIOR: In the paper it is written that VLBI should allow the separation of geometrical deformations from mass transport phenomena. Does that mean you intend to directly measure the Love numbers h and l without mixing with k?

ONG: Not at the moment.

MELCHIOR: The number h characterizes the ground variation directly. In the text it is said that it would therefore be desirable for gravimeters to be co-located with VLBI stations. In that use, gravimeters alone will not be sufficient. You should also have horizontal pendulums. Do you have an idea of the precision sought? For example, if you have a radial motion of 40 cm, should you, say, get 1% of that figure?

ONG: A precision of 5 - 10% of that figure is probably adequate.

MELCHIOR: Could you measure the deformations with a precision of 1%?

ONG: A precision of 1% of a 40 cm effect would amount to 4mm. At the present we can obtain 4 cm accuracy in all three components of short baselines. This is about 10% of the effect. Sub-cm precision for intercontinental baselines is beyond the present state of the art.

WERNER: An instrument of that size (radio telescope) should suffer from unexpected variations in position of the electrical centre; has the movement of the electrical centre been monitored relative to nearby marks to ascertain the size of this motion.

MACDORAN†: The electrical phase centre of the station is not the point of "antenna location" in a VLBI solution. The concept of a VLBI station location is at the intersection of antenna axes (i.e., the intersection of the elevation and azimuth axes). Such intersection of axes can be easily measured relative to a nearby geodetic control point. It is because of the method of multi-source simultaneous solution for baseline, astronomical and instrumental parameters that it naturally dictates the axes intersection to be the only spatially invariant point at each station.

GUBBAY: I believe there is a settling time for it and I believe movements have been noted at Tidbinbilla during the first six months of operation. Small movements, but they are being measured.

*Paper presented by K.M. ONG †Post symposium written reply

GUBBAY, J.S.
LYNN, K.J.W.
LEGG, A.J.
ROBERTSON, D.S.
Space Research Group
Weapons Research Establishment
Adelaide
AUSTRALIA

Proc. Symposium on Earth's Gravitational Field & Secular Variations in Position (1973),396-405.

COMPARISON OF TWO INTERCONTINENTAL BASELINES BY VLBI

ABSTRACT

Compact components, ≤ .001 arcsec, of several radio sources were observed in the course of VLBI observations at S-band between NASA-JPL Deep Space Stations located in South Africa, Australia, and California USA. During the southern summer of 1971-72, the stations were equipped with H-maser frequency standards of sufficiently high stability to allow phase coherent integration of the data, thus improving the system threshold and reducing the doppler fringe frequency reading error to better than 1 mHz.

The primary aim of the experiments was to monitor the secular behaviour of the fringe amplitude due to the compact components and consequently two successive observations were made on each source. However, the data were analysed to determine errors in the assumed baselines as well as the relative clock drifts and to improve the determination of source positions. There is some evidence for the existence of an error in the hour angle of both baselines of about + .07 s. The error in the length of the projection of the trans-Pacific baseline on the equatorial plane was not significant. A present difficulty in determining this length for the southern VLBI and its solution is explained.

1. Introduction

During the southern summer of 1971-72, two stations of the NASA-JPL Deep Space Network, DSS 51 at Hartebeesthoek, South Africa and DSS 41 at Island Lagoon, South Australia, co-operated in a series of three interferometer experiments (see Table 1).

TABLE 1

Interferometer experiments using independent H-maser frequency standards

Epoch		Western Station Designation	Eastern Station Designation
357-8	1971	DSS 51, Hartebeesthoek, near Johannesburg, South Africa	DSS 41, Island Lagoon, near Woomera, South Australia
21	1972		
44-5	1972		
52-3	1972	DSS 41	DSS 12, Goldstone, California United States of America

G. Nicolson and P. Harvey of the South African CSIR were responsible for the conduct of the experiments at the South African terminal. This series was followed within a few days by an experiment between DSS 12 near Goldstone in California and the Australian station, DSS 41. The three stations taking part in experiments across the two intercontinental baselines were equipped with 26 m antennae, maser front ends and Hydrogen maser frequency standards.

The trans-Pacific experiment was conducted in conjunction with A. T. Moffet and D. Shaffer of the California Institute of Technology and D. Spitzmesser of the Jet Propulsion Laboratory. The only significant difference in equipment configuration from that adopted for the southern baseline experiments was the substitution of the S-band synthesizer by a multiplier chain at one station.

Cohen and Shaffer 1971 took the results of a survey for compact components using a trans-Pacific baseline between the 64 m telescope at Goldstone, California and the 26 m telescope at Tidbinbilla, Australia, to determine the position of compact components. Their position determinations were among the first using VLBI techniques with independent local oscillators. The accuracy of these positions was limited by the stability of the station rubidium frequency standards and by the single parameter atmospheric model adopted.

In our experiments, both ionospheric and atmospheric contributions to the phase path were taken into account. The ionospheric model adopted for computing corrections to the observed doppler difference frequency was that given by ONDRASIK & MULHALL (1969). Here the real ionosphere is replaced by a curved slab of ionization with the same vertical total electron content. Stanford University and F. Hibberd of the University of Armidale supplied values of total electron content for the American and Australian observations respectively. These values were obtained by measurements of Faraday rotation using signals from geostationary satellites. No total electron content information was available from South Africa. Values for this site were inferred from locally obtained F-region critical-frequencies (supplied by the South African CSIR Telecommunication Group) using the method described by MULHALL, ONDRASIK & THULEEN (1970) together with scale heights calculated from the Armidale data.

The atmospheric contribution to phase path was calculated using a standard US atmosphere for a latitude of 35° and an average water vapour content. The height of the observing telescope above sea level was the significant parameter in producing differences between observing sites.

2. Description of Method

If $\vec{B}$ represents the retarded baseline vector (NASA LS35 station solution) and $\vec{\ell}$ the unit vector in the direction of an extragalactic source and c the velocity of light, then T, the time lapse between the arrival of corresponding segments of the waveform at the respective stations can be expressed

$$T = \frac{1}{c} \vec{B} \cdot \vec{\ell}$$

The bandwidth of the data is only 14.3 kHz and therefore T cannot be determined to better than about 0.5 microsec. This is equivalent to an uncertainty of about 150 m in the projection of the baseline in the direction of the source. Due to the rotation of the earth $\vec{\omega}$ however, the angle between $\vec{B}$ and $\vec{\ell}$ varies continuously and the time derivative of the lapse time, i.e. the doppler difference frequency ν, divided by the observing frequency F, becomes

$$\frac{\nu}{F} = \frac{dT}{dt} = \frac{1}{c}\vec{\omega} \times \vec{B} \cdot \vec{\ell}$$

The difference S, between the observed frequency ν_o, and the expected ν_o, is given by

$$S = \frac{1}{\Delta T} \int_o^{\Delta T} (\nu_o - \nu_p)dt = \frac{\phi}{\Delta T} \qquad (1)$$

where ϕ is the total phase accumulated over the integration time ΔT, and can be determined to approximately 0.1 cycle. The hydrogen maser frequency standards used at the stations were sufficiently stable to allow phase coherent integration over the whole data record of 660s, giving an accuracy of ± 0.15 mHz in the measurement of S. This is equivalent to an intrinsic error in the equatorial component of the baseline distance of about 0.3m, assuming that there are no other sources of error. Contributions to S arise from:

1) errors in right ascension of source
2) errors in declination of source
3) possible error in baseline length, and
4) possible errors in frequency standards or "bias".

There are other possible contributions to S, such as the atmosphere and the ionosphere, but for the moment let us restrict ourselves to these four sources of error.

Errors 3 and 4 are common to all sources, although in the case of 3 the contribution to S of a constant error in baseline length will be different for different sources. Suppose we observe n sources twice each. This provides 2n values of S and we have 2n + 2 unknowns.

Let a_m and b_m be the errors in the assumed values of right ascension and declination of the mth source. Let e be the error in the length of the projection of the baseline on the equatorial plane (=R), and let d be the frequency difference between the two station frequency standards or "bias". Then for the 2n values of S obtained there are n sets of dual equations of the form:

$$S_{2m-1} = a_m \frac{\delta S_{2m-1}}{\delta(RA)} + b_m \frac{\delta S_{2m-1}}{\delta(DEC)} + e \frac{\delta S_{2m-1}}{\delta R} + d \qquad (2)$$

$$S_{2m} = a_m \frac{\delta S_{2m}}{\delta(RA)} + b_m \frac{\delta S_{2m}}{\delta(DEC)} + e \frac{\delta S_{2m}}{\delta R} + d \qquad (3)$$

Referring to equation 2, S_p depends upon errors in right ascension, declination, R, and the bias d. Therefore, if S_p is plotted against $\frac{\delta S}{\delta R}p$, the scatter of the points from a best fit line will depend upon the errors in right ascension and declination.

The best fit line will have a gradient equal to e and the value of S given by this line when $\frac{\delta S}{\delta R}$ equals zero will be d. Using these values of e and d in equations 2 and 3 the right ascensions and declinations of the n individual sources can be readily calculated from the n pairs of equations.

To find the best fit line, the assumption has been made that the population of sources is large enough to be regarded as having a normal distribution in right ascension and declination errors, i.e. the assumption that the following equation is valid.

$$\sum_{2n} \left\{ \frac{S_p - (d + e \frac{\delta S_p}{\delta R})}{W_p} \right\}^2 = \text{Minimum} \qquad (4)$$

e and d are found by differentiating this equation with respect to e and d. The two resulting equations can then be solved for e and d. W_p is a weighting factor depending upon the derivation of the reference source positions.

The weight to be attached to an observation when determining the best fit line is a function of the ionospheric and tropospheric contributions to S. The contribution of these regions to S is proportional to the electrical length of the path through them but the models used for these regions are imperfect. The path length is a function of the right ascension and declination of the star so that the weighting factor W_p will also be a function of the position of the star.

The weight is also a function of the errors in the reference positions of the stars. The Kristian and Sandage optical positions are taken to have an accuracy of ~0.5 arcsec. The contribution to S due to a position error is also a function of the position of the star.

We have therefore defined the weighting factor W_p to be

$$W_p = \left\{ (0.5 \frac{\delta S_p}{\delta(RA)})^2 + (0.5 \frac{\delta S_p}{\delta(DEC)})^2 + (\frac{1}{20} T_p)^2 + (\frac{1}{10} I_p)^2 \right\}^{\frac{1}{2}} \qquad (4)$$

where RA and DEC are the right ascension and declination of the star used for the p^{th} observation and T and I are the corrections to S due to the troposphere and ionosphere. The factors of $\frac{1}{20}$ and $\frac{1}{10}$ reflect the confidence that we have in our models for the two regions. The possibility of the optical and radio positions being different would give an additional contribution to W_p. We have no quantitative data about this, so are unable to include it.

3. Results

Figure 1 represents the trans-Pacific results. The reference positions for the sources are those of the optical counterparts of each source. The best fit line gives e = -5.3 and d = -0.1 see Table 2. The points in figure 2 are obtained when the reference positions are VLBI determinations either by NASA/JPL or MIT. In this case W_p consists only of the terms representing the relative likely error in the atmospheric correction.

Figure 3 displays the results obtained using the Southern VLBI, South Africa to Australia. The baseline and bias errors are assumed unchanged for the three experiments and the results are plotted together. The reference positions have been determined optically and the weighting factors W corresponding to the optical case have been adopted to obtain the best fit line. The outstanding feature of this plot is that the points cover a very narrow range in $\frac{\delta S}{\delta R}$ because no accurate high declination optical determinations were available. The wide range in the value of $\frac{\delta S}{\delta R}$ within the declination viewing limits would otherwise allow better baseline and bias solutions in this case than

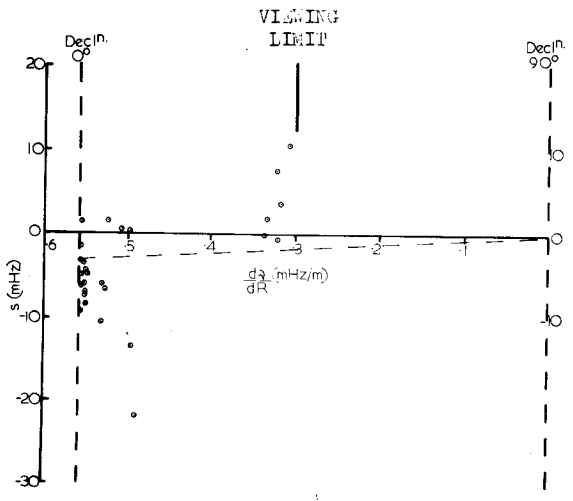

Figure 1. Trans-Pacific results

Plot of frequency residuals against the effect in mHz of an error of +1m in equatorial distance R
Reference positions were determined optically
(KRISTIAN & SANDAGE 1970)

TABLE 2

Baseline	Reference Sources	Figure	Error in Equatorial Projection e(m)	Bias d(mHz)
Trans-Pacific	Optical	1	-5.3	-0.1
Trans-Pacific	VLBI	2	-0.5	-3.9
Southern	Optical	3	11.8	-16.6
Southern	Various	4	-67.9	26.4

for the trans-Pacific interferometer.

The same condition obtains in Figure 4 where the reference positions include any available positions determined by long or short baseline radio interferometers or by optical means that are accurate to about a second of arc or better. The common sky of the southern interferometer does not extend to declinations above +16° and the positions of the high declination southern sources observed, P0332-40, P0438-43, and P0537-441 are not sufficiently well known yet. Consequently the best fit solutions for figures 3 and 4 are of very little value. However, accurate optical positions for these sources are being determined by B. Peterson at Mt Stromlo.

Figure 5 compares the distribution in right ascension error among the sources observed across the Pacific and for the southern interferometer respectively. The error in the hour angle of the baseline is taken to be the value of the mode of the distribution to avoid the effect of "rogue" values. The error in the hour angle of the two baselines appears to be similar and in the same sense.

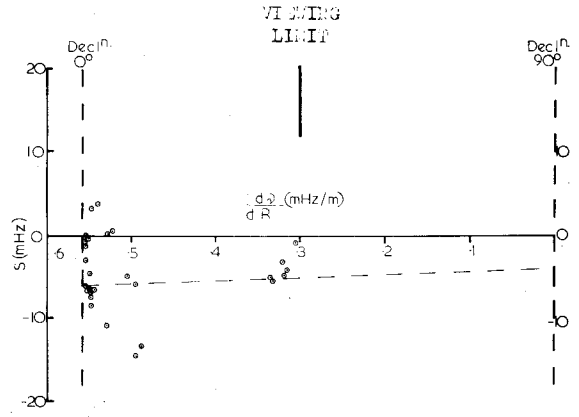

Figure 2. Trans-Pacific results

Plot of frequency residuals against the effect in mHz of an error of +1m in equatorial distance R
Reference positions were determined by VLBI
(JPL and MIT results)

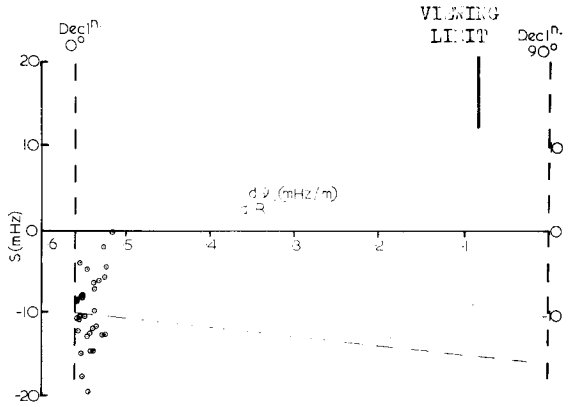

Figure 3. Trans-Indian results

Plot of frequency residuals against the effect in mHz of an error of +1m in equatorial distance R
Reference positions were determined optically
(KRISTIAN & SANDAGE 1970)

Faraday rotation observations are available in Australia and in California on a continuing basis and will probably soon become available in South Africa. However, X-band receivers will be available at the NASA-JPL stations in Australia and at this observing frequency the effect of the ionosphere is negligible. Dual frequency observations would yield optimum results.

Our experiments were not designed for the purpose of geodetics, but they have yielded some geodetic

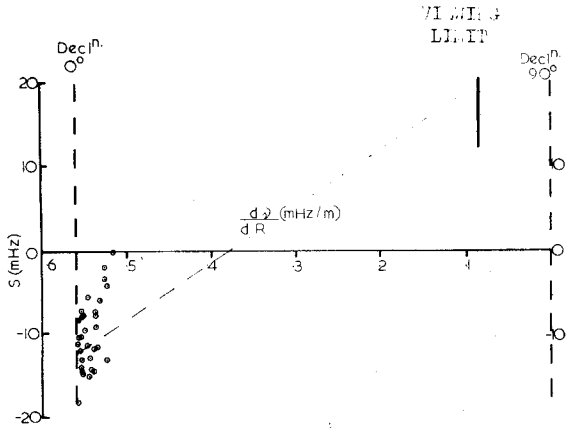

Figure 4. Trans-Indian results

Plot of frequency residuals against the effect in mHz of an error of +1m in equatorial distance R
Reference positions were determined by various techniques

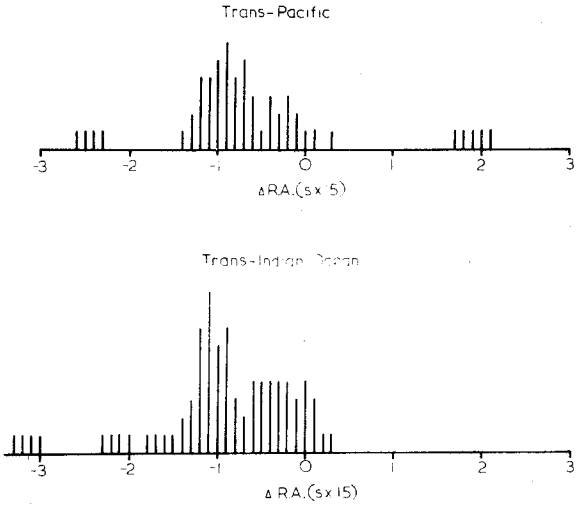

Figure 5. Frequency distribution of right ascension errors (arcsec)

information. The length of the projection of the trans Pacific baseline on the equatorial plane, R, seems to be accurate, but there is a significant error in the hour angle of this baseline. To obtain the true baseline therefore, the assumed baseline must be rotated eastwards. There is some evidence that this also applies to the southern baseline.

A VLBI experiment, or series of experiments, could be designed to yield a baseline accuracy of about 1m in R and an accuracy in baseline hour angle of .01 s. A sampling rate of 1 to 2M bits/sec would be required to provide a corresponding accuracy in the determination of the component of the baseline along the earth's axis.

Short-baseline connected-element interferometry can provide positions of the required degree of accuracy but the centroid of the object thus observed at low resolution does not appear to correspond to the VLBI objects. The position for P0438-43 obtained by Wade in 1973 using the NRAO interferometer would be consistent with an intercontinental baseline error of a few hundred meters.

Two pairs of trans-Pacific observations were taken on 3C279 and each pair was treated independently. The observations were not successive in this instance, the first and third and the second and fourth forming the two pairs. The agreement between the two positions obtained for 3C279 was better than 0.1". The discrepancy between the two values of declination and the MIT value was also within this limit but the right ascensions differed from the MIT value by -.07 s. This is probably due to an error in the hour angle of the assumed baseline which has been discussed. Table 3 sets out the difference between our trans-Pacific positions of several sources and those determined by FANSELOW et al (1973), of JPL, or by ROGERS et al (1973), of MIT and in one case, the position of the optical component given by KRISTIAN & SANDAGE (1970).

TABLE 3

TRANS-PACIFIC RESULTS (OF FIGURE 2)

POSITION SOLUTION MINUS REFERENCE POSITION

Source	RA Err(S*15)	Dec Err (arcsec)	References
NRA0190	-1.230	23.16	JPL
P2134+00.4	-2.407	7.608	JPL
P0106+01	0.504	-5.456	JPL
P1055+01	-1.157	-2.204	JPL
3C273	-0.881	-0.576	MIT
P1741-3.8	-0.292	-1.160	JPL
3C279	-1.008	-0.052	MIT
3C279	-1.003	-0.002	MIT
P1510-08	-0.739	-1.050	K&S
3C454.3	-0.750	-0.7374	JPL
P2345-16	-0.294	0.513	JPL
3C345	0.858	0.950	JPL
4C39.25	0.008	0.171	JPL
VR042.22.1	1.883	1.593	JPL

4. Conclusions

Although our series of observations was designed to study temporal variations of quasar components of angular diameter $\leq$ .001 arcsec., useful geodetic and source-positional information has been obtained. This was in spite of the fact that individual observations were made sequentially rather than being spaced so as to cover a reasonable range of hour angle.

It is by no means certain that when one component dies and another is born that the new one will

occupy the same position as the old one. Accuracies of the order of 0.01 arcsec are on the horizon and one will soon be able to detect such differences in position of successive components, if they exist.

For an inertial reference system for geodetic purposes one will need a population of extra galactic sources so that these small differences will average to zero.

5. References

BROSCHE, P., WADE, C.M. & HJELLMING, R.M. 1973. *Proc. IAU Conference, Perth, Australia,* on "New Problems in Astrometry".

COHEN, M.H. & SHAFFER, D.B. 1971. *Astronom. J.* 76, pp.91-100

FANSELOW et al, 1973. Personal communication.

KRISTIAN, J. & SANDAGE, A. 1970. *Ap. J,* 1962, 391.

MULHALL, B.D., ONDRASIK, V.J. & THULEEN, K.L. 1970. *JPL Technical Report.* 32-1499, p.45.

ONDRASIK, V. & MULHALL, B.D. 1969. *JPL Space Programs Summary* 37-57, II, p.23

ROGERS, A.E.E., COUNSELMAN III, C.C., HINTEREGGER, H.F., KNIGHT, C.A., ROBERTSON, D.S., SHAPIRO, I.I, & WHITNEY, A.R. 1973. - To be submitted to *Astrophysical Letters.*

6. Discussion

ROBERTS: When you are able to observe the source for many hours, is it not possible to solve for both the baseline and the position of the source?

GUBBAY: Yes, and we will, eventually, but can't do it at present because the hydrogen masers have left as they were in Australia only for the Mariner Mars experiment. For good geodetic work, I would certainly favour hydrogen masers although in the last paper there was some reference to modern caesium systems. Maybe our chairman (HIBBARD) could differentiate between the older caesium systems we use, and which have very poor short term stability like the old rubidium, and the modern caesium system.

HIBBARD: There is a new Hewlett Packard caesium standard not yet available in Australia which is ten to a hundred times better in general short term stability and a little better in absolute frequency. We are referring to seven parts in 10^{12} in absolute frequency, and it is suggested this stability is more like a part in 10^{13} over some hundreds of seconds. This is extremely good and when these are scattered around the stations, you'll find a lot more work can be done. There will be no abundance of hydrogen masers.

ANON: Could the caesium tube be shortened? Is it a problem of epoch? MACDORAN's paper stated that a caesium tube is satisfactory over a short baseline and not a long baseline.

ONG: It is mainly that over a short baseline, you could make a more rapid measurement of sources during a three hour period. You would avoid using a caesium standard for over three hours. It would drift too much.

MARKOWITZ: The table in your paper gives comparisons of baselines in terms of frequency. What is required for geodetic applications are lengths. Will you be expressing these comparisons in terms of length?

GUBBAY: What I have done is to express a comparison in right ascension. As far as the baseline is concerned, I can only say that I am comparing not the baseline but the quality of the results. In the case of the trans-Pacific line we can get some kind of an answer, i.e., less than ±5 m. The LS35 solution is pretty accurate. I agree we should come out with errors in metres. Less than a metre (0.3 m) for the trans-Pacific line for the equatorial distance. In the case of the trans-Indian, the results are not trustworthy. Table 2, column 4, lists the respective errors in equatorial projection in metres; column 5 shows the corresponding relative clock drifts in mHz.

LLOYD, I. D.
School of Surveying
University of New South Wales
Kensington N.S.W. 2033
Australia

Proc. Symposium on Earth's Gravitational Field & Secular Variations in Position (1973), 406-409.

ON THE SCALE AND ORIENTATION OF GEODETIC REFERENCE SYSTEMS FROM VLBI

ABSTRACT

Since all points on the Earth's surface must be considered to be in motion relative to one another, the optimum strategy is to hold one station fixed and refer the motion of all points on the Earth to this station. The next step is to use the current technologies to measure the vector between pairs of geodetic stations within the instantaneous reference system. The final step is to relate the instantaneous reference systems to one another and then extract the data on earth dynamics.

Given an acceptable geodetic reference system for long term studies of the Earth, the problem then becomes one of adding scale and orientation to the network of geodetic stations. This paper examines the *method* by which these goals can be achieved and the possible *consequences* on the extracted information, using the technique of VLBI.

1. Introduction

For long term studies in earth physics a Geodetic Reference System should be such that it is possible to relate observations directly to it and to have secular variations in position simply related to changes in co-ordinates between epochs. An example of a convenient system is given by (MATHER 1973):

1. At any epoch replacing earth by an instantaneous rigid body model;
2. Adopting a three-dimensional cartesian system centred at the geocentre;
3. Letting x_3 axis coincide with the axis of rotation;
4. Letting x_1x_3 plane contain the axis of rotation and one point on the earth's surface.

Ideally, this one point on the earth's surface should be the only fixed station, to which the motion of all other points is referred. Then provided that the instantaneous reference systems can be related to one another, earth dynamic studies require the high precision measurements of the vector between pairs of geodetic stations within the instantaneous reference system.

VLBI observations can define the vector between the optical centres of the two radio telescopes within the co-ordinate system of the observed radio sources, to resolutions approaching 10 cm (HINTEREGGER ET AL 1972). Then provided the many parameters involved in the transformation to the instantaneous reference system can be evaluated, we have our requirements apparently fulfilled (LLOYD 1973). However, the *scale* and *orientation* for the baseline within the reference system is indeterminate from observations on unknown sources. So that, while VLBI can relate points on the earth's surface to one another to very high precision within an arbitrary reference system at any instant, external observations are required to define the scale and absolute orientation with respect to the accepted geodetic reference system.

2. The Basic Problem

The measured quantities in the VLBI technique are the time delay and the fringe frequency, where the time delay can be considered to be the time difference taken for the radio wavefront to reach the two radio antennae from the source, and the fringe frequency is the difference between the doppler frequencies at the two antennae. Hence, the measurements are differential quantities and VLBI can be considered as a geometrical device relating parameters of the baseline vector and source vectors. An analogy can be made with the measurements of directions by a theodolite in a triangulation net where each observed quantity is related to the position of the observer and that of the target. In the case of the theodolite measurements an arbitrary adjustment can be made which is completely consistent within itself but which does not yield the practical co-ordinates required (called a free net adjustment). To obtain the answer which we want from the triangulation adjustment in terms of real co-ordinates, the co-ordinate system must be uniquely defined. For directions reduced to a projection plane two points are held fixed or one point plus an externally observed azimuth (giving orientation to the net) and one observed distance (giving scale) are held fixed during the adjustment. Similarly, with VLBI observations, either internal control or external observations or conditions are required to obtain an unambiguous solution for the parameters with respect to the reference system.

The basic problem can now be summarised. In an adjustment of VLBI observations to distant radio sources, internal control must come from holding several source co-ordinates fixed. But these co-ordinates can only be estimated from earth-based VLBI which assumes a known baseline vector. But of course, baseline vectors are really the unknowns and also, by fixing the source positions, errors will be introduced into the extracted earth dynamic parameters, due to the proper motions of the sources.

3. Discussion

While a network of VLBI baselines cannot be tied to the geodetic reference system by VLBI observations alone, it can form an internally consistent arrangement fixed to two observed sources. Therefore, since geophysicists are really more interested in relative movements on the earth, rather than absolute distances between points on the earth's surface, it might appear attractive to perform experiments and holding the two sources fixed at their best known values. The error here would be in assuming that the two fixed sources had negligible proper motions over several years, at about the 0.001 arc second level, an assumption which is without justification.

It can be said that for unambiguous results in earth dynamics, besides VLBI observations, external observations or measurements using a different principle appear essential. These observations are required to scale the space, introduce orientation of the geodetic net with respect to the geodetic reference system, and isolate the proper motions of the sources.

It appears that accurate scaling observations over more than one VLBI baseline, besides introducing the unknown scale to the space, can also isolate the proper motion of the sources. This is because, while accurate scaling will show a change in the chord distance between the two earth points due to plate tectonics, the change in distance as recorded by VLBI will also include the proper motion effects of the fixed source parameters. An example of a very accurate scaling device is laser ranging to artificial earth satellites.

The observation of absolute orientation need only be made at one location, such as the reference point through which the x_1x_3 plane is defined, but the measurement must have precision equivalent to that of

VLBI and scaling. As a minimum requirement it must be possible to measure at different epochs either the direction of one baseline, or one source within the reference system. A suitable technique is not available at the moment.

4. Conclusion

The goal of modern geodesy is to relate points on the earth's surface to one another within a geodetic reference system. VLBI could be considered as the workhorse within such a programme relating geodetic stations within an arbitrary reference system. However, to obtain parameters within the defined reference system will require observations of scale (with respect to the velocity of light) and of absolute orientation, by means of different observing techniques. The combination of VLBI observations and laser ranging observations would be an exciting venture and a step towards the achievement of this requirement.

5. References

HINTEREGGER, H. F. ET AL 1972. "Precision Geodesy via Radio Interferometry: First Results" *Science* Vol. 178, 396.

LLOYD, I. D. 1973. "Geodetic Applications of Very Long Baseline Interferometry" *UNISURV Report* G-19 p. 81.

MATHER, R. S. 1973. "Geodetic Reference Systems for Long Period Studies in Earth Physics" *UNISURV Report* G-19 p. 1.

6. Discussion

GUBBAY: I think it is a little severe to state that VLBI has no means of finding its own reference system; because without knowing anything about baselines, either its length or orientation, we can determine the declination of a source in this way. Let us consider a thought experiment where your sources are spread through the whole range of $\pm 90^{o}$; if we had sufficient time to observe all sources, then that source with the greatest peak fringe frequency lies on the equator. The peak frequency of the other sources are related through declination only. If you get the peak frequency of one source and compare it with the maximum ...

LLOYD: You get the source closest to the equator.

GUBBAY: You have a continuous spread ....

LLOYD: You have a line of sources separated by nothing; but you don't have this line in reality.

GUBBAY: This was a thought experiment; in practice the relation between them is $\cos(\mathrm{Decl}^{n}\ A)/\cos(\mathrm{Decl}^{n}\ B)$ .....

LLOYD: Yes; but this is not practical at all. What you do is make observations on discrete sources. Set up parametric equations and there is no way of putting in control internally to give absolute values.

ANGUS-LEPPAN: Is this reference system you propose consistent with reference systems for other types of observations?

LLOYD: I did not mention a reference system specifically as this can apply to any reference system. Ideally we'd like a reference system such as that pointed out by MATHER which has various

properties, one of which is that observations should be directly related to the reference system. Secondly the parameters you are after should be easily extracted from this system. I am in full agreement with the system he quotes.

I showed a Cartesian system here but I did not say how it was defined. The system defined by MATHER where the z-axis coincides with the instantaneous rotation axis, the origin coincides with the instantaneous geocentre and the x-axis is defined in the following manner. The x-z plane contains one Earth fixed point. And that is very suitable for VLBI observations. Unfortunately we have to fix the co-ordinates of one or two extra-terrestrial sources. The only way this can be done is to combine several different types of observational techniques and bring them together. The problem is one of establishing an absolute orientation with a few cm precision.

KAULA, W.M.
Department of Planetary & Space Science
University of California
Los Angeles, California 90024
United States of America

Proc.Symposium on Earth's Gravitational Field & Secular Variations in Position (1973),410-412.

GEOPHYSICAL IMPLICATIONS OF LUNAR LASER RANGING

ABSTRACT

Laser distance measurements to the Apollo retroreflector packages are currently being made regularly by the McDonald Observatory with an accuracy of 15 cm. A new station being constructed on Maui has an accuracy goal of 2 or 3 cm. The results over two and a half years have been fit with an accuracy of 3 m. Improvements in the theory of the moon's angular motion about its centre of mass and in lunar orbit calculations are expected to give better agreement between theory and experiment soon. Future results are expected to include measurement of polar motion to a few cm, UT-1 to 100 microsec, and crustal movement to a few cm. Repeated station location measurements with a mobile station at a network of fundamental sites spaced perhaps 1000 km apart, when supplemented by accurate absolute gravity measurements, seem capable of providing a reliable reference framework for the measurement of the dynamics of the Earth's crust and upper mantle.

1. Text

This paper is a team report. The report by BENDER ET AL (1973)* covers developments till early 1973. This paper brings that report up-to-date and discusses some of the predicted applications for geophysical uses.

The instrumental jitter is ±2½ nsec or ±50 cm in range. A normal point obtained from a 15 min. span has an uncertainty of ±15 cm in range from the telescope to the retro-reflector on the moon. A three parameter (the position of the moon with respect to the telescope) fit of 5 or 6 hours of data has an rms residual of ±11 cm. So it would appear that the data itself has an accuracy of ±15 cm.

From the point of view of the data analyst, the main objection is that the data are not a completely continuous record. In a typical month, there are data for only 14 days. The gaps in the data are 9 days (around new moon), 2 days, and two of 1 day each. As with artificial satellite tracking, these gaps in the data contribute much more to uncertainty in the results than the instrumental inaccuracy.

As discussed by BENDER ET AL (1973), considerable progress has been made. The best information available in 1969 leads to residuals of several hundred metres. A solution for a reasonable number of parameters (21) enables the residuals to be brought down below ±3 m for a three year long data record. Since BENDER ET AL (1973), when it was felt that the main reason for the ±3 m were the physical librations, a new model for the physical librations has been generated by Eckhardt considering the third degree harmonic terms and the non-linear iteration terms. The present situation

* copies distributed to symposium participants

for a long data span is about ±0.5 m for the relative position of the retro-reflectors and ±1 m for the orbital error.

The ±1 m residual also depends on a tidal acceleration of 38 sec per century^2, confirming the values found by other techniques in recent years.

The current modeling work, mainly by J.G. Williams, is trying to work out some discrepancies between numerical integration and iteration theories in the physical librations. The ±1 m error does not prevent much smaller geophysical effects from showing up. Discrepancies between two points on the same day, e.g., errors in UT1 and in the polar wobble, are caused by differences in range at different times of day for the same station. These effects are at the 0.2 m level, smaller than the estimate of the accuracy of the BIH pole position (0.4 m).

Error analyses (KAULA 1973) confirm that the spectral separation by the Earth's rotation enables determination of geophysical and geodetic parameters to much smaller uncertainties than the total uncertainty of the system. The following are some results from error analyses of hypothetical spans for 440 days of data. ±15 cm instrumental uncertainty was assumed, and 97 parameters were solved for.

Stations in Texas & Hawaii, plus: -				Australia	Crimea	Azores
Station Drift	E-W cm/yr /yr	-	4.5	4.1	4.4	4.4
	N-S cm/yr	-	25	18	19	20
Wobble	13.25d cm	-	2.6	1.5	1.5	1.6
	13.66 cm	-	3.8	1.8	1.9	2.1
	14.11 cm	-	3.0	1.7	1.6	1.9
	27.33d cm	-	5.6	2.8	3.7	3.1
Rotation	13.25d 10^{-6}s	-	18	10	9	11
	13.66 10^{-6}s	-	34	20	22	24
	14.11 10^{-6}s	-	21	13	12	14
	27.33d 10^{-6}s	-	211	80	128	159
Tidal Love No.	h	-	-	0.60	0.29	0.49	0.44

The reason why east-west drift is so much better determined than north-south drift is that the effect of station drift on the signal will be sinusoidal with a period of 24 hours; the phase depends on longitude and the amplitude depends on the distance from the rotation axis. The error ellipsoid for position determination from laser ranging has its longest axis parallel to the rotation axis and its shortest in the longitude direction.

The main weaknesses in the error analysis are the truncated rotation and wobble spectra and the assumption of day-to-day randomness of gaps in the data. However, it is evident that the main need is a southern hemisphere station to get better coverage of the orbit, as well as more sensitivity to polar wobble.

2. References

BENDER, P.L., CURRIE, D.G., DICKE, R.H., ECKHARDT, D.H., FALLER, J.E., KAULA, W.M., MULHOLLAND, J.D., PLOTKIN, H.H., POULTNEY, S.K., SILVERBERG, E.C., WILKINSON, D.T., WILLIAMS, J.G. & ALLEY, C.O. 1973. The Lunar Laser Ranging Experiment. *Science* 182,229-238.

KAULA, W.M. 1973. Potentialities of Lunar Laser Ranging for Measuring Tectonic Motions. *Phil.Trans.R.Soc.Lond.A* 274,185-193.

3. Discussion

HOLDAHL: You mentioned a 1000 km spacing for observing stations. Do you think a spacing of VLBI or Lunar Laser Ranging stations of less than 1000 km would produce greater advantages than have already been obtained by use of current terrestrial methods?

KAULA: I referred to one of laser ranging to satellites and the moon or VLBI. All three might have a certain role, but the global role of lunar ranging or VLBI or the regional role of satellites involve many obstacles that have to be dealt with. From the point of view of geophysics and the determination of secular motion, regional determinations are more important than long wave determinations of secular motion.

MUELLER: On the last slide that you showed were there three stations observing four reflectors?

KAULA: Two reflectors. There were two and the three stations adding on to the Hawaii station, the third station. The table was published in (KAULA 1973). A similar analysis has also been made by Counselman. Bender has also made an analysis, which was not a conventional error analysis but defines systematic error contributions.

Proc. Symposium on Earth's Gravitational Field & Secular Variations in Position (1973), 413-432.

LUCK, J. McK.
MILLER, M.J.
MORGAN, P.J.
Division of National Mapping
Department of Minerals & Energy
Canberra ACT
A U S T R A L I A

THE NATIONAL MAPPING LUNAR LASER PROGRAM

ABSTRACT

National Mapping is reassembling the AFCRL Laser Ranger at Orroral in the ACT for the purpose of Laser Ranging. The site was chosen after a careful examination of many factors including number of clear/usable nights, 50%; level of precipitable water vapour, less than 10 mms; level of logistical support available, high; night sky contamination assessed as zero and average atmospheric seeing quality, normally less than 2 arc seconds. The determination of the site and the granting of the necessary approvals is now complete after almost nine months of continuous activity.

The proposed configuration of the hardware is to use a modified cassegrain (Nasmyth) focus position of a 1.5 metre astronomical telescope to transmit and receive photons generated by a 4 stage ruby laser operating initially with a power of 3 Joules, once every five seconds with a 10 nanosecond pulse width. Plans are in hand to reduce the pulse width as expertise becomes available. Timing will be at the one nanosecond level, consequently the initial limitation will be due to pulse length.

Tracking will be accomplished by a servo-loop working from the main field optics and an image dissecting tube with a digital step size of 0.6 arc seconds to both the equatorial and declination axis. A feature of the system is the ability to track on a lunar object, usually a region of high contrast, and then to offset from a known lunar point to the retroreflecter which corresponds to the optical axis of the system.

The object of this program is to monitor the secular changes in position that occur as a direct result of: variations in the rotational speed of the earth and its inclination, commonly referred to as polar motion; crustal motion, commonly referred to as continental drift, and hopefully, long term changes in gravitation, tidal coupling and the variation of astronomical constants.

1. Introduction

To augment its programs of studying secular geodetic changes and monitoring polar motion, the Division of National Mapping is installing a Lunar Laser Ranger (LLR) at Orroral Valley in the Australian Capital Territory. It consists of a 150 cm Ritchey-Chretien telescope used in the modified Cassegrain (Nasmyth) configuration, a one gigawatt pulsed ruby laser, a minicomputer for telescope and laser control and data acquisition, and associated control electronics.

The equipment was made available to the Division as a long term loan from NASA in cooperation with the Smithsonian Astrophysical Observatory. It was formerly operated by the US Air Force Cambridge Research Laboratories at Mount Lemmon in Arizona.

Briefly, its principle of operation is to fire a laser pulse three nanoseconds long through the telescope which collimates the pulse to 2 arc seconds of beam divergence. The pulse impinges on one of the retroreflectors placed on the Moon's surface by Apollo astronauts and returns through the telescope

to a pulse detector which stops a nanosecond counter started by the outgoing pulse. Twice the telescope-retroreflector distance is therefore measured in terms of the velocity of light.

A minimum set of three observatories well separated in latitude and longitude, and three lunar retroreflectors well separated in selenocentric latitude and longitude will, if operated simultaneously or in cooperation over an extended time period, permit the determination of the vectors GT, GM, MR, (figure 1) relative to an inertial reference frame for each of the stations and each of the retroreflectors.

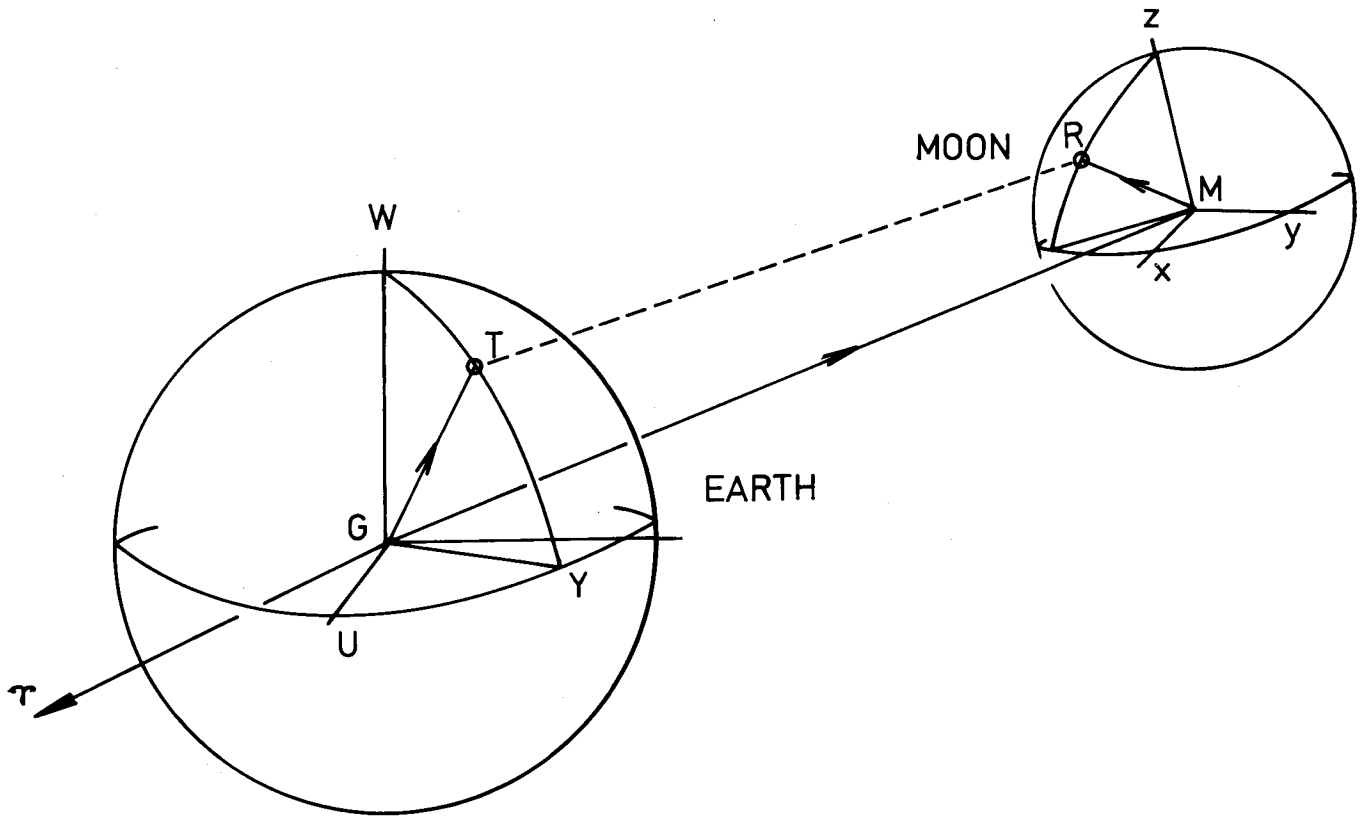

Figure 1.
Earth-Moon System

2. Site Selection and Preparation

Prime site requirements are geologically stable bedrock foundations, clear sky and good seeing, and low precipitable water vapour. Logistics is an important consideration in view of the limited budget available.

2.1 Region

The US agencies concerned require that the LLR be located in Australia for Geodetic reasons. A study of the geology of Australia showed that the ACT was a suitable location. It was early recognised that placing the LLR in reasonable proximity to the Mount Stromlo Photographic Zenith Tube (PZT) would provide a unique opportunity for comparing two entirely different techniques in measuring the polar motion and, indeed, continental drift, while similar comparisons against Very Long Baseline Interferometry would be feasible if the LLR were close to radio telescopes which exist at tracking stations in the ACT. The Division's general interest in earth satellite tracking by Doppler methods and foreseeably by laser satellite tracking reinforced the desirability of the ACT as a site. Finally, the convenience of proximity to Head Office was not ignored.

A possible site at Siding Spring in northern NSW, adjacent to the Anglo Australian 150 inch telescope was considered. While the percentage of clear nights per year there is undoubtedly greater than in the ACT, it lacks geodetic and positional astronomy facilities, is remote, and is inferior to the ACT in freedom from precipitable water vapour.

2.2 Precipitable Water Vapour

Since the wavelength, $6943A^{o}$, of the emitted ruby laser pulse is close to an atmospheric water vapour absorption band, it is an operational requirement that the level of precipitable water vapour in the atmosphere be minimum, less than 10mm for optimum performance.

Firstly, a comparative study was made of the monthly mean values of water vapour in the Coonabarabran (Siding Spring) and Canberra regions using relative humidity data supplied by the Canberra Bureau of Meteorology, and a formula (REITAN 1963) for converting monthly mean dewpoints $D^{o}F$ to total precipitable water vapour at sea level, u:

$$\ln u = -0.981 + 0.0341\ D$$

Table 1 shows that the Canberra region is superior in this respect, even more so considering the fact that Canberra has considerably more rainy days than Coonabarabran. Studies at Mount Stromlo Observatory by HYLAND (1973) indicate that on clear nights there the frequency distribution of precipitable water vapour ranges from 4 to 18 mm and peaks at 6 to 8 mm.

Secondly, daily radiosonde data acquired in 1971-2 by the Bureau of Meteorology at its Wagga, NSW, station were analysed to give the total precipitable water vapour profile against pressure (altitude). The other nearest station is at Nowra, NSW, but as it is a coastal station it was considered unsuitable for either comparison or averaging; the Bureau considered that the Wagga data was suitable for our purposes, especially as the mean motion of the sonde is towards Canberra.

From the wet and dry bulb temperatures and pressure profiles obtained from the radiosondes, the mixing ratios m(z), defined as the ratios of the mass of water vapour to the mass of dry air at altitude z, were read from aerological diagrams at various pressures. Now the pressure p(z) at altitude z is given by

$$p(z) = -\int_z^\infty g\rho(x)dx$$

where $\rho(x)$ is the density at height x. Also, the amount of water vapour in a volume element $A\delta z$ at height z is

$$\delta w(z) = m(z)\rho(z)A\delta z$$

whence

$$W(\infty) - w(h) = \frac{A}{g}\int_{p(h)}^{\infty} m(z)dp(z)$$

Since $W(\infty) = 0$, the total precipitable water vapour above unit surface at height h, i.e. $w(h)/A$, was obtained by simple numerical integration. Typically, after converting to pressure, w(950 mbar) - w(850 mbar) = 5mm. The altitude of the collimation tower site at Orroral Valley tracking station, 1400 metres, corresponds approximately to a pressure of 850 mbar; the mean monthly results subdivided by class of cloud cover are given in table II.

TABLE I

Comparison of Precipitable Water Vapour

Canberra and Coonabarabran

Monthly Mean Precipitable Water Vapour at Sea Level (u mm), by Formula (REITAN 19)					
Month	Canberra	C'bran	Month	Canberra	C'bran
Jan	21.4	25.3	Jul	14.6	16.3
Feb	23.6	26.1	Aug	14.6	15.7
Mar	20.5	24.6	Sep	16.3	16.3
Apr	19.3	22.0	Oct	16.8	18.0
May	16.8	18.6	Nov	19.9	21.4
Jun	15.2	16.8	Dec	20.5	23.6

TABLE II

Precipitable Water Vapour - Canberra

Precipitable water vapour (mm) Canberra region, 1972, altitude 1400 metres							
Month	Cloud Cover 0/8-2/8	3/8-5/8	6/8-8/8	Month	Cloud Cover 0/8-2/8	3/8-5/8	6/8-8/8
Jan	9.7	10.5	13.5	Jul	4.5	7.4	6.0
Feb	14.9	12.4	15.1	Aug	5.2	4.5	5.6
Mar	14.0	14.5	13.3	Sep	5.5	4.9	6.9
Apr	8.8	7.4	8.4	Oct	6.0	7.5	4.8
May	7.4	8.4	7.3	Nov	9.0	7.5	10.0
Jun	5.1	3.3	5.6	Dec	6.4	5.7	8.6

2.3 Cloud Cover

The Bureau of Meteorology and Mount Stromlo Observatory made available their observations of cloud cover at various times of every day in the period June 1970 to December 197 2. The observations at Fairbairn Airport, Canberra, were made professionally every three hours; at Mount Stromlo Observatory by the regular night assistants at 9 pm, midnight and 3 am; and at other stations, at 9 am and 3 pm. The comparison between Mount Stromlo and Orroral Valley uses the Fairbairn data set as an interpolator. Table III shows the percentage of days in the period having each of three classes of cloud cover at each station. Note that Yarralumla is very close to Mount Stromlo. Table IV gives the monthly values for Orroral Valley at 9 am and 3 pm. The Division's own informal observations suggest that, at night, the incidence of cloud cover may be even less than the tables indicate.

TABLE III

Cloud Cover - Comparison

Percentage of days with given cloud cover, 1970-2

Time	Station	0/8-2/8	3/8-5/8	6/8-8/8
9 am	Orroral Valley	42	17	41
	Fairbairn	35	18	47
	Yarralumla	35	15	50
3 pm	Orroral Valley	33	22	45
	Fairbairn	30	26	44
	Yarralumla	31	23	46
9 pm	Fairbairn	47	20	33
	Mt Stromlo	40	13	47
Midnight	Fairbairn	47	15	38
	Mt Stromlo	38	11	51

TABLE IV

Cloud Cover - Orroral Valley

Percentage of Days with Given Cloud Cover, Orroral Valley, ACT

Month	Period Averaged	9am			3pm		
		0/8-2/8	3/8-5/8	6/8-8/8	0/8-2/8	3/8-5/8	6/8-8/8
Jan	1971-2	28	13	59	16	27	57
Feb	1971-2	28	16	56	18	24	58
Mar	1971-2	29	16	55	31	25	44
Apr	1971-2	47	15	38	47	18	35
May	1971-2	42	18	40	36	20	44
Jun	1972	64	7	29	53	14	33
Jul	1970-2	53	11	36	46	24	30
Aug	1970-2	32	25	43	25	25	50
Sep	1970-2	47	18	35	40	21	39
Oct	1970-2	50	20	30	34	26	40
Nov	1970-2	40	20	40	27	22	51
Dec	1970-1	47	19	34	38	25	37

In summary, the Orroral site is superior to a Mount Stromlo site in both cloud cover and precipitable water vapour aspects.

2.4 Seeing and Fog

An 8 inch reflecting telescope was tested against the Oddie telescope at Mount Stromlo and taken to Orroral where, on several nights, double stars of close separation were observed to assess the seeing. The operational requirement of the LLR is that, to achieve the desired pointing accuracy and signal-to-noise ratio, the beam direction and beam divergence should be stable to better than two arcseconds. On each occasion double stars of separation less than 1".5 were readily resolved. MEINEL (1963) indicates that, in testing for a medium large telescope, a test aperture of at least 10 cm is required so that the large scale blurring effect characteristic of seeing disturbances in large telescopes is observed rather than mere image motion observed by small telescopes.

An interesting point is that, in general, the seeing at the collimation tower was much superior to the seeing on the valley floor 400 metres below.

The site is situated on a level part of the slope of Mount Orroral, as in figure 2. It is expected that deterioration of the seeing as the air flow encounters a knoll (KIEPENHEUER 1962) will not be serious as the knolling is small and the telescope will be 28 feet above ground level.

Advantage was taken of the valley profile (figure 2) to determine the height of the inversion layer above the valley floor. On two nights, one clear and the other with fog in the valley, observations of wet and dry bulb temperatures and barometric pressure were taken at regular intervals both across the valley and along it. The graphs of dry temperature against scale height, shown normalised in figures 3 and 4, clearly indicate that the normal inversion layer lies well below the collimation tower. This is confirmed by the fact that not once during 1973 was there fog at that site.

2.5 Geological Surveys

An extensive series of seismic and resistivity tests of both valley and collimation tower sites was conducted by the Bureau of Mineral Resources to verify the geodetic stability of the sites. (The valley floor was included as it was a logistically desirable site). Figure 5 is a plan of the geophone arrays used in the seismic survey at the tower site, and figure 6 shows the bedrock profiles relative to the surface. A massive bedrock outcrop with a 30 foot diameter flat top was chosen as the prime area of interest; the tests established that, within interpretable limits, the outcrop was at the very worst, a large tor sitting solidly on bedrock and surrounded by highly weathered granitic material. Electrical resistivity tests confirmed this finding. The valley floor site was not so suitable, bedrock there being some 10 metres from the surface in all cases.

2.6 Logistics

Within the ACT, Mount Stromlo is undoubtedly the best site from the point of view of access, proximity to Head Office, and building and technical services, water, power and communications facilities.

Access to the Orroral collimation tower site is possible through a locked gate under most weather conditions in four-wheel drive vehicles; it has standard US configured power and telephone readily available, but no water. It is within reasonable daily travelling distance from Canberra, and is collocated with a major technical facility, the Orroral Valley STDN Tracking Station.

For the preceding reasons, the tower site has been chosen for erection of the LLR.

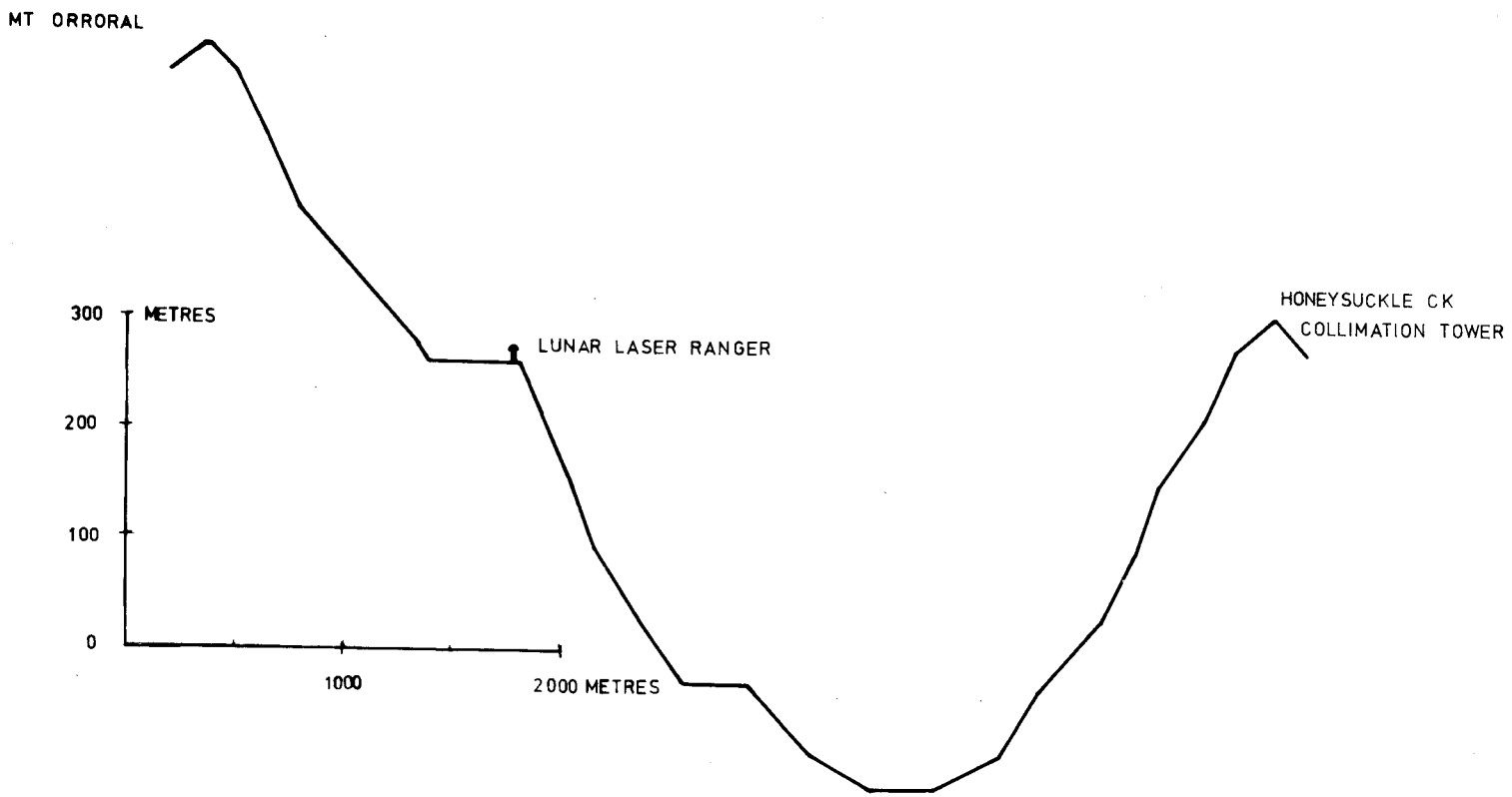

Figure 2. Longitudinal Section Across Orroral Valley

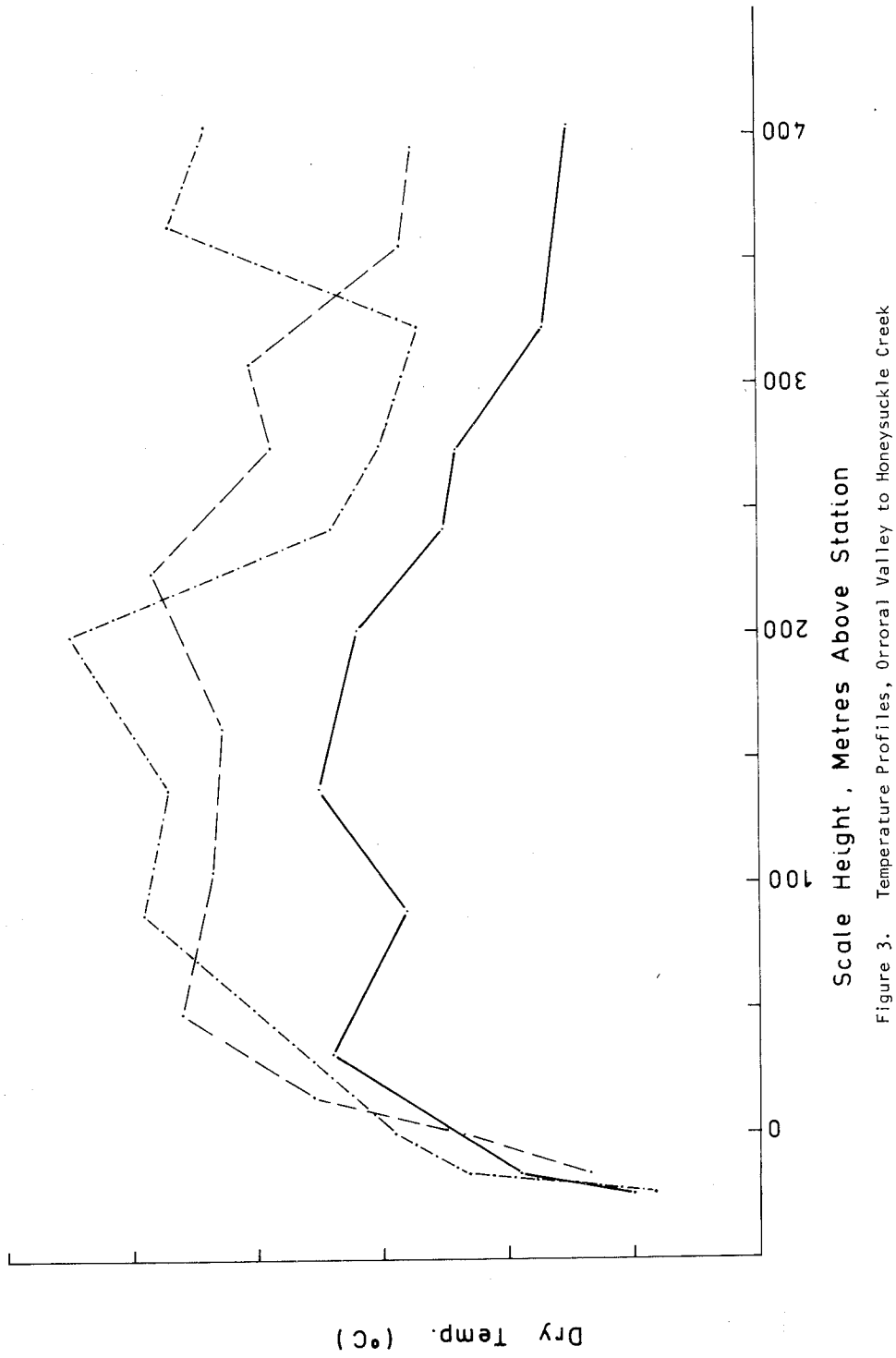

Figure 3. Temperature Profiles, Orroral Valley to Honeysuckle Creek

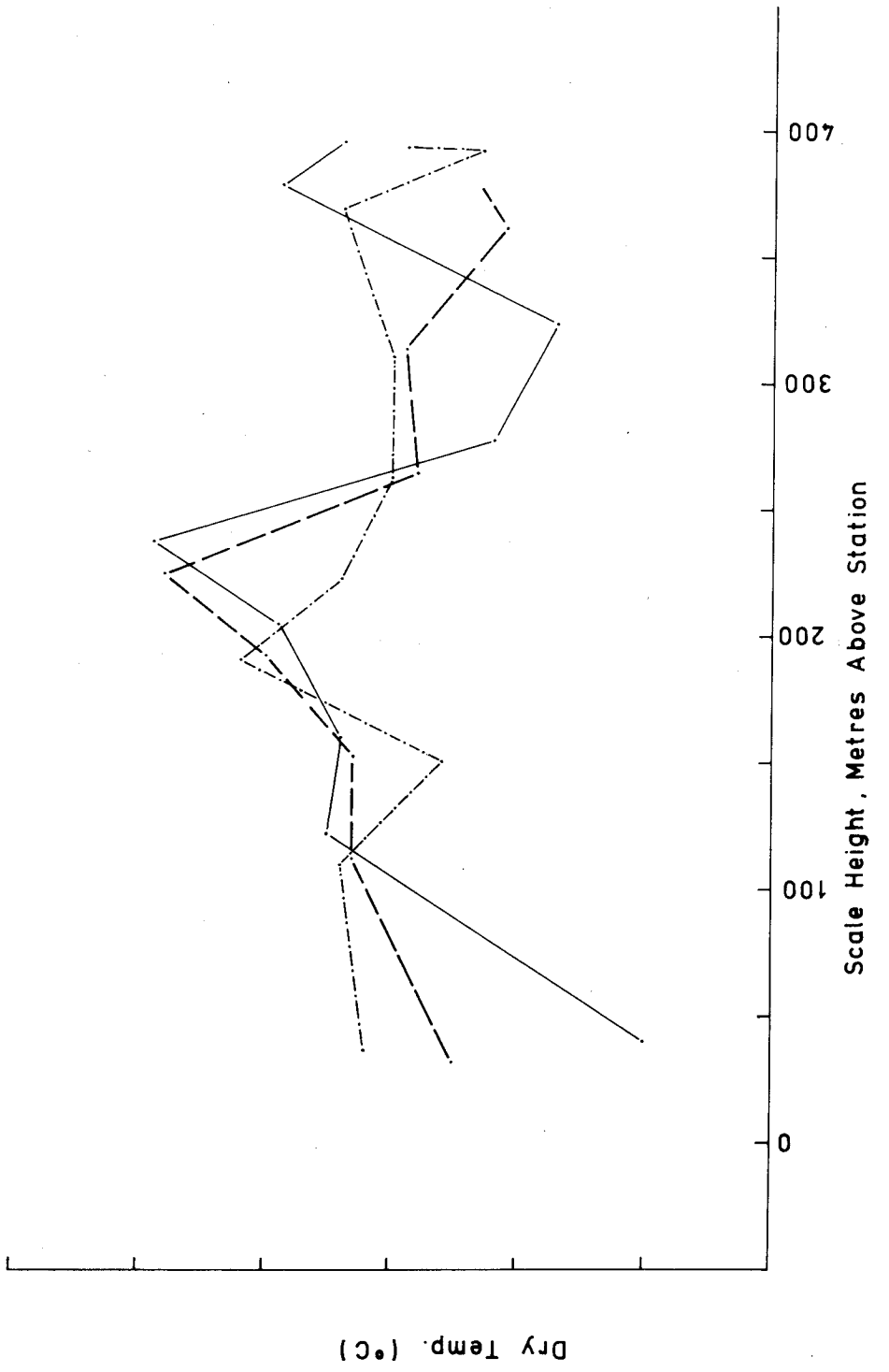

Figure 4. Temperature Profiles, Orroral Valley to Orroral Collimation Tower

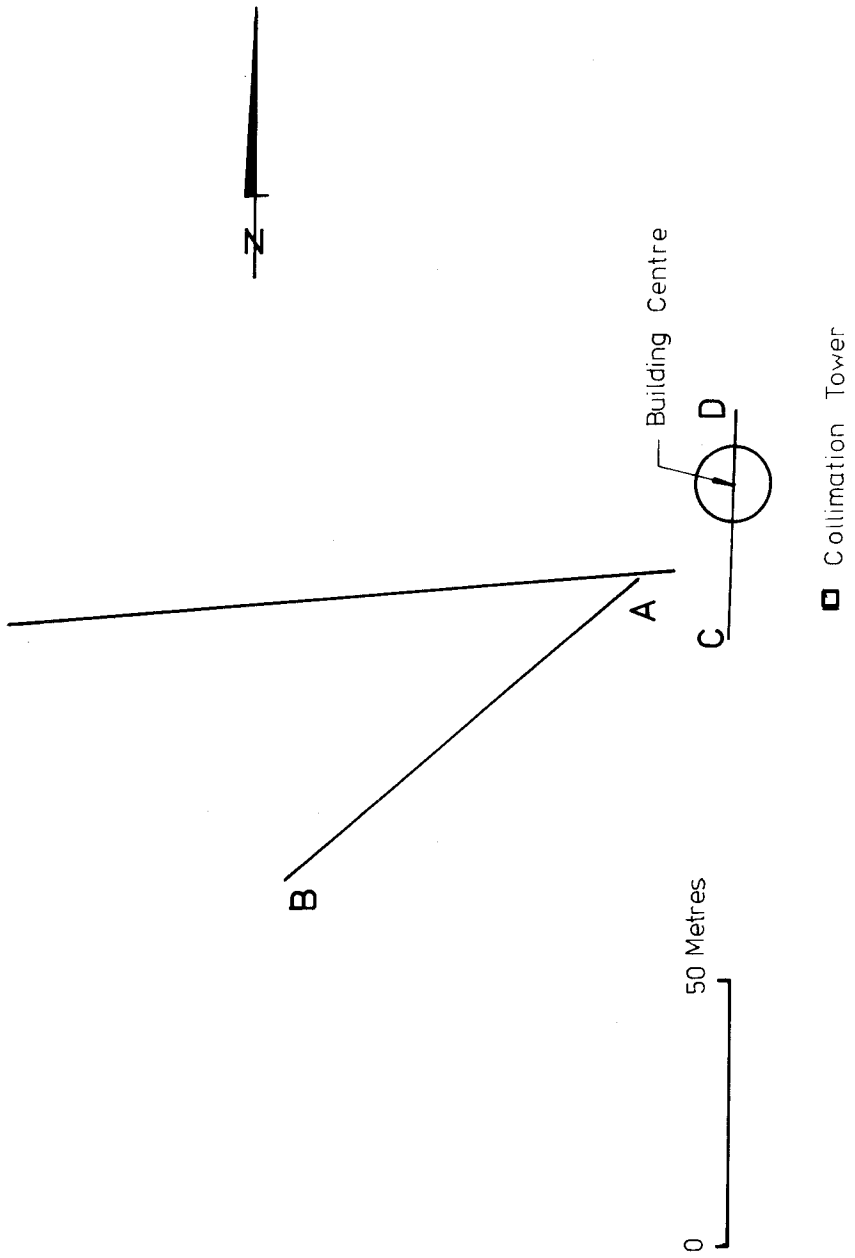

Figure 5. Plan of Seismic Geophone Arrays

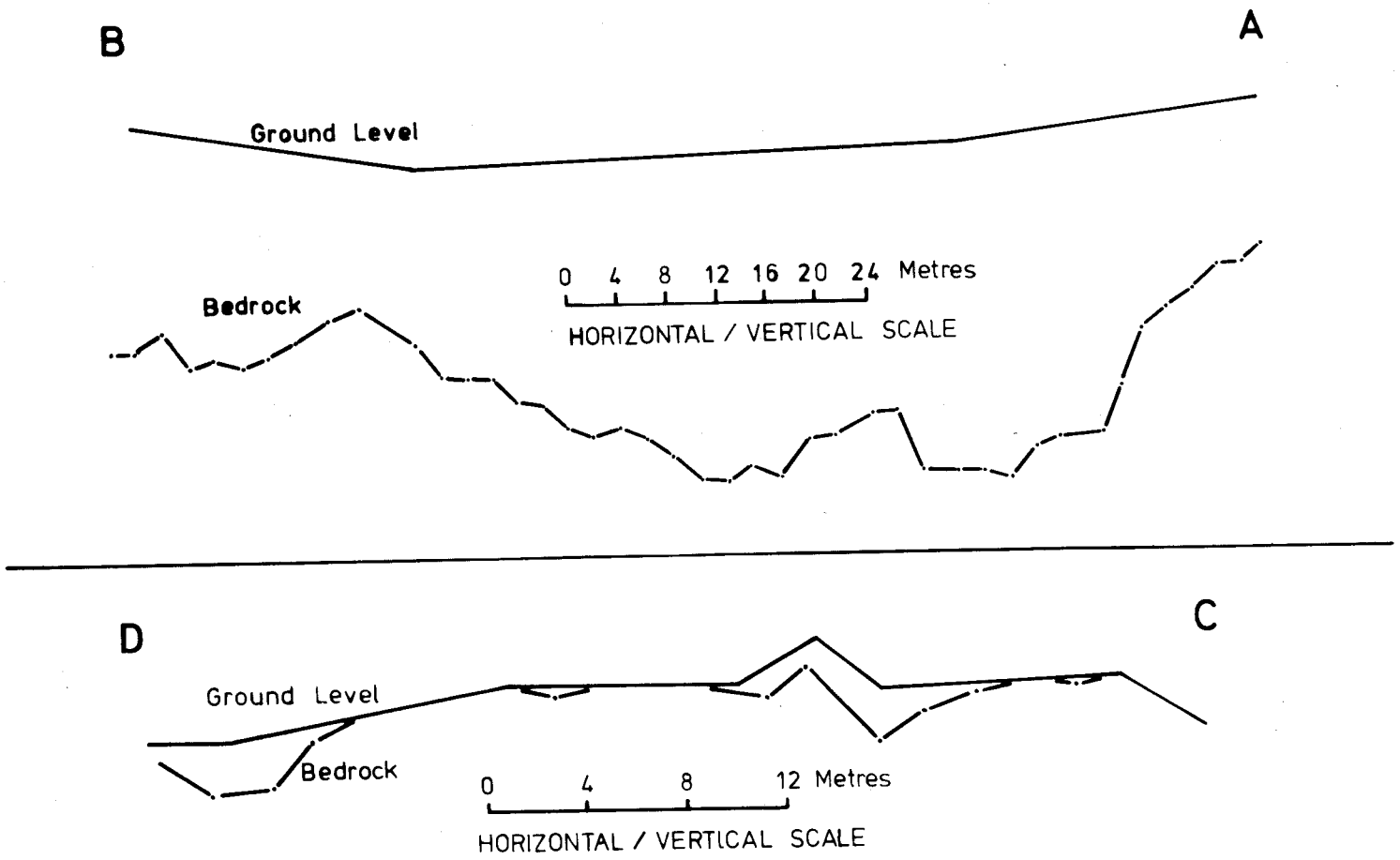

Figure 6. Bedrock Profile

2.7 Site Preparation

The current (November 1973) state of site preparation is that all necessary approvals have been obtained from the appropriate government departments, and that the area surrounding the selected rock has been cleared of those trees which would interfere with observations and access. The top of the rock has been cleared of weathered material preparatory to construction of the dome building for which tenders have been called. The 28'6" dome to surmount the brick structure has been ordered from the Ash-Dome company in the USA.

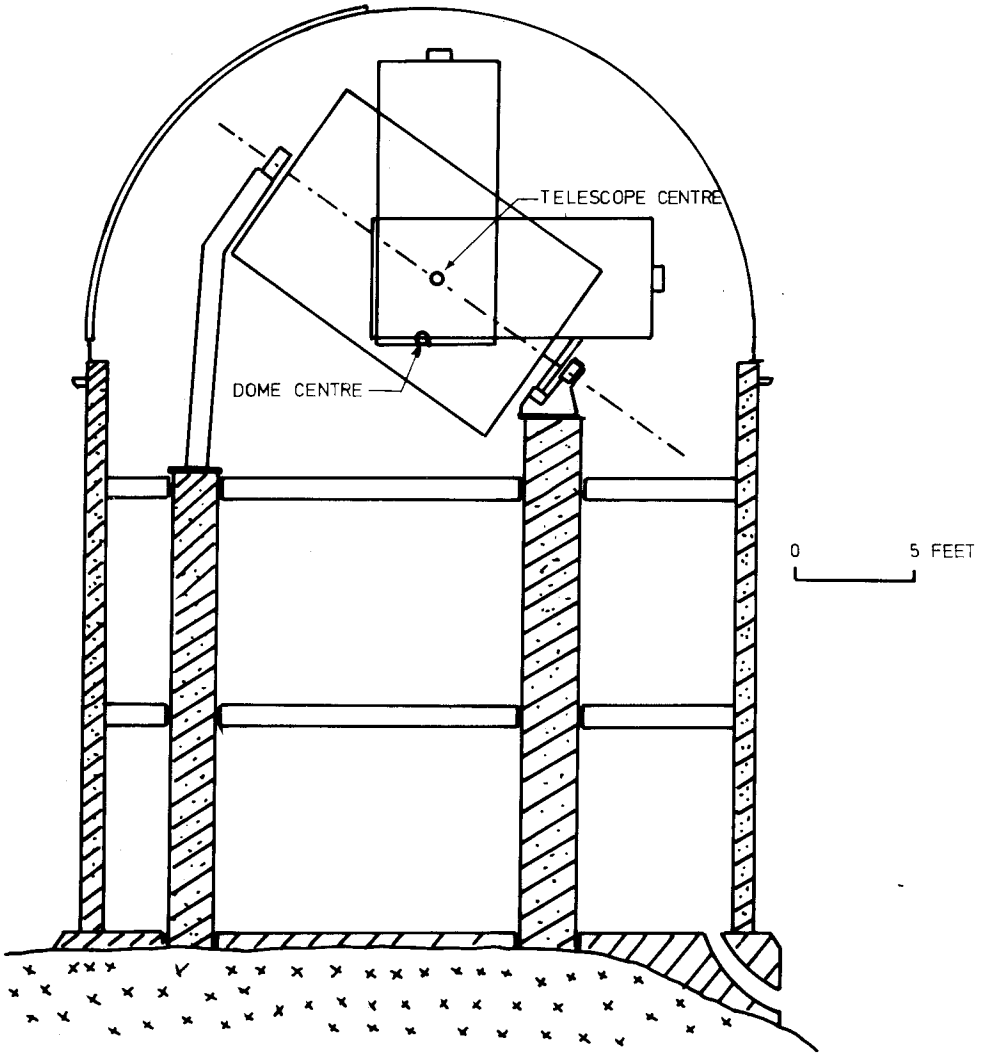

Figure 7. Lunar Ranger Building Cross Section

3. The Building

3.1 Construction

The building is to be a 28'6" external diameter double brick cylinder 25' high (LUCK et al in press) surmounted by a standard hemispherical Ash-Dome. The intersection of the telescope axes

will be 28'7" above the ground floor. There will be three floors - ground, intermediate and observation floors. Figures 7 and 8 show the layout of the building. The observation floor will contain the telescope, control console and laser pulse forming networks. The intermediate floor will be air-conditioned and will contain the control computer and its principal peripherals, the National Mapping clock ensemble, VLF receivers and associated electronic equipment, working space and room for the installation of control racks for future geodetic instruments. The ground floor will house loading bay, heavy power and air conditioning plant, toilet and meal table. The building will be constructed by contract from the Australian Department of Works.

3.2 Telescope Piers

The essential feature of the internal building is the set of three 18 inch piers to support the telescope legs. To ensure firmness and stability, they will be sunk four feet into the rock, and tied by 14 inch concrete beams just below each floor, including the ground floor. However, each pier will be mechanically isolated everywhere from the building by neoprene filled gaps so that no vibrations induced in the building by wind or other movement will be transmitted to the telescope.

4. The Telescope

4.1 Mounting

The telescope was built by Astro Mechanics Inc, Austin, Texas, to a minimum weight specification. It is supported at the south end by two vent legs whose feet are 15 feet apart, and at the north end by a pedestal containing the RA drive. Between them a strong rectangular frame carries two stub axles which form the declination axis and two stub axles forming the polar axis. The declination axles support the declination cube, a strong square box on which the laser box itself is mounted, and above and below which are mounted the Serrurier trusses which carry the spider of the secondary mirror, and the primary mirror. The telescope is to be assembled shortly in a workshop to check its operating condition prior to final reassembly.

4.2 Optics

BUCHROEDER et al (1972) have described the telescope optics. The essential features are shown in figure 9 and comprise an aluminised f2.5 152 cm CerVit primary slightly over-parabolised, a 40 cm gold coated hyperboloidal secondary which increases the effective focal ratio to f8, and a 23 cm x 15 cm elliptical, dichroic beamsplitter whose coating reflects 96% of light at 6943A^{o} but transmits most of the light 10A^{o} away. The beamsplitter, at 45^{o} to the optical axis, directs the laser beam to and from an aperture in the declination cube which gives optical access to the laser optical system.

The bulk of white light collected by the telescope passes through the dichroic beamsplitter and another 45^{o} glass plate situated in the centre hole of the primary in order to compensate coma and aberration introduced by the beamsplitter. This beam is then further split, part going to a visual eyepiece and part to the automatic tracker in the Cassegrain position. The eyepiece is placed on a graduated and calibrated X-Y stage so that the telescope can be set on a known lunar feature, such as a peak in a crater, then offset precisely to the position of the adjacent retroreflector array which is, of course, invisible but whose selenodetic coordinates are known. The offset can be computer calculated and, in the future, controlled.

The tracker consists of an ITT F4011 image dissector which is sufficiently sensitive to detect departures from the central position of features in full moon, daylight or possibly illuminated by

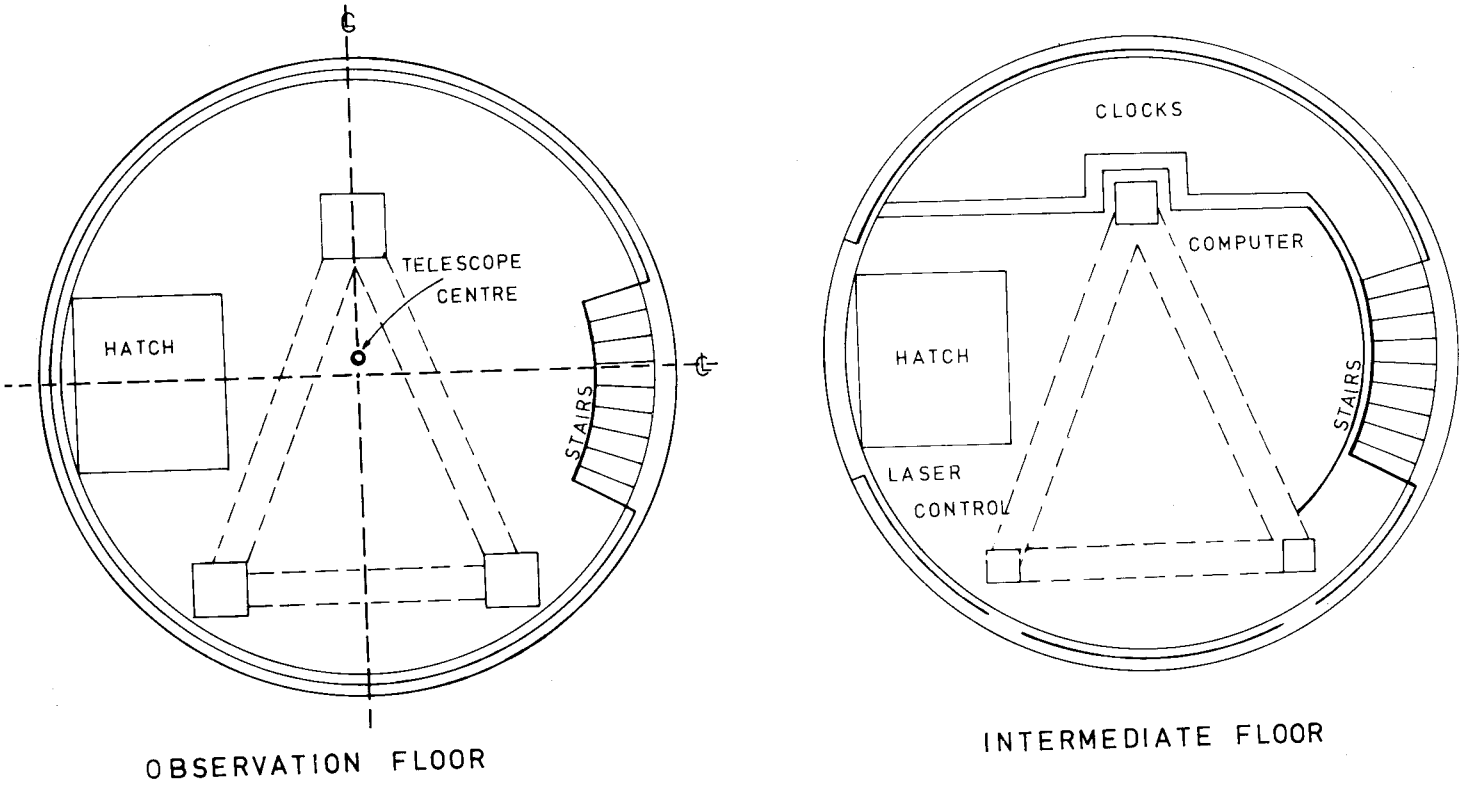

Figure 8. Lunar Ranger Building Floor Plans

earthshine. The correcting signals from the dissector tube drive stepping motors in 0.6 arcsecond steps in declination and hour angle to bring the feature back to centre position. This method of tracking obviates the need for a conventional clock or sidereal drive, and is equally suitable for tracking the moon, stars, or high altitude earth satellites.

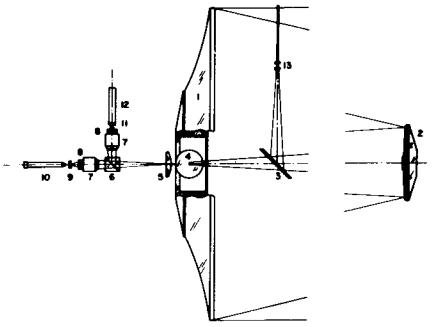

152-cm diam telescope. (1) 152-cm f/2.5 hyperboloid CER-VIT primary mirror. (2) 40-cm hyperboloid CER-VIT secondary mirror. (3) 23 X 15-cm elliptical dichroic beamsplitter (99% reflectivity at 694.3 nm). (4) 23 X 15-cm elliptical compensator plate. (5) 14-cm field lens. (6) 76-mm dichroic cube beamsplitter. (7) Nikkor-H 35-mm f/1.8 camera lens and portrait attachment. (8) Spherical aberration corrector plate. (9) Field flattener and reference reticle. (10) 40X microscope on X-Y stage. (11) Field flattener bonded to face of image dissector tube. (12) ITT F4011 image dissector tube. (13) Laser interfacing lenses.

Figure 9. Telescope Optics. (From BUCHROEDER et al 1972)

5. The Laser

5.1 Laser Generator

The laser was originally built by Hughes Aircraft. It consists basically (CARTER et al 1972) (see figure 10) of a mechanical Q-switched ruby laser oscillator to provide the initial pulse of 0.2 Joule in 17 nanoseconds, four cascaded ruby amplifier lasers each with gain 1.5, a Pockels cell to rapidly chop the pulse to 3 nanoseconds, turning prisms and mirrors to render the laser box reasonably compact, and a diverging lens matched to the telescope optical system and placed precisely at its focal point so that the beam emerging from the telescope is parallel to within 2 arcseconds. The laser has already been test fired in the Q-switched 17 ns pulse mode. Tests with another ruby laser revealed no radio interference to the tracking station antennae.

5.2 Receiver

The beam returns from the moon via a transmit-receive mirror through a tunable Etalon filter which permits only light of the ruby wavelength to reach the detecting photomultiplier tube whose output stops a time interval counter started approximately 2.5 seconds earlier by the outgoing pulse. The photomultiplier is sufficiently sensitive to detect a single return photon. That such a return photon comes from the original pulse rather than stray moonlight is ensured with high proba-

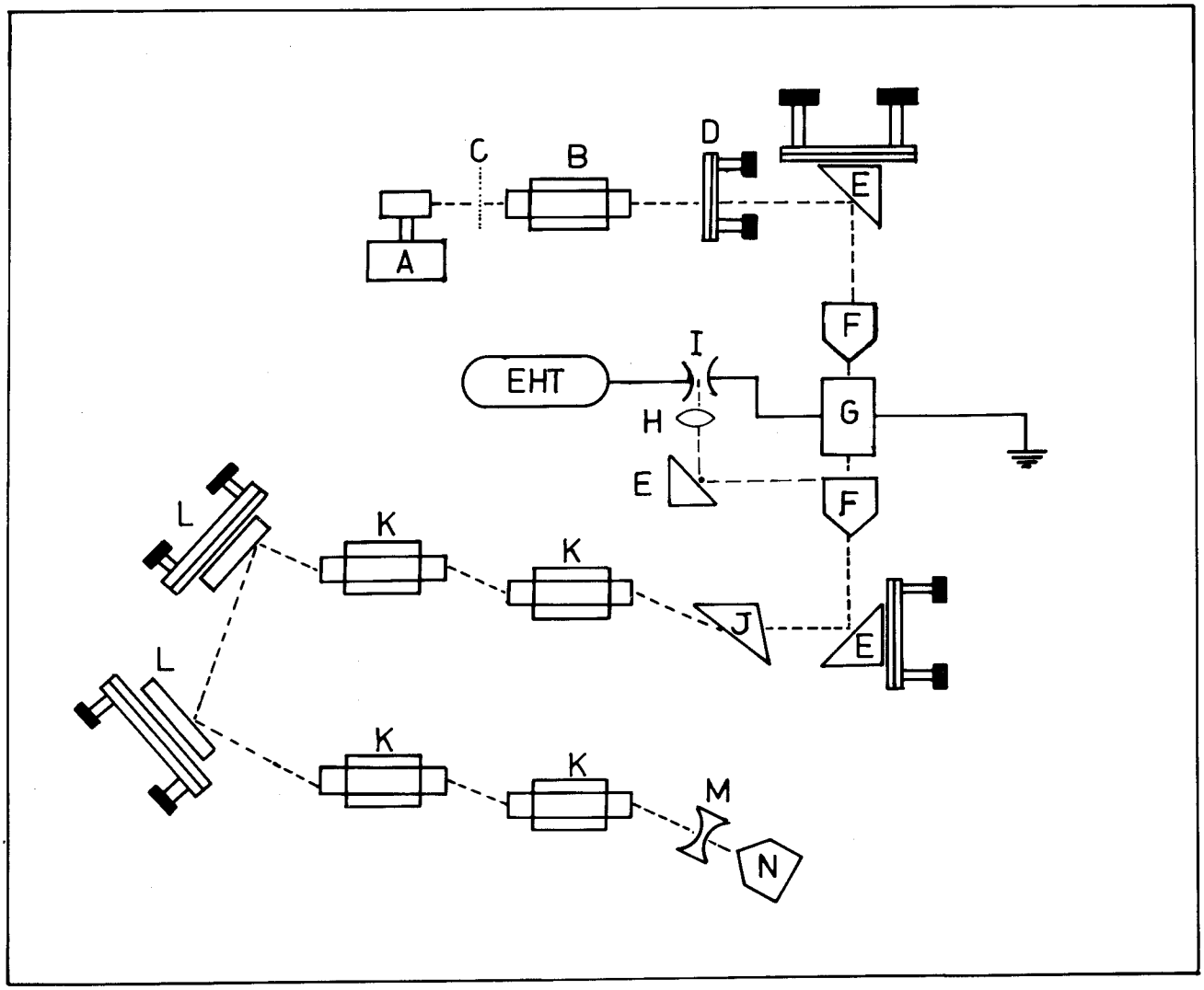

Figure 10. Laser box

(A) Rotating prism Q-switch. (B) Ruby laser. (C) Aperture stop.
(D) Sapphire mirror. (E) Turning prisms. (F) Glan polarising prisms.
(G) Pockels cell. (H) Focusser. (I) Spark gap. (J) Brewster prism.
(K) Ruby amplifiers. (L) Turning mirrors. (M) Diverging lens.
(N) Circulariser, turns beam to dichroic beamsplitter.

bility by three types of filtering: frequency filtering by the Etalon filter; spatial filtering by optical stops so placed that even errors in telescope collimation will impede the photon; and time filtering by gating the photomultiplier with a window one or two microseconds wide about the expected return time.

The single photon sensitivity of the receiver is required since the original 150 cm beam has expanded, assuming 2 arcsecond divergence, to a diameter of 4 km at the moon, whereas only 1/3 square metre is returned by the retroreflector array, that is only one part in 4×10^7 is returned. A similar attenuation occurs between the moon and earth on the homeward journey. The atmosphere absorbs a considerable proportion of the energy in each direction, as do the numerous optical surfaces in the laser, telescope and receiver.

5.3 Shot Sequence

The laser firing sequence is controlled by an on-line computer, which also computes and sets the range gate by means of Chebyshev polynomials interpolating the lunar ephemeris initially to be provided by the Jet Propulsion Laboratory, Pasadena, California. The firing sequence will initially be 200 shots at 5 second intervals, repeated to each of the available lunar retroreflectors, particularly the American ones at Hadley's Rille, Fra Mauro and Mare Tranquillitatis. It is hoped eventually to reduce the interval between shots to the limit of 3 seconds required for the capacitor banks of the pulse forming networks to recharge between shots.

6. RANGE EQUATIONS

FAJEMIROKUN (1971), KAULA (1973) and MUELLER et al (1972) have described the range equations and analysed them numerically from different standpoints for various needs. A brief description follows, together with suggestions for obtaining the sidereal time, polar motion components and continental drift explicitly from the adjustment solutions, these quantities being of particular interest to the Division which is very well placed to compare these quantities determined by the LLR against determinations by its PZT.

6.1 Topocentric Coordinates of a Retroreflector

The distances will be expressed eventually in terms of X, Y, Z components in the very nearly inertial geocentric ecliptic coordinate system at epoch 1950.0, say. Conventional rotation matrices (MUELLER 1969) $R_1(\alpha)$, $R_2(\beta)$, $R_3(\gamma)$, denoting rotations of α,β,γ about the X,Y,Z axes respectively,,and Lucas matrices L_1, L_2, L_3 such that

$$\frac{\partial R_1(\alpha)}{\partial \alpha} = L_1 R_1(\alpha)$$

will be employed throughout.

Let $[U,V,W]^T$ be cartesian coordinates in a geodetic system of the laser station T, and let $[X_p,Y_p,Z_p]^T$ be its coordinates in the 1950.0 ecliptic system. Then

$$\begin{bmatrix} U \\ V \\ W \end{bmatrix} = \begin{bmatrix} (N + h) \cos \phi \cos \lambda \\ (N + h) \cos \phi \sin \lambda \\ [N(1-e^2) + h] \sin \phi \end{bmatrix} \qquad (1)$$

in standard notation.

If ε_o is the obliquity of the ecliptic 1950.0, z_1, θ_1 and ζ_o are precession parameters (HMSO 1961), ε, $\Delta\varepsilon$ and $\Delta\psi$ are nutation parameters, x_p and y_p are the instantaneous coordinates of the pole relative to the CIO of 1903.0 and S is the current sidereal time, then

$$\begin{bmatrix} X_p \\ Y_p \\ Z_p \end{bmatrix} = R_1(\varepsilon_0)R_3(\zeta_0)R_2(-\theta_1)R_3(z_1)R_1(-\varepsilon)R_3(\Delta\psi)R_1(\varepsilon+\Delta\varepsilon)R_3(-S)R_1(y_p)R_2(x_p)\begin{bmatrix} U \\ V \\ W \end{bmatrix} . \qquad (2)$$

Similarly, if ψ,θ,Φ, are the Euler angles of the orientation of the selenodetic coordinate system, and $[x_m,y_m,z_m]^T$ are the coordinates of the retroreflector R in the selenodetic system, its coordinates $[X_m, Y_m, Z_m]^T$ in the 1950.0 ecliptic system will be

$$\begin{bmatrix} X_m \\ Y_m \\ Z_m \end{bmatrix} = R_1(\varepsilon_0)R_3(\zeta_0)R_2(-\theta_1)R_3(z_1)R_1(-\varepsilon)R_3(-\psi)R_1(\theta)R_3(\Phi)\begin{bmatrix} x_m \\ y_m \\ z_m \end{bmatrix} . \qquad (3)$$

The geocentric 1950.0 equatorial coordinates of the lunar centre M, $[X_{cq},Y_{cq},Z_{cq}]^T$ are obtained from a lunar ephemeris and transformed to the 1950.0 ecliptic system by

$$\begin{bmatrix} X_c \\ Y_c \\ Z_c \end{bmatrix} = R_1(\varepsilon_0)\begin{bmatrix} X_{cq} \\ Y_{cq} \\ Z_{cq} \end{bmatrix} . \qquad (4)$$

Reference to figure 1 then shows that the coordinates $[X_{m_t}, Y_{m_t}, Z_{m_t}]^T$ of the retroreflector relative to the telescope are

$$\begin{bmatrix} X_{m_t} \\ Y_{m_t} \\ Z_{m_t} \end{bmatrix} = \begin{bmatrix} X_c \\ Y_c \\ Z_c \end{bmatrix} + \begin{bmatrix} X_m \\ Y_m \\ Z_m \end{bmatrix} - \begin{bmatrix} X_p \\ Y_p \\ Z_p \end{bmatrix} . \qquad (5)$$

The measured distance d obtained by lunar laser ranging is

$$d = (X_{m_t}^2 + Y_{m_t}^2 + Z_{m_t}^2)^{\frac{1}{2}} .$$

6.2 Observation Equations

The design matrix A of the observation equations in the adjustment is (CARTER et al 1972)

$$A = \frac{\partial D}{\partial x} = \frac{\partial D}{\partial X_t} \cdot \frac{\partial X_t}{\partial x} \qquad (6)$$

where D is the column vector of parametrised distances d_i,

$$X_t = [X_{m_t}, Y_{m_t}, Z_{m_t}]^T,$$

and X is the column vector of all the parameters.

The partial derivatives of particular interest are those concerned with sidereal time, polar motion and continental drift.

6.2.1 Sidereal Time and Polar Motion

The sidereal time S can be modelled as

$$S = UTC + B^t T + \Delta\psi \cos\varepsilon + S_1 \tag{7}$$

where UTC is a uniform time scale, $B^t T$ is the usual conversion in terms of t, the number of Julian centuries elapsed since 1900 Jan 0.5UT, $\Delta\psi \cos\varepsilon$ is the equation of the equinoxes and S_1 is a model of the variation in the rate of rotation of the earth:

$$\begin{aligned} S_1 = {} & s_1 \cos(2\pi.36525t) + s_2 \sin(2\pi.36525t) \\ & + s_3 \cos(2\pi.100t) + s_4 \sin(2\pi.100t) \\ & + s_5 \cos(2\pi.86t) + s_6 \sin(2\pi.86t) \end{aligned} \tag{8}$$

The first two terms of S_1 represent the diurnal variation which may be better determined by laser ranging than by Photographic Zenith Tubes, since observations can cover all hours of the day in the course of the month, while the other terms represent annual and Chandler variations. The expression for the partial derivative in s_1 is

$$\frac{\partial X_t}{\partial s_1} = \frac{\partial X_t}{\partial S} \cdot \frac{\partial S}{\partial s_1} = R_1(\varepsilon_0) P^t N^t L_3 R_3(-S) R_1(y_p) R_2(x_p) \begin{bmatrix} U \\ V \\ W \end{bmatrix} \cos(2\pi.365252t)$$

where P^t is written for the precession matrices and N^t for the nutation matrices. Similar expressions hold for the other coefficients. Again, the polar motion terms x_p and y_p can be similarly modelled in terms of diurnal, annual and Chandler periods.

6.2.2 Continental Drift

The simplest model of continental drift relative to an absolute geodetic datum is to let

$$\begin{bmatrix} U \\ V \\ W \end{bmatrix} = \begin{bmatrix} U_o + ut \\ V_o + vt \\ W_o + wt \end{bmatrix}$$

from which is obtained representatively

$$\frac{\partial X_t}{\partial u} = -R_1(\varepsilon_0) P^t N^t R_3(-S) R_1(y_p) R_2(x_p) \begin{bmatrix} t \\ o \\ o \end{bmatrix} \tag{10}$$

These proposals are currently conjectural. Numerical experiments by KAULA suggest that station drift parameters, especially in the east-west direction, will be well determined although, naturally, highly correlated with station location, and that sidereal time and polar motion parameters should include monthly and bimonthly terms as well.

7. Acknowledgment

The authors wish to thank the Canberra Bureau of Meteorology for providing data and assistance; the Bureau of Mineral Resources for conducting the geophysical surveys; and staff of the Australian National University for advice on siting and building. The Director of the Weapons Research Establishment, South Australia, kindly made available a pulsed ruby laser for radio interference tests. They are grateful to Mr R. CAMERON for the loan of his eight inch telescope. They thank the Director of the STDN facility at Orroral Valley for his good offices, and finally, the officers of the Division of National Mapping who have contributed towards this project.

8. References

BUCHROEDER, R.A., ELMORE, L.H., SHACK, R.V. & SLATER, P.N. 1972. *The Design, Construction and Testing of the Optics for a 147-cm Aperture Telescope.* Final Report for AFCRL, Bedford, Mass. USA. Contract F19628-72-C-0047.

CARTER, W.E., ECKHARDT, D.H. & ROBINSON, W.G. 1972. *AFCRL Lunar Laser Instrumentation Status Report.* AFCRL Report 72-0615.

FAJEMIROKUN, F.A. 1971. *Applications of Laser Ranging and VLBI Observations for Selenodetic Control.* Report No.157, Department of Geodetic Science, Ohio State University, for NASA Manned Spacecraft Centre, Houston, Texas, USA. Contract NAS (9-9695 1971)

HMSO. 1971. *Explanatory Supplement to the Astronomical Ephemeris.*

HYLAND, A.R. 1973. Private Communication.

KAULA, W.M. 1973. *Phil.Trans.Roy.Soc. Lond. A* 274,185-193.

KIEPENHEUER, K.O. 1962. "Le Choix des Sites d'Observatoires Astronomiques" in ROSCH, J.(ed) *IAU Symposium No.*19.

LUCK, J. McK., MILLER, M.J. & MORGAN, P.J. *Proc.Astron.Soc. of Australia.* In Press.

MEINEL, A.B. 1963. "Astronomical Seeing and Observatory Site Selection" in KUIPER, G.P. & MIDDLEHURST, B.M. (eds). *Telescopes.* 158.

MUELLER, I.I., FAJEMIROKUN, R.A. & PAPO, H.B. 1972. *Report to Annual Meeting of COSPAR.* Madrid

MUELLER, I.I. 1969. *Spherical and Practical Astronomy as applied to Geodesy.* Frederick Ungar Publishing Co. New York.

REITAN, D. 1963.*J. App. Meteorology.* 2, 776.

9. Discussion

PLOTKIN: We hear something of the difficulties involved. We are using beams which are 2 - 3 arcsec in diameter and most astronomical telescopes while they can guide accurately, cannot point absolutely in that sense. The Hawaiian station is one of the few attempts to do absolute pointing with an instrument that large.

MORGAN†: Whether or not this will increase the nights per lunation on which data can be acquired is still not certain.

† Post-symposium comment.

CARTER, W. E.
WILLIAMS, J. D.
Institute for Astronomy
University of Hawaii
Hawaii

Proc.Symposium on Earth's Gravitational Field & Secular Variations in Position (1973),433-441.

UNIVERSITY OF HAWAII LURE OBSERVATORY

ABSTRACT

The University of Hawaii Institute for Astronomy is constructing a lunar laser ranging observatory at the summit of Mt. Haleakala, Maui, Hawaii. The project is funded by the National Aeronautics and Space Administration and the design, construction, and operation of the station are being closely coordinated with the LURE Team.

Instrumentation has been developed at the University of Maryland, Wesleyan University, JILA National Bureau of Standards and the University of Colorado, University of Texas, University of Hawaii, and NASA Goddard Space Center.

The laser is frequency doubled Nd YAG operating at three pulses per second; each pulse is 200 picoseconds (FWHM) in duration, and contains 250 millijoules of energy at 5320 Å.

The laser is coupled into a 40 cm aperture refractor telescope. The telescope expands and collimates the laser pulses, and directs them toward a 68 cm diameter altitude-azimuth mounted flat mirror referred to as a lunastat. The lunastat is positioned so that the reflected beam is pointed at the desired target by fully automatic, computer controlled absolute pointing or by offset guiding techniques.

The return signal is received by a multi-lensed telescope referred to as the lurescope. The light collected by eighty 19 cm aperture achromatic lenses is routed to a common focus, spatially and optically filtered, beamsplit, and detected by two photomultiplier tubes. The output of each PMT is connected to one channel of a dual channel multi-event timer system.

The event timer determines the epoch of each start and stop event, on the station timescale, with a resolution of 100 picoseconds. The total uncertainty of each range measurement is approximately 500 to 600 picoseconds. An observation consists of several range measurements.

Two mini-computers are used to generate range predictions, retrieve and store range data, control the telescope drive, read and store meteorological data, and perform numerous other housekeeping duties.

Current planning anticipates ranging to begin in mid 1974.

1. Introduction

The University of Hawaii's Institute for Astronomy is currently constructing a lunar laser ranging observatory at the 3050-meter summit of Mt. Haleakala, Maui, Hawaii. The project is funded by NASA under contract NASW-2326, with J. T. Jefferies as Principal Investigator. The design, construction, and operation of the station is being closely coordinated with the LURE team and many of the major components of the system are being built by D. CURRIE ET AL at the Department of Physics and Astronomy, University of Maryland; J. FALLER ET AL at Wesleyan University and the Joint Institute for Laboratory Astrophysics, National Bureau of Standards and the University of Colorado; and by H. PLOTKIN ET AL, NASA Goddard Space Center, Maryland.

2. The Observatory

Figure 1 is a cutaway east elevation of the University of Hawaii LURE Observatory.

At the north end of the observatory a 9-meter diameter dome (Ash Dome Inc.) houses the receive telescope (Lurescope). The Lurescope dome is connected to the main building by an enclosed hallway.

The main building, containing the control and timing electronics, the laser and transmitter system, and support facilities, is a 9 x 19 - m prefabricated steel structure. A 0.5-meter crawl space beneath the raised working level accommodates the air conditioning, electrical distribution and sanitary systems. An articulated light path used to route a portion of the laser light to the Lurescope for the purposes of tuning the narrow bandpass filer and calibrating the timing system, is also located in the crawl space.

The transmitter system is located near the south end of the observatory and is constructed on two levels. The lower level is a laboratory environment that houses the laser and interfacing optics, the lunastat drive and pointing electronics, and the pointing optomechanical instrumentation. The upper level, reached by stairway from the laboratory area, is enclosed in a 7-meter diameter dome (Ash Dome Inc.) and contains the primary optics of the refractor feed telescope and the lunastat. The isolated instrument pier extends from beneath the laboratory level to the upper level. All the optomechanical components of the transmitter system, including the laser, interfacing optics, pointing instrumentation, feed telescope, and lunastat are mounted on this common pier.

3. The Laser

The Nd YAG laser system (figure 2), developed by GTE Sylvania, Electronic Systems Group of Mountain View, California, under a NASA Goddard Space Center contract, provides three pulses per second, each pulse being approximately 200 picoseconds in duration (FWHM) and containing 250 millijoules of energy at 5320 Å.

The basic elements of the system are: a mode locked oscillator, a regenerative amplifier, three single pass amplifiers, and a CsD*A (caesium dideuterium arsenate) frequency doubling crystal.

The oscillator cavity is formed by two reflectors spaced at approximately 1 meter and supported on isolation-mounted Invar rods. The oscillator head contains a 3.8-mm diameter by 70-mm rod, pumped continuously by two tungsten-halogen incandescent lamps. Mode locking is accomplished by a Data Light Inc. acousto-optic mode locker operated at 75 MHz. The output of the oscillator is a 150 MHz train of 200 picosecond duration pulses each containing approximately 2 nanojoules of energy at 10 640 Å.

Upon command, a pair of pockels cells switch a single pulse out of the train and inject it into the regenerative amplifier. After 12 passes of the pulse through the regenerative amplifier, which utilizes a 6-mm diameter by 76-mm rod apertured to 3 mm, the pulse is switched out, expanded and routed to the single pass amplifiers. The pulse passes through two 6-mm diameter by 76-mm amplifiers, is further expanded and passes through a 9.5-mm diameter by 76- millimetre saturated amplifier. The 200 picosecond pulse then contains approximately 500 millijoules of energy at 10 640 Å and has a beam divergence of approximately three times the diffraction limit.

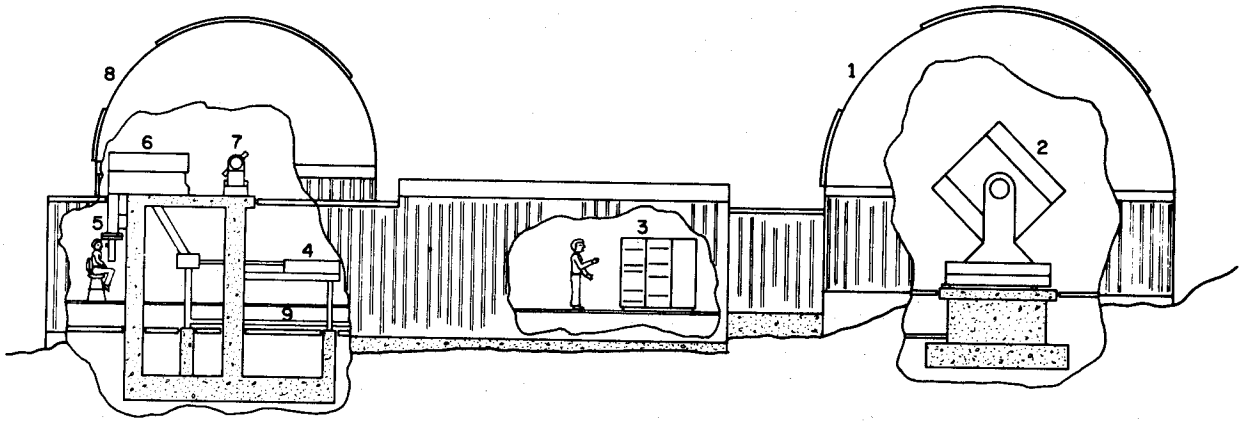

Figure 1. University of Hawaii LURE Observatory

1. 9-Meter Diameter Dome
2. Lurescope
3. Control & Timing Electronics
4. Laser
5. Pointing Instrumentation
6. Feed Telescope
7. Lunastat
8. 7-Meter Diameter Dome
9. Calibration Light-Link

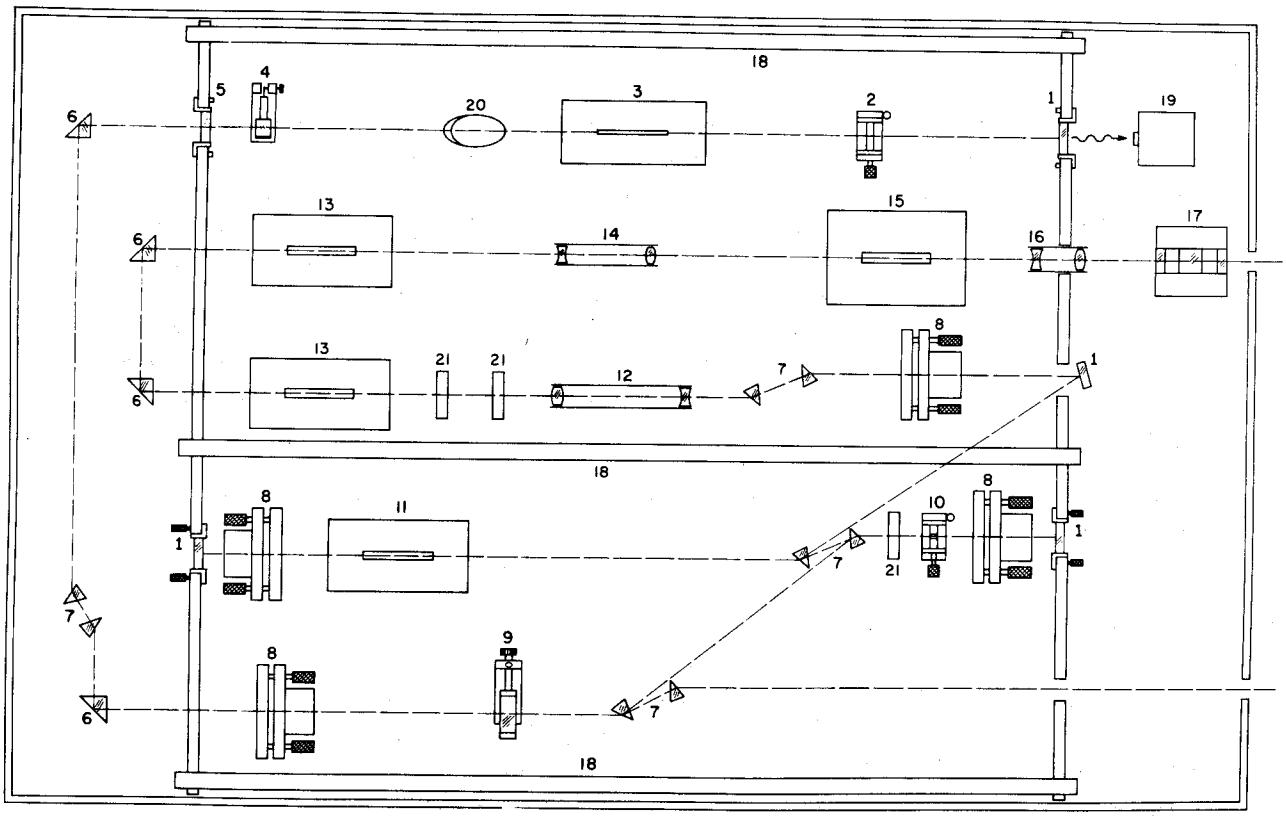

Figure 2. Laser

1. 99.9% Mirror
2. Aperture
3. Oscillator Head (3.8 x 70 mm rod)
4. Acousto-Optical Modulator
5. 98% Mirror
6. Turning Prism
7. Calcite Prisms
8. Pockels Cell
9. Beam Height Adjustment
10. Aperture
11. Regenerative Amplifier (6 x 76 mm rod)
12. Beam Expander Telescope
13. Single-Pass Amplifier (6 x 76 mm rod)
14. Beam Expander Telescope
15. Single-Pass Amplifier (9.5 x 76 mm rod)
16. Beam Expander Telescope
17. CsD*A Doubling Crystal
18. Invar Mounting Rods
19. Photo-detector
20. Brewster Plate
21. $\lambda/4$ Plate

The infrared is frequency-doubled by a CsD*A crystal to produce the desired 5320 Å light. The doubling crystal further deteriorates the beam collimation to 6 - 8 times the diffraction limit. Residual infrared is stripped-off by reflection from two dichroic mirrors prior to coupling into the transmitter system.

4. The Transmitter

Figure 3 is a sketch of the laser transmitter system (CARTER 1973). The collimated laser light is routed to a diverging lens. The diverging lens creates a diverging cone of light that appears to emanate from a point lying in the focal plane of the telescope objective. The diverging light is routed by reflection from a dichroic beamsplitter to the 40-cm diameter objective. The objective recollimates the expanded beam and transmits it toward the Lunastat. The reflected beam is pointed by accurate positioning of the lunastat and exits the enclosing observatory dome through a window of 75 cm diameter. A portion of the transmitted beam is intercepted by a cube corner and retroreflected. Approximately 0.2% of the reflected light passes through the dichroic beamsplitter and is routed to the pointing ocular which is mounted on a precise X-Y stage. The entire system, including the laser, is mounted on a common rigid frame concrete instrument pier.

5. The Lunastat

The Lunastat was constructed by Goerz-Inland Systems Division, Kollmorgen Corporation of Pittsburgh, Pennsylvania. A 70 cm diameter ultra-lightweight (25 kg) fused quartz optical flat, loaned for the duration of the project by the Optical Sciences Center, The University of Arizona, is the principal optical component. The mounting is altitude-azimuth; stabilized castings and maximum symmetry on construction have been used to minimize structural flexure and temperature related distortions of the mount. The design incorporates previously developed units consisting of mechanical axis, direct coupled torque motor drive, d.c. tachometer, and Inductosyn electronic shaft encoder. The axis wobble is <2.0 arcseconds; the encoder has a resolution of 0.36 arcsecond. The electronic logic, control, and readout units are standard production items. Both manual and computer control modes are available.

A two axis electronic level has been built into the instrument to provide a real time measurement of tilt, and appropriate corrections are made in formulations of the pointing commands.

6. Feed Telescope

The principal imagery element of the feed telescope is the 40 cm diameter f/11 achromatic objective. The two elements of the objective are widely airspaced ($\sim$ 20 cm) for the purpose of eliminating spherochromatism. The objective is diffraction-limited, monochromatically, over the visible spectrum, and image splitting by wavelength selection allows the objective to be used simultaneously for three distinct purposes: transmitting laser pulses, visual viewing, and electronic viewing.

The laser transmitting path and the two viewing optical paths are interfaced to the objective by use of a 2.5 cm thick, 33 cm diameter fused quartz beamsplitter located approximately 152 cm from the objective. The beamsplitter is dielectric coated to have >99.5% reflection at the laser wavelength of 5320 Å region. Light passing through the beamsplitter does suffer significant optical aberrations; an array of three optically flat corrector plates is used to compensate these

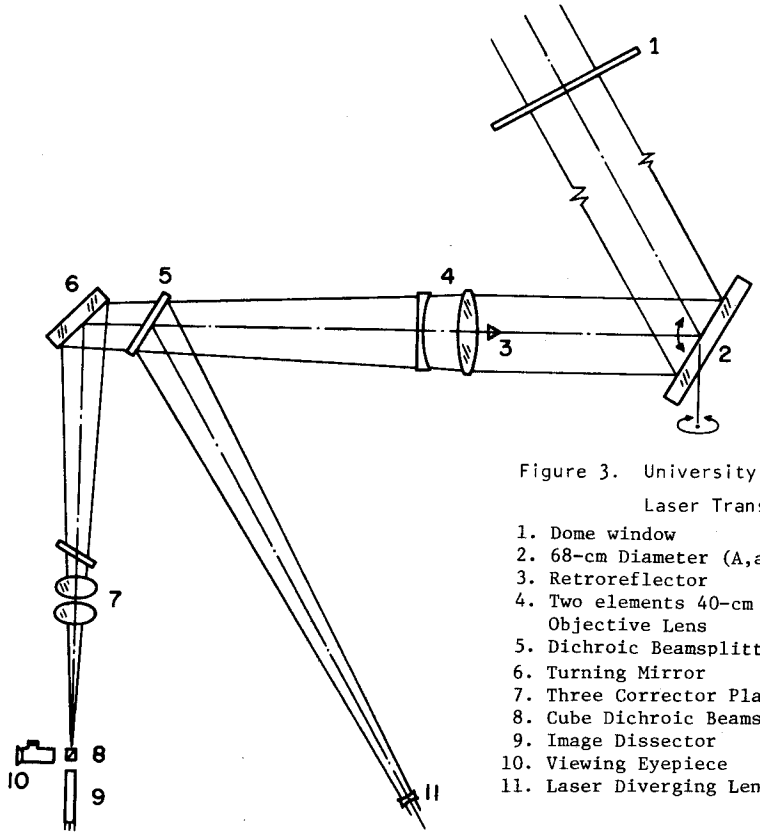

Figure 3. University of Hawaii Laser Transmitter System

1. Dome window
2. 68-cm Diameter (A,a) Mounted Flat
3. Retroreflector
4. Two elements 40-cm Diameter Objective Lens
5. Dichroic Beamsplitter
6. Turning Mirror
7. Three Corrector Plates
8. Cube Dichroic Beamsplitter
9. Image Dissector
10. Viewing Eyepiece
11. Laser Diverging Lens

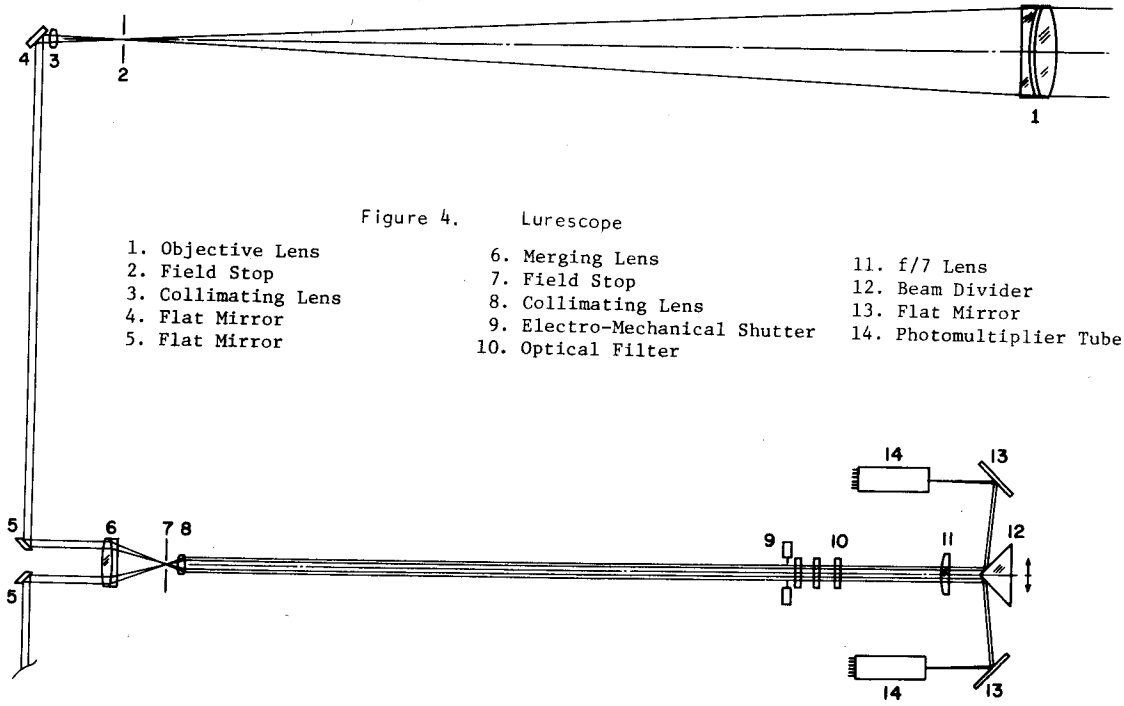

Figure 4. Lurescope

1. Objective Lens
2. Field Stop
3. Collimating Lens
4. Flat Mirror
5. Flat Mirror
6. Merging Lens
7. Field Stop
8. Collimating Lens
9. Electro-Mechanical Shutter
10. Optical Filter
11. f/7 Lens
12. Beam Divider
13. Flat Mirror
14. Photomultiplier Tube

aberrations. This light is further subdivided, by use of a cube dichroic beamsplitter, and routed to an ocular and image dissector tube mounted on the X-Y stage.

The feed telescope body and optical mounts were constructed by the University of Hawaii, in-house. The optical components were fabricated by Hudson Precision Optical Co., Inc. of Hudson, New Hampshire.

The feed telescope optics were designed by R.A. Buchroeder.

7. Relative Pointing System

The feed telescope, described above, has a nominal focal plane scale of 48 arsec/mm, resulting in a lunar image approximately 3.8 cm in diameter. A precise X-Y positioning stage, Yosemite Laboratory of Berkeley, California, is attached rigidly to the telescope tube and carries an assembly containing both an observer eyepiece and an image dissector tube, ITT F4012 RP. The stage is driven by stepping motors, Superior Electric Inc. type LS50-1006, having 500 steps per rotation. Each full rotation of the motors translates the stage 0.254 cm, making a single step equal to approximately 0.22 arcseconds. Maximum deviation from linearity over the entire 10-cm travel, each axis, is 0.0020 mm. Orthogonality of the axes is better than 10 arcseconds and flatness to travel is better than 0.0020 mm over the entire travel. Total positioning uncertainty over the full 10-cm x 10-cm field is less than 0.25 arcseconds. Temperature effects, about 1 part in 10^5 per degree centigrade, are insignificant over a range $\pm 3^{o}$C expected for the observatory ambient temperature.

Positioning of the stage may be controlled from a manual control panel or by computer command. A one-pulse-per-rotation shaft encoder is mounted on each drive motor. The total number of steps is recorded and the position is inferred directly. Whole numbers of rotations are checked for coincidence with the encoder pulse as a check against loss or addition of spurious counts. The laser will be aligned to the center of the stage travel as nearly as conveniently possible, and the actual coordinates will serve as fiducial. Offsets thus will be measured relative to the laser coordinates. Star fields and lunar features will be used to calibrate the focal plane distortions.

Use of two modes of relative pointing is anticipated. The modes differ, however, only in the means used to generate the basic lunar rate, i.e., by computer control or electronic tracker control of the Lunastat. The first method uses absolute methods continually to update the pointing, and the observer is required only to apply small corrections as required for deficiencies in the computer modelling. It is the ultimate goal that computer pointing be developed to the level of accuracy that the observer may be eliminated from the system and truly absolute pointing methods used.

The second method uses an image dissector tube as a sensor to lock onto and track a reference lunar feature. The observer still must make small pointing corrections as the offset changes with time. Comparison of electronic tracking and computer pointing will be used to improve the absolute point program model.

8. The Receiver (Lurescope)

FALLER's group built the receiver referred to as the Lurescope (FALLER 1972). The Lurescope consists of a "bundle" of 19-cm aperture refractor telescopes that are optically coupled to form a single image.

For the laser ranging a second field stop is placed in the common focal plane. The light passing through this spatial filter is collimated, routed through an optical filter, (typically, 2 to 3 Å) beamsplit, and routed to two photomultiplier tubes. Figure 4 is a schematic of the optical elements of a typical channel.

The Lurescope has an altitude-azimuth mount. The vertical axis has oil bearings; the horizontal axis has mechanical bearings. The drives are torque motors coupled to the axes by metal rollers. Twenty-bit, 1.2 arcsecond, optical shaft encoders measure the rotations about each axis. The primary method of pointing is absolute, under the control of Data General Corporation Super Nova Computer. A guide telescope is provided for manual guiding and/or for the observer to "touch-up" the computer pointing.

9. University of Maryland Event Timer System

Currie's group developed a clock system that is capable of measuring the epoch of individual events with a resolution of 100 picoseconds and, by differencing, determine the interval between two events occurring within a few seconds of one another to approximately 200 picoseconds. Figure 5 is block diagram of the system.

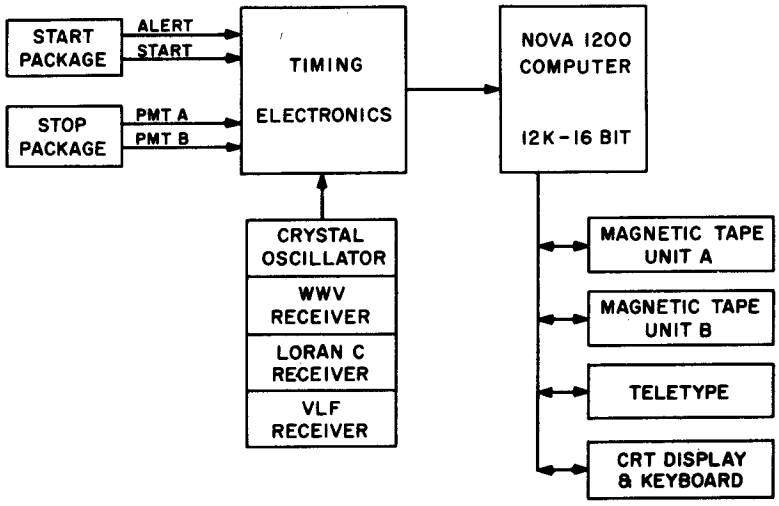

Figure 5. Event Timer System

The crystal oscillator, Austron-Sulzer Model 1250, provides a 10 MHz driving frequency to the event timer unit. The epoch of the event timer is set to UTC via WWVH and Loran C broadcasts, and the frequency of crystal oscillator is monitored and adjusted via Loran C and VLF broadcasts.

The event timer counts the 10 MHz crystal oscillator signal continuously, maintaining epoch to 100 nanoseconds. Events happenings within any particular cycle are timed relative to the end of the cycle by a vernier system. Receipt of an event begins the charging of a capacitor from a constant-current source. The charging continues from the time the event is received until the start of the second following 10 MHz cycle. At the end of the charging period, the capacitor is discharged at a current 125 times smaller than the charging current. The discharge period is measured by an 80 MHz counter that is phase locked to the 10 MHz clock with a resolution of ± 1 cycle. This resolution is equivalent, with the 125 times scaling factor, to 100 picoseconds. The event timer has two independent channels, and each channel can accept 4 events at intervals as short as 20 nanoseconds. The dual channel, multiple event, low dead time features of the event timer allow operation with high background noise and considerable latitude in operating and calibration methods.

The epoch of each event is read by the computer (Data General Nova 1200) and the determination of the type of event and interval between particular events is performed by the computer.

The relatively high repetition rate of the laser, 3 Hz, makes it difficult for an operator to monitor the progress of the ranging operations and decide when a sufficient number of rangings have been recorded for an acceptable measurement. To assist, a histogram of the predicted minus measured range residuals is displayed in real time on a CRT display. The full data set is stored on magnetic tape.

10. Accuracy of Ranges

The uncertainty associated with each range measurement arises from several factors, e.g. the finite laser pulse width, event timer resolution, discriminator walk, and PMT jitter.

Studies conducted at the University of Maryland indicate that PMT jitter is presently the most significant item, with a magnitude of 400 to 500 picoseconds for the best available useful tubes.

The total additional uncertainty contributed by the laser pulse width ($\simeq$ 200 picoseconds FWHM), event timer ($\pm$ 100 picoseconds per event), discriminator walk (100 picoseconds), and other lesser sources may be expected to increase the total uncertainty to 500 - 600 picoseconds per range measurement.

The uncertainty associated with the mean range of N measurements diminishes as the square root of N, making it not unreasonable to achieve an uncertainty of $\pm$ 100 picoseconds for an observation (set of measurements).

11. Conclusions

Current plans are to have the new LURE Observatory operational early in 1974. A staff of 6 to 9 full-time employees will operate the system whenever, during each lunar cycle, background noise and pointing capabilities will allow a reasonable yield of range measurements.

12. References

BUCHROEDER, R. A. 1972. 16-inch f/11 Refractor. Lunar Laser Transmitter System, Design Report prepared for the University of Hawaii, Institute for Astronomy.

CARTER, W. E. 1973. *The Lunar Laser Ranging Pointing Problem*, Department of Civil Engineering, University of Arizona.

FALLER, J. 1972. *The Apollo Retroreflector Arrays and a New Multi-lensed Receiver Telescope*, Space Research XII, Akademie-Verlag Berlin, 211-217.

Proc.Symposium on Earth's Gravitational Field & Secular Variations in Position (1973),442-453.

MORITZ, H.
Technical University at Graz
A 8010 Graz
Austria
&
Department of Geodetic Science
The Ohio State University
Columbus Ohio 43210
United States of America

THE ROLE OF STATISTICAL TECHNIQUES IN THE DETERMINATION OF THE EARTH'S GRAVITATIONAL FIELD

ABSTRACT

The paper discusses the statistical structure of the terrestrial gravity field and applications to physical geodesy. Among these applications are least squares prediction (interpolation and extrapolation) of gravity anomalies and deflections of the vertical, and least squares collocation; the collocation method permits an optimal simultaneous determination of geodetic positions and of the terrestrial gravity field by combining different data of any kind -- terrestrial angle, distance and gravity measurements as well as data from advanced satellite techniques.

1. Introduction

The classical statistical technique in geodesy is least-squares adjustment. Here the observational errors are treated on a statistical basis. R.A. HIRVONEN (1956) was the first to recognize that the irregularities of the anomalous gravity field make a statistical treatment of gravity anomalies meaningful and useful. W.M. KAULA (1959) made a comprehensive statistical analysis of the gravity anomaly field, which provided a basis for many subsequent investigations.

In the terminology of stochastic processes, the field of the gravity anomalies is treated as a two-dimensional stochastic process on a sphere. Therefore, least squares prediction techniques for stochastic processes were adapted to the interpolation and extrapolation of gravity (MORITZ 1962) and extensively applied (RAPP 1964; SOLTAU 1970).

Statistical methods may also be used for estimating the accuracy of the predicted gravity anomalies and of quantities derived from them, such as geoidal heights, deflections of the vertical, etc. A comprehensive presentation of these developments until 1966 is found in chapter 7 of (HEISKANEN & MORITZ 1967). The present paper attempts to review subsequent developments and to illustrate the methods by treating some aspects in more detail.

2. Statistics of the Gravity Field

Let the spherical harmonic expansion of the gravity anomaly Δg be written as

$$\Delta g = \sum_{n=2}^{\infty} \sum_{m=0}^{n} \left(\bar{a}_{nm} \bar{R}_{nm}(\theta,\lambda) + \bar{b}_{nm} \bar{S}_{nm}(\theta,\lambda) \right) \qquad (1),$$

where $\bar{R}_{nm}$ and $\bar{S}_{nm}$ are fully normalized surface harmonics:

$$\bar{R}_{nm}(\theta,\lambda) = \bar{P}_{nm}(\cos\theta)\cos m\lambda \quad ; \quad \bar{S}_{nm}(\theta,\lambda) = \bar{P}_{nm}(\cos\theta)\sin m\lambda \tag{2},$$

$\bar{P}_{nm}(\cos\theta)$ being a fully normalized Legendre function (IBID,section 1-14); θ (co-latitude) and λ (longitude) are spherical co-ordinates. Then the covariance function of the gravity anomaly is given by (IBID.section 7-3)

$$C(\psi) = \sum_{n=2}^{\infty} c_n P_n(\cos\psi) \tag{3},$$

where $P_n(\cos\psi)$ are the conventional Legendre polynomials, ψ being the spherical distance, and the coefficients c_n are expressed in terms of the coefficients $\bar{a}_{nm}$ and $\bar{b}_{nm}$ by

$$c_n = \sum_{m=0}^{n} \left(\bar{a}_{nm}^2 + \bar{b}_{nm}^2 \right) \tag{4}.$$

This covariance function fully describes the (wide sense) statistical behaviour of the anomalous gravitational field. The coefficients c_n are called degree variances and frequently denoted by σ_n^2.

A comparison of recent values for σ_n^2 is given by RAPP (1973b,table 3). They conform remarkably well to Kaula's rule of thumb (KAULA 1966b): he suggests that the root mean square value of a potential harmonic coefficient of degree n could be estimated by

$$\pm \frac{10^{-5}}{n^2} \tag{5}.$$

This corresponds to degree variances

$$\sigma_n^2 = \gamma^2 (n-1)^2 (2n+1) \frac{10^{-10}}{n^4} \tag{6},$$

where γ is a mean value of gravity (980 gal).

RAPP (1972) investigated a series of analytical models to improve this rule of thumb, recommending

$$\sigma_n^2 = \frac{a(n-1)}{(n-2)(n+b+cn^2)} \tag{7},$$

with

$$a = 251.6 \text{ mgal} \; ; \quad b = 12.93 \; ; \quad \text{and} \quad c = 0.00071 \tag{8}.$$

LAURITZEN (1973) and TSCHERNING (1972b) used a closed analytical expression for the covariance function which amounts to putting

$$\sigma_n^2 = A\frac{n-1}{n-2} \tag{9}.$$

A review of statistical analysis of data distributed over a sphere, which is applicable to the gravity field, is given in (KAULA 1967).

The autocovariances of any other quantity of the anomalous gravity field, such as geoidal heights

or deflections of the vertical, and their cross-covariances are derived by covariance propagation. See (HEISKANEN & MORITZ 1967,section 7.7) - the theory given there for error covariance functions applies without change to other covariance functions - and (MORITZ 1970a,section 7).

A theoretical and numerical investigation of the covariance structure of geoidal heights, gravity anomalies, vertical deflections, and anomalous gravity gradients is found in (MEISSL 1971). TSCHERNING (1972b) made analytical and numerical evaluations of various covariance functions.

For local purposes, the Earth's surface may be approximated by a plane. The plane theory of the covariance structure of the gravity field is somewhat simpler than the spherical theory and was investigated by several authors; cf. (SHAW ET AL 1969; GRAFAREND 1971a; GRAFAREND 1971b; GRAFAREND 1973a; GRAFAREND 1973b).

Grafarend points out that for vector fields $s_i (i=1,2)$ such as deflections of the vertical, homogeneity and isotropy do not imply that all covariances depend only on the distance r; instead, the general form of a homogeneous and isotropic covariance tensor C_{ij} corresponding to the vector s_i is

$$C_{ij}(P,Q) = \Psi(r)\,\delta_{ij} + \{\,\Omega(r) - \Psi(r)\,\}e_i e_j \qquad (10),$$

where $\Psi(r)$ and $\Omega(r)$ are arbitrary functions and the direction enters through the unit vector e_i from point P to point Q; δ_{ij} denotes the components of the unit matrix. He also tested this structure in empirical deflection fields (GRAFAREND 1971c; GRAFAREND 1972a).

GROTEN (1972) investigated effects due to non-uniform distribution of data, incomplete elimination of trends (anisotropy, non-stationarity, etc) and their influence on linear regression prediction.

An important negative result concerning the interpretation of the anomalous gravity field as a stochastic process was obtained by LAURITZEN (1973). He proved that it is impossible to find a stochastic process, harmonic outside a sphere, which is both Gaussian and ergodic.

Therefore MORITZ (1972,section 8) proposed to use, instead of an interpretation as a stochastic process, an interpretation in terms of a covariance analysis of individual functions as rigorously elaborated already by WIENER (1930); cf. also (DOOB 1949). This also takes into account that in reality there is only one individual Earth's gravity field and not a phase space of many such fields.

3. Least-Squares Prediction and Collocation

Least-squares prediction was applied, not only to gravity anomalies, but also to deflections of the vertical (HEITZ 1969; GRAFAREND 1971a; GRAFAREND 1971b).

Least-squares filtering, which is closely related to prediction, was applied for removing inertial noise from airborne gravimeter data (MORITZ 1967; MEISSL 1970; SZABO & ANTHONY 1971).

The usual least-squares prediction is linear since the results s_i are obtained as linear functions of the data x_j, of form

$$s_i = B_{ij} x_j \qquad (11),$$

summation over subscripts occurring twice is implied. Optimum linear estimates are the best among all estimates, linear and non-linear, if the quantities under consideration are normally distributed. As we have just seen, however, the assumption of normal distribution for the anomalous gravity field leads to difficulties. Therefore KAULA (1967) and GRAFAREND (1972b) considered non-linear prediction in the form of a series

$$s_i = B_{ij} x_j + C_{ijk} x_j x_k + D_{ijk\ell} x_j x_k x_\ell + \ldots\ldots \qquad (12).$$

So far however, linear estimation is almost exclusively used.

The decisive generalization of linear least-squares prediction to a general theory of estimation of any element of the anomalous gravitational field (gravity anomalies, geoidal heights, deflections of the vertical, harmonic coefficients of the geopotential) from arbitrary, even heterogeneous data was given by KRARUP (1968; 1969); this method was called least-squares collocation. He also clarified the relation between least-squares collocation and least-squares adjustment, by exhibiting collocation as an adjustment in Hilbert space with a kernel function; for prediction of time series this had been done by PARZEN (1961). More on the Hilbert space aspect may be found in (TSCHERNING 1971; TSCHERNING 1973).

In a different but equivalent approach, which is simpler by avoiding the use of Hilbert space, least-squares collocation was applied to the solution of a number of problems in physical geodesy, such as the discrete geodetic boundary value problem, the application of aerial gravimetry, the geodetic use of gradiometer measurements, and the combination of gravimetry with satellite-determined harmonics and with astro-geodetic data (MORITZ 1970a).

A somewhat different line of development, already foreshadowed in (KAULA 1963), leads to the incorporation of parameters representing systematic effects. For the case of gravity this was done in (MONGET 1969), (MONGET & ALBUISSON 1971), (LAUER 1971), (MORITZ 1969) and (MORITZ 1970c), where also applications to other fields of geodesy are outlined. This line of development finally leads to a joint least-squares determination of geometric positions and of the gravity field ("Integrated Geodesy"). Cf. (KRARUP 1971; EEG & KRARUP 1973); here we shall follow the presentation given in (MORITZ 1972).

The basic model for least-squares collocation including systematic parameters is

$$x = AX + s + n \qquad (13).$$

Here x, the "measurement", is a vector formed by the observations; X is the vector of the non-stochastic parameters; A is the "sensitivity matrix" characterizing the influence of the parameters X on the measurement x; and s, the "signal", and n, the "noise", are two different random vectors of zero mean.

The noise n is nothing else than the random measuring error of the quantity x, and s represents the effect of the anomalous gravity field on this quantity. The part AX comprises, after linearization by Taylor's theorem:

1. the effect of the reference ellipsoid and of the normal gravity field;
2. geometric parameters such as point co-ordinates; and
3. systematic errors and trends (e.g., gravimeter drift).

Now it is easily seen that *every* geodetic measurement can be split up according to equation 13. As an example, consider gravity g

$$g = \gamma + \Delta g + n_g \qquad (14).$$

Here, normal gravity γ represents AX, the gravity anomaly Δg stands for s, and n_g signifies the measuring error.

For geometrical quantities such as azimuths, horizontal angles or zenith distances, AX represents the corresponding ellipsoidal ("geodetic") quantity, and s is nothing else than the "reduction to the reference ellipsoid" as described in (HEISKANEN & MORITZ 1967,section 5.4 & 5.5). In a similar way, satellite observations (variations of orbital elements, directions, distances, doppler and altimeter data, etc) may be treated.

The formulas for least-squares collocation may be derived from two different minimum principles:

1. From a suitable generalization of the well known adjustment principle

$$v^T P\, v = \text{minimum},$$

where P is the weight matrix, v is a random vector, and ^{T} denotes its transpose.

2. From the condition that the standard error of the result be minimized.

This is in full analogy to least-squares adjustment; again, the two different minimum principles turn out to be equivalent.

The basic computational formulas are as follows. The parameter vector X is given by

$$X = (A^T \overline{C}^{-1} A)^{-1} A^T \overline{C}^{-1} x \qquad (15),$$

then any signal s_P may be obtained from

$$s_P = C_P^T \overline{C}^{-1} (x - AX) \qquad (16).$$

The signal s_P may be any quantity of the anomalous gravity field; an anomalous potential T, a geoidal height N, a component of the deflection of the vertical (ξ or η), a gravity anomaly Δg, etc.

The matrix $\overline{C}$ is the covariance matrix of the vector x, it consists of a signal part C, and a noise part D:

$$\overline{C} = C + D \qquad (17).$$

D is the error covariance matrix, representing the effect of the random measuring errors n. In adjustment computations, only the matrix D is considered and it is called the variance-covariance

matrix.

The signal covariance matrix C is the characteristic novelty in least-squares collocation; it represents the effect of the anomalous gravity field on the quantities under consideration.

The essential point is that the signal covariances, for any measured element, must be derived from a single basic covariance function by covariance propagation, as we have seen in section 2.

The matrix C_P^T is the row vector

$$C_P^T = (C_{P1}, C_{P2}, \ldots, C_{Pq}) \qquad (18),$$

representing the signal covariances between s_P and the measurements x; it is likewise to be derived from covariance propagation.

Equation 15 is analogous to the equation determining the parameters in least-squares adjustment, with the important difference that in adjustment by parameters, we have the error covariance matrix D instead of $\overline{C}$, whereas in collocation, the signal covariances C enter as well through equation 17.

Equation 16 is analogous to the basic equation for least squares prediction; cf. (HEISKANEN & MORITZ 1967,p.268). In fact (LOC.CIT.,equation 7.63) is a special case of equation 16, if there are no measuring errors (n=0, D=0, $\overline{C}$ = C) and no systematic parameters (A=0), and if both the measurements x and the signal s_P to be computed are gravity anomalies.

The present method may thus be regarded as a combination of least-squares adjustment and least-squares prediction into a unified scheme. It gives a solution which is optimal in the sense that it gives the most accurate results obtainable on the basis of the available data.

It should be emphasized that the estimated quantity s_P and the measurements making up the vector

$$x^T = (x_1, x_2, \ldots, x_q)$$

may be of different nature; for example, x_1 may be a measured gravity anomaly, x_2 may be a terrestrial baseline, x_3 may be a component of the deflection of the vertical, x_4 may be a satellite range-rate, etc, whereas s_P may be a geoidal height to be computed.

The accuracy of the estimated quantities X and s_P may be evaluated by formulas which are generalizations of the corresponding formulas for least-squares adjustment and least-squares prediction.

An attractive feature of collocation is the fact that the signal s and the noise n, which often have a similar order of magnitude, are treated on an equal statistical basis.

We remark that all calculated quantities s, whatever they are, refer to one and the same anomalous gravity field, so that our method is indeed self-consistent.

This field, besides being optimal in the sense of highest accuracy, is also the smoothest gravity field that is compatible with the given data. Therefore it can be analytically continued down to sea level without any difficulties.

The usual solution of problems of physical geodesy by means of integral formulas may be considered as limiting cases of collocation solutions when the coverage by gravity measurements becomes continuous.

In fact however, the case of discrete measurements, which underlies least-squares collocation, is much more realistic than the case of continuous gravity coverage. Interpolation and vertical reduction, essential in the classical procedures are, so to speak, built in now; data of different kinds can be combined; and measuring errors are automatically adjusted.

As an idealization, we might assume that *all* geodetic measurements (from triangulation to advanced dynamic satellite techniques) obtained so far are combined into a single solution set out in equations 15 and 16, to give the best result for the Earth's geometry and gravity field. As a matter of fact, this cannot be fully and literally realized in practice because it would involve the inversion of an excessively large $\overline{C}$ matrix.

The inversion of the $\overline{C}$ matrix constitutes, in fact, the main computational problem with this method. On the other hand, the inversion of $\overline{C}$ must be performed only once for a given set of data; any desired quantity s_p, of the anomalous gravity field, and also its accuracy, may then be computed with the same matrix $\overline{C}^{-1}$.

This, in practice, the number of data to be combined is limited by the size of the matrix that can be inverted in the computer. This presupposes suitable representative selection of the data and some working "from the large to the small" in several steps; cf. (MORITZ 1973a).

BJERHAMMAR (1971) and KOCH & LAUER (1971) advocated the use of Kalman filtering and prediction; BJERHAMMAR (1973b) and MORITZ (1973a) investigated the relation between stepwise collocation and the Kalman method.

4. Applications of Collocation

TSCHERNING (1970) applied collocation to the determination of the geoid in Scandinavia from astro-geodetic deflections of the vertical and from gravity; for a comparison with least-squares prediction see (HEITZ & TSCHERNING 1972).

Rapp compared the collocation procedure of MORITZ (1970b) with the adjustment procedure of RAPP (1969); his results are given in (RAPP 1973a) and presented at this symposium (RAPP 1973b).

An application of collocation to the determination of zonal harmonics from satellite observations is described in (MORITZ & SCHWARZ 1973) and (SCHWARZ 1973). The mathematical formulation of this problem leads to a linear system of the form

$$Ms + n = x \qquad (19),$$

where the vector x comprises (essentially) the observed variations in the orbital elements such as $\Delta\Omega$ and $\Delta\omega$, n represents the measuring errors, and s consists of the unknown spherical harmonic coefficients (or more precisely, the deviations of these coefficients from the corresponding coefficients for the normal gravity field); since there are infinitely many such coefficients, the vector s is an infinite vector. The matrix M represents the influence of these coefficients on the

observations x; it has a finite number of rows and infinitely many columns.

The usual way of solving equation 19 is to truncate the infinite vector s so as to get an over-determined system, which is solved by the adjustment of parameters. It may however, also be solved by collocation, with the result

$$s = C M^T (M C M^T + D)^{-1} x \qquad (20).$$

Here C represents the covariance matrix of the vector s; it is an infinite diagonal matrix whose elements are closely related to the degree variances σ_n^2 (section 2), and D is the error covariance matrix for the observations x.

The collocation solution appears to have certain advantages over the conventional method. It maintains the proper balance between the order of magnitude of coefficients and of measuring errors by treating them on an equal statistical basis, thus taking seriously the fact that especially for higher coefficients, their error has almost the same order of magnitude as the coefficients themselves. Furthermore collocation separates the individual coefficients in an optimal way and gives values for all infinitely many coefficients - the best values obtainable on the basis of the given data; if a higher coefficient can no more be reliably determined, then collocation gives a value close to zero.

The improvement of the statistical model by including gravity field covariances also leads to more realistic accuracy estimates for the resulting coefficients.

5. Acknowledgment

This paper incorporates research performed in co-operation with the Department of Geodetic Science, of the Ohio State University under Contract F19628-72-C-0120 sponsored by Air Force Cambridge Research Laboratories, and work done under Grant No 1474 of the Austrian "Fonds zur Förderung der wissenschaftlichen Forschung".

6. References

BJERHAMMAR, A. 1969. *Linear Prediction and Filtering.* Division of Geodesy, Royal Institute of Technology, Stockholm.

BJERHAMMAR, A. 1971. Prediction and Filtering of Non-Stationary Stochastic Processes in Geodesy. *XV General Assembly, IUGG*, Moscow.

BJERHAMMAR, A. 1973a. *Methods of Estimation of Physical Geodesy.* International Summer School in the Mountains, Ramsau Austria.

BJERHAMMAR, A. 1973b. *A General Model for Optimal Prediction and Filtering in the Linear Case.* International Summer School in the Mountains, Ramsau Austria.

DOOB, J.L. 1949. Time Series and Harmonic Analysis. In (NEYMAN, J. ed.) *Proceedings of the Berkeley Symposium on Mathematical Statistics and Probability.* University of California Press, 303.

EEG, J. & KRARUP, T. 1973. Integrated Geodesy. *Internal Rep.* 7, Danish Geodetic Institute, Copenhagen.

GRAFAREND, E. 1971a. Statistische Modelle zur Prädiktion von Lotabweichungen. *Vermessungstechnik* 19, 66-68.

GRAFAREND, E. 1971b. A Combined Gravimetric-Astrogeodetic Method for Telluroid and Vertical Deflection Analysis. In: Beiträge aus der BRD zur Vorlage bei der XV. Generalversammlung der IUGG. *Veröffentlichungen der Deutschen Geodätischen Kommission B* 188, 23-36.

GRAFAREND, E. 1971c. Isotropietests von Lotabweichungsverteilungen in Westdeutschland I. *Z.f. Geophys.* 37, 719-733.

GRAFAREND, E. 1972a. Isotropietests von Lotabweichungsverteilungen in Westdeutschland II. *Z.f.Geophys.* 38,243-255.

GRAFAREND, E. 1972b. Nichtlineare Prädiktion. *Z.f.VermessWes.* 97,245-255.

GRAFAREND, E. 1973a. *Geodetic Stochastic Processes.* International Summer School in the Mountains, Ramsau Austria.

GRAFAREND, E. 1973b. *Geodetic Prediction Concepts.* International Summer School in the Mountains, Ramsau Austria.

GROTEN, E. 1972. Some Numerical Aspects of Linear Regression Prediction. *Fifth Symposium on Mathematical Geodesy*, Florence.

HEISKANEN, W.A. & MORITZ, H. 1967. *Physical Geodesy.* Freeman, San Fransisco.

HEITZ, S. 1969. Eine astronomisch geodätische Geoidbestimmung für Westdeutschland. *Veröffentlichung der Deutschen Geodätischen Kommission B* 167, Munich.

HEITZ, S. & TSCHERNING, C.C. 1972. Comparison of Two Methods of Astrogeodetic Geoid Determination based on Least Squares Prediction and Collocation. *Tellus* XXIV,271-276.

HIRVONEN, R.A. 1956. On the Precision of the Gravimetric Determination of the Geoid. *Trans.Am. geophys.U.* 37,1-8.

KAULA, W.M. 1959. Statistical and Harmonic Analysis of Gravity. *J.geophys.Res.* 64,2401-2421.

KAULA, W.M. 1963. Determination of the Earth's Gravitational Field. *Revs.geophys.* 1,507-551.

KAULA, W.M. 1966a. Global Harmonic and Statistical Analysis of Gravimetry. In "Gravity Anomalies: Unsurveyed Areas". *Geophys.Monograph* 9,American Geophysical Union,Washington DC.

KAULA, W.M. 1966b. Tests and Combination of Satellite Determinations of the Gravity Field with Gravimetry. *J.geophys.Res.* 71.5303-5314.

KAULA, W.M. 1967. Theory of Statistical Analysis of Data Distributed over a Sphere. *Revs.geophys.* 5,83-107.

KOCH, K.R. & LAUER, S. 1971. Automation der Isoliniendarstellung mit Hilfe des Wiener - und des Kalman - Filters. *Publication* 2,Institute of Theoretical Geodesy,University of Bonn.

KRARUP, T. 1968. *A framework for least-squares determination of the potential of the Earth.* Report to Members of IAG Special Study Group 5:31.

KRARUP, T. 1969. A Contribution to the Mathmatical Foundation of Physical Geodesy. *Publication* 44, Danish Geodetic Institute,Copenhagen.

KRARUP, T. 1971. *Introducing Integrated Geodesy.* Lecture - Technical University of Berlin (May).

LAUER, S. 1971. Kovarianzen, Power-Spektren und Prädiktionen im lokalen Schwerefeld. In "Beiträge aus der BRD zur Vorlage bei der XV Generalversammlung der IUGG". *Veröffentlichungen der Deutschen Geodätischen Kommission B* 188,37-49,Munich.

LAURITZEN, S.L. 1973. The Probabilistic Background of some Statistical Methods in Physical Geodesy. *Publication* 48,Danish Geodetic Institute,Copenhagen.

MEISSL, P. 1970. Probabilistic Error Analysis of Airborne Gravimetry. *Rep.*138,Department of Geodetic Science,The Ohio State University,Columbus Ohio.

MEISSL, P. 1971. A Study of Covariance Functions Related to the Earth's Disturbing Potential. *Rep.*151,Dept. of Geodetic Science,The Ohio State University,Columbus Ohio.

MONGET, J.M. 1969. Une Nouvelle Méthode d'Analyse Statistique des Données Gravimetriques.*Bull.géodés.* 94,427-441.

MONGET, J.M. & ALBUISSON, M. 1971. A New Statistical Treatment of Gravity Data. *Bull.géodés.* 102, 451-466.

MORITZ, H. 1962. Interpolation and Prediction of Gravity and their Accuracy. *Rep.* 24,Institute of Geodesy,Photogrammetry & Cartography,The Ohio State University,Columbus Ohio.

MORITZ, H. 1967. Optimum Smoothing of Aerial Gravity Measurements. *Rep.* 81,Dept. of Geodetic Science,The Ohio State University,Columbus Ohio.

MORITZ, H. 1969. A General Theory of Gravity Processing. *Rep.* 122,Dept. of Geodetic Science,The Ohio State University,Columbus Ohio.

MORITZ, H. 1970a. Least Squares Estimation in Physical Geodesy. *Rep.* 130,Dept. of Geodetic Science, The Ohio State University,Columbus Ohio; *Veröffentlichungen der Deutschen Geodätischen Kommission A* 69.

MORITZ, H. 1970b. Combination of Satellite Harmonics and Gravimetry. *Rep.*146,Dept. of Geodetic Science,The Ohio State University,Columbus Ohio.

MORITZ, H. 1970c. A generalized Least-Squares Model. *Studia geophys.et geodaet.*14,353-362.

MORITZ, H. 1972. Advanced Least Squares Methods. *Rep.* 175,Dept. of Geodetic Science,The Ohio State University,Columbus Ohio.

MORITZ, H. 1973a. Stepwise and Sequential Collocation. *Rep.* 202,Dept. of Geodetic Science,The Ohio State University,Columbus Ohio.

MORITZ, H. 1973b. Determination of the Gravity Field by Collocation. *Boll.di geodes.e scienzi affini* XXXII,1-13.

MORITZ, H. & SCHWARZ, K.P. 1973. On the Computation of Spherical Harmonics from Satellite Observations. *Boll.di geodes.e scienzi affini* XXXII,185-200.

PARZEN, E. 1961. An Approach to Time Series Analysis. *Ann.math.statistics* 32,951-989.

RAPP, R.H. 1964. The Prediction of Point and Mean Gravity Anomalies Through the use of a Digital Computer. *Rep.* 43,Dept. of Geodetic Science,The Ohio State University,Columbus Ohio.

RAPP, R.H. 1966. A Fortran Program for the Computation of Localized Gravity Anomaly Statistics. *Rep.* 74,Dept. of Geodetic Science,The Ohio State University,Columbus Ohio.

RAPP, R.H. 1969. Analytical and Numerical Differences Between Two Methods for the Combination of Gravimetric and Satellite Data. *Boll. geofis.teorica appl.* 11,108-118.

RAPP, R.H. 1972. Geopotential Coefficient Behaviour to High Degree and Geoid Information by Wavelength. *Rep.* 180,Dept. of Geodetic Science,The Ohio State University,Columbus Ohio.

RAPP, R.H. 1973a. Numerical Results from the Combination of Gravimetric and Satellite Data using the Principles of Least-Squares Collocation. *Rep.* 200,Dept. of Geodetic Science,The Ohio State University,Columbus Ohio.

RAPP, R.H. 1973b. The Earth's Gravitational Field from the Combination of Satellite and Terrestrial Data. *Proc.Symposium on Earth's Gravitational Field & Secular Variations in Position*,51-75.

SCHWARZ, K.P. 1973. Even Zonal Harmonics from Satellite Observations by Collocation. *First International Symposium,The use of Artificial Satellites for Geodesy & Geodynamics*,Athens.

SHAW, L., PAUL, I & HENRIKSON, P. 1969. Statistical Models for the Vertical Deflection from Gravity Anomaly Models. *J.geophys.Res.* 74,4259-4265.

SOLTAU, G. 1970. Möglichkeiten zur kartographischen Darstellung des Schwerefeldes. *Veröffentlichungen des Deutschen Geodätischen Kommission B* 179.

SZABO, B. & ANTHONY, D. 1971. Results of AFCRL's ExperimentalAerial Gravity Measurements. *Bull.géodés.* 100,179-202.

TSCHERNING, C.C. 1970. *Geoid Determination by Collocation.* Meeting of Nordic Geodetic Commission, Helsinki.

TSCHERNING, C.C. 1971. *Collocation Methods in Harmonic Spaces.* Tagung Freie Randwertaufgaben, Bonn.

TSCHERNING, C.C 1972a. Representation of Covariance Functions Related to the Anomalous Potential of the Earth Using Reproducing Kernels. *Internal Rep.* 3,Danish Geodetic Institute, Copenhagen.

TSCHERNING, C.C. 1972b. On the Relation Between the Variation of the Degree Variances and the Variation of the Anomalous Potential. *V Symposium on Mathematical Geodesy*,Florence.

TSCHERNING, C.C. 1973. *Application of Collocation.* International Summer School in the Mountains, Ramsau Austria.

WIENER, N. 1930. Generalized Harmonic Analysis. *Acta math.* 55,117; (Reprint: MIT Paperback Series 51 1966).

7. Discussion

TAPLEY: I have a question related to the original model

$$\mathbf{x} = \mathbf{AX} + \mathbf{s} + \mathbf{n}.$$

In the presentation you assumed that the signal **S** was a random variable with zero mean at the observation point and with a non-zero mean elsewhere. You combined the s' as a zero mean plus **n**. Is this a type of phenomenon you would ordinarily encounter in geodesy; e.g., one which is zero at the observation point and non-zero elsewhere?

MORITZ: Well, it is not zero at the observation point and non-zero elsewhere. It's just the average over the whole Earth. For example, if **s** is the gravity anomaly, the integral or mean of the gravity anomaly over the whole Earth is zero, which is equivalent to there being no zero degree harmonic.

TAPLEY: This is not the point. You separate the signal into two parts which you denote as **s** at points other than the observation point, and **s'** at the observation point. You then combine **s'** with **n** and make the assumption that this combination (s'+n) has zero mean and known covariance. Then the expected value of this quantity is always assumed to be zero at the observation point.

MORITZ: Yes; at the observation point and everywhere else.

TAPLEY: However, you obtain an estimate for **s** in your final results. The estimate cannot be forced to be below s_P which corresponds to an estimate at the point.

MORITZ: Going back to the original report, one has $M\{n\} = 0$ and $M\{s\} = 0$. The **s** is the predicted value. It is the expected value taking into account the given measurements.

TAPLEY: Your estimate is your bias; then it cannot be forced to be zero elsewhere.

MORITZ: Let us consider the simplest case of the gravity anomaly. Let us say you have a measured value Δg, and you want to predict it another point. The average at any point will be zero. If one has no observations, then the best estimate is the value zero. But as soon as one has obtained some sample values, the best estimate will no longer be the value zero.

TAPLEY: Now if you go to another point and have a sample at another point, and if it is forced to be zero at one point, this implies that the results will be zero at any other collocated point.

MORITZ: No. The thing in mathematical terms is the expectation and the conditional expectation on the basis of one observed sample. Here the expected value of Δg is zero. The expectation of Δg at P on the assumption that Δg has been observed, is just the prediction formula. The difference between conditional expectation and ordinary expectation is the basic point.

TAPLEY: That requires a knowledge of the covariance matrix C_P. Getting a value for C_P is halfway to having the problem solved. Will any C_P satisfy the paper's assumption that you can always force the mean to zero?

MORITZ: It will not, because if we can compute a covariance function, then one knows the gravity field over the whole Earth and then one does not need statistics. But this is the case in statistical applications everywhere.

TAPLEY: One other question related to the observation relation applied to estimation. You know there will be observation errors $\Delta\omega$ or random errors in the covariances D. Why not go ahead and tackle the problem by estimating the unknown parameters directly with standard minimum variance, maximum likelihood or least squares algorithms?

MORITZ: If we use this approach, then the quantities J_2 and J_3 are considered as parameters and not as measured quantities. But I just want to consider them as random quantities in order to treat signal quantities and measurements on an equal statistical basis.

TAPLEY: But they are apparently considered as random quantities. When you write down the sigma, you treat your covariance matrix associated with your estimate of the observations as random observation noise.

MORITZ: But if you use this approach, one doesn't get any C matrix, only a D matrix.

TAPLEY: You get a D', not a C or an a priori estimate associated with the expected value as

equal to zero.

GRAFAREND: It was a question of having a case of truncating the series; and if you truncate, you have aliasing. The defect to the presented solution is that you have a biased solution. You avoid truncation, but you introduce bias.

TAPLEY: But with the observation relationships being non-linear .....

MORITZ: I think it is unbiased. It depends on what you understand by bias. Grafarend and I disagree on this.

KAULA: This problem is identical with what the seismologists call the inversion problem. They come into it from an entirely different direction because they have a highly under-determined situation. The question is how much of a continuum the data can resolve. Moritz' equation has been derived by JACKSON (*Geophys.J.R.astr.Soc.* 28,p.97, 1972) and by WIGGINS (*Revs.geophys.* 10,p.251,1972). With regard to the matrix C, there is quite a variety of diverse possibilities apart from a simple diagonal matrix, e.g., optimizing a certain function such as minimizing the temperature at the bottom in thermal convection. A powerful tool applicable here is singular value analysis: finding the diagonal roots and the pre- and post-multiplying unitary matrices, to give the relationships to these roots of the parameters on the one hand and the data on the other. This is an interesting technique which could be used in gravity field problems, particularly in analyzing radar altimetry of the oceans, where the parameters are not so obvious as in the case of satellite perturbation analysis for spherical harmonics.

SEEBER, G.
Geodetic Institute *
University of Bonn
Bonn
Federal Republic of Germany

Proc.Symposium on Earth's Gravitational Field & Secular Variations in Position (1973),454-462.

DATA EVALUATION BY COVARIANCE ANALYSIS, EXERCISED ON PHOTOGRAPHIC SATELLITE OBSERVATIONS

ABSTRACT

As an example of a multiparametric stochastic process of vector-type, some plates obtained with a high accuracy sidereal driven satellite camera are studied.

Subject of analysis is the set of residuals, obtained after reduction with different models. If beside the white noise there is any statistical information left, it produces correlations between the residuals, which can be described using different characteristical functions.

Quantitative tests show, that with simple models it is possible to extract the whole information out of the plates, so that a directional accuracy of a few tenths of arcseconds can be expected.

In connection with precise Laser distances such direction measurements can contribute to geodynamical studies.

1. Introduction

The increasing accuracy of laser distance measurements to satellites reaching the order of decimeters (PLOTKIN et al 1973) opens new possibilities for the study of geodynamic effects (DUNN et al 1973). One method for the determination of secular variations in the relative position of two or more points is the measuring of base-chord lengths (KOLACZEK & WILSON 1973) using simultaneous distance and direction observations to satellites. The advantage of this combined method is that only two stations are involved in observation at the same time. The simultaneous operation of four lasers, which would be necessary for the geometrical solution of pure distance-measurements (CAMPBELL et al 1973) has to cope with great difficulties.

The disadvantage of the combined method is seen in the limited accuracy obtainable for direction observations, which generally is assumed to be 1" (KOLACZEK & WILSON 1973). Regarding the formula for the propagation of errors (equation 1) for the base-chord length b, which corresponds to figure 1 it is evident that best results are obtained with γ as large as possible; a small angle γ will nullify the advantage of the high distance accuracy.

$$m_b^2 = \cos^2\alpha\, m_{s_1}^2 + \cos^2\beta\, m_{s_2}^2 + h_S^2 \frac{m_\gamma^2}{\rho^2} \qquad (1)$$

---

* *Now at: Institut für Theoretische Geodasie, Astronomische Station, Technische Universität Hannover, FRG*

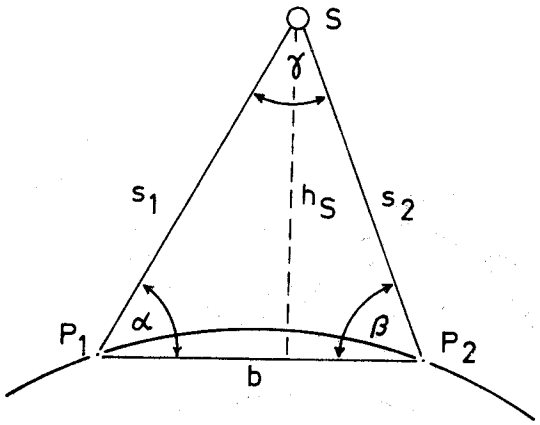

Figure 1. Determination of Base-Chord b with Simultaneous Range and Direction Observations to S

The method described could be much more powerful if it were possible to determine directions with an accuracy in the order of 0".1. The presented paper deals with the question whether such accuracy for camera observations is attainable and how it can be proved.

2. Review of theoretical foundations

In plate reduction we have to solve a transformation-and-interpolation-problem. Star positions in the star catalogue and on the photographic plate are considered as two fields of identical points which can be transformed into each other using a set of transformation parameters AX obtained in a least squares solution.

Using these parameters it is possible to transform the unknown information of the plate, i.e. the satellite positions, into equatorial directions. If the set of parameters AX - the functional model - is able to describe the whole transformation process, the residuals v after transformation contain only a pure random part n (white noise, resulting from the measuring errors). If the functional model is not sufficient, the residuals contain another part, the "signal term" s, hence

$$v = s + n$$

In general we can write according to figure 2

$$x = AX + s + n \qquad (2)$$

where x stands for the observations. Equation 2 is the general form of the collocation concept (MORITZ 1973).

The next step is the decide whether the "signal" term s exists, that means whether there is any information left in the set of residuals, *or* if the residuals contain only "white noise", which

would mean

$$v = n$$

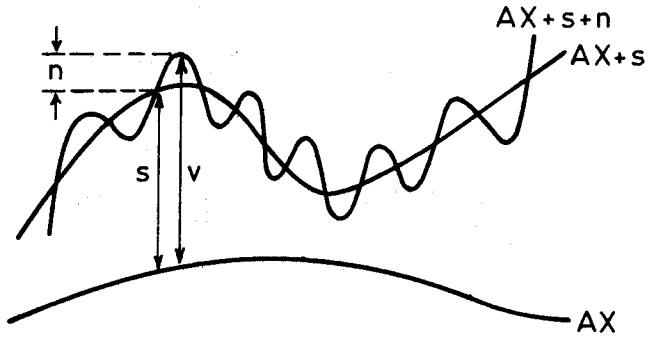

Figure 2. Concept of Collocation

If the term s exists, there are two possibilities to proceed:

a) the mathematical model AX can be supplemented with further parameters. (In plate reduction we have the important advantage that the basic concept of projection is known).

b) application of the collocation method using equation 2. In this case the unknown signal-term in the satellite point can be estimated - with respect to the signals of the surrounding star points - by means of least squares interpolation.

The answer on the question whether there are signals s left in the residuals or not can be given by estimating the two or more parametric correlation functions. These functions are also needed for the determination of the matrix C in the well known formula 3 for least squares interpolation (MORITZ 1973).

$$s_P = C_P^T C^{-1} v \qquad (3)$$

where P stands for the interpolated point.

In the case of plate reduction we find a stochastic process of vector-type in a two dimensional space (plate). The general form for the two-point-correlation-function of the residuals is

$$E\{\xi_i(\underline{r}_1)\xi_j(\underline{r}_2)\} = \Phi_{ij}(\underline{r}_1,\underline{r}_2) \qquad (4)$$

where $\underline{r}_1$, $\underline{r}_2$ describe the two points between which the correlations are to be determined and ξ_i, ξ_j are the components of the random variable $\underline{v}$, described in the coordinate system i, j (figure 3).

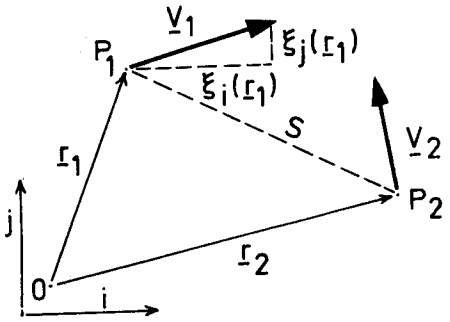

Figure 3. The Random Variable $\underline{v}$ (Residuals After Plate Reduction)

Practical work can be made much easier, if the stochastic process is, in a statistical sense, *homogeneous*, that means invariant against translation, and *isotropic*, that means invariant against rotation. In the homogeneous case equation 4 becomes

$$\Phi_{ij}(\underline{r}_1, \underline{r}_2) = \Phi_{ij}(\underline{r}_2 - \underline{r}_1) \qquad (5)$$

and in the isotropic case

$$\Phi_{ij}(\underline{r}_1, \underline{r}_2) = \Phi_{ij}(|\underline{r}_2 - \underline{r}_1|) = \Phi_{ij}(s) \qquad (6)$$

For more details see SEEBER (1972).

It can be shown that, in a statistical homogeneous and isotropic stochastic process, the two-point-correlation-functions of vector-type (2 dimensions) can be described by only two characteristical functions (OBUCHOW 1958). These functions have only one independent variable, the distance s between the two observation points, and are called "longitudinal" correlation function L(s) and "lateral" correlation function Q(s). They can be determined by dividing the residuals $\underline{v}$ in one component in the direction of s and another perpendicular to it (figure 4).

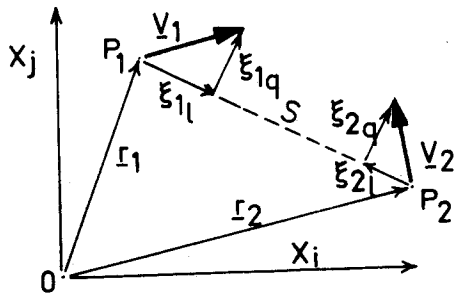

Figure 4. Components for L(s) and Q(s) in a Moving Coordinate System P_1P_2

Then we have

$$L(s) = E\{\xi_{1\ell}\xi_{2\ell}\} \qquad Q(s) = E\{\xi_{1q}\xi_{2q}\} \tag{7}$$

In this way $L(s)$ and $Q(s)$ are defined in a coordinate system which is moving with the observation points. In a fixed system $x_i x_j$ we find (SEEBER 1972), (OBUCHOW 1958), (GRAFAREND 1972)

$$\Phi_{ij}(\underline{r}_1,\underline{r}_2) = Q(s)\delta_{ij} + \frac{L(s)-Q(s)}{s^2} x_i x_j. \tag{8}$$

Equation 8 is named after the first investigators TAYLOR and KARMAN.

For correlation functions between three and more points the necessary number of such invariant distance functions increases considerably (IBID). These correlations functions are required for non-linear collocation problems, if the signal-level of the observation is very high (IBID).

For several problems, especially in plate reduction, it is better to refine the mathematical model AX in equation 2 until the linear formula 3 is sufficient and the correlation matrix C can be calculated by only two functions namely $L(s)$ and $Q(s)$. In addition these two functions enable us to see if there is any information left in the field of residuals after reduction.

3. Numerical Investigations

As observation material some plates were chosen, obtained with the new sidereal driven ballistic satellite camera BMK 46/18/1:4, 5 at the satellite station Bonn-Todenfeld (SEEBER 1972). This camera is equipped with a new type objective ASTRO-TOPAR of high geometrical accuracy. Distortion is smaller than 5 Micron.

Correlation analysis was done with the residuals after reduction using a 6-parameter-photogrammetric model. The set of residuals for one plate is shown in figure 5. The mean error of unit weight m_o for this plate was $\pm 2{,}6\mu m$.

The corresponding two-point-correlation functions $L(s)$ and $Q(s)$ are shown in figure 6. It is evident that no information is left in the residuals; hence the signal-term s is zero and only the noise-term n exists. Consequently any least squares estimation efforts are unnecessary in this case.

As a comparison, figure 7 shows residuals with a high content of information (neglected refraction correction) leading to strong correlations (figure 8). Furthermore it is evident that the field of residuals is neither homogeneous nor isotropic (figure 9). As a consequence the use of equations 2 and 3 requires a set of numerous functions $L(s)$ and $Q(s)$ for a single plate. Moreover, it cannot be expected that the linear method 3 is sufficient, therefore non-linear prediction methods with three, or more, point correlation functions have to be used.

A much simpler way is to use the physical knowledge about the whole process and correct the observations before the reduction. Doing that we obtain immediately "white noise" as is shown in figures 5

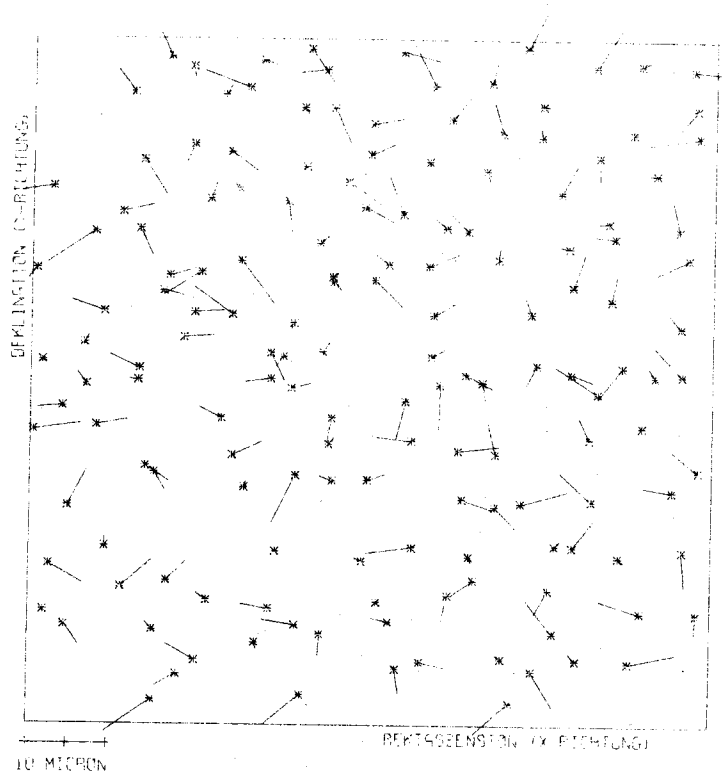

Figure 5. Residuals After Plate Reduction, 6 Parameters

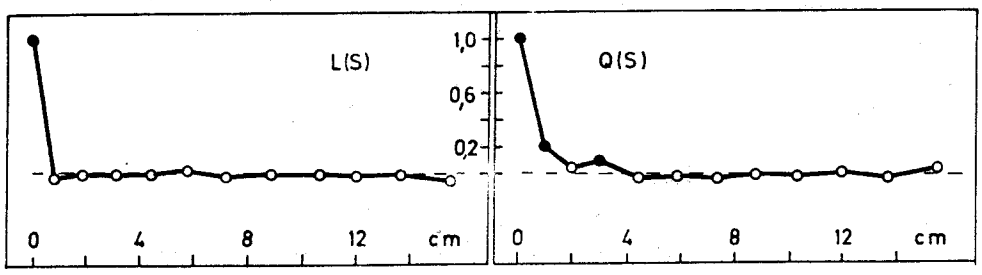

Figure 6. Longitudinal (left) and Lateral (right) Correlation Functions, Model with 6 Parameters

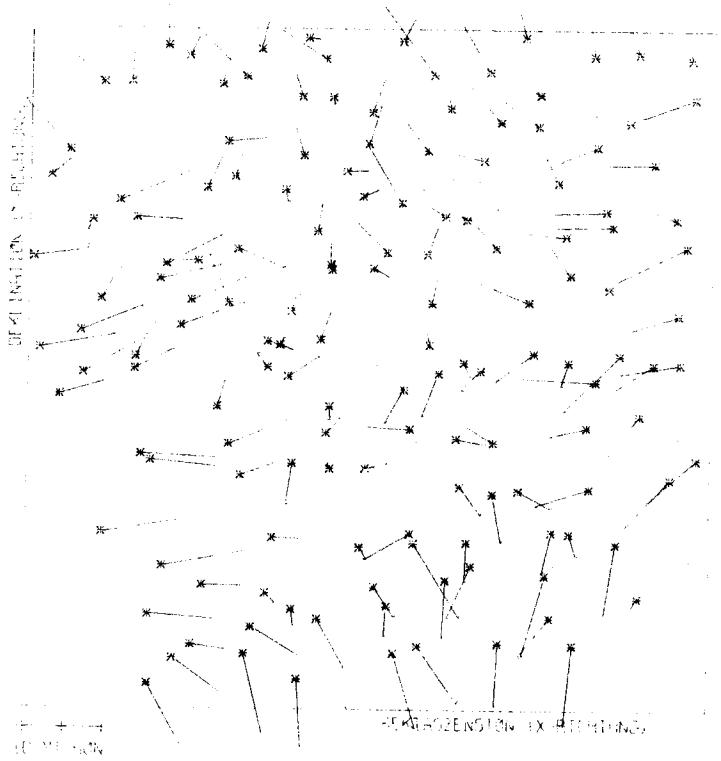

Figure 7. Residuals after Reduction with an Insufficient Model (Neglected Refraction Correction)

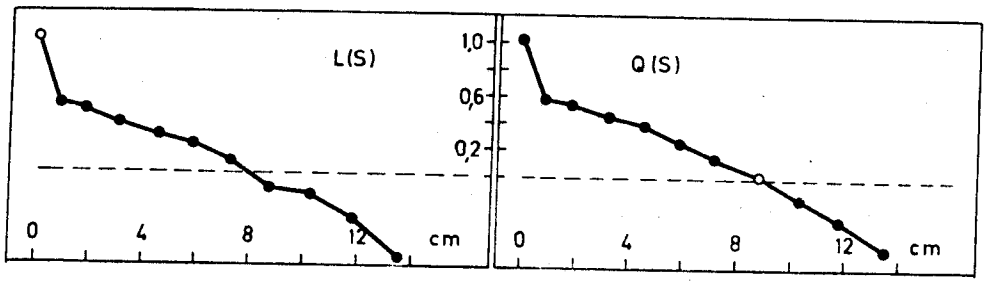

Figure 8. Longitudinal (L(s)) and Lateral (Q(s)) Correlation Functions for an Insufficient Model

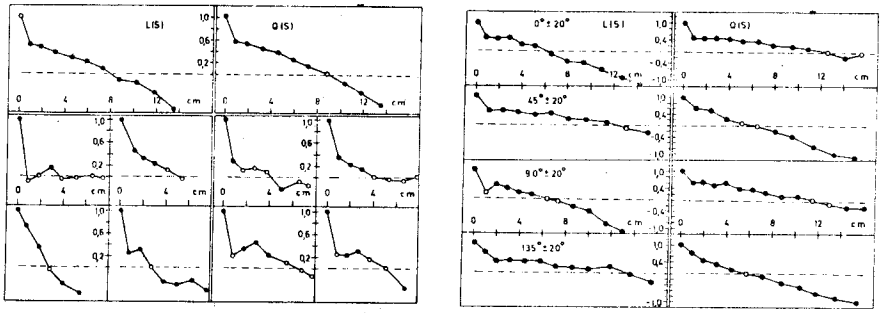

Figure 9. Test on Homogeneity (left, 4 Parts of a Plate) and Isotropy (right, 4 directional Classes)

and 6. This holds also for a simple astrometric interpolation model with 6 parameters, so that the use of simple models for the reduction of BMK-plates is sufficient if the physical knowledge about the projection process is applied.

As a consequence, the transformation error, resulting from a least squares solution, is very small. Figure 10 gives an impression of the transformation errors for the whole plate corresponding to a simple model (left) and a more sophisticated one (right).

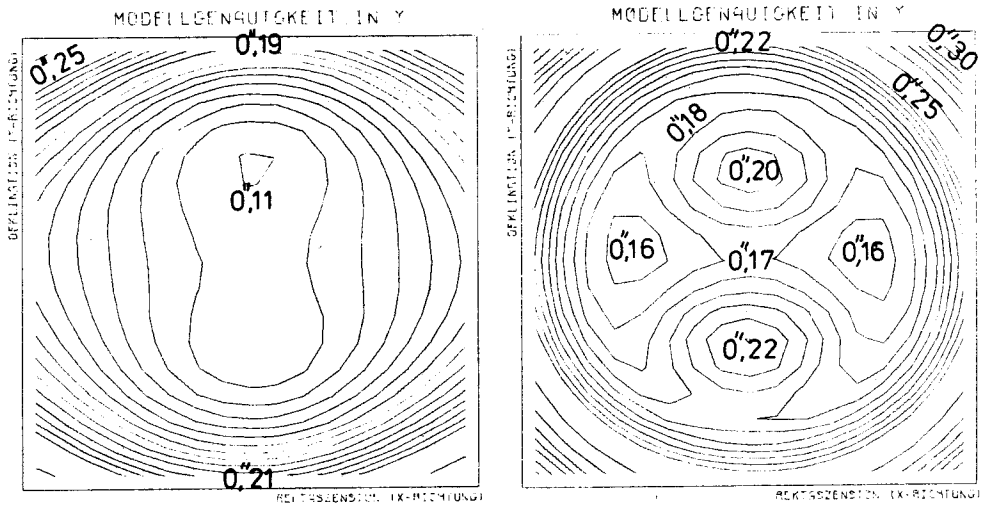

6 parameters 12 parameters

Figure 10. Mean Error of an Adjusted Fictitious Point all over the Plate for a Simple Model (left) and a More Sophisticated One (right)

Apart from the inconsistencies in the star catalogues amounting to several tenths of arcseconds, the directional accuracy of 0".1 may be regarded as realistic since all information has been pulled out of the residuals.

4. Conclusion

Data evaluation by covariance analysis is a powerful tool for testing the realistic accuracy obtainable in directional observations to satellites. Using a camera like the BMK such directions can be determined with an accuracy of a few tenths of arcseconds. In combination with laser distance measurements it is possible to contribute to the study of secular variations in position.

5. References

CAMPBELL, J., SEEBER, G. & WITTE, B. 1973. Kombination von Doppler-, Laser- und photographischen Beobachtungen in Satellitennetzen. *Deutsche Geodätische Kommission, Reihe B.* Heft Nr.200, München.

DUNN, P.J., KOLENKIEWICZ, R. & SMITH, D.E. 1973. Techniques for the Analysis of Geodynamic Effects using Laser Data. *First International Symposium on the Use of Artificial Satellites for Geodesy and Geodynamics.* Athens.

GRAFAREND, E. 1972. Nichtlineare Prädiktion. *Zeitschrift für Vermessungswesen*, 97, 245-255

KOLACZEK, B. & WILSON, P. 1973. On the Use of Base-Chord Lengths for the Investigation of Local Crustal Movements. *First International Symposium on the Use of Artificial Satellites for Geodesy and Geodynamics.* Athens.

MORITZ, H. 1973. Neuere Ausgleichungs- und Prädiktionsverfahren. *Zeitschrift für Vermessungswesen* 98, 137-146.

OBUCHOW, A.M. 1958. Statistische Beschreibung stetiger Felder. In, GOERING, H. *Sammelband zur statistischen Theorie der Turbulenz.* Berlin.

PLOTKIN, H.H., JOHNSON, Th.S. & MINOTT, P.O. 1973. Progress in Laser Ranging to Satellites: Achievements and Plans. *First International Symposium on the Use of Artificial Satellites for Geodesy and Geodynamics,* Athens.

SEEBER, G. 1972. Über das stochastische Verhalten von photographisch bestimmten Stern- und Satellitenkoordinaten. *Deutsche Geodätische Kommission*, Reihe C, Heft 178, München.

6. Discussion

GRAFAREND: Do you have an estimate of the confidence band of your correlation function for the isotropic case?

SEEBER: Yes, but they are small; of the order of 10%.

HAGIWARA, Y.
Earthquake Research Institute
University of Tokyo
Tokyo
Japan

Proc.Symposium on Earth's Gravitational Field & Secular Variations in Position (1973),463-474.

TRUNCATION ERROR ESTIMATE AND TRUNCATED GRAVITY ANOMALY

ABSTRACT

Stokes' integration of the gravity anomaly is extended over the whole surface of the Earth in determining geoidal height. If the integration is made over an area restricted to a spherical cap, a truncation error in geoidal heights results from neglecting the remaining regions. A truncation error is also defined in the Vening Meinesz integration for deflections of the vertical. COOK (1951) was the first to investigate truncation errors for geoidal height and deflection of the vertical. MOLODENSKII ET AL (1962) later derived truncation formulas by using a truncation coefficient Q_n.

The present paper is devoted to obtaining a mathematical relationship between the Molodenskii coefficient Q_n and Cook's truncation function q_n by means of the "truncated gravity anomaly". Maps of the world-wide distribution of truncation errors are also presented.

The truncation procedure produces low-order terms of spherical harmonics. This implies that a truncated gravity anomaly is caused by an anomalous density distribution which is different from that of the "real" Earth. The centre of a geoid calculated from the truncated gravity anomaly may not coincide with one of the "real" geoid. In other words, the truncation procedure apparently removes or shifts a part of the Earth's masses. In the present paper, the 0-th and 1-st order terms that result from the truncation of the satellite gravity anomaly are estimated as a few mgal.

1. Introduction

Gravimetric geoidal height and deflection of the vertical are obtained at a point P on the Earth's surface by the Stokes and Vening Meinesz integrations, respectively, which are extended over the whole surface of the Earth. The Stokes and Vening Meinesz functions converge into zero with spherical distance from the point P, so that it may be natural to think that we can approximately calculate the geoidal height and deflection of the vertical by respectively integration the Stokes and Vening Meinesz functions over an area restricted to a spherical cap around P. The convergence of the above-mentioned functions however, is so slow that the effects of neglecting the remote zones on the integrations are not small. Such an effect is called "truncation error" by DE WITTE (1967).

The truncation error was first investigated by COOK (1951), who published tables of truncation errors for the geoidal height up to a truncation angle 30°, and for the deflection of the vertical up to 18°. Probably not aware of Cook's work, MOLODENSKII ET AL (1962) later derived truncation error formulas by using the truncation coefficient Q_n, which is called the "Molodenskii coefficient" by DE WITTE (1967). The primary motivation of Molodenskii et al. was not to obtain the truncation errors but functions of rapid convergence instead of the Stokes and Vening Meinesz functions.

HIRVONEN & MORITZ (1963) discussed the truncation errors by using Molodenskii coefficients Q_n, and a similar discussion appears in the famous textbook "Physical Geodesy" authored by HEISKANEN & MORITZ (1967). However, in their papers, there is no description of Cook's work and the truncation error formula for the Vening Meinesz integration derived by Molodenskii et al. The truncation error

formulas for the Vening Meinesz integration introduced in these papers are equal to neither Cook's nor Molodenskii's.

DE WITTE (1967) pointed out that Cook's method is valid for the treatment of Vening Meinesz truncation errors. In order to distinguish Cook's truncation coefficient from the Molodenskii coefficient Q_n, de Witte defined q_n anew, which he called the "Vening Meinesz kernel function", and "Cook's truncation function" by MATHER (1970). HAGIWARA (1972) obtained a mathematical relation between Q_n and q_n, showing that Cook's truncation formula for the Vening Meinesz integration is essentially identified with the one derived by Molodenskii et al.

DE WITTE (1967) obtained a table of Molodenskii coefficients Q_n up to order $n = 25$, actually estimating the truncation errors for the geoidal height and deflection of the vertical at Meade's Ranch, the North American Geodetic Datum Station, by applying Q_n to the satellite gravity anomaly obtained by GUIER (1965), and concluding that the truncation errors are not negligibly small.

It may be possible to obtain the gravimetric geoid by means of numerical calculation of the Stokes integral of terrestrial gravity anomalies extending up to a spherical distance, together with truncation error considerations based on satellite gravimetry. However, such a treatment brings forward a fundamental problem which needs to be solved. It corresponds to the difference between the shape of an ellipsoid on which the terrestrial gravimetry is based, and that of a satellite determined ellipsoid. The centre of the former ellipsoid may not coincide with that of the latter.

Such a non-coincidence of position also generates errors in the geoidal estimation in combining terrestrial gravity anomalies with satellite ones. Although the positional relation is absolutely impossible to be solved from the gravimetry only, this kind of problem still remains to be considered further in physical geodesy. MATHER (1970) discussed the zero-order term of geopotential on truncation errors as caused by the difference between the shapes of the ellipsoids. From the other point of view, the author also discusses the associated problem in the present paper, defining the "truncated gravity anomaly" in a fashion similar to the Molodenskii treatment in the truncated Stokes function.

2. Molodenskii Truncation

The geoidal height is obtained by calculating the Stokes integration on extension over the whole surface of the Earth. Letting α and ψ be the azimuth and angular distance respectively, the geoidal height is

$$N = \frac{R}{4\pi G} \int_0^{2\pi} d\alpha \int_0^{\pi} \Delta g \, S(\cos \psi) \sin \psi \, d\psi \qquad (1),$$

where R is the mean radius of the Earth, G is the mean gravity over the Earth's surface, Δg the gravity anomaly and S is Stokes' function, given by a series of Legendre polynomials as follows:

$$S(\cos \psi) = \sum_{n=2}^{\infty} \frac{2n + 1}{n - 1} P_n(\cos \psi) \qquad (2).$$

When the integration with respect to ψ is extended only upto an angular distance ψ_o, the effect of

neglecting distant regions beyond ψ_o on the integration, which was called "truncation error" by DE WITTE (1967), is

$$\Delta N = \frac{R}{4\pi G} \int_0^{2\pi} d\alpha \int_0^{\pi} \Delta g \, S(\cos \psi) \sin \psi \, d\psi \qquad (3).$$

Introducing a truncation function

$$\bar{S}(\cos \psi) = \begin{cases} 0 & \text{for } 0 \leq \psi < \psi_o \\ S(\cos \psi) & \text{for } \psi_o \leq \psi \leq \pi \end{cases} \qquad (4),$$

equation 3 can be re-written as

$$\Delta N = \frac{R}{4\pi G} \int_0^{2\pi} d\alpha \int_{\psi_o}^{\pi} \Delta g \, \bar{S}(\cos \psi) \sin \psi \, d\psi \qquad (5).$$

We then expand $\bar{S}(\cos \psi)$ in a series of Legendre polynomials in the form

$$\bar{S}(\cos \psi) = \sum_{n=0}^{\infty} \frac{2n+1}{2} Q_n P_n(\cos \psi) \qquad (6),$$

where Q_n, which was called the "Molodenskii coefficient" by de Witte (IBID), was originally tabulated by MOLODENSKII ET AL (1962). On substituting equation 6 in equation 5, we get

$$\Delta N = \frac{R}{2G} \sum_{n=2}^{\infty} Q_n \, \Delta g_n \qquad (7),$$

where Δg_n is the n-th order spherical harmonic of Δg.

3. Truncated Gravity Anomaly

It is convenient for treatments of the truncation of Stokes' integral to define a "truncated Legendre function" given by

$$R_n^m(\cos \psi) = \begin{cases} 0 & \text{for } 0 \leq \psi < \psi_o \\ P_n^m(\cos \psi) & \text{for } \psi_o \leq \psi \leq \pi \end{cases} \qquad (8).$$

If the above function is expanded in a spherical harmonic series, we have

$$R_n^m(\cos \psi) = \sum_{k=m}^{\infty} \frac{2k+1}{2} \frac{(k-m)!}{(k+m)!} R_{nk}^m P_k^m(\cos \psi) \qquad (9).$$

The coefficient R_{nk}^m is determined by the orthogonality condition of Legendre polynomials, so that

$$R^m_{nk} = \int_{\psi_o}^{\pi} P^m_n(\cos\psi)\, P^m_k(\cos\psi)\, \sin\psi\, d\psi \tag{10}.$$

Now, suppose the case of $m = 0$ in equation 10. For brevity, replacing R^0_{nk} by R_{nk}, and putting $\mu_o = \cos\psi_o$, we obtain

$$R_{nk} = \int_{\psi_o}^{\pi} P_n(\cos\psi)\, P_k(\cos\psi)\, \sin\psi\, d\psi$$

$$= \begin{cases} \frac{1}{2n+1}\left\{1 + \mu_o\left(P_n(\mu_o)\right)^2 + 2\sum_{m=1}^{n-1} P_m(\mu_o)\left(\mu_o P_m(\mu_o) - P_{m+1}(\mu_o)\right)\right\} & \text{for } n=k \\ \frac{1}{(n-k)(n+k+1)}\left\{kP_n(\mu_o)\left(P_{k-1}(\mu_o) - \mu_o P_k(\mu_o)\right) - nP_k(\mu_o)\left(P_{n-1}(\mu_o) - \mu_o P_n(\mu_o)\right)\right\} & \text{for } n\neq k \end{cases} \tag{11}.$$

Especially

$$R_{00} = 1 + \mu_o \quad ; \qquad \text{and} \qquad R_{11} = (1 + \mu_o^3)/3 \tag{12}.$$

Applying equation 2 to equation 11, we obtain

$$\int_0^{\pi} R_n(\cos\psi)\, S(\cos\psi)\, \sin\psi\, d\psi = \sum_{k=2}^{\infty} \frac{2k+1}{k-1} R_{nk} \tag{13}.$$

Furthermore, supposing $m = 1$, equation 10 becomes

$$R^1_{nk} = \int_{\psi_o}^{\pi} P^1_n(\cos\psi)\, P^1_k(\cos\psi)\, \sin\psi\, d\psi$$

$$= n(n+1)\, R_{nk} + P^1_n(\cos\psi_o)\, P_k(\cos\psi_o)\, \sin\psi_o \tag{14}.$$

The global distribution of the gravity anomaly is usually expressed by spherical harmonics as

$$\Delta g = G \sum_{n=2}^{\infty} (n-1) \sum_{m=0}^{n} \left(C_{nm}\cos m\alpha + S_{nm}\sin m\alpha\right) P^m_n(\cos\psi) \tag{15}.$$

If a "truncated gravity anomaly" is defined in a fashion similar to 4 by

$$\overline{\Delta g} = \begin{cases} 0 & \text{for} \quad 0 \leq \psi < \psi_o \\ \Delta g & \text{for} \quad \psi_o \leq \psi \leq \pi \end{cases} \tag{16},$$

equation 16 can be expressed as

$$\overline{\Delta g} = G \sum_{n=2}^{\infty} (n-1) \sum_{m=0}^{n} \left(C_{nm}\cos m\alpha + S_{nm}\sin m\alpha\right) R^m_n(\cos\psi) \tag{17}.$$

This is a spherical harmonic expression of the truncated gravity anomaly, where attention should be paid to the fact that the Legendre function in equation 15 has been replaced by the truncated

Legendre function in equation 17.

The truncation of the geoidal height can readily be treated by using the truncated gravity anomaly. Instead of equation 5, the truncation error of the geoidal height is given by

$$\Delta N = \frac{R}{4\pi G} \int_0^{2\pi} d\alpha \int_0^{\pi} \overline{\Delta g}\, S(\cos\psi) \sin\psi\, d\psi \qquad (18).$$

Substitution of equations 2 and 17 into equation 18 gives

$$\Delta N = \frac{R}{2G} \sum_{n=2}^{\infty} \Delta g_n \sum_{k=2}^{\infty} \frac{2k+1}{k-1} R_{nk} \qquad (19).$$

On comparing equation 19 with equation 7, we obtain the Molodenskii coefficient as a series in R_{nk}:

$$Q_n = \sum_{k=2}^{\infty} \frac{2k+1}{k-1} R_{nk} \qquad (20).$$

By the way, Q_n is also obtained directly from the relation 13.

4. Truncation of the Vening Meinesz Integral

In a fashion similar to the truncation of the geoidal height in the Stokes integration, the truncation error of the Vening Meinesz integration is defined as

$$\begin{pmatrix} \Delta\xi \\ \Delta\eta \end{pmatrix} = \frac{1}{4\pi G} \int_0^{2\pi} \begin{Bmatrix} \cos\alpha \\ \sin\alpha \end{Bmatrix} d\alpha \int_{\psi_o}^{\pi} \Delta g \frac{dS}{d\psi} \sin\psi\, d\psi \qquad (21).$$

If we rewrite the above by using the truncated gravity anomaly, we have

$$\begin{pmatrix} \Delta\xi \\ \Delta\eta \end{pmatrix} = \frac{1}{4\pi G} \int_0^{2\pi} \begin{bmatrix} \cos\alpha \\ \sin\alpha \end{bmatrix} d\alpha \int_{\psi_o}^{\pi} \overline{\Delta g} \frac{dS}{d\psi} \sin\psi\, d\psi \qquad (22).$$

Differentiating both sides of equation 2 with respect to latitude ϕ and longitude λ, and taking the following relations into account,

$$\left.\begin{aligned} \frac{\partial P_n(\cos\psi)}{\partial\phi} &= \frac{dP_n(\cos\psi)}{d\psi} \frac{\partial\psi}{\partial\phi} = P_n^1(\cos\psi)\cos\alpha \\ \frac{\partial P_n(\cos\psi)}{\partial\phi} &= \frac{dP_n(\cos\psi)}{d\psi} \frac{\partial\psi}{\partial\lambda} = P_n^1(\cos\psi)\sin\alpha\cos\phi \end{aligned}\right\} \qquad (23),$$

and

$$\int_0^{\pi} R_n^1(\cos\psi) \frac{dS}{d\psi} \sin\psi\, d\psi = -\sum_{k=2}^{\infty} \frac{2k+1}{k-1} R_{nk}^1 \qquad (24),$$

we obtain

$$\begin{pmatrix} \Delta\xi \\ \Delta\eta \end{pmatrix} = -\frac{1}{2G} \sum_{n=2}^{\infty} \frac{1}{n(n+1)} \begin{pmatrix} \partial\Delta g_n/\partial\phi \\ \partial\Delta g_n/(\cos\phi\ \partial\lambda) \end{pmatrix} \sum_{n=2}^{\infty} \frac{2k+1}{k-1} R^1_{nk} \tag{25}.$$

Similarly to equation 7, we assume the following formula by using a newly defined coefficient Q^*_n:

$$\begin{pmatrix} \Delta\xi \\ \Delta\eta \end{pmatrix} = -\frac{1}{2G} \sum_{n=2}^{\infty} Q^*_n \begin{pmatrix} \partial\Delta g_n/\partial\phi \\ \partial\Delta g_n/(\cos\phi\ \partial\lambda) \end{pmatrix} \tag{26}.$$

Comparing the above with equation 25, we prove

$$Q^*_n = \frac{1}{n(n+1)} \sum_{n=2}^{\infty} \frac{2k+1}{k-1} R^1_{nk} \tag{27}.$$

Cook's truncation function q_n is similarly given by

$$q_n = -\frac{1}{2} \sum_{k=2}^{\infty} \frac{2k+1}{k-1} R^1_{nk} \tag{28}.$$

Taking equations 14 and 20 into account, Q^*_n can be expressed as

$$Q^*_n = Q_n + \frac{1}{n(n+1)} S(\cos\psi_o)\, P^1_n(\cos\psi_o) \sin\psi_o \tag{29}.$$

A table of Q^*_n was presented by HAGIWARA (1972). Figure 1 shows low-order terms of Q_n and Q^*_n.

Similarly we obtain the relation between Q_n and q_n as

$$q_n = -\frac{n(n+1)}{2} Q_n - \frac{1}{2} S(\cos\psi_o)\, P^1_n(\cos\psi_o) \sin\psi_o \tag{30}.$$

Figure 2a shows the truncation error in the Stokes integration in the case of $\psi_o = 20^o$, using spherical harmonic coefficients given by GAPOSCHKIN & LAMBECK (1970). It is noticed in the figure that the error of the geoidal heights amounts to ±30 m or so. The truncation error of the meridian deflection of the vertical amounting to 3.0 sec or so arranges zonally as shown in figure 2b; on the contrary, that of the prime vertical deflection indicates a sectorial distribution (see figure 2c)

5. Zero and First Order Terms Caused by Truncation

The gravity anomalies are caused by subterranean distribution of anomalous masses. When we define a truncated gravity anomaly, we must bear in mind that such a gravity anomaly corresponds to a mass distribution which may be different from that of the real Earth. The truncation procedure apparently removes or shifts a part of the Earth's masses. The geoidal height is based on the assumption that the spherical functions of zero and first order terms of the disturbing potential are equal to zero.

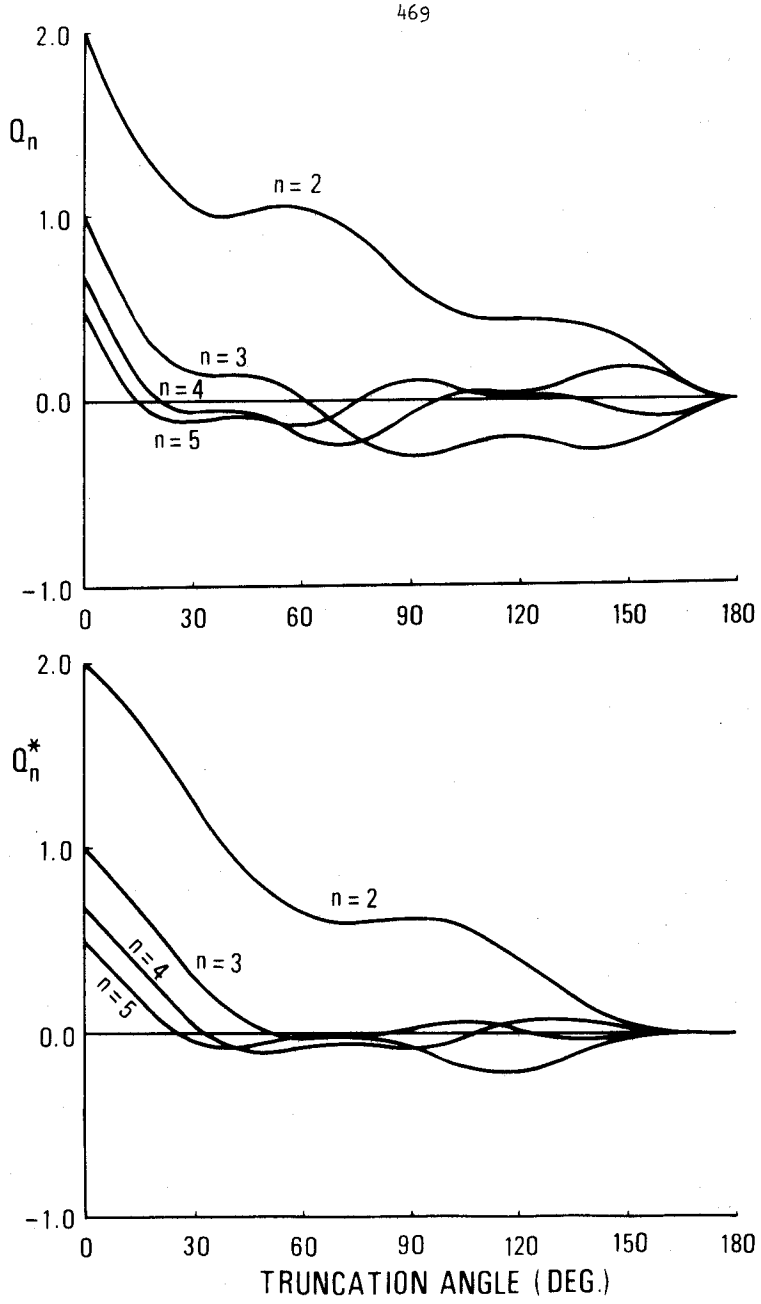

Figure 1. Q_n and Q_n^*

The assumption of the zero-order term implies that the global mean of the gravity anomaly is adopted as zero, and that of the first order terms is equivalent to setting the centre of the reference ellipsoid at the centre of the Earth's mass. If the centre of a geoid calculated from the truncated gravity anomaly does not coincide with that of the real geoid, the problem of the forbidden terms may come up.

We assume that the truncated gravity anomaly is expressed in the form

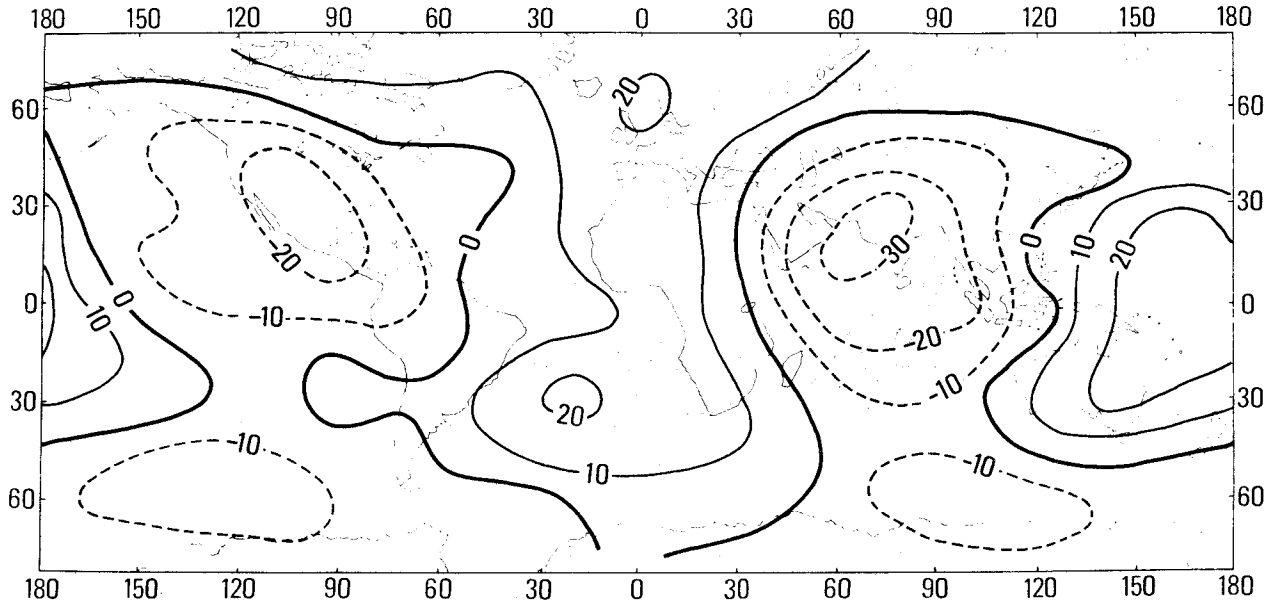

Figure 2a. Truncation Error Distribution for the Geoidal Height (Metres)

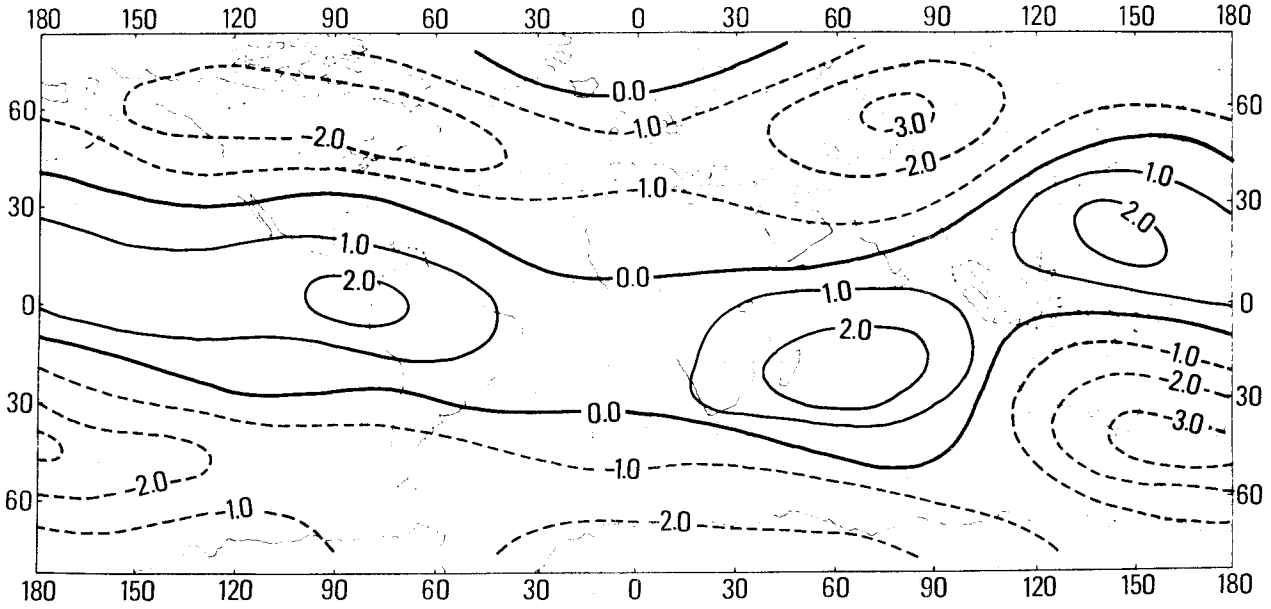

Figure 2b. Truncation Error Distribution for the meridian Deflection of the Vertical (sec.)

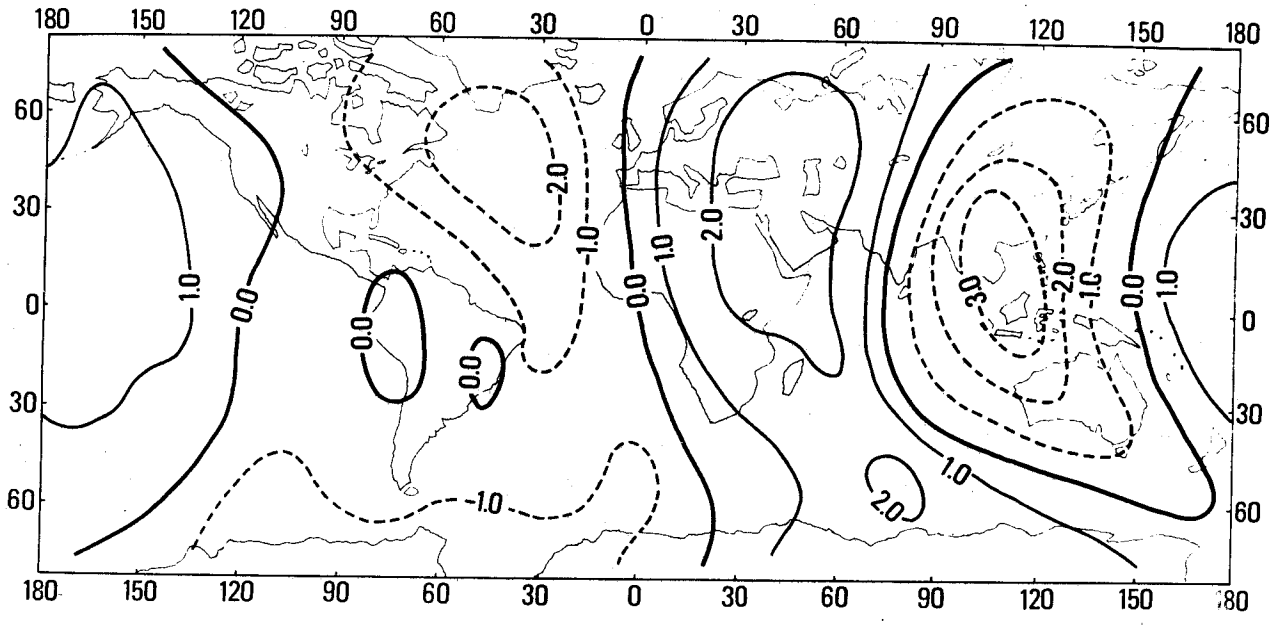

Figure 2c. Truncation Error Distribution for the Prime-Vertical Deflection of the Vertical (sec.)

$$\overline{\Delta g} = G \sum_{n=0}^{\infty} \sum_{m=0}^{n} \left(A_{nm} \cos m\alpha + B_{nm} \sin m\alpha\right) P_n^m(\cos \psi) \qquad (31).$$

In this case, attention is required to ensure that the series includes zero and first order terms. If there is no change in the masses due to the truncation procedure, these terms become zero, and

$$A_{nm} = (n-1)\, C_{nm} \qquad \text{and} \qquad B_{nm} = (n-1)\, S_{nm} \qquad \text{for} \quad n \geq 2.$$

From equations 17 and 31, together with the orthogonality condition of spherical harmonics, the following relations are derived.

$$A_{00} = \frac{1}{2G} \sum_{n=2}^{\infty} R_{n0}\ \Delta g_n \quad ; \quad A_{10} = \frac{3}{2G} \sum_{n=2}^{\infty} R_{n1}\ \Delta g_n$$

and

$$\begin{pmatrix} A_{11} \\ B_{11} \end{pmatrix} = \frac{3}{2G} \sum_{n=2}^{\infty} \frac{R^1_{n1}}{n(n+1)} \begin{pmatrix} \partial \Delta g_n / \partial \phi \\ \partial \Delta g_n / (\cos \phi\ \partial \lambda) \end{pmatrix} \qquad (32),$$

where A_{00}, A_{10}, A_{11} and B_{11} are functions of ϕ and λ.

Figures 3a to 3d show the global distributions of these terms, i.e., $A_{00}G$, $A_{10}G$, $A_{11}G$ and $B_{11}G$ in mgal

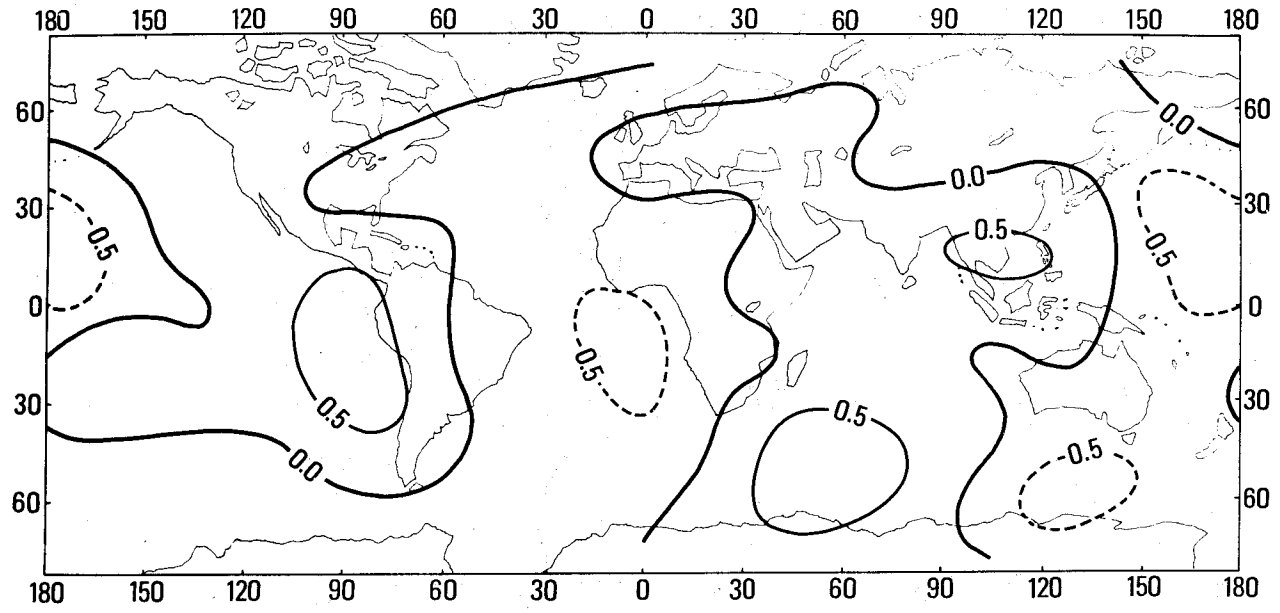

Figure 3a. Global Distribution of $A_{00}G$ (mgal)

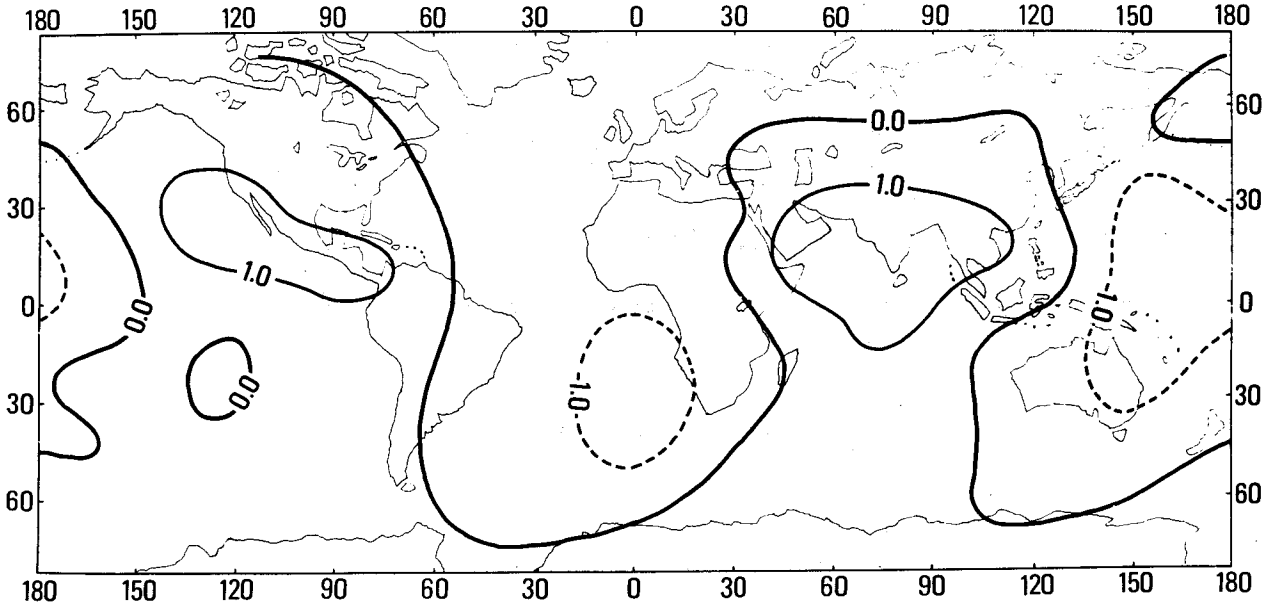

Figure 3b. Global Distribution of $A_{10}G$ (mgal)

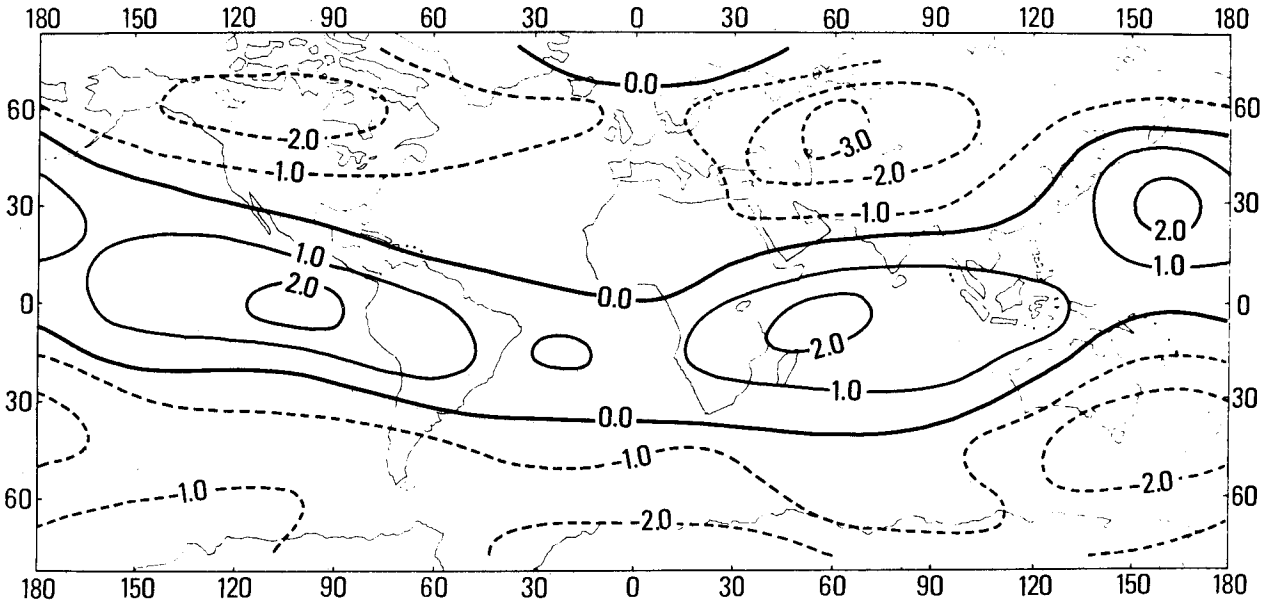

Figure 3c. Global Distribution of $A_{11}G$ (mgal)

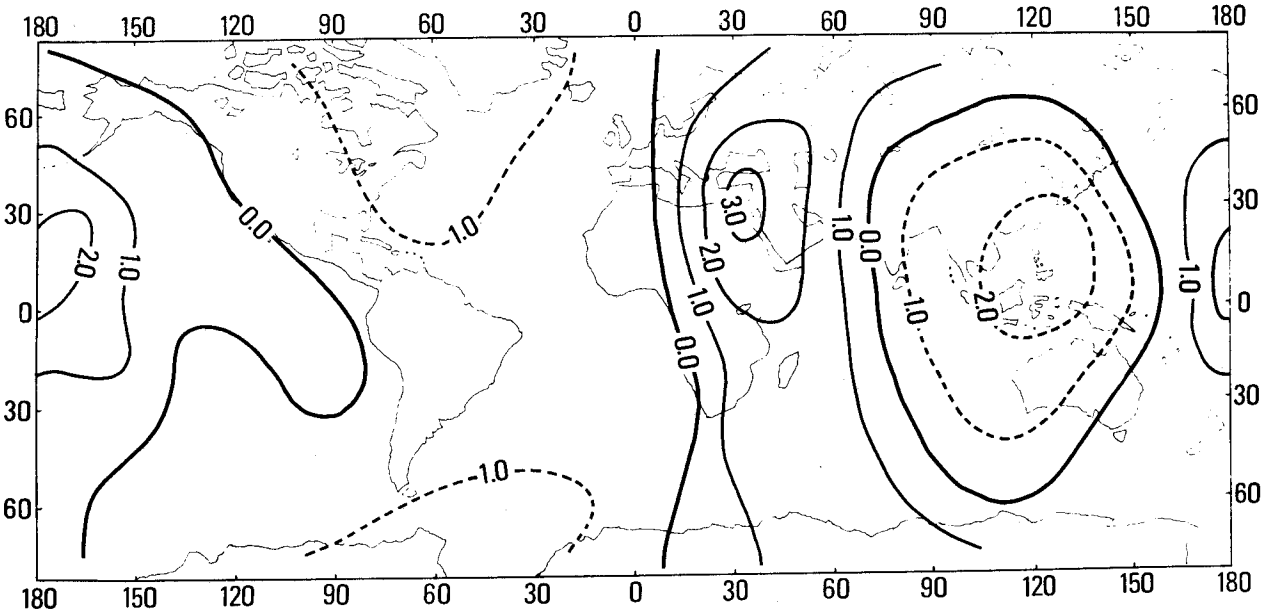

Figure 3d. Global Distribution of $B_{11}G$ (mgal)

for the case of $\psi_o = 20^o$, respectively, which are computed by using the coefficients given by GAPOSCHKIN & LAMBECK (1970). We see in the figures that $A_{00}G$ and $A_{10}G$ take small values below ±1 mgal, but $A_{11}G$ and $B_{11}G$ amount to ±3 mgal or so. The pattern of $A_{10}G$ resembles that of the truncation error of the geoidal height shown in figure 2a. $A_{11}G$ and $B_{11}G$ represent zonal and sectorial effects like the truncation errors in the meridian and prime vertical deflections of the vertical as seen in figures 2b and 2c respectively.

Although the determinations of these zero and first order terms are made, the problem of whether the centre of the reference ellipsoid coincides with that of the Earth's mass or not, still remains, because it is absolutely impossible to solve such an uncertainty from gravity data only. It should be emphasized however, that these zero and first order terms may correspond to the mass removal caused by the truncation procedure. Consideration of the truncation effect of zero and first order terms may be necessary when estimating a geoidal height and a deflection of the vertical from the terrestrial gravity anomaly distribution over an area within an angular distance of ψ_o, together with the satellite gravity anomalies over the remaining regions of the Earth's surface.

6. Acknowledgments

The author would like to express his cordial gratitude to Professor R. Mather of the University of New South Wales for reading the paper on his behalf at the Symposium.

7. References

COOK, A.H. 1951. A Note on the Errors Involved in the Calculation of Elevations of the Geoid. *Proc. R.Soc. A* 208,133-141.

DE WITTE, L. 1967. Truncation Errors in the Stokes and Vening Meinesz Formulae for Different Order Spherical Harmonic Gravity Terms. *Geophys.J.R.astr.Soc.* 12,449-464.

GAPOSCHKIN, E.M. & LAMBECK, K. 1969. 1969 Smithsonian Standard Earth II. *Smithsonian astrophys.Obs. Spec.Rep.* 315,Cambridge Mass.

GUIER, W.H. 1965. Recent Progress in Satellite Geodesy. *Proc.Sixth Winter Convention on Military Electronics* III B,42-46.

HAGIWARA, Y. 1972. Truncation Error Formulas for the Geoidal Height and the Deflection of the Vertical. *Bull.geodes.* 106,453-466.

HEISKANEN, W.A. & MORITZ, H. 1967. *Physical Geodesy.* Freeman,San Fransisco.

HIRVONEN, R.A. & MORITZ, H. 1963. Practical Computation of Gravity at High Altitude. *Rep.*27, Institute of Geodesy, Photogrammetry & Cartography,The Ohio State University,Columbus Ohio.

MATHER, R.S. 1970. The Geocentric Orientation Vector for the Australian Geodetic Datum. *Geophys.J. R.astr.Soc.* 22,55-81.

MOLODENSKII, M.S., EREMEEV, V.F. & YURKINA, M.I. 1962. *Methods for the Study of the External Gravitational Field and Figure of the Earth.* Israel Program for Scientific Translations, Jerusalem.

BJERHAMMAR, A.
Kungl. Tekniska Hogskolan
Institutionen for Geodesi
S-100 44 Stockholm 70
Sweden

Proc. Symposium on Earth's Gravitational Field & Secular Variations in Position (1973), 475-488.

ON THE DISCRETE BOUNDARY VALUE PROBLEM

ABSTRACT

The author made in (1963) and (1964) a re-definition of the principal problem of physical geodesy. The solution of this problem gives all quantities needed in modern geodesy as disturbance potentials, geoidal heights, vertical deflection and predicted values of the gravity anomaly. The solutions are valid for points in space and at the surface of the Earth. Various numerical solutions of this problem have been presented and this paper gives a summary of the present situation with references to the work of PICK (1965), FORSTNER (1966), MORITZ (1964), (1970), (1972), (1972a), REIT (1967), BJERHAMMAR (1968b), (1969), HOTINE (1969), KRARUP (1969), GROTEN (1970), BARLIK (1970) and HEIT & TSCHERNING (1971).

1. Formulation of the Problem

In classical geodesy, the principal problem was considered as one where gravity was given all over the physical surface of the Earth. This continuous approach was first treated in a more general way by MOLODENSKY (1948) and the general problem is normally called the problem of Molodensky.

For most geodetic applications we only know gravity at discrete points and the boundary value problem was later defined in the following way:

> A finite number of gravity data is given for a non-spherical surface, and it is required to find such a solution that the boundary values for the gravity data are satisfied in all given points (BJERHAMMAR 1963; BJERHAMMAR 1964). (*Collocation* in the classical mathematical sense).

2. Solution

An internal sphere was introduced for the solution of the previous problem. All boundary values of the physical surface were reduced down to this internal sphere using an integral equation for harmonic functions. See BJERHAMMAR (1963; 1968b), REIT (1967), KRARUP (1969), MORITZ (1970), TSCHERNING (1971) and LAURITZEN (1973).

This new approach was first received with considerable scepticism. For example PICK (1965) questioned the general stability of the solution. J.J. Levallois also expressed his opinion that he disagrees with the general approach and he has also given a "proof" for the impossibility of downward continuation. MORITZ (1964) was the first scientist who gave the new procedure full support and the author is grateful for many valuable discussions concerning this subject. MORITZ (1970) writes :

> "Solution of the Bjerhammar's Problem
>
> Let the gravity anomalies Δg_1, Δg_2 ..... Δg_n at n points on the Earth's surface, at elevations h_1, h_2, ... h_n, be known from observations; to determine a gravity field consistent with these observations.
>
> This formulation of the main problem of gravimetric geodesy, due to Bjerhammar is indeed more realistic than the usual formulation in terms of a boundary-value problem, since we observe at discrete points only. The solution of

> this problem is not unique. It may therefore be restricted by the additional requirement that the computed gravity field be as smooth as possible. This requirement makes sense because then there will be no spurious irregularities that do not correspond to reality.
>
> In a way, the non-uniqueness of the solution of Bjerhammar's problem corresponds to the non-uniqueness of the problem of interpolation. Thus we may expect that optimum interpolation - in the sense of least standard error, will correspond to an optimum solution of Bjerhammar's problem - in the sense of an optimally smooth gravity field. The remark at the end of section 3 indicates the possibility for such a correspondence to exist, and the solution to be described now will bear this out.
>
> In the solution we shall use another idea of Bjerhammar, analytical continuation of the free air anomaly Δg down to sea level. For the usual case, that the measured gravity anomalies are assumed to be known at every point of the Earth's surface, this method has been described in (HEISKANEN & MORITZ 1967,section 8-10)"

HOTINE (1969) made a detailed presentation of the method and also gave his support for the new technique. In these new early descriptions of the method, there was always included a direct computation of the reduced gravity anomaly Δg^* at the internal sphere. The numerical presentation of the reduced Δg was given with the use of power series or grids having constant gravity inside each surface element. In order to test the validity of the method, several test models were analyzed. A numerical model with several thousand tons of mass in one single point outside the internal sphere was properly evaluated without any serious difficulties (BJERHAMMAR 1969). The accuracy of the solution was improved with increasing power of the applied polynomial giving a bias smaller than the rounding errors. For this giant mass concentration in one single point outside the sphere, all vertical deflections had errors less than 0".3. The study showed that the final results improved considerably when adding a correction for residuals at the observation points, using the classical formulas for the computation of the vertical deflections. In practical application we can consider all external mass to be located in a very large number of points with, for example, one million times smaller mass. For each such point, we can make a corresponding gravity reduction and the residual errors will be less than 1 part in 10^6 for each point. The individual errors will be positive as well as negative and the total error will have a tendency to cancel. It can easily be proved that the errors cancel exactly when the external mass can be "focused" into points below the sphere.

KRARUP (1969) was the first mathematician who studied this technique in a more advanced way and he stated (IBID,p.9)

> "As far as I can see, the most important point of view introduced in physical geodesy since the appearance of Molodensky's famous articles, is Bjerhammar's idea of calculating an approximation of the potential by collocation, at the points where gravity anomalies have been measured, of potentials that are regular down to a certain sphere inside the surface of the Earth.
>
> From the classical theory this idea looks very venturesome, because we know that the actual potential of the Earth is not regular down to the Bjerhammar sphere. Nor does the evidence Bjerhammar produces in support of his idea seem convincing to me at all. As we shall see later on from the point of view of the new potential theory, very much can be said in favour of the determination of the potential by interpolation methods as well as the use of potentials that are regular outside the Bjerhammar sphere.
>
> There is a very close connection between the problem of the Bjerhammar sphere and the problem of the convergence of series in spherical harmonics or better the question of approximation of potentials by series in spherical harmonics, and here I believe we have reached the very core of the foundation of physical geodesy."

In studying this new technique, Krarup makes use of the following theorem which he calls the Runge theorem (IBID,p.54) :

> " Given any potential regular outside the surface of the Earth and any sphere in

the interior of the Earth. For every closed surface surrounding the Earth (which may be arbitrarily near the surface of the Earth) there exists a sequence of potentials regular in the whole space outside the given sphere and uniformly converging to the given potential on and outside the given surface.

This theorem is extremely important. In fact it permits a mathematical treatment of physical geodesy .....".

In the Appendix of his book, Krarup gives the following proof.

"Proof of Runge's theorem.
I want to prove that any potential in an open bounded region Ω can be approximated by potentials regular in an open sphere Σ containing Ω in its interior. The region Ω is supposed to be bounded by a surface ω which is sufficiently regular, i.e., by having finite curvature all over. This condition could be weakened very much, but I do not think it would be of interest in this connection. It is, however important that $\Sigma - \Omega$ is connected. "

It shouldn't perhaps be necessary to deal further with these questions, but Krarup's contribution has gained exceptional interest among geodesists. Furthermore, this very important work is based upon advanced studies with the use of functional analysis, and most geodesists will probably have difficulties when reading it. We will therefore try to explain some of the operations and also give some additional comments.

First we note that the Runge theorem as defined on page 54 of Krarup's publication is not quite identical with that which he wants to prove in the Appendix. It is, for example, added that $\Sigma - \Omega$ should be connected. There is no explanation for this restriction and we simply note that the Runge theorem is valid for harmonic polynomials if and only if the complement $(C\Omega)$ is connected. However, Krarup instead uses the notation $\Sigma - \Omega$. We also note that Krarup has not anticipated any harmonic polynomial and therefore his restriction is not mandatory.

It is of interest to note that Krarup on page 54, quite correctly restricts his Runge theorem with the use of a closed surface surrounding the Earth "which can come arbitrarily near the surface of the Earth." This restriction is essential for the Runge theorem and it must be required that the given potentials are harmonic in the neighbourhood of this region Ω. This means we cannot come down all the way to the actual surface of the Earth when using this theorem. The potentials could very well misbehave in the space between our region Ω and the physical surface of the Earth. This we have to remember in our further analysis. Krarup uses two lemmas for this proof and we quote:

" Lemma 1. For every function f continuous in $\Omega+\omega$ and 0 on ω we have that from

$$\int_{\Omega} f \cdot \psi \, d\Omega = 0 ,$$

for all potentials ψ regular in Σ follows

$$\int_{\Omega} f \cdot \phi \, d\Omega = 0,$$

for all potentials ϕ regular in Ω."

In the proof, Krarup defines a Hilbert space H consisting of functions, not necessarily potentials, f defined in Ω so that

$$\int_{\Omega} f^2 d\Omega \quad \text{is finite.}$$

Then Krarup writes

" Since functions of the type f in Lemma 1 are dense in H we have Lemma 2. In the Hilbert space H any element orthogonal to every potential ψ regular in Σ and restricted to Ω is orthogonal to every element ϕ of H that is a regular potential in Ω. "

However if lemma 1 goes to lemma 2 for a class of f, dense in H, then this is not true for all f in H, and this is unfortunately necessary for the proof used by Krarup. (The theorem can be proved using the technique outlined below.)

The next step could be a re-formulation of the Krarup proof, but it seems more natural to look into the basic definition of our problem. We easily see that if we want a strict proof for the geodetic approach, then we cannot accept the Runge theorem because the potential can very well misbehave between the compact set and the physical surface. However, the Runge theorem is a step in the correct direction, but it is not the complete answer. Fortunately we can use a well known theorem for potential theory by *Keldych* which we give in a geodetic version (see KELDYCH & LAVRENTIEFF 1937).

> *Let E be a compact set with a connected complement CE. Then every function continuous on the boundary E* can be uniformly approximated on E* with harmonic polynomials if and only if there are no unstable points at the boundary (i.e., there are no points on E* where the complement CE is thin).***

For the geodetic use of this theorem we put a sphere in the interior of the Earth and make an inversion of our model. The infinity point now comes in the interior of the sphere.

A proof can be outlined in the following way. We note that non-stable points cannot be approached from the complement by a cone. The stable points are dense in the boundary. The space of functions continuous on E* is denoted C and the space of measures μ on E* with the potential in the open complement of E equal to zero is denoted M. F is the linear subspace of C generated by elementary harmonic functions $\Phi_n^a(x)$

$$\Phi_n^a(x) = H_n(x-a) \cdot |x-a|^{-(2n+1)}, \quad n \geq 0,$$

where $H_n(x)$ is a harmonic polynomial of order n, a is the given point and x the actual point. Here F is dense in C (and thus uniform approximation is possible) if and only if zero is the only measure orthogonal to F. This is obvious from the well-known Hahn-Banach theorem. (The measures μ are orthogonal to F if and only if

$$\int \Phi_n^a(x)\, d\mu = 0 \qquad \text{for all } n.)$$

We have a connected complement CE and the measure μ is orthogonal to F if and only if it is in M. Furthermore M contains only the zero measure if and only if there are no unstable points on E* (#)

This problem has been carefully studied by several authors and we make reference to the work of KELDYCH & LAVRENTIEFF(1937), DENY (1939) and LANDKOF (1972). (After small modifications we also prove the Krarup-Runge theorem.)

This very general theorem can be called the *central theorem of physical geodesy*. As a special case, we obtain the Runge theorem which we re-formulate in the following way.

** Furthermore we also note that the potential is determined all over in the space when it is defined as a continuous function over the surface of the Earth.

(#)Note that the theorem is not restricted to uniform approximations with the use of a sphere.

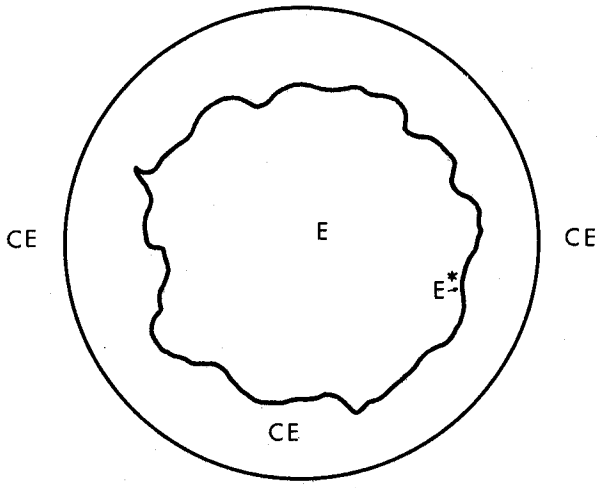

Figure 1. The Compact Set

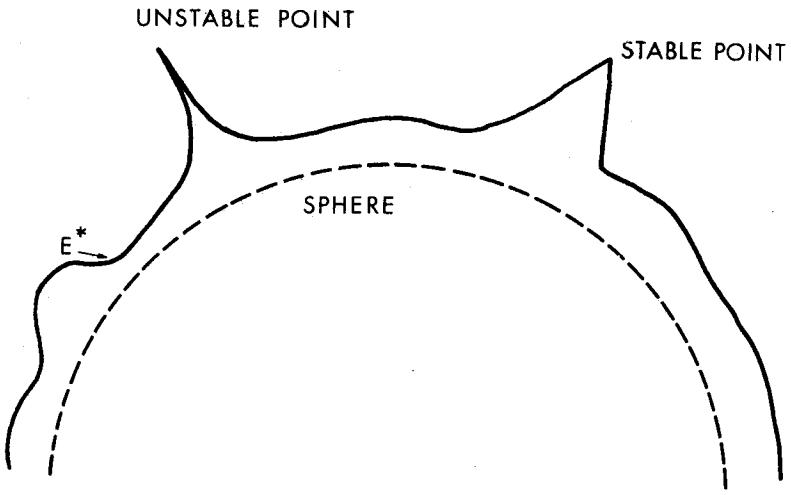

Figure 2. After Inversion

Let the compact E have the boundary E*. Then every function harmonic on E and in the neighbourhood of E U E* can be uniformly approximated on E. The approximating functions can be harmonic polynomials if and only if the complement of E is connected.

We note that the Runge theorem includes no restrictions on the surface. The Keldych theorem is more general but includes restrictions on the surface. These restrictions are without practical importance for geodetic application.†

We now go back to our original formulation of the boundary value problem (BJERHAMMAR 1963). It is obvious that Krarup didn't accept our discrete approach without using the Runge theorem of uniform approximation. A uniform approximation is of course no necessary tool for the acceptance of a discrete solution that fits in all given points. We are fully entitled to use any solution that fits all given points. We will always have sufficient harmonics for a fit of this type if we restrict the study to geodetic applications. The next question will be if our selected estimator will be better if the Keldych theorem is satisfied. Still we cannot give a limit for the maximum error of our selected estimate, but we know that the errors of some selected integral norm can be arbitrarily good. By increasing the number of observations, we can perhaps approach this limiting value.

The theorems of Keldych have a limited impact upon our discrete approach because it postulates a continuous approach. We have only observed a small subset of the original domain of boundary values and an infinite number of degenerations will be included in our solutions. In the practical applications, we have perhaps upto one million observations but we cannot handle more than a few thousand in a simultaneous computer run. In such situations we will find it useful to give solutions that minimize some additional norms for the residuals. *The contribution of Krarup has been extremely rewarding for the study of all these problems.*

LAURITZEN (1973) writes:

> "We shall not consider these difficulties in detail, but a way to overcome them (KRARUP 1969) is to search for the potential among functions, regular and harmonic, outside a sphere which is contained in the Earth's interior, the so called *Bjerhammar sphere*. Of course, this does not solve the problem, but because of the very important theorem of Runge (see IBID) we can in this way find an approximation to the potential which in some sense is arbitrarily good. "

The Runge theorem plays an important role in the present theory but to some extent it seems to be misinterpreted and we make the following remarks:

1. The errors in our geodetic approach cannot be made arbitrarily small because the effect of the Earth tide (sun and moon) is not negligible.
2. If observations are only made at discrete points, then the Runge theorem says nothing about the correctness of the predictions for intermediate points. (Probably uniform approximation will require that the measured points are uniformly distributed.)**

Continuous approach: A completely unbiased solution does not exist in the general case. However, the bias can be made arbitrarily small with the use of uniform approximation.

Discrete approach: An infinite number of unbiased estimators can be found. The unbiasedness is normally restricted to linear functions of the observations and cannot generally be extended to the continuous case.

---

† Note that already the Dirichlet problem will have no solution when unstable points are included. Therefore the Runge-Krarup approach suffers from the same limitations with respect to the surface.

** In a private note, L. Hörmander has verified the uniform convergence for the two-dimensional case when using equidistant spacing.

3. Observation Errors

Our uniform approximation is only possible if no observation errors are included. However, in all physical models we find observation errors. For various reasons we cannot avoid observation errors ε of the following two categories:

1. $E\{\varepsilon_1\} = 0$ (accidental) $\varepsilon_1 \in \varepsilon$
2. $E\{\varepsilon_2\} \neq 0$ (systematic) $\varepsilon_2 \in \varepsilon$

We will also recognize combinations of these errors. It is obvious that the ε_2-type of errors will give an additional bias in our final answer; for example, calibration errors. Our solution will of course be influenced by the model bias ε_3 which however, can be made arbitrarily small by uniform approximation. We have

3. $\varepsilon_3 \geq 0$ (systematic).

This means that we always will be exposed to systematic errors. It can therefore be justified to accept a more simple physical explanation for our approach.

4. Numerical Solution

The following integral equation was used for the numerical solution of the gravity reduction to an internal sphere (BJERHAMMAR 1962; BJERHAMMAR 1963; BJERHAMMAR 1964).

$$\Delta g_j = \frac{r_j^2 - r_o^2}{4\pi r_j} \iint \frac{\Delta g^*}{r_{ji}^3} \, ds \qquad (1),$$

or in matrices

$$\Delta g = K \, \Delta g^*.$$

Any element k of the matrix K is obtained with the use of the formula

$$K_{ji} = \sum_{n=0}^{\infty} (2n + 1) \left(\frac{r_o}{r_j} \right)^{n+2} P_n(\cos \omega_{ji})$$

or

$$K_{ji} = \frac{(r_j^2 - r_o^2) r_o^2}{r_{ji}^3 r_j} .$$

where ds = surface element of the sphere, Δg_j = gravity anomaly at the fixed point,
Δg^* = gravity anomaly at the internal sphere, r_o = radius of sphere,
r_{ji} = distance between the fixed point at the surface of the Earth (or in space) P_j and the moving point on the internal sphere,
r_j = geocentric distance to the actual point, and
r_i = distance between the centre of the Earth and the intersection of the surface of the Earth and a radius vector through the moving point.

4.1 Iterative Approach

In the first approach the measured gravity anomalies were used as approximate Δg^* values, and the residuals were used for corrections

$$\Delta g^* = \Delta g_o + \left\{ \Delta g_o - \frac{r_j^2 - r_o^2}{4\pi r_j} \iint \frac{\Delta g}{r_{ji}^3} \, ds \right\} .$$

For further details see (BJERHAMMAR 1962; BJERHAMMAR 1963; BJERHAMMAR 1969). MORITZ (1964) presented a "trick" (also given by BJERHAMMAR (1964))

$$\Delta g^* = \Delta g_o + \frac{r_j^2 - r_o^2}{4\pi r_j} \iint \frac{\Delta g_o - \Delta g}{r_{ji}^3} \, ds .$$

It is obvious that this solution is only an approximation of the previous solution above. For large values of $(r_j - r_o)$ this type of solution gives a considerable loss of accuracy. A number of different iterations are described in (BJERHAMMAR 1969).

4.2 Power Series (Least Squares Solution)

See also FORSTNER (1966), REIT (1967) and GROTEN (1970).

$$\Delta g^* = \Delta g + c_1 h + c_2 h^2 + c_3 h^3 + \ldots\ldots + c_n h^n \qquad (2),$$

where h is the height above the sphere.

4.3 Spherical Harmonic Solution

$$\Delta g = \frac{GM}{r_j} \sum_{n=2}^{\infty} \left(\frac{r_o}{r_j} \right)^n (n-1) \sum_{m=0}^{n} P_{nm}(\sin \phi) \left(C_{nm} \cos m\lambda + S_{nm} \sin m\lambda \right) \qquad (3),$$

where

G = Newtonian constant and M is the mass of the Earth

4.4 Matrix Solution (non-singular case)

$$\Delta g = K \, \Delta g^*, \quad \text{with} \qquad \Delta g^* = K^{-1} \Delta g \qquad (4).$$

4.41 Matrix Solution with Singular K-matrix

$$(\Delta g - K \Delta g^*)^T (\Delta g - K \Delta g^*) = \min \; ; \; \Delta g^* = (K^T K)^{-1} K^T \Delta g = K_{01}^{-1} \Delta g$$

See(BJERHAMMAR 1964).

4.42

$$(\Delta g^*)^T (\Delta g^*) = \min \; ; \qquad \Delta g^* = K^T (K K^T)^{-1} \Delta g = K_{10}^{-1} \Delta g$$

(BJERHAMMAR 1968a)

4.43

$$(\Delta g - \hat{\Delta g})^T (\Delta g - \hat{\Delta g}) = \min, \quad \text{where} \qquad \hat{\Delta g} = K \, \Delta g^*,$$

with the constraint

$$(\Delta g^*)^T \Delta g^* = \min \quad ; \quad \Delta g^* = K^T(KK^T)^{-1}K(K^TK)^{-1}K^T \Delta g = K_{11}^{-1} \Delta g \quad \text{(IBID)}.$$

These three solutions are very general and can be used with *weights* in the classical way.

4.44

With an infinite dimensional matrix K(∞×n) we transcribe 4.42 for a finite number of observations

$$\frac{1}{4\pi} \iint (\Delta g^*)\, d\sigma = \min ,$$

where σ is the unit sphere. The elements of KK^T are here obtained after integration over the sphere. An arbitrary element is then for the points P_j and P_i

$$(KK^T)_{ji} = \frac{1}{4\pi} \iint \sum_{n=0}^{\infty} (2n+1) \left(\frac{r_o}{r_j}\right)^{n+2} P_n(\cos \omega_j) \sum_{\underline{n}=0}^{\infty} (2\underline{n}+1) \left(\frac{r_o}{r_i}\right)^{\underline{n}+2} P_{\underline{n}}(\cos \omega_i)\, d\sigma.$$

After an expansion in spherical harmonics, we obtain (also in 4.46:5)

$$(KK^T)_{ji} = \sum_{n=0}^{\infty} (2n+1) \left(\frac{r_o^2}{r_j r_i}\right)^{n+2} P_n(\cos \omega_{ji}) \; ; \quad \text{thus } K_{10}^{-1} \text{ is also defined.}$$

4.45

We replace Δg all over by T in equation 1. Then we have the true Poisson formula

$$T_j = \frac{r_j^2 - r_o^2}{4 r_o} \iint \frac{T^*}{r_{ji}^3}\, d\sigma; \qquad K_{ji} = \sum_{n=0}^{\infty} (2n+1) \left(\frac{r_o}{r_j}\right)^{n+1} P_n(\cos \omega_{ji}),$$

K_{ji} being the elements of the K matrix.
Using the technique of 4.44, we obtain

$$\frac{1}{4\pi} \iint (T^*)^2\, d\sigma = \min; \qquad \text{or} \quad ||T^*||^2 = \min.$$

The elements of KK^T are obtained in the corresponding way (also in 4.46:1)

$$(KK^T)_{ji} = \sum_{n=0}^{\infty} (2n+1) \left(\frac{r_o^2}{r_j r_i}\right)^{n+1} P_n(\cos \omega_{ji}).$$

The solutions of 4.44 and 4.45 can also be obtained with the theory of Hilbert spaces with reproducing kernels.

4.46 Mean Values

The spherical harmonics of order n will be denoted T_n for the disturbance potential and Δg_n for the gravity anomaly. Then we have the relations

$$T_j = \sum T_n^* \left(\frac{r_o}{r_j}\right)^{n+1} \qquad ; \qquad \Delta g_j = \sum \Delta g_n^* \left(\frac{r_o}{r_j}\right)^{n+2}$$

$$T_j = \sum r_o \, \Delta g_n^* \, (n-1)^{-1} \left(\frac{r_o}{r_j} \right)^{n+1} \quad ; \quad \Delta g_j = \sum \frac{1}{r_o} \, T_n^* \, (n-1) \left(\frac{r_o}{r_j} \right)^{n+2} .$$

With the use of these basic harmonics, we compute the following mean values after an integration over the internal sphere. The integrated means are denoted $E(T_j T_i)$, $E(\Delta g_j, \Delta g_i)$ etc., when the two points in question are P_i and P_j. Furthermore we introduce the special notations

$$E(T_n^* \, T_n^*) = s_n^2 \qquad \text{and} \qquad E(\Delta g_n^* \, \Delta g_n^*) = \sigma_n^2 .$$

$$||T|| = \min$$

4.46:1 $$E(T_j T_i) = \sum s_n^2 \, (2n+1) \left(\frac{r_o^2}{r_j r_i} \right)^{n+1} P_n(\cos \omega_{ji})$$

4.46:2 $$E(\Delta g_j \Delta g_i) = \frac{1}{r_o^2} \sum s_n^2 \, (2n+1) \, (n-1)^2 \left(\frac{r_o^2}{r_j r_i} \right)^{n+2} P_n(\cos \omega_{ji})$$

4.46:3 $$E(T_j \Delta g_i) = \frac{1}{r_i} \sum s_n^2 \, (2n+1) \, (n-1) \left(\frac{r_o^2}{r_j r_i} \right)^{n+1} P_n(\cos \omega_{ji}).$$

$$||\Delta g|| = \min$$

4.46:4 $$E(T_j T_i) = r_o^2 \sum \sigma_n^2 \, (2n+1) \, (n-1)^{-2} \left(\frac{r_o^2}{r_j r_i} \right)^{n+1} P_n(\cos \omega_{ji})$$

4.46:5 $$E(\Delta g_j \Delta g_j) = \sum \sigma_n^2 \, (2n+1) \left(\frac{r_o^2}{r_i r_j} \right)^{n+2} P_n(\cos \omega_{ji})$$

4.46:6 $$E(T_j \Delta g_i) = \frac{r_o^2}{r_i} \sum \sigma_n^2 \, (2n+1) \, (n-1)^{-1} \left(\frac{r_o^2}{r_j r_i} \right)^{n+1} P_n(\cos \omega_{ji})$$

The summation can be taken from 3 to infinity for all Legendre polynomials. Order one must be excluded in two of the expressions. Order two is anyway eliminated with the use of the reference ellipsoid. In our following study, we consider σ_n^2 and s_n^2 given constants (degree variances).

The presented means have a special meaning in the theory of stochastic processes. Furthermore equation 4.46:1 can be used as a reproducing kernel in Hilbert space. Our study is simply a least squares application. (The stochastic process approach has been questioned by Lauritzen who proved that ergodicity is not prevailing. See (LAURITZEN 1973).)

4.47

For points on the sphere and outside the sphere we can estimate gravity, disturbance potentials and vertical deflections in a general system which is valid for the singular as well as the non-singular case. (Estimates for points below the physical surface have no physical meaning.)

Gravity :

$$\Delta g_j = k_g \, \Delta g_i^* = k_g \, K_g^T \, (K_g K_g^T)^{-1} \, \Delta g_i = k_{gg} K_{gg}^{-1} \, \Delta g_i$$

Disturbance Potential:

$$T_j = f_T \Delta g^* = f_T K_g^* (K_g K_g^T)^{-1} \Delta g_i = k_{Tg} K_{gg}^{-1} \Delta g_i$$

or

$$T_j = k_T T^* = k_T K_T^* (K_T K_T^T)^{-1} T_i = k_{TT} K_{TT}^{-1} T_i .$$

The individual elements are defined by

$$K_{gg} = \sum_{n=0}^{\infty} k_n (2n+1) t^{n+2} P_n(\cos \omega_{ji}) = k_{gg} \rightarrow \frac{t^2 - t^4}{\rho^3} \quad \text{for } k_n = 1 \text{ and } \rho = (1+t^2 - 2t \cos \omega_{ji})^{\frac{1}{2}}$$

$$K_{TT} = r_o^2 \sum_{n=2}^{\infty} k_n (2n+1) (n-1)^{-2} t^{n+1} P_n(\cos \omega_{ji}) = k_{TT} ; \quad \text{and}$$

$$r_j \sum_{n=2}^{\infty} k_n (2n+1) (n-1)^{-1} t^{n+2} P_n(\cos \omega_{ji}) = k_{Tg} \rightarrow r_j t^2 \left(\frac{2}{\rho} - 3\rho + 1 - 5t \cos \omega_{ji} - 3t \cos \omega_{ji} \ln \phi\right) \text{ for } k_n = 1 \text{ where } \phi = (1 + \rho - t \cos \omega_{ji})^{\frac{1}{2}}.$$

Vertical Deflections:

$$\xi_j = -\frac{1}{\gamma_j} \frac{\partial T_j}{\partial x} = -\frac{1}{\gamma_j} f_x K_{gg}^{-1} \Delta g \qquad \begin{Bmatrix} f_x \\ f_y \end{Bmatrix} \rightarrow \begin{Bmatrix} \cos \alpha_{ji} \\ \sin \alpha_{ji} \end{Bmatrix} t^3 \sin \omega_{ji} \left(\frac{2}{\rho^3} - 8 + \frac{3(\rho+1)^2}{2\rho\phi} - 3 \ln \phi\right) \text{ for } k_n = 1.$$

$$\eta_j = -\frac{1}{\gamma_j} \frac{\partial T_j}{\partial y} = -\frac{1}{\gamma_j} f_y K_{gg}^{-1} \Delta g$$

Three important types of solutions are obtained as special cases

I: $k_n = 1$ and $t = r_o/r_j$		non singular (BJERHAMMAR 1964)
II: $k_n = \sigma_n^2$ and $t = r_o^2/r_j r_i$		$\|\|\Delta g^*\\| = \min$ (cf.MORITZ 1970)
III: $k_n = s_n^2 (n-1)^2 (1/r_o^2)$ and $t = r_o^2/r_j r_i$		$\|\|T^*\\| = \min$ (cf.KRARUP 1969)

The "non-parametric solution" of BJERHAMMAR (1964) minimizes the $||\Delta g^*||$ norm with $\sigma_n^2 = (r_i/r_o)^{n+2}$. The "covariance" matrix is here asymmetric. High order harmonics are given low weights. The solution by Bjerhammar (IBID) gives the solution of MORITZ (1970) if r_j is replaced by $r_j r_i / r_o$. Furthermore this solution is identical with the solution of KRARUP (1969) because $r_o \Delta g_n^* = T_n^* (n-1)$. Krarup and Moritz excluded potentials that are not rotation invariant. Here we accept the symmetric as well as the non-symmetric cases. No probabalistic meaning of the covariances is anticipated. The Moritz solution is obtained as a limiting value from our solution 4.42 above (BJERHAMMAR 1968b) when using infinite points at the "sphere".

4.48 Antireduction

If a very large number of unknowns are used, then we cannot use the methods available now for the inversion of the corresponding matrices. For most cases, it is unnecessary to compute the inverse and the methods of Gauss or Cholesky are useful for the back

substitution. Still it will be very difficult to include all observations and therefore we use the method of antireduction in order to find the best solution. The technique is based upon the following procedure. With our discrete approach we find a solution that satisfies the boundary values at n given points. The total set of measured points includes N observations. Gravity is now computed for all N points with the use of our previous solution for n points. The residual gravity anomaly is then obtained for all these points. The final solution is then of the following type for the disturbance potential

$$T = \frac{1}{4\pi r_j} \iint \Delta g \sum_{n=2}^{\infty} (2n+1)(n-1)^{-1} \left(\frac{r_o}{r_j} \right)^n P_n(\cos \omega) ds + \frac{1}{4\pi r_j} \iint \Delta G \sum_{n=2}^{\infty} (2n+1)(n-1)^{-1} P_n(\cos \omega) ds,$$

where

ΔG = residual gravity anomaly.

If still higher accuracy is wanted, then we continue with iterative methods. Molodensky's technique will probably be useful.

The choice between a least squares solution (or stochastic processes) and the non-singular approach is not critical when antireduction is included.

Finally it should be noted that our non-singular solution in all cases gives a better condition number than the corresponding solution with rotation invariant potentials. However, only the least squares types of solution have a quite symmetrical K_{gg}-matrix. A somewhat simpler computational technique can be used in the symmetrical case. This computational gain is obtained at the cost of a general loss of the non-stationary parts of the solution.

4.5 Filtering

Our solution with generalized inverses is re-written

$$\Delta g^* = QK^T(KQK^T)^{-1} K(K^T R^{-1} K)^{-1} K^T R^{-1} \Delta g = \lim_{\delta \to 0} QK^T(KQK^T + \delta R)^{-1} \Delta g,$$

with

$$(\Delta g - k \Delta g^*)^T R^{-1} (\Delta g - K \Delta g^*) = \min \qquad \text{and} \qquad (\Delta g^*)^T Q^{-1} \Delta g^* = \min.$$

This solution gives an *unbiased* estimate of Δg^* for any Δg.

If we restrict our estimate to observations with $E\{\Delta g\} = 0$ then we have an *unbiased* estimate also for $\delta \neq 0$ and we can write

$$\Delta g^* = QK^T(KQK^T + R)^{-1} \overline{\Delta g} \qquad \text{for} \qquad E\{\overline{\Delta g}\} = 0.$$

Here KQK^T is positive definite. We can now use this solution for a prediction of Δg anywhere at the surface of the Earth or in space. The final prediction $\hat{x}$ is then (for $Q = I$)

$$\hat{x} = u \Delta g^* = u K^T(KK^T + R)^{-1} \overline{\Delta g}.$$

This expression can be re-written with the obvious notation

$$\boxed{\hat{x} = k(\overline{K} + R)^{-1}\,\overline{\Delta g}} \qquad \text{where} \qquad \overline{\Delta g} = \Delta g - E\{\Delta g\}\ .$$

It is easily verified that this type of solution satisfies the condition

$$(\Delta g^*)^T\ \Delta g^* + (\Delta g - K\,\Delta g^*)^T\ R^{-1}\ (\Delta g - K\,\Delta g^*) = \min.$$

5. Acknowledgment

The author is grateful for the comments given by professors J. Deny, L.I. Hedberg, Lars Hörmander and H. Shapiro.

6. References

BARLIK, M. 1970. Kwestia Tozwiazania Problemu Bjerhammara. *Geodezja i Kartografia.*

BJERHAMMAR, A. 1963. *Gravimetric Geodesy Free from Density Estimate through Analysis of Discrete Gravity Data.* Research Institute for Geodetic Sciences, Alexandria Va.

BJERHAMMAR, A. 1964. A New Theory of Geodetic Gravity. *Trans.R.Inst.Techn.* 243, Stockholm, 75 pp.

BJERHAMMAR, A. 1968a. A Generalized Matrix Algebra. *Trans.R.Inst.Techn.* ,Stockholm.

BJERHAMMAR, A. 1968b. *On Gravity.* 129 pp, Kungl.Tekniska Hogskolan,Stockholm.

BJERHAMMAR, A. 1969. On the Boundary Value Problem of Physical Geodesy. *Tellus* XXI,451-516.

BJERHAMMAR, A. 1973. *Theory of Errors and Generalized Matrix Inverses.* Elsevier,Amsterdam.

CHOVITZ, B.H. 1972. Downward Continuation of the Potential from Satellite Altitudes. *Fifth Symposium on Mathematical Geodesy (Second Hotine Symposium)*,Florence.

DENY, J. 1949. Systemes Totaux de Fonctions Harmoniques. *Ann.de l'Inst.Fourier.*

FORSTNER, W. 1966. Studies on the Problem of Bjerhammar. *Trans.R.Inst.Techn.* ,Stockholm.

GOLUB, G & REINSCH, C. 1970. Singular Value Decomposition and Least Squares Solutions. *Num.Math.* 14, 403-420.

GROTEN, E. 1970. Some Remarks on the Downward Continuation of Gravity. In *Advances in Gravimetry*, Pittsburgh Pa.

HEITZ, S. & TSCHERNING, C.C. 1971. Comparisons of Two Methods of Astro-geodetic Geoid Determinations based on Least Squares Prediction and Collocation. *Tellus* XXIV,271-275.

HOTINE, M. 1969. Mathematical Geodesy. *ESSA Monograph* 2,Washington, DC.

KELDYCH, M. & LAVRENTIEFF, M. 1937. *Compte.rendue.Acad.Sci.*,1788,Paris.

KRARUP T. 1969. A Contribution to the Mathematical Foundation of Physical Geodesy. *Meddelelse* 44,80 pp,Geodaetisk Institut, København.

LANDKOF, N.S. 1972. *Foundations of Modern Potential Theory.* Springer, Berlin.

LAURITZEN, S.L. 1973. The Probabilistic Background of some Statistical Methods in Physical Geodesy. *Meddelelse* 48,96 pp,Geodaetisk Institut,København.

MESCHKOWSKI, H. 1962. *Hilbertsche Räume mit Kernfunktionen.* Springer, Berlin.

MORITZ, H. 1964. The Boundary Value Problem of Physical Geodesy. *Rep.* 46,Dept. of Geodetic Science, The Ohio State University,Columbus Ohio.

MORITZ, H. 1970. Least Squares Estimation in Physical Geodesy. *Rep.* 130,Dept. of Geodetic Science, The Ohio State University,Columbus Ohio.

MORITZ, H. 1972. Advanced Least Squares Methods. *Rep.* 175,Dept. of Geodetic Science, The Ohio State University,Columbus Ohio.

MORITZ, H. & SCHWARZ, K.P. 1972. On the Computation of Spherical Harmonics from Satellite Observations. *Fifth Symposium on Mathematical Geodesy (Second Hotine Symposium)*,Florence.

MORRISON, F. 1969. Validity of the Expansion for Potential Near the Surface of the Earth. *Proc. Fourth Symposium on Mathematical Geodesy*,95-105,Trieste.

PICK, M. 1965. On the Shape of the Earth by using Analytical Continuation for Function. *Studia geophys.et geodaet.*9,3.

REIT, B.G. 1967. *On the Numerical Solution of the Gravimetrical Integral Equation of Bjerhammar.* Geodesy Division, Royal Institute of Technology,Stockholm.

7. Discussion*

QURESHI: You are inverting upward continuation. Why don't you call this downward continuation?

MORITZ: It is a downward continuation. Downward continuation cannot be done in an elementary way. So the obvious way is to use the integral approach, via upward continuation.

DOOLEY: Referring to this theorem; that we modify the gravity field by a small amount and get an analytical solution at any depth. This is in conflict with what we have always been taught that if you have a mass at a certain depth - a point mass - it gives a very sharp anomaly and this simply cannot be continued any further without divergence.

MORITZ: This is the familiar case of a mass point causing singularity on analytical continuation. But it is still true that by modifying the external gravity field by a small amount, one can continue it downward. The downward continuation will be rather irregular, but it will exist. It will be something like approximating a delta function by an analytical function.

* Paper presented by H. MORITZ.

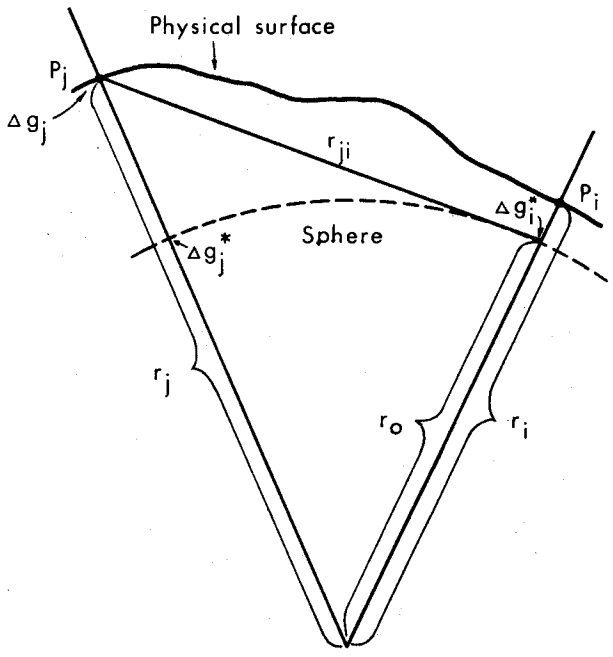

Figure 3. The Physical Surface and the Sphere

TAPLEY, B.D.
SCHUTZ, B.E.
Dept. of Aerospace Engineering & Engineering Mechanics
The University of Texas at Austin
Austin Texas 78712
United States of America

Proc. Symposium on Earth's Gravitational Field & Secular Variations in Position (1973), 489-508.

A COMPARISON OF ESTIMATION METHODS FOR THE REDUCTION OF LASER RANGE OBSERVATIONS **

ABSTRACT

The accuracy, stability and convergence characteristics of the classical batch estimation algorithm is compared with the characteristics of the sequential estimation algorithm. The relationship of each of these methods to the least squares collocation algorithm is described. The accuracy of the estimate obtained with each of these methods is compared by examining the converged state estimate and the observations from the Beacon Explorer-C satellite. It is concluded that, for the same estimation accuracy, the rectified sequential estimation algorithm has a faster convergence and a larger initial radius of convergence. Furthermore the results indicate that it can be used to study the evolution of the estimates of constant parameters such as tracking station co-ordinates.

1. Introduction

In recent years, the accuracy of the observations of near-Earth satellites has undergone dramatic improvement. For instance, laser ranging systems currently measure the range between a tracking station and an orbiting satellite to within 50 cm. It is expected that such accuracy will improve to within 5 to 10 cm. Satellite observations with this precision are of interest in the study of various phenomena such as the determination of the shape and physical composition of the Earth as well as studies of solid Earth tides, tectonic plate motion, and polar motion. However, to employ observations of such accuracy in the study of these phenomena, estimates of the position and velocity of the satellite must be obtained to an accuracy commensurate with the observation precision.

There are two fundamental factors which limit the accuracy with which the orbit of a satellite can be determined and predicted. These two factors are:

1. The computational procedure used to reduce the observations and to predict the future motion of the satellite; and
2. The accuracy with which the mathematical model used to describe the satellite's motion is known.

There are two basic procedures for processing satellite observations to obtain an estimate of the orbit of a space vehicle. The methods are referred to as batch processors and sequential processors. The sequential orbit determination procedure processes each observation at the time point at which it is received and an estimate of the state is obtained at that time. On the other hand, the batch processor , which obtains the estimate at some reference epoch, requires that the entire sequence of observations be processed before the estimate of the state can be made. Both batch and sequential estimation algorithms are founded on the assumption that the non-linear equations of motion and observation-state equations can be linearized with reference to some a priori solution. Then the deviation from the reference solution can be determined by the application of linear estimation

** This research was supported by AFOSR under Grant # 72-2233

techniques.

Errors of four basic types influence the accuracy of linear estimators:

1. errors due to linearization assumptions;
2. errors introduced in the computational procedures;
3. errors which occur in the observation process; and
4. errors due to inaccuracies in the mathematical model used to describe the dynamical process.

While it is anticipated that the last two error sources will influence both the batch and the sequential estimation algorithms in the same manner, errors due to the first effects may lead to differences in the estimate obtained by these algorithms, especially during the initial iterations.

The least-squares batch estimation algorithms are widely used in most geodetic work and in the majority of the real-time operational orbit determination programs. There have been few applications of sequential orbit determination algorithms to real time data reduction and even fewer detailed numerical comparisons between the characteristics of the batch type algorithms and the sequential algorithms in their applications to the reduction of real tracking data. While the formal mathematical equivalence between the sequential estimation algorithm and the batch estimation algorithm can be shown, the extended sequential estimation algorithm which rectifies the reference trajectory at each observation point, will yield the same numerical estimate as the batch algorithm only if the solution is iterated to convergence. Furthermore, the well known problem of "divergence" of the sequential estimate in the presence of a small state error covariance matrix has led to the convention of propagating the state error covariance matrix in a state noise compensated mode. The observation residuals obtained with this algorithm are significantly different from the residuals obtained with the batch algorithms, and this fact has lead to some reluctance to use the sequential estimation algorithm for many orbit determination applications.

In the following discussion, the derivation of both the batch and the sequential estimation algorithms are reviewed, and their computational characteristics, as determined by application to the problem of reducing precise laser ranging observations to a near-Earth satellite, are compared. The question of the nature of the convergence as well as the radius of convergence for each algorithm is also considered. The number of iterations, a pertinent quantity in determining the computing time required for convergence by both methods, is also considered.

The mathematical foundations for the batch estimation algorithms are reviewed by TAPLEY (1973). The derivations for the sequential estimation algorithm reside in the classic works of KALMAN (1960), and KALMAN & BUCY (1961). Additional references on estimation theory, which discuss both batch and sequential methods, include BRYSON & HO (1969), DEUTSCH (1965), JAZWINSKI (1970) and LIEBELT (1967).

2. Problem Formulation

The equations which govern the motion of a satellite in orbit about a central body can be expressed as

$$\dot{\vec{r}} = \vec{v}, \qquad \dot{\vec{v}} = -\frac{\mu \vec{r}}{r^3} + \vec{R}(\vec{r},\vec{v},\vec{\alpha},t) \tag{2.1},$$

where $\vec{r}$ is the position vector measured from the mass centre, $\vec{v}$ is the velocity vector, μ the gravitational parameter, and $\vec{R}$ is a vector of perturbations which depend on $\vec{r}$, $\vec{v}$, and the set of model

parameters $\vec{\alpha}$. For example, $\vec{R}$ may be due to the effects of atmospheric drag, the non-central components of the central body gravitational force, the gravitational attractions of other bodies, etc. The parameters $\vec{\alpha}$ represent any unknown parameters whose value must be estimated during the estimation procedure, e.g., the mass of a third body, the spherical harmonic coefficients, $C_{\ell m}$ and $S_{\ell m}$, for the central body gravitational field, etc. Equations 2.1 can be expressed in first-order form as follows

$$\dot{\eta} = f(\eta,\alpha,t) \qquad \dot{\alpha} = 0 \tag{2.2}$$

where the six-dimensional vectors η and $f(\eta,\alpha,t)$ are defined as follows:

$$\eta^T = [\vec{r}^T : \vec{v}^T], \quad f^T(\eta,\alpha,t) = [\vec{v}^T : (-\mu\vec{r}/r^3 + \vec{R})^T] \tag{2.3}$$

The state vector X consists of all time dependent variables or constant parameters required to determine uniquely the evolution of the satellite's motion. With this definition, the n-dimensional state vector X can be expressed as follows:

$$X^T = [\eta^T : \alpha^T] \tag{2.4}$$

and the state equations become

$$\dot{X} = F(X,t), \qquad X(t_o) = X_o \tag{2.5}$$

where $F^T(X,t) = [f^T(\eta,\alpha,t) : 0]$. With X_o specified, the evolution of the dynamic system will be determined uniquely by the solution to equation 2.5. In the usual orbit determination problem, X_o will not be known perfectly and observations of the motion must be made to determine the best estimate of X_o.

Usually the state vector cannot be observed directly. Instead, the observation will be a non-linear function of the state. Since the observations are usually influenced by random observation error, the observation-state relationship can be expressed as

$$Y_i = G(X_i,t_i) + \varepsilon_i \tag{2.6}$$

where Y_i is a p-vector of observations of the state X_i at the epoch t_i, $G(X_i,t_i)$ is a non-linear function relating the state and the observations, and ε_i is a p-vector of observation errors.

Examination of equations 2.5 and 2.6 indicate that the basic equations of interest are non-linear. To apply linear estimation theory, equations 2.5 and 2.6 must be replaced by an equivalent set of linear equations. To accomplish this, a Taylor series expansion about some reference trajectory at each point in the time interval of interest can be used. If the definitions

$$\begin{aligned} x(t) &= X(t) - X^*(t), \qquad t_o \leq t \leq t_\ell \\ \text{and} \\ y_i &= Y_i - G(X_i^*,t_i), \qquad i = 1, \ldots\ldots \ell \end{aligned} \tag{2.7}$$

are used, where $X^*(t)$ indicates the reference trajectory, then the deviation from the reference trajectory and the observation associated with this deviation can be expressed as

$$\dot{x}(t) = A(t)\,x(t), \qquad x(t_o) = x_o, \qquad t_o \leq t \leq t_\ell$$

and (2.8),

$$y_i = \tilde{H}_i x_i + \varepsilon_i , \qquad i=1, \ldots\ldots \ell$$

where terms of $O\{(x_i - x_i^*)^2\}$ are neglected, and where $A(t) = [\partial F/\partial X]^*$ and $\tilde{H}_i = [(\partial G/\partial X)]^*$. The symbol $[\ ]^*$ indicates that the quantity in the brackets is evaluated on the reference solution.

By noting that the first of equations 2.8 has the solution

$$x_i = \Phi(t_i,t_k)x_k \tag{2.9}$$

where $\dot{\Phi}(t_i,t_k) = A(t)\,\Phi(t_i,t_k)$, $\Phi(t_k,t_k) = I$, the observation sequence y_i, $(i=1,\ldots,\ell)$, can be reduced to a single epoch. If

$$y = \begin{pmatrix} y_1 \\ y_2 \\ . \\ . \\ y_\ell \end{pmatrix}, \qquad H = \begin{pmatrix} \tilde{H}\,\Phi(t_1,t_k) \\ \tilde{H}_2\Phi(t_2,t_k) \\ . \\ . \\ \tilde{H}_\ell\Phi(t_\ell,t_k) \end{pmatrix}, \qquad \varepsilon = \begin{pmatrix} \varepsilon_1 \\ \varepsilon_2 \\ . \\ . \\ \varepsilon_k \end{pmatrix},$$

then the observation sequence can be represented as

$$y = H x_k + \varepsilon \tag{2.10}$$

The m-vector y, where $m = p \times \ell$, will represent the entire set of observations used in the estimate. Generally, $m > n$, but if a few observations are to be combined with an a priori estimate, $m \leq n$ is permissible. The observation error ε_i is assumed to satisfy the a priori statistics:

$$E\{\varepsilon_i\} = 0, \qquad E\{\varepsilon_i\varepsilon_j^T\} = R_i\,\delta_{ij} \tag{2.11}$$

where δ_{ij} is the Kronecker delta and where R_i is a $p \times p$ positive definite matrix.

Given an estimate of the state $\hat{x}_j = E\{x_i|y_i, \ldots, y_j\}$, and the associated state error covariance matrix $P_j = E\{(x_j-\hat{x}_j)(x_j-\hat{x}_j)^T|y_1, \ldots, y_j\}$, the estimate and the covariance matrix at a future time t_k is given by the expressions

$$\bar{x}_k = \Phi(t_k,t_j)\,\hat{x}_j, \qquad \bar{P}_k = \Phi(t_k,t_j)\,P_j\,\Phi^T(t_k,t_j) \tag{2.12}$$

The predicted estimate of the state at the time, t_k, can be treated as an observation whose associated error is $\eta_k = x_k - \bar{x}_k$. It is a straightforward procedure to show that, for an unbiased estimate $\hat{X}_j$,

$$E\{\eta_k\} = 0 \quad , \quad E\{\eta_k\eta_k^T\} = \bar{P}_k \tag{2.13}$$

Hence, combining equation 2.12 with equation 2.10, the following observations and a priori estimates of the state at a time t_k are available:

$$y_k = H_k x_k + \varepsilon_k \quad ; \qquad \bar{x}_k = x_k + \eta_k \tag{2.14}$$

If the state vector x_k is an n-vector of constant parameters, then the state transition matrix will

reduce to the identity matrix for all values of time, i.e., $\Phi(t_i,t_k) = I$. Equations 2.14 can be used to combine a priori estimates x_k with new observations y_k where the observation errors are assumed to satisfy equations 2.11 and 2.13.

3. Minimum Variance Estimate

If the best linear, unbiased, minimum variance estimate of x_k is sought, given equations 2.11, 2.13 and 2.14, the estimate will be determined by the following expression

$$\hat{x}_k = \left(H_k^T R_k^{-1} H_k + \bar{P}_k^{-1}\right)^{-1} \left(H_k R_k^{-1} y_k + \bar{P}_k^{-1} \bar{x}_k\right) \tag{3.1}$$

In equation 3.1, the vector y_k may be only a single observation or it may include an entire batch of observations. The a priori estimate $\bar{x}_k$ may represent the estimate of the initial conditions propagated to the time t_k, or it may be based on the reduction of a previous batch of data. The computation of the estimate $\hat{x}_k$ requires the inversion of an $n \times n$ matrix and if the dimension n is large, this inversion can lead to computational difficulties.

If the a priori estimate is zero, i.e., if $\bar{x}_k = 0$, then equation 3.1 reduces to

$$\hat{x}_k = \left(H_k^T R_k^{-1} H_k + \bar{P}_k^{-1}\right)^{-1} H_k^T R_k^{-1} y_k \tag{3.2}$$

Note that equation 3.2 still retains the covariance matrix $\bar{P}_k$ associated with the estimate $\bar{x}_k = 0$ and the estimate $\hat{x}_k$ will be different than the estimate obtained if no a priori information is available. The no a priori information case is characterized by the limit as $\bar{P}_k \to \infty$. For this case, equation 3.1 reduces to

$$\hat{x}_k = \left(H_k^T R_k^{-1} H_k\right)^{-1} H_k^T R_k^{-1} y_k \tag{3.3}$$

Note that if the observation noise covariance matrix R_k is replaced by an observation weighting matrix W_k, where $W_k = R_k^{-1}$, the expressions in equations 3.1, 3.2 and 3.3 give the weighted least squares estimation algorithms. Furthermore, if the observation errors and the a priori values for the initial conditions satisfy Gaussian distributions, then equation 3.1 is also the maximum likelihood estimate.

The primary differences between the different estimation algorithms lie in the nature of the a priori information. In this regard, the least squares collocation algorithm described by MORITZ (1970) can be shown to be equivalent to the algorithm given by equation 3.2, i.e., the minimum variance estimate for the case $\bar{x}_k = 0$. This equivalence is discussed in a subsequent paragraph.

In describing the computational algorithm for implementing equation 3.1, it is convenient to define the following matrix expressions

$$L = H^T R^{-1} H + \bar{P}_o^{-1} = \sum_{i=1}^{\ell} H_i^T R_i^{-1} H_i + \bar{P}_o^{-1}$$

and

$$M = H^T R^{-1} y = \sum_{i=1}^{\ell} H_i^T R_i^{-1} y_i + \bar{P}_o^{-1} \bar{x}_o \tag{3.4}$$

where $H_i = \tilde{H}_i\ \Phi(t_i,t_o)$. With these definitions, equation 3.1 becomes

$$\hat{x}_o = L^{-1}\ M \tag{3.5}$$

Then the procedure for computing the batch estimate of x can be summarized as follows:

Given: X^*_o, $\bar{x}_o$, $\bar{P}_o$ and y_i, i=1, ...ℓ,

Batch computational algorithm

1. Compute $L_o = \bar{P}_o^{-1}$, $M_o = \bar{P}_o^{-1}\ \bar{x}_o$, set $t_k = t_1$, $t_{k-1} = t_o$.

2. Integrate: From t_{k-1} to t_k

$$\dot{X}^* = F(X^*,t),\quad X^*(t_{k-1}) = X^*_{k-1}$$

$$\dot{\Phi}(t,t_{k-1}) = A(t)\ \Phi(t,t_{k-1});\qquad \Phi_{k-1} = \Phi(t_{k-1},t_o) \tag{3.6}$$

3. Compute:

$$\tilde{H}_k = \partial G(X^*_k,t_k)/\partial X_k,\quad H_k = \tilde{H}_k\ \Phi(t_k,t_o),\quad N_k = H_k^T R_k^{-1}$$

$$L_k = L_{k-1} + N_k H_k \tag{3.7}$$

$$M_k = M_{k-1} + N_k y_k$$

4. Test: if $k = \ell$, go to 5; if $k < \ell$, increase k by 1 and return to 2.

5. Compute

$$\hat{x}_o = L_\ell^{-1}\ M_\ell \tag{3.8}$$

Note that in the algorithms summarized by equations 3.7, L_k is a symmetric $n \times n$ matrix and consequently computation of only the upper half of the matrix is necessary. If it is assumed that the vector y_k is a p-vector, and that the observations are correlated, i.e., the $p \times p$ matrix, $E[\varepsilon_k \varepsilon_k^T] = R_k$ has non-zero off-diagonal elements, then the elements in L_k, which must be computed, can be expressed as follows :

$$(L_{ij})_k = (L_{ij})_{k-1} + \sum_{\ell=1}^{p}\sum_{m=1}^{p} \left(H_{\ell i}\ \sigma^{-1}_{\ell m}\ H_{mj}\right)_k,\ i=1, \ldots ,n;\ j=1, \ldots , n \tag{3.9}$$

If the observations are uncorrelated, i.e., if $\sigma_{\ell m} = 0$, $\ell \neq m$, then each observation can be included independently and equation 3.9 reduces to the following convenient form

$$(L_{ij})_k = (L_{ij})_{k-1} + \sigma_k^{-1}\ (H_i H_j)_k,\ i=1, \ldots ,n\ ;\ j=1, \ldots ,n \tag{3.10}$$

The remaining elements are obtained by noting that $L_{ij} = L_{ji}$ for all i and j. Using the symmetric property of L_ℓ can have a significant effect on the computation speed. Furthermore, by forcing symmetry through requiring that $L_{ji} = L_{ij}$, the matrix L_ℓ is guaranteed to be symmetric and positive definite.

4. Sequential Estimation Algorithms

The algorithms given in equations 3.1, 3.2 and 3.3 are referred to as batch estimation algorithms since all of the observations are reduced before the estimate can be obtained. Equation 3.1 can be used as the starting point for developing a sequential estimation algorithm in which the observations can

be included sequentially as they are obtained.

The following matrix identity is a fundamental relationship between the batch and sequential estimation algorithms (see TAPLEY (1973))

$$P_k = \left(H_k^T R_k^{-1} H_k + \bar{P}_k^{-1}\right)^{-1} = \left(I - K_k H_k\right)\bar{P}_k \qquad (4.1),$$

where

$$K_k = \bar{P}_k H_k^T \left(H_k \bar{P}_k H_k^T + R_k\right)^{-1} .$$

The $n \times n$ matrix P_k in equation 4.1 is the covariance matrix associated with the estimate $\hat{x}_k$. Note, in examining equation 4.1, that the first expression requires an $n \times n$ matrix inversion, while the second expression requires the computation of K_k. As can be seen by examining equation 4.2, the computation of K_k requires inverting a $p \times p$ matrix, where p is the dimension of the observations. If a single scalar observation is processed, then the computation of P_k would be obtained by a single scalar division. If the identity given in equation 4.1 is substituted into equation 3.1, it is a straightforward algebraic procedure to rearrange the results to obtain the following expression for the estimate of x

$$\hat{x}_k = \bar{x}_k + K_k\left(y_k - H_k \bar{x}_k\right) \qquad (4.3),$$

where

$$\bar{x}_k = \Phi(t_k, t_{k-1})\, \hat{x}_{k-1} ,$$

and

$$\bar{P}_k = \Phi(t_k, t_{k-1})\, P_{k-1}\, \Phi^T(t_k, t_{k-1}). \qquad (4.4).$$

Note that equation 4.3 obtains the estimate $\hat{x}_k$ as a linear combination of the predicted estimate $\bar{x}_k$ plus a weighting factor multiplied by the difference between the observation y_k and the predicted observation $\bar{y}_k = H_k \bar{x}_k$. The a priori or predicted value of the estimate and the associated a priori covariance matrix are given by equations 4.4. Equation 4.3 can be used to obtain the updated estimate when only a single observation is included by a single scalar division. Whereas, to include the single observation using the batch estimation algorithm would require that an $n \times n$ matrix be inverted. The procedure for computing the estimate with a sequential estimation algorithm can be summarized in the following equations:

Sequential Estimation Algorithm

Given : $X_{k-1} = X^*_{k-1}$, $\bar{x}_{k-1} = \hat{x}_{k-1}$, $\bar{P}_{k-1} = P_{k-1}$, y_i, $(i=k, \ldots, \ell)$

Compute :

1.

$$\dot{X}^* = F(X^*, t), \quad X^*(t_{k-1}) = X^*_{k-1}, \quad t_{k-1} \leq t \leq t_k$$

$$\dot{\Phi} = A(t)\Phi, \quad \Phi(t_{k-1}, t_{k-1}) = I \qquad (4.5).$$

2.

$$\bar{x}_k = \Phi(t_k, t_{k-1})\hat{x}_{k-1}$$

$$\bar{P} = \Phi(t_k, t_{k-1})\, P_{k-1}\, \Phi^T(t_k, t_{k-1}) \qquad (4.6).$$

3.

$$K_k = \bar{P}_k H_k^T (H_k \bar{P}_k H_k^T + P_k)^{-1}$$

$$y_k = Y_k - G(X_k^*, t_k) \tag{4.7}$$

4.

$$\hat{x}_k = \bar{x}_k + K_k (y_k - H_k \bar{x}_k)$$

$$P_k = I - K_k H_k \bar{P}_k \tag{4.8}$$

5.

$$\hat{X}_k = X_k^* + \hat{x}_k \tag{4.9}$$

6. If $k < \ell$, index k and return to 1.

Examination of the above algorithm indicates that as $P_k \to 0$, the estimation procedure will become insensitive to the observations and the estimate will diverge due either to errors introduced in the linearization procedure, computational errors, or errors due to an incomplete mathematical model. Modifications of the algorithm which account for the model errors are discussed by TAPLEY & INGRAM (1971; 1973).

In order to minimize the effects of the errors due to linearization assumptions, the extended form of the sequential estimation algorithm can be used. The extended or rectified sequential estimation algorithm can be obtained by noting that the best estimate of the state of the vehicle will usually be closer to the true trajectory than the initial reference trajectory. As a consequence, the current best estimate can be used to linearize the non-linear equations and to propagate the estimate between observation points. If the current trajectory is updated or rectified to include the local estimate of the error, i.e., if $X_{k-1}^* = \hat{X}_{k-1}$, then the value of x_{k-1} in equation 4.4 will be zero, and as a consequence, the predicted value $\bar{x}_k$ will always be zero. This follows since the state deviation is governed by a system of linear differential equations and if the initial conditions are zero, the solution, or the predicted value, will always be zero for any subsequent time point. Hence, if $\bar{x}_k$ is zero, the sequential estimation algorithm can be expressed in the following extended or rectified form:

Rectified Sequential Estimation Algorithm

Given : $\hat{X}_{k-1}, P_{k-1}, Y_k, \quad (k=1, \ldots, \ell)$

Compute :

1.

$$\dot{\bar{X}} = F(\bar{X}, t), \quad \bar{X}_{k-1} = \hat{X}_{k-1}$$

$$\dot{\Phi} = A(t)\Phi, \quad \Phi(t_{k-1}, t_{k-1}) = I \tag{4.10}$$

2.

$$\bar{P}_k = \Phi(t_k, t_{k-1})\, P_{k-1}\, \Phi^T(t_k, t_{k-1})$$

$$K_k = \bar{P}_k H_k^T (H_k \bar{P}_k H_k^T + R_k)^{-1} \tag{4.11}$$

3.

$$\hat{X}_k = \bar{X}_k + K_k [Y_k - G(\bar{X}_k, t_k)]$$

$$P_k = I - K_k H_k \bar{P}_k \tag{4.12}$$

4. If $k < \ell$, increase k by one and return to 1.

Note that the linear terms $\bar{x}_k = \Phi(t_k,t_{k-1})\hat{x}_{k-1}$ and $H_k\bar{x}_k$ which appeared in equations 4.6 and 4.8 are not present in equations 4.11 and 4.12. All higher order terms which were neglected in the Taylor series expansion used to linearize the original non-linear problem are zero also.

The symmetric property of the covariance matrix $\bar{P}_k$ can be used to reduce the computations in the same manner as described in the batch estimation algorithms. Note that the a priori covariance matrix $\bar{P}_k = \Phi(t_k,t_{k-1})\, P_{k-1}\, \Phi^T(t_k,t_{k-1})$ will satisfy the following matrix differential equation

$$\dot{\bar{P}} = A(t)\,\bar{P} + \bar{P}\,A^T(t), \qquad \bar{P}(t_{k-1}) = P_{k-1} \tag{4.13},$$

where $A(t) = \partial F(\bar{X},t)/\partial X$. Equations 4.13 can be used to replace the n × n matrix integration expressed by the second of equations 4.10 as well as the two n × n matrix multiplications implied by the first of equations 4.11. Furthermore, since $\bar{P}$ is symmetric, only $\{n\times(n+1)\}/2$ of the n × n equations in 4.13 must be integrated. The remaining elements in $\bar{P}$ are obtained by requiring that $(\bar{P})_{ij} = (\bar{P})_{ji}$, for all i,j. Note however, that the $\{n \times (n+1)\}/2$ system of equations must be integrated as a coupled system and this can lead to numerical difficulties. The solution for $\Phi(t_k,t_{k-1})$ can be obtained as n-independent solutions to a system of n-differential equations. Further discussions of these questions are given by TAPLEY (1973).

5. Least Sqaures Collocation Estimate

Consider the special case where a priori statistics on the initial state are given as $x_o \sim \{0,\bar{P}_o\}$; that is, the initial state estimate is $\bar{x}_o = 0$ and the associated state error covariance matrix is $\bar{P}_o$. Then the least squares estimate with a priori data, as given in equation 3.1, can be expressed as follows

$$\hat{x}_k = \left(H_k^T R_k^{-1} H_k + P_k^{-1}\right)^{-1} H_k^T R_k^{-1} y_k = P_k H_k^T R_k^{-1} y_k \tag{5.1}.$$

Note that in this expression, an n × n matrix must be inverted in order to obtain the estimate x_k. The state error estimate covariance matrix P_k can be written in the following equivalent form

$$P_k = \left(H_k^T R_k^{-1} H_k + \bar{P}_k^{-1}\right)^{-1} = \bar{P}_k - \bar{P}_k H_k^T \left(H_k \bar{P}_k H_k^T + R_k\right)^{-1} H_k \bar{P}_k \tag{5.2}$$

Note that the last expression in equation 5.2 requires inverting a p × p matrix where p is the dimension of the observation data vector which is to be reduced. Equation 5.2 is referred to as the fundamental identity, the Schurr identity, or the inside-out rule in various places in the literature. If the last expression in equation 5.2 is substituted for P_k in equation 5.1, the following result is obtained.

$$\hat{x}_k = \left(\bar{P}_k - \bar{P}_k H_k^T \{H_k \bar{P}_k H_k^T + R_k\}^{-1} H_k \bar{P}_k\right) H_k^T R_k^{-1} y_k \tag{5.3}$$

Algebraic re-arrangement leads to the following expressions

$$\begin{aligned}\hat{x}_k &= \bar{P}_k H_k^T \left(I - \{H_k \bar{P}_k H_k^T + R_k\}^{-1} H_k \bar{P}_k H_k^T\right) R_k^{-1} y_k \\ &= \bar{P}_k H_k^T \left(H_k P_k H_k^T + R_k\right)^{-1} \left(H_k \bar{P}_k H_k^T + R_k - H_k \bar{P}_k H_k^T\right) R_k^{-1} y_k \end{aligned} \tag{5.4}$$

Then, cancelling the two identical terms in the second bracket in equation 5.4, and noting that $R_k(R_k)^{-1} = I$, the following equivalent expression for the estimate of x_k is obtained

$$\hat{x}_k = \bar{P}_k H_k^T (H_k \bar{P}_k H_k^T + R_k)^{-1} y_k \tag{5.5}.$$

Equation 4.6 is identical to the expression given by MORITZ (1970) and by MORITZ & SCHWARZ (1972). This equivalence can be seen by noting the following similarities in notation

$$\bar{P}_k = C_{ss}, \quad H_k = A^T, \quad R_k = C_{nn}, \text{ and } \hat{x}_k = s \tag{5.6}.$$

Note that in these investigations Moritz & Schwarz point out the difficulty in obtaining $\hat{x}_k$ using equation 5.5 because the matrix to be inverted is of the same dimension as the observation data vector, i.e., it is a $p \times p$ matrix where $p >> n$. As a consequence, if the dimension of the data vector is much larger than the parameters to be estimated, equation 5.5 is an extremely inconvenient algorithm to use. On the other hand, the equivalent estimate for $\hat{x}_k$, given by equation 5.1, requires the inversion of only an $n \times n$ matrix, where n is the size of the parameter vector to be estimated. Note that either equations 5.1 or 5.5 may be used, depending on the size of the matrix to be inverted. For the case $p = n$, the computational requirements involved using either equation 5.1 or 5.5 will be identical. If $p < n$, then equation 5.5 should be used and if the a priori estimate of x_k, i.e., $\bar{x}_k$ is not zero, then for $p < n$, equation 4.3 should be used.

As a final remark, it should be noted that the expressions 5.1 through 5.6 indicate the equivalence between the least squares with a priori data and the least squares collocation proposed by Moritz & Schwarz, and the expressions demonstrate that the least squares collocation is a special case of the general least squares method. It is well known in studies related to minimum variance, maximum likelihood, and least squares estimation theory, that the estimate obtained will be dependent on the a priori data, and if a priori estimates of the initial values of the parameters are available, complete equivalence between methods can be established only when identical a priori data are used. Furthermore, the least squares estimate with a priori data will always give a different answer from that obtained with the conventional least squares estimate, as given by equation 3.3, i.e., the case when $\bar{P}_k = \infty$, since a different set of a priori statistics will be used in these two approaches.

6. Comparison of Batch and Sequential Estimation Algorithms

In the previous section, the algebraic equivalence of the sequential, the batch estimation and the least squares collocation algorithms have been shown. The extended sequential estimation algorithm which rectifies the trajectory at each observation point will be equivalent to the estimate obtained by these algorithms only if the data is iterated to obtain a converged solution for the trajectory. It is anticipated that the rectified sequential estimation algorithm will converge more quickly because the effects of linearization are minimized and, furthermore, that the estimate on any given iteration will be more accurate. As a corollary, the region of convergence for the extended or rectified sequential estimation algorithm will be larger than for the regular sequential estimation algorithm or for the batch estimation algorithm. It should be noted further that the batch estimation algorithm requires the inversion of an $n \times n$ matrix, where n is the dimension of the state vector, while for uncorrelated observations, the sequential estimation algorithm requires only a sequence of scalar divisions.

In order to compare the numerical performance of both the batch and sequential algorithms, a set of high-accuracy laser ranging observations of the Beacon Explorer-C satellite obtained by the Goddard Space Flight Center was used. The Beacon Explorer-C (BE-C) or Explorer 27 was launched with a Scout vehicle on April 29, 1965, from Wallops, Virginia, to study the ionosphere and the shape of the Earth. The orbit characteristics are 940 km perigee height, 1315 km apogee height, an eccentricity of 0.025, an inclination of 41.2°, and a period of 107.8 minutes. The BE-C was equipped with a laser retro-reflector array as well as beacons for atmospheric studies. The satellite is aligned with the Earth's magnetic field. The observations were obtained with the Goddard Space Flight Center tracking station (GODLAS) and a mobile station SENLAS located at Seneca Lake, New York, approximately 400 km due north of GODLAS. The set of observations was originally obtained in conjunction with an experiment conducted by D.E. Smith of Goddard Space Flight Center, aimed at measuring the Earth's polar motion (SMITH ET AL 1972b). In addition, the data have been used to evaluate the effect of solid Earth tides on the BE-C satellite (KOLENKIEWICZ ET AL 1973b). Of the approximately six months of data obtained by GODLAS and SENLAS, a sequence of four consecutive passes beginning September 2, 1970, was used in this investigation. This is the densest set of data obtained during the entire tracking period due mainly to favourable weather during these dates. The station locations are shown in figure 1, and the ground track for a typical four-pass sequence is shown in figure 2. The station co-ordinates for the study reported in this paper were those determined by SMITH ET AL (1972a), shown in table 1, where the height is that above the reference ellipsoid, where a_e = 6,378,155 m and f = 1/298.255.

T a b l e 1

Station Co-ordinates

Station	Geodetic Latitude ° ' "	Geodetic Longitude ° ' "	Height m
GODLAS	39 01 13.880	283 10 18.500	18.8
SENLAS	42 42 04.881	283 10 17.203	200.0

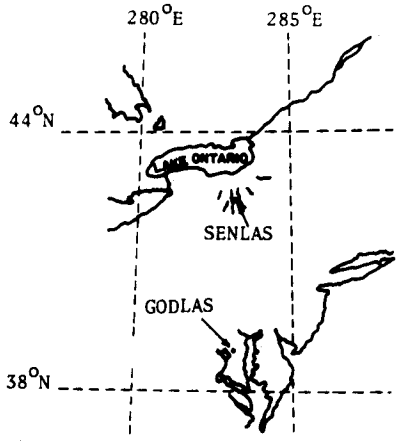

Figure 1. Tracking Station Locations (from SMITH ET AL 1972a)

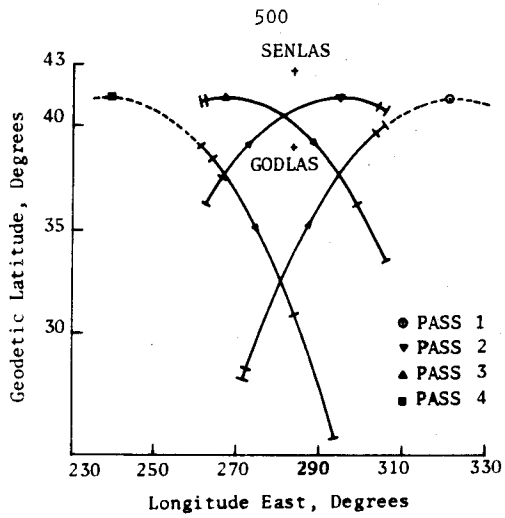

Solid Line Indicates Satellite Being Observed

Figure 2. Beacon Explorer-C Ground Tracks (From SMITH ET AL 1972a)

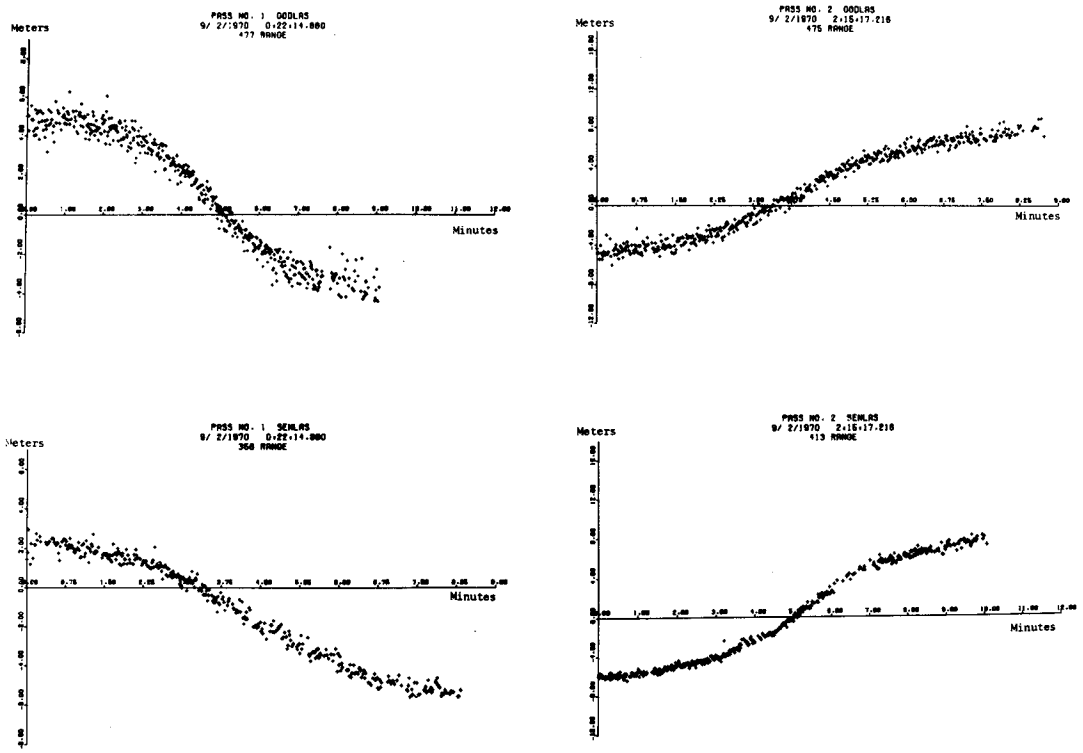

Figure 3a. Batch Processor Range Residuals for Passes 1 and 2

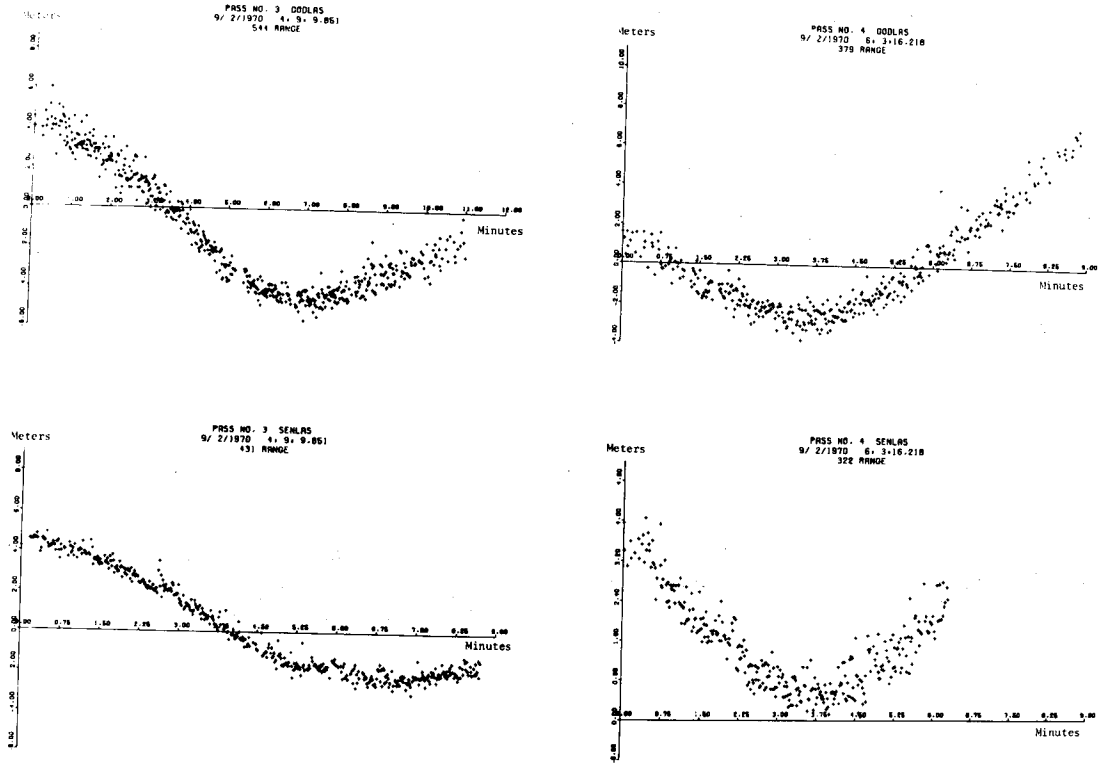

Figure 3b. Batch Processor Range Residuals for Passes 3 and 4

Figures 3a and 3b show the observation residual patterns obtained when the sequence of BE-C range observations are reduced using a batch processor which iterates to convergence. The residuals from the GODLAS station are shown at the top of each figure, while the SENLAS residuals are shown at the bottom. Note that the scatter has an amplitude of approximately 50 cm. Note also that the observation residual has a bias of approximately 8 m in amplitude. This bias is most likely due to the gravitational model used for the computation. The SAO Standard Earth II (GAPOSCHKIN & LAMBECK 1970) was used for this study. KOLENKIEWICZ ET AL (1973a), using the Goddard Earth Model I (GEM I) (LERCH ET AL 1972), obtained somewhat smaller residual patterns. However, since the specific accuracy is not of interest in this study, and since only the qualitative nature of the residuals are of interest, further consideration will not be given to the geopotential models. In addition, the effects of atmospheric drag were not included in this study. It has been determined in independent studies (SMITH ET AL 1972b) that drag does not significantly influence the motion of the BE-C satellite during the period studied. This fact is not surprising in view of the high altitude of the BE-C satellite and the short data arc examined (four revolutions). Further details on the nature of the numerical computations are given by SCHUTZ ET AL (1973).

In figures 4a and 4b, the observation residuals obtained during the first pass of the sequential estimation algorithm are shown. Due to the rapid convergence of the extended sequential estimation algorithm, the converged results are essentially identical to the results shown on the first iteration through the data. Note that the basic character of the observation residuals are quite different from the batch results during the first three passes, but they show a close agreement during the fourth pass. For instance, in the initial phase of the third pass, the model bias error is on the order of

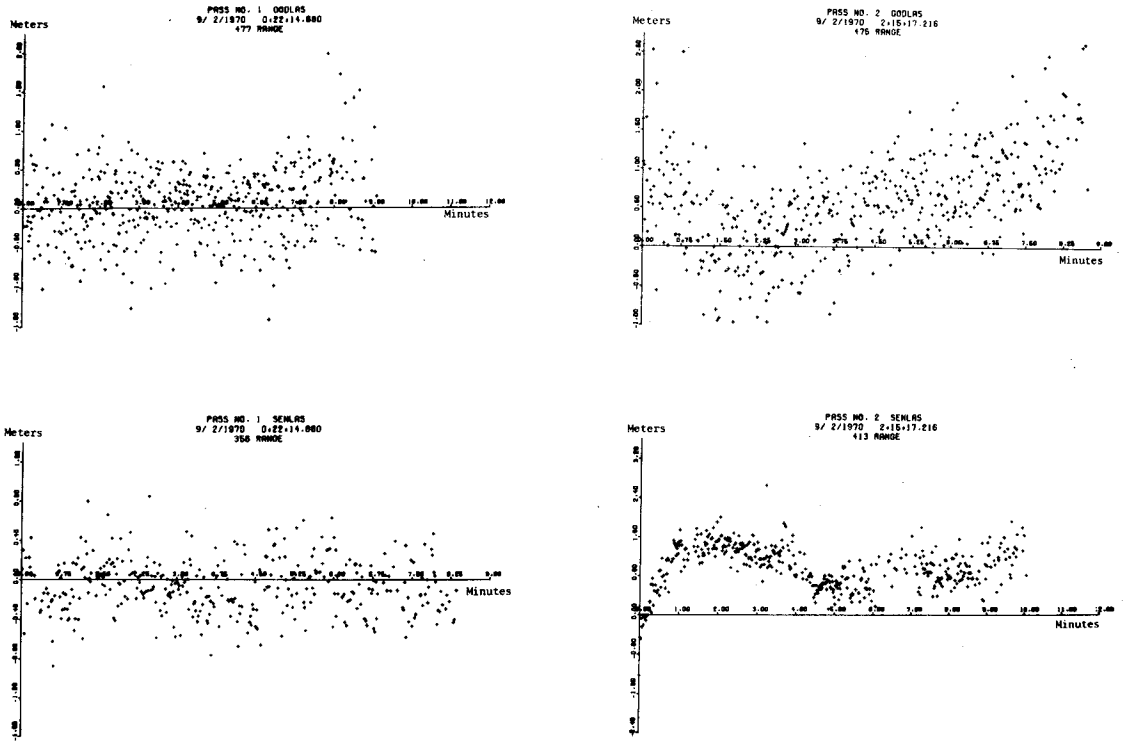

Figure 4a. Sequential Processor Range Residuals for Passes 1 and 2

33 m. The scatter about the bias is on the order of 50 cm for the GODLAS data and on the order of 35 cm for the SENLAS data, indicating that the actual observation accuracies are somewhat better than the formal observation accuracy of 1 m which is assigned to the data. It should be noted that the initial state estimate obtained on the first iteration agreed with the converged iteration estimate to less than 0.1m in position and less than 0.1 mm per second in velocity.

Although the observation residual patterns generated by the sequential and the batch estimation algorithms are quite different, as shown in figures 3 and 4, the agreement between the estimates can be evaluated by converting the estimates to a common epoch. The epoch used for the batch estimation algorithms was the initial time and a comparison can be made by taking the final sequence estimate, i.e., the estimate at the final time on the fourth pass, and integrating backwards through four passes to the initial time. The resulting state obtained by backward integration can then be compared with the estimate of the initial conditions obtained by the batch estimation algorithm. Table 2 shows the converged estimates of the conditions at the initial epoch obtained by the batch and sequential estimation algorithms. The a priori values for the initial covariance matrix $\overline{P}_o^1$, assumed elements of of 250,000 m^2 for the position component elements of the covariance matrix and 100 m^2s^{-2} respectively, for the elements of the velocity components. The matrix was assumed to be diagonal with no off-diagonal elements. Note that two iterations are required by the batch algorithm for less than 10cm accuracy in the converged solution for an a priori state which differs from the converged value by 75 m (case 1), whereas the extended sequential requires one iteration. If the a priori state error is larger, e.g. 600 m (case 2), then four iterations are required by the batch estimation algorithm to achieve convergence to this accuracy, while the extended sequential estimation algorithm still

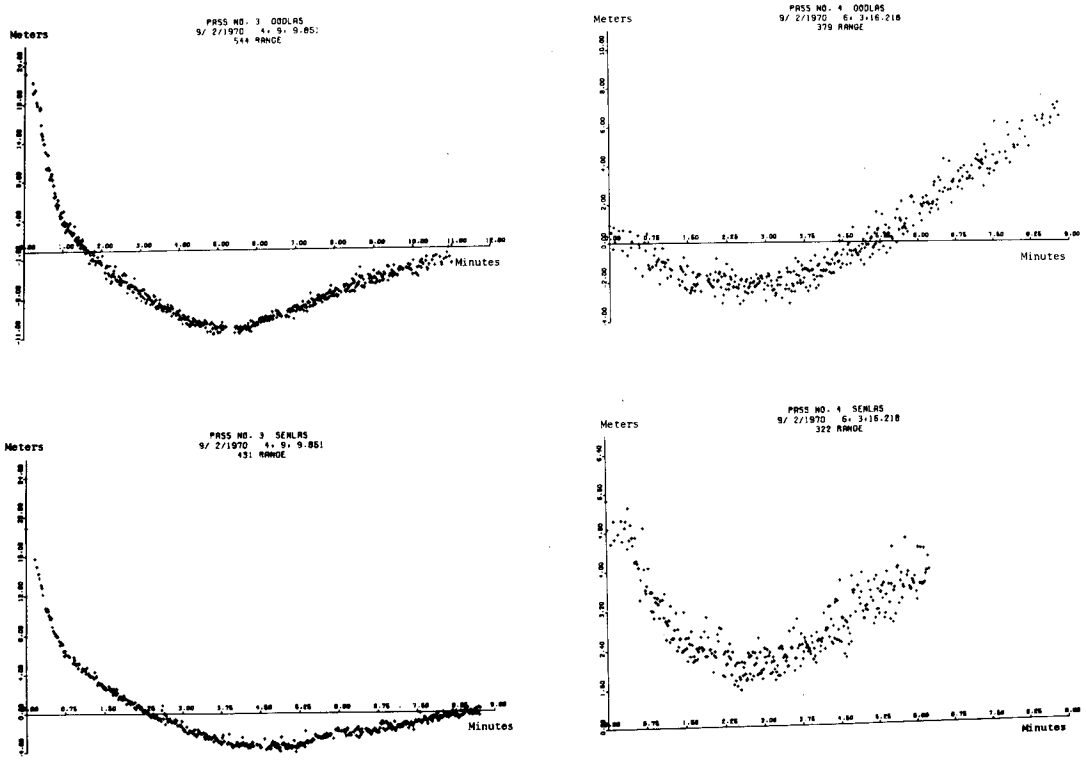

Figure 4b. Sequential Processor Range Residuals for Passes 3 and 4

achieves the same accuracy as before in one iteration. Further details on these computations are given by SCHUTZ ET AL (1973).

Comparison of the converged batch and extended sequential estimates of the initial state shows agreement to less than 10 cm in position and to less than 1 mm per second in velocity. A further question which should be considered relates to the accuracy of the predicted state; i.e., whether the disagreement in the epoch state estimates have a significant influence on the magnitude of the predicted error. An examination of the residual patterns during the first four revolutions shows no discernible difference in the residual pattern. Table 3 shows a comparison of the predicted residuals during the 42nd revolution using the predicted state obtained with the estimated sequential and batch initial conditions, as given in table 2. In addition, table 3 shows the difference in the predicted states during the 42nd revolution. Note that the predicted positions agree to less than 1 m, while the velocity components agree to less than 1 m sec^{-1}. From these results, it can be seen that the batch estimation algorithm and the extended sequential estimation algorithm yield converged estimates for the initial state which agree to less than 10 cm in position. Since the observations being reduced have a formal accuracy of 1 m, the estimates obtained by the two algorithms agree to well within the formal accuracy assigned to the observations.

The extended sequential estimator has a distinct advantage over the batch algorithms in problems

Table 2

Converged Epoch Estimates for Case 1 and Case 2 Initial Conditions

Estimator	CONVERGED SOLUTIONS X	Y	Z	$\dot{X}$	$\dot{Y}$	$\dot{Z}$	No.of Iterations for< 10 cm Converged Values
Case 1							
Batch $(\bar{P}_o = \infty)$	-1531394.255	-6310301.372	3397639.175	6610.939326	338.148095	3443.581299	2
Batch $(\bar{P}_o = \bar{P}_o^{-1})$	.255	.372	.175	.939326	.148095	.581299	2
Extended Sequential $(\bar{P}_o = \bar{P}_o^{-1})$	.201	.383	.280	.939336	.148192	.581172	1
Case 2							
Batch $(\bar{P}_o = \infty)$	-1531394.255	-6310301.372	3397639.175	6610.939326	338.148095	3443.581299	4
Batch $(\bar{P}_o = \bar{P}_o^{-1})$	.255	.372	.175	.939326	.148095	.581299	4
Extended Sequential $(\bar{P}_o = \bar{P}_o^{-1})$	.201	.383	.277	.939336	.148190	.581175	1

Table 3

Prediction for 42nd Revolution

Pass Begins:September 5 1970 2:8:31.6693 UTC; Estimation Epoch: September 2 1970 0:22:14.8805 UTC

Estimators	Time From Beginning of Pass (sec)	Batch Residual	Sequential Residual	Predicted State Differences (No Filtering) Based on Filtering 6 Hours Data Commencing Sept. 2 1970 ΔX	ΔY	ΔZ	$\Delta\dot{X}$	$\Delta\dot{Y}$	$\Delta\dot{Z}$
Converged Batch	0.	-49.9	-50.3	0.473	-0.186	0.063	0.000	0.000	0.000
- 1 Iteration	179.93271	-56.0	-56.0	0.452	-0.248	0.006	0.000	0.000	0.001
Extended Sequen-	335.93261	-4.7	-4.4	0.420	-0.296	-0.043	-0.001	0.001	0.000
tial									
Converged Batch	0.	-49.9	-50.7	1.020	-0.367	0.090	0.000	0.000	0.000
-Converged Exten-	179.93271	-56.0	-56.1	0.072	-0.506	-0.021	0.000	0.001	0.001
ded Sequential	335.93261	-4.7	-4.0	0.903	-0.615	-0.117	-0.001	0.001	0.000

Units: m & m sec^{-1}

involving the determination of constant parameters. If the state vector includes the satellite position and velocity as well as constant parameters, e.g., station co-ordinates, then the state estimate at each observation time provides the evolution with time of the estimate of those parameters. To illustrate this fact, figure 5 shows the evolution of the height above the reference ellipsoid for GODLAS obtained with the laser range observation of the BE-C satellite described previously. It can be seen that if the last half of data in, say, the third pass had

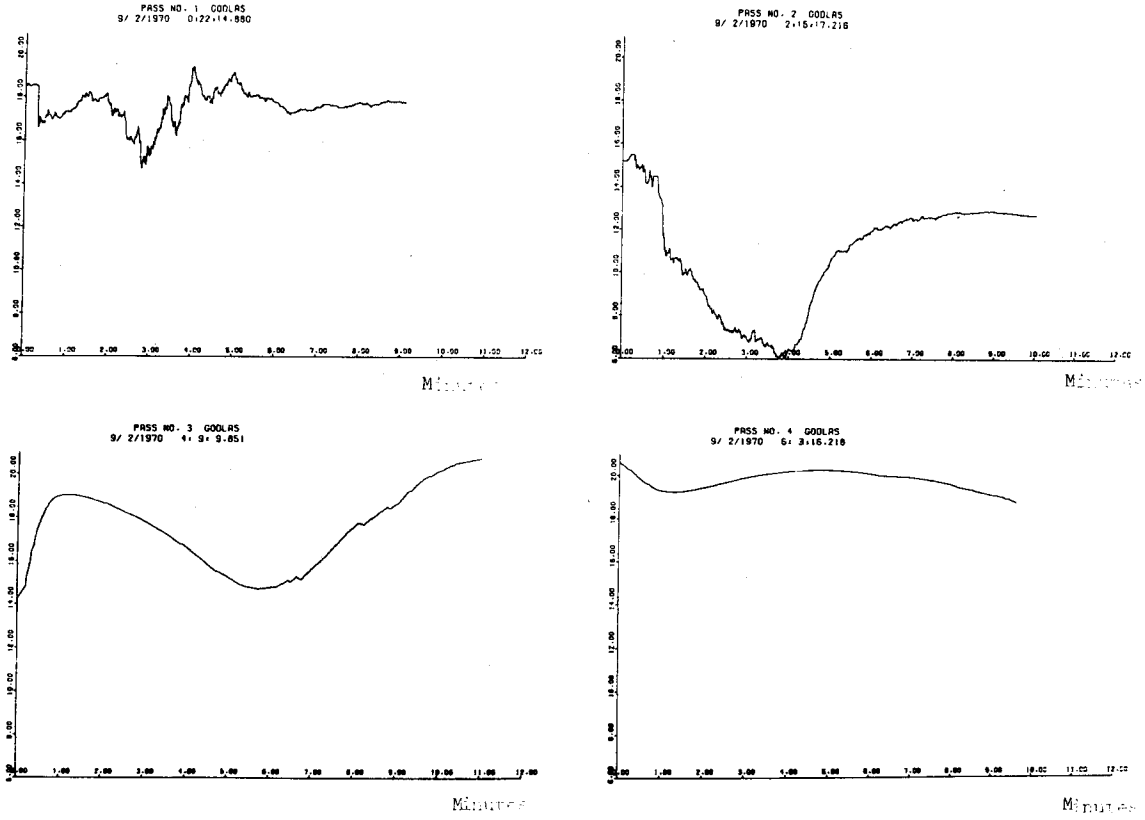

Figure 5. GODLAS Height Estimate in Metres from Extended Sequential Filter

not been included, the estimated height would have been considerably different from that at the end of the pass. The wide variations as well as the large observation residuals are, in fact, due to geopotential model errors. It can be shown that the second pass estimate is less affected by the model error and consequently the best estimate of the station co-ordinates will be obtained using data from two consecutive passes. Further details are given by SCHUTZ ET AL (1973b).

Finally, the question of the convergence properties of the estimation algorithms were studied. The results obtained do not show absolute bounds for the radius of convergence, but are intended to simply ascertain whether any significant differences exist. To generate specific initial conditions, each component of the converged batch estimate of the epoch was multiplied by a percentage factor. The a priori batch estimate with a priori information, diverges at 0.2%, whereas the extended sequential estimate diverges at 2.5%. It can be seen from figure 6 that converged sequential solutions are obtained with greater initial state errors It is important to note that the extended sequential estimate converges for a 3% initial error using the values adopted for $\overline{P}_o$ in this investigation, but diverged for larger values of $\overline{P}_o$ (SCHUTZ ET AL 1973a). This indicates the importance of the a priori covariance matrix. The results shown here indicate that the extended sequential algorithm has a significantly larger radius of convergence than the batch algorithms. The results also indicate the importance of the a priori information on the initial state errors in increasing the radius of convergence of both the batch and the sequential estimation algorithms.

7. Conclusions

The conclusions to be drawn from examination of the results presented in the previous section can be summarized as follows:

1. The least squares batch, sequential and least squares collocated algorithms are equivalent if the same a priori statistical information is used by each algorithm.
2. Using laser range observations of a near-Earth satellite obtained over four revolutions for which the observation accuracy is on the order of 50 cm, the estimates obtained with the batch and the extended sequential estimation algorithms are numerically equivalent to an order of 10 cm in position and 0.1 mm per second in velocity.
3. The extended sequential estimation algorithm which rectifies the trajectory at each observation point, converges to within 10 cm of the converged solution in one iteration, while the number of iterations required by the batch estimation algorithm is more dependent on the a priori data used.
4. The region of convergence for the extended sequential estimation algorithm appears to be approximately 10 times larger than the region of convergence for the batch estimation algorithm for the two station BE-C data examined in this study.
5. The extended sequential estimation algorithm provides the evolution of constant parameter estimates, such as tracking station co-ordinates and the effect of model error on the estimates can be determined directly.

From these above conclusions, the general conclusion can be reached that the sequential estimation algorithm is a useful approach to a number of problems in precision orbit determination for near-Earth and near planetary satellites. Where identical a priori data and identical modeling are included, the estimation accuracies agree to an extremely high precision with the batch results. However, the estimates are usually obtained with fewer iterations.

8. References

BRYSON, A.E. & HO, Y.-C. 1969. *Applied Optimal Control.* Blaisdell, Waltham Mass.

DEUTSCH, R. 1965. *Estimation Theory.* Prentice-Hall, Englewood Cliffs NJ.

FELLER, W. 1966. *Introduction to Probability Theory.* John Wiley, New York NY.

GAPOSCHKIN, E.M. & LAMBECK, K. 1970. 1969 Smithsonian Standard Earth II. *Smithsonian astrophys. Obs.Spec.Rep.*315, Cambridge Mass.

JAZWINSKI, A.H. 1970. *Stochastic Processes and Filtering Theory.* Academic Press, New York.

KALMAN, R.E. 1960. A New Approach to Linear Filtering and Prediction Problems. *J.Basic eng.*(ASME Trans.) 82D,35.

KALMAN, R.E. & BUCY, R.S. 1961. New Results in Linear Filtering and Prediction Theory. *J.Basic eng.*(ASME Trans.) 83D

KOLENKIEWICZ, R., SMITH, D.E. & DUNN, P.J. 1973a. Gravity Field Effects on Satellite Laser Ranging Data. *EOS (Trans.Am.geophys.U)* 54,126.

KOLENKIEWICZ, R., SMITH, D.E. & DUNN, P.J. 1973b. A Re-Evaluation of the Tidal Perturbation of the Beacon Explorer-C Spacecraft. *EOS (Trans.Am.geophys.U.)* 54,232.

LERCH, F.J., WAGNER, C.A., SMITH, D.E., SANDSON, M.L., BROWND, J.E. & RICHARDSON, J.A. 1972. Gravitational Field Models for the Earth (GEM 1 and 2). *Rep. X*-553-72-146, Goddard Space Flight Center, Greenbelt Md.

LIEBELT, P.E. 1967. *An introduction to Optimal Estimation.* Addison-Wesley, Reading Mass.

MORITZ, H. 1970. Least Squares Estimation in Physical Geodesy. *Rep.* 130,Dept. of Geodetic Science, The Ohio State University, Columbus Ohio.

MORITZ, H. & SCHWARZ, K. 1972. On the Computation of Spherical Harmonics from Satellite Observations. *Boll. geodes.e scienze affini* XXXII,185-200.

SCHUTZ, B.E., MCMILLAN, J.D. & TAPLEY, B.D. 1973a. *A Comparison of Estimation Methods for the Reduction of Laser Observations of a Near-Earth Satellite.* AAS/AIAA Astrodynamics Conference, Vail Colorado.

SCHUTZ, B.E., CONDON, S.P. & TAPLEY, B.D. 1973b. Sequential Filtering Applied to Short-Arc Analysis of Laser Tracking Data for Geodesy. *EOS (Trans.Am.geophys.U.)* 54.

SJOGREN, W.L., MULLER, P.M., GOTTLIEB, P., WONG, L., BUECHLER, G., DOWNS, W. & PRISLIN, R. 1971. Lunar-Surface Mass Distribution from Dynamical Point-Mass Solution. *The Moon.* 2,388.

SMITH, D.E., KOLENKIEWICZ, R. & DUNN, P.J. 1972a. Geodetic Studies by Laser Ranging to Satellites. in (HENRIKSEN, S.W. ed.) *The Use of Artificial Satellites for Geodesy.* William Byrd Press, Richmond Va.

SMITH, D.E., KOLENKIEWICZ, R., DUNN, P.J., PLOTKIN, H.H. & JOHNSON, T.S. 1972b. Polar Motion from Laser Tracking of Artificial Satellites. *Science* 178,405.

TAPLEY, B.D. & INGRAM, D.S. 1971. Orbit Determination in the Presence of Unmodeled Accelerations. *Proc.Second Symposium on Nonlinear Estimation Theory.* San Diego, Western Periodicals, Hollywood California.

TAPLEY, B.D. & INGRAM, D.S. 1973. Orbit Determination in the Presence of Unmodeled Accelerations. *IEEE Trans. on Automatic Control* AC-18,369-373.

TAPLEY, B.D. & SCHUTZ, B.E. 1972. *Estimation of Unmodeled Forces on a Lunar Satellite.* 23rd Congress of the International Astronautical Federation, Vienna.

TAPLEY, B.D. 1973. Statistical Orbit Determination. In (TAPLEY, B.D. & SZEBEHELY, V. ed.) *Recent Advances in Dynamical Astronomy.* D. Reidel, Dordrecht.

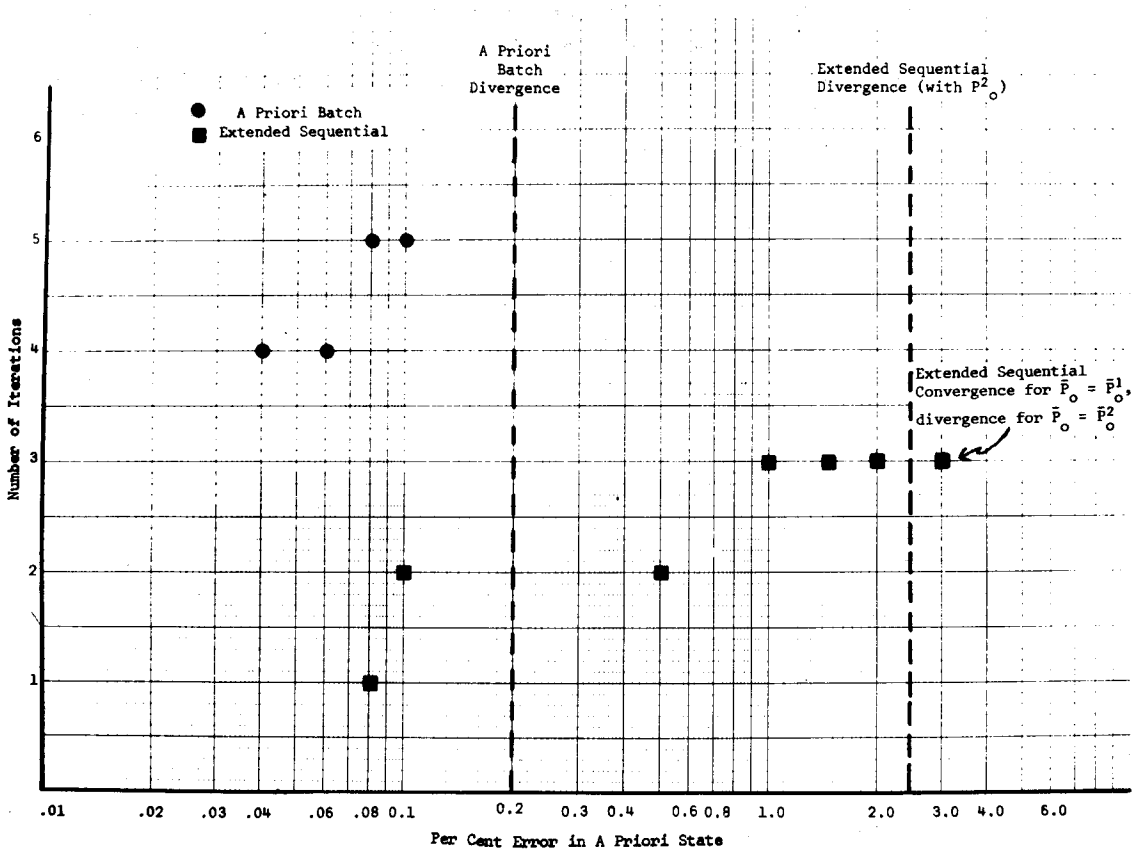

Figure 6. Radius of Convergence

9. Discussion

GRAFAREND: May I comment on some work I have done. I calculated the covariance function for the gravity anomalies, vertical deflections and the height anomalies, and assumed I had a Markov process for the gravity field. The procedure worked well for the gravity field and the vertical deflection field, but I had difficulties with the undulation fields as I had a singularity problem. So one basic assumption in the concept of approaching the Kalman-Bucy type of filter is that one has a Markov process. Did you assume a Markov process?

TAPLEY: No; as a matter of fact, the slide I used was a least squares algorithm. This made no assumption on the statistical nature. All I had really assumed was that the covariance matrices associated with the observation was a specified weighting matrix; and we get the least squares recursive formulation by just doing the manipulation shown. The Markov assumption is not essential. It is an essential assumption if one wants to use the Kalman-Bucy filter. But we are not required to assume that model. If one wants to do batch recursive computation, it is not an essential assumption.

KAULA: What type of covariance do you use in trying to model error sources which are not homogeneous but dying out with distance? It seems to me some sort of overlapping batch processing has to be done to get covariances more realistic than simple exponentials.

TAPLEY: Yes; we have considered several alternate representations. The exponential representation dies with time. It has the disadvantage that it is a rather artificial type approximation and will not predict very well. Alternate models which overcome this difficulty have been studied. But with the exponential model, if you want to go from one batch to another, then the exponential model has to be modified.

MELCHIOR, P.
Observatoire Royal de Belqique
Bruxelles
Belgium

Proc.Symposium on Earth's Gravitational Field & Secular Variations in Position (1973),509-521.

ON EARTH TIDE MODELS FOR THE REDUCTION OF HIGH PRECISION QUASI-RADIAL RANGE MEASUREMENTS

ABSTRACT

The problem of the Earth's deformation is one of spherical elasticity of the sixth order. The importance of Earth tides in astronomy and geophysics is emphasised by their relation to the precession-nutation and tesseral tide problems, the secular retardation of the Earth's rate of rotation due to the dissipation of energy in sectorial tides, the periodic variations in the rate of rotation due to zonal tides, satellite orbit perturbations due to variations in the Earth's potential, and the radial deformations in laser distance measurements.

The possibility that dynamical effects would be produced in the Earth's liquid core was pointed out by Poincare, and developed by Jeffreys, Vicente and Molodensky. An experimental confirmation is presented. The role of the Earth tide phenomenon in geodetic space research is also described, along with perturbing effects due to regional tectonic features. Instrumental developments are critical in the acquisition of precise data; the calibration problem is fundamental for a correct comparison with Earth models and the reduction of quasi-radial range measurements.

1. Text

We are concerned during this Symposium with the possibility of correcting the Earth-Moon or Earth-satellites distance measurements from the effects of tidal deformations with a precision of 1 cm.

The Earth-Tide theory as well as the observations use the well known Love numbers for a representation of all types of solid-Earth deformations.

The main difficulty in the interpretation of Earth tide observations in terms of these Love parameters is due to the indirect effects of the oceanic tides.

This very clearly appears in clinometric measurements, in satellite orbit perturbations and at a lower degree (but in any case not negligible) in gravimetric measurements.

The deformation component needed for correcting the laser distance measurements to the Moon and satellites is obviously the radial displacement. Unfortunately it cannot be measured directly with geodynamical instruments. The classical way to derive it consists of a combination of tidal gravity and tidal tilt measurements which respectively give the amplitude ratios to a rigid Earth described by the coefficients

$$\delta = 1 + h - \frac{3}{2} k \qquad (1)$$

and

$$\gamma = 1 + k - h \qquad (2).$$

Then

$$k = 4 - 2(\gamma + \delta) \qquad (3)$$

and

$$h = 5 - 3\gamma - 2\delta \qquad (4).$$

h is the elastic parameter of interest as it characterizes the static radial deformation

$$\xi = h \frac{W}{g} \quad ,$$

W being the tidal potential.

However it is not permissible to derive h as given by equation 4 if the observed quantitites γ, and δ are disturbed by important regional superficial effects like ocean loading, oceanic attraction and also thermic or barometric perturbations.

Thermic and barometric perturbations strongly affect the clinometric measurements but they can be eliminated fairly well if sufficiently deep stations (minimum 50 m depth) are installed and if periods of observations of a minimum of one year are available.

The problem of investigating and eliminating the ocean loading and the consequent change of potential and attraction, is quite different. There are three ways of progressing in that difficult question:

(a) By making observations with good and well calibrated instruments in the very centre of continents and from there, develop trans-continental profiles. Such profiles are now observed in the United States (by Kuo), Europe (by Melchior and Kuo, Honkasalo, Bonatz, Stuckenbroker, and others) and Asia (by Melchior and Ducarme).

(b) By making a computation of the ocean loading effects on the basis of a model of the crust constitution and a precise cotidal chart. This procedure is developed by J.T. Kuo, W. Farrel, D. Bower and B. Pertsev.

(c) By concentrating our attention not on the semi-diurnal components but on the diurnal ones. The diurnal tides have, by chance, very little amplitudes in the main oceans.

Indeed, it can be observed from table 1 that the γ factor which is extremely sensitive to oceanic indirect effects, remains very homogeneous and stable all across Europe for each of the three main diurnal components although the oceanic tides have important amplitudes and a very complicated distribution around the European coasts. But their diurnal components are always of very small amplitude. Therefore let us consider, as a first step, the results obtained for the diurnal waves. These waves are of primary importance in astronomy and geophysics: they are tesseral waves and are produced by the same part of the tidal potential as the astronomical precession and nutation (MELCHIOR 1973, volume 4).

For example:

K_1 wave is associated with the precession;
P_1 wave is associated with the semi-annual nutation; and
O_1 wave is associated with the fornightly nutation.

As they are of tesseral nature, liquid core dynamical effects can modify their amplitudes by resonance as demonstrated by Poincaré. This effect has been calculated for several Earth models by Jeffreys & Vicente, and by Molodensky.

The O_1 wave frequency, being far from the resonance frequency, can be considered as representing the pure static deformation.

As the O_1 wave has a period of $25^h\ 49^m$, it is out of the strong diurnal noise of 24 hour period and

Table 1

Dynamical Effects of the Earth's Liquid Core on the Tesseral Diurnal Waves

A. CLINOMETRIC MEASUREMENTS - HORIZONTAL EW COMPONENT.

	N	AMPLITUDE FACTORS K1	P1	O1	Q1	PHASE K1	P1	O1	Q1	INSTR
BELGIUM										
SCLAIGN.1 EW	2512	0.7519	0.697	0.6825	0.656	7.31	13.59	10.54	16.35	VM 1
SCLAIGN.1 EW	2512	0.0058	0.018	0.0081	0.042	0.44	1.48	0.68	3.66	VM 31
SCLAIGN.2 EW	544	0.7269	0.654	0.6883	0.730	8.82	13.56	8.82	11.70	VM 67
SCLAIGN.2 EW	544	0.0153	0.049	0.0203	0.103	1.21	4.34	1.69	8.10	VM 67
SCLAIGN.3 EW	1718	0.7697	0.740	0.6879	0.834	8.31	13.34	7.35	12.86	VM 55
SCLAIGN.3 EW	1718	0.0072	0.023	0.0098	0.051	0.53	1.80	0.81	3.48	VM 55
DOURBES 1 EW	3062	0.7544	0.724	0.6671	0.637	-2.24	-3.93	0.29	1.45	VM 8
DOURBES 1 EW	3062	0.0028	0.009	0.0039	0.020	0.22	0.73	0.33	1.81	VM 8
DOURBES 2 EW	2924	0.7545	0.725	0.6670	0.571	2.61	3.93	8.76	6.44	VM 28
DOURBES 2 EW	2924	0.0031	0.010	0.0042	0.022	0.23	0.80	0.36	2.21	VM 28
KANNE EW	1678	0.7520	0.688	0.7186	0.629	-7.85	-3.34	-14.49	-11.37	VM 72
KANNE EW	1678	0.0086	0.029	0.0117	0.061	0.66	2.41	0.93	5.55	VM 72
LUXEMBURG										
LUXEMBG. EW	410			0.6458				-5.39		VM 65
LUXEMBG. EW	410			0.0418				5.79		VM 65
WALFERD.1 EW	1176	0.7591	0.737	0.6816	0.637	-3.09	-1.38	0.88	-3.37	VM 42
WALFERD.1 EW	1176	0.0042	0.014	0.0057	0.030	0.33	1.11	0.49	2.75	VM 42
WALFERD.2 EW	870	0.7553	0.728	0.6395	0.602	-5.13	-7.34	-4.09	5.53	VM 42
WALFERD.2 EW	870	0.0058	0.019	0.0078	0.040	0.44	1.50	0.71	3.88	VM 12
WALFERD.3 EW	320	0.7338	0.764	0.6727	0.590	-4.21	-2.91	-7.60	-17.72	TSB 16
WALFERD.3 EW	320	0.0178	0.057	0.0241	0.121	1.40	4.26	2.05	11.79	TSB 16
CZECHOSLOVAKIA										
PRIBRBL. EW	846	0.7321	0.622	0.6917	0.693	-14.87	-19.22	-15.29	-21.97	VM 77
PRIBRBL. EW	846	0.0084	0.028	0.0112	0.058	0.65	2.59	0.93	4.83	VM 77
GERMANY										
BAD GRUND EW	312	0.7554	0.687	0.6787	0.636	6.79	5.39	11.75	14.90	VM 64
BAD GRUND EW	312	0.0082	0.027	0.0111	0.058	0.64	2.37	0.97	5.38	VM 64
TIEFEN. EW	1048	0.7330	0.793	0.6745	0.634	2.42	3.85	3.10	1.37	SW
TIEFEN. EW	1048	0.0098	0.028	0.0141	0.072	0.20	0.57	0.29	1.48	SW
AUSTRIA										
GRAZ EW	598	0.7359	0.826	0.6476	0.603	15.40	18.13	19.62	31.60	VM 44
GRAZ EW	598	0.0123	0.040	0.0166	0.087	0.96	2.80	1.47	8.30	VM 44
HUNGARY										
SOPRON EW	91	0.7558		0.6965	0.664	-1.40		5.27	2.94	VM 44
SOPRON EW	91	0.0122		0.0188	0.104	0.97		1.55	8.86	VM 44
SWEDEN										
DANNEM. EW	2954	0.7353	0.680	0.7100	0.712	-5.02	-8.09	-0.47	5.73	VM 38
DANNEM. EW	2954	0.0039	0.013	0.0054	0.027	0.31	1.09	0.43	2.21	VM 38
FINLAND										
LOHJA EW	780	0.7163	0.616	0.6983	0.716	0.35	7.56	2.83	3.68	VM 89
LOHJA EW	780	0.0085	0.029	0.0112	0.059	0.68	2.69	0.92	6.07	VM 89

VM VERBAANDERT - MELCHIOR QUARTZ PENDULUM
SW SCHWEYDAR PENDULUM
TSB TSUBOKWA ELECTROMAGNETIC PENDULUM

T a b l e 1 (Continued)

Dynamical Effects of the Earth's Liquid Core on the Tesseral Diurnal Waves

B. GRAVIMETRIC MEASUREMENTS - VERTICAL COMPONENT
****

RECENT TIDAL GRAVITY PROFILES /PROVISIONNAL RESULTS/
****

			FACT.AMPLITUDE				PHASE				INSTR
		N	K1	P1	O1	Q1	K1	P1	O1	Q1	
FUNDAMENTAL STATION FOR CALIBRATION											
BRUXELLES	V	606	1.1505	1.164	1.1641	1.176	0.23	-0.23	-0.01	-0.32	G 84
BRUXELLES	V	606	0.0017	0.005	0.0023	0.011	0.08	0.26	0.11	0.56	G 84
BRUXELLES	V	168	1.1482		1.1641	1.175	0.19		0.11	1.52	G 721
BRUXELLES	V	168	0.0033		0.0041	0.022	0.16		0.20	1.07	G 721
BRUXELLES	V	80	1.1499		1.1643	1.158	-0.18		0.06	-0.24	G 730
BRUXELLES	V	80	0.0040		0.0055	0.024	0.19		0.27	1.19	G 730
BRUXELLES	V	158	1.1500		1.1642	1.167	0.30		0.25	-0.44	G 804
BRUXELLES	V	158	0.0022		0.0032	0.017	0.11		0.15	0.84	G 804
BRUXELLES	V	50	1.1477		1.1642	1.152	-0.35		-0.14	-1.01	G 761
BRUXELLES	V	50	0.0025		0.0043	0.018	0.13		0.21	0.91	G 761
BRUXELLES	V	76	1.1489		1.1642	1.156	0.20		0.05	0.38	A 210
BRUXELLES	V	76	0.0039		0.0043	0.020	0.19		0.21	0.99	A 210
BRUXELLES	V	70	1.1503		1.1642	1.186	-0.23		-0.23	-0.20	L 258
BRUXELLES	V	70	0.0061		0.0069	0.031	0.30		0.34	1.51	L 258
BRUXELLES	V	80	1.1403		1.1643	1.160	0.71		0.21	-0.61	L 298
BRUXELLES	V	80	0.0037		0.0051	0.025	0.19		0.25	1.25	L 298
BRUXELLES	V	1694	1.1443	1.140	1.1643	1.113	-0.08	0.43	-0.50	-0.31	AA145
BRUXELLES	V	1694	0.0051	0.014	0.0075	0.038	0.25	0.72	0.37	1.99	AA145
BRUXELLES	V	916	1.1575	1.252	1.1616	1.202	-0.49	0.66	-0.42	-2.14	AA160
BRUXELLES	V	916	0.0089	0.024	0.0134	0.071	0.18	0.49	0.27	1.45	AA160
BRUXELLES	V	522	1.1456	1.190	1.1647	1.153	-1.02	-3.26	-0.27	-1.10	AA191
BRUXELLES	V	522	0.0052	0.017	0.0065	0.032	0.26	0.84	0.32	1.60	AA191
TRANS EUROPEAN PROFILE											
BIDSTON	V	200	1.1676		1.1572	1.166	0.36		0.17	-0.93	G 721
BIDSTON	V	200	0.0021		0.0030	0.016	0.10		0.15	0.77	G 721
CAMBRIDGE	V	60	1.1359		1.1366	1.257	-3.96		-0.14	0.98	G 721
CAMBRIDGE	V	60	0.0090		0.0133	0.065	0.46		0.67	2.98	G 721
HERSTM.	V	114	1.1409		1.1491	1.161	0.55		0.17	-1.91	G 721
HERSTM.	V	114	0.0023		0.0036	0.018	0.12		0.18	0.89	G 721
OOSTENDE	V	104	1.1375		1.1688	1.196	0.48		0.27	-0.33	G 730
OOSTENDE	V	104	0.0031		0.0043	0.021	0.15		0.21	0.99	G 730
WALFERD.	V	72	1.1524		1.1632	1.140	0.47		-0.05	-2.26	G 804
WALFERD.	V	72	0.0043		0.0056	0.031	0.22		0.28	1.55	G 804
WALFERD.	V	110	1.1399		1.1540	1.155	0.18		0.27	0.18	A 206
WALFERD.	V	110	0.0033		0.0044	0.021	0.17		0.22	1.04	A 206

Table 1 (Continued)

Dynamical Effects of the Earth's Liquid Core on the Tesseral Diurnal Waves

B. Gravimetric Measurements - Vertical Component

Recent Tidal Gravity Profiles / Provisional Results/

Trans European Profile (continued)

STRASBOURG	V	78	1.1342	1.1442	1.170	0.12	-0.36	-0.87	G 730
STRASBOURG	V	78	0.0021	0.0028	0.016	0.11	0.14	0.78	G 730
STRASBOURG	V	76	1.1372	1.1552	1.168	0.15	-0.04	3.52	A 206
STRASBOURG	V	76	0.0022	0.0033	0.021	0.11	0.17	1.00	A 206
CLERMONT/F	V	98	1.1569	1.1720	1.195	0.79	-0.09	-1.99	G 804
CLERMONT/F	V	98	0.0025	0.0033	0.016	0.13	0.16	0.78	G 804
GRASSE/NI	V	96	1.1439	1.1583	1.172	0.39	0.22	2.18	G 804
GRASSE CE	V	96	0.0039	0.0058	0.030	0.20	0.29	1.49	G 804
BORDEAUX	V	86	1.1567	1.1544	1.137	0.91	0.06	-1.22	G 804
BORDEAUX	V	86	0.0027	0.0045	0.021	0.14	0.22	1.05	G 804
CHUR	V	130	1.1470	1.1652	1.165	-0.09	0.30	-0.15	G 804
CHUR	V	130	0.0018	0.0028	0.013	0.09	0.14	0.64	G 804
TORINO	V	90	1.1199	1.1585	1.142	-2.21	-0.76	-0.91	G 730
TORINO	V	90	0.0036	0.0051	0.025	0.18	0.25	1.25	G 730
BONN	V	42	1.1438	1.1769	1.181	1.02	-0.70	0.68	A 210
BONN	V	42	0.0080	0.0141	0.086	0.41	0.69	4.20	A 210
HANNOVER	V	32	1.1446	1.1574	1.168	-0.46	-0.73	1.36	L 260
HANNOVER	V	32	0.0045	0.0077	0.039	0.23	0.39	1.89	L 260
FAEROE	V	78	1.1953	1.1452	1.138	1.34	1.38	-4.30	G 730
FAEROE	V	78	0.0041	0.0063	0.030	0.20	0.32	1.50	G 730

G GEODYNAMICS L LACOSTE ROMBERG
AA ASKANIA GS 11 A ASKANIA GS 15

can thus be derived with the highest precision by a harmonic analysis of the very long series of data available (tables 1A and 1B).

Moreover the theoretical amplitude of the O_1 wave is comparatively large as it is one of the main tidal waves (with M_2 and K_1), being :

in inclination	0''006;
in gravity	31 µgal; and
in geoid radial deformation	10 cm.

These amplitudes have to be multiplied by sin 2ϕ for gravity and radial deformation (ϕ is the latitude of the place considered) and by cos 2ϕ or sin ϕ for north-south or east-west inclination components.

We are therefore of the opinion that the excellent results obtained for O_1 allow us to derive the static value of Love parameters from Earth ground observations as follows:

$$\gamma(O_1) = 0.6788 \pm 0.0056,$$

$$\delta(O_1) = 1.1628 \pm 0.0008,$$

$$k = 0.317 \pm 0.011 ,$$

$$\boxed{h = 0.638 \pm 0.017} ,$$

and

$$k/h = 0.497 \pm 0.022.$$

It is to be observed that a theoretical check exists for the ratio k/h, which is:

$$k/h \leq \frac{3}{2} \frac{C}{Ma^2} = 0.499.$$

The equal sign corresponds to homothetic deformations (MELCHIOR 1973,volume 3-p.114).

For the other tesseral diurnal tidal waves, the Earth core dynamical effects have to be taken into account. The experimental results given in table 1 demonstrate with confidence their reality.

The following values of h are then derived:

For wave K_1 with period 23^h56^m $\quad h = 0.474 \pm 0.015$

For wave P_1 with period 24^h04^m $\quad h = 0.574 \pm 0.076$

(see table 2).

Table 2

Experimental Results

/28,568 days of registration/

	$\gamma = 1 + k - h$	$\delta = 1 + h - \frac{3}{2}k$	h	k	k/h
K1 165.555	0.7429±0.0045	1.1485±0.0028	0.474±0.015	0.217±0.011	0.458±0.026
P1 163.555	0.7054±0.0157	1.1550±0.0300	0.574±0.076	0.279±0.068	0.487±0.119
O1 145.555	0.6788±0.0056	1.1628±0.0008	0.638±0.017	0.317±0.011	0.497±0.022
Q1 135.655	0.6504±0.0207	1.1588±0.0095			
THEORETICAL MODELS					
**********					
MOLODENSKY MODEL 1					
K1 165.555	0.734	1.136	0.521	0.256	0.491
P1 163.555	0.699	1.154	0.594	0.294	0.494
O1 145.555	0.688	1.161	0.617	0.305	0.494
MOLODENSKY MODEL 2					
K1 165.555	0.730	1.142	0.528	0.258	0.489
P1 163.555	0.697	1.158	0.593	0.290	0.489
O1 145.555	0.686	1.164	0.614	0.300	0.488

γ: /1/ 14 STATIONS EQUIPPED WITH VM QUARTZ PENDULUMS-18056 DAYS OF REGISTRATION/

δ: /2/ 18 STATIONS EQUIPPED WITH GRAVIMETERS - 10512 DAYS OF REGISTRATION/

The fundamental parameter determining the resonance frequency in the diurnal tesseral waves is the *flattening* of the core which determines the possible movements with respect to the mantle.

As a first approximation one cannot do anything other than to adopt the hydrostatic flattening derived from Clairaut theory : 1/393 (BULLEN & HADDON 1973) which corresponds to a difference in the equatorial and polar semi-diameters of the core of 9 km, the equatorial radius best value being now determined as

$$R = 3483 \text{ km} \pm 3 \text{ km}.$$

It is to be hoped that an observed flattening will be very soon derived directly from seismology.

Very precise Earth tide measurements of very long duration could permit us to determine the resonance frequency and obtain more information concerning core motions.

Figure 1 shows that, according to a very elementary Molodensky model, this frequency is near to the ψ_1 line in the tidal spectrum.

Analysis of long records has recently been made to try to determine the amplitudes of the secondary waves ψ_1, ϕ_1, π_1, J_1, Q_1, M_1 and OO_1 in the tidal spectrum.

Unfortunately the mean square errors are still high as their theoretical amplitude is extremely small but some preliminary results are encouraging. Special careful analysis is being undertaken to improve these results.

Moreover it is to be noted that in all the European trans-continental gravity profiles, the phase of the O_1 wave is not significantly different from zero, even in the Faeroe Islands and at a near-shore coastal station like Oostende.

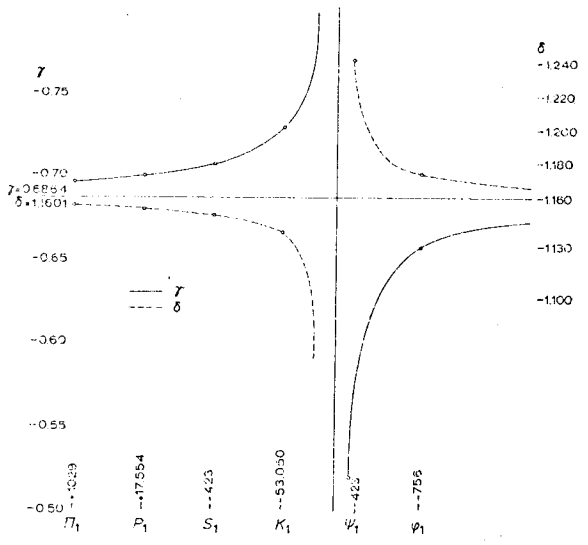

Figure 1.

2. Semi-diurnal Waves

The results of many stations are now available, e.g., see presentations at the IUGG Moscow General Assembly in 1971, and at the 7th International Symposium on Earth Tides at Sopron in 1973; also see tables 1 and 3. Only some very typical examples of the perturbations due to the loading and attraction effects of the oceanic tides will be given here: we have selected some coastal or insular stations, and compare the amplitude factors obtained for the diurnal O_1 wave with the main semi-diurnal wave M_2:

Table 3

Semi - Diurnal Tidal Waves as Given in Europe for the Vertical Component

		N	M2	N2	S2	K2	M2	N2	S2	K2	INSTR
			AMPLITUDE FACTORS				PHASE				
BRUXELLES	V	606	1.1865	1.178	1.207	1.154	3.16	2.52	-0.69	1.96	G 84
BRUXELLES	V	606	0.0013	0.006	0.003	0.008	0.06	0.31	0.13	0.41	G 84
BRUXELLES	V	168	1.1793	1.182	1.199		3.16	2.10	1.84		G 721
BRUXELLES	V	168	0.0023	0.012	0.004		0.11	0.59	0.19		G 721
BRUXELLES	V	80	1.1771	1.157	1.210		3.16	3.89	0.89		G 730
BRUXELLES	V	80	0.0030	0.014	0.006		0.14	0.67	0.28		G 730
BRUXELLES	V	158	1.1821	1.186	1.205		3.16	2.80	0.86		G 804
BRUXELLES	V	158	0.0017	0.009	0.003		0.08	0.45	0.16		G 804
BRUXELLES	V	50	1.1704	1.134	1.200		3.16	3.62	0.09		G 761
BRUXELLES	V	50	0.0029	0.012	0.008		0.14	0.60	0.40		G 761
BRUXELLES	V	76	1.1991	1.152	1.218		3.16	3.28	1.58		A 210
BRUXELLES	V	76	0.0032	0.015	0.005		0.16	0.74	0.25		A 210
BRUXELLES	V	70	1.1903	1.181	1.209		3.16	1.60	1.35		L 258
BRUXELLES	V	70	0.0046	0.022	0.007		0.22	1.06	0.36		L 258
BRUXELLES	V	80	1.1872	1.160	1.206		3.17	4.55	2.32		L 298
BRUXELLES	V	80	0.0031	0.015	0.006		0.15	0.75	0.30		L 298
BIDSTON	V	200	1.1600	1.188	1.184		0.99	0.15	1.02		G 721
BIDSTON	V	200	0.0017	0.009	0.003		0.09	0.43	0.16		G 721
CAMBRIDGE	V	60	1.2069	1.148	1.130		4.21	4.87	-0.20		G 721
CAMBRIDGE	V	60	0.0052	0.027	0.010		0.25	1.35	0.49		G 721
HERSTMONC.	V	114	1.1213	1.143	1.144		0.99	0.12	2.06		G 721
HERSTMONC.	V	114	0.0012	0.006	0.003		0.06	0.30	0.13		G 721
OOSTENDE	V	104	1.0753	1.085	1.139		4.61	0.77	4.65		G 730
OOSTENDE	V	104	0.0025	0.012	0.005		0.13	0.61	0.24		G 730
WALFERD.	V	72	1.1867	1.173	1.192		2.37	3.19	0.93		G 804
WALFERD.	V	72	0.0035	0.020	0.006		0.17	0.98	0.30		G 804
WALFERD.	V	110	1.1854	1.184	1.192		2.47	3.03	1.12		A 206
WALFERD.	V	110	0.0022	0.011	0.004		0.11	0.53	0.20		A 206

T a b l e 3 (Continued)

Semi - Diurnal Tidal Waves as Given in Europe for the Vertical Component

STRASBOURG	V	78	1.1693	1.154	1.189	1.94	2.37	1.52	G 730
STRASBOURG	V	78	0.0018	0.010	0.003	0.09	0.50	0.15	G 730
STRASBOURG	V	76	1.1842	1.207	1.185	1.96	3.50	0.36	A 206
STRASBOURG	V	76	0.0022	0.013	0.004	0.11	0.61	0.20	A 206
CLERMONT/F	V	98	1.2038	1.202	1.217	3.85	2.26	2.30	G 804
CLERMONT/F	V	98	0.0014	0.007	0.003	0.07	0.32	0.13	G 804
GRASSE/NI	V	96	1.1816	1.159	1.191	2.47	1.78	1.63	G 804
GRASSE CE	V	96	0.0017	0.008	0.003	0.08	0.43	0.16	G 804
BORDEAUX	V	86	1.2044	1.137	1.230	7.36	7.67	4.42	G 804
BORDEAUX	V	86	0.0028	0.013	0.007	0.14	0.65	0.33	G 804
CHUR	V	130	1.1894	1.167	1.195	2.23	2.71	1.48	G 804
CHUR	V	130	0.0014	0.006	0.003	0.07	0.31	0.14	G 804
TORINO	V	90	1.1790	1.175	1.192	1.68	1.69	0.92	G 730
TORINO	V	90	0.0027	0.014	0.005	0.13	0.66	0.23	G 730
BONN	V	42	1.2025	1.189	1.231	1.85	1.68	-0.91	A 210
BONN	V	42	0.0075	0.044	0.018	0.36	2.12	0.86	A 210
HANNOVER	V	32	1.1801	1.191	1.187	1.29	3.43	-0.23	L 260
HANNOVER	V	32	0.0033	0.015	0.007	0.16	0.74	0.35	L 260
HANNOVER	V	32	1.1825	1.170	1.204	1.29	2.14	0.22	L 298
HANNOVER	V	32	0.0045	0.021	0.010	0.22	1.02	0.46	L 298
FAEROE	V	78	1.5770	1.494	1.470	0.15	3.46	-6.99	G 730
FAEROE	V	78	0.0059	0.027	0.013	0.21	1.02	0.49	G 730

1)	*Gravity Tide*	$\delta(O_1)$	$\delta(M_2)$
	Spitsbergen	1.12	0.57
	Faeroe	1.14	1.57
	Oostende (B)	1.17	1.07
	Kerguelen	1.17	1.00
2)	*Clinometric Tide*	$\gamma(O_1)$	$\gamma(M_2)$
	Sclaigneaux (B)	0.68	0.8
	Spitsbergen	0.62	5.5

Such results for M_2 cannot be directly interpreted in terms of Love numbers.

Corrections due to the oceanic effects must be calculated according to procedures described by several authors (FARREL 1972; BOWER 1970; KUO 1969). Then the corrected results available show a tendency of M_2 to agree with those previously described of O_1. However such a procedure will only be successful if we have at our disposal a correct model of the cotidal charts for all the oceans.

This is far from being the case and therefore J.T. Kuo proposes to solve the inverse problem; that

is, to try to improve these cotidal charts on the basis of shore and island solid Earth tide measurements. A first application of this technique has recently been presented by JACHENS & KUO (1973). But obviously very much has to be done to make progress in that way. Precise observations of Earth tides are needed in all parts of the world and not only, as at present, in some restricted areas (North America, Europe, Japan).

Trans-World tidal gravity profiles are just now expanded to build such a network which would serve as the reference for satellite mapping of the solid Earth and oceans.

Table 4 gives the semi-amplitude of radial deformation of the geoid corresponding to the 18 main waves. It must be observed that in practice, the maximum deviation will never reach the total of the amplitudes indicated as the diurnal components have sin 2ϕ as a factor, while the semi-diurnals have $\cos^2\phi$ as factor and the long period ones have $(1 - 3 \sin^2\phi)$ as factor.

The possible deformation of the crust has been computed for the experimentally obtained value of h : 0.638.

It shows that a precision of 5% could be sufficient actually to ensure a correction of the measurements precise to 1 cm. The calibration of the tidal instruments is presently precise to 1% or sometimes 0.5%, but systematic errors of 3% or so have sometimes been found and accordingly corrected. This problem of calibration cannot be underestimated (see Annex).

3. Conclusions

The main needs at present are:

1) A correct model of the Earth's core for the evaluation of resonance effects on diurnal tidal waves.

2) A correct model of the Earth's crust and the oceanic cotidal charts for the evaluation of semi-diurnal deformations.

3) Well calibrated instruments correctly installed in a world-wide net of Earth tide stations to check the model results.

4. Annex

Some Remarks Concerning Earth Tide Instruments

The tidal amplitudes are so small that much care has to be taken in the installation and the maintenance of the instruments to avoid systematic influences and to avoid a too high level of noise.

Unfortunately many instruments have not been installed in optimum conditions and the results obtained at these stations have to be discarded in a general analysis.

The criteria to be applied to check the quality of the stations are as follows.

1. *Gravimeters*

Amplitudes to be measured are between 1 µgal and 45 µgal; they must be installed in thermostatized underground rooms (depth from 2 to 3 m).

Levels insensitivity points must have been checked, calibrations must have been made every week and must show a fairly smooth linear change with time or no change at all.

Results of table 1B obtained with 11 different instruments at Bruxelles show the possible agreement to be obtained.

2. *Clinometers*

Amplitudes to be measured are between 0''0002 and 0''0090; they must be installed at a minimum depth of 50 m and completely isolated from any thermic influence including those due to weekly maintenance.

Table 4

Radial Deformations in Centimetres

H = 0.638			
	FREQUENCY	GEOID	CRUST
DIURNAL COMPONENTS		AMPLITUDE FACTOR SIN 2ϕ	
Q1	-13.3986609	1.93	1.23
O1	-13.9430356	10.08	6.43
M1	-14.4966939	0.79	0.50
P1	-14.9589314	4.69	2.99
S1	-15.0000020	0.11	0.07
K1	-15.0410686	14.18	9.05
J1	-15.5854433	0.79	0.50
001	-16.1391017	0.71	0.45
TOTAL		33.07	21.07
SEMI DIURNAL COMPONENTS		AMPLITUDE FACTOR $\cos^2\phi$	
2N2	27.8907130	0.61	0.39
N2	28.4397295	4.65	2.96
M2	28.9841042	24.30	15.50
L2	29.5284789	0.69	0.44
S2	30.0000000	11.30	7.21
K2	30.0821373	3.08	1.96
TOTAL		44.63	28.43
LONG PERIOD COMPONENTS		AMPLITUDE FACTOR /1-3 $\sin^2\phi$ /	
SA	0.0410668	0.31	0.20
SSA	0.0821373	1.95	1.24
MM	0.5443747	2.21	1.41
MF	1.0980331	4.19	2.67
TOTAL		8.66	5.52

They must be provided with an automatic calibration system and their calibration must show a fairly smooth linear change with time or no change at all.

Results of table 5 obtained in the same laboratory with different instruments show possible agreement or discrepancy obtained.

3. *For All Types of Instruments*

Diurnal waves results (K_1 P_1 O_1) must have have been published as they reflect particularly well the environment qualities.

5. References

BOWER, D.R. 1970. Some Numerical Results in the Determination of the Indirect Effect. (Presented to 6th Symposium on Earth Tides,Strasbourg) *Obs.R.Belg.Comm.A9,S.géophys.* 96,106-112.

BULLEN, K.E. & HADDON, R.A.N. 1973. The Ellipticities of Surfaces of Equal Density Inside the Earth. *Physics of the Earth and Plan.Int.* 7,199-202.

T a b l e 5
Comparison of Three Different Instruments at Walferdange Underground Laboratory

	N	K1	P1	O1	Q1	K1	P1	O1	Q1	INSTR.
WALFERD.1 EW	1176	0.7591	0.737	0.6816	0.637	-3.09	-1.38	0.88	-3.37	VM 42
WALFERD.1 EW	1176	0.0042	0.014	0.0057	0.030	0.33	1.11	0.49	2.75	VM 42
WALFERD.2 EW	870	0.7553	0.728	0.6395	0.602	-5.13	-7.34	-4.09	5.53	VM 12
WALFERD.2 EW	870	0.0058	0.019	0.0078	0.040	0.44	1.50	0.71	3.88	VM 12
WALFERD.3 EW	320	0.7338	0.764	0.6727	0.590	-4.21	-2.91	-7.60	-17.72	TSB 16
WALFERD.3 EW	320	0.0178	0.057	0.0241	0.121	1.40	4.26	2.05	11.79	TSB 16

	N	M2	N2	S2	K2	M2	N2	S2	K2	INSTR.
WALFERD.1 EW	1176	0.8771	0.949	0.730	0.763	-8.53	-4.83	-13.90	-12.40	VM 42
WALFERD.1 EW	1176	0.0020	0.010	0.004	0.012	0.13	0.64	0.31	0.90	VM 42
WALFERD.2 EW	870	0.9205	0.956	0.774	0.793	-9.71	-6.43	-13.96	-13.15	VM 12
WALFERD.2 EW	870	0.0021	0.011	0.004	0.013	0.13	0.68	0.33	0.97	VM 12
WALFERD.3 EW	320	0.8054	0.865	0.753	0.750	-8.94	-3.62	-13.13	-10.23	TSB 16
WALFERD.3 EW	320	0.0053	0.026	0.011	0.037	0.38	1.74	0.85	2.83	TSB 16
WALFERD.1 NS	1110	0.6261	0.662	0.630	0.626	-5.10	-5.16	-1.91	-1.57	VM 10
WALFERD.1 NS	1110	0.0028	0.015	0.006	0.017	0.25	1.28	0.51	1.50	VM 10
WALFERD.2 NS	1240	0.6556	0.695	0.635	0.643	0.18	-2.82	7.92	2.11	VM 56
WALFERD.2 NS	1240	0.0024	0.013	0.005	0.014	0.21	1.06	0.45	1.29	VM 56
WALFERD.3 NS	310	0.6041	0.645	0.747	0.677	-6.95	-14.26	4.22	-28.92	TSB 15
WALFERD.3 NS	310	0.0080	0.041	0.017	0.056	0.75	3.64	1.33	4.75	TSB 15

VM VERBAANDERT-MELCHIOR QUARTZ PENDULUM
TSB TSUBOKAWA ELECTROMAGNETIC PENDULUM
N NUMBER OF DAYS

FARREL, W.E. 1972. Deformation of the Earth by Surface Loads. *Revs.geophys. and space phys.* 10, 761-797.

JACHENS, R.C. & KUO, J.T. 1973. The O_1 Tide in the North Atlantic Ocean as Derived from Land-Based Tidal Gravity Measurements. *7th Symposium on Earth Tides.* Sopron.

KUO, J.T. 1969. Static Response of a Multilayered Medium Under Inclined Surface Loads. *J.geophys. Res.* 74,3195-3206.

MELCHIOR, P. 1973. *Physique et Dynamique planetaires, Vol. 3 et 4.* Vander, rue Defacqz 21, 1050 Bruxelles.

6. Discussion

SAKUMA: Presently it is believed that the velocity of gravitational waves is equal to the velocity of light, but this has not yet been proved. Do you think it might be possible to determine this value by measuring the phase of the Earth tides due to the sun? Because gravitational waves should take about eight minutes to the Earth from the sun.

MELCHIOR: This is a difficult question because of the precision of phase. We can barely investigate the diurnal wave in that case. The speed of the paper is one limiting factor. It is 2-3 cm per hour (or 3 mm per 6 minutes). It could be done. Tidal measurements do not use high speed recorders as we are mainly concerned with long period waves.

KAULA: Your paper does not mention the use of pressure sensors at the bottom of the oceans. What are the possibilities in this area?

MELCHIOR: I have no personal experience of these measurements, but I do know measurements are being made for the improvement of tidal charts at amphidromic points. But I have no personal comments.

LAMBECK, K.
Institut de Physique du Globe
Université Paris VI
quai Saint-Bernard 75230 Paris
&
Groupe de Recherches de Géodésie Spatiale
Centre National d'Etudes Spatiales
91 Bretigny sur Orge
France

Proc. Symposium on Earth's Gravitational Field & Secular Variations in Position (1973), 522-528.

DETERMINATION OF EARTH AND OCEAN TIDES FROM THE ANALYSIS OF SATELLITE ORBITS

1. Solid Earth Tides

The elastic deformation of the Earth due to the variable lunar and solar attraction has been reviewed most recently by SLICHTER (1972). Observations of these deformations provide estimates of the Earth's mean elastic parameters. If the potential of the attracting force U_n is harmonic in degree n, the elastic response is also assumed to be harmonic in degree n, and in the classical definition of LOVE (1909), (see also JEFFREYS 1962) the additional potential resulting from the deformation is defined at the Earth's surface R, as

$$\Delta U_n = k_n U_n(R)$$

or, at a point r exterior to the Earth, as

$$\Delta U_n(r) = k_n \left(\frac{R}{r}\right)^{n+1} U_n(R) = k_n \left(\frac{R}{r}\right)^{2n+1} U_n(r)$$

The principal tidal terms occur for degree 2. The harmonics of zero order give the zonal tides, the first order harmonics the diurnal tides and the second order harmonics the semi-diurnal tides. Similar definitions define the actual deformation at the Earth's surface. Thus the radial deformation at the surface is defined as $h_n U_n(R)/g$ (g is gravity at the surface) and the horizontal deformations are in longitude (λ) $\frac{\ell_n}{g} \frac{\partial U_n}{\partial \phi}(R)$, and in latitude ($\phi$) $\frac{\ell_n}{g \cos \phi} \frac{\partial U_n}{\partial \lambda}(R)$. The Love numbers h_n k_n ℓ_n are integral measures of the Earth's elastic properties and relate in a complex manner to such parameters as the density, bulk modulus and rigidity variations throughout the Earth. They present most satisfactory transfer parameters between complex theory on the one hand and refined measurements on the other hand, although their interpretation is not always free from ambiguity.

In their classical definition, the Love numbers define the response of a radially symmetric, perfectly elastic, Earth to the perturbing potentials. This theoretical response is now best determined from seismology where the elastic parameters can be measured directly as a function of depth. These calculations have been most recently performed by FARRELL (1972). This study, as well as earlier ones, showed that the Love numbers are not very sensitive to the choice of mantle model; an oceanic type upper mantle giving almost identical results as a continental type upper mantle. Thus, if the theoretical response corresponded to reality, there would be little value in observing the solid tides as they provide only an insensitive global measure of the elasticity of the Earth. Before the development of seismology, however, solid tide observations played an important role in establishing the existence of the dense and liquid core.

The theoretical response is strongly modified or influenced by the fluid parts of the Earth, and to a lesser extent by the Earth's anelastic properties. A modification of some interest is the possible resonance effect due to inertial coupling between the elastic mantle and fluid core as propounded by the theories of JEFFREYS & VICENTE (1957) and which predict, for some of the diurnal tides, a rapid change in the value of k_2 with frequency. Solid tide observations have until now, not been very successful in distinguishing between the variously proposed models mainly because the oceans perturb the tide observations (SLICHTER 1972; BLUM et al 1973). In any case, it would appear that these resonances may tell us more on how to solve an interesting mathematical problem rather than tell us about the physics of the coupling mechanism itself.

The Earth is not a purely elastic body, for if it were, it would still be vibrating under the combined effect of all the earthquakes since its origin. Energy is therefore dissipated, and in the case of the tidal problem this dissipation results in a slight delay in the response to the attracting potential. Observation of this lag is of greater intrinsic value than the Love numbers themselves as it provides a measure of the Earth's global imperfections in elasticity at the tidal frequencies and provides a key parameter in the understanding of the evolution of the Earth-Moon system. Observations of this lag have until now not been particularly conclusive also because the measurements are perturbed by the ocean tides.

2. Ocean Tides

Ocean tides have been reviewed recently by HENDERSHOTT & MUNK (1970) and HENDERSHOTT (1973). Long records of ocean tides exist along many of the world's coast lines and these are extremely valuable for predicting the tides locally. But such observations are very much influenced by the coastline configurations and the shallow coastal seas and they are hardly representative of the mid-ocean tides. The best observational data of the latter comes from island stations that are little disturbed by local sea floor topography and all such records show that the undisturbed tide is little more than a meter. The available island measurements do not suffice for establishing the global pattern accurately, and the recent development of pressure tide gauges for measuring the tides in the open sea have made no impact yet on the global tide solutions. Our present knowledge of the open ocean tides comes from the more or less complete solutions of the Laplace tidal equations and a number of solutions for the M_2 tide (the principal semi-diurnal lunar tide) have been published recently. PEKERIS & ACCAD (1969) give solutions assuming a rigid Earth with, as boundary conditions, an impermeable coastline and allowing explicitly for dissipation in shallow seas. HENDERSHOTT (1972) allows for the effect of the tidal yielding of the solid Earth on the ocean tide and also attempts to evaluate the effect of the Earth's deformation under the variable ocean load (see also FARRELL 1972). Hendershott's boundary conditions are that the tide must correspond to the observed coastal values and dissipation is allowed for by allowing flow normal to the coastlines. The solutions of PEKERIS & ACCAD and of HENDERSHOTT agree in many areas but important discrepancies exist in, for example, the Pacific Ocean, pointing to the need for both improved theory and for more observational data. The S_2 ocean tide (the principal semi-diurnal solar tide) has been computed by BOGDANOV & MAGARIK (1967). No numerical solutions appear to exist for the other semi-diurnal tides or for the diurnal tides, although DIETRICH (1944) gives empirical cotidal charts for the O_1 (a nearly diurnal tide of solar origin) and K_1 (also nearly diurnal and of solar and lunar origin) tides as well as observed aplitudes along the coastlines and for some island sites.

3. Solid - Ocean Tide Interaction

The importance of the ocean tide interference with the solid tide has been demonstrated by the variable results obtained from surface measurements (for example, KUO et al 1970; PERTSEV 1969; BLUM & HATZFELD 1970; BERGER & LOVBERG 1970; SLICHTER 1972). The ocean loading of the continents appears to perturb all tide measurements, even those in the middle of the continents and although local tides are oftem most important (for example, LAMBERT 1970) even very distant tides will contribute to the observed combined tide (KUO et al 1970; PERTSEV 1969). In general, the ocean tides are not well enough known to be able to correct for this loading and improvements in the solid tide studies can only come about if there is also an improvement in our knowledge of the ocean tide (HENDERSHOTT & MUNK 1970). We cannot separate fully, at present, the fluid and solid tides through lack of mathematical completeness of the ocean tide solutions and through lack of global observational ocean tide data in particular for the components other than the principal components. Progress in interpreting the solid tidal measurements in terms of phase lags, resonances or geological variations, can only be achieved by a concomitant progress in ocean tide solutions. It is possible to use the Earth tide measurements as constraints in these solutions in the sense that any departures from a theoretical response can be used as an integral of the ocean tide. The value of such constraints still has to be proved but in view of the numerical solutions extreme sensitivity to small changes in boundary conditions, it would seem probable that any additional constraints will be of value. The foregoing remarks are equally valid for tidal studies from terrestrial measurements as for tidal studies from satellite orbit analyses, the only difference being that the two provide different constraints and as such the two methods are entirely complementary (LAMBECK et al 1973; 1974).

4. Satellite Methods for Tidal Studies

The tidal potential $\Delta U(r)$ at the satellite causes an additional force function that has to be taken into account when the satellite's equations of motion are integrated. This potential introduces perturbations in the motion of close Earth satellites and KAULA (1964; 1969) has given the necessary formalism. The frequencies of these tidal perturbations are governed by the frequencies of the satellite motion around the Earth and the perturbing body's motion in space and the principal perturbations will tend to group around the principal terms in the lunar and solar motion. Thus the semi-diurnal M_2 tide will give perturbations with periods near fourteen days and the solar S_2 tide will give perturbations with periods near six months. Also, as the satellite measures the integral effect of the tidal potential, the longer the period of the perturbation, the larger will be its amplitude. Thus the S_2 tide even though on the Earth's surface it has less than one half the amplitude of the M_2 tide it will cause perturbations in the satellite motion an order of magnitude larger than the M_2 perturbations. In the special cases where the satellite parameters and the Sun's or Moon's elements combine so as to give very long period orbital perturbations, tides that are very small on the Earth can give rise to very large orbital perturbations. The amplitudes of the tidal perturbations are proportional to the Love numbers. For most discussions of the tides, only the potential component of degree 2 is considered as the others are small. In particular, at the satellite height the potential decreases rapidly with increasing degree due to the term $(R/r)^{2\ell+1}$ in $\Delta U(r)$. Thus with the satellite methods it is k_2 that is observed. The difference between the observed phase of the perturbation and the phase of the perturbing potential assuming a perfectly elastic Earth, gives a measure of the phase lag. This lag has a value of at most one or two degrees

and is very much more difficult to observe with confidence than k_2. Some typical periods and amplitudes of the tidal orbital perturbations are given in Table 1.

Due to the ocean-continent distribution and the variable sea floor topography, the ocean tides, when expressed in terms of spherical harmonics will contain all harmonics of degree zero to infinity but the convergence appears to be rapid (see the solution of HENDERSHOTT 1972). This tide generates a potential which is readily expressed by a surface density layer representation and which gives an additional term to the force function acting on the satellite. We would expect that this ocean tide would generate perturbations of the same frequency as the solid tide due to that term in the ocean tide expansion that has the same degree and order as the solid tide. In addition, we could expect further perturbations resulting from the other harmonics in the ocean tide expansion. But most of these further perturbations are of short period - near the period of revolution of the satellite about the Earth - and as such do not build up into measurable perturbations (LAMBECK et al 1973). If the tidal potential is of degree 2 and order m, then the principal ocean tide perturbations, having the same frequencies as the solid tide perturbations, are caused by the ocean harmonics of degree and order 2,m ; 4,m ; 6,m etc, with a rapid decrease in importance. Table 2 gives some orders of magnitude. In general, the ocean perturbations are equal to about 10% of the solid tide. One observes therefore, a combined solid-ocean tide. Or, if the perturbation in an element ε due to the principal lunar tide is written as

$$(\delta\varepsilon)_{st} = k_2 \phi \cos \gamma$$

the ocean tide perturbation with the same frequency γ is

$$(\delta\varepsilon)_{ot} = (C_{22} \psi_{22} + C_{42} \psi_{42} + C_{62} \psi_{62}) \cos \gamma$$

where the C are coefficients in the ocean tide expansion (LAMBECK & CAZENAVE 1973; LAMBECK et al 1974). We observe

$$(\delta\varepsilon)_{obs} = (k_2\phi + C_{22} \psi_{22} + C_{42} \psi_{42} + \dots) \cos \gamma$$

The factors ϕ and ψ depend on the orbital parameters and one could imagine that a separation of the k_2 and C is possible if different satellite orbits or different orbital elements are analysed. This is only partially true. The principal ocean term has exactly the same dependence on the orbital elements as the solid tide and a separation of k_2 and C_{22} is not possible. A separation of these terms from C_{42} (and eventually from C_{62} if very precise tracking data becomes available) is possible and we can imagine an iterative procedure where we solve for

$$(k_2 + \frac{\psi}{\phi}22\ C_{22}),\ C_{42} \text{ and } C_{62}$$

and introduce the last two parameters as constraints in the solution of the Laplace tidal equations and compute the value C_{22} and hence k_2. In exactly the same way, a separation of the phase lags resulting from the solid Earth and the oceans is not possible from the analysis of tidal perturbations alone and we can again envisage the above iterative approach.

5. Results

Love numbers have been estimated from orbital perturbations by KOZAI (1968), NEWTON (1968), ANDERLE (1971), DOUGLAS et al (1972), SMITH et al (1973) and LAMBECK et al (1974). Of these studies only the last considered the ocean tides. LAMBECK & CAZENAVE (1973) showed that the apparently aberrant results for Love numbers obtained by the various investigators resulted from their neglect of the ocean tide, and LAMBECK et al (1974) have applied the ocean corrections to the results of the earlier investigators to give a value for $k_2 = 0.306$ and a phase lag of 0.5 degrees (see Table 3). The latter leads to a mantle Q of about 60, a value in reasonable agreement with seismic results (LAGUS & ANDERSON 1968). The studies of LAMBECK & CAZANAVE (1973) and LAMBECK et al (1973; 1974) lead to the following conclusions:

i) There is an important interaction between Earth and ocean tides as observed from orbit analyses. Neglect of the latter tides can introduce errors in k_2 of as much as 15% and of several degrees in phase;

ii) the ocean tide models, even the comparatively well known M_2 tide, are inadequate for making the precise ocean corrections, particularly for the important diurnal tides;

iii) the solid Earth tidal parameters computed from the satellite orbits are not yet very conclusive, even when corrected for the ocean tides. This is in part due to ii) but also due to residual non-tidal perturbations remaining in the satellite orbit parameters and due to inadequate tracking data. Better results can be expected in the future if precise laser tracking data, well distributed in space and time, can be collected from the already existing satellites and from the new small and dense satellite to be launched by the Centre National d'Etudes Spatiales in 1974 for gravimetric and tidal studies;

iv) a complete separation of fluid and solid tides is not possible from the analysis of satellite orbits alone, but the ocean tidal parameters that can be estimated can be used as constraints in the numerical tide solutions. This is also the case for the surface measurements of the bodily tide but in the former case the constraints, being the harmonics of degree 2 and 4 (and possibly 6 in the future) are of a global nature whereas the surface measurements provide constraints on the regional tides;

v) the ocean tide effect on the satellite orbit is frequency dependent (due to near resonances between the forcing function and the free periods of the oceans) and as such one must analyse the satellite orbits for specific tidal terms rather than solve for a single parameter that will present some average effect as has been done by SMITH et al (1973) and DOUGLAS et al (1972) as this leads to results that have no clear physical interpretation even though they may describe well the orbital perturbations of a particular satellite. This frequency dependence also makes the approach through latitude dependent Love numbers (KAULA 1969) impractical.

6. References

ANDERLE, R. 1971. Refined geodetic results based on doppler satellite observations. *US Naval Weapons Laboratory, Technical Report. TR - 2889.*

BERGER, J. & LOVBERG, R. 1970. Earth strain measurements with a laser interferometer. *Science* 170,286.

Table 1
Amplitudes and Periods of Perturbations in the inclination of GEOS-1 and GEOS-2 due to some tidal Components

Satellite	Tide	Period (days)	Δi (arcsec)
GEOS-1	M_2	11.7	0.17
GEOS-1	S_2	55.7	0.40
GEOS-1	K_1	160.7	0.95
GEOS-2	M_2	15.3	0.30
GEOS-2	S_2	432.7	4.03
GEOS-2	K_1	255.1	1.04

Table 2

Amplitudes of the Orbital Perturbations in i and Ω due to the Second and Fourth Harmonics in the Ocean M_2 Tide and Compared with the Corresponding Earth Tide

		Inclination i			Ascending Node Ω			
		Earth Tide M_2	Ocean Tide M_2		Earth Tide M_2	Ocean Tide M_2		Period (days)
			Second Harmonic	Fourth Harmonic		Second Harmonic	Fourth Harmonic	
7010901	(PEOLE)	0''06	0''011	0''016	0''26	0''043	0''056	9
6503201	(BE-C)	0''16	0''025	0''017	0''19	0''032	0''002	10
6508901	(GEOS-1)	0''19	0''029	0''005	0''13	0''020	0''015	12
6406401	(BE-B)	0''31	0''051	0''009	0''12	0''019	0''018	13
6402601	(TRANSIT)	0''33	0''056	0''013	0''08	0''014	0''004	14
6800201	(GEOS-2)	0''32	0''052	0''005	0''15	0''025	0''023	15

Table 3
Summary of Results Obtined by Other Authors and Corrected for Ocean Tidal Parameters

Author	Satellite	Tidal	Element Analysed	k_2 Observed	k_2 Corrected	δ_2 Observed	δ_2 Corrected
Kozai	5900101	$K_1^m + K_1^S$	i	0.22	0.24	-5°5	-1°5
Kozai	6000902	$K_1^m + K_1^S$	i	0.31	0.34	1°3	3°7
Kozai	6206001	$K_1^m + K_1^S$	i	0.32	0.34	0°7	6°7
Newton	Mean of four Polar Satellites	M_2	i	0.27	0.30	1°5	-5°5
Newton		M_2	Ω	0.29	0.32	1°7	-5°6
Newton		S_2	i	0.34	0.36	1°6	-3°4
Newton		S_2	Ω	0.33	0.36	1°2	-3°8
Douglas et al.	6508901	$K_1 + S_2$	i	0.22	0.25		
	6800201	$K_1+S_2+P_1$	i	0.31	0.33		
Smith et al.	6502801	$K_1+S_2+P_1$	i	0.25	0.28	3°2	5°
Lambeck et al.	6800201	M_2	i + Ω	0.29			9°
		Arithmetic Mean			0.309		0°5

BLUM, P.A. & HATZFELD, D. 1970. Etude régionale de l'influence océanique sur l'inclinaison; Premiers résultats à la station de Moulis. *Comm. A-9, Ser.Geophys. 96. Obs.Roy.Belgique.* 102-105.

BLUM, P.A., HATZFELD, D. & WITTLINGER, G. 1973. Résultats expérimentaux sur la fréquence de résonance due à l'effet dynamique du noyau liquide. *C.R.Acad.Sc.Paris. Ser.B,* 277,241-244.

BOGDANOV, K.T. & MAGARIK, V.A. 1967. Numerical solutions for the world's semi-diurnal (M_2 and S_2) tides. *Dokl. Akad. Nauk SSSR, 172.* 1315-1317.

DEITRICH, G. 1944. Die schwingungssysteme der halb - und eintagigen tiden in den ozeanen. *Veroffentl. Meereskunde, Univ. Berlin.* A 41. 7-68.

DOUGLAS, B.C., KLOSKO, S.M., MARSH, J.G. & WILLIAMSON, R.G. 1972. Tidal perturbations on the orbits of Geos 1 and Geos 2. *NASA/GSFC Report X.* 553 - 72 - 475. Greenbelt, Md.

FARRELL, W.E. 1972. Deformation of the Earth by surface loads. *Rev.Geophys.Space Phys.* 10. 761-797.

HENDERSHOTT, M.C. 1972. The effects of solid Earth deformations on global ocean tides *Geophys. J. Roy.Ast.Soc.* 29. 389-402

HENDERSHOTT, M.C. 1973. Ocean tides. *Transactions American Geophysical Union.* 54. 76-86.

HENDERSHOTT, M. & MUNK, W. 1970. Tides. *Ann.Rev.Fluid Mech.* 21, 205-224.

JEFFREYS, H. 1962. *The Earth.* (4th ed.) Cambridge University Press.

JEFFREYS, H. & VICENTE, R.O. 1957. The theory of nutation and the variation of latitude. *Mon.Not.R.astr.Soc.* 117, 142-161.

KAULA, W.M. 1964. Tidal dissipation by solid friction and the resulting orbital evolution. *Reviews of Geophysics.* 2, 661-685.

KAULA, W.M. 1969. Tidal friction with latitude dependent amplitude. *Astron.Journ.* 74, 1108-1114.

KOZAI, Y. 1968. Love's number of the Earth derived from satellites observations. *Publ.Astron. Soc.Japan.* 20, 24-26.

KUO, J.T., JACHENS, R.C., EWING, H. & WHITE, G. 1970. Transcontinental tidal gravity profile across the United States. *Science.* 168, 968.

LAGUS, P.L. & ANDERSON, D.L. 1968. Tidal dissipation in the Earth and planets. *Phys.Earth Planet Interiors.* 1, 505-510.

LAMBECK, K. & CAZENAVE, A. 1973. Fluid tidal effects on satellite orbit and other temporal variations in the geopotential. *Bull.Groupe Recherches Géodesie Spatiale.* 7.

LAMBECK, K., CAZENAVE, A. & BALMINO, G. 1973. Solid Earth and fluid tides from satellite orbit analyses, in Veis, G.(ed). *The use of artificial satellites for geodesy and geodynamics.* Technical University of Athens. In press.

LAMBECK, K., CAZENAVE, A. & BALMINO, G. 1974. Solid Earth and ocean tides estimated from satellite orbit analyses *Revs.geophys.Space Phys.* 12 (May)

LAMBERT, A. 1970. The response of the earth to loading by the ocean tides around Nova Scotia. *Geophys.J.Roy.astr.Soc.* 19, 449-477.

LOVE, A.E.H. 1909. *Some problems in geodynamics.* Cambridge University Press.

NEWTON, R.R. .1968. A satellite determination of tidal parameters and Earth deceleration. *Geophys.J.Roy.astr.Soc.* 14, 505-539.

PEKERIS, C.L. & ACCAD, Y. 1969. Solution of Laplace's equations for M_2 tide in the world oceans. *Philos.Trans.Roy.Soc.*, London, Ser.A. 265. 413-436.

PERTSEV, B.P. 1969. The effect of ocean tides upon Earth tide observations. *Comm., A.9, Ser.Geophys.* 96, Obs.Roy.Belgique, 113-115.

SLICHTER, L.B. 1972. Earth Tides. In ROBERTSON, E.C.(ed.) *The Nature of the Solid Earth.* McGraw Hill, 285-320.

SMITH, D.E., DUNN, P.J. & KOLENKIEWICZ, R. 1973. Earth tidal amplitude and phase. *Nature.* 244. 498.

MUELLER, I.I.
Department of Geodetic Science
The Ohio State University
Columbus Ohio 43210
United States of America

Proc. Symposium on Earth's Gravitational Field & Secular Variations in Position (1973), 529-553.

EARTH PARAMETERS FROM GLOBAL SATELLITE TRIANGULATION AND TRILATERATION

Abstract

Results obtained from 159-station global satellite triangulation and trilateration (including Baker-Nunn, BC-4, PC-1000 camera observations, SECOR, C-Band radar and EDM distance measurements) indicate differences in the semidiameter and orientation of the Earth compared to results obtained from dynamic satellite solutions. Geoidal undulations obtained can be made consistent with dynamically determined ones at the expense of slight changes in the currently accepted parameters defining the gravity field of the level ellipsoid.

1. Introduction

The global triangulation and trilateration forming the basis of this paper was performed as part of the US National Geodetic Satellite Program. A summary of the networks involved in the adjustments reported here (solutions WN) is presented in table 1. The data for the MPS and BC networks was obtained through the National Space Science Center. The Defence Mapping Agency provided observations for the SECOR and the SA networks (Topographic Center and Aerospace Center respectively). The sources for the constraint information are listed in table 2. Figure 1 shows the combined network

Table 1

Basic Information on the OSU Solutions (Networks)

OSU Solution (Network)	No. of Stations	No. of Observations	No. of Constraints Used[8]					$^{6}\sigma_o$	[7]Reference
			Origin	Relative Position	Scale (Length)	Height	Directional		
[1]MPS	66	28,744	Inner	9	7	63	-	1.07	188
[2]BC	49	30,302	Inner	2	7	48	-	2.80	193
[3]SECOR	50	28,844	Inner	14	-	37	9	1.37	195
[4]SA	14	2,524	Inner	3	1	14	-	2.50	196
[5]WN	159	90,444	Inner	43	11	158	-	1.02	199

[1]MPS includes 14 PC-1000 stations, 15 MOTS-40 stations, 1 PTH-100 station, 7 C-Band stations, 6 European stations (8000 series), and 23 SAO stations (9000 series).

[2]BC includes all 49 stations of BC-4 Worldwide Geometric Satellite Network.

[3]SECOR includes 37 SECOR stations of the Equatorial Network and 13 collocated BC-4 Camera Stations.

[4]SA includes 9 PC-1000 stations of South American Densification Net and 5 BC-4 stations.

[5]WN includes all networks at [1], [2], [3], & [4], namely, MPS (less 1 C-Band Station 4742), BC, SECOR & SA.

[6]A posteriori standard deviation of unit weight.

[7]OSU Department of Geodetic Science Report No.

[8]No constraints imposed on station position.

Table 2

Summary of Constraint Types with the Source Information

Code	Constraint Type	Source (Agency)*
	Relative Position	
1	BC-4 - Baker-Nunn	SAO, NGS
2	BC-4 - SECOR	DMA/TC
3	BC-4 - BC-4	NGS
4	Others	OSU
	Height	
5	MSL (mean sea level heights)	CSC, NGS, NWL
6	Geoidal Undulations	OSU (RAPP 1973)
	Length (Chord)	
7	North America	NGS
8	Europe	NGS, DGFI
9	Africa	NGS
10	Australia	NGS, DNP
11	C-Band	NASA/Wallops Isl.

* CSC - Computer Sciences Corporation
NGS - National Geodetic Survey
DGFI - Deutsche Geodätisches Forschungsinstitut
NWL - Naval Weapons Laboratory
DMA/TC - Defence Mapping Agency Topographic Center
SAO - Smithsonian Astrophysical Observatory
DNP - Division of National Mapping, Australia

(WN). Different symbols indicate the various instruments utilized in the observations. Concentric symbols show collocated stations or nearby stations with relative positions from known geodetic surveys. The straight lines between some of the stations illustrate the location of the baselines.

2. Reference Ellipsoid, Origin and Orientation

The least squares adjustment of the observations was performed in terms of Cartesian co-ordinates of the tracking stations. The results are also converted into geodetic co-ordinates (latitude, longitude and height) referenced to a rotational ellipsoid of the following parameters:

$$a = 6\ 378\ 155.00 \text{ m} \quad ; \quad b = 6\ 356\ 769.70 \text{ m}.$$

The corresponding flattening is

$$f = 1/298.249\ 498\ 5 = 0.003\ 352\ 897\ 507.$$

The origin of the co-ordinate system (or the centre of the above *reference ellipsoid*) is free as determined through "inner" constraints explained in (BLAHA 1971). The orientation of the system is inherent in the optical observations, through the star positions in the SAO catalogue (referenced to the FK4 system) updated to their apparent positions at the epoch of observation, and through UT1, x and y (co-ordinates of the true pole with respect to the CIO) as derived by BIH. Thus the positive

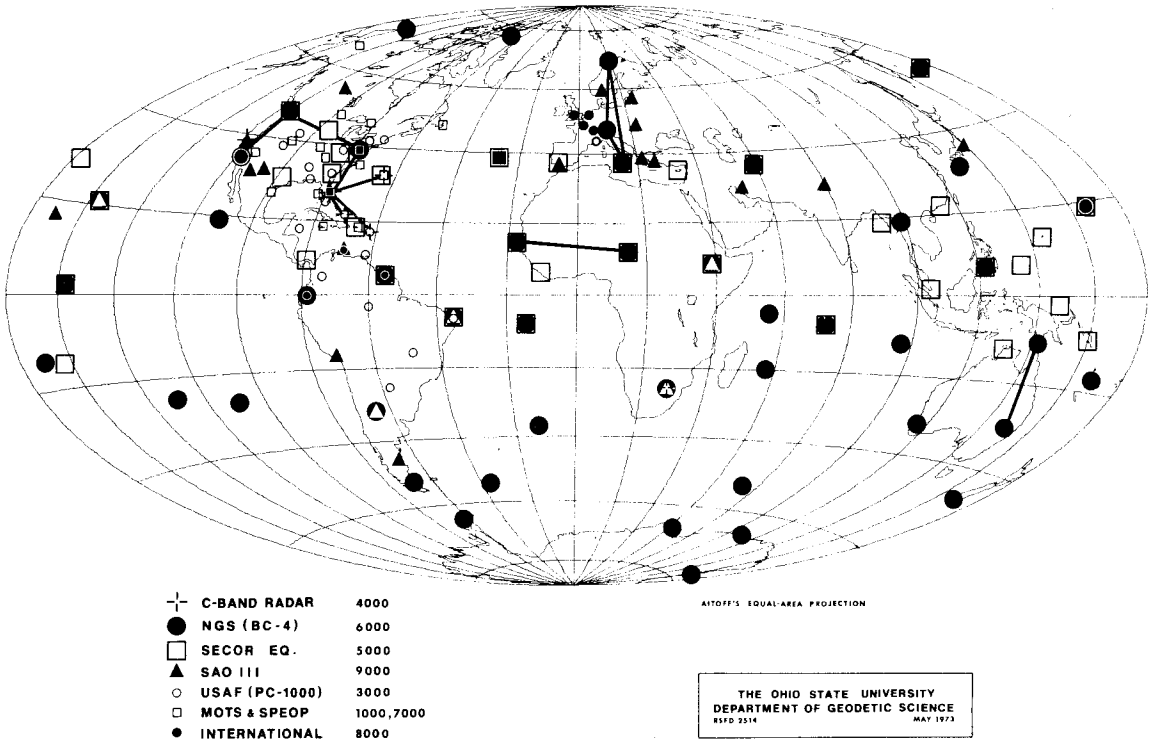

Figure 1. OSU Geometric Satellite Network (WN)

end of the axis u is in the direction of the Greenwich Mean Astronomical Meridian (and the zero geodetic meridian of the reference ellipsoid); the positive w axis passes through the Conventional International Origin (and coincides with the minor axis of the reference ellipsoid). The axis v completes the right handed co-ordinate system in the direction of the 90°(E) meridian, and with the u axis defines the plane of the average terrestrial (geodetic) equator.

3. Scale

The scale in the solution is defined through the dominating nearly 30,000 SECOR range observations, through the lengths of eight EDM (Geodimeter or Tellurometer) and three C-Band baselines, and also through a special procedure using constrained ellipsoidal heights.

3.1 SECOR Observations

The SECOR observations have an a posteriori standard deviation of ±4.1 m or approximately one part per million (MUELLER ET AL 1973b). The scale is propagated into the network through fifteen optical stations whose relative positions with respect to the nearby SECOR stations are maintained in the adjustment with their survey co-ordinate differences entered as weighted constraints.

3.2 Baselines

The available EDM and C-Band baselines are listed in table 3. The chord distances shown are entered in the adjustment as weighted constraints with weights computed from their estimated a priori

Table 3

Chord Constraints

Station-Station	Chord Distance (m)	$\sigma \times 10^6$ [1]	Source Code [2]
6002 - 6003	3 485 363.232	1.00	7
6003 - 6111	1 425 876.452	1.11	7
6006 - 6065	2 457 765.810	1.43	8
6016 - 6065	1 194 793.601	1.18	8
6063 - 6064	3 485 550.755	1.18	9
6023 - 6060	2 300 209.803	2.00	10
6032 - 6060*	3 163 623.866	2.00	10
6006 - 6016	3 545 871.454	1.00	8
3861 - 7043	1 531 562.9	1.33	7
4082 - 4050*	10 909 592	1.33	11
4082 - 4742*	7 362 142	2.00	11
4082 - 4740	1 593 106	2.00	11
4082 - 4081	1 230 691	2.00	11
4082 - 4061	2 288 026	2.00	11
4742 - 4280*	3 977 684	2.00	11

1 Used in computing the weights

2 Refer to table 2

* Rejected from the solution

standard deviations as listed in the table. The reasons for rejecting the east-west Australian tellurometer line (6032 - 6060) are explained below. Three C-Band lines were also rejected because of suspected errors in the survey co-ordinates of the terminal stations [Kauai (4742) in Hawaii and Pretoria (4040) in South Africa] needed to tie them to the nearest optical stations (9012 and 9002 respectively). Though these four lines were not constrained, at the end of the analysis, two of them (6032 - 6060 and 4082 - 4050) compared well with the lengths computed from the adjusted co-ordinates (see table 8). Thus the only station with survey co-ordinates in definite error is Kauai.

To get a feel for the quality of the EDM baselines listed in table 3, four preliminary adjustments of the BC network were performed in which the four longest scalars were individually constrained to their measured lengths, and their effect on the other (unconstrained) baselines investigated. The results are shown in table 4 in the form of the differences "adjusted - measured" lengths(Δd). Only independent lines longer than 2000 km are shown since the adjusted length of a short line, due to the geometry resulting from the high altitude of PAGEOS, the satellite used in the BC net, is not reliable. From the table it is clear that holding the east-west Australian line (3032 - 6060) to its measured value results in unreasonably larger differences of generally opposite signs than in any other case.

To verify the suspicion that something is wrong with the given measured value of line 6032 - 6060, a free adjustment was performed, in which both the origin and the scale constraints were "free" (BLAHA 1971). It is expected that the variances obtained from such an adjustment would primarily reflect the geometry of the situation. In other words, the variances of the various lengths would be due to the geometry of the network and free of the quality of the measured lengths. If the estimated variances of the measured lengths $(\sigma_d^{msrd})^2$ are added to those obtained from the free adjustment $(\sigma_d^{free})^2$, an estimate is obtained for the maximum expected variances of the length differences

Table 4

Adjusted - Given Lengths (m)

Solution	BC-8	BC-9	BC-10	BC-11
Line Fixed	6002 - 6003	6063 - 6064	6032 - 6060	6006 - 6016
6002 - 6003	0.0	-8.6	33.8	12.4
6006 - 6016	-13.3	-20.9	22.1	0.0
6063 - 6064	6.1	0.0	40.5	19.1
6023 - 6060	-9.5	-14.6	12.4	-0.7
6032 - 6060	-29.5	-36.6	0.0	-17.5
$\sum \Delta d$ (m)	-46.2	-83.6	108.8	13.3
$\sum \frac{\Delta d}{\text{length}} \times 10^6$	-2.89	-5.23	6.81	0.83

$(\sigma_d^{est})^2$. If an actual length difference is found to be 2 - 3 times greater than this estimated standard deviation, the measured length becomes suspect. The result of such analysis is shown in table 5.

From this table it is seen again that line 6032 - 6060 is out of bounds.

Another way of evaluating the effect of a scalar is through the semi-diameter of an ellipsoid best fitting the geoid resulting from a solution (see more of this in section 3.3). In this method, the undulations for each station are computed (ellipsoidal height - mean sea level height) and, after suitable transformations for shift of origin, are compared with some standard set of undulations, in this case with those in (PAPP 1973). The average difference N of these two sets of undulations is equivalent, with opposite sign, to the difference between the semi-diameter of the reference ellipsoid (a = 6 378 155 m) and that of the level ellipsoid of the same flattening to which the "standard" undulations refer.

Three sets of such comparisons were performed. One with the baselines constrained with weights corresponding to the standard deviations listed in table 3, one with all lines constrained to 1:3 M, and one with 1:30 M. Within each set, the adjustment was performed with all 6000 series EDM lines constrained and also without the line 6032-6060 (seven lines). The results are shown in table 6. In addition to the semi-diameter of the best-fitting level ellipsoid, the table also contains the

Table 5

Adjusted - Measured Lengths (Δd) from a Free Adjustment

Line	σ_d^{free} (m)	σ_d^{msrd} (m)*	$\sigma_{\Delta d}^{est}$ (m)	Δd (m)
6002 - 6003	4.2	3.5	5.5	-5.0
6006 - 6016	4.5	3.5	5.7	-17.2
6063 - 6064	4.4	4.1	6.0	2.4
6023 - 6060	4.4	4.6	6.4	-12.1
6032 - 6060	4.3	6.3	7.6	-33.1

* From table 3.

average standard deviations of a single co-ordinate ($\sigma^2 = \sigma_u^2 + \sigma_v^2 + \sigma_w^2$) as well as those of the heights (σ_H) and the ratios (adjusted - measured lengths)/lengths : $\sum(\Delta d/\text{length})$.

Table 6

Comparison of Seven- or Eight-Baseline Solutions

Solution	No. of Lines Constrained	Type of Constraint	$\sum \frac{\Delta d}{\text{length}} \times 10^6$	a (level ellipsoid) 6 378 000 + (m)	σ (m)	σ_H (m)
BC D12	8	As In	0.81	124.1 ± 11.0	6.3	8.1
BC D 2	7	table 3	0.19	118.4 ± 11.2	6.2	8.3
BC D 7	8	1:3 M	0.08	128.0 ± 10.8	6.1	7.7
BC D 8	7		0.04	119.7 ± 11.2	6.2	7.9
BC D 9	8	1:30 M	0.02	127.0 ± 10.7	5.9	7.2
BC D10	7		0.01	118.0 ± 11.2	6.0	7.3

From the table it is evident that though the varying type and number of constraints do not change significantly, the quality of the co-ordinates in the seven baseline solutions (D2, D8, D10) is better, as the adjusted lengths agree better with their measured values, than in the eight-baseline solutions (D12, D7, D9). It is also seen that the inclusion of the single east-west Australian line increases the semi-diameter by the unreasonable amount of 6 - 9 m (1 - 1.5 parts per million) in all cases.

On the basis of the results in tables 4 to 6 and also based on other calculations not reported here, the measured value of the Australian line 6032 - 6060 was rejected as a useful constraint.

The high standard deviations attached to the semi-diameters of the level ellipsoids in table 6 also indicates the questionable value of only seven or eight baselines in scaling a global network regardless of their individual quality. The inclusion of height constraints in the solution is an attempt for a better scale.

3.3 Use of Constrained Ellipsoidal Heights as Scalars

The use of geodetic (ellipsoidal) heights as weighted constraints as a contribution to the scale requires a more detailed explanation (figure 2). The height H above a geocentric reference ellipsoid

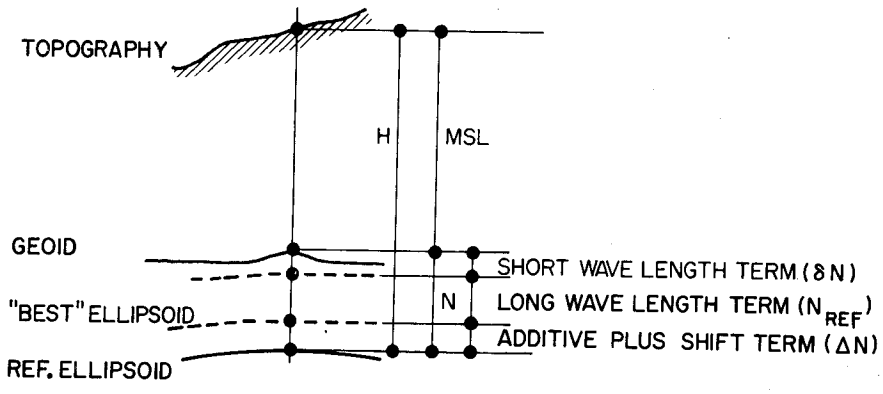

Figure 2. Height Components

has two main components:

- the orthometric (mean sea level) height (MSL); and
- the geoid undulation (N).

In this geocentric case, N consists of a long-wavelength component N_{REF}, a short-wavelength term δN, and an additive part Δa. The term N_{REF} generally corresponds to regional gravitational effects and can be computed for example from a truncated spherical harmonic series. The short-wavelength part δN corresponds to local gravity or mass disturbances and is generally not contained in the spherical harmonic representation. The additive part Δa is the so-called zero degree term which may exist due to the fact that the ellipsoid may not be of the same size (though it is of the same flattening) as the "best" (mean Earth) *level ellipsoid* to which the undulation N_{REF} is referenced. Since the N_{REF} undulations are, within reasonable limits, insensitive to the semi-diameter of the level ellipsoid, it is difficult to define a correct value for Δa. If the reference ellipsoid is *non-geocentric*, as is the case in this solution, an additional height term dH arises due to the "shift" of the origin (ellipsoidal centre) with respect to the geocentre. Thus the geodetic height may have the following components:

$$H = MSL + N \tag{1}$$

and

$$N = N_{REF} + \delta N + \Delta N \tag{2},$$

where (HEISKANEN & MORITZ 1967,p.207)

$$\Delta N = \Delta a + dH = \Delta a + u_o \cos\phi \cos\lambda + v_o \cos\phi \sin\lambda + w_o \sin\phi \tag{3},$$

Δa = a(level ellipsoid) - a(reference ellipsoid),

u_o, v_o, w_o are the co-ordinates of the geocentre with respect to the centre of the reference ellipsoid (origin); and

ϕ, λ are the geodetic co-ordinates of the station to which H refers.

In practice, at most satellite tracking stations, the quantity $MSL+N_{REF}$ is well known, and generally it constitutes the largest portion of the total height above the level ellipsoid. The additive plus shift term ΔN can be determined empirically through an iterative interpolation procedure as described later. Since $(MSL + N_{REF} + \Delta N)$ constitute the largest portion of the total height above the *reference ellipsoid* , it seems reasonable not to ignore this, admittedly partial, information on the height of the station and to include it in the adjustment as a constraint $(H_{CONSTR} = MSL + N_{REF} + \Delta N)$ with such a weight that the adjustment should be able to "pull out" the only remaining component, the short-wavelength term δN, together with possible errors in H_{CONSTR}. In this solution, the standard deviations used in computing the weights vary from ±2.5 m to ±8 m depending mostly on the location of the station, from the point of view of the extent of the available surface gravity observations in the area which was included in the spherical harmonic expansion for N_{REF} (RAPP 1973).

In trying to determine the "best" scale for the solution or, which is the same, the "best" additive term Δa, the first step is to establish the relationship between them. The problem differently stated is the determination of the relationship between the additive term and the semi-diameter of the "best" level ellipsoid to which the quantity N_{REF} refers. The meaning of the term "best" will be elaborated on later in this section. This is accomplished empirically from a set of solutions with height constraints containing different additive terms, from Δa = 0 to 30 m. The shift term dH initially is estimated from comparisons with various dynamic solutions, resulting in the

co-ordinates u_o, v_o and w_o needed in equation 3. These solutions result in sets of geodetic heights (H_{WNi}) above the reference ellipsoid and also in sets of undulations after subtracting the MSL:

$$N_{WNi} = H_{WNi} - MSL.$$

These undulations thus refer to the reference ellipsoid of a = 6 378 155 m, whose origin is set by the inner constraint. Disregarding the short-wavelength term, the relationship between the undulations N_{WNi} and N_{REF} is given by equations 2 and 3, from where, for any station and for the solution WNi:

$$(N_{WNi} - N_{REF}) - (\Delta a_i + u_{oi}\cos\phi\cos\lambda + v_{oi}\cos\phi\sin\lambda + w_{oi}\sin\phi) = 0.$$

Since the quantity $(N_{WNi} - N_{REF})$ is known at all stations, the parameters Δa_i, u_{oi}, v_{oi}, w_{oi} can be calculated (iterated) from least squares adjustments for each set "i". This is the same as determining the size (scale) and the origin of the level ellipsoid which fits best the geoid defined for a given set by the undulations N_{WNi}. Its size is

$$a_i = 6\,378\,155 + \Delta a_i$$

and its origin with respect to the origin of the reference ellipsoid is defined by the co-ordinates u_{oi}, v_{oi} and w_{oi}. After some iterations, these co-ordinates hardly change from solution (set) to solution (set), regardless of the initial selection of Δa; thus the relationship between the input additive term and the resulting semi-diameter, $a = f(\Delta a)$, becomes straightforward and linear.

This empirically determined relationship is shown in figure 3, as the dashed line drawn from the lower left corner towards the upper right. The corresponding ordinate is on the right hand side of the diagram. The line now allows either to pick the correct initial additive term which when used in the height constraints, would result in an a priori defined semi-diameter (scale), or to determine which semi-diameter (scale) would correspond to an a priori defined additive term. As an example, if the semi-diameter of the level ellipsoid best fitting the geoid was to be 6 378 142 m, the WN solution would require height constraints computed with an additive term of -15 m.

The next question, of course, is just how big should this desired semi-diameter be. Putting it differently, what criterion should be used to select the "best" scale ? If the scale was to be determined only from the EDM and C-Band baselines and/or the SECOR observations, these questions would not arise since the scale would be inherently defined. The use of weighted height constraints, as explained above, provides a unique tool to select the scale to fit some criterion. There could be several non-inclusive criteria, e.g.,

(1) The lengths of the EDM baselines as computed from the adjusted co-ordinates of the terminal stations should be
   - (a) exactly the same as the given lengths in table 3, or
   - (b) their differences should be within the limit of one (average) standard deviation,

   or (c) within a certain limit, e.g., 1:1,000,000, etc.

(2) Same as (1) but for the C-Band baselines.

(3) The scale difference as determined from the station co-ordinates of the WN solution and from the same co-ordinates of *some* dynamic solution should be
   - (a) exactly zero,
   - (b) within the limit of one standard deviation of the scale difference factor,
   - (c) within 1:1,000,000, etc.

(4) The scale difference as determined in (3) should be within a certain limit with respect to *all* the dynamic solutions.

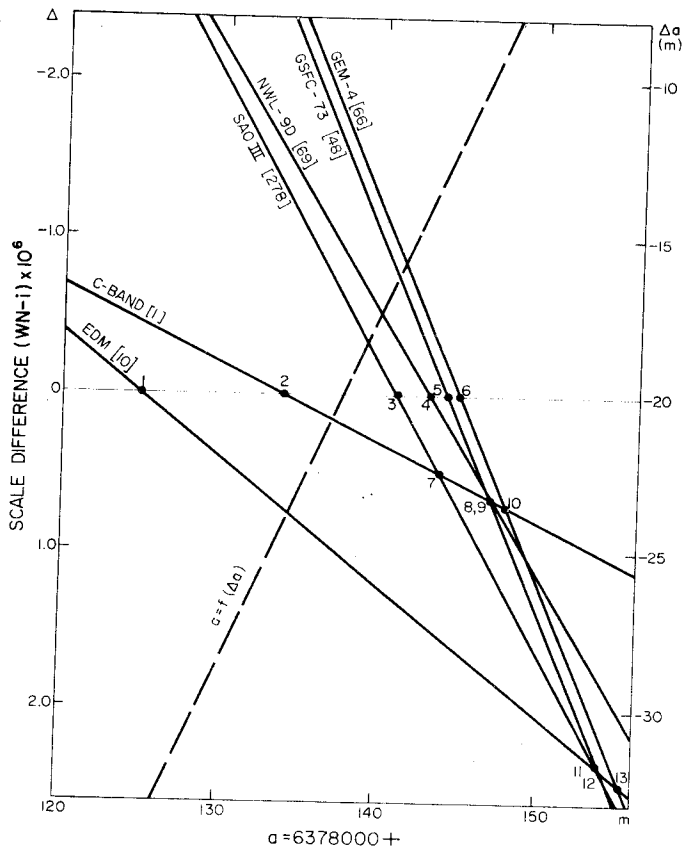

Figure 3. Determination of Scale

(5) The scale difference should be within a certain limit with respect to all the dynamic solutions *and* the EDM and C-Band baselines.

In order to be able to enforce any of the above criteria, first the relationship between the scale difference factor and the semi-diameter has to be established. This is accomplished again empirically by determining the scale differences between the different WNi solutions (used to determine the function a = f(Δa)) and the EDM and C-Band baselines and the dynamic solutions NWL-9D (ANDERLE 1973), SAO III (GAPOSCHKIN ET AL 1973), GEM 4(LERCH ET AL 1972), GSFC 73 (MARSH ET AL 1973). The method of calculating the scale difference factor is described in (KUMAR 1972), and the results are shown in figure 3 where, with the ordinate on the left hand side, the scale differences are plotted against the semi-diameters corresponding to the various Δa's used in the height constraints. The numbers on the lines indicate relative weights based on the uncertainties of the scale-difference determinations. It can be seen that the lines representing the geometric (EDM and C-Band) scale differences are much less well determined than the dynamic ones. As an example, the scale-difference factor between the WNi solution computed with Δa = -15 m (a = 6 378 142 m), and the solutions NWL-9D is -0.18×10^{-6}; the GEM 4 is -0.68×10^{-6} (the dynamic scales are larger). Also, the lengths of the EDM baselines from the adjustment differ from their directly measured values by 1.38×10^{-6} (the measured values are smaller).

The diagram is used by recognizing the importance of the various intersection points, marked by numbers. For example, point 1 illustrates the fact that if the semi-diameter of the level ellipsoid

was 6 378 125 m, the difference between the adjusted chord lengths and their given values would be zero; point 4 shows that with an a = 6 378 143 m, there would be no scale difference between WNi and NWL-9D. Fourteen similar intersection points are listed in table 7 with weights and interpretation.

From the table it is immediately clear that taking the weighted mean of the intersection points from the "geometric" scalars (points 1 and 2), the "best" semi-diameter is 6 378 125.8 m, while from the "dynamic" lines (points 3 - 6) it is 6 378 142.0 m. The difference of some 16 m, or about 2.5 parts in a million, seems to be real but unexplained at this time. The combined weighted mean from points 1 - 6 is 6 378 141.7 m; while from all the points (1 - 14), it is 6 378 142.7 m.

For the solution reported here (WN14), the criterion for the scale is (5) above; i.e., that the scale should correspond well to all geometric and dynamic information available at present. Based on the above numbers and on previously published parameters, a = 6 378 142 m was *selected*. This then requires an adjustment in which the scale is defined, in addition to the SECOR, EDM and C-Band observations, through height constraints with the initial additive constant $\Delta a = -15$ m. As can be seen from figure 3, at this semi-diameter, the maximum scale difference expected between WN14 and any of the dynamic solutions is about 0.8×10^{-6}, and with respect to the EDM about 1.4×10^{-6} or 1:700,000 which is about the average standard deviation of the EDM baselines. Using this scale, the resulting geoid undulations

$$N = H_{WN14} - MSL - \Delta N \qquad (4),$$

with

$$\Delta N(\text{metres}) = -13 - 23.2 \cos\phi \cos\lambda - 2.9 \cos\phi \sin\lambda + 2.7 \sin\phi$$

Table 7

Determination of Scale

Point	Interpretation	Weight	a (m)	Weighted Mean a (m)
1	WN = EDM	10	6 378 125.0	6 378 125.8 (from points 1 & 2)
2	WN = C-Band	1	6 378 133.7	
3	WN = SAO III	278	6 378 140.8	6 378 141.7 (from points 1 - 6)
4	WN = NWL 9D	69	6 378 143.0	
5	WN = GSFC 73	66	6 378 144.9	6 378 142.0 (from points 3 - 6)
6	WN = GEM 4	48	6 378 144.1	
7	C-Band = SAO III	1	6 378 143.6	6 378 142.7 (from points 1 - 14)
8	C-Band = GSFC 73	1	6 378 146.8	
9	C-Band = NWL 9D	1	6 378 147.1	
10	C-Band = GEM 4	1	6 378 147.8	
11	EDM = SAO III	10	6 378 153.7	
12	EDM = GSFC 73	8	6 378 154.0	
13	EDM = GEM 4	9	6 378 155.2	
14	EDM = NWL 9D	9	6 378 160.5	

are consistent with dynamically computed ones when the following set of constants defining the gravity of the level ellipsoid are used (HEISKANEN & MORITZ 1967, p.64):

$f = 1/298.25$ (flattening) ; $\omega = 0.729\,211\,514\,67 \times 10^{-4}$ sec^{-1} (rotational velocity);

$a = 6\,378\,142$ m ; and

$W_o = 6\,263\,688.00$ kgal m (geopotential on the geoid).

Derived from these are the following parameters:

$k^2M = 3.986\,009\,22 \times 10^{14}$ m^{3}sec^{-1} (gravitational constant × Earth mass);

$\gamma_e = 978.032\,26$ cm sec^{-2} (equatorial normal gravity); and

$J_2 = 1\,082.6863 \times 10^{-6}$ (second degree harmonic).

All the above constants are in good agreement with their current best estimates. The parameters in equation 4 ($\Delta a = -13 \pm 0.7$ m, $u_o = -23.2 \pm 0.9$ m, $v_o = -2.9 \pm 0.8$ m, $w_o = 2.7 \pm 1.2$ m) are the result of fitting an ellipsoid to the WN14 geoid as explained earlier in this section, and they represent the size and position of the best fitting level ellipsoid with respect to the reference ellipsoid (of the same flattening). In the case of a good global station distribution, the centre of this level ellipsoid is the "geometric" centre of the geoid. If this point is assumed to be identical with the centre of mass, then the above co-ordinates may be viewed as its co-ordinates with respect to the origin of the reference ellipsoid, and with opposite signs they can be used to shift the WN14 co-ordinates to the geocentre:

$$\begin{aligned} u(\text{geocentric}) &= u_{WN14} + 23.2 \text{ m} \\ v(\text{geocentric}) &= v_{WN14} + 2.9 \text{ m} \\ w(\text{geocentric}) &= w_{WN14} - 2.7 \text{ m} \end{aligned} \qquad (5).$$

It should be pointed out again that the selection of the semi-diameter 6 378 142 m was arbitrary. Had the lowest extremity in table 7 been chosen (6 378 125 m), the gravitational parameters (keeping f, ω and the geoidal undulations the same) still would not become completely unreasonable:

$W_o = 6\,263\,705.35$ kgal m ; $k^2M = 3.986\,009\,68 \times 10^{14}$ m^{3}sec^{-1}

$\gamma_e = 978.037\,62$ cm sec^{-2} ; $J_2 = 1\,082.695\,6 \times 10^{-6}$.

Thus the question of what is the "best" semi-diameter still needs to be answered.

4. Comparison of the Results

4.1 Comparisons with Geometric Information

In addition to solution WN14, two other adjustments were also performed with the same data. The only differences were that in one of them (WN12), the weighted height constraints were not applied; thus the scale is defined through the SECOR, EDM and C-Band data. In the other (WN16), the EDM and C-Band lengths were not entered as weighted constraints; thus the scale is through the SECOR and the weighted height constraints.

Table 8 contains differences between the adjusted and given chord lengths (table 3) from the three solutions. The lines originating from Station 4742 (Kauai) are not listed for reasons explained earlier. Comparing solutions WN14 and WN12, the effect of including the heights is not very significant. The average length discrepancy decreases 0.48×10^{-6} in the case of EDM, and 0.60×10^{-6} in the C-Band case, both numbers being within the noise level. At first glance, the difference between WN14 and WN16 seems to be significant since the average length discrepancy increases by about

Table 8

Chord Length Comparisons (Solutions WN12, 14 and 16)

Type	Line	Adjusted - Given Length					
		WN12		WN14		WN16	
		m	ppm	m	ppm	m	ppm
EDM	6002 - 6003	8.3 ± 2.5	2.38	2.7 ± 2.3	0.78	5.9 ± 3.0	1.70
	6003 - 6111	2.7 ± 1.4	1.90	2.3 ± 1.4	1.60	11.4 ± 3.1	8.00
	6006 - 6065	7.7 ± 2.1	3.13	6.1 ± 2.0	2.47	19.9 ± 3.5	8.13
	6016 - 6065	-2.8 ± 1.3	2.30	-2.9 ± 1.3	2.47	-18.9 ± 3.4	15.87
	6006 - 6016	2.7 ± 2.2	0.77	1.3 ± 2.1	0.37	1.6 ± 3.3	0.46
	6063 - 6064	13.7 ± 2.4	3.94	10.6 ± 2.3	3.03	15.2 ± 2.8	4.37
	6023 - 6060	7.9 ± 3.1	3.42	5.9 ± 3.0	2.55	9.6 ± 3.8	4.16
	6032 - 6060*	-2.4 ± 3.9	0.76	-4.5 ± 3.6	1.42	-2.9 ± 3.7	0.92
	3861 - 7043	2.2 ± 1.8	1.44	1.5 ± 1.8	0.99	7.6 ± 3.7	5.00
C-Band	4082 - 4050*	26.5 ± 6.9	2.42	-5.2 ± 3.9	0.48	-4.2 ± 4.0	0.39
	4082 - 4740	2.0 ± 2.7	1.25	1.3 ± 2.7	1.90	6.6 ± 5.0	4.13
	4082 - 4081	3.0 ± 2.3	2.40	2.3 ± 2.3	0.79	17.9 ± 6.2	14.49
	4082 - 4061	-0.4 ± 3.6	0.19	-1.5 ± 3.6	0.65	2.1 ± 6.1	0.93
Average	EDM		2.22		1.74		5.40
	C-Band		1.56		0.96		4.98
	All		2.02		1.50		5.27

4×10^{-6} or 1:250,000 for both types of observations. Close inspection, however, reveals that though the inclusion of the EDM and C-Band chords in the solution improves the positions of stations 6111 (Wrightwood), 6065 (H.Peissenberg) and 4081 (Grand Turk), it does not otherwise contribute to the overall scale determination significantly. If the above mentioned stations are left out of the comparison, the average length discrepancies in the WN16 solution decrease to 2.76×10^{-6} for the EDM and 1.81×10^{-6} for the C-Band, both within the noise level from WN14 (about 1×10^{-6}).

The above conclusion is also strengthened by the content of table 9 where the average standard deviations of the co-ordinates and the heights are compared from the three solutions. It is seen that while the inclusion of the weighted heights decreases standard deviations significantly, the exclusion of the geometric scalars hardly changes the results.

Table 9

Standard Deviation Comparisons
(Solutions WN12, 14 and 16)

Solution	Constituent Networks								WN_i	
	BC		SECOR		MPS		SA			
	σ	σ_H	σ	σ_H	σ	σ_H	σ	σ_H	σ	σ_H
WN12	4.4	5.0	4.2	4.8	6.9	7.6	5.2	5.9	5.5	6.2
WN14	3.5	3.2	2.8	2.4	4.8	2.9	4.1	3.0	3.9	2.9
WN16	3.5	3.2	2.8	2.4	4.9	2.9	4.1	3.0	4.0	2.9

All units in metres

4.2 Comparisons with Dynamic Solutions

Table 10 is a compilation of transformation parameters between the WN co-ordinates and those from the dynamic solutions NWL-9D, SAO III, GEM-4 and GSFC-73. The method of computing the parameters is described in (KUMAR 1972). In the table the positive angles ω, ψ and ε are counter-clockwise rotations about the w, v and u axes respectively, as viewed from the end of the positive axis. The scale difference factor Δ is in units of ppM. In the transformations the variances of both sets of the co-ordinates are taken into account. Taking the variances of the WN solutions as standard, those of the dynamic solutions are scaled by the weight factors indicated. These numbers are also indicative of the over-optimism over the quality of some of the published solutions. For example, a weight factor of 25 would indicate that the published standard deviations of a given solution need to be multiplied by $\sqrt{25} = 5$.

T a b l e 10

Relationships Between Various Dynamic and the WN Systems

(Dynamic - WN14)

Solution	NWL-9D			SAO III			GEM-4	GSFC-73
Sta. Considered	5000	6000	all	6000	9000	all	all	all
No. Stations	12	22	32	47	22	73	30	26
Weight Factor*	1.5	7.75	4	2	2	2	50	22
Δu(m)	15.6 ±1.6	16.8 ±1.1	15.9 ±1.0	16.8 ±1.5	10.7 ±2.1	13.9 ±1.3	14.5 ±1.6	13.7 ±1.5
Δv(m)	13.1 ±1.5	9.6 ±1.1	10.3 ±1.0	12.8 ±1.5	13.6 ±2.2	13.6 ±1.3	11.6 ±1.6	12.9 ±1.4
Δw(m)	-7.8 ±2.0	-3.2 ±1.1	-3.4 ±1.1	-5.2 ±1.5	-15.7 ±2.3	-10.4 ±1.3	1.9 ±1.7	-1.7 ±1.9
Δ (10^{-6})	0.74±0.15	0.26±0.05	0.29±0.04	-0.50±0.05	0.74±0.15	-0.17±0.04	0.93±0.11	0.96±0.11
ω ('')	0.73±0.03	0.70±0.01	0.71±0.01	0.51±0.02	0.26±0.03	0.37±0.01	-0.02±0.02	-0.38±0.02
ψ ('')	-0.11±0.04	-0.15±0.01	-0.15±0.01	0.15±0.02	0.08±0.04	0.15±0.01	0.12±0.03	0.19±0.03
ε ('')	0.23±0.07	-0.17±0.01	-0.14±0.01	-0.18±0.02	0.07±0.03	-0.03±0.01	0.17±0.02	0.24±0.03
σ_o^2	0.65	0.91	0.87	0.83	1.20	1.14	1.11	1.09

* Weight Factor = $\sigma_{o,i}^2 / \sigma_{o,WN14}^2$

As it is seen there is good agreement between the translational elements Δu-s and Δv-s of the main (all stations inclusive) dynamic solutions and a discrepancy of about 8.5 ± 1.7 m with respect to the geometric values (see equation 5). The largest discrepancy occurs in the Δw components, where there seems to be a 12.3 ± 2.1 m difference between the SAO III and the GEM-4 solutions. Eliminating the SAO III value, all Δw's, including the geometric one, are within the noise level.

The weighted mean shifts from the main dynamic solutions (excluding Δw from SAO III), or the co-ordinates of the geocentre with respect to the WN14 origin, are listed in table 11. The quantity $r_o = \sqrt{u_o^2 + v_o^2}$ is the distance of the WN14 origin from the rotation axis of the Earth. Calculating the same number from the JPL-LS 37 co-ordinates of the Deep Space Network (stations DSN1 = 4711, DSN2 = 4712, DSN4 = 4714, DSN6 = 4742 and DSN7 = 4751) as published in (GAPOSCHKIN ET AL 1973), one gets r_o = 25.9 ± 2.5 m, which value is nearest to the one calculated from the geometric fit.

The differences in scale between dynamic solutions are significant (see figure 3 for comparison). The largest discrepancy is between the SAOIII and GSFC-73 with $\Delta = (1.13 \pm 0.12) \times 10^{-6}$, which is

Table 11

Shifts to the Geocentre (Solution WN14)

Source	u_o (m)	v_o (m)	w_o (m)	r_o (m)
1. Dynamic Comparison	14.8 ± 1.4	11.8 ± 1.3	-1.8 ± 1.6	18.9 ± 1.9
2. Geometric Fit (eqn.5)	23.2 ± 0.9	2.9 ± 0.8	-2.7 ± 1.2	23.4 ± 1.2
3. Weighted Mean of 1 & 2	20.7 ± 1.2	5.3 ± 1.1	-2.4 ± 1.4	21.4 ± 1.6
4. JPL/DSN				25.9 ± 2.5

larger than what one would expect from the noise. The other dynamic scales are within near noise level and, on the average, differ from the scale of the WN14 solution by

$$\Delta = (0.12 \pm 0.08) \times 10^{-6}$$

or about one part in 8.3 million. The largest discrepancies occur in the orientation of the various dynamic systems with respect to each other and to WN14. In the rotation about the w axis (ω), the largest difference occurs between the NWL-9D and the GSFC-73 solutions, where $\omega = 1''.1$, or about 34 m on the equator (figure 4). The other differences are smaller but significant. These rotations may be partly due to the definition of the zero meridian in the case of purely electronic systems (e.g., Doppler), partly to the various definitions of vernal equinox in the star catalogues used, and also to its motion with respect to inertial space, in the case of optical observations. The latter alone requires a correction to the FK4 right ascensions amounting to $+0''.65$ at 1960.0, changing with a rate of $+1''.36$ per century (MARTIN & VAN FLANDERN 1970).

The rotations about the axes u and v are even more confusing. Figure 5 illustrates the situation at the pole. The weighted means of the dynamic solutions are $\psi = 0''.02 \pm 0''.02$ and $\varepsilon = -0''.04 \pm 0''.02$. The discrepancy between the poles as determined separately from the SAO III 6000 stations and then from the 9000 stations is unexplained at this time. It is interesting to note that the weighted mean pole and zero meridian positions computed from the dynamic solutions hardly differ from those of the WN14 solution.

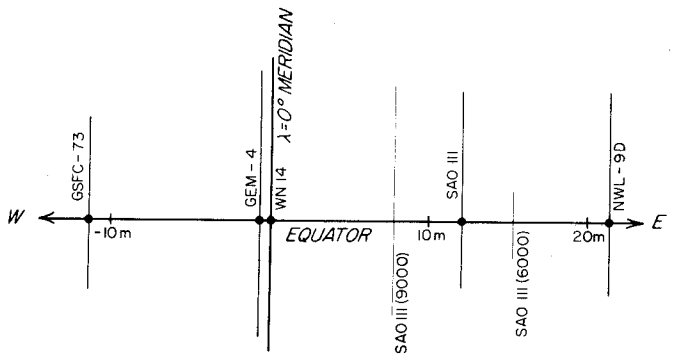

Figure 4. Dynamic Zero Meridians Relative to the WN14 Zero Meridian

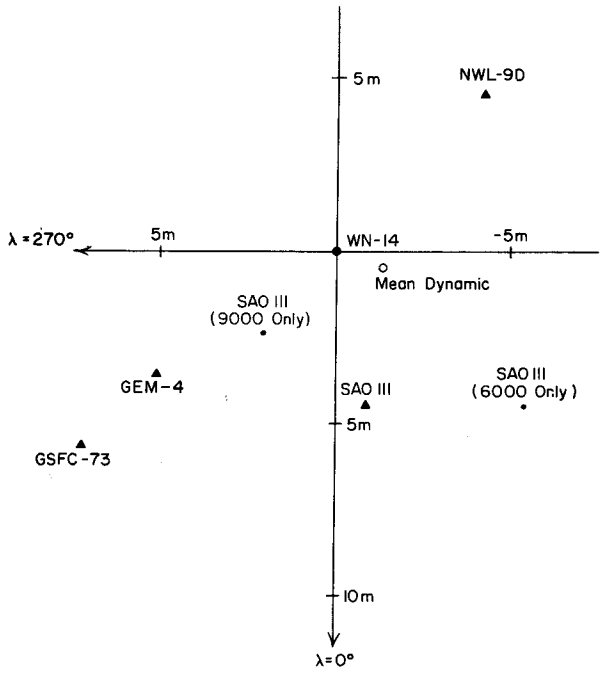

Figure 5. Dynamic Pole Positions Relative to the WN14 Pole

The only general conclusion that one can draw from the rotation parameters is that the co-ordinate systems used in the dynamic solutions need to be more carefully defined and conditions enforcing these definitions more strongly applied than evidenced from the solutions discussed.

4.3 Comparison with Geodetic Datums

Table 12 is a summary of datums. Table 13 summarizes the relationships between the various geodetic datums and the WN14 system for those datums where stations were located.

5. Cartesian Co-ordinates From Solutions WN12 and WN14

Table 14 is a summary of the Cartesian co-ordinates of solutions WN12 and WN14. As mentioned earlier the former differs from the latter only in that in it, the heights are not constrained. The resulting scale in WN12 is such that when the co-ordinates are transformed to a geocentric rotational ellipsoid of $a = 6\ 378\ 154$ m and $1/f = 298.2495$, they produce geoid undulations consistent with dynamically determined ones with $k^2M = 3.986\ 008\ 91 \times 10^{14} m^3 sec^{-2}$ and $\gamma_e = 978.028\ 47$ cm sec^{-2}. Derived from these constants are the values $W_o = 6\ 263\ 675.76$ kgal m and $J_2 = 1\ 082.6797 \times 10^{-6}$. These values together with those mentioned at the end of section 3.3 seem to be the extreme limits within which the truce must lie, provided that the dynamically determined undulations are correct.

Comparisons with geoid undulations from satellite and surface gravimetric solutions in case of the WN14 solution show an rms residual of ±6.1 m, with an average of only -0.3m. Similar comparison with the WN12 solution, where the heights are not constrained, shows that the rms of the residuals is ±16.1 m, and the average -0.2 m.

Table 12

Geodetic Datums

Code	Datum	Ellipsoid	Origin	Latitude	Longitude
1	Adindan (Ethiopia)	Clarke 1880	STATION Z5 ADINDAN	22°10'07".110	31°29'21".608
2	American Samoa 1962	Clarke 1866	BETTY 13 ECC	-14 20 08.341	189 17 07.750
3	Arc-Cape (South Africa)	Clarke 1880	Buffelsfontein	-33 59 32.000	25 30 44.622
4	Argentine	International	Campo Inchauspe	-35 58 17	297 49 48
5	Ascension Island 1958	International	Mean of three stations	-07 57	345 37
6	Australian Geodetic	Australian National	Johnston Memorial Cairn	-25 56 54.55	133 12 30.08
7	Bermuda 1957	Clarke 1866	FT. GEORGE B 1937	32 22 44.360	295 19 01.890
8	Berne 1898	Bessel	Berne Observatory	46 57 08.660	07 26 22.335
9	Betio Island, 1966	International	1966 SECOR ASTRO	01 21 42.03	172 55 47.90
10	Camp Area Astro 1961-62 USGS	International	CAMP AREA ASTRO	-77 50 52.521	166 40 13.753
11	Canton Astro 1966	International	1966 CANTON SECOR ASTRO	-02 46 28.99	188 16 43.47
12	Christmas Island Astro 1967	International	SAT.TRI.STA. 059 RM3	02 00 35.91	202 35 21.82
13	Chua Astro (Brazil-Geodetic)	International	CHUA	-19 45 41.16	311 53 52.44
14	Corrego Alegre (Brazil-Mapping)	International	CORREGO ALEGRE	-19 50 15.140	311 02 17.250
15	Easter Island 1967 Astro	International	SATRIG RM No. 1	-27 10 39.95	250 34 16.81
16	European	International	Helmert Tower	52 22 51.45	13 03 58.74
17	Graciosa Island (Azores)	International	SW BASE	39 03 54.934	331 57 36.118
18	Gizo, Provisional DOS	International	GUX 1	-09 27 05.272	159 58 31.752
19	Guam	Clarke 1866	TOGCHA LEE NO. 7	13 22 38.49	144 45 51.56
20	Heard Astro 1969	International	INTSATRIG 0044 ASTRO	-53 01 11.68	73 23 22.64
21	Iben Astro, Navy 1947 (Truk)	Clarke 1866	IBEN ASTRO	07 29 13.05	151 49 44.42
22	Indian	Everest	Kalianpur	24 07 11.26	77 39 17.57
23	Isla Socorro Astro	Clarke 1866	Station 038	18 43 44.93	249 02 39.28
24	Johnston Island 1961	International	JOHNSTON ISLAND 1961	16 44 49.729	190 29 04.781
25	Kusaie, Astro 1962, 1965	International	ALLEN SODANO LIGHT	05 21 48.80	162 58 03.28
26	Luzon 1911 (Philippines)	Clarke 1866	BALANCAN	13 33 41.000	121 52 03.000
27	Midway Astro 1961	International	MIDWAY ASTRO 1961	28 11 34.50	182 36 24.28
28	New Zealand 1949	International	PAPATAHI	-41 19 08.900	175 02 51.000
29	North American 1927	Clarke 1866	MEADES RANCH	39 13 26.686	261 27 29.494
30	*NAD 1927 (Cape Canaveral)	Clarke 1866	CENTRAL	28 29 32.364	279 25 21.230
31	*NAD 1927 (White Sands)	Clarke 1866	KENT 1909	32 30 27.079	253 31 01.306
32	Old Bavarian	Bessel	Munich	48 08 20.000	11 34 26.493
33	Old Hawaiian	Clarke 1866	OAHU WEST BASE	21 18 13.89	202 09 04.20
34	Ordnance Survey G.B. 1936	Airy	Herstmonceux	50 51 55.271	00 20 45.882
35	Pico de las Nieves (Canaries)	International	PICO DE LAS NIEVES	27 57 41.273	344 25 49.476
36	Pitcairn Island Astro	International	PITCAIRN ASTRO 1967	-25 04 06.97	229 53 12.17
37	Potsdam	Bessel	Helmert Tower	52 22 53.954	13 04 01.153
38	Provisional S.American 1956	International	LA CANOA	08 34 17.17	296 08 25.12
39	Provisional S. Chile 1963	International	HITO XVIII	-53 57 07.76	291 23 28.76
40	Pulkovo 1942	Krassovski	Pulkovo Observatory	59 46 18.55	30 19 42.09
41	South American 1969	South American 1969	CHUA	-19 45 41.653	311 53 55.936
42	Southeast Island (Mahe)	Clarke 1880		-04 40 39.460	55 32 00.166
43	South Georgia Astro	International	ISTS 061 ASTRO POINT 1968	-54 16 38.93	323 30 43.97
44	Swallow Islands (Solomons)	International	1966 SECOR ASTRO	-10 18 21.42	166 17 56.79
45	Tananarive	International	Tananarive Observatory	-18 55 02.10	47 33 06.75
46	Tokyo	Bessel	Tokyo Observatory (old)	35 39 17.51	139 44 40.50
47	Tristan Astro 1968	International	INTSATRIG 069 RM No. 2	-37 03 26.79	347 40 53.21
48	Viti Levu 1916 (Fiji)	Clarke 1880	MONAVATU (latitude only) SUVA (longitude only)	-17 53 28.285	178 25 35.835
49	Wake Island, Astronomic 1952	International	ASTRO 1952	19 17 19.991	166 38 46.294
50	Yof Astro 1967 (Dakar)	Clarke 1880	YOF ASTRO 1967	14 44 41.62	342 30 52.98
51	Palmer Astro 1969	International	ISTS 050	-64 46 35.71	295 56 39.53
52	Eftate	International	Belle Vue IGN	-17 44 17.400	168 20 33.250

*Local datums of special purpose, based on NAD 1927 values for the origin stations.

Table 13

Relationship Between Various Geodetic Datums and the WN System (Datum - WN14)

Datum No.	Datum Name[1]	No. of Stations	Δu (m)*	Δv (m)*	Δw (m)*	ω (″)**	ψ (″)**	ϵ (″)**	Δ (×10⁶)
1	Adindan (Ethiopia)	2	184 ±19	21 ±11	-200 ± 6				
2	American Samoa 1962	1	119 ± 8	-105 ± 8	-413 ±10				
3	Arc Cape (South Africa)	1	152 ± 7	126 ± 7	298 ±10				
5	Ascension Island 1958	1	227 ± 7	- 93 ± 7	- 58 ± 8				
6	Australian Geodetic	3	118.2± 5.0	41.1± 6.2	-121.0± 6.9	1.03±0.18	0.99±0.18	-0.25±0.22	-1.20±0.71
10	Camp Area Astro 1961/62(USGS)	1	111 ±10	148 ± 9	-238 ±10				
12	Christmas Island Astro 1967	1	-115 ± 9	-224 ±12	529 ± 8				
15	Easter Island Astro 1967	1	-182 ±10	-138 ±10	-128 ±11				
16	European-50 (W)[2]	11	133.3± 9.5	114.2±15.9	152.2± 9.2	-1.76±0.38	0.01±0.31	-0.38±0.44	-7.30±1.14
	European-50 (All stations)[3]	16	134.3± 9.1	152.7± 8.0	144.6± 8.8	-0.41±0.20	0.27±0.30	-0.51±0.22	-7.24±0.88
17	Graciosa Island (Azores)	1	123 ±17	-147 ± 9	37 ±17				
20	Heard Astro 1969	1	182 ±12	56 ±12	-114 ±14				
22	Indian[4]	1	-165 ±17	-711 ±10	-228 ±11				
23	Isla Socoro Astro	1	-134 ±12	-206 ± 7	-503 ± 9				
24	Johnston Island 1961	1	-161 ±13	51 ±25	211 ±13				
26	Luzon 1911 (Philippines)	1	151 ±10	51 ± 7	111 ± 8				
27	Midway Astro 1961	1	-377 ± 7	84 ± 7	-279 ± 9				

*If (Datum - Geocenter) is sought add to the tabulated values of Δu, Δv, Δw the respective quantities -21m, -5 m, 2 m see Table 11

**ω, ψ, ϵ when positive, represent counterclockwise rotations about the respective w, v, u axes, as viewed from the end of the positive axis.

Table 13 (cont'd)

Datum No.	Datum Name[1]	No. of Stations	Δu (m)*	Δv (m)*	Δw (m)*	ω(″)**	ψ(″)**	ε(″)	Δ(×10⁶)
28	New Zealand 1949	1	- 61 ± 8	41 ± 9	-192 ± 9				
29	North American 1927 (W)[5]	8	30.6± 7.3	-170.3± 4.5	-134.9± 6.8	0.21±0.20	0.59±0.21	-0.45±0.23	-7.91±0.45
	North American 1927 (E)[6]	13	56.4± 6.9	-144.6± 4.4	-196.4± 4.3	1.01±0.19	-0.01±0.16	0.54±0.14	2.15±0.62
	North American (All Stations)[7]	21	57.1± 2.2	-147.9± 2.6	-187.5± 2.9	0.86±0.06	0.23±0.06	0.33±0.11	0.80±0.27
36	Pitcairn Island Astro	1	-167 ±12	-168 ±11	- 60 ±11				
39	Provisional South Chile 1963	1	0 ± 8	-196 ± 8	- 93 ± 9				
41	South American 1969[9]	10	54.4± 5.5	30.0± 4.8	42.9± 4.9	-0.63±0.17	0.17±0.12	-0.12±0.13	6.67±0.59
42	Southeast Island (Mahe)	1	54 ± 8	186 ± 8	272 ± 9				
43	South Georgia Astro	1	820 ± 8	-101 ±11	291 ±11				
46	Tokyo	1	183 ±10	-506 ± 9	-686 ± 9				
47	Tristan Astro 1968	1	654 ±14	-420 ±11	622 ±13				
49	Wake Island Astronomic 1952	1	-260 ± 7	67 ±12	-140 ± 8				
50	Yof Astro 1967 (Dakar)	1	55 ± 6	-143 ± 7	- 95 ± 7				
51	Palmer Astro 1969	1	-218 ± 9	- 8 ±12	-226 ±12				

*If (Datum - Geocenter) is sought add to the tabulated values of Δu, Δv, Δw the respective quantities -21m, -5 m, 2 m see Table 11.

**ω, ψ, ε when positive, represent counterclockwise rotations about the respective w, v, u axes, as viewed from the end of the positive axis.

Table 13 (cont'd)

[1] See Table 12 for datum description and other related information.

[2] Stations included are Tromso (6006), Catania (6016), Hohenpeissenberg (6065), Wippolder (8009), Zimmerwald (8010), Haute Provence (8015), Nice (8019), Meudon (8030), San Fernando (9004), Dionysos (9091) and Harestua (9426).

[3] Stations included are as in #2 and Mashhad (6015), Malvern (8011), Naini Tal (9006), Shiraz (9008) and Riga (9431).

[4] Based on p. 70, Bulletin Geodesique, 107, 1973.

[5] Stations included are Goldstone (1030), Colorado Springs (3400), Vandenberg AFB (4280), Wrightwood II (6134), Moses Lake (6003), Edinburg (7036), Denver (7045) and Organ Pass (9001).

[6] Stations included are Blossom Point (1021), Fort Myers (1022), E. Grand Forks (1034), Rosman (1042), Bedford (3401), Semmes (3402), Hunter AFB (3648), Aberdeen (3657), Homestead (3861), Beltsville (6002), Greenbelt (7043), Jupiter (7072) and Sudbury (7075).

[7] Stations included are as in #4 and #5 above.

[8] Stations included are Brasilia (3414), Asunction (3431), Bogota (3477), Paramaribo (6008), Quito (6009), Villa Dolores (6019), Natal (6067), Arequipa (9007), Curacao (9009) and Comodoro Rivadavia (9031).

Table 14

Summary of Cartesian Coordinates (Solutions WN12 and WN14)

STATION		SOLUTION WN-12						SOLUTION WN-14					
NO	NAME	U	V	W	σ_u	σ_v	σ_w	U	V	W	σ_u	σ_v	σ_w
1021	BLOSSOM POINT	1118021.8	-4876331.7	3942970.9	3.1	4.0	4.2	1118023.1	-4876323.4	3942963.9	2.8	2.6	2.8
1022	FORT MYERS	807850.8	-5652004.0	2833509.0	2.6	3.3	3.3	807851.9	-5651989.6	2833500.2	2.2	1.9	2.3
1030	GOLDSTONE	-2357249.2	-4646346.4	3668312.5	6.1	4.4	4.7	-2357242.9	-4646338.5	3668306.8	5.6	3.3	3.2
1032	ST. JOHN'S	2602704.3	-3419179.7	4697621.1	49.1	89.5	29.9	2602688.6	-3419228.9	4697637.3	39.3	46.7	13.8
1033	FAIRBANKS	-2299292.3	-1445690.5	5751823.3	7.5	10.0	10.5	-2299282.6	-1445693.7	5751811.6	6.9	9.7	5.7
1034	E. GRAND FORKS	-521708.3	-4242074.9	4718726.5	3.5	4.0	4.4	-521704.5	-4242064.3	4718716.8	3.1	3.0	2.7
1042	ROSMAN	647495.9	-5177948.0	3656714.4	3.1	3.6	4.0	647497.5	-5177935.6	3656705.9	2.8	2.4	2.8
3106	ANTIGUA	2801840.5	-5372180.7	1868548.5	4.1	4.6	4.9	2801838.3	-5372164.6	1868538.6	3.7	3.3	4.3
3334	STONEVILLE	-84969.1	-5327986.3	3493434.3	15.6	14.0	10.8	-84963.8	-5327974.9	3493428.3	13.6	6.8	9.0
3400	COLORADO SPRINGS	-1275239.4	-4798062.9	3994229.5	16.3	12.4	8.6	-1275207.2	-4798029.3	3994208.3	9.1	5.1	5.7
3401	BEDFORD	1513134.8	-4463580.1	4283061.2	3.5	5.3	4.6	1513136.1	-4463576.8	4283055.8	3.2	3.4	3.0
3402	SEMMES	167256.1	-5481980.4	3245042.6	4.2	4.3	4.6	167259.7	-5481971.0	3245037.0	3.9	2.8	3.5
3404	SWAN ISLAND	642485.7	-6053942.4	1895690.5	5.0	5.3	5.5	642491.4	-6053940.3	1895688.6	4.7	3.7	4.9
3405	GRAND TURK	1919482.1	-5621096.5	2315780.1	3.6	5.6	4.9	1919482.9	-5621088.1	2315775.3	3.3	3.5	4.0
3406	CURACAO	2251802.9	-5816929.0	1327197.4	2.8	3.5	3.8	2251800.2	-5816912.9	1327191.1	2.4	2.1	3.4
3407	TRINIDAD	2979092.9	-5513532.6	1181126.8	5.2	5.1	5.9	2979091.1	-5513530.9	1181129.3	4.7	3.4	5.3
3413	NATAL	5186366.4	-3654225.1	-653022.7	3.4	2.9	3.2	5186348.4	-3654222.4	-653018.9	2.1	2.2	2.7
3414	BRASILIA	4114987.8	-4554148.5	-1732166.1	9.9	8.4	7.9	4114977.8	-4554142.5	-1732154.0	7.7	6.1	7.2
3431	ASUNCION	3093056.1	-4870100.4	-2710845.8	8.5	9.3	12.5	3093045.4	-4870081.7	-2710823.0	7.6	6.5	10.8
3476	PARAMARIBO	3623293.6	-5214213.7	601514.0	3.4	3.3	3.6	3623277.3	-5214210.7	601515.3	2.2	2.0	3.0
3477	BOGOTA	1744649.6	-6114305.6	532205.2	10.4	13.7	9.8	1744650.2	-6114296.7	532208.6	10.2	6.6	9.6
3478	MANAUS	3185705.4	-5514574.5	-347713.2	19.3	35.4	35.8	3185777.0	-5514585.9	-347703.2	18.7	14.5	35.1
3499	QUITO	1280834.0	-6250966.2	-10605.5	3.8	5.9	4.5	1280834.2	-6250955.9	-10600.6	3.6	3.4	4.1
3648	HUNTER AFB	832562.6	-5349553.4	3360596.4	4.1	5.0	5.4	832566.2	-5349540.7	3360585.3	3.6	2.5	3.6
3657	ABERDEEN	1186786.1	-4785205.1	4032892.3	3.4	5.0	4.5	1186787.1	-4785193.1	4032882.3	3.1	3.0	3.0
3661	HOMESTEAD	961766.7	-5679170.6	2729883.8	3.3	3.8	3.7	961767.9	-5679156.6	2729883.5	3.0	2.3	2.6
3902	CHEYENNE	-1234689.4	-4651235.9	4174763.4	28.6	32.1	11.3	-1234700.7	-4651242.8	4174758.6	8.6	6.3	6.3
3903	HERNDON	1088960.0	-4842973.2	3991763.9	12.3	15.5	11.4	1088989.7	-4843005.4	3991776.6	12.1	8.5	8.9
4050	PRETORIA	5051614.8	2726608.6	-2774181.0	4.4	3.8	5.5	5051608.1	2726603.3	-2774166.8	3.2	3.2	4.4
4061	ANTIGUA	2801594.5	-5372540.2	1868034.3	4.2	4.7	5.0	2801592.3	-5372523.9	1868024.4	3.8	3.5	4.3
4081	GRAND TURK	1920409.9	-5619426.1	2319133.4	3.7	5.7	5.0	1920410.9	-5619417.8	2319128.5	3.3	3.6	4.0
4082	MERRITT ISLAND	910567.9	-5539130.2	3017974.8	2.9	3.8	3.7	910567.2	-5539113.2	3017965.3	2.6	2.4	2.8
4280	VANDENBERG AFB	-2671883.7	-4521217.3	3607495.0	4.3	4.4	4.8	-2671873.8	-4521210.5	3607490.4	3.8	3.3	3.6
4740	BERMUDA	2308008.6	-4874314.8	3393092.0	3.8	5.4	5.1	2308007.3	-4874298.2	3393082.1	3.3	3.1	3.8
5001	HERNDON	1088874.4	-4842954.9	3991857.8	4.9	10.2	7.9	1088849.4	-4842948.7	3991840.2	3.6	3.0	3.7
5201	MOSES LAKE	-2127810.4	-3785912.3	4656011.9	2.7	2.8	3.7	-2127802.2	-3785911.5	4656012.1	2.3	2.2	2.4
5410	MIDWAY ISLANDS	-5618764.5	-250231.5	2997243.8	2.9	3.2	4.1	-5618754.1	-250237.5	2997250.2	2.3	2.8	3.6
5648	FORT STEWART	794687.3	-5360063.7	3353093.5	4.2	5.0	5.5	794691.0	-5360051.1	3353082.4	3.6	2.5	3.6
5712	PARAMARIBO	3623307.1	-5214190.5	601672.3	3.4	3.3	3.6	3623289.8	-5214188.0	601673.2	2.1	2.0	2.9
5713	TERCEIRA	4433654.4	-2268159.2	3971673.1	2.7	2.8	3.8	4433637.8	-2268153.2	3971656.8	2.0	2.2	2.5

Table 14 (cont'd)

STATION		SOLUTION WN-12						SOLUTION WN-14					
NO	NAME	U	V	W	σ_u	σ_v	σ_w	U	V	W	σ_u	σ_v	σ_w
5715	DAKAR	5084479.9	-1853580.1	1612763.8	2.3	2.5	3.1	5084468.8	-1853580.1	1612760.1	1.6	2.0	2.3
5717	FORT LAMY	6023416.1	1617949.5	1331651.2	2.7	2.8	3.3	6023410.7	1617946.5	1331655.8	2.0	2.0	2.7
5720	ADDIS ABADA	4900750.1	3968255.1	966348.3	2.7	2.9	3.4	4900749.1	3968253.0	966354.7	2.0	2.1	2.9
5721	MASHHAD	2604406.6	4444124.9	3750345.7	2.6	2.8	3.5	2604404.8	4444122.3	3750344.3	2.1	2.1	2.7
5722	DIEGO GARCIA	1905122.3	6032294.5	-810726.4	4.2	5.5	4.8	1905127.0	6032287.5	-810716.2	3.5	4.1	4.3
5723	CHIANG MAI	-941713.7	5967448.6	2039317.5	3.1	3.3	4.1	-941709.4	5967445.0	2039322.9	2.5	2.3	3.5
5726	ZAMBOANGA	-3361953.2	5365845.5	763623.6	3.0	3.3	3.8	-3361946.8	5365837.0	763627.8	2.3	2.2	3.2
5730	WAKE ISLAND	-5858583.8	1394474.9	2093844.7	2.8	3.1	3.8	-5858574.6	1394467.2	2093847.4	2.1	2.5	3.1
5732	PAGO PAGO	-6099984.0	-997345.6	-1568577.0	5.7	4.4	4.9	-6099970.5	-997355.3	-1568570.9	3.6	3.5	4.1
5733	CHRISTMAS ISLAND	-5885350.8	-2448375.3	221663.1	4.4	3.5	4.6	-5885333.9	-2448380.4	221670.7	2.7	2.9	3.9
5734	SHEMYA	-3851806.1	396416.1	5051343.3	3.2	3.7	4.9	-3851799.0	396409.3	5051342.0	2.7	3.3	3.9
5735	NATAL	5186368.5	-3654226.0	-653022.6	3.3	2.8	3.1	5186350.6	-3654223.7	-653018.9	2.0	2.1	2.5
5736	ASCENSION ISLAND	6118355.5	-1571763.1	-878558.4	3.3	2.9	3.3	6118340.3	-1571761.9	-878553.6	2.3	2.2	2.7
5739	TERCEIRA	4433646.0	-2268192.2	3971663.3	2.7	2.8	3.8	4433629.3	-2268186.2	3971647.0	2.0	2.2	2.5
5744	CATANIA	4896444.1	1316129.4	3856628.4	2.4	2.8	3.2	4896437.7	1316125.0	3856626.2	1.8	2.2	2.3
5907	WORTHINGTON	-449391.6	-4600910.6	4380315.4	5.8	13.8	13.5	-449417.5	-4600905.5	4380280.1	4.2	3.2	4.5
5911	BERMUDA	2308010.4	-4873778.3	3394476.1	3.6	4.9	5.2	2307991.2	-4873773.2	3394463.4	2.6	2.3	3.0
5912	PANAMA	1142664.4	-6196104.1	988340.8	4.8	9.1	7.0	1142644.5	-6196109.1	988336.6	3.1	3.4	4.1
5914	PUERTO RICO	2349423.9	-5576023.2	2010340.5	13.5	21.1	9.7	2349456.9	-5576027.1	2010342.6	10.5	7.0	6.4
5915	AUSTIN	-744066.7	-5465234.3	3192485.8	5.6	15.3	12.8	-744091.1	-5465238.7	3192467.4	3.8	3.8	4.7
5923	CYPRUS	4363335.9	2862258.8	3655280.7	2.5	2.7	3.3	4363332.2	2862254.9	3655280.7	1.9	2.1	2.4
5924	ROTA	5093565.8	-565319.1	3784273.1	2.4	3.1	3.8	5093556.2	-565322.3	3784268.3	1.9	2.6	2.9
5925	ROBERTS FIELD	6237376.8	-1140241.8	687740.0	3.0	3.1	3.6	6237366.3	-1140241.5	687740.2	2.3	2.6	3.0
5930	SINGAPORE	-1542556.4	6186964.6	151827.8	3.3	3.9	4.0	-1542549.4	6186956.7	151833.8	2.6	2.7	3.4
5931	HONG KONG	-2423919.1	5388254.8	2394863.9	3.1	3.5	4.3	-2423914.9	5388250.3	2394869.2	2.5	2.5	3.6
5933	DARWIN	-4071578.3	4714767.0	-1366533.3	4.3	4.4	4.3	-4071568.4	4714253.3	-1366528.3	3.2	3.2	3.7
5934	MANUS	-5367671.7	3437861.4	-225419.4	3.6	3.5	3.8	-5367663.1	3437869.9	-225416.0	2.5	2.5	3.3
5935	GUAM	-5059832.6	3591194.2	1472759.4	2.9	3.0	3.4	-5059825.7	3591186.0	1472762.5	2.1	2.2	2.8
5937	PALAU	-4433470.5	4512939.3	809955.3	3.1	3.2	3.7	-4433463.6	4512930.3	809958.7	2.2	2.2	3.2
5938	GUADALCANAL	-5915106.0	2146873.2	-1037912.8	4.4	3.9	4.0	-5915096.5	2146860.8	-1037909.5	3.0	3.0	3.5
5941	MAUI	-5467771.9	-2381242.7	2254024.0	3.5	3.2	4.4	-5467757.3	-2381246.7	2254033.8	2.5	2.8	3.8
6001	THULE	546566.4	-1389993.6	6180242.4	2.7	2.7	4.4	546568.7	-1389993.7	6180236.7	2.6	2.4	3.4
6002	BELTSVILLE	1130762.7	-4830837.6	3994709.9	2.2	2.7	3.1	1130764.9	-4830831.9	3994704.0	2.0	1.7	1.9
6003	MOSES LAKE	-2127839.9	-3785864.2	4656037.4	2.5	2.7	3.5	-2127832.1	-3785863.0	4656037.2	2.1	2.0	2.3
6004	SHEMYA	-3851806.8	396416.1	5051341.7	3.2	3.7	5.0	-3851797.5	396409.4	5051340.5	2.7	3.3	3.9
6006	TROMSO	2102930.3	721674.1	5958181.7	2.7	3.3	4.4	2102927.4	721660.5	5958180.8	2.4	2.9	2.9
6007	TERCEIRA	4433653.3	-2268156.9	3971671.0	2.7	2.7	3.8	4433637.3	-2268151.4	3971655.0	2.0	2.2	2.5
6008	PARAMARIBO	3623257.3	-5214236.7	601534.8	3.4	3.3	3.6	3623241.0	-5214233.7	601536.1	2.1	2.0	2.9
6009	QUITO	1280834.0	-6250966.2	-10805.5	3.8	5.9	4.5	1280834.2	-6250955.9	-10800.6	3.6	3.4	4.1
6011	MAUI	-5466039.2	-2404429.3	2242224.6	4.4	3.4	3.9	-5466018.6	-2404431.5	2242224.4	3.0	2.9	3.3

Table 14 (cont'd)

STATION		SOLUTION WN-12						SOLUTION WN-14					
NO	NAME	U	V	W	σ_u	σ_v	σ_w	U	V	W	σ_u	σ_v	σ_w
6012	WAKE ISLAND I	-5858578.8	1394516.4	2093817.4	2.9	3.2	3.8	-5858569.3	1394508.7	2093820.3	2.1	2.6	3.2
6013	KANOYA	-3565901.4	4120723.2	3303426.9	4.0	5.2	5.9	-3565892.8	4120713.6	3303428.3	3.3	4.4	4.9
6015	MASHHAD	2604355.4	4444169.2	3750321.7	2.6	2.9	3.5	2604353.3	4444166.0	3750320.5	2.1	2.2	2.6
6016	CATANIA	4896394.6	1316176.2	3856670.7	2.4	2.8	3.2	4896388.3	1316172.1	3856668.2	1.8	2.2	2.2
6019	VILLA DOLORES	2280630.7	-4914547.7	-3355417.9	2.7	3.6	5.2	2280627.1	-4914543.2	-3355402.8	2.4	2.7	3.7
6020	EASTER ISLAND	-1858621.5	-5354898.4	-2095762.3	6.0	6.1	6.9	-1858614.3	-5354894.4	-2095749.0	5.4	4.5	5.5
6022	TUTUILA	-6099975.9	-997357.7	-1568593.6	4.8	3.9	5.2	-6099961.7	-997362.2	-1568585.5	3.4	3.6	4.7
6023	THURSDAY ISLAND	-4955391.2	3842255.7	-1163855.5	4.5	3.9	4.7	-4955386.8	3842247.8	-1163847.4	3.2	3.0	4.0
6031	INVERCARGILL	-4313830.4	891340.6	-4597277.7	4.4	4.2	5.3	-4313825.3	891333.9	-4597265.8	3.4	3.9	3.8
6032	CAVERSHAM	-2375426.0	4875557.6	-3345424.5	3.7	4.3	5.0	-2375420.6	4875546.7	-3345411.1	3.3	3.2	3.9
6038	SOCORRO ISLAND	-2160989.6	-5642717.9	2035360.0	2.9	3.8	4.4	-2160980.9	-5642710.5	2035367.8	2.5	2.8	3.8
6039	PITCAIRN ISLAND	-3724775.0	-4421234.4	-2686094.4	7.9	7.2	7.3	-3724765.9	-4421237.6	-2686084.7	6.2	5.4	5.5
6040	COCOS ISLAND	-741986.1	6190803.6	-1330567.1	4.7	4.8	4.7	-741981.7	6190792.9	-1330546.3	4.5	3.7	4.2
6042	ADDIS ABABA	4900752.0	3968255.1	966318.9	2.7	2.9	3.4	4900750.7	3968252.7	966325.3	2.0	2.1	2.9
6043	CERRO SOMBRERO	1371376.5	-3614750.6	-5055947.1	3.5	4.2	7.0	1371375.9	-3614750.3	-5055927.8	3.3	3.8	4.8
6044	HEARD ISLAND	1098098.5	3684617.0	-5071900.1	6.9	6.7	11.1	1098097.9	3684606.6	-5071873.1	6.8	6.2	7.8
6045	MAURITIUS	3223434.7	5045343.6	-2191818.0	3.6	4.0	4.6	3223432.0	5045336.3	-2191805.7	3.2	3.1	3.9
6047	ZAMBOANGA	-3361983.5	5365820.6	763620.5	3.1	3.4	3.8	-3361976.9	5365811.9	763624.7	2.4	2.3	3.2
6050	PALMER STATION	1192679.3	-2451013.2	-5747052.4	5.0	6.3	9.8	1192678.8	-2451015.6	-5747034.2	4.9	6.1	6.1
6051	MAWSON STATION	1111337.1	2169270.2	-5874355.2	5.0	4.2	7.3	1111336.1	2169262.7	-5874334.1	4.9	3.7	4.4
6052	WILKES STATION	-902611.4	2409530.0	-5816569.9	4.6	4.4	7.4	-902608.8	2409522.1	-5816551.8	4.4	4.0	5.4
6053	MCMURDO STATION	-1310854.8	311262.9	-6213294.3	4.8	4.8	7.4	-1310852.3	311257.5	-6213276.5	4.6	4.5	4.3
6055	ASCENSION ISLAND	6118349.3	-1571749.2	-878601.3	3.3	2.9	3.4	6118334.2	-1571748.3	-878596.5	2.3	2.3	2.8
6059	CHRISTMAS ISLAND	-5885350.2	-2448374.4	221663.6	4.3	3.4	4.5	-5885333.5	-2448379.0	221671.1	2.7	2.9	3.8
6060	CULGOORA	-4751655.0	2792065.7	-3200174.2	4.5	4.0	4.7	-4751650.0	2792058.1	-3200164.0	3.3	3.3	3.7
6061	SOUTH GEORGIA IS.	2999921.2	-2219366.3	-5155267.1	3.9	5.9	7.8	2999915.6	-2219369.3	-5155246.0	3.7	5.7	5.3
6063	DAKAR	5084479.3	-1653496.4	1612858.7	2.4	2.6	3.2	5084467.4	-1653495.8	1612855.1	1.7	2.1	2.5
6064	FORT LAMY	6023394.4	1617934.2	1331731.7	3.3	3.1	3.7	6023386.7	1617931.9	1331733.2	2.7	2.6	3.2
6065	HOHENPEISSENBERG	4213570.2	820833.7	4702786.5	2.6	3.0	3.6	4213564.6	820830.0	4702784.4	2.0	2.4	2.3
6066	WAKE ISLAND II	-5858580.7	1394474.0	2093843.0	2.9	3.2	3.8	-5858571.2	1394466.4	2093846.0	2.1	2.6	3.2
6067	NATAL	5186415.0	-3653935.9	-654280.7	3.3	2.8	3.1	5186397.1	-3653933.3	-654276.9	2.1	2.2	2.6
6068	JOHANNESBURG	5084837.1	2670346.5	-2768109.3	4.2	3.5	5.3	5084830.4	2670341.2	-2768095.2	3.0	2.9	4.2
6069	TRISTAN DA CUNHA	4978430.9	-1086871.1	-3823187.7	8.3	6.6	10.4	4978421.7	-1086874.0	-3823167.8	6.5	6.4	8.1
6072	CHIANG MAI	-941707.8	5967462.5	2039307.4	5.9	5.1	4.9	-941702.1	5967455.1	2039311.6	5.7	4.0	4.3
6073	DIEGO GARCIA	1905134.3	6032292.0	-810742.3	3.7	4.8	4.7	1905134.1	6032282.4	-810732.7	3.4	3.7	4.2
6075	MAHE	3602824.5	5238240.2	-515957.7	4.2	4.6	4.5	3602820.6	5238240.7	-515948.3	3.8	3.6	4.0
6078	PORT VILA	-5952307.7	1231910.5	-1925983.7	19.9	9.4	16.6	-5952303.4	1231904.9	-1925972.5	9.7	8.0	12.4
6111	WRIGHTWOOD I	-2448862.8	-4667992.3	3582759.4	3.0	3.2	3.8	-2448853.3	-4667985.8	3582754.9	2.6	2.1	2.4
6123	POINT BARROW	-1881807.4	-812435.3	6019599.3	4.9	4.6	7.1	-1881799.4	-812439.0	6019590.7	4.6	4.4	4.5
6134	WRIGHTWOOD II	-2448916.5	-4668082.4	3582454.1	3.0	3.2	3.8	-2448907.0	-4668075.9	3582449.6	2.6	2.1	2.4

Table 14 (cont'd)

STATION		SOLUTION WN-12						SOLUTION WN-14					
NO	NAME	U	V	W	σ_u	σ_v	σ_w	U	V	W	σ_u	σ_v	σ_w
7036	EDINBURG	-828491.0	-5657486.5	2816825.5	3.8	3.9	4.0	-828487.0	-5657471.3	2816816.0	3.5	2.4	2.9
7037	COLUMBIA	-191294.8	-4967308.3	3903264.5	3.2	3.5	3.9	-191291.0	-4967293.9	3903252.6	2.9	2.2	2.4
7039	BERMUDA	2308214.8	-4873614.8	3394568.4	3.7	5.3	5.0	2308213.4	-4873598.3	3394558.5	3.3	3.1	3.6
7040	SAN JUAN	2465050.9	-5534945.5	1985522.2	4.0	4.4	4.7	2465049.5	-5534930.0	1985513.1	3.7	3.2	4.0
7043	GREENBELT	1130706.5	-4831337.2	3994141.4	2.2	2.7	3.1	1130708.6	-4831331.3	3994135.5	2.0	1.7	1.9
7045	DENVER	-1240475.1	-4760256.0	4048997.8	4.6	4.2	4.7	-1240470.2	-4760242.1	4048985.3	4.2	2.8	2.9
7072	JUPITER	976261.3	-5601416.4	2880251.4	2.5	3.3	3.3	976261.3	-5601399.9	2880241.9	2.2	1.8	2.3
7075	SUDBURY	692618.7	-4347090.4	4600487.7	4.0	5.7	5.4	692620.7	-4347076.5	4600475.4	3.7	3.8	3.4
7076	KINGSTON	1384159.2	-5905680.0	1966554.4	4.3	5.8	5.9	1384158.7	-5905662.0	1966545.7	4.1	4.4	5.3
8009	WIPPOLDER	3923429.9	299866.1	5003013.3	13.3	13.1	15.2	3923397.4	299869.4	5002975.5	8.5	10.1	6.9
8010	ZIMMERWALD	4331312.7	567499.7	4633118.9	7.9	10.9	11.5	4331307.0	567490.8	4633108.3	5.7	8.3	5.4
8011	MALVERN	3920186.9	-134806.7	5012776.2	12.8	16.5	15.5	3920153.5	-134804.5	5012734.8	8.9	14.3	6.9
8015	HAUTE PROVENCE	4578328.1	457945.6	4403204.8	6.4	10.7	10.2	4578322.1	457936.5	4403195.3	4.2	8.0	4.4
8019	NICE	4579469.1	586582.7	4386428.4	6.3	10.6	10.1	4579463.2	586573.5	4386419.2	4.1	7.9	4.3
8030	MEUDON	4205629.1	163695.4	4776550.9	9.0	12.3	11.8	4205626.9	163683.4	4776540.6	6.5	9.7	5.8
9001	ORGAN PASS	-1535755.1	-5167026.6	3401047.1	4.6	3.9	3.8	-1535750.7	-5167014.4	3401039.4	4.2	2.8	2.7
9002	OLIFANTSFONTEIN	5056115.1	2716514.0	-2775782.9	4.2	3.6	5.3	5056108.4	2716508.7	-2775768.8	3.0	3.0	4.2
9004	SAN FERNANDO	5105589.8	-555269.7	3769680.6	6.3	12.9	8.5	5105581.5	-555271.5	3769676.0	3.4	10.0	4.0
9005	TOKYO	-3946751.4	3366303.2	3698830.3	11.2	10.3	9.8	-3946730.5	3366286.1	3698822.9	9.2	9.0	7.5
9006	NAINI TAL	1018153.3	5471119.3	3109622.2	14.2	10.9	9.6	1018164.5	5471108.7	3109625.6	12.4	5.5	6.0
9007	AREQUIPA	1942762.4	-5804101.6	-1796905.8	2.8	4.0	5.3	1942760.9	-5804088.2	-1796900.9	2.5	2.9	4.4
9008	SHIRAZ	3376872.6	4403990.0	3136250.1	8.1	10.3	9.5	3376875.2	4403976.2	3136257.3	6.8	6.1	6.1
9009	CURACAO	2251613.5	-5816933.6	1327169.7	2.8	3.5	3.8	2251810.7	-5816917.6	1327163.4	2.4	2.1	3.4
9010	JUPITER	976276.2	-5601418.8	2880244.0	2.5	3.3	3.3	976276.2	-5601402.2	2880234.5	2.1	1.8	2.3
9011	VILLA DOLORES	2280578.9	-4914584.8	-3355398.8	2.7	3.6	5.3	2280575.3	-4914580.2	-3355383.7	2.4	2.7	3.7
9012	MAUI	-5466088.5	-2404310.5	2242188.7	4.5	3.4	3.9	-5466067.8	-2404312.7	2242180.4	3.0	2.9	3.3
9021	MOUNT HOPKINS	-1936799.1	-5077719.4	3331926.1	7.3	6.8	6.4	-1936789.3	-5077714.7	3331922.7	7.1	5.3	5.3
9028	ADDIS ABABA	4903727.7	3965208.6	963853.2	2.8	2.9	3.4	4903726.6	3965206.3	963859.6	2.1	2.1	2.9
9029	NATAL	5186459.3	-3653074.6	-654317.9	3.4	2.9	3.2	5186441.4	-3653071.9	-654314.1	2.1	2.2	2.7
9031	CONCORDIA R*DAVIA	1693795.5	-4112354.3	-4556644.1	8.4	9.4	14.3	1693797.3	-4112353.1	-4556622.0	8.3	8.8	11.2
9051	ATHENS	4606866.7	2029708.0	3903567.4	6.0	12.6	8.9	4606861.5	2029692.2	3903562.2	4.2	10.3	4.4
9091	DIONYSOS	4595164.1	2039433.4	3912675.8	6.0	12.6	8.9	4595158.9	2039417.6	3912670.6	4.2	10.3	4.4
9424	COLD LAKE	-1264834.5	-3466912.6	5185449.2	5.2	6.5	7.7	-1264831.9	-3466915.4	5185450.9	4.7	5.5	4.3
9425	EDWARDS AFB	-2450022.2	-4624438.2	3635041.1	3.1	3.2	3.8	-2450012.7	-4624431.6	3635036.6	2.6	2.2	2.4
9426	HARESTUA	3121262.6	592607.0	5512720.9	9.6	11.4	15.5	3121261.3	592605.7	5512723.0	8.6	9.4	5.8
9427	JOHNSTON ISLAND	-6007458.1	-1111834.2	1825730.0	10.9	20.6	8.8	-6007428.7	-1111852.5	1825733.9	8.9	19.8	8.6
9431	RIGA	3183691.2	1421439.3	5322819.8	13.1	11.7	14.7	3183897.6	1421426.7	5322814.7	12.3	9.4	7.0
9432	UZHGOROD	3907423.8	1602394.2	4763932.7	10.2	12.6	13.7	3907419.2	1602378.6	4763922.1	7.9	10.4	5.9

6. Acknowledgment

This investigation was partially sponsored through NASA Grant No. NGL 36-008-093. Some free computer time was provided by The Ohio State University Computer Center.

Grateful acknowledgment is given to the organizations mentioned in the introduction for supplying the observational data, the basic ingredients of this work, and other information always without reservations or delay.

The author wishes also to acknowledge his appreciation to M. Kumar, J.P. Reilly, N.K. Saxena and T. Soler for their part in handling the computer work, and for other assistance, many times on call beyond duty.

7. References

ANDERLE, R.J. 1973. Transformation of Terrestrial Survey Data to Doppler Satellite Datum. *J.geophys.Res.* (in press).

BLAHA, G. 1971. Inner Adjustment Constraints with Emphasis on Range Observations. *Reports of the Department of Geodetic Science* 148,The Ohio State University,Columbus Ohio.

GAPOSCHKIN, E.M., VEIS, G. & LATIMER, J. 1973. Smithsonian Institution Standard Earth III Coordinates. *First International Symposium, The Use of Artificial Satellites for Geodesy and Geodynamics.* Athens.

HEISKANEN, W.A. & MORITZ, H. 1967. *Physical Geodesy.* Freeman,San Fransisco.

KUMAR, M. 1972. Coordinate Transformation by Minimizing Correlations Between Parameters. *Reports of the Department of Geodetic Science* 184,The Ohio State University,Columbus Ohio.

LERCH, F.J. ET AL. 1972. Gravitational Field Models for the Earth. *International Symposium on Earth Gravity Models and Related Problems.* St. Louis Missouri.

MARSH, J.G., DOUGLAS, B.C. & KLOSKO, S.M. 1973. A Global Station Co-ordinate Solution Based Upon Camera and Laser Data - GSFC 1973. *First International Symposium,The Use of Artificial Satellites for Geodesy and Geodynamics.* Athens.

MARTIN, C.F. & VAN FLANDERN, T.C. 1970. Secular Changes in the Lunar Ephemeris. *Science* 168,246-247.

MUELLER, I.I. & WHITING, M.C. 1972. Free Adjustment of a Global Satellite Network (Solution MPS-7). *Reports of the Department of Geodetic Science* 188,The Ohio State University,Columbus Ohio.

MUELLER, I.I., KUMAR, M., REILLY, J.P. & SAXENA, N. 1973a. Free Geometric Adjustment of the DOC/DOD Cooperative Worldwide Geodetic Satellite (BC-4) Network. *Reports of the Department of Geodetic Science* 193,The Ohio State University,Columbus Ohio.

MUELLER, I.I., KUMAR, M & SOLER, T. 1973b. Free Geometric Adjustment of the SECOR Equatorial Network. *Reports of the Department of Geodetic Science* 195,The Ohio State University, Columbus Ohio.

MUELLER, I.I. & KUMAR, M. 1973c. Geometric Adjustment of the South American Satellite Densification (PC-1000) Network. *Reports of the Department of Geodetic Science* 196,The Ohio State University,Columbus Ohio.

MUELLER, I.I., KUMAR, M., REILLY, J.P., SAXENA, N. & SOLER, T. 1973d. Global Satellite Triangulation and Trilateration for the National Geodetic Satellite Program. *Reports of the Department of Geodetic Science* 199,The Ohio State University,Columbus Ohio.

RAPP, R.H. 1973. Comparison of Least Squares and Collocation Estimated Potential Coefficients. *Reports of the Department of Geodetic Science* 200,The Ohio State University,Columbus Ohio.

8. Discussion

MELCHIOR: Can you tell me where the BIH zero meridian is, and where CIO is?

MUELLER: Theoretically, the BIH zero meridian and CIO should be exactly those of WN14, for they were enforced in this solution.

MELCHIOR: The NWL solution has also been adjusted to that.

MUELLER: These numbers (transformation parameters) are based on the published co-ordinates and there is no agreement. We have done a lot of thinking since this thing was noticed last June and there is no easy explanation. In the dynamic solution, due to the fact that some of the harmonic coefficients are enforced to be zero, some biasing can happen to the co-ordinate systems. I hope that next summer we can have a conference on the topic to resolve this problem.

BOMFORD: A variety of co-ordinates are being produced for stations on the world network. In Europe, no co-ordinate system has yet been adopted because every four years at the IAG more information is produced which people think should be included. I ask our colleagues from the United States if WN14, which I think is an excellent solution, is likely to be adopted in any formal way? Do we wait till we go to Grenoble in 1975, by which time there is likely to be some more information? What is likely to happen?

MUELLER: I think this is a political question. I really cannot answer this at all. We have to keep producing improved solutions and let someone else decide on which of the systems should be used. A scientist always *uses* the best current solution and not an earlier *adopted* one. My suggestion is : Don't wait for an international body to adopt a solution. A user should decide on which set suits his needs and then determine the relations between this system and all other available systems.

RAPP, R.H.
Department of Geodetic Science
The Ohio State University
Columbus Ohio 43210
United States of America

Proc.Symposium on Earth's Gravitational Field & Secular Variations in Position (1973),554-558.

ADJUSTED PARAMETERS OF A MEAN EARTH ELLIPSOID

ABSTRACT

Independent estimates of **a**, J_2, kM_E (of the solid Earth), R_o (scale factor for lengths), γ_e (equatorial gravity) and a fixed ω are used in a weighted least squares adjustment to determine adjusted values for the variable parameters assuming a rotational bi-axial equipotential ellipsoid as the figure of reference. The adjusted values are:

$kM_E = (3.986\ 003\ 4 \pm 0.000\ 002\ 3) \times 10^{14}\ m^3 sec^{-2}$;

$\gamma_e = 978\ 031.69 \pm 0.77$ mgal;

$f = 1/(298.256\ 36 \pm 0.001\ 47)$;

$R_o = 6\ 363\ 674.98 \pm 2.50$ m;

$a = 6\ 378\ 139.0 \pm 2.51$ m; and

W_o (the geoid potential) = 6 263 681.62 kgal m.

1. Introduction

The estimation of the parameters of a mean Earth ellipsoid is one of the important goals of geodetic work. This paper is written to briefly summarize the results found recently for mean Earth ellipsoid parameters using currently available data. A more detailed paper is currently in preparation.

2. Dynamic Ellipsoid Parameters

We define the ellipsoid of interest to be an equipotential bi-axial ellipsoid. We consider the following quantities related to this ellipsoid:

ω, the rotational velocity of the ellipsoid. We adopt the value for ω as used in the Geodetic Reference System 1967: $\omega = 0.729\ 211\ 514\ 67 \times 10^{-4}$ (IAG 1971). This value is considered fixed.

kM_E, the geocentric gravitational constant of the Earth excluding the atmosphere. A current estimate of kM including the atmosphere is $kM_{E+A} = 3.986\ 008\ 0 \times 10^{14} m^3 sec^{-2}$ (ESPOSITO & WONG 1972). Discussions with Esposito indicate that a reasonable standard deviation for this estimate is $\pm 0.000\ 002\ 5 \times 10^{14} m^3 sec^{-2}$. To determine kM_E we subtract the mass of the atmosphere given by OLCZAK (1970) as $kM_A = 0.000\ 003\ 4 \times 10^{14} m^3 sec^{-2}$, yielding $kM_E = (3.986\ 004\ 6 \pm 0.000\ 002\ 5) \times 10^{14} m^3 sec^{-2}$ for the value to be used in this paper.

γ_e, equatorial gravity. Given a set of gravity anomalies referred to an arbitrary gravity formula, a new gravity formula (a γ_e, and a flattening) can be derived by least squares techniques (HEISKANEN & VENING MEINESZ 1958,p.76). Using a set of 24,260 1° × 1° mean free air anomalies a best estimate of γ_e was determined to be $978\ 030.9 \pm 1$ mgal where the flattening implied by the gravity formula was fixed at 1/298.256. In determining

this γ_e, all anomalies were given equal weights and a Potsdam correction of -14 mgal (IAG 1971) was used.

f, the flattening. The flattening was not directly estimated. Instead we choose to use a determination of J_2, the second degree zonal potential coefficient, as carried out by WAGNER (1972). The value of J_2 used was $(1082.635 \pm 0.011) \times 10^{-6}$. J_2 can be almost directly related to the flattening using equations given by COOK (1959) or HEISKANEN & MORITZ (1967, p.73).

R_o, the scale factor for lengths is defined to be (BURSA 1969)

$$R_o = kM/W_o \qquad (1),$$

where W_o is the potential on the geoid. If we know the geocentric positions of points on the geoid, we can determine W_o from (IBID)

$$W_o = \frac{kM_E}{r_i}\left(1 + \sum_{\ell=2}^{N}\left(\frac{a}{r_i}\right)^{\ell}\sum_{m=0}^{\ell}\left(\overline{C}_{\ell m}\cos m\lambda + \overline{S}_{\ell m}\sin m\lambda\right)\overline{P}_{\ell m}(\sin\Phi)\right) + \frac{\omega^2 r_i^2}{2}\cos^2\Phi \qquad (2),$$

where: r_i = the geocentric radius to the geoid point;
Φ = the geocentric latitude; and
$\overline{C}_{\ell m}, \overline{S}_{\ell m}$ = fully normalized potential coefficients.

Considering equation 1, we can see that R_o can be estimated (almost) independently of kM. The R_o is not completely independent of kM since the scale of the geocentric radius depends on the kM used in a satellite solution for geocentric station co-ordinates.

In order to estimate R_o we used the recent solution of the SAO Standard Earth III, and the Goddard Earth Model (GEM) 6. Both of these solutions used a $kM_{E+A} = 3.986\,013 \times 10^{14} m^3 sec^{-2}$ for their primary scale determination. Since we have decided to use a $kM_{E+A} = 3.986\,008\,0 \times 10^{14} m^3 sec^{-2}$ as our best estimate, we scaled the station co-ordinates of the SE III and GEM 6 using the $\Delta kM/3kM$ change discussed by KAULA (1967). After this a value of R_o was estimated separately for each solution with a weighted mean value of $R_o = 6\,363\,676.0 \pm 4.0\ m$ being found. The standard deviation assiged to R_o was computed considering the following factors:

- neglect of higher degree potential coefficients,
- errors in the potential coefficients,
- errors in the station co-ordinates,
- consistency of the R_o values from each solution, and
- the error in kM.

a, the equatorial radius may be computed from some or all of the above data. For example, the data needed for computing W_o, can be used to determine an equatorial radius. For this paper, however, we wish to determine an "a" from methods independent of previous data used. Such a method lies within the recent results from the geometrical satellite triangulation networks. In a presentation SCHMID (1972) indicated an equatorial radius from his geometric net to be on the order of 6 378 130 m. MUELLER (1973) gave a result for his geometric analysis only, of 6 378 125.8 m. Consideration of this data leads us to use an equatorial radius estimate of 6 378 128 ± 6 m where the standard deviation is based on accuracy considerations for the WN14 solution as given in (IBID).

3. The Adjustment

At this point we note that we need adopt only four parameters to completely define our mean Earth ellipsoid. If we use such a procedure, however, we will be forced to choose which of the above parameters are most reliable. An alternative procedure is to use all our data estimates and carry out a weighted least squares adjustment.

To formulate our adjustment model we first re-write equation 2-61 from (HEISKANEN & MORITZ 1967,p.67) to put it in the form:

$$\frac{1}{R_o} = \frac{W_o}{kM} = \frac{\tan^{-1} e'}{ae} + \frac{1}{3}\frac{\omega^2 a^2}{kM} \qquad (3).$$

We then write (IBID,equation 2-73) in the following form:

$$kM_E = \gamma_e a\, b \left(1 - m - \frac{m}{6}\frac{e'\, q'_0}{q_0}\right)^{-1} \qquad (4)$$

where all terms not defined here may be found in the reference quoted. Equations 3 and 4 were conceptually modified to incorporate J_2 as a shape (or flattening) parameter instead of the first (e) or second (e') eccentricity.

Considering equations 3 and 4 as our basic functional model, a generalized least squares adjustment was carried out. The a priori values and the standard deviations of the parameters kM_E, γ_e, J_2, R_o and **a** were assigned as previously discussed. The adjusted values were then obtained after the adjustment. A summary of the "a priori" values and the adjusted values are given in table 1.

Table 1

Adjustment of Earth Parameters

	A Priori	Adjusted	Units
ω*	7.292 115 146 7	7.292 115 146 7	$\times 10^{-5}$ sec^{-1}
kM_E	3.986 004 6 ±0.000 002 5	3.986 003 4 ±0.000 002 3	$\times 10^{14}$ m^{3}sec^{-2}
γ_e	978 030.9 ± 1.0	978 031.69 ± 0.77	mgal
J_2	1082.635 ± 0.011	1082.635 ± 0.011	$\times 10^{-6}$
R_o	6 376 676.0 ± 4.0	6 363 674.98 ± 2.50	m
a	6 378 128.0 ± 6.0	6 378 139.00 ± 2.51	m
kM^+_{E+A}	3.986 008 0	3.986 006 8	10^{14} m^{3}sec^{-2}
$W^+_o = \frac{kM_E}{R_o}$	6 263 682.5	6 263 681.62	kgal m
1/f +	298.257 18	298.256 36 ±0.001 47	

+ Derived Quantities * Fixed

The adjusted values given in table 1 are best estimates on the basis of the data available. As these change, so will the adjusted values. For example, if we let our a priori estimate of a have a standard deviation of 200 m, the adjusted value of "a" will be increased by 2.34 m.

4. Conclusions

The main results given in this paper are the numerical values given in table 1. They represent the results obtained by utilizing more data than the minimum needed to define an equipotential ellipsoid. The a priori values are based on current estimates of the parameters with, hopefully, realistic standard deviations.

The adjustment model incorporating R_o was chosen preferable to one incorporating W_o because W_o is strongly dependent on kM and thus estimates of W_o and kM would be correlated. The use of R_o eliminates most of the correlation although a small amount remains through the dependence of the magnitude of the geocentric radius on the adopted value of kM on the satellite solution. The potential correlation between R_o and kM was considered by performing adjustments where the correlation coefficient between R_o and kM was varied between 0.1 and 0.9. The effect on the results was less than 1 part in 10^7 and considered negligible.

The technique described in this paper allows us to use estimates of all the parameters defining a mean Earth ellipsoid and thus does not force us into the position of choosing what might be considered by some to be the most reliable parameters.

5. Acknowledgment

The computer time used in this study was provided by the Instruction and Research Computer Center of The Ohio State University.

Mr. D.P. Hajela carried out the necessary derivations for the adjustment procedures described here and prepared the necessary computer programs for carrying out the adjustment.

6. References

BURSA, M. 1969. Potential of the Geoidal Surface, the Scale Factor for Lengths and Earth's Figure Parameters from Satellite Observations. *Studia geophys. et geodet.* 13,337-358.

ESPOSITO, P.B. & WONG, S.K. 1972. Geocentric Gravitational Constant Determined from Mariner 9 Radio Tracking Data. *International Symposium on Earth Gravity Models & Related Problems*, St. Louis Mo.

IAG 1971. *Geodetic Reference System 1967.* Special Publication,International Association of Geodesy, Paris.

HAJELA, D.P. 1973. *Earth Model Parameter Adjustment Procedure.* (unpubl.) Department of Geodetic Science,The Ohio State University,Columbus Ohio.

HEISKANEN, W.A. & MORITZ, H. 1967. *Physical Geodesy.* Freeman,San Fransisco.

HEISKANEN, W.A. & VENING MEINESZ, F.A. 1958. *The Earth and its Gravity Field.* McGraw Hill,New York.

KAULA, W.M. 1967. Comparison and Combination of Satellites with Other Results for Geodetic Parameters. In (VEIS, G. ed.) *The Use of Artificial Satellites for Geodesy, Vol.II.* National Technical University,Athens.

MUELLER, I.I. 1973. Earth Parameters from Global Satellite Triangulation and Trilateration. In *Proceedings of Symposium on Earth's Gravitational Field & Secular Variations in Position*, University of New South Wales,Kensington NSW.

OLCZAK, T. 1970. The Earth Ellipsoid and Some Physical Constants Associated with It. *Acta Geophysica Polonica* XVIII(3-4) (Transl. Defence Mapping Agency Aerospace Center TC-1729,1971)

SCHMID, H. 1972. Presentation to 5th Symposium on Mathematical Geodesy (2nd Hotine Symp.),Florence.

WAGNER, C.A. 1972. Earth Zonal Harmonics from Rapid Numerical Analysis of Long Satellite Arcs. *Doc. X*-553-72-341, Goddard Space Flight Center, Greenbelt Md.

GRAFAREND, E.W.
Institut für Theoretische Geodäsie
Universität Bonn
Bonn
Federal Republic of Germany

Proc. Symposium on Earth's Gravitational Field & Secular Variations in Position (1973), 559.

VARIATIONAL PRINCIPLES AND THE ELLIPSOIDAL DATUM

ABSTRACT

Variational principles for the best fitting of a reference figure, for instance an ellipsoid, relative to a planetary figure are analysed in respect of their sensitivity. General orthonormal series solutions are presented for global criteria. Spectra of four difference norms (Euclidian distance, gradient distance, curvature distances) of a geoidal with respect to a rotational symmetric ellipsoidal surface are given and physically interpreted. Relative to a spherical integration surface, the principal semi-axis of a rotational ellipsoid is due to 6,378,132 m, ..., 120 m, ... , 140 m respectively for the Euclidian distance, the gradient distances and the invariant and the invariant curvature distances; its flattening 1/298.2553, ... .2553, ... .2571, ... .2448, ... .2494 respectively.

GODFREY, J.S.
Division of Fisheries & Oceanography
CSIRO
Cronulla NSW
A U S T R A L I A

Proc. Symposium on Earth's Gravitational Field & Secular Variations in Position (1973), 560-564.

MEAN SEA LEVEL: THE OCEANOGRAPHER's POINT OF VIEW

ABSTRACT

Oceanographers obtain a fair approximation to mean sea level in the open ocean, using water density measurements. The assumptions underlying this method will be discussed, together with the observational basis for these assumptions

Further assumptions and measurements are needed to extrapolate from mean sea levels in deep water to the shore, where results can be compared with geodetic levelling. HAMON & GREIG (1972) have used these techniques in the east Australian region, to obtain results very different to those from geodetic levelling. Independent oceanographic considerations support the Hamon-Greig picture over the geodetic results. These considerations are outlined.

1. Introduction

This paper is concerned with a discrepancy between the distribution of mean sea level along the east Australian coast, as found on one hand by geodetic levelling on land, and on the other by steric levelling at sea. The aim is to discuss and to some extent amplify the results of HAMON & GREIG (1972); it will be assumed that the reader is unfamiliar with oceanographic methods and assumptions.

The Division of National Mapping of the Australian Department of National Development recently reported the results of an extensive levelling survey of the Australian continent (ROELSE et al 1971). Among other studies, this report dealt with levelling from one tide gauge to the next, around the coast. A particularly striking feature to emerge from this work was that mean sea level appeared to rise quite strongly and steadily from Coffs Harbour, near the Queensland-New South Wales border, to Bamaga at the tip of Cape York. The total rise was 1.75 ± 0.5 metres; the error estimate makes generous allowance for random errors, due to permitted misclosures in third-order levelling. From Coffs Harbour south to Eden (near the New South Wales-Victorian border), the mean sea level was found to be relatively flat.

We concern ourselves here only with the mean sea level in this region, from Bamaga to Eden.

2. The Discrepancy

HAMON & GREIG (1972) collected all available measurements of steric sea level, relative to an assumed "level of no motion" at a depth of about 1300 metres below the sea surface, between the edge of the continental shelf and about 700 km offshore (the terms will be explained shortly). The pattern they obtained was quite different from the geodetic result: they found steric sea level to be essentially flat from 10°S to 30°S - i.e. from about the latitude of Bamaga to that of Coffs Harbour - and to drop sharply by about 50 cm from the latitude of Coffs Harbour to that of Eden (38°S).

Within the geographic "bins" used by HAMON & GREIG for averaging purposes, the individual observations

differed from one another by amounts of order 10 cm; thus the observations are definitely not consistent with a rise of anything like 175 cm from Coffs Harbour to Bamaga.

3. The Steric Levelling Technique

The ocean is typically 4000 metres deep; the steric levelling technique is based on the assumption that at any depth below about 1000 metres, there is very little *steady* motion. More specifically, it is assumed that the pressure, averaged over tides and transient meteorological phenomena, is constant along any geopotential surface deep down in the ocean - i.e. the isobar map at such depths is flat (since flow should follow the isobars in the ocean, the two statements are equivalent). We shall discuss this important assumption in the next section; if it is temporarily accepted, the steric levelling method may be simply explained.

The method consists of measuring temperature and salinity at various depths above the assumed "level of no motion". From these, the water density may be accurately inferred from the equation of state for seawater. Furthermore, order-of-magnitude estimates of terms in the equations of motion for seawater show that the hydrostatic relation should hold with great accuracy - i.e. the rate of increase of pressure with depth $\partial p/\partial z$ must equal water density ρ times the acceleration due to gravity g:

$$\frac{\partial p}{\partial z} = -g\,\rho \qquad (1)$$

Therefore the density data may be used to integrate upwards from the "level of no motion", to find what depth of water is needed to produce the constant pressure at that level. If the water is warm and light at all depths, a slightly greater height of seawater is needed to produce the constant pressure than is required in regions where the water is cold and dense. For example, water in offshore parts of the East Australian Current is typically warmer by several degrees than water on the inshore side; so the steric levelling technique indicates that the sea surface should stand higher offshore than inshore, by an amount that is sometimes as high as 50 cm.

4. "The Level of No Motion" Assumption

This is the crucial assumption underlying the steric levelling method, and we must discuss why oceanographers believe it to be valid. Three arguments will be advanced in favour of it. First, the ocean above about 1000 metres is quite inhomogeneous - the temperature of the surface water varies from typical values of $1^{\circ}C$ near the poles to $25^{\circ}C$ or more near the equator - whereas from 1500 metres to the bottom, the water is homogeneous within about $1^{\circ}C$, over the whole world ocean. This suggests that the water has moved to level out major horizontal density differences; there is thus little potential energy to drive flow at these great depths.

Secondly, five direct observations of currents at depths below 2000 metres have been made in the east Australian region, by tracking floats that are carefully weighted to drift at the appropriate depth. The highest speed found was 10 cm/sec, whereas surface currents directly above were generally of order 100 cm/sec (BOLAND & HAMON 1970).

Finally, if the contour plots of steric sea level truly reflect the mean sea level, then ocean currents should run parallel to steric level contours, just as winds in the atmosphere follow the isobars. The reason is that on a geopotential surface just below the sea surface, high mean sea

sea level implies high pressure; thus contour maps of steric sea level should also serve as isobar maps. Direct observation of currents, in the East Australian Current and elsewhere in the ocean, indicate that this is consistently the case: errors (which are due to the current measurement as much as to the steric levelling technique) are of order 20-30%.

5. Extrapolation to the Coast

Steric levelling can only be performed in deep water: some other method must be found to extrapolate from beyond the edge of the continental shelf, when steric levelling is possible, in to the coast. To do this, we can in principle use the statement that pressure gradients associated with slope in the sea surface should be balanced (to within terms of order 10%) by Coriolis forces; in particular, a net southward surface current should imply (in the southern hemisphere) a rise in mean sea level from the coast, eastward towards the continental slope. Rather little quantitative information is available about average currents over the Australian continental shelf: but it is known that really strong currents, potentially capable of causing a 20 cm rise in sea level from the coast to the edge of the continental shelf, are present only along the coasts of south Queensland and northern and central New South Wales. Currents from Sydney southwards are rather weak, and directed (on average) towards the south, whereas nearshore currents in the Coral Sea are weak and generally directed towards the north.

Consequently, HAMON & GREIG concluded that extrapolation of steric levels to the coast should not qualitatively change the result quoted earlier: mean sea level should be roughly flat along the north Queensland coast, and should fall about 50 cm (perhaps a few centimetres more) from southern Queensland down to Eden.

6. Other Oceanographic Evidence

Fairly elaborate numerical models of the ocean have been run recently; one in particular, due to BRYAN & COX (1968) was found to give a surprisingly good qualitative representation of the East Australian Current (GODFREY, in press). In this model, the crucial element determining the dynamics of the current system was, precisely, the slope of mean sea level along the shoreline: this slope could *not* be balanced by Coriolis forces (water cannot flow out of the coast). Instead the pressure gradient accelerated the current, and there was a close correlation between the slope of mean sea level at the shoreline, and the strength of the longshore current.

Applied to the East Australian Current, the model suggests that the strong southward current region - south Queensland and north to central New South Wales - should also be a region of strong fall in mean sea level towards the south: whereas the weak northward current region (northern Queensland) should be a region of slow fall in mean sea level towards the north.

These deductions are compatible with HAMON & GREIG's results, but not with geodetic results.

7. Conclusion

Over recent decades, oceanographers have made a number of theoretical studies of ocean circulation, based on the Navier-Stokes equations (essentially, Newton's laws of motion, applied to fluids). The result is a body of theory which, though by no means rigorous, nevertheless provides a coherent

qualitative explanation of a number of very different oceanographic phenomena. In the light of this theory, it is difficult to see how the slope of mean sea level along the east Australian coast found by geodetic levelling could be consistent with observed oceanographic phenomena in the region.

8. References

BOLAND, F.M. & HAMON, B.V. 1970. The East Australian Current 1965-1968. *Deep-Sea Res.* 17,777-794.

BRYAN, K. & COX, M.D. 1968. A Non-linear Model of an Ocean Driven by Wind & Differential Heating: Part 1 ..... *J.Atm.Sci.* 25,945-978.

GODFREY, J.S. 1974. On the Dynamics of the Western Boundary Current in BRYAN & COX's (1968) Numerical Model Ocean. *Deep-Sea Res.* (in press).

HAMON, B.V. & GREIG, M.A. 1972. Mean Sea Level in Relation to Geodetic Land Leveling around Australia. *J.geophys.Res.* 77,7157-7162.

ROELSE, A., GRANGER, H.W. & GRAHAM, J.W. 1971. The Adjustment of the Australian Levelling Survey 1970-1971. *Tech.Rep.* 12,Division of National Mapping,Canberra.

9. Discussion

MUELLER: Could you tell us how close the isobaric surface at 1300 m depth is to an equipotemtial surface? In the case of a rotating homogeneous ellipsoid, there is no difference between an equipotential and an isobaric surface. It could be that the discrepancies observed here in Australia and elsewhere are due to the assumption that the isobaric surface is not really an equipotential surface.

GODFREY: If you don't have pressure surfaces coincident with potential surfaces in the oceans or in the atmosphere, you must have flow - at least in the open ocean. This comes out in order of magnitude estimates of the Coriolis force which turns out to be much larger than other forces. The only thing that balances a pressure gradient is flow along isobars.

MUELLER: It could be possible to assume that the departure of about ½ m or so over such long distances can be due to differences between those two reference surfaces?

GODFREY: Off-shore that could happen. You could have a smooth rise ....

MUELLER: This is of course the only place where you can make your comparisons.

GODFREY: If you have such a slope at the edge of the continental shelf, then that pressure gradient will have to drive a current. You can't have Coriolis forces there.

TAPLEY: What is this magic number 1300 m?

GODFREY: It does not matter very much what depth you take. In the next paper (by STURGES), 2000 m is used in the Atlantic, while a lot of people use 1000 m depth in the Pacific. It is largely a matter of history. However, whatever depth you use, provided the depth is low enough, you do not get very large errors. STURGES gives a figure for it.

ANGUS-LEPPAN: What happens from 75 km off-shore to the shore. Do you measure the profile over the last 75 km?

GODFREY: You reverse the principles and work backwards. If you know the currents parallel to the shore, you can work out the slope of the sea surface. The sea surface heights are measured directly off-shore and the currents worked out from it. Close in, we can measure the currents and then work out the slope of the sea surface. The flow is generally southward, and you work inwards from there to get the sea surface height at the coast.

ANGUS-LEPPAN: The slope is deduced from the current?

GODFREY: Yes, but we do not have good observations for currents. You can only get a qualitative figure; it is of the order of 5-10 cm.

GRAFAREND: What is the definition of the "heights" you refer to ? Are they dynamical heights or normal heights?

GODFREY: They are what's called "dynamic" heights.

LAMBERT: How do you know that the isobaric surface 1300 m down is parallel to the isobaric surface at the top?

GODFREY: At 1300 m, the isobaric surface follows the equipotential surface. At the sea surface it does not, as the latter is a free surface.

LAMBERT: Do you believe that the equipotential surface at the surface is parallel to the equipotential surface 1300 m down?

GODFREY: I believe if you took two equipotential surfaces, one at 1300 m and the other at the sea surface, the upper one will intersect the real ocean surface.

LAMBERT: The point is that you are taking as a datum the equipotential surface 1300 m down, and assuming that there is a surface parallel to it that is going to coincide with zero elevation.

HOLDAHL: They (the oceanographers) are assuming it is parallel in the dynamic sense but not in the geometric sense.

WERNER: Your term "bar" - does it refer to a normal atmosphere?

GODFREY: Yes. When we refer to 1300 dbar, we refer to a location where a pressure gauge would measure a pressure of 1300 dbar. We don't really mean 1300 m.

STURGES, W.
Department of Oceanography
Florida State University
Tallahassee Florida
UNITED STATES OF AMERICA

Proc.Symposium on Earth's Gravitational Field & Secular Variations in Position (1973),565-572.

DISCREPANCY BETWEEN GEODETIC AND OCEANOGRAPHIC LEVELLING ALONG CONTINENTAL BOUNDARIES

ABSTRACT

On the basis of levelling results on land, sea level along US coasts is found to rise to the north, with a total change in level of about 1 m. For comparison, the variation of sea level along continental boundaries is studied from a variety of oceanographic data. Along the western boundaries of the Atlantic and Pacific oceans, sea level *falls* approximately 80 cm between the equator and 40° N or S. Along the eastern boundaries, the change in level is about one-third this amount. This meridional slope is shown to be the correct amount required by the change, with latitude, of surface slope across the boundary currents. The meridional slope along the inshore edge of the Gulf Stream has the correct sign and magnitude to be balanced by the gradient of the Reynolds stresses. In the east-west direction, sea level along the Pacific coast of the United States stands about 70 cm higher than along the Atlantic coast, in agreement with levelling. It is argued that if the cause of the discrepancy in the north-south direction is an extremely small systematic error in levelling, it would have a much smaller impact on the parent field than if the error lies in some fundamental concept in physical oceanography.

1. Introduction

Sea level on the Pacific coast of the United States stands higher than on the Atlantic coast. This result has been apparent in the United States levelling network for nearly fifty years. The evidence from oceanographic data is about as old, but the agreement between these observations has been recognised by few oceanographers. A renewed interest in information about sea level near the coasts has been stirred by recent work in geodesy, especially the promise of very high accuracy altimeters in satellites and also by new work in numerical simulation models of ocean circulation in which slopes of sea level appear along coastal boundaries.

The most recent published analysis of first-order levelling in North America has shown (BRAATEN & McCOMBS 1963), in the 1963 Special Adjustment, that sea level along the Pacific coast stands 62 cm higher than along the Atlantic coast, in agreement with earlier levelling work. The uncertainty in the levelling was estimated to be about 6 cm. Over the latitudes of comparison, 32°N to 42°N, the difference between the two coasts is independent of latitude (see STURGES 1967, figure 1). On the basis of oceanic (or steric) levelling, MONTGOMERY (1969) has estimated that the sea-level difference between the two coasts should be 70 cm, in close agreement with the results of geodetic levelling.

2. Sea-level Differences from Hydrographic Data

One of the major reasons for the difference in sea level across the American continent has long been recognised as the difference in density of the waters of the Atlantic and Pacific oceans. REID (1961a) has shown that the surface of the Pacific Ocean should stand higher than the Atlantic by 40 cm on the basis of geopotential relative to the 1000 db surface. This difference increases with deeper reference surfaces; MONTGOMERY (1969) showed that the deepest significant reference surface is

probably near 2000 db.

These differences discussed by REID, however, pertain to the zonally *averaged* level of the oceans. The largest slopes in the ocean are found in boundary currents, however, so it is clear that sea level *at the coasts* will depart considerably from the ocean-wide averages. In order to examine this effect, figure 1 shows, for the Atlantic and Pacific oceans, the height of steric sea level near the coasts. The quantity plotted is the geopotential anomaly of the sea surface relative to a deep pressure surface. (The anomaly is divided by gravity, to convert to length units.) To use this technique to infer sea-surface slope is usually called *steric levelling*. The data from the Pacific Ocean, relative to 1000 db, are from REID (1961b). In the Atlantic, relative to 2000 db, the data are from ANATI (1973), based on IGY data, and from DEFANT (1941). A single point in the Caribbean, from GORDON (1967), was adjusted from his map (1200 db) to 2000 db. Aside from the few points that are annual averages -- MONTGOMERY (1969), STURGES (1968) -- the data contain scatter caused by seasonal variations. PATTULLO et al (1955) have shown that these variations are typically 5 to 10 cm.

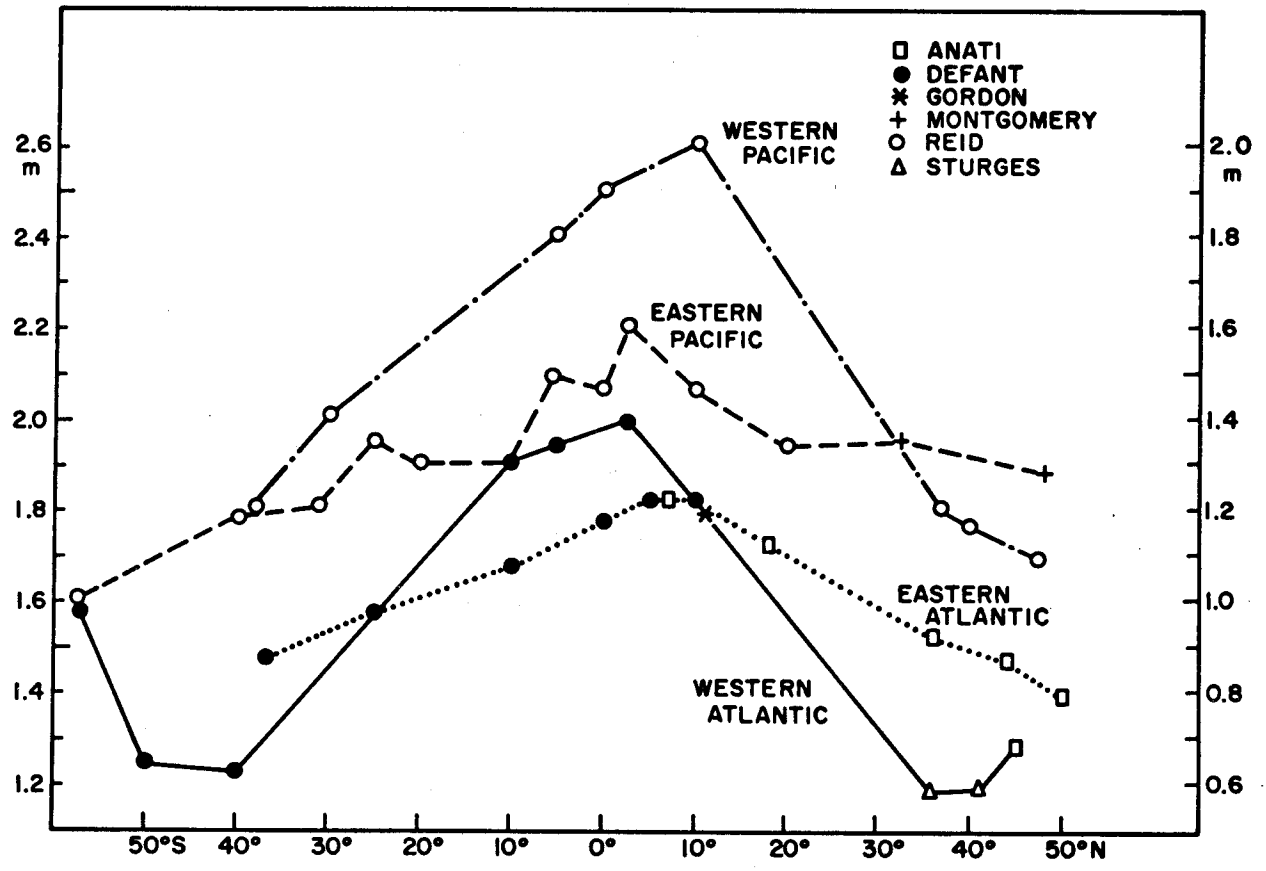

Figure 1. Dynamic height of the sea surface near continental boundaries versus latitude: Left ordinate, for Atlantic data, is relative to 2000 db; right ordinate, for Pacific data, is relative to 1000 db. Equivalence between the two scales is based on Montgomery's values and holds exactly only in the north-east Pacific.

The two scales in figure 1 (relative to 1000 db in the Pacific, relative to 2000 db in the Atlantic) are offset by 61 cm, the geopotential anomaly of the 1000-2000 db layer reported by MONTGOMERY (1969), for Ocean Weather Station Papa in the North Pacific.

The data in figure 1 are intended to apply as nearly as possible to *coastal* values, even though the data are obtained in water 1000 m to 2000 m deep. In regions with a narrow continental shelf, inside a weak boundary current, the change in level between deep water and the coast is a few centimeters at most; the change is also negligibly small at low latitudes. Inside a western boundary current, however, extrapolation to the coast would introduce large errors (by this technique), so no data points are included in figure 1 for these regions. As a result, we lose some detail in between; nevertheless, the average slope is correct.

A number of features in figure 1 deserve discussion. In both oceans, at low latitudes, the western side stands higher than the eastern side, as has long been recognised. The slope is reversed at higher latitudes. As REID (1961b) showed, for the Pacific, this difference closely parallels the wind stress at the sea surface. The cross-over for the Atlantic data in figure 1 is at a latitude which seems too low, but this problem is probably caused by the scatter of observations and relatively small difference in slope of the two lines.

There is a systematic difference in level between the Pacific and the Atlantic, caused by the density differences between the two oceans, and this difference is evident in figure 1. This difference is in agreement with the results of geodetic levelling across the United States, as mentioned above. It is also evident, however, that the coastal height depends on latitude, although the difference across the United States is a very weak function of latitude.

The difference across the American continent is a minimum at low southern latitudes; the apparent zero difference at 10°S is not reliable, in light of seasonal variability.

The single data point inside the Caribbean Sea is from GORDON (1967, figure 8). Near the Panama Canal, sea level (on Gordon's map) stands 5 cm higher; the resulting difference, near 8°N, between the Western Atlantic and Eastern Pacific is an estimate of the difference in sea level across the Panama Canal. This difference, near 8° to 10°N, is about 20 cm, but is subject to error from seasonal effects. The levelling across the Panama Canal, as cited by REID (1961a) gives a difference of 3/4 ft (23 cm) with the same sign as given here; the Pacific stands higher. Again, the levelling results agree with the findings of oceanic levelling.

The oceanic levelling is affected by the deep pressure surface used as a basis for the calculations. It has been shown (STURGES 1974) that the uncertainty introduced by this choice is only a few centimeters.

3. North-south Slope of Sea Level along North America

A feature that is apparent in Figure 1 is the meridional slope along each coast. The observation that sea level stands high at low latitudes is consistent with the primary thermal effect. In the Atlantic Ocean, the northeast trade winds, on the average, blow nearly perpendicularly into the coast of the American continent. The result is a piling-up of water there, balanced directly by the wind stress. One is struck by the observation (e.g. STOMMEL's 1965, figure 96), that the direction and magnitude of the annual mean wind stress and the orientation of the coastline seem to be optimised with regard to this piling-up of water at low latitudes. ANATI's figure 3 (sea surface topography

relative to 200 db) suggests that the sea surface along the northeast coast of Brazil, near 0° to $5^{\circ}N$, stands about 30 cm higher than in the open ocean at about $30^{\circ}N$.

The slope of sea level along a coastal boundary will be an important effect in connection with the boundary currents. This effect is examined by consideration of the momentum balance in the cross-stream and down-stream directions.

4. Momentum Balance in the Cross-stream Direction

It is generally accepted that the flow in a western boundary current is in geostrophic balance in the cross-stream direction. That is, the momentum balance is given, to a very good approximation, by

$$fv = i_x g \tag{1}$$

where f is the Coriolis parameter, v is the down-stream velocity (here to the North, taken to be in the y-direction), i_x is the slope of the sea surface in the x-direction, and g is gravity. The total change in level across the flow, Δh, is given by the cross-stream integral of equation 1 after rearranging,

$$\Delta h = \frac{f\bar{v}X}{g} \tag{2}$$

where $\bar{v}$ is the average surface speed over the width X. To see the effect of a current flowing to a different latitude, we differentiate equation 2 with respect to y:

$$\frac{\delta \Delta h}{\delta y} = \frac{f}{g}\frac{\delta \bar{v}X}{\delta y} + \frac{\bar{v}X}{g}\frac{\delta f}{\delta y} \tag{3}$$

the left-hand side is the meridional slope of sea level along the coast, if the offshore edge of the current is assumed to remain level. The coastal slope can be corrected for slope of the offshore edge, as discussed below.

The first term on the right in equation 3 is the meridional change in the surface transport per unit depth. The second term is the result of variation of the Coriolis parameter with latitude. If these terms can be evaluated, they will provide an independent test of the meridional slope shown in figure 1. I have computed the necessary values from available observations in a single boundary current, the Gulf Stream. The values are given in table 1. The quantity $\bar{v}X$ was computed from the surface velocity at each section, and the total change in level, Δh, was calculated from equation 2. There seemed to be a small variation in $\bar{v}X$ over the latitude range of the available data, although there is a trend; the standard deviation is only 8% of the average value. Some of this scatter is surely observational error, but it is about the same magnitude as the variations in total transport as reported by SCHMITZ & RICHARDSON (1968). Presumably at lower latitudes, where the major flow is toward the west, the $\bar{v}X$ term may vary substantially. The total meridional slope of the sea surface required by the data in table 1 (through equation 3) is $2.8 \pm .3$ cm/deg. It should be emphasised that the data in table 1 (with two exceptions) are from direct velocity observations, and are independent of the density observations used for figure 1. The lowest latitude point, from the Caribbean Sea, is from geostrophic calculations; this point is included for completeness, but is not included in any calculations that follow. WARREN & VOLKMANN's (1968) velocity field was computed from hydrographic data plus Swallow floats. In all other cases, velocity was observed directly;

for some observations the surface velocity was determined by GEK, which in turn was calibrated with LORAN.

TABLE 1

Average surface transport in the Gulf Stream from direct observations.
The change in level across the stream, Δh, is computed from the geostrophic relation.

Latitude	$\bar{v}X$	Δh	Source
13° 0'N	$88 \times 10^7 cm^2/s$	30 cm	GORDON 1967
24°20'	110	68	RICHARDSON, SCHMITZ & NIILER 1969
24°45'	102	64	RICHARDSON, SCHMITZ & NIILER 1969
25°30'	111	71	RICHARDSON, SCHMITZ & NIILER 1969
25°40'	100	65	WEBSTER 1961
27°26'	108	75	RICHARDSON, SCHMITZ & NIILER 1969
28°21'	106	75	RICHARDSON, SCHMITZ & NIILER 1969
30° 0'	111	83	WEBSTER 1965
30°20'	114	86	RICHARDSON, SCHMITZ & NIILER 1969
32°24'	117	94	RICHARDSON, SCHMITZ & NIILER 1969
35° 0'	100	86	WEBSTER 1965
35°45'	117	103	WORTHINGTON & KAWAI 1970
38° 0'	123	103	VON ARX 1953
38° 0'	121	112	WARREN & VOLKMANN 1968
38°06'	109	101	WORTHINGTON 1954
Mean	110 ± 8		

The question of the slope of the offshore edge was investigated by forming averages of hydrographic data in areas beyond the edge of the Gulf Stream, where a substantial accumulation of hydrographic data was available. The results of that study suggest that sea level in mid-ocean, i.e. beyond the edge of the Gulf Stream, rises slightly to the North with an average slope of 0.8 ± .2 cm/deg latitude; this slope, of course, is relative to the slope of the 3000 db surface, which may be assumed negligible for the present purpose. The meridional change in total elevation across the Gulf Stream, as required by the results in Table 1 (from 25° to 38°N), is 2.8 ± .3 cm/deg. The difference between these slopes, 2.0 ± .4 cm/deg. must appear as a north-south slope of sea level along the inshore edge of the current. Sea level should fall to the North by this amount.

5. Momentum Balance in the Downstream Direction

It is appropriate to determine whether the meridional slope found, in the preceding section, on the inshore edge of the Gulf Stream can be reconciled with the momentum equation in the downstream direction. We can omit the details (see STURGES 1974) and merely give the result: the balance is between the longshore pressure gradient, caused by the sea-surface slope, and a term involving the so-called Reynolds stresses.

The Reynolds stress term may be evaluated from the results of SCHMITZ & NIILER (1969) in the Florida Current. Their figure 1g gives the distribution of Reynolds stress across the stream near 30°N; the gradient at the inshore edge is calculated to be $+2.5 \times 10^{-4}$ cm/sec^2. The magnitude of the pressure gradient caused by the slope of the sea surface is $\sim 2 \times 10^{-4}$ cm/sec^2. The conclusion, therefore, is that the Reynolds stress term has the correct sign and approximate magnitude to balance the pressure gradient associated with the surface slope determined from equation 3.

In summary: the slope along the coast of the Western Atlantic indicated in figure 1 from 12°N to 36°N is -2.5 cm/deg. The uncertainties in the data are approximately ± 2 cm in the annual average at 36°, ± 5 cm at 12°, and ± 5 cm from the slope of the 2000 db surface (on the inshore edge of the stream). The two *independent* estimates of slope are thus -2.5 ± .5 cm/deg from steric levelling (figure 1), compared with -2.0 ± .4 cm/deg from geostrophic levelling. The two methods are independent, and the two results agree quite well.

6. Comparison with Land Levelling

The results of geodetic levelling (BRAATEN & McCOMBS 1963) are that sea level should rise strongly from South to North along US coasts, with a slope of 2.8×10^{-7} on both coasts. This discrepancy has been discussed elsewhere (STURGES 1967; STURGES 1968).

The slope along the Atlantic coast, as found by levelling, is in sharp contrast with the value of -2×10^{-7} (-2.2 cm/deg) found in the present paper. More recent work, done since the special levelling adjustment of 1963 (S. HOLDAHL, private communication) suggests that the slope indicated by levelling along the US Pacific coast is even larger than was found by BRAATEN & McCOMBS. A similar disagreement with levelling results in Australia has been discussed by HAMON & GRIEG (1972). In a previous study of sea level along the Pacific coast, it was shown (STURGES, 1967) that the geodetic levelling results are at variance with the oceanic results.

The "confrontation" may be described as follows. The oceanic results involve the density field, the observed currents, and the well-known equations of motion. Two independent methods give, quantitatively, the same result (in this paper). A third method, independent of the first two, gives qualitatively the same result. To put it colloquially, "it all hangs together." To change the oceanographic results will require a first-order (i.e. large) change in our understanding of at least one of the quantities involved.

By contrast, the presence of an extremely small systematic error in the geodetic levelling - a few microns per sight - would account for the discrepancy between the two sets of results, and would involve no difficulties with the understanding of any fundamental processes. My own personal inclination is to take this second choice. One suspects strongly, on the basis of the oceanographic results put forward here, that the geodetic levelling contains systematic errors.

By contrast, the levelling results in Brazil (RODRIGUEZ 1970) indicate that sea level should rise 29 cm from Imbituba (28°S) to Fortaleza (4°S). This slope agrees refreshingly well with that shown in figure 1.

It is obviously necessary that the present discrepancy between land levelling and oceanic levelling be resolved, in order that we may use their combined results to provide urgently-needed information about circulation, geodesy, and other areas of importance near our coasts.

7. Acknowledgment

I am happy to thank Dr R. B. Montgomery for several helpful discussions throughout the course of this work, which was supported by the Office of Naval Research, Contract N00014-67A-0235-0002.

8. References

ANATI, David A. Some aspects of the relative geostrophic flow in the North Atlantic Gyre. *J.Mar.Res.* (in press).

BRAATEN, N.F. & McCOMBS, C.E. 1963. Mean sea level variations as indicated by a 1963 adjustment of first-order levelling in the United States. Unpublished technical report, US Coast & Geodetic Survey, Washington.

DEFANT, A. 1941. Die relative Topographie einzelner Druckflachen in Atl.Ozean. *Meteor.Werke.* 6/2.

GORDON, A.L. 1967. Circulation of the Caribbean Sea. *J.Geophys.Res.* 72(24), 6207-6223.

HAMON, B.V. & GRIEG, M.A. 1972. Mean sea level in relation to geodetic land levelling around Australia. *J.Geophys.Res.*77, 7157-7162.

MONTGOMERY, R.B. 1969. Comments on oceanic levelling. *Deep-Sea Res.* 16, *Suppl.*147-152.

PATTULLO, J, MUNK, W., REVELLE, R. & STRONG, E. The seasonal oscillation in sea level. *J.Mar.Res.* 14, 88-155. 1955.

REID, J.L. Jr. 1961a. On the temperature, salinity, and density differences between the Atlantic and Pacific oceans in the upper kilometer. *Deep-Sea Res.* 7(4). 265-275.

REID, J.L. Jr. 1961b. On the geostrophic flow at the surface of the Pacific Ocean with respect to the 1000 decibar surface. *Tellus.* 13. 489-502.

RICHARDSON, W.L., SCHMITZ, W.J. & NIILER, P.P. 1969. The velocity structure of the Florida Current from the Straits of Florida to Cape Fear. *Deep-Sea Res.* 16, *Suppl.*225-231.

RODRIGUEZ, L.V. 1970. Brasilian National System of first-order levelling. In *Report on the symposium on coastal geodesy.* Munich, July 1970: R. SIGL (ed), Inst. Astronom. Phys.Geodesy, Munich.

SCHMITZ, W.J. Jr. & NIILER, P.P. 1969. A note on the kinetic energy exchange between fluctuations and mean flow in the surface layer of the Florida Current. *Tellus.* 21(6), 814-819.

SCHMITZ, W.J. Jr. & RICHARDSON, W.S. 1968. On the Transport of the Florida Current. *Deep-Sea Res.* 15(6), 679-693.

STOMMEL, Henry. 1965. *The Gulf Stream.* 2nd ed. Univ. of Cal.Pr. Berkeley, 248 pp.

STURGES, Wilton. 1967. Slope of sea level along the Pacific Coast of the United States. *J.Geophys.Res.* 72, 3627-3637.

STURGES, W. 1968. Sea-surface topography near he Gulf Stream. *Deep-Sea Res.* 15, 149-156.

STURGES, W. 1974. Sea-level slope along continental boundaries. *J.Geophys.Res.* 79.

von ARX, W.S. 1952. Notes on the surface velocity profile and horizontal shear across the width of the Gulf Stream. *Tellus.* 3, 211-214.

WARREN, B.A. & VOLKMANN, G.H. 1968. Measurement of volume transport of the Gulf Stream south of New England. *J.Mar.Res.* 26(2), 110-126.

WEBSTER, F. 1961. The effect of meanders on the kinetic energy balance of the Gulf Stream. *Tellus.* 13, 392-401.

WEBSTER, F. 1965. Measurements of eddy fluxes of momentum in the surface layer of the Gulf Stream. *Tellus.* 17. 239-245.

WORTHINGTON, L.V. 1954. Three detailed cross-sections of the Gulf Stream. *Tellus.* 6(2), 116-123.

WORTHINGTON, L.V. & KAWAI, H. 1970. Comparison between deep sections across the Kuroshio and the Florida Current and Gulf Stream. In *'A Treatise on the Kuroshio*, eds: STOMMEL & YOSHIDO. Univ. Tokyo Press.

9. Discussion *

MARKOWITZ: Are the geodesists wrong? Is this discrepancy due to an error in the levelling?

HOLDAHL: It is very unlikely that the total discrepancy could be due to the accumulation of random levelling errors. The results of a recent adjustment showed the discrepancy between San Fransisco and Los Angeles to be 491 mm, whereas the standard error of the adjusted elevation difference between these points was only 40 mm.

MARKOWITZ: Then there is a genuine discrepancy?

HOLDAHL: Yes.

MUELLER: STURGES believes there is some systematic error in the levelling which no one knows anything about. This matter was discussed at the Fourth GEOP conference in Boulder last August, but I still dont understand after that session and the two presentations so far made here, what the basic reference surface is to which steric heights are referred. This is still a mystery to me. How do you define this surface which is 700 - 2000 m down?

GODFREY: The forces of pressure and gravity are essentially the same. The pressure is there because of gravity.

SYDENHAM: This can be resolved by the use of the (Division of) National Mapping laser ranging profiler which has actually picked up effects similar to this. This is an aircraft flown laser terrain profile recorder which has already, in tests, picked up about ½ m difference in sea surface in South Australian waters. It has a similar problem because it uses an isobaric surface for positioning reference.

BUCHWALD (Chairman): I think we all agree that this is a problem which needs resolving ....

WERNER: I notice from your comparison between geodetic levelling and (steric levelling), there is agreement with geodetic results when comparisons are made along a latitude circle. Along a meridian there is disagreement. I don't expect an answer but just introduce the point for discussion.

* Paper presented by J.S. GODFREY

MITCHELL, H. L.
University of Western Australia
Nedlands WA 6009
Australia

Proc. Symposium on Earth's Gravitational Field & Secular Variations in Position (1973), 573-584.

SEA-SURFACE TOPOGRAPHY IN GEODESY WITH PARTICULAR REFERENCE TO AUSTRALIA

ABSTRACT

The relationship between the physical ocean surface and the more elusive geoid provides a problem worthy of attention in geodesy, as well as in oceanography. Co-operation between these two disciplines can feasibly lead to results which would have application to geodetic techniques. These points are discussed in the light of current methods and accuracies.

Present-day knowledge of the existence, and causes, of separation between the two surfaces is summarized, but progress in the study of the phenomenon in Australia is considered in detail. Areas of concern and possible techniques for study in this vicinity point to possible future activity in the field of sea-surface topography.

1. Definition of Sea-Surface Topography

The sea-surface topography is represented by the separations, ζ, along the vertical, between the ocean surface and the geoid. The values, which are of positive sign when the sea-surface is above the geoid, vary both with position on the geoid and with time. The heights are also dependent on the particular equipotential surface which is accepted as being the geoid. However, provided that the reference surface is used consistently and is chosen at approximately the mean position of the sea-surface, this effect, in practice, is not significant.

The sea-surface topography is often represented by the *mean* rather than instantaneous, value of ζ, over a period of time, which will be signified here by $\overline{\zeta}$.

It is useful for the following discussion to recognise ζ as being composed of two parts:

(i) a known portion, for which corrections can be estimated, and

(ii) a remaining, unexplained portion.

2. Interest in Sea-Surface Topography

The determination of $\overline{\zeta}$ has significance in practical geodesy, as it enables the definition of the position of the geoid at those places where, and at the times when the ocean surface is available. This may enable objects on and above the physical surface to be related to the geoid more easily than by conventional methods, or even where existing methods are impossible. Applications, related to height determinations, could include:

(i) height datum comparisons, both inter-continental and intra-continental. The former has application to satellite tracking, for example, by permitting observation station heights to be tied to one geoid. An accuracy of datum extension of 10 cm corresponds to one part in 10^8 of the earth's radius.

(ii) determination of geoid heights at sea. Elevations to 1 m are necessary for free-air corrections to 0.3 mgal for gravity reductions.

(iii) determination of altitudes of satellites relative to the geoid, which may be provided over the oceans by altimeter measurements of the distance between the satellite and sea-surface. This technique will be discussed further below.

In oceanography, interest lies in the value of the separation ζ, rather than in the spatial position of either the ocean surface or the geoid. Areas of concern include tides, ocean currents and water density, air-pressure and wind effects, tsunamis and surface waves. Although it may seem, therefore, that such interests are not relevant to geodesy, it must be stressed that the converse is true. Geodetic determinations of the sea-surface topography would assist oceanographic study of the ζ function which may be used, in turn, in the geodetic applications mentioned above.

The problem of sea-surface topography in geodesy is to determine and explain the unknown portion of the sea-surface topography in order to be able to specify ζ to an accuracy which is suitable for present purposes. Oceanographic knowledge presently provides estimates of ζ. If sample values of the true separation can be collected, it seems feasible that the value of sea-surface topography could be provided to an accuracy of 10 cm. The required level of accuracy of ζ depends on its intended use, but 10 cm seems adequate for geodetic purposes, as mentioned above. This approach to the problem assumes that the separation between the geoid and sea-surface cannot generally be determined whenever required and would, instead, be calculated if necessary using such data as ocean conditions. The following sections discuss the present state of knowledge of the expected and apparent sea-surface topographies, particularly around Australia.

3. Present Knowledge of the Existence of ζ

Observations of ζ are presently supplied by connections between geodetic levelling networks and tide-gauges. Levelling provides heights of the physical surface of the earth above an equipotential surface. The tide-gauges can be used to relate the sea-surface, or usually the mean sea-surface over a time period, to the physical surface. By combining levelling and tide-gauge observation, therefore, the sea-surface can be related to an equipotential surface.

Levelling in the United European Levelling Network, as reported by LEVALLOIS (1960) showed some variations between sea-level and levelled heights. If the levelling results were assumed to be correct, then sea-level had an apparent elevation of +28 cm at Kemi, Finland, an apparent elevation of +14 cm at Cascais, Portugal, and of -34 cm at Genoa on the Mediterranean Sea. Generally sea-levels had apparent elevations of the order of $\pm$10 cm in this network.

The first order levelling net of France of 1969 indicated that differences in sea-level around the coastline were up to half a metre (LEVALLOIS & MAILLARD 1970).

U.S. experience, as reported by STURGES (1967) and BRAATEN & McCOMBS (1963), based on the levelling used in the 1963 adjustment by the U.S. Coast and Geodetic Survey indicated that the sea-surface slopes upward from North to South by about 50 cm along both the Pacific and Atlantic coasts, and that at a given latitude, the Pacific Ocean is higher than the Atlantic Ocean.

The 1970 re-adjustment of the geodetic levellings of Great Britain, connected to about six gauges, showed maximum and minimum sea-levels to differ by 29 cm, between Aberdeen in Scotland and Newlyn in the south (KELSEY 1970).

RODRIGUEZ (1970) reported that, according to the Brazilian levelling, the sea-level variation is 41 cm between Rio de Janeiro and Fortaleza, which are separated by over 1500 km of coastline.

In Australia, since 1945, 160 000 km of levelling, mainly third order, has been undertaken under the direction of the Division of National Mapping of the Department of Minerals and Energy for the National Mapping Council of Australia. The network is described by LEPPERT (1970) and by ROELSE ET AL (1971). During the survey, connections were made to about 30 tide-gauges around the mainland coastline, with the intention of connecting the various local datums based on Mean Sea Level (Ibid). The results also provide an estimate of the sea-surface topography around this country. The levelling net, after adjustment, indicated that, if ζ at Port Lincoln in the Great Australian Bight was adopted as zero then ζ at Cape York would be of the order of 2 m. Further details of this result are given by ROELSE ET AL (1971).

To account for any effect of gravity variation on the results, an orthometric correction has been applied to the levelled height differences in the Australian net. The gravity values used in this correction were based on *theoretical* (normal) gravity values referred to the Reference System 1967 (ROELSE ET AL 1971, p. 65).

The levelling has also been converted into *geopotential* differences using *observed* gravity, (MITCHELL 1973). Potential differences, ΔW, between bench-marks in the levelling, were formed from the observed height differences Δh, using the relation:

$$\Delta W = \tfrac{1}{2}(g_1 + g_2)\Delta h \qquad (1)$$

g_1 and g_2, the gravity values at the two bench-marks, were interpolated from surrounding values available at 0.1 degree intervals. Bench-marks were at a spacing of the order of 3 km. However, the values of ζ in units of geopotential differences when compared with those in terms of height, were found to have been altered by amounts which are not significant in this discussion (Ibid).

The apparent sea-surface topography must be viewed in the light of the accuracy of the levelling results.

PETROV's analysis of reports about the United European Levelling Network showed that errors in the levelling do not permit any significance to be attached to sea-surface topography given by that net, as mentioned above (PETROV 1965, p. 247).

The accuracy of the levelling in the Australian network has been studied by ROELSE ET AL (1971) who, in their report on the adjustment, note that "...most of the levelling in the network was observed to third order standard" (Ibid, p. 75). This standard requires that the two levellings of any section between bench-marks must not differ by more than $12\sqrt{K}$ mm where K is the distance, in kilometres, between bench-marks, (NATIONAL MAPPING COUNCIL OF AUSTRALIA 1970). ROELSE ET AL (p. 76) have adopted a value of about $8.1\sqrt{K}$ mm for the precision of the *adjusted* orthometric levelling. It is estimated (Ibid, Annexure F) that the standard deviation of a height at the coastline when referred to a height at an origin towards the centre of the continent, via the adjusted orthometric levelling, is of the order of 35 cm. This is significantly less than the 200 cm variation in sea-level which has been shown by the levelling results. Thus, the existence

of the sea-surface topography is not explained by the errors expected from type of levelling survey carried out in Australia.

Systematic errors in the levelling could exist undetected, to produce the apparent ζ values, but discussion on this would, at the moment, seem to be largely speculative.

The change in the shape of the geoid during tides in the equipotential surfaces (MELCHIOR 1966; JENSEN 1950) is not sufficient to contribute significantly to the apparent sea-surface topography.

4. Known Sources of Sea-Surface Topography

Although the surface of an undisturbed homogeneous liquid should coincide with an equipotential surface, the sea-surface, in practice, is not expected to fulfill such a condition exactly. Known sources of separations between the surfaces are summarized below. Where possible, they will be related to the Australian sea-surface topography result.

Under generation in a wind field, waves and swell may have heights up to the order of 10 m and periods up to 15 sec. (e.g. SCOTT 1968). However, because of their periodicity and comparatively high frequency, these waves are generally considered to be filtered, by the mechanism of the tide-gauges, from their records. Thus, the state of the sea and swell should not have contributed to the sea-surface topography indicated by the Australian survey.

Large values of ζ are also caused by the tidal fluctuations. Their effect on sea-surface topography is assumed to vary with time according to

$$\zeta_{tides} = \sum_{i=1}^{n} a_i \cos (2\pi f_i t + \Phi_i) \qquad (2)$$

where $a_i \cos (2\pi f_i t + \Phi_i)$ represents one of n tidal constituents. A mean of observations over a suitable period of time should therefore eliminate tidal influence. The effectiveness of the mean depends on the period over which it is taken, and on the amplitudes, a_i, and frequencies, f_i, of the tides. Means of sea-level produced from tide-gauge records over a number of years as in the case of the Australian survey, may be considered to be free from the variable effects of any tides which have a magnitude of more than a few centimetres.

Subtraction of the tide-height from an observed level of the sea-surface is generally only an accurate process if records of the tides over a number of years are available for that particular point, as evidenced by co-range charts given by EASTON (1970).

UNOKI & ISOZAKI (1965) have discussed the influence of tides on ζ within enclosed bays and harbours, although the order of magnitude of the effect was only centimetres. Little other mention has been found in the literature on the position dependent effect of the tides.

Two oceanographic phenomena which significantly affect sea-surface topography are the distribution of water density and the existence of ocean currents. They are closely related and may be discussed simultaneously.

Theoretically, the value of ζ at a given time and place is assumed to depend on the average density in a column of water between the surface and a specified equipotential surface deep in the ocean. Density is a function of salinity and temperature, which are measurable, and of pressure, which depends on the dynamic depth. Variations of ζ with time and position may therefore be calculated from differences in density. The surface of less dense water is higher, with respect to the geoid, than that of more dense water.

Ocean current positions are also indicative of the density-induced portion of sea-surface topography. The currents arise as a result of the pressure differences, which result from the density distribution. Their flow is modified by the Coriolis effect, so that, for example, currents in the southern hemisphere circulate in an anticlockwise direction around areas of high ζ value. The situation is analogous to the relationship between atmospheric winds and barometric pressure differences. The complete theory of ocean water densities and currents, and their relationships to sea-surface topography is complex (DIETRICH 1957, pp. 291 et seq; FOMIN 1964; NEUMANN 1968; SVERDRUP ET AL 1942, pp. 389 et seq).

The effects of ocean currents and density in practical cases have been considered by BOWDEN (1960), DONN ET AL (1964, pp. 247 et seq), LISITZIN (1965), STURGES (1967; 1968). See also a review by HAMON (1970). LISITZIN (1965, p. 16) has produced a world map of density effects on the sea-surface, showing the resultant variation in ζ around the Australian coast to be of the order of 80 cm. Other papers indicating ζ values due to density in waters around Australia have been published by HAMON (1961; 1965 A,), HAMON & TRANTER (1971), WYRTKI (1962 A; 1962B) and HAMON & GREIG (1972). The density data, which has been collected principally by the Division of Fisheries and Oceanography, CSIRO, Australia, shows a contribution of about 60 cm to the apparent variation of sea-surface topography between Port Lincoln and Cape York (MITCHELL 1973). The existence of time variations of ζ due to density is illustrated by the changes in ocean current positions near Australia (WYRTKI 1960; 1961; HAMON & KERR 1968), but lack of complete data makes it difficult to estimate accurately the change of ζ with time.

The possibility of correcting for density variations depends directly on the available salinity and temperature data. It must be noted, however, that the density/current influence is one of the major contributors to variable sea-surface topography.

Interaction between the atmosphere and the oceans produces a number of variations of ζ with both position and time. The variation of observed sea-level due to barometric pressure is generally given by the linear relationship

$$\zeta_{barom} = \alpha \Delta p \qquad (3)$$

where Δp is the deviation of the atmospheric pressure from a standard value which is independent of time and position, and α is a constant. Theoretically, α has a value of -1.01 cm mbar^{-1} (HAMON 1966, p. 2883). However analysis of sea-level records in conjunction with air-pressure records has not always produced a value for this factor of -1.01 cm mbar^{-1} (DONN ET AL 1964, pp. 247 et seq; EASTON & RADOK 1970 A, p. 6; HAMON 1958, pp. 189 et seq; 1962; 1966; LISITZIN & PATTULLO 1961, p. 845; ISOZAKI 1969).

However, using this value of α and air-pressure observations, obtained from *Bureau of Meteorology (Monthly)* the corrections needed to reduce all mean levels of the sea-surface in the Australian survey to a standard atmospheric pressure, have been calculated (MITCHELL 1973). The corrections reduced the apparent variation in ζ around Australia by the order of 10 cm.

Another atmospheric action on sea-level, often operating simultaneously with barometric pressure effects, is wind. The magnitude of the influence is dependent on the depth and width of the continental shelf and on the velocity of the wind acting across the shelf towards the shore. Various formulae can be used to estimate this effect (e.g. STURGES 1967, p. 3630; HAMON 1958, p. 191; CREPON 1970; SILVESTER 1970). Theoretically, the influence of winds on a long term mean sea level is expected to be negligible (STURGES 1967; HAMON 1958). Studies of the tide-gauges used in the Australian survey (EASTON 1968) and of their records (EASTON 1967 A, 1967 B, 1970; EASTON & RADOK 1968, 1970 A, 1970 B) have produced some information on wind effects at these sites. Most notable is the evidence of a persistent 15 cm effect at Mackay (EASTON 1970, pp. 47 and 252).

Some minor effects on the value of ζ as determined by the conventional process with tide-gauges, can be considered to have negligible influence on the Australian results. These include:

(i) tsunamis,

(ii) the secular change in ζ which is only of the order of 0.5 mm per year around Australia (IAPO 1955),

(iii) erroneous gauge recording. The faults described in the reports on the gauges and their recording, should not be significant in this discussion (EASTON 1967 A, 1967 B, 1968, 1970; EASTON & RADOK 1968, 1970 A),

(iv) river flow past the tide gauges, a number of which are situated in rivers or near their mouths (EASTON 1968). The river flow at individual gauges is not considered likely to produce ζ effects as a regular function of position on the coastline, and should not, therefore, affect the overall picture of ζ variation around Australia.

5. Investigation of Anomalous Sea-Surface Topography

Around Australia, the apparent sea-surface topography is presently only partially accounted for by known oceanographic phenomena.

It must therefore be considered as a possibility that the estimate of $\overline{\zeta}$ by the networks of height or geopotential differences over this continent is erroneous. A latitude dependent systematic error of 0.3 mm per km would explain a significant portion of the apparent sea surface topography. It is, therefore, important to recognise that any future determination of the sea-surface relative to the geoid should, if possible, be independent of the existing levelling.

The most significant known cause of a deviation between the *mean* sea-surface and the geoid is undoubtedly that of ocean water density. It is credible that its contribution may be larger than indicated in the above discussion. It is plausible that the relationship between the measured densities at sea and the sea-surface topography is imperfect, being affected, for example, by sea bed topography, ocean current eddies or friction, to an extent which is presently underestimated.

Attention could be paid to wind effects on the sea-surface. Although not expected to produce a full metre variation in sea-level, their contribution could nevertheless be significant. Extensive study should at least prove conclusively either that the wind effects are not significant or that they are worthy of further study. The vast areas of shallow water less than 200 m deep in the Gulf of Carpentaria, Arafura Sea and Torres Strait regions arouse interest.

The possibility of a position dependent tidal influence could be examined.

Estimates of the effect of river flow past tide-gauges in Australia would reduce the uncertainty in present values of the sea-surface topography.

6. Sea Surface Topography from Satellite Altimetry

As it is possible that erroneous levelling or tide-gauge results contribute to the apparent sea-surface topography around Australia, a determination of ζ independent of the levelling or potential networks would assist further investigation of the problem. Satellite altimetry has been considered as one suitable method for determining sea-surface topography (STURGES 1971). The principles may be explained with the aid of Figure 1, which shows the development of a portion of the surface which contains the verticals through successive satellite positions. Along any vertical, the following scalars, which are shown positive in the diagram, are involved:

(i) a, the distance, measured by an altimeter, between the satellite and the instantaneous sea-surface,

(ii) h_{si}, the height of the satellite above the ith spheroid. Two reference surfaces are included to indicate that there are many spheroids, with various dimensions and positions, to which reference may be made,

(iii) N_i, the separation between the geoid and the ith spheroid.

The required value of ζ is then given by

$$\zeta = h_{si} - a - N_i \qquad (4)$$

Such an altimetering system has been planned for the GEOS-C satellite, and in the following summary of the application of satellite altimetry, GEOS-C is emphasized.

Errors in the value of a, which will be measured from GEOS-C by an altimeter reflecting a *radar* beam from the sea-surface, will result from refraction through the atmosphere. Corrections must be made to minimise the errors (WEIFFENBACH 1971, p. 1-3; SIRY 1971, p. 7-30). The state of the sea at the time of the satellite's passage, which will also affect the measured value of a, may have to be determined to apply necessary corrections, (WEIFFENBACH 1971, pp. 1-6). Possibly the altimeter readings themselves will provide an estimate of the sea-state (SHAPIRO ET AL 1971).

The spheroid height is obtained by either tracking the satellite from stations whose co-ordinates are known, or by predicting the satellite height using knowledge of the gravity field combined with corrections obtained from tracking. The former method, which relates the satellite height to a local spheroid, cannot be applied to the Australian problem as heights of observation stations cannot be determined independent of the levelling processes. The latter method, however, relates the satellite height to a geocentric spheroid. The determination of h_{si} is possibly the major cause of errors propagated into ζ.

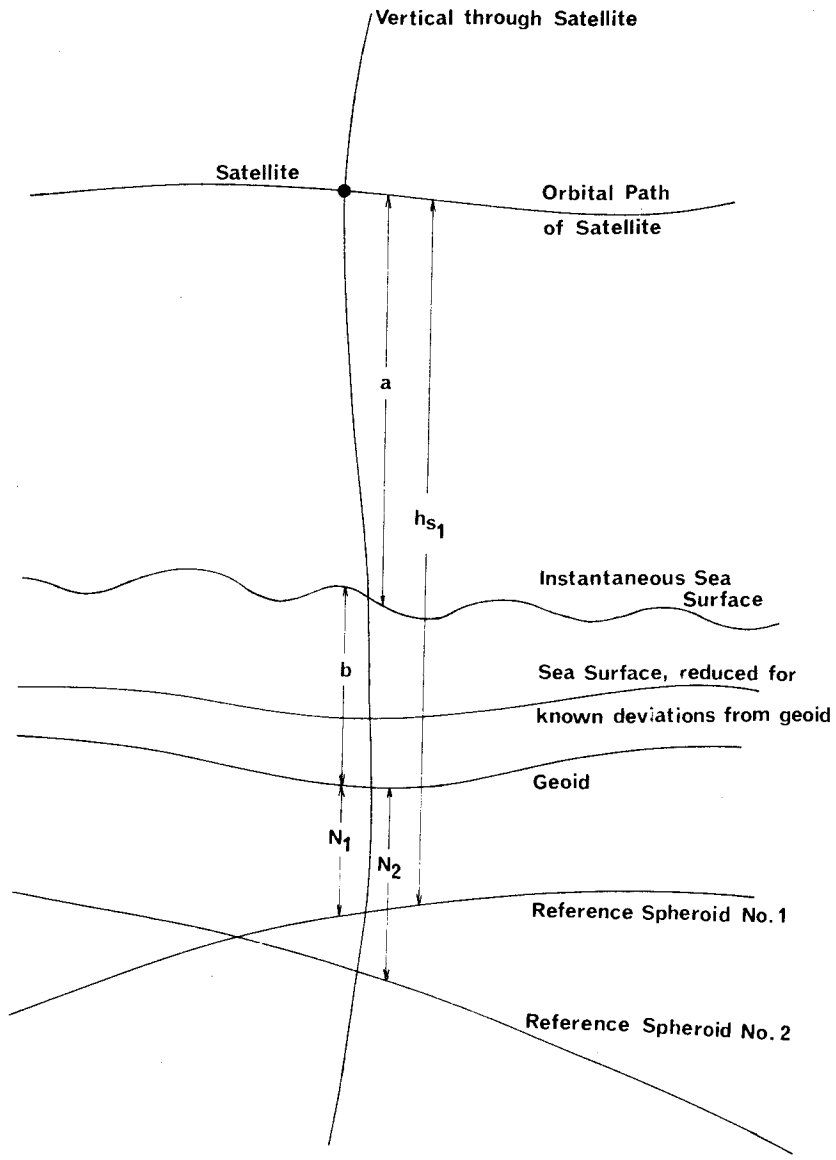

Figure 1

Of the two main methods of determining the geoid-spheroid separation, i.e. the astro-geodetic levelling and gravimetric method, the former cannot be applied to the Australian situation. It relates the geoid to a *local* spheroid. The gravimetrically determined geoid is related to the geocentric spheroid and also has the advantage, for satellite altimetry, of being determinable on the continental shelf and in the open ocean. Although the value of N on continental shelves around Australia must presently be extrapolated from land areas, the *possibility* of development to 10 cm accuracy will make possible the future use of satellite altimetry to determine the sea-surface topography around this continent.

Because the altimeter will operate for many hours over lifetime of a satellite, 1.5 to 2 years, a large number of values of a and h_{si}, obtained on many different orbital crossings, will be involved in the determination of the sea-surface topography. For GEOS-C, typical estimates are of the order of 20 observations per one degree square (WEIFFENBACH 1971, pp. 1 - 9; CHOVITZ 1971). Thus, unlike tide-gauge records only a limited number of observations of the ocean surface are obtained by satellite altimetry. The corrections for known ζ influences will be more difficult to calculate, unless they are suitably meaned by as few as 20 measurements over 10^4 km^2 of ocean. Hopefully, the determination of sea and swell conditions by the altimeter itself will enable satisfactory corrections to be computed for the influence of surface waves as mentioned previously. Although a large number of observations will be taken over a square kilometre of ocean, the tides, whose spring range may be as large as 10 m around the mainland Australian coastline (EASTON 1970, p. 159) are likely to influence results. Tide-gauge recording during the altimeter's operation would be imperative, therefore, but difficulty will arise as the times and ranges of these tides on the continental shelf and, more particularly, at sea, cannot be extrapolated from coastal values. Corrections for barometric pressure, which may be of the order of 15 cm under typical conditions, can easily be applied.

The mean of the number of observations taken should be effectively free from the time influences of surges and ocean-density variations.

Australia, being a large area surrounded by ocean and covered by homogeneous levelling and gravity networks, seems suited to an application of satellite altimetry to check the unexpectedly large values of ζ. However, the region lacks sufficient tracking facilities to ensure that errors in h_{si} are kept to acceptable levels. The feasibility of satellite altimetry's application to this continent also depends on the accuracy of the determination of the geoid-spheroid separation, and of the tidal conditions, on the continental shelf areas.

Attention is drawn to the possibility that ζ varies across the continental shelf. This would require careful consideration in the analysis of altimetry results, as well as in any eventual application of sea-surface topography to geodetic techniques.

7. Summary

It is suggested that, through the use of satellite altimetry, the presently uncertain portion of the sea surface topography may be deduced. Such a determination would be particularly valuable in Australia where the position variation of the mean ζ value is exceptionally large. Oceanographic research or studies of the levelling survey, based on the results from satellite altimetry may provide a more complete knowledge of the sea-surface topography which could, in turn, be usefully applied to geodetic methods.

8. Acknowledgments

The major part of the work for this article was carried out while the author was a Commonwealth Post-Graduate Scholar at the School of Surveying, University of N.S.W.

9. References

BERBERT, J. H. & LOVELESS, F. M. 1971. *A Satellite Altimeter Bias Recovery Simulation.* Goddard Space Flight Centre X-550-71-224.

BOWDEN, K. F. 1960. The Effect of Water Density on the Mean Slope of the Sea Surface. *Bull Geodes.* 55, pp. 93 - 96.

BRAATEN, N. F. & McCOMBS, C. E. 1963. *Mean Sea Level Variations as Indicated by a 1963 Adjustment of First Order Levelling in the U.S.* I.U.G.G., I.A.G., General Assembly, Berkeley.

Monthly Climate Data - Surface, Australia. Commonwealth of Australia, Department of Science. Bureau of Meteorology - Monthly.

CHOVITZ, B. H. 1971. Refinement of the Geoid from GEOS-C Data, *Sea Surface Topography from Space.* NOAA Technical Report ERL 228 - AOML 7 - 2, p. 2 - 1.

CREPON, M. 1970. The Influence of Wind on Sea Level. *Report on the Symposium on Coastal Geodesy.* Munich, July 1970, pp. 453 - 462.

DIETRICH, G. 1957. *General Oceanography.* Interscience.

DONN, W. L., PATTULLO, J.G.. & SHAW, D. M. 1964. Sea Level Fluctuations and Long Waves. *Res in Geophys.* 2, pp. 243 - 269.

DOODSON, A. T. 1928. The Analysis of Tidal Observations. *Phil. Trans. Roy. Soc. Lond.* A227, pp. 223 - 245.

DOODSON, A. T. 1960. Mean Sea Level and Geodesy. *Bull Geodes.* 55, pp. 69 - 88.

EASTON, A. K. 1967 A. *Tidal Programme 1966 - 1967.* Memorandum No. 2, Horace Lamb Centre for Oceanographical Research. Flinders University of South Australia.

EASTON, A. K. 1967 B. *Tidal Programme 1966 - 1967.* Memorandum No. 3, Horace Lamb Centre for Oceanographical Research. Flinders University of South Australia.

EASTON, A. K. 1968. *A Handbook of Selected Australian Tide Gauges.* Survey Paper No. 6, Horace Lamb Centre for Oceanographical Research. Flinders University of South Australia.

EASTON, A. K. 1970. *The Tides of the Continent of Australia.* Research Paper No. 37, Horace Lamb Centre for Oceanographical Research. Flinders University of South Australia.

EASTON, A. K. & RADOK, R. 1968. *Tidal Programme 1966 - 1967.* Memorandum No. 4, Horace Lame Centre for Oceanographical Research. Flinders University of South Australia.

EASTON, A. K. & RADOK, R. 1970 A. *Tidal Programme 1966 - 1968.* Memorandum No. 5, Horace Lamb Centre for Oceanographical Research. Flinders University of South Australia.

EASTON, A. K. & RADOK, R. 1970 B. *Australia's Changing MSL Surface.* Survey Paper No. 9, Horace Lamb Centre for Oceanographical Research. Flinders University of South Australia. Also: *Report on the Symposium on Coastal Geodesy.* Munich, July 1970, pp. 267 - 278.

FOMIN. L. M. 1964. *The Dynamic Method in Oceanography.* Elsevier.

HAMON, B. V. 1958. Mean Sea Level Variation on the Coast of New South Wales. *Aust. Surv.* 17, pp. 188 - 199.

HAMON, B. V. 1961. *The Structure of the East Australian Current.* CSIRO Australia, Division of Fisheries and Oceanography. Tech. Paper 11.

HAMON, B. V. 1962. The Spectrums of Mean Sea Level at Sydney, Coffs Harbour and Lord Howe Island. *J. Geophys. Res.* 67(13), pp. 5147 - 5155 (Correction: 1963, J. Geophys. Res., 68, p. 6033).

HAMON, B. V. 1965 A. Geostrophic Currents in the South-Eastern Indian Ocean. *Aust. J. Marine & Freshwater Res.* 16(3), pp. 255 - 271.

HAMON, B. V. 1965 B. The East Australian Current 1960 - 1964. *Deep Sea Res.* 12, pp. 899 - 921.

HAMON, B. V. 1966. Continental Shelf Waves and the Effects of Atmospheric Pressure and Wind Stress on Sea Level, *J. Geophys. Res.* 71, pp. 2883 - 2893.

HAMON, B. V. 1970. A Review of "Current-Effect" on Sea Level. *Report on the Symposium on Coastal Geodesy.* Munich, July 1970, pp. 395 - 410.

HAMON, B. V. & GREIG, M. A. 1972. Mean Sea Level in Relation to Geodetic Land Levelling around Australia. *J. Geophys. Res.* 77(36), pp. 7157 - 7162.

HAMON, B. V. & KERR, J. D. 1968. Time and Space Scales of Variations in the East Australian Current from Merchant Ship Data. *Aust. J. Marine & Freshwater Res.* 19, pp. 101 - 106.

HAMON, B. V. & TRANTER, D. J. 1971. The East Australian Current. *Aust. Natural Hist.* 17(4), pp. 129 - 133.

HUDSON, E. F. 1971. A Geodetic and Oceanographic Satellite Altimeter System. *Am. Inst. of Aeronautics and Astronautics Space Systems Meeting.* Denver, Colorado, July, 1971.

ISOZAKI, I. 1969. An Investigation on the Variations of Sea Level due to Meteorological Disturbances on the Coast of Japanese Islands (III). On the Variation of Daily Mean Sea Level. *J. Oceanographical Soc. Jap.* 25(2), pp. 91 - 102.

INTERNATIONAL ASSOCIATION OF PHYSICAL OCEANOGRAPHY 1955. *Secular Variation in Sea Level.* I.U.G.G., Publication Scientifique No. 13.

JENSEN, H. 1950. Formulas for the Astronomical Correction to Precise Levelling. *Bull Geodes.* 17, pp. 267 - 277.

KELSEY, J. 1970. Considerations Arising from the 1970 Readjustment of the Geodetic Levellings of Great Britain, *Report on the Symposium on Coastal Geodesy.* Munich, July 1970, pp. 331 - 338.

LEPPERT, K. 1970. The Australian Levelling Net Adjustment. Progress to April 1970. *Report on the Symposium on Coastal Geodesy.* Munich, July 1970, pp. 223 - 231.

LEVALLOIS, J. J. 1960. Symposium sur le Niveau Moyen des Mers en Europe Occidentale, (Liverpool, October 1959). *Bull Geodes.* 55, pp. 25 - 37.

LEVALLOIS, J. J. & MAILLARD, J. 1970. The New French 1st Order Levelling Net - Practical and Scientific Consequences. *Report on the Symposium on Coastal Geodesy.* Munich, July 1970, pp. 300 - 330.

LISITZIN, E. 1965. The Mean Sea Level of the World Ocean. *Commentationes Physico-Mathematicae.* Societas Scientarium Fennica. 30(7).

LISITZIN, E. & PATTULLO, J. G. 1961. The Principle Factors Influencing the Seasonal Oscillation of Sea Level. *J. Geophys. Res.* 66(3), pp. 845 - 852.

LUNDQUIST, C. A. & GIACAGLIA, G. E. O. 1969. Possible Geopotential Improvement from Satellite Altimetry. *Smithsonian Astro-physical Observatory Special Report No. 294.*

MARTIN, C. F. 1971. Optimum Usage of Ground Stations for GEOS-C Orbit Determination. *Sea Surface Topography from Space.* NOAA Technical Report ERL 228 - AOML 7-2, pp. 9 - 1.

MATHER, R. S., BARLOW, B. C. & FRYER, J. G. 1971. *A Study of the Earth's Gravitational Field in the Australian Region.* IUGG, General Assembly, Moscow.

MELCHOIR, P. J. 1966. *The Earth Tides.* Pergamon.

MITCHELL, H. L. 1972. Relationships between Mean Sea Level and the Australian Levelling Survey. *UNISURV Report* G-17. University of New South Wales, Kensington NSW, pp.43-58.

MITCHELL, H. L. 1973. Relations between Mean Sea Level and Geodetic Levelling in Australia. *UNISURV Report* S-9. University of New South Wales, Kensington NSW.

NATIONAL MAPPING COUNCIL OF AUSTRALIA 1970. *Standard Specifications and Recommended Practice for Horizontal and Vertical Control Surveys.* Division of National Mapping, Canberra, as amended.

NEUMANN, G. 1968. *Ocean Currents.* Elsevier, Amsterdam.

OAKES, J. B. 1971. GEOS-C Radar Altimeter Characteristics. *Sea Surface Topography from Space.* NOAA Technical Report ERL 228-AOML 7-2, p. 18 - 1.

PATTULLO, J. G. 1962. Seasonal Changes in Sea Level. *The Sea* (M.N. Hill, ed.), Ch. 22, Vol. 2, pp. 485 - 496. Interscience.

PATTULLO, J. G., MUNK, W., REVELLE, R. & STRONG, E. 1955. The Seasonal Oscillation in Sea Level. *J. Mar. Res.* 14(1), p. 88.

PETROV, V.D. 1965. Use of Mean Sea Level Surfaces in Processing Levelling Results. *Geodesy and Aerophotography.* 4, pp. 246 - 248.

RODRIGUEZ, L. V. 1970. Brazilian National System of First Order Levelling. *Report on the Symposium on Coastal Geodesy.* Munich, July 1970, pp. 363 - 366.

ROELSE, A., GRANGER, H. W. & GRAHAM, J. W. 1971. *The Adjustment of the Australian Levelling Survey 1970 - 1971.* Division of National Mapping, Technical Report 12, Canberra.

SCOTT, J. R. 1968. Some Average Sea Spectra. *Quart. Trans. Roy. Inst. Nav. Arch.* 110, pp. 233 - 239.

SHAPIRO, A., ULIANA, E. A. & YAPLEE, B. S. 1971. Radar Pulse Shape Versus Ocean Wave Height. *Sea Surface Topography from Space*. NOAA Technical Report ERL 228 - AOML 7 - 2, p. 11 - 1.

SILVESTER, R. 1970. Computation of Storm Surge. *Proc. Twelfth Coastal Eng. Conf.* Washington, September 1970.

SIRY, J. W. 1971. Sat. Altitude Determination Uncertainties. *Sea Surface Topography from Space*. NOAA Technical Report ERL 228 - AOML 7 - 2, p. 7 - 1.

STURGES, W. 1967. Slope of Sea Level along the Pacific Coast of the United States. *J. Geophys. Res.* 72(14), pp. 3627 - 3637.

STURGES, W. 1968. Sea Surface Topography near the Gulf Stream. *Deep Sea Res.* 15, pp. 149 - 156.

STURGES, W. 1971. Comments on Ocean Circulation with Regard to Satellite Altimetry. *Sea Surface Topography from Space*. NOAA Technical Report ERL 228 - AOML 7 - 2, p. 24 - 1.

SVERDRUP, H. U., JOHNSON, M. W. & FLEMING, R. H. 1942. *The Oceans: Their Physics, Chemistry and General Biology*. Prentice-Hall.

UNOKI, S. & ISOZAKI, I. 1965. Mean Sea Level in Bays, with Special Reference to the Mean Slope of Sea Surface due to the Standing Oscillation of the Tide. *Oceanographical Mag.* 17(1-2), pp. 11 - 35.

WEIFFENBACH, G. C. 1971. An Observational Philosophy for GEOS-C Satellite Altimetry. *Sea Surface Topography from Space*. NOAA Technical Report ERL 228 - AOML 7 - 2, p. 6 - 1.

WYRTKI, K. 1960. *Surface Circulation in the Coral and Tasman Seas*. CSIRO Aust., Division of Fisheries and Oceanography, Technical Paper No. 6.

WYRTKI, K. 1961. *Physical Oceanography of the Southeast Asian Waters*. NAGA Report, Vol. 2, Scripps Institution of Oceanography, La Jolla, California.

WYRTKI, K. 1962 A. Geopotential Topographies and Associated Circulation in the South-Eastern Indian Ocean. *Aust. J. Marine and Freshwater Res.* 13, p. 1 - 17.

WYRTKI, K. 1962 B. Geopotential Topographies and Associated Circulation in the Western South Pacific Ocean. *Aust. J. Marine and Freshwater Res.* 13, pp. 89 - 105.

MATHER, R.S.
School of Surveying
The University of New South Wales
Kensington NSW 2033
Australia

Proc.Symposium on Earth's Gravitational Field & Secular Variations in Position (1973),585-599.

THE INFLUENCE OF STATIONARY SEA SURFACE TOPOGRAPHY ON GEODETIC CONSIDERATIONS

ABSTRACT

The comparison of the results of geodetic levelling with the mean level of the sea as defined by tide gauge readings, has indicated the apparent existence of widespread departures of sea level from an equipotential surface of the Earth's gravitational field.

While the evidence available at present for the existence of this quasi-stationary sea surface topography is confined to coastal regions, there should be repercussions of fundamental significance in high precision geodesy if this phenomenon were to prevail over the global oceans with amplitudes and wavelengths which are not negligible. This arises primarliy through the widespread adoption of "mean sea level" as a datum for elevations, and affects global determinations of the highest resolution in both physical geodesy and vertical crustal motion studies.

These problems are summarized and desirable goals indicated for satellite altimetry and laser ranging techniques which would not only eliminate the errors arising from the assumption outlined above, but also confirm the global characteristics of stationary sea surface topography in non-coastal areas.

1. Introduction

1.1 Preamble

It has been widely reported in the literature (see Appendix 1) that Mean Sea Level as defined by the mean of tide gauge readings over some limited epoch, does not correspond to a single equipotential surface of the Earth's gravitational field insofar as the latter is implied from the results of a continental geodetic levelling operation. This phenomenon has been called stationary *sea surface topography* (APEL 1972) and its possible existence on a world wide scale poses problems in geodetic terms due to the reliance on Mean Sea Level as a means for providing the datum of reference for first order geodetic levelling on a global scale. The evidence available at present for providing some estimate of the possible magnitude of this phenomenon is summarized in Appendix 1.

On the basis of this evidence, sea surface topography which is quasi-stationary, could be expected to have amplitudes as great as 2 m and wavelengths as great as 8000 km if the coastal samples were representative of the Earth's oceans as a whole. Without making a case one way or the other for the existence of such a possibility, it is of interest to assess the effect it has on relevant geodetic considerations. In the first instance, it can be stated that Mean Sea Level does indeed provide an adequate global datum for first order geodetic levelling *insofar as* the results of levelling can be combined with those obtained from horizontal survey methods, to give position in three dimensions with a precision of 1 part in 10^6 in each co-ordinate.

First order geodetic levelling retains the capacity to provide a higher relative resolution than any of the other traditional geodetic processes at the present time. It is relatively simple in both principle and procedure, though somewhat laborious to execute. The resolution obtained from first

order levelling procedures is approximately 30 times superior to the requirements of geodesy at 1 part in 10^6. This resolution is admittedly lost on transformation of the results of levelling to notions of position in three dimensions, where the best results obtained to date are generally conceded as having a precision approaching ±6 m in each co-ordinate.

The superior resolution of first order geodetic levelling is used at present primarily for either sophisticated engineering projects which are of local relevance, or for vertical crustal motion studies where global considerations, which should be of consequence, are not resolved with an equivalent degree of certainty due to the levelling being referred in all cases to the regional definition of Mean Sea Level. On the basis of the extrapolation of coastal estimates of quasi-stationary sea surface topography to the global oceans, the possibility of an uncertainty of up to ±2 m should be anticipated in the inter-connection between two such studies due to a lack of continuity in the definition of the datum for levelling. This figure is an order of magnitude greater than the internal precision expected from a continental network of first order geodetic levelling.

Present practice in the measurement of vertical crustal motion, relies on the resolution of the phenomenon afforded in most instances by orthometric elevations. The latter are referred to a datum usually provided by a convenient tide gauge. The Mean Sea Level datums so defined are assumed to be situated on a unique equipotential surface of the Earth's gravitational field called the *geoid*. It cannot be considered desirable to base extended studies over long time spans with reference to a surface whose shape and Earth space position in relation to the Earth's surface, change as a function of time, even on excluding tidal phenomena. This is a characteristic which can be expected from the geoid if constant mass re-distributions were to take place in the Earth's interior.

It is evident that if the definition of the geoidal datum for elevations on a world-wide basis is to match the resolution of first order geodetic levelling,

(a) the definition should characterize a particular epoch; and

(b) the existence of stationary sea surface topography, which must be construed as a non-gravitational phenomenon, will have to be allowed for,

The first is necessary due to reported secular variations in sea level (e.g., DONN ET AL 1964). The second would call for an averaging procedure in the definition of the geoid. It is therefore of interest to re-examine the geoidal concept in the context of determinations of secular variations in position with an ultimate goal of 1 part in 10^8.

1.2 A Guide to Notation

1.2.1 Recurring Symbols

A_n = surface harmonic of degree n having the form

$$A_n = \sum_{m=0}^{n} p_{nm}(\sin \phi) \left(A_{1nm} \cos m\lambda + A_{2nm} \sin m\lambda\right)$$

a = equatorial radius of the ellipsoid of reference

dS = element of area on the surface of integration

dt = interval of time between two contiguous epochs

$d\sigma$ = element of surface area on unit sphere

e = eccentricity of meridian ellipse

f = flattening of meridian ellipse

$f(\psi)$ = Stokes' function $\equiv$ $\operatorname{cosec} \frac{1}{2}\psi + 1 - 5 \cos \psi - 6 \sin \frac{1}{2}\psi - 3 \cos \psi \log\left(\sin \frac{1}{2}\psi(1 + \sin \frac{1}{2}\psi)\right)$

G = gravitational constant

G_n = surface harmonic of degree n in the expansion of

$$\Delta g' = \sum_{n=0}^{\infty} G_n, \quad n \neq 1$$

g = observed gravity at the surface of the Earth

$\overline{g}$ = mean value of gravity along local vertical between the Earth's surface and the geoid.

h = elevation above ellipsoid

h' = orthometric elevation

h_d = height anomaly

$\vec{i}$ = set of unit vectors along the axes of the X_i Cartesian co-ordinate system

$m = \frac{a\omega^2}{\gamma_e}$

$\vec{N}$ = unit vector normal to dS (dσ)

R = mean radius of the Earth

r = distance between the element of surface area dS and the point of computation P

T = time

U = potential of the reference system

U_o = potential of the equipotential reference ellipsoid

V_d = disturbing potential

W = geopotential

W_o = potential of the geoid

X_i = geocentric rectangular Cartesian co-ordinate system $X_1X_2X_3$, with the X_3 axis coincident with the axis of rotation, and the X_1X_3 plane defining the meridian of reference

α = azimuth

γ = normal gravity due to the reference system; subscript $_o$ refers to values on the reference ellipsoid; subscript $_e$ refers to equatorial value

Δg = gravity anomaly at the surface of the Earth

$\Delta g' = \Delta g - 2\frac{\delta W}{R}$

ΔW = geopotential difference with respect to the geoid

δW = geopotential difference between elevation datum and the geoid

λ = longitude, positive east

τ = epoch of observation

ρ = density of crustal material

ϕ = latitude, positive north

ψ = angular distance at geocentre between the point of computation P and the element of surface area dS (dσ)

ν = radius of curvature of the reference ellipsoid in the prime vertical normal section

ω = angular velocity of rotation of the Earth

$$\vec{\nabla} = \sum_{i=1}^{3} \frac{\partial}{\partial X_i} \vec{i}$$

1.2.2 Convention

$a = b + o\{b^2\}$ $\equiv$ terms whose order of magnitude is equivalent to or less than b^2 have been neglected

2. The Sea Surface and the Geoid

As pointed out in the introduction, the adoption of the definition of the geoid as *the equipotential surface of the Earth's gravitational field corresponding to Mean Sea Level*, poses no problems in the context of determinations of position in Earth space to 1 part in 10^6; co-ordinates of geodetic stations being computed on a three dimensional geocentric or quasi-geocentric Cartesian co-ordinate system X_i, on combining the observational data from both horizontal surveys and levelling operations. The required relations are

$$X_1 = (\nu + h) \cos\phi \cos\lambda \; ; \quad X_2 = (\nu + h) \cos\phi \sin\lambda \; ; \quad X_3 = [\nu(1 - e^2) + h] \sin\phi \qquad (1),$$

where all the symbols are described in section 1.2. The ellipsoidal elevation h needs to be known to o{6 m} to ensure that the precision of the X_i's are equivalent to those of the horizontal co-ordinates on a global basis. Regional determinations call for differences in ellipsoidal elevations between adjacent geodetic stations to be evaluated to o{±30 cm}. Conversely global solutions for geocentric position obtained from geometrical satellite geodesy (e.g, MARSH ET AL 1973) could be used to deduce ellipsoidal elevations to this same precision using procedures similar to that summarized in Appendix 2.

The results obtained by the use of the latter procedure obviate the necessity for the definition of orthometric elevations and the geoid vis-a-vis the reference ellipsoid, whose Earth space position is implicit in the numerical magnitudes of the ellipsoidal elevations, and the Earth's surface. It is not uncommon at the present time, to deduce geoid heights (e.g., IBID) with a resolution at the 5% level, from orthometric elevations supplied in the case of most tracking stations by the local geodetic authority (e.g., NASA 1971).

If it were pessimistically assumed that sea surface topography were to exist in a stationary state with amplitudes equivalent to the maximum reported in Appendix 1, and with long wavelengths in the non-coastal oceanic regions, a further 2% uncertainty would be introduced into the computed values of the geoid heights at the tracking stations. This would be difficult to detect if the resolution were only at the level of 1 part in 10^6. This uncertainty is of course introduced on account of the probability that each regional height datum would not lie on a unique equipotential surface of the Earth's gravitational field.

It is also necessary to take into account the nature of orthometric elevations when attempting to deduce geoid heights from three dimensional solutions. It is conventional to define orthometric elevations h' in terms of the observed difference of geopotential ΔW with respect to mean sea level which is assumed to coincide with the geoid, by the equation

$$h' = \frac{\Delta W}{\bar{g}} \qquad (2),$$

where $\bar{g}$ is the mean value of gravity as sampled along the local vertical between the Earth's surface and the geoid. If the Earth's surface were assumed to be planar, any value g_p at P on the vertical is related to observed gravity g at the surface of the Earth by a relation of the form

$$g_p = g + \frac{(\Delta h)^i}{i!} \frac{d^i g}{dh^i} - 4\pi G \int_0^{\Delta h} \rho \, dh \qquad (3),$$

where Δh is the depth of P below the Earth's surface and the differential coefficients $d^i g/dh^i$ are free air effects. Errors occur in the value of $\bar{g}$ due to errors in the values assumed for ρ as the stratification of matter between the Earth's surface and the geoid are not known. As the error $e_{h'}$ in h' due to an error $e_{\bar{g}}$ in $\bar{g}$ is obtained from equation 2 as

$$\frac{e_{h'}}{h'} = \frac{e_{\bar{g}}}{\bar{g}} \qquad (4),$$

it follows that errors in $\bar{g}$ due to incorrect modeling of the Earth's crust will have to be held to below 1 part in 10^5 in mountainous areas if orthometric heights are to be unaffected by crustal model errors in excess of the estimated precision of first order geodetic levelling over continental extents. Table 1 gives estimates of the magnitudes of errors in h' as functions of both h' and crustal modeling errors expressed as percentages of the value (ρ = 2.67 g cm^{-3}) most commonly adopted as a mean density for the upper crust.

T a b l e 1

Errors in Orthometric Heights Due to Crustal Density Errors (100% = 2.67)

Errors expressed as parts per million in orthometric elevations

h (m)	Percentage density error				
	10	20	30	40	50
500	11	23	35	46	57
1 000	23	46	77	91	124
3 000	68	137	206	274	342
5 000	114	228	343	457	571
7 000	160	320	480	640	800
10 000	228	457	685	914	1142

As it is extremely unlikely on present trends that the stratification of crustal matter between the Earth's surface and the geoid will be known well enough such that $e_{\bar{g}}$ could in fact be kept to $o\{\pm 10^{-5}\bar{g}\}$, it could be argued that a plausible but nevertheless arbitrary model could be adopted for the Earth's crust. This would define not only both h' and N without ambiguity, but also the equipotential surface for this prescribed mass distribution which coincides with average mean sea level over the oceans, assuming that no stationary sea surface topography exists.

While orthometric height differences will continue to be a basic high precision geodetic measurement, it is difficult to put forward a forceful case for the retention of the concept of orthometric elevations in the context of geodesy to 1 part in 10^8. A corollary to this contention is the irrelevance of defining the geoid *in continental areas* to this same order of precision. This conclusion is by no means new, having been the basis for the decision taken in the nineteen-fifties to use geopotential differences as the means for representing the results of first order geodetic levelling in lieu of orthometric elevations.

Two points have to be taken into consideration when re-assessing the role of the geoid vis-a-vis geodetic levelling. The *first* is the consequence of the various Mean Sea Level datums not lying on the same equipotential surface of the Earth's gravitational field. While this will not cause concern when attempting to use the results of levelling in conjunction with three-dimensional co-ordinates

obtained from satellite solutions to 1 part in 10^6, it has effects of significance on determinations in physical geodesy where formulations at the present time are based on the ability to refer all differences of geopotential ΔW to a common surface of equal potential $W = W_o$.

The *second* problem arises in the use of geodetic levelling techniques for the evaluation of vertical crustal movement, which at the time of writing, is largely based on measurements of differential changes obtained on re-levelling the same network of benchmarks

(a) after some finite but limited time lapse; and

(b) in relation to a datum surface which is assumed to be invariant in Earth space between successive levellings.

The definition of vertical crustal motion in the short term is unlikely to be improved by the use of geopotential differences ΔW in lieu of orthometric elevations, to any significant extent. The fundamental technique itself founders on the assumptions which are implicit in the adopted surface of reference and which could cause concern in long period studies when attempting to relate results from different areas into a single cohesive dynamic Earth model. It is of relevance to note that the practice of defining vertical crustal motion instead of a three dimensional crustal motion vector, is testimony to the superiority of first order geodetic levelling over all three dimensional position determinations which have been made to date.

These two questions are dealt with in the following sections.

3. Stationary Sea Surface Topography and Solutions in Physical Geodesy

The following is a revised presentation in a convenient summary form, of an aspect of an earlier development (MATHER 1973a). All basic definitions in physical geodesy are framed in the context of the system afforded by the physical surface of the Earth and the telluroid which is the locus of the points Q $(\phi_a,\lambda_a,U=U_o+\Delta W)$ illustrated in figure 1, in relation to points P $(\phi_g,\lambda_g,W=W_o+\Delta W)$ defining the Earth's surface. The disturbing potential V_{dp} at P is given by the generalized Bruns' equation

$$V_{dp} = W_o - U_o + \gamma h_{dp} + o\{f^2 V_d\} \qquad (5).$$

The validity of equation 5 is not questionable so long as no interpretation is forced on the value W_o which is the geopotential of the datum of reference for the geodetic levelling from which the geopotential differences ΔW are measured. U_o is conventionally assumed to be the potential of the reference system on the surface of the equipotential ellipsoid of reference $U = U_o$. Such a concept, while questionable in geophysical terms, is totally acceptable in the geodetic sense.

The gravity anomaly Δg is defined as (e.g., MATHER 1971,p.101)

$$\Delta g = g_p - \gamma_{p'} = g_p - \left\{\gamma_o - \frac{2\Delta W}{a}\left\{1 + f + m - \tfrac{1}{2}\frac{\Delta W}{a\gamma} - 2f\sin^2\phi + o\{f^2\}\right\}\right\} \qquad (6),$$

this being an instance of a free boundary value problem where it is assumed that the co-ordinates (ϕ_g,λ_g) are sufficiently well known to eliminate second order effects on the results (MATHER 1973a, p.16).

At the time of writing, Δg is considered to be the basic observed quantity in solutions of the geodetic

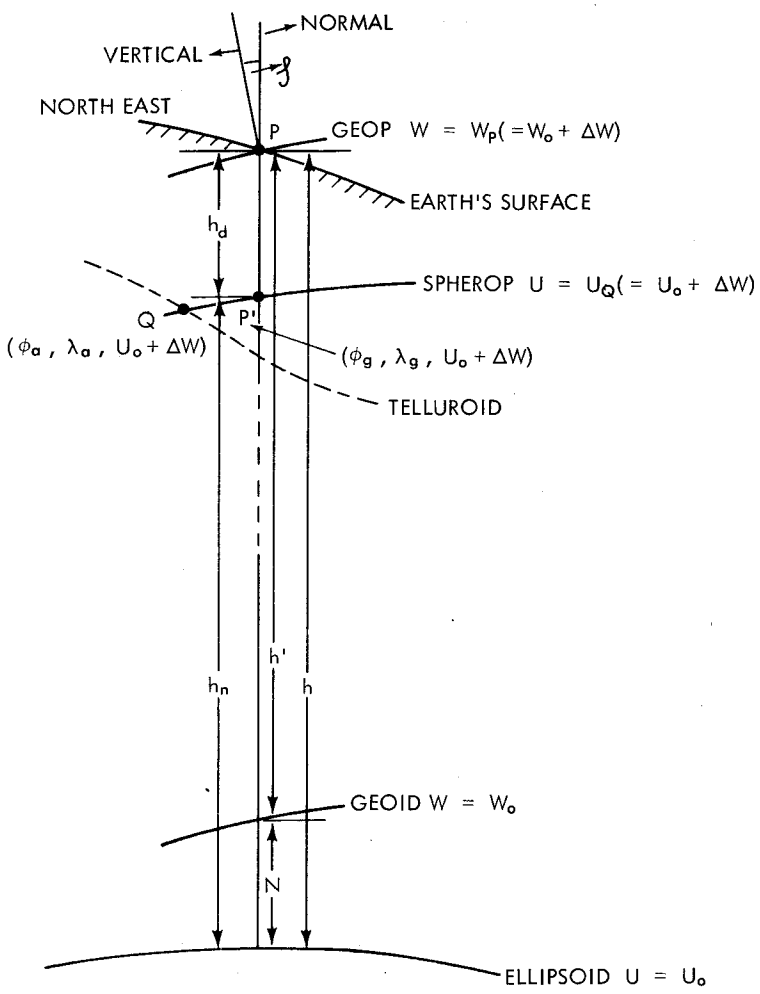

Figure 1. Systems of Elevations

boundary value problem, being used to solve integrals which are of the type

$$V_{dp} = \frac{1}{2\pi} \iint \left(V_d \, \vec{\nabla} \cdot \vec{N} \, \frac{1}{r} - \frac{1}{r} \, \vec{\nabla} \cdot \vec{N} \, V_d \right) dS \qquad (7).$$

The gravity anomaly Δg is introduced into equation 7 by the use of the inter-relation between equation 5 and the expression (IBID, p. 18)

$$\Delta g = - \frac{\partial V_d}{\partial h} + h_d \frac{\partial \gamma}{\partial h} + o\{f \, \Delta g\} \qquad (8).$$

Problems arise when the geopotential differences ΔW are referred to the equipotential surface ($W = W_o + \delta W$) of the Earth's gravitational field which does not coincide with the geoid ($W = W_o$). These are, of course, the various local estimates of the geoid , which is defined as the equipotential surface which best fits Mean Sea Level as sampled at a limited selection of tide gauge stations distributed globally. Individual tide gauges situated on the equipotential surface ($W = W_o + \delta W$) will not, in the general case, coincide with the geoid ($W = W_o$). The disturbing potential V_{dp} at a point

P whose geopotential difference has been established in such a manner, can be more accurately described by the equation

$$V_{dp} = W_p - U_p = (W_o + \delta W - U_o) + \gamma h_d + o\{f^2 V_d\} \quad (9).$$

The use of equation 9 along with the simplified relation

$$\frac{\partial \gamma}{\partial h} = -\frac{2\gamma}{R} + o\{f \frac{\partial \gamma}{\partial h}\} \quad (10)$$

and equation 8, gives the gravity anomaly in such a case as

$$\Delta g = -\frac{\partial V_d}{\partial h} - \frac{2}{R}(V_d - (W_o + \delta W - U_o)) + o\{f \Delta g\} \quad (11).$$

W_o is at best known to $o\{\pm 10$ kgal m$\}$ at the present time, while the most pessimistic estimate of δW on the basis of the evidence currently available can be put at $o\{\pm 2$ kgal m$\}$, with equivalent uncertainties of $o\{\pm 3$ mgal$\}$ and $o\{\pm \frac{1}{2}$ mgal$\}$ respectively in Δg. The first effect is of zero degree while the second is likely to have wavelengths as great as 10^3 to 10^4 km. The effect of tide gauges not lying on the same equipotential surface of the Earth's gravitational field, which can be interpreted as being due to the existence of stationary sea surface topography, influences the solution of the geodetic boundary value problem. This effect can be illustrated with the least complexity and adequate accuracy, by formulating its consequences in the Stokesian case where the Earth is represented without any matter exterior to the bounding equipotential which constitutes the Earth's surface.

Equation 7 is well known to transform according to the relation

$$V_{dp} = \frac{1}{2\pi} \iint \frac{1}{r}\left\{\Delta g + \frac{3V_d}{2R} - \frac{2}{R}(W_o + \delta W - U_o)\right\} dS \quad (12),$$

on using equation 11 and the relation

$$\vec{\nabla} \cdot \vec{N} \frac{1}{r} = -\frac{1}{2Rr}$$

which is valid in the case of a spherical equipotential surface. It is standard practice to adopt a spherical harmonic representation

$$V_d = \sum_{n=0}^{\infty} \frac{A_n}{R^{n+1}}, \quad n \neq 1 \quad (13)$$

for the disturbing potential as a means of combining the effects of the gravity anomaly and the disturbing potential, when the use of the conventional procedure using equation 11 gives

$$\Delta g = -\frac{\partial V_d}{\partial h} - \frac{2}{R}\{V_d - (W_o + \delta W - U_o)\} + o\{f \Delta g\} = \sum_{n=0}^{\infty} (n-1)\frac{A_n}{R^{n+2}} + \frac{2}{R}(W_o + \delta W - U_o) + o\{f \Delta g\}, \; n \neq 1 \quad (14).$$

Equation 12 can therefore be written as

$$V_{dp} = \frac{1}{4\pi} \iint \frac{1}{r} \sum_{n=0}^{\infty} (2n + 1) \frac{A_n}{R^{n+2}} \, dS, \quad n \neq 1 \qquad (15).$$

Stokesian practice calls for the replacement

$$A_n = \frac{R^{n+1}}{n-1} G_n$$

which is valid on the surface of a sphere of radius R. G_n is the n-th degree harmonic in the representation of the amended gravity anomaly $\Delta g'$ which is given by the equations

$$\Delta g' = \sum_{n=0}^{\infty} G_n = \sum_{n=0}^{\infty} (n - 1) \frac{A_n}{R^{n+2}}, \; n \neq 1 = \Delta g - 2 \frac{W_o - U_o}{R} - 2 \frac{\delta W}{R} \qquad (16),$$

the second equality following from equation 11.

The continuation of the Stokesian manipulation, including the term of zero degree, gives

$$V_{dp} = \frac{1}{4\pi} \iint \frac{1}{r} \sum_{n=0}^{\infty} \frac{2n + 1}{n - 1} G_n \, dS, \quad n \neq 1$$

$$= - \frac{R \, G_o}{4\pi} \int_0^{\pi} \int_0^{2\pi} \cos \tfrac{1}{2}\psi \, d\psi \, d\alpha + \frac{1}{4\pi R} \iint f(\psi) \, \Delta g' \, dS$$

$$= 2(W_o - U_o) - R \, M\{\Delta g\} + 2M\{\delta W\} + \frac{1}{4\pi R} \iint f(\psi) \left(\Delta g - 2\frac{\delta W}{R}\right) dS \qquad (17),$$

as the term $(W_o - U_o)$ has no effect through Stokes' integral being a term of zero degree. On using equation 9, and if $M\{\ \}$ refers to the global mean value, equation 17 becomes

$$h_d = \frac{W_o - U_o}{\gamma} + \frac{2 \, M\{\delta W\} - \delta W_p}{\gamma} - \frac{R}{\gamma} M\{\Delta g\} + \frac{R}{4\pi\gamma} \iint f(\psi) \left(\Delta g - 2\frac{\delta W}{R}\right) d\sigma \qquad (18).$$

$M\{\delta W\} = 0$ if the geoid is defined as the mean equipotential surface through the global set of elevation datums. The net effect $e_{h_{dp}}$ of the existence of stationary sea surface topography on the solution h_{dp} of the boundary value problem at P is therefore

$$e_{h_{dp}} = - \frac{\delta W_p}{\gamma} - \frac{1}{2\pi\gamma} \iint f(\psi) \, \delta W \, d\sigma \qquad (19).$$

Notes

(i) Equation 19 defines effects of consequence in practical evaluations in physical geodesy as δW holds the same sign over large extents of surface area.

(ii) It was implied in an earlier study (MATHER 1973a,p.87) that an iterative procedure would be necessary if quasi-stationary sea surface topography were widespread phenomena with significant amplitudes and wavelengths. The use of equation 19 would however restrict the iterative procedure to merely the correction terms which would be more economic to compute. The expression at 19 can be considered to be of adequate accuracy for all foreseeable practical solutions of the geodetic boundary value problem.

(iii) The earlier study referred to above estimated that the existence of values of $o\{\pm 2$ kgal m$\}$ for δW with wavelengths of 4000 km would contribute errors of $o\{\pm 30$ cm$\}$ to determinations of geoid heights in ocean areas if not allowed for by procedures similar to those outlined above.

(iv) As a corollary, it would appear at first glance that no determination of stationary sea surface topography by a combination of satellite altimetry, physical geodesy

and tidal analysis, as illustrated in figure 2, can be achieved without resorting to an iterative procedure. A first iteration excluding the effect embodied in equation 19, should define the stationary sea surface topography to o{±30 cm} as discussed at (iii). Consequently, δW in equation 19 can still be as large as o{±0.3 kgal m}, giving effects of o{±5 cm} in h_d. The apparently less plausible long wavelengths in the stationary sea surface topography cause greater systematic errors in the solution of the geodetic boundary value problem.

(v) An alternative technique with some appeal, especially when repeating the solution to get rid of small systematic effects, is the use of randomization techniques on the value of δW when using equation 19. The use of such techniques on the gravity data is not advisable as in the first instance, it precludes the use of equation 19.

(vi) It is important to note particulars of elevation datums when compiling gravity data banks so that δW can be correctly computed.

4. Geodetic Reference Systems for Determination of Vertical Crustal Motion

The techniques in use at present for the determination of vertical crustal motion can at best, be classified as regional in concept rather than global. The basic principles utilized, more from necessity rather than by design, can be summarized as follows. Points of reference (benchmarks) are selected to represent the terrain in the region considered. These benchmarks are linked during a selected epoch (τ = T) by first order geodetic levelling procedures to some datum of reference, usually a convenient tide gauge which is assessed as lying "outside" the area subject to vertical crustal motion. The levelling is repeated at a subsequent epoch (τ = T + dT) and the differences in geopotential between the levellings at each benchmark, as converted to their linear equivalents, give an estimate of vertical crustal motion.

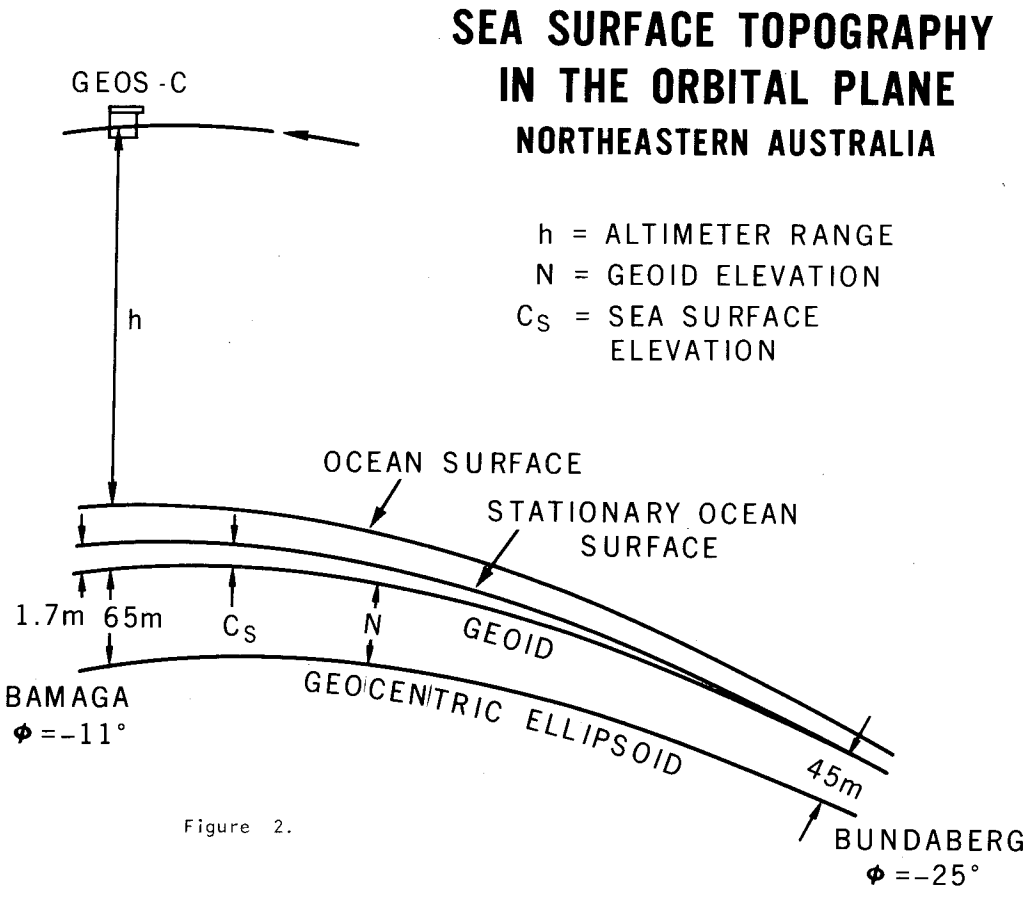

Figure 2.

The technique described above makes the following assumptions.

(i) The location of the datum for elevations is invariant in Earth space between epochs

(ii) The change in geopotential obtained between the epochs at any benchmark is a measure of the Earth space displacement along the local vertical.

The validity of the first assumption or any departures from its basic premise, is partly dependent on the criteria adopted for the definition of the observation space. It is possible to define a three dimensional Cartesian system of reference X_i for position in Earth space such that the differences between the co-ordinates $X_i(\tau = T + dT)$ and $X_i(\tau = T)$ give the displacement vector of the point considered in Earth space (MATHER 1973b). Elevation datums which were incorporated in such a world wide network of geodetic control would provide space characteristics of global relevance for determinations of vertical crustal motion using levelling techniques *only if* there were no change in the shape and spacing between adjacent geops (equipotential surfaces of the Earth's gravitational field) in Earth space. This follows from the nature of the levelling process where the level is always set tangential to the instantaneous surface geop prior to observing incremental differences in orthometric elevations.

The latter contention is therefore based on the same foundation as the assumption at (ii) above. It is however inconsistent with the concept of crustal motion at *some* order of magnitude, as the latter implies changes in the Earth space position of a proportion of the mass elements constituting the Earth. It is therefore more desirable in principle, that studies of vertical crustal motion be based on observations referred to a system of geodetic reference with an unambiguous location in Earth space, *provided no loss of resolution occurs in doing so.*

Assuming that it is considered desirable to evaluate vertical crustal motion as opposed to the crustal motion vector, i.e., it is necessary to determine incremental changes in position along the local vertical, the surface of reference adopted should be such that its normal approximates closely to the direction of the local vertical. It is common knowledge that the normals of an ellipsoid of revolution which has the same volume as the geoid, and is concentric with the geocentre, do not depart from surface verticals by amounts much in excess of $o\{\frac{1}{3}$ mrad$\}$. Three dimensional Cartesian co-ordinates X_i obtained in the manner referred to earlier for all benchmarks in the region of vertical crustal motion determination, can be converted to positional parameters (ϕ,λ,h) with respect to the ellipsoid, if desired, using procedures similar to that described in Appendix 2. The changes

$$dh = h(\tau = T + dt) - h(\tau = T)$$

obtained at any benchmark using such a system of reference, would be a measure of vertical crustal motion which is free from the errors of assumption given at (i) and (ii) above.

The adoption of this procedure would be of practical relevance only if the resulting estimate of vertical crustal motion had the same resolution as the results obtained from first order geodetic levelling. If this were possible, the three dimensional technique would, in addition, completely define the crustal motion vector in Earth space. The precision requirements for the geocentric co-ordinates in such a solution would be $o\{\pm 10$ cm$\}$ in each co-ordinate. While no such achievements have been realized to date, there is promise that recent technological developments could well result in this happening in the foreseeable future by the use of global networks of either laser ranging systems to satellites and the moon, or VLBI.

The advantages of doing so are

(a) the total definition of the crustal motion vector, as opposed to the vertical component only;

(b) the global relevance of the results; and

(c) an independence from temporal variations in the shape and Earth space position of the equipotential surfaces of the Earth's gravitational field.

The main obstacles to implementation are logistic. It is all important to have a truly global network of ground stations to comprise the fundamental geodetic net. It is equally important to fabricate transportable systems to complement the fixed stations. Observations to extra-terrestrial objects which are banded in declination may cause a weakness in determinations of the X_3 co-ordinate, as pointed out by Kaula for determinations from laser ranging to the moon (KAULA 1973).

In the final analysis, the goal of four dimensional position determinations for the crustal motion vector must be the resolution of vertical crustal motion with the same precision as that presently achieved by first order geodetic levelling.

5. References

APEL, J. (ed) 1972. Sea Surface Topography from Space. *NOAA Tech.Rep.* ERL 228-AOML 7,Vols. 1 & 2, Boulder Colorado.

BALAZS, E.I. 1973. *Local Mean Sea Level in Relation to Geodetic Levelling Along the United States Coastlines.* National Geodetic Survey, Rockville Md.

DE ALENCAR, J.C.M. 1968. *Sistema Nacional de Livelamento de 1ª Ordem.* Fundacão IBGE, Instituto Brasileiro de Geografia,Divisão de Geodésia e Topografia,Sao Paulo.

DONN, W.L., PATTULLO, J.G., & SHAW, D.M. 1964. Sea Level Fluctuations and Long Waves. In (ODISHAW, H ed.). *Research in Geophysics, Volume 2.* M.I.T. Press, Cambridge Mass,243-269.

HAYASHI, T. 1969. A Study on the Vertical Movements of the Earth's Crust by Means of Precise Levelling. *Bull.geog.Surv.Inst.* XV,Part 1,1-67.

KAULA, W.M. 1973. Potentialities of Lunar Laser Ranging for Measuring Tectonic Motions. *Phil.Trans. R.Soc.Lond.A* 274,185-193.

KELSEY, J. 1970. Considerations Arising from the 1970 Readjustment of the Levellings of Great Britain. In (SIGL, R. ed.) *Report on the Symposium on Coastal Geodesy.* Institute for Astronomical & Physical Geodesy, Technical University,Munich,331-338.

LEVALLOIS, J.J. & MAILLARD, J. 1970. The New French 1st Order Levelling Net - Practical and Scientific Consequences. *Op.cit.*,331-338.

MARSH, J.G., DOUGLAS, B.C. & KLOSKO, S.M. 1973. A Global Station Co-ordinate Solution based upon Camera and Laser Data. *Rep.X*-592-73-171,Goddard Space Flight Center,Greenbelt Md,64 pp.

MATHER, R.S. 1971. The Analysis of the Earth's Gravity Field. *Monograph* 2,School of Surveying, The University of New South Wales,Kensington NSW.

MATHER, R.S. 1973a. A Solution of the Geodetic Boundary Value Problem to Order e^3. *Rep. X*-592-73-11,Goddard Space Flight Center,Greenbelt Md,127 pp.

MATHER, R.S. 1973b. Four Dimensional Studies in Earth Space. *Bull.geodês.* 108,187-209.

MITCHELL, H.L. 1973. Relations between Mean Sea Level and Geodetic Levelling in Australia. *UNISURV Rep.* S9,University of New South Wales,Kensington NSW,264 pp.

NASA 1971. *NASA Directory of Observation Station Locations,* Vols 1 & 2. NASA Goddard Space Flight Center,Greenbelt Md.

ROELSE, A., GRANGER, H.W. & GRAHAM, J.W. 1971. The Adjustment of the Australian Levelling Survey 1970-1971. *Tech.Rep.* 12,Division of National Mapping,Canberra,81 pp & App.

ROSSITER, J.R. 1967. An Analysis of Annual Sea Level Variations in European Waters. *Geophys.J.R. astr.Soc.* 12,259-299.

STURGES, W. 1973. Sea Level Slope Along Continental Boundaries. Submitted to *J.geophys.Res.*

TROVAAG, O & JELSTRUP, G. 1956. Presisjonsnivellement i Sør-Norge. *Geodet. Publ.* 5,Norges Geografiske Oppmaling,Oslo,170 pp.

6. Appendix 1

Reported Stationary Topography of Mean Sea Level

REGION	OCEAN/SEA	APPROXIMATE POSITION ESTIMATED STATIONARY COASTAL TOPOGRAPHY (+VE N,E)										
		Latitude		Longitude		From Geodetic Levelling				From Steric Levelling		
		deg N		deg E		Slope		Epoch	Source	Slope (m)	Epoch	Source
		From	To	From	To	(m)	(rad)					
AUSTRALIA												
North East	Pacific	-30	-11	153	142	+1.75	+0.74	1966-68	7	+0.2 ±0.1	1960-64	6
South East	Southern;Tasman	-35	-30	136	153	+0.30	+0.17	1966-68	7	+0.35±0.1	1960-64	6
South	Southern	-35	-35	118	136	-0.82	-0.52	1966-68	7	0.0 ±0.1	1960-64	6
South West	Indian	-35	-29	118	115	-0.31	-0.45	1966-68	7	+0.0 ±0.1	1960-64	6
North West	Indian;Timor	-29	-17	115	137	+0.38	+0.17	1966-68	7	+0.5 ±0.1	1960-64	6
North	Carpentaria	-17	-11	137	142	+1.16	+1.38	1966-68	7	+0.05±0.1	1960-64	6
BRAZIL	Atlantic	-24	-4	-42	-38	+0.41	+0.17	1949-57	2	+0.4 ±0.1	*	9
EUROPE (WESTERN)												
Malaga-Genoa	Mediterranean	37	44	-4	9	-0.04	-0.06	1950.0	5			
Cadiz-Dieppe	Atlantic	37	50	-6	2	0.00	0.00	1950.0	5			
Dieppe-Cuxhaven	North	50	53	2	9	+0.21	+0.34	1950.0	5			
DENMARK	North;Baltic	55½	55½	9½	12½	0.02	+0.06	1950.0	5	-0.09±0.1	1950.0	8
FINLAND	Baltic	60½	65½	27	24½	0.03	+0.06	1950.0	5	+0.03±0.1	1950.0	8
GREAT BRITAIN	Atlantic;North	50	57	-5½	-2	+0.29	+0.34	1950.0	4	+0.13±0.1	1950.0	8
JAPAN East	Pacific	32	35	132	140	-0.18	-0.23	1950.0	3			
West	Japan	35	40	132	140	+0.03	0.00	1950.0	3			
NORWAY South	North;Atlantic	59	63½	10	9	+0.01	+0.00	1916-53	10	+0.04±0.1	1950.0	8
North West	Atlantic	63½	70	9	19	-0.03	-0.06	1950.0	5	+0.03±0.1	1950.0	8
SWEDEN	Baltic	58½	65	11	21	+0.31	+0.34	1950.0	5	+0.09±0.1	1950.0	8
UNITED STATES												
East Coast (N)	Atlantic	33	45	-81	-67	+0.00	+0.00	1966.9	1	+0.0 ±0.1	*	9
East Coast (S)	Atlantic	24½	33	-80	-81	+0.33	+0.34	1966.9	1	-0.2 ±0.1	*	9
Gulf Coast	Gulf of Mexico	24½	29	-87	-95	+0.49	+0.52	1966.9	1			
West Coast (S)	Pacific	33	35	-117	-121	0.32	+0.17	1969.3	1	-0.1 ±0.1	*	9
West Coast (N)	Pacific	35	48½	-121	-125	0.63	+0.40	1969.3	1	-0.2 ±0.1	*	9

KEY TO SOURCE :- 1 = BALAZS 1973 2 = DE ALENCAR 1968,p.11 3 HAYASHI 1969,p.18
4 = KELSEY 1970,p.366 5 = LEVALLOIS & MAILLARD 1970, p.330
6 = MITCHELL 1973,p.105 7 = ROELSE ET AL 1971 8 ROSSITER 1967,p.292
9 = STURGES 1973,figure 1 10 = TROVAAG & JELSTRUP 1956, p.167

* No epoch specified. See uncertainty estimates in previous column.

7. Appendix 2

RECOVERY OF VERTICAL COMPONENT

ADOPT A REFERENCE ELLIPSOID, HENCE (a,f)

$$\nu = \frac{a}{\left[1-(2f-f^2)\sin^2\phi\right]^{1/2}}$$

$$X_1 = (\nu+h)\cos\phi \quad \cos\lambda$$

$$X_2 = (\nu+h)\cos\phi \quad \sin\lambda$$

$$X_3 = \left[\nu(1-f)^2 + h\right] \quad \sin\phi$$

$$\lambda = \tan^{-1}(X_2/X_1)$$

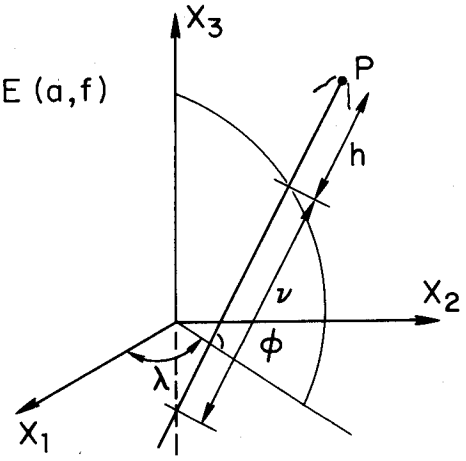

ITERATE BETWEEN

$$\phi = \tan^{-1}\left[\frac{X_3(\nu+h)\sin\lambda}{X_2\left[\nu(1-f)^2+h\right]}\right] = \tan^{-1}\left[\frac{X_3(\nu+h)\cos\lambda}{X_1\left[\nu(1-f)^2+h\right]}\right]$$

$$h = \frac{X_1}{\cos\phi\cos\lambda} - \nu = \frac{X_2}{\cos\phi\sin\lambda} - \nu = \frac{X_3}{\sin\phi} - \nu(1-f)^2$$

8. Discussion

WALCOTT: Are there differences between geodetic re-levelling and tidal changes at the same location? I ask this because the European map of recent crustal movements shows some peculiarities when you get near the coast. Contours tend to smooth out and not show the closures forming domes and basins which are mapped inland.

HOLLWEY: As far as the British Isles are concerned, the answer is "Yes".

MELCHIOR: On page 5 of your Compendium (TITLE: *Quasi-Stationary Sea Surface Topography and Variations of Mean Sea Level with Time - An Interim Compendium (1973)* - Final Version to appear shortly in *UNISURV Rep.* G-Series,University of New South Wales), you state that only a limited number of organizations were able to provide information. But you do not mention the Permanent Service for Mean Sea Level.

MATHER: I wrote to Dr. Lennon and he referred me to the *Report of the Symposium on Coastal Geodesy*

(SIGL, R. ed., Munich 1970) as a "state of the art" document and considerable material from that source has been incorporated.

MELCHIOR: It is a matter of great concern for IUGG how the Permanent Services are really working, and what kind of data they provide to geodesists and geophysicists. We are really in a very difficult situation in the Union because the ICSU is channelling money to the Permanent Services. At the last meeting of the Union Executive Committee, we discussed the situation and in a few weeks, I shall send documents to all Associations and to many interested geodesists concerning data provided by the Permanent Services. In this case, the Permanent Service on Mean Sea Level should provide a lot of data, not only to oceanographers but also to geodesists. It should be a first task for IAG to say what they expect to receive from this service and if they are satisfied; and if something has to be improved. Such a meeting as this could say something about it.

If the work of this service is satisfactory (I hope so), or if you need more help from such a service - for I expect you will in preparing such a compendium - I should expect that the Permanent Service of Mean Sea Level should help.

MATHER: All I can say is that when I wrote to national government agencies in various parts of the world, those who replied wanted to have a copy of the compendium. Presumably the data is not readily available.

RAPP: On the equation that you showed for the effect of MSL, you had the integration of Stokes' function times δW. Implicitly you said that δW changed from place to place, e.g., you had (one value for a) datum like Australia and another for NAD, etc. A more difficult problem occurs in the case of the 70% of the Earth's surface which is oceanic. How accurately do people who measure gravity at sea measure their heights? This is going to change for every one of your points. For example, for Australia, you have one correction for *all* points, but at sea, unless you can determine very uniquely the height of the gravity meter with respect to sea level, you have a problem.

BARLOW: I think the gravity meters themselves have limited resolution and no one worries at all about this effect.

MATHER: We are really concerned about effects which retain the same sign over large areas. If it changes sign often, then the effect is minimized.

MUELLER: I did not catch one of your comments about disagreement in the meridian and agreement in the prime vertical. What did you mean by that?

MATHER: On levelling across a continent generally along a parallel, and on comparing the steric levelling with the geodetic levelling, good agreement is obtained from the data available at present.

RAPP: I might remark that STURGES' answer to that is the way the sun shines on the levelling staffs.

MATHER: I have read that comment.

HOLLWEY, J. R.
Department of Land Surveying
North East London Polytechnic
E N G L A N D

Proc. Symposium on Earth's Gravitational Field & Secular Variations in Position (1973), 600-621.

SEA LEVEL VARIATIONS IN TIME AND SPACE ALONG THE EAST COAST OF ENGLAND

1. Introduction

In many respects, the problems arising from variations in the level of the sea from place to place become more complex when we introduce a fourth dimension of time into the situation. It follows that with the introduction of this extra dimension, there will be a repetition of connections by geodetic levelling to tidal observatories. Furthermore, with an improvement in the quality of our measuring systems both at the Observatory and in the geodetic levelling, the opportunity is lost to sweep into a category of observational error any results which do not fit a very simple model of the natural phenomena involved. This leaves open the question of a more complex model to fit the results or the possibility of a source of error in the observations not hitherto considered.

The United Kingdom is fortunate in possessing a Second and Third Geodetic Levelling Network of a standard sufficiently reliable to permit comparison. As well, the main island is sufficiently small to permit detailed study of results from both geodetic levelling and tidal observatories. At the same time, it is sufficiently large for this result to be meaningful. The oceanographic and meteorological conditions provide a variation in data and geological information is both detailed and reliable.

Considering first the situation exposed by the completion of the Third Geodetic Levelling, this is illustrated by figure 1; a more detailed study of these results is given in CARMODY & BURNETT (1960).

The conclusions from the levelling alone points to rise of Dunbar relative to Newlyn of 0.58ft, but from the tidal observations alone, assuming Mean Sea Level has risen at Dunbar and Newlyn at the same rate, there seems to be evidence of a rise of Dunbar relative to Newlyn of 0.17ft. It will also be seen from figure 1 that Felixstowe and Newlyn seem to move in sympathy and that the critical area of uncertainty is the coastline from the Thames estuary to the Firth of Forth. Along this stretch of coast, there are now reliable tidal observatories at Southend, Lowestoft, Immingham and North Shields. Note: the Felixstowe Observatory is no longer in use. It is this stretch of coast which I am examining here in some detail.

2. The Determination of Mean Sea Level

No uniform method of reduction of sea level observations exists; ROSSITER (1958) lists the following ways in which the basic daily mean is normally computed -

A. Direct average of 1, 3, 6 or 8 heights per day at fixed hours.

B. Direct average of 24 or 25 hourly heights.

C. Numerical filters applied to hourly heights.

D. Direct average of high and low water heights.

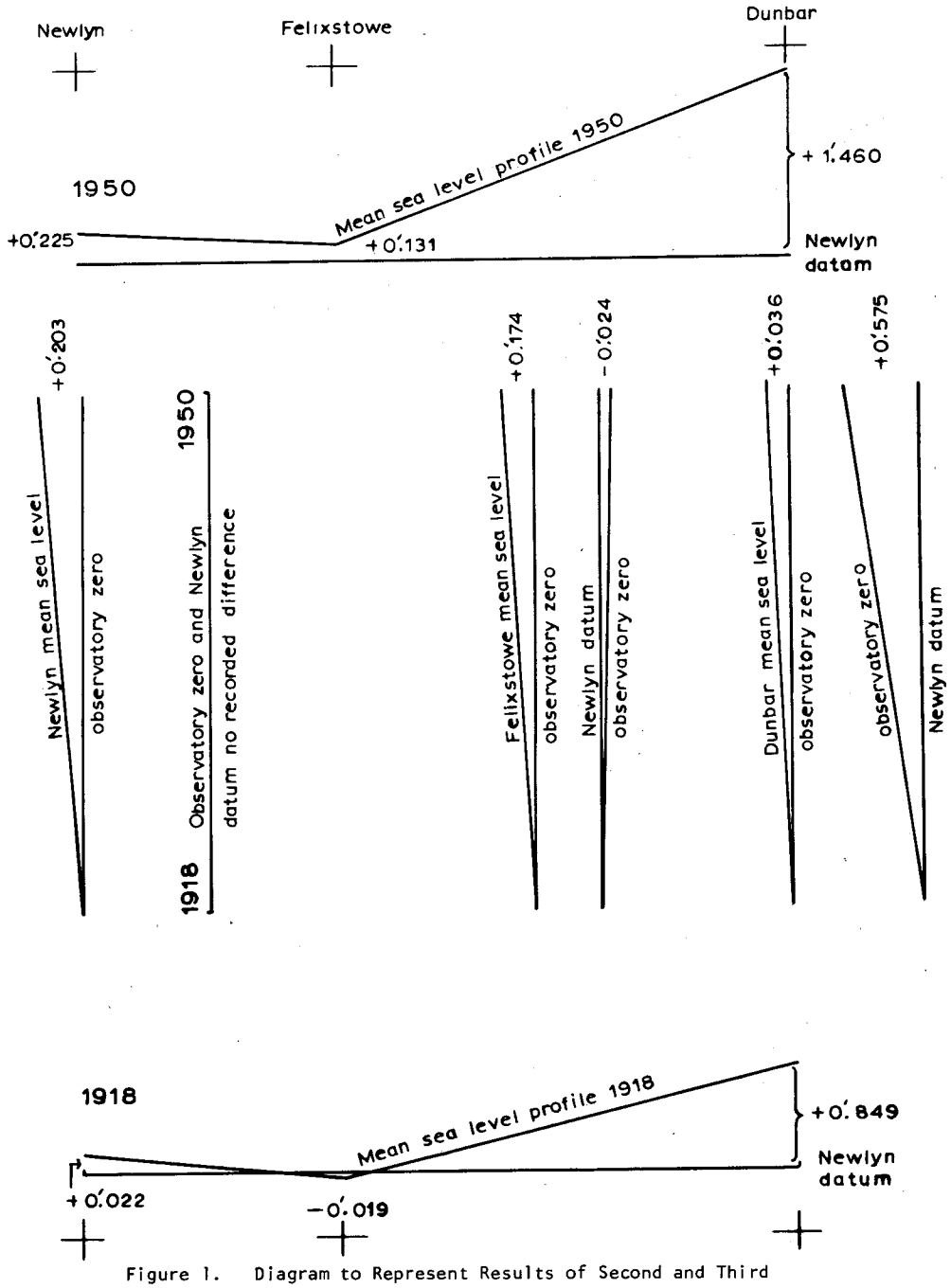

Figure 1. Diagram to Represent Results of Second and Third Geodetic Levelling of the United Kingdom

E. Integration of daily records of sea level changes by planimeter.

to which I would add -

F. The average of hourly heights taken during the hours of daylight. For example, the mean of 12 or 13 consecutive observations in every 24 hours.

It is obvious that A) can only be meaningfully used in regions where tidal ranges are small. Similarly, D) and F) must be treated with considerable caution, although they are commonly the resort of survey parties establishing a temporary datum. B), C) and E) give results which are commonly described as Mean Sea Level.

If, however, we adopt a definition which seems the most suitable for the problem of geodesy, namely:

"the level which results from processing a set of sea observations in such a way that the contributions made by the tidal oscillations are removed" (LENNON, 1965)

the following points emerge:

Let Mean 'Sea' Level so defined be Zo and let the contributions made by the tidal oscillations at time t be Y_t, then the level of the sea at time t is given by h_t, where

$$h_t = Zo + Y_t. \tag{1}$$

If a harmonic tidal constituent be represented by

$$\zeta_H = R \cos (\sigma H + pD - \varepsilon) \qquad \text{(after ROSSITER, 1958)}$$

with R the amplitude and ε the phase lag, both constant at any one place σ the speed in degrees per mean solar hour, p the speed in degrees per mean solar day, H the time in hours, and D the time in days, then

$$Y_t = \sum_{i=1}^{n} . \; R_i \; . \cos (\sigma_i H + p_i D - \varepsilon_i) \tag{2}$$

where R_i, σ_i, p_i and ε_i represent values unique for each one of n tidal constituents significant at the locality.

The problem is now reduced to one of combining values of ζ_H in such a way that in their summation

$$\Sigma Y_t \simeq 0 \quad \text{or} \quad \int_0^{24} Y_t \simeq 0.$$

This is most nearly achieved by a numerical filter of which the X_o filter of Doodson (DOODSON & WARBURG 1941) is the most suitable. It can be shown that:

$$\sum_{i=0}^{m-1} R \cos (\sigma q t_i + pD - \varepsilon) = (\sin \tfrac{qm\sigma}{2} \,/\, \sin \tfrac{q\sigma}{2}) \, R \cos (pD - \varepsilon + \tfrac{m-1}{2} \, q\sigma) \tag{3}$$

where terms are as above and in addition the summation sequence involves m values at intervals of q hours. Further, H in equation (1) is related to q and t_i by $t_i q = H$

From equation (3) it is possible to devise a numerical filter which enables a quantity X_o to be evaluated which approximates to the LENNON (1965) definition of Mean Sea Level. For each day,

$$X_o = \frac{1}{30}(h_{17} + h^1_{19} + h^1_{22} + h_0 + h_1 + 2h_3 + h_5 + h_6 + 2h_8 + h_9$$

$$+ h_{10} + 2h_{11} + 2h_{13} + h_{14} + h_{15} + 2h_{16} + h_{18} + h_{19}$$

$$+ 2h_{21} + h_{23} + h_{24} + h^{11}_2 + h^{11}_5 + h^{11}_7)$$

where h^1_n is the height at hour n on the previous day, h_n is the height at hour n on the current day, and $h^{11}n$ is the height at hour n on the following day.

The efficiency of the X_o filter and in particular the tidal coefficients it removes is illustrated by figures 2 and 3.

A comparison of the daily means computed by taking the mean of the 24 hour readings and by using the X_o filter was carried out for the years 1967, 1968 and 1969 for the four east coast observatories mentioned above. The result of this comparison is given by table 1 below.

TABLE 1

	Southend	Lowestoft	Immingham	N.Shields
Max. -ve diff. 1967	-0.73	-0.50	-0.58	-0.66
Max. +ve diff. 1967	+0.49	+0.43	+0.54	+0.40
Max. -ve diff. 1968	-0.63	-0.61	-0.89	-0.51
Max. +ve diff. 1968	+0.66	+0.55	+0.57	+0.47
Max. -ve diff. 1969	-0.66	-0.72	-0.74	-0.68
Max. +ve diff. 1969	+0.50	+0.70	+0.68	+0.38
Neap Tide Range	11.0	3.4	10.4	6.0
Spring Tide Range	17.1	6.4	20.9	14.1

Units Feet

Using the various daily values, it is found that in the two sets of 144 monthly means differences for the same month of 0.048 ft. occur in only one case; for the remainder, differences between 0.015 and 0.04 ft. occur in only seven cases, and in all other cases differences are less than 0.015 ft. It seems that for the conditions pertaining along the east coast it is unnecessary to use the filtered values. This conclusion agrees with theory as expressed by table 2, obtained by use of tables 1 and 3 of ROSSITER (1958).

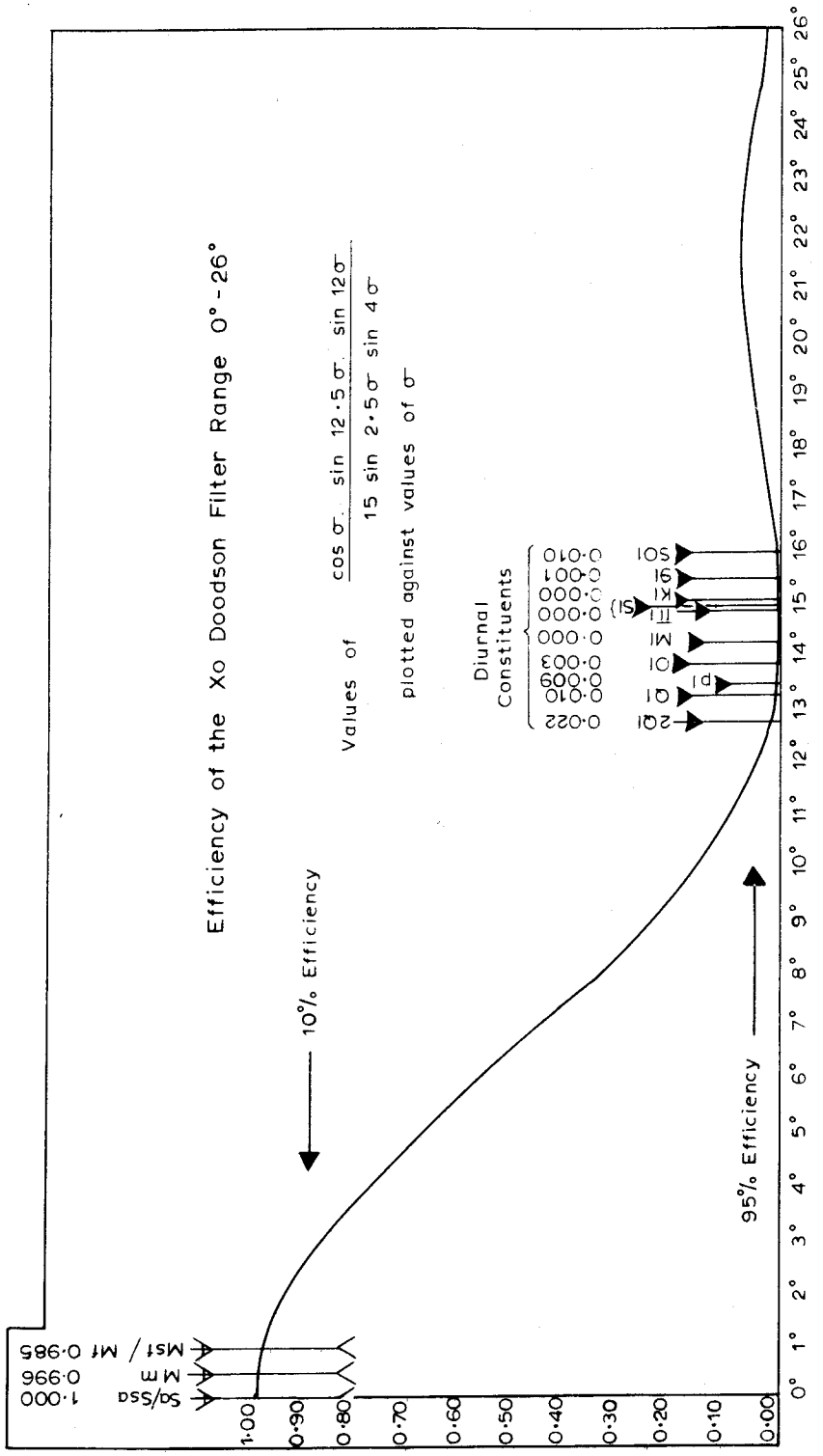
Efficiency of the Xo Doodson Filter Range 0° - 26°
Values of cos σ . sin 12·5 σ . sin 12 σ / 15 sin 2·5 σ sin 4 σ
plotted against values of σ
Diurnal Constituents
2Q1 0·022
σ1 0·010
Q1 0·009
ρ1 0·003
O1 0·000
M1 0·000
(S1) 0·000
K1 0·000
J1 0·001
OO1 0·010
10% Efficiency
95% Efficiency
Sa/Ssa 1·000
M3 0·996
Ms1 / M1 0·985
1·00 0·90 0·80 0·70 0·60 0·50 0·40 0·30 0·20 0·10 0·00
0° 1° 2° 3° 4° 5° 6° 7° 8° 9° 10° 11° 12° 13° 14° 15° 16° 17° 18° 19° 20° 21° 22° 23° 24° 25° 26°

Figure 2

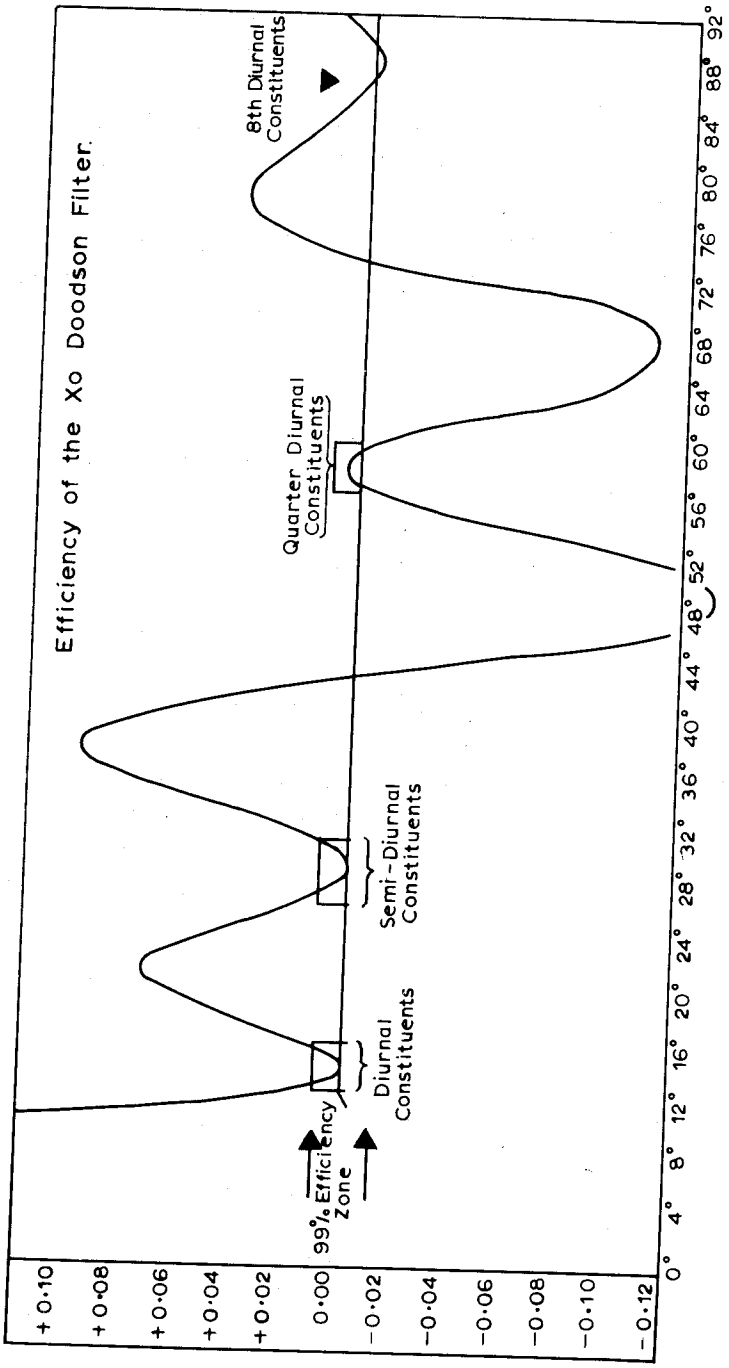
Efficiency of the Xo Doodson Filter.
8th Diurnal Constituents
Quarter Diurnal Constituents
Semi-Diurnal Constituents
Diurnal Constituents
99% Efficiency Zone
+0·10
+0·08
+0·06
+0·04
+0·02
0·00
−0·02
−0·04
−0·06
−0·08
−0·10
−0·12
0°
4°
8°
12°
16°
20°
24°
28°
32°
36°
40°
44°
48°
52°
56°
60°
64°
68°
72°
76°
80°
84°
88°
92°

Figure 3

Table 2

Coefficients of Contributions from Listed Tidal Constituents								
	30 day Means							
To X_o Value	K_1	O_1	M_2	N_2	M_3	M_4	M_6	MSf
	.0001	.0002	-.0000	-.0001	.0001	-.0000	-.0000	.0155
24h Value	-.0027	.0040	-.0005	.0021	-.0006	-.0006	-.0006	.0155
	365 day Means							
To X_o Value	.0000	-.0000	-.0000	-.0000	-.0000	-.0000	-.0000	.0127
24h Value	.0000	-.0007	-.0003	.0000	-.0001	.0002	-.0001	.0127

Note: The maximum contribution to the mean over the period specified is obtained by multiplying the amplitude of the constituent by the coefficient given above.

3. Variations of Monthly Mean Sea Level at the Four Observatories (1967-69)

Monthly Mean Sea Level at each of the four stations varies during the period considered within a range of approximately 1ft. (300mm) and with a standard deviation of 0.2 to 0.3ft (60 to 90mm). Regardless of methods used to process the hourly height these statistics remain unchanged. Against this background it was decided to establish how far the variation pattern might be related between stations and how far monthly values at one station might be predicted from one or more adjacent stations.

The method of correlation and regression analysis used, the statistical processes involved, and the computer program are not relevant to this paper and are fairly standard; here I am only concerned with the results obtained.

Figure 4 illustrates the changes in monthly mean sea level over the period January 1967 to December 1969 at the four stations Southend, Lowestoft, Immingham and North Shields. It is evident from the graphs that there is a close relationship. In 26 cases sea level changes from month to month at all stations with the same sign, in 7 of the 9 remaining cases, 3 out of 4 of the changes are the same. In April/May 1967 the two northerly stations show an increase followed by a decrease in May/June 1967 whilst the southerly stations show successively a decrease followed by an increase.

Examining the statistics in table 3, the Immingham correlations are in all cases the strongest. Not surprisingly Immingham/North Shields (0.925) is the strongest, but this is closely followed by the Immingham/Southend figure (0.910). CARTWRIGHT (1967) draws artention to the way in which daily means at Southend and Immingham are closely related and this result seems to be repeated with monthly means. The weakest correlation is given by North Shields/Southend (0.773) which is still, however, very significant.

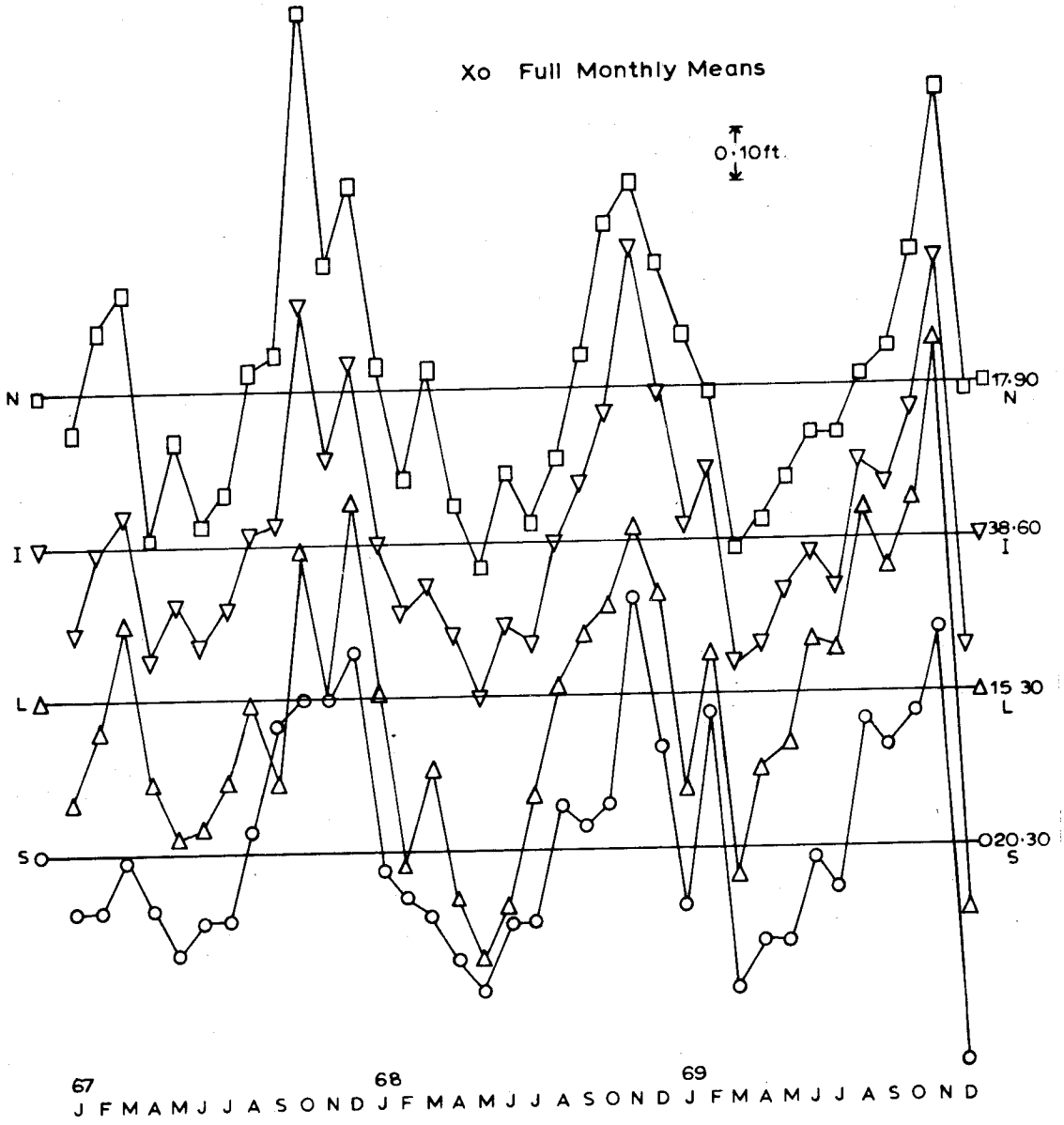

Figure 4

The results of a multiple (or where necessary linear) correlation of all combinations of 3 of the 4 stations are given in table 4. On the basis of the regression equation, it should be possible to predict monthly mean sea level at one station given monthly means at one or more of the other stations. In table 5 are given the results of such a prediction for Southend 1961 using 3 of the regression equations. The ability of this treatment to detect unreliable monthly means, as for instance Immingham May 1961, is more significant than its use in prediction. In addition, isolated gaps might be more successfully filled by this method than by prediction from harmonic constituents.

For example, the predicted values for North Shields December 1969 are all consistently lower than observed. In that month only 16 daily means were obtained and it might have been better to use a predicted monthly mean for purposes of an investigation into changes of Mean Sea Level.

TABLE 3

X_o Full Month Monthly Means Correlation Coefficients

	Lowestoft	Immingham	N.Shields
Southend	0.851	0.910	0.773
Lowestoft	-	0.882	0.776
Immingham	-	-	0.925

TABLE 4

X_o Full Month Regression Analysis Between Monthly Means

Ref.	Std. Dev. of Variable	Intercept $\times 10^{-2}$	Regression Coeff. of Independent Variables			Multiple Correl. Coeff.	Std. Err. of Est. $\times 10^{-2}$	Degs. of F'dom	F Value
Southend			Low.	Imm.	N.Sh.				
020/1	0.223	-20.219	+0.110	+1.185	-0.387	0.930	0.085	3:32	68.813
020/5		- 9.792	+0.175	+0.710		0.916	0.092	2:33	85.915
020/6		+ 8.096	+0.510		+0.247	0.869	0.113	2:33	51.062
020/7		-23.862		+1.338	-0.420	0.928	0.085	2:33	102.963
020/8		+ 9.805	+0.687			0.851	0.119	1:34	89.120
020/9		-14.393		+0.899		0.910	0.094	1:34	164.247
20/10		+ 8.246			+0.673	0.773	0.143	1:34	50.424
Lowestoft			South.	Imm.	N.Sh.				
020/02	0.276	-26.945	+0.257	+1.041	-0.192	0.892	0.130	3:32	41.344
020/11		-21.322	+0.341	+0.765		0.890	0.130	2:33	62.535
020/12		- 6.066	+0.771		+0.317	0.871	0.139	2:33	51.856
020/13		-33.078		+1.392	-0.300	0.888	0.130	2:33	61.676
020/14		- 6.096	+1.052			0.851	0.147	1:34	89.120
020/15		-26.310		+1.077		0.882	0.132	1:34	118.989
020/16		+ 0.295			+0.836	0.776	0.176	1:34	51.416
Immingham			South.	Low.	N.Sh.				
020/03	0.226	+20.812	+0.380	+0.144	+0.441	0.979	0.048	3:32	243.647
020/17		+23.889		+0.338	+0.534	0.961	0.064	2:33	199.674
020/18		+19.941	+0.491		+0.486	0.975	0.052	2:33	317.721
020/19		+21.838	+0.586	+0.319		0.933	0.084	2:33	110.762
020/20		+19.894	+0.922			0.910	0.094	1:34	164.247
020/21		+27.589		+0.722		0.882	0.108	1:34	118.989
020/22		+23.989			+0.817	0.925	0.027	1:34	202.193
North Shields			South.	Low.	Imm.				
020/04	0.256	-31.202	-0.432	-0.092	+1.535	0.941	0.090	3:32	83.002
020/23		+23.292	+0.469	+0.398		0.805	0.156	2:33	30.372
020/24		-26.972		-0.167	+1.229	0.929	0.097	2:33	104.194
020/25		-29.242	-0.464		+1.465	0.940	0.090	2:33	125.831
020/26		- 0.095	+0.887			0.773	0.165	1:34	50.424
020/27		+ 6.923		+0.720		0.776	0.164	1:34	51.416
020/28		-22.565			+0.048	0.925	0.098	1:34	202.193

F. Distribution:

D. of F.	5%	2½%	1%
3 : 32	2.90	3.56	4.46
2 : 33	3.28	4.14	5.32
1 : 34	4.13	5.50	7.45

TABLE 5

Actual and Predicted Monthly Mean Sea Level: Southend 1961 (units feet)

Month	Actual Mean+	Predicted 020/5	Res.	Predicted 020/8	Res.	Predicted 020/9	Res.
Jan.	20.10	20.00	-.10	20.18	+.08	19.99	-.11
Feb.	20.28	20.13	-.15	20.22	-.06	20.13	-.15
Mar.	20.40	20.21	-.19	20.36	-.04	20.19	-.21
Apr.	20.08	20.08	0	20.18	+.10	20.09	+.01
May	20.45	(20.21)	-.24	20.38	-.07	(20.19)	-.26
June	20.21	20.18	-.03	20.28	-.07	20.19	-.02
July	20.38	20.18	-.20	20.30	-.08	20.18	-.20
Aug.	20.21*	20.20	-.01	20.25	+.04	20.21	0
Sept.	20.35	20.34	-.01	20.24	-.11	20.40	+.05
Oct.	20.38	20.48	+.10	20.34	-.04	20.55	+.17
Nov.	20.68	20.47	-.21	20.48	-.20	20.48	-.20
Dec.	20.57	20.44	-.13	20.54	-.03	20.43	-.14
		σ = .15		σ = .09		σ = .16	
		Prediction 020/5 uses Immingham & Lowestoft		Prediction 020/8 uses Lowestoft only		Prediction 020/9 uses Immingham only	

NOTES: + Source Monographie 21 (IUGG), Monthly and Annual Mean Heights of Sea Level 1959-61 except *where corrected value given in Monographie 30.

() Immingham Data indicated as being unreliable

4. Results and Differences in Height of Mean Sea Level

The relationship between tidal observatory datums will depend, inter alia, upon the adjustment of the connecting geodetic levelling. Three alternative relationships are given in table 6.

TABLE 6

Corrections to Reduce Monthly Mean Value (X_o Full Month) of Sea Level to A.O.D. Newlyn (ft)

	(1) Reduction based on pract. Adj.effectively 2nd Geodetic Levelling	(2)-(1)	(2) Reduction based on 2nd Scientific Adj. of 3rd Geod. Levelling	(3)-(2)	(3) Reduction based on limited Adj. of 3rd Geod. Levelling
Southend	-20.000	+0.200	-19.800	+0.030	-19.770
Lowestoft	-15.010	+0.094	-14.916	+0.054	-14.862
Immingham	-37.695	+0.063	-37.532	+0.101	-37.431
N.Shields	-16.952	+0.248	-16.704	+0.107	-16.597

For the whole period under review, the alternative height A.O.D. Newlyn of mean sea level is given in table 7 and the "slopes" in table 8.

TABLE 7

Mean Sea Level 1967-68-69, A.O.D. Newlyn Various Network Adjustments
(ft.)

	Southend (20.318)	Lowestoft (15.282)	Immingham (38.627)	N.Shields (17.925)
M.S.L. based on Adj. (1)	0.318	0.272	0.932	0.973
M.S.L. based on Adj. (2)	0.518	0.366	1.095	1.221
M.S.L. based on Adj. (3)	0.548	0.420	1.196	1.328

TABLE 8

Slope Mean Sea Level 1967-68-69 Various Network Adjustments
(ft.)

	Adj. (1)	Adj. (2)	Adj. (3)
Southend - Lowestoft	- 0.046	- 0.152	- 0.128
Southend - Immingham	+ 0.614	+ 0.577	+ 0.648
Southend - N. Shields	+ 0.655	+ 0.703	+ 0.780
Lowestoft - Immingham	+ 0.660	+ 0.729	+ 0.776
Lowestoft - N.Shields	+ 0.701	+ 0.855	+ 0.908
Immingham - N.Shields	+ 0.041	+ 0.126	+ 0.132

5. Magnitude of Possible Errors in the Results of Differences in Height of Mean Sea Level

There are two possible courses of error in the results given above. Firstly, the levelling is liable to error. Secondly, the observations of the sea level and the reduction to monthly and annual means are liable to error.

Considering the levelling, we find that an estimate of the precision per mile of the Third Geodetic Levelling (computed using the IAG Oslo 1948 formulae) is 0.00469 ft. $\sqrt{M}$ (1.13mm $\sqrt{K}$). For a free network extending from Southend to North Shields, this gives a figure of 0.08 ft. The results of the adjustment can be illustrated by the differences in the difference in height between the

FBM's at Ipswich and Hexham given by table 9.

TABLE 9

(units ft.)	Ipswich to Hexham
(1) Second Geodetic Levelling	+ 512.086
(2) Second Scientific Adjustment of the Third Geodetic Levelling	+ 512.2097
(3) Adjustment of Limited Network of Third Geodetic Levelling	+ 512.2520

The magnitude of the total corrections applied from Ipswich to Hexham in the second scientific adjustment is -0.0442 being made up of -0.0481 from Hexham to Bulmer, +0.0889 from Bulmer to Caster and -0.0850 from Caster to Ipswich.

The difference between the Second and Third Geodetic Levelling seems to point to a rise of land in the north relative to the south east, but there is an uncertainty of around 0.1 ft.

There is a further uncertainty in the connection to the Southend Tidal Observatory of the order of 0.05 ft.

Considering the observations of sea level, table 10 gives an estimate of the standard errors in gauge reductions. This does not, however, express the full uncertainty in the determination of mean sea level. To these values must be added a more fundamental uncertainty of around 0.1 ft. arising from the unreliability of the stilling well type of tide gauge (see LENNON 1968).

TABLE 10

	Correction to reduce observations reduced to tide gauge zero to heights A.O.D. Newlyn second scientific adjustment (ft)		Estimated Standard errors (feet)	
			Gauge Reduction	Levelling Connection
Southend	Add	0.200	± 0.075	± 0.05
Tilbury	Add	0.198	± 0.060	Not Sig.
Lowestoft	Subtract	14.916	± 0.100	" "
Immingham	Subtract	37.532	± 0.050	" "
N. Shields	Subtract	6.704	± 0.100	" "

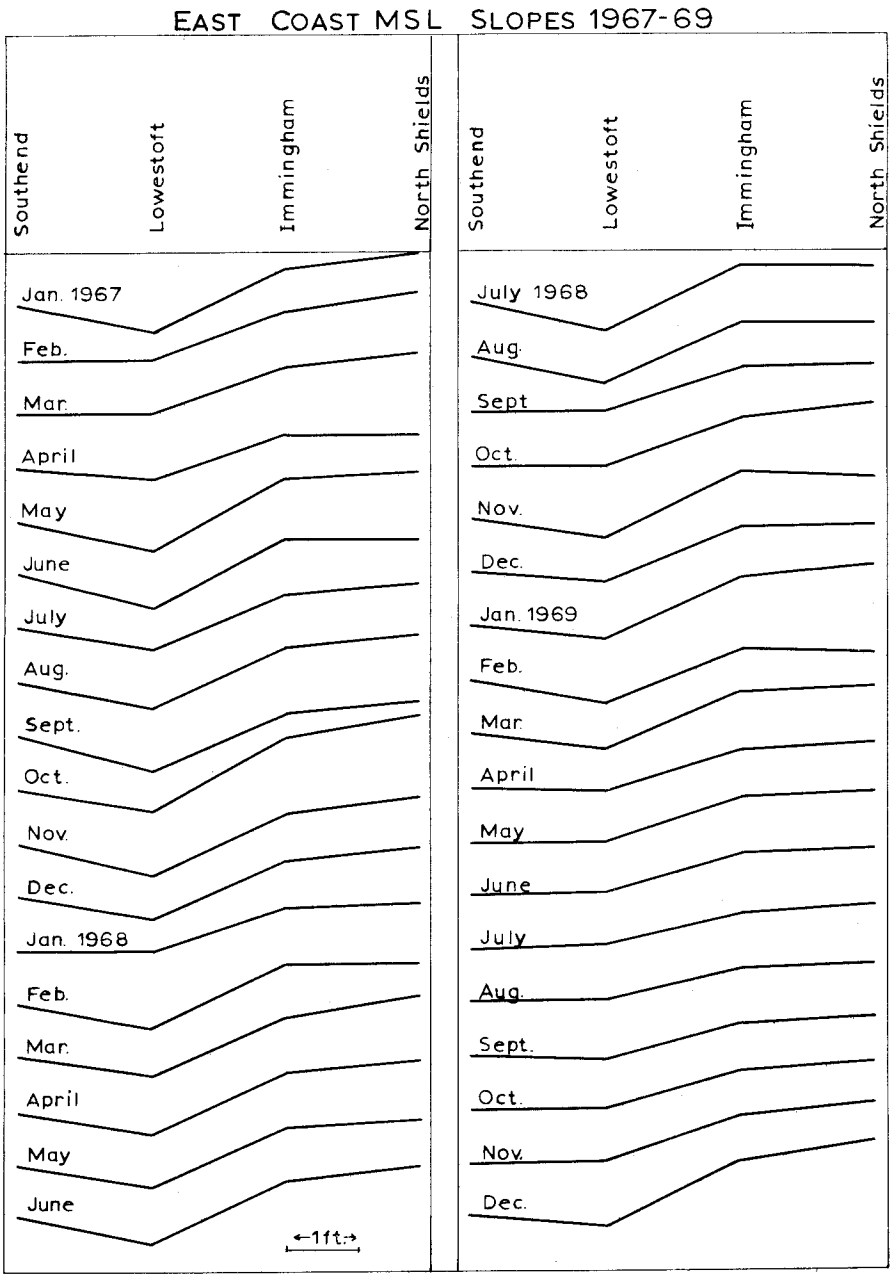
EAST COAST MSL SLOPES 1967-69
Southend
Lowestoft
Immingham
North Shields
Jan. 1967
Feb.
Mar.
April
May
June
July
Aug.
Sept.
Oct.
Nov.
Dec.
Jan. 1968
Feb.
Mar.
April
May
June
←1ft.→
Southend
Lowestoft
Immingham
North Shields
July 1968
Aug.
Sept
Oct.
Nov.
Dec.
Jan. 1969
Feb.
Mar.
April
May
June
July
Aug.
Sept.
Oct.
Nov.
Dec.

Figure 5.

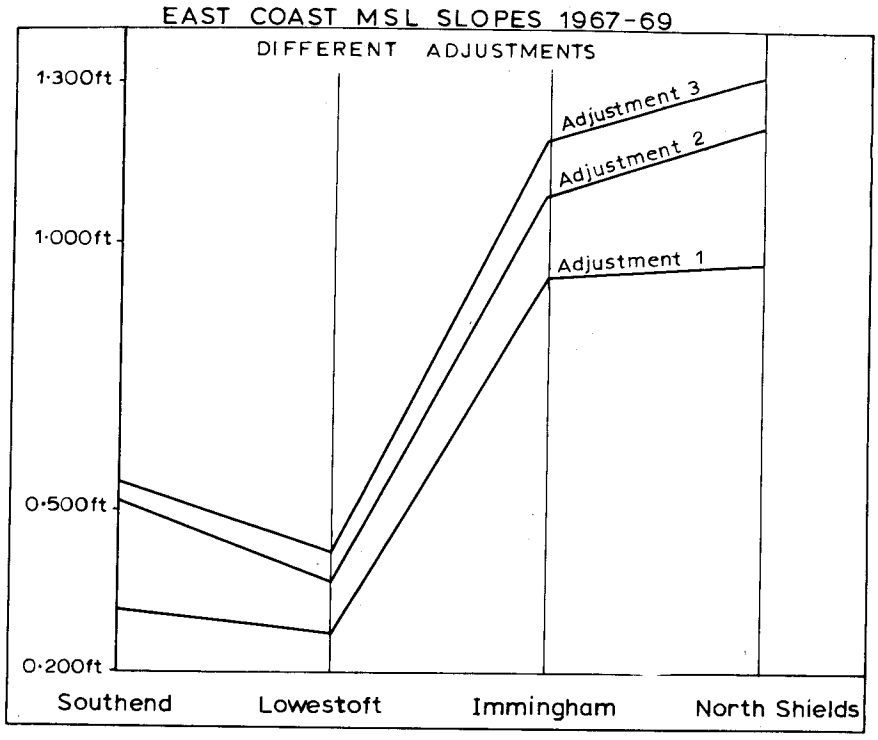
EAST COAST MSL SLOPES 1967-69
DIFFERENT ADJUSTMENTS
1·300ft
1·000ft
0·500ft
0·200ft
Adjustment 3
Adjustment 2
Adjustment 1
Southend
Lowestoft
Immingham
North Shields

Figure 6

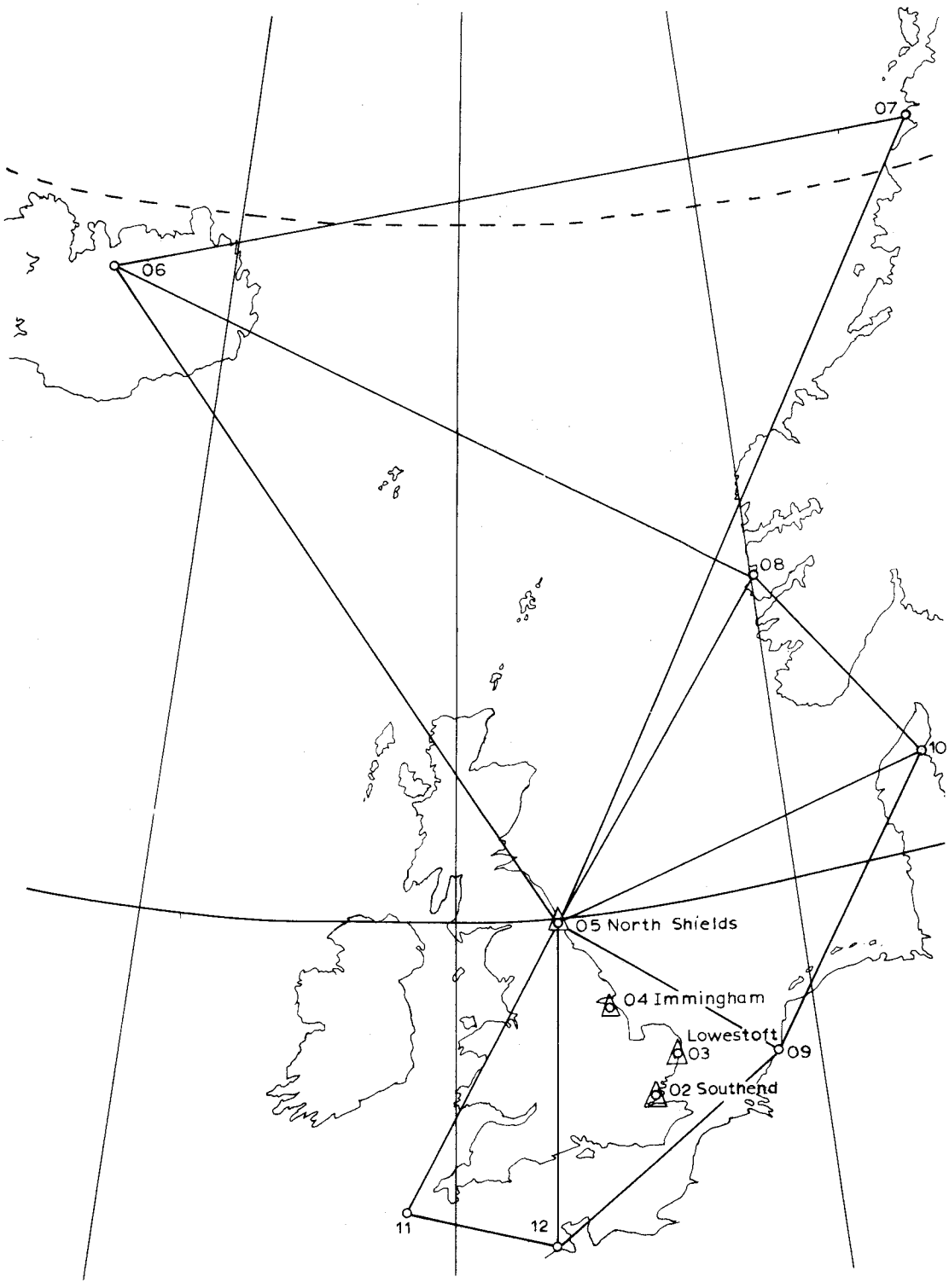

Figure 7. Location of Barometric Pressure Stations
North Shields Triads

6. Validity of Results

Bearing in mind the uncertainties expressed above, the validity of the results detailed in tables 7 and 8 may be examined. The standard deviations computed from the monthly variation of "slope" (see figure 5) are not in themselves a measure of reliability. Part of the differences from month to month may be due to the different magnitude of the seasonal influences and none of the difference can be attributed to the errors in the levelling or to the systematic errors in the sea level measuring and recording system. The standard deviations do, however, indicate a steadiness in the combined sea level measuring and recording system.

Considering each result (see figure 6)

Southend to Lowestoft

The negative "slope" with quite a large variation from month to month produces a standard deviation nearly as large as the "slope". This is hardly a significant result. The inherent errors of the tide gauge and the possible errors in the connections to the Southend Tidal Observatory reinforce this conclusion. Theindications are that from Southend to Lowestoft there is a slight negative "slope" for the period being considered in this study. This "slope" is about the same magnitude as the uncertainty in the result.

Southend to Immingham

The close correlation found elsewhere between the behaviour of these two tide gauges is reflected in the smaller standard deviation. Uncertainties in the levelling and in the tide gauge records make it unlikely that this result can be expressed to better than ±0.15 ft. and to regard the "slope" as 0.58 ft. with a standard error of 0.15 ft. seems reasonable.

Southend to North Shields

This result indicates a northward continuation of the "slope" detected from Southend to Immingham. The uncertainties in this result are, however, greater than in the previous case; the North Shields tide gauge is less reliable and the less steady determination of the "slope" indicated by the greater standard deviation points to an estimate of 0.70 ft. with a standard error of 0.2 ft.

Summarising, we have -

TABLE 11

	Slope*	Standard Error
(1) Southend - Immingham	+ 0.58	± 0.15
(2) Southend - N.Shields	+ 0.70	± 0.20
(3) Lowestoft - Immingham	+ 0.73	± 0.25
(4) Lowestoft - N.Shields	+ 0.85	± 0.30

* Based on second scientific adjustment of the 3rd Geodetic Levelling

The Immingham to North Shields "slope" is only slightly more significant than the Southend to Lowestoft result. It is, however, an extension of the Southend to Immingham "slope" and there is ample evidence to regard this result as indicative of a slight positive "slope" to the north.

In conclusion, the evidence supports a general thesis that there is a slope of Mean Sea Level for the period 1967-69 from the mouth of the Thames to the Tyne.

Possible errors in the levelling and sea level observations and reductions are not sufficient to cast serious doubt on this thesis. The magnitude of the slope is around 0.7 ft.

7. The Meteorological Contribution to Changes in Sea Level Along the East Coast of England.

The meteorological conditions over the North Sea and the eastern part of the North Atlantic are generally regarded as significantly contributing to changes in sea level along the east coast of England. The response of the southern North Sea to the meteorological changes over this larger area will take the form of water movements and surface gradients. In a theoretical sense, it is possible to deduce this response from a knowledge of the spatial and time distribution of the forcing function; this is $f(\tau, B)$ where τ is the mean wind stress and B is the air pressure. Such deductive studies would be extremely difficult and the practice has been to seek relationships by means of a regression analysis between the time variations of sea level at a given station and the forcing functions, see ROSSITER (1967).

Wind stress is a function of wind velocity and its influence on water movements and surface gradients will depend upon its velocity and direction. In the absence of systematically observed values of these quantities a further relationship must be assumed; that is that wind velocity W is a function of the air pressure gradient ΔB. In effect, the assumptions that are made are that $\tau \propto W$, $W \propto \Delta B$ and hence $\tau \propto \Delta B$. It is arguable that τ is more correctly proportional to W^2; for such a case, however, it is probable that W^2 is only proportional to ΔB^2 when ΔB^2 is a function of the mean of the squares of daily differences of barometric pressure. This information was not readily available from the sources used and this line of investigation was not pursued.

It follows that the forcing function was assumed to be represented by three variables; firstly, the mean monthly air pressure over the selected area, secondly the wind velocity and, thirdly, the wind direction. For purposes of the regression, the second and third of these variables were represented, the relationships above being accepted, by the mean monthly air pressure gradients along the three sides of a triangle.

Ideally this triangle should be as nearly equilateral in form as possible, as such a triad will most effectively represent all wind vectors.

On this basis, the eleven stations where monthly mean air pressure was known were grouped to form a variety of triads. The choice of the triad or triads which would be most significant was not easy and only samples of the full set of results are given.

In tabular form these are:

	Southend	Lowestoft	Immingham	North Shields
1. A three triad network which covers whole sea area north of the tidal station ("Theoretical best")	014/2 (02 06 08) (06 07 08) (02 08 09)	015/2 (03 06 08) (06 07 08) (03 09 10)	015/2 (04 06 08) (06 07 08) (04 09 10)	015/2 (05 06 08) (06 07 08) (05 09 10)

	Southend	Lowestoft	Immingham	North Shields
2. A three triad network which gives largest multiple correlation coefficient ("Actual best")	014/10 (04 06 08) (04 09 08) (08 09 10)	014/6 (02 06 08) (06 07 08) (02 09 08)	014/8 (05 06 08) (05 08 09) (05 11 12)	014/10 (04 06 08) (04 08 10) (04 09 10)
3. SaSsa + Density + triad which involves nearest air pressure station to tidal station and covers most of sea area ("Theoretical triad")	019/2 (02 06 08) level of Sig. 1% (F = 4.775)	019/2 (02 06 08) Level of Sig. 1% (F = 9.050)	019/2 (04 06 08) Level of Sig. 1% (F = 10.655)	019/2 (05 06 08) Level of Sig. 1% (F = 29.590)
4. SaSsu and Density + triad which gives largest MCC selected ("best response") from all reasonable combinations of the 11 stations	019/5 (04 06 08) (F = 4.944)	-19/6 (04 06 10) (F = 14.719)	019/6 (04 06 10) (F = 12.675)	019/4 (04 06 08) (F = 29.900)

8. Prediction of Mean Sea Level from Results of the Regression Analysis

Mention is made in ROSSITER (1967) of evaluation of the height of sea level under isobaric conditions from the results of a regression analysis of mean sea level observations at 97 stations. When a similar method was used here to estimate the difference of height of sea level under both isobaric conditions and conditions ofuniform density between the four stations, it was found that the isobaric contribution is largely cancelled out by the contribution from assumed density.

Table 12 compares the normal and isobaric (1015 millibars) heights AOD Newlyn 2nd Scientific Adjustment.

TABLE 12

1967-69 Units of ft.

	Southend	Lowestoft	Immingham	North Shields
h_n	+0.518	+0.366	+1.095	+1.221
h_i	+0.501	+0.278	+1.046	+1.109
$(h_n - h_i)$	+0.016	+0.088	+0.049	+0.112
$(h_n - h_i)$ cm +0.5	+2.7	+1.5	+3.4	

These figures substantially agree with table 9 and figure 9 of ROSSITER (1967); the -3cm anomaly at North Shields having been replaced by a +3.4 cm value.

If a larger barometric pressure had been selected for the isobaric surface, the apparent "slope" of 0.70 ft. from Southend to North Shields would nearly disappear. For example, 1050 millibars gives an isobaric height with uniform density as in table 13.

TABLE 13

	Southend	Lowestoft	Immingham	N.Shields
h_i	+0.293	-0.084	+0.556	+0.205
$(h_n - h_i)$	+0.225	+0.450	+0.539	+1.016

This poses the question as to the contribution of the longshore mean current and whether it reinforces the barometric contribution. The whole of the predictions made in this section are based upon the regression analyses. We find for the four formulae used the statistics given in table 14.

TABLE 14

	S_o	ϕ	R	F
Southend	22.279	16.323	0.765	4.775
Lowestoft	27.554	16.350	0.853	9.050
Immingham	22.567	12.602	0.871	10.655
N.Shields	25.567	9.314	0.947	25.590

Where S_o is the standard deviation of the dependent variable, i.e. the monthly mean sea level values,

ϕ is the standard error of the estimate,
R is the multiple correlation coefficient,
F is the F value.

From these figures, it is apparent that much of the season variation is unaccounted for at Southend compared with the results at Immingham and North Shields. The ratio of R^2 Southend to North Shields is 58.5 : 90 which indicates that over four times as much of the variation is unaccounted for at Southend as at North Shields and that factors which have not been taken into account and play only a minor role in effecting sea level at North Shields are significant at Southend. Furthermore, the significance of these unknown factors increases from north to south. (100 -90) : (100 -76) : (100 -73) : (100 -58)
10 : 24 : 27 : 42

9. Conclusions

The available evidence points clearly to an apparent upward slope of mean sea level from the Thames estuary northwards. In 1950 this apparent slope over some 360 miles (580 km) was of the order of 1.3 ft. (40 cm); this compares with an earlier determination in 1918 of 0.85 ft. (26 cm) based on a different geodetic levelling. However, these results are confused by seeming land movement which may be of the magnitude of 0.2 ft. (6 cm) or of 0.6 ft. (18 cm). In 1968 the mean sea level slope over 270 miles (440 km) of the same coastline was found to be 0.7 ft. (21 cm); unfortunately, a value over the whole length of the original coastline was not possible.

Investigations into the possible sources of error in the levelling and sea level measurement are sufficient to account for some of the variation in the slope with time, and residual uncertainties

may be accounted for by crustal movements. Systematic errors such as suggested by EDGE (1959) and SIMONSEN (1965) are not of sufficient magnitude to account for the slope.

Accordingly, an oceanic or meteorological origin for the slope which is found in many north-south coastlines, must be sought. Techniques involving the statistical treatment of a fairly simple model proved fairly successful when considering annual values. ROSSITER (1967). When monthly values of mean sea level are used, even when the annual and semi-annual tide is allowed for, the results of a statistical treatment of the simple model are not particularly satisfactory. It would seem that a more complex model is needed.

This paper is somewhat negative in that it is establishing a physical or apparent physical feature of the sea level topography, but offers no explanation of its origin. It would seem that the following is needed:

a) A more detailed study of the environment of each tidal observatory. For example, the Southend station may not be stable.

b) A more detailed study of the process of levelling to a tidal observatory. This process is subject to errors arising from local deviations of the vertical due to the variable attraction of the vertical by the oceanic tide (LENNON 1961), and due to the variable crustal loading from the same source.

c) A more complete study of the changes, month by month, in the marine environment. There is a surprising lack of detailed information over periods of greater than a few days.

(d) A more complex model than that of ROSSITER (1967) of the interaction of the oceanic and meteorological effects on the sea level topography must be designed.

10. References

CARMODY & BURNETT. 1960. Geodetic Levelling and Mean Sea Level in Great Britain. *Bull.Geodes.* Vol.55

CARTWRIGHT. 1967. A Unified Analysis of Tides and Surges around North Britain. *Phil.Trans.Roy.Soc.* A.263.

DOODSON & WARBURG. 1941. Admiralty Manual of Tides. HMSO, London.

EDGE. 1959. Some Considerations Arising from the Results of the Second and Third Geodetic Levelling of England and Wales. *Bull.Geodes.*51.

LENNON, G.W. 1961. Attraction of Vertical by Oceanic Tides. *Geophys.J.R.astr.Soc.* Vol.1, p.15.

LENNON, G.W. 1965. A Note on the Routine Reduction of Tidal Records to give Mean Sea Level, using an IBM 1620. *Cahiers Oceanographiques.* 17, 389.

LENNON, G.W. 1968. The Evaluation of Tide Gauge Performance through the Van de Casteele Test. *Cahiers Oceanographiques.* 20.

ROSSITER, J.R. 1958. Note on Methods of Determining Monthly and Annual Values of Mean Water Level. *International Hydrographic Review XXXV*, no.1, p.105-116.

ROSSITER, J.R. 1967. An Analysis of Annual Sea Level Variations in European Waters. *Geophys.J.R.astr.Soc.* 12, p.259-299.

SIMONSEN, O. 1965. *Global Aspect of the Astronomical Correction for Levelling of High Precision.* The Danish Geodetic Institute, Copenhagen.

11. Discussion

BUCHWALD (Chairman): I can now see why I was chosen as chairman - hoping that, as a mathematician, I'd stay neutral.

HOLDAHL: I have a question regarding changes in height due to loading by ocean tides. How far inland can this effect be detected? 10 km? 150 km? Or more? MELCHIOR may wish to comment.

MELCHIOR: When we had one station in Czechoslavokia which is at the centre of Europe, and at 1500 m depth, loading effects were still sensible; and if you look at the paper I have distributed you will see that in Europe we have an advance of phase of $2\frac{1}{2}^{\circ}$ in gravity tides in east Switzerland. Not only the Altantic ocean influences events but also the Pacific.

HOLDAHL: In other words, you say that the whole of England would be affected?

MELCHIOR: Yes.

WALCOTT: It may be worth mentioning that Land's End (Newlyn) which is the fundamental bench mark in England, has the largest ocean tide displacement effect known in the world.

HOLLWEY: That is most interesting. It is just a datum and you could change the datum to a point in the Midlands and it would not really matter. It's only a reference point for heighting.

SYDENHAM: Is there any plan to modify the levelling using the Channel Tunnel as a reference line under a large stretch of sea surface?

HOLLWEY: Once the Channel Tunnel is built, we will certainly level through it.

GRAFAREND: What we are really measuring in levelling is the difference of potential. But I do not see from this point of view why we need to have any datum for heights. Why do we need to have a datum for heights?

HOLLWEY: We don't need MSL as a datum. But we do need some point as a reference.

GRAFAREND: What for?

BOMFORD: We need some numbers, and for numbers you must have a datum.

GRAFAREND: You can use any arbitrary number.

HOLLWEY: What you need to know is whether point A is higher than point B.

GRAFAREND: Right. Therefore we need only differences.

HOLLWEY: This is what we really have in the United Kingdom.

ANGUS-LEPPAN: There are practical reasons why we should have a physical datum. If you adjust your levelling net to Mean Sea Level instead of an equipotential surface, you distort the whole system. This is why we have to solve the problem of whether MSL is an equipotential, and if not, whether the difference is significant in practice.

HOLLWEY: I would not adjust to M S L or a particular equipotential surface. What we seek for a level net is consistency within itself.

GRAFAREND: The problem in geodesy is that every nation has its own height datum. It is absurd for every country to have this. We perhaps need a global datum. For example take Europe, where nearly every country has its own datum and there are datum problems in adjusting data across national boundaries.

HOLDAHL: Are you familiar with the reasons why corrections are not applied to levelling observations to compensate for loading by ocean tides? As I see it, ocean loading would produce an effect similar to the Earth tide which disturbs a large area and has a short period. The effect on height determination would be small and random if good levelling procedures were used. I was wondering whether this was the way English geodesists have reasoned?

HOLLWEY: The presence of the 12 cm Earth tide at Newlyn indicates that the magnitude is such that there there is an argument for examining possible corrections. The effect is, as you say, simultaneous and should in the normal case be cancelled out. The next stage in this argument is that there is no need to keep a record of time of observation which could be correlated with the tidal effect. This is a foolish extension of the argument because once you have no record you cannot prove that the effect is cancelled out. At the moment, as no record is kept, we cannot make such an analysis.

BUCHWALD: I use my prerogative as chairman to sum up. Regarding the two metre slope in the sea surface between the north and south of the east coast (of Australia), the work of GODFREY and his co-workers is an attempt in my opinion, to explain the phenomenon using the dynamics of the ocean and it does not really matter what datum we use and so on. Neither the dynamics nor the statics of the ocean as known at present, explains this two metre difference. Both oceanographers and geodesists should work at it to see if there is some systematic reason why there is this difference.

HIBBARD, L. U.
National Standards Laboratory
CSIRO
Australia

Proc. Symposium on Earth's Gravitational Field & Secular Variations in Position (1973), 622-636.

THE STABILITY OF MICROWAVE FREQUENCY STANDARDS AND THEIR EFFECTS ON SECULAR VARIATION STUDIES

ABSTRACT

Atomic resonances in the microwave region are the present basis for accurate frequency, time interval and time standards. Rubidium standards are light in weight and cheap enough for any purpose requiring an accuracy of 5×10^{-10} and stability (> 100 s) of 10^{-12}. Commercial caesium beam standards are the workhorse of the frequency standard industry. Only the most stringent applications call for a better performance. Individual clocks are accurate over long periods to better than 10^{-11} and for some years past a batch of clocks has been used to maintain a continuous long term accuracy better than 10^{-12}.

The hydrogen maser is comparatively expensive and cumbersome but not excessively so for the most demanding applications calling for stability. Its accuracy (10^{-12}) approaches that of the best laboratory caesium beam standards and its stability (> 10 s) of 10^{-14} is better by more than an order of magnitude.

A revolution in technique is now in progress with the extension of electronic capabilities to terahertz regions. The stabilization of masers and lasers by atomic beams or by absorption cells gives promise of accuracies beyond 10^{-13} together with reductions in magnetic sensitivity, weight and size.

1. Introduction

For some secular variation studies accurate measurement of time interval is essential, for others stable measurement is of greater importance. At the present time, the most accurate time standards are not the most stable. The current definition of the SI second (BEEHLER ET AL 1965) is based on a caesium hyperfine resonance and there is no more accurate alternative available. Long baseline interferometry (LBI) workers, however, prefer the hydrogen maser because it is over an order of magnitude more stable. At this stage it is not as accurate but this situation could change. On the other hand both devices might be superseded by standards which may or may not be envisaged at the moment.

2. Quartz Crystal Frequency Standards

The quartz oscillator is not an absolute standard of frequency and it has serious drift and rate-of-drift effects. For times less than 0.1 s a quartz oscillator has a stability better than most atomic devices and high frequency (100 MHz) crystals are appreciably better than low frequency (5 MHz) types in this respect. For longer times, good crystals have a drift rate as low as 5×10^{-10} per day and a stability of 5×10^{-12}, the lower frequencies having the better performance.

If crystal oscillators are switched off for a period they take a long while to settle down again to their best performance and may then differ by 10^{-9} or more from the previous value. Despite these faults, they play an indispensable role with all frequency standards either passive or active. For passive standards, crystals supply a basic frequency from which the atomic excitation is synthesized. For active standards, they supply a similar synthesized frequency for comparison with the atomic oscillation. In both cases, the quartz oscillator is servo-controlled by the atomic device, but the short-term stability (< 0.1 s) is due to the quartz oscillator alone. All other frequencies and clock signals are subsequently derived from the quartz oscillator.

3. Atomic Frequency Standards

The caesium beam standard (MOCKLER 1961; GLAZE 1970) is a passive device in which a high frequency magnetic field synthesized from a relatively low frequency quartz oscillator is made to interact with a collimated beam of neutral caesium atoms and gives rise to a transverse deflection of the beam. The basic elements of such a standard are shown in figure 1. Atoms are evaporated from a narrow slit in an oven and pass through a deflecting magnet in which there is an intense magnetic field gradient. The field magnetically polarizes each atom and the field gradient acts on the resulting magnetic moments and produces sideways deflections. By this means atoms in a particular hyperfine state are separated and channelled through an interaction region and a second deflecting magnet to a detector. The hyperfine states of alkali atoms are caused by coupling of the spins of the outermost electron and the nucleus. The spins, in general, either align in the same direction or in the opposite direction. As each spin has an associated magnetic moment there is an energy due to interaction of these magnetic dipoles. Transitions between one hyperfine state and another are produced by a suitable magnetic field which resonates with the energy difference between the two states,

$$\text{i.e. } h\nu = E_1 - E_2$$

where ν is the frequency, E_1 and E_2 the energies and h is Planck's constant. Such a field applied in the interaction region changes the hyperfine state of the atoms in flight and on subsequent passage through the second magnetic deflector changes the number which reach the detector. Variations in the detector output are an indication of resonance between the atoms and the rf field and are used to servo-control the frequency of the basic quartz oscillator. The accuracy of such a standard depends on the interaction time and hence on the length of the interaction space. However, if the path is made very long, the number of atoms which can be focussed through it is reduced and the detector signal may be impaired by 'shot' noise. For this reason, a short but intense beam can be comparable with a long weaker beam as regards accuracy. Excellent commercial caesium beam standards have been made by several companies and are being used in considerable numbers; nevertheless the best laboratory standards use beam lengths of some metres. The commercial standards are designed for continuous operation but the laboratory standards to date have been used on an intermittent basis and require other continuously operating standards to be used as flywheels.

The hydrogen maser (figure 2) (RAMSEY 1965; RAMSEY 1972) uses a hexapole magnetic lens to select a beam of hydrogen atoms by focussing them through the small entrance to a quartz bulb. Unwanted atoms are defocussed and discarded. The atoms that enter the bulb take about a second to escape through the same hole and during this time interact with the field in a resonant cavity.

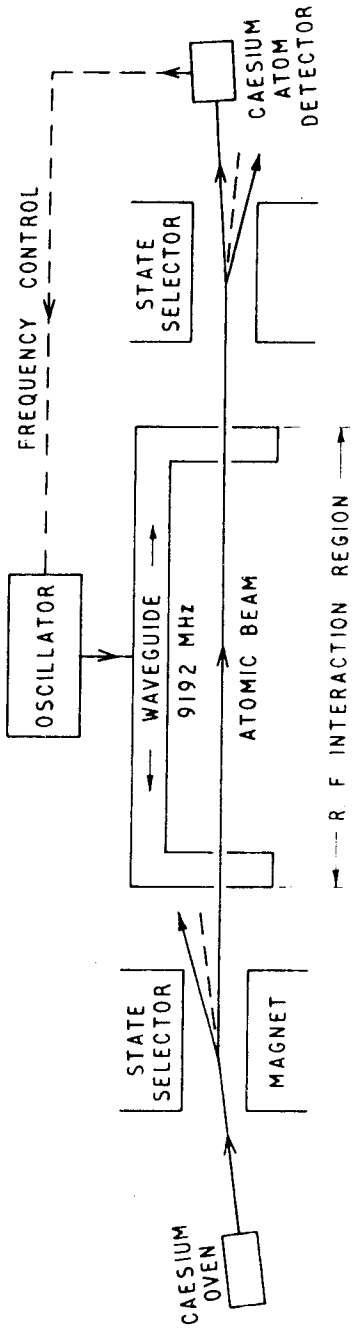

Figure 1. Caesium Beam Frequency Standard

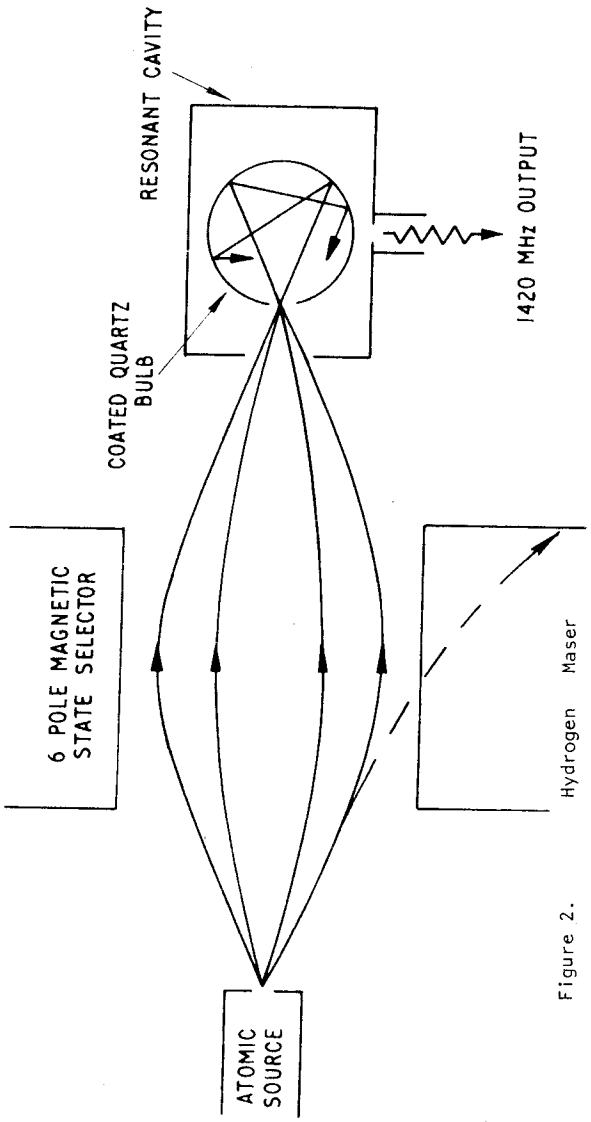

Figure 2. Hydrogen Maser

The field stimulates the atoms to change the hyperfine state and in so doing to emit energy at the hyperfine frequency of 1420 MHz. The cavity field builds up by itself and oscillates continuously without requiring an auxiliary oscillator. However it is still found necessary to servo-lock a basic quartz oscillator to the maser in order to be able to generate the clock pulses and other frequencies that are required of a standard. The maser is a continuous 'active' oscillator and achieves its superior stability because of the long interaction time, while the atoms bounce around inside the bulb. In this sense it is equivalent to a very long beam. The bulb not only confines the atoms but its temperature also determines the mean squared velocity $\overline{v^2}$ of the interacting atoms and hence a 'second-order doppler' frequency correction $\overline{v^2}/2C^2$ due to the 'time dilatation' effect of special relativity. The high stability due to containment is offset by a loss in absolute accuracy caused by phase shifts during the wall collisions. The best wall surface is Teflon and even with this there is an accumulated frequency change of about 2 parts in 10^{11} at room temperature. The uncertainties in this figure as yet prevent the full realization of the maser's capabilities.

There is not a clear cut 'best' standard. If the hydrogen maser were to receive as much development effort as has been applied to the caesium beam it may surpass it in accuracy as well as stability. This can only be decided in the future but in the meantime the same might be said of other contenders. Thallium is an attractive alternative to caesium for a beam standard; however, there are some technical problems and any ultimate advantage hardly seems to warrant the effort.

Historically the hydrogen maser grew out of attempts to make a passive beam device with a folded-up interaction path. More recently there has been advocacy (HELLWIG 1970 A) for a return from the active to the passive concept and to make the atoms emerging from the containment bulb pass through a second state selector to a detector. Another variant proposed is to couple rf power into and out of the resonant cavity and to detect the dispersion signal caused by the atoms (HELLWIG & BELL 1972). Each of these proposals has compensating disadvantages and is still left with the 'wall shift' uncertainty. The program at the CSIRO National Standards Laboratory is directed at minimizing the wall shift uncertainty of the H maser by operating at a temperature (> 80°C) at which the shift for Teflon is known to pass through zero (VESSOT ET AL 1970; ZITZEWITZ & RAMSEY 1971). The outstanding problem is to establish this temperature accurately and to be able to reestablish it whenever there is a possibility that it might have changed.

4. Frequency Stability

Frequency stability, which is identical with time-interval stability, is fashionably described in terms of the 'Allan Variance' $\sigma^2_{\Delta f/f}(2, t)$ which is equal to $\frac{1}{2}\langle(f_{n+1} - f_n)^2\rangle$ where f_n is the average frequency measured over the nth interval of time 't'. Typical plots of the square root of the 'Allan Variance' against t are shown in figure 3 for the caesium and hydrogen standards. Corresponding results for commercial rubidium standards are also included as these, together with the commercial caesium standards, are the only ones readily available off the shelf for general use. The rubidium standard uses optical pumping of rubidium vapour in a buffer gas and as a consequence is not in the category of an absolute standard. The typical drift rate is better than 10^{-11} per month but is sufficient to necessitate periodic recalibration at intervals of a year or two. Despite this low price and size make it the best choice for most applications.

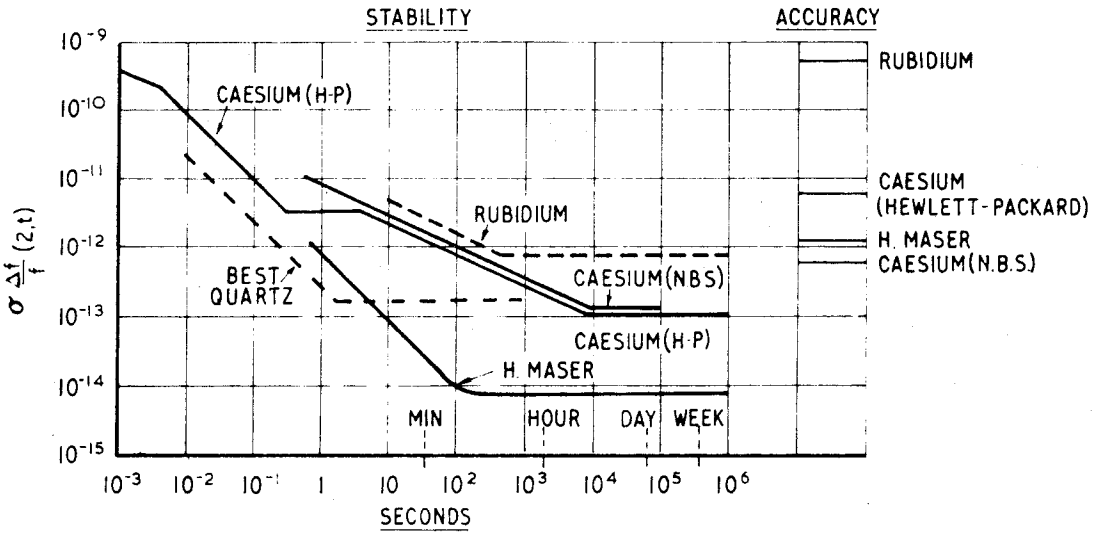

Figure 3. Frequency Stability of Atomic Standards

The long caesium beams have all been custom built by standards laboratories and have not as yet been developed for more general use. Hydrogen masers have not had as much attention for standards laboratory use but have been developed in a semi-commercial way and small numbers have been transported to remote users for LBI and space purposes. They have been most successful in applications requiring very high stability over periods of hours. They are transportable rather than portable. The smallest developed to date has a weight of some 500-600 lbs and requires 4 men to move it (LEVINE & VESSOT 1970). Transportation by plane and even by satellite is practicable. While undoubtedly expensive and complex they are not excessively so when considered in relation to the military, astronomical or space applications for which they have been developed. Already there are prospects that operating lifetimes of the order of 10 years will be achieved without major overhaul. Given skilled attention and some duplication of equipment to allow servicing, adequate continuity and indefinite high quality performance can be expected.

The frequency stability characteristics of all standards improve with time interval for intervals up to some seconds, and then level off as shown in figure 3. In general there are characteristic regions in which the stability of a standard is determined by different causes. For short times the subsidiary crystal determines the performance, and noise effects give rise to a 1/t characteristic. For longer times the stability may improve as $1/\sqrt{t}$ and a final levelling off is interpreted as 'flicker' type behaviour.

Commercial atomic standards operate continuously and typically receive no attention until a noticeable defect occurs. Their stability is often very good, approaching 10^{-13} for periods of weeks or months. However they can change abruptly in frequency and rate but should stay within their overall accuracy specification. Representative accuracy figures for the various standards are also shown in figure 3. The latest commercial caesium beam by Hewlett-Packard is specified to 7 parts in 10^{12} in accuracy. The accuracy of the best laboratory caesium standards is about 5 in 10^{13} for some hours (GLAZE 1970). To achieve indefinite long term accuracy of this order they employ a substantial number of quartz crystals and/or commercial caesium or rubidium standards to supply the continuity. High accuracy is maintained by regular and systematic evaluation of the possible errors of the caesium beam and frequent measurement of the frequencies and rates of the subsidiary standards.

The best laboratory hydrogen masers (HELLWIG ET AL 1970) require periodic reevaluation of the 'wall shift' in order to maintain accuracy to 1 in 10^{12}. Improvement to 1 in 10^{13} is forseeable with better understanding of the wall effect. The resonant cavity must be kept accurately tuned to the maser frequency and this can be done automatically or periodically. However the best stability of 1 in 10^{14} or better is only achieved when the cavity tuning is left alone. The transportable masers have not been designed for 'self' evaluation of the wall shift and the completed maser must be checked against other standards if the best accuracy is required. Despite this they are the best available standards for LBI use. For lunar ranging (LURE TEAM 1970) which requires timing accuracies of about 1 nanosecond in 2.5 seconds the rubidium standard is adequate although a commercial caesium standard would not be extravagant as it does not require recalibration.

5. Long Baseline Radio Interferometry

With the current LBI technique, beats between the incoming radio waves and a locally synthesized signal are simultaneously recorded on tape at the separate stations and cross-correlated at a later date. The computer which does the correlation can compensate for disagreements in the synthesized frequencies and the time epochs and even in the rates-of-change of frequency. It is more important for the frequencies to be stable or to drift stably over the recording period than it is for them to be known absolutely or to be in the closest agreement. Recent experiments show that time synchronization can be established retrospectively by LBI studies to within ± 1 nanosecond and that frequency differences can be measured to some parts in 10^{14} (KLEMPERER 1972). Not only do the LBI programs not suffer from current time and frequency inaccuracies but a valuable byproduct of them is an accurate method of intercontinental synchronization of epoch and frequency. The ± 1 ns accuracy of time comparison is largely set by atmospheric delays which are equivalent to a few metres of path (MATHUR ET AL 1970). Important variations are caused by water vapour and barometric pressure. The LBI and Lunar Ranging programs allow these effects to be studied in their own right and this in turn will lead to further improvement in accuracy.

It should be noted that in both the LBI and lunar ranging cases and presumably any other distance measuring situation, frequency and time interval are not the primary quantities in the measurement. The quantities that are determined are the numbers of wavelengths of the radiation under consideration. Time only enters the equations after the velocity of light is inserted. Thus the question as to whether our frequency standards remain invariable over centuries, while interesting in its own right, is not relevant to the studies under consideration.

6. World Time and Frequency

A number of countries produce standard frequency and time broadcasts that are disseminated widely. These are generated from caesium standards, either by long laboratory types or by batches of commercial units. Some claim an accuracy approaching 5 parts in 10^{13} and a number are synchronized in time to a microsecond. This has been achieved by radio, satellite and US Navy flying clock programs (RAMASASTRY ET AL 1973; WINKLER 1970), but there is as yet no accepted or regular procedure. Individual broadcasts are monitored by other centres and the results are collated by an international agency. From all of this an international standard (SMITH 1972) is derived by assigning weights to the various measured broadcast frequencies. The resultant differences between the international standard frequency and the component standards are published and corrections may be applied in retrospect as desired by these stations and by those relying on them.

'Real time' accuracy in the derivative centres can only be achieved by having a local 'flywheel' standard which is continuously compared with radio broadcasts and checked by any other means that are available. Radio propagation errors can be quite large and variable and, because of multiple path interference, ambiguities of some tens of microseconds can arise in remote parts of the globe. These can be resolved by continuously recording more than one broadcast and comparing them with locally generated standards. The local standard requires at least a couple of commercial caesium standards if the distance from a broadcast centre is large. In the northern hemisphere coordination of standards is also achieved via the Loran C networks. The 8 Loran chains comprising a total of 30 stations are synchronized to within ± 5 μs. With knowledge of the published variations an accuracy of $\pm \frac{1}{2}$ μs can be achieved (KLEMPERER 1972).

Synchronization to 0.1 μs is possible by the use of stationary satellites (RAMASASTRY ET AL 1973) but this is an inconvenient and expensive process as it requires simultaneous two way transmissions of timing signals and suitably positioned stations. Two clocks differing by 1 in 10^{12} will drift apart by 0.1 μs in a day. Thus weekly synchronization is desirable if 1 μs timing accuracy is to be maintained. This is a strong argument for improving clock stability beyond the present limits. Stability is more important than accuracy in this respect as coordination of time is becoming more necessary every day, whereas accuracy of time scale and frequency are more than adequate for all known requirements.

7. Aircraft Collision Avoidance

The most promising method of aircraft collision avoidance is one based on the simultaneous emission of radio pulses from every aircraft (BRENNAN 1971). For this to be effective the aircraft clocks must be synchronized with ground stations over substantial areas. A proposed specification for synchronism of individual ground stations for this purpose already calls for a timing accuracy of 60 ns. The more densely populated areas of the northern hemisphere can be expected to move towards a system of time coordination approaching this accuracy and a comparable global system is likely in the foreseeable future. In addition to the substantial technical problems of improving clock stability, accuracy and coordination over large areas the requirements for widespread nanosecond intelligence raise to a practical everyday level some hitherto academic aspects of relativity.

8. Relativistic Time and Frequency Corrections

The experiment by HAFELE in 1971 has conclusively resolved any doubts concerning both the clock paradox and the variation of clock rate with gravitational potential (HAFELE 1972).

By flying a batch of four caesium clocks round the world as quickly as possible on commerical airlines he eliminated from both corrections any considerations of light propagation, doppler shift, change of photon energy and frequency etc. The results clearly demonstrate that moving a clock around the earth in the direction of rotation slows the clock compared with a clock that is stationary on the earth, and one proceeding in the opposite direction speeds up. The effect of the earth's gravitational field was likewise evaluated and good agreement was obtained. Both effects are in agreement with general relativity, although the first effect can be 'derived' from the restricted principle. The expression for a clock moving eastward at the equator with velocity v and height h relative to the ground is (HAFELE 1972)

$$\frac{\Delta t}{t_o} = \frac{t - t_o}{t_o} = \frac{gh}{c^2} - \frac{2R\Omega v + v^2}{2c^2}$$

t is the time recorded by the flying clock,
t_o is the time recorded by a clock on the earth's surface,
R is the radius of the earth,
Ω is the angular velocity of the earth,
g is the acceleration due to gravity at the earth's surface.

In HAFELE's experiment the integrated components of time increase for one complete circuit of the earth were

	Time gain in nanoseconds	
	Eastward	Westward
Gravitational 'red shift'	144 ± 14	179 ± 18
Kinematic time dilatation	- 184 ± 18	96 ± 10
Predicted total time increase	- 40 ± 23	275 ± 21
Observed total time increase	- 59 ± 10	273 ± 7

Even for small velocities v at sea level the expression for Δt becomes $\Delta t = -\frac{R\Omega v t_o}{c^2} = -\frac{2\pi R^2 \Omega}{c^2} = -\frac{dV}{c^2}$ where d is the distance travelled ($2\pi R$) and V is the velocity of the rotating earth's surface. This result, which is independent of v, is identical with the time difference term in special relativity when time is coordinated by Einstein's convention using light signals. The discrepancy is of the opposite sign if the information is conveyed in the opposite direction. This is no problem but must always be calculated and allowed for.

To a good accuracy, clocks at rest at sea level keep the same relativistic time independently of latitude differences thus clocks conveyed around the Earth along a meridian at low velocity do not require correction (COCKE 1966).

The magnitude of the gravitational shift $\frac{gh}{c^2}$ is 1.09×10^{-13} per km. For two ground stations with substantial difference in altitude this effect cannot be ignored. The US Naval Observatory at Washington is responsible to the US Government for maintenance of the nation's time scales. However the National Bureau of Standards at Boulder is responsible for all standards of measurement including frequency and time interval. The US Naval Observatory controls Loran C emissions with the help of 16 selected commercial caesium clocks (WINKLER ET AL 1970) and thus has a major influence on the coordination of time throughout the northern hemisphere.

The NBS derives standard frequencies from a 3.66 meter caesium beam and broadcasts round the world (GLAZE 1970). In 1968 the two standards differed by 9.8×10^{-13} and a coordinated standard was agreed upon by subtracting a 1.8×10^{-13} correction due to the gravitational effect of the differing altitudes and then splitting the difference. In the forseeable future the 1.8×10^{-13} effect will be the predominant adjustment.

9. New Proposals For Frequency Standards

The standards that have been discussed have been in use for frequency and time measurement for a number of years and any immediate requirements would have to be satisfied by one or more of them. They are capable of further refinement but the limits are well understood. However it is to be expected that there will be major developments in the future as regards accuracy, size etc. arising from proposals that have already been made. Any attempt to plan long term centres for secular variation studies would require a study to be made of these future trends. It will not be possible here to do more than briefly outline a few of the more promising schemes and the progress to date (HELLWIG 1970 B; BASHKIN 1972).

10. Ion Storage Standard

The hydrogen maser selects and confines neutral atoms in a container and the limits of accuracy are due to collisions with the container walls and the tuning of the resonant cavity. A proposal has been made to confine massive hydrogen-like ions such as Hg^+ in a suitable configuration of electric fields and to make a passive frequency standard based on induced hyperfine transitions (SCHUESSLER 1971). A highly sophisticated technique is proposed in which the ions are produced in the trap by electron bombardment and then polarized by spin-exchange collisions with a beam of caesium atoms which itself has been fully polarized by the same means as used in a conventional caesium beam device.

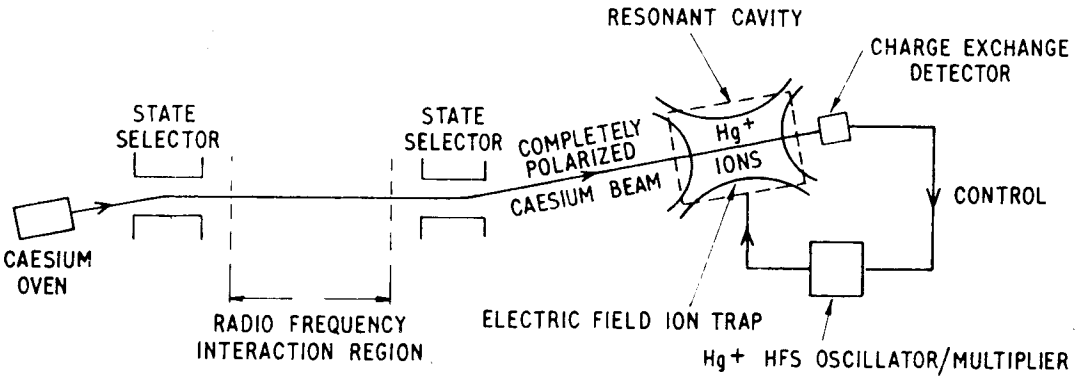

Figure 4. Hg^+ Ion Storage Frequency Standard

The effect of an applied radio-frequency field in inducing hyperfine transitions in the ions is then sensed by the effects (charge-exchange) of the same collisions with the polarized caesium beam. Some aspects of the proposal have been demonstrated using $(He^3)^+$ ions (SCHUESSLER ET AL 1969) and it is clear that there are many desirable features. Compared with the hydrogen maser the wall effect is calculated at parts in 10^{17} instead of 10^{11}. The hyperfine frequency is some 30 times higher and storage times are much greater. These both contribute to a very much higher line Q and the passive system reduces dependence on cavity tuning. All factors known to affect accuracy can be reduced to less than 1 in 10^{14} except the relativistic second order doppler shift $-\frac{v^2}{2c^2}$. This requires that the ion temperature be controlled to a few degrees. The proposal has many desirable features but will need a lot of proving and engineering if it is to leave a laboratory environment.

11. Atomic Beam Fine-Structure Standard

With the exception of the ammonia maser, existing atomic frequency standards rely on magnetic hyperfine structure. One reason for this is that microwave techniques have in the past restricted the radio frequencies to some tens of gigahertz, which is a very small energy difference when compared with normal electronic transitions. A new breed of standards is now being made possible by the progressive extension of radio techniques to much higher frequencies.

An atomic beam standard operating in the terahertz (10^{12}) region has been proposed and the forecast made of accuracy 'better than 10^{-15}'(STRUMLA 1972). The scheme (figure 5) utilizes a beam of neutral zero-spin atoms such as Mg or Ca which are excited by a discharge inside the oven to the lowest excited state, a metastable triplet P level.

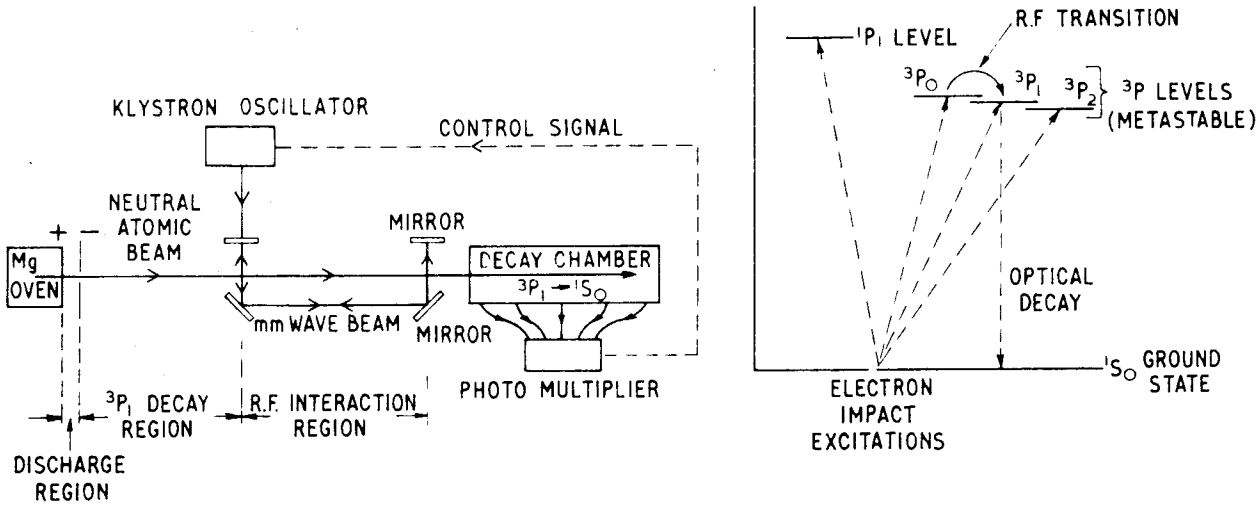

Figure 5. Mg Beam Fine Structure Frequency Standard

The $^3P_1$ state is not very long lived and decays to the ground state in milliseconds leaving $^3P_0$ and $^3P_2$ atoms in the beam which then passes through an interaction region where magnetic fine-structure transitions are induced between the $^3P_0$ and $^3P_1$ levels by an appropriate radio frequency field (601 GHz for Mg, 1564 GHz for Ca). The $^3P_1$ atoms so formed decay rapidly to the ground state emitting photons which serve as an indicator of the resonance of the applied frequency. The line width as with all beam standards is determined by the interaction time and the frequency is 100 times higher than for caesium so the line Q and the stability are increased 100 fold. Once again an important limitation of accuracy is set by the second order doppler shift.

12. Stabilized Laser Standards

There is intense activity at present to stabilize optical and infrared lasers to accuracies comparable with the frequency standards that have been discussed. In parallel with this, the interlocking of microwave and laser frequencies is gradually being achieved by an extension of traditional radio techniques (BRADLEY ET AL 1972; BOYNE 1971). The methods are cumbersome and impermanent as yet and typically involve the stabilization and interlocking of several intermediate maser and laser oscillators using Schottky diode multiplier/mixers. It is not impossible however that a simple, well engineered standard with associated electronics will be achieved within the next few years and may serve to define both length and time standards in the same instrument.

Traditionally the Fabry-Perot type lasers have been stabilized by accurate control of the mirror spacing using the 'Lamb dip' of the gain/frequency profile as an indication of resonance. This dip arises because, in general, moving molecules experience a doppler shifted electromagnetic field and only those molecules with a particular velocity are necessarily resonant with the field. If the field is exactly right the resonance occurs only with molecules having little or no component of velocity in the direction of the laser beam. Such molecules will resonate with the laser beams in both directions at the same time and hence experience greater saturation effects. This can show up as a dip at the centre of the doppler broadened resonance line. It is possible to produce a similar effect by inserting an absorbing medium outside the discharge region but inside the optical resonator (figure 6). In this case saturation of the absorption occurs giving rise to an emission effect when the laser is tuned close to the centre of the absorption resonance. If the absorbing level of the molecules has a long natural lifetime and the optimum pressure is used, the saturated absorption linewidth can be a magnitude or so narrower than the normal Lamb dip giving rise to a more accurate indicator for control of frequency. This has been done most successfully with the He-Ne laser and a CH_4 absorber (BARGER & HALL 1969) leading to a reproducibility of 10^{-11} and a stability of 10^{-13} over a 10 s averaging time (BAY ET AL 1972; HELLWIG ET AL 1972). The latest stability results are shown in figure 8 superimposed on those of other standards.

There are other possibilities with different lasers and absorbing media and very promising results have already been achieved leading to more accurate determinations of the velocity of light (EVENSON ET AL 1973; BARGER & HALL 1973). Even greater frequency stability is proposed by the use of the absorption cell technique in a ring laser (BASOV ET AL 1971).

Other proposals have been made for optical laser stabilization by interrogating conventional atomic beams (BASHKIN 1972). In one of these (ORAEVSKY 1968), the rf interaction region of a caesium beam device is replaced by a similar Ramsay-type interaction region with an optical system arranged so that the atomic beam crosses the laser beam twice at right angles (figure 7).

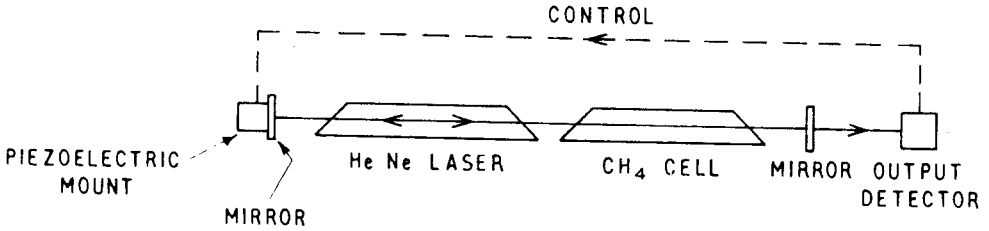

Figure 6. Methane Stabilized He Ne Laser

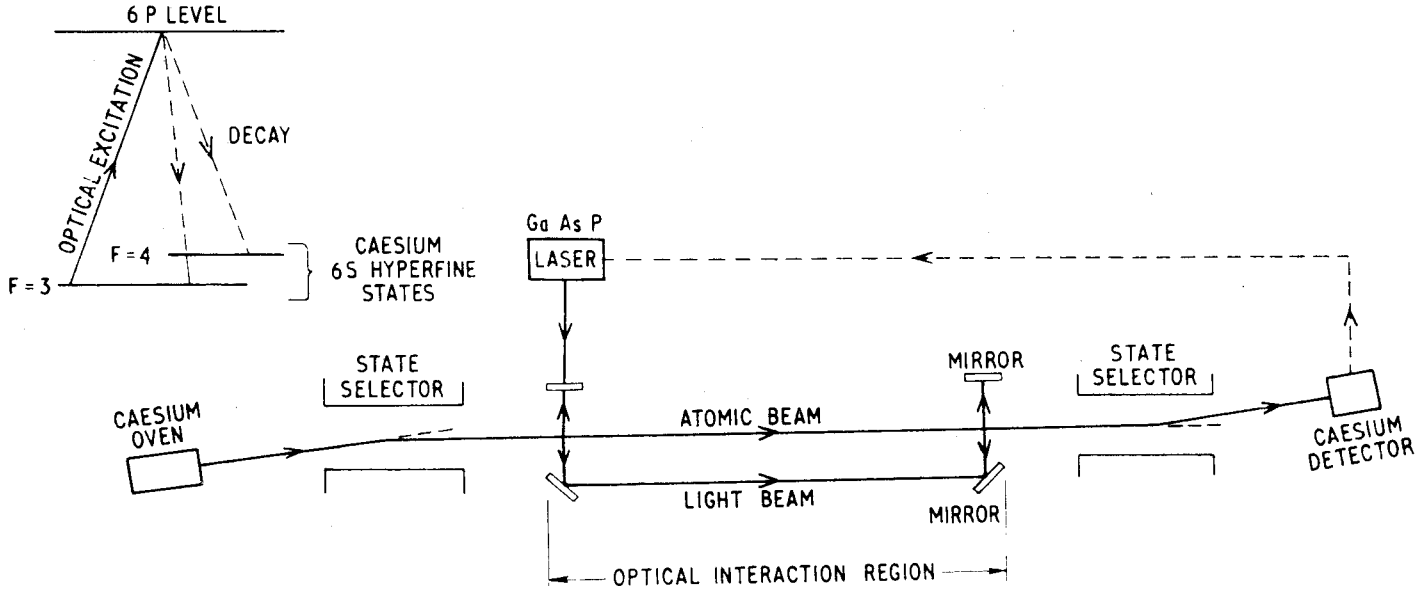

Figure 7. Laser Stabilization By Atomic Beam

In this case a GaAsP solid state laser would provide a suitable frequency to excite the caesium atoms of the selected hyperfine state to a 6P level. The atoms would decay rapidly back to the 6S ground state but would populate the empty hyperfine level and give rise to a signal in the output beam detector.

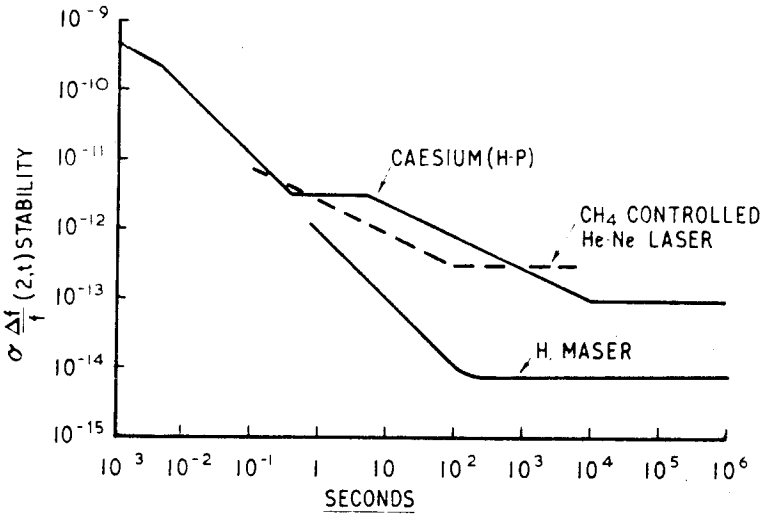

Figure 8. Methane - Stabilized Laser

13. Conclusion

There is an embarrassingly large number of proposals for the next generation of frequency standards with accuracy potentials exceeding 10^{-13}. It is likely that one at least of these will achieve the claims made for it and at the same time equal or improve on the best existing accuracy and stability and provide a compact, transportable device comparatively insensitive to magnetic fields and other environmental effects. For the next few years, however, reliance must be placed on the proven existing devices with rubidium standards for bread and butter requirements too demanding for quartz crystals, commercial caesium beams for more important purposes, and hydrogen masers for long baseline interferometry.

A long term research facility for secular variation studies would probably require all three of these devices.

14. References

BARGER, R. & HALL, J. 1969. *Phys.Rev.Letts*, 22, No. 1: 4.

BARGER, R. & HALL, J. 1973. *Appl.Phys.Letts*, 22, No. 4: 196.

BASHKIN, A. 1972. *Soviet J.Quantum Electronics*, 1, No. 5: 437.

BASOV, N., BELENOV, E., DANILEIKO, M. & NIKITIN, V. 1971. *Soviet J.Quantum Electronics*, 1, No. 1: 28.

BAY, Z., LUTHER, G. & WHITE, J. 1972. *Phys.Rev.Letts*, 29, No. 3: 189.

BEEHLER, R., MOCKLER, R. & RICHARDSON, J. 1965. *Metrologia*, 1, No. 3: 114.

BOYNE, H. 1971. *IEEE Trans.Instrum. Measmt*, IM-20: 19.

BRADLEY, C., EDWARDS, J., KNIGHT, D., ROWLEY, W. & WOODS, P. 1972. P. 295 *Atomic Masses & Fundamental Constants 4* (ed. J. Sanders and A. Wapstra) Plenum Press, London.

BRENNAN, J. 1971. *Proc.Precise Time & Time Interval, Strategic Planning Mtg*, 1: 305 (US Naval Observatory).

COCKE, W. 1966. *Phys.Rev.Letts*, 16: 662.

EVENSON, K., WELLS, J., PETERSEN, F., DANIELSON, B. & DAY, G. 1973. *Appl.Phys.Letts*, 22, No. 4: 192.

GLAZE, D. 1970. *IEEE Trans.Instrum.Measmt* IM-19, No. 3: 156.

HAFELE, J. 1972. *Science*, 177, No. 4044: 166, 168.

HELLWIG, H. 1970 A. *Metrologia*, 6, No. 2: 56.

HELLWIG, H. 1970 B. *Metrologia*, 6, No. 4: 118.

HELLWIG, H., VESSOT, R., LEVINE, M., ZITZEWITZ, P., ALLAN, D. & GLAZE, D. 1970. *IEEE Trans. Instrum.Measmt* IM-19, No. 4.

HELLWIG, H. & BELL, H. 1972. *Metrologia*, 8:96.

HELLWIG, H., BELL, H., KARTASCHOFF, P. & BIRGQUIST, J. 1972. *J.Appl.Phys.* 43, No. 2: 450.

KLEMPERER, W. 1972. *Proc.IEEE*, 60, No. 5: 602.

LEVINE, M. & VESSOT, R. 1970. *Radio Science*, 5, No. 10: 1287.

LURE Team 1970. *Science*, 167: 458.

MATHUR, N., GROSSI, M. & PEARLMAN, M. 1970. *Radio Science*, 5, No. 10: 1253.

MOCKLER, R. 1961. *Advances in Electronics and Electron.Phys.* 15.

ORAEVSKY, A. 1968. *IEEE Trans.Instrum Measmt*, IM-17, No. 4: 346.

RAMASASTRY, J., ROSENBAUM, B., MICHELINI, R & KUEGLER, G. 1973. *IEEE Trans.Instrum.Measmt*, IM-22, No. 1.

RAMSEY, N. 1965. *Metrologia*, 1, No. 1: 7.

RAMSEY, N. 1972. *IEEE Trans.Instrum.Measmt* IM-21, No. 2: 90.

SCHUESSLER, H., FORTSON, E. & DEHMELT, H. 1969. *Phys.Rev.* 187: 5.

SCHUESSLER, H. 1971. *Metrologia*, 7, No. 3: 103.

SMITH, H. 1972. *Proc.IEEE*, 60, No. 5: 479.

STRUMLA, F. 1972. *Metrologia*, 8: 85.

VESSOT, R., LEVINE, M., ZITZEWITZ, P., DEBELY, P. & RAMSEY, N. 1970. P. 27, *Proc.Int.Conf. Precision Measurement and Fundamental Constants, August 1970*, at National Bureau of Standards, Gaithersburg, Md, USA. (ed. Langenberg and Taylor).

WINKLER, G., HALL, R. & PERCIVAL, D. 1970. *Metrologia*, 6: 126.

WINKLER, G. 1970. *Proc.Precise Time & Time Interval (PTTI), Strategic Planning Mtg*, 1: 129 (US Naval Observatory).

ZITZEWITZ, P. & RAMSEY, N. 1971. *Phys.Rev.* A3: 51.

15. Discussion

WHITTEN (Chairman): I wish to mention some work that was done in the Cascade Mountains (USA). There is a tunnel there available to physicists at the University of Washington. VALI & BOSTROM used a hydrogen maser to control the strain experiment for which they used a laser interferometer. They found there was a sudden step change. This emphasizes the necessity for redundancy such as you have pointed out. They assumed that in this case, it was the hydrogen maser and not some sudden step change in the strain field.

HIBBARD: The hydrogen maser could have had automatic tuning. Automatic tuning causes changes in the frequency.

GUBBAY: You mentioned the sensitivity to Doppler in some of these lasers. Which of them is least sensitive and why aren't they all as sensitive?

HIBBARD: Do you mean lasers or atomic beam devices?

GUBBAY: Atomic beam devices.

HIBBARD: Firstly, you have to know the velocity as they come out of the hole. If you don't know the velocity, a thermal distribution is assumed. That's not quite right. You collimate. A good long collimator is what you like; you then get a different system. The slower atoms are knocked on by the faster ones. You've got to know the velocity distribution. The hydrogen maser is the only device where you know that.

GUBBAY: Wouldn't you get interaction between particles which would destroy the monochromatic light?

HIBBARD: It is not monochromatic. An atom is being "scanned" for half a second or so and is changing its velocity after each collision. First order Doppler effects cancel out. In the case of the caesium beams, you get a Doppler reduction by "scanning" at right angles. The original ammonia maser effectively "scanned" in length.

WHITTEN: Thank you for preparing your paper which I am sure will serve as a reference document for some time.

NASON, R.D.*
U.S. Geological Survey
Menlo Park, California
United States of America

Proc. Symposium on Earth's Gravitational Field & Secular Variations in Position (1973),637-639.

OBSERVATION SITES FOR SECULAR VARIATION STUDIES *

ABSTRACT

In an astronomical Earth-surveying program using movable telescopes to study Earth deformation, the usefulness of the measurements will depend on the long-term stability of the permanent survey marks. In areas of weak rock or soil on sloped ground, there will be a tendency for the survey mark to move slowly downhill. In areas where underground oil or water is being withdrawn, the ground surface may "subside", together with horizontal movements. Seasonal moisture or freezing changes in soil can cause movements of several centimetres.

Most causes of local instability can be avoided by careful installation of survey marks. But for complete certainty, the local position of an astronomical survey mark should be carefully measured to nearby or distant reference marks using geodetic triangulation, trilateration, and/or levelling. If local movement does occur, the reference measurements will show the amount of movement for a site correction. Having the astronomical survey mark be part of an existing geodetic network, or extending an existing network to the observation site, will improve the value of the results.

1. Text *

I am very sorry that Dr. Nason cannot be here to speak on "Observation Sites for Secular Variation Studies". Bob Nason is a good friend and colleague of mine. He has shown a very keen interest in searching for and locating those special areas where fault creep may be observed and measured. I will not attempt to give you his thoughts on the subject assigned to him but for a few moments I wish to describe some aspects of the crustal movement program in California and the relevance of some of the discussion we have had this week.

More than 40 years ago, seismologists in California who were working with geodesists in developing a program for detecting crustal movement, recommended establishing eight traverse or triangulation schemes crossing the San Andreas Fault system. Near the fault, monuments were spaced 25 m apart, then at 50 and 100 m spacing and eventually at 1 to 2 km for a total distance of 25 or more km on each side of the fault. The closer spacings were designed for the use of 50 m invar tapes but, unfortunately, many of the sites were not ideally located. Many marks were damaged or destroyed by highway development, etc. The original program specified a re-survey every ten years or an immediate re-survey following an earthquake. Through the years additional networks were established, some for monitoring crustal movement but many for the overall requirement of geodetic control for large scale mapping, highway construction, etc. Today, there are about 10,000 geodetic points throughout this area. Many of them are monitored on a repeat basis to detect crustal deformation. Crustal deformation occurs in relatively short wavelengths in comparison to the total extent of the area.

---

* Text is that of a talk given by C.A. WHITTEN, Chairman of Session L, in lieu of the paper by R.D. NASON who was unable to attend.

I will quickly review what has been learned concerning movement along the broad San Andreas system. North of San Fransisco, near Fort Ross, repeat surveys show strain accumulation at a rate approximating 1 in 10^6 per year. There is no evidence of creep. Near San Fransisco, the San Andreas fault seems to be locked, but on the east side of the Bay there is evidence of creep of a few mm per year along the Hayward and Calaveras faults. Further south, near Hollister, the rate increases to 12 to 14 mm per year and near Cholame the rate of creep is as large as 35 mm per year. Near the bend in the fault system at the junction with the Garlock fault, there is evidence of north-south compression and in the piece of pie shaped segment between the two faults there is evidence of elongation. Repeat geodetic levelling indicates subsidence in this latter block. The horizontal measurements show a slight left lateral creep on the Garlock fault but the major system seems to be locked. Near the southern end of the system, there is evidence of continuing movement across the Imperial Valley. Some of this movement may be creep along the various faults that comprise the total system in this region. There is an urgent need for more closely spaced survey points and more frequent monitoring.

Two weeks ago there was a crustal movement symposium in Bandung, Indonesia. James Savage presented a paper on work being done by the U.S. Geological Survey on the west side of the San Andreas fault near Hollister. They have a network of nine points concentrated in a region about 5 km on a side. The measurements indicate that if there is any strain accumulation it is only about 2 in 10^7 per year. They are using a Geodolite for the measurements. Recently I saw a demonstration of a new distance measuring instrument called the Mekometer. It is available to geodesists and can measure distances to 1 part in 10^7. Seismologists are asking geodesists to measure distances accurate to a millimetre or a fraction of one. When we think in terms of how 1000 km laser range baseline measurements accurate to 3 or 4 cm might be used, such lines would be of tremendous assistance to the geodetic community for controlling the accumulation of error that occurs in the classical geodetic networks.

I want to refer to another paper presented at Bandung. Dr. Fujita, who is present here, presented a very interesting paper on the re-triangulation in Japan. After listening to the discussion on collocation techniques this week, I am suggesting a variation in technique which might be applied by geodesists in the United States or in Japan. Dr. Fujita used the primary triangulation net in Japan, adjusting two sets of observations, separated by approximately 60 years. He held six points "fixed" along the full length of the country. Of course, this produced some distortion. I wish to suggest a technique which would essentially hold all points fixed. Then look at the corrections to the observed directions, treating them in a statistical manner such as Moritz and his colleagues have suggested. Use the differences of corrections to directions to determine strain accumulation. Where there are discontinuities, earthquakes have occurred. Those values would determine strain release.

It may be that some slight variation in this procedure is necessary. But following the philosophy of holding all points fixed, because of the strength obtained in combining observational data, permit some slight relaxation at those points where the corrections from this adjustment process indicate that relaxation should occur. It would require an inverse sigma type of application plus iterative computations to arrive at optimum results. I am convinced this type of study is worthwhile. Strain accumulation follows a systematic pattern. Where there are discontinuities, these are clearly defined as the displacements which occur at the time of an earthquake. The signal to noise ratio is such that the noise is often a little greater than the signal we are seeking. Thus, considerable expertise in statistical methods is required to obtain meaningful results.

I suggest this as something I gained from this symposium this week and hope it might be applied to blocks of geodetic data in attempting to get a clearer picture of what happens in crustal deformation.

KAULA, W.M.
Department of Planetary & Space Science
University of California
Los Angeles, California 90024
United States of America

Proc.Symposium on Earth's Gravitational Field & Secular Variations in Position (1973),640-642.

MOTIONS INFERRED FROM REMANENT MAGNETISM, FRACTURE ZONE ORIENTATIONS, AND EARTHQUAKE SLIP VECTORS

1. Text

For tectonic plates of more than 5000 km extent, the standard deviations of relative motion determinations are less than 0.6 cm/year. This uncertainty applies to the motion averaged over the last five million years. Within the accuracy of the data, the motion has been steady for the last ten million years. The resolution of the remanent magnetic data is about 100,000 years.

In a symposium discussing secular variations in position, it seems appropriate to review the evidence which has persuaded most solid Earth geophysicists that major segments of the Earth's lithosphere are moving at steady rates on the order of 5 cm/yr with respect to each other. A knowledge of the accuracy and limitations of these determinations is necessary to plan the application of geodetic techniques most effectively to these problems. Fortunately such a review is facilitated by the recent comprehensive analysis of MINSTER ET AL (1974). Their analysis synthesizes and updates the determinations of the four classic papers, (MCKENZIE & PARKER 1967), (MORGAN 1968), (LE PICHON 1968) and (ISACKS ET AL 1968), which clinched the plate tectonics revolution.

The study by MINSTER ET AL (1974) analyzed three data types:

- remanent magnetic stripes centred on ocean rises;
- oceanic fracture zones; and
- seismic slip vectors.

The analysis was extremely detailed and thorough: the paper is 57 pages long and has 121 references. Special attention was paid to statistical techniques, and iterative procedures were used to avoid convergence to non-global optima.

The first data type was measurement of magnetic fields on 68 profiles across ocean ridges. For these data, the digitization interval is 1.7 km, corresponding on the average to about 30,000 years of sea floor spreading. Since it takes more than one data point to infer a variation and since there is some variation in signal strength due to topographic irregularities, lithological variations, etc, the true resolution is conservatively estimated to be about 100,000 years. For regions of average or rapid spreading, data out to magnetic anomaly three (about five million years) were used, and for regions of slow spreading, data to anomaly five (ten million years) were used. For comparisons with radiometrically dated magnetic intensity sequences, the marine magnetic profiles are corrected for both latitude and orientation.

The second data type was orientation of 62 oceanic fracture zones: locations where oceanic rises are offset by strike-slip fractures. If these fractures are strike-slip, and if the plate motions are rigid, then the fractures must lie along parallels about the pole of rotation between plates. Hence

each fracture zone orientation is an estimate of the rotation pole, but not of rate.

The third data type was 106 earthquake slip vectors. When an earthquake occurs, it is expressible as a double couple. There is a break in the material and motion of the material on one side of the break with respect to the other, but there is no nett volumetric change from an earthquake. In the signal radiated from an earthquake, in two quadrants the onset of the longitudinal P wave will coincide with a dilatation, and in the other two, to a compression. The systematic variations with azimuth in an earthquake of this initial signal are analysed to get the direction of motion of the earthquake.

In three dimensions there is an ambiguity -- there are two principal directions in which an earthquake could occur. At this point, geological interpretation is used to determine which nodal direction is reasonable. In the case of strike-slip faults like the San Andreas, it is obvious that the motion does not occur at right angles to the fault. In faults which involve under thrusting, the determination is less strong. In the analysis by Minster and co-workers, it was arbitrarily assumed that no slip vector is known to better than 10°.

The analysis took into account twelve plates:

- the LE PICHON (1968) six (Pacific, Americas, Eurasia, India, Antractic, and Africa),
- plus separation of South America from North America,
- the Nazca and Cocos plates separate from an Antarctic, and
- the Arabian plate from the Eurasian.

The slip vectors also indicate a Bering plate separate from the North American. The twelfth plate was the Somali plate whose motion with respect to the African plate could not be discriminated from zero. Minster et al were very careful to omit any slip vectors which caused any confusion at all. For example they omitted all seismic data along the Alpide belt from the Mediterranean to New Guinea.

Any motion of points on a sphere relative to each other can be described as rotation about a specific pole, so locations of these poles as well as rates of rotation are required. Since the location of the pole is defined by sines and cosines of latitude and longitude, the problem is non-linear. It is possible to converge from a least squares solution to a false minimum. The procedure adopted by MINSTER ET AL (1974) was first a solution for relative motion between triplets of plates. Next, from best solutions for these sets of triplets, for quadruplets of plates. Finally they worked stepwise to a set of 12 plates. In this process, they made findings about separating off the Bering and South American plates from the North American plate and so forth. For plates of more than 5000 km (all except Cocos, Arabia and Bering), the standard deviation of relative motion averages ±0.3 cm yr^{-1}. The maximum for major plates is ±0.6 cm yr^{-1}. The uncertainties for the Cocos and Arabic plates are ±1.2 cm yr^{-1}. The distribution of the residuals fits a chi-square test very well.

In two places, comparisons with geodetic data can be made. In Tadzhikistan, the closure rate between the Indian and Eurasian plates is 3.8 cm yr^{-1}, compared to the 2.0 cm yr^{-1} measured on the Hissaro fault. In California, the slip rate between the North American and Pacific plates is 5.5 cm yr^{-1}, compared to 3.2 cm yr^{-1} measured on the San Andreas fault. In both these places, about half the motion is obviously being taken up by complexes of subsidiary faults about the main fault.

A second analysis by MINSTER ET AL (1974) estimated motion relative to an absolute frame. They adopted the hot spot hypothesis and at 20 places in the world, such as the Hawaiian volcano chain,

used radioactive dating as a guide to the rate and direction of motion of the plate with respect to a set of hypothetical hot spots. They used seven chains in the Pacific, three in the Indian Ocean, five in the south Atlantic, three in the north Atlantic and two in North America.

These chains were carried back ten million years, twice as long as used for relative analysis. From a best fit, an estimate of absolute motion was obtained. The internal uncertainty of the results was less than 1 cm yr^{-1}. There are three interesting things about this hot spot frame.

1. It coincides very closely with the frame defined by minimizing the velocity normal to compressive belts of the over-riding plates, i.e., the typical situation being an oceanic plate going underneath a continental plate. In this case, the continental plate is staying still and the oceanic plate is the one that is moving.
2. It is very close to minimizing the nett rotation of the entire lithosphere.
3. It is close to a frame minimizing continental motion and maximizing oceanic motion.

The task of geodetic techniques is thus to measure variations from the steady states determined mainly from remanent magnetism. Considering that

1. the motions from earthquake slip vectors over the last seventy years agree fairly well with those from remanent magnetism (DAVIES & BRUNE 1971); and
2. earthquakes are not known to extend more than 1000 km (KELLEHER ET AL 1973),

it is probable that measurable variations in motion are confined to zones of less than 1000 km width about plate margins.

2. References

DAVIES, G.F. & BRUNE, J.N. 1971. Regional and Global Fault Slip Rates from Seismicity. *Nature Physical Science* 229,101-107.

KELLEHER, J., SYKES, L. & OLIVER, J. 1973. Possible Criteria for Predicting Earthquake Locations and Their Application to Major Plate Boundaries of the Pacific and the Carribean. *J.geophys.Res.* 78,2547-2585.

MCKENZIE, D.P. & PARKER, R.L. 1967. The North Pacific: An example of Tectonics on a Sphere. *Nature* 216,1276-1280.

ISACKS, B., OLIVER, J. & SYKES, L.R. 1968. Seismology and the New Global Tectonics. *J.geophys.Res.* 73,5855-5899.

LE PICHON, X. 1968. Sea Floor Spreading and Continental Drift. *J.geophys.Res.* 73,3661-3697.

MINSTER, J.B., JORDAN, T.H., MOLNAR, P. & HAINES, E. 1974. Numerical Modeling of Instantaneous Plate Tectonics. *Geophys.J.R.astr.Soc.* (in press).

MORGAN, W.J. 1968. Rises, Trenches, Great Faults, and Crustal Blocks. *J.geophys.Res.* 73,1959-1982.

3. Discussion

DOOLEY: One phenomenon which is prominent in sea floor spreading is that the spreading on each side of an oceanic ridge is quite symmetrical. Has this been used?

KAULA: Symmetry has not been assumed. The results obtained are consistent with symmetry, however.

GRAFAREND, E.W.
Institut für Theoretische Geodäsie
University of Bonn
Bonn
Federal Republic of Germany

Proc.Symposium on Earth's Gravitational Field & Secular Variations in Position (1973) ,643-659.

A LOD AND WOBBLE ANALYSIS OF GENERALIZED EULER-LIOUVILLE TYPE BASED ON VIRIAL PLANETARY EQUATIONS

ABSTRACT

Four dimensional geodesy is based on longitude, latitude and gravity variations in time. The classical analysis of the length of day (LOD) and of the Earth's wobble has its origins in the Euler - Liouville equation. For three different Earth models (rigid, liquid, elastic) the virial method as an alternative tool is applied to generalize the Euler - Liouville problem. Numerical solutions are are discussed for the different models.

1. Introduction

Geodesy can be understood as the science defining estimable, unique space-time co-ordinates, especially of points on the surface of the Earth or other planets. There are two central problems characterizing geodesy:

- the problem of finding *holonomic* space-time co-ordinates; and
- the geodetic *datum* problem.

In three dimensional geodesy these problems are the following:
All geodetic instruments, for example levelling instruments, theodolites, gyro-compasses. satellite cameras, satellites, refer to gravitation. Related to the *local* gravity vector the so-called "natural" or astronomical co-ordinate system is introduced; therefore the local measurement triad (east, north, vertical), which is orthonormal, characterizes this system. But it is easy to prove that co-ordinates measured along these axes are *anholonomic*, non-integrable, therefore non-unique. The determination of co-ordinate differences between two points is path-dependent. In order to give an example we note that the Cartesian co-ordinate differences along east,north, vertical, calculated from measurements of the azimuth, the vertical angle, and the distance, are non-integrable. There is no way to arrive at *global* unique co-ordinates from co-ordinate differences if we have no further information about the size and shape of the gravity field. In geodesy, two ways have been gone to change this situation. A.Marussi introduced in 1949 the three co-ordinates astronomical longitude, astronomical latitude and geopotential and proved that these co-ordinates are *holonomic*. He succeeded in transforming co-ordinate differentials from the natural triad into the mentioned holonomic one by introducing in general, nine integrating factors of the Pfaff-Frobenius-Cartan type. This transformation, today called the Marussi transformation, is characterized by gravity gradients and the Euclidian norm of the gravity vector. For more details see (GRAFAREND 1971;GRAFAREND 1972; GRAFAREND 1973a,b,c). In geodesy, the Marussi co-ordinate system was not a breakthrough for practice. The *geocentric* co-ordinate system along the triad to Greenwich, orthogonal to Greenwich, and parallel to the rotation vector of the Earth *turned out to be holonomic*, alternatively. This frame had the advantage to coincide with our natural feelings about the embedding of the Earth in a three dimensional Euclidian world.

The Pfaff-Frobenius-Cartan type of transformation from co-ordinates along the natural anholonomic triad into the holonomic geocentric triad depends only on the local astronomical longitude and astronomical latitude. Added to the three natural co-ordinates along east, north, vertical, we have a five dimensional geodetic concept! The *geodetic datum problem* has its origin in the fact that we can measure only co-ordinate differences, but we have to know global co-ordinates. A geodetic net must be fixed for translation, rotation and scale. Free net adjustment problems with singular normal equations are typical.

Classical three-dimensional geodesy is based on the assumption of a rigid Earth. This is a very good first order approximation, but modern geodetic concepts reflect this restriction. Of course, we have crustal movements etc for a real non-rigid Earth. Time dependent or four-dimensional co-ordinates have to be introduced. The question of holonomity and datum are very open for discussion.

Against this background, we introduce the most general four-dimensional continuum concept at this point. For a plastic-elastic Earth, we will refer to four-dimensional moving frames (4D-Cartan frames) of, in general, anholonomic type in section 2. The concept of dislocation is included.

All text books referring to the dynamics of such a continuum, introduce the so-called Euler-Liouville equation plus some intuitive feeling how the inertial moments change with the rotational speed of the Earth, and some parameters characteristic of the mechanical behaviour - the Love numbers. This concept has the disadvantage not to reflect to the now classical theory of plasticity and elasticity. For example, in elasticity Lame's constants or another set of two constants describe an isotropic material. The main difficulty in deriving a second order dynamical equation, the moment of momentum, is the fact that the vector form of this moment is independent of plastic-elastic effects. In section 3 we present our solution to this problem: the technique of tensorial virial equations. We succeed in formulating a general dynamic equation for a plastic-elastic-liqiud-viscous body, including couple stress. This is an important tool to introduce the hydromagnetic coupling of the core and the mantle of the Earth.

Sections four to six are examples of different mechanical models. We start with rigid body displacements and calculate the free precession of the Earth. Then we study Maclaurin type equilibrium figures for liquid body displacements. Finally we describe the second order dynamic virial equation of second rank tensor type for an elastic body displacement which includes Lame's constants!

2. Four Dimensional Moving Frames (4D-Cartan Frames)

The material points of a continuous medium at the ideal or initial state (at time zero) occupy a region B that consists of the material volume V and the surface S. The position of a material point P in this region is denoted by a curvilinear co-ordinate X^K, K=1,2,3, or by a vector P that extends from an origin O of the co-ordinates to the point P. After the total deformation (plastic and elastic deformation) takes place, at time t, the material point of V + S go into a region b consisting of a spatial volume v and its surface s. A point p in the deformed or final state may be represented by a new set of curvilinear co-ordinates x^k, k=1,2,3, or a position vector p that extends from the origin C of the new co-ordinates to the point p. Often it is advantageous to select these two reference frames to be non-identical. In the description of *motion* of a continuous body, we shall find a definite need for the use of these two types of co-ordinates. Following the current terminology, we shall call X^K the material or *Lagrangian* co-ordinates and x^k the spatial or *Eulerian*

co-ordinates. The position vector $\mathbf{P}$ of a point P in B and $\mathbf{p}$ of one in b referred respectively to rectangular co-ordinates Z^K and z^k, are given by

$$\mathbf{P} = Z^K E_K \quad , \qquad \mathbf{p} = z^k e_k \qquad 2(1),$$

where E_K and e_k are the rectangular base vectors in Z^K and z^k. Of course, there is a mapping $Z^K(X)$ and $z^k(x)$. For example, the base vectors e_k at time zero can be directed to the mean ecliptic (1950.0) system. Infinitesimal vectors $d\mathbf{P}$ in B and $d\mathbf{p}$ in b may be expressed as

$$d\mathbf{P} = G_K dX^K \quad , \qquad d\mathbf{p} = g_k dx^k \qquad 2(2),$$

where in general for *anholonomic co-ordinates* $G_K \neq \partial P/\partial X^K$ and $g_k \neq \partial p/\partial x^k$. The situation is very typical for geodetic problems. In 1972 I proved that co-ordinates along the "natural" triad east, north, vertical are anholonomic. If F is the Frobenius matrix of integrating factors mapping the anholonomic co-ordinates dX onto the holonomic co-ordinates dZ one-to-one; F: $dX \rightarrow dZ$, the transformation of the base vectors is due to

$$G_K = F_K^M E_M \quad , \qquad g_k = f_k^m e_m \qquad 2(3).$$

The base vectors $G_K(X)$ and $g_k(x)$ are moving frames of the 3D type. Their parameters are the three components of their position vector. The deformed or final infinitesimal vector $d\mathbf{p}$ consists of the *plastic* part $d\mathbf{p}_{plast}$ and the *elastic* part $d\mathbf{p}_{el}$.

$$d\mathbf{p} = d\mathbf{p}_{plast} + d\mathbf{p}_{el} \qquad 2(4)$$

defined by the line integrals

$$\oint d\mathbf{p} \neq 0 \quad , \qquad \oint d\mathbf{p}_{plast} \neq 0 \quad , \qquad \oint d\mathbf{p}_{el} = 0 \qquad 2(5).$$

In order to understand better these two fundamental types of deformation, let us refer for a moment to holonomic co-ordinates Y^K, and thus base vectors $H_K = \partial P/ Y^K$. Y^K may be represented by the holonomic Marussi co-ordinates astronomical longitude, astronomical latitude and geopotential at the initial state. The misclosure of the plastic infinitesimal vector $d\mathbf{p}_{plast}$ is due to Cartanian torsion. The squares of the lengths of the infinitesimal vectors $d\mathbf{P}$ and $d\mathbf{p}$ in B and b are respectively

$$dS^2 = d\mathbf{P}\cdot d\mathbf{P} = G_{KL}\, dX^K\, dX^L, \qquad ds^2 = d\mathbf{p}\cdot d\mathbf{p} = g_{k\ell}\, dx^k dx^\ell \qquad 2(6).$$

$$G_{KL}(X) = G_K \cdot G_L \quad , \qquad g_{k\ell}(x) = g_k \cdot g_\ell \qquad 2(7)$$

are the covariant metric tensors of B and b respectively. For comparison purposes it will often be necessary to *shift* vectors and tensors to the same system in parallel transport. For example, by definition, components of position vectors $\mathbf{P}$ and $\mathbf{p}$ in X^K and x^k

$$P^K = \mathbf{P}\cdot G^K \quad , \qquad p^k = \mathbf{p}\cdot g^k \qquad 2(8).$$

Suppose now we want to shift $\mathbf{p}$ to the point P(X) in parallel transport. If p^K are the components of $\mathbf{p}$ in X^K, then

$$p = p^K G_K(X) = p^k g_k(x) \qquad 2(9)$$

or by taking inner products with G^L and g^ℓ, we get

$$p^K = g^K_{.k} p^k, \qquad p^k = g^k_{.K} p^K \qquad 2(10),$$

where

$$g^K_{.k}(X,x) = G^K(X) \cdot g_k(x), \qquad g^k_{.K}(X,x) = g^k(x) \cdot G_K(X) \qquad 2(11)$$

are the *shifters* required for this parallel transport. The shifters relate components of a vector in two co-ordinate systems. They are *two-point* tensor fields. We say that *a body has undergone a rigid-body displacement wherever* $ds^2 = dS^2$ *for all material points.* Therefore the difference $(ds^2 - dS^2)$ is a measure of the deformation produced during a displacement. If at time t, we look upon the motion

$$dX^k = A^k_K \, dX^K, \qquad dX^K = A^K_k \, dx^k \qquad 2(12),$$

then by substitution we get

$$dS^2 = c_{k\ell}(x,t) \, dx^k dx^\ell, \qquad ds^2 = C_{KL}(X,t) \, dX^K dX^L \qquad 2\,(13)$$

for all

$$c_{k\ell} := G_{KL}(X) \, A^K_k \, A^L_\ell \qquad 2(14)$$

$$C_{KL} := g_{k\ell}(x) \, A^k_K \, A^\ell_L \qquad 2(15),$$

then

$$ds^2 - dS^2 = 2E_{KL}(X,t) \, dX^K dX^L = 2e_{k\ell}(x,t) \, dx^k dx^\ell \qquad 2(16)$$

for all

$$2E_{KL} = C_{KL}(X,t) - G_{KL}(X) \qquad 2(17)$$

$$2e_{k\ell} = g_{k\ell}(x) - c_{k\ell}(x,t) \qquad 2(18),$$

which are respectively called *Lagrangian and Eulerian strain tensors.* Our procedure was quite obvious: we transformed the metric tensor $g_{k\ell}$ within ds^2 into the metric tensor C_{KL} from the x^k into the X^K system. This was necessary in order to compare the displacement in the same base system.

Formally we can call

$$c_k(x,t) = G_K(X) \, A^K_k(t) \qquad 2(19)$$

and

$$C_K(X,t) = g_k(x) \, A^k_K(t) \qquad 2(20)$$

the *new base vectors.* The base vectors are dependent on *the position co-ordinates and the time.* They form *four-dimensional moving frames or 4D-Cartan frames.* c_k is called the *Cauchy base vector,*

C^K the *Green base vector*. Finally figure 1 is a brief summary of the geometrical situation .

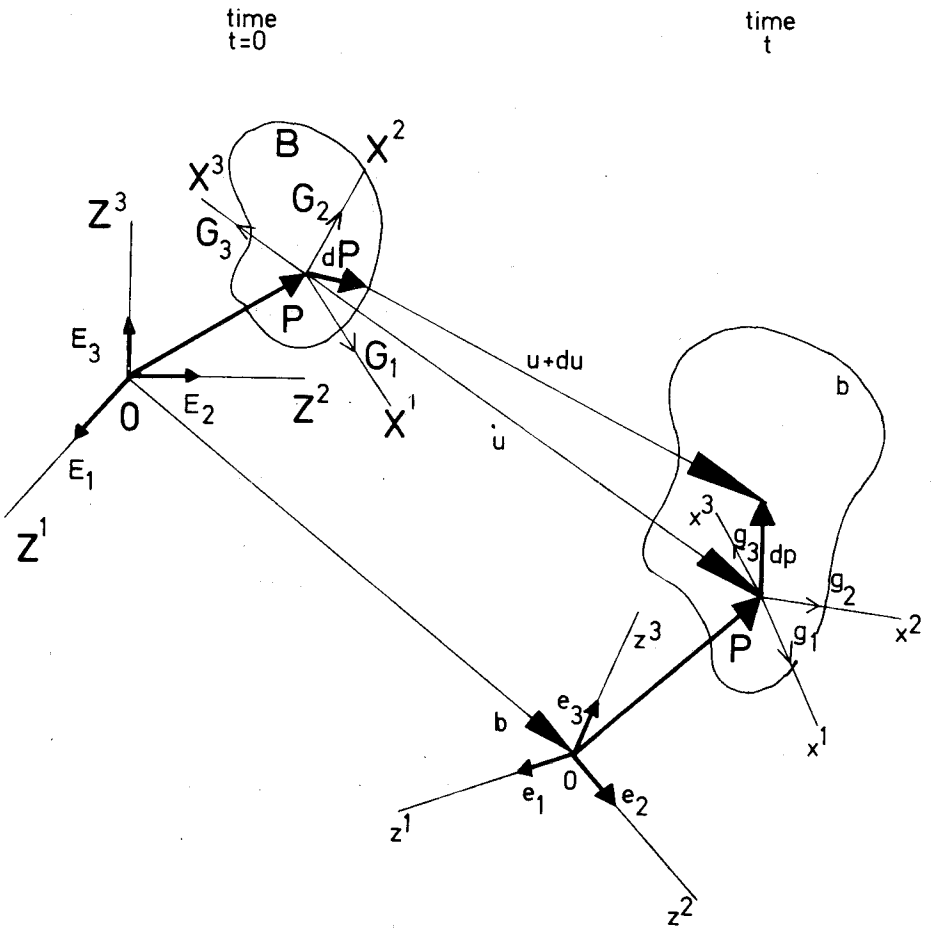

Figure 1. Base Vectors, Displacement Vector and Co-ordinate Systems.

The *displacement vector* is defined as the vector that extends from a material point in the undeformed body to the same material point in the deformed body. Thus

$$u = p - P + b = U^K G_K = u^k g_k \qquad 2(21).$$

If we represent respectively **dp** and **dP** in the 4D-Cartan frames,

$$\mathbf{dp} = C_K \, dX^K = (G_K + U_{M;K} \, G^M) \, dX^K \qquad 2(22)$$

and

$$\mathbf{dP} = c_k \, dx^k = (g_k - u_{m;k} \, g^m) \, dx^k \qquad 2(23),$$

the Lagrangian and Eulerian strain tensors are related to the displacement vector by

$$2E_{KL} = C_{KL} - G_{KL} = U_{K;L} + U_{M;K} U^M{}_{;L} \qquad 2(24)$$

and

$$2e_{k\ell} = g_{k\ell} - c_{k\ell} = u_{\ell;k} - u_{m;k} u^m{}_{;\ell} \qquad 2(25)$$

The semicolon indicates covariant partial differentiation. In the "Small Displacement Theory", the displacement components are considered small. Thus any product of these components and their various gradients may be neglected:

$$2E_{KL} \doteq 2e_{k\ell} \doteq u_{k;\ell} + u_{\ell;k} \qquad 2(26).$$

The differences between U_K and u_k disappear.

In the kinematics of continuous media, time rates of vectors and tensors associated with the material points play an important role. In the determination of the time rate of change of field quantities carried by a material point, one must take into account not only the change at a fixed spatial point (*local change*) but also the change in the field as observed by the particle due solely to its motion (*convective change*). The *material derivative* of an absolute spatial vector $f^k(x,t)$ is defined by

$$\frac{D}{Dt} f^k(x,t) = \frac{\partial f^k}{\partial t} + \frac{\delta f^k}{\delta t} = \frac{\partial f^k}{\partial t} + f^k{}_{;\ell} \frac{dx^\ell}{dt} \qquad 2(27),$$

where the partial time derivative $\partial f^k/\partial t$ is taken with X held constant and the intrinsic derivative $\delta f^k/\delta t$ with t held constant.

In the experimental determination of geometrical and physical properties of the Earth, it is necessary to know how the motion of the observer will affect the measurements. It is evident that for those properties that are independent of the motion of the observer, measurements made in one frame of reference are sufficient to determine their values once and for all.

In the formulation of physical laws, it is desirable to introduce quantities which are independent of the observer or the frame of reference. Such quantities are called *objective*. For example, the location of a point will appear different to observers located at different places, and therefore is not objective. Similarly the velocity of a point will appear to be different to observers moving with respect to each other. Hence again it is not objective. On the other hand, distances and angles are objective quantities since they are independent of the frame of reference.

Attempts to secure the invariance of physical laws of motion from the observer have produced one of the great triumphs of twentieth century physics. Newton's laws of motion have long been known to be valid only in a special frame of reference, the *inertial or Galilean* reference frame. Attempts to free the principles of classical mechanics from the motion of an observer were resolved by A. Einstein in his general theory of relativity, by rejecting these principles altogether and denying an objective meaning for the concept of time and distance.

While we wish to stay in the domain of classical mechanics, we will find that in the description of materials and dynamic processes, the axiom of objectivity plays a central role. To formulate these physically evident facts, let us consider a point x in a reference frame F. In another frame of reference F^1 this point will appear as x^1. The relation between x and x^1 must be such that the distance and the angle are preserved. The most general transformation of space and time that satisfy these conditions are of the form

$$x^1 = Ax + b, \qquad t^1 = t - a \qquad 2(28),$$

where A(t) is an arbitrary real valued non-singular orthogonal matrix, b(t) is an arbitrary point, and a is a constant. Both A and b are continuously differentiable functions of time t alone. The orthogonality condition for the matrix A requires that

$$\mathbf{A}\,\mathbf{A}^T = \mathbf{A}^T\mathbf{A} = \mathbf{I} \qquad 2(29),$$

where $\mathbf{A}^T$ denotes the transposed $\mathbf{A}$ and $\mathbf{I}$ the unit matrix. Suppose $\mathbf{x} = \mathbf{x}(X,t)$ represents the motion of the body B. Then

$$\mathbf{x}^1(X,t^1) = \mathbf{A}(t)\,\mathbf{x}(X,t) + \mathbf{b}(t) \qquad 2(30)$$

indicates that for $t = t^1$, the two frames F and F^1 may move with respect to each other in an arbitrary rigid motion. In rectangular co-ordinates $\mathbf{A}(t)$ for det A = 1 and b(t) represent, respectively, the rotation and the translation of one frame with respect to the other; they behave like moving frames or 4D-Cartan frames.

We have to note that for quantities which are independent of time, objectivity does not come into play. For time dependent quantities, however, the situation is different. If $\mathbf{e}$ is a vector in an inertial frame, it will appear in another frame prime as

$$\mathbf{e}^1 = \mathbf{A}\,\mathbf{e} \qquad 2(31),$$

where $\mathbf{A}$ is a function of time. Because of equations (28),

$$\Omega^* = \frac{DA}{Dt}\,A^T \qquad 2(32)$$

is antisymmetric, since

$$\Omega^* + \Omega^{*T} = \frac{DA}{Dt}\,A^T + A\,\frac{DA^T}{Dt} = \frac{D}{Dt}(A\,A^T) = 0 \qquad 2(33).$$

The dual, Ω, of the matrix Ω^* is a vector, related by

$$\Omega^*_{ij} = \delta_{ij}{}^{k}\,\Omega_k, \qquad \Omega_i = \frac{1}{2}\,\delta_i{}^{jk}\,\Omega^*_{jk} \qquad 2(34)$$

$\delta_{ij}{}^{k}$ denotes the generalized Kronecker symbol, in this case the Levi-Civita symbol. We differentiate (31).

$$\frac{De}{Dt} = \frac{DA^T}{Dt}\,e^1 + A^T\,\frac{De^1}{Dt} \qquad 2(35).$$

It is our aim to resolve the equation along the instantaneous co-ordinate axes of the moving frame.

$$A\,\frac{De}{Dt} = -\,\Omega^*\,(Ae) + \frac{D}{Dt}(Ae) \qquad 2(36).$$

Thus the "velocity" vector is not objective.

3. The Virial Equations of the Various Orders in 4D-Cartan Frames

A technique very much in vogue for treating the integro-differential equations of physical geodesy is to take the moments of the equations concerned. The moment equations have the advantage of allowing simple physical interpretations. The virial method as developed in the context, is mainly the method of moments applied to the solution of rigid, hydrodynamical and elastic problems in which the gravitational field of the matter is taken into account. If we apply the virial method to the equations of motion, we must involve the moments of the distribution of density, stress tensor, for example, pressure, velocity, and gravitational potential.

(a). Let us consider a distribution of mass in a volume v. The frame of reference is for a moment fixed at the centre of mass. Then the choice of the reference frame requires

$$I = \int_v dX\ \rho(X)\ |X|^2 \qquad 3(1),$$

$$I_i = \int_v dX\ \rho(X)\ x_i = 0 \qquad 3(2),$$

$$I_{ij} = \int_v dX\ \rho(X)\ x_i\ x_j \qquad 3(3),$$

and

$$I_{ijk\ldots} = \int_v dX\ \rho(X)\ x_i\ x_j\ x_k \ldots \qquad 3(4),$$

where $\rho(X)$ is the density at the point X. I is the moment of inertia, I_i defining the origin of the mass centre, I_{ij} the moment of inertia tensor.

(b) The prevailing distribution of stresses σ_{ij} similarly leads to a consideration of the moments.

$$\Sigma_{ij} = \int_v dX\ \sigma_{ij} \qquad 3(5),$$

$$\Sigma_{ijk} = \int_v dX\ \sigma_{ij}\ x_k = \int dX\ \sigma_{ijk} \qquad 3(6),$$

and

$$\Sigma_{ijk\ell\ldots} = \int_v dX\ \sigma_{ij}\ x_k x_\ell \ldots. \qquad 3(7),$$

and for a distribution of isotropic pressure $\sigma_{ij} = -p\,\delta_{ij}$

$$\Pi = \int_v dX\ p \qquad 3(8),$$

$$\Pi_i = \int_v dX\ p\ x_i \qquad 3(9)$$

and

$$\Pi_{ij..} = \int_v dX\ p\ x_i\ x_j \ldots.. \qquad 3(10).$$

(c) For a description of the macroscopic motion, we have to refer to the total kinetic energy of the motions in the system.

$$T = \frac{1}{2}\int_v dX\ \rho(X)\ |V|^2 \qquad 3(11),$$

$$T_{ij..} = \frac{1}{2}\int_v dX\ \rho(X)\ v_i v_j \ldots. \qquad 3(12),$$

$$T_{ij|k} = \frac{1}{2}\int_v dX\ \rho(X)\ v_i v_j x_k \qquad 3(13),$$

and

$$T_{ij|k\ell..} = \frac{1}{2}\int_v d\mathbf{X}\ \rho(\mathbf{X})\ v_i v_j x_k x_\ell .. \qquad 3(14),$$

where $|\mathbf{V}|^2 = v_1^2 + v_2^2 + v_3^2$ is the square of the velocity of a material point at $\mathbf{X}$. T_{ij} is the kinetic energy tensor.

(d) The gravitational effect at a point x, due to a distribution of matter with density $\rho(\mathbf{X})$, is determined by the Newtonian potential.

$$V(\mathbf{X}) = G\int_v d\mathbf{X}^1 \quad \frac{\rho(\mathbf{X}^1)}{|\mathbf{X} - \mathbf{X}^1|} \qquad 3(15)$$

and

$$V_{ij}(\mathbf{X}) = G\int_v d\mathbf{X}^1\ \rho(\mathbf{X}^1)\ \frac{(x_i - x_i^1)(x_j - x_j^1)}{|x - x^1|^3} \qquad 3(16).$$

G denotes the constant of gravitation. Associated with the gravitational potential is the potential energy.

$$W = -\frac{1}{2}\int_v d\mathbf{X}\ \rho(\mathbf{X})\ V(\mathbf{X}) \qquad 3(17)$$

and

$$W_{ij} = -\frac{1}{2}\int_v d\mathbf{X}\ \rho(\mathbf{X})\ V_{ij}(\mathbf{X}) \qquad 3(18).$$

(e) We consider a continuous medium of material points described in terms of a density $\rho(\mathbf{X},t)$ and a stress $\sigma_{ij}(\mathbf{X},t)$. Further we suppose that beside the surface force, the only volume force to which the body motions are subject is that derived from its own gravitation. Under these assumptions, the dynamical equation governing the motions, *referred to an inertial frame of reference*, is given by

$$\rho\frac{D}{Dt}v_i = \partial_j \sigma_{ij} + \rho\,\partial_i V \qquad 3(19),$$

where following equation 2(27),

$$\frac{D}{Dt} = \frac{\partial}{\partial t} + v_j\,\partial_j \qquad 3(20)$$

is the material derivative. The virial equations of the various orders are now obtained by simply multiplying the basic dynamical equation, successively by 1, x_j, x_{jk}, $x_j x_k x_\ell$, etc, and integrating over the entire volume v instantaneously occupied by the body.

(f) *The Equations of the First Order*

The equations of the first order are obtained by integrating equation 3(19) over the instantaneous volume V occupied by the body.

$$\frac{D}{Dt}\int_v d\mathbf{X}\ \rho\ v_i = \int_v d\mathbf{X}\ \frac{\partial}{\partial x_j}\sigma_{ij} + \int_V d\mathbf{X}\ \rho\ \frac{\partial V}{\partial x_i} \qquad 3(21),$$

and

$$\frac{D}{Dt}\int_v d\mathbf{X}\ \rho(\mathbf{X},t) = \frac{DM}{Dt} = 0 \qquad 3(22)$$

especially the *local* condition $D\rho/Dt = 0$.

The volume integral $\int_V dx\ \partial_j\ \sigma_{ij}$ can be transformed by the Gaussian integral therein into a surface integral

$$\int_V dX \quad \partial_j \sigma_{ij} \quad = \int_s ds_j \quad \sigma_{ij} \quad = \int_s ds \; n_j \; \sigma_{ij} \qquad 3(23)$$

s denotes the *free surface* bounding the volume v and $ds_j = n_j\, ds$ an element of this surface. n_j is the surface normal vector.

Due to the condition that the normal component of the stress must vanish on a *free boundary*, this surface integral must vanish. By equation 3(15), the second integral in equation 3(21) results zero too, on account of the antisymmetry of the integral in X and X^1.

$$\int_V dX \quad \rho \frac{\partial v}{\partial x_i} \quad = \quad - \quad G \int_V dX \int_V dX^1 \rho(X) \; \rho(X^1) \quad \frac{x_i - x_i^1}{|X - X'|^3} \quad = 0 \qquad 3(24).$$

Thus we are left with the fundamental result

$$\frac{D}{Dt} \int_V dX \; \rho \; v_i \quad = \quad \frac{D^2}{Dt^2} \int_V dX \; \rho \; x_i \quad = \quad \frac{D^2}{Dt^2} I_i \quad = 0 \qquad 3(25)$$

expressing the *uniform motion of the centre of mass*.

(g) *The Equations of the Second Order*

We multiply equation 3(13) by x_j and integrate over the deformed volume v

$$\int_V dX \; \rho \; \frac{Dv_i}{Dt} \; x_j = \int_V dX \; \rho \left\{ \frac{D}{Dt}(v_i x_j) - v_i v_j \right\} \quad = \quad \frac{D}{Dt} \int_V dX \; \rho \; v_i x_j - 2T_{ij}$$

$$= \int_V dX \; (\partial_k \sigma_{ik}) x_j \quad + \int_V dX \; \rho \; x_j \partial_i V \quad = \quad \int_V dX \; \partial_k \sigma_{ijk} - \sum_{ij} + W_{ij} \qquad 3(26).$$

Now we understand that σ_{ijk} are the components of *couple stress* in the deformed state. We note that we have written for $(\partial_k \sigma_{ik}) x_j = \partial_k (\sigma_{ik} x_j) - \sigma_{ik} \partial_k x_j = \partial_k (\sigma_{ijk}) - \sigma_{ij}$. Finally we obtain from equation 3(26) the basic equation 3(27)

$$\frac{D}{Dt} \int_V dX \; \rho \; v_i x_j \quad = \quad 2T_{ij} \quad + \quad S_{ij} - \sum_{ij} + W_{ij} \qquad 3(27).$$

Of course, $\int_V dX \; \partial_k \sigma_{ijk} = \int_s ds \; n_k \sigma_{ijk} = S_{ij}$ by the Gaussian identity. Let us specialize for a moment that we have

1. no plastic effects : $\sigma_{ij} = \sigma_{ji}$; and
2. no couple stresses : $\sigma_{ijk} = 0$.

Then

$$\frac{1}{2} \; \frac{D}{Dt} \int_V dX \; \rho \; (v_i x_j - v_j x_i) \quad = \quad 0 \qquad 3(28)$$

and

$$\frac{1}{2} \; \frac{D}{Dt} \int_V dX \; \rho \; (v_i x_j + v_j x_i) \quad = \quad \frac{1}{2} \frac{D^2}{Dt^2} \int_V dX \quad \rho \; x_i x_j = \frac{1}{2} \frac{D^2 I_{ij}}{Dt^2} \qquad 3(29).$$

Hence we must have

$$\frac{1}{2} \; \frac{D^2}{Dt^2} I_{ij} \quad = \quad 2T_{ij} \quad + W_{ij} \quad - \quad \sum_{ij} \qquad 3(30).$$

(h) *The Equations of Higher Order*

Up to now the reader will be familiar with the virial method. For higher order virial equations, we have to split

$$\int_v dx\ \rho\ \frac{Dv_i}{Dt}\ x_j x_k x_\ell \cdots\cdots \qquad 3(31)$$

by

$$\int_v dx\ \ \rho\{\frac{D}{Dt}(v_i x_j x_k x_\ell \cdots) - (v_i v_j x_k x_\ell \cdots) - (v_i x_j v_k x_\ell \cdots\cdots) - \cdots\cdots\ \} \qquad 3(32).$$

For us, the virial equations in four dimensional moving frames are now most important.

(i) The Second Order Virial Equations in a Moving Frame

From physics it is well known that the virial equations - up to the second order identical with the *first and second laws of motion of Cauchy* - are not objective, but the couple stress tensor is! We apply here only the result of section 2 that

$$\mathbf{A}\frac{D\mathbf{v}}{Dt} = -\Omega^*(\mathbf{Av}) + \frac{D}{Dt}(\mathbf{Av}) \qquad 3(33)$$

for any vector $\mathbf{v}$. Let us denote

$$\mathbf{V} = \mathbf{A}\frac{D\mathbf{x}}{Dt}, \qquad \mathbf{v} = \frac{D\mathbf{x}}{Dt} \qquad 3(34);$$

the velocities in the inertial frame resolved along the instantaneous axes of the moving frame and with respect to an observer at rest in the moving frame, respectively, we can write

$$\mathbf{A}\frac{D\mathbf{x}}{Dt} = \mathbf{V} = \mathbf{v} - \Omega^*\mathbf{x} \qquad 3(35)$$

and

$$\mathbf{A}\frac{D^2\mathbf{x}}{Dt^2} = \frac{D\mathbf{V}}{Dt} = -\Omega^*\mathbf{V} \qquad 3(36).$$

Our basic dynamical equation can therefore be re-written in the form

$$\rho\ \frac{DV_i}{Dt} - \rho\ \Omega^*_{ij}\ V_j = \partial_j\sigma_{ij} + \rho\ \partial_i V \qquad 3(37).$$

To obtain the second order virial equations in a moving frame, we have only to multiply equation 3(37) by the co-ordinates x_j of the deformed state and integrate over the volume v occupied by the material body.

$$\frac{D}{Dt}\int_v dx\ \rho\ V_i x_j = \int_v dx\ \rho\ V_i v_j + \int_v dx\ \rho\ \Omega^*_{im} V_m x_j + S_{ij} - \Sigma_{ij} + W_{ij} \qquad 3(38).$$

Finally we express V(v).

$$\frac{D}{Dt}\int_v dx\,\rho\,v_i x_j - \frac{D}{Dt}\int_v dx\ \rho\ \Omega^*_{im}x_m x_j = \int_v dx\ \rho\ v_i v_j + \int_v dx\ \rho\ \Omega^*_{im}(v_m x_j - v_j x_m) - \int_v dx\ \rho\ \Omega^*_{im}\Omega^*_{m\ell}x_\ell x_j + S_{ij} - \Sigma_{ij} + W_{ij} \qquad 3(39),$$

or alternatively

$$\frac{D}{Dt}\int_V dX\,\rho\, v_i x_j - \frac{D}{Dt}(\Omega^*_{im} I_{mj}) = 2T_{ij} + S_{ij} - \Sigma_{ij} + W_{ij} - \Omega^*_{ik}\Omega^*_{k\ell} I_{\ell j} + \int_V dx\,\rho\,\Omega^*_{im}(v_m x_j - v_j x_m) \qquad 3(40)$$

Why is this equation so important? As an equation of the type of the moment of the momentum, it balances for a general body of rigid - liquid - elastic - plastic type the different influences. We like to point out that this equation even includes couple stress and dislocations. In the next chapters we will present examples for body displacements of rigid, hydrostatic and elastic type. The inclusion of couple stress is under the influence of magnetohydrodynamical effects, essential.

4. Example 1: Rigid Body Displacement

Let us assume $ds^2 = dS^2$, that is, a rigid body displacement, with no stress $\sigma_{ij} = 0$, no couple stress $\sigma_{ijk} = 0$, $\frac{D}{Dt}\rho = 0$, $v_i = 0$. We apply the second order virial equations 3(40) in a moving frame.

$$-\left(\frac{D}{Dt}\Omega^*_{im}\right) I_{mj} + \Omega^*_{ik}\Omega^*_{k\ell} I_{\ell j} = W_{ij} \qquad 4(1).$$

Thus we have found the classical Eulerian dynamical equation for a rigid body in the form of a second rank tensor formula. The dual vector equation is a result of "antisymmetrization"

$$0 = \delta_{ijk} W_{jk} = -\delta_{ijk}\left(\frac{D}{Dt}\Omega_{jm}\right) I_{mk} + \delta_{ijk}\Omega_{j\ell}\Omega_{\ell m} I_{mk} \qquad 4(2).$$

W_{ij} is symmetric, therefore $\delta_{ijk} W_{jk} = 0$ in our Cartesian notation. Of course equation 2(34) holds:

$$I_{ij}\frac{D\Omega_j}{Dt} + \delta_{ijk}\Omega_j\Omega_\ell I_{k\ell} = 0 \qquad 4(3).$$

We note that $\delta_{ijk}\delta_{pqk} = \delta_{ip}\delta_{jq} - \delta_{iq}\delta_{jp}$. It is important that for a self-gravitating body under no outer moments, the vector equation of the moment is balanced! If we call A, B and C the eigenvalues along the eigen vectors of I_{ij}, we arrive at the familar formula

$$\left.\begin{aligned} A\frac{D\Omega_1}{Dt} - (B - C)\Omega_2\Omega_3 &= 0 \\ B\frac{D\Omega_2}{Dt} - (C - A)\Omega_3\Omega_1 &= 0 \\ C\frac{D\Omega_3}{Dt} - (A - B)\Omega_1\Omega_2 &= 0 \end{aligned}\right\} \qquad 4(4).$$

In the case we have other volume couples, we will find an inhomogeneous system! For a symmetric body, A = B; we will study the displacement in more detail:

$$C \frac{D\Omega_3}{Dt} = 0, \qquad \Omega_3 = \Omega_{30} = \text{const.} \tag{4(5)}$$

$$A \frac{D\Omega_1}{Dt} - (A - C)\, \Omega_{30}\, \Omega_2 = 0 \tag{4(6)}$$

and

$$A \frac{D\Omega_2}{Dt} + (A - C)\, \Omega_{30}\, \Omega_1 = 0 \tag{4(7)}$$

We start with $\Omega_1 = \Omega_{10} \sin \delta t$, $\Omega_2 = \Omega_{10} \cos \delta t$, and

$$\delta = \frac{A - C}{A}\, \Omega_{30} = \left(1 - \frac{C}{A}\right) \Omega_{30} \tag{4(8)}$$

The precession frequency δ is periodical with

$$\boxed{T_p = 2\pi\delta^{-1} = \frac{2\pi A}{(A - C)\Omega_{30}}} \tag{4(9)}$$

With the dynamical parameters A, C, Ω_{30} of the Earth we find $T_p = 10$ months, which differs from the measured Chandler period of 14 months. Elastic-plastic effects cause this defect.

5. Example 2: Hydrostatic Body Displacement of Maclaurin Type

Let us assume $ds^2 \neq dS^2$ for a liquid body, that is the stress is isotropic by $\sigma_{ij} = - p\, \sigma_{ij}$, no couple stress $\sigma_{ijk} = 0$, $s_{ij} = 0$, $\sum_{ij} = - \Pi\, \delta_{ij}$, $D\Omega/Dt = 0$.

We apply the second order virial equations 3(40) in this uniformly rotating frame.

$$2T_{ij} + W_{ij} + \Omega^2 I_{ij} - \Omega_i\, \Omega_k\, I_{kj} + \delta_{ij}\, \Pi + 2\delta_{i\ell m}\, \Omega_m \int_V \mathbf{dx}\, \rho\, u_\ell\, x_j = \frac{D}{Dt} \int \mathbf{dx}\, \rho\, v_i\, x_j \tag{5(1)}$$

Under static conditions when there are *no relative motions*, in the rotating frame considered, and which are of interest, $- v_i = 0$ - it is convenient to choose the x_3 axis to be along the direction of the rotation vetor Ω which gives

$$W_{ij} + \Omega^2 (I_{ij} - \delta_{i3} I_{3j}) = - \delta_{ij}\, \Pi \tag{5(2)}$$

The equilibrium figures of *Maclaurin spheroidal type* represent the solution of equation 5(2) when

1. the configuration is of uniform density; and
2. the rotational axis is further assumed to be an axis of symmetry:

$$W_{11} + \Omega^2 I_{11} = W_{33} = - \delta_{ij}\, \Pi \tag{5(3)}$$

$$W_{11} = W_{22} \tag{5(4)}$$

and

$$I_{11} = I_{22} \tag{5(5)}$$

Let us have a look for solutions of the ellipsoidal type. From classical potential theory we find for the energy potential tensor W_{ij} for a homogeneous ellipsoid

$$\frac{W_{ij}}{\pi G \rho} = -2A_i\, I_{ij} \tag{5(6)}$$

where the moment of inertia tensor is due to

$$I_{ij} = \frac{1}{5} M a_i^2 \delta_{ij} \qquad 5(7)$$

and the mass

$$M = \frac{4}{3} \Pi a_1 a_2 a_3 \qquad 5(8).$$

a_i are the eigenvalues in the eigen directions of an ellipsoidal canonical two-form. The index symbols are defined by

$$A_i = a_1 a_2 a_3 \int_0^\infty du\left[(a_1^2 + u)(a_2^2 + u)(a_3^2 + u)\right)^{-\frac{1}{2}} \qquad 5(9).$$

Inserting for W_{11} and W_{33} gives

$$-2(\pi G\rho)A_1 I_{11} + \Omega^2 I_{11} = -2(\pi G\rho)A_3 I_{33} \qquad 5(10)$$

and

$$\frac{\Omega^2}{\pi G\rho} = 2\left(A_2 - \frac{a_3^2}{a_1^2} A_3\right) \qquad 5(11).$$

If $a_1 = a_2 > a_3$, the integrals defining the A_i's are elementary:

$$A_1 = A_2 = \frac{(1 - e^2)}{e^3} \sin^{-1} e - \frac{1 - e^2}{e^2} \qquad 5(12)$$

and

$$A_3 = \frac{2}{e^2} - \frac{2(1 - e^2)^{\frac{1}{2}}}{e^3} \sin^{-1} e \qquad 5(13),$$

where $e^2 = 1 - a_3^2/a_1^2$, defines the eccentricity of the meridional sections. Substituting for A_1 and A_3 in equation 5(11), we have Maclaurin's formula

$$\frac{\Omega^2}{\pi G\rho} = \frac{2(1 - e)^{\frac{1}{2}}}{e^3} (3 - 2e^2) \sin^{-1} e - \frac{6}{a^2}(1 - e^2) \qquad 5(14),$$

plotted in figure 2.

6. Example 3: Elastic Body Displacement of LOD and Wobble Type

Let us assume $ds^2 \neq dS^2$ for an elastic body, especially within the "Small Displacement Theory" of isotropic type, i.e.,

$$\sigma_{ij} = \lambda(\mathrm{tr}\, e_{k\ell})\, \delta_{ij} + 2\mu\, e_{ij} \qquad 6(1),$$

where λ and μ are Lame's constants, with no couple stress $\sigma_{ijk} = 0$, $S_{ij} = 0$. We apply the second order virial equations 3(40) in a moving frame,

$$\frac{D}{Dt}\int_v dx\, \rho\, v_i x_j - \frac{D}{Dt}(\Omega^*_{im} I_{mj}) = 2T_{ij} - \sum_{ij} + W_{ij} - \Omega^*_{ik}\Omega^*_{k\ell} I_{\ell j} + \int_v dx\, \rho\, \Omega^*_{im}(v_m x_j - v_j x_m) \qquad 6(2)$$

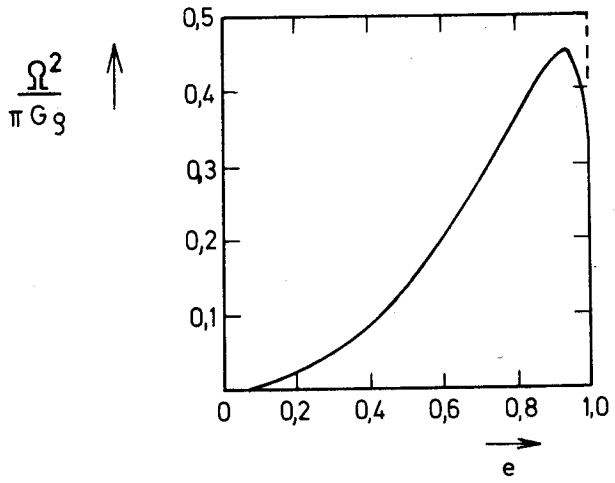

Figure 2. The Square of the Angular Velocity in Units of $\pi G\rho$ along the Maclaurin Sequences

For the data of the Earth: mean density $\rho = 5.514$ g cm^{-3}, $G = 6.674 \times 10^{-8}$ cm^3 g^{-1} sec^{-2}, and $\Omega = 7.292 \times 10^{-5}$ sec^{-1}, the value of $(\Omega^2/\pi G\rho)$ is about 0.025, not too far away from an eccentricity of about 0.00672.

generalizing the Euler - Liouville equations for a deformable body. The global stress tensor is now due to

$$\sum_{ij} = \int_V dX\ \sigma_{ij} = \delta_{ij} \int_V dX\ \lambda(\mathrm{tr}\ e_{k\ell}) + 2\int_V dX\ \mu\ e_{ij} \qquad 6(3)$$

in general, for inhomogeneous elastic bodies, and the Lame's constants λ and μ are functions of the position within the body. Inserting from equation 2(25) of the displacement vector leads to

$$2e_{k\ell} = u_{k;\ell} + u_{\ell;k}, \qquad \mathrm{tr}\ e_{k\ell} = \frac{1}{2}(\partial_1 u_1 + \partial_2 u_2 + \partial_3 u_3) \qquad 6(4).$$

The structure of equation 6(2) is very similar to the structure of the Eulerian dynamical equations for a rigid body. This will be quite obvious if we rewrite equation 6(2)

$$\frac{D}{Dt}\left(-\Omega^*_{im} I_{mj} + \int_V dX\ \rho\ v_i x_j\right) + \int_V dX\ \rho\ \Omega^*_{ik}\left(\Omega^*_{k\ell} I_{\ell j}/M - v_k x_j + v_j x_k\right) = W_{ij} + 2T_{ij} - \sum_{ij} \qquad 6(5).$$

It is very interesting that in the dual vector equation of 5(2), the right hand side quantities W_{ij}, T_{ij}, $\sum_{ij}$ vanish because of their symmetry. Therefore we have to work with equation 6(2)! Of course, this statement is true for the "liquid" equation 5(1), too.

The well known procedure of perturbation theory leads simply to the classical LOD and wobble analysis, but in our case in terms of Lame's constants, avoiding the concept of Love numbers. Finally, if we are only interested in the static situation we will have no relative motions:

$$-\frac{D}{Dt}(\Omega^*_{im} I_{mj}) = -\sum_{ij} + W_{ij} - \Omega^*_{ik}\,\Omega_{k\ell}\,I_{\ell j} \qquad 6(6).$$

For more details of how to solve equation 6(2), the reader is referred to MUNK & MACDONALD (1960, p.38 et seq.).

7. References

BOCCHIO, F. 1970. Su Alcune Applicazioni de Interesse Geodetico delle Connessioni non Simmitriche. *Acad.Naz.Linc.*, Rome,p.343.

CHANDRASEKHAR, S. 1969. *Ellipsoidal Figures of Equilibrium.* Yale University Press, New Haven Conn.

DE WIT, R. 1967. Differential Geometry of nonlinear Continuum Theory of Dislocations. In (KROENER, E ed.) *IUTAM - Symposium on "The Generalized Cosserat Continuum and the Continuum Theory of Dislocations with Applications", Freudenstadt/Stuttgart 1967.* Springer-Verlag, Berlin.

GRAFAREND, E. 1971. The Object of Anholonomity and a Generalized Riemannian Geometry for Geodesy. *Boll.Geof.Teor.Appl.* 13,241.

GRAFAREND, E. 1972. Three Dimensional Geodesy and Gravity Gradients. *Rep.* 174,Dept. of Geodetic Science,The Ohio State University,Columbus Ohio.

GRAFAREND, E. 1973a. Attempts for a Unified Theory of Geodesy. *Boll.geodesia e Scienze Affini* 32, 231.

GRAFAREND, E. 1973b. Gravity Gradients and Three Dimensional Net Adjustments without Ellipsoidal Reference. *Rep.* 202,Dept. of Geodetic Science,The Ohio State University,Columbus Ohio.

GRAFAREND, E. 1973c. *Cartan Frames and a Foundation of Physical Geodesy.* International Summer School in the Mountains, Ramsau Austria.

GRAFAREND, E & SCHAFFRIN, B 1973. Unbiased Free Net Adjustment. *Surv.Rev.* (in press).

GROSSMAN, N. 1973. Marussi Theorem and Holonomic Measurables. *J.geophys.Res.* (in press)

HOTINE, M. 1969. Mathematical Geodesy. *ESSA Monograph* 2,Washington DC.

KROENER, E. 1960. *Arch.Rat.mech.Anal.* 4,273.

MARUSSI, A. 1949. Fondements de Geometrie Differentielle Absolue du Champ Potential Terrestre. *Bull.géodes.* 14,411.

MUNK, W.H. & MACDONALD, G.J.F. 1960. *The Rotation of the Earth.* Cambridge University Press.

SCHOUTEN, J.A. 1954. *Ricci-Calculus.* Berlin.

8. Discussion

LAMBECK: I am a little disturbed by your dislike for the Love numbers. It is generally recognized that they offer very convenient ways of describing integral effects of the Earth's elastic (and anelastic) properties, in particular, when the details of the distribution of the elastic parameters within the Earth are not adequately known. In this sense they act as transfer parameters between observations and theory. Once observed, they then have to be interpreted in terms of the physics of the Earth. I agree that due to the multiplicity of types of Love numbers, this question of interpretation is most difficult.

GRAFAREND: This approach is rigorous if you accept stress-strain relationships of this kind. The problem of Love numbers is that they are really intuitive, and specialists introduce concepts like non-linear Love numbers. The original paper of Love gives a number of definitions of Love numbers. The problem of Love numbers is that they depend on the model being used.

KAULA: The Love numbers are rigorous for spherical Earth models. For a Maxwell rheology you can use complex Love numbers. More realistic rheologies may lead to more complicated Love operators.

GRAFAREND: Right. If one had spherical symmetry the problem would be solved. Why is no one working with the classical approach used in physics where you have continuum mechanics and where, for example, you refer to elasticity, you have Lamé's constants? Everyone in seismology is working with elastic constants. I don't see too many reasons why we need Love numbers for this purpose.

LAMBECK: You have oversimplified the problem. In seismology one measures directly the Lame parameters as a function of position and Love numbers do not enter into the problem. For tidal loading and rotational studies, however, one must also consider oceanic, atmospheric and liquid core effects and these cannot usually be treated in the same way as can the elastic mantle. In particular, these fluid effects can differ depending on the problem. For example, whether or not the axis of rotation is variable or whether the forcing function has a frequency close to the free oscillation of the fluid part. Your approach is an interesting one but I do not see how you can include these various effects with any more certitude than one can interpret the Love numbers now.

WHITTEN (Chairman): GRAFAREND told us he has worked two years on this paper. We should not expect to grasp its full meaning in a few minutes. Unfortunately we have to move on to the next paper .....

MORGAN, P.
Division of National Mapping
Department of Minerals & Energy
Canberra ACT 2600
Australia

Proc. Symposium on Earth's Gravitational Field & Secular Variations in Position (1973), 660-673.

CRUSTAL VELOCITY AND STRAIN

ABSTRACT

Historically geodesists have measured displacements relative to an assumed or known fixed position and made these observations available for the computation of other geodetic/geophysical parameters. Strain analysis performed in such a manner is usually accomplished in a Lagrangian system of co-ordinates and results in numerous approximations, many of which break down at, or close by, yield point which accompanies earthquakes.

A more powerful approach appears to be via the determination of velocity fields. In this approach a particle or point is tracked through the prevailing velocity field, which may not be constant with time. The system of co-ordinates used in such an analysis is Eulerian and has the immediate advantage that the differential of the velocity field, the Jacobian, contains both the rotationally symmetric part and anti-symmetric part, without approximation of the strain rate tensor.

A number of methods of determining the strain rate tensor from observations over meso and maro areas are developed with the view of determining and monitoring the state of strain of an area, as it is changes of state that appear to be most important. Continental motion most probably can be viewed as a continuous process with peaks in state of strain which must be relieved by violent crustal motions.

1. Preamble

The historical role of geodesy, the study of the size and shape of the Earth, was directed towards the attainment of national, and just lately global, networks which adequately describe, for most mapping purposes, the parametric relationship between points in such networks as well as the surface on which these points lie. These networks are essential for national mapping programs, communications and the distribution of essential commodities. Having fulfilled these requirements, at least in the so-termed developed sector, geodesy was in danger of having completed its mission just as physics was in the time of Lord Kelvin.

In today's world, geodesy is no longer the simple study of the Earth's size and shape but also of secular changes that take place in its size and shape.

It can be argued that all changes and advancements in the applied sciences, as distinct from the pure sciences, are derived from a basic need or series of such needs. In our present world a basic need is the understanding of volcanic and seismic activity and the possibly interrelated phenomena of polar motion, particularly Chandlerian motion, with the view of predicting such events on a global as well as a local scale.

This paper addresses itself to the gathering and possible interpretation of suitable geodetic observations for investigations into the secular nature of the behaviour of the planet Earth under the

assumption that descriptive parameters are not constant with time, nor are they constant in space.

2. An Introduction to Elastic Theory and Crustal Movement

2.1 The Strain Tensor

Consider a general spatial region over which a geodetic network is laid. The region is initially unstressed and a general point in the area has arbitrarily assigned to it co-ordinates

$$X_p = \begin{pmatrix} x \\ y \\ z \end{pmatrix}_p$$

in the geocentric system. The squared length of a differential element is therefore represented as follows (BORG 1963)

$$d\ell_p^2 = dx^2 + dy^2 + dz^2 = dX_p^T \cdot dX_p \qquad (1).$$

If the area is now subjected to strain such that this general point moves relative to the origin of the system, then its new position, X_1, can be expressed as a function of the old position as follows:

$$X_1 = X_p + \begin{pmatrix} h_1(X_p) \\ h_2(X_p) \\ h_3(X_p) \end{pmatrix} = G(X_p) \qquad (2).$$

The differential element of length must reflect this change and a state of strain is introduced as a result of changes in the differential element. This state of strain is defined as the difference in square length, viz, state of strain, given by

$$\text{State of Strain} = dX_1^T \cdot dX_1 - dX_p^T \cdot dX_p \qquad (3),$$

where the differential element dX_1 can be expressed, by virtue of the above functional dependency, as:

$$dX_1 = J\,dX_p = \begin{pmatrix} \frac{\partial g_1(X_p)}{\partial x_p} & \frac{\partial g_1(X_p)}{\partial y_p} & \frac{\partial g_1(X_p)}{\partial z_p} \\ \frac{\partial g_2(X_p)}{\partial x_p} & \frac{\partial g_2(X_p)}{\partial y_p} & \frac{\partial g_2(X_p)}{\partial z_p} \\ \frac{\partial g_3(X_p)}{\partial x_p} & \frac{\partial g_3(X_p)}{\partial y_p} & \frac{\partial g_3(X_p)}{\partial z_p} \end{pmatrix} \cdot \begin{pmatrix} dx_p \\ dy_p \\ dz_p \end{pmatrix} \qquad (4).$$

It is convention to refer to J as the Jacobian although the more common geodetic nomenclature is the partial differential matrix of the function with respect to the parameters.

Substitution of equation set 4 into equation set 3 yields after simplification:

$$\text{State of Strain} = dX_p^T\,(J^T \cdot J - I)\,dX_p \qquad (5).$$

The important quantity here is $J^T \cdot J - I$, which is directly proportional to the classically defined strain tensor η:

$$\eta = \tfrac{1}{2}(J^T \cdot J - I) \qquad (6)$$

It is important to note that η has been derived without any restrictions and may be used for large strains, as all second order terms are included. In particular it is to be noted that the co-ordinate system is Lagrangian rather than the classical Eulerian system.

Expounding upon the last statement, it has been assumed historically that in equation set 2, there is no essential difference between X_p and X_1 and that all displacements are small linear displacements. That is, the differentials are performed about the new point rather than the old point. In essence this can be interpreted as follows:

> The Eulerian system specifies the conditions at each point in the deformed region whereas the Lagrangian system attempts to follow the motion of a particle, the survey peg, in the deformed region, thereby relating all subsequent positions by functions to the initial position.

Of necessity the changes must be small if the Eulerian system is to be used as second order terms are defined to be zero, that is, the derived tensor η has as its symmetric components those elements which make up the Eulerian rotationally symmetric strain tensor. The non symmetric terms are the second order effects. The diagonal elements of η represent the elongation/contraction of the network while the off-diagonal terms refer specifically to the non-uniform shear deformation to which the region is being subjected.

2.2 The Stress Tensor

When a region is subject to strain (deformation), it is being elongated/contracted or sheared by forces acting on the boundaries or faces of the region. These forces must have resultant forces, which are manifested by deformation. The stress that a region undergoes during the deformation is defined to be equal to the force acting per unit area, i.e.,

$$\text{Stress} = \frac{\partial \text{ Force}}{\partial \text{ Area}} = \frac{\partial F}{\partial A} = \frac{\partial}{\partial A} F \, .$$

Generalizing this definition to three-dimensional forces,

$$F = \begin{pmatrix} F_x \\ F_y \\ F_z \end{pmatrix} \quad \text{and, after considering a multifaced body for which} \quad A = \begin{pmatrix} A_x \\ A_y \\ A_z \end{pmatrix},$$

the following stress tensor is obtained:

$$T = \left(\frac{\partial}{\partial A} \right) \cdot F^T = \begin{pmatrix} \frac{\partial}{\partial A_x} \\ \frac{\partial}{\partial A_y} \\ \frac{\partial}{\partial A_z} \end{pmatrix} \cdot \left(F_x, F_y, F_z \right) \qquad (7),$$

that is,

$$T = \begin{pmatrix} \frac{\partial F}{\partial A_x^x} & \frac{\partial F}{\partial A_x^y} & \frac{\partial F}{\partial A_x^z} \\ \frac{\partial F}{\partial A_y^x} & \frac{\partial F}{\partial A_y^y} & \frac{\partial F}{\partial A_y^z} \\ \frac{\partial F}{\partial A_z^x} & \frac{\partial F}{\partial A_z^y} & \frac{\partial F}{\partial A_z} \end{pmatrix} = \begin{pmatrix} \sigma_x & \tau_{xy} & \tau_{xz} \\ \tau_{yx} & \sigma_y & \tau_{yz} \\ \tau_{zx} & \tau_{zy} & \sigma_z \end{pmatrix} \qquad (8).$$

This strain tensor is symmetric by virtue of the necessary static equilibrium and moment conditions that must hold for differential elements. Consequently it can be resolved into principal components

if necessary. In particular the main diagonal elements represent normal forces while off-diagonal elements represent shearing forces.

2.3 The Strain Rate Tensor

The strain and stress tensors reflect the state existing in a region after an initial epoch at which the region was unstrained. This is a non-recoverable epoch or condition and, since these states may be continually changing, it is also necessary to consider changes in these tensors. That is the secular change of the strain and stress tensors is of great interest in determining the state of the Earth.

Consider only the variation that is the first order differential of the strain tensor, since the stress tensor is related to it by Hooke's law. Then, to first order accuracy, the following holds for equation set 6:

$$\delta\eta = \tfrac{1}{2}[(\delta J^T)\, J + J^T\, (\delta J)] \qquad (9).$$

From equation set 4, it is evident that the basic definition of the Jacobian is

$$J^T = \begin{pmatrix} \frac{\partial}{\partial x} \\ \frac{\partial}{\partial y} \\ \frac{\partial}{\partial z} \end{pmatrix} \cdot G^T(X_p).$$

Under the assumption that the second derivatives are continuous and the variables are independent, then

$$J^T = \begin{pmatrix} \delta\frac{\partial}{\partial x} \\ \delta\frac{\partial}{\partial y} \\ \delta\frac{\partial}{\partial z} \end{pmatrix} \cdot G^T(X_p) = \begin{pmatrix} \frac{\partial}{\partial x} \\ \frac{\partial}{\partial y} \\ \frac{\partial}{\partial z} \end{pmatrix} \cdot \delta G^T(X_p) \qquad (10).$$

By definition $G(X_p)$ is a spatial field of points. At the initial epoch, X_p and X_1 are coincident but the survey point is being subjected to pressure to force a separation. That is, it has velocity and possibly acceleration which may be time dependent.

Now

$$G^T(X_p) = \frac{\partial G^T}{\partial X_p} \cdot \delta X_p + \frac{\partial G^T}{\partial t} \cdot \delta t.$$

From the above definition,

$$\frac{\partial G^T}{\partial X_p} \cdot \delta X_p = 0,$$

and hence

$$G^T(X_p) = \dot{G} \cdot \delta t.$$

Consequently

$$\delta J^T = \begin{pmatrix} \frac{\partial}{\partial x} \\ \frac{\partial}{\partial y} \\ \frac{\partial}{\partial z} \end{pmatrix} \cdot G^T\, \delta t = \dot{J}\, \delta t \qquad (11).$$

Substituting equation set 11 into equation sets 9, and noting that $J = I$ by virtue of the fact that $\begin{bmatrix} h_1(X_p) \\ h_2(X_p) \\ h_3(X_p) \end{bmatrix}$ of equation set 2 must be replaced by $\begin{bmatrix} h_1(t) \\ h_2(t) \\ h_3(t) \end{bmatrix}$, then equation set 9 reduces to the following well known equation which defines the strain rate tensor, also referred to as the rate of deformation matrix:

$$\frac{\delta \eta}{\delta t} = \dot{\eta} = \tfrac{1}{2}(\dot{J}^T + \dot{J}) \qquad (12).$$

Thus at this stage it becomes practical to solve for those forces and/or stresses that control crustal movement, and their secular changes. Elastic theory is outside the scope of these discussions which will now centre on how best to obtain $G(X_p)$. Full discussions on elastic theory have been presented by TIMOSHENKO & GOODIER (1951), LOVE (1920) and SOKOLNIKOFF (1956).

3. The Photogrammetric Model

Using the notation indicated in section 7.2, the well known collinearity condition equation can be expressed as follows:

$$x_p - x_o = - f[M_1(X_p - X_o)/M_3(X_p - X_o)]$$

and

$$y_p - y_o = - f[M_2(X_p - X_o)/M_3(X_p - X_o)] \qquad (13).$$

The augmentation of these equations to accept the velocity concept is conceptually very simple since the following definition can be made:

$$X_1 = X_p + V_p(t)$$

and as a consequence X_1 is substituted in the above for X_p.

The solution of the augmented collinearity condition equations is in accordance with the normal conventions and procedures. In particular it can be expected that some ground survey will have taken place and hence some additional observations on the unknown parameter set will be available. This can be represented as:

$F(L_a^1, X_a) = 0$ for the image space, and $G(L_a^2, X_a) = 0$ for the object space.

This is the classical dual observation set on the same unknown parameters which was fully treated by BROWN (RCA54), except that additional observations are on the unknown object space parameters associated with ground points and not on the camera station and its orientation.

The classical solution of this problem can be expressed as follows, using the notation of UOTILA (1967)

$$\begin{bmatrix} A_1^T(B_1P_1^{-1}B^T)^{-1}A_1 & A_2^T \\ A_2 & -B_2P_2^{-1}B_2^T \end{bmatrix} \cdot \begin{bmatrix} X \\ -K_2 \end{bmatrix} = \begin{bmatrix} -A_1(B_1P_1^{-1}B^T)^{-1}W_1 \\ -W_2 \end{bmatrix} \qquad (14).$$

In an effort to determine the conditions under which a solution can be obtained, it is more instructive to introduce the fixed and/or known points into the model by means of the following conditions:

$$F(L_a^1, X_a) = 0, \qquad G(L_a^2, X_a) = 0, \qquad \text{and} \qquad H(X_a) = 0 \tag{15}$$

The solution of the system is an augmented form of equation set 14:

$$\begin{bmatrix} A_1^T(B_1P_1^{-1}B^T)^{-1}A_1 & A_2^T & C^T \\ A_2 & -B_2P_2^{-1}B_2^T & 0 \\ C & 0 & 0 \end{bmatrix} \cdot \begin{bmatrix} X \\ -K_2 \\ -K_c \end{bmatrix} = \begin{bmatrix} -A_1^T(B_1P_1^{-1}B^T)^{-1}W_1 \\ -W_2 \\ -W_3 \end{bmatrix} \tag{16}$$

where

$$C = \frac{\partial G}{\partial \text{parameter}} .$$

It is to be noted that for observation equation work, B = I, resulting in considerable simplification of the above. The necessary and sufficient condition for solution is:

$$(2n + m) + (p + q) > (2n + m) > (p + q),$$

where
- n is the number of photographic images observed,
- m is the number of ground survey observations,
- p is the number of unknown parameters, and
- q is the number of conditions being impressed.

Unfortunately there is also a stability condition that has to be met if a numerical value is to be obtained. That is, if the p+q sector is ill-determined then this has the effect that in the above equation, the first condition is not satisfied.

A full exposé of methods of handling the analytic photogrammetric problem may be found in the various publications of Brown.

4. The Geodetic Model

The augmentation of geodetic short arc formulae to accommodate velocity terms is similar in theory to that proposed in the photogrammetric model except that the observations cannot be made at a single epoch. Consequently in a dynamic environment the same spatial point cannot be observed at a number of different epochs and allowances must be made for this fact.

The direct problem is normally associated with the determination of the point under observation, P_2, from an initial point P_1 It is characterized in this context by the following relationship:

$$\begin{bmatrix} \phi_2 \\ \lambda_2 \\ A_{21} \end{bmatrix} = F(\phi_1, \dot{\phi}_1, \lambda_1, \dot{\lambda}_1, A_{12}, S, t).$$

The inverse problem is associated with an assumed knowledge of station values and the need to deduce the parameters specifying the separation. It is characterized as follows :

$$\begin{bmatrix} S \\ A_{12} \\ A_{21} \end{bmatrix} = G(\phi_1, \dot{\phi}_1, \lambda_1, \dot{\lambda}_1, \phi_2, \dot{\phi}_2, \lambda_2, \dot{\lambda}_2, t).$$

It is this form which is equivalent to the mathematical model that is normally used in least squares solutions $L_a = F(X_a)$. However it is considered important to derive both cases. The method used follows that developed by CLARK (1963) in proving the Puissant form of the direct and indirect problem.

4.1 The Direct Geodetic Problem

Consider now figure 1, the equivalent sphere polar triangle. The spatial co-ordinates of the two points P_1 and P_2 are functions of time in the aforementioned prescribed manner. Applying the cosine law to the observed triangle P_1-P_2-Pole, (Δ-P_1-P_2-Pole), and simplifying by the application of double angle formulae yields :

$$\sin(\phi_2 + \dot{\phi}_2\Delta t) = \sin(\phi_1 + \dot{\phi}_1\Delta t)\cdot\cos\left(\frac{S}{N_E}\right) + \cos(\phi_1 + \dot{\phi}_1\Delta t)\cdot\sin\left(\frac{S}{N_E}\right)\cos A_{12} \qquad (19).$$

Defining $\phi_2 = \phi_1 + d\phi$, and expanding equation 19 by means of double angle expressions yields:

$$\sin(\phi_1+ \dot{\phi}_2\Delta t)\cdot\cos d\phi + \sin d\phi\cdot\cos(\phi_1+ \dot{\phi}_2\Delta t) = [\sin\phi_1\cdot\cos(\dot{\phi}_1\Delta t) + \sin(\dot{\phi}_1\Delta t)\cdot\cos\phi_1]\cdot\cos\left(\frac{S}{N_E}\right)+$$

$$[\cos\phi_1\cdot\cos(\dot{\phi}_1\Delta t) - \sin\phi_1\cdot\sin(\dot{\phi}_1\Delta t)]\cdot\sin\left(\frac{S}{N_E}\right)\cdot\cos A_{12} \qquad (20).$$

Now the left hand side of equation 20 can be expressed, after trigonometrically expanding the double angles, followed by a power series expansion of all small quantities to the third order and re-arrangement as:

$$\sin\phi_1\cdot\left(1 - \frac{(\dot{\phi}_2\cdot\Delta t)^2}{2} + \frac{\cos\phi_1}{\sin\phi_1}(\dot{\phi}_2\cdot\Delta t)\right) + \cos\phi_1\cdot d\phi\left(1 - \frac{(\dot{\phi}_2\cdot\Delta t)^2}{2} - \frac{\sin\phi_1}{\cos\phi_1}(\dot{\phi}_2\cdot\Delta t)\right) -$$

$$\sin\phi_1\cdot\frac{(d\phi)^2}{2}\left(1 - \frac{(\dot{\phi}_2\cdot\Delta t)^2}{2} + \frac{\cos\phi_1}{\sin\phi_1}(\dot{\phi}_2\cdot\Delta t)\right) - \cos\phi_1\frac{(d\phi)^3}{6}\cdot\left(1 - \frac{(\dot{\phi}_2\cdot\Delta t)^2}{2} - \frac{\sin\phi_1}{\cos\phi_1}(\dot{\phi}_2\cdot\Delta t)\right) \qquad (21).$$

Treating the right hand side of equation 20 in the same manner yields the following:

$$\sin\dot{\phi}_1\cdot\left(1 - \frac{(\dot{\phi}_1\cdot\Delta t)^2}{2} + \frac{\cos\phi_1}{\sin\phi_1}(\dot{\phi}_1\cdot\Delta t)\right) + \frac{S}{N_E}\cdot\cos A_{12}\cdot\cos\phi_1\cdot\left(1 - \frac{(\dot{\phi}_1\cdot\Delta t)^2}{2} - \frac{\sin\phi_1}{\cos\phi_1}(\dot{\phi}_1\cdot\Delta t)\right) -$$

$$\frac{S^2}{2N_E^2}\cdot\sin\phi_1\cdot\left(1 - \frac{(\dot{\phi}_1\cdot\Delta t)^2}{2} + \frac{\cos\phi_1}{\sin\phi_1}(\dot{\phi}_1\cdot\Delta t)\right) - \frac{S^3}{6N_E^3}\cdot\cos\phi_1\cdot\cos A_{12}\cdot\left(1 - \frac{(\dot{\phi}_1\cdot\Delta t)^2}{2} - \frac{\sin\phi_1}{\cos\phi_1}(\dot{\phi}_1\cdot\Delta t)\right) \qquad (22).$$

Now defining

$$1 - \frac{(\dot{\phi}_1\cdot\Delta t)^2}{2} - \frac{\sin\phi_1}{\cos\phi_1}\cdot(\dot{\phi}_1\cdot\Delta t) = I_1 \; ; \qquad 1 - \frac{(\dot{\phi}_2\cdot\Delta t)^2}{2} - \frac{\sin\phi_1}{\cos\phi_1}\cdot(\dot{\phi}_2\cdot\Delta t) = I_2 \; ;$$

$$1 - \frac{(\dot{\phi}_1\cdot\Delta t)^2}{2} + \frac{\sin\phi_1}{\cos\phi_1}\cdot(\dot{\phi}_1\cdot\Delta t) = J_1 \; ; \text{ and } \; 1 - \frac{(\dot{\phi}_2\cdot\Delta t)^2}{2} + \frac{\sin\phi_1}{\cos\phi_1}\cdot(\dot{\phi}_2\cdot\Delta t) = J_2 \qquad (23),$$

and introducing these definitions yields, after re-arrangements the following expression for $d\phi$, the difference in latitude at some standard epoch:

$$d\phi = \tan\phi_1\cdot\frac{J_2}{2I_2}\cdot(d\phi)^2 + \frac{(d\phi)^3}{6} + \frac{S}{N_E}\cdot\cos A_{12}\cdot\frac{I_1}{I_2} - \frac{S^2}{2N_E^2}\cdot\tan\phi_1\cdot\frac{J_1}{J_2} - \frac{S^3}{6N_E^3}\cdot\cos A_{12}\cdot\frac{I_1}{I_2} + \tan\phi_1\frac{J_1 - J_2}{I_2} \qquad (24).$$

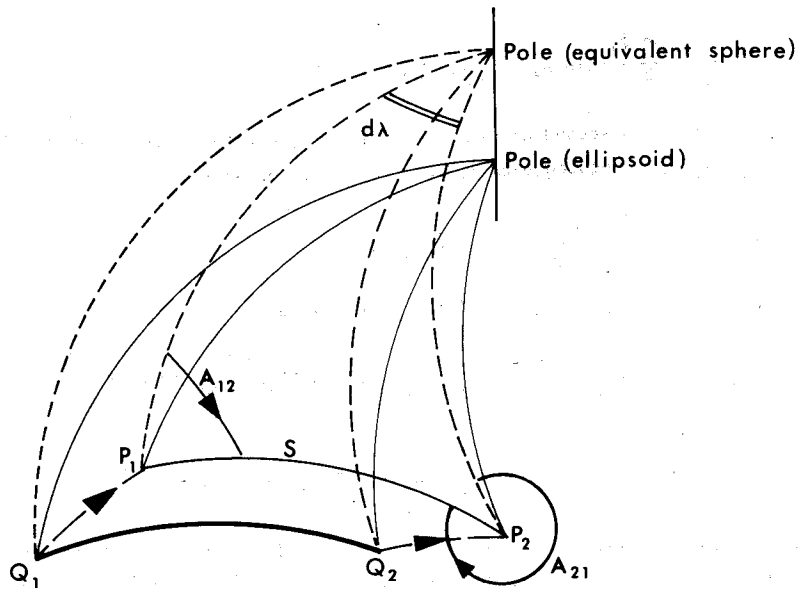

$$P_1 = Q_1 + \begin{bmatrix} \dot{\phi}_1 \cdot \Delta t \\ \dot{\lambda}_1 \cdot \Delta t \end{bmatrix} \qquad P_2 = Q_2 + \begin{bmatrix} \dot{\phi}_2 \cdot \Delta t \\ \dot{\lambda}_2 \cdot \Delta t \end{bmatrix}$$

Figure 1: The Polar Triangles at Observation and Standard Epoch

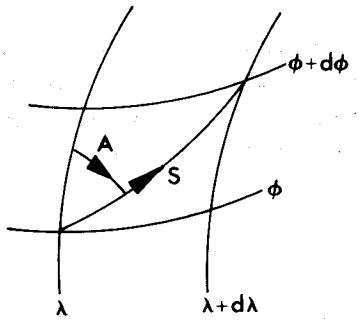

Figure 2: The Differential Figure

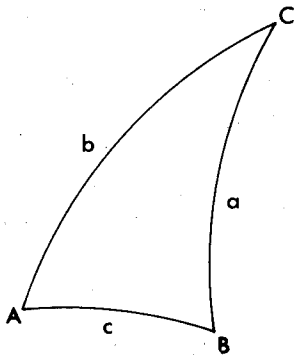

Figure 3: The Spherical Triangle

Consider now the differential geodetic figure - figure 2 - from which the relationship

$$d\phi = \frac{S}{N_E} \cdot \cos A_{12}$$

is derived. When substituted into equation 24, the following relationship is obtained under the additional initial assumption that $I_1 = I_2 = J_1 = J_2 = 1$:

$$d\phi = \frac{S}{N_E} \cdot \cos A_{12} - \frac{S^2}{N_E^2} \cdot \frac{\tan \phi_1}{2} \cdot \sin^2 A_{12} - \frac{S^3}{6N_E^3} \cdot \cos A_{12} \cdot \sin^2 A_{12} \qquad (25).$$

Now neglecting terms higher than second order, since their contribution is less than 5×10^{-6} for a 100 km line, then the following updated expression for $d\phi$ is obtained:

$$d\phi = \frac{S}{N_E} \cdot \cos A_{12} - \frac{S^2}{2N_E^2} \tan \phi_1 \sin^2 A_{12},$$

which is re-substituted into equation 24, yielding after simplification:

$$d\phi = \frac{S}{N_E} \cdot \cos A_{12} \cdot \frac{I_1}{I_2} - \frac{\tan \phi_1}{2} \cdot \frac{S^2}{N_E^2} \cdot \left(\frac{J_1}{I_2} - \frac{J_2}{I_2} \cos^2 A_{12} \right) - \frac{S^3}{6N_E^3} \cdot \cos A_{12} \cdot \left(\frac{I_1}{I_2} - 1 + \sin^2 A_{12} + 3 \sin^2 A_{12} \cdot \tan^2 \phi_1 \cdot \frac{J_2}{I_2} \right) + \tan \phi_1 \cdot \left(\frac{J_1 - J_2}{I_2} \right) \qquad (26).$$

Under the assumption that the velocity field is not too irregular and that we are considering lines less than 100 km long, the definition equation set 23 can be used to simplify equation 26 if $I_1 \sim I_2$ and $J_1 \sim J_2$. Under these assumptions, it reduces to:

$$d\phi = \frac{S}{N_E} \cdot \cos A_{12} \cdot \left(\frac{I_1}{I_2} \right) - \frac{\tan \phi_1}{2} \cdot \frac{S^2}{N_E^2} \cdot \frac{\sin^2 A_{12}}{I_2} + \tan \phi_1 \cdot \left(\frac{J_1 - J_2}{I_2} \right) - \frac{S^3}{6N_E^3} \cdot \cos A_{12} \sin^2 A_{12} \cdot \left(1 + 3 \tan^2 \phi_1 \cdot \frac{J_2}{J_1} \right) \qquad (27).$$

It is now necessary to transfer from the equivalent sphere to the ellipsoid; i.e., the spherical distance $N_E d\phi$ must be converted into an ellipsoidal meridian section of equivalent length. Mathematically, the following must hold:

$$N_E \, d\phi_{sphere} = M_m \, d\phi_{ellipse} \qquad (28).$$

Before accomplishing this, it is to be remembered that N_E is the radius of the equivalent sphere at point P_2 and $M_m d\phi_{ellipse}$ best defines the meridional arc if M_m is evaluated at the midpoint of the arc, i.e., at the latitude $\phi_1 + \frac{1}{2}d\phi$. To get at this unknown point, it is necessary to determine the variation of M_m at P_1 and then to approach it by the application of the differential quantity $\frac{1}{2}\delta\phi$. To the first order this can be represented as:

$$M_m = M_1 + \frac{\partial M}{\partial \phi} \frac{\delta \phi}{2}.$$

But

$$M = a(1 - e^2 \sin^2 \phi)^{-3/2} \cdot (1 - e^2) = \frac{a(1 - e^2)}{W^{3/2}},$$

and hence

$$\frac{\partial M}{\partial \phi} = \frac{3M \cdot (e^2 \cdot \sin \phi \cdot \cos \phi)}{W^2}$$

which yields the following value M_m at the desired point:

$$M_m = M_1 \cdot \left(1 + \frac{3}{2W^2} \cdot (e^2 \cdot \sin \phi_1 \cdot \cos \phi_1) \cdot \delta\phi \right) \qquad (29)$$

or, in terms of $1/M_m$ after binomial expansion:

$$\frac{1}{M_m} = \frac{1}{M_1} \cdot \left(1 - \frac{3}{2W^2} (e^2 \cdot \sin \phi_1 \cdot \cos \phi_1) \cdot \delta\phi \right) \qquad (30).$$

Unfortunately the quantity $\delta\phi$ is the unknown and steps will have to be taken to overcome it. This can be achieved in an iterative manner as follows:

$$d\phi = \frac{S}{M_1}\cdot\cos A_{12}\,\frac{I_1}{I_2} - \frac{\tan\phi_1}{2}\,\frac{S^2}{N_1M_1}\,\frac{\sin^2A_{12}}{I_2} - \frac{S^3}{6N_1^2M_1}\cdot\cos A_{12}\cdot\sin^2A_{12}\cdot\left(1 + 3\tan^2\phi_1\,\frac{J_2}{I_2}\right) +$$

$$\frac{N_1}{M_1}\cdot\tan\phi_1\cdot\left(\frac{J_1 - J_2}{I_2}\right) - \frac{3}{2W_1^2}\cdot\left(e^2\cdot\sin\phi_1\cdot\cos\phi_1\right)\cdot\delta\phi^2 \qquad (31),$$

where

$$\delta\phi = \frac{S}{N}\cdot\cos A_{12}\cdot\frac{I_1}{I_2} - \frac{\tan\phi_1}{2}\cdot\frac{S^2}{N_1^2}\cdot\frac{\sin^2A_{12}}{I_2} - \frac{S^3}{6N_1^3}\cdot\cos A_{12}\cdot\sin^2A_{12}\cdot\left(1 + 3\tan^2\phi_1\cdot\frac{J_2}{I_2}\right) + \tan\phi_1\cdot\left(\frac{J_1 - J_2}{I_2}\right) \qquad (32).$$

The separation in longitude between P_1 and P_2 at the initial epoch must now be considered. Referring to figure 1:

$$d\lambda = \lambda_{P_2} - \lambda_{P1} = \lambda_2 + \dot\lambda_2\cdot\Delta t - \lambda_1 - \dot\lambda_1\cdot\Delta t = \lambda_2 - \lambda_1 + (\dot\lambda_2 - \dot\lambda_1)\cdot\Delta t = d\lambda + d\dot\lambda\cdot\Delta t \qquad (33).$$

Applying the sine rule to $\Delta - P_2 - P_1 -$ Pole the following relationship which implies an equivalent sphere to the ellipsoid at P_2, as well as the equivalence of spherical and ellipsoidal azimuths, is obtained:

$$\frac{\sin(d\lambda)}{\sin\left(\frac{S}{N_2}\right)} = \frac{\sin A_{12}}{\cos(\phi_2 + \dot\phi_2\cdot\Delta t)} \qquad (34).$$

Substitution of equation 33 into this and simplification after expansion will yield the following closed form which pre-supposes the solution of the latitude problem:

$$d\lambda + d\dot\lambda\cdot\Delta t = \arcsin\left(\sin\left(\frac{S}{N_2}\right)\frac{\sin A_{12}}{\cos(\phi_2 + \dot\phi_2\cdot\Delta t)}\right) \qquad (35).$$

It may be convenient, although unnecessary at this stage, to expand equation 35 by a power series formula.

Finally the back azimuth must be computed. The technique for the determination is similar to that developed for latitude and longitude, in that equivalent spheres are used. Also the solution is dependent on a knowledge of $d\phi$ and $d\lambda$ and since it is assumed that $\dot\phi_i$ and $\dot\lambda_i$ are known, the method can be used for a wide variety of back azimuths in addition to the back azimuth of the observed section.

Referring to figure 3, the following cyclic spherical relationships are formed:

$$\frac{\tan\frac{1}{2}(a + b)}{\tan\frac{1}{2}c} = \frac{\cos\frac{1}{2}(A - B)}{\cos\frac{1}{2}(A + B)} \quad ; \text{ and } \quad \frac{\tan\frac{1}{2}(A + B)}{\cot\frac{1}{2}c} = \frac{\cos\frac{1}{2}(a - b)}{\cos\frac{1}{2}(a + b)} \qquad (36).$$

Substitution of the necessary parameters takes place, usually into equation 36, together with the condition that:

$$\tfrac{1}{2}(A + B) = \tfrac{1}{2}(A_{12} + 360 - A_{21}) = \tfrac{1}{2}(A_{12} + 180 - A_{12} - dA),$$

where $dA = A_{21} - A_{12} - 180,$

i.e.,

$$\tan \tfrac{1}{2}(A + B) = \tan\left(90 - \frac{dA}{2}\right) = \cot\left(\frac{dA}{2}\right).$$

After manipulation and simplification, the following form, which may be subjected to power series expansions, results:

$$dA = 2 \arctan\left\{\frac{\sin[\frac{1}{2}(\phi_1 + \dot{\phi}_1 \cdot \Delta t + \phi_2 + \dot{\phi}_2 \cdot \Delta t)]}{\cos[\frac{1}{2}(\phi_1 + \dot{\phi}_1 \cdot \Delta t - \phi_2 - \dot{\phi}_2 \cdot \Delta t)]} \cdot \tan(d\lambda + d\dot{\lambda} \cdot \Delta t)\right\} \tag{37}.$$

4.2 The Inverse Geodetic Problem

The inverse geodetic problem by Puissant type equations cannot be stated in explicit terms. It is therefore necessary to approach the problem in an iterative manner involving much initial simplification.

Expand equation 35 by power series to yield:

$$d\lambda + d\dot{\lambda} \cdot \Delta t = \frac{S}{N_2} \cdot \sin A_{12} \cdot \sec(\phi_2 + \dot{\phi}_2 \cdot \Delta t) \cdot \left\{1 - \frac{S^2}{6N_2^2} \cdot \left[1 - \sin^2 A_{12} \cdot \sec^2(\phi_2 + \dot{\phi}_2 \cdot \Delta t)\right]\right\} \tag{38},$$

and degenerate this equation by use of the fact that $S^2/(6N_2^2) << 1$, of the order of 6×10^{-5} for a 50 km line, into

$$S \sin A_{12} = (d\lambda + d\dot{\lambda} \cdot \Delta t) \cdot \cos(\phi_2 + \dot{\phi}_2 \cdot \Delta t) \cdot N_2 \tag{39}.$$

Consider now equation 32 which can also be degenerated by approximation into:

$$d\phi = \frac{S}{M_1} \cdot \cos A_n \cdot \frac{I_1}{I_2} \tag{40}.$$

Substitution of this first order equation into equation 39 yields:

$$\tan A_{12} = \frac{(d\lambda + d\dot{\lambda} \cdot \Delta t)}{d\phi} \cdot \frac{I_1}{I_2} \cdot \frac{N_2}{M_1} \cos(\phi_2 + \dot{\phi}_2 \cdot \Delta t).$$

S may now be determined from either equation 39 or equation 40. Using these values of S and A_{12}, an updated value of $S \cdot \sin A_{12}$ is computed from equation 38, and similarly $S \cdot \cos A_{12}$ from equation 31. The procedure is cycled until sufficient accuracy is obtained, oscillating between the alternative equations for efficiency of convergence.

The final quantity A_{21} is directly determined from a knowledge of dA as outlined in the direct geodetic problem.

4.3 General Remarks on the Geodetic Model

The equations and methods developed in this section are far from satisfactory for incorporation into an adjustment scheme as it is a non-trivial matter to obtain the partial derivatives or to form observation equations directly. A number of alternatives exist, not the least of which is the desirability of using equations other than the Puissant type. The developments of such forms is not

within the scope of this paper.

5. Summary

In summary it has been shown that it is possible to derive geodetic/photogrammetric models to determine a velocity field from observations of moving stations over a suitable time scale. KAULA (1973) has performed similar derivations and simulations for lunar laser ranging which will account for global plate tectonics while the geodetic model is expected to cover individual plate boundaries and other macro areas and the photogrammetric method could be expected to cover meso areas such as glaciers and volcanic regions.

The principal advantages of the velocity concept can be summarized as follows:

1) It provides rigorous derivations of the forces, stresses and strains that an area is undergoing. In particular, the yield point can be approached without fear of model breakdown.

2) Few surveys, except for pure photogrammetric cases, can be accomplished in time scales which are sufficiently short that all observations can be regarded as occurring at a standard epoch.

3) The passage of stress waves through a spatial field can be modelled by incorporating time into the velocity function active at the point.

4) In a secular environment where there are no fixed points available, the velocity approach allows a single centre of mass point of the array to be chosen and all data to be made relative to this point.

The principal disadvantage of the system is the increased complexity of the mathematical models associated with the deformations.

National Mapping has only this last field season begun surveys of which the principal aim has been the detection of crustal movement, although in certain instances the Australian Geodetic Datum can be used as a benchmark for future work. This traverse work, in conjunction with the high precision satellite and lunar programs, has necessitated that theoretical investigations into the most efficient and best data analysis methods for elucidating geophysical information from geodetic observations, be undertaken. In this regard, all the above developments have been checked against static cases for correctness.

Work is continuing on deriving simpler equations to handle the velocity concept and, where practical, of incorporating extra-terrestrial data into the model for its added strength at the macro level.

6. Acknowledgments

Many people have contributed to the ideas expressed in this paper. However, Mr. J. McK. Luck has been especially helpful in providing a most useful sounding board and in organizing the final production.

7. Notation

The following notations have been used.

7.1 Section 2

$X_p = \begin{pmatrix} x \\ y \\ z \end{pmatrix}_p$ a vector of space rectangular geocentric co-ordinates. In particular it usually applies to the co-ordinates of the point at the initial epoch

$X_1 = \begin{pmatrix} x \\ y \\ z \end{pmatrix}_p$ the same, but at epoch $t \neq 0$, i.e., at some epoch other than the initial epoch

$h_i(X_p)$ function of spatial co-ordinates

$h_i(t)$ velocity function with respect to time

η strain tensor

F three-dimensional vector of rectangular forces

A vector of face areas of a body being subjected to general three-dimensional forces

J the Jacobian

T stress tensor

$\dot{\eta}$ strain rate tensor

7.2 Section 3

x_p, y_p observed plate co-ordinates relative to the fiducial centre

x_o, y_o the calibrated values of the optical centre relative to the fiducial centre

f calibrated focal length

X_p a vector of ground station co-ordinates in a Cartesian rectangular system

X_o a vector of camera station co-ordinates in the co-ordinate system of X_p

$M = \begin{pmatrix} M_1 \\ M_2 \\ M_3 \end{pmatrix}$ the general rotation matrix ω, ϕ, χ

$V_p(t)$ a vector of velocity function not embodying X_p in any functional relationship

F, G, H general matrix functions

L_a the adjusted or true observations

L_b the observations to be adjusted

X_a the adjusted/true parameters

A $\partial F / \partial X_a$

B $\partial F / \partial L_a$

$P = \Sigma^{-1}$ a weight matrix of observations

X a vector of unknown parameters

X_o a vector of approximations to unknown parameters

K_i a vector of Lagrangian multipliers

W_i $F(L_b, X_o)$

7.3 Section 4

$\phi_i, \lambda_i, A_{ij}$ geodetic latitude, longitude and azimuth

$\dot{\phi}_i, \dot{\lambda}_i$ time rate of change of ϕ_i and λ_i

S	arc length - normal section
t	time
Δt	time interval
F,G	general matrix functions
(Δ - P_1- P_2- Pole)	the triangle with vertices P_1, P_2,Pole
M	the meridional radius of curvature of the ellipsoid
N	the prime vertical radius of curvature of the ellipsoid

8. References

BORG, S.F. 1963. *Matrix - Tensor Methods in Continuum Mechanics.* Van Nostrand,Princeton NJ.

BROWN, D.C. RCA54. Results in Geodetic Photogrammetry 1, The Precise Determination of the Location of Bermuda from Photogrammetric Observations of Flares Ejected from Juno II. *Rep.* 54, Radio Corporation of America.

BROWN, D.C. ET AL 1964. *Research in Mathematical Targeting, Volumes I,II & III.* Reports perpared for Rome Air Development Center, Griffiths Air Force Base, New York, under contract AF 30(602)-3007.

CLARK, D. 1963. *Plane and Geodetic Surveying,Volumes I & II.* (5th ed) Constable,London.

KAULA, W.M. 1973. Potentialities of Lunar Laser Ranging for Measuring Tectonic Motions. *Phil.Trans. R.Soc.Lond.A* 274,185-193.

LOVE, A.E.H. 1920. *A Treatise on the Mathematical Theory of Elasticity.* (3rd ed) Cambridge University Press.

SOKOLNIKOFF, I.S. 1956. *Mathematical Theory of Elasticity.* (2nd ed) McGraw-Hill,New York.

TIMOSHENKO, S. & GOODIER, J.N. 1951. *Theory of Elasticity.* (2nd ed) McGraw-Hill,New York.

UOTILA, U.A. 1967. *Introduction to Adjustment Computations with Matrices.* (Unpublished Lecture Notes) Department of Geodetic Science,The Ohio State University,Columbus Ohio.

SAKUMA, A.
Bureau International des Poids et Mesures
92310 Sèvres
France

Proc. Symposium on Earth's Gravitational Field & Secular Variations in Position (1973), 674-684.

A PERMANENT STATION FOR THE ABSOLUTE DETERMINATION OF GRAVITY APPROACHING ONE MICRO-GAL ACCURACY

ABSTRACT

This paper describes the first permanent station for the absolute determination of gravity at the International Bureau of Weights and Measures. The station presently consists of an absolute apparatus of a few micro-Gal accuracy based on a symmetrical free rise and fall observation of a corner reflector in vacuum. Periodic determinations of g by the apparatus permits one to monitor the small variations of g arising from the Earth tide and various geophysical causes including the secular effects. The principal sources of errors in the apparatus are discussed and it is predicted that a final accuracy of 1 μGal can be obtained by the symmetric free rise and fall principle, provided that the local Earth tide and the vertical gradient of g are measured with sufficient accuracy. A tendency of the secular variation of g of the order of 10 μGal per year is reported. An Earth tide recording gravimeter and a transportable absolute gravity apparatus, both of which have recently been completed at this station, are also described.

1. Introduction

Since the centre of gravity of the Earth is difficult to determine with sufficient accuracy from the terrestrial stations, the modern techniques for the absolute determination of g (presently accurate up to a few micro-Gal) (SAKUMA 1971) have been considered as the most reliable means of monitoring the variations of the physical condition of the Earth, e.g., secular change of g, sea level, tectonic motions, etc. Thus it has been proposed (LEVALLOIS 1971) and recommended by the International Association of Geodesy (IAG RESOLUTIONS 1971) that permanent stations be established for absolute gravity measurements on different sites of the Earth.

Presently there exist two stations for this purpose; the first has been in operation since 1967 (TRAVAUX IAG 1968) at the International Bureau of Weights and Measures (BIPM), Sèvres, FRANCE, while the second is being constructed at the International Latitude Observatory, Mizusawa, JAPAN. Several other future sites are also foreseen. This paper presents the present state of the BIPM Station where improvements in the accuracy of the apparatus have been continuously made in parallel with the periodical measurement of g. The aim of this work is to attain a final accuracy of one micro-Gal. When this accuracy is assured, new possibilities, such as an absolute determination of the Earth tide, crustal deformation due to air mass, polar motion effect on the variation of gravity and so on, will be open in geophysical studies.

2. Principle

The single principle involved in the ultimate absolute determination of g to better than 1 part in 10^8 is the observation from an inertial reference point of free fall motion in the gravity field. In comparison with, for example, the simple free fall method, the method of symmetrical free rise

and fall (VOLET 1947) is the most promising due to its inherent high precision and its relative freedom from systematic errors such as air resistance, timing errors, etc. In this symmetrical free rise and fall method, employed at the BIPM Station, an object - a corner reflector - is projected vertically upwards and crosses two defined horizontal stations : S_1, S_h whose separation H is known. Two independent time intervals corresponding to the upward and downward passages across each station : T_1, T_h are measured and the value of g is obtained from

$$g = \frac{8H}{T_1^2 - T_h^2} \qquad (1).$$

If the vertical gradient of g is constant along the trajectory, the value of g obtained from equation 1 corresponds to that at height

$$Z = \frac{H}{6} + \frac{h}{3} \qquad (2)$$

downward from the apex of the trajectory, where h is the distance between the apex and the upper station.

In spite of its principal advantages, this symmetrical method has been employed only by three standard laboratories :

- National Physical Laboratory, England (COOK 1967);
- National Standards Laboratory, Australia (BELL 1973); and
- B I P M, France.

The main reasons preventing the use of this method are that the launching of an object in vacuum with severe limits of rotation and vertical deviation of the trajectory, is much more difficult to realize than the simple free fall, and that the mechanical shocks caused by the launching of the object are liable to produce an additional disturbance of the observation by which the advantage of the method may be cancelled out. Thus the two essential problems to be resolved for high precision absolute gravimetry are

1) how to correctly launch the projectile; and
2) how to realize an inertial reference point which is free from shocks, ground motion and other perturbing effects.

These problems become predominant at a level of accuracy of 0.1 mGal and these have been the key points for the gravimetry at BIPM on which important efforts have been made.

3. Description of the Apparatus

The essential part of the absolute gravity apparatus at the BIPM is a Michelson type interferometer in vacuum (figure 1). A corner reflector forming one mirror in the vertical beam of the interferometer is used as the projectile. The two horizontal stations are installed in the trajectory as the conjugate planes of two mirrors forming an end standard of 0.8 m length made of fused silica, placed in the horizontal beam of the interferometer.

The timing signals, which are white light fringes with a half width corresponding to a vertical displacement of 0.06 μm of the falling corner reflector, are detected by a photomultiplier when the optical path difference between the horizontal and the vertical is null. The frequency of the fringes is very high, about 30 MHz; in addition the effective surface of each mirror is made very small, 0.2 cm^2, in order to assure a highly planar surface on the mirrors and to avoid the

intersection (roof) of the two orthogonal mirrors. Furthermore the solid angle of the light source seen by the interferometer is made small in order to get good parallelism of the light beam in the long trajectory. Thus an ordinary white light source is not sufficient to give a good S/N ratio ($\sim$ 40 dB) for the fringes, and so a xenon flash lamp is synchronously triggered with each passage of the corner reflector at the two stations in upward and downward motions (SAKUMA 1963).

3.1 Length Measurement

The length of the end standard of 0.8 m is determined by direct comparison with the primary standard line of a Kr86 lamp in the same interferometer used for the measurement of g (figure 1). The use of the same interferometer for the two measurements eliminates several sources of the systematic errors due to the individual difference of interferometers, lack of flatness, difference of aperture, phase shifts in thin film, effects of polarization and so on. For this length measurement, the movable corner reflector in the vertical beam is fixed midway between the two stations so that the conjugate plane of the end mirror in the vertical beam is formed in the horizontal beam at the centre of the two mirrors of the end standard. Thus the length of the standard is obtained as the addition of the two distances measured by the intermediate of the conjugate plane with 0.8 m optical path difference.

For the phase determination of the standard, the horizontal optical path is finely modulated by the piezo-electric element: PZT.1 on which a corner reflector is fixed. This fine optical path length modulating device is also used for the fine adjustment of the symmetry of the white light fringe

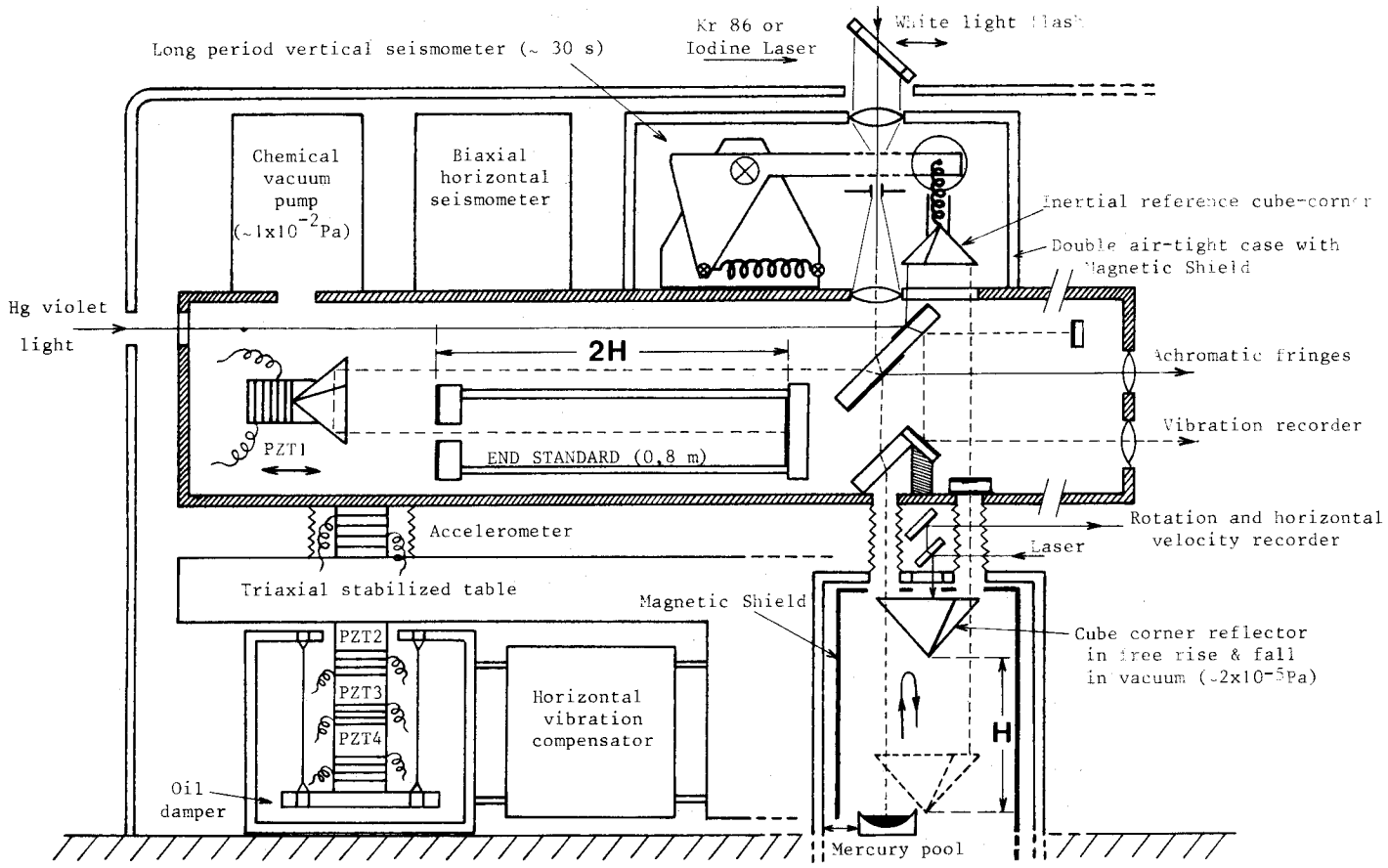

Figure 1. Schematic Diagram of the Absolute Gravimetry Apparatus at B I P M.

pattern and for checking the alignment of the interferometer. Because of the large optical path difference of 0.8 m, the visibility of the interference of the Kr86 primary standard line decreases to only 5%. Nevertheless, by using a low-noise photomultiplier cooled to -50°C, the length of the standard can be measured with 1×10^{-9} precision. This high precision length measurement was the first experimental proof that the present metre definition by Kr86 has a reproducibility of one part in 10^9. This proof was reconfirmed (CCDM 1973) recently by several standard laboratories when the new wavelength standard became available. This improved standard which uses saturated molecular absorption lasers ($^{127}I_2$ laser for example), gives a precision of 1×10^{-10}. A determination of the wavelength of an iodine stabilized laser made recently by the g apparatus gave

$$\lambda(^{127}I_2, \text{"g"}) = 632\ 991\ 231.1 \pm 0.6 \text{ fm.}$$

The uncertainty in the wavelength (1×10^{-9}) comes from the uncertainty of the Kr86 standard. This value is in good agreement with the value:

$$\lambda(^{127}I_2, \text{"g"}) = 632\ 991\ 231.0 \text{ fm}$$

recommended by the 5th Consultative Committee for the Definition of the Metre (June 1973 at BIPM). Thus this good agreement of the wavelength shows that the length measurements made in the gravity apparatus at BIPM did not contain a systematic errors exceeding 1×10^{-9}. (Moreover the use of this new wavelength standard greatly facilitates the length measurement in the apparatus, in addition to increasing the absolute stability of the unit of length up to 1×10^{-10}.)

The obliquity correction must be applied for the length measurement by the interferometric method. This correction is due to the curvature of the interference wave caused by a finite dimension of the light source and in the present apparatus, the theoretical correction attains 2.8 parts in 10^8 of the length standard. This correction agrees with the experimental result obtained by the extrapolation to null dimension of the light source with 2% accuracy. The resulting uncertainty of the length standard is $\pm 6 \times 10^{-10}$.

The inhomogeneity of illumination in the interferometer, combined with the lack of flatness of the mirrors also causes a systematic error in the length measurement but this effect can be verified experimentally and reduced to below 1×10^{-9} in the standard. Thus it is presently possible to determine a length standard of around 1 m with an accuracy of 1 part in 10^9.

3.2 Projectile and Catapult

Figure 2 shows schematically the composition of the projectile and the catapult. The projectile (figure 2.1 and figure 3) is composed of a pair of corner reflectors, 10 cm high, weighing 430 g, arranged back to back with their apices at the same point so that the optical centre of a corner reflector coincides with the centre of gravity to within 10 µm. The three mirrors of each corner reflector are fixed on a duralumin support in which the six holes are made every sixty degrees around its vertical centre axis to let pass freely the light beams of the interferometer. This duralumin support also has a central hole in the vertical direction and the top of the hole is slightly tapered. This tapered top of the projectile rests before launching on a conical piece (4) attached at its top to the elastic cord (3) of the catapult and at its bottom to a cylindrical piece (6) by means of the nylon wire (5). The piece (6) is also attached to a weak elastic cord (7) so that (6) moves always in the vertical direction. Before launching, the projectile sits on an elevator table (8) and is turned around its vertical axis so that the light beam (2) falls correctly in a specified hole.

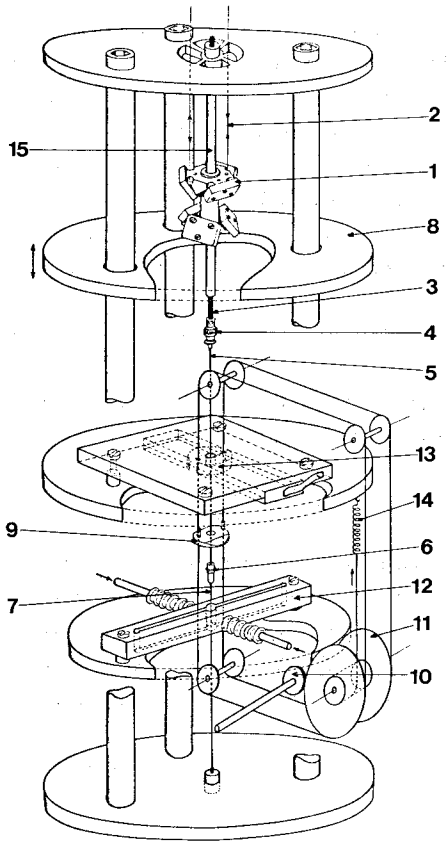

Figure 2. Schematic Drawing of the Catapult with the Corner Reflector in Flight

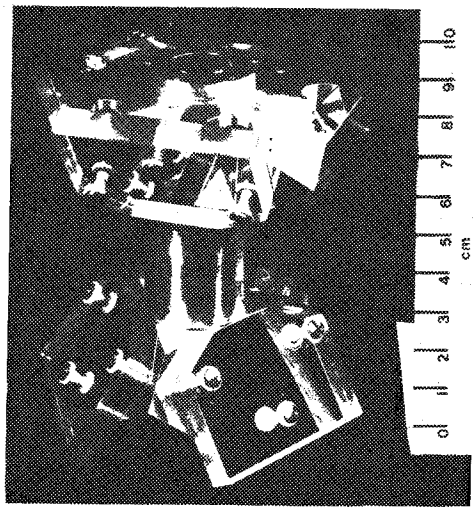

Figure 3. Projectile: Double Cube Corner Reflector for Absolute Measurement of Gravity
430 g. right angle ±5 μrad
flatness: ∿ λ/50 on ϕ = 12 mm

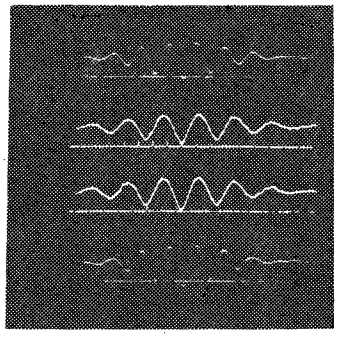

Figure 4. Four White Light Fringes with 20 MHz Time Base
1 & 4: Rise and Fall at Lower Station with increased sweep speed
2 & 3: Rise and Fall at Upper Station with Normal Sweep Speed

Then the table (8) goes down slowly and leaves the projectile hanging on the conical piece (4). An annular piece (9) placed co-axially with the wire (5) can be displaced vertically by rotating a shaft with clutch (10) and by a pulley (11). By these mechanisms the piece (6), guided by the ring (9), is engaged into a hole of the release (12) by the pressure of compressed air. Then the ring (9) goes up to be locked into a fixed stage (13) and the shaft (10) is declutched. When the piece (6) is released, the projectile is accelerated by the traction of the elastic cord (3). After an accelerated rise of about 0.3 m, the piece (6) touches and is stopped by the fixed stage (13). Likewise the conical piece (4) is also stopped so that the projectile enters in its free rise. By the shocks given by the piece (6) to the fixed stage (13), the locked ring (9) is liberated and it sits on the piece (6) by the downward traction of the spring (14). After the free rise and fall, the projectile (1) falls on the piece (4) and the elastic cord (3) is stretched. During this braked fall, the two pieces (6) and (9) follow this downward motion of the projectile by means of the traction of the spring (14). During this motion, one friction disc in the pulley (11) absorbs the kinetic energy so the projectile is stopped smoothly without rebouncing.

This catapult throws the projectile while giving it a rotation of less than 0.01 rad per sec, and with a horizontal velocity of $\sim$ 0.2 mm per sec. The mass of the moving part of the catapult is only 20 g and there is no moving element during the free rise and fall of the projectile. Moreover the whole of the catapult is mounted on a vibration absorber. Therefore the mechanical vibration due to the operation of the catapult is much smaller than the ground motion. At the beginning of the free rise, the projectile is observed to oscillate longitudinally with 18 kHz and 0.04 μm amplitude, but this oscillation decays rapidly with a 6 ms time constant. Therefore a free rise time of 50 ms (18 cm rise) is allowed before entering the lower station of the g measurement. After this decay time, the free oscillation is less than 0.1 nm amplitude. The catapult is adjusted so that at the apex of the normalized trajectory, the optical centre of the corner reflector rises vertically 5 cm above the upper station (45 cm from the lower station). In this normalized flight the four white light fringes appear every 0.2 s and this periodicity is convenient to change uniformly the capacitances of the xenon flash tube. The elastic cord (3) produces some electrostatic charge by its contraction. This effect on the projectile (1) is avoided by a metallic tube (15) placed around the elastic cord. This electrostatic shield by the tube (15) maintains a constant capacitance of $\sim$ 20 pF of the projectile against the Earth during the flight. Due to this constancy of the capacitance, the effect of electrostatic force on the projectile in flight is confirmed to be negligible, even though the projectile is charged artificially up to several hundred volts.

3.3 Stabilized Table and Inertial Reference

The anti-vibrating devices employed for the gravity measurement are shown in figure 1.

The Michelson interferometer in the horizontal vacuum chamber is mounted on the suspended table by metallic wires. This wire suspension with oil damping attenuates the horizontal acceleration due to the rapid ground motion (> 5 Hz) over thirty times. Thus the relative vibrations of mirrors in the interferometer become negligible (< 0.1 nm). For vibration control in the vertical direction, an electronic feed-back device is used between the vertical accelerometer and the piezo-electric driver PZT-2, so that the output of the accelerometer tends to null. By means of this device the rapid ground motion (5 Hz $\sim$ 50 Hz) is attenuated over ten times without using a soft suspension (spring) which is liable to derange the vertical and the horizontal position of the interferometer. The other piezo-element PZT-3 is driven by an auxiliary long-period vertical seismometer to compensate the long period microseisms due to the ocean waves (0.15 $\sim$ 0.3 Hz). Another piezo-element PZT-4 is used for the fine adjustment of the horizontal of the table against the instability of the concrete piers. The residual vibration of the interferometer with respect to the corner reflector suspended

by a long period seismometer is measured and recorded during the gravity measurements. This seismometer is carefully protected from the variation of the terrestrial magnetic field due to traffic, microbarometric pressure change and the temperature drift. The horizontal acceleration due to the ocean waves also excites this vertical seismometer because of weak coupling between the two directions, so that a horizontal compensator is presently being made.

The residual acceleration of the inertial reference corner reflector is presently $\sim$ 2 μGal (1 second average) and 0.5 μGal is expected in the near future.

3.4 Time Measurements

The time intervals of the flight, 0.6 s at the lower station and 0.2 s at the upper station, are measured in two steps. First, 50 ns resolution is obtained with 20 MHz counters. Next, 0.1 ns resolution is achieved by means of a photographic record of an oscilloscope display of the white light fringes with a 20 MHz time base (figure 4).

In order to assure sub-nanosecond accuracy, careful checks of the chronographs are required. These checks test the perturbation due to the gate operation, the effects of standing waves due to impedance mismatching, non-linearity of the oscilloscope sweep, fluctuation of the electron transit in the photomultiplier, parallax in the photographic record, time base jitter, and so on. Presently, the time measurements are accurate to 0.2 ns to 0.6 ns for a corresponding uncertainty of 1 μGal in g. This is due principally to the noise of the white light fringes. This uncertainty will be improved in the future by a factor of two (0.5 μGal). Practically, the chronographs are designed for three successive time measurements: T_r, rise time in crossing the two stations; T_h, up and down crossing at the upper station; and T_f, fall time crossing the two stations. By comparing the two times T_r and T_f, the coefficient of the residual air resistance on the projectile can be determined as a function of the pressure in vacuum chamber. By virtue of the symmetrical free fall, the air resistance effect on the value of g was negligible up to 1 Pa (CIPM 1970). On higher vacuum, < 0.05 Pa, the time difference

$$\Delta T = T_f - T_r$$

was found to be proportional to the pressure with a coefficient of +16 μs per Pa. Therefore the pressure variation should exceed no more than 1×10^{-5} Pa during the free rise and fall of the projectile to ensure that the influence of air resistance on g is less than 1 μGal. Fortunately, the pressure variation due to outgassing because of the operation of the catapult in a vacuum of 2×10^{-5} Pa was within the limit of the sensitivity of a vacuum gauge; that is $\leq 2 \times 10^{-6}$Pa. Thus the effect of air resistance is negligible (< 0.2 μGal) for the measurements of g when the symmetrical free fall is employed. The time difference for an ideal vacuum was obtained by an extrapolation to be

$$\Delta T_{po} = +5.3 \pm 0.5 \text{ ns.}$$

This residual time is explained by the velocity of the light c. The white light fringes at the lower station arrive at the photodetector after travelling an additional distance of

$$2H = 0.8 \text{ m} \quad (2.67 \text{ ns times c})$$

compared with the white light fringes at the upper station. So the measured rise time is decreased by 2.67 ns, and the measured fall time is increased by the same quantity, resulting in a measured time difference of +5.34 ns. This time delay has no influence on the value of g in the case of the symmetrical free fall method, but in the case of simple free fall, this correction due to the finite velocity of light must be applied.

The observation of this time difference of +5.3 ns confirms the accuracy of the time measurements. In addition, the comparison of this time difference obtained in each measurement of g permits the detection of accidental perturbations which may occur during the experiment.

3.5 Earth Tide Recording Gravimeter

The gravimetric Earth tide perturbs the mean value of g by as much as +110 µGal and - 160 µGal, with a maximum gradient of ±0.8 µGal per minute at the BIPM station.

Therefore it is necessary to know the correction for the Earth tide with 0.5% accuracy in amplitude and 1 minute accuracy in phase (0.5 degree phase accuracy for the semi-diurnal waves) in order to compare the mean value of g from day to day with 1 µGal accuracy. On the other hand, a systematic phase delay of several minutes has been identified in the theoretical Earth tide by comparison with the absolute determination data. For these reasons, a new Earth tide station has been completed in October 1973 at an underground site 40 m north of the absolute station of the BIPM and the existence of the phase delay of the theoretical tide has been confirmed by this apparatus. The principal part of the apparatus is an old gravity meter, type Western (< 1956), modified at the BIPM so that the Earth tide can be measured with a short response time ($\sim$ 20 s) by a null method using a symmetrical electrostatic compensation of the tidal force. This apparatus has been installed on a stabilized table in a constant pressure well with an optimum temperature control ($\sim$ 0.01 mK). The instrumental drift is presently found to be +3 µGal per day. This combination of the two types of gravity apparatus, absolute and relative, is of mutual benefit; the real correction of the Earth tide now becomes available for the absolute apparatus, and the absolute apparatus gives the possibility to study and calibrate the long term drift of the relative apparatus.

4. Experimental Results

All experimental results of the absolute determination of g since October 1966 are shown in figure 5. The significant discrepancies of 20 $\sim$ 40 µGal are noted, especially that between the data of 1969 and that of 1972-1973. These differences in g are still unexplained.

In spite of careful verifications of the absolute apparatus, no instrumental drifts of such magnitude have been identified up till now. The variation of the underground water table was surveyed for this period with the collaboration of the Bureau of Geological and Mining Research (BRGM), Paris, but no correlation was found.

Several more years will be necessary to clarify the observations in figure 5, but when the data prior to 1969 are taken into account, the minimum value of g appears around 1969. In the same year, the tidal wave of 18.61 year period due to the Moon's nodal regression also passed its minimum value. The calculated variation of g due to this wave is only 4 µGal peak-to-peak at this station and the correction due to this wave is already applied to the data of figure 5. On the other hand, it is said that the response of the Earth to this long period (18.61 years) wave is not yet well understood (MICHELSON 1973). Furthermore, in view of the fact that geyser activity and polar motion observations also indicate 19 year periodicity (NOAA 1972; OKUDA 1968), this tidal wave motion probably affects the Earth much more strongly than classical tidal theory indicates.

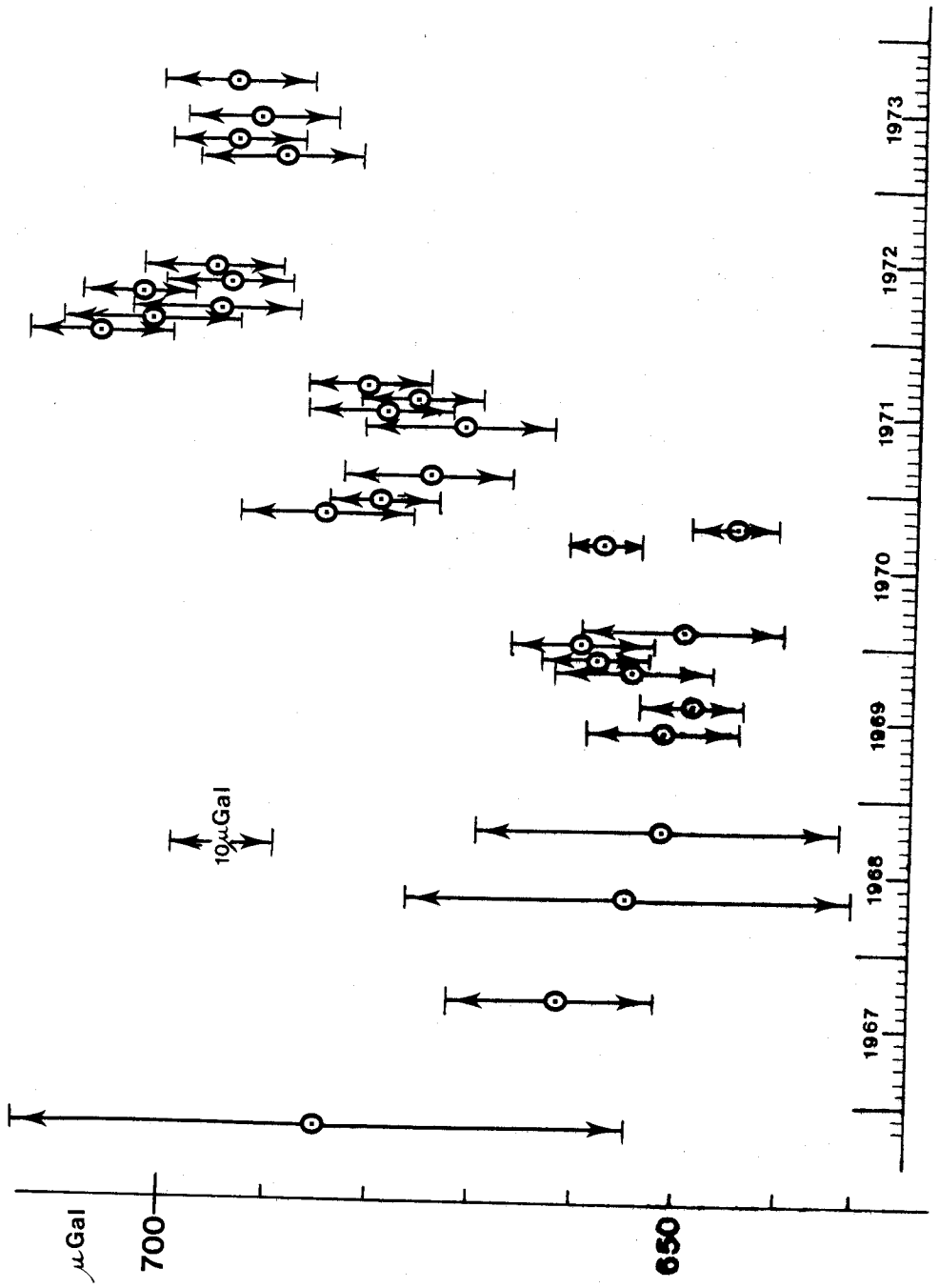

Figure 5. Monthly Mean of Absolute Value of Gravity with Scatter of Single Measurement at SEVRES POINT A2 (Apparatus Site).

B I P M : g_{A2} = 980 925 000 μGal + Values on Graph

5. Transportable Absolute Gravity Apparatus

This apparatus, constructed by the National Institute of Metrology (IMGC), Torino, Italy, with the technical assistance of the BIPM, also employs the principle of symmetrical free rise and fall. The instrumental details of this apparatus are very similar to those of the fixed apparatus at the BIPM. Nevertheless, it is worth noting three differences which facilitate the transportation of the instrument and the calculation of g, namely:

1) The determination of g is made in a low vacuum of about 0.1 Pa for which the secondary vacuum pump is not required;

2) Instead of the end standard of length, a stabilized laser is employed with a reversible interferometric fringe counting method; and

3) The vibration effect is compensated automatically by an inertial reference corner reflector forming itself the end mirror of the horizontal beam.

This apparatus, 1.4 m high and with a 0.5 × 0.5 m section, consists of two separable main parts; a Michelson interferometer in a pressure tight case weighing $\sim$ 40 kg, and a catapult in a vacuum cylinder weighing $\sim$ 60 kg. This apparatus can be transported in a small truck.

A first preliminary result was recently obtained by this apparatus, transported to the BIPM and installed on a pier where the value of g is already known. The mean value of 25 measurements of g (about one hour) was in agreement to within ±0.02 mGal with the value obtained by the fixed apparatus.

A final precision of 0.01 mGal will be obtained by this transportable apparatus and its accuracy and repeatability will be checked by the fixed apparatus of the BIPM.

This apparatus has been of interest to several geophysical and standards laboratories for their studies. So a project for its industrial production by a French firm is presently in progress. This kind of apparatus will be useful not only for the creation of absolute stations and for the calibration of the gravity net, but also, by means of periodical gravity ties by the apparatus, for the study of the global evolution of the gravity field of the Earth.

6. Conclusion

The accuracy of the absolute determination of gravity is now steadily approaching one μGal and there are no further essential metrological difficulties preventing the realization of this goal. The results obtained at the absolute station of the BIPM have been significantly improved by the direct observation of the Earth tides and they no longer rely upon the theoretical calculation for the correction of this effect. Also, new observations of the underground water level will be started at the BIPM. Such activities lie in the domain of geophysical studies, but it is nevertheless the responsibility and interest of metrological laboratories such as the BIPM to confirm that the apparatus functions correctly. With such an apparatus to provide accurate data, geophysicists can then make the interpretations necessary to arrive at a better understanding of the Earth.

7. References

BELL, G.A. ET AL 1973. *Metrologia* 9,47.

CCDM 1973. Rapport, 5e Comité Consultatif pour la Définition du Metre. (In press).

CIPM 1970. Procès-Verbaux, Comité International des Poids et Mesures, Tome 38,49.

COOK, A.H. 1967. A New Determination of the Acceleration Due to Gravity at the National Physical Laboratory,England. *Phil.Trans.R.Soc.Lond.A* 261,211.

IAG RESOLUTIONS 1971. Resolutions No 12 & 13,XV General Assembly of IAG, Moscow. *Bull.géodés.* 102, 403.

LEVALLOIS, J.J. 1971. Quelques Conséquences Géophysiques des Nouvelles Méthodes de Haute Précision des Mesures Absolues de **g**. *Bull.géodés.* 99,111.

MICHELSON, I. 1973. Private Communication. Illinois Institute of Technology.

NOAA 1972. *Earthquake Information Bulletin* 23,Nov.-Dec. 1972,National Oceanic & Atmospheric Administration, Boulder Colorado.

OKUDA, T. 1968. *Publication of the International Latitude Observatory of Misuzawa* 4(2),231.

SAKUMA, A. 1963. *Bull.géodés.* 69,249.

SAKUMA, A. 1971. *Spec.Publ.* 343,US National Bureau of Standards,Boulder Colorado,p.447.

TRAVAUX IAG 1968. *Travaux de l'Assoc.Int.Géodés.* 23,273 & 367.

VOLET, CH. 1947. *Comptes Rendus Acad.Sci.* 224,1815.

8. Discussion

HOPKINS: It seems to me that in the measurement of absolute gravity, we are using length standards and time standards using hyperfine transitions which themselves use the value of **g**. Aren't we involving something we are looking for in the search?

MARKOWITZ: The value of **g** does not enter directly into the present quantum definitions of the units of either length or time. The possible variations in **g** are too small to have any significant effect.

(For a "conversation" by D. ECKHARDT on developments in absolute gravimetry at the Air Force Cambridge Research Laboratories, Bedford Mass., see p.716)

SYDENHAM, P.H.
Cooney Observatory
University of New England
Armidale NSW 2351
A U S T R A L I A

Proc.Symposium on Earth's Gravitational Field & Secular Variations in Position (1973),685-690.

DEVELOPMENT AND USE OF A TEST FACILITY FOR COMPARING LONG-LENGTH STANDARDS

ABSTRACT

Secular variations in the Earth's shape can be measured by a number of ways of which direct length changes are the most obvious. A long-term program aims at the provision of basic knowledge about the stability of long-length (decametres) standards especially over ultra-long periods. To date, two generations of 10m test-base have been built and the stability o Invar and quartz standards tested to parts in 10^{12} per hour drift. A superior facility, currently under construction, enables both temperature and pressure to be controlled for 5m length devices. It is situated 300 m underground to make use of natural environmental control. Strainmeters, tested on these bases, have been installed to monitor rock strain: they have provided long-term data on the secular relative ground movement to parts in 10^{12} per hour uncertainty. The contribution of the program in its relation to surface geodetic survey are that improved techniques seem feasible to raise the accuracy of short bases beyond current EDM capability.

1. Metrological consideration of strainmeters

For a variety of reasons it is desirable to measure relative ground movements - continental drift, expanding earth, tidal studies and global shape changes come to mind. There exists many means by which this can be performed - EDM, taping, Viasala interference multiplication, VLBI, satellite triangulation, lunar ranging, strain and creep-meters, tilt and gravity variations and even visual inspection. Each has its own field of useful application in the study of the Earth.

Common to all is a necessary hierarchy of metrological requirements. Firstly, the process must possess adequate stability (or repeatibility, depending whether it is a continuous or discrete measurement process). The more stable the process the more that can be learnt within a given time-scale. Next, and only next, comes the need for accuracy of either the absolute interval length or of the differences in length.

The research reported here relates to the measurement of both relative and absolute values of intervals in the region of 1-100m. This includes earth strainmeters, metrological length standards for industrial and surveying practice and scientific strain meters for use in basic research such as gravity wave detection.

To date the emphasis of this program, conducted in the Cooney Observatory near Armidale in NSW, Australia, has been on the stability and installation problems of nanostrain extensometers. Here accuracy is needed to only a few percent compared with required stabilities of parts in 10^{10} or better.

2. The Need for a Stabilised Test Base

The easiest way to test the stability of a length standard is to mount it on a base-line that is more

stable by an order of magnitude. This approach works well in the standards laboratory-to-industrial relationship but not so well in the standards situation where the ultimate standard is being improved - the new device could well be superior to the existing authority. An approach used to avoid this dilemma is to build two devices and compare them against each other. Provided systematic secondary effects are eliminated it is reasonable (but never totally certain) to suggest that one device alone exhibits no greater than the total drift observed. It is like the scientific basis - all is right until proven wrong. When identical devices agree there is room for some doubt as each could be systematically effected. A slightly better process is to use two different systems where possible, leaping from one to the other as the foundation for the next stage of development.

At present the international standard of length uses krypton radiation and provides knowledge of absolute length to within parts in 10^9. It requires sophisticated equipment and demanding technique. Molecular absorption stabilisation of laser radiation is almost certainly about to replace krypton giving length reproduceability to parts in 10^{10}. It is however, one thing to have basic stable radiation available and another to apply it to practical measurement: usually some basic accuracy is lost in the process.

Recent research has developed ways to apply mechanical length standards (quartz tube and tensioned-catenary) to rockstrain measurement with stabilities of parts in 10^{10} per hour drift. Theoretical considerations show that both mechanical and optical standards, given a controlled environment, exhibit similar practical and theoretical limits (three or four orders of magnitude difference at present) so which is the ultimate is really a matter of the point in time of development that the question is asked. In strainmeter designs, it is the relative stability that is vital, not the absolute length; this enables their performance to be pushed further in some respects than absolute standards.

The obvious way to research strainmeters is to set them up on a stable baseline - the Earth, for instance, or a geodetic-tape base. These suffice to parts in 10^7 over short-time periods but this is totally inadequate for state-of-the-art nanostrainmeter research. Beyond this a new approach is needed. This program (the only of its kind) uses substantial steel structures that are length stabilised by controlling their temperature to fine limits. These bases are supported to be free of the influence of rock-strains.

3. Thermally-controlled Bases

In 1968 the need arose, in connection with an industrial 10m length measuring device, to provide a stable base of 12m length (SYDENHAM 1969) that could be used to determine the repeatibility of a wire-on-drum length measuring transducer to parts in 10^6 over several months. The first design of base used (a cross-section is given in figure 1) internally-circulated water that was temperature controlled to 0.01K. It realised stability of parts in 10^7 per day and parts in 10^6 per annum being measured relative to tensioned Invar wires. This work indirectly led to a new form of earth-strain meter - the tensioned catenary design.

In 1971 the chance arose (in connection with the earth-strain program started in the Cooney Observatory at that time) to build an improved version of the 1968 measuring base, placing it deep underground (SYDENHAM 1972a).

Naturally improved thermal background stability and hanging arrangements realised milliKelvin control and for a while stability measurements were found to be limited (by inherent creep in Invar) to

parts in 10^8 per hour even after many months of waiting.

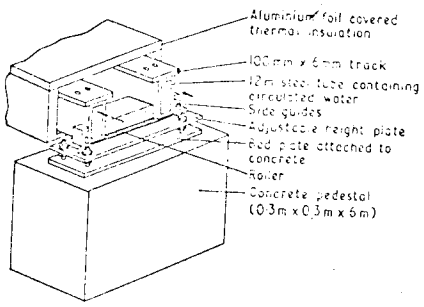

Figure 1. The first measuring base.

In 1972 the control system was improved (SYDENHAM 1973a) by distributing the heating throughout the 10m base, as shown in figure 2. At the same time the use of tensioned-quartz canes was made practicable and the combined result were several periods (of 100-200 hr duration) when the stability of quartz relative to the steel base held constant to within parts in 10^{11} per hour. Long term relative stability was also studied (IBID).

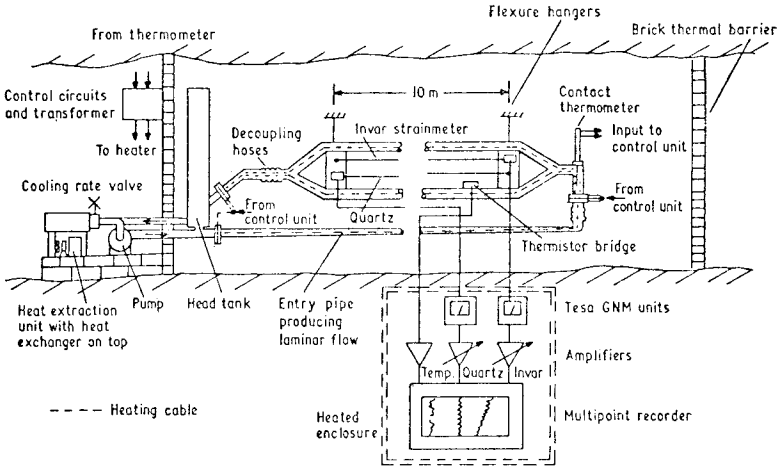

Figure 2. Cooney Observatory open-sided measuring base.

In early 1973 it was established that the random drift normally observed in the records was mainly caused by set-point instability in the contact-thermometer controller. The design was subsequently changed to use a micro-Kelvin sensitivity thermistor sensor as the proportional input to an industrial SCR controller; this greatly reduced the thermal fluctuations giving continuous average thermal stability to within ±2μK per hour drift. It is apparent that this can still be improved by an order of magnitude as the servo control system is not, as yet, tuned.

To date, it seems that instability in controlled temperature quartz and steel is still undetectable. This is discussed further, later in this paper. Figure 3 shows the drift of Invar and quartz.

In the middle of 1972 it became obvious that the control and design of the first base was inadequate - pressure on the standard could not be controlled and ambient thermals were not isolated sufficiently.

To overcome these disadvantages, and to provide a superior test base where both optical and mechanical methods could be intercompared to parts in 10^{12} or better, a new design was implemented.

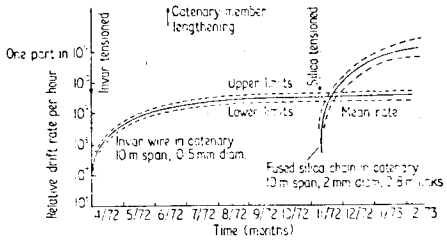

Figure 3. Drift of Invar and quartz relative to steel

The second design, designated the coaxial base, uses concentric cylinders of water to provide better shielding and has a double level, piggy-back, control, coarse on the outer, fine control in the inner jacket. The inner measurement chamber is supported on flexure diaphragms and by flotation.

The whole unit hangs from a single-point support with vibration isolation between the unit and the ground. It has been situated in a deeper underground chamber than the earlier version. It is envisaged that stability, down to natural Brownian limits, will be reached (parts in 10^{15}). Figure 4 shows the side view.

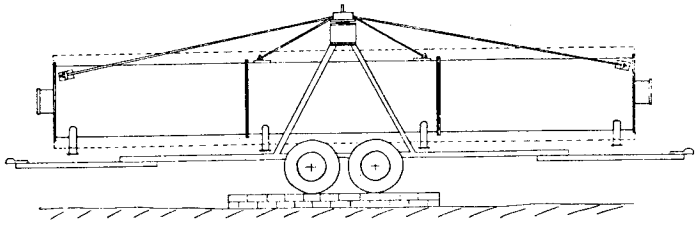

Figure 4. Side view of 5m, double-jacketed, coaxial measuring base

At the time of writing the coaxial unit was close to initial testing, but due to delay in the iodine absorption stabilised laser development it has not yet been used for intercomparison.

4. On Secular Earth Movement Measurement

The research program is designed to be integrated with earth-strain measurements. One long-term aim is to produce a strainmeter that can be used with the ease of a gravity meter (but for less expense). One example of this spinoff from the stabilised-base research was the logical deployment of a 10m quartz catenary strainmeter (sectioned in figure 5) alongside an existing 10m quartz-tube design (SYDENHAM 1972b). During 1973 they have both produced visually identical strain records (SYDENHAM 1973b) drifting relative to each other only 5 parts in 10^{12} per hour for a 500h period. The high fidelity enables the recorded secular drifts of the observatory area to be accepted with a high degree of confidence. It has been shown, in this way (figure 6) that the area undergoes quite large secular strain variations and that any harmonic analysis of tides should be carried out on

carefully chosen records obtained during quiet background periods.

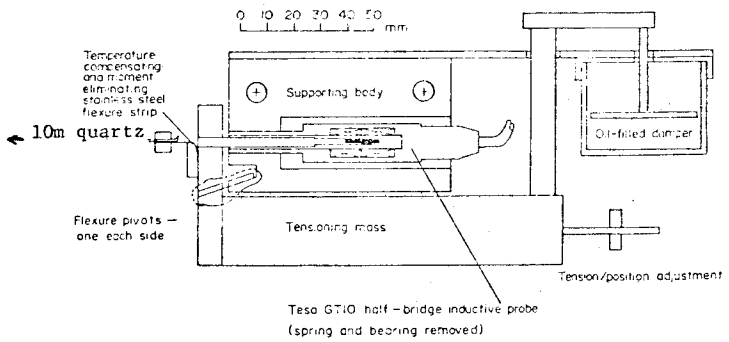

Figure 5. Tensioning and measuring head of quartz catenary strainmeter.

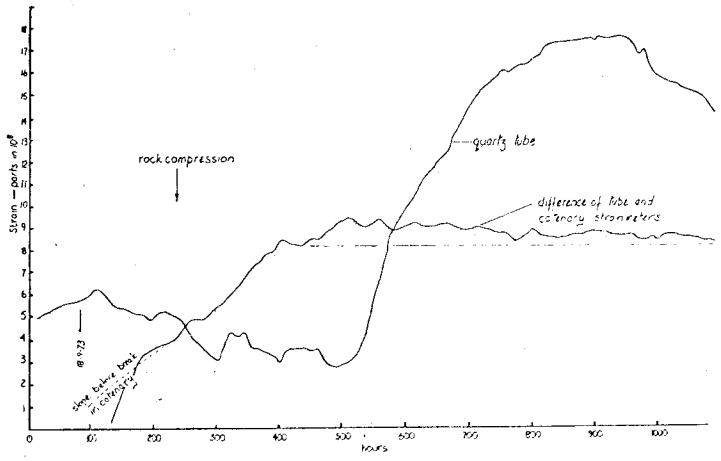

Figure 6. Secular drift in Cooney Observatory region

5. The Future

The past two years of research by the Cooney group have realised gradual improvement in strainmeter designs. Quality nanostrain data is now being obtained with a very simple 1m long mechanical design (PETERS & SYDENHAM 1973). Much has been learned about the drift of the instruments and their installation. Mounting instability has also been studied (JEFFREY & SYDENHAM 1973) showing that this part of the strainmeter loop is the significant source of creep during the first few months of a new installation.

Two laser components (SYDENHAM & BLAIR 1973), forming part of a multi-coordinate array, are about to be completed. By 1974, these, plus other strainmeters, will provide data for strain tensor investigation.

If the coaxial measuring base does realise stabilities of parts in 10^{15} it could become routine to look for gravity wave reception - a currently unsolved new area of gravity phenomena.

The information produced so far on the stability of mechanical instruments now enables a new path to be developed (manpower allowing). This is to find ways to use the stable lengths for defining highly precise baselines on the surface. Tides and secular movements produce surface changes, maximising around parts in 10^7 so there is still room for improvement in surface surveying. Although this suggests a return to a kind of relatively slow taping procedure or Colby-bar approach, on order of magnitude gain over EDM could prove useful in many areas of geodetic survey, especially in ground settlement monitoring.

At present this is being pursued (on a less precise scale) with the development and appraisal of a 50-100m range automated wire-drum transducer (SYDENHAM 1970) for the Melbourne Underground Loop Railway Authority. It is hoped this unit will enable trilateration of streets to be made with an accuracy of 0.1mm, filling the gap below EDM equipment capability.

6. Acknowledgment

Research is supported by a continuing Australian Research Grants Committee Award (providing for laser strainmeter, stabilised-laser and general research needs); by a two-year Nuffield Foundation Award (to build and test the coaxial measuring base); and from various University funds. The Bureau of Mineral Resources, Canberra, and the University jointly operate the tiltmeter installation.

7. References

JEFFREY, G.J. & SYDENHAM, P.H. 1973. Stability of Strainmeter Mounts. *Geophys.J.R.astr.Soc.* 32(2), 185-193.

PETERS, J.D. & SYDENHAM, P.H. 1973. *Earth tides recorded with 1m internal mechanical strainmeter.* (Submitted).

SYDENHAM, P.H. 1969. A length stablised 12m measuring base. *J.Phys.E: Sci.Instrum.* Ser 2, 2, 523-525.

SYDENHAM, P.H. 1970. Numerically-controlled position using trilateral coordinates. *Int.J.Mach.Tool Des.Res.* 10, 327-335

SYDENHAM, P.H. 1972a. An improved 10m length stabilised base. *J.Phys.E: Sci.Instrum.* 5, 421-424.

SYDENHAM, P.H. 1972b. Progress in the design of tensioned-wire earth strainmeters. *Geophys.J.R.astro. Soc.* 29, 319-327.

SYDENHAM, P.H. 1973a. Nanometre stability of Invar and quartz suspended in catenary. *J. Phys.E: Sci.Instrum.* 6, 572-576.

SYDENHAM, P.H. 1973b. *2000h comparison of quartz-tube and quartz-catenary strainmeters.* (Submitted).

SYDENHAM, P.H. & BLAIR, D.P. 1973. *Measurement of earth strain using laser interferometry.* Ian Clunies Ross conference on laser applications, Melbourne.

BARLOW, B.C.
COUTTS, D.A.
Bureau of Mineral Resources, Geology & Geophysics
Department of Minerals & Energy
Canberra A C T 2600
Australia

SYDENHAM, P.H.
Department of Geophysics
University of New England
Armidale NSW 2351
Australia

Proc. Symposium on Earth's Gravitational Field & Secular Variations in Position (1973), 691-698.

TIDAL DEVIATIONS OF THE VERTICAL AT ARMIDALE, AUSTRALIA

ABSTRACT

Deviations of the vertical are being recorded at the Cooney Geophysical Observatory near Armidale, New South Wales, using a pair of Verbaandert-Melchior horizontal pendulums. Problems associated with the installation and operation of the apparatus have been largely overcome. Since the pendulums were installed in 1971 only two periods of reliable records longer than 29 days have been obtained. These data have been scaled and will now be forwarded to the International Centre for the Earth Tides for detailed analysis. Various non-tidal effects still appear on the current records and are probably due to site defects.

1. Introduction

Since 1961 the International Association of Geodesy has repeatedly recommended that Earth tides should be recorded in the southern hemisphere, and particularly in Australia at the antipodes of Europe.

Although more than 300 stations are now observing Earth tides, the stations are not uniformly distributed internationally. Central Europe is comparatively well-served with stations which have records extending over many years. Significant data have been obtained from a number of stations across the USSR, in Japan, and in North America. It is known that various groups in Australia, New Zealand, South America and Antarctica are attempting to record reliable Earth tide signals, but, as far as the authors are aware, no Earth tide data from the southern hemisphere have yet been published.

This paper describes the installation and operation of a pair of Verbaandert-Melchior horizontal pendulums in the Cooney Geophysical Observatory near Armidale, New South Wales. This is a co-operative project by the Bureau of Mineral Resources, Geology and Geophysics (BMR) and the Department of Geophysics, University of New England (UNE) to measure tidal deviations of the vertical.

It was expected that analysis of recent data would be completed in time for presentation at this conference, but unavoidable delays have made this impossible. Nevertheless, continuous recordings from both pendulums have been obtained over two periods of more than 29 days, and the data have now been scaled and are being checked before transmittal to the International Centre for the Earth Tides for detailed analysis.

In common with other groups seeking to obtain reliable observations of the tidal variations in tilt we have experienced considerable difficulty in the installation and operation of apparatus. It is clear that the present site is not ideal, and non-tidal effects continually appear in the records.

Preliminary analysis of the data showed that the principal components of the tides can be separated, but that it may be difficult to determine their amplitudes and phases to the desired accuracy.

2. Installation of the Pendulums

The Verbaandert-Melchior horizontal pendulums ORB 53 and ORB 54 were obtained by BMR from Professor Paul Melchior in 1963. Because of difficulties in obtaining a suitable site and because of the unavailability of staff for this project the pendulums remained unused for some years. In 1970 UNE established the Cooney Geophysical Observatory in an abandoned mine in the Hillgrove area 28 km east of Armidale (see figure 1). BMR and UNE agreed to install and operate the pendulums as a co-operative project at that site.

The Cooney Observatory has been described in several earlier papers (e.g., GREEN & SYDENHAM 1971) and is shown in figures 2, 3 & 4. The pendulums are installed at the innermost end of the Upper Cooney tunnel about 170 m from the tunnel mouth so that the rock cover exceeds 100 m. The pendulums are isolated from the main part of the tunnel and the cross-cut by three brick partitions with sealing doors, so that the occasional ventilation of other parts of Upper Cooney do not produce significant temperature variations in the pendulum observation chamber.

As far as possible the installation follows the procedures laid down by MELCHIOR (1966). A niche measuring 0.4 by 0.4 by 0.8 m was cut into the end face of the tunnel without the use of explosives. The rock is a garnetiferous carbonaceous slate and is extremely hard. Sets of fracture planes in three directions are clearly seen in the rock floor of the niche. Water weeps into the niche through various fractures, and has caused considerable difficulty. The pendulums are mounted on stainless steel pins glued with Araldite into holes drilled into the floor of the niche. As recommended by Melchior great care was taken to ensure that each pin is a close fit in its hole and that the shape of the bottom of the pin matches the shape of the bottom of the hole. The ceiling, back and side walls of the niche were sheathed with galvanised iron to catch and divert water entering the niche. The floor of the niche was sealed with a layer of Readibond (epoxy-resin plastic). A hinged glass door closes the front of the niche.

Moisture has been a persistent problem; fogging of the glass door of the niche was finally cured by blowing freeze-dried air on to those portions of the glass that transmit the light rays to and from the pendulum mirrors. A small amount of this dried air is allowed to weep into the niche to prevent entry of moist air from the observation chamber.

Imperfections in the pendulum mirrors, particularly that mounted on ORB 54, made sharp focusing of the traces impossible and it was necessary to re-silver these mirrors.

Automatic calibration apparatus was obtained from Melchior and installed in the observation chamber. Two of the stainless steel pins have oversized heads and support the crapaudines (expandable bearing plates) under the drift leg of each of the pendulums. The apparatus which automatically changes the height of the mercury bottle was installed close to the tunnel ceiling in order to obtain a pressure head of 1.5 m between the mercury bottle and the crapaudines.

The recorders and the light sources are mounted on a brick and concrete table 5 m from the niche. It was necessary to widen the tunnel at this place in order to allow access past the table to the niche. A pair of timing lights, mounted close to the niche and at the same height as the mirrors on the pendulums, provide a flash of light each hour in response to a signal from a Bulova Accutron clock.

To improve ventilation in the chamber when it is occupied for extended periods, air is sucked from the ceiling of the chamber and evacuated into the main part of the tunnel by a domestic vacuum cleaner.

The portion of the tunnel immediately before the observation chamber serves as a light trap and workroom. Ambient pressure is recorded in this workroom; other apparatus is being installed to record other parameters in the observation chamber, including temperatures of chamber air, niche air, rock floor of the niche, and interstitial water.

The installation commenced in August 1971 and several of the features were not installed until much later.

The records are changed weekly by UNE staff, who also make adjustments for drift as required.

3. Azimuths and Co-ordinates

The true bearing of the Upper Cooney Tunnel is 53° 13' 11". The narrowness of the observation chamber prevents the mounting of the pendulums with the preferred N-S and E-W orientations. Tilt is measured in the mean azimuths 54° 59' and 142° 05'; this limits the accuracy of determination of amplitudes and phases of the various components. The co-ordinates of the observation site are :-

Latitude (Australian National Spheroid)	30° 34' 43" S
Longitude (Australian National Spheroid)	151° 53' 36" E
Elevation (Australian Height Datum - mean sea level)	649.9 m

The acceleration due to gravity referred to absolute datum (IGSN 71) is 9 791 662 $\mu m\ s^{-2}$ (BMR gravity station number 7291-0646).

4. Records Obtained

During the period August 1971 to July 1972 and August 1972 to June 1973 the records obtained were unsatisfactory for scaling and analysis for one or more of the following reasons:

(a) Problems due to moisture in the niche, condensation on optics, etc.

(b) Extremely high drift of one or both pendulums for several months following initial installation and following later work necessary to eliminate moisture problems.

(c) Slipping clutches in the drive mechanism of the recorder drums.

(d) Inadequate resetting of light spots during periods of medium drift.

(e) Failures of timing mechanism due to clock and relay faults.

(f) Disturbance from experimental heating rings on lenses.

(g) Failure of small refrigerator used to freeze-dry air.

During July and August 1972, a 29-day continuous set of recordings was obtained on both pendulums. No resets were made during this period as the drift rates of both pendulums were small. The records are usable but have the following defects:

(a) Poorly focused traces, particularly from ORB 54.

(b) Timing problems necessitating the use of earthquake arrival times to verify universal time datum.

(c) Incorrect setting of the calibrator arm and hence poor calibration of amplitudes.

These data were partly scaled and analysed, the principal tidal components being resolved in the records from one pendulum. The azimuths of the pendulums were not available until March 1973. By then the behaviour of the pendulums suggested that the scaled data were suspect and should be confirmed by a second set if possible.

During June and July 1973 a 37-day continuous set of recordings was obtained on both pendulums. These records are usable but have the following defects:

(a) Poorly focused traces, particularly from ORB 54.

(b) Minor problems causing intermittent faults in the drum drives and timing apparatus.

(c) High drift on ORB 53 necessitating resets about every ten days.

(d) Several periods of noise continuous over several hours or several days.

(e) Small tares, usually without recovery but occasionally with recovery over several hours.

The first two are instrumental faults, corrected by re-silvering the mirrors and other repairs. The remaining faults have continued since that time. Both the noise and the tares have become more frequent, so that the June-July period data remain the best obtained to date. These records have been scaled and are being analysed at present.

The data from both sets of continuous records are being checked and re-formatted before transmittal to Brussels for detailed analysis.

5. Non-Tidal Effects in the Records

Records from the pendulums show a number of interesting non-tidal effects during the 27-month recording period:

1. Drift.
2. Small tares.
3. Bays, both large and small.
4. Teleseismic and microseismic noise.
5. Discordant noise.

1. Drift

When the pendulums were first installed, both had drift rates of several hundred milliseconds of arc (mseca) per day. These drift rates fluctuated and even reversed during the first three months. Since then the measured drift rates have always been less than 70 and generally less than 30 mseca/day. Each pendulum has shown drift rates less than 5 mseca/day for periods of about 2 months. The drift rates of both pendulums are acceptable , although not as small as those quoted by MELCHIOR (1966) and others.

MELCHIOR (IBID) lists several instrumental, geophysical and tectonic effects as probable causes of drift. Movement in one of the pendulum supports, or in the fractures in the floor of the niche, was initially suspected at Cooney. The pendulums were interchanged on their supports in May 1972 in an attempt to improve focus, and were changed back again in August 1973. Thus half the recording period to date

has been made with the pendulums interchanged, but the drift data do not suggest any particular effect as the probable cause of drift.

2. Small Tares

Small offsets or tares in the trace of one pendulum occur several times each week (figures 6 and 7). They range from 1-10 mm on the record (4-40 mseca) and recovery is rarely seen to occur. Almost without exception, these tares occur in the trace of only one pendulum and are in the direction of the apparent drift. It follows that their cause is instrumental and lies in the pendulum apparatus or in the support pins. It is possible that the observed drift is mainly or totally due to the accumulated effect of such tares.

3. Bays, Both Large and Small

Large bays, during which the trace is displaced 20-400 mm, are rare. Both pendulums are affected and recovery appears to be complete. The shape of the trace is similar to that recorded after the environment has been thermally disturbed, the displacement occurring over 5-20 hours. These bays are thought to be due to thermal effects. Smaller bays of 5-20 mm amplitude and lasting $\frac{1}{2}$ - 2 hours occur every few months. These bays are also thought to be of thermal origin (figure 5)

4. Teleseismic and Microseismic Noise

Distant earthquakes, local tremors, rock-bursts, and man-made explosions contribute noise to the records (figures 5, 6 & 7). Individual arrivals of energy occur simultaneously on the traces of both pendulums. The noise level is frequently high during normal working hours, even though the observatory itself is unattended. It is likely that this daytime noise is generated by mining activity in the area. Although no mines are worked within 1 km of the site, ore is treated in a plant on the hill above the observatory. Several periods of unexplained noise have continued without break for periods of 2-6 days.

5. Discordant Noise

Discordant noise affects one pendulum only, or affects both pendulums over a period with different arrival times for individual energy packets. Time differences of 10-40 minutes are observed. No explanation for this noise has been found.

6. Need for Further Work

Several recent papers have indicated that a niche excavated in the end wall of a tunnel is not an ideal site for the recording of tidal tilt because of unequal stress relief parallel and transverse to the axis of the tunnel. Moreover the present site does not permit the pendulums to be oriented north-south and east-west. A better site may be found in the centre of one of the large chambers of Lower Cooney, but is likely to have the same noise level as the present site. LENNON & BAKER (1973) discuss the discrepancies in the tilt attenuation factors and phases reported by various Earth tide stations in central Europe. Tilt records from a number of stations yet to be established throughout Australia are required, but there is so little activity in this field (SYDENHAM 1973) that it is impossible to forecast when these data will be available.

The analysis of tilt data from the present site will be of interest because it will be first data from this part of the globe. Nevertheless it should be treated with reserve until joined by data from other sites. It is impossible to distinguish between regional and global influences in the data from only one site.

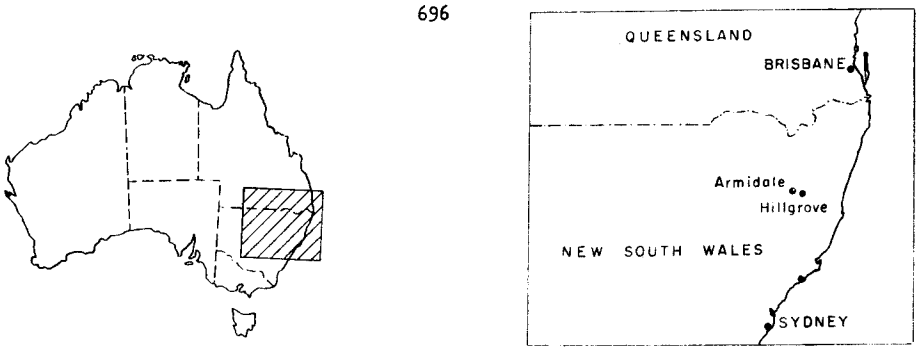

Figure 1

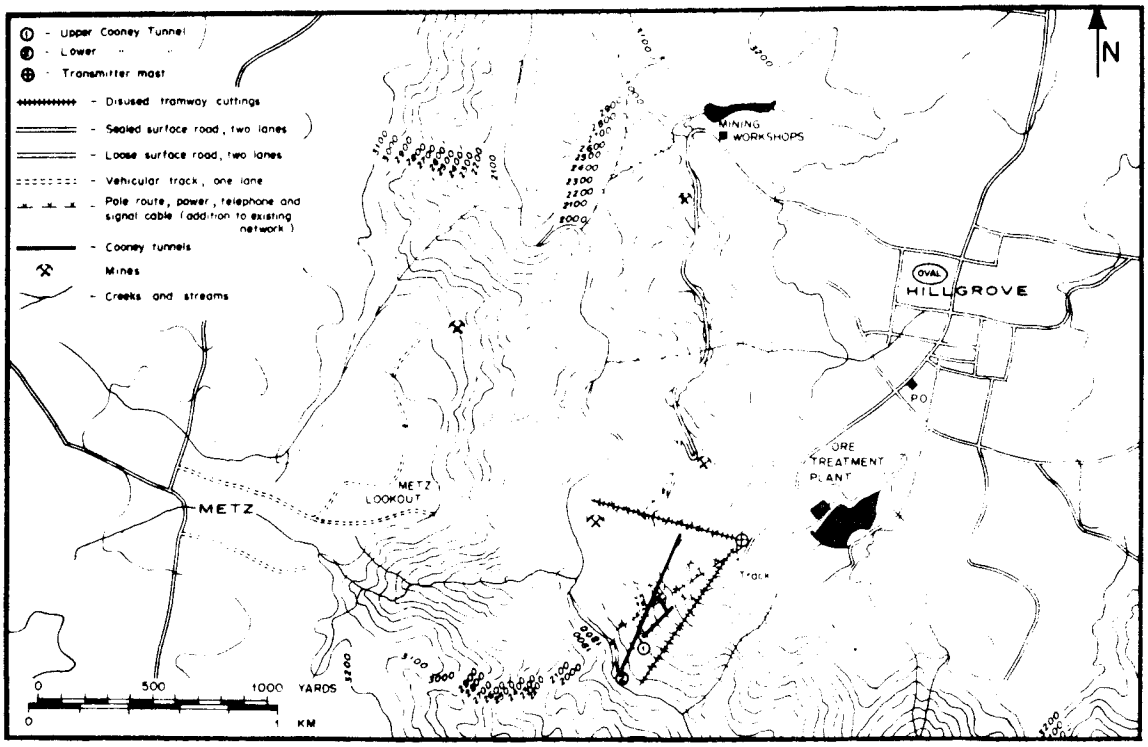

Figure 2

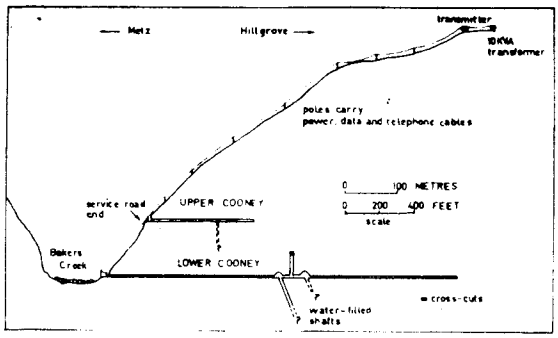

Figure 3

COONEY GEOPHYSICAL OBSERVATORY SITE, HILLGROVE, NSW.

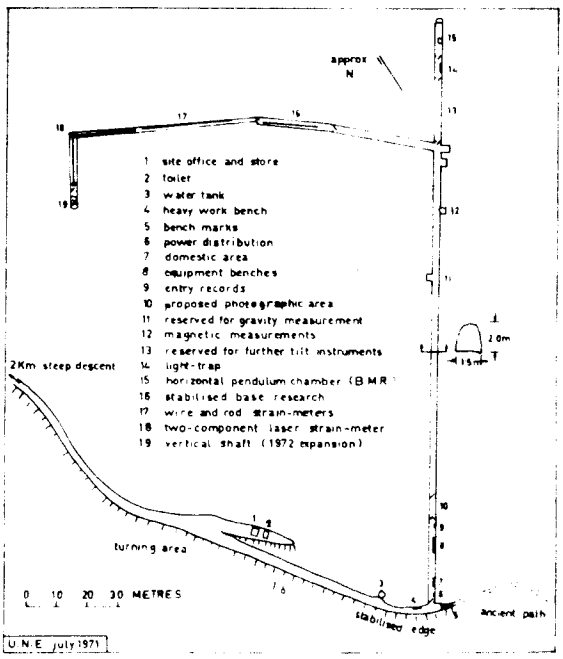

Figure 4

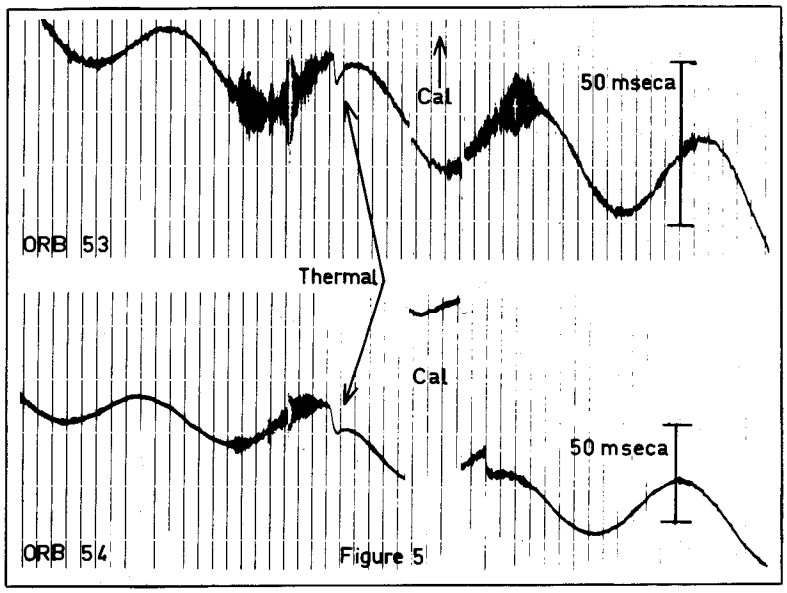

Figure 5

Explanatory notes for figures 5, 6 and 7

1. Each figure is a half scale reproduction of simultaneous photographic records produced by the two horizontal pendulums ORB 53 and ORB 54.
2. Vertical lines are hourly time marks produced photographically.
3. The 50 mseca bar shown against each trace indicates the response of the pendulum to a tilt of 0.050 seconds of arc. During these periods of recording ORB 53 is more sensitive than ORB 54 because it is operating with a longer period.
4. Each trace includes one example of the offset produced by the auto-calibrator and crapaudine system. This offset corresponds to about 90 mseca.
5. The various figures show examples of non-tidal effects in the recent records.

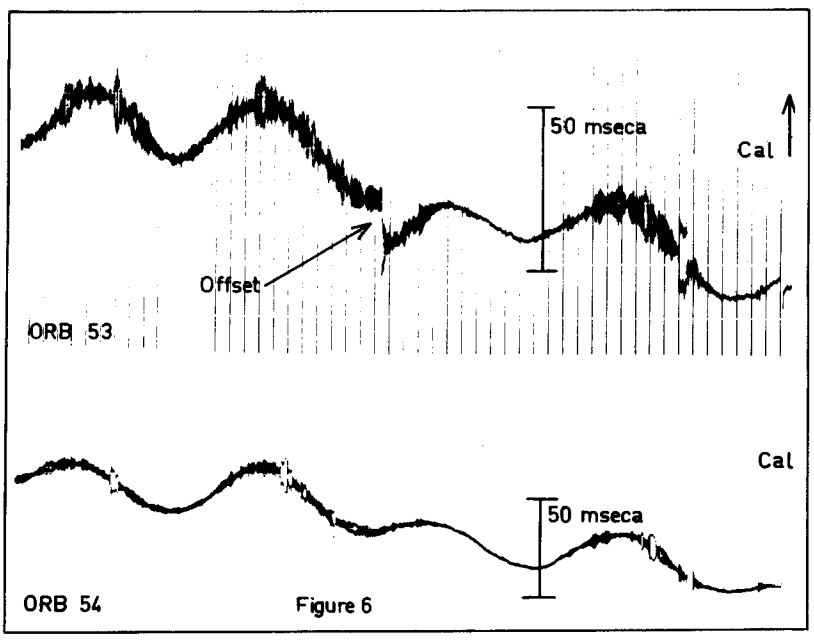

Figure 6

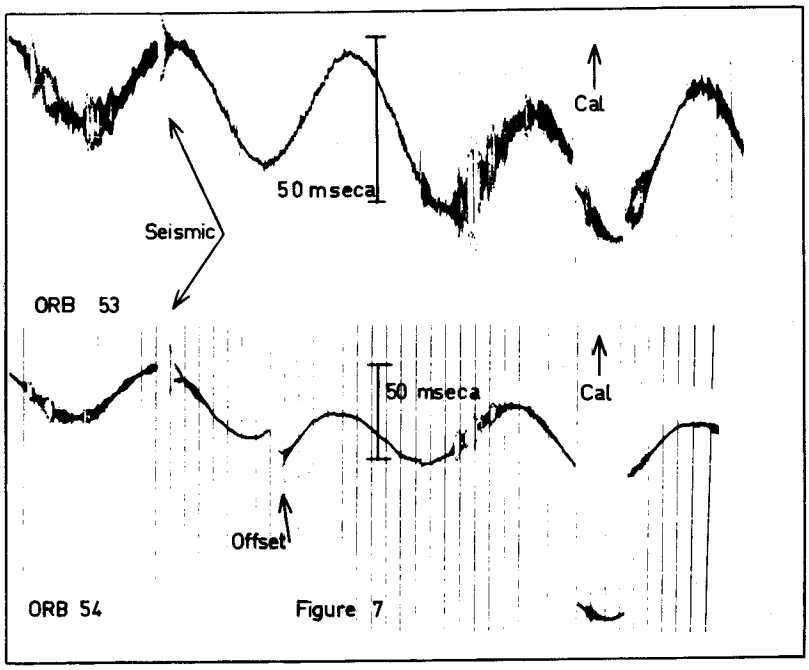

Figure 7

7. References

GREEN, R. & SYDENHAM, P.H. 1971. The Cooney Geophysical Observatory. *Aust.phys.* 8,167-172.

LENNON, G.W. & BAKER, T.F. 1973. The Earth Tide Signal and its Coherency. *Q.J.R.astr.Soc.* 14, 161-182.

MELCHIOR, P. 1966. *The Earth tides.* Pergamon,Oxford.

SYDENHAM, P.H. 1973. Strain Measurement in Australia with Particular Reference to Cooney Observatory. *Phil.Trans.R.Soc.Lond. A* 274, 323-330.

WERNER, A.P.H.
ANDERSON, E.G.
The School of Surveying
The University of New South Wales
Kensington NSW 2033
Australia

Proc.Symposium on Earth's Gravitational Field & Secular Variations in Position (1973),699-701.

INTERNATIONAL UNITS (S.I. UNITS) IN GRAVIMETRY

ABSTRACT

It is attempted to show that it would be beneficial for geodesists to follow practising geophysicists in introducing S.I. Units and ISO proposals for uniform mathematical notation (ISO 1961).

1. Introduction

International bodies such as the International Standards Organization (ISO)* and related commissions have recommended the use of S.I. Units. Governments are preparing new Weights and Measures Acts which will recognise S.I. Units; among these are France (1977), Germany (1978) and, surprisingly, the United States.

Appropriate standards of S.I. Units have been published in many countries. The draft proposal ISO/DIS 31/1, February 1973, Part 1, for "Quantities and Units in Space and Time" reads, among other items:

1.10.2 acceleration due to gravity, acceleration of free fall $g_m = 9.806\ 65\ m/s^2$,

1.10.b Gal = 1 cm/s^2, conversion factor 1 Gal = 0.01 m/s^2.

This proposal means that there is no word for the unit of *standard gravity* other than that used so far. 980.665 Gal are simply written as shown above. Rules for multiples and sub-multiples are that tertiary powers of ten should be used. Table 1 shows acomparison of Old, acceptable but not S.I., and proper S.I. Units proposed in this paper.

2. The Argument

Articles preceded by a legend of notation and definitions or clear references to national standards reveal a degree of individual style of notation and inconsistent use of units and dimensions which make understanding unnecessarily difficult. Naturally authors follow a well established tradition and the majority of geodesists may not have concerned themselves with aspects of international standardization other than that effected through their respective organizations such as the IAG, the IUGG or the FIG. There is also the strong feeling that the *Gal* is an unassailable term because it has found recognition by the ISO (ISO DIS 31/1). This is a misinterpretation of the intention of that body. Some terms are considered "tolerable" but their use is discouraged, simply because their definition defies the first fundamental rule that all units must be derived from the six basic units,

* I.S.O. - also called the International Organization for Standardization

Table 1

OLD	ACCEPTABLE BUT NOT S.I.	PROPOSED PROPER S.I.
GRAVITY		
1 Gal = 1 cm/s^2	1 Gal = 0.01 m/s^2	10^{-2}m kg $s^{-2}kg^{-1}$ = 10^{-2}N kg^{-1}
1 milliGal	1 mGal = 10^{-5} m/s^2	10^{-5}N kg^{-1}
1 microGal	1 μGal = 10^{-8} m/s^2	10^{-8}N kg^{-1}
1 gravity unit	10^{-1} mGal = 10^{-6} m/s^2	μN kg^{-1}
		(Note that the convenience of the old expression is retained)
POTENTIAL		
(Generally) W = g cm^2s^{-2}	(newton.metre = joule) N m = J	As ISO
GRAVITATIONAL POTENTIAL = Work per unit mass = force • length per unit mass		
W = cm^2s^{-2} (implying W = g $cm^2s^{-2}g^{-1}$	Not considered by ISO (Could be written thus - W = $10^{-4}m^2s^{-2}$ = 10^{-2}Gal m s^{-2})	N m kg^{-1} = J kg^{-1}
GEOPOTENTIAL NUMBER		
kiloGal.metre	Not considered by ISO	10^5J kg^{-1}
DYNAMIC HEIGHT		
metre	Not considered by ISO	m

of which the kg, m and second of time are of interest to us here. The second fundamental rule states that all units should be expressed with the aid of prescribed prefixes and multiples of the tertiary powers of ten. Obviously the *Gal* being 0.01 m/s^2, does not obey this rule and cannot therefore be expected to be accepted as a S.I. derived unit.

However, this is not the central argument. The need for serious consideration of changing from the *Gal* and the *kiloGal.metre* to the N kg^{-1} and the J kg^{-1} is seen to be derived from the following considerations which are divided into:

a. administrative reasons; and

b. technical reasons.

a. Adminstrative Reasons

1. All educational institutions have or are about to change to S.I.
2. Editors could control the selection and checking, etc. of papers and thus have some influence on reducing the publication explosion.
3. Information scientists could efficiently assess and catalogue specialist papers. This is a most important aspect because non-specialists would have a better grasp of the scope of numerical results.
4. Practising geophysicists have begun to work in S.I.

b. Technical Reasons

1. Newton spoke of *the force of gravity*; therefore the S.I. Unit for force is the *Newton* or N m kg s^{-2}. Geodesists naturally prefer to think and compute in terms of what they can measure, e.g., the metre, the second of time and the Gal. One could even leave the Gal as a word and it would

still be clearly understood to represent 0.01 m s^{-2} or 10^{-2}N kg^{-1}. Mass, force and acceleration are taught in that order and the degree of difficulty of understanding increases with each term in that order; metre per second squared conveys acceleration but says nothing of its reason; Newton per kilogram reveals the reason but loses the elegance of appearing as an acceleration. A derived S.I. Unit must show its basic components (in this case m, kg, s or N and kg) unless it is given a new name. It is interesting to note that the Oxford Dictionary (CONCISE,4th ed. 1959) defines gravity as a force - "degree of intensity of this measured by acceleration", while MUELLER & ROCKIE (1966) define *gravity* as "centrifugal force" or "gradient of the geopotential".

2. If one accepts the definition of gravity as "gradient of the geopotential" and that in itself is clearly understood to be "work per unit mass" in gravimetry, i.e., joule per kilogram, then it is reasonable to retain that approach for the derivations of the geopotential and to think of acceleration in terms of *force per unit mass*. If one speaks of force it should be seen as such by its dimensions of Newton.

3. Conclusion

It seems that it would be more appropriate to think of *force per unit mass* for the non-S.I. Unit of the *Gal*; likewise the geopotential can be expressed in units of *joule per kilogram* instead of the kiloGal metre which is a term conveying very little meaning to those trained in S.I. Units.
The computations of corrections to gravity would become consistent and not fraught with the present danger inherent in having centimetres and metres side by side. If the *Gal* is seen as 0.01 m s^{-2}, certain dimensional difficulties arise when computing corrections. No good author will write solely for the initiated.

The gravitational constant, being $6.67 \times 10^{-8} cm^3 g^{-1} s^{-2}$ would read

$$k = 6.67 \times 10^{-11} m^3 kg^{-1} s^{-2}$$

in S.I. Units.

4. References

ISO 1961. *Mathematical Signs and Symbols for use in Physical Sciences and Technology.* Recommendation R 31 ,Part XI (1st ed.). International Standards Organization.

MUELLER, I.I. & ROCKIE, J.D. 1966. *Gravimetric and Celestial Geodesy.* Ungar,New York.

ANGUS-LEPPAN, P. V.
School of Surveying
University of New South Wales
Kensington N.S.W. 2033
Australia

Proc.Symposium on Earth's Gravitational Field & Secular Variations in Position (1973),702-709.

A SYSTEM OF OBSERVATIONS FOR FOUR-DIMENSIONAL GEODESY

ABSTRACT

Four-dimensional geodesy is a convenient term for those new high-precision observation techniques which yield position and gravity and, within a short time span, their variations. This data has applications in many areas of earth physics.

The measurements are approaching an accuracy of one part in 10^8. A global network of observing stations is required to obtain full accuracy, and this is consistent with the geophysical need for a fundamental station on each continental plate. Continuous monitoring of position and time at this station should be supplemented by periodic observations at a number of subsidiary stations spread over the plate.

The siting and marking of the stations requires care to avoid local movements and to ensure that the instrumental positions can be initially defined and later redefined precisely after a lapse of decades, or even centuries. In practice it is not possible to site all fundamental observing instruments at one observatory and they need to be connected in time and position by surveys of ultra high precision.

Coordinating bodies are needed on a national and international level to ensure that the observing programs, the data storage, the analyses and the research in this area are interrelated for optimum benefit.

1. Four-Dimensional Geodesy

New techniques of measurement are providing geodetic results of such high accuracy that the changes, with time, in position, length and gravity need to be taken into account. Conversely the measurements yield valuable data in the form of rates of change of these elements with time. Time becomes an active element, so that it is appropriate to use the term four-dimensional geodesy (4-D geodesy) in these studies.

The precision of measurement is approaching 10 cm for position, 10 microgals for gravity and one part in 10^8 for intercontinental distances (FALLER ET AL 1972; SMITH ET AL 1972A; SAKUMA 1971; KELLERMAN 1972). Since these accuracies are of the same order of magnitude as the annual variation of position and gravity, it should be possible to detect changes within a time span of about three years and to define rates of change within ten years.

In order to make valid comparisons it is essential that all results be referred to the same reference system. Within a framework where all elements, even the so-called fundamental constants, may be changing, this is a requirement fraught with difficulties. The time span of observations is several decades, at least; the observing stations are spread over the whole globe; and the observations involve objects in earth-based and celestial coordinate systems.

This problem has been investigated by Mather who has proposed a special reference frame for long-term studies (MATHER 1972; 1973). His solution involves adopting a rigid body model for the earth and applying corrections to account for any variations from the model. Appropriate expressions are derived for transforming astronomical observations into the system. Since the emphasis is on determining movements of continental plates, a single station is chosen as reference, and movements in longitude are all referred to its longitude. Shifts in the position of the geocentre - the earth's centre of mass - are vital, and will require to be monitored by periodic high-precision measurements of gravity.

Within this framework the data should be expressed in a form made familiar by star catalogues. The data should be given for a particular epoch, say 1975.0, with the 'proper motion' of each element listed, in addition.

2. Applications

4-D geodesy brings a new emphasis on time and the need for a special reference frame. It also introduces a closer relationship between geodesy and other earth sciences. Data from geodesy is applicable to many of the problems currently being investigated in geophysics, geodynamics and oceanography (KAULA 1971; LAMBECK 1972).

Variations in the position of the earth's axis of rotation and in the rate of rotation will be measured by continuous observing programmes to yield results accurate to about 10 cm and 100 μs (MELCHIOR & YUMI 1972). Greater accuracy in polar motion and rotation will help resolve problems in the possible mechanisms of the variations, such as the relationship between earthquakes and the Chandler motion and between rotation, atmospheric circulation and the coupling between the core and the mantle (KAULA 1971; MELCHIOR & YUMI 1972; MANSINHA ET AL 1970). Detailed data on continental plate motion will show whether present motion is the same as the average over past millions of years; whether there are differential movements; whether plates are subject to flexure or vertical movements. The measurements will fill in details in the picture of global tectonics which has emerged over the past decade. This indicates that continental plates are moving apart, with related sea floor spreading from mid-ocean ridges, while elsewhere the plates are colliding with one plate being subduced or forced under the other (le PICHON 1968; HEIRTZLER ET AL 1968; DEWEY & HORSFIELD 1970; le PICHON ET AL 1973).

Satellite geodesy should improve the determination of the gravitational field in two ways: improved accuracy from laser ranging should yield more accurate values for the low order harmonics, and satellites carrying radar altimeters should provide a higher resolution. Anomalies in the low order harmonics show a correlation with tectonic features (HIDE & MALIN 1970), but until more laser range data is available for analysis, the accuracy will not be sufficient for the unambiguous definition of the anomalies (LAMBECK 1972).

In relation to the earth's elasticity, the new observations will provide data on earth tides and the response of continental margins to tidal loading. It will be possible to determine the Love number k and to investigate its apparent variations in different regions of the globe (SMITH ET AL 1972B).

The launching of the GEOS C satellite in 1974 will provide measurements of the geoid surface over ocean areas, from which, in the first instance, the gravitational field can be determined to a higher resolution (APEL 1972). If the geoid is known independently, then geoid - sea level relationships, such as open ocean tides, sea surface slopes, and ocean circulation can be studied (APEL 1972).

3. Measurements

The measurements of 4-D geodesy include laser ranging to satellites (SMITH ET AL 1972A), laser ranging to the moon (BENDER ET AL 1973), very long baseline interferometry (VLBI) (SHAPIRO & KNIGHT 1970) and high precision gravimetry (SAKUMA 1971). Each method of observation has its limitations on accuracy. Laser ranging to both satellites and the moon is affected by the atmosphere and the inherent accuracy of the instruments but these are no longer limiting factors (FALLER ET AL 1972; SAASTAMOINEN 1973). In satellite ranging, uncertainties in the gravitational field, earth tides, radiation pressure and atmospheric drag, all of which cause perturbations of the orbit, are the factors which limit the accuracy (KAULA 1966). In lunar ranging it is again the perturbations of the satellite orbit - in this case the lunar librations - which are the limiting factors (WILLIAMS ET AL 1973; FALLER ET AL 1972).

Altimeter results from GEOS C are expected to be accurate to slightly better than one metre when observing in the high energy mode. Later altimeters, as in the SEASAT series of satellites of the EOPAP programme, should be accurate to 10 cm. The limitations are in the instrumentation, the directional guidance and the effects of ocean waves and other surface irregularities.

In VLBI the volume of data required and the high rate of acquisition have caused difficulties but these have been effectively overcome (SHAPIRO & KNIGHT 1970). The system is capable of giving the required precision but the atmospheric corrections place a limit on the accuracy. Because of the great length of the baselines, there is no similarity between the paths traversed through the atmosphere at the two ends (JONES 1969; SHAPIRO & KNIGHT 1970; KELLERMAN 1972).

Doppler measurements of satellites are generally considered to be of lower accuracy but the method has given results consistent to one metre, in the determination of polar motion (BEUGLASS & ANDERLE 1972). It has been stated that the instruments are capable of an accuracy of 5 cm (SMITH 1971). The remaining limitation on the accuracy is the uncertainty in the atmospheric correction. The advantages of the Doppler system are the ease of obtaining observations, the number of satellites available and the 24 hour capabilities, independent of weather.

4. The Ideal System

In order to obtain the full accuracy of the methods, satellite and lunar laser ranging require a global distribution of observing stations. This is consistent with the geophysical need for a fundamental station on each major continental plate. The problems are on the southern land masses: South America, Africa and Australia, and in Asia where until recently scientific cooperation was very difficult. A satisfactory distribution would be a very minimum of six stations, one each in North and South America, Europe, Southern Africa, Eastern Asia and Australia.

Each station would constitute the fundamental geodetic observatory for its region. Facilities would include the two laser ranging systems, antenna for interconnection of stations by VLBI,

Doppler satellite instruments and a base for absolute gravity measurements. A continuous programme of observations would include laser satellite and lunar ranging and Doppler measurements. The VLBI and gravity measurements would be taken at regular intervals.

In addition to the fundamental station, each region would require a number of main stations set up for periodic observations according to a set programme. Here observations would be made using transportable equipment for satellite ranging, Doppler measurements, gravity and possibly interferometry using wide-band transmitters carried by satellite or on the moon. With a 1 000 km spacing, it would require about 15 stations for the Australian continent and its margins. For a 500 km spacing, the requirement would increase to 40 stations. In addition it would be desirable to add a coverage of stations on appropriately situated islands so as to cover oceanic regions.

5. Location of Stations

Apart from normal siting requirements the fundamental stations should be chosen for stability in position over a long term, extending over several decades and possibly centuries. On a regional scale, they should avoid coastal areas where tidal loading may be difficult to model, and zones of known instability due to crustal collision, faulting, earthquake or volcanic activity. On a local scale, site investigation will be needed to avoid local faulting, subsidence or known local earthquake zones.

The objective is to be able to relate, to mm accuracy, positions of all observations taken over the full time span, and to ensure that movements are representative of the whole region. A system of reference marks will be necessary. The marks will probably be in three sets, each set comprising four marks or more. One set will be the stable monuments, set in bedrock and not easily accessible. The next set will be the working monuments, conveniently situated for connecting to the instruments by precise survey. The third set will be the recovery marks placed, for safety, at some distance from disturbing influences on the observing site. The marks will all be interconnected by precise survey. Since there are four marks in each set it will be easy to detect the disturbance of one or two marks.

The same considerations hold for main stations, though they need not be applied so strictly. They may be situated especially for observing a disturbing factor such as fault movement or coastal tide loading.

Because of the accuracy requirement, the definition of the "instrument centre" to which measurements refer, requires careful consideration. The centre may be defined implicitly in the calibration process, or it may depend on the physical form of the equipment. The design of the instrument should provide a clear and direct definition of the centre for the connection to the working monuments by precise survey.

6. The System in Practice

The situation in practice will fall short of the ideal. It may not be possible to set up all observing systems in each of the six continental regions. The instruments are unlikely to be sited together in one geodetic observatory. It may not be possible to arrange a full coverage of main stations over each continent and oceanic region.

As a result one of the problems arising will be the determination of relative positions of different observing systems, so as to compare results. This will be, in effect, tying together the elements of the geodetic observatory. Conventional ground surveys, if carried out to the highest precision, will be sufficiently accurate for plan position over distances up to about 100 km. Care will be necessary in transforming the measurements into the appropriate reference system. Transfer of heights by precise levelling involves an extra difficulty because the datum for those heights is the geoid. The difference in geoid ellipsoid separation can only be carried to the required accuracy for short distances, well under 100 km.

From these considerations it is clear that in most cases the methods of 4-D geodesy will be required to determine the relative positions. It will also be necessary to interrelate the stations in terms of their gravity values, and, during observing periods, their time systems. These determinations should provide no difficulties.

7. The System in Australia

In Australia there are some activities relating to 4-D geodesy. The Division of National Mapping is setting up a lunar laser ranger near Canberra, as part of its Time Service. Initially the results are not expected to be in the 10 cm accuracy class. There is considerable activity in VLBI by the Space Research Group of the Weapons Research Establishment and others, but not directed towards geodetic results. A joint project has been proposed, involving groups in the U.S.A. and the School of Surveying, University of New South Wales (UNSW), to be sponsored by SAO and the Australian Research Grants Committee. If supported, this project will make use of the Tidbinbilla antenna to measure three base-lines of a trans-Pacific network. In gravimetry, the CSIRO's National Standards Laboratory is active in absolute gravity measurement, and the Bureau of Mineral Resources, which already has gravity stations of the National ISOGAL network distributed through Australia, has no formal plans to measure time variations in the gravity field. There is at present no prospect of setting up a satellite laser ranging instrument. This leaves a serious gap in the world-wide network, and in the types of measurement to be undertaken in Australia. In particular it leaves Australia with no participation in international studies, which are currently being planned, of the ocean surface using satellite altimeters.

A further element is necessary in 4-D geodesy: research and development. Much essential development is being undertaken by the National Mapping Division in setting up its lunar laser system. The UNSW School of Surveying has commenced a programme of research on a small scale but this has so far not been directly related to observing systems. In Australia the difficulty in this and other aspects of 4-D geodesy is that while the activities of the National Mapping Division include the applied aspects of geodesy, there is no body to take responsibility and provide funds for scientific geodesy. It will be unfortunate if, as a result, there is limited Australian participation in this new phase of geodesy.

8. Coordination of Activities

The activities under discussion cover a wide geographical range and a diversity of measuring techniques. They share common aims, so it is obvious that coordinating bodies are necessary on national and international levels. It is envisaged that these bodies would have an advisory role. Each national committee would keep in touch with the activities of 4-D geodesy, making assessments to ensure that the coverage was comprehensive and encouraging new projects where necessary. The committee might need to take a hand in the 'housekeeping' functions such as the provision and survey of adequate reference

marks, facilities for retaining records of data and distributing data. The national committees would be the channels of communication with the international committee. This committee would have an analogous function in relation to the programmes in the various member nations.

The existing coordinating bodies in Australia are probably similar to those elsewhere. The Academy of Science has a National Committee on Geodesy and Geophysics (ANCOGG) which has a small Sub-Committee on Geodesy. This sub-committee is too limited as the scope of activities required in 4-D geodesy go far beyond its scope. On the other hand, ANCOGG has interests in a great range of fields besides those involved in 4-D geodesy, and even so does not encompass the whole of 4-D geodesy. There is a clear case for the establishment of an ad hoc body to carry out the functions of coordination in four-dimensional geodesy.

9. References

APEL, J. R. (ed.) 1972. *Sea Surface Topography from Space*, NOAA Tech. Rep., ERL 228-AOML 7, Florida, Oct. 1971.

BENDER, P. L. ET AL 1973. The Lunar Laser Ranging Experiment. *Science*, 182,229.

BFUGLASS, L. K. & ANDERLE, R. J. 1972. Refined Doppler Satellite Determinations of the Earth's Polar Motion. *Use of Artificial Satellites for Geodesy*, eds. Henriksen, S. W., Mancini, A. & Chovitz, G. H. Am. Geophys. Union, Geophysical Monograph 15, pp. 181-186.

DEWEY, J. F. & HORSFIELD, B. 1970. Plate Tectonics, Orogeny and Continental Growth. *Nature*, No. 225, pp. 251-257.

FALLER, J. E. ET AL 1972. Geodesy Results Obtainable from Lunar Retroflectors. *Use of Artificial Satellites for Geodesy*, ed. Henriksen, S. W., Mancini, A. & Chovitz, G. H., Am Geophys. Union, Geophysical Monograph 15, pp. 261-264.

HEIRTZLER, J. R., DICKSON, G. O., HERRON, E. M., PITTMAN, W. C. & le PICHON, X. 1968. Marine magnetic anomalies, geomagnetic field reversals, and motions of the ocean floor and continents. *Journal of Geophysical Research*, vol. 73, p. 2119.

HIDE, R. & MALIN, S. R. C. 1970. Novel Correlations between Global Features of the Earth's Gravitational and Magnetic Fields. *Nature*, vol. 225, p. 605.

JONES, H. E. 1969. Geodetic ties between continents by means of radio telescopes. *Canadian Surveyor*, XXIII, 4, pp. 377-388.

KAULA, W. M. 1966. *Theory of Satellite Geodesy*. Blaisdell Pub. Co. 124 p.

KAULA, W. M. 1971. Geophysical Implications of Lunar Ranging to the Moon. *IUGG/IAG Lunar Ranging Symposium*, Moscow.

KELLERMAN, K. I. 1972. Intercontinental Radio Astronomy. *Scientific American*, Feb. 1972, pp. 72-83.

LAMBECK, K. 1972. The Earth's Gravity Field: its Determination and its Interpretation. Nederlands Geodetisch Tijdschrift, Vol. 2, No. 3, pp. 41-54.

le PICHON, X. 1968. Sea Floor Spreading and Continental Drift. *Journal of Geophysical Research*. Vol. 73, p. 3661.

le PICHON, X., FRANCHETEAU, J. & BONNIN, J. 1973. *Plate Tectonics*. Developments in Geotectonics, Vol. 6. Elsevier, Holland.

MANSINHA, L. ET AL (eds) 1970. *Earthquake Displacement Fields and the Rotation of the Earth*. Springer-Verlag, New York.

MATHER, R. S. 1972. Earth Space. *UNISURV Report G17*, School of Surveying, University of N.S.W., pp. 1-41.

MATHER, R. S. 1973. Geodetic Reference Systems for Long Period Studies in Earth Physics, *UNISURV Report G19*, School of Surveying, University of N.S.W.; also *GSFC Publication X-592-73-85*, Geodynamics Program Division, Goddard Space Flight Centre, Greenbelt, Maryland.

MELCHIOR, P. & YUMI, S. (eds) 1972. *Rotation of the Earth*. Int. Astronomical Union, D. Reidel Pub. Co. 244 p.

SAASTAMOINEN, J. 1973. Contributions to the Theory of Atmospheric Refraction, Part II, B. Electromagnetic Ranging of Satellites. *Bul. Geodesique*, No. 107, pp. 17-34.

SAKUMA, A. 1971. Observations Experimentales de la Constance de la Pesanteur au Bureau des Poids et Mesures, *Bull. geodes.*, 100, pp. 159-163.

SHAPIRO, I. I. & KNIGHT, A. 1970. Geophysical Applications of Long-Baseline Radio Interferometry. *Earthquake Displacement Fields and the Rotation of the Earth*, eds. L. Mansinha et al, D. Reidel Pub. Co., Holland, pp. 284-301.

SMITH, D. E. 1971. Precision Tracking Systems of the Immediate Future: A Discussion. In: *Sea Surface Topography from Space*, NOAA Tech. Rep., ERL 228-AOML 7, Vol. 1, Florida, Oct. 1971, pp. 10-1 - 10-9.

SMITH, D. E., KOLENKIEWICZ, R. & DUNN, P. T. 1972 A. Geodetic Studies by Laser Ranging to Satellites. *Use of Artificial Satellites for Geodesy*, ed. Henriksen, S. W., Mancini, A. & Chovitz, G. H., Am. Geophys. Union, Geophysical Monograph 15, pp. 187-196.

SMITH, D. E. ET AL 1972 B. Polar Motion from Laser Tracking of Artificial Satellites. *Science*, Vol. 178, No. 4059, pp. 405-407.

WILLIAMS, J. G., ECKHARDT, D. H., KAULA, W. M. & SLADE, M. A. 1973. Lunar Physical Librations and Laser Ranging. *Lunar Dynamics and Observational Coordinate Systems*, COSPAR - IAU - LSI Colloquium, Houston. *Moon*, 1973.

10. Discussion

MELCHIOR: I am still not clear on the problem of Doppler accuracy. We get a precision of 80 cm from the Navy Navigation Satellite. If we had satellites at a greater distance, say 3000 km with 3 frequencies, you could have a higher precision with Doppler.

ANGUS-LEPPAN: Yes. I have carefully not mentioned future possibilities. Particularly with Doppler there are possible new developments just over the horizon.

MELCHIOR: When you are proposing some programs, don't you think there are existing in the Geodynamics Project some working groups who *should* deal with the problem and have probably not done so?

WALCOTT: There are the necessary organizations at the international level but not at the national level.

BOULANGER: Yes.

MELCHIOR: I am a member of working group six in the Geodynamics Commission; this working group deals with problems of the rotation of the Earth, changes in gravity, tides, etc, and they have until now, not made anything very clear.

BOULANGER: We have several regions in the Soviet Union where velocities of vertical crustal movements reach 120 mm yr^{-1}. It is not possible to use such precise measurements without fixing the time of measurements. It is quite easy to see in this problem of measurements for four-dimensional geodesy as spoken of four years ago by Kukkämäkki, Levallois and Marussi. A special study group should be formed to look into this matter; perhaps firstly the question of international programs. In geodesy it is very important and it must be an inter-union organization.

MELCHIOR: The Geodynamics Project is precisely such an inter-union project and with some working groups; and some of those groups are working.

DOOLEY: In the context of measuring changes in gravity, I would like to mention that the (Australian) Bureau of Mineral Resources, in conjunction with the Division of National

Mapping, is setting up two networks in New Guinea for measuring crustal movements in two regions of rapid movement and we plan to make gravity measurements across these zones. Secondly, with the help of Boulanger's group, we have a very accurate net of gravity measurements covering the whole of Australia. It is planned that in ten to twenty years from now, this net will be re-measured with a view to detecting changes in gravity in this way. You also state that your system should have at least one station on every continental plate. I would suggest that you need at least two fundamental stations to each plate, as it requires three parameters to define the relative motion of two plates. It is not possible to get relative rotation from one station.

ANGUS-LEPPAN: The proposal is to have one station at which you take regular observations and a number of other stations where you have a program of periodic observations.

DOOLEY: It will depend on whether you measure relative azimuth at these stations. If you measure only distance, and you are on the one plate, the distances should stay the same. You should measure at least three distances between two plates.

ANGUS-LEPPAN: The proposal was in terms of fixing position each time with respect to the basic frame, rather than distance.

SIRY, J.W.
National Aeronautics & Space Administration
Washington DC 20546
United States of America

VONBUN, F.O.
Geodynamics Program Division
Goddard Space Flight Center
Greenbelt Md 20771
United States of America

Proc.Symposium on Earth's Gravitational Field & Secular Variations in Position (1973),709-715.

FUTURE APPLICATIONS OF LASER RANGING SYSTEMS

1. Text

The NASA Earth and Ocean Physics Applications Program (EOPAP) will make extensive use of the advanced laser tracking capabilities which are now being developed. The Earth Dynamics portion of the program will involve laser tracking of satellites in order to make very accurate measurements of the Earth's crustal and rotational motions. Tectonic plate motions of the order of a centimetre per year; and polar motion anomalies of the order of a couple of centimeters in half a day will be monitored to provide basic information about earthquake processes and their possible correlation with the motion of the Earth's rotational pole. The Ocean Dynamics missions of EOPAP will also depend on the power of the laser approach to give the accurate orbital positions needed for the interpretation of the

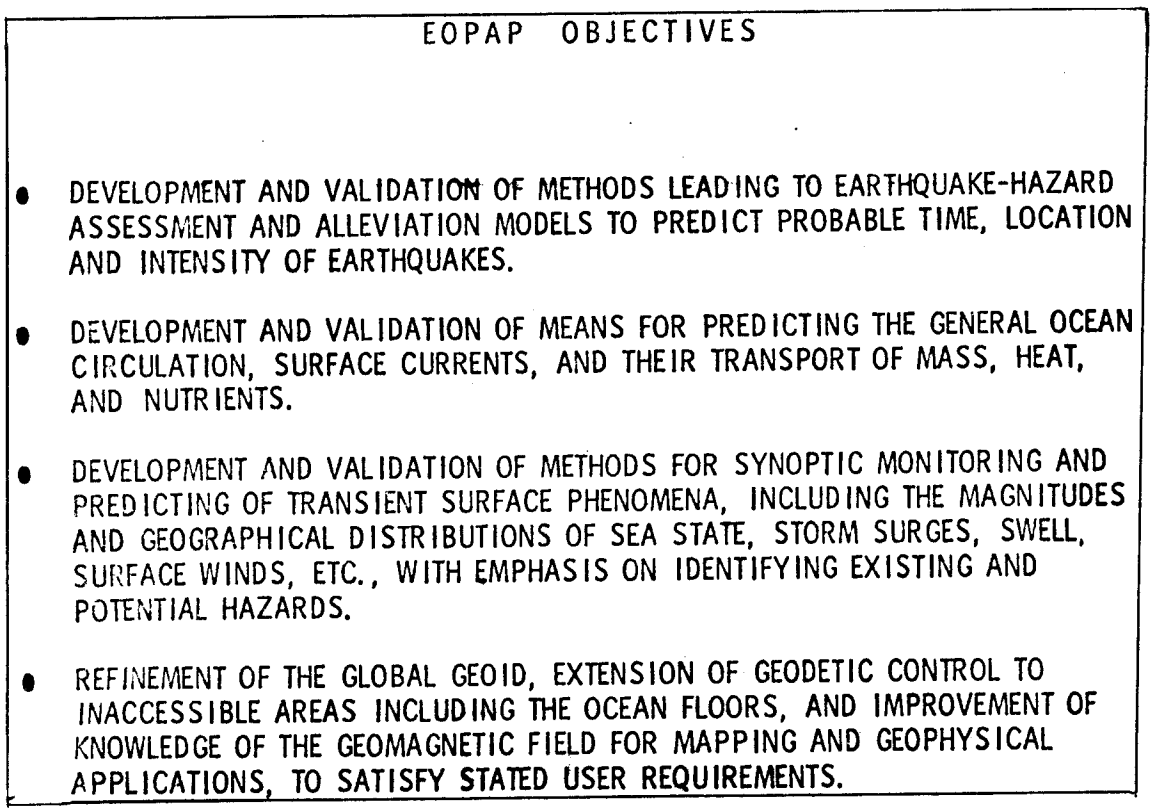

Figure 1

MEASUREMENT REQUIREMENTS SUMMARY

MEASUREMENT	ACCURACY
• CRUSTAL MOTION	1 cm / year
• POLAR MOTION, EARTH ROTATION	2 cm / 0.5 day
• SATELLITE ORBITS	10 cm
• GRAVITY FIELD / GEOID	10 cm
• SEA SURFACE TOPOGRAPHY	10 cm

Figure 2

altimeter data (see figures 1 & 2; NASA 1972).

The evolution of laser tracking system accuracies is indicated in figure 3. The EOPAP flight missions which will take advantage of these capabilities are listed in figure 4 (NASA 1972; VONBUN 1972). Laser tracking will be used to determine the altitude of the GEOS-C spacecraft as its altimeter measures sea surface topography in the western north Atlantic next year. Lasers having a 10 cm range accuracy located at Wallops Island, Bermuda, Cape Kennedy and Goddard will track this satellite and provide the kind of accurate geometrical position reference needed both to calibrate the altimeter and to determine topographical features of the ocean after the instrument has been validated. Results of an analysis of the accuracies attainable with laser tracking data from Goddard, Cape Kennedy and Bermuda are indicated in figures 5 and 6 (BERBERT 1973).

LAGEOS, a dense, spherical, retroreflector studded satellite, to be launched into an orbit of high altitude and inclination in 1976, will be a key element of the EOPAP endeavour. LAGEOS will be the

LASER TRACKING SYSTEM ACCURACIES

1970	50 cm
1973	10 cm
1975	5 cm

Figure 3

NASA EARTH AND OCEAN PHYSICS APPLICATIONS PROGRAM (EOPAP)

MISSIONS EMPLOYING LASER RANGING

GEOS-C	1974
LAGEOS	1976
SEASAT I	1978
GEOPAUSE	1979
SEASAT II	1982

Figure 4

first flight mission devoted exclusively to laser ranging applications. The satellite and its orbit will be designed especially to minimize errors associated with retroreflection from the satellite's corner cube array, and uncertainties in orbital perturbations due to gravitational and radiation pressure effects. A network of lasers having 5 cm range tracking accuracy will be deployed to provide the data needed for determining accurate LAGEOS orbits, and to monitor the motions of the ensemble of large tectonic plates which form the Earth's cover. Polar motion and variations in the

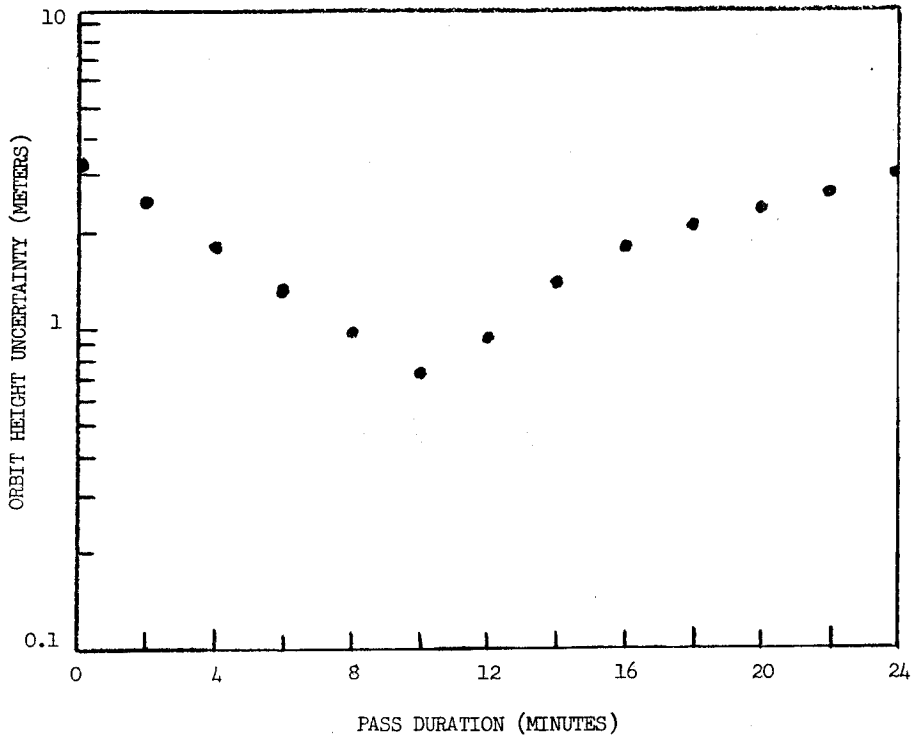

Figure 5. GEOS-C Height Uncertainty Corresponding to Laser Tracking from Goddard, Cape Kennedy, and Bermuda for a Typical SE - NW Arc
Detailed assumptions are listed in figure 6, and discussed in (BERBERT 1973)

Laser Observations (1 per 10 seconds)		
Range Bias	ΔR	20 cm
Range Noise	σR	20 cm
Azimuth Noise	σA	30 arc sec
Elevation Noise	σE	30 arc sec
Time Bias at Reference Site (Goddard)	Δt	0 μsec
Time Bias at Other Sites	Δt	50 μsec
Gravity Field		
Spherical Harmonic Coefficients		0.25 (APL 3.5 - SAO M1)
GM		1×10^{-6}
Survey		
Reference Site		(0, 0, 0) metres
Other Sites		
Cape Kennedy		(1.0,0.5,0.7) metres
Bermuda		(1.0,0.9,0.8) metres

Figure 6. A Priori Error Estimates for Orbit Height Recoveries

Earth's rotational rate will also be determined by this LAGEOS system consisting of the dedicated satellite and the associated laser network (figure 7).

The San Andreas Fault Experiment (SAFE), aimed at detecting and measuring motions some 100 km from the fault line, will also take advantage of the LAGEOS capabilities to achieve more accurate results. Sites already occupied at Quincy and San Diego will be supplemented by additional stations at other

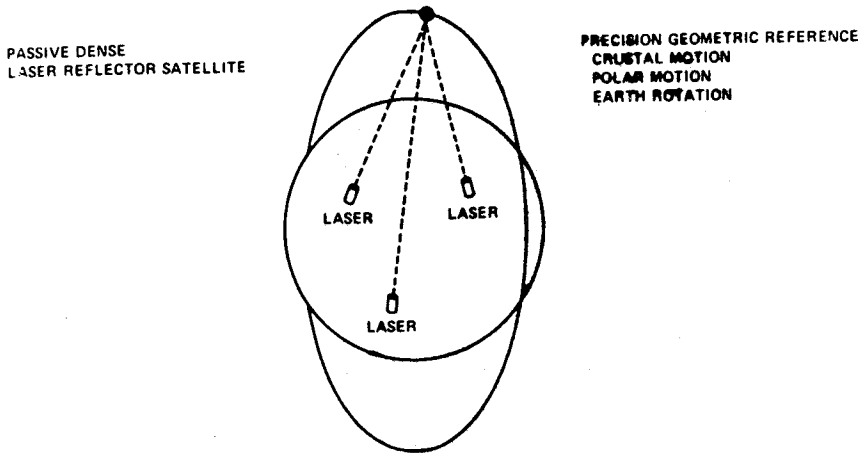

Figure 7. LAGEOS

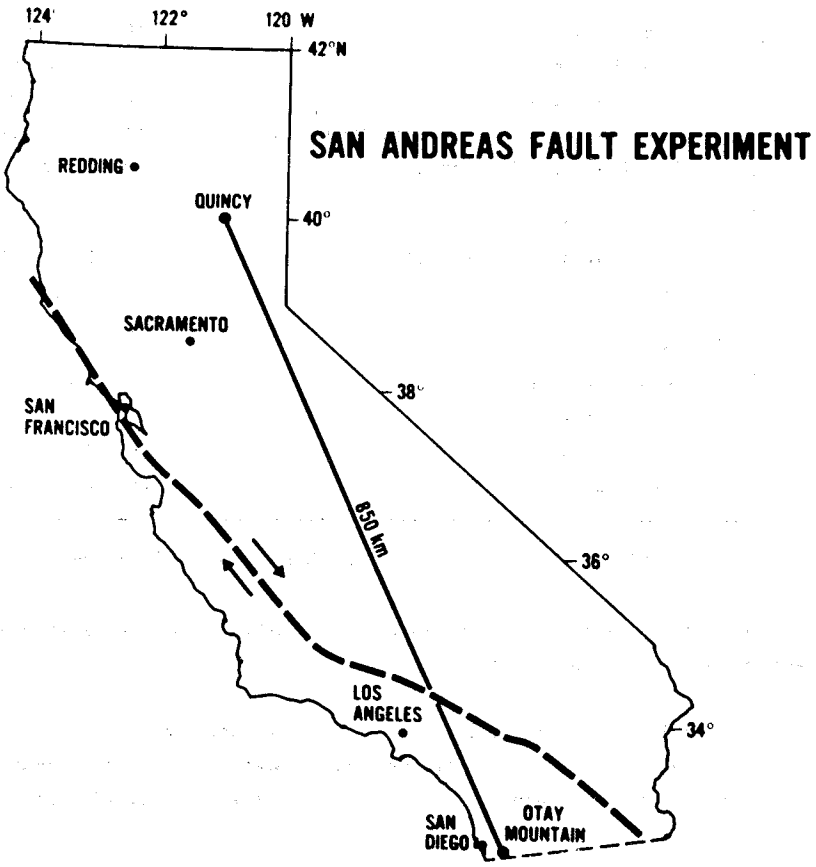

Figure 8.

locations in western North America (figure 8).

A longer look into the future outlined in the general EOPAP plan reveals the SEASAT-A, GEOPAUSE and SEASAT-B spacecraft envisioned for launching in 1978, 1979, and 1982 respectively. It is anticipated that SEASAT-A will be tracked by lasers deployed both globally and in local regions in the manner planned for GEOS-C. The improved capabilities developed for the LAGEOS program will also be used to good advantage in support of SEASAT.

GEOPAUSE, in a circular, polar orbit at a distance of about 30,000 km will also be tracked by the advanced ground laser complex (SIRY 1971). Thought is being given, too, to the possibility of operating a laser system in the GEOPAUSE satellite and using it to track retroreflectors on the ground. Uncertainties associated with orbital perturbations due to the geopotential will be negligibly small for this high orbit. The satellite will be above the horizon for four or more lasers simultaneously in many parts of its orbit; hence the prospect of eliminating tracking system biases on a continuing basis is opened up. Observation of polar motion and variations in the Earth's rotation rate in time intervals of less than half a day will also be possible. It will be practical in addition, to monitor crustal motion both in the small, in terms of effects occurring near fault

zones, and in the large, in terms of the gross motions of the tectonic plates relative to one another.

2. References

BERBERT, J.H. 1973. Laser Network Survey and Orbit Recovery. *International Symposium, Use of Artificial Satellites for Geodesy and Geodynamics*, Athens.

NASA 1972. *NASA Earth and Ocean Physics Applications Program*. National Aeronautics & Space Administration, Washington DC.

SIRY, J.W. 1971. A Geopause Satellite System Concept. *Space Science Reviews* 14(2), 314-341; and *Third International Symposium, Use of Artificial Satellites for Geodesy*, Washington DC.

VONBUN, F.O. 1972. Earth and Ocean Physics Applications Program (EOPAP). *XXIII International Astronautical Congress*, Vienna.

3. Discussion

HOLDAHL: In the diagram showing locations where you would send your portable lasers, the array seems quite dense (Ed: See diagram in paper by SIRY in this volume). Do you think the methods you described can compete with conventional geodetic methods at distances less than 300 km?

SIRY: Rule of thumb has it that conventional geodetic methods have a resolution of 1 part in 10^6. So once you go beyond 100 km, you are not operating at the 10 cm level. That's the rationale for using these techniques at the 300 km level.

HOLDAHL: What is the minimum spacing at which the observing stations should be placed? †

SIRY: Let's put it this way; beyond 100 km you would have difficulties in doing work to 10 cm accuracy with conventional techniques. You can improve on this by a factor of 2 to 5 by using satellite techniques.

WALCOTT: Isn't 1 part in 10^6 pessimistic? Aren't we up to 2 parts in 10^7?

ANGUS-LEPPAN: These are instrumental accuracies; but you are measuring through the atmosphere and I don't think the question of refraction has been solved to 1 part in 10^6.

---

†Post Symposium Comment by HOLDAHL: The rule of thumb mentioned should not be applied to detection of height changes. Error in height changes, when computed from levellings, is proportional to the square root of the distance between the observation point and the reference point. For distances less than 1000 km, precise levellings can detect height changes with an uncertainty less than 10 cm.

DISCUSSION ON SESSION "M" - METROLOGY (G.A. BELL AS CHAIRMAN)

ECKHARDT: Air Force Cambridge Research Laboratories (AFCRL) is presently supporting the development of a new, second generation laser-interferometer absolute gravity system which offers significant improvements over the original instrument constructed by Faller and Hammond with the support of AFCRL and the National Bureau of Standards. The method employed in both instruments is to drop one reflector of the two-beam Michelson interferometer and to determine the distance fallen in known time intervals by direct measurement in terms of interference fringes.

The original instrument which was designed to be transported and was successful in that it was taken to eight different sites and, after spending between one and two weeks total set-up, operate and take down time, absolute values with a precision of better than ±0.05 mGal were obtained at most sites. The apparatus was bulky and when packed for shipment had a total weight of about 2500 lb packed into about 20 shipping containers.

The aim of the new instrument is to decrease the time required to obtain an absolute value of gravity with a precision of at least as good as ±0.05 mGal to about 2 or 3 days and to cut the total weight to at most 800 lb. This is being accomplished by making some radical changes in the mechanical design and employing present day state-of-the-art electronics and computing equipment to give rapid computation of results.

The mechanical design has evolved with the express purpose of removing the necessity of having an ultra high vacuum. This removes the approximately 100 lb weight of the high vacuum pump and cuts the time by at least one full day besides greatly simplifying the problem of using trouble free materials in the vacuum chamber. Reliability will be increased because the tendency for clean surfaces to stick together will not exist in the moderate vacuum needed with the new design.

The main feature of the new design is that the freely falling reflector is enclosed in a small evacuated chamber which falls along with the reflector. These both fall in a larger vacuum chamber but since the air which comes in contact with the falling object is falling with the acceleration of gravity, air resistance cannot affect the measurement. The vacuum required in the outer chamber need be no better than 10^{-2} mm of Hg to prevent gaseous turbulence and to avoid air drag slowing its fall. The interior of the small chamber requires a vacuum of only 10^{-3} mm of Hg to place all possible air resistance effects beyond the level of consideration. While the mechanism required for separating the reflector from the small chamber during the fall is somewhat elaborate, it should be very reliable and be able to withstand many repetitions of operation.

The electronics system will make digital time measurements between a large number (50 to 500) of interference fringes and will thus make independent measurements of **g** and the gravity gradient as well as detect seismic motions occurring during the fall of the object. The digital data will be processed immediately by an on line process and control mini-computer. This will save all the time and trouble required with the original instrument to prepare data for computation and get co-ordinated with a computer facility at or near a field site.

The overall height of the instrument is about 1.5 m, while the use of aluminium in place of stainless steel and a lighter base permissible because of the new design, have also contributed to improvement in total weight. The progress of the state-of-the-art in electronics has resulted in electronic and computation systems that do much more than in the original instrument while its weight has been cut by a factor of two or three.

The future of absolute gravity instruments lies in two directions:

- portable instruments with precisions of between 0.01 mGal and 0.10 mGal; and
- fixed stations with precisions in the 0.001 mGal range.

The technology for producing such portable instruments is well in hand and if there were demand for a large enough quantity, they could become production items in the same sense that gravimeters have. The work of Sakuma at Bureau International des Poids et Mesures (BIPM) has shown that the technology for 0.001 mGal precision is available but the size and complexity of his instrument prove that it is not obtained without a great deal of extra effort and expense.

AUTHOR INDEX

Names in italics refer to participants
Entries in italics refer to contributions presented at this symposium

SUBJECT INDEX